RIKEN Accelerator Progress Report

2011

vol. 45

BOOK & CD-ROM

独立行政法人理化学研究所　仁科加速器研究センター

RIKEN Nishina Center for Accelerator-Based Science

RIKEN Accelerator Progress Report 2011

***vol.* 45**

独立行政法人理化学研究所　仁科加速器研究センター
RIKEN Nishina Center for Accelerator-Based Science
Wako, Saitama, 351-0198 JAPAN

GRAVURE & HIGHLIGHTS OF THE YEAR

« Selection process of gravure and highlights »

Gravure and highlights will be selected by two-steps process. In the first step, referee will recommend manuscript for gravure or highlight. With the above recommendation, the editors will then give secondary recommendation.

After the following 1 and 2 are comprehensively considered, the editor-in-chief will draft a manuscript idea which will be thoroughly discussed by the editors for the final decision:

1. Approval based on the editor's judgment as an expert/non-expert in the field (thereby agreeing with the referee's recommendation)
2. Additional recommendation based on the editor's expertise.

Current Status of SAMURAI

K. Yoneda, T. Isobe, N. Iwasa,[*1] T. Kobayashi,[*1] Y. Kondo,[*2] T. Kubo, K. Kusaka, T. Motobayashi, T. Murakami,[*3] T. Nakamura,[*2] J. Ohnishi, H. Otsu, H. Sakurai, H. Sato, Y. Satou,[*4] K. Sekiguchi,[*1] Y. Shimizu, Y. Togano,[*5] and K. Yoshida

This report describes the current status of a spectrometer that has been constructed in RIBF, called SAMURAI (Superconducting Analyzer for MUltiparticles from RAdio Isotope beams with 7 Tm bending power). A schematic illustration of SAMURAI is shown in Fig. 1. SAMURAI comprises a large superconducting dipole magnet and various types of particle detectors. SAMURAI is characterized by large momentum acceptance and angular acceptance for particles emitted in fast RI beam reactions and hence serves as a useful tool for experiments requiring multiparticle coincidence measurements. SAMURAI will be used in a variety of experimental studies such as breakup reactions, knockout reactions, polarized-deuteron-induced reactions, and nuclear equation-of-state studies. In our current planning, invariant-mass spectroscopy using breakup reactions is the major usage in the early stage of operation, and SAMURAI's multiparticle detection capability is particularly suitable for this purpose. Combined with the high-intensity RI beams available at RIBF, SAMURAI facilitates studies of unbound states of unstable nuclei, thus enabling investigations that have been out of our experimental reach so far.

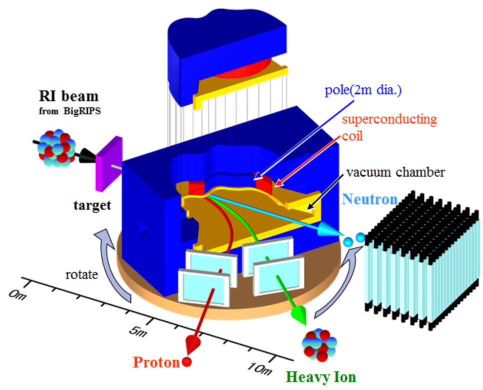

Fig. 1. Schematic view of SAMURAI. The magnet is a superconducting dipole magnet with a large bending power of 7 Tm and a large pole gap of 80 cm. Heavy-ion detectors, neutron detectors, and proton detectors are installed around the magnet. The detector configuration changes depending on experimental requirements.

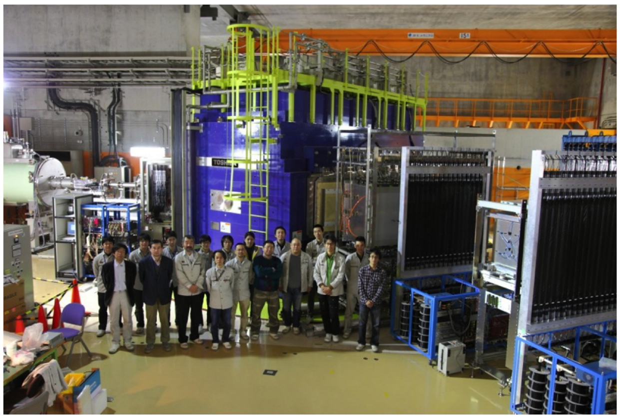

Fig. 2. Photo of experimental setup for the commissioning experiment. The setup consists of a large bending magnet with surrounding particle detectors. The beam comes from the left side, and heavy-ion detectors after the magnet are seen on the right side of the photo.

A major part of the construction of SAMURAI was funded by a four-year budget that started in fiscal year 2008. The construction of magnets and experimental devices, which are covered in the construction budget, will be completed in February 2012. Then, SAMURAI will be ready for a commissioning experiment scheduled in March 2012 and the following first series of physics experiments scheduled in May 2012.

Figure 2 shows a photo of the SAMURAI experimental setup for the commissioning experiment. The setup includes a large bending magnet, detectors for incoming beam particles, detectors for heavy ions after the target, a neutron detector at forward angles, and γ-ray detectors around the target. In the following paragraphs, a brief report of the detectors and experimental devices is provided. The overall description of the detector system has been included in a previous report [1)].

Construction of the superconducting dipole magnet was completed in June 2011. The designed maximum magnetic field of 3.08 T was achieved in the excitation test. Magnetic field maps were preliminarily measured and were compared with the results of TOSCA calculations. Details can be found in anothre report[2)]. The beamline to SAMURAI is being prepared. A moving stage was introduced for STQ18, superconducting quadrupole magnets right after a dipole magnet that works as a beamline branch to SAMURAI and ZeroDegree Spectrometer; with this arrangement, STQ18 can be used in both beamlines. For radiation safety, a beam stopper and a radiation shutter, which

*1 Department of Physics, Tohoku University
*2 Department of Physics, Tokyo Institute of Technology
*3 Department of Physics, Kyoto University
*4 Department of Physics and Astronomy, Seoul National University, Korea
*5 Extreme Matter Institute EMMI, GSI, Gremany

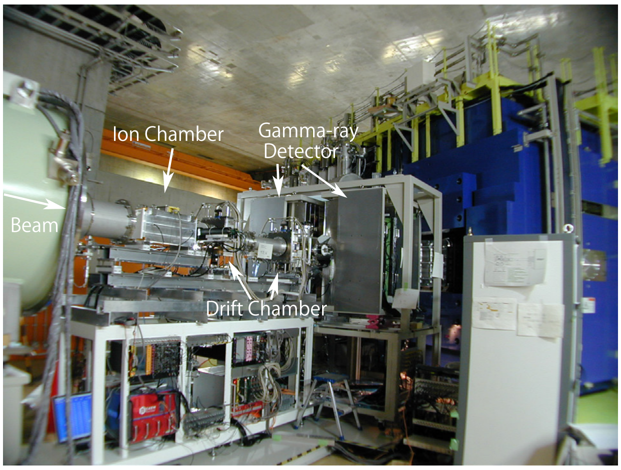

Fig. 3. Photo of experimental setup before the magnet. A STQ magnet, an ionization chamber, two tracking detectors, and a NaI(Tl) array around the target are seen.

are made of 350-mm-thick and 600-mm-thick stainless steel SUS304, respectively, were installed in the beamline. A superconducting triplet quadrupole magnet, STQ25, which serves as the last beam-focusing element for the SAMURAI target position, was installed. STQ25 is placed on a linear rail that moves 2.5 m along the beamline, in order to allow for configurational flexibility for the detectors and targets. The design of the vacuum system that connects to the built-in vacuum chamber in the gap of the dipole magnet was fixed; its construction will be completed in February 2012 [3].

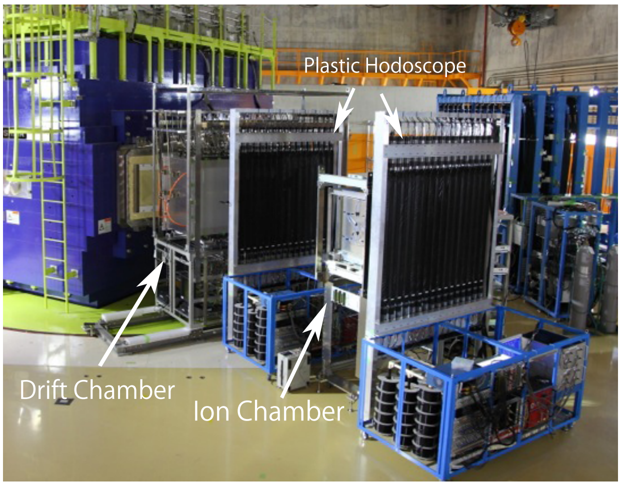

Fig. 4. Photo of experimental setup after the magnet. Charged particles are tracked by a drift chamber after the particles are bent and are identified by an ionization chamber and a plastic hodoscope.

The detectors for incoming beam particles consist of plastic scintillation detectors for timing measurements, drift chambers for beam tracking, and an ionization tors have been installed in the beamline, as shown in Fig. 3. For heavy-ion fragments, two drift chambers before and after the magnet for tracking, an ionization chamber for energy loss measurements, and plastic scintillator hodoscopes for timing measurements are installed (Fig. 4).

Figure 5 shows a neutron detector array, called NEBULA (NEutron-detection system for Breakup of Unstable nuclei with Large Acceptance), which will be placed at forward angles [4]. NEBULA consists of four sets of detector arrays, and each set consists of 60 neutron detection plastic scintillators (120 mm $\times$ 120 mm $\times$ 1800 mm), which are arranged in two layers to cover an area of 1.8 m (V) $\times$ 3.6 m (H). In addition, charged-particle-veto scintillators are placed in front of the neutron detector modules. At present, 50% of the neutron detection scintillators have been funded and are ready for use.

Fig. 5. Photo of neutron detector NEBULA. 60 scintillation detector modules are included in each frame, covering an area of 1.8 m(V) $\times$ 3.6 m(H).

In the commissioning experiment, the performances of all the detectors are checked with heavy-ion beams, and the basic characteristics are studied. Data for magnetic rigidity calibration will be acquired by using RI beams having narrow momentum spreads and with known magnetic rigidity, which is measured precisely in the BigRIPS. The overall resolution and acceptance will be checked by measuring the breakup reactions of ^{15}C, ^{17}B, and ^{14}Be.

References

1) K. Yoneda *et al.*.: RIKEN Accel. Prog. Rep. **43**, 178 (2010).
2) H. Sato *et al.*.: In this report; J. Ohnishi *et al.*: In this report.
3) Y. Shimizu *et al.*.: In this report.
4) Y. Kondo *et al.*.: In this report.

Well-developed deformation in ^{42}Si

S. Takeuchi, M. Matsushita,[*1] N. Aoi, P. Doornenbal, K. Li,[*2] T. Motobayashi, H. Scheit, D. Steppenbeck, H. Wang,[*2] H. Baba, D. Bazin,[*3] L. Càceres,[*4] H. Crawford,[*5] P. Fallon,[*5] R. Gernhäuser,[*6] J. Gibelin,[*7] S. Go,[*8] S. Grévy,[*4] C. Hinke,[*6] C. R. Hoffman,[*9] R. Hughes,[*10] E. Ideguchi,[*8] D. Jenkins,[*11] N. Kobayashi,[*12] Y. Kondo,[*12] R. Krücken,[*6] T. Le Bleis,[*13] G. Lee,[*12] J. Lee, A. Matta,[*14] S. Michimasa,[*8] T. Nakamura,[*12] S. Ota,[*8] M. Petri,[*5] T. Sako,[*12] H. Sakurai, S. Shimoura,[*8] K. Steiger,[*6] K. Takahashi,[*12] M. Takechi, Y. Togano, R. Winkler,[*3] and K. Yoneda

[Nuclear structure, in-beam γ-ray spectroscopy]

Neutron-rich Si isotopes are of interest because of their possible sub-shell closure at $Z = 14$. In particular, the nucleus of ^{42}Si could be of a doubly-closed shell, since it has 14 protons and 28 neutrons, where both 14 and 28 are (sub)magic numbers appearing by the spin-orbit splitting. Several experimental studies have been performed to investigate the structure of ^{42}Si. However, the experimental information is limited due to the low production yield. In the two-proton removal reaction experiment performed at NSCL[1)], the small cross section was interpreted as a substantial $Z = 14$ sub-shell closure in ^{42}Si. Contrary to this, the disappearance of the $Z = 14$ and $N = 28$ spherical shell closures in ^{42}Si was suggested from the observation of a γ line corresponding to the $2^+ \rightarrow 0^+$ transition with the energy of 770(19) keV in the same reaction performed at GANIL[2)]. The purpose of the present study is to investigate excited states above the 2^+ state to deduce information on the nuclear shape and/or the shell evolution. Through this study, an explanation will be provided for these conflicting results. In this study, we measured the two-proton removal reaction of the ^{44}S nucleus[3)], in which the excited states of interest in ^{42}Si can be populated selectively.

Figure 1(a) shows a γ-ray energy spectrum obtained from the two-proton removal reaction of ^{44}S associated with the de-excitation γ-rays in ^{42}Si, in which Doppler-shift effects were corrected. The prominent peak at $E_\gamma = 742(8)$ keV in Fig. 1(a) agrees with that of the reported de-excitation γ ray of the $2^+ \rightarrow 0^+$ transition with $E_\gamma = 770$ keV[2)] within a 1.5 standard deviation. In addition, several γ lines were observed at $E_\gamma = 1431(11)$, 2032(9), and 2357(15) keV. These lines were not identified in the earlier experiments[1,2)] and are newly found in the present measurement. Among these transitions, the γ line for 1431 keV was observed even in a γ-γ coincidence spectrum, as shown in Fig. 1(b). We note that the population of the yrast states, the 4^+ states in ^{42}Si, was largely enhanced due to the property of fragmentation-like reactions[4)]. Therefore, we tentatively assigned the 1431-keV γ line as the $4^+ \rightarrow 2^+$ transition.

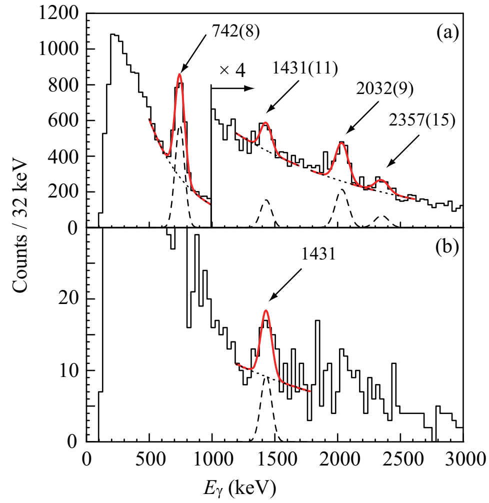

Fig. 1. (a) A Doppler-shift corrected γ-ray energy spectrum and (b) that obtained in the γ-γ coincidence with 742-keV γ rays measured in the C(^{44}S,^{42}Si γ) reaction. Solid curves show a χ^2-fitting result obtained using Gaussian functions (dashed curves) and an exponential curve as the background (dotted curve).

In the present study, the excitation energies of the 2^+ and 4^+ states were clearly determined as 742(8) keV and 2173(14) keV, respectively. The energy ratio between the 4^+ and 2^+ states, $E(4^+)/E(2^+) = 2.93$, indicates a well-developed deformation of the ^{42}Si nucleus despite its neutron magic number $N = 28$.

*1 Department of Physics, Rikkyo University
*2 State Key Laboratory of Nuclear Physics and Technology, Peking University
*3 National Superconducting Cyclotron Laboratory (NSCL)
*4 Grand Accélérateur National d'Ions Lourds (GANIL)
*5 Lawrence Berkeley National Laboratory (LBNL)
*6 Physik-Department, Technische Universität München
*7 LPC-ENSICAEN, IN2P3-CNRS et Universite de Caen
*8 CNS, University of Tokyo
*9 Argonne National Laboratory (ANL)
*10 Department of Physics, University of Richmond
*11 Department of Physics, University of York
*12 Department of Physics, Tokyo Institute of Technology
*13 University of Frankfurt/Helmholtzzentrum für Schwerionenforschung GmbH (GSI)
*14 Institut de Physique Nucléaire, Orsay

References
1) J. Fridmann et al.: Phys. Rev. C **74**, 034313 (2006).
2) B. Bastin et al.: Phys. Rev. Lett. **99**, 022503 (2007).
3) S. Takeuchi et al.: RIKEN Accel. Prog. Rep. **44**, 13 (2011).
4) P. Fallon et al.: Phys. Rev. C. **81**, 041302 (2010).

The first precision measurement of the deeply bound pionic state in ^{121}Sn at RIBF

T. Nishi,[*1] G.P.A. Berg,[*2] H. Fujioka,[*3] H. Geissel,[*4] R.S. Hayano,[*1] N. Inabe, K. Itahashi, S. Itoh,[*1] D. Kameda, T. Kubo, H. Matsubara,[*5] S. Michimasa, K. Miki,[*6] H. Miya,[*5] M. Nakamura, S. Noji,[*5] S. Ota,[*5] K. Suzuki,[*7] H. Takeda, K. Todoroki,[*1] K. Tsukada[*8], T. Uesaka, H. Weick,[*4] K. Yoshida

[Pionic atom, Precision spectroscopy]

Recent studies revealed that chiral condensate formed at the normal nuclear density can be deduced via precision spectroscopy of pionic atoms.[1,2] We performed a precision measurement of a pionic atom using the missing-mass spectroscopy of the ^{122}Sn(d,^{3}He) reaction. This experiment serves as a pilot experiment for systematic precision studies of deeply bound pionic atoms at the RIKEN RI beam factory (RIBF)[3]. Here, the latest analysis results are reported.

The left-side panel of Fig. 1 shows the position spectrum of ^{3}He in the ^{122}Sn(d,^{3}He) reaction for reaction angles smaller than 1° on a dispersive focal plane. Large binding energies appear at the right side of this spectrum. The vertical, dashed line in the figure corresponds to the quasi-free π^- production threshold. The peaks observed in the position range [-40 mm, 10 mm] are assigned to the pionic bound states, thus representing the first such observation of these states in ^{121}Sn. The right-side panel of Fig. 1 shows a theoretically calculated Q-value spectrum of the ^{122}Sn(d,^{3}He) reaction with a resolution of 300 keV (FWHM)[4]. The measured and calculated spectra are in good agreement with each other. From a comparison with the theoretical spectrum, the achieved experimental resolution is estimated to be comparable with the 400 keV that was achieved in a previous experiment[1], although this spectrum is the result of a 16-hour-long measurement, which is only 1/7 of the time of the previous one.

Figure 2 shows a scatter plot of the measured events. The angular dependences of the peaks are clearly different, indicating different momentum transfers for the peaks. This was the first observation of the angular distribution of the pionic atom cross section in the (d,^{3}He) reaction.

In conclusion, for the first time we measured the deeply bound pionic ^{121}Sn atom and the angular distribution of its cross section. The resolution was at least as good as that in the previous experiment. The data-collection time was reduced dramatically, which is essential for systematic spectroscopy. The conditions were not perfect in this pilot experiment and there is still room for improvements, especially of the optics. Although we are still working on the energy and cross-section calibrations, the results presented here indicate the potential of the RIBF facility for systematic high-precision spectroscopy of deeply bound pionic atoms.

This work is supported by a Grant-in-Aid for Scientific Research on Innovative Areas (No. 22105517).

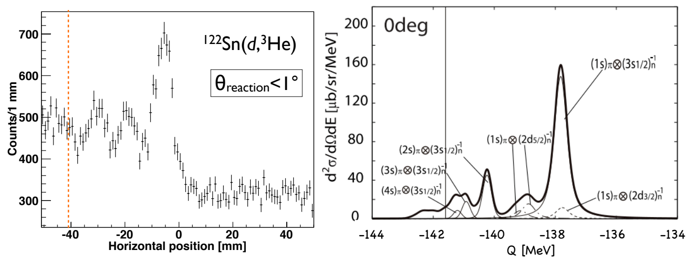

Fig. 1. (Left) Acceptance-corrected horizontal position spectrum of ^{3}He for reaction angles < 1 ° at a dispersive focal plane. The vertical dashed line represents the quasi-free π^- production threshold. (Right) Theoretically calculated Q-value spectrum for the ^{122}Sn(d,^{3}He) reaction with a resolution of 300 keV (FWHM)[4].

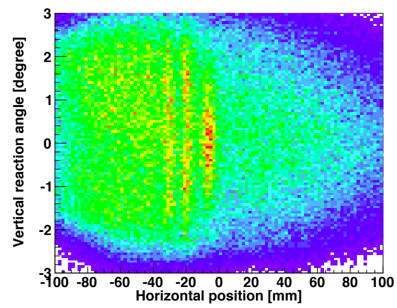

Fig. 2. Scatter plot of the acceptance-corrected horizontal position of ^{3}He and the vertical reaction angle of the ^{122}Sn(d,^{3}He) reaction.

*1 Department of Physics, University of Tokyo
*2 JINA and Department of Physics, University of Notre Dame
*3 Division of Physics and Astronomy, University of Kyoto
*4 GSI, Germany
*5 Center for Nuclear Study, University of Tokyo
*6 Research Center for Nuclear Physics, Osaka University
*7 Stefan Meyer Institute, Austrian Academy of Sciences
*8 Department of Physics, Tohoku University

References

1) K. Suzuki *et al.*: *Phys. Rev. Lett.* **92**, 072302 (2004).
2) E. E. Kolomeitsev, N. Kaiser, and W. Weise, *Phys. Rev. Lett.* **90**, 092501 (2003).
3) K. Itahashi *et al.*: *RIBF Proposal* **No.054** (2008).
4) N. Ikeno *et al.*, *Eur. Phys. J. A* **47**, 161 (2011)

Measurement of ^{12}Be$(p,n)^{12}$B reaction at 200A MeV in inverse kinematics

K. Yako,[*1] H. Sakai,[*2] H. Baba,[*2] M. Dozono,[*2] T. Fujii,[*3] N. Inabe,[*2] S. Kawase,[*3] T. Kawabata,[*4] Y. Kikuchi,[*3] K. Kisamori,[*3] T. Kubo,[*2] Y. Kubota,[*3] H. Matsubara,[*3] S. Michimasa,[*3] K. Miki,[*5] H. Miya,[*3] M. Kurata-Nishimura,[*2] S. Noji,[*3] C.S. Lee,[*3] T. Ohnishi,[*3] S. Ota,[*2] Y. Sasamoto,[*3] M. Sasano,[*2] Y. Shimizu,[*2] S. Shimoura,[*3] M. Takaki,[*3] H. Takeda,[*2] T.L. Tang,[*3] H. Tokieda,[*3] T. Uesaka,[*2] Z.Y. Xu,[*1] R. Yokoyama,[*3] and R.G.T. Zegers[*6]

[Nuclear structure, spin-isospin excitation, charge-exchange reaction, inverse kinematics]

Charge-exchange reactions at intermediate energies are excellent probes of spin-isospin excitations in nuclei, which are characterized by changes in the spin and the isospin ($\Delta S = \Delta T = 1$). The (p,n) and (n,p) reactions are among the most successful probes in the spin-isospin studies of stable nuclei owing to the simple reaction mechanism. Therefore, we constructed a facility at SHARAQ where (p,n) reactions on unstable nuclei can be studied in inverse kinematics.

In June 2011, we performed the measurement of the ^{12}Be(p,n) reaction as the first (p,n) measurement in inverse kinematics at RIBF. The ^{12}Be nucleus is a neutron-rich nucleus with a large isospin asymmetry factor $\epsilon \equiv (N-Z)/A = 0.33$. Although the neutron number $N = 8$ indicates a simple structure, it is known to possess exotic properties, e.g., breaking of $N = 8$ p-shell closure[1)] and cluster/molecular structure like $2\alpha + 4n$ configuration[2)]. It is interesting to see how these properties change the aspects of Gamow-Teller (GT, $\Delta S = \Delta T = 1, \Delta L = 0$) and spin-dipole (SD, $\Delta S = \Delta T = \Delta L = 1$) excitations.

A primary beam of ^{18}O was accelerated up to 250A MeV, and it was focused on the production target of 20-mm-thick Be at BigRIPS-F0, yielding a secondary ^{12}Be beam of 200A MeV by projectile fragmentation. ^{12}Be with a purity of 95% was selected at F3 and then transported in the achromatic mode to a liquid hydrogen target with a thickness of 14 mm at the pivot position of SHARAQ (S0). The size of the beam spot was $\sigma = 7$ mm (5 mm) in the horizontal (vertical) direction on the target. The typical beam intensity was 5×10^5 counts/s with a 100 pnA primary beam.

The missing mass spectra of the ^{12}Be(p,n) reaction were derived from the scattering angle of the neutron ($\theta_{\rm lab}$) and its kinetic energy (T_n). These were measured by the time-of-flight (TOF) method using a set of newly developed neutron counters (WINDS)[3)]. To obtain clean TOF spectra for relatively slow neutrons with $T_n < 2$ MeV, A beam buncher at RILAC was operated with a frequency that was 1/4 of base frequency of the cyclotrons, so that the interval of beam bunches was 122 ns[4)]. SHARAQ and the detectors at its focal plane (S2) were used to tag the residual nucleus (^{12}B) or its decay products (^{11}B or ^{10}B).

Figure 1 shows the spectrum of the ^{12}Be$(p,n)^{12}$B reaction with tagging of ^{12}B at S2, covering the excitation energy region of 0 to 3.4 MeV. Here, the angular distributions of GT and SD components are expected to have peaks at $\theta_{\rm cm} = 0°$ ($T_n \sim 0$ MeV) and 8–12° ($T_n = 4.5$–8.0 MeV), respectively. The observed locus is due to the GT transition to the ground state of ^{12}B. Data analysis for the GT and SD strengths is in progress.

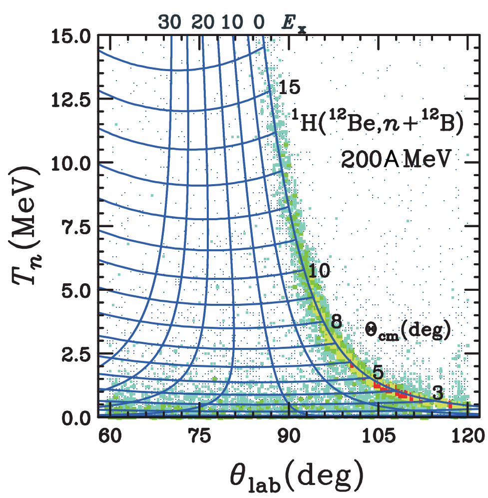

Fig. 1. Preliminary spectrum of the ^{12}Be$(p,n)^{12}$B reaction with tagging of ^{12}B at S2.

*1 Department of Physics, University of Tokyo
*2 RIKEN Nishina Center
*3 CNS, University of Tokyo
*4 Department of Physics, Kyoto University
*5 RCNP, Osaka University
*6 NSCL, Michigan State University

References
1) T. Suzuki and T. Otsuka: Phys. Rev. C **56**, 847 (1997).
2) Y. Kanada-En'yo *et al.*: Phys. Rev. C **68**, 014319 (2003).
3) K. Yako *et al.*: "Development of WINDS: wide-angle inverse-kinematics neutron detectors for SHARAQ", elsewhere in this Report.
4) K. Suda *et al.*: "Operation of the RILAC prebuncher at the fourth subharmonic frequency to provide pulsed ^{18}O beams for RIBF", elsewhere in this Report.

Decay spectroscopy in the vicinity of ^{100}Sn - test experiment

M. Lewitowicz,[*1] I. Čeliković,[*1,*2] G. de France,[*1] H. Baba, D. Bazin,[*3] N. Fukuda, R. Gernhauser,[*4] N. Inabe, D. Kameda, T. Kubo, K. Steiger,[*4] S. Nishimura, H. Suzuki, and H. Takeda

[Nuclear structure, ^{100}Sn, Gamow-Teller transition]

The ^{100}Sn nucleus has been the subject of many experimental and theoretical efforts[1–9]. This nucleus presumably the heaviest doubly magic and particle-stable nucleus with N=Z, is serving as one of the most important cases for testing nuclear structure models. One way to obtain experimental information on the structure of nuclei is through studies of Gamow-Teller (GT) beta-decay. The ^{100}Sn nucleus dominantly decays with an electron capture via a pure GT transition converting a $g_{9/2}$ proton into a $g_{7/2}$ neutron with one-unit change both in spin and isospin, making this nucleus an exceptionally interesting case. There is a prediction that mainly a single 1^+ state is populated[8] which can be confirmed by measuring γ-ray cascade emitted after the β-decay of ^{100}Sn. Combining the measured excitation energy with the β-endpoint energy would give the ^{100}Sn-^{100}In mass difference. The large QEC window for the ^{100}Sn decay allows almost full GT-strength to be observed experimentally. Moreover, the accurate analysis of the decay properties associated to model predictions might elucidate a problem of the missing GT strength[10].

In the project "Decay spectroscopy in the vicinity of ^{100}Sn", we aim at building an unambiguous level scheme of ^{100}In as well as ^{100}Sn β-decay properties, using a high-intensity ^{124}Xe beam at RIKEN Radioactive Ion Beam Factory (RIBF).

In December 2011, a one-day in-beam test was performed in order to optimize the settings of the in-flight separator BigRIPS for the ^{100}Sn production and selection.

Nuclei around ^{100}Sn were produced by the fragmentation from a 345 MeV/nucleon $^{124}Xe^{52+}$ beam with an intensity of ~9 pnA impinging on a Be target. The following two different configurations were used to be carefully evaluated.

One configuration (A) was consisting of a 4 mm Be target at the F0 focal plane and 3 mm thick Al wedges located at F1 and F5, while in the other one (B), an 8 mm Be target with 0.2 mm of W foil (used to enhance the production of $^{100}Sn^{49+}$) (F0) and Al wedges of 1.4 mm (F1) and 0.7 mm (F5).

The particle identification (PID) was done using focal plane detectors of the BigRIPS with the standard Bρ - ΔE - TOF method. Parallel - Plate Avalanche Counters (PPACs) at F3, F5 and F7 were used for the Bρ measurements. Plastic scintillators were placed at F3 and F7 for the TOF measurement. The ΔE information was obtained by ionisation chamber placed at F7. At the final focal plane F12, beam particles were implanted and energy measured by silicon strip detectors surrounded by a Ge array for γ-ray detection. Figure 1 shows the PID plot with respect to atomic number Z and the mass to charge ratio A/Q for configuration with 8 mm target. The 9 counts of ^{100}Sn shown in the PID plot were collected in 6.5 hours. A confirmation of the identification in Z and A/Q was obtained by observation of characteristic γ lines of known isomers in ^{98}Cd and ^{96}Pd.

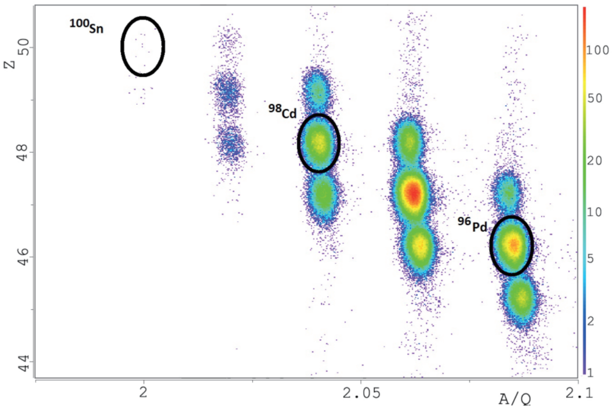

Fig. 1. A particle identification plot with respect to the atomic number Z and the mass-to-charge ratio A/Q for configuration with 8 mm target.

A preliminary result for the production rate of ^{100}Sn is 2.2 particles/h and 1.4 particles/h, while the total count rate measured by the timing signal of the plastic scintillator at the final focal plane was around 30 pps and 60 pps for the configurations A and B respectively.

References
1) R. Schneider et al.: Z. Phys. A **348**, 241 (1994).
2) M. Lewitowicz et al.: Phys. Lett. B **332**, 20 (1994).
3) M. Chartier et al.: Phys. Rev. Lett. **77**, 2400 (1996) .
4) K. Sümmer et al.: Nucl. Phys. A **616**, 341 (1997).
5) T. Faestermann et al.: Eur. Phys. J. A **15**, 185 (2002).
6) D. Bazin et al.: Phys. Rev. Lett. **101**, 232501 (2008).
7) C. Hinke et al.: Nature (to be published).
8) H. Grawe et al.: AIP Conf. Proc. **481** 177 (1999).
9) A. Bobyk et al.: Acta Phys. Pol. B **31**, 953 (2000).
10) B. A. Brown: Phys. Rev. C **50**, 2270 (1994).

*1 GANIL, France
*2 Institute "Vinča", Belgrade University, Serbia
*3 NSCL, USA
*4 TU München, Germany

Production-cross-section measurement of neutron-rich radioactive isotopes using a ^{238}U beam at 345 MeV/nucleon

N. Fukuda, D. Kameda, H. Takeda , T. Ohnishi, N. Inabe, and T. Kubo

[Production cross sections, In-flight fission]

Since the commissioning of the RIBF in 2007, a variety of RI beams have been produced at BigRIPS [1] using the in-flight fission of ^{238}U beam at 345 MeV/nucleon, and their production cross sections have been deduced from the measured production yields[2,3]. These measured production cross sections are important in designing the RI-beam experiments, allowing accurate estimates of the RI-beam intensities. In this article, we report the measured production cross sections for a wide range of neutron-rich radioactive isotopes.

The experimental conditions are summarized in Table 1. We conducted the measurements with two different target materials, beryllium and lead, in order to investigate the reaction mechanism. The abrasion-fission (AF) process is dominant in the case of the beryllium target; the Coulomb-fission (CF) process, in the case of the lead target. For the beryllium target, we conducted measurements with three different $B\rho$ settings in order to examine the $B\rho$ dependence of the cross section. The $B\rho$ settings were optimized such that the total trigger rate should be less than a few kilohertz.

The method of isotopic separation and particle identification is described in Ref[2]. The total ^{238}U beam doses required for deducing the cross section were obtained by measuring the light charged particles that were recoiling out of the target.

The measured cross sections of the isotopes produced with the Be and Pb targets are shown in Fig. 1, along with the predictions from the LISE++ simulations based on the AF and CF, models[4], respectively. The parameters used in the model are the standard ones that have been determined to fit the GSI cross section data. A fairly good agreement is observed between the measurement and the LISE++ simulation results. However, discrepancies between them are found for Sn and the $Z \leq 18$ isotopes for the Be target, and the Ag, Cd, In, Ba isotopes for the Pb target. A major reason for the discrepancies could be uncertainty of the $B\rho$ distributions in the transmission estimation. Finally, it should be emphasized that the present work is the first application of the AF model and aims to evaluate.

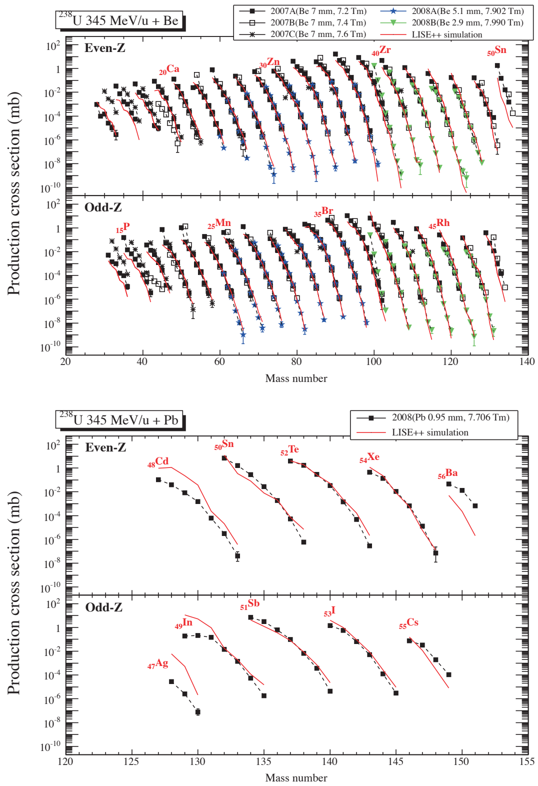

Fig. 1. Production cross sections of the isotopes produced by the in-flight fission of a ^{238}U beam for the Be (upper panel) and Pb (lower panel) targets. The measured cross section are shown by the symbols. The red lines show the predictions from the LISE++ simulations.

References
1) T. Kubo: Nucl. Instr. and Meth. **B 204**, 97 (2003).
2) T. Ohnishi et al.: J. Phys. Soc. Jpn. **77**, 083201 (2008).
3) T. Ohnishi et al.: J. Phys. Soc. Jpn. **79**, 073201 (2010).
4) O.B. Tarasov and D. Bazin: Nucl. Instr. and Meth. **B 266**, 4657 (2008), and references therein; LISE++ manual, Michigan State University, http://groups.nscl.msu.edu/lise/lise.html.

Table 1. Summary of experimental conditions.

Target	Be 7 mm			Pb 1.5 mm	Be 5.1 mm	Be 2.9 mm	Pb 0.95 mm + Al 0.3 mm
$B\rho$ (Tm)	7.2	7.4	7.6	7.0	7.902	7.990	7.706
dp/p	±1%	±1%	±2%	±0.1%	±3%	±3%	±3%
Degrader	None	None	None	None	F1: 1.29 mm	F1: 2.18 mm	F1: 2.56 mm, F5: 1.8 mm
F2 slit (mm)	±30	±30	±30	±50	±13.5	±15.5	±15

New result on production of ^{277}Cn by ^{208}Pb+^{70}Zn reaction

T. Sumita,[*1] K. Morimoto, D. Kaji, H. Haba, K. Ozeki, Y. Kudou, R. Sakai, A. Yoneda, A. Yoshida, H. Hasebe, K. Katori, N. Sato,[*2] Y. Wakabayashi,[*2] S. Mitsuoka,[*2] S. Goto,[*3] M. Murakami,[*3] Y. Kariya,[*3] F. Tokanai,[*4] K. Mayama,[*4] M. Takeyama,[*4] T. Moriya,[*4] E. Ideguchi,[*5] T. Yamaguchi,[*6] H. Kikunaga,[*7] J. Chiba,[*1] and K. Morita

[^{277}Cn, excitation function, GARIS]

The production and decay property of an isotope of the 112$^{\mathrm{th}}$ element, ^{277}Cn, were investigated by irradiating ^{208}Pb targets with a ^{70}Zn beam. We observed one decay chain of ^{277}Cn and measured the excitation function.

Only four decay events originating from ^{277}Cn, produced by the ^{208}Pb(^{70}Zn, n) reaction, were reported until now. Two of them were reported by a research group at GSI, Germany[1)], and the other two by a group at RIKEN[2)]. We performed an experiment to obtain additional information on the production and decay of ^{277}Cn.

A ^{70}Zn beam was derived from the RILAC. The typical beam intensity was $2.8\times10^{12}\,\mathrm{s}^{-1}$. Targets were prepared by vacuum evaporation of metallic lead onto carbon backing foils with a thickness of 60 μg/cm^2. The gas-filled recoil ion separator, GARIS[3)], was used as the recoil separator. The experimental setup is almost the same as that in the previous experiment[2)].

The experiments were performed with ^{70}Zn beam at 347.5, 351.5, and 355.5 MeV. The experimental conditions are listed in Table 1. The energy loss of the beam in the target was calculated by using range-energy table[4)]. The production cross section was derived by assuming the transmission of GARIS to be 80%[3)]. The excitation energy of the compound nuclei (E^*_{CN}) at the middle of the target was estimated by using the predicted masses[5)] of ^{278}Cn and the experimental masses of the beam and target.

Table 1. Summary of the experimental conditions. E_{in}: beam energy in front of target. E^*_{CN}: excitation energy of the compound nuclei. T_{av}: average target thickness. σ: production cross section.

E_{in} (MeV)	E^*_{CN} (MeV)	T_{av} (μg/cm^2)	Dose ($\times10^{18}$)	Number of events	σ (pb)
351.5	15.3 ± 2.5	580	9.7	1	$0.078^{+0.18}_{-0.065}$
347.5	12.0 ± 2.9	660	5.1	0	<0.25
355.5	18.1 ± 2.8	640	8.2	0	<0.15

At a beam energy of 351.5 MeV, one event was observed. The observed decay chain is shown in Fig. 1, in which the measured energies, decay times, and positions of the implantation of evaporation residue and decay events are specified. The spectroscopic information of the isotope ^{277}Cn and its decay daughters ^{273}Ds and ^{269}Hs will be improved.

From the results of the present study, the production cross section was deduced to be $0.078^{+0.18}_{-0.065}$ pb. At other energies, no event was observed. Combining the results of the present and previous[2)] experiments, the production cross section is deduced to be $0.17^{+0.16}_{-0.10}$ pb at average $E^*_{\mathrm{CN}}=15.2$ MeV. At $E^*_{\mathrm{CN}}=12.0$ and 18.1 MeV, 1σ upper limit (68% confidence level) was calculated to be 0.25 and 0.15 pb, respectively. Although statistical errors are still large, the optimum E^*_{CN} value to produce the ^{277}Cn isotope would be around 15 MeV.

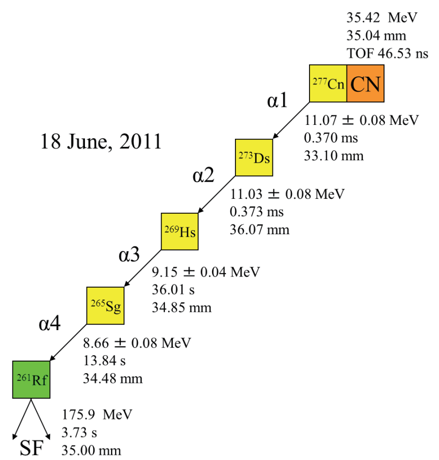

Fig. 1. Decay chain observed in ^{208}Pb(^{70}Zn, n)^{277}Cn reaction. Measured energies, decay times, and positions are indicated in the figure.

*1 Faculty of Science and Technology, Tokyo University of Science
*2 Advanced Science Research Center, Japan Atomic Energy Agency
*3 Department of Chemistry, Niigata University
*4 Department of Physics, Yamagata University
*5 Center for Nuclear Study, University of Tokyo
*6 Department of Physics, Saitama University
*7 Research Center for Electron Photon Science, Tohoku University

References

1) S. Hofmann et al.: Eur. Phys. J. A **14** (2002) 147.
2) K. Morita et al.: J. Phys. Soc. Jap. **76** (2007) 043201.
3) K. Morita et al.: J. Phys. Soc. Jap. **73** (2004) 1738.
4) L. C. Northcliffe and R. F. Schilling: Nucl. Data Tables A **7** (1970) 233.
5) W. D. Myers and W. J. Swiatecki: Nucl. Phys. A **601** (1996) 141.

Development of mountable controller for VME modules

H. Baba, T. Ichihara, T. Ohnishi, S. Takeuchi, K. Yoshida, Y. Watanabe, S. Ota,[*1] and S. Shimoura[*1]

At the RIKEN RIBF, a network-distributed DAQ system is used[1)]. The dead time of the system is determined by the number of readout channels per CAMAC/VME controller. The bus frequency is limited by the system specification. To achieve a higher speed, either the number of readout channels or the interrupt latency should be reduced.

Recently, FPGA-based controllers have been distributed by companies. CC/NET[2)] and VM-USB[3)] are CAMAC and VME controllers that can run as a list sequencer on an FPGA. They can achieve the intrinsic readout speed of buses. Moreover, the interrupt latency is quite shorter than that of the usual PC-to-VME system. These controllers are very good. However, it is almost impossible to install many controllers for reducing the readout channel per controller. It is assumed that one controller should handle several slave modules and that the controllers and crates are expensive.

In this study, we have developed a new small VME controller to achieve the best readout speed. The concept behind the controller is referred to as "1 controller for 1 module," and the cost of the controllers is low. A photograph of the controller is shown in Fig. 1. This controller consists of FPGA (Xilinx, XC3S50AN, Spartan 3AN) and USB2.0 slave (FTDI, FT2232H Hi-speed Dual USB UART/FIFO) chips. The FPGA covers the VME operation modes of A32/A24/A16, D32/D16, Read/Write, and block transfer (BLT). VME data are transferred to a PC though the USB chip. The FPGA is synchronized with a 60 MHz clock signal from the USB chip. This controller can connect to the VME bus; however, it uses only power lines. In other words, a VME module can be handled without a VME crate.

Figure 2 shows the timing chart of the interrupt response and block transfer. The FPGA is configured such that when the interrupt signal is generated, 34 data are read from a CAEN V792 QDC and transferred to the USB chip. The timing chart is obtained by ChipScope Pro[4)], which is a debug tool to inspect the interior of the FPGA. The sampling clock frequency is 50 MHz. *VME IRQ1** is the interrupt signal from CAEN V792. *VME AS** (Address Strobe), *DS** (Data Strobe), and *DTACK** (Data Acknowledge) are VME bus signals used to perform handshake. First, VME data are stored in the FPGA FIFO memory (*FPGA FIFO WR_EN*). Subsequently, data is transferred to the USB FIFO memory (*USB FIFO WR_EN**). Note that an asterisk (*) following the signal name represents inverted signals. The transaction time of this sequence is only 7.8 μs. The controller can achieve the intrinsic speed of VME. The worst interrupt latency is only 16.6 ns since the FPGA checks the *VME IRQ** signal every 16.6 ns (synchronized with a 60 MHz clock). This value corresponds to a speed that is 1000 times higher than the speed of the usual PC-to-VME system.

The production cost of the controller is about 20,000 yen. This price is very low, and it is possible to install this controller for all VME modules at the RIKEN RIBF. The development of the CAMAC mountable controller is currently being planned.

*1 Center for Nuclear Study, University of Tokyo

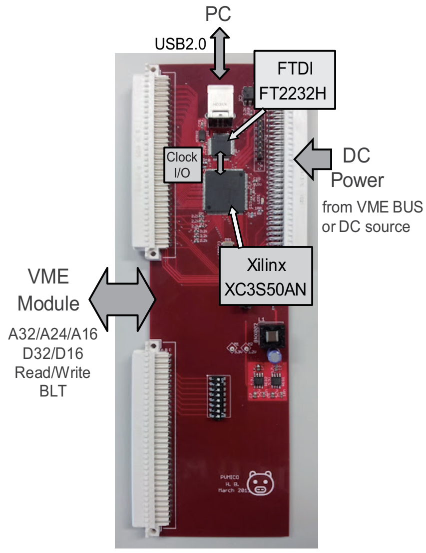

Fig. 1. Photograph of the mountable controller.

References
1) H. Baba et al.: Nucl. Inst. Meth. A **616** (2010) 65.
2) Y. Yasu et al.: Comp. High Ene. Nucl. Phys. (2003) 24.
3) *Wiener VM-USB User Manual.*
4) *Xilinx ChipScope Pro Software and Cores User Guide.*

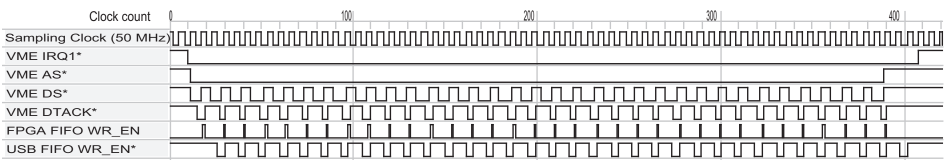

Fig. 2. Timing chart of the response of the interrupt signal and 34 data block read.

The EUROBALL RIKEN Cluster Array Project (EURICA)

S. Nishimura, H. Baba, P. Doornenbal, E. Ideguchi,[*1] T. Isobe, M. Kurata-Nishimura, Z. Li, G. Lorusso, A. Odahara,[*2] T. Nakao, P.-A. Söderström, D. Steppenbeck, H. Sakurai, T. Sumikama,[*3] H. Watanabe, Z. Xu,[*4] K. Yoshinaga[*3] and the EURICA Collaboration[1)]

[Nuclear structure, β-decay, unstable nuclei]

A new project, EURICA (**EU**roball **RI**ken **C**luster **A**rray) which proposes to utilize the EUROBALL Cluster detectors for experimental campaigns at the RIBF, has been approved by the EUROBALL Owners Committee on July 27th, 2011. The EURICA is an open project that has been launched as a research campaign with the main aim of conducting isomeric and β-delayed γ-spectroscopy of nuclei with extreme proton-to-neutron ratios[2)].

The experimental arrangement, which consists of 12 seven-element germanium Cluster detectors and their support was formerly used as the RISING at GSI[3)], shown in Fig. 1; it has been transported and installed at the F11 focal point at RIBF. The EURICA Cluster detectors are supported by two independent hemispherical supporting-frames mounted on a 4 m long rail system. In total, 84 Cluster capsules (7 × 12 Cluster detectors) are arranged to form a spherical shape with an inner diameter of 38-cm. Each energy signal from the Cluster capsule is processed by fully digital electronics using DGF-4C modules from XIA, with an expected energy resolution of better than 3 keV at $E\gamma$ = 1.3 MeV[3)]. The photopeak efficiency of the EURICA is about 15% at $E\gamma = 662$ keV. The advantage of EURICA is that it can study the low-lying states of nuclei with one order of magnitude higher detection efficiency for single γ-ray detection, i.e., two orders of magnitude higher for $\gamma\gamma$-coincidence, compared to the previous β-decay spectroscopy experiment conducted at RIBF[4)].

An infrastructure of liquid N_2 pipeline will be available in March 2012 to keep the germanium detector operational. An "active stopper" detector, consisting of double-sided silicon-strip detectors, will be placed at the center of the EURICA for the detection of the β-rays and the implantation of heavy ions. For fast γ-ray detection, $LaBr_3$(Ce) detectors will be also installed in the space of missing Cluster detectors.

Commissioning of the EURICA has been scheduled for March 2012 so that it can be ready for the first experimental campaign in June 2012. The overall beam time at the RIBF available for EURICA is estimated to be 40-50 % of the overall beam time available from 2012 until June 2013. Most of the PAC-approved EURICA programs are requesting the use of ^{238}U at a current of $I = 5$ pnA. The ^{238}U beam has so far been delivered at a maximum current of $I = 3.5$-4 pnA in the ^{238}U beam series conducted in October -December 2011[5)]. The collaboration would like to thank the EUROBALL Owners Committee for the loan of the germanium detectors, the PreSpec Collaboration for the use of the readout electronics of the Cluster detectors, and GSI for the technical support provided to the EURICA project at RIBF.

*1 CNS, University of Tokyo
*2 Department of Physics, Osaka University
*3 Department of Physics, Tokyo University of Science
*4 Department of Physics, The University of Tokyo

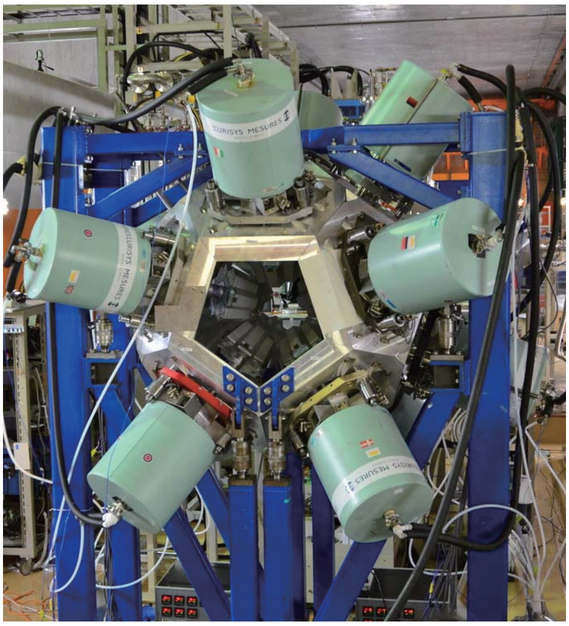

Fig. 1. The EURICA setup. The 12 EUROBALL Cluster detectors and support structure, formerly used for the RISING stopped beam campaign at GSI, have been installed at the F11 focus of Zero-Degree Spectrometer.

References

1) http://ribf.riken.jp/EURICA.
2) The EURICA Project: Submitted to the Gammapool Owners Committee (July 2011)
3) H.J. Wollersheim et al.: Nucl. Instr. Meth. A **537**, 637 (2005).
4) H. Watanabe, et al.: Phys. Lett. B **696**, 185-190 (2011); S. Nishimura, et al.: Phys. Rev. Lett. **106**, 052502 (2011); T. Sumikama, et al.: Phys. Rev. Lett. **106**, 202501 (2011); H. Watanabe, et al.: Phys. Lett. B **704**, 270-275 (2011).
5) The status of RIBF accelerator in this progress report.

Monopole strength function of deformed superfluid nuclei†

M. Stoitsov,[*1] M. Kortelinen,[*1] T. Nakatsukasa C. Losa,[*2] and W. Nazarewicz,[*1]

[Nuclear structure, random phase approximation]

One of the major challenges in the many-body problem is the microscopic description of the collective motion involving hundreds of strongly interacting particles. Here, of particular interest is the response of the system to a time-dependent external field. In the nuclear case, in the small-amplitude limit of nearly harmonic oscillations about the equilibrium, the associate phenomena include the presence of a variety of vibrational modes and characteristic distribution of electromagnetic, particle, and beta-decay strength.

A majority of nuclei exhibit strong nucleonic pairing that profoundly impacts their collective motion. Away from the stability line, another factor affecting nuclear correlations and dynamics is the presence of low-lying particle continuum that provides a vast configuration space for nucleonic excitations. Therefore, to understand a variety of nuclear modes throughout the nuclear chart, a consistent treatment of many-body correlations and continuum is required.

This study focuses on the multipole strength in superfluid deformed heavy nuclei. The theoretical method is the quasi-particle random-phase approximation (QRPA) applied to the self-consistent configuration obtained by means of the nuclear density functional theory (DFT). QRPA represents the small amplitude limit to the time-dependent DFT method or time-dependent Hartree-Fock-Bogoliubov (TDHFB) method. In the absence of pairing, QRPA reduces to the usual random phase approximation (RPA) built atop the Hartree-Fock (HF) equilibrium.

The main obstacle in the conventional matrix formulation of (Q)RPA is the computation of matrix elements of the residual interactions and their storage. The recent breakthrough came from the realization that the explicit computation and storing the huge (Q)RPA matrices can be avoided by taking advantage of self-consistent DFT solutions and directly employing the linear response theory to them. Indeed, in the finite-amplitude method (FAM)[1)], the (Q)RPA matrix equations are recast into the set of self-consistent equations with respect to (Q)RPA amplitudes, which significantly reduces the computational efforts. The FAM has been applied in the RPA variant to Skyrme energy density functionals (EDFs) to study giant dipole resonances and low-lying pygmy dipole modes[2)]. Recently, in its QRPA extension, FAM was used to study monopole resonances in a spherical dripline nucleus ^{174}Sn[3)].

We have constructed a FAM program based on the deformed HFB code in the harmonic-oscillator-basis representation HFBTHO[4)]. We have employed a method for solving the FAM equations based on the Broyden iterative scheme[5)]. Further, we have studied the performance of the method and compared it with that of the standard QRPA diagonalization method. An example of the result is shown in Fig. 1 for the monopole strength in deformed ^{24}Mg. This calculation has been done within a small model space of five major shells. In the standard method, it is difficult to increase the model space, even with a supercomputer. In contrast, in the FAM, we are able to make a calculation with the model space of 20 major shells on a single laptop computer. We also demonstrate that FAM solutions can be obtained with no more than 40 iterations at modest memory requirements of about of 0.5 GB, for large model spaces corresponding to fission isomers in the actinides or neutron-rich deformed nuclei.

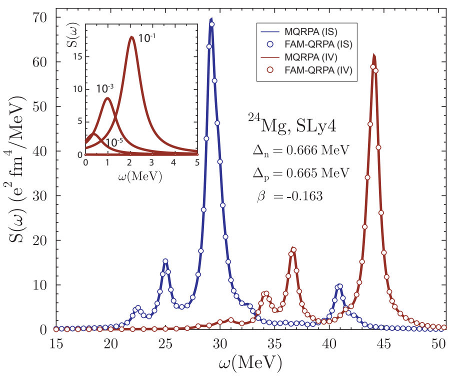

Fig. 1. The isoscalar (blue circles) and isovector (red circles) monopole strength in oblate-deformed paired minimum of ^{24}Mg. The isoscalar and isovector strength obtained with the conventional matrix formulation are shown by blue and red lines, respectively.

† Condensed from the article in Phys. Rev. C **84**, 041305(R) (2011)

*1 Department of Physics & Astronomy, University of Tennessee, USA
*2 International School for Advanced Studies, SISSA, Italy

References

1) T. Nakatsukasa, T. Inakura, and K. Yabana, Phys. Rev. C **76**, 024318 (2007).
2) T. Inakura, T. Nakatsukasa, and K. Yabana, Phys. Rev. C **80**, 044301 (2009); Phys. Rev. C **84**, 021302 (2011).
3) P. Avogadro and T. Nakatsukasa, Phys. Rev. C **84**, 014314 (2011).
4) M. Stoitsov et al., Comp.. Phys. Comm., **167**, 43 (2005).
5) C.G. Broyden, Math. Comput. **19**, 577 (1965); D.D. Jonson, Phys. Rev. B **38**, 12807 (1988).

Separation of a Slater determinant wave function with a neck structure into spatially localized subsystems

Y. Taniguchi and Y. Kanada-En'yo*[1]

[Nuclear structure, cluster]

Nuclear systems often exhibit multicenter structures having spatially localized subsystems, as observed in cluster structures and fusion/fission processes. In order to gain an in-depth understanding of nuclear systems with subsystems, wave functions of each subsystem should be defined microscopically.

An orthonormal set of spatially localized single-particle wave functions is obtained by diagonalizing the coordinate operator for the major axis of a necked system. Consider the following Slater determinant wave function $|\Phi\rangle$ having a two-center structure:

$$|\Phi\rangle = \hat{\mathcal{A}}|\tilde{\varphi}_1, \tilde{\varphi}_2, ..., \tilde{\varphi}_A\rangle,$$

where $\hat{\mathcal{A}}$ is the antisymmetrization operator, A is the mass number of the system, and $\tilde{\varphi}_1$, ..., $_A$ are single-particle wave functions. Note that $|\Phi\rangle$ is invariant except for the normalization under any linear transformation of single-particle wave functions, i.e., $\{\tilde{\varphi}_i\} \to \{\varphi_i\}$, that gives nonzero determinants.

In order to separate the system into two subsystems, namely, I and II, subsystem wave functions are defined as follows. First, single-particle wave functions are transformed in order to diagonalize norm and coordinate operators $\hat{z}$,

$$|\varphi_i\rangle = \sum_j |\tilde{\varphi}_j\rangle c_{ji},\ \langle\varphi_i|\varphi_j\rangle = \delta_{ij},\ \langle\varphi_i|\hat{z}|\varphi_j\rangle = z_i\delta_{ij},$$

where $z_1 \leq z_2 \leq \cdots \leq z_A$. The eigenvalue z_i indicates the mean position of the ith nucleon. φ_i are classified into two groups $\{\varphi_1, \cdots, \varphi_{A_1}\}$ and $\{\varphi_{A_1+1}, \cdots, \varphi_A\}$ according to the distribution of z_i. The wave function of each subsystem is defined using the localized single-particle wave functions.

The present method is used for separating an antisymmetrized molecular dynamics (AMD) wave functions[1,2] of ^{10}Be into α + ^{6}He subsystems. An AMD wave function is obtained by energy variation after the angular momentum projection.[3] By analyzing the mean position z_i of nucleons determined by the present method, the single-particle wave functions φ_i can be separated into two subsystems. Figure 1 shows the linear density distributions of the dominant components, which are separated into α and ^{6}He clusters, of the ground state in ^{10}Be. The total linear density distributions have necks at $z \sim 0$ fm, and single-particle orbits localize the left and right parts. Four nucleons that have z_i to the left of the neck position and form an α cluster, and six nucleons that have z_i to the right of the neck form a ^{6}He cluster. Thus, the ^{10}Be system can be separated into two clusters by using the proposed separation method.

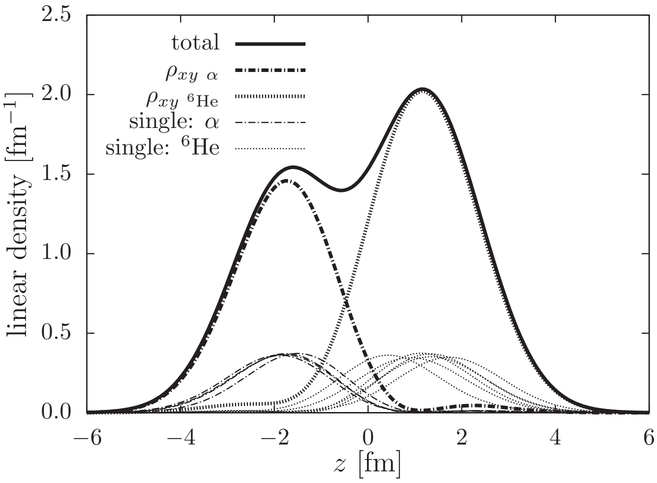

Fig. 1. Linear density distributions of intrinsic wave functions of the dominant components of the ground state of ^{10}Be. The thin dot-dashed and dotted lines represent single-particle wave functions for α and ^{6}He clusters, respectively. The thick dot-dashed and dotted lines represent α and ^{6}He clusters, respectively. The solid lines represent total wave functions. The units for linear densities and z are in fm^{-1} and fm, respectively.

The proposed method is simple and applicable to a wide variety of approaches based on the Slater determinant wave function, e.g., the HF method. Moreover, this method is useful for the analysis of systems that have spatially localized subsystems observed in cluster structures and nuclear reactions.

- - - - -

References

1) A. Ono, H. Horiuchi, T. Maruyama, and A. Ohnishi, Prog. Theor. Phys. 87, 1185 (1992).
2) Y. Kanada-En'yo and H. Horiuchi, Prog. Theor. Phys. 93, 115 (1995).
3) Y. Kanada-En'yo, H.Horiuchi, and A. Dote, Phys. Rev. C 60, 064304 (1999).

*1 Department of Physics, Kyoto University, Japan

Double spin asymmetry of single electron production in polarized proton-proton collisions at $\sqrt{s} = 200$ GeV

K.R. Nakamura[*1] for the PHENIX Collaboration

It is important to understand gluon polarization in proton for understanding the spin structure of the nucleon. In proton-proton collisions, heavy flavor quarks are mainly produced by gluon-gluon interactions at the partonic level. In PHENIX, the quarks are detected by observing electrons from semileptonic decays of the quarks (single electrons). Therefore, the longitudinal spin asymmetry of single electron production can provide information on the gluon polarization[1)].

The measurement of electrons in PHENIX includes a large fraction of background electrons. The background source mainly consists of electron pairs from Dalitz decays of neutral mesons and photon conversions (photonic electrons). To reject the photonic electrons effectively, a new position-sensitive Cherenkov counter, Hadron Blind Detector (HBD), is used for this measurement.

The background electron pairs are produced with a small opening angle. Therefore, on the HBD, their signals are merged and a cluster with twice the charge of a single electron is produced. In my previous study, yield spectra of "single electron clusters" and "merged clusters" were obtained on the HBD and a clearly decrease in the number of photonic electrons by a cluster charge selection was confirmed[2)]. While the single electron clusters mainly consist of single electrons, they also include photonic electrons. The amount of photonic electrons is estimated by studying the spatial charge distribution on the HBD around the projected point of the reconstructed track. From the estimated value, the yield of single electrons can be calculated.

The cross section of single electron production is estimated using the single electron yield. Figure 1 shows the cross section obtained from such an analysis, apart from the previous results obtained from measurements performed in 2005 and 2006. The cross section obtained in the present study is consistent with the previously obtained cross section. Since analysis methods used for the measurements of 2005 and 2006 were different, the consistency supports the validity of the new analysis method.

The dilution factor is also estimated from the yield of single electrons for use in the spin asymmetry analysis. The estimation shows an improvement by a factor of about 1.5 compared to the dilution factors obtained with the 2005 and 2006 measurements. The improvement is a consequence of the event selection being based on HBD signals for rejecting the photonic electrons.

*1 Department of Physics, Kyoto University, Kitashirakawa-Oiwake, Sakyo, Kyoto 606-8502, Japan

Using the improved dilution factor, the double spin asymmetry of single electron production is calculated. Figure 2 shows the result of the spin asymmetry analysis. By calculating the combination of points in the low-momentum region ($p_T < 1.5$ GeV/c), a combined asymmetry A_{LL} ($0.5 < p_T < 1.5$ GeV/c) of (3.1 ± 5.5 (stat.) ± 5.7 (syst.)) $\times 10^{-3}$ is obtained.

A paper reporting these results is under preparation, and it is expected be published in 2012.

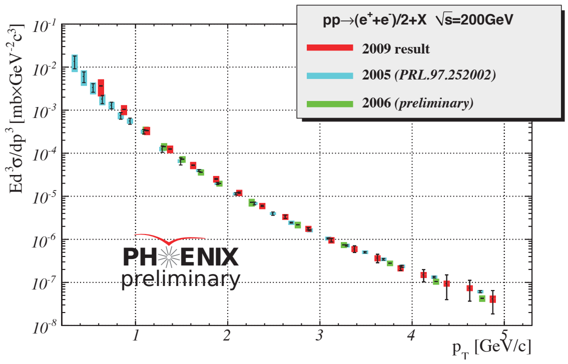

Fig. 1. Cross section of single electron production in proton-proton collisions at $\sqrt{s} = 200$ GeV. The spectra with red, green, and blue error bands represent results from the measurement of the present study and previous measurements of 2005 and 2006, respectively.

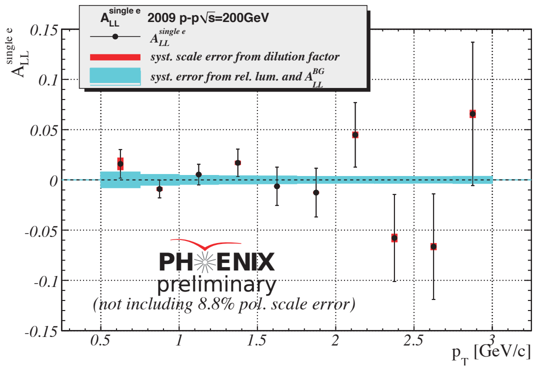

Fig. 2. Double spin asymmetry of single electron production. The red bar and the blue band represent the systematic error in the estimation of the dilution factor and the combined systematic error in the relative luminosity and background asymmetry, respectively.

References
1) I. Bojak, Phys. Rev. D **67** (2003) 034010.
2) K.R. Nakamura and Y. Akiba, RIKEN Accel. Prog. Rep. **44** (2011) 65.

Commissioning and operation of silicon vertex detector for PHENIX experiment in RHIC Run-11

M. Kurosawa,*1 Y. Akiba, H. Asano,*2 R. Akimoto,*3 O. Drapier,*4 A. Enokizono, F. Gastaldi,*4 T. Hachiya, J. Koster,*1 E. Mannel,*5 R. Pak,*5 C. Pancake,*6 H. Sako,*7 S. Sato,*7 E. Shaft,*6 W. Sondheim,*8 M. Stepanov,*9 A. Taketani, and the PHENIX VTX group

The PHENIX experiment is aimed at elucidating the spin structure of nucleons and studying the hot and dense matter at Relativistic Heavy Ion Collider (RHIC), Brookhaven National Laboratory (BNL). With the aim of enhancing the physics capability of PHENIX for spin and heavy-ion programs, the PHENIX detector was upgraded with a silicon vertex tracker (VTX) in Dec, 2010. The VTX comprises a four-layer barrel detector built from two inner silicon pixel detectors and two outer silicon strip detectors. The main roles of the VTX are precision measurements of the decay position of heavy-flavor decays and the precision reconstruction of jet axis with large acceptance[1)] of VTX.

After the installation of VTX in the PHENIX detector and the commissioning of VTX, physics data were successfully taken with the VTX. This report presents the results of the commissioning and discusses the performance of the pixel detectors that we had developed and constructed.

In the commissioning stage, the adjustment of the trigger timing and noise threshold level for the pixel detectors was performed.

The PHENIX detector front end modules (FEMs) need to function with the same clock signal as the RHIC accelerator. The granule timing module (GTM) fans out a copy of the clock to all the FEMs. On the other hand, the FEMs send the collision trigger to a digital circuit on the readout chip of the pixel ladder. In order to take a hit data, the timing for storing the data into a four-event FIFO needs to be adjusted with the trigger timing. This timing was adjusted by changing a parameter of the delay units on the readout chip.

The relation between a hit event rate and trigger latency is shown in Fig. 1. The hit event rate is defined as the ratio between the number of hit events for one readout chips and that for all readout chip. The timing adjustment needs to be completed within one beam clock cycle. The trigger latency was set to 9.6 beam clock.

The threshold voltage for each readout chip was adjusted to be above the noise level. Figure 2 shows a typical plot of the hit event rate vs. threshold DAC values. The average adjusted threshold was 180, which corresponds to 3,700 electrons. This was considerably lower than the 14,000 electrons of the minimum ionizing particle (MIP). After the adjustment, the noise rate reduced to 10^{-6}.

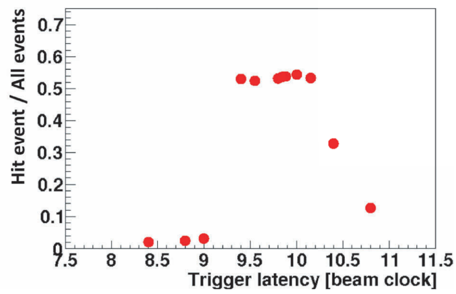

Fig. 1. Plot of hit event rate vs. trigger latency.

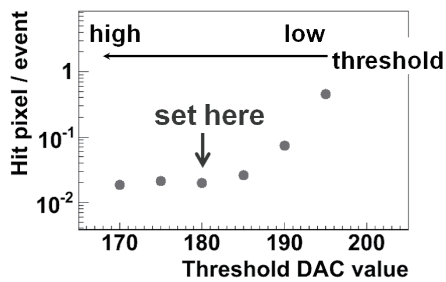

Fig. 2. Plot of hit event rate vs. threshold DAC value.

The 200 GeV/c Au+Au collision run was started in early May and ended in middle of June. Three billion events of the physics data were successfully taken with VTX during this period.

In summary, the VTX was successfully commissioned for the 200 GeV/c Au+Au run. The trigger latency was adjusted to be within one beam clock cycle. The average threshold level was one quarter of the MIP level and the noise rate was 10^{-6}. In all, three billion events were recorded with VTX in the 200 GeV/c Au+Au run.

*1 RIKEN BNL Research Center, USA
*2 Department of Physics, Kyoto Univ., Japan
*3 Center for Nuclear Study, Univ. of Tokyo, Japan
*4 LLR, Ecole Polytechnique, CNRS-IN2P3, France
*5 Brookhaven National Laboratory, USA
*6 Stony Brook University, USA
*7 JAEA, Advanced Science Research Center, Japan
*8 Los Alamos National Laboratory, USA
*9 University of Massachusetts, USA

References
1) Y. Akiba et al.: In this report

No-go theorem for critical phenomena in large-N_c QCD

Y. Hidaka and N. Yamamoto*2

The phase structure of quantum chromodynamics (QCD) at finite temperature T and finite baryon chemical potential μ_B is not well understood despite its phenomenological importance. Although it has been established by lattice QCD simulations that the thermal chiral transition at $\mu_B = 0$ is a crossover in real QCD, the fate of the chiral transition at nonzero μ_B has not been fully understood. In particular, not only the location, but even the existence of the QCD critical point(s) has not yet been confirmed.

In this work, we derive exact results on the chiral phase transition in large-N_c QCD[1]. Critical phenomena and associated soft modes are forbidden in flavor-symmetric QCD at finite μ_B for a nonzero quark mass m_q as long as the coordinate (T, μ_B) is outside the pion condensed phase in the corresponding QCD phase diagram at finite isospin chemical potential $\mu_I = 2\mu_B/N_c$.

We first recall the rigorous QCD inequalities[2]. We work with the Euclidean and flavor-symmetric QCD with N_f flavors and consider the Dirac operator at $\mu_B = 0$, which is given by $\mathcal{D} = D + m_q$, with $D = \gamma_\mu(\partial_\mu + igA_\mu)$. The operator D is anti-Hermitician and preserves chiral symmetry, i.e., $D^\dagger = -D$ and $\gamma_5 D \gamma_5 = -D$. From these properties, we have the γ_5-Hermiticity $\gamma_5 \mathcal{D} \gamma_5 = \mathcal{D}^\dagger$ and the positivity $\det \mathcal{D} \geq 0$.

Let us take a generic flavor nonsinglet fermion bilinear $M_\Gamma = \bar\psi \Gamma \psi$ and consider a set of correlation functions $C_\Gamma(x,y) \equiv \langle M_\Gamma(x) M_\Gamma^\dagger(y)\rangle_{\psi,A} = -\langle \mathrm{tr}[S_A(x,y)\Gamma S_A(y,x)\bar\Gamma]\rangle_A$, with $S_A(x,y) \equiv \langle x|\mathcal{D}^{-1}|y\rangle$ is a propagator from y to x in a background gauge field A; the symbols $\langle\ \cdot\ \rangle_{\psi,A}$ and $\langle\ \cdot\ \rangle_A$ denote the full average and the average over the gauge field, respectively, and $\bar\Gamma \equiv \gamma_0 \Gamma^\dagger \gamma_0$. From the γ_5-Hermiticity and the positivity of the measure, we have $C_\Gamma \leq \langle \mathrm{tr}[S_A(x,y) S_A^\dagger(x,y)]\rangle_A$. The inequality is saturated when $\Gamma = i\gamma_5 \tau_a$, with traceless flavor generators τ_a.

The asymptotic behavior of C_Γ at large distance $|x-y|$ can be written as $C_\Gamma \sim e^{-m_\Gamma |x-y|}$, with m_Γ being the mass of the lowest meson state in channel Γ. Then, the inequalities among correlators lead to the inequalities among meson masses, $m_\Gamma \geq m_\pi$, where m_π is the mass of the pseudoscalar pion. Note that the derivation of the QCD inequalities involves the assumption that j_Γ is not a flavor singlet. This condition is necessary; otherwise the flavor disconnected diagrams ($\sim \langle \mathrm{tr}[\Gamma S_A(x,x)]\,\mathrm{tr}[\bar\Gamma S_A(y,y)]\rangle_A$) also contribute and the above argument breaks down. The flavor disconnected diagrams are subleading compared with the connected diagrams in the $1/N_c$ expansion. Hence, in the leading order of the $1/N_c$ expansion, the QCD inequalities are also applicable to the flavor singlet channel. In particular, it follows that $m_\sigma \geq m_\pi$. Here m_σ is the mass of the flavor singlet scalar σ, which has the quantum number of the chiral condensate $\langle\bar\psi\psi\rangle$.

Let us consider the thermal chiral phase transition in large-N_c QCD at $\mu_B = 0$ and $m_q > 0$. In this case, a pion becomes massive because of the explicit breaking of chiral symmetry, that is, $m_\pi > 0$. If there exists a second-order chiral transition at some critical temperature $T = T_c$ at $\mu_B = 0$, the screening mass in the σ-meson channel vanishes, that is, $m_\sigma = 0$. However, the inequality, which is valid irrespective of T, leads to the finite bound $\sim N_c^0$ for m_σ, $m_\sigma \geq m_\pi > 0$. This constraint clearly contradicts the fact that $m_\sigma = 0$ at $T = T_c$. Therefore, we arrive at the conclusion that the second-order chiral transition and associated soft modes are forbidden in large-N_c QCD at $\mu_B = 0$ for any $m_q > 0$. This is our first no-go theorem. From this theorem, we infer that large-N_c thermal chiral transition at $\mu_B = 0$ for $m_q > 0$ is either of first order or a crossover.

This inequality can be generalized to the case of finite μ_I, although it cannot be applied to the case of finite μ_B owing to the lack of positivity of the fermion determinant. The inequality for finite μ_I is $m_\sigma \geq m_{\pi_\pm}$, which implies that the second-order chiral transition is not allowed at finite μ_I where $m_{\pi_\pm} > 0$.

It is known that a class of observables in large-N_c QCD at finite μ_B, including the chiral condensate, exactly coincide with those of QCD at finite μ_I outside the pion condensed phase (the large-N_c orbifold equivalence[3,4]). Using this equivalence, we conclude that the chiral phase transition is forbidden at finite μ_B for any nonzero quark mass outside the pion condensed phase in the corresponding phase diagram of QCD at finite μ_I. This is our second no-go theorem.

References

1) Y. Hidaka and N. Yamamoto, Phys. Rev. Lett. **108**, 121601 (2012).
2) D. Weingarten, Phys. Rev. Lett. **51**, 1830 (1983); E. Witten, Phys. Rev. Lett. **51**, 2351 (1983); S. Nussinov, Phys. Rev. Lett. **52**, 966 (1984); D. Espriu, M. Gross, and J. F. Wheater, Phys. Lett. **B146**, 67 (1984).
3) M. Bershadsky and A. Johansen, Nucl. Phys. **B536**, 141 (1998); M. Schmaltz, Phys. Rev. D **59**, 105018 (1999); M. J. Strassler, arXiv:hep-th/0104032; P. Kovtun, M. Ünsal, and L. G. Yaffe, JHEP **0312**, 034 (2003); P. Kovtun, M. Unsal, and L. G. Yaffe, JHEP **0507**, 008 (2005).
4) A. Cherman, M. Hanada, and D. Robles-Llana, Phys. Rev. Lett. **106**, 091603 (2011); A. Cherman and B. C. Tiburzi, JHEP **1106**, 034 (2011); M. Hanada and N. Yamamoto, JHEP **1202**, 138 (2012).

*2 Institute for Nuclear Theory, University of Washington

Nucleus from string theory[†]

K. Hashimoto[*1] and T. Morita[*2]

[Holography, AdS/CFT correspondence, Nuclear physics]

In generic holographic QCD, we find that baryons are bound to form a nucleus, and that its radius obeys the empirically-known mass number (A) dependence $r \propto A^{1/3}$ for large A. Our result is robust, since we use only a generic property of D-brane actions in string theory. We also show that nucleons are bound completely in a finite volume. Furthermore, employing a concrete holographic model (derived by Hashimoto, Iizuka, and Yi, describing a multi-baryon system in the Sakai-Sugimoto model), the nuclear radius is evaluated as $\mathcal{O}(1) \times A^{1/3}$ [fm], which is consistent with experiments.

To describe atomic nuclei directly by strongly coupled quark dynamics, QCD, is a long-standing problem in nuclear physics and particle physics. It was only recent that lattice QCD simulations reproduce qualitatively the nuclear forces. Recent progress in solving strongly coupled gauge theories with a new mathematical tool of superstring theory, the AdS/CFT correspondence[1)], has been proven to be truly powerful in application to QCD (called holographic QCD).

In this letter, we show by quite a generic argument in superstring theory and the AdS/CFT correspondence that non-supersymmetric QCD-like theories in the large N_c limit host nuclei, multi-baryon bound states. Furthermore, we can show also that the resultant nuclei have the important nuclear property in the real world: Finiteness of the nuclear size, and its mass-number dependence. That is, the radius of the holographically realized nuclei is shown to be proportional to $A^{1/3}$ where A is the mass number (the baryon number) of the nucleus.

In deriving these, we do not rely on any specific model of holographic QCD. What we use is only the following two known facts: (i) Baryons are D-branes in any gravity dual of QCD-like gauge theories, (ii) D-brane effective actions are a dimensionally reduced Yang-Mills (YM) theory. From these two, the formation of the nuclei and the mass-number dependence of the nuclear size follow. Therefore our finding is quite robust and universal for any holographic description of non-supersymmetric QCD-like gauge theories, at the large N_c and at the strong coupling.

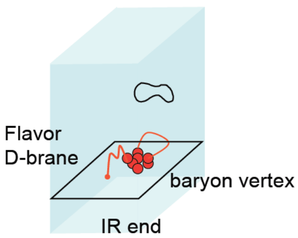

Fig. 1. A schematic picture for the gravity dual of QCD-like confining gauge theories with A baryons.

Fig. 2. The density distribution of the nucleus. Darker color means smaller density. Ignoring the surface defect, we find a homogeneous density distribution.

Our derivation is divided into two steps.

1. The system with a large number of baryons in generic holographic QCD is described effectively by a simple bosonic matrix quantum mechanics. It is a pure YM action dimensionally reduced to 1 dimension,
$$S = c \int dt \, \mathrm{tr}_A \left[\frac{1}{2}(D_t X^I)^2 + \frac{g^2}{4}[X^I, X^J]^2 \right]. \quad (1)$$
where $I = 1, \cdots, D$. The eigenvalues of the $A \times A$ matrix X^i ($i = 1,2,3$) are location of the A baryons in our space, and $X^{\hat{i}}$ ($\hat{i} = 4, \cdots, D$) is for holographic directions.
2. The system allows a non-perturbative vacuum at which the eigenvalues of X^i form a ball-like distribution, which is nothing but a nucleus. The size shows the mass-number dependence $A^{1/3}$.

Together with the explicit matrix model[2)] where input parameters are only the ρ meson mass and the NNπ coupling, we obtain the nuclear radius $R \sim \mathcal{O}(1) \times A^{1/3}$ [fm], which is consistent with the standard experimental observation.

References
1) J. M. Maldacena, Adv. Theor. Math. Phys. **2**, 231 (1998) [Int. J. Theor. Phys. **38**, 1113 (1999)] [arXiv:hep-th/9711200].
2) K. Hashimoto, N. Iizuka, P. Yi, JHEP **1010**, 003 (2010). [arXiv:1003.4988 [hep-th]].

† Condensed from the article in Phys. Rev. **D84**, 046004 (2011)
*1 Mathematical Physics Laboratory, RIKEN Nishina Center
*2 Crete Center for Theoretical Physics, Department of Physics, University of Crete, Greece

Aoki phases in the lattice Gross-Neveu model with flavored mass terms

M. Creutz,[*1] T. Kimura,[*2,*3] and T. Misumi[*4]

Since the pioneering work,[1)] the rich phase structure in the lattice Wilson fermion has been extensively studied: there emerges a parity-broken phase (Aoki phase) at a finite lattice spacing. The full phase diagram reflects the masses possessed by each of the original doublers.

In this report we study the parity-broken phase structure for staggered fermions with the flavored mass terms.[2–4)] We use the two-dimensional lattice Gross-Neveu models as toy models of QCD.[5)] To study the parity broken phase structure we propose the generalized staggered Gross-Neveu model with the γ_5-type 4-point interaction, which is given by

$$\begin{aligned} S = & \frac{1}{2}\sum_{n,\mu}\eta_\mu\bar{\chi}_n(\chi_{n+\mu}-\chi_{n-\mu}) + \sum_n \bar{\chi}_n(M+M_f)\chi_n \\ & -\frac{g^2}{2N}\sum_{\mathcal{N}}\Big[(\sum_A \bar{\chi}_{2\mathcal{N}+A}\,\chi_{2\mathcal{N}+A})^2 \\ & \qquad +(\sum_A i(-1)^{A_1+A_2}\bar{\chi}_{2\mathcal{N}+A}\,\chi_{2\mathcal{N}+A})^2\Big], \quad (1) \end{aligned}$$

where we define two-dimensional coordinates as $n = 2\mathcal{N}+A$ with the sublattice $A=(A_1,A_2)$ $(A_{1,2}=0,1)$. χ_n is a one-component fermionic field. $(-1)^{A_1+A_2}$ corresponds to the natural definition of γ_5 for this fermion which is expressed as $\Gamma_{55}=\gamma_5\otimes\gamma_5$ in the spinor-taste explicit expression. $\eta_\mu=(-1)^{n_1+\cdots+n_{\mu-1}}$ corresponds to γ_μ. As the flavored mass term we choose the Adams-type one, which is given by $M_f = \Gamma_5\Gamma_{55} \sim \mathbf{1}\otimes\gamma_5+\mathcal{O}(a)$ with the following chirality matrix $\Gamma_5 = -i\eta_1\eta_2\sum_{\rm sym}C_1C_2$, $C_\mu=\frac{1}{2}(T_\mu+T_{-\mu})$ where T_μ is an operator causing the spatial translation. (The chirality matrix in general dimensions is defined as $\Gamma_5\equiv-(i)^{d/2}\eta_1\cdots\eta_d\sum_{\rm sym}C_1\cdots C_d$.) This mass term assigns the positive mass $(m=+1)$ to one taste and the negative mass $(m=-1)$ to the other taste depending on $\pm$ eigenvalues for $\Gamma_5\Gamma_{55}$ which we call the flavor-chirality. With bosonic auxiliary fields $\sigma_\mathcal{N}$, $\pi_\mathcal{N}$, and integrating the fermion field, the partition function and the effective action with these auxiliary fields are given by

$$S_{\rm eff} = \frac{1}{2g^2}\sum_{\mathcal{N}}(\sigma_\mathcal{N}^2+\pi_\mathcal{N}^2) - {\rm Tr}\,\log D, \quad (2)$$

with

$$\begin{aligned} D_{n,m} = & (\sigma_\mathcal{N}+i(-1)^{A_1+A_2}\pi_\mathcal{N})\delta_{n,m} \\ & +\frac{\eta_\mu}{2}(\delta_{n+\mu,m}-\delta_{n-\mu,m})+(M+M_f)_{n,m}. \quad (3) \end{aligned}$$

By solving the saddle point equation, $\delta S_{\rm eff}/\delta\sigma_\mathcal{N} = \delta S_{\rm eff}/\delta\pi_\mathcal{N}=0$, and imposing $\pi=0$, we obtain the phase boundary as shown in Fig. 1.

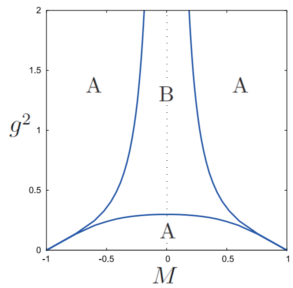

Fig. 1. Aoki phase structure for the staggered fermion with the flavored mass $\Gamma_5\Gamma_{55}$. "A" stands for a parity symmetric phase and B for Aoki phase.

To obtain the chiral limit of this model, we need to introduce two independent couplings g_σ^2 and g_π^2.[5)] We have to tune parameters to restore $O(2)$ rotation symmetry for (σ,π). In Fig. 2 we depict the phase boundary $M(g_\pi^2)$ naively derived from the above gap equations for $g_\sigma^2 = 0.4$. The fine-tuned point $(-0.286, 0.243)$ as a crosspoint is located near the self-crossing point. The true phase boundaries are composed of the three parts. The fine-tuned point is located slightly to the right and below the self-crossing point.

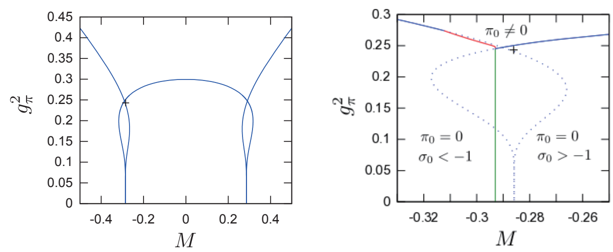

Fig. 2. The phase boundaries of the Aoki phase and the fine-tuned point shown as a cross. In the extended version, blue and red lines are 2nd and 1st order π_0 boundary, and green one is of 1st order σ_0 transition.

References
1) S. Aoki, Phys. Rev. **D30** (1984) 2653.
2) D. H. Adams, Phys. Rev. Lett. **104** (2010) 141602; Phys. Lett. **B699** (2011) 394.
3) C. Hoelbling, Phys.Lett. **B696** (2011) 422.
4) M. Creutz, T. Kimura, T. Misumi, JHEP **12** (2010) 041.
5) S. Aoki and K. Higashijima, Prog. Theor. Phys. **76** (1986) 521.

† Condensed from the article in Phys.Rev.**D83** (2011) 094506.
*1 Physics Department, Brookhaven National Laboratory
*2 Department of Basic Science, University of Tokyo
*3 Mathematical Physics Laboratory, RIKEN Nishina Center
*4 Yukawa Institute for Theoretical Physics, Kyoto University

Results for RIKEN superconducting electron cyclotron resonance ion source with 28 GHz microwave†

Y. Higurashi, J. Ohnishi, T. Nakagawa, H. Haba, M. Tamura,[*1] T. Aihara,[*1] M. Fujimaki, M. Komiyama, A. Uchiyama,[*1] and O. Kamigaito

In the last three decades, the beam intensity of highly charged heavy ions from electron cyclotron resonance (ECR) ion sources has increased dramatically. For example, the beam intensity of Ar^{8+} increased from few ten μA[1)] to 2 mA[2)]. One of the driving forces behind this the development is the semi-empirical formula proposed by R. Geller,[3)] wihch predicts that the performance is improved using higher magnetic field strength and frequencies. Based on this formula, a few advanced ECR ion sources (e.g. VENUS at LBL and SECRAL at Lanzhou) that have a microwave frequency higher than 18 GHz were constructed and gave excellent results in the last decade.[4,5)]

At RIKEN, we constructed a new superconducting ECR ion source (SC-ECR ion source)[6)] to increase the beam intensity of highly charged heavy ions for the Radio Isotope Beam Factory (RIBF) project. This ion source can produce a flexible mirror magnetic field, from classical B_{min} to the so-called "flat" B_{min}[7)]. In 2009, we obtained the first beam with 18 GHz and produced a highly charged U beam, which was ten times as high as that of the RIKEN 18 GHz ECR ion source. In the spring of 2011, we injected 28 GHz microwaves into the ion source and obtained the first beam. So far, we have tried to produce highly charged heavy ions and have performed several test experiments to investigate the effect of the key parameters of the ECR ion source on the beam intensity.

Figure 1 shows the beam intensity of $^{124}Xe^{25+}$ ions as a function of the injected RF power. The magnetic field strength on the RF injection side (B_{inj}), the minimum magnetic field of the mirror magnetic field (B_{min}), the magnetic field strength on the beam extraction side (B_{ext}), and the radial magnetic field strength on the inner wall of the plasma chamber (B_r) were 3.15, 0.62, 1.83 and 1.86 T, respectively. The typical gas pressure was about 3.3×10^{-5} Pa. The biased disc position and the voltage were tuned to maximize the beam intensity. The beam intensity increased linearly with the RF power up to 1.3 kW.

In order to investigate the effect of frequency on the beam intensity, the B_{inj}, B_{min}, B_{ext}, and B_r for 18 GHz were maintained at 2.1, 0.4, 1.17 and 1.2 T, respectively. These values are 18/28 times the values for 28 GHz microwave operations as described previously. This implies that the mirror ratio and B_{min}/B_{ecr} for 18 GHz are the same as those for 28 GHz. Note that we used the same RF power (500 W) and extraction voltage (20 kV) in both cases. Figure 2 shows the charge state distribution of the Xe ion beam with 28 and 18 GHz. the gas pressure, biased disc position and disc voltage were tuned to maximize the beam intensity of Xe^{25+} ions. The beam intensity of Xe^{25+} for 28 GHz microwaves is almost three times that for 18 GHz microwaves.

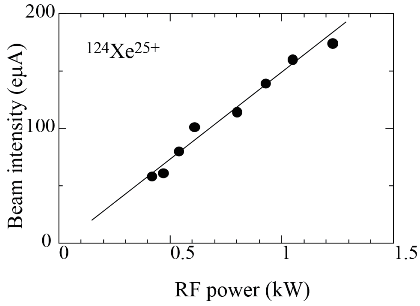

Fig. 1. Beam intensity of Xe^{25+} as a function of RF power.

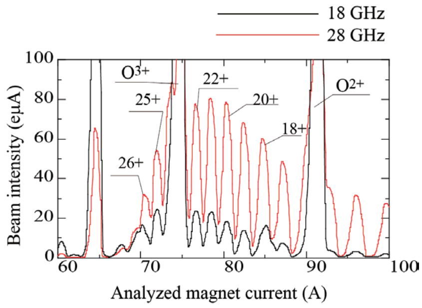

Fig. 2. Charge state distribution of the Xe ion beam with 28 GHz (red line) and 18 GHz (black line) microwaves. The ion source was tuned to produce Xe^{25+} for both cases.

References
1) N. Chan Tung, S. Dousson, R. Geller, B. Jacquot, M. Lieuvin, Nucl. Instr. & Methods **174** (1980) 151.
2) Y. Higurashi, et al, Nucl. Instrum. Methods A **510** (2003) 206.
3) R. Geller, et al, in: Proc. 8th Int. Workshop on ECRIS, East Lansing, 1987, 1, unpublished.
4) H. W. Zhao,L. et al, Rev. Sci. Instrum. **81** (2010) 02A202.
5) C. Lyneis, et al, Rev. Sci. Instrum. **81** (2010) 02A201
6) T. Nakagawa et al., Rev. Sci. Instrum. **81** (2010) 02A320.
7) G. D. Alton, and D. N. Smithe, Rev. Sci. Instrum. **65** (1994) 775.

† Condensed from a contributed paper published as part of the Proceedings of the 14th International Conference on Ion Source, Giardini-Naxos, Sicily, Italy, September 2011

*1 SHI Accelerator Service, Ltd.

Development of carbon nanotube and sputter-deposition carbon foil for stripping uranium beams

H. Hasebe, H. Kuboki, H. Okuno, H. Imao, I. Yamane, N. Fukunishi, M. Kase, and O. Kamigaito

We have developed carbon foils (C-foils) as a charge stripper for stripping the uranium (U) beam in the acceleration chain at the RIKEN RI Beam Factory. To increase the lifetime of the C-foil, the fabrication mechanism of C-foils has been enhanced many times[1–3] and a rotating-cylinder stripper device to enlarge the total irradiated area has been developed as well[4,5].

Many types of C-foils have been tested including commercial ones and the samples fabricated in other laboratories or companies. Among them, the carbon nanotube (CNT) foil was tested with U beams in Nov. 2009. We measured the charge distribution of the C-foil and found that the most probable charge state of a 250 μg/cm^2 thick CNT foil was 66+, which was lower than that of the C-foil fabricated by a sputter-deposition method (SDC-foil)[3]. However, the most probable charge state shifted to 69+ after the beam irradiation. This value was almost the same as that for the SDC-foil. However, CNT foils were found to still not be applicable as a stripper because the efficiency of the stripped beam using CNT foils was worse than that for SDC-foils already used.

Fabrication of large C-foils for the rotating-cylinder stripper device was also challenging. The idea of depositing carbon on CNT was proposed. A 250 μg/cm^2 thick sheet of CNT was attached to the holder. Next, a 50 μg/cm^2 thick carbon layer was deposited on both sides of the holder using the magnetron sputtering system. Thus, the overall thickness of the foil (CNT-SDC-foil) was 350 μg/cm^2 (50(SDC)+250(CNT)+50(SDC) μg/cm^2). This new foil possessed flexibility and mechanical strength, attributed to the properties of CNT, while a standard SDC-foil is very hard and fragile. In addition, the beam efficiency for the CNT-SDC-foil was expected to be better than that for the pure CNT-foil because SDC layers enhanced the efficiency.

The lifetime of the new CNT-SDC-foil on the rotating-cylinder stripper device was tested with a U beam in June 2011. The revolution rate was 0.05 rpm. The beam intensity was 1 electric μA. No damage such as a crevice or pinhole was observed even after 40 hours of irradiation.

The CNT-SDC-foil was used for the U beam time from October to December 2011. The beam intensity was maximally 10 electric μA. The spot size had an elliptical shape with 10 mm (horizontal) and 5 mm (vertical). In June, the shifting of charge distribution to a higher state occurred in 24 hours. The time taken was shorter for this instance because of the increased beam intensities. 7 foils were used in the entire beam time, and the lifetimes of 6 foils were estimated. Figure 1 shows the appearances of 1 new CNT-SDC-foil and 7 used foils. The total charge irradiated on each foil is also given in the figure. The total charge irradiated on the 1st one was 1.38 C, this foil was replaced with a new one before its lifetime. The foil tested in June was used again as the 2nd one. The 3rd, 4th, 6th, and 7th foils cracked during irradiation. However, in the usage of these foils, the beam was temporarily stopped at the cracking positions. The lifetime of the 7th foil could not be estimated because it was mostly used for tuning beams with low intensity.

In conclusion, the lifetimes of these new foils were drastically extended to be 2-5 C (practically 4-5 days), while those of fixed SDC-foils were 20-40 mC. These new CNT-SDC-foils successfully made it possible to provide stable U beams with higher intensity.

References
1) H. Hasebe et al., Nucl. Instr. Meth. A**590** (2008) 13.
2) H. Hasebe et al., Nucl. Instr. Meth. A**613** (2010) 453.
3) H. Hasebe et al., Nucl. Instr. Meth. A**655** (2011) 57.
4) H. Ryuto et al., Nucl. Instr. Meth. A**569** (2006) 697.
5) H. Hasebe et al., RIKEN Accel. Prog. Rep. **44**, p. 114 (2011).

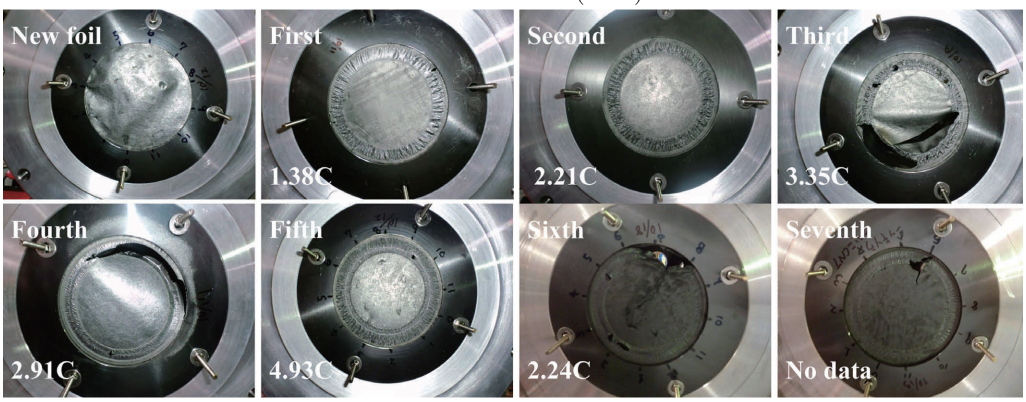

Fig. 1. Total irradiated charges for each CNT-SDC-foil used in U beam time is shown in the figure.

Achieved Luminosity at SCRIT Electron Scattering Facility

S. Wang,[*1] T. Adachi,[*1] M. Hara,[*2] T. Hori,[*2] S. Ichikawa,[*2] R. Kitazawa,[*1] K. Koizumi,[*3] K. Kurita,[*3] Y. Miyashita,[*2] R. Ogawara,[*3] T. Ohnishi,[*2] T. Suda,[*1] H. Takehara,[*4] T. Tamae,[*1] S. Tamaki,[*3] M. Togasaki,[*3] and M. Wakasugi[*2]

[Luminosity, unstable nuclei, electron scattering]

It had already been confirmed that electron scattering off unstable nuclei can be realized by SCRIT method[1)] and luminosity of nearly 10^{26}cm^{-2}s^{-1} was achievable with the trapped ion of 10^6 at electron beam current 80 mA at KSR[2)]. Due to low beam current and short lifetime of KSR (maximum $\sim$ 100 mA with lifetime 100 s), SCRIT Electron Scattering Facility,whose performance is much inproved compared to KSR, had already been constructed for the further R&D study of SCRIT at Nishina Center[3)].

In the current experiments, the energy of electron beam is set to 150 MeV and the stored beam current is around 250 mA with lifetime about 200 minutes. Ions of stable ^{133}Cs are still employed as target. To study the achievable luminosity at the new facility, elasctic scattering electrons from trapped ions are measured by a detection system, which consists of a drift chamber, plastic scintillation detectors and two calorimeters, as shown in Fig.1. The trajectories and energy of scattered electrons are determined by the drift chamber and calorimeters. A pair of plastic scintillation detectors is placed in front of each calorimeter to define the solid angle. The detection system coveres the scattering angle from 25° to 50°.

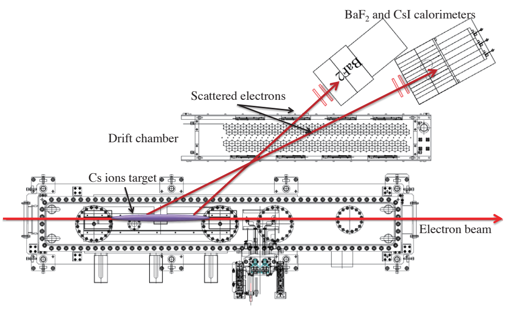

Fig. 1. Detection system for scattered electrons

Figure 2(a) and (b) show the vertex distribution and energy spectra of scattered electrons with and without trapped Cs ions. Vertices of those events, whose energy loss in the calorimeter is over 100 MeV, are shown in Fig.2(a) and the trapping region is from -25 cm to 25 cm, which is consistent with the design value. The sharp peaks around -35 cm, -15 cm and 40 cm are attributed to beam halo hitting the thick terminal electrodes. Figure 2(b) shows the energy spectra of the events from trapping region. The scattered electrons from the trapped Cs ions are clearly observed.

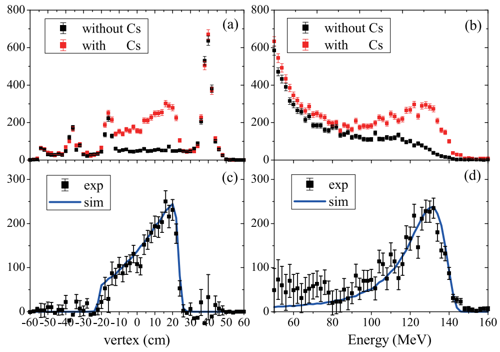

Fig. 2. Vertex distributin and energy spectra. Red(black) points in (a) and (b) show the events with(without) Cs ion trapping. Black points are experimental data and the blue line is simulated result in (c) and (d).

The black points in Fig.2(c) and (d) show the subtracted spectra from Fig.2(a) and (b), and the blue lines show the result of a Geant4 simulation, which assumes that the energy of scattered electrons is 150 MeV, the density distribution of trapped Cs ions is uniformed and elactic cross setion of ^{133}Cs calculated by DREPHA[4)] was also taken into account. The experimental data are well reproduced by the simulation, which demonstrates that the trapped Cs ions are uniformly distributed and the events above 100 MeV in Fig.2(d) are consistent with elastic scattering. Considering the solid angle of two calorimeters and the elastic scattering cross section, the achieved luminsoity is estimated to be 9.0×10^{26} cm^{-2}s^{-1} with electron beam current 200 mA.

References
1) M. Wakasugi et al.: Phys. Rev. Lett. **100**, 164801 (2008).
2) T. Suda et al.: Phys. Rev. Lett. **102**, 102501 (2009).
3) M. Wakasugi et al.: RIKEN Accel. Prog. Rep. **43**, (2010) P.1.
4) B. Dreher, DREPHA: a phase-shift calculation code for elastic electron scattering.

*1 Research Center for Electron Photo Science, Tohoku University, Japan
*2 RIKEN Nishina Center, Japan
*3 Department of Physics, Rikkyo University, Japan
*4 Department of Electrical Engineering, Nagaoka University, Japan

RIKEN Accel. Prog. Rep. 45 (2012)

Diffusive behavior of garnet-type compounds

J. Sugiyama,[*1] H. Nozaki,[*1] M. Harada,[*1] S. Ohta,[*1] K. Shimomura,[*2] K. Ohishi, and D. Tomono

[Lithium diffusion, solid electrolyte, battery]

In order to fabricate an all solid-state lithium-ion battery for improving safety and volumetric energy density, a solid electrolyte is unambiguously one of the key materials, because the present electrolytes are in a liquid state. Very recently, a novel garnet-type compound, $Li_{6.75}La_3Zr_{1.75}Nb_{0.25}O_{12}$, was found to exhibit the highest Li-ion conductivity ($\sigma_{Li} \sim 10^{-3}$ S/cm) at ambient T[1,2] among several oxide electrolytes. Note that this σ_{Li} is lower only by one order of magnitude than σ_{Li} for the present liquid electrolyte, and is almost comparable to σ_{Li} for a gel electrolyte[3]. Here, the chemical formula of the novel garnet-type compound is represented by $Li_xLa_3Zr_{x-5}Nb_{7-x}O_{12}$, and σ_{Li} is known to depend on x; i.e. the $\sigma_{Li}(x)$ curve exhibits a maximum at $x = 6.75$[1,2], for reasons currently unknown.

On the contrary, we found that μ^+SR provides information on a self-diffusion coefficient of Li^+ ions (D_{Li}) in oxides, through the change in the fluctuating nuclear magnetic field[4-6]. Therefore, in order to investigate the change in D_{Li} with x in the garnet-type compounds, we have measured ZF- and LF-μ^+SR spectra for the powder samples of $Li_5La_3Nb_2O_{12}$, $Li_6La_3Zr_1Nb_1O_{12}$, $Li_{6.75}La_3Zr_{1.75}Nb_{0.25}O_{12}$, and $Li_7La_3Zr_2O_{12}$ in the T range between 50 and 480 K.

The ZF- and LF-spectra were well fitted by a combination of a dynamic Kubo-Toyabe function from the garnet-type phase and a time-independent background signal from the titanium cell. Furthermore, the initial asymmetry (A_0) is almost a full value (~ 0.24) even at 100 K, indicating that all the implanted μ^+s locate at the vicinity of O^{2-} ions so as to make a stable μ^+-O bond in the lattice.

Figure 1 shows the T dependences of the field distribution width (Δ) and the field fluctuation rate (ν) for the four samples. As T increases from 100 K, Δ decreases monotonically with T until around 275 K, then Δ decreases rapidly with T above 275 K. This suggests that something, most likely the Li^+ ions start to diffuse above around 275 K. Indeed, ν increases with T with increasing slope ($d\nu/dT$) until 350 K, around which ν reaches a maximum. Above 350 K, it is very difficult to estimate ν precisely, because $\nu >> \Delta$. In other words, although ν is expected to increase with T in the manner given by the formula; $\nu = \nu_0 \exp(-E_a/k_BT)$ even above 350 K, such behavior is hidden due to a motional narrowing of the spectrum. Here, it should be noted that the $x = 6.75$ sample exhibits the highest σ_{Li} at ambient T in the four samples, while ν for the $x = 6.75$ sample is lower than that for the $x = 6$ sample in the whole T range measured. Since all the samples are insulating at 300 K, D_{Li} should be proportional to σ_{Li}. In order to estimate D_{Li} from ν, we need information on the jump distance, the number of the sites to jump, and the occupancy of such sites. We are, therefore, attempting to measure neutron diffraction data on these samples.

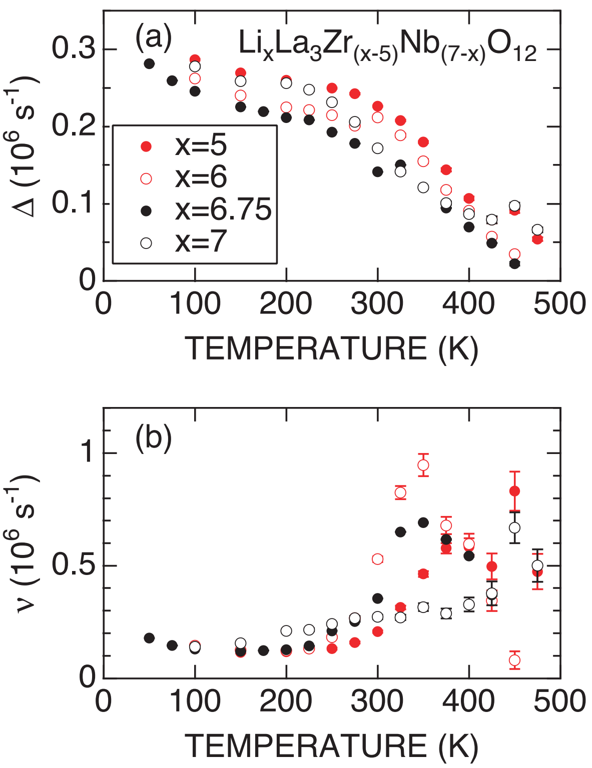

Fig. 1. T dependences of Δ and ν for $Li_xLa_3Zr_{x-5}Nb_{7-x}O_{12}$ with $x = 5$, 6, 6.75, and 7.

References
1) S. Ohta *et al.*, J. Power Sources **196**, 3342 (2011).
2) S. Ohta *et al.*, J. Power Sources **202**, 332 (2012).
3) N. Kamaya *et al.*, Nature Mater. **10**, 682 (2011).
4) J. Sugiyama *et al.*, Phys. Rev. Lett. **103**, 147601 (2009).
5) J. Sugiyama *et al.*, Phys. Rev. B **82**, 224412 (2010).
6) J. Sugiyama *et al.*, Phys. Rev. B **84**, 054430 (2011).

*1 Toyota Central Research and Development Labs., Inc.
*2 KEK

Screening of heteromorphic self-incompatibility genes in buckwheat by using heavy-ion beam irradiation†

Y. Yasui,*1 M. Mori,*2 J. Aii,*3 T. Abe, D. Matsumoto,*1 S. Sato,*3 Y. Hayashi, O. Ohnishi,*1 and T. Ota*4

The different forms of flowers in a species have attracted the attention of many evolutionary biologists, including Charles Darwin. In *Fagopyrum esculentum* (common buckwheat), the occurrence of dimorphic flowers, namely short-styled and long-styled flowers, is associated with a type of self-incompatibility (SI) called heteromorphic SI. The floral morphology and intra-morph incompatibility are both determined by a single genetic locus named the *S*-locus. Plants with short-styled flowers are heterozygous (*S/s*) and plants with long-styled flowers are homozygous recessive (*s/s*) at the *S*-locus. Despite recent progress in our understanding of the molecular basis of flower development and plant SI systems, the molecular mechanisms underlying heteromorphic SI remain unresolved.

By examining differentially expressed genes in the styles of the two floral morphs, we successfully identified four short-style-specific genes (*SSG1 - SSG4*) that are expressed only in short-styled plants. To investigate the function of the four *SSG*s and the physical linkage between *S*-locus and the four *SSG*s, we conducted mutagenesis procedure by using heavy-ion beam irradiarion. Buckwheat seeds were irradiated with accelerated ^{20}Ne ions (135 MeV/nucleon) in a dose range of 75 Gy to 100 Gy. The linear energy transfer (LET) of ^{20}Ne^{10+} was 63.4 keV/μm. Flower morphology was observed for 1,400 M_1 plants grown in a closed experimental room. During the mutagenesis screening of buckwheat, a single chimeric plant possessing a branch that sets long-styled flowers on a short-styled plant was obtained. In spite of our great interest in its SI phenotype, we were unable to determine what kind of SI response the long-styled flowers of this plant showed, because mating by using pollen grains from these flowers was unsuccessful on the pistils of both long- and short-styled plants, and mating by using pollen grains from both long- and short-styled plants was unsuccessful on the pistils of these flowers. Nevertheless, PCR analysis of the genomic DNA of this chimeric plant yielded intriguing results. PCR successfully amplified *SSG2* and *SSG3* from the total DNA of the short-styled part of the plant and not the long-styled part of the plant. On the other hand, PCR successfully amplified *SSG1* and *SSG4* from DNA isolated

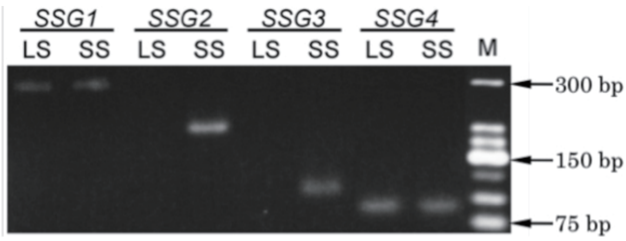

Fig. 1. PCR amplification of gene fragments for *SSG1 - SSG4* by using genomic DNA isolated from the chimeric plant as template. LS, template DNA extracted from the long-styled branch; SS, template DNA extracted from the short-styled branch; M, molecular marker.

from both short- and long-styled parts of the plant (Fig. 1). Considering that *SSG2* and *SSG3* are tightly linked and separated by about 100 kb[1)], this result suggests that somatic deletion of the region that includes *SSG2* and *SSG3* occurred in the chimeric plant and raises the possibility that these genes are located at the *S*-locus, which determines the floral phenotype.

BLAST search identified no homologs with *SSG2*. Furthermore, examination of the *SSG2* alleles in 20 short-styled plants identified one that contained a large deletion. The plant that harbored the allele did not have any apparent defects and this cast doubt on the significance of *SSG2* in heteromorphic SI. On the other hand, homology between *SSG3* and *Arabidopsis thaliana ELF3* was detected. Phylogenetic analysis based on the deduced amino acid sequences showed that *SSG3* is not an ortholog but a paralog of *ELF3*. We named this new gene *S-LOCUS EARLY FLOWERING 3* (*S-ELF3*).

In this study, we screened and identified one of the most promising candidate genes for buckwheat heteromorphic SI by using multiple molecular approaches. In near future, mutagenesis with heavy-ion beams will certainly play a fundamental role in the identification of the function of *S-ELF 3* in the buckwheat heteromorphic SI system for which no method has been established for genetically transforming the species.

References
1) Y. Yasui et al. : PLoS ONE **7**, e31264 (2012).

† Condensed from the article in PLoS ONE **7**, e31264 (2012)
*1 Graduate School of Agriculture, Kyoto University
*2 Research Institute for Bioresources and Biotechnology, Ishikawa Prefectural University
*3 Faculty of Applied Life Science, Niigata University of Pharmacy and Applied Life Science
*4 Department of Evolutionary Studies of Biosystems, The Graduate University for Advanced Studies

Ion beam technology used to create sake yeasts

M. Yokobori,*[1] K. Minamisawa,*[1] T. Takahashi,*[1] K. Masuda,*[1] Y. Hayashi, and T. Abe

The Northern Laboratory, at the Saitama Industrial Technology Center, carries out research involving the production and utilization of microbes for (1) sake making and producing fermented food products, (2) the characterization and utilization of microbes for sake making and fermented food products, (3) the characterization of microbes used in fermentation, and (4) research and development for their safe use. It is also responsible for maintenance and distribution of original sake yeasts to sake breweries in Saitama prefecture. There is a demand for new yeasts from these breweries. Therefore, we attempted making new sake yeasts by using mutation breeding, which produces yeasts with the characteristic ability to produce fragrance or acid, with eight different Saitama yeasts.

Heavy-ion beam irradiation and chemical treatment were used for artificial mutation. A Fe-ion beam (90MeV/u) was used to irradiate yeasts cultured with an agar medium at 400 Gy. A C-ion beam (135 MeV/u) was used to irradiate the yeast suspension culture at 400 Gy. Ethyl methane sulfonic acid was used for chemical mutagenesis. After mutation processing, the yeasts were cultured on a plate containing either cerulenin or cycloheximide for selection of resistant mutants. We acquired 260 cerulenin resistant strains (we expected a characteristic fragrance from these) and 305 cycloheximide resistant strains (we expected a characteristic acidity from these).

We inoculated each stock into koji extract with dry koji and cultured it at 15 ℃. We measured the weight, acidity, and flavor component. After the removal of the yeasts that were inferior in fermentability or produced a considerable amount of ethyl acetate, we selected yeasts that produced a significant amount of ethyl caproate (main component of the fragrance of ginjoshu), had very high or very low acidity, and had good fermentability. Finally, we selected 20 stocks that produced a high level of ethyl caproate, or had very high or very low acidity level. Furthermore, we narrowed them down to four stocks by small-scale sake making with 55 g of total rice (1 dan-jikomi with dry koji and pre-gelatinized rice). We then selected AFH10, FFC6, and F0C4 by small-scale sake making with 1 kg of total rice (3 or 2 dan-jikomi with dry koji and steamed rice). We offered these three stocks for a sake production test using 60 kg of total rice. Saitama E yeast was used as a control. The sake meters of mash in the three stocks were higher than in the control. F0C4 lagged in the production of alcohol in the latter part of mash fermentation. The acidities of mash were lower in the three stocks than in the control and were particularly low in AFH10 and F0C4. The aminoacidities of mash in the three stocks were higher than in the control, and they were particularly high in F0C4. The yeast density of mash was low in F0C4, and the extinction rate of mash was low in FFC6.

With the regard to produced refined sake, in F0C4, the level of ethyl caproate was high and acidity was low. The low alcohol content of this sake was its negative feature. Because it had high aminoacidity, there are concerns about the rapid deterioration of this sake.

AFH10 was smooth with lightness and had a flavor typical of sake. FFC6 was full and gorgeous, and its taste was light. F0C4 was superior in fragrance as well, although we felt that a little added flavor came from the process of brewing, probably because of high amino acidity.

As a result, we selected the FFC6 (the cerulenin resistant strain, irradiated with a Fe-ion beam in Saitama F yeast) for its clear characteristics and good fermentability, and we offered it for production on a practice scale at the breweries in Saitama. The tendency of delayed fermentation was observed at low temperature during the latter part of mash fermentation, and a longer duration was requied to finish fermentation. The rate of alcohol production was low and amino acidity was high, and yet, a gorgeous fragrance was obtained and the acidity was low. Three types of sake (Junmai-daiginjoshu, Junmai-ginjoshu, Gingo-namazake), brewed using FFC6, were produced at three breweries in Satama, and introduced in the market in November 2011 (Fig. 1). They are collectively known as 'Nishina Homare' (in honor of Nishina), named after Yoshio Nishina, the father of nuclear physics in Japan and one of RIKEN's most eminent scientists.

We decided to distribute the FFC6 stock as the new yeast named "Saitama G yeast" for Ginjoshu.

Fig. 1. Three types of Japanese sake called "Nishina Homare" produced using Saitama G yeast. Right: Gingo-namazake, Center: Junmai-daiginjoshu, Left: Junmai-ginjoshu

*1 Northern Laboratory, Saitama Industrial Technology Center

The Completion of RIBF Cyclopedia

—An exhibition hall was opened on the 1F of the RIBF bldg.

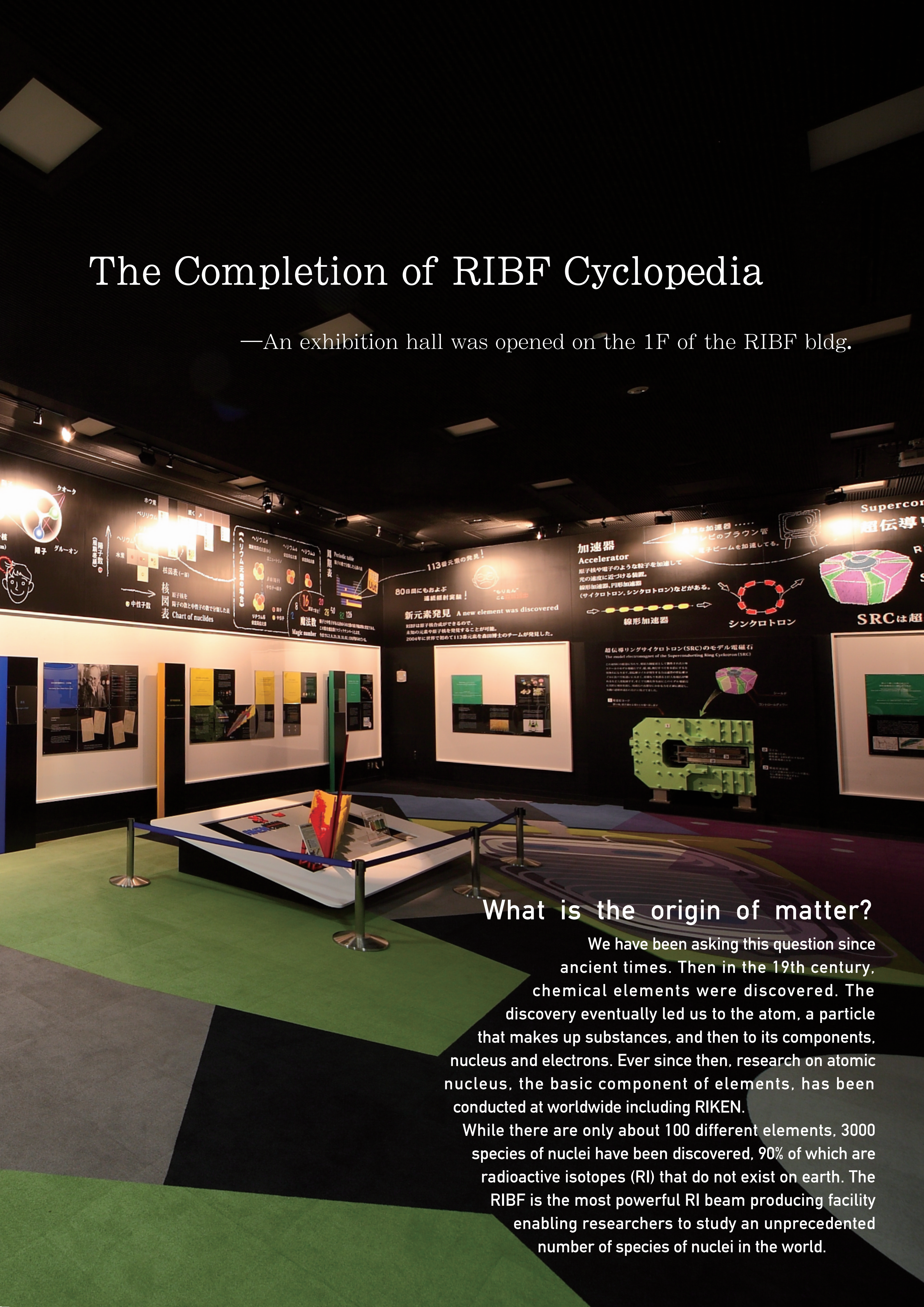

What is the origin of matter?

We have been asking this question since ancient times. Then in the 19th century, chemical elements were discovered. The discovery eventually led us to the atom, a particle that makes up substances, and then to its components, nucleus and electrons. Ever since then, research on atomic nucleus, the basic component of elements, has been conducted at worldwide including RIKEN.

While there are only about 100 different elements, 3000 species of nuclei have been discovered, 90% of which are radioactive isotopes (RI) that do not exist on earth. The RIBF is the most powerful RI beam producing facility enabling researchers to study an unprecedented number of species of nuclei in the world.

RIBF CYCLOPEDIA

PANEL EXHIBIT

1 Introduction

RI Beam Factory and Nishina Center for Accelerator-Based Science are introduced.
Other related topics also shown.

2 The Origin of RIBF

Dr. Nishina developed the first cyclotron ever to be constructed outside the U.S. where it was first created. His disciples continue to pioneer innovative research in the field of nuclear physics worldwide. The history behind the establishment of Nishina Center and RIBF is explained.

3 Basic Knowledge of Atomic Nuclei

Basic knowledge required to understand nuclear physics is explained, including size of atomic nuclei, chart of nuclide, and nuclear force.

4 Research

New nuclei and element have been discovered at RIBF. Previously unknown phenomena of nuclei can be investigated using RIBF. Industrial application of the beams produced at RIBF is also promoted.

5 RIBF Facilities

RIBF is an innovative accelerator facility that houses the world's most powerful Superconducting Ring Cyclotron (SRC) and other types of cyclotrons. The state-of-the-art facility is introduced.

Pilot Electromagnet for SRC

Before constructing SRC, pilot 1/6-scale magnets were used for measurements of magnetic force between them. This was helpful in designing the actual machine.

Model of RIBF

A full model of RIBF simulates the beam current with press of a button.

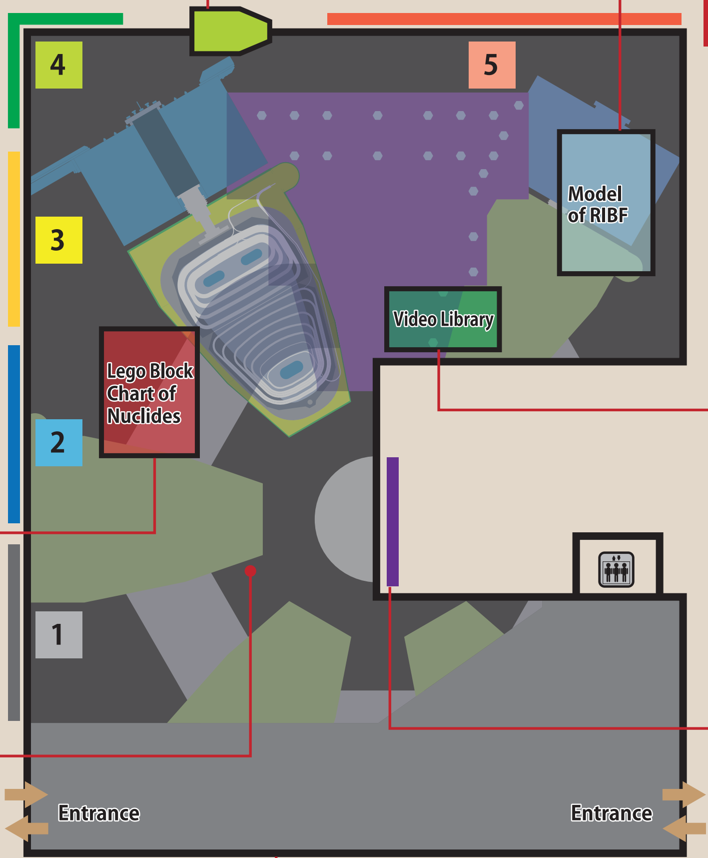

Lego Block Chart of Nuclides

Chart of Nuclides is a two-dimensional graph that shows all nuclei.
The three-dimensional Chart of Nuclides using Lego block allows a better visualization and understanding of the characteristics of atomic nucleus.

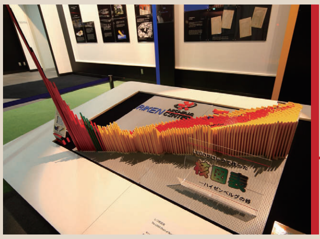

Video Library

Research being conducted at RIBF and its facilities are introduced in a 3D video. Other RIBF related images and topics are also shown.

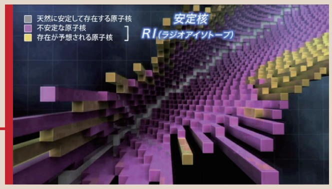

Full-Scale Drawing of Control Dewar

Helium control dewar at the center of SRC is like a gigantic thermos that stores liquid helium. The full-scale drawing is proportionate to the SRC floor design.

Full-Scale Floor Design of SRC

The image of RIBF's largest accelerator, SRC, is drawn on the floor. Photographs alone do not convey the actual size of SRC, but by standing on top of the full-scale size floor design of SRC, one can actually get a grasp of its grand size.

Dr. Yoshio Nishina and his No.2 Cyclotron

Nishina Center was named after Dr. Nishina, the father of modern physics in Japan, and one of the great predecessors who worked in RIKEN.
This is a dynamic, almost full-scale photograph of Dr. Nishina sitting atop his cyclotron.
(Photographed by Ken Domon)

*The exhibition may change depending on season and program

C O N T E N T S

2. Atomic and Solid State Physics (Muon)

3. Radiochemistry and Nuclear Chemistry

I. PREFACE

Preface

The Great East Japan Earthquake and the Fukushima Daiichi nuclear disaster wrought by the earthquake turned the greatest accomplishments of nuclear research for the advancement of humankind into a dangerous endeavor. Even in such a dire situation, however, many personnel at Nishina Center worked hard to readjust the accelerator, and despite serious power shortages, restored beam time almost beyond the achievable limit. There were staff members who went to Fukushima immediately following the Earthquake to conduct a radiation survey and provide other support as well as participate in soil investigation. This volume of the Accelerator Progress Report contains a special section to record what we have done in response to the 2011 Fukushima nuclear disaster.

In spite of the shorter beam time available in 2011, the present volume of RIKEN Accelerator Progress Report (APR) contains many more important works done at the Radioisotope Beam Factory (RIBF). These are glimpses of the tremendous power of this facility, which is gradually becoming apparent. Several significant papers based on RIBF activity have been specially selected by the editorial committee of APR to be featured in "Frontispiece" and "Highlights of the Year," together with papers from other activities in the Nishina Center, namely, hadron physics, theory, and applications. The amazing yield of deeply bound pionic states in ^{121}Sn observed by Nishi et al. showed the real versatility of RIBF reigning over hot topics in hadron physics. Because it is the world's only synergetic-use laboratory, Nishina Center's APR contains progress reports submitted by external users of RIBF and the RIKEN Muon Facility at the Rutherford Appleton Laboratory in the UK.

On April 1, 2011, T. Uesaka arrived at a chief scientist post of newly created Spin Isospin Laboratory in the RIBF division. Uesaka, Sakurai, and one more new chief scientist expected in 2013 will be the driving force of RIBF science for the next 10 years. In theoretical research, T. Hatsuda, another new chief scientist, started the Quantum Hadron Physics Laboratory. With his arrival, the Nishina Center now has a diverse and synergistic theoretical research.

The RIKEN BNL Research Center created the Computing Group headed by T. Izubuchi. This group is dedicated to large-scale physics computations such as lattice quantum chromodynamics (QCD). We expect Hatsuda and Izubuchi together to achieve breakthroughs using supercomputer *K* in Kobe. On July 1, a new research body, the Astro-Glaciology Research Unit, was inaugurated in the RIBF division. This unit, headed by Y. Mochizuki, analyzes Antarctic ice cores as footprints of supernova explosions and giant solar flares to correlate them with large climate changes and/or nucleosynthesis.

Last year is also remembered as a year of awards. We at Nishina Center are all very proud of Dr. Yasushige Yano, the former director of Nishina Center, for being awarded the prestigious Gersh Budker Prize. The Suwa Award given to H. Okuno, N. Fukunishi, J. Ohnishi, N. Sakamoto, K. Kuno, T. Kawaguchi, T. Semba, and T. Mitsumoto is a proof that the Japanese style of academic-industrial alliance created by Yoshio Nishina has come to fruition. The MEXT Commendation for Science and Technology given to T. Ohnishi is the applause for the BigRIPS performance. Furthermore, while the earthquake disaster prevented us from holding Nishina Laboratory's 80th anniversary celebration, the excellent news of Dr. Y. Akiba receiving the Nishina Memorial Prize more than made up for it.

In JFY 2011, the 4-year construction of the Superconducting Analyser for MUlti particles from RAdio Isotope beams (SAMURAI) was completed. The EUro RIken Crystal Array (EURICA) was also put in place. SAMURAI and EURICA finished their shakedowns and are already starting PAC-approved experiments. The Self-Confining RI Ion Target (SCRIT) achieved its luminosity goal of 10^{27}/cm^{2}s. Finally, the long-awaited Rare-Radioisotope Ring was approved for construction by RIKEN headquarters. The construction will be completed in 2012, and we expect the first results within 3 years.

At the very end of JFY2011, the RIBF Cyclopedia was inaugurated on the first floor of the RIBF building where visitors can learn about RIBF science from A to Z, with 3D video, a full-sized color-coded carpet mapping out the sectors of Superconducting Ring Cyclotron, and variety of displays.

Our research is not immune to the aftermath of the Earthquake or the economic downturn. Even so, however, we have achieved many milestones, and there are many more to come. Let us celebrate each of these auspicious events by drinking Nishina-Homare, RIBF-made Sake, newly branded in 2011.

Hideto En'yo
Director,
RIKEN Nishina Center for Accelerator-Based Science

II. RESEARCH ACTIVITIES I
(Nuclear-Particle Physics)

1. Nuclear Physics

Non-yrast structure of ^{110}Mo†

H. Watanabe*1

[Nuclear structure, unstable nuclei]

The neutron-rich nucleus ^{110}Mo has been investigated by means of γ-ray spectroscopy following the β-decay of ^{110}Nb, produced using in-flight fission of a ^{238}U beam at 345 MeV/nucleon at the RIBF facility. The nuclei of interest were separated and transported through the BigRIPS spectrometer[1,2], operated with a 6-mm-thick wedge-shaped aluminum degrader at the first dispersive focal plane for purification of the secondary beams. The identification of nuclei by their atomic number and the mass-to-charge ratio was achieved on the basis of the ΔE-TOF-$B\rho$ method, where ΔE, TOF, and $B\rho$ denote energy loss, time of flight, and magnetic rigidity, respectively. A total of 5.2×10^4 ^{110}Nb ions were implanted into an active stopper consisting of nine double-sided silicon-strip detectors (DSSSD) stacked compactly. Each DSSSD has a thickness of 1 mm with a 50 mm × 50 mm active area segmented into sixteen strips on both sides in the vertical and horizontal dimensions. The DSSSDs also served as detectors for electrons following β-decay and internal-conversion processes. The implantation of an identified particle was associated with the subsequent electron events that were detected in the same DSSSD pixel. Gamma rays were detected by four Compton-suppressed Clover-type Ge detectors arranged around the DSSSD telescope in a close geometry. Further details of a particle-identification spectrum and data-analysis techniques are given in Ref.[3].

Figure 1 exhibits the level scheme of ^{110}Mo, established by means of β-delayed γ-ray spectroscopy following the decay of ^{110}Nb. Prior to the present work, the ground-state band in ^{110}Mo has been known up to the 10^+ state by measuring the prompt γ rays from the spontaneous fission of ^{248}Cm[4]. In addition to the 214-, 386-, and 532-keV γ rays that belong to the ground-state band, seven new transitions have been unambiguously observed in a singles γ-ray spectrum measured in coincidence with β rays subsequent to implantation of ^{110}Nb, as shown in Fig. 2.

A least-squares fit of the summed gated time spectra for the γ rays at energies of 281, 421, 463, 487, and 494 keV yields a half-life of 75(9) ms, which is in agreement with the value of 81(6) ms deduced from the time distribution of the 214-keV γ ray within experimental errors. These values are consistent with $T_{1/2} = 86(6)$ ms extracted from an independent analysis of β-decay half-lives[5].

The second 2^+ level (2_2^+) is proposed at 494 keV, decaying by the 281- and 494-keV transitions which directly feed the yrast 2^+ and 0^+ states, respectively. In deformed even-even nuclei, a quasi-γ band is built on the low-lying 2_2^+ state. In the present analysis, the limited statistics preclude us from confirming the coincidence relationship between the 281- and 214-keV γ rays. Nevertheless, the assignment of the 2_2^+ state at 494 keV is justified, since only the energy sum for the 281−214-keV cascade agrees with the energy of the 494-keV γ ray within experimental errors among the newly observed γ rays. This observation is consistent with the decay pattern from the 2_2^+ state to the lower-lying 2_1^+ and 0_1^+ levels, as confirmed for even $_{42}$Mo and $_{44}$Ru isotopes in this neutron-rich region.

† Condensed from the article in Phys. Lett. B **704**, 270 (2011)

*1 RIKEN Nishina Center

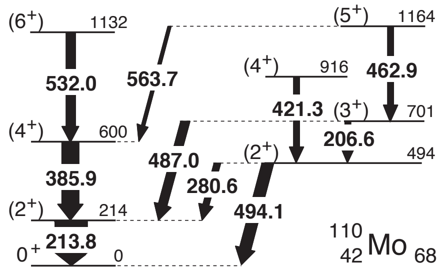

Fig. 1. Partial level scheme of ^{110}Mo established in the present work. The widths of arrows represent relative intensities of γ rays.

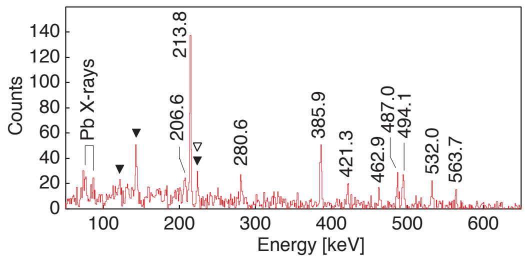

Fig. 2. γ-ray energy spectrum measured in coincidence with β rays detected within 250 ms after implantation of ^{110}Nb. Contaminants from ^{110}Tc and ^{109}Mo are indicated with filled and open triangles, respectively.

References

1) T. Kubo: Nucl. Instrum. Methods B **204**, 97 (2003).
2) T. Ohnishi et al.: J. Phys. Soc. Jpn. **77**, 083201 (2008).
3) H. Watanabe et al.: Phys. Lett. B **696**, 186 (2011).
4) W. Urban et al.: Eur. Phys. J. A **20**, 381 (2004).
5) S. Nishimura et al.: Phys. Rev. Lett. **106**, 052502 (2011).

Decay spectroscopy of neutron-rich nuclei with CAITEN

K. Steiger,[1] S. Nishimura,[2] Z. Li,[2] R. Chen,[2] T. Faestermann,[1] R. Gernhäuser,[1] C. Hinke,[1] R. Krücken,[1,3] M. Kurata-Nishimura,[2] G. Lorusso,[2] Y. Miyashita,[4] K. Sugimoto,[4] T. Sumikama,[4] H. Watanabe,[2] and K. Yoshinaga[2]

[Nuclear structure, shell model, unstable nuclei, β decay]

An experiment in fall 2010 at RIBF investigated neutron-rich nuclei in the neighborhood of ^{30}Ne and ^{36}Mg. These nuclei were produced by relativistic projectile fragmentation of a 345 AMeV ^{48}Ca primary beam which was delivered from the superconducting ring cyclotron SRC with an average intensity of 70 pnA. The secondary cocktail beam was separated and identified with the BigRIPS[1)] fragment separator and the ZeroDegree spectrometer (ZDS). The beam was used for two simultaneous experiments: An in-beam γ-ray spectroscopy experiment[2)] using a secondary target and the DALI2 array[3)] at the position F8 of BigRIPS and a parasitic β-decay experiment at F11 of ZDS which is the topic of this report. The unambiguous particle identification was achieved by measuring the energy loss (ΔE), time of flight (TOF) and magnetic rigidity ($B\rho$) event-by-event before and behind the secondary target (Fig. 1). The identified fragments were implanted in the CAITEN[4)] detector (Cylindrical Active Implantation Target for Efficient Nuclear-decay study). The main part of this detector is a 4×10^4-fold segmented plastic scintillator with the shape of a hollow cylinder. To reduce background decay events the scintillator was moved axially (20-40 rpm) and vertically (2 mm/s) similar to a tape-transport system. Implantations and decays were correlated in time and space. A background subtraction was performed to remove random correlations. γ-rays were detected with three germanium clover detectors. For the first time β-delayed γ-rays were measured in the neutron-rich isotopes ^{37,38}Si. In Fig. 2 the β-delayed γ-spectrum after the decay of ^{37}Al is shown. With β-γ-γ coincidences five new γ transitions could be placed in a tentative level scheme of the daughter nucleus ^{37}Si. Due to the large Q_β value β-delayed neutron emission is also possible. Applying the same methods after the decay of ^{30}Ne the low-energy level structure of ^{30}Na which was reported in Ref. 5 could be reproduced.

Half-life values for the implanted nuclei were measured and tentative level schemes of other daughter nuclei could be determined. The analysis of the data is currently in progress.

Supported by BMBF (06MT9156), DFG (EXC 153, KR2326/2-1), KAKENHI (19340074) and RIKEN President's Fund (2005).

*1 Physik Department, Technische Universität München, Germany
*2 RIKEN Nishina Center
*3 TRIUMF, Vancouver, Canada
*4 Department of Physics, Tokyo University of Science

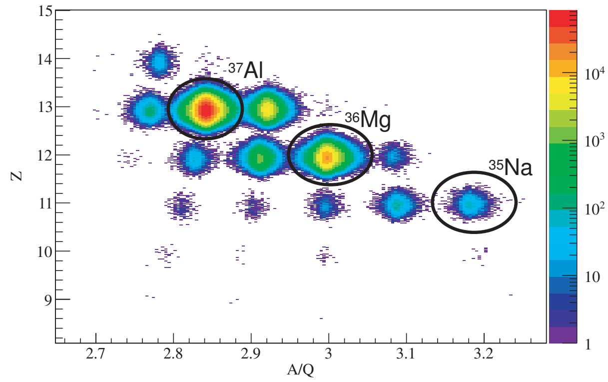

Fig. 1. Particle identification of ZDS for the ^{36}Mg setting. The nuclear charge Z is plotted against the mass over charge ratio A/Q.

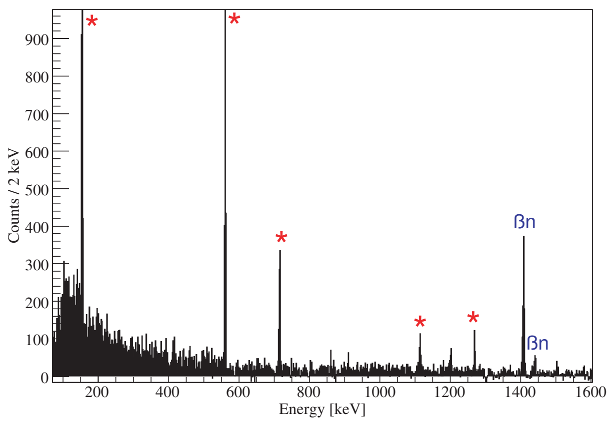

Fig. 2. γ-spectrum after the β-decay of ^{37}Al. The correlation time of implantations and decays is 10 ms. New transitions attributed to ^{37}Si are marked with asterisks (*). Already known transitions in the β-n daughter ^{36}Si are labeled with (βn).

References

1) T. Kubo: Nucl. Instr. and Meth. B 204 (2003) 97.
2) J. Lee et al.: RIKEN Acc. Rep. 44 (2011) 12.
3) S. Takeuchi et al., RIKEN Acc. Rep. 36 (2003) 148.
4) S. Nishimura et al.: RIKEN Acc. Rep. 41 (2008) 149.
5) V. Tripathi et al.: Phys. Rev. C 76 (2007) 021301.

In-beam γ-ray spectroscopy of ^{38,40}Si

M. Matsushita,[*1] S. Takeuchi, N. Aoi, P. Doornenbal, J. Lee, H. Scheit, D. Steppenbeck, H. Wang,[*2] K. Li,[*2] H. Baba, D. Bazin,[*3] L. Càceres,[*4] H. Crawford,[*5] P. Fallon,[*5] R. Gernhäuser,[*6] J. Gibelin,[*7] S. Go,[*8] S. Grévy,[*4] C. Hinke,[*6] C. R. Hoffman,[*9] R. Hughes,[*10] E. Ideguchi,[*8] D. Jenkins,[*11] N. Kobayashi,[*12] Y. Kondo,[*12] R. Krücken,[*6] T. Le Bleis,[*13] G. Lee,[*12] A. Matta,[*14] S. Michimasa,[*8] T. Motobayashi, T. Nakamura,[*12] S. Ota,[*8] M. Petri,[*5] T. Sako,[*12] H. Sakurai, S. Shimoura,[*8] K. Steiger,[*6] K. Takahashi,[*12] M. Takechi, Y. Togano, R. Winkler,[*3] K. Yoneda and K. Ieki,[*1]

[Nuclear structure, in-beam γ-ray spectroscopy]

The enhancement of nuclear collectivity in neutron-rich Si isotopes is reported by the recent studies[1–4], which show the lowering of the energies of the first 2^+ (2_1^+) excited state from ^{34}Si(N = 20) to ^{42}Si(N = 28). This indicates that the neutron shell closure at N = 28 does not persist in ^{42}Si even though the regular magic number N = 28. In addition to the 2_1^+ excited state, information on a higher excited state such as 4^+ is necessary in order to clarify whether these enhanced collectivities attribute to the nuclear vibrational motion or the rotational motion. In-beam γ-ray spectroscopies of the ^{38,40,42}Si nucleus[5] using multi-nucleon removal reactions were performed at RIBF in order to observe excited states higher than the 2_1^+ excited states and to systematically investigate the evolution of the nuclear shape (collective motion) and collectivity in Si isotopes.

The ^{44}S and ^{40}S beams were produced by a projectile fragmentation reaction of the ^{48}Ca primary beam with a typical intensity of around 70 pnA. The primary beam bombarded a 15 mm-thick Be target placed in the F0 focal plane of BigRIPS at 345 MeV/nucleon. Intensities of the ^{44}S and ^{40}S beams were around 7×10^4 pps in both cases. The secondary beams bombarded a reaction target of 2.54 g/cm^2-thick C located in the F8 focal plane in the ZeroDegree Spectrometer. ^{38,40}Si isotopes were produced by the multi-nucleon removal reactions of ^{44}S and ^{40}S, respectively, and were identified using the ZeroDegree Spectrometer. The de-excitation γ-rays of ^{38,40}Si was observed using a DALI2 γ-ray detector array[7] surrounding the reaction target.

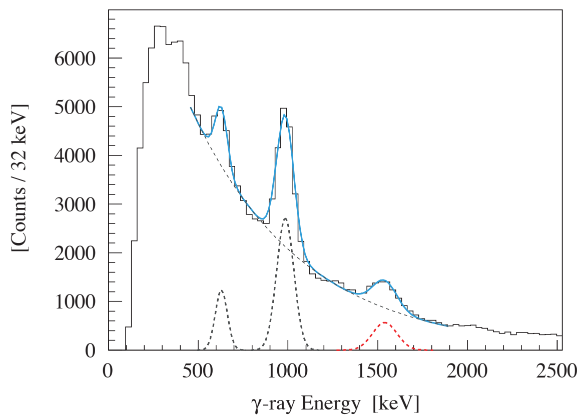

Fig. 1. Doppler shift corrected γ-ray energy spectrum of C(^{44}S,^{40}Si+γ) reaction. A new γ-ray transition was observed at 1500 keV.

The Doppler shift corrected γ-ray energy spectrum of the C(^{44}S,^{40}Si+γ) reaction is shown in Fig. 1. Three photopeaks were cleary observed in this spectrum. The photopeaks at around 600 keV and 1000 keV correspond to the known γ-ray transition that Campbell et al. previously observed at 638 keV [2] and the ground state transition from the 2_1^+ excited state (986 keV)[2], respectively. The other photopeak at around 1500 keV in this spectrum is a newly observed γ-ray transition, which is a candidate for the $4^+ \rightarrow 2^+$ transition in ^{40}Si. Further analysis in this regard is currently in progress.

[*1] Department of Physics, Rikkyo University
[*2] State Key Laboratory of Nuclear Physics and Technology, Peking University
[*3] National Superconducting Cyclotron Laboratory (NSCL)
[*4] Grand Accélérateur National d'Ions Lourds (GANIL)
[*5] Lawrence Berkeley National Laboratory (LBNL)
[*6] Physik-Department, Technische Universität München
[*7] LPC-ENSICAEN, IN2P3-CNRS et Universite de Caen
[*8] CNS, University of Tokyo
[*9] Argonne National Laboratory (ANL)
[*10] Department of Physics, University of Richmond
[*11] Department of Physics, University of York
[*12] Department of Physics, Tokyo Institute of Technology
[*13] University of Frankfurt/Helmholtzzentrum für Schwerionenforschung GmbH (GSI)
[*14] Institut de Physique Nucléaire, Orsay

References

1) R. W. Ibbotson et al.: Phys. Rev. Lett. 80, 2081 (1998)
2) C. M. Campbell et al.: Phys. Rev. Lett. 97, 112501 (2006)
3) C. M. Campbell et al.: Phys. Lett. B 652, 169 (2007)
4) B. Bastin et al.: Phys. Rev. Lett. 99, 022503 (2007)
5) S. Takeuchi et al.: RIKEN Accel. Prog. Rep. 44, 13 (2011).
6) T. Kubo: Nucl. Instr. and Meth. B 204, 97 (2003)
7) S. Takeuchi et al.: RIKEN Accel. Prog. Rep. 36, 148 (2003).

Inclusive breakup cross sections of the neutron-rich nuclei ^{29}Ne, ^{33,35,37}Mg, and ^{39,41}Si

N. Kobayashi,[*1] T. Nakamura,[*1] Y. Kondo,[*1] N. Aoi, H. Baba, S. Deguchi,[*1] N. Fukuda, G. S. Lee,[*1] H. S. Lee,[*2] N. Inabe, M. Ishihara, Y. Kawada,[*1] R. Kanungo,[*3] T. Kubo, M. Famiano,[*4] M. Matsushita, T. Motobayashi, T. Ohnishi, N. A. Orr,[*5] H. Otsu, R. Barthelemy,[*4] H. Sakurai, S. Kim,[*2] T. Sako,[*1] T. Sumikama,[*6] Y. Satou,[*2] K. Takahashi,[*1] H. Takeda, S. Takeuchi, R. Tanaka,[*1] N. Tanaka,[*1] Y. Togano,[*7] and K. Yoneda

[Halo nuclei, Coulomb breakup, nuclear structure]

Shell evolution in the neutron-rich region and formation of halo structures have recently attracted considerable attention. A recent study[1)] on the Coulomb breakup of ^{31}Ne suggested that the nucleus has a halo structure and pointed to the dominance of a loosely bound valence neutron in a p- or s-orbital; these features can be attributed to a change in the conventional shell order. Hamamoto[2)] interpreted the Coulomb breakup data in terms of a p-wave neutron halo and a deformed ^{30}Ne core. Therefore, the investigation of shell evolution and possible halo structures of neutron-rich nuclei in the vicinity of ^{31}Ne is of great interest.

The present study is aimed at identifying new halo nuclei heavier than ^{31}Ne and clarifying their shell configurations on the basis of inclusive Coulomb and nuclear breakup. Breakup measurements can be used to quantitatively investigate the characteristics of the halo structure through the evaluating of the separation energy and spectroscopic factor for a single-particle orbital[3)]. Coulomb breakup is useful for investigating the soft $E1$ excitation, which is a unique feature of halo nuclei. Nuclear breakup is useful for investigating the single-particle properties of the valence neutron, which could form a halo.

Here, we focus on the neutron-rich nuclei ^{29}Ne, ^{33,35,37}Mg, and ^{39,41}Si near the drip line from $N = 20$ to $N = 28$. The separation energies of these nuclei are less than about 2 MeV, although some of the mass values have a large uncertainty. According to the conventional shell order, the valence neutron of these nuclei occupies the high-ℓ orbital $f_{7/2}$, which hinders the tunneling effect and the formation of a halo. On the other hand, the shell melting effect, deformation, and weak binding may result in the dominance of a p- or s-orbital and thus enhance the halo properties.

In the present experiment, we measured the one-neutron removal cross sections (σ_{-1n}) on lead and carbon targets. The Coulomb breakup cross section (σ_{CB}) was determined by using the formula:

$$\sigma_{\mathrm{CB}} = \sigma_{-1n}(\mathrm{Pb}) - \Gamma\sigma_{-1n}(\mathrm{C}). \quad (1)$$

Here, σ_{-1n}(Pb) and σ_{-1n}(C) are the cross sections for lead and carbon targets. Γ was estimated to be in the approximate range 1.6–2.6[1)]. In addition, we measured the momentum distributions of the core fragments and γ-rays for the carbon target. The experimental details have been described in last year's report[4)].

Preliminary results of the cross sections σ_{CB}, σ_{-1n}(Pb), and σ_{-1n}(C) are shown in Fig. 1. σ_{CB} for ^{37}Mg is as large as that for ^{31}Ne which has a halo structure. Therefore, it is suggested that ^{37}Mg has a halo structure and its valence neutron is in a p- or s-orbital. The cross section of ^{41}Si is larger than that of ^{39}Si, which suggests that a valence neutron in the low-ℓ orbital is significant in ^{41}Si. Further analysis is in progress.

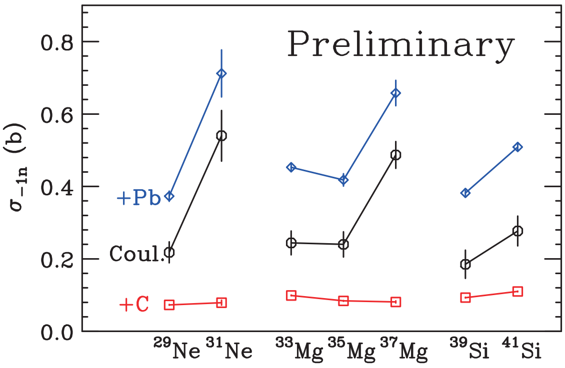

Fig. 1. Cross sections of ^{29,31}Ne, ^{33,35,37}Mg, and ^{39,41}Si. Open circles, diamonds, and squares represent the data for σ_{CB}, σ_{-1n}(Pb), and σ_{-1n}(C), respectively. The cross sections for ^{31}Ne are taken from Ref. 1).

*1 Department of Physics, Tokyo Institute of Technology
*2 Seoul National University, Korea
*3 Saint Mary's University, Canada
*4 Western Michigan University, USA
*5 LPC-Caen, ENSICAEN, IN2P3-CNRS, Université de Caen, France
*6 Department of Physics, Tokyo University of Science
*7 ExtreMe Matter Institute EMMI, GSI, Germany

References
1) T. Nakamura *et al.*: Phys. Rev. Lett. **103**, 011302 (2009).
2) I. Hamamoto: Phys. Rev. C. **81**, 021304 (2010).
3) V. Maddalena: Phys. Rev. C. **63**, 024613 (2001).
4) N. Kobayashi *et al.*: RIKEN Accel. Prog. Rep. **44**, 15 (2011).

Proton elastic cross sections of the drip-line nucleus ^{24}O at RIBF energies

V. Lapoux,[*1] H. Otsu, S.Boissinot,[*1] H. Baba, R.J. Chen, E.C. Pollacco,[*1] Y. Blumenfeld,[*2] F. Flavigny,[*1] S. Franchoo,[*2] N. Fukuda, P. Gangnant,[*3] F. Hammache,[*2] Ch. Houarner,[*3] N. Inabe, D. Kameda, J.F.Libin,[*3] C. Louchart,[*1] A. Matta,[*2] M. Matsushita, T. Motobayashi, L. Nalpas,[*1] E. Yu. Nikolskii, M. Kurata-Nishimura, A. Obertelli,[*1] T. Onishi, E. Rindel,[*2] Ph. Rosier,[*2] H.Sakurai, F. Saillant,[*3] M.Takechi, S. Takeuchi, Y. Togano, K.Yoneda, A.Yoshida and K.Yoshida

[Unstable nuclei, shell structure, magic number, elastic scattering]

Low-lying resonances or new magic shells represent stringent tests for the nuclear theories and their modeling of the nuclear interaction. These last years it was shown that several effects are playing a crucial role in the nuclear models, for the understanding of the location of the neutron drip-line and the spectroscopy of exotic nuclei: the inclusion of 3 nucleon forces[1)], the influence of the proton-neutron interaction[2)] and the continuum-coupling treatment. These effects and the characteristics of the new magic shell gap[2)] created at N=16 between the 2*s1/2* and the 1*d3/2* shells can be investigated in the case of the last bound O isotope, ^{24}O, associated to the theoretically interpreted as an enhancement of the neutron shell gap. At MSU, via invariant mass method, possible states were indicated[3)] above S_n =4.19 (14) MeV, around 4.5 and 5.3 MeV, but not clearly identified. ^{24}O having no bound excited state, the (p,p') reaction was measured with the light charged particle spectroscopy technique giving access to both bound and unbound states.

The RIBF57 experiment was realized in the F8 area by combining the intense secondary RIBF beams and the state-of-the-art particle detector array MUST2[4)]. ^{24}O was produced in BigRIPS[5)] at 263 MeV/n with unique average intensities, 1100/s (maximum for primary intensity at 180 particle nA) from the fragmentation on a Be target of the ^{48}Ca beam at 345 MeV/n. A block of 4 2-stage (Si+CsI) telescopes located at ~23 cm downstream the 2.7 mg/cm^2-thick CH_2 reaction target covered lab. angles between (65-90) deg. Each MUST2 of 10x10 cm^2 active area, provides identification, energies and trajectories of the light particles. The (p,p') kinematics were obtained by the correlations of the proton energy with the scattering angle deduced from the proton trajectory and the incident tracks reconstructed by the 3 PPACs in F8. The incident and outgoing particles were identified by Bρ-TOF-ΔE technique in BigRIPS, and in the ZDS[6)], respectively. Via the missing mass method, the ^{24}O excitation spectra (Ex) are extracted. The data for ^{24}O(p,p') corresponded to the 3 settings of ZDS, tuned with Bρ centered on 1. ^{24}O for the elastic, 2. ^{23}O from ^{24}O decay, for inelastic to states above S_n , and 3. ^{22}O, for states above S_{2n}.

[*1] CEA Saclay IRFU/SPhN, France
[*2] CNRS-IN2P3, IPNO, France [*3] GANIL, France

The extraction of the kinematics and of the Ex spectra were checked on the ^{22}O(p,p'), the reference measurement done at 262.5 MeV/n. The ^{22}O elastic data were compared with calculations (Fig.1) done within the optical model potential (OMP) framework, using the KD[7)] global nucleon-nucleus potential. The (p,p) cross sections were measured for ^{24}O (Fig.1) and also for the contaminants of the ^{22,24}O beams, ^{21}O, ^{23}F, and ^{23}O, ^{25}F respectively. By comparison to OMP calculations, the characteristics of the OMP at RIBF energies will be obtained. From the $^{21-24}$O(p,p) elastic data, the matter density root mean square radii will be extracted via coupled-channel calculations using microscopic density-dependent optical potentials[8)].

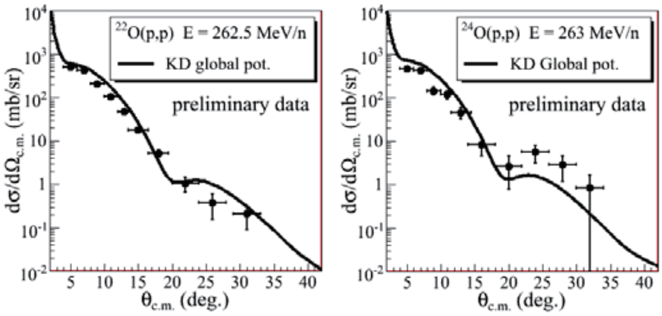

Fig.1.Elastic cross sections for ^{22}O(p,p)^{22}O and ^{24}O(p,p)^{24}O.

The preliminary Ex spectra for ^{24}O, obtained in exclusive conditions, for proton in coincidence with O isotopes in ZDS, either with $^{22-24}$O or with $^{22-23}$O were extracted with a low statistics (less than 100 counts for the whole data set). Possible structures are indicated: one above Sn; three above S_{2n}. The data analysis is still under progress to determine the maximum likelihood of the Ex structures as possible resonant states and to extract the parameters, Ex and width.

References

1) T. Otsuka et al., Phys. Rev. Lett. 105, 032501 (2010).
2) T. Otsuka *et al.*: Phys. Rev. Lett. **91**, 179202 (2003).
3) C.R. Hoffman *et al.*: Phys.Lett.B **672**, 17 (2009).
4) E.C. Pollacco *et al.*: Eur. Phys. J. A **25**, 287 (2005)
5) T. Kubo *et al.*: NIM. in Phys. Res., B **204**, 97 (2003).
6) T. Ohnishi *et al.*: J. Phys. Soc. Jpn. **77**, 083201 (2008).
7) A. Koning and J. P. Delaroche, Nucl. Phys. ***A 713***, 231 (2003).
8) M. Dupuis *et al.* Phys. Rev. C **73**, 014605 (2006).

Elastic scattering of ^{23,25}F from proton target

R.J. Chen, H. Otsu, V. Lapoux,[*1] S. Boissinot,[*1] H. Baba, A. Matta,[*2] E. Pollacco,[*1] Y. Blumenfeld,[*2] F. Flavigny,[*1] S. Franchoo,[*2] N. Fukuda, P. Gangnant,[*3] F. Hammache,[*2] C. Houarner,[*3] N. Inabe, D. Kameda, J.F. Libin,[*3] C. Louchart,[*1] M. Matsushita, T. Motobayashi, L. Nalpas,[*1] E.Y. Nikolskii, M.K. Nishimura, A. Obertelli,[*1] T. Onishi, E. Rindel,[*2] P. Rosier,[*2] H. Sakurai, F. Saillant,[*3] M. Takechi, S. Takeuchi, Y. Togano, K. Yoneda, A. Yoshida, and K. Yoshida

[Elastic scattering, Neutron-rich nuclei, Surface properties, Optical model potential (OMP)]

Nuclear structures of neutron-rich nuclei have attracted considerable attention because of their exotic properties, such as neutron halo and neutron skin. For example, in neutron halo nuclei, a very weakly bound nucleon can tunnel into the classically forbidden region, giving rise to a diffuse tail surrounding a well-bound core, due to low binding energy[1)]. Recently, with the development of the radioactive isotope beam, such exotic properties can be studied through elastic scattering in inverse kinematics. Experimental studies on light neutron-rich nuclei showed that ^{22}C, ^{23}N, and ^{24}O are the last bound nuclei of their respective isotopic chains, whereas the addition of only one more proton extends the drip line for the flourine isotopes to ^{29}F[2)]. In order to understand such phenomena, we study herein the neutron number dependence of the density of flourine isotopes, by measuring the proton elastic scattering with a ^{23}F and ^{25}F beam at 289 and 298 MeV/nucleon, respectively.

Secondary beams were produced by bombarding a 15-mm-thick Be target with a ^{48}Ca beam at 345 MeV/nucleon with an average intensity of 120 particle nA. The beams of interest were separated and purified using a 15 mm-thick Al degrader at the focal point F1, and were then identified event-by-event by measuring the energy loss, magnetic rigidity, and time-of-flight at BigRIPS. The intensities of ^{23}F and ^{25}F secondary beams were approximately 9.6×10^3 (purity 23%) and 330 (purity 1.3%) cps, respectively. The profiles of secondary beams were obtained with 3 sets of parallel plate avalanche counters (PPAC), with a position resolution of approximately 2.8 mm (FWHM). Inside the vacuum chamber at F8, a polyethylene CH_2 foil with a thickness of 2.7 mg/cm^2 was used as a proton target for the (p,p) scattering measurement, and a carbon foil with a thickness of 0.78 mg/cm^2 was used for subtracting the contribution of carbon in the CH_2 foil. The energy and scattering angle of recoil protons were measured using 4 sets of MUST2 telescopes[3)] which were located at 23 cm downstream of the target, covering an angular region from 30° to 90° in the laboratory frame. The details of the setup are described in Ref.[4)]. Protons were identified by measuring the energy loss and total energy with the double-sided silicon strip detector (DSSD) and the CsI detector, respectively. For low-energy protons that stopped inside the DSSD, the time-of-flight between the PPAC and DSSD was used, instead of the total energy, for the particle identification. The ^{23,25}F(p,p) and (p,p') reaction channels were selected by analyzing outgoing heavy residual nuclei in ZeroDegree Spectrometer (ZDS) and analyzing protons in MUST2 telescope. The counts of the elastic scattering reaction were obtained by integrating the measured excitation energy spectrum from −2 to 2 MeV. We note that the counts should include the contribution from the inelastic scattering reaction populating the low-energy bound excited states of ^{23,25}F due to the limited energy resolution (approximately 2.1 MeV in FWHM).

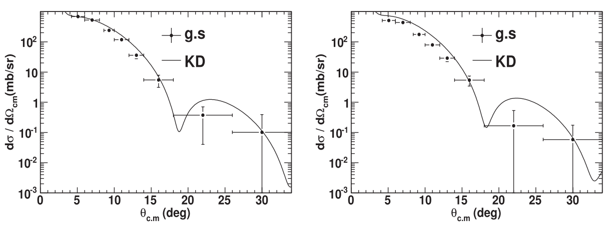

Fig. 1. Differential cross sections for the ^{23}F(p,p) (left) and ^{25}F(p,p) (right) reactions.

The differential cross sections for the ^{23}F(p,p) and ^{25}F(p,p) reactions in the center-of-mass (c.m.) system are shown in the left and right panels of Fig. 1, respectively. The solid line represents the results of the DWBA calculation with KD optical model potential[5)] using Fresco code[6)]. A theorectical analysis with a folding potential model for the extraction of density distribution is in progress.

References

1) A. DiPietro et al., Phys. Rev. Lett 105, 022701 (2010).
2) H. Sakurai et al., Phys. Lett. B 448, 180 (1999).
3) E. Pollacco et al., Eur. Phys. J. A 25, 287 (2005).
4) V. Lapoux et al., RIKEN Accel. Prog. Rep., 44 (2001).
5) A.J. Koning et al., Phys. A713, 231 (2003).
6) I.J. Thompson, Comput. Phys. Rep. 7, 167 (1988).

*1 CEA-Saclay, DSM/IRFU SPhN, F-91191 Gif sur Yvette Cedex, France
*2 Institut de Physique Nucle aire, IN2P3-CNRS, F-91406 Orsay, France
*3 GANIL, CEA/DSM - CNRS/IN2P3, BP 55027, F-14076 Caen Cedex5, France

Gamow-Teller transitions from ^{56}Ni†

M. Sasano,[*1,*2,*3] G. Perdikakis,[*1,*2] R.G.T. Zegers,[*1,*2,*4] Sam M. Austin,[*1,*4] D. Bazin,[*1] B. A. Brown,[*1,*2,*4] C. Caesar,[*5] A. L. Cole,[*6] J.M. Deaven,[*1,*2,*4] N. Ferrante,[*7] C.J. Guess,[*8] G. W. Hitt,[*9] M. Honma,[*10] R. Meharchand,[*1,*2,*4] F. Montes,[*1,*2] J. Palardy,[*7] A. Prinke,[*1,*2,*4] L. A. Riley,[*7] H. Sakai,[*11] M. Scott,[*1,*2,*4] A. Stolz,[*2] T. Suzuki,[*12,*13,*14] L. Valdez,[*1,*2,*4] and K. Yako[*15]

[Nuclear structure, shell model, unstable nuclei, electron captures]

Charge-exchange (CE) reactions at intermediate energies ($T_p \geq 100$ MeV/u) have long been used to investigate isovector (change in isospin $\Delta T = 1$) spin-flip ($\Delta S = 1$) excitation modes in stable nuclei[1)]. An important application of CE reactions is study of the GT transition, which is characterized by no angular momentum transfer ($\Delta L = 0$) and mediated through the $\vec{\sigma}\tau_{\pm}$ operator, and whose strength is directly connected with weak matrix element of an allowed-β-decay or electron capture (EC). Especially, the GT strengths in medium-heavy nuclei are key ingredients for understanding roles of weak interaction (EC and β-decay) in late stellar evolution[2–4)]. To extend such CE-reaction study to unstable nuclei has been strongly needed, because many nuclei playing dominant roles in stellar weak processes are unstable (e.g., see Table I in Ref.[3)]). However, such experiments have been challenging; successful experiments have focused on the study of relatively light nuclei and at low excitation energies (see e.g.[5–7)]).

In this study, a new experimental technique to measure the CE (p,n) reaction in inverse kinematics with unstable isotopes of any mass and up to high excitation energies was developed and used to study ^{56}Ni(p,n) reaction at 110 MeV/u. Gamow-Teller transition strengths from ^{56}Ni leading to ^{56}Cu were obtained and compared with shell-model predictions in the pf shell using the KB3G and GXPF1A interactions. The calculations with the GXPF1A interaction reproduced the experimental strength distribution much better than the calculations that employed the KB3B interaction, indicating deficiencies in the spin-orbit and proton-neutron residual potentials for the latter. The experiment was performed at NSCL, Michigan State University in 2010 when one of the authors, M. Sasano, was under the employment of NSCL, and the main results were published in Ref.[8)] in November 2011, after he moved to RIKEN Nishina Center. This work was supported by the US NSF (Grants No. PHY-0822648 (JINA), No. PHY-0606007, No. PHY-0758099, No. PHY-0922615, and No. PHY-1068217).

References

1) F. Osterfeld, Rev. Mod. Phys. **64**, 491 (1992).
2) K. Langanke and G. Martínez-Pinedo, Rev. Mod. Phys., **75** 819 (2003), and references therein.
3) A. Heger and S. E. Woosley and G. Martínez-Pinedo and K. Langanke, Astro Phys. J., **560** 307 (2001).
4) W. R. Hix *et al.*, Phys. Rev. Lett., **91** 201102 (2003).
5) T. Nakamura *et al.*, Phys. Lett., **B493**, 209 (2000).
6) R.G.T. Zegers *et al.*, Phys. Rev. Lett., **104**, 212504 (2010).
7) Y. Satou *et al.*, Phys. Lett., **B697**, 459 (2011).
8) M. Sasano et al., Phys. Rev. Lett. **107**, 202501 (2011).

† Condensed from the article in Phys. Rev. Lett. **107**, 202501 (2011)

*1 NSCL, Michigan State University
*2 JINA, Michigan State University
*3 RIKEN Nishina Center (from Oct. 1st, 2011 to the present)
*4 Department of Physics and Astronomy, Michigan State University
*5 GSI Darmstadt
*6 Physics Department, Kalamazoo College, Kalamazoo
*7 Department of Physics and Astronomy, Ursinus College
*8 Department of Physics, University of Massachusetts Lowell
*9 Khalifa University of Science, Technology & Research
*10 Center for Mathematical Sciences, University of Aizu
*11 RIKEN Nishina Center
*12 Department of Physics, College of Humanities and Sciences, Nihon University
*13 CNS, University of Tokyo
*14 National Astronomical Observatory of Japan
*15 Department of Physics, University of Tokyo

The parity-transfer reaction (^{16}O, ^{16}F) for studies of pionic 0^- mode

M. Dozono, T. Uesaka, M. Sasano, S. Shimoura,*1 S. Michimasa,*1 S. Ota,*1 H. Matsubara,*1 Y. Sasamoto,*1 S. Noji,*1 H. Tokieda,*1 H. Miya,*1 S. Kawase,*1 R. Tang,*1 Y. Kikuchi,*1 K. Kisamori,*1 M. Takaki,*1 Y. Kubota,*1 C. S. Lee,*1 T. Fujii,*1 R. Yokoyama,*1 H. Sakai, T. Kubo, K. Yoshida, Y. Yanagisawa, N. Fukuda, H. Takeda, D. Kameda, N. Inabe, K. Yako,*2 T. Wakasa,*3 K. Fujita,*3 S. Sakaguchi,*3 H. Sagawa,*4 M. Yamagami,*4 and M. Ichimura

[Nuclear structure, Spin-isospin response, Charge-exchange reaction]

The pion is the most important particle for understanding nuclear forces. The pseudo-scalar nature of the pion leads to a strong tensor correlation, which plays a characteristic role in nuclear structure. The investigation of tensor correlation in nuclei is thus indispensable in understanding the fundamental nature of a nuclear many-body system.

The spin-isospin excitations provide a unique opportunity to study the tensor correlation effects in nuclei. The spin-dipole (SD) 0^- excitations are of particular interest as they carry the same quantum number as a pion. Recently, the effects of tensor correlations on the 0^- excitations have been investigated by using self-consistent HF+RPA calculations[1)]. From the calculations, it was found that the tensor correlations produce a strong hardening (shifting toward a higher excitation energy) effect on the collective 0^- resonance, and the effect is very sensitive to the magnitude of the tensor strength. Therefore, from the study of 0^- states, we are able to identify the tensor correlation effects. However, in spite of this importance, experimental information on 0^- states is very limited because of a lack of experimental tools that would be suitable for 0^- studies.

In this report, we propose a new probe, a parity-transfer reaction for the 0^- study. The parity-transfer reaction is a direct nuclear reaction where the probe particle changes from the initial 0^+ state to the final 0^- state ($0^+ \rightarrow 0^-$). This reaction has advantages over other reactions used so far. Table 1 shows the J^π states that are excited by using the parity-transfer reaction and traditional reactions such as $(p,n)[1/2^+ \rightarrow 1/2^+]$ and $(d,^2\mathrm{He})[1^+ \rightarrow 0^+]$. With all the traditional reaction probes, it is very difficult to separate 0^- states from the 1^- and 2^- states as these SD states are excited with the same $\Delta L = 1$. On the other hand, the new probe, the parity-transfer reaction, excites only one J^π component with each ΔL. Thus, the J^π components can be assigned by only the angular distribution. In addition, due to its unique feature as an exclusive probe of unnatural-parity states, the contribution from the natural-parity 1^- excitation is negligible. Thus, the parity-transfer reaction can be a powerful tool for reliable determination of the 0^- strength distribution.

Table 1. The spin-parity states excited via the parity-transfer reaction and traditional reactions.

	$\Delta L = 0$	$\Delta L = 1$	$\Delta L = 2$	$\cdots$
Parity-trans.	0^-	1^+	2^-	$\cdots$
(p,n) etc.	$0^+, 1^+$	$0^-, 1^-, 2^-$	$1^+, 2^+, 3^+$	$\cdots$

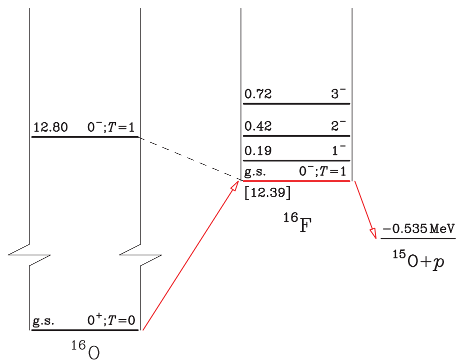

Fig. 1. Energy level diagram for ^{16}F

This technique is based on the transition from the 0^+ g.s. of ^{16}O to the 0^- g.s. of ^{16}F (See Fig. 1). The RIBF accelerators, which provide heavy ion beams of 345 MeV/A, in combination with the SHARAQ spectrometer, which affords high-resolution particle spectroscopy, offer the sole opportunity for studies of the parity-transfer (^{16}O, ^{16}F) reaction at an energy of 200–300 MeV/A. In this energy region, the single-step process is dominant, and thus, we can extract the nuclear structure information reliably. In order to confirm the validity of the method of the parity-transfer reaction, we plan to perform a ^{12}C(^{16}O, ^{16}F)^{12}B experiment at 250 MeV/A. Once this new method is established, it will open new opportunities for the study of the 0^- strengths in nuclei and for exclusive excitation feeding to the unnatural-parity states in general.

*1 Center for Nuclear Study, University of Tokyo
*2 Department of Physics, University of Tokyo
*3 Department of Physics, Kyushu University
*4 Center for Mathematics and Physics, University of Aizu

References
1) C. L. Bai *et al.*, Phys. Rev. Lett. **105**, 072501 (2010).

N/Z Dependence of π^-/π^+ Ratio from Heavy Ion Reaction of 400 MeV/nucleon

M. Sako[*1], T. Murakami[*1], Y. Ichikawa[*1], K. Ieki[*3], Y. Ikeda[*3], S. Imajo[*1], T. Isobe, S. Ebesu[*1], M. Matsushita[*3], J. Murata[*3], Y. Nakai, S. Nishimura, M. Nitta[*3], H. Sakurai, R. Sameshima[*1], E. Takada[*2], and K. Yoshinaga[*4]

[Symmetry energy, pion ratio, high density]

As we have already mentioned in the previous RIKEN Accel. Prog. Rep.[1)2)], the density dependence of nuclear symmetry energy $E_{sym}(\rho)$ is one of the most attractive subjects in nuclear physics. According to the transport model calculation (IBUU04)[3)], detailed studies of the pion yield ratio, $Y(\pi^-)/Y(\pi^+)$, in central nucleus-nucleus collisions at intermediate energies would provide significant constraints on $E_{sym}(\rho)$ at high densities ($\rho > \rho_0$).

The theoretical calculations[3)] predicted that the incident energy dependence and N/Z dependence of the pion yield ratio are strongly related to the behavior of $E_{sym}(\rho)$ in the supra-normal density region ($\rho > \rho_0$). We have already reported the energy dependence of the pion ratio[2)]. In 2011, we performed a comparative study on the pion yield ratio in In(^{28}Si, $\pi^\pm$)X[2)] and In(^{132}Xe, $\pi^\pm$)X[1)] reactions, which we had measured for beam energies of 400 MeV/nucleon at HIMAC with a compact centrality filter and a pion range counter in order to estimate the N/Z ratio dependence of the pion yield ratio. The total number of charged pions was estimated by using ΔE_i-ΔE_j correlations obtained experimentally for π^+ events, because we had demonstrated that π^+ events could be clearly identified by the $\pi^+ \to \mu^+ + \nu_\mu$ decay when π^+ stops in one of the elements of the range counter.

Figure 1 shows the pion yield ratio as a function of the kinematic energy of the pions in a mid rapidity frame(E_{rap}). Curves fitted to the experimental data by using a power function are shown in Fig. 1, and the slope of the fitted curves shows the N/Z dependence. We roughly estimated the integrated pion yield ratio. The preliminary results are 1.40 ± 0.22 and 2.46±0.46 for In+^{28}Si and In+^{132}Xe, respectively, and seem to be qualitatively consistent with the transport model prediction[4)].

We performed systematic experiments to investigate N/Z dependence of the pion yield ratio in further detail. We measured the pion yield ratio in CsI(^{129,132,136}Xe,$\pi^\pm$)X reaction for a beam energy of 400 MeV/nucleon at HIMAC. We configured the data acquisition system to perform high-statistics experiments and performed measurements at 45° and 90° in the laboratory system. For comparison, we also measured the pion yield ratio in Si(^{129,132,136}Xe,$\pi^\pm$)X reaction for a beam energy of 400 MeV/nucleon. We used Xe isotope beams to avoid the Z dependence between each reaction because the coulomb effect is different between charged pions. After finishing the data analysis, we will put constraint on the density behavior of the symmetry energy by comparing the energy dependence and N/Z dependence of the pion yield ratio obtained from experiments with those from transport model calculation.

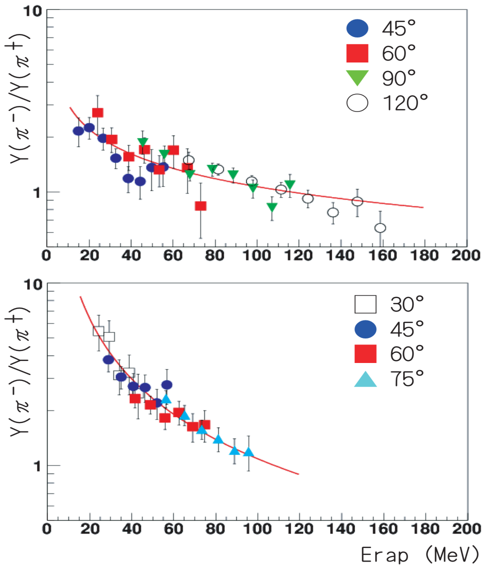

Fig. 1. Pion yield ratio as a function of kinematic energy in a mid rapidity frame for In+^{28}Si collisions (upper) and In+^{132}Xe collisions (bottom) at 400 MeV/nucleon. Solid lines are curves fitted by using a function of $Cx^{-\alpha}$. The slope parameters (α) are $(4.5 \pm 0.5) \times 10^{-1}$ and $(11.0\pm 0.8)\times 10^{-1}$ for In+^{28}Si and In+^{132}Xe, respectively.

*1 Department of Physics, Kyoto University, Kyoto, Japan
*2 Department of Accelerator and Medical Physics, NIRS, Chiba, Japan
*3 Department of Physics, Rikkyo University, Tokyo, Japan
*4 Department of Physics, Tokyo University of Science, Tokyo, Japan

References
1) T. Murakami et al., RIKEN Accel. Prog. Rep. **43**, 26 (2010).
2) M. Sako et al., RIKEN Accel. Prog. Rep. **44**, 20 (2011).
3) Bao-An Li, Gao-Chan Yong, and Wei Zuo, Phys. Rev. C **71**, 014608 (2005).
4) Zhigang Xiao et al. Phys. Rev. Lett. **102**, 062502(2009).

Search for short-lived isomers in neutron-rich $Z \sim 60$ nuclei produced by in-flight fission of 345 MeV/nucleon ^{238}U

R. Yokoyama, [*1] D. Kameda, T. Kubo, N. Inabe, N. Fukuda, H. Takeda, H. Suzuki, K. Yoshida, K. Kusaka, K. Tanaka, Y. Yanagisawa, M. Ohtake, H. Sato, Y. Shimizu, H. Baba, M. Kurokawa, D. Nishimura, T. Ohnishi, N. Iwasa, [*2] A. Chiba, [*2] T. Yamada, [*2] E. Ideguchi, [*1] S. Go, [*1] T. Fujii, [*1] H. Nishibata, [*3] K. Ieki, [*4] D. Murai, [*4] S. Momota, [*5] Y. Sato, [*6] J. Hwang, [*6] S. Kim, [*6] O. B. Tarasov, [*7] D. J. Morrissey, [*7] B. M. Sherrill, [*7] and G. Simpson, [*8]

[In-flight fission, neutron-rich nuclei, short-lived isomer]

In-flight fission of the ^{238}U beam, which is one of the most advantageous features of RIBF, enables the production of highly neutron rich radioisotopes (RIs) with a wide range of atomic masses. However, little is known about medium-heavy-to-heavy nuclides, especially their excited states. In-flight fission is expected to excite some isomeric states that are sufficiently long-lived to be measured by γ-ray spectroscopy at the end of the separator beam line.

In 2011, neutron-rich isotopes in the $Z \sim 60$ region were investigated, by the in-flight fission of a 345 MeV/nucleon ^{238}U beam. The RI beams were identified in an event-by-event plot of their proton number (Z) versus mass-to-charge ratio (A/Q). This plot (called the PID plot) was obtained by the measurement of the magnetic rigidity ($B\rho$), time of flight (TOF), and energy loss (dE) in the BigRIPS separator. A total kinetic energy (TKE) detector was installed in the F12 focal plane, at the end of the BigRIPS beamline, in order to identify heavier elements with different atomic charge states. The TKE detector consists of 20 layers of Si detectors and is designed to stop all ions of interest.

This condition is adequate to search for new isomeric states with half-lives on the order of microseconds or sub-microseconds. We carried out γ-ray measurements at F12 and searched for isomers by gating on each RI in the PID. These measurements also serveed as confirmation of the PID plot since the events gated by known isomeric γ-rays were plotted.

The γ-rays from the isomeric states were detected by four clover-type HPGe detectors placed around the TKE detector. Each detector consists of four crystals which make adding back Compton-scattered events in the neighboring crystals possible, to improve the signal-to-noise ratio. The energy and timing of the γ-rays triggered by the RI beam within a time window of 20 μs after arrival were measured. In order to reduce the background from beam irradiation, the γ-events close to the implantation timing of the beam were excluded.

Thus, we have confirmed some of the known isomers. Figure 1 shows the preliminary energy spectra and the decay curves of the delayed gamma-rays for ^{154}Nd and ^{156}Nd. These isomers are reported in the reference[1]. The γ-ray energies and half-lives obtained in this study are consistent with those in the reference. In addition, potential candidates for new isomers have been identified. Further analysis of these isomers is in progress.

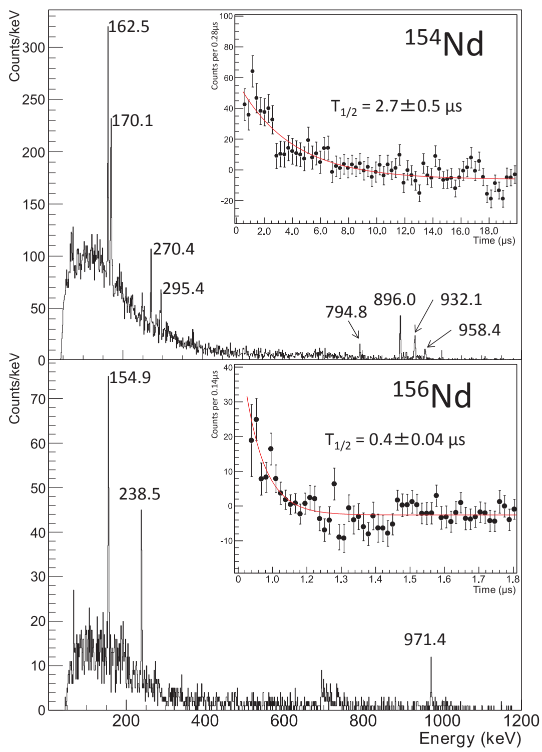

Fig. 1. γ-ray energy spectra for ^{154}Nd and ^{156}Nd.

References
1) G. S. Simpson *et al.*, Phys. Rev. C 80, 024304 (2009)

*1 Center for Nuclear Study, University of Tokyo
*2 Department of Physics Tohoku University
*3 Department of Physics, Osaka University
*4 Department of Physics, Rikkyo University
*5 School of Environmental Science and Engineering, Kochi University of Technology
*6 Department of Physics and Astronomy, Seoul National University
*7 National Superconducting Cyclotron Laboratory Michigan State University
*8 LPSC-IN2P3

Search for new isotopes near the proton drip-line by using projectile fragmentation of ^{124}Xe

N. Inabe, T. Kubo, H. Suzuki, N. Fukuda, H. Takeda, D. Kameda, K. Yoshida, K. Kusaka, K. Tanaka, Y. Yanagisawa, M. Ohtake, H. Sato, Y. Shimizu, H. Baba, M. Kurokawa, D. Nishimura, N. Iwasa[*1], A. Chiba[*1], Y. Okoda[*1], E. Ideguchi [*2], S. Go[*2], R. Yokoyama[*2], T. Fujii[*2], K. Ieki [*3], D, Murai [*3], H. Nishibata[*4], S. Momota[*5], M. Lewitowicz [*6], G. DeFrance[*6], I. Celikovic[*6], K. Steiger[*7], D. J. Morrissey[*8], and D. P. Bazin[*8]

[New isotope, Proton drip-line, ^{124}Xe beam, Projectile fragmentation, BigRIPS]

We have performed search for new isotopes in the very proton-rich regions of Nb~Pd and Te~Xe by using projectile fragmentation of ^{124}Xe. These new isotopes are located at or very close to the proton drip-line.

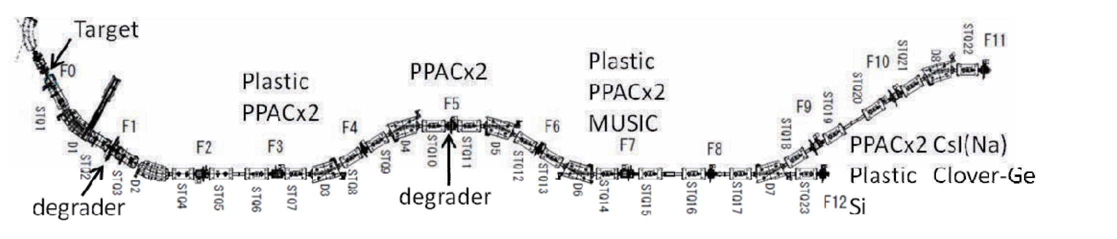

Fig.1 Schematic drawing of the experimental setup.

A schematic drawing of the experimental setup is shown in Fig. 1. A ^{124}Xe beam at 345 MeV/u impinged on a Be target at F0. The produced fragments were collected and separated by the BigRIPS separator,[1] and identified by using beam-line detectors placed at the F3, F5, F7 and F12 focuses as indicated in Fig. 1. The isotope separation was made by the two-stage separation mode, in which wedge-shaped energy degraders were employed at both F1 and F5 focuses. We adopted this mode in order to improve the isotope purity of proton-rich fragments, which was expected to be poor due to contaminants originating from low-energy tail of the fragment momentum distribution. We optimized the BigRIPS settings, such as target and degrader thickness, slit openings at F1, F2, F5 and F7 focuses, and $B\rho$ values, based on simulations using the code LISE++[2]. The experimental conditions of the present measurements are summarized in Table 1, including the BigRIPS settings.

The particle identification (PID) was performed using the ΔE-TOF-$B\rho$ method, which allows the event-by-event determination of atomic number Z and mass-to-charge ratio A/Q of fragments. The energy loss (ΔE) was measured by an ion chamber (MUSIC) at F7. The time-of-flight (TOF) between F3 and F7 was measured by using thin plastic scintillators. The fragment trajectory (positions and angles) was measured at F3, F5 and F7 by using PPACs in order to make trajectory reconstruction. This allows precise determination of fragment $B\rho$ values.[2] The Si stack detectors were placed at F12 to measure the total kinetic energies (TKE) of fragments. The Si stack detectors were surrounded by four clover-type Ge detectors, in order to measure delayed γ-rays emitted from isomers of stopped fragments. The TKE provided us with additional information for the PID. The observation of known isomeric γ-decays allowed us to confirm the PID calibration. We used delayed γ-rays from ^{80m}Y for the Nb~Pd setting and those from ^{106m}Sb for the Te~Xe setting.

We observed a few candidates of new isotopes according to our on-line analysis. Detailed analysis is in progress.

*1 Department of Physics, Tohoku University
*2 Center for Nuclear study, The University of Tokyo
*3 Department of Physics, Rikkyo University
*4 Department of Physics, Osaka University
*5 School of Environmental Science and Engineering, Kochi University of Technology
*6 Grand Accelerateur National d' Ions Lourds, France
*7 Physik Department, Technische University at Munchen, Germany
*8 National Superconducting Cyclotron Laboratory, Michigan State University, USA(MSU)

Table 1 Summary of the experimental conditions

	Nb~Pd	Te~Xe
Target	Be 4 mm	
Degrader (F1/F5)	Al 2.85 mm / Al 1.97 mm	
Central particle	^{85}Ru	^{105}Te
$B\rho$ (D1) (Tm)	5.113	5.300
Momentum Acc. (%)	±2	-2~1.5
Slit width (mm) F2	±20	-15~20
F5	±95	±95
F7	±20	±10
^{124}Xe intensity (pnA)	7.6	8.9
Running time (hrs)	21.8	19.6
Ave. total rate (kcps)	~1.7	~1.3

References

1) T. Kubo: Nucl. Instr. Meth. **B 204**, 97 (2003).
2) O. B. Tarasov and D. Bazin: a manual of the code LISE++ available at http://www.nscl.msu.edu/lise/.
3) T. Ohnishi et al.: Jpn. J. Phys. Soc. Jpn. **79**, 073201 (2010).

Production rate measurement of very proton-rich Sn isotopes by using projectile fragmentation of 345-MeV/nucleon ^{124}Xe

H. Suzuki, T. Kubo, N. Inabe, N. Fukuda, H. Takeda, D. Kameda, K. Yoshida, K. Kusaka, K. Tanaka, Y. Yanagisawa, M. Ohtake, H. Sato, Y. Shimizu, H. Baba, M. Kurokawa, D. Nishimura, N. Iwasa,[*1] A. Chiba,[*1] Y. Okoda,[*1] E. Ideguchi,[*2] S. Go,[*2] R. Yokoyama,[*2] T. Fujii,[*2] K. Ieki,[*3] D. Murai,[*3] H. Nishibata,[*4] S. Momota,[*5] M. Lewitowicz,[*6] G. DeFrance,[*6] I. Celikovic,[*6] K. Steiger,[*7] D. J. Morrissey,[*8] and D. P. Bazin[*8]

[NUCLEAR REACTION, Projectile fragmentation, Proton-rich nuclei]

We have performed the measurement of the production rate for highly proton-rich Sn isotopes, including ^{100}Sn, by using the BigRIPS separator[1]. These isotopes have been produced by the projectile fragmentation of a primary beam of ^{124}Xe at 345 MeV/nucleon. We have also measured the momentum distribution of these fragments. The production rates of ^{100}Sn and its neighboring isotopes have attracted considerable attention, because the ^{100}Sn nucleus is the heaviest doubly magic nucleus with the same proton number (Z) and neutron number (N). The study of the momentum distribution is very important, because the behavior of its low-momentum tail determines the purity of the in-flight isotope separation when proton-rich isotopes are produced in our energy domain.

The experiment was performed in December 2011 using a primary beam of ^{124}Xe at an energy of 345 MeV/nucleon. The typical intensity of the beam was around 8 particle nA. The ^{124}Xe beam was impinged on a 4-mm-thick Be target. The projectile fragments were collected and analyzed using BigRIPS and sent to the final focal plane at F12. Particle identification was performed at the second stage of BigRIPS on the basis of the measured time of flight (TOF), energy loss (ΔE), and magnetic rigidity ($B\rho$). TOF was measured using two plastic scintillation counters placed at F3 and F7 with a central flight length of 47 m. At F7, an ion chamber with an active area having a diameter of 230 mm[2] was installed to measure the ΔE values. To deduce the $B\rho$ values precisely, the trajectories of the fragments were reconstructed from the positions and angles measured with PPACs at F3, F5, and F7. First-order ion-optical transfer matrices were obtained by performing a simulation using the ion-optics code COSY INFINITY[3]. To confirm the particle identification, delayed γ rays from the isomeric states of ^{94}Pd were measured using three clover-type high-purity germanium detectors located at F12.

The analysis is now in progress, and the obtained results are preliminary. Figure 1 shows a two-dimensional plot of Z versus mass-to-charge (A/Q) ratio for ^{100}Sn-production setting. The production rates of ^{100,101,102}Sn are shown in Table 1. The rate for ^{100}Sn was $(1.1 \pm 0.2) \times 10^{-4}$ cps/pnA, and it is about 1/10 of the rate obtained by LISE++ calculation with the parameters of EPAX2. The production rate of other Sn isotopes are also lower than the corresponding calculated rate.

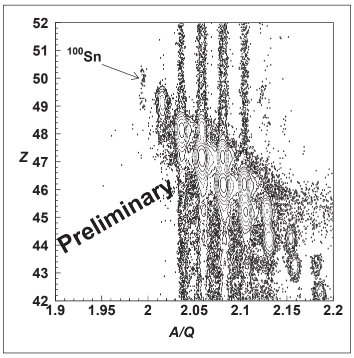

Fig. 1. Two-dimensional plot of Z vs. A/Q for ^{100}Sn-production setting (Preliminary).

Table 1. The production rates [cps/pnA] of ^{100,101,102}Sn (Preliminary).

Nuclei	Experiment	LISE++
^{100}Sn	$(1.1 \pm 0.2) \times 10^{-4}$	9.4×10^{-4}
^{101}Sn	$(7.0 \pm 0.8) \times 10^{-3}$	5.0×10^{-2}
^{102}Sn	$(4.6 \pm 1.2) \times 10^{-1}$	2.2×10^{0}

In summary, we performed the production of proton-rich Sn isotopes, including ^{100}Sn, at BigRIPS using a primary beam of ^{124}Xe at 345-MeV/nucleon. We measured the production rates and momentum distribution for ^{100}Sn and neighboring nuclei. Further data analysis is now in progress.

*1 Department of Physics, Tohoku University
*2 Center for Nuclear Study, University of Tokyo
*3 Department of Physics, Rikkyo University
*4 Department of Physics, Osaka University
*5 School of Environmental Science and Engineering, Kochi University of Technology
*6 Grand Accelerateur National d'Ions Lourds, France
*7 Physik Department, Technische Universität München, Germany
*8 National Superconducting Cyclotron Laboratory, Michigan State University, USA

References

1) T. Kubo et al.: Nucl. Instr. and Meth. **B 204**, 97 (2003)
2) H. Otsu et al.: RIKEN Accel. Prog. Rep. **42**, 163 (2009)
3) K. Makino and M. Berz: Nucl. Instr. and Meth. **A 558**, 346 (2006)

Search for new isomers near the N=Z line by using projectile-fragmentation of ^{124}Xe

S. Go,[*1] D. Kameda, T. Kubo, N. Inabe, N. Fukuda, H. Takeda, H. Suzuki, K. Yoshida, K. Kusaka, K. Tanaka, Y. Yanagisawa, M. Ohtake, H. Sato, Y. Shimizu, H. Baba, M. Kurokawa, D. Nishimura, N. Iwasa,[*2] A. Chiba,[*2] Y. Okoda,[*2] E. Ideguchi,[*1] R. Yokoyama,[*1] T. Fujii,[*1] K. Ieki,[*3] D. Murai,[*3] H. Nishibata,[*4] S. Momota,[*5] M. Lewitowicz,[*6] G. DeFrance,[*6] I. Celikovic,[*6] K. Steiger,[*7] D. J. Morrissey,[*7] and D. P. Bazin [*7]

Spectroscopy around doubly-magic nuclei ^{100}Sn is of great importance for studying the closure of nuclear shells at $N = Z = 50$, and this region has a rich variety of nuclear structures.[1−3)] A feature of great interest in this region is the presence of isomeric states that exist because of proton and neutron interaction owing to the large overlap of wave functions between the proton and the neutron.[4)] In addition, the structure of this region is of astrophysical importance as the rapid proton capture process lies around ^{100}Sn.[5)]

An isomer search experiment was performed at RIBF in December 2011. The search region was around Z = 40-50. Nuclei were produced by the fragmentation reaction of the ^{124}Xe beam at an energy of 345 MeV/u on a ^{9}Be target of 4 g/cm^2 thickness. Beam intensity of the primary ^{124}Xe beam was about 8 pnA. A secondary beam was selected using the BigRIPS separator and transported along the BigRIPS beam line.[6)] Particle identification was based on the ΔE-TOF-$B\rho$ method, in which the energy loss of the particle (ΔE), time of flight (TOF), and magnetic rigidity ($B\rho$) were measured to deduce the atomic number Z and the mass-to-charge ratio A/Q of particle. The TOF was measured using plastic scintillators and PPAC placed on focal planes. The average total counting trigger rate at F7 was about 1.5 kcps. To implant the isotopes and to measure ΔE and total energy E. A stack of Si detectors is placed on the final focal plane F12.

γ-rays emitted from the excited nuclei were detected by 4 clover-type Ge detectors placed around the Si detectors. The signals were digitized by CAMAC ADC (ORTEC AD413A). The dynamic range of TDC was up to 20 μs. Many known isomers were observed in this experiment. This information served as confirmation of the particle identification of the beam.

The observed γ-ray spectrum of ^{96}Pd is presented in Fig. 1. Each γ-ray spectrum was summed up in all germanium detectors. To reduce the background due to beam irradiation, the timing gate after 300 ns from the prompt γ-ray emission was adopted. Strong peaks were observed at 106.2, 325.2, 683.7, and 1415.3 keV. The decay curve gated by the isometric γ-ray, 106.2 keV, is presented in the inset of Fig. 1. The half life is preliminarily deduced to be 1.9(40) μs. This value agrees with the value reported inRef. 7, 2.2μs within errors.

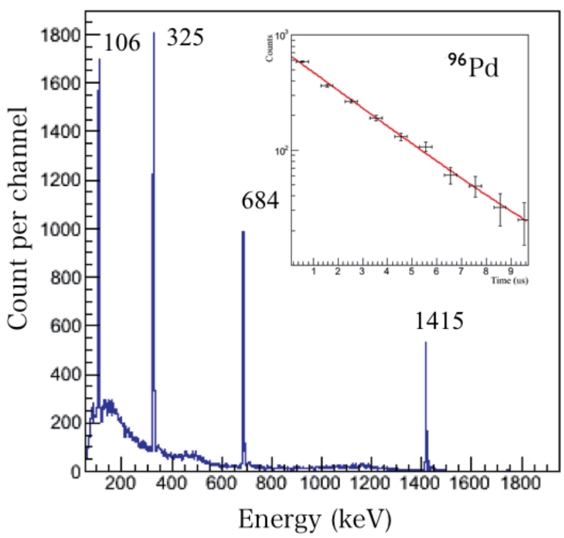

Fig. 1. γ-ray energy spectrum of ^{96}Pd. Inset shows a decay curve spectrum for 106 keV transition.

Further analysis of the new isomer search is now in progress.

References
1) B. Cederwall et al., Nature **469**, 68 (2011).
2) A. Blazhev et al., Phys. Rev. C **69**, 064304 (2004).
3) A. D. Becerril et al, Phys. Rev. C **84**, 041303 (2011).
4) A. Afanasjev et al., Phys. Rev. C **71**, 064318 (2005).
5) C. Mazzocchi et al., Phys. Rev. Lett. **98**, 212501 (2007).
6) T. Kubo., Nucl. Instr. and Meth. B **204**, 97 (2003).
7) L. Batist et al., Nucl. Phys. A **624**, 185 (1997).

*1 Center for Nuclear Study, The University of Tokyo
*2 Department of Physics, Tohoku University
*3 Department of Physics, Rikkyo University
*4 Department of Physics, Osaka University
*5 School of Environmental Science and Engineering, Kochi University of Technology
*6 Grand Accelerateur National d' Ions Lourds, France
*7 National Superconducting Cyclotron Laboratory, Michigan State University USA(MSU).

Resonance states in ^{27}P using Coulomb dissociation and their effect on the stellar reaction ^{26}Si(p,γ)^{27}P†

Y. Togano,[*1] T. Gomi,[*1] T. Motobayashi, Y. Ando,[*1] N. Aoi, H. Baba, K. Demichi,[*1] Z. Elekes,[*2] N. Fukuda, Zs. Fülöp,[*2] U. Futakami,[*1] H. Hasegawa,[*1] Y. Higurashi,[*1] K. Ieki,[*1] N. Imai, M. Ishihara, K. Ishikawa,[*3] N. Iwasa,[*4] H. Iwasaki,[*5] S. Kanno,[*1] Y. Kondo,[*3] T. Kubo, S. Kubono,[*6] M. Kunibu,[*1] K. Kurita,[*1] Y. U. Matsuyama,[*1] S. Michimasa,[*6] T. Minemura, M. Miura,[*3] H. Murakami,[*1] T. Nakamura,[*3] M. Notani,[*6] S. Ota,[*6] A. Saito,[*1,*6] H. Sakurai, M. Serata,[*1] S. Shimoura,[*6] T. Sugimoto,[*3] E. Takeshita,[*1] S. Takeuchi, K. Ue,[*5] K. Yamada, Y. Yanagisawa, K. Yoneda, and A. Yoshida

[^{208}Pb(^{27}P,p^{26}Si)^{208}Pb, Coulomb dissociation, Nuclear astrophysics]

The stellar reaction ^{26}Si(p,γ)^{27}P was studied by considering Coulomb dissociation of ^{27}P at 54 MeV/nucleon[1)]. The ^{26}Si(p,γ)^{27}P reaction rate was deduced on the basis of measured cross sections to resonance and continuum states in ^{27}P.

The γ-ray from the decay of ^{26}Al is an excellent observable to constrain nucleosynthesis models[2)]. The ^{26}Si(p,γ)^{27}P reaction might affect the production of ^{26}Al since the reaction reduces the amount of ^{26}Si, which produces ^{26}Al via its β^+ decay. The aim of the present work is to improve the estimate of the ^{26}Si(p,γ)^{27}P reaction rate by using experimentally obtained inputs.

The experiment was performed at the RIBF. A ^{27}P beam was produced from a 115 MeV/nucleon ^{36}Ar beam and separated by RIPS. The typical ^{27}P intensity was 2.8 kcps, which corresponds to 1% of the total secondary beam intensity. A lead plate with a thickness of 125 mg/cm^2 was used as a secondary target. The beam trajectory was obtained by using two PPACs placed at upstream of the target. The momentum vector of reaction products, ^{26}Si ions and protons, were measured by a position-sensitive silicon telescope and a plastic scintillator hodoscope. The relative energies between the ^{26}Si ions and protons were reconstructed by using the measured momentum vectors.

The ^{26}Si-p relative energy spectrum obtained for the ^{27}P + Pb reaction is shown in Fig. 1. The peaks at 0.32 and 0.81 MeV correspond to the known resonances in ^{27}P[3)]. To explain the structure above the second peak, we consider the third and fourth resonances. The fit results of the lower peak at 1.37 MeV suggest the existence of third excited state in ^{27}P. This state can be analogous to the 1.94 MeV state with a spin-parity of $5/2^+$ in the mirror nucleus ^{27}Mg. The peak at 2.2 MeV may be the sum of unresolved states.

The E2 components of the resonant strength $\omega\gamma$(E2) of the three resonance states at low relative energy were estimated to deduce the the ^{26}Si(p,γ)^{27}P reaction rate. They were obtained to be $(6.5\pm1.3)\times10^{-11}$ MeV, $(6.0\pm1.1)\times10^{-11}$ MeV, and $(1.10\pm0.27)\times10^{-11}$ MeV respectively by using the obtained cross sections. The total $\omega\gamma$ value (E2 + M1) for the first resonance was deduced to be $1.9^{+1.9}_{-1.1}\times10^{-9}$ MeV by using the M1 component estimated through shell model calculations with USDB effective interaction[4)]. The associated error was from the difference between the experimental result and the shell model calculation result for ^{27}P. This $\omega\gamma$ value indicates that the resonant capture reaction through the first resonance in ^{27}P is the dominant process at stellar temperatures from 0.1 to 3 GK.

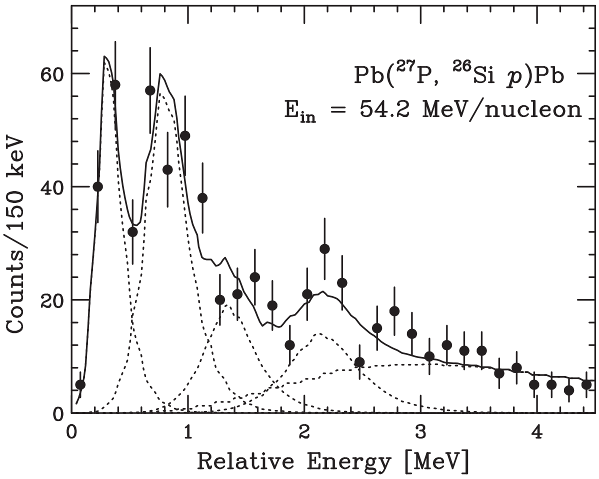

Fig. 1. ^{26}Si-p relative energy spectrum in the ^{27}P + Pb reaction. The solid curve represents the best fit by five components: four resonances and one direct capture component represented individually by the dotted curves.

† Condensed from an article in Phys. Rev. C **84**, 035808 (2011)
*1 Department of Physics, Rikkyo University
*2 Institute of Nuclear Research of the Hungarian Academy of Sciences (ATOMKI), Hungary
*3 Department of Physics, Tokyo Institute of Technology
*4 Department of Physics, Tohoku University
*5 Department of Physics, University of Tokyo
*6 Center for Nuclear Study, University of Tokyo

References
1) Y. Togano et al.: Phys. Rev. C **84**, 035808 (2011).
2) R. Diehl et al.: Astron. Astrophys. Suppl. Ser. **97**, 181 (1993).
3) J. A. Caggiano et al.: Phy. Rev. C **64**, 025802 (2001).
4) W. A. Richter, S. Mkhize and B. A. Brown: Phy. Rev. C **78**, 064302 (2008).

N=16 shell closure in ^{24}O

K. Tshoo,*1 Y. Satou,*1 T. Nakamura,*2 H.C. Bhang,*1 S. Choi,*1 Y. Kondo,*2 N. Aoi, S. Deguchi,*2 F. Delaunay,*3 J. Gibelin,*3 T. Honda,*4 M. Ishihara, Y. Kawada,*2 N. Kobayashi,*2 T. Kobayashi,*5 F.M. Marques,*3 M. Matsushita,*4 Y. Miyashita,*6 T. Motobayashi, Y. Nakayama,*2 N.A. Orr,*3 H. Otsu, H. Sakurai, S. Shimoura,*7 D. Sohler,*8 T. Sumikama,*6 S. Takeuchi, K.N. Tanaka,*2 N. Tanaka,*2 Y. Togano, K. Yoneda, K. Yoshinaga,*6 T. Zheng,*9 Z.H. Li, Z.X. Cao*9

[Nuclear structure, Neutron-rich nuclei, Magic number, Shell structure]

In the oxygen isotopes, new shell closures at N = 14[1–3] and 16[4–6] near the neutron drip line have been extensively studied both experimentally and theoretically. The measured low $E2$ transition probability $B(E2)$ and high excitation energy of the first 2^+ state, $E_x(2_1^+)$, in ^{22}O[1] show the spherical nature of the N = 14 shell. However, since the $B(E2)$ value in principle depends only on the proton distribution, proton inelastic scattering, which is sensitive to both the neutron and proton distributions, was performed by Becheva *et al.*[3]. They reported a quadrupole transition parameter β_2 (= 0.26 ± 0.04) smaller than those of ^{18,20}O, indicating the nearly spherical nature of the N = 14 shell. For ^{24}O, β_2 was not measured despite it being critical for the study of the systematics for the magic nature of ^{24}O.

We report on the 2_1^+ excitation energy of ^{24}O measured in the inverse kinematics of the proton inelastic scattering, along with β_2 of the first excited state for the first time. The β_2 value was deduced by a phenomenological distorted wave Born approximation (DWBA) analysis.

Fig. 1 shows the systematics of the 2_1^+ excitation energy (upper panel) and the quadrupole transition parameter β_2 (lower panel) comparing with those of previous studies for even-even oxygen isotopes between N = 10 and N = 14[3,7,8]. As the neutron number N increases from 12 to 16, the 2_1^+ excitation energy also increase rapidly while β_2 decreases. The solid lines were obtained by using the shell model calculation code NUSHELL[9] and the USDB interaction[10]; the β_2 values were derived by employing Bernstein's prescription[11] with the $B(E2)$ values obtained from the shell model calculation. These shell model calculations predict the ratio of the neutron to proton quadrupole matrix elements M_n/M_p to be 2.60, in good agreement with ^{22}O data (M_n/M_p = 2.5 ± 1.0)[3]. The calculations results reproduce the neutron number systematics of both $E_x(2_1^+)$ and β_2 well, especially those of ^{22}O and ^{24}O. The systematics of $E_x(2_1^+)$ and β_2 in the Z = 8 isotopes clearly shows the robustness of the N = 16 shell closure at Z = 8.

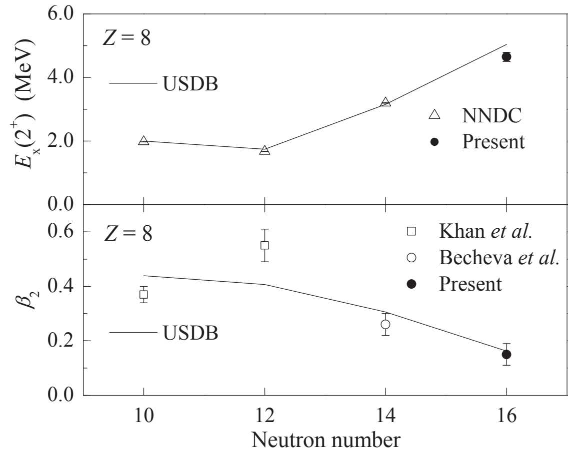

Fig. 1. $E_x(2_1^+)$ (upper panel) and $\beta_2(2_1^+)$ (lower panel). The present results are for N = 16. The open triangles are the observed 2_1^+ energies taken from Ref. 7. The β_2 values for $^{18-22}$O measured in Refs. 3 and 8 are indicated by open squares and an open circle, respectively. The solid lines represent the results of shell model calculations performed by using the USDB interaction.

*1 Department of Physics and Astronomy, Seoul National University, Korea.
*2 Department of Physics, Tokyo Institute of Technology, Japan.
*3 LPC Caen, ENSICAEN, Université de Caen, CNRS/IN2P3, Caen, France.
*4 Department of Physics, Rikkyo University, Japan.
*5 Department of Physics, Tohoku University, Japan.
*6 Department of Physics, Tokyo University of Science, Japan.
*7 Center for Nuclear Study, University of Tokyo, Japan.
*8 Institute of Nuclear Physics (ATOMKI), Debrecen, Hungary.
*9 School of Physics and State Key Laboratory of Nuclear Physics and Technology, Peking University, Beijing, China.

References

1) P.G. Thirolf *et al.*, Phys. Lett. B **485**, 16 (2000).
2) M. Stanoiu *et al.*, Phys. Rev. C **69**, 034312 (2004).
3) E. Becheva *et al.*, Phys. Rev. Lett. **96**, 012501 (2006).
4) T. Otsuka, *et al.*, Phys. Rev. Lett. **87**, 082502 (2001).
5) C.R. Hoffman *et al.*, Phys. Rev. Lett. **100**, 152502 (2008).
6) C.R. Hoffman *et al.*, Phys. Lett. B **672**, 17 (2009).
7) NNDC database (2011), http://www.nndc.bnl.gov.
8) E. Khan *et al.*, Phys. Lett. B **490**, 45 (2000).
9) B.A. Brown and W.D.M. Rae, MSU-NSCL report (2007).
10) B.A. Brown and W.A. Richter, Phys. Rev. C **74**, 034315 (2006).
11) A.M. Bernstein, V.R. Brown, and V.A. Madsen, Phys. Lett. B **103**, 255 (1981).

Structure study of ^{10}He by ^{11}Li(d,^{3}He) transfer reaction

A. Matta,[*1] D. Beaumel,[*1] H. Otsu,[*2] N. Aoi,[*2] M. Assie,[*1] H. Baba,[*2] S. Boissinot,[*3] R. Chen,[*2] F. Delaunay,[*4] N. de Sereville,[*1] S. Franchoo,[*1] J. Gibelin,[*4] F. Hammache,[*1] H. Wang,[*2] N. Imai,[*5] N. Kobayashi,[*6] T. Kubo,[*2] Y. Kondo,[*6] Y. Kawada,[*6] V. Lapoux,[*3] J. Lee,[*2] M.Nishimura,[*2] T. Motobayashi,[*2] T. Nakamura,[*6] L. Nalpas,[*3] E. Nikolskii,[*2,10] A. Obertelli,[*3] E. Pollacco,[*3] T. Sako,[*6] H. Sakurai,[*2] A. Sanchez-Benitez,[*7] J-A. Scarpaci,[*1] I. Stefan,[*1] D. Suzuki,[*8] K. Takahashi,[*6] M. Takechi,[*2] S. Takeuchi,[*2] R. Wolski,[*9] K. Yoneda,[*2]

[Nuclear structure, unbound nuclei]

The first experimental evidence of the ^{10}He system forming a resonant state was obtained from the study of the ^{11}Li +CD2 $\rightarrow$ ^{10}He+X reactions at 61 AMeV performed at RIKEN, on the RIPS line[1)]. The experiment was carried out using the invariant mass method in the ^{8}He+n+n channel. Since various experimental work has been carried out using the invariant mass method and the double charge exchange[2)] and (p,2p) [3,4)] reactions. Recently, some results using the missing mass method were obtained from the (t,p) transfer reaction[5)]. All these works lead to ambiguities on the position of the first resonant state of the unbound ^{10}He system, located in the 1-1.5 MeV region above the two neutrons emission threshold. Some theoretical work predicted a never observed state a few keV above the two neutron threshold[6)] using a three body model.

The experiment was performed in july 2010 at the RIKEN RIPS facility, producing a secondary beam of ^{11}Li at 50 AMeV on a CD_2 target. At forward angle, a wall of four MUST2 telescopes[7)] were coupled with four 20μm thick silicon detectors in order to perform an E-ΔE identification of the light particles, and separation of ^{4}He and ^{3}He. At zero degree, a fifth MUST2 telescope and a two stages plastic detector were used for identification of heavy residues of reaction in coincidences. In addition a ^{9}Li beam at 50 AMeV was used to perform a reference experiment.

The excitation energy spectrum of ^{10}He, obtained requiring coincidences between a ^{3}He and an ^{8}He, is presented in fig.1 and show a resonant state 1.4(1) MeV above the ^{8}He+n+n threshold. The angular distribution associate with this state has been extracted and is being interpreted through DWBA in order to extract a spectroscopic factor. State of higher energy of excitation are also under analysis, requiring coincidences with ^{6}He and ^{4}He around zero degrees.

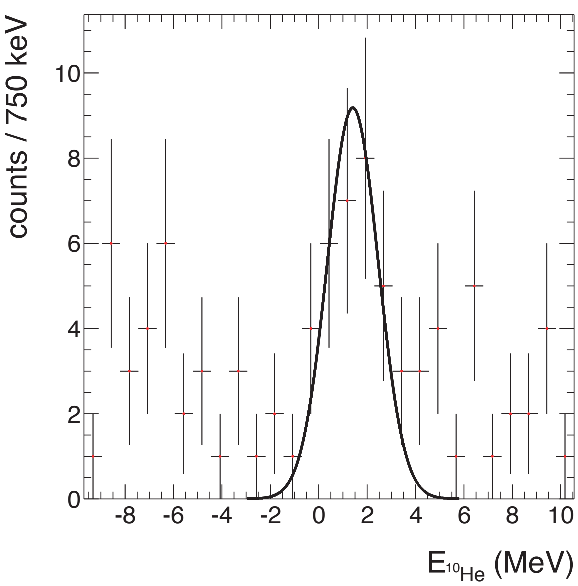

Fig. 1. *The ^{10}He spectrum obtained from ^{11}Li(d,^{3}He) reaction data. Coincidences between ^{3}He and ^{8}He were required. The black line is a fit using the convolution of a Breit-Wigner with a Gaussian.*

References
1) A. Korsheninnikov *et al*, Phys. Lett. B 326, 31-36 (1994)
2) A. Ostrowski *et al*, Phys. Lett. B 338, 13-19 (1994)
3) T. Kobayashi *et al*, Nucl. Phys. A 616, 223-230 (1997)
4) H. Johansson *et al*, Nucl. Phys. A 847, 66-88 (2010)
5) M. Golovkov *et al*, Phys. Lett. B 672, 22 29 (2009)
6) Aoyama, Nuc. Phys. A 722, 474-479 (2003)
7) E. Pollacco *et al*, Eur. Phys. Jour. A 25, 287-288 (2005)

*1 Institut de Physique Nucleaire, Orsay Cedex, France
*2 Riken, 2-1 Hirosawa, Wako, Saitama 351-0198, Japan
*3 CEA/IRFU/SPhN, CEA Saclay, Gif-sur-Yvette, France
*4 LPC, Universite de Caen ,Caen, France
*5 KEK, 1-1 Oho, Tsukuba-shi, Ibaraki-ken, 305, Japan
*6 Tokyo Institute of Technology,O-okayama,Tokyo, Japan
*7 Departamento de FA, Universidad de Huelva, Huelva, Spain
*8 NSCL, Michigan State University, Michigan, USA
*9 Institute of Nuclear Physics, Krakow, Polan
*10 National Research Centre “Kurchatov Institute”, Moscow, Russia

Attempt to synthesize a new neutron-deficient isotope, ^{216}U

Y. Wakabayashi,[*1] K. Nishio,[*1] S. Mitsuoka,[*1] K. Morita, K. Morimoto, D. Kaji, H. Haba, T. Sumita, A. Yoneda and Y. Gono

[Nuclear structure, shell model, unstable nuclei]

Synthesis of neutron-deficient actinide nuclei close to the N = 126 shell closure is important to understand the stability of the N = 126 closed shell[1)] and to predict the limit of existence for elements with N = 126. These nuclei also allow us to study the structure of the actinide nuclei with a spherical shape. Actinide nuclei with N = 126 have been produced up to uranium (^{218}U), and the lightest uranium isotope produced so far is ^{217}U. A campaign has been started to investigate the nuclei in this region. We have chosen the reaction ^{82}Kr + ^{138}Ba to produce ^{216}U (N = 124) in the fusion-evaporation reaction as the first step. The cross section is important to extend our study to produce unknown nuclei such as ^{220}Pu with N = 126 (in the reaction ^{82}Kr + ^{140}Ce). We have also attempted to find the isomeric states in ^{216,217}U to study the nuclear properties of these nuclei.

An experiment to produce ^{216}U using the ^{138}Ba(^{82}Kr, $4n$)^{216}U reaction was performed at the RIKEN Linear Accelerator (RILAC) facility. The bombarding energy, 378 MeV, was chosen on the basis of the largest cross section for ^{216}U predicted by the code HIVAP[2)]. We also used a beam energy of 363 MeV to examine the energy dependence of the cross section for other isotopes. ^{82}Kr^{12+} beams of 384 and 397 MeV were supplied from RILAC and made to bombard a rotating ^{138}BaCO$_3$ target foil. The corresponding beam energies at the middle of the target were 363 and 378 MeV, respectively. The rotating target wheel had a diameter of 10 cm and was rotated at 1000 rpm. ^{138}BaCO$_3$ targets with thickness in the range 347$\simeq$507 μg/cm^2 were prepared by sputtering a 99%-enriched ^{138}Ba on 1.5-μm-thick aluminum foils, and they were also covered with 65 μg/cm^2 aluminum by sputtering. A gas-filled recoil ion separator (GARIS) was used to collect evaporation residues (ERs) and to separate them from the ^{82}Kr beam and other reaction products. The separated recoils were implanted in a position-sensitive strip detector (PSD; 58 × 58 mm^2). Two microchannel plates (MCPs) were used in timing detectors to obtain the time-of-flight (TOF) signal of the ERs. The presence of the signal in the timing detectors was also used to distinguish the α-decay in the PSD from recoil implantation. In this experiment, the ^{138}Ba targets were irradiated with a ^{82}Kr beam with an intensity of about 200 particle nA on average, and beam doses of 4.3 × 10^{17} and 7.8 × 10^{16} were accumulated at 397 MeV and 384 MeV, respectively.

*1 Japan Atomic Energy Agency

The identification of the isotope produced was made by using an α-decay chain and recoil implantation in the PSD with the help of known α-decay properties (energy and lifetime) of the descendants and the position correlation between implanted ERs and subsequent α-decays. Figure 1 shows an α-α correlation spectrum for the correlated chain obtained at both beam energies, 384 and 397 MeV. For ^{217}U ($3n$), we observed 10 events at 397 MeV and 8 events at 384 MeV. The obtained cross sections were 120 ± 60 pb and 0.5 ± 0.2 nb, respectively, and were consistent with the HIVAP calculation. Similarly, the cross sections for the isotopes, such as ^{217}Pa, ^{215}Th, and ^{213}Ac, agreed with the calculation. The decay chain from ^{216}U was not identified, and the upper limit cross section was obtained to be 10 pb. Additional irradiation experiments are necessary to study the production of ^{216}U.

We observed an energy difference of about 150 keV for ^{217}U, which is shown by arrows labeled ^{217}U and ^{217m}U in Fig. 1. This may indicate the population of the isomeric state in ^{217}U. Further irradiation experiments will help in identifying the isomer.

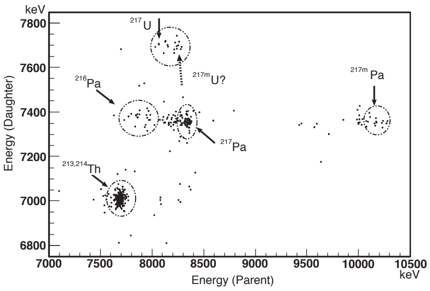

Fig. 1. Two dimensional spectrum of α-α correlation. The X and Y axis denote the α-particle energy emitted from the parent nucleus and daughter nucleus, respectively. The time difference between implanted ERs and the α-decay of the parent nucleus and between the α-decays of the parent and daughter nuclei was set to 100 ms and 2 s, respectively. These events were measured within the horizontal position of the same strip (∼3.6 mm width) and a vertical window of ±3 mm in the PSD. The energy of the implanted ERs was selected from the range 45 $\simeq$ 85 MeV. Each circle with an arrow and label shows a parent nucleus in an α-chain.

References

1) H. Koura and T. Tachibana, Btsuri (in Japanese), 60, (2005) 717.
2) W. Reisdorf and M. Schadel, Z. Phys. A343 (1992) 47.

Active target measurement of the ^{22}Mg + alpha system in inverse kinematics

N.N. Duy[*1], S. Kubono,[*2] H. Yamaguchi,[*2] D. Kahl,[*2] T. Hashimoto,[*2] S. Ota,[*2] Y. Wakabayashi,[*3] T. Komatsubara,[*4] T. Teranishi,[*5] S. Kato,[*6] N. Iwasa,[*7] T. Yamada,[*7] Y.K. Kwon,[*8] A. Kim,[*9] Y.H. Kim,[*9] J. Song,[*9] J. Hu,[*10] and Y. Ito.[*11]

The ^{22}Mg(α,p)^{25}Al reaction at low incident energies plays an important role in rp-process nucleosynthesis. It is believed that the process takes place under extremely high-temperature and high-density conditions. Because the ^{22}Mg nucleus is thought to be a waiting point, the evolution of nucleosynthesis can proceed through three mechanisms: proton capture ^{22}Mg(p,γ)^{23}Al; β^+ decay ^{22}Mg(β^+)^{22}Na; and the ^{22}Mg(α,p)^{25}Al reaction ,which is thought to dominate even if its cross section is underestimated by a factor of 100.[1)] Because of its dominance, the reaction affects the ^{22}Na abundance as well as the yield of the 1.275 MeV gamma ray and causes isotopic anomalies in meteorites, called the Ne-E problem.[2)] In addition, the ^{22}Mg(α,p)^{25}Al reaction is related to the nuclear structure of ^{26}Si immediately above the α threshold (E = 9.17 MeV). Though only limited numbers of level are known for ^{26}Si, many more levels should exist above the threshold, since many levels have been identified in the mirror nucleus ^{26}Mg. Of particular interest is the possible α structure of some of the levels predicted by the threshold rule for finding α-cluster states. The nonstatistical contribution from resonances with large α widths would enhance the cross section as compared to calculations using models such as the one with the NON-SMOKER code[3)] based on the Hauser-Feshbach model. There was an effort toward extracting the reaction rate[4)], but its accuracy is still limited because of a lack of precise experimental data. In order to obtain experimental data of the stellar reaction ^{22}Mg(α,p)^{25}Al, we performed a direct measurement in inverse kinematics in the center-of-mass energy range from 1 to 4.2 MeV, corresponding to Gamow windows at temperatures from 1 to 3 GK, which are of astrophysical interest. We carried out the experiment by means of the thick-target method, using the active-target detector MSTPC[5)] with a radioactive beam of ^{22}Mg produced by CRIB (CNS Radioactive Ion Beam separator) at the Center for Nuclear Study (CNS), The University of Tokyo.[6)] The ^{22}Mg beam was produced via the ^{3}He(^{20}Ne,^{22}Mg)n reaction. Primary beams of ^{20}Ne of 6.2 MeV/u energy bombarded a cryogenic gas target[7)] of ^{3}He cooled to 90 K with 2.5 μm Harvar windows. See table 1 for details.

*1 Institute of Physics, Vietnamese Academy of Science and Technology.
*2 Center for Nuclear Study, Graduate School of Science, Univ. of Tokyo.
*3 JAEA, Japan.
*4 Department of Physics, University of Tsukuba, Japan.
*5 Department of Physics, University of Kyushu, Japan.
*6 Department of Physics, University of Yamagata, Japan.
*7 Department of Physics, University of Tohoku, Japan.
*8 Department of Physics, ChungAng University, Korea.
*9 Department of Physics, Seoul University, Korea.
*10 Institute of Modern Physics, Chinese Academy of Science.
*11 Low Energy Experimental Nuclear Physics Gr., Univ. of Tsukuba.

Table 1. Conditions of radioactive beam production.

^{20}Ne	Target	Purity	^{22}Mg at F3
700 enA	0.72696 mg/cm^2	30%	1.2 x 10^3 cps

The target and detection system were set at the focal plane of CRIB, as shown in Fig.1. The target was a gas mixture of ^{4}He+CO_2 (10%) at 140 Torr at room temperature filled in a chamber in which electrode structures of MSTPC and arrays of silicon detector telescopes were installed.

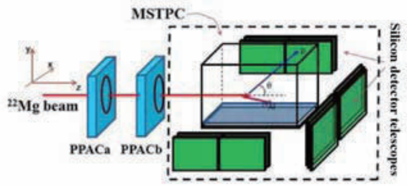

Fig 1. Setup of the ^{22}Mg(α,p)^{25}Al experiment.

The trajectory and timing information of incoming ^{22}Mg were obtained using the beam monitors for particle identification. The monitors also provided event-trigger signals. In the experiment, the events due to the elastic scattering ^{22}Mg(α,α)^{22}Mg or the ^{22}Mg(α,p)^{25}Al reaction were distinguished from those due to production of beam contaminants based on the Bragg curves of the outgoing ^{22}Mg and ^{25}Al, which were determined from the energy loss measured by the MSTPC, as shown in Fig. 2. On the other hand, protons and alphas were detected by the silicon detector telescopes.

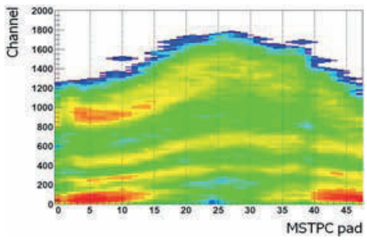

Fig 2. Energy loss spectra of ^{22}Mg, ^{21}Na, and ^{20}Ne in the gas target were measured by the MSTPC. A Bragg curve can be deduced from the spectra to obtain the events of interest.

The data analysis is underway. Extraction of the experimental cross section and R-matrix analysis[8)] to obtain the reaction rate will be performed in future.

References

1) J.L. Fisker et al: The Astrophys. J, L63 (2004).
2) M. Arnould et al: Astron. Astrophys, 64, 195-213 (1978).
3) T. Rauscher: http://nucastro.org/reaclib.html#ns_web.
4) http://dissertations.ub.rug.nl/faculties/science/2007/a.matic
5) T. Hashimoto et al: CNS Annual Rep., (2008) p.17.
6) S. Kubono et al: Eur. Phys. J, A 13 (2002), p. 217.
7) H.Yamaguchi et al: Nucl.Instrum.Meth. A589(2008) 150.
8) A. M. Lane et al: Rev. Mod. Phys. 30 (1958) 257.

2. Nuclear Physics (Theory)

Photoabsorption of ^{4}He using realistic nuclear interactions[†]

W. Horiuchi,[*1] Y. Suzuki,[*2*1] and K. Arai,[*3]

[Nuclear reaction, ab initio calculation, ^{4}He]

Nuclear strength or response functions of electroweak interactions provide us with important information on the resonant and continuum structures of the nuclear system as well as the detailed properties of the underlying interactions. In this report, we focus on the photoabsorption of ^{4}He. The experimental study of (γ, p) and (γ, n) reactions on ^{4}He has a long history spanning the last half century. Unfortunately, the experimental data presented so far are in serious disagreement[1,2]. We investigate this issue with a full four-body calculation using bare realistic interactions.

The photoabsorption of ^{4}He occurs mainly through the electric dipole ($E1$) transition, and the cross section $\sigma_\gamma(E_\gamma)$ can be calculated by the formula

$$\sigma_\gamma(E_\gamma) = \frac{4\pi^2}{\hbar c} E_\gamma \frac{1}{3} S(E_\gamma), \tag{1}$$

where $S(E)$ is the strength function for the $E1$ transition

$$S(E) = \boldsymbol{\mathcal{S}}_{\mu f} |\langle \Psi_f | \mathcal{M}_{1\mu} | \Psi_0 \rangle|^2 \delta(E_f - E_0 - E). \tag{2}$$

The symbol $\mathcal{M}_{1\mu}$ denotes the $E1$ operator, and Ψ_0 and Ψ_f are the wave functions of the ground state with energy E_0 and of the final state with the excitation energy E_f of ^{4}He, respectively. The symbol $\boldsymbol{\mathcal{S}}_{\mu f}$ indicates a summation over μ and all possible final states f. The recoil energy of ^{4}He is ignored, and as a result E_γ is equal to the nuclear excitation energy E.

The Hamiltonian consists of two- and three-body interactions. The kinetic energy of the center of mass motion is subtracted. As the NN potential, we employ Argonne $v8'$ (AV8$'$)[3] and G3RS[4] potentials that contain central, tensor, and spin-orbit terms. The reproduction of the two- and three-body thresholds is vital for a realistic calculation of $\sigma_\gamma(E_\gamma)$. For this purpose, we add a three-nucleon force (3NF) and adopt a purely phenomenological potential[5], which is determined such that it fits inelastic electron form factor from the ground state to the first excited state of ^{4}He as well as the binding energies of ^{3}H, ^{3}He, and ^{4}He.

The wave functions of the states are approximated through a combination of explicitly correlated Gaussians with double global vectors[6]. With this method, all the observed levels of ^{4}He below 26 MeV are well reproduced using bare realistic nuclear interactions[6,7]. The strength function is evaluated using the complex scaling method[8], which makes a continuum state that has an outgoing wave in the asymptotic region damp at large distances, thus enabling us to avoid an explicit construction of the continuum state.

We display in Fig. 1 the total photoabsorption cross section $\sigma_\gamma(E_\gamma)$. The two potentials give qualitatively the same results, although a careful examination reveals that the resonance energy and the width given by the AV8$'$+3NF potential are slightly smaller than those obtained with the G3RS+3NF potential. The calculation predicts a sharp increase in the photoabsorption cross section from the threshold, which is observed in several measurements[2,9], excluding the data of Ref.[1]. Our result is consistent with the other theoretical calculations[11,12] starting from the realistic interactions, particularly with regard to the cross section near the threshold. Our calculation is based on an *ab initio* calculation, and hence, we expect that the discrepancy observed in the low energy region will be resolved experimentally in the future.

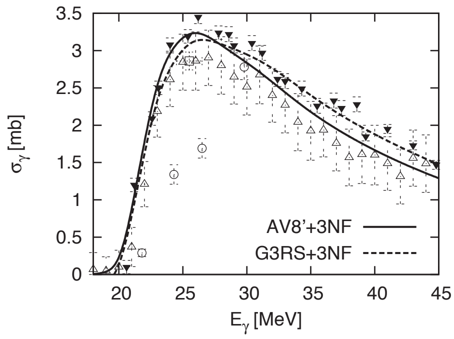

Fig. 1. Comparison of the photoabsorption cross section between the theory and the experiment. The threshold energy of ^{3}H+p is 19.82 MeV. The data are plotted as follows: closed triangle[9], open square[10], open circle[1], and open triangle[2].

References

1) T. Shima *et al.*, Phys. Rev. C **72**, 044004 (2005).
2) S. Nakayama *et al.*, Phys. Rev. C **76**, 021305 (2007).
3) B.S. Pudliner *et al.*, Phys. Rev. C **56**, 1720 (1997).
4) R. Tamagaki, Prog. Theor. Phys. **39**, 91 (1968).
5) E. Hiyama *et al.*, Phys. Rev. C **70**, 031001 (2004).
6) Y. Suzuki *et al.*, Few-Body Syst. **42**, 33 (2008).
7) W. Horiuchi and Y. Suzuki, Phys. Rev. C **78**, 034305 (2008).
8) S. Aoyama *et al.*, Prog. Theor. Phys. **116**, 1 (2006).
9) Yu.M. Arkatov *et al.*, Sov. J. Nucl. Phys. **10**, 639 (1970).
10) D.P. Wells *et al.*, Phys. Rev. C **46**, 449 (1992).
11) D. Gazit *et al.*, Phys. Rev. Lett. **96**, 112301 (2006).
12) S. Bacca, Phys. Rev. C **75**, 044001 (2007).

† Condensed from Phys. Rev. C **85**, 054002 (2012).
*1 RIKEN Nishina Center, Japan
*2 Department of Physics, Niigata University, Japan
*3 Division of General Education, Nagaoka National College of Technology, Japan

Role of the tensor interaction in He isotopes with a tensor-optimized shell model†

T. Myo,[*1] A. Umeya,[*2] H. Toki,[*3] and K. Ikeda

[Nuclear structure, Unstable nuclei, Tensor interaction, Tensor-optimized shell model]

The nucleon-nucleon (NN) interaction has distinctive features. There exist strong tensor interaction at intermediate distance caused by pion exchange and strong repulsion at a short distance caused by quark dynamics. It is important to investigate the nuclear structure in relation with the above characteristics of the NN interaction. Recently, we have been able to express the strong tensor correlation in a reasonable shell model space[1,2]. We name this method as Tensor Optimized Shell Model (TOSM), in which the wave function is constructed with full optimization of the two particle-two hole ($2p2h$) states involving the high momentum component induced by the tensor interaction[3]. The Unitary Correlation Operator Method (UCOM) is used to treat the short-range repulsion. We combine two methods, TOSM and UCOM to describe nuclei using bare interaction.

We have applied TOSM+UCOM to the He isotopes. The results using the bare AV8′ NN interaction are shown in Fig. 1. The excitation energy spectra reproduce the experiments[4] well, so that we can discuss the structure differences between energy levels. We report the detailed structures of ^{6}He, in particular, the effect of tensor interaction on the splitting energy between 0_1^+ and 0_2^+. In Table 1, we compare the Hamiltonian components in two 0^+ states of ^{6}He measured from those of ^{4}He. In the calculation, we take the length parameters of the hole states as 1.5 fm, which corresponds to the value of $\hbar\omega$ being 18.43 MeV. This is done to exclude the continuum effect in ^{6}He.

In Table 1, it is found that the 0_1^+ ground state has a larger tensor contribution than the 0_2^+ case. This is related to the large mixing of the $p_{1/2}$ component in ^{4}He caused by the tensor interaction[2,3]. When the last two neutrons occupy the $p_{3/2}$ orbit in ^{6}He, these neutrons do not disturb the ^{4}He structure so much. This causes the gain of the tensor contribution in ^{6}He(0_1^+), which enhances the kinetic energy because of the high momentum nature of the tensor interaction. In case of the $(p_{1/2})^2$ configuration in the 0_2^+ state, two neutrons are blocked to occupy the orbit owing to the excited $p_{1/2}$ neutron from the ^{4}He core by the tensor interaction. This Pauli-blocking effect does not increase the tensor contribution in ^{6}He(0_2^+) from that of ^{4}He. Those different couplings between ^{4}He and last neutrons explain the difference in the Hamiltonian components in two states of ^{6}He, and results in the splitting energy as a net value. There are same mechanisms seen in other He isotopes, which are discussed in our paper[5]. There is also the discussion of the effect of the genuine three-body force on the splitting energy in ^{5}He[6].

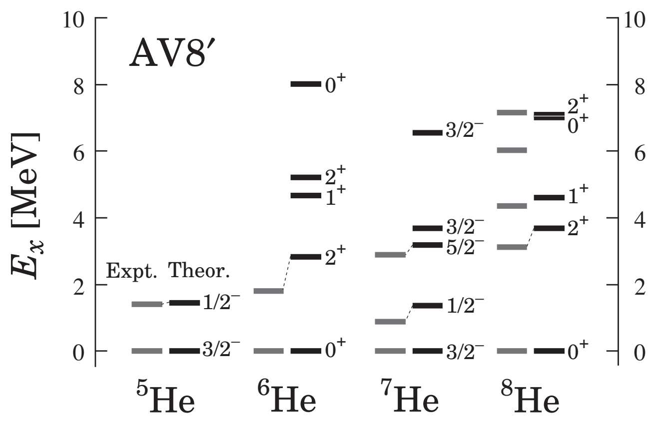

Fig. 1. Excitation energies of He isotopes with TOSM+UCOM.

Table 1. Various energy components in ^{6}He in comparison with ^{4}He. Units are given in MeV.

^{6}He(J^π)	E	Kinetic	Central	Tensor	LS
0_1^+	8.95	53.04	−27.75	−12.02	−4.04
0_2^+	21.90	34.30	−14.06	−0.17	2.11

† Condensed from the article in Phys. Rev. C**84**, 034315 (2011)

*1 General Education, Faculty of Engineering, Osaka Institute of Technology
*2 Human Science and Common Education, Faculty of Engineering, Nippon Institute of Technology
*3 Research Center for Nuclear Physics, Osaka University

References

1) T. Myo, S. Sugimoto, K. Kato, H. Toki and K. Ikeda, Prog. Theor. Phys.**117**, 257 (2007).
2) T. Myo, H. Toki and K. Ikeda, Prog. Theor. Phys.**121**, 511 (2009).
3) K. Ikeda, T. Myo, K. Katō and H. Toki, Lecture Notes in Physics **818** "Clusters in Nuclei" Vol. 1, pp165-221, Springer, (2010).
4) F. Skaza *et al.*, Nucl. Phys. A**788**, 260c (2007), and references therein.
5) T. Myo, A. Umeya, H. Toki and K. Ikeda, Phys. Rev. C**84**, 034315 (2011).
6) K. M. Nollett, S. C. Pieper, R. B. Wiringa, J. Carlson and G. M. Hale, Phys. Rev. C**99**, 022502 (2012).

RIA analysis of proton-elastic scattering from He isotopes

K. Kaki*1

[Nuclear reaction, RIA, unstable nuclei]

The author calculates observables of proton elastic scattering from the helium isotopes, and discusses relations between observables and nuclear distributions of the isotopes by comparison of the calculated results with experimental data. The calculations are based on relativistic impulse approximation (RIA) at incident proton energy: 71 MeV for ^{4,6,8}He, 300 and 500 MeV for ^{4}He, and 0.7GeV for ^{6}He. The present report, however, shows some of results for ^{8}He at 71 MeV.

The Dirac equation containing the optical potential is described in momentum space as follows:

$$\{\gamma^0 E - \boldsymbol{\gamma}\cdot\boldsymbol{p}' - m\}\ \Psi(\boldsymbol{p}') - \int \frac{d^3p}{(2\pi)^3}\ \hat{U}(\boldsymbol{p}',\boldsymbol{p})\ \Psi(\boldsymbol{p}) = 0, \qquad (1)$$

where $\Psi(\boldsymbol{p})$ is given by the Fourier transformation of the wave function in coordinate space.

In accordance with the prescription of the RIA[1], the optimal factorization is taken into account, the Dirac optical potential is given in the well-known $t\rho$ forms:

$$\hat{U}(\boldsymbol{p}',\boldsymbol{p}) = -\frac{1}{4}\mathrm{Tr}_2\left\{\hat{M}_{pp}(\boldsymbol{p},\frac{\boldsymbol{q}}{2}\to\boldsymbol{p}',\frac{\boldsymbol{q}}{2})\ \hat{\rho}_p(\boldsymbol{q})\right\} -\frac{1}{4}\mathrm{Tr}_2\left\{\hat{M}_{pn}(\boldsymbol{p},\frac{\boldsymbol{q}}{2}\to\boldsymbol{p}',\frac{\boldsymbol{q}}{2})\ \hat{\rho}_n(\boldsymbol{q})\right\}. \qquad (2)$$

where $\hat{\rho}_p$ and $\hat{\rho}_n$ are density matrices for protons and neutrons, respectively. The relativistic density matrix $\hat{\rho}$ depends only on the momentum transfer q, as follows;

$$\hat{\rho}(\boldsymbol{q}) = \rho_S(q) + \gamma_2^0\rho_V(q) - \frac{i\boldsymbol{\alpha}_2\cdot\boldsymbol{q}}{2m}\rho_T(q), \qquad (3)$$

where each term is a Fourier transformation of a coordinate-space density which is provided by the relativistic mean-field theory (RMFT)[2].

In the generalized RIA[1] the scalar Feynman amplitude consists of the direct and exchange parts, each of which represents a sum of four Yukawa terms characterized by coupling constants, masses and cutoff masses. In the present calculation, the IA2 parameterization of Ref.[1] is used.

Modified distributions are taken, which are obtained by compressing ($a < 1.0$) the proton and expanding ($a > 1.0$) neutron profiles in different way. Tab.1 shows the root-mean-square radius of the distributions, and the radius deduced from the charge radius[3]. In the table 'pa' means model distributions of ^{4}He core + four neutrons. The 1st number is the parameter 'a' for ^{4}He core, and 2nd one for four neutron.

Fig.1 shows differential cross section and analyzing power for proton-elastic scattering from ^{8}He at 71 MeV, corresponding to the Tab.1. It is seen that the model distribution of pa=0.85 with spreading neutrons reproduces differential cross section well though no distribution succeeds to predict the analyzing power data.

*1 Department of Physics, Shizuoka University

References

1) J.A.Tjon and S.J.Wallace, Phys.Rev.**C35** (1987) 280; Phys.Rev.**C36** (1987) 1085.
2) Y.Sugahara and H.Toki, Nucl.Phys.**A579** (1994) 557.
3) P. Mueller *et al.*, Phys. Rev. Lett. **99**, 252501 (2007).
4) S.Sakaguchi, Docroral Dissatation, Univ. of Tokyo, 2008

Table 1. Root-mean-square radius of proton and neutron for ^{8}He.

modified distribution	proton	neutron
pa=0.80/12	1.720	3.657
pa=0.85/11	1.792	3.396
pa=0.90/an	1.936	3.422
charge	1.808	-

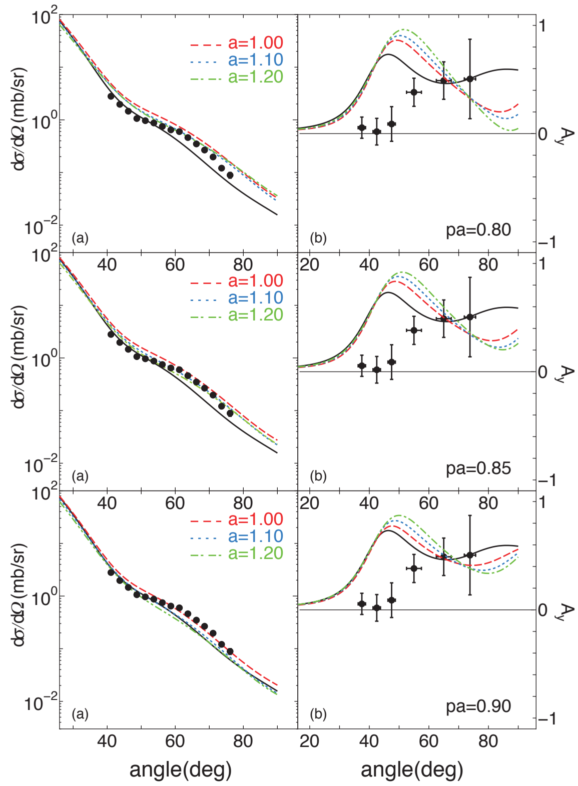

Fig. 1. Differential cross section and analyzing power for proton-elastic scattering from ^{8}He at 71 MeV. Dots are experimental data[4]. Solid lines are of RMFT density.

Energy dependence of K^--"pp" effective potential derived from coupled-channel Green's function

T. Koike and T. Harada[1]

In order to elucidate the nature of the antikaon-nucleon ($\bar{K}N$) interaction in high density nuclear matter, it is important to clarify whether the "deeply-bound kaonic nucleus" exists. In particular, the $[\bar{K} \otimes \{NN\}_{I=1}]_{I=1/2}$, $J^\pi = 0^-$ bound state, which is referred to as "K^-pp" here, is suggested to be the lightest and most fundamental kaonic nucleus. A new experimental search of K^-pp via the ^{3}He(in-flight K^-, n) reaction has been planned at J-PARC as an E15 experiment. We have theoretically discussed the expected spectra for the ^{3}He(in-flight K^-, n) reaction. We have assumed a phenomenological single-channel K^--"pp" (complex) effective potential between the K^- and the "pp"-core nucleus[1,2] having the form of

$$U^{\rm eff}(E;r) = (V_0 + i\,W_0\,f(E)\,)\exp[-(r/b)^2], \qquad (1)$$

where $f(E)$ is the phase space suppression factor of the $K^-pp \to \pi\Sigma N$ decay modes[3] and E is the energy measured from the K^-pp threshold.

In the single-channel framework, the energy-dependence of $U^{\rm eff}$ in Eq.(1) plays an important role in determining the spectrum shape[2]. Thus, the validity of our calculations relies in part on whether the energy dependence of Eq.(1) is appropriate. For this purpose, we have extended the previous K^-pp single channel description to the $\bar{K}(NN)$-$\pi(\Sigma N)$ coupled-channel (CC) description, because the energy dependence of Eq.(1) should originate from the elimination of the $\pi\Sigma N$ channel in such a CC scheme.

We investigate a single-channel K^--"pp" equivalent local potential $\tilde{U}^{\rm eff}$, which is derived from CC Green's functions for $K^-(pp)$-$\pi(\Sigma N)$ systems[4]. We find that the calculated Im $\tilde{U}^{\rm eff}$ becomes shallower as E approaches $K^-pp \to \pi\Sigma N$ decay threshold energy $\simeq -100$ MeV when no bound state exists in the $\pi(\Sigma N)$ channel, whereas the shape of $\tilde{U}^{\rm eff}$ is not precisely Gaussian, as is shown in Figure 1. Figure 2 shows the imaginary part, strength $W^{\rm eff}(E)$, corresponding to the Gaussian potential as a function of the energy E, which is deduced from $\tilde{U}^{\rm eff}$ with the help of the volume integrals. The results are as follows:

- If no bound state exists in the $\pi(\Sigma N)$ channel, Im $\tilde{U}^{\rm eff}$ approximates to the phase space factor $f(E)$ that is used in Eq.(1) near the $K^-pp \to \pi\Sigma N$ decay threshold, as indicated by the solid curve in Figure 2.
- If a bound state exists in the $\pi(\Sigma N)$ channel, the energy dependence of Im $\tilde{U}^{\rm eff}$ considerably differs from that of Eq.(1) owing to the modification of the phase volume via a pole that is located near the $\pi\Sigma N$ threshold, as shown by the dashed curve in Figure 2.

These energy dependences of $\tilde{U}^{\rm eff}$ are expected to have a significant influence on the extraction of the binding energy and width of the K^-pp state from the experimental spectrum.

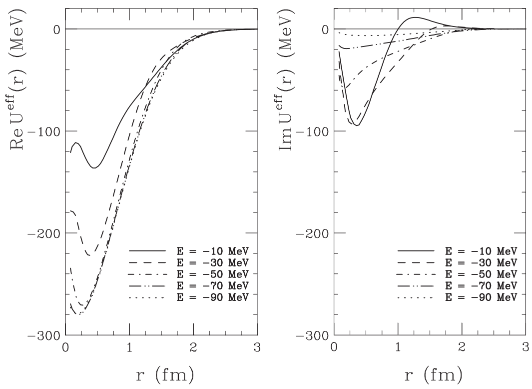

Fig. 1. Real (left) and imaginary (right) parts of the equivalent local potential $\tilde{U}^{\rm eff}$ for the K^--"pp" channel in the case that the binding energy and width of K^-pp are consistent with those calculated in Ref.[5]. The energy E, which is measured from the K^-pp threshold, is varied from -10 MeV to -90 MeV.

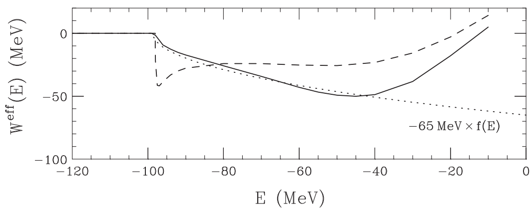

Fig. 2. Energy dependence of the imaginary part $W^{\rm eff}(E)$ of the K^--(pp) equivalent local potential $\tilde{U}^{\rm eff}$. The solid and dashed lines denote the cases when the $\pi(\Sigma N)$ channel has a bound state and no bound state, respectively. The dotted line denotes the fitted curve of $W_0 \times f(E)$ of Eq.(1).

References
1) T. Koike and T. Harada, Phys. Lett. **B652**, 262 (2007).
2) T. Koike and T. Harada, Phys. Rev. **C80**, 055208 (2009).
3) J. Mareš, E. Friedman and A. Gal, Phys. Lett. **B606**, 295 (2005).
4) T. Koike and T. Harada, Hyperfine Interact **210**, 80 (2012)
5) T. Yamazaki and Y. Akaishi, Phys. Lett. **B535**, 70 (2002).

*1 Research Center for Physics and Mathematics, Osaka Electro-Communication University

s-shell Λ-hypernuclei with ΛN-ΣN coupling

A. Umeya,[*1] T. Myo,[*2] and E. Hiyama

[Nuclear structure, Hypernuclei, ΛN-ΣN coupling interaction]

One of the purposes of hypernuclear study is to obtain information on baryon-baryon interaction from the structures of hypernuclei. For this purpose, high-resolution γ-ray experiments have been performed. By combining the data and the theoretical studies, we succeeded in extracting information about spin-dependent terms such as spin-spin and spin-orbit forces of the ΛN interaction. The present work is focused on the study of ΛN-ΣN coupling interaction, whose properties are still an open question in hypernuclear physics.

For investigating the ΛN-ΣN coupling, many authors studied the structure of ${}^4_\Lambda$H, ${}^4_\Lambda$He, and ${}^5_\Lambda$He by taking the ΛN-ΣN coupling explicitly. Furthermore, at the J-PARC facility, production of neutron-rich hypernuclei such as ${}^6_\Lambda$H and ${}^9_\Lambda$He has been planned. In addition, an experiment has been performed to produce ${}^7_\Lambda$He at Jefferson Laboratory.

The aim of the present work is to perform *ab initio* like calculations for neutron-rich hypernuclei with realistic interactions, including the ΛN-ΣN coupling, using the tensor-optimized shell model (TOSM).[1] TOSM is based on the shell model, and can explicitly take into account the tensor force of NN and YN interactions. A TOSM wave function is constructed with $2p2h$ states involving the high-momentum component induced by tensor interaction. Also, the Unitary Correlation Operator Method (UCOM)[2] is used in the TOSM framework to treat short-range correlation. In UCOM, a shift operator is introduced for every nucleon pair and nucleon-hyperon pair in hypernuclei in order to reduce the short-range amplitude of the relative pair wave functions. We initiate this study by focusing on s-shell Λ-hypernuclei of ${}_\Lambda$H and ${}_\Lambda$He isotopes, and we calculate the energy spectra of ${}^4_\Lambda$H and ${}^5_\Lambda$He.

In this report, we consider the $0s_{1/2}$ orbit for both nucleons and the Λ hyperon states as the hole states. For the particle states, we consider $l_{\max} = 14$ in the energy variation calculation, where $l_{\max}$ is the maximum number of orbital angular momenta and determines the model space of TOSM. We employ the AV8′ potential[3] for the NN interaction. We employ the ΛN, ΣN, and ΛN-ΣN potentials with central, spin-orbit, and tensor terms[4] that simulate the scattering phase shifts given by NSC97f.[5]

Figure 1 shows the Λ separation energies B_Λ in the ${}^4_\Lambda$H (0^+), ${}^4_\Lambda$H (1^+), and ${}^5_\Lambda$He $(1/2^+)$ states. For the ${}^4_\Lambda$H states, we compare our results with few-body calculations[6] with the same potentials as those used in our work. For the ${}^5_\Lambda$He state, we compare our results with those in Ref. 7, in which the G3R3 potential[8] is used for the NN interaction. In the present calculation, our results do not reflect sufficient binding energies and show that the ${}^4_\Lambda$H (1^+) and ${}^5_\Lambda$He $(1/2^+)$ states are unbound.

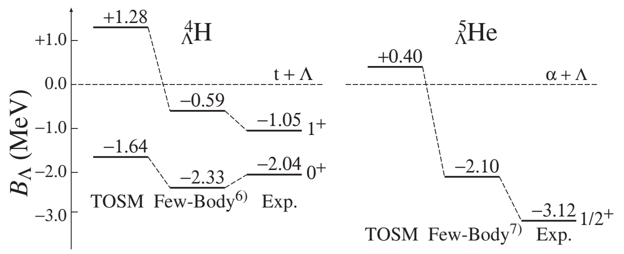

Fig. 1. Calculated Λ separation energies B_Λ in the ${}^4_\Lambda$H (0^+), ${}^4_\Lambda$H (1^+), and ${}^5_\Lambda$He $(1/2^+)$ states, together with the few-body calculation results[6,7] and experimental data. Energy is measured from the t + Λ (α + Λ) threshold in ${}^4_\Lambda$H (${}^5_\Lambda$He).

We are considering the following improvements to obtain sufficient binding energies. First, we intend to extend the model space of TOSM. In the present calculation, the model space with $l_{\max} = 14$ is not enough to obtain sufficient energy convergence. Second, we can vary the parameters of the shift operators of UCOM in order to determine their most suitable values. In the present calculation, the parameters of the shift operators for the YN relative states are same as those for the NN relative states. However, the few-body calculations[6] for the ${}^5_\Lambda$He $(1/2^+)$ state suggest that the correlation function in the YN interaction is different from that in the NN interaction, especially for the short-range region. This implies that the parameters of the shift operators of UCOM for the YN relative state should be determined independently. With these improvements, our calculation may yield sufficient binding energies for s-shell Λ-hypernuclei.

*1 Human Science and Common Education, Faculty of Engineering, Nippon Institute of Technology
*2 General Education, Faculty of Engineering, Osaka Institute of Technology

References

1) T. Myo *et al.*: Prog. Theor. Phys. **117**, 257 (2007).
2) H. Feldmeier *et al.*: Nucl. Phys. A **632**, 61 (1998).
3) B.S. Pudliner *et al.*: Phys. Rev. C **56**, 1720 (1997).
4) S. Shinmura (private communications).
5) Th.A. Rijken *et al.*: Phys. Rev. C **59**, 21 (1999).
6) E. Hiyama *et al.*: Phys. Rev. C **65**, 011341(R) (2001).
7) H. Nemura *et al.*: Phys. Rev. Lett. **89**, 142504 (2002).
8) R. Tamagaki: Prog. Theor. Phys. **39**, 91 (1968).

Four-body resonances of ^{7}B using the complex scaling method†

T. Myo,*1 Y. Kikuchi,*2 and K. Katō,*3

[Nuclear structure, Unstable nuclei, Cluster model, Resonance, Mirror symmetry]

Recently, the new experiment on ^{7}B has been reported[1]. The ^{7}B nucleus is known as an unbound system beyond the proton drip-line and can decay not only to two-body ^{6}Be+p channels, but also to many-body channels of ^{5}Li+2p and ^{4}He+3p.

In this report, we present our recent study on the resonance spectroscopy of ^{7}B. We employ the cluster-orbital shell model (COSM) of the ^{4}He+p+p+p four-body system, and describe the many-body resonances under the correct boundary conditions by using the complex scaling method. We adopt the Hamiltonian, the nuclear part of which reproduces the ^{4}He-n scattering data and the ^{6}He energy[2,3]. The mirror nucleus of ^{7}B is ^{7}He, which is also an unbound system with respect to the one-neutron emission. It is interesting to examine the mirror symmetry between ^{7}B and ^{7}He.

We show the level structures of ^{5}Li, ^{6}Be and ^{7}B in Fig. 1. It is found that the present calculations agree with the observations and predict more energy levels.

For ^{7}B, we evaluate the S-factors of the ^{6}Be-p components to examine the coupling behavior between ^{6}Be and a last proton, where the 0^+_1 and 2^+_1 states of ^{6}Be are chosen. To compare the structures of ^{7}B and ^{7}He, we obtain the S-factors of the ^{6}He-n components of ^{7}He. The S-factors are shown in Fig. 2. In the $3/2^-$ ground states of ^{7}B and ^{7}He, the sizable difference between the A=6(2^+_1) components is seen. The other four excited states of two nuclei show the similar values. These results indicate that the mirror symmetry is broken only in the ground states of ^{7}B and ^{7}He, while the excited states of two nuclei keep the symmetry. The reason of the different 2^+ coupling is that the ^{7}B ground state is located closely to the ^{6}Be(2^+_1)+p decaying channel by 0.45 MeV, as shown in Fig. 1. In ^{7}He, on the other hand, the corresponding energy difference between ^{7}He($3/2^-_1$) and ^{6}He(2^+_1)+n channel is 1.46 MeV[3], larger than the case of ^{7}B. The small energy difference between ^{7}B and ^{6}Be(2^+_1) enhances the ^{6}Be(2^+_1)-p component in ^{7}B as the coupling to the open channel of ^{6}Be(2^+_1)+p. The origin of the small energy difference between two states is the Coulomb repulsion, which shifts the entire energies of the ^{7}B states up.

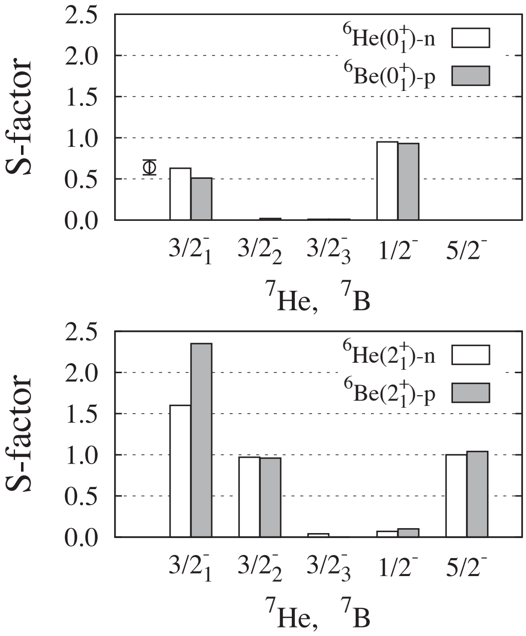

Fig. 2. S-factors of ^{7}B and ^{7}He, in which the daughter nuclei are the 0^+_1 (upper) and 2^+_1 (lower) states. The open circle is the experiment of the ^{7}He($3/2^-$) state[4].

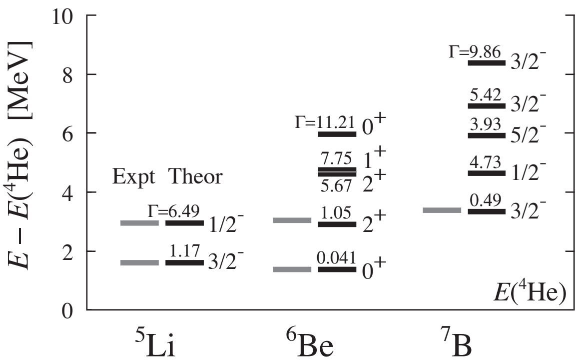

Fig. 1. Energy levels of ^{5}Li, ^{6}Be and ^{7}B measured from the threshold energy of ^{4}He and valence nucleons. Units are in MeV. Black and gray lines are theory and experiments, respectively. Small numbers are decay widths.

References
1) R. J. Charity *et al.*: Phys. Rev. C**84**, 014320 (2011).
2) T. Myo, R. Ando and K. Katō: Phys. Rev. C**80**, 014315 (2009).
3) T. Myo, R. Ando and K. Katō: Phys. Lett. B**691**, 150 (2010).
4) F. Beck *et al.*: Phys. Lett. B**645**, 128 (2007).

† Condensed from the article in Phys. Rev. C**84**, 064306 (2011)

*1 General Education, Faculty of Engineering, Osaka Institute of Technology
*2 Research Center for Nuclear Physics, Osaka University
*3 Graduate School of Science, Hokkaido University

Structure of ${}^{10}_{\Lambda}$Be studied with the four-body cluster model†

Y. Zhang,*1 E. Hiyama,*1 and Y. Yamamoto*1

[Hypernucleus, energy spectrum, cluster models]

Recently, at the Thomas Jefferson National Accelerator Facility (JLab), search experiments were performed for p-shell and sd-shell hypernuclei by $(e, e'K^+)$ reactions on the targets ^{7}Li, ^{10}B, etc. The structure of ${}^7_\Lambda$He has been studied in close relation to the ^{7}Li $(e, e'K^+){}^7_\Lambda$He experiment[1]. In the present work, we investigate the structure of ${}^{10}_\Lambda$Be related to the ^{10}B $(e, e'K^+){}^{10}_\Lambda$Be experiment to predict the energy spectrum of ${}^{10}_\Lambda$Be up to the $\alpha+\alpha+n+\Lambda$ threshold. In the core nucleus ^{9}Be, the ground state is the only bound state of the $\alpha+\alpha+n$ three-body system, and all the excited states lie above the three-body threshold as resonant states. When a Λ particle is attached to these three-body states, it is expected that the resultant four-body states are more stable than the parent three-body states due to the glue-like role of the Λ particle. As a result, there should be some bound states and sharp resonant states below the $\alpha+\alpha+\Lambda+n$ four-body threshold in ${}^{10}_\Lambda$Be.

The $\alpha+\alpha+N+\Lambda$ four-body problem is solved by using the Gaussian Expansion Method (GEM)[2,3], where the Pauli principle between nucleons belonging to two α clusters is taken into account by using the orthogonality condition model (OCM). The interactions $V_{\Lambda N}$, $V_{N\alpha}$ and $V_{\alpha\Lambda}$ that we take are the same as those in Ref.[1] For $V_{\alpha\alpha}$, we employ the potential that has often been used in the OCM-based cluster-model study of light nuclei, with a phenomenological $\alpha\alpha n$ three-body force as in Ref.[4].

In Fig. 1, we show the calculated energy spectra of ${}^{10}_\Lambda$Be and the core nucleus ^{9}Be. The ground state of ^{9}Be is bound by 1.58 MeV below the $\alpha+\alpha+n$ three-body threshold. Owing to the additional Λ particle, the corresponding ground state of ${}^{10}_\Lambda$Be becomes rather deeply bound, by about 4 MeV, and it is split into the doublet states 1^- and 2^- due to the ΛN spin-spin interaction. Furthermore, the $5/2^-$ and $1/2^+$ resonant states of ^{9}Be become bound (3^-, 2^-_2, 0^+ and 1^+_1 states in ${}^{10}_\Lambda$Be) due to the attraction between Λ and the ^{9}Be core. It is interesting to see that the order of the (3^-, 2^-_2) and (0^+, 1^+_1) doublets is reversed from ^{9}Be to ${}^{10}_\Lambda$Be. This is because the energy gain due to the addition of the Λ particle is larger in the compactly coupled state ($5/2^-$) than in the loosely coupled state ($1/2^+$).

Above the ${}^9_\Lambda$Be$+n$ threshold, we find several resonant states. Here, these states are obtained by the bound state approximation, that is, by taking the lowest eigenstate of the Hamiltonian for each spin-parity state. Just above the ${}^9_\Lambda$Be$+n$ threshold, there appear four lower states 1^-_2, 0^-, 2^+_1 and 3^+. For the 1^-_2 and 0^- states, the dominant configuration is ^{9}Be$(1/2^-)+\Lambda(0s)$. About 0.2 MeV above, we have the 2^+_1 state and 3^+ states, whose configuration is ^{9}Be$(5/2^+)+\Lambda(0s)$. The parent state ^{9}Be$(1/2^-)$ of the former states lies at almost the same position as the parent state ^{9}Be$(5/2^+)$ of the latter states. However, we find that the energy gain of the resultant 1^-_2 and 0^- is larger than that of the 3^+ and 2^+_1 states because of Λ-core attraction. This is considered to be because the structure of the negative parity states in ^{9}Be is more compact than that of the positive parity states. There appear four higher states, 2^-_3, 1^-_3, 1^+_2 and 2^+_2, about 4 MeV below the $\alpha+\alpha+n+\Lambda$ four-body breakup threshold. The dominant configuration of the 2^-_3 and 1^-_3 states is ^{9}Be$(3/2^-_2)+\Lambda(0s)$, and that of the 1^+_2 and 2^+_2 states is ^{9}Be$(3/2^+)+\Lambda(0s)$. Calculations are in progress to identify the states that could be produced by the ^{10}B$(e, e'K^+){}^{10}_\Lambda$Be reaction.

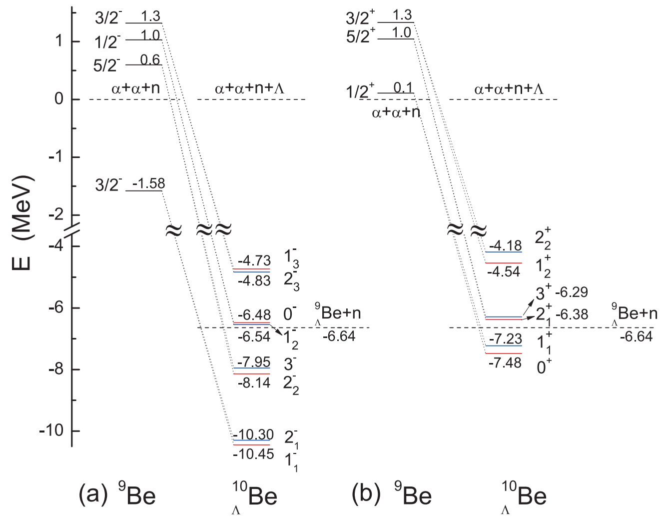

Fig. 1. Calculated energy spectra of the (a) low-lying negative parity states and (b) low-lying positive parity states of ${}^{10}_\Lambda$Be together with those of the core nucleus ^{9}Be.

References

1) E. Hiyama, Y. Yamamoto, T. Motoba and M. Kamimura, Phys. Rev. C **80**, 054321 (2009).
2) M. Kamimura, Phys. Rev. A **38**, 621 (1988).
3) E. Hiyama, Y. Kino and M. Kamimura, Prog. Part. Nucl. Phys. **51**, 223 (2003).
4) E. Hiyama, M. Kamimura, Y. Yamamoto and T. Motoba, Phys. Rev. Lett. **104**, 212502 (2010).

† Condensed from the article published in Nucl. Phys. **A 881** 288-297 (2012)

*1 Nishina Center for Accelerator-Based Science, RIKEN

Rotational structure of $\alpha + {}^{12}\mathrm{C}(0_2^+)$ and 4α-particle condensate

Y. Funaki, T. Yamada,[*1] S. Ohkubo,[*2] H. Horiuchi,[*3] G. Röpke,[*4] P. Schuck[5] and A. Tohsaki[*3]

[Nuclear structure, Cluster model, Alpha particle]

It is established that α-clustering plays an important role in the structure of light nuclei.[1] Several papers[2–5] have shown that the Hoyle state, the second 0^+ state in ^{12}C, having only about one-third of the saturation density can be described to a good approximation as a product state of three α-particles condensed into the lowest mean field $0S$-orbit.[4,6] The concept of α-particle condensation has been extended to ^{16}O, and the 4α-particle condensate state was recently investigated by the present authors. In the study presented in Ref.7, we utilized the 4α Orthogonality Condition Model (OCM) and solved the four-body problem in a large model space of 4α-particles. We found the sixth 0^+ state to be a candidate for the 4α-codensate state, which has a large occupation probability of 61% in a single-α orbit. The 0_6^+ state was also shown to have a large component of the $\alpha+$ Hoyle state, indicating that the state can be regarded as the analog to the Hoyle state.

In this short study, we investigate the non-zero spin excited states in ^{16}O, which are analogous to the Hoyle state, i.e., family members of the 0_6^+ state. Calculations are performed with the 4α OCM, which has also been considered in Ref.7.

On the basis of the calculations, we found that some states characteristically have a large component of the $\alpha+$ Hoyle state, where the α-particle orbits around the Hoyle state in S, P, D, F, and G waves for $J^\pi = 0^+, 1^-, 2^+, 3^-$, and 4^+, respectively. In Fig. 1, we show the energy spectra as a function of $J(J+1)$. Naturally one can suppose that these states form rotational bands between the Hoyle state and α-particle, i.e., $K^\pi = 0^+$ for the positive parity states and $K^\pi = 0^-$ for the negative parity states. It is further interesting to see that the 0_6^+ state at 16.5 MeV strays off the $J(J+1)$ rotational line and gets more strongly bound. This indicates that it has a structure that is rather different from that of the other rotational members. One can say that when the α-particle rotates around the Hoyle state in an S-wave, it seems to drop into the S-orbit, which is already occupied by the three α-particles in the Hoyle state, leading to the 0_6^+ state gaining energy. This might be interpreted as a transition from the local condensate to the complete condensate (also see Ref. 8). On the other hand, above the 0_6^+ state, we found four states that have relatively large S-factors in a channel of the $\alpha+$ Hoyle state (see the crosses in Fig. 1). They could be the bandhead of the $\alpha+$ Hoyle rotational band. They were fragmented and the average excitation energy was pushed up above the rotational line because of the existence of the 0_6^+ state and since the two configurations, those of the 4α-condensate and the $\alpha+$ Hoyle rotation, cannot be orthogonal to each other. This novel interpretation of these states should be confirmed through experiments in a future study.

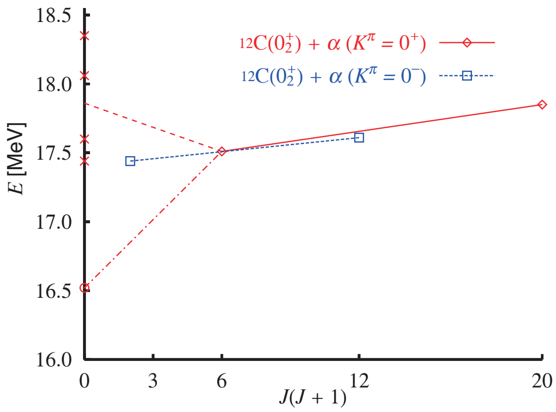

Fig. 1. (Color online) Rotational band of the $\alpha+$ Hoyle state. The dotted line originates from the average excitation energy of the four 0^+ states above the 0_6^+ state at 16.5 MeV, which are denoted by crosses and have rather large $\alpha+$ Hoyle state components.

References

1) K. Wildermuth and Y. C. Tang, *A Unified Theory of the Nucleus* (Vieweg, Braunschweig, 1977).
2) A. Tohsaki *et al.*, Phys. Rev. Let. **87**, 192501 (2001).
3) Y. Funaki *et al.*, Phys. Rev. C **67**, 051306(R) (2003); **80**, 064326 (2009); Eur. Phys. J. A **24**, 321 (2005)
4) T. Yamada *et al.*, Euro. Phys. J. A **26**, 185 (2005).
5) M. Chernykh *et al.*, Phys. Rev. Lett. **98**, 032501(2007); **105**, 022501 (2010).
6) H. Matsumura *et al.*, Nucl. Phys. A **739**, 238 (2004).
7) Y. Funaki *et al.*, Phys. Rev. Lett. **101**, 082502 (2008).
8) S. Ohkubo and Y. Hirabayashi, Phys. Lett. B **684**, 127 (2010).

[*1] Laboratory of Physics, Kanto Gakuin University, Yokohama 236-8501, Japan
[*2] Department of Applied Science and Environment, University of Kochi, Kochi 780-8515, Japan
[*3] Research Center for Nuclear Physics (RCNP), Osaka University, Osaka 567-0047, Japan
[*4] Institut für Physik, Universität Rostock, D-18051 Rostock, Germany
[*5] Institut de Physique Nucléaire, CNRS, UMR 8608, Orsay, F-91406, France

Proton inelastic diffraction by a black nucleus and the size of excited nuclei†

K. Iida,*1 S. Koide,*1 A. Kohama, and K. Oyamatsu*2

[Nuclear reaction, proton inelastic scattering, nuclear radius, black-sphere model]

The size of an atomic nucleus is one of the most fundamental quantities that characterize matter in these nuclei. It is well known for β stable nuclei in the ground state thanks to systematic measurements of electron and proton elastic differential cross sections.[1] This helps clarify the equation of state of nuclear matter near the saturation point[2]. For excited states of β stable nuclei, however, it is not straightforward to deduce the nuclear size, because elastic scattering off an excited target is hard to measure. Alternatively, one can use proton *in*elastic differential cross sections in deducing the size of excited nuclei, but all one may be able to determine is the transition density, which implicitly reflects only the density distribution of the excited nuclei.[3]

As a feasibility study, we apply the black-sphere picture to the analyses of proton inelastic scattering data for $T_p \sim$1000 MeV and systematically derive a length scale characterizing the size of a low-lying β stable nucleus using the empirical data for the diffraction peak angle in the proton inelastic differential cross section at an incident energy of $\sim$1000 MeV. Basically, this approach is a straightforward extension of the case of proton elastic scattering,[4] which is closely related to the method developed by Blair[5] for alpha scattering by assuming elastic diffraction by a circular black disk of radius R_0 and inelastic diffraction by a black nucleus with small multipolar deformations from a sphere of radius R_0. We allow this radius to change from R_0, define it as a_l for the excited state with spin l, and derive a_l by comparing the inelastic diffraction patterns obtained in the Fraunhofer approximation with the experimental ones. Note that the resulting black-sphere radius does not correspond to the size of the nucleus excited by the incident proton, but rather is related to the transition density and is hence expected to lie between the sizes in the ground and excited states. Even so, systematic derivation of the black-sphere radius from the inelastic channels is useful for predicting how the size in the excited state depends on the excitation energy $E_{\rm ex}$.

In the present analysis, we focus on even-even nuclei. We find that for ^{12}C, ^{58,60,62,64}Ni, and ^{208}Pb, the value of a_l obtained from the inelastic channel is generally larger than that obtained from the elastic channel and tends to increase with $E_{\rm ex}$, with a few exceptions in which case the black-sphere radius decreases with $E_{\rm ex}$ in its central value but can be regarded as unchanged, allowing for error bars. This is consistent with the behavior of the transition radii obtained systematically from the electron inelastic scattering off ^{208}Pb.[7] The increase is remarkable for the Hoyle state (Fig. 1), a feature consistent with the alpha clustering picture.[3] We hope that the present analysis could develop into a systematic drawing of the black-sphere radii of isomers and nuclei in other characteristic excited states over a chart of the nuclides.

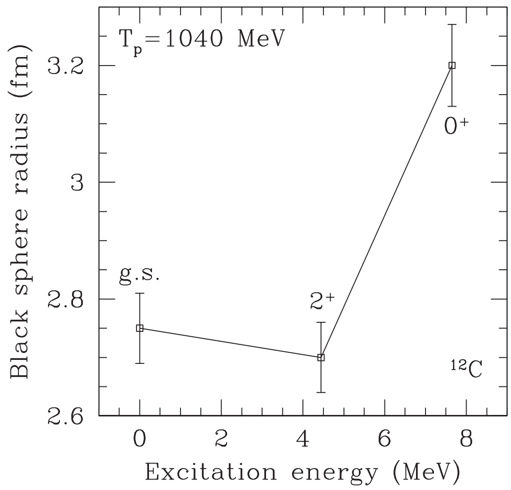

Fig. 1. The black-sphere radius of ^{12}C, obtained from the data in Ref.[6], as a function of the excitation energy.

† Condensed from the article in Mod. Phys. Lett. A **27**, 1250020 (2012).

*1 Department of Natural Science, Kochi University
*2 Department of Human Informatics, Aichi Shukutoku University

References

1) C.J. Batty *et al.*: Adv. Nucl. Phys. **19**, 1 (1989).
2) K. Oyamatsu and K. Iida: Prog. Theor. Phys. **109**, 631 (2003).
3) M. Takashina: Phys. Rev. C **78**, 014602 (2008).
4) A. Kohama, K. Iida, and K. Oyamatsu: Phys. Rev. C **72**, 024602 (2005).
5) J.S. Blair: Phys. Rev. **115**, 928 (1959).
6) R. Bertini *et al.*: Phys. Lett. **45B**, 119 (1973).
7) J. Friedrich, N. Voegler, and H. Euteneuer: Phys. Lett. **64B**, 269 (1976).

Shape fluctuations in the ground and excited 0^+ states of ^{30,32,34}Mg†

N. Hinohara,[*1] K. Sato, K. Yoshida,[*2] T. Nakatsukasa, M. Matsuo,[*2] and K. Matsuyanagi[*3]

[Nuclear structure, collective model, unstable nuclei]

Currently, the low-lying states of neutron-rich nuclei with N of around 20 are attracting considerable interest, because the spherical configurations associated with the neutron magic number disappear in the ground states. The increase in the $E(4_1^+)/E(2_1^+)$ energy ratio and $B(E2; 2_1^+ \to 0_1^+)$ from ^{30}Mg to ^{34}Mg indicate a quantum transition from spherical to deformed shapes taking place around ^{32}Mg. Excited 0^+ states were found in ^{30}Mg and ^{32}Mg in the recent experiments[1,2], and the clarification for the nature of the low-lying states using microscopic theories is challenging. The excited 0_2^+ state of ^{30}Mg is interpreted as a prolate state that coexists with the spherical ground state, while the 0_2^+ state of ^{32}Mg is suggested as a spherical state coexisting with the deformed ground state. However, the available calculations overestimate the excitation energy of ^{32}Mg.

We investigated the large-amplitude collective dynamics of shape phase transition in the low-lying states of $^{30-36}$Mg by solving the collective Schrödinger equation. The collective masses and potential of the five-dimensional quadrupole collective Hamiltonian were microscopically derived using the constrained Hartree-Fock-Bogoliubov plus local quasiparticle random-phase approximation (CHFB+LQRPA) method[3].

Figure 1 shows a comparison of the calculated excitation energies with the experimental data. The lowering of the excitation energies of the 2_1^+ and 4_1^+ states from ^{30}Mg to ^{34}Mg is well clarified in this calculation. The properties of the 2_1^+ and 4_1^+ states gradually change from vibrational to rotational with increasing neutron number. The calculated excitation energies of the 0_2^+ states are 1.353 and 0.986 MeV for ^{30}Mg and ^{32}Mg, respectively, which are in fair agreement with the experimental data[1,2]. In particular, the very low excitation energy of the 0_2^+ state in ^{32}Mg is well reproduced.

We have investigated the probability densities of finding a shape with a specific value of β. In the ground states from ^{30}Mg to ^{34}Mg, the peak position moves towards a larger value of β, which indicates the development of quadrupole deformation. The distribution for ^{32}Mg is much broader than those for ^{30}Mg and ^{34}Mg. The probability densities of the excited 0_2^+ states are composed of two bumps. In ^{30}Mg, the bump at the small deformation, which corresponds to the spherical configuration, is considerably smaller than the major bump around $\beta \approx 0.3$. Thus, we can regard the 0_2^+ state of ^{30}Mg to be a prolately deformed state, and the shape coexistence picture where the deformed excited 0^+ state coexists with the spherical ground state approximately holds in ^{30}Mg. In the case of ^{32}Mg, the probability density of the excited 0^+ state exhibits a very broad distribution extending from the spherical to deformed regions up to $\beta \approx 0.5$, with a prominent peak at $\beta \approx 0.3$. The range of the shape fluctuation in the 0_2^+ state in β direction is almost the same as that in the 0_1^+ state. Thus, the result of our calculation yields a physical picture for the 0_2^+ state in ^{32}Mg that is quite different from the interpretation of a "spherical excited state" based on the inversion picture of the spherical and deformed configurations.

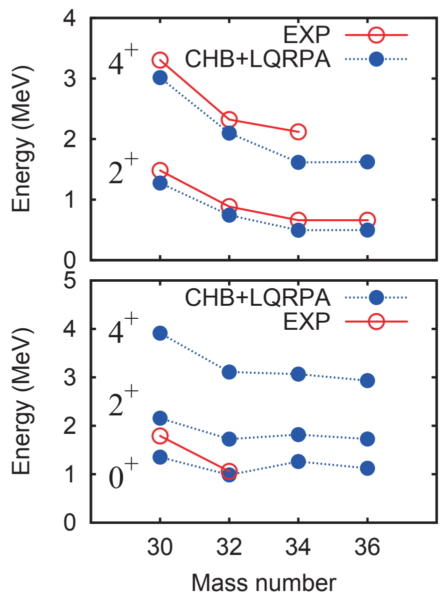

Fig. 1. Comparison of calculated excitation energies with experimental data. The upper panel shows the excitation energies of the 2_1^+ and 4_1^+ states, and the lower one shows those of the 0_2^+, 2_2^+, and 4_2^+ states.

† Condensed from the article in Phys. Rev. C **84**, 061302 (2011)
*1 Department of Physics and Astronomy, University of North Carolina at Chapel Hill, USA
*2 Department of Physics, Faculty of Science, Niigata University
*3 Yukawa Institute for Theoretical Physics, Kyoto University

References
1) W. Schwerdtfeger et al.: Phys. Rev. Lett. **103**, 012501 (2009).
2) K. Wimmer et al.: Phys. Rev. Lett. **105**, 252501 (2010).
3) N. Hinohara et al.: Phys. Rev. C **82**, 064313 (2010).

Neutron-skin effects on pygmy dipole resonances

T. Inakura,*1

[Nuclear structure, RPA, unstable nuclei]

Electric dipole ($E1$) excitation has been used as an important tool for investigating a nuclear structure. The low-lying $E1$ excitation, which is often called pygmy dipole resonances (PDR), is sensitive to nuclear properties at the nuclear surface and at a low density. Thus, the observed properties of the PDR may provide us with information on the neutron skin or halo.

From the theoretical aspect, many microscopic studies are conducted to investigate the nature of the PDR. However, different models predict different pictures. Piekarewicz[1)] showed that the calculated PDR strength is strongly correlated with the neutron skin thickness. In contrast, Reinhard and Nazarewicz[2)] suggested a very weak correlation between the skin thickness and the PDR strength by using a covariance analysis, which investigates the parameter dependence of various properties. However, these conclusions were drawn from calculations for only several spherical nuclei. It is thus desirable to perform a systematic calculation for the PDR for spherical and deformed nuclei, to reveal the correlation.

We have carried out ax systematic calculation of the $E1$ responses using the fully self-consistent random phase approximation (RPA) with the Skyrme interaction in the three-dimensional coordinate representation. The calculation was performed for even-even nuclei up to zirconium isotopes from the proton drip-line to neutron drip-line nuclei[3)].

First, we define the PDR strength fraction

$$f_{\rm PDR} = \frac{\int_0^{10{\rm MeV}} d\omega\, \omega S(\omega;\hat{D})}{\int_0^{\infty} d\omega\, \omega S(\omega;\hat{D})}, \qquad (1)$$

where $S(\omega;\hat{D}) = \sum_{n\in{\rm RPA}} |\langle n|\hat{D}|0\rangle|^2 \delta(\omega - E_n)$ is the $E1$ strength. This is equal to the ratio of the cross section for less than 10 MeV to the total photoabsorption cross section. In Fig.1, we plot the PDR fraction $f_{\rm PDR}$ as a function of the neutron skin thickness, defined by the difference in the radius of neutrons and protons: $\Delta R_{\rm rms} = \sqrt{\langle r_n^2\rangle} - \sqrt{\langle r_p^2\rangle}$. The $f_{\rm PDR}$ in each isotopic chain shows a linear correlation with the $\Delta R_{\rm rms}$ in the specific region of neutron number $N = 28 - 34$ and $N > 50$. Although the position of the kinks depends on the isotopic chain, the slopes have an almost universal value for all isotopes in the range of 0.18∼0.20 fm^{-1}.

Next, we discuss the parameter dependence of the correlation between the PDR and the skin thickness

*1 Theoretical Nuclear Physics Laboratory, RIKEN Nishina Center

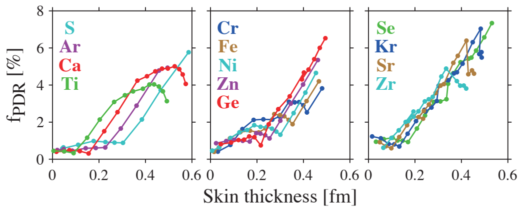

Fig. 1. Calculated PDR strength fraction as a function of the neutron skin thickness.

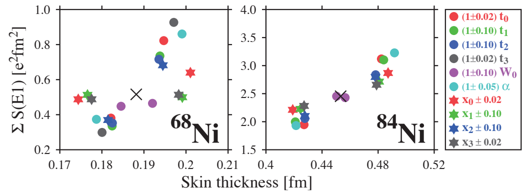

Fig. 2. Parameter dependence of the correlation in ^{68}Ni and ^{84}Ni between PDR strength and skin thickness.

$\Delta R_{\rm rms}$. Although Ref.[2)] showed a weak parameter dependence of the correlation, the calculated nucleus ^{68}Ni ($\Delta R_{\rm rms} = 0.19$ fm) is not located in the region ($N > 50$), where the linear correlation appears. To confirm and investigate the parameter dependence of the linear correlation, we perform a simple but similar analysis for ^{68}Ni and ^{84}Ni. We slightly modified each parameter value for every 10 parameters of the Skyrme interaction, and the subsequently calculated PDR strengths are shown in Fig. 2. The calculated points for ^{68}Ni are scattered around the cross symbol obtained with the original SkM* interaction. This indicates a weak correlation in ^{68}Ni. In the case of ^{84}Ni, the calculated points form a narrow ellipse, which implies that there is a strong correlation in ^{84}Ni between the PDR strengths and $\Delta R_{\rm rms}$. A strong correlation is also seen in ^{24}O and ^{54}Ca, which have a prominent PDR.

In summary, we carried out the systematic calculation of the low-lying $E1$ strengths. We found that the PDR strengths correlated linearly with the neutron skin thickness in the region where the PDR was stronger. The correlation was weak outside this region. This result is simultaneously consistent with the correlations reported in Refs.[1)] and[2)].

References

1) J. Piekarewicz, Phys. Rev. **C 73** (2006), 044325.
2) P.-G. Reinhard and W. Nazarewicz, Phys. Rev. **C 81** (2010), 051303.
3) Tsunenori Inakura, Takashi Nakatsukasa, and Kazuhiro Yabana, Phys. Rev. **C 84** (2011), 021302.

Shape transition in neutron-rich Cr isotopes around $N = 40$

K. Sato, N. Hinohara[*1], T. Nakatsukasa, M. Matsuo[*2], K. Matsuyanagi[*3]

[Nuclear structure, unstable nuclei, shape transition]

Atomic nuclei exhibit a variety of shapes depending on the proton and neutron numbers, and the underlying shell structure reveals a clue that can help in understanding the equilibrium shapes. Although it is a magic number for the harmonic oscillator potential, the collectivity of isotones with $N = 40$ changes significantly with the proton number. In neutron-rich Cr and Fe isotopes around $N = 40$, the onset of collectivity associated with a spherical-to-deformed shape transition has been suggested by recent experimental data.[1)]

To describe transitional nuclei, we have to go beyond the small-amplitude approximation around the equilibrium shape owing to a possible large-amplitude shape fluctuation. Here, we study the shape transition in Cr isotopes with the five-dimensional quadrupole collective Hamiltonian approach.[2)] The collective Hamiltonian is characterized by the collective potential and inertial functions; these are functions of the deformation parameters (β, γ) in general. The Inglis-Belyaev (IB) cranking formula has been widely used for calculating the inertial functions. However, it is well known that the IB cranking formula does not contain the contributions from the time-odd components of the mean field and that it overestimates excitation energies.

To overcome the limitations of the IB cranking formula, we employ the constrained Hartree-Fock-Bogoliubov plus local quasiparticle random-phase approximation (CHFB+LQRPA) method[3)] for determining the collective potential and inertial functions in the collective Hamiltonian. This method comprises the CHFB equation and the LQRPA equations, which are an extension of the usual QRPA equations to the non-equilibrium points at each mesh point in the (β, γ) plane. After quantizing the collective Hamiltonian, we solve the collective Schrödinger equation to obtain the excitation energies.

In Fig. 1, we show the excitation energies of the 2_1^+ and 4_1^+ states, their ratios $R_{4/2} = E(4_1^+)/E(2_1^+)$, and the spectroscopic quadrupole moments of the 2_1^+ states calculated for $^{58-66}$Cr, in comparison with the available experimental data. In this study, we used the pairing-plus-quadrupole model including the quadupole-pairing interaction. For calculating the spectroscopic quadrupole moments, we used the effective charges $(e_n, e_p) = (0.5, 1.5)$. The excitation energies as well as their ratios are well reproduced by the calculated results. The decrease in the excitation energies and increase in $R_{4/2}$ indicate that the deformation stabilizes as the neutron number increases. The calculated spectroscopic quadrupole moments have a negative sign, thus indicating prolate shapes, and the magnitude increases from $N = 34$ to $N = 40$. This behavior of the excitation energies and the spectroscopic quadrupole moments suggests that a spherical-prolate shape transition may have occured between $N = 34$ and $N = 40$. Details of this calculation will be presented in a forthcoming paper.[6)]

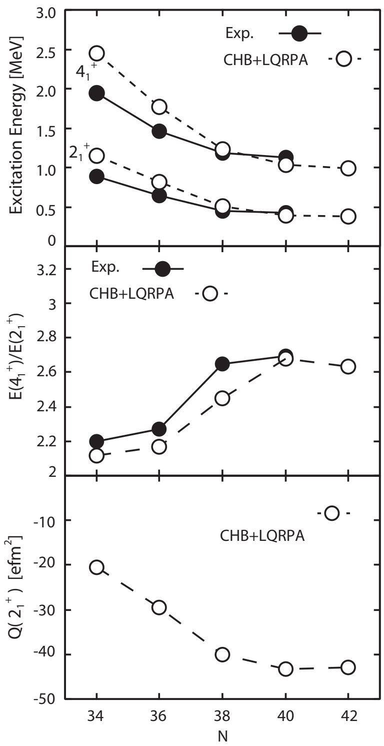

Fig. 1. Excitation energies of the 2_1^+ and 4_1^+ states (*top*), their ratios $R_{4/2}$(*middle*), and spectroscopic quadrupole moments (*bottom*) calculated using the CHFB+LQRPA method, in comparison with the experimental data. 1,4,5)

*1 Department of Physics and Astronomy, University of North Carolina at Chapel Hill
*2 Department of Physics, Niigata University
*3 Yukawa Institute for Theoretical Physics, Kyoto University

References

1) A. Gade et al.: Phys. Rev. C **81**, 051304 (2010).
2) A. Bohr and B. R. Mottelson: *Nuclear Structure*, Vol. II (W. A. Benjamin Inc., 1975; World Scientific, 1998).
3) N. Hinohara, K. Sato, T. Nakatsukasa, M. Matsuo, and K. Matsuyanagi: Phys. Rev. C **82**, 064313 (2010).
4) S. Zhu et al.: Phys. Rev. C **74**, 064315 (2006).
5) N. Aoi et al.: Phys. Rev. Lett. **102**, 012502 (2009).
6) K. Sato et al.: in preparation.

Shape changes and large-amplitude collective dynamics in neutron-rich Cr isotopes†

Kenichi Yoshida and Nobuo Hinohara

[Nuclear structure, density functional theory, quadrupole collectivity]

Atomic nuclei have a variety of equilibrium shapes, and shape changes are observed along their isotopic or isotonic chain. The mean-field approximation gives us an intuitive picture of the nuclear shape. However, we have to go beyond it to describe the shape-phase transition that is the dynamical change of the mean-field potential associated with the large-amplitude collective motion.

A self-consistent mean-field model employing the effective interaction or the nuclear energy-density functional (EDF) can successfully describe the ground-state properties[1]. Recent advances in the computing capability together with the highly developed techniques in the nuclear EDF method allow us to determine the ground-state properties of nuclei, including deformation in the entire mass region of the nuclear chart.

Magic number or shell closure is an essential concept in understanding stability against deformation. The subshell closure at 40 created by the gap between $1g_{9/2}$ and $2p_{1/2}, 1f_{5/2}$ orbitals has attracted much attention for several reasons[2]. Half-life measurements have indicated that neutron-rich ^{66}Fe is deformed with a quadrupole deformation β of about 0.26[3]. Since the Cr isotopes lie at the mid-proton $1f_{7/2}$ shell, protons could additionally destabilize a nucleus with a spherical shape and induce deformation. Experimental evidence of nuclear shape changes is related to low-lying quadrupole collectivity. The observed small excitation energy of the 2_1^+ state of neutron-rich Cr isotopes indicates that deformation develops toward $N = 40$[4].

In this study, on the basis of the nuclear EDF method that is closely related to the mean-field approximation, we develop a new framework of the microscopic theory of large-amplitude collective motion employing a quadrupole collective Hamiltonian approach for axially symmetric nuclei.

Since the β deformation is considered to primally govern the quadrupole collectivity in neutron-rich Cr isotopes, we start from the $(1+2)$D (vibration in the β direction and rotations about the two axes that are perpendicular to the symmetry axis) quadrupole collective Hamiltonian:

$$\mathcal{H}_{\rm coll} = \frac{1}{2}\mathcal{M}_\beta(\beta)\dot{\beta}^2 + \frac{1}{2}\sum_{i=1}^{2}\mathcal{J}_i(\beta)\omega_i^2 + V(\beta). \qquad (1)$$

With Pauli's prescription, we requantize Eq. (1) and construct the collective Schrödinger equation. The collective potential $V(\beta)$ is calculated by solving the constrained Hartree-Fock-Bogoliubov (CHFB) equation. The microscopic Hamiltonian is constructed from the Skyrme and pairing EDFs. Following the discussion in Ref. 5), the vibrational mass $M_\beta(\beta)$ and the rotational mass $\mathcal{J}_i(\beta)$ are evaluated using the local normal mode and the spurious mode on top of the CHFB state.

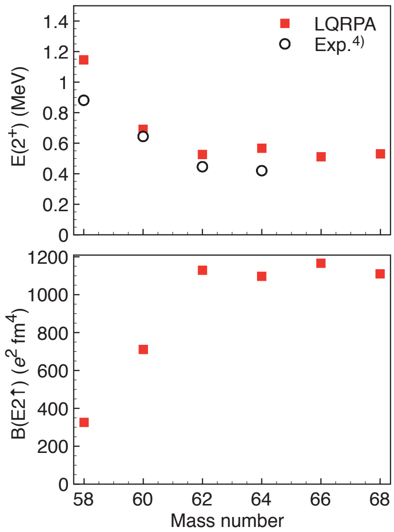

Fig. 1. Upper: Excitation energy of the 2_1^+ state in Cr isotopes as a function of the mass number. Lower: The $B(E2; 0_1^+ \to 2_1^+)$ value.

When the neutron number increases from that in ^{58}Cr, the excitation energy of the 2_1^+ state drops toward ^{62}Cr, as shown in Fig. 1. The transition probability $B(E2; 0_1^+ \to 2_1^+)$ increases at the same time. The present calculation reproduces the experimental results well. From the investigation of the collective wave functions, we reach the conclusion that ^{60}Cr is located close to the critical point of the shape-phase transition, and the onset of deformation takes place at around $N = 38$. Large-amplitude dynamics plays a dominant role in the shape changes in neutron-rich Cr isotopes.

† Condensed from article in Phys. Rev. C **83**, 061302R (2011).

References

1) M. Bender et al., Rev. Mod. Phys. **75**, 121 (2003).
2) P.-G. Reinhard et al., Phys. Rev. C **60**, 014316 (1999).
3) M. Hannawald et al., Phys. Rev. Lett. **82**, 1391 (1999).
4) A. Gade et al., Phys. Rev. C **81**, 051304R (2010).
5) N. Hinohara et al., Phys. Rev. C **82**, 064313 (2010).

Systematic investigation for low-lying $E1$ modes of heavy nuclei around $N = 82$ using Cb-TDHFB

S. Ebata,[*1] T. Nakatsukasa, and T. Inakura

[Nuclear structure, heavy nucleus]

The low-lying electric dipole ($E1$) mode is often called Pygmy dipole resonance (PDR) and known as a characteristic excited state of neutron-rich nuclei. Furthermore, PDR is important in order to understand the nucleosynthesis on the r-process path[1]. Despite the increased capability of generating and measuring unstable nuclei with new radioisotope beam facilities, it is still difficult to study nuclei on the r-process path. Hence, we strongly need a method to predict and analyze the excited state of exotic nuclei in the very neutron-rich and heavy region, such as nuclei on the r-process path. For a systematic theoretical investigation of exotic nuclei, we need to consider the effects of deformation and pairing correlation.

We had proposed the canonical-basis time-dependent Hartree-Fock-Bogoliubov (Cb-TDHFB) theory in the three-dimensional coordinate-space representation for the wide-scale study of nuclear dynamics, which can account for any type of deformation while treating the pairing correlation in the Bardeen-Cooper-Schrieffer (BCS)-like approximation. The Cb-TDHFB equations can be derived from the full TDHFB equation, and are composed of time-dependent formulations for the canonical basis, the occupation probability $\rho_l(t) = |v_l^2(t)|$, and the pair probability $\kappa_l(t) = u_l(t)v_l(t)$. $u_l(t)$ and $v_l(t)$ correspond to the time-dependent BCS factors for the canonical pair of states $\phi_l(\boldsymbol{r}, t)$ and $\phi_{\bar{l}}(\boldsymbol{r}, t)$. Details of the Cb-TDHFB equations and the adopted functionals are given in Ref.2. The results for light and heavy nuclei utilizing Cb-TDHFB have been reported previously[2,3].

We carried out a systematic investigation of the low-lying $E1$ strength for heavy isotopes around $N = 82$. We solved the Cb-TDHFB equations in real time and computed the linear response of the nucleus. For the linear-response calculation, we added an external field $\hat{V}_{\rm ext}(\boldsymbol{r}, t) \equiv -k\hat{F}\delta(t)$ to the ground state of the nucleus, where $\hat{F}$ is a one-body operator and k is an arbitrary small parameter. In this study, we selected the $E1$ operator, $\hat{F}_{E1} = (N/A)\sum_p \hat{r}_p - (Z/A)\sum_n \hat{r}_n$, here $r = (x, y, z)$. We obtained the strength function $S(\hat{F}_{E1}; E)$ through the Fourier transformation of the time-dependent expectation value of $\hat{F}_{E1}$[2]. To quantify the low-lying $E1$ strength, we used the following ratio:

$$\frac{m_1(E_c)}{m_1} \equiv \frac{\int^{E_c} E \times S(E1; E)dE}{\int E \times S(E1; E)dE}, \qquad (1)$$

where E_c is a cut-off energy. We presumed $E_c = 10$ MeV in the present calculation.

Figure 1 shows the results for heavy neutron-rich even-even isotopes with $Z = 38 - 56$ and $N = 76 - 90$, as a function of the neutron number. We can see a sudden jump in the ratio at $N = 82 \to 84$ for each isotopic chain. These results show a neutron shell effect on the low-lying $E1$ strength. A similar shell effect around $N = 50$ is reported in Ref.4. We can also see constant PDR ratios for $N = 76 - 82$. In light stable nuclei, the calculated low-lying $E1$ strength is usually very small[2,4]. However, $^{130-136}$Xe and ^{136,138}Ba, which are stable nuclei, have 1.5% of the PDR ratio. The ratio even increases as the proton number decreases. These features suggest that the PDR in heavy nuclei has different properties from that in light nuclei.

Currently, we are investigating the origin of these differences between heavy stable nuclei and neutron-rich light nuclei. We also plan to use this method to investigate other excitation modes (monopole, quadrupole, scissors, etc.) and heavy ion-collision dynamics.

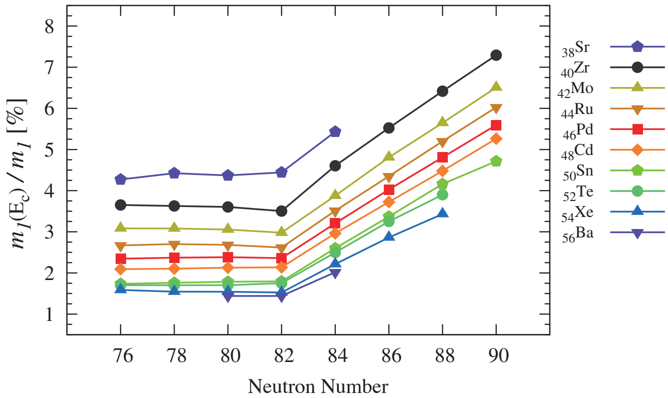

Fig. 1. Neutron number dependence of the low-lying $E1$ ratio defined by Eq.(1) for $Z = 38–56$ (Sr to Ba) with $N = 76–90$.

References

1) S. Goriely: Phys. Lett. B **436**, 10 (1998).
2) S. Ebata *et al.*: Phys. Rev. C **82**, 034306 (2010).
3) S. Ebata *et al.*: RIKEN Accel. Prog. Rep. **44**, iv (2010).
4) T. Inakura, T. Nakatsukasa and K. Yabana: Phys. Rev. C **84**, 021302 (2011).

*1 Center for Nuclear Study, University of Tokyo

Shell-model fits for Sn isotopes

M. Honma,[*1] T. Otsuka,[*2,*3] T. Mizusaki,[*4] and M. Hjorth-Jensen[*5]

[NUCLEAR STRUCTURE, shell model]

The Sn isotopes provide us with an ideal test for conventional shell-model calculations on the basis of the microscopic effective interaction theory and also the knowledge of nuclear forces. Because of the Z=50 semi-magic structure, the deformation is not significant, and the the shell-model description within a limited one-major shell is expected to be reasonable. In fact, shell-model calculations using an effective interaction derived microscopically from a realistic nucleon-nucleon potential have been successfully applied to the analysis of new experimental data and also the prediction for unobserved properties[1)].

However, such a microscopic approach is not necessarily successful in the middle of the neutron shell as shown in Ref.[2)] for example, where the excitation energy of the 2_1^+ state is predicted to be too high by 0.4MeV for ^{118}Sn. On the other hand, it has been shown that the microscopic effective interaction can be improved for a practical use by fitting to the experimental data. Therefore, it is interesting to investigate how accurately the structure of Sn isotopes can be described by using such a fitted effective interaction. We report the results of such an attempt.

The adopted model space consists of five single-particle orbits $1d_{5/2}$, $0g_{7/2}$, $0h_{11/2}$, $2s_{1/2}$ and $1d_{3/2}$ in which the Sn isotopes are described by valence neutrons, and the $T = 1$ part of the two-body interactions is relevant. We start with an effective interaction obtained in a microscopic way as described in Ref.[3)] using the N^{3}LO interaction[4)]. A series of fitting calculations was carried out with 313 experimental energy data including 29 binding energies. We utilized the Linear-Combination (LC) method as in our previous approach[5)]. We found that only a small modification was necessary to improve the microscopic interaction. In fact a reasonable convergence was obtained by varying only 22 LC's of 165 Hamiltonian parameters (5 single-particle energies and 160 two-body matrix elements). In the final fit, the rms deviation of 147 keV was obtained.

As an example of the results, the excitation energies of the yrast states of even-N isotopes are shown in Fig.1. One can find a reasonable agreement between the experimental data and the shell-model results throughout the isotope chain. The quality of the fit is similar for odd-N isotopes. The predicted ground-state spin of ^{101}Sn is $7/2^+$ rather than $5/2^+$, in good agreement with recent experimental observation.[6)] The fit of the binding energy is basically successful for heavier isotopes, but the shell-model result begins to show underbinding as approaching ^{100}Sn. This result suggests the development of a kind of collectivity which can not be described by the present model space. Such a picture can be consistent with the large B(E2) values below $N = 64$ observed in recent measurements[7)].

This fitted interaction can be a good starting point for extending the model space so as to describe the ^{100}Sn core excitations and also for the study of more neutron-rich isotopes.

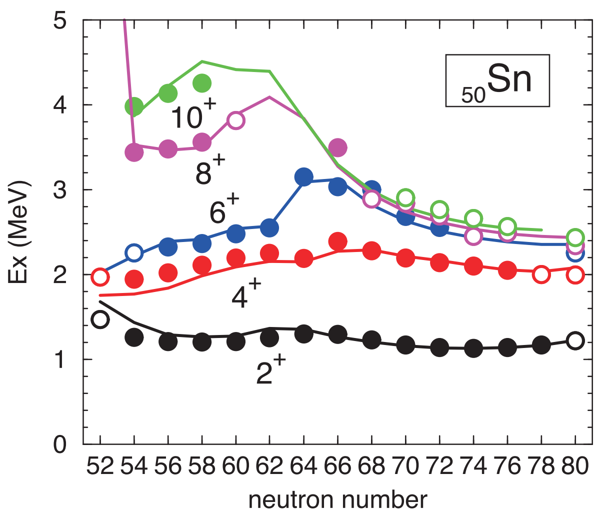

Fig. 1. Comparison of excitation energies of even-spin yrast states between the experimental data (symbols) and the shell-model results (lines). Experimental data are taken from Ref.[8)] Open symbols indicate that the spin assignment is uncertain. The shell-model results are obtained by using the efficient shell-model code MSHELL[9)].

*1 Center for Mathematical Sciences, University of Aizu
*2 Department of Physics, University of Tokyo
*3 Center for Nuclear Studies, University of Tokyo
*4 Institute of Natural Sciences, Senshu University
*5 Department of Physics and Center of Mathematics for Applications, University of Oslo

References
1) A. Banu *et al.*: Phys. Rev. C **72**, 061305(R) (2005).
2) P. Guazzoni *et al.*: Phys. Rev. C **78**, 064608 (2008).
3) M. Hjorth-Jensen *et al.*: Phys. Rep. **261**, 125 (1995).
4) D. R. Entem *et al.*: Phys. Rev. C **68**, 041001(R) (2003).
5) M. Honma *et al.*: Phys. Rev. C **80**, 064323 (2009).
6) I. G. Darby *et al.*: Phys. Rev. Lett. **105**, 162502 (2010).
7) A. Ekström *et al.*: Phys. Rev. Lett. **101**, 012502 (2008).
8) Data extracted using the NNDC WorldWideWeb site from the ENSDF database.
9) T. Mizusaki: RIKEN Accel. Prog. Rep. **33**, 14 (2000).

Anomalous behaviors of two neutron transfer in neutron-rich Sn isotopes

H. Shimoyama*[1] and M. Matsuo*[2]

[Nuclear structure, Two-neutron transfer, Neutron-rich nuclei]

Recently, the study of two neutron transfer in unstable nuclei have been attracting attention[1–4]. In this work we have studied two neutron transfer with $L = 0$ populating 0^+_{gs} and excited 0^+ states, and we show that the pairing vibrations in neutron-rich Sn isotopes have anomalous features[4].

We describe the two-neutron transfer by means of the Hartree-Fock-Bogoliubov (HFB) mean-field theory and the continuum quasiparticle random phase approximation[3] (QRPA). The Skyrme functional with the parameter SLy4 is adopted. For the pairing interaction, we choose the density-dependent-delta-interaction.

Figure 1 shows the calculated pair-addition transfer strength of the low-lying pairing vibrational transfer and the strength of the ground state transfer. We define the pair-additional strength:

$$B(Pad0; gs \to i) = \sum_i |\langle \Psi_i | P^\dagger_{00} | \Psi_0 \rangle|^2 \qquad (1)$$

where $P^\dagger_{00} = \int \boldsymbol{r}^2 Y_{00}(\hat{\boldsymbol{r}})\,\psi^\dagger_q(\boldsymbol{r}\downarrow)\,\psi^\dagger_q(\boldsymbol{r}\uparrow)$ is the pair-additional operator with $L = 0$. And we evaluate the ground state transfer strength

$$B(Pad0; gs \to gs) = \left|\sqrt{\pi}\int r^2 \tilde{\rho}(r) dr\right|^2 \qquad (2)$$

using HFB pair density $\tilde{\rho}(r)$. The isotopes with A = 132-140 have large strengths of the pairing vibration. These strengths are several times larger than in other isotopes and almost the same value as that of the ground state transfer. Usually the intensity of pairing vibrational transfer is significantly weaker than the ground state transfer, for instance the strength ratio in stable Sn isotopes ($A \sim 120$) are less than 10% in Fig.1[5]. However the ratio amounts to 60-90% in the $A = 132$-140 isotopes.

Figure 2 shows the transition density of the pair-addition vibrational modes in Sn isotopes with A = 120-130 and A = 132-140. The pairing vibrational modes in the $A = 132$-140 isotopes have significant amplitude extending far outside of the nucleus($r = 15$ fm). These long tails are related to the weak binding features of the systems. The Hartree-Fock single-particle energies above the $N = 82$ shell gap are $e_{2f7/2}$ = -1.99 MeV, $e_{3p3/2}$ = -0.25 MeV and $e_{3p1/2}$ = 0.26 MeV in ^{132}Sn. The transfer of two neutrons into the weakly bound p orbits is an important element to produce the long tail.

We predict emergence of the anomalous pairing vibration in neutron-rich Sn isotopes beyond $N = 82$ shell closure. We regard it anomalous because of the large transfer strength and the long tail of the transition density.

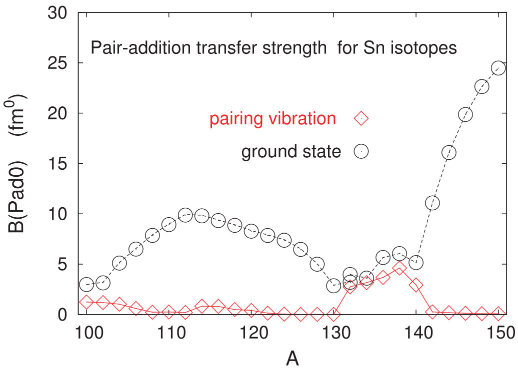

Fig. 1. The pair-addition strengths associated with pairing vibratioal state (diamonds) and with the ground state(circles).

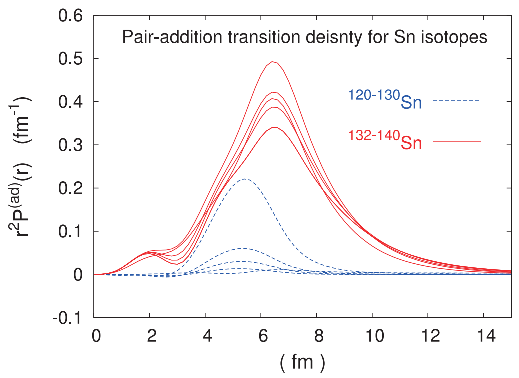

Fig. 2. The pair-addition transition densities with the pairing vibrational mode in $^{132-140}$Sn (solid curves) and $^{120-130}$Sn (dashed curves).

References
1) I. Tanihata *et al.*: Phys. Rev. Lett. **100**, 192502 (2008).
2) E. Khan *et al.*: Phys. Rev. C **80**, 044328 (2004), Phys. Rev. C **80**, 044328 (2009).
3) M. Matsuo *et al.*: Phys. Rev. C **82**, 0243418 (2010).
4) H.Shimoyama *et al.*: Phys. Rev. C **84**, 044317 (2011).
5) R. A. Broglia *et al.*: in*Advances in Nuclear Physics* vol.6, edited by M. Baranger and E. Vogt, (Plenum, New York, 1973),p.287-457.

*1 Graduate School of Science and Technology, Niigata University
*2 Department of Physics, Faculty of Science, Niigata University

Nuclear Schiff moment of ^{129}Xe

N. Yoshinaga[*1] and K. Higashiyama[*2]

[Electric dipole moments, Nuclear Schiff moments]

The permanent electric dipole moment (EDM) of a particle or an atom provides us with important information that can help improve our fundamental understanding of nature with regard to the simultaneous violation of parity (P) and time-reversal (T) invariance. The EDM of a neutral atom is mainly induced by the nuclear Schiff moment, since the electron EDM is very small and the nuclear EDM is shielded by outside electrons according to the Schiff theorem[1)]. The Schiff moments have been theoretically calculated through various mean-field approaches, but no study has so far been carried out by considering the viewpoint of the shell model.

In this work, we calculate the nuclear Schiff moment arising from the P- and T-violating nucleon-nucleon interaction by considering the pair-truncated shell model (PTSM). Collective nucleon pairs with angular momenta of zero and two are the basic ingredients of the model. Systematic studies have previously been carried out for the even-even and odd-mass nuclei in the region of mass $A \approx 130$[2)]. Calculations have reproduced the energy levels and electromagnetic transitions well.

The nuclear Schiff moment operator may be written as[3)]

$$\boldsymbol{S} = \frac{1}{10}\sum_{i=1}^{A} e_i \left({r_i}^2 - \frac{5}{3}\left\langle r^2 \right\rangle_{\mathrm{ch}} \right) \boldsymbol{r}_i, \tag{1}$$

where $\left\langle r^2 \right\rangle_{\mathrm{ch}}$ is the mean square radius of the nuclear charge distribution, $\boldsymbol{r}_i$ indicates the ith nucleon position, and e_i denotes the charge ($e_i = e$ for protons and $e_i = 0$ for neutrons). The nuclear Schiff moment arising from the two-body interaction that breaks the P and T invariance can be calculated by using the first-order perturbation theory as

$$S = \sum_{i \neq 0} \frac{\langle \Phi_0 | \, \hat{S}_z \, | \Phi_i \rangle \langle \Phi_i | \, \hat{V}_{\mathrm{PT}} \, | \Phi_0 \rangle}{E_0 - E_i} + c.c., \tag{2}$$

where $|\Phi_0\rangle$ represents the PTSM wave function of the $1/2^+$ state (the ground state) with energy E_0 and $|\Phi_i\rangle$ denotes the wave functions of the $1/2^-$ states with excitation energies E_i. The operator $\hat{V}_{\mathrm{PT}}$ is the P- and T-violating nucleon-nucleon interaction, and it is assumed to be of the following form for simplicity:

$$\hat{V}_{\mathrm{PT}} = B \left[\boldsymbol{\sigma}^{(-)} \cdot \boldsymbol{r} \right] \tau_z^{(+)} + \left[\boldsymbol{\sigma}^{(+)} \cdot \boldsymbol{r} \right] \tau_z^{(-)}, \tag{3}$$

with $\boldsymbol{\sigma}^{(\pm)} = \boldsymbol{\sigma}^{(1)} \pm \boldsymbol{\sigma}^{(2)}$ $\tau_z^{(\pm)} = \tau_z^{(1)} \pm \tau_z^{(2)}$ and $\boldsymbol{r} = r^{(1)} - r^{(2)}$, where B is the interaction strength (in units of MeV/fm). The calculated Schiff moment of the $1/2^+_1$ state in ^{129}Xe is

*1 Department of Physics, Saitama University
*2 Department of Physics, Chiba Institute of Technology

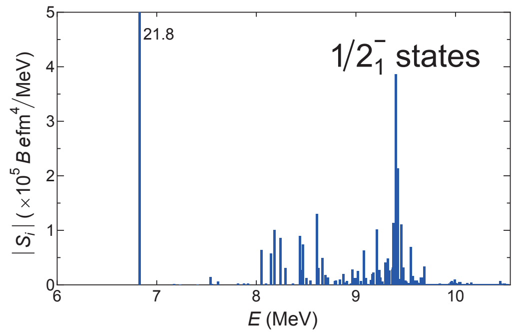

Fig. 1. Absolute values of components S_i.

$$S = 4.17 \times 10^6 B \; e\,\mathrm{fm}^4/\mathrm{MeV}. \tag{4}$$

To identify the microscopic origin of the nuclear Schiff moment, we calculate the absolute value of each component S_i, which is defined by

$$S_i = \frac{\langle \Phi_0 | \, \hat{S}_z \, | \Phi_i \rangle \langle \Phi_i | \, \hat{V}_{\mathrm{PT}} \, | \Phi_0 \rangle}{E_0 - E_i}. \tag{5}$$

In Fig. 1, the calculated absolute values of S_i are plotted against the excitation energy E_i. It is found that of all components, the component S_1 corresponding to the lowest $1/2^-$ state with an excitation energy (E_1) of 6.83 MeV is dominant.

According to Dzuba et al.[4)], the EDM of a neutral ^{129}Xe atom can be expressed in terms of the nuclear Schiff moment S as

$$d\left(^{129}\mathrm{Xe}\right) = 0.38 \times 10^{-17} \left(\frac{S}{e\ \mathrm{fm}^3} \right) \ e\ \mathrm{cm}. \tag{6}$$

Using the upper limit for the experimental EDM for the neutral ^{129}Xe atom $\left(\left| d_n \left(^{129}\mathrm{Xe}\right) \right| < 4.1 \times 10^{-27}\ e\ \mathrm{cm}^{5)} \right)$ and Eqs. (4) and (6), we obtain the upper limit for the interaction strength:

$$B\ (\mathrm{MeV/fm}) = 2.6 \times 10^{-16}. \tag{7}$$

References

1) L. I. Schiff: Phys. Rev. **132**, 2194 (1963).
2) K. Higashiyama and N. Yoshinaga: Phys. Rev. C **83**, 034321 (2011).
3) V. F. Dmitriev and R. A. Sen'kov: Phys. Rev. Lett. **91**, 212303 (2003).
4) V. A. Dzuba et al.: Phys. Rev. A **66**, 012111 (2002).
5) M. A. Rosenberry et al.: Phys. Rev. Lett. **86**, 22 (2001).

Application of tops-on-top model to triaxial, strongly deformed bands in odd-odd nucleus ^{164}Lu†

K. Tanabe*1,*2 and K. Sugawara-Tanabe*1,*3

[Nuclear structure, TSD bands, Top-on-top model, Electromagnetic transition rates]

We have attempted to describe the triaxial, strongly deformed (TSD) bands in the odd-odd nucleus ^{164}Lu[1,2] in terms of the "tops-on-top model," which is an extension of the "top-on-top model"[3–5] and includes two valence nucleons in each single-j orbital. Our Hamiltonian is given by

$$\begin{aligned} H &= H_{\rm rot} + H_{\rm sp}(\vec{j}_1) + H_{\rm sp}(\vec{j}_2)\,; \\ H_{\rm rot} &= \sum_{k=x,y,z} A_k(I_k - j_{1k} - j_{2k})^2, \\ H_{\rm sp}(\vec{j}_i) &= \frac{V_i}{j_i(j_i+1)}\big[\cos\gamma(3j_{iz}^2 - \vec{j}_i^{\,2}) \\ &\quad -\sqrt{3}\sin\gamma(j_{ix}^2 - j_{iy}^2)\big] \quad (i = 1, \text{or } 2), \quad (1) \end{aligned}$$

where $A_k = 1/(2\mathcal{J}_k)$. For rigid-body moments of inertia, as defined in Ref.[3], inequalities of $\mathcal{J}_x \geq \mathcal{J}_y \geq \mathcal{J}_z$ hold good within the range $0° \leq \gamma \leq 60°$. In the Nilsson Hamiltonian $H_{\rm sp}(\vec{j}_i)$ $(i = \pi, \nu)$, the oscillator strengths satisfy the condition $\omega_x^2 \geq \omega_y^2 \geq \omega_z^2$ within the same range of γ. These inequalities are also consistent with the radii of the oscillator satisfying the condition $R_x \leq R_y \leq R_z$. We get $\mathcal{J}_x = \mathcal{J}_y$, $\omega_x^2 = \omega_y^2$, and $R_x = R_y$ at $\gamma = 0°$, and $\mathcal{J}_y = \mathcal{J}_z$, $\omega_y^2 = \omega_z^2$, and $R_y = R_z$ at $\gamma = 60°$. We state that the period of the γ-dependence of the hydrodynamical moments of inertia does not agree with that of the Nilsson Hamiltonian, even when the sign of γ is changed. In order to simulate the evolution of the intrinsic structure with increasing angular momentum I, we assume I-dependence of the moments of inertia $\mathcal{J}_k$, with parameters c_1 and c_2, as employed in Refs.[3–5].

Two positive-parity TSD bands (TSD3 and TSD2) and one negative-parity TSD band (TSD1) are identified for ^{164}Lu[2]. The parity of TSD2 has been confirmed to be positive[2] rather than negative[1]. The proton single-particle orbital is assumed to be $i_{13/2}$, as in the other odd-A Lu isotopes, but the neutron single-particle orbital is not definite. It is suggested in Ref.[1] that the neutron orbital is $i_{13/2}$ for the TSD3 band, as the band starts from the 13^+ state, and $h_{9/2}$ for the TSD1 band, though this band starts from the 14^- state. The neutron orbital for TSD1 is suggested to be $j_{15/2}$ in Ref.[2]. In actual numerical analysis, we perform exact diagonalization of H in Eq. (1) by applying the Lanczos method. In the figure below, we compare the theoretical energy levels relative to the reference, *i.e.*, $E^* - aI(I+1)$, with the experimental TSD2 and TSD3 levels[2] for ^{164}Lu. We assume that the valence proton and neutron are in the $\pi i_{13/2}$ and $\nu i_{13/2}$ orbitals and that parameters are the $V_\pi = V_\nu = 2.3$MeV, $\mathcal{J}_0 = 82$MeV^{-1}, $c_1 = -8$, and $c_2 = 41$. We introduce an attenuation factor of 0.55 for the term $-\sum_{k=x,y,z} I_k(j_{\pi k} + j_{\nu k})/\mathcal{J}_k$ appearing in the Coriolis term and for $\sum_{k=x,y,z} j_{\pi k}j_{\nu k}/\mathcal{J}_k$ in the recoil term. The experimental TSD band levels are well

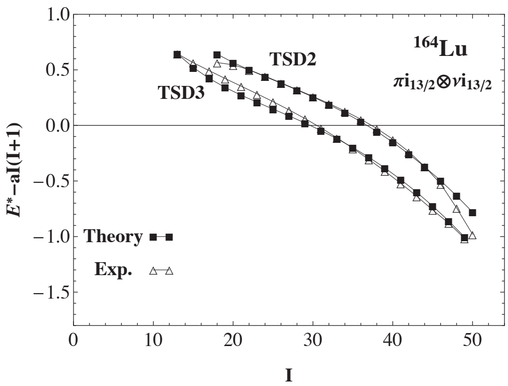

reproduced in terms of the tops-on-top model. The calculated alignment of $\langle I_x^2\rangle^{1/2}$ and $\langle R_x^2\rangle^{1/2}$ in the TSD2 band is one unit lesser than that in the TSD3 band, showing "wobbling" motion of $\vec{R}$ in the TSD2 band. In the table, we show the predicted values of $B(E2)_{\rm in}$, $B(E2)_{\rm out}$, and $B(M1)_{\rm out}$.

^{164}Lu(theory)			
I	$B(E2)_{\rm out}$ $((eb)^2)$	$B(E2)_{\rm in}$ $((eb)^2)$	$B(M1)_{\rm out}$ $((\mu_{\rm N})^2)$
24	0.254	1.141	0.0051
26	0.235	1.150	0.0046
28	0.219	1.159	0.0041
30	0.205	1.165	0.0038
32	0.192	1.171	0.0032

References

1) S. Törmänen *et al.*: Phys. Lett. B **454**, 8 (1999).
2) P. Bringel *et al.*: Phys. Rev. C **75**, 044306 (2007).
3) K. Tanabe and K. Sugawara-Tanabe: Phys. Rev. C **73**, 034305 (2006); **75**, 059903(E) (2007).
4) K. Tanabe and K. Sugawara-Tanabe: Phys. Rev. C **77**, 064318 (2008).
5) K. Sugawara-Tanabe and K. Tanabe: Phys. Rev. C **82**, 051303(R) (2010).

† Condensed from the article in press, J. Phys. Conf. Ser., Rutherford Centennial Conference on Nuclear Physics, 8-12 August 2011, The University of Manchester, UK.

*1 Theoretical Nuclear Physics Laboratory, RIKEN Nishina Center, Wako, Saitama 351-0198
*2 Department of Physics, Saitama University, Sakura-Ku, Saitama 338-8570
*3 Otsuma Women's University, Tama, Tokyo 206-8540

Finite amplitude method for the quasi-particle random-phase approximation†

P. Avogadro*1 and T. Nakatsukasa

[Nuclear structure, random-phase approximation]

Elementary modes of excitation in nuclei provide valuable information about the nuclear structure. The random-phase approximation (RPA) based on energy density functionals (EDFs) is a leading theory applicable to both low-lying excited states and giant resonances. Although the fully self-consistent treatment of residual (induced) interactions for realistic energy functionals is becoming increasingly prevalent, RPA calculations for deformed nuclei are still computationally demanding. At present, the use of quasi-particle random-phase approximation (QRPA) for deformed superfluid nuclei is limited to axially deformed cases.

In Ref. 1), the finite amplitude method (FAM) was proposed as a feasible method for obtaining a solution of the RPA equation. The FAM allows us to calculate all the induced fields with the use of a finite difference method, which involves the use of a computational program of the static mean-field solutions. Recently, the FAM has been applied to electric dipole excitations in nuclei by using the Skyrme energy functionals[2)]. These developements in conjunction with fast algorithms for linear systems open the possibility of systematically exploring nuclear excitations over the entire nuclear chart.

So far, the FAM has been used for obtaining solutions of the RPA equation without the pairing correlations. It is well known, however, that almost all but magic nuclei show superfluid features. Therefore, a further improvement of the method is highly desirable for its application to QRPA equations including correlations in the particle-particle and hole-hole channels. The purpose of the present study is to generalize the FAM to superfluid systems, which would enable us to perform a QRPA calculation by utilizing a static Hartree-Fock-Bogoliubov (HFB) code with minor modifications. Our final goal is the construction of a fast computer program for the fully self-consistent and triaxially deformed QRPA. This paper is the first step toward the goal, and it presents the basic equations of the FAM for the QRPA and shows the first result for spherical nuclei. We convert the spherically symmetric HFB code called HFBRAD[3)] to the QRPA code.

Below, we present the FAM formulae for the QRPA. The linear response equation is given by $A\vec{x} = \vec{b}$, where

$$\vec{x} \equiv \begin{pmatrix} X_{\mu\nu} \\ Y_{\mu\nu} \end{pmatrix}, \quad \vec{b} \equiv \begin{pmatrix} F^{20}_{\mu\nu} \\ F^{02}_{\mu\nu} \end{pmatrix},$$

and

$$A\vec{x} = \begin{pmatrix} (E_\mu + E_\nu - \omega)\, X_{\mu\nu}(\omega) + \delta H^{20}_{\mu\nu}(\omega) \\ (E_\mu + E_\nu + \omega)\, Y_{\mu\nu}(\omega) + \delta H^{02}_{\mu\nu}(\omega) \end{pmatrix},$$

with

$$\begin{aligned} \delta H^{20}_{\mu\nu}(\omega) &= U^\dagger \delta h V^* - V^\dagger \delta\Delta^{(-)*} V^* \\ &+ U^\dagger \delta\Delta^{(+)} U^* - V^\dagger \delta h^T U^* \end{aligned} \quad (1)$$

and

$$\begin{aligned} \delta H^{02}_{\mu\nu}(\omega) &= -V^T \delta h U + U^T \delta\Delta^{(-)*} U \\ &- V^T \delta\Delta^{(+)} V + U^T \delta h^T V. \end{aligned} \quad (2)$$

Denoting h and Δ collectively as $\mathcal{H} \equiv (h, \Delta)$, the induced fields $\delta\mathcal{H}$ are calculated by the FAM formulae

$$\delta\mathcal{H} = \frac{\mathcal{H}\left[\bar{U}^*_\eta, \bar{V}^*_\eta; U_\eta, V_\eta\right] - \mathcal{H}\left[U^*, V^*; U, V\right]}{\eta}. \quad (3)$$

$(\bar{U}^*_\eta, \bar{V}^*_\eta; U_\eta, V_\eta)$ are given by

$$\begin{aligned} \bar{U}^*_\eta &\equiv U^* + \eta V X, \quad \bar{V}^*_\eta \equiv V^* + \eta U X, \\ U_\eta &\equiv U + \eta V^* Y, \quad \text{and} \quad V_\eta \equiv V + \eta U^* Y \end{aligned}$$

for the calculation of $\delta h(\omega)$ and $\delta\Delta^{(+)}$. For $\delta\Delta^{(-)}$, they are given by

$$\begin{aligned} \bar{U}^*_\eta &\equiv U^* + \eta V Y^*, \quad \bar{V}^*_\eta \equiv V^* + \eta U Y^*, \\ U_\eta &\equiv U + \eta V^* X^*, \quad \text{and} \quad V_\eta \equiv V + \eta U^* X^*. \end{aligned}$$

Here, $\mathcal{H}$ is the HFB Hamiltonian and η is an arbitrary small parameter used to validate the linearization. We have demonstrated that the method works efficiently for the monopole excitation in Sn isotopes. Readers are referred to our original paper for details of the formulae and the numerical procedure.

References
1) T. Nakatsukasa, T. Inakura, and K. Yabana, Phys. Rev. C **76**, 024318 (2007).
2) T. Inakura, T. Nakatsukasa, and K. Yabana, Phys. Rev. C **80**, 044301 (2009).
3) K. Bennaceur and J. Dobaczewski, Comp.. Phys. Comm., **168**, 96 (2005).

† Condensed from the article in Phys. Rev. C **84**, 014314 (2011)
*1 Università degli Studi di Milano

Local energy density functional for proton pairing correlations

M. Yamagami,[*1] J. Margueron,[*2] H. Sagawa,[*1] and K. Hagino[*3]

[Pairing correlations, Neutron-rich nuclei, Density functional theory]

The repulsive Coulomb force reduces proton pairing gaps by about 25%. In Ref.[1)], the authors proposed a method in which the explicit Coulomb effect can be taken into account by reducing the strength of the effective interaction in the proton pairing channel by 10% compared with the neutron strength ($V_p = 0.9V_n$) for a wide range of mass number and neutron excess. The validity of this method is shown by performing fully self-consistent Hartree-Fock-Bogoliubov (HFB) calculation with the Gongy force and Coulomb force. A similar treatment has been found to work for a three-body model calculation for the ^{17}Ne nucleus[2)].

In this study, we compare two renormalization methods for the local energy density functional of the pairing channel (pair-DF): (1) renormalization of the Coulomb effect to the proton pairing strength, and (2) renormalization of the Coulomb effect to the isovector-density ($\rho_1 = \rho_n - \rho_p$) dependence in the pair-DF.

We propose a pair-DF $\tilde{h}_\tau(\mathbf{r}) = \frac{1}{2}V_\tau g_\tau(\mathbf{r})\tilde{\rho}_\tau(\mathbf{r})$ that includes the linear and quadratic ρ_1 terms in addition to the usual isoscalar density ($\rho = \rho_n + \rho_p$) term:[3)]

$$g_\tau(\mathbf{r}) = 1 - \eta_0\left(\frac{\rho}{\rho_0}\right) - \eta_1\left(\frac{\tau_3\rho_1}{\rho_0}\right) - \eta_2\left(\frac{\rho_1}{\rho_0}\right)^2.$$

Here, $\tau_3 = 1(-1)$ for $\tau = n$ (p). $\tilde{\rho}_\tau$ is the pairing density, and $\rho_0 = 0.16$ fm^{-3}. Under the assumption $V_p = V_n$ or $V_p = 0.9V_n$, the phenomenological parameters $(V_n, \eta_0, \eta_1, \eta_2)$ are determined by minimizing the r.m.s. deviation between the result of the HFB calculation with the Skyrme SLy4 force and the 298 experimental pairing gaps (159 neutron gaps and 139 proton gaps).

In Fig. 1, the neutron pairing gaps in Ca, Ni, Sn, and Pb isotopes and the proton pairing gaps in $N = 20, 28, 50$, and 82 isotones are shown. The results in the case of $V_p = 0.9V_n = -373.75$ MeV fm^{-3} and $\eta_1 = 0.585$ are compared with those in the case of $V_p = V_n = -396.47$ MeV fm^{-3} and $\eta_1 = 0.270$. Here, $(\eta_0, \eta_2) = (0.75, 2.5)$ is used in both cases.

The two pair-DFs give almost the same results for the neutron and proton pairing gaps from the proton drip line to the neutron drip line, except for nuclei with $Z > N$. The identical results can be obtained by optimizing η_1 for each V_p/V_n.

We also compare the neutron (proton) r.m.s. deviation σ_n (σ_p) by analyzing the experimental pairing gaps for even-even nuclei in the region $20 \leq A \leq 254$. The results obtained under the assumption $V_p = 0.9V_n$ are $\sigma_p = 0.317$ MeV and $\sigma_n = 0.325$ MeV, while those under the assumption $V_p = V_n$ are $\sigma_p = 0.289$ MeV and $\sigma_n = 0.317$ MeV.

We conclude that the predicting power of our Coulomb effect renormalization methods are almost identical for various isotopes in the nuclear chart. The Coulomb effect can be taken into account in terms of the linear ρ_1 dependence.

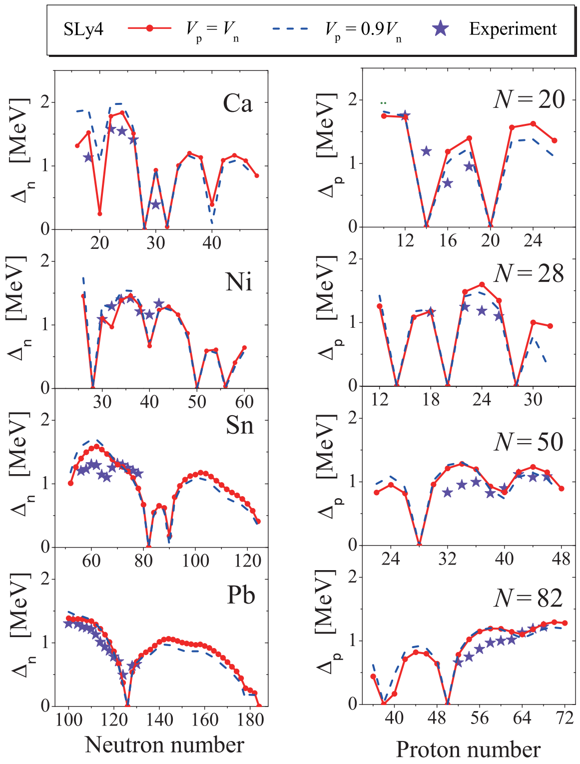

Fig. 1. Neutron pairing gaps in Ca, Ni, Sn, and Pb isotopes (left) and proton pairing gaps in $N = 20, 28, 50$, and 82 isotones (right). The results obtained under the assumptions $V_p = V_n$ and $V_p = 0.9V_n$ are compared. See text for details.

References
1) H. Nakada and M. Yamagami, Phys. Rev. C **83**, 031302(R) (2011).
2) T. Oishi, K. Hagino, and H. Sagawa, Phys. Rev. C **84**, 057301 (2011).
3) M. Yamagami, Y. R. Shimizu, and T. Nakatsukasa: Phys. Rev. C **80**, 064301 (2009).

*1 Department of Computer Science and Engineering, University of Aizu, Aizu-Wakamatsu, Fukushima 965-8580, Japan
*2 Institut de Physique Nucléaire, Université Paris-Sud, IN2P3-CNRS, F-91406 Orsay Cedex, France
*3 Department of Physics, Tohoku University, Sendai 980-8578, Japan

Diabatic separation of overlapping resonances: A theorem introducing a new concept of resonance channel space

Isao Shimamura

[Resonance theory, overlapping resonances, unstable states]

A resonance affects scattering processes strongly. In potential scattering, the phase shift $\delta(E)$ at scattering energies E near the central energy E_r of the resonance with width Γ is represented by the Breit-Wigner formula, i.e., the sum of a slowly varying background $\delta_b(E)$ and a rapidly varying component $\cot^{-1}[(E_r - E)/(\Gamma/2)]$ denoted by $\delta_r(E)$. When resonances overlap, i.e., when two or more resonances occur within their widths, the rapidly changing part $\delta(E) - \delta_b(E)$ of the phase shift takes the form of the sum of $\delta_r(E)$ with different pairs of E_r and Γ.

An isolated resonance in a multichannel process is described by an S matrix of the Breit-Wigner form, which is symmetric (satisfying the time reversal symmetry) and unitary (satisfying the flux conservation law). The eigenvalues $\exp(2i\eta_\alpha)$ and the corresponding eigenvectors of the S matrix define the eigenphases $\eta_\alpha(E)$ and the eigenchannels α. The sum of $\eta_\alpha(E)$, called the eigenphase sum, satisfies the same Breit-Wigner formula as the phase shift $\delta(E)$ for potential scattering.[1] The cross sections for the respective channels show a resonance at a common energy E_r.

The interference between N (>1 and not too many) overlapping resonances in a multichannel process leads to cross sections that are extremely complex for resonance analysis. In fact, no explicitly symmetric and unitary representation of the S matrix is known for this case for general N.[1] The resonance information is hard to extract even from the eigenphase sum $\delta(E)$. Figure 1a shows an example of $\delta(E)$ in He($^1P^o$), which gives the wrong impression of only two resonances occurring in the energy region of the figure.

A few years ago, however, the time-delay matrix $Q(E) = i\hbar S dS^\dagger/dE$ (the dagger indicating Hermitian conjugate), representing a multichannel generalization of the time delay in potential scattering, was numerically shown to have a salient feature: when N resonances overlap, its N eigenvalues $q_i(E)$ represent N Lorentzian profiles $L_\nu(E)$ avoiding each other around their crossing points, the values of all the other $q_i(E)$ being very small. An example is found in Fig. 1b, which shows as many as five overlapping resonances.[2] The occurrence of this feature was theoretically proved for double resonances ($N = 2$) in Ref. 3.

Recently, a new theorem has been proved that shows this feature to be observable for any N.[4,5] Furthermore, as a part of this theorem, the sum of all $q_i(E)$, i.e., the trace of the Q matrix, $\mathrm{Tr}\, Q$, has been proved to be a simple sum of N Lorentzian profiles, provided the background S matrix is independent of E.[4,5] Each Lorentzian represents a diabatic, or separate resonance with well-defined E_r and Γ, clearly disentangling the intricate resonance interference (see Fig. 1c).

A resonance state can decay into any open channel of the same symmetry as this resonance state. All processes associated with these channels are affected by this common resonance state. This is also the case with the eigenchannels defined by the S-matrix eigenvectors. The resonance decays into all these eigenchannels, contrary to the general expectation in the early sixties.[1] However, the above new theorem also indicates that the N overlapping resonances can decay only into the N channels defined by the eigenvectors of the Q matrix corresponding to the avoided Lorentzian profiles, provided the background S matrix is independent of E. Thus, the whole channel space can be clearly and uniquely divided into "resonance channel space" and its complement completely irrelevant to the resonances in the asymptotic region of the configuration space.[4,5]

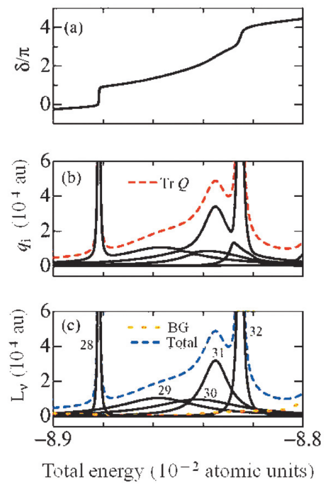

Fig. 1. An example of He($^1P^o$) overlapping resonances.[2]

References

1) I. Shimamura: *Advances in Quantum Chemistry, Vol. 63, Unstable States in the Continuous Spectra, Part II*, edited by C. A. Nicolaides and E. Brändas (Academic, New York, 2012), Chap. 4.
2) K. Aiba, A. Igarashi, and I. Shimamura: J. Phys. B: At. Mol. Opt. Phys. **40**, F9 (2007).
3) I. Shimamura, J. F. McCann, and A. Igarashi: J. Phys. B: At. Mol. Opt. Phys. **39**, 1847 (2006).
4) http://iopscience.iop.org/0953-4075/labtalk-article/47367.
5) I. Shimamura: J. Phys. B: At. Mol. Opt. Phys. **44**, 201002 (2011) (IOPSelect).

Pairing reentrance in hot rotating nuclei†

N. Quang Hung*1 and N. Dinh Dang

[Nuclear structure, pairing, BCS theory, rotation, thermal fluctuations]

It is well-known from Mottelson-Valatin prediction that pairing correlation decreases with total angular momentum and/or rotational frequency and vanishes at a given critical total angular momentum M_c or rotational frequency ω_c[1]. However, at $M \geq M_c$ (or $\omega \geq \omega_c$), the increase of temperature T will relax the tight packing of quasiparticles around the Fermi surface and makes some levels become partially unoccupied, therefore, available for scattered pairs. As a result, when T increases up to some critical value T_1, the pairing correlation is energetically favored, and pairing correlation reappears. As T goes higher, the increase of a large number of quasiparticles eventually breaks down the pairing at $T_2 > T_1$. This phenomenon is called thermally assisted pairing correlation or anomalous pairing, and later as pairing reentrance[2]. However, the experimental extraction of the pairing correlation in hot nuclei is not simple. Therefore a detection of the pairing reentrance effect by using experimentally extracted pairing gaps seems to be elusive. Meanwhile, the heat capacity has been extracted from the experimental nuclear level densities. A recent calculation of the hot rotating ^{72}Ge nucleus within the shell model Monte Carlo (SMMC) approach has found a local dip in the heat capacity at a rotation frequency of 0.5 MeV at $T \approx 0.45$ MeV, and a corresponding local maximum on the temperature dependence of the logarithm of level density[3]. Such irregularities are associated with the signatures of the pairing reentrance. The goal of this work is to study the pairing reentrance effect within a different microscopic approach, which bases on the BCS theory at finite temperature and total angular momentum, taking into account thermal fluctuations in terms of quasiparticle number fluctuation. The later has been found to be very important for finite nuclear systems, especially for light nuclei[4]. The corresponding approach is called the FTBCS1 plus angular momentum, which has been derived in detail in Ref[5] and successfully applied to study the pairing properties of hot rotating systems.

The numerical calculations are carried out for two realistic ^{60}Ni and ^{72}Ge nuclei. The latter is considered in order to have a comparison with the results obtained within the SMMC approach. The results obtained show the appearance of the pairing reentrance in the pairing gap at finite M and T [see e.g. Fig. 1 (a)]. Instead of decreasing with increasing T , the gap first increases with T then decreases at higher T.

† Condensed from the article in Phys. Rev. C **84**, 054324 (2011)

*1 Tan Tao University, Duc Hoa, Long An Province, Vietnam

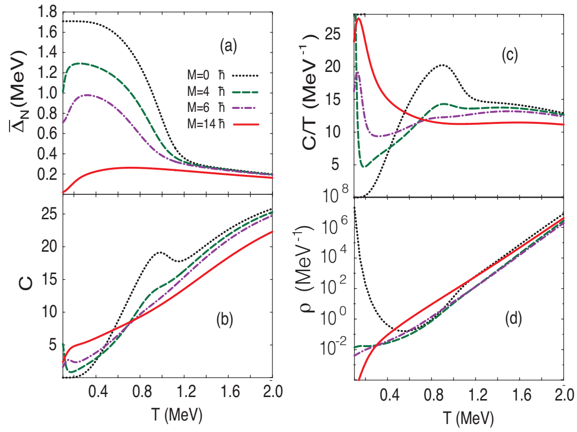

Fig. 1. Level-weighted neutron pairing gap $\bar{\Delta}$ (a), heat capacity C (b), heat capacity divided by temperature C/T (c), and level density ρ (d) for ^{60}Ni obtained within the FTBCS1 at different values of angular momentum M as functions of T.

It is demonstrated that the heat capacity C [Fig. 1 (b)], or rather C/T [Fig. 1 (c)] , and the level density ρ [Fig. 1 (d)] can be used to experimentally identify the pairing reentrance effect. The pairing reentrance leads to a clear depletion in the temperature dependence of the heat capacity, whereas the level density weakly changes from a convex function of T to a concave one. The later contradicts the claim of the SMMC calculations, which turns out to be an artifact caused by unphysically large values of the heat capacity at low T.

The numerical calculations were carried out using the RIKEN RICC system. NQH acknowledges the support by the National Foundation for Science and Technology Development (NAFOSTED) of Vietnam through Grant No. 103.04-2010.02.

References

1) B.R. Mottelson and J.G. Valatin, Phys. Rev. Lett. 5, 511 (1960).
2) T. Kammuri, Prog. Theor. Phys. 31, 595 (1964); L. G. Moretto, Nucl. Phys. A 185, 145 (1972); R. Balian, H. Flocard and M. Veneroni, Phys. Rep. 317, 251 (1999).
3) D. J. Dean, K. Langanke, H. A. Nam, and W. Nazarewicz, Phys. Rev. Lett. **105**, 212504 (2010).
4) N. Dinh Dang and V. Zelevinsky, Phys. Rev. C 64, 064319 (2001); V. Zelevinsky, B.A. Brown, N. Fazier, and M. Horoi, Phys. Rep. 276, 85 (1996).
5) N. Quang Hung and N. Dinh Dang, Phys. Rev. C 78, 064315 (2008).

Viscosity of hot nuclei†

N. Dinh Dang

[NUCLEAR STRUCTURE, shear viscosity, entropy, giant dipole resonance, hot nuclei, quark-gluon plasma, perfect liquid, Green-Kubo relation, entropy density, thermal pairing, phonon damping model]

In the verification of the condition for applying hydrodynamics to nuclear system, it turned out that the quantum mechanical uncertainty principle requires a finite viscosity for any thermal fluid. Kovtun, Son and Starinets (KSS)[1)] have conjectured that the ratio η/s of shear viscosity η to the entropy volume density s is bounded below for all fluids, namely the value

$$\frac{\eta}{s} = \frac{\hbar}{4\pi k_B} \simeq 5.24 \times 10^{-23} \text{ Mev s} . \tag{1}$$

is the universal lower bound (the so-called KSS bound or KSS unit). Although several theoretical counter examples have been proposed, no fluid that violates this lower bound has ever been experimentally found so far. Given this conjectured universality, there has been an increasing interest in calculating the ratio η/s in different systems.

In the present article, by using the Kubo relation and the fluctuation-dissipation theorem, the shear viscosity η and the ratio η/s have been extracted from the experimental systematics for the width of giant dipole resonance (GDR) in copper, tin and lead regions at $T \neq 0$, and compared with the theoretical predictions by four independent theoretical models, namely, the phonon damping model (PDM)[2)], the adiabatic model (AM), the phenomenological thermal shape fluctuation model (pTSFM), and the Fermi liquid drop model (FLDM). The calculations adopt the value $\eta(0) = 1.0^{+0.2}_{-0.4} \times u$ ($u = 10^{-23}$ Mev s fm^{-3}) as a parameter, which has been extracted by fitting the giant resonances at $T = 0$ and fission data. The analysis of numerical calculations shows that the shear viscosity η increases between (0.5 - 2.5)u with increasing T from 0.5 up to $T \simeq 3$ - 3.5 MeV for $\eta(0) = 1u$. At higher T, the PDM, AM, and pTSFM predict a saturation, or at least a very slow increase of η, whereas the FLDM shows a continuously strong increase of η, with T. At $T = 5$ MeV, the PDM estimates η between around (1.3 - 3.5)u.

All theoretical models predict a decrease of the ratio η/s with increasing T up to $T \simeq 2.5$ MeV. At higher T, the PDM, AM, and pTSFM show a continuous decrease of η/s, whereas the FLDM predicts an increase of η/s, with increasing T. The PDM fits best the empirical values for η/s extracted at $0.7 \leq T \leq 3.2$ MeV for all three nuclei, ^{63}Cu, ^{120}Sn, and ^{208}Pb. At $T =$ 5 MeV, the values of η/s predicted by the PDM reach $3^{+0.63}_{-1.2}$, $2.8^{+0.5}_{-1.1}$, $3.3^{+0.7}_{-1.3}$ KSS units for ^{63}Cu, ^{120}Sn, and ^{208}Pb, respectively. Combining these results with the model-independent estimation for the high-T limit of η/s, which is $2.2^{+0.4}_{-0.9}$ KSS units, one can conclude that the value of η/s for medium and heavy nuclei at $T = 5$ MeV is in between (1.3 - 4.0) KSS units, which is about (3 - 5) times smaller (and of much less uncertainty) than the value between (4 - 19) KSS units predicted by the FLDM for heavy nuclei. This estimation also indicates that nucleons inside a hot nucleus at $T =$ 5 MeV has nearly the same ratio η/s as that of the quark-gluon plasma, around (2 - 3) KSS units, at $T >$ 170 MeV discovered at the Relativistic Heavy Ion Collider (Brookhaven National Laboratory) and the Large Hadron Collider at CERN.

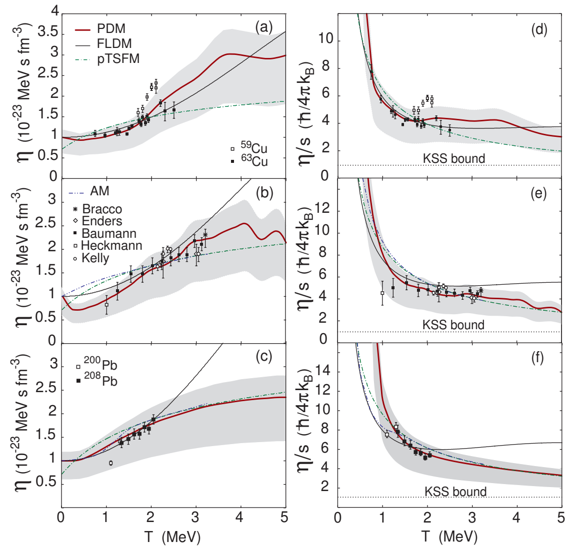

Fig. 1. Shear viscosity $\eta(T)$ [(a) - (c)] and ratio η/s [(d) - (f)] as functions of T for nuclei in copper [(a) and (d)], tin [(b) and (e)], and lead [(c) and (f)] regions. The gray areas are the PDM predictions by using $0.6u \leq \eta(0) \leq 1.2u$. The color lines denote the predictions by the models, whose names are shown in (a) and (b) and in the text. Data points have been extracted by using the corresponding experimental widths and energies for the GDR for these isotopes.

† Condensed from the article in Phys. Rev. C **84**, 034309 (2011)

References

1) P.K. Kovtun, D.T. Son, and A.O. Starinets, Phys. Rev. Lett. **94**, 111601 (2005).
2) N.D. Dang and A. Arima, Phys. Rev. Lett **80**, 4145 (1998).

Nucleus-nucleus interaction potential in heavy-ion collision

L. Guo,[*1] and T. Nakatsukasa

[time-dependent Hartree-Fock, interaction potential]

The nucleus-nucleus interaction potential in heavy-ion collision gives important information on the reaction dynamics. Various approaches have been employed to investigate internuclear potentials. Among these methods, the microscopic time-dependent Hartree-Fock (TDHF) with density-constraint (DC)[1] method is one of the successful approaches in a sense the nuclear structure and nuclear dynamics are treated in a unified framework and there are no free parameters in the description of the nuclear dynamics.

Our study aims at investigating some alternative methods to deduce the internuclear potential in the framework of the TDHF theory. The first of these methods is to employ the time-even (ev) TDHF hamiltonian, the second is to employ the boost-invariant (bi) TDHF hamiltonian, and the third is to employ the energy density functional (EDF) theory by using the frozen density (FD) approximation; the corresponding parameters are denoted as $h_{\rm ev}$, $h_{\rm bi}$, and FD in Fig. 1.

The first method involves solving the Schrödinger equation $\hat{h}\phi_i = \epsilon_i\phi_i$, where $\hat{h}$ is replaced with the ev-TDHF Hamiltonian at each time step. During the process of searching for the lowest solution, all the time-even fields in the Skyrme functional except the nuclear density are renewed. The energy expectation with respect to the Slater determinant of the ev single particle state, $E_{\rm ev} = \langle\Phi_{\rm ev}|\hat{H}|\Phi_{\rm ev}\rangle$, is the collective potential energy. The nucleus-nucleus potential at a given relative distance R is defined as

$$V_{\rm ev}(R) = E_{\rm ev} - E_{A1} - E_{A2}, \tag{1}$$

where E_{A1} and E_{A2} are the ground-state binding energies of the projectile and the target.

In the second method, the Hamiltonian in the Schrödinger equation is replaced with the bi-TDHF Hamiltonian defined in Ref.[2] $\hat{h} = \hat{h}^{\rm TDHF}_{\rm bi}(t)$. Similar to the ev-TDHF method, the boost-invariant energy $E_{\rm bi}$ in this method is expressed as $E_{\rm bi} = \langle\Phi_{\rm bi}|\hat{H}|\Phi_{\rm bi}\rangle$. The internuclear potential calculated with the bi-TDHF Hamiltonian is then expressed as

$$V_{\rm bi}(R) = E_{\rm bi} - T_{\rm R} - E_{\rm A1} - E_{\rm A2}, \tag{2}$$

where T_R is the instantaneous translational energy between the two nuclei.

The third method, FD-EDF, assumes that the densities of the projectile and the target remain constant and equal to their respective ground state densities ρ_p and ρ_T. By using the FD-EDF method, the interaction potential can be obtained as

$$V_{\rm FD}(R) = E[\hat{\rho}_{P+T}](R) - E[\hat{\rho}_P] - E[\hat{\rho}_T], \tag{3}$$

in terms of the energy functional E.

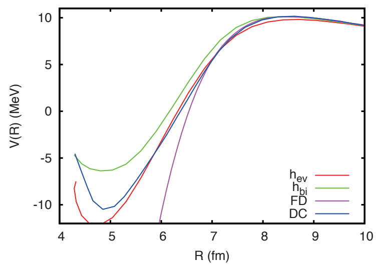

Fig. 1. Nucleus-nucleus interaction potentials for ^{16}O $+^{16}$ O, with Sly5 interaction and center of mass energy $\rm E_{cm}$ = 34 MeV, obtained with the ev-TDHF method (red line), bi-TDHF calculation (green line), FD-EDF method (purple line), and DC-TDHF results from Ref. [1] (blue line).

Fig. 1 shows our calculated nucleus-nucleus interaction potentials for the collision ^{16}O $+^{16}$ O obtained using the ev-TDHF method, bi-TDHF calculation, and FD-EDF method. For comparison, the DC-TDHF result from Ref.[1] is included in the figure. As the FD-EDF method does not consider the Pauli principle, the binding of the colliding system is overestimated. Near the Coulomb barrier, the overlap of the two densities is small, allowing FD-EDF to be compared with other methods. For a small relative distance, the potential calculated using FD-EDF should increase if the Pauli principle is accounted for. Potentials calculated with the ev-TDHF and bi-TDHF methods well reproduce the DC-TDHF results in the approaching process, until the Coulomb barrier is approached. When the approaching process develops further until the first touch, the potential from the ev-TDHF calculation also well reproduces the DC-TDHF results, whereas the potential from the bi-TDHF calculation becomes larger than that of DC-TDHF owing to the underestimation of the instantaneous collective kinetic energy. In order to verify the reliability of our method, more calculations for heavy systems are currently being peformed.

*1 Present address: College of Physical Sciences, Graduate University of Chinese Academy of Sciences, Beijing 100049, China

References

1) A. S. Umar, and V. E. Oberacker: Phys. Rev. **C 74**, 021601(R) (2006).
2) L. Guo, J. A. Maruhn, and P.-G. Reinhard: Phys. Rev. **C 76**, 014601 (2007).

Nuclear force in the parity-odd sector and the LS forces

K. Murano,[*1] for HAL QCD Collaboration

[Lattice QCD calculations, Nuclear forces]

Recently, a new method to extract the nucleon-nucleon (NN) potential on the basis of lattice Quantum Chromo Dynamics (QCD) has been proposed[1]. The potential is constructed from the Nambu-Bethe-Salpeter (NBS) wave function at the center of mass frame which is defined by

$$\phi(\vec{r};\vec{k}) = \langle 0|p(\vec{x})n(\vec{y})|p(+\vec{k})n(-\vec{k})\rangle, \vec{r} \equiv \vec{x} - \vec{y} \quad (1)$$

where $E = k^2/m_N$, with m_N being the nucleon mass. p and n denote the local composite nucleon operators.The NBS wave functions satisfy the following Schrödinger-type equation[2]:

$$\left(\frac{k^2}{m_N} + \frac{\nabla^2}{m_N}\right)\phi(\vec{r};\vec{k}) = \left[P^+V^{(+)} + P^-V^{(-)}\right]\phi(\vec{r};\vec{k}), \quad (2)$$

where P^+ (P^-) denotes a projection operator for parity plus (minus); and $V^{(+)}$ ($V^{(-)}$) potential projected onto the parity-plus (minus) sector. It is decomposed as

$$V^{(\pm)} = \Big[V_0^{(\pm)}(r) + V_\sigma^{(\pm)}(r)\vec{\sigma}_1\cdot\vec{\sigma}_2 + V_T^{(\pm)}(r)S_{12} + V_{LS}^{(\pm)}(r)\vec{L}\cdot\vec{S} + (\mathrm{NNLO})\Big], \quad (3)$$

where $V_0^{(\pm)}$ and $V_\sigma^{(\pm)}$ denote the central and spin-dependent central forces respectively; $V_T^{\pm}$ denotes the tensor force; and $V_{LS}^{(\pm)}$, the spin-orbit force. After calculating the NBS wave function from the lattice, potentials are obtained by solving Eq. 3. The method has been successfully applied to the potentials in the parity-even sector in the leading order of the derivative expansion, i.e., the central force ($V_0^{(+)}$,$V_\sigma^{(+)}$) and the tensor force ($V_T^{(+)}$) are obtained for various cases, including NN, YN, and YY systems (where Y represents a hyperon). In contrast, the method has not yet been applied to the forces in the parity-odd sector or to the spin-orbital force. In particular, the spin-orbit force is important in explaining the ls splitting of (hyper) nuclear spectra and the magic numbers of nuclei.

In this paper, we report our first attempt at determining the NN potentials in the parity odd sector including the spin-orbit force in lattice QCD. We calculated the NBS wave functions for a state in which a proton and a neutron collide with each other with a relative momentum of $\vec{k}$. First, we projected the NBS wave functions to parity-minus sector, as

$$\phi(\vec{r})^{(-)} = \left\{\phi(\vec{r};\vec{k}) - \phi(\vec{r};-\vec{k})\right\}/2. \quad (4)$$

Secondly, we projected the NBS wave function $\phi^{(-)}$ to the $^3P_0$ ($J = A_1, L = T_1$), $^3P_1$ ($J = T_1, L = T_1$) and $^3P_2$ ($J = E, L = T_1$) states based on the cubic group. Finally, by using these NBS wave functions, we solved Eq. 3 for $V_C^{(-)}$, $V_T^{(-)}$, and $V_{LS}^{(-)}$.

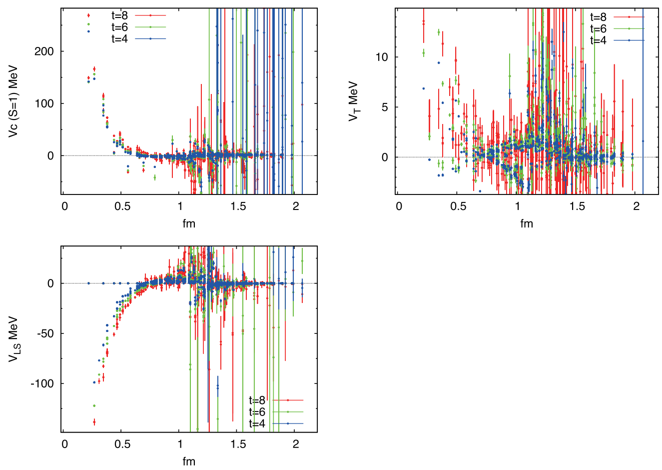

Fig. 1. Odd-parity potentials $V_C^{(-)}$, $V_T^{(-)}$, and $V_{LS}^{(-)}$ obtained from three NBS wave functions for $^3P_0$, $^3P_1$, and $^3P_2$.

The results are shown in Fig. 1. Although statistical errors are still large, we see that our preliminary results show qualitative features. (1) V_C is repulsive at all distances. In particular, it has a repulsive core at a short distance. (2) V_T is positive and quite small. (3) V_{LS} is large and negative. These features qualitatively agree with those of phenomenological potentials[3].

These calculations were performed using the University of Tsukuba Supercomputer system (T2K), with $N_f = 2$ CP-PACS gauge configurations on a $16^3 \times 32$ lattice at $a \simeq 0.16$ fm and $m_\pi \simeq 1100$ MeV.

References

1) N. Ishii, S. Aoki and T. Hatsuda, Phys. Rev. Lett. **99**, 022001 (2007).
2) S. Aoki, T. Hatsuda and N. Ishii, Prog. Theor. Phys. **123**, 89 (2010).
3) R. B. Wiringa, V. G. J. Stoks and R. Schiavilla, Phys. Rev. C **51**, 38 (1995).

*1 RIKEN Nishina Center, RIKEN

Variational calculation of ^{4}He tetramer ground and excited states using a realistic pair potential†

E. Hiyama and M. Kamimura[1]

[few-body problem, ultra cold atom]

In early 1970's, Efimov pointed out a possibility of having an infinite number of three-body bound states even when none exist in the separate two-body subsystems[1)]. This occurs when the two-body scattering length is much larger than the range of the two-body interaction.

In atomic systems, triatomic ^{4}He (trimer) have been expected to have bound states of Efimov type since the realistic ^{4}He-^{4}He interactions[2)] give a large ^{4}He-^{4}He scattering length ($\simeq$ 115Å), much greater than the potential range ($\sim$ 10Å), and a very small ^{4}He dimer binding energy ($\simeq$ 1.3 mK).

The main purpose of the present work is to perform accurate calculations of the ^{4}He tetramer ground and excited states using a realistic pair potential. We employ the Gaussian expansion method (GEM) for *ab initio* variational calculations of few-body systems[3)]. The method has been proposed and developed by the present authors and collaborators and applied to various types of three-, four- and five-body systems in nuclear physics and exotic atomic/molecular physics.

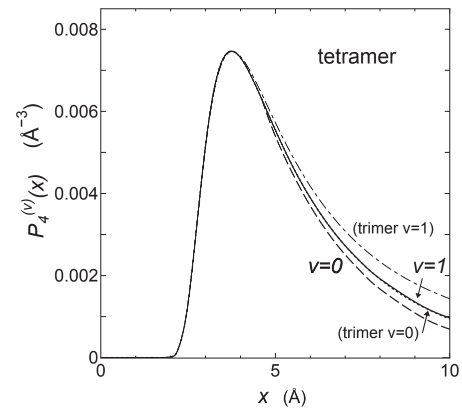

Fig. 1. Short-range structure of the pair correlation function. The dashed line stands for the tetramer ground ($v = 0$) state and the solid line for the excited ($v = 1$) state. For the sake of comparison, additionally shown are the dotted line for the trimer ground state and the dash-dotted line for the trimer excited state. The solid, dotted and dash-dotted lines have been multiplied by factors 2.76, 1.36 and 19.8, respectively.

We have 558.98 mK for the ground state and 127.33 mK for the excited state of the tetramer. The tetramer excited state is located only by 0.93 mK below the trimer ground state (126.40 mK). The former is in good agreement with the literature calculations, while the latter supports the result of 127.5 mK by Ref.[4)]. As shown in Fig.1, we find that the strong short-range correlation seen in the dimer appears also in the ground and excited states of the trimer and tetramer precisely in the same shape. This gives a foundation to an a *priori* assumption that a pair correlation function to simulate the short-range part of the dimer wavefunction is incorporated in the three-(four-) body wave function from the beginning.

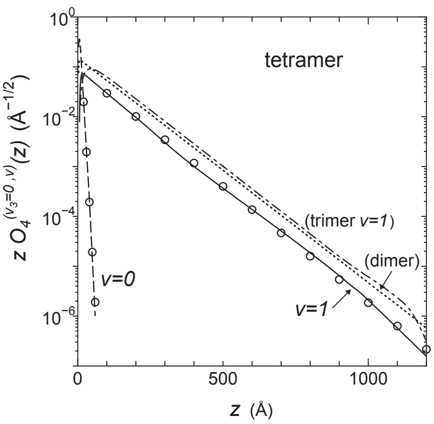

Fig. 2. Asymptotic behavior of the overlap function $\mathcal{O}_4^{(v_3=0,v)}(z)$, multiplied by z, between the trimer ground state ($v_3 = 0$) and the tetramer states ($v = 0, 1$). Open circles represent the exact asymptotic behavior.

As shown in Fig.2, we find that the asymptotic behavior of the tetramer excited state is in good agreement with the open circles up to 1000$\mathring{A}$. In this way, we succeed in describing short-range correlation and asymptoic behavior using our method.

† To be published in Phys. Rev. A

*1 Department of Physics, Kyushu University

References

1) V. Efimov, Yad. Fiz. **12**, 1080 (1970) [Sov. J. Nucl. Phys. **12**, 589 (1971)].
2) For example, R.A. Aziz, V.P.S. Nain, J.S. Carley, W.L. Taylor and G.T. McConville, J. Chem. Phys. **70**, 4330 (1979).
3) E. Hiyama, Y. Kino and M. Kamimura, Prog. Part. Nucl. Phys. **51**, 223-307 (2003).
4) R. Lazauskas and J. Carbonell, Phys. Rev. A **73**, 062717 (2006).

Deviations from the universal Efimov scenario in helium trimers

P. Naidon, E. Hiyama, and M. Ueda,*1

[Universality, few-body physics]

In 1970, nuclear physicist Vitaly Efimov found a curious effect[1] while looking at the problem of three nucleons interacting with short-range interactions. He considered the limit of resonant interactions, occurring when the interactions can almost or hardly bind two of these particles together, with no angular momentum. In other words, the interaction supports an s-wave bound or virtual two-body state (or *dimer*) with nearly zero binding energy, which corresponds to a divergence of the s-wave scattering length a. Because the scattering length becomes very large, much larger than the range of the interactions, most of the low-energy physics of the three particles depends on this length.

However, V. Efimov found that an effective $1/R^2$ attraction appears between the three particles (here, R denotes their hyper-radius) and pushes them to short distances from each other, where an extra length scale, known as the three-body parameter Λ, is required to account for the effect of the short-range interactions at these distances. Furthermore, the effective $1/R^2$ attraction can bind the three particles together to make three-body bound states (or *trimers*), and because the form of this attraction makes the Schr inger equation scale-invariant, the spectrum of these trimers is also scale invariant. Therefore, there is an infinite tower of trimers, whose sizes and energies can be related from one trimer to the next by multiplying by a universal scaling factor, approximately 22.7. It was particularly striking to find the existence of an infinity of trimers, whereas the dimer can hardly exist.

Although this Efimov effect is very general and applicable to any kind of particles, the conditions required for its realisation do not occur very often in Nature. For many years, the only example of such special three-body binding was the two trimers of helium-4 atoms. Recently, it has been possible to change at will the scattering length between ultra-cold atoms, and Efimov trimers made of various kinds of atoms could be observed indirectly or directly [2]. However these experiments could only probe the first two trimers of the infinite Efimov series, which lie at the limit of applicability of the Efimov theory. While confirming qualitatively the features of the theory (such as the scaling invariance), these experiments revealed significant deviations as well.

In order to understand these deviations, we considered the simplest system exhibiting the Efimov effect: three atoms of helium-4. The two-body interaction potential for these atoms is rather well-known, thus

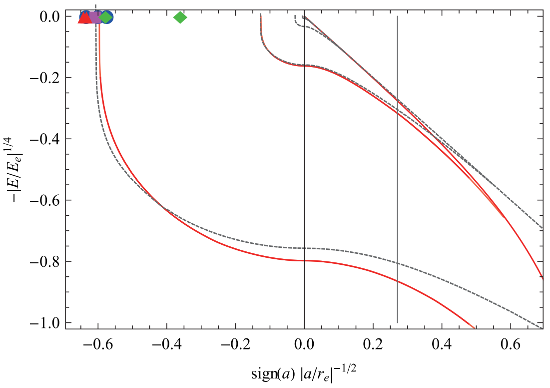

Figure 1. Computed energy of the first two Efimov trimers of helium-4 atoms as a function of the inverse scattering length $1/a$ (quantities are normalised in units of the effective range r_e). The red curves show the results obtained with realistic helium-4 potentials. The dashed curves show the Efimov theory. The symbols show recent experimental observations of the dissociation point of the first Efimov trimer with other kinds of atoms.

it is possible to make an ab-initio calculation of the trimer states, rather than employing effective or approximate theories like the Efimov theory. We solved the problem numerically by using the Gaussian expansion method [3]. To simulate the change of scattering length that is induced by a magnetic field in ultra-cold experiments, we multiplied the interaction potential by a scaling coefficient λ close to unity.

The computed trimer energies as a function of scattering length are shown in Fig. 1, where deviations from the universal Efimov trimer can be seen. We then replaced the complicated helium-4 two-body interaction potential by simpler potentials, such as local or separable Gaussian potentials, but having the same scattering lengths and effective ranges. We found that adjusting a small three-body interaction in addition to these simple two-body interactions could reproduce very well our previous calculations. This shows that the deviations from Efimov theory for the first two trimers can be characterised by only three parameters. Moreover this description is consistent with recent measurements involving other kinds of atoms.

References
1) V.N.Efimov, Sov. J. Nucl. Phys. 12, 589 (1970).
2) F.Ferlaino and R.Grimm, Physics 3, 9 (2010).
3) E. Hiyama, Y. Kino, and M. Kamimura, Prog. Part. and Nucl. Phys. 51, 223 (2003).

*1 Department of Physics, University of Tokyo

Compilation of experimental nuclear reaction data from RIKEN

N. Furutachi,[*1] M. Aikawa,[*1] V. Devi,[*2] D. Ichinkhorloo,[*3] M. Kimura,[*4] A. Makinaga,[*2] T. Matsumoto,[*5] M. Odsuren,[*2] N. Otuka,[*6] K. Tsubakihara,[*2] K. Yamamoto,[*2] and K. Kato[*1]

[Nulcear reaction, Database, NRDF, EXFOR]

Nuclear reaction data are essential for the development of the basic nuclear science, as well as applications such as nuclear engineering and radiation therapy. It is very important to compile experimental nuclear reaction data and construct their database. The Hokkaido University Nuclear Reaction Data Centre (JCPRG)[1)] compiles domestic nuclear reaction data and provides the compiled data to nuclear data users. JCPRG has developed its own database, NRDF, since 1974, and it also contributes to the international nuclear reaction database EXFOR. The compiled nuclear reaction data are available on the online search systems of NRDF[2)] and EXFOR[3)], respectively. In this article, we report on our activities in 2011 concerning the experimental nuclear reaction data produced at RIKEN facilities.

Table 1 lists the number of papers compiled in 2010 and 2011. We compiled nuclear reaction data from the 20∼30 papers published in a year. For the papers published in 2011, we have compiled 6 papers[4–9)] that report the data obtained at RIBF. They are easily accessible by a unique accession number (1 alphabet and 4 digits, as shown in the reference, e.g., E2324) in the EXFOR search system[3)]. Owing to the cooperation provided by the authors, the numerical data published in figures have been received from the authors and compiled into the NRDF and EXFOR databases. In addition, some of these EXFOR files could be proofread by authors for achieving better quality.

JCPRG established a collaborative research contact with RIKEN Nishina Center in 2010, in order to advance the compilation process and make the availability of the nuclear reaction data produced at RIBF to users possible. For this collaborative research, improvement in the database format is necessary. Owing to the recent development of experimental techniques, nuclear reactions have become more complex than before. Such nuclear reaction data are occasionally difficult to compile in the present database formats. For example, data from sequential reactions and breakup reactions from among the unstable nuclear reactions performed at RIBF are sometimes difficult to compile in the EXFOR format. Therefore, we need to discuss and consider the improvement of the database format in order to compile such data.

To achieve completeness and rapidness in RIBF data compilation, we plan to extend the survey scope of our papers to conference proceedings beyond peer-reviewed journals. In the case of the compilation of proceedings, data need to be compiled through a careful discussion with authors about their reliability because they may be preliminary.

In December 2011, we held the RIBF ULIC mini-workshop in order to report on the present data compilation status and to discuss the future development required to compile the experimental nuclear reaction data obtained at RIBF. We have discussed several topics: the feasibility of extending the compilation scope to unpublished RIKEN data and/or conference proceedings, problems of the present database format, the data searching system, and the future plan. In addition, a practical procedure for the efficient compilation of RIKEN data has been discussed, and we have agreed to cooperate for searching papers for compilation. JCPRG continuously devotes efforts to improve the completeness and usability of the experimental nuclear reaction data produced at RIBF. The details of our activities are presented on our website[1)].

Table 1. Numbers of compiled papers for which experiments have been performed at the RIKEN facilities and all domestic facilities (Total), respectively. The data for 2010 and 2011 are shown for comparison.

Publication year	RIKEN	Total
2010	8	21
2011	6	17

*1 Faculty of Science, Hokkaido University
*2 Meme Media Laboratory, Hokkaido University
*3 Graduate School of Science, Hokkaido University
*4 Creative Research Institution, Hokkaido University; Present Affiliation: Faculty of Science, Hokkaido University
*5 Meme Media Laboratory, Hokkaido University; Present Affiliation: Department of Physics, Kyushu University
*6 Nuclear Data Section, International Atomic Energy Agency

References

1) http://www.jcprg.org/
2) Nuclear Reaction Data File (NRDF); http://www.jcprg.org/nrdf/
3) EXchange FORmat (EXFOR); http://www.jcprg.org/exfor/
4) H. Haba *et al.*, Phys. Rev. C **83** (2011) 034602 (E2324)
5) Y. Satoh *et al.*, Phys. Lett. B **697** (2011) 459 (E2325)
6) H. Yamaguchi *et al.*, Phys. Rev. C **83** (2011) 034306 (E2326)
7) J. L. Lou *et al.*, Phys. Rev. C **83** (2011) 034612 (E2327)
8) K. Sekiguchi *et al.*, Phys. Rev. C **83** (2011) 061001(R) (E2346)
9) T. Yamaguchi *et al.*, Nucl. Phys. A **864** (2011) 1 (E2350)

3. Hadron Physics

Photoproduction of $\Lambda(1405)$ and $\Sigma^0(1385)$ on proton at $E\gamma = 1.5$–3.0 GeV at SPring-8/LEPS

Y. Nakatsugawa for LEPS collaboration

[SPring-8, LEPS, photoproduction, $\Lambda(1405)$]

$\Lambda(1405)$ is assigned as a p-wave q^3 baryon in a quark model. However, it is also suggested that $\Lambda(1405)$ has a non-q^3 structure, for instance, as a meson-baryon molecular state. Some theoretical works, using a chiral Lagrangian model and coupled unitary model, predict the line shape of $\Lambda(1405)$ as $\pi\Sigma^0$ and $\overline{K}N$[1]. Its 2-pole structure has also been suggested[2]: one pole strongly couples to $\pi\Sigma^0$ and the other to $\overline{K}N$. On the other hand, $\Sigma^0(1385)$ is firmly established as a q^3 state baryon. The difference in the internal structures of $\Lambda(1405)$ and $\Sigma^0(1385)$ may appear in the photoproduction cross sections and/or photon beam asymmetries of these two hyperons[3]. Recently, differential cross sections for the $\gamma p \to K^+\Lambda(1405)$ and $\gamma p \to K^+\Sigma^0(1385)$ reactions were measured by LEPS collaboration[4]. However, the statistics were limited. Therefore, a new experiment was carried out at SPring-8/LEPS with a liquid hydrogen target and linearly polarized photon beam. In order to detect the decay products of hadrons, a TPC has been installed surrounding the target and used together with the LEPS spectrometer.

To obtain the yields of $\Lambda(1405)$ and $\Sigma^0(1385)$ separately, we are focusing on the following two reactions considering certain cut conditions:

(1) $\gamma p \to K^+\Sigma^0(1385) \to K^+\Lambda\pi^0 \to K^+p\pi^-\ \pi^0$

(2) $\gamma p \to K^+\Lambda(1405) \to K^+\ \Sigma^\pm\pi^\mp \to K^+n\pi^+\pi^-$

The spectrum of $\Sigma^0(1385)$ was extracted from reaction (1) using the following cut conditions: (i) K^+ was detected in the forward spectrometer, (ii) a proton and a π^- were detected in the TPC, (iii) a $\Lambda(1116)$ was identified using the invariant mass of $p\pi^-$. Fig.1 shows the missing mass spectrum of $\gamma p \to K^+X$ ($MM(K^+\pi^+\pi^-)$) after cuts (i),(ii), and (iii). Fig.1 a)-c) comrespond to a) $1.5<E\gamma<2.0$GeV, b) $2.0<E\gamma<2.4$GeV and c) $2.4<E\gamma<3.0$GeV, respectively. The bump structure of $\Sigma^0(1385)$ can be seen around $1.38\text{GeV}/c^2$. Because $\Lambda(1405)$ is prohibited from decaying into $\Lambda\pi^0$ by isospin conservation, the yield of $\Sigma^0(1385)$ can be estimated from its decay branching ratios.

The spectrum of $\Lambda(1405)$ was obtained from reaction (2) considering the following cut conditions: (iv) K^+ was detected in the forward spectrometer, (v) a π^+ and a π^- were detected in the TPC, and (vi) a neutron was identified using the missing mass of $\gamma p \to K^+\pi^+\pi^-X$. It is should be noted that because of a strong interference of the isospin 0 and 1 terms of the $\Sigma\pi$ scattering amplitudes, the line shape of $\Lambda(1405)$ could be different in the $\Sigma^-\pi^+$ and $\Sigma^+\pi^-$ decay modes.[1] In order to separate both decay modes, a kinematic fit with two constraints, $MM(K^+\pi^+\pi^-) = M(n)$ and $MM(K^+\pi^\pm) = M(\Sigma^\pm)$, was applied. Bumps of $\Lambda(1405)$ can be seen around 1.4 GeV in Fig.2: a) $\Sigma^-\pi^+$ decay mode and b) $\Sigma^+\pi^-$ decay mode. The isospin interference term is canceled by summing the spectra of the $\Sigma^-\pi^+$ and $\Sigma^+\pi^-$ modes. Fig.3 shows the combined spectra in three energy bins: a) $1.5<E\gamma<2.0$GeV, b) $2.0<E\gamma<2.4$GeV and c) $2.4<E\gamma<3.0$GeV.

In order to discuss the cross sections of $\Sigma^0(1385)$ and $\Lambda(1405)$ and the line shape of $\Lambda(1405)$, more precise studies of backgrounds and acceptance calculation are required. All plots will be revised soon.

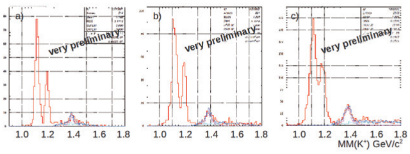

Fig. 1. $MM(K^+)$ after selection cuts (i),(ii), and (iii)

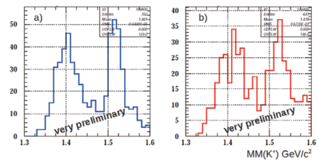

Fig. 2. $MM(K^+)$ after selection cuts (iv),(v), and (vi)

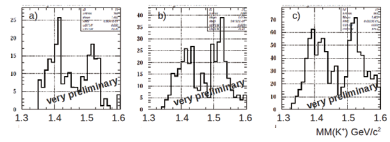

Fig. 3. The combined spectra of $\Sigma^-\pi^+$ and $\Sigma^+\pi^-$ modes

References

1) J. C. Nacher, E. Oset, H. Toki, and A, Ramos: Phys. Lett.B **455**, 55(1999).
2) D. Jido, J. A. Oller, E. Oset, A. Ramos, and U.-G. Meissner: Nucl. Phys. A **755**, 669(2005).
3) Y. Oh, C. M. Ko, and K. Nakayama : Phys. Rev.C **77**, 045204(2008).
4) M. Niiyama *et al.*: Phys. Rev.C **78**, 035202(2008).

Measurement of flavor asymmetry of light quark sea of the proton in the E906/SeaQuest Drell-Yan experiment

S. Miyasaka*[1], Y. Goto, Y. Miyachi*[2], K. Nakano*[1], F. Sanftl*[1], S. Sawada*[3], T.-A. Shibata*[1], and S. Takeuchi*[1]

A proton consists of valence quarks, sea quarks, and gluons. The sea quarks include antiquarks. The numbers of anti-down ($\bar{d}$) and anti-up ($\bar{u}$) quarks in the proton were previously thought to be equal, on the basis of SU(2) flavor symmetry. The result of the 1991 NMC experiment[1)] at CERN, however, indicated the asymmetry of these, making the discovery of the Gottfried sum rule violation. We, the E906/SeaQuest experiment group at Fermi National Accelerator Laboratory (Fermilab), will measure the $\bar{d}/\bar{u}$ ratio in the region of large Bjorken x using the Drell-Yan process, as shown in Fig. 1. The Drell-Yan process occurs in hadron-hadron collision when a quark of one hadron and an antiquark of the other hadron annihilate into a virtual photon. Then, a muon pair is created as follows: $q + \bar{q} \rightarrow \gamma^* \rightarrow \mu^+ + \mu^-$. The E906/SeaQuest experiment is a fixed-target experiment. A proton and a deuteron are used as the targets. The $\bar{d}/\bar{u}$ ratio is obtained by comparing the Drell-Yan events in $p + p$ and $p + d$ collisions.

The E906/SeaQuest experiment follows the E866/NuSea experiment[2)] at Fermilab. In the E866/NuSea experiment, the $\bar{d}/\bar{u}$ ratio was measured over a wide Bjorken x range, $0.015 < x < 0.35$, as shown in Fig. 2. The $\bar{d}/\bar{u}$ ratio is as large as 1.7 at $x \simeq 0.2$. Moreover, the ratio seems to be smaller than 1 at high x, although this is not yet conclusive owing to the limited statistical accuracy. Because no theoretical models can reproduce the decrease in the ratio to less than 1, a new characteristic of the proton structure is indicated. Therefore, it is very important to measure the ratio at high Bjorken x, hence, in the E906/SeaQuest experiment, the ratio is measured in the range $0.1 < x < 0.45$. In the E866/NuSea experiment, an 800-GeV proton beam was used, while in the E906/SeaQuest experiment, a 120-GeV proton beam is used. Since a lower enegy beam is used in the E906/SeaQuest experiment, the number of recorded events might increase by a factor of 50 at high x in comparison with that in the E866/NuSea experiment. The anticipated accuracy is 10 times better at $x \simeq 0.3$.

Three tracking stations are used in the E906/SeaQuest experiment. Each station is equipped with trigger hodoscopes and drift chambers for tracking. The Japanese groups (RIKEN, KEK, Tokyo Institute of Technology, and Yamagata University) are in charge of one of the stations. The trigger hodoscopes were successfully set up by February 2011, and the drift chambers were installed in March 2011. Cabling to the data acquisition systems was completed in autumn 2011. We tested the drift chambers with cosmic rays. Clear signals due to the cosmic rays were derived from the drift chambers. The signals were triggered by the hodoscopes. We then proceeded extrtact TDC data pertaining to the cosmic rays using the data acquisition systems. The first beam for commissioning will be available by the end of February 2012.

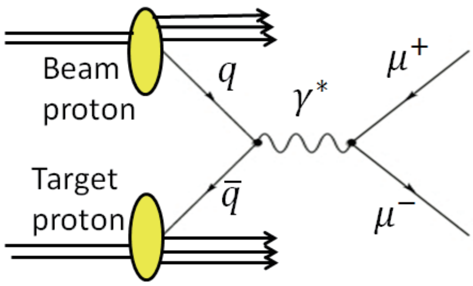

Fig. 1. Schematic representation of the Drell-Yan process.

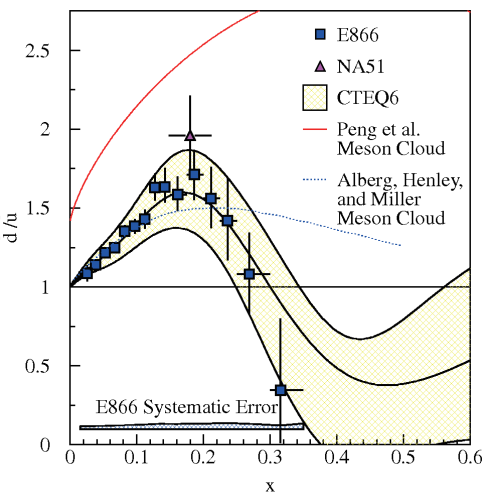

Fig. 2. Flavor asymmetry, $\bar{d}/\bar{u}$, as a function of x.

References
1) P. Amaudruz *et al.*: Phys. Rev. Lett. **66**, 2712 (1991).
2) R. S. Towell *et al.*: Phys. Rev. D **64**, 052002 (2001).

*1 Tokyo Institute of Technology
*2 Yamagata University
*3 KEK

Fragmentation function measurements with the Belle detector

R. Seidl, M. Leitgab,[*1] A. Vossen,[*2] F. Giordano,[*1] N. Kobayashi,[*3] M. Grosse-Perdekamp,[*1] A. Ogawa,[*4*5] C. Hulse[*6] and G. Schnell,[*6*7]

[fragmentation, spin, QCD]

The precise knowledge of fragmentation functions (FF) is needed for any semi-inclusive deep inelastic scattering (SIDIS) or proton-proton (pp) measurement including at least one final state hadron with the exception of jet measurements. The majority of the knowledge on unpolarized fragmentation functions were obtained at LEP whose energies are around the Z mass and above. Recently also hadronic cross sections in SIDIS and pp were used in global analyses to extract fragmentation functions. However, one important missing piece is the knowledge of fragmentation functions at energy scales close to the existing polarized measurements to extract the spin structure of the nucleon and in particular at high fractional energies $z >$ 0.7. These regions are especially important to the RHIC measurements of the gluon spin's contribution to the proton as mostly high z particles are selected. The gluon fragmentation function enters in e^+e^- annihilation only through the QCD evolution w hich requires a large lever arm in the collision energy scale Q. The Belle experiment at a scale of only 10 GeV can provide this and will thus in turn reduce the uncertainty on the gluon fragmentation function. The measurements of fragmentation functions for pions, kaons and protons are currently ongoing with results expected soon. In addition spin-dependent fragmentation functions can be applied as polarimeters for the parton's spin in the nucleon. The chiral-odd Collins fragmentation function is described by a non-uniform azimuthal modulation of the yield of a detected final state hadron relative to the spin direction and momentum direction of the initial quark. The modulation is described by a sine modulation which in the case of e^+e^- becomes a cosine modulation of the sum of the two angles defined by the two hadrons in opposite hemispheres relative to the production plane spanned by the lepton axis and the quark axis (approximated by the thrust axis). First results for charged pion pairs, were obtained by the Belle collaboration[1]. They were since then improved by a significantly larger amount of statistics[2]. The results from the Belle data were included in a global fit together with the HERMES[3] Collins moments on a proton target and the COMPASS[4] results on a deuteron target to obtain the first, still model-dependent extraction of u and d quark transversity distributions of the nucleon[5]. Another chiral-odd fragmentation function is the interference fragmentation function (IFF) which again can be cleanly obtained from e^+e^- annihilation and then used in SIDIS or pp collisions to access transversity. Unlike the Collins FF, which requires an explicit dependence on the transverse momentum of the final state hadron, the IFF is sensitive to the azimuthal orientation of the plane spanned by two final state hadrons of different sign and therefore any transverse momenta are integrated over. This makes this function preferable as QCD evolution is known. Belle has first measured the IFF in charged pion pairs[6] (see Fig. 1) this year and this data together with HERMES data[7] has been used to extract transversity as well[8] which seems to coincide with the extraction obtained using the Collins asymmetries. Further measurements of different final states for the Collins FF and IFF are ongoing and more sophisticated, explicitly transverse momentum dependent measurements are being prepared.

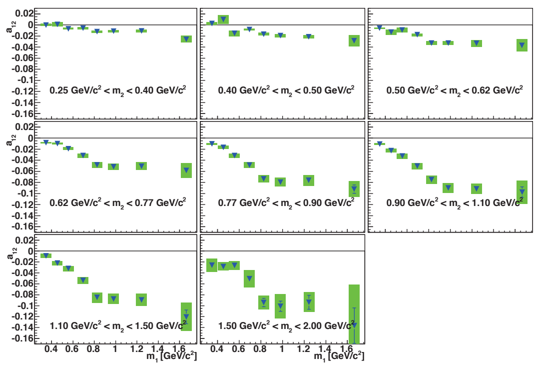

Fig. 1. IFF related cosine modulations for the 8×8 m_1, m_2 binning as a function of m_1 for the m_2 bins, where $1, 2$ stands for the hemisphere.

References
1) R. Seidl *et al.*, Phys. Rev. Lett. **96**, 232002 (2006).
2) R. Seidl *et al.*, Phys. Rev. D **78**, 032011 (2008).
3) A. Airapetian *et al.*, Phys. Rev. Lett. **94**, 012002 (2005).
4) V. Y. Alexakhin *et al.*, Phys. Rev. Lett. **94**, 202002 (2005).
5) M. Anselmino *et al.*, Phys. Rev. D **75**, 054032 (2007).
6) A. Vossen *et al.*, Phys. Rev. Lett. **107**, 072004 (2011).
7) A. Airapetian *et al.*, JHEP **0806**, 017 (2008).
8) A. Bacchetta, A. Courtoy, M. Radici, Phys. Rev. Lett. **107**, 012001 (2011).

*1 University of Illinois, Urbana, IL, U.S.A.
*2 University of Indiana, Bloomington, ID, U.S.A.
*3 Tokyo Institute of Technology, Japan
*4 Brookhaven National Laboratory, Upton, NY, U.S.A
*5 RIKEN BNL Research Center, Upton, NY, U.S.A
*6 University of the Basque Country, Bilbao, Spain
*7 Ikerbasque, Spain

Comparison of elliptical flow for six particles in 200 GeV Au+Au collision in RHIC-PHENIX

Y. Ikeda

In relativistic heavy ion collision, participants are geometrically well separated. The initial geometry of the collision system is oval because of non-central collision. A large azimuthal anisotropy of particle emission that depends on the initial geometry has been found. Experimentally, this azimuthal anisotropy is extremely important because it is related to the initial stage of collision. In particular, elliptical anisotropy, which is the second term of the Fourier series, is believed to carry the initial geometrical anisotropy. The large v_2 can be evidence for the short mean-free path of the particles in the hot dense medium. The measured v_2 increases with p_T in the low-p_T (soft) region, as shown by hydrodynamical calculations, in which fast thermalization is assumed in the initial stage and the share viscosity is thought to be small for the entire entropy density range. [1)2)]

The v_2 measurement in RHIC-PHENIX has so far been limited to the low-p_T region with abundant yield because of the complex statistics, which in turn can be attributed to the poor resolution of the reaction-plane detectors. A new reaction-plane detector RxP with higher resolution was installed to measure the elliptical flow in RHIC-PHENIX experiment.[3)] RxP allowed us to measurments in the carry out azimuthal anisotropy higher-p_T region, above 3 GeV/c. The obtained v_2 values for π, K, p, d, Λ, and Φ are shown in Fig. 1.

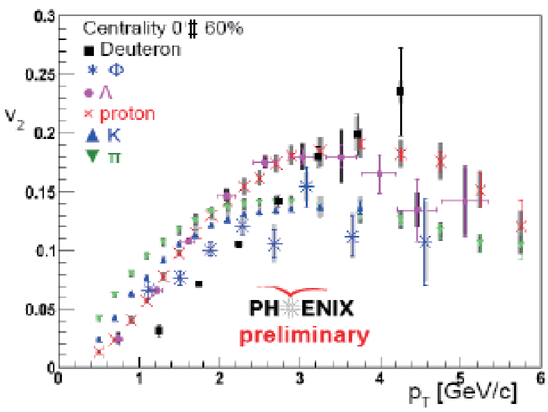

Fig.1 v_2 versus p_T for six particles.

The new plot is drawn using v_2/n_q as the vertical axis and KE_T/n_q as the horizontal axis, where n_q is the number of constituent quarks for a hadron and KE_T (= $m_T - m$) is the transverse kinetic energy. Six particles of v_2/n_q are consistent at $KE_T/n_q < 0.8$ GeV. The agreement between the v_2 values of six different particles indicates the success of quark coalescence mechanism [3)4)] for hadron generation. Φ meson is a very important parameter for verifying of quark coalescence picture, because it is a meson with n_q = 2, while its mass is heavy and comparable to that of a proton and a Lambda baryon and cross section of hadron scattering is small. The consistency of Φ meson with other hadrons implies that v_2 of the hadrons is generated by partons in the Quark Gluon Plasma phase before phase transition and that it has a small effect on the hadron scattering. The unified trend between v_2/n_q and KE_T/n_q is not observed at $KE_T/n_q > 0.8$ GeV. This divergence is understandable from the consideration that particles in the high-p_T region do not follow the hydrodynamical evolution and suffer considerable energy loss while traversing the hot medium.

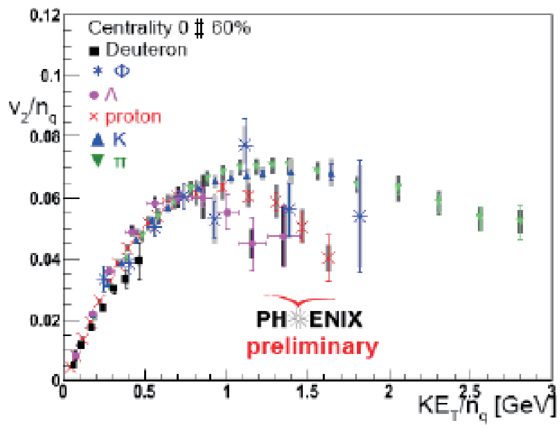

Fig. 2 v_2 versus KE_T on quark number scaling.

References

1) P. Houvinen, P.E. Kolb, U.W. Heinz, P.V. Ruuskanen, and S.A. Voloshin, Phys. Lett. B503, 58 (2001)

2) S. S. Adler et al., (PHENIX Collaboration), Phys. Rev. Lett. 91, 182301 (2003)

3) E, Richardson et al., Nucl. Intsr. And Mass. A vol636, 99, (2010)

4) R.J. Fries, B. Muller, C. Nonaka, S.A. Bass, Phys. Rev. Lett. 90, 202303 (2003)

5) R.J. Fries, B. Muller, C. Nonaka, S.A. Bass, Phys. Rev. C68, 044902 (2003)

Two-particle correlations with higher harmonic flow subtractions in Au+Au $\sqrt{s_{NN}} = 200$ GeV collisions at RHIC-PHENIX†

T. Todoroki *1 for the PHENIX Collaboration

[Quark gluon plasma, jet quenching, parton energy loss]

The quark gluon plasma (QGP) is the phase of matter at a high energy density and the existence of which is predicted by quantum chromodynamics. High-energy heavy-ion collisions are considered to be a unique tool to realize such a high-density state, and the study of the matter properties is an important issue in addition to the confirmation of QGP generation. Measurements of di-hadron correlations are useful in understanding the interplay between hard-scattered and soft-collective partons in QGP.

In $\sqrt{s_{NN}} = 200$ GeV Au+Au collisions, di-hadron correlations having a double hump structure[3)] are observed at the away side in azimuthal direction and long range pseudo-rapidity correlations are observed at near side, while these structures of correlations are not seen in $\sqrt{s} = 200$ p+p collisions. Therefore, these phenomena can be considered to be characteristic of heavy ion collisions, and a detailed study may reveal new features of QGP properties.

Recently it has been suggested via AMPT model simulations that the double hump structures at away side can be described by the triangular flow[2)] originating from the fluctuations of initial collision geometry. Eq.(1) is the definition of triangular and higher harmonic flow, where ϕ indicates the azimuthal angle of emitted hadrons and Ψ_n denotes the nth harmonic reaction plane.

$$v_n =< \cos n(\phi - \Psi_n) > \qquad (1)$$

The existence of a higher harmonic flow including triangular flow is confirmed[3,4)] and magnitudes of v_3 and v_4 are in the same level of elliptic flow v_2. Contributions from higher harmonic flow to the two particle angular correlations have to be subtracted, as suggested by AMPT. The double hump structure in most central collisions(0-1%) with a large pseudo-rapidity gap($|\Delta\eta| > 1$) between the di-hadron pair is well described[4)] with the contributions from higher-order harmonics, v2, v3, and v4. With consideration of the fact that flow measurements require a sufficient pseudo-rapidity gap to exclude the auto correlations from the hard process, the correlations with a large pseudo-rapidity gap have essentially the same information as higher harmonic flow. Therefore, it is important to select the pairs without a pseudo-rapidity gap when studying the interplay between hard and soft partons.

† Results from RHIC experimental operations in 2007

*1 Graduate School of Pure and Applied Sciences, University of Tsukuba

For this purpose, di-hadron correlation without a rapidity gap has been investigated for the data of Au+Au collisions at $\sqrt{s_{NN}} = 200$ GeV taken in the 2007 run. The v_n of charged hadrons within $|\eta| < 0.35$ is measured with the event plane determined at $1.0 < \eta < 2.8$. Figure 1 shows the results of di-hadron correlations after v_2, v_3, and v_4 contributions are subtracted. In most central collisions,the double hump structure at the away side is almost vanished, which is similar to the case with the pseudo-rapidity gap. However, when centrality reaches up to the level of mid-central collisions, the amplitude of the double hump structure increases.

The result shows that higher harmonics cannot necessarily explain the di-hadron angular correlation in non-central collisions and suggests that the interplay between the hard and soft process plays a role in generating the characteristic correlation patterns in heavy ion collisions.

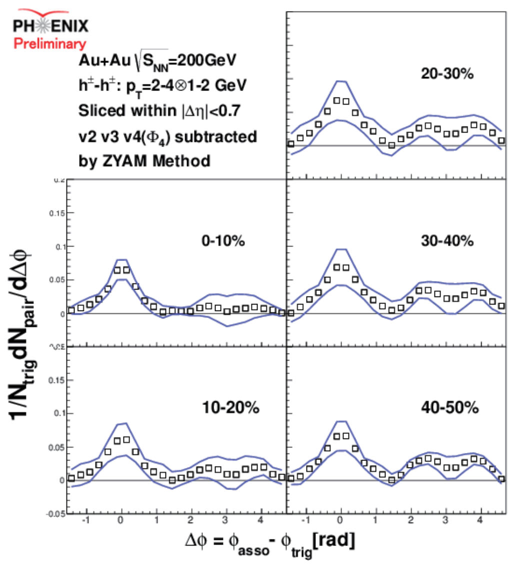

Fig. 1. Pair yield per a trigger with p_T selection p_T^{trig}=2-4, p_T^{asso}=1-2[GeV/c] in Au+Au $\sqrt{s_{NN}}$ =200 GeV collisions from 0% to 50% centrality. Contributions from v_2, v_3, and v_4 are subtracted.

References
1) A. Adler *et al*, Phys. Rev. C. **78**, 014901 (2008).
2) B. Alver *et al*, Phys. Rev. C **81**, 054905 (2010).
3) A. Adare *et al*, Phys. Rev. Lett. **107**, 252301 (2011).
4) K. Adamodt *et al*, Phys. Rev. Lett. **107**, 032301 (2011).

Contributions of higher order flow harmonics in two particle correlations in Au+Au collisions at $\sqrt{s_{NN}} = 200$ GeV

C.-H. Chen,*1

[heavy ion collision, two particle correlations, higher harmonic flow]

The two particle azimuthal correlation method has been proved as an extremely powerful method to study jet properties in quark-gluon plasma (QGP) [1]. The correlation function (CF), is assumed to have two components: the underlying event background (FL), and jet components (JF), and it can be written as

$$CF(\Delta\phi) = JF(\Delta\phi) + FL(\Delta\phi) \tag{1}$$

where $\Delta\phi$ is the azimuthal difference between two particles. The shape of the underlying event background can be described by Eq. 2

$$\begin{aligned} FL(\Delta\phi) = b_0(1 &+ 2v_2^a v_2^b cos(2\Delta\phi) \\ &+ 2v_3^a v_3^b cos(3\Delta\phi) \\ &+ 2v_4^a v_4^b cos(4\Delta\phi)...) \end{aligned} \tag{2}$$

where $v_n^{(a,b)}$ is the n-th order Fourier coefficient of the particle angular distribution of the trigger and partner particles. b_0 is the level of the underlying event background, which should be determined separately.

The v_n of the particles are measured by PHENIX at the Relativistic Heavy Ion Collider at Brookhaven National Laboratory [2]. The background level, b_0, is determined by the method called "absolute normalization"[3] in Au+Au collisions. In $p+p$ collisions, b_0 is determined by a method called "ZYAM" , which stands for "zero yield at minimum" [4].

Fig. 1 is the inclusive photon-charged hadron azimuthal correlation function, where the p_T of the inclusive photons are 2-3 GeV/c, and the p_T of the inclusive charged hadrons are 1-2 GeV/c. The centrality in Au+Au collisions is 0-20%.

The left column of Fig. 1 is flow background with only v_2 modulation. The first row is the per trigger yield Au+Au CF, where the magenta curve represents the flow background. The jet function is plotted in the second row as black points. The red points are the CF of p+p plotted as a reference. With the v_2 background, the double peak structure in away side is consistent with previous measurement [4]. The third row shows the Fourier spectra of the Au+Au jet function (plotted as black points) compared with two different $p+p$ cases. The solid red curve represents the unmodified $p+p$, and the red dashed curve represents $p+p$ with away side fully suppressed. The third harmonic C_3 in Au+Au is significantly higher than in $p+p$.

The v_3 term is included in the flow function in the second column. The subtracted jet function in the second row shows that the double peak structure is significantly reduced, and there is a pedestal-like structure under the jet correlation function.

The Fourier spectra in the third row show that the third harmonic is significantly reduced, which is not surprising because we included the v_3 contribution in the flow and removed them. The last column has v_2, v_3, and v_4 in the flow subtraction. We can see that the subtracted jet function resembles a broadened and suppressed jet sitting on a flat pedestal.

In summary, the jet shape in Au+Au two particle correlations depends heavily on the shape of the underlying event background. When we add the v_3 and v_4 contribution, the double peak structure in away side disappears.

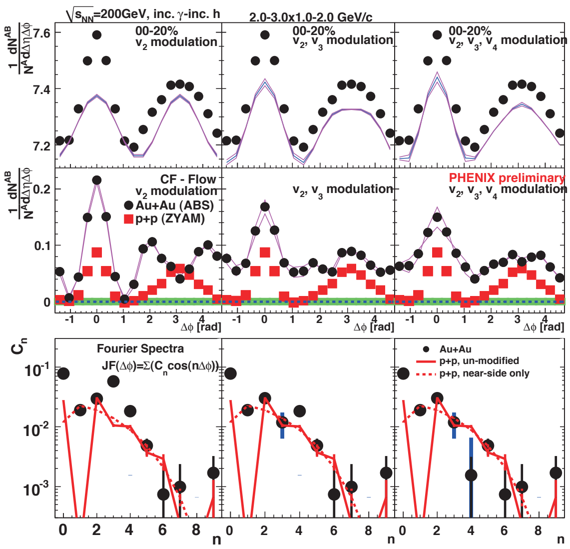

Fig. 1. Comparison of jet shape in Au+Au under different background modulations with $p+p$.

*1 Riken Brookhaven Research Center, Brookhaven National Laboratory

References
1) A. Adare et al.: Phys. Rev. C 78, 014901 (2008)
2) A. Adare et al.: Phys. Rev. Lett. 107, 252301 (2011)
3) Anne Sickles, Michael P. McCumber, Andrew Adare: Phys. Rev. C 81, 014908 (2010)
4) S. S. Adler et al.: Phys. Rev. Lett. 97, 052301 (2006)

Analysis of Single Electrons in PHENIX Cu+Cu Collisions at Center-of-Mass Energy 200 GeV per Nucleon Pair

Stephen Baumgart for the PHENIX Collaboration

The interaction of heavy flavor with the nuclear medium generated in a heavy-ion collision can be studied via the nuclear modification factor ($R_{AA} \equiv \frac{dN^e_{CuCu}/dp^e_t}{<N_{coll}>dN^e_{pp}/dp^e_t}$ where N_{coll} is the number of binary collisions and dN/dp_t is the invariant yield). The PHENIX collaboration previously measured the single electron spectra in $\sqrt{s_{NN}} = 200$ GeV $p+p$[1] and $Au+Au$[2] collisions. These results show that heavy flavor electron spectra are suppressed at higher p_t in the Au+Au system. This is probably due to a combination of radiative and collisional energy loss.

The PHENIX central arms were used for data collection[3]. Track geometry, energy depoisited in the calorimetry and Cherenkov ring shape are used to help identify electron candidates. A cocktail of electron sources is used to subtract electrons not from heavy flavor. Photonic conversions and π^0 Dalitz decays constitute the primary sources of background. Other light mesons, including the η,$\eta^{'}$,ρ,ω, ϕ, and K_{e3}, also contribute. The pion spectra from the same Cu+Cu data set are fit and then the high-p_t ratios as measure in p-p collisions are used in conjection with m_t scaling to describe the spectra of electron sources. The K_{e3} spectrum is calculated using a full simulation of the detector. They only contribute at very low momenta because the $c\tau$ of these decays is significant compared to the dimensions of the detectors.

Photonic conversions in the detector material represent a signifcant contribution to the total cocktail. These can be simulated via tracks passing through the PHENIX detector but due to uncertainties of material distribution it is desirable to cross-check this photonic electron spectrum against converter results. Direct virtual photons from the initial collision also contribute to the total background. The QCD prediction for the photon spectrum in a p+p collision can be scaled by number of collisions to the Cu+Cu system. The kinematics of the electrons generated by these photons was calculated and added to the cocktail.

As an alternative method of calculating the background, a brass cylinder of known radiation lengths was placed inside the PHENIX detector, surrounding the beam pipe, for a fraction of the data-taking period. Since the number of extra electrons generated by the presence of this converter is known, the ratio of non-photon electrons to photonic runs in the data-taking runs without the converter can be calculated. This serves as a cross-check for the cocktail method.

Converter results are consistent with those measured via cocktail. Because of the relationship of photonic

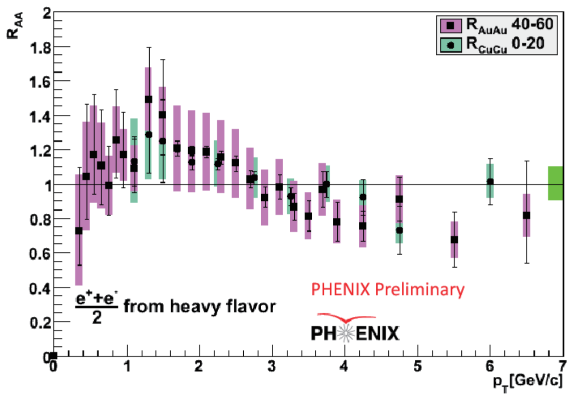

Fig. 1. Comparison of R_{AA} at centrality 0 to 20% Cu+Cu [$N_{coll} = 151.8$](circles) to 40 to 60% Au+Au [$N_{coll} = 90.65$](squares)

electrons to other sources of background in the cocktail via the ratio of $\frac{\pi^0 \rightarrow \gamma\gamma}{\pi^0 \rightarrow \gamma e^+ e^-}$, the converter check also helps to verify the full cocktail.

A spectrum of electrons from decays of charm and beauty mesons was obtained after subtracting the cocktail. The nuclear modification of various centrality ranges in the Cu+Cu system can be compared with Au+Au (Fig. 1). Central $\sqrt{s_{NN}} = 200$ GeV Cu+Cu collisions (0 to 20% centrality) are consistent with mid-peripheral $\sqrt{s_{NN}} = 200$ GeV Au+Au collisions (40 to 60% centrality).

The spectra of electrons from heavy flavor (charm and bottom decays) has been succesfully measured in $\sqrt{s_{NN}} = 200$ GeV Cu+Cu collisions by use of cocktail background subtraction method. The photonic background was verfied by use of a converter of known radiation lengths to provide a secondary means of background calculation. Preliminary results indicate that the heavy flavor electron spectra in $\sqrt{s_{NN}} = 200$ GeV Cu+Cu are not highly suppressed at higher transverse momenta, in contrast to central Au+Au collisions at $\sqrt{s_{NN}} = 200$ GeV but consistent with peripheral Au+Au collisions with roughly equivalent number of collisions.

References

1) S.S. Adler *et al.* (PHENIX), Phys. Rev. Lett. **97** 252002 (2005).
2) S.S. Adler *et al.* (PHENIX), Phys. Rev. Lett. **94** 082301 (2005).
3) K. Adcox *et al.* (PHENIX), Nucl. Inst. Method **A499** 469-479 (2003)

Measurement of J/ψ photo-production at mid-rapidity and forward rapidity in Au+Au collisions at $\sqrt{s_{NN}} = 200$ GeV

A. Takahara[*1], Y. Akiba[*2] , E. T. Atomssa[*3], M. Chiu[*4], T. Gunji[*1], H. Hamagaki[*1], J. Nystrand[*5], S. White[*4], K. Skjerdal[*5], Z. C. del Valle[*6]

[Nuclear structure]

We present the measurements of the photoproduction of J/ψ in ultra-peripheral Au+Au collisions at $\sqrt{s_{NN}} = 200$ GeV at RHIC. The measurement of J/ψ in UPC serves an important role in determining the gluon density in nuclei at small Bjorken x, where the gluon density is expected to be suppressed due to the gluon shadowing effect[1–3]. PHENIX has measured the integrated cross section of J/ψ in UPC in 2004[4]. However, due to less statistical data, it was very difficult to constrain the theoretical calculations on the gluon distribution in nuclei. The measurement for J/ψ photoproduction in UPC as a function of transverse momentum p_T and rapidity y has been done using data taken in 2007 and 2010, where, respectively, 3 and 9 times larger statistics were achieved compared to that in 2004. The requirement of UPC event selection is that there should be only two electron (muon) tracks in the central arms (forward muon spectrometer) and that at least one neutron should be detected. Figure 1 shows the invariant mass spectra of dielectrons and dimuons in UPC events. Figure 2 shows the preliminary results of the p_T distribution of J/ψ cross section in UPC, where the black, blue, and red curves correspond to the cross section at mid-rapidity with one neutron tagged by a zero degree calorimeter, (ZDC) and to -2.2<y<-1.2 and 1.2<y<2.2 with two neutrons tagged on both sides of ZDC, respectively. From Fig.2 , the cross section at mid-rapidity in low p_T is very large as compared to that at forward-rapidity.

The upper limit of integrated cross section for coherent J/ψ production was extracted to be 46.7±13±15 μb^{-1}. The value was determind by integration from 0 to 0.4. Since the cross section without any nuclear effects such as gluon shadowing is expected to be 118 μb[5]. Figure 3 shows the cross section as a function of y, where neutrons are tagged on both sides.

Measurement of J/ψ in UPC has been performed by using 2007 and 2010 data. Studies for both neutron tagging and theoretical understanding are underway.

*1 Department of Physics, University of Tokyo
*2 RIKEN BNL
*3 Stony Book University
*4 Brookhaven National Laboratory
*5 CERN
*6 Department of Physics, Lund University

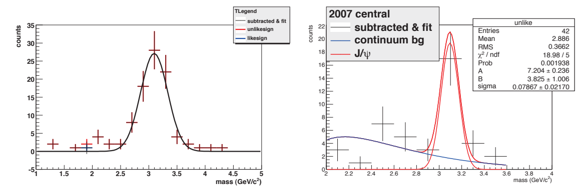

Fig. 1. 2010 North arm (dimuon) and 2007 central arm (dielectron) invariant mass yields.

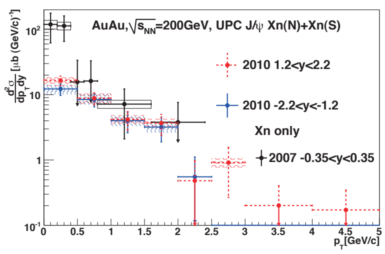

Fig. 2. PHENIX 2010 dimuon (Red and Blue) and 2007 dielectron(black) UPC J/ψ $\frac{d^2\sigma}{dp_T dy}$. Dielectron distribution has a significant 0 p_T peak, but the same peak can not be found from dimuon distribution.

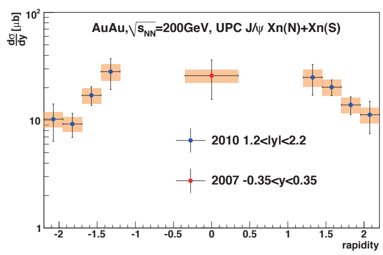

Fig. 3. PHENIX 2010 RUN UPC J/ψ $\frac{d\sigma}{dy}$ distribution

References

1) G. Baur, K. Hencken, D. Trautmann, S. Sadovsky, and Y. Kharlov: Phys. Rept. B, 359 (2002).
2) C. A. Bertulani, and S. R. Klein, J. Nystrand, Ann. Rev. Nucl. Part. Sci. B, 271 (2005).
3) A. Baltz et al.: Phys. Rept. B 171 (2008).
4) S. Afanasiev PHENIX Collaboration: Phys. Lett. B 321(2009).
5) A. L. Ayala Filho, V. P. Goncalves, and M. T. Griep Phys. Rev. C 78, 044904 (2008)

Improved measurement of direct photon production in $p+p$ collisions at $\sqrt{s}=200$ GeV and its x_T scaling

K. Okada

In hadron-hadron collisions, direct photons are used to probe the initial condition of quantum chromodynamics (QCD) hard scatterings. In leading order process, direct photons are produced from quark-anti quark ($q+\bar{q}$) annihilation and quark-gluon ($q+g$) scattering processes. Since the photon has neither an electric nor a strong charge, once it is produced, it can be detected without disturbance.

The PHENIX experiment[1] has measured the invariant cross section of direct photon production in the mid-rapidity region in $p+p$ collisions at $\sqrt{s}=200$ GeV over a wide range of transverse momentum (p_T)[2,3]. In the previous publication[2], the highest p_T was 15 GeV/c from the data set with the integrated luminosity ($\int Ldt$) of 0.24 pb^{-1}. With improved statistics ($\int Ldt = 8.0$pb^{-1}), the p_T reach was significantly increased up to 25 GeV/c. The result is well described by the next-to-leading order perturbative QCD calculation.

To compare various experimental results, Fig. 1 shows measurements for $p+p$ and $p+\bar{p}$ collisions as a function of x_T ($x_T \equiv 2p_T/\sqrt{s}$), where $\sqrt{s}$ is the center of mass energy of the collision. Points are scaled by $\sqrt{s}^{4.5}$. In the $2\rightarrow 2$ process, when the final products go to 90° to the incoming axis in the center of mass system, x_T corresponds to the momentum fraction of the initial parton in the incoming (anti-)proton. In the original parton model, in which the parton distribution does not depend on the energy scale and no additional higher-twist contributions are considered, the power given to $\sqrt{s}$ is $n=4$.

Remarkably, Fig. 1 shows that all but two experimental results are on a common curve. In fact, for the direct photon process the power ($n=4.5$) is consistent with the next-to-leading order perturbative QCD expectations[4].

References
1) K. Adcox *et al.*: Nucl. Inst. Meth. A **499**, 469 (2003)
2) S.S. Adler *et al.*: Phys. Rev. Lett. **98**, 012002 (2007)
3) A. Adare *et al.*: Phys. Rev. C **81**,034911 (2010)
4) F. Arleo *et al.*: Phys. Rev. Lett. **105**, 062002 (2010)

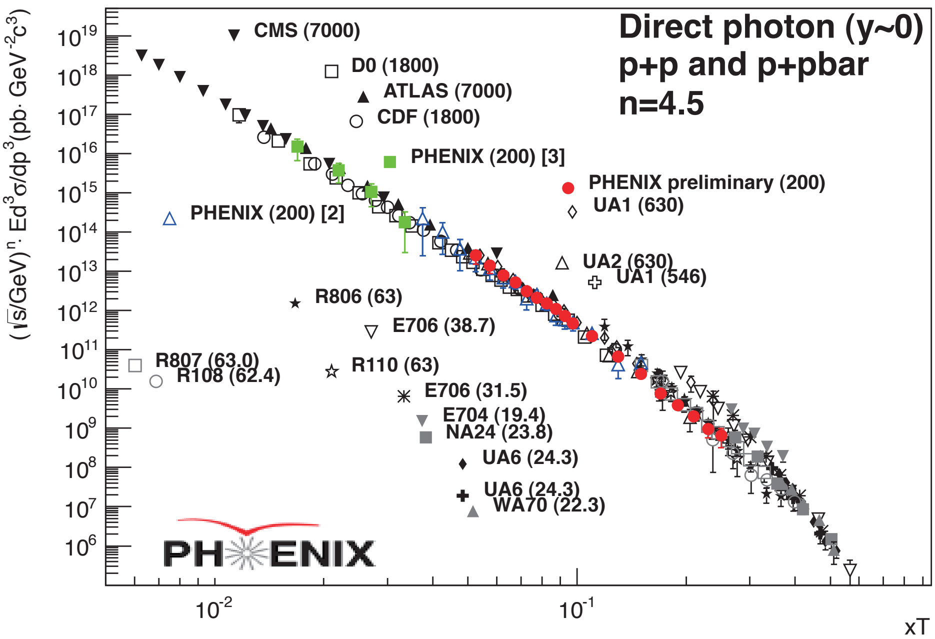

Fig. 1. Various direct photon cross section measurements in $p+p$ and $p+\bar{p}$ collisions scaled by $\sqrt{s}^{4.5}$ on $x_T \equiv 2p_T/\sqrt{s}$. The legend shows the symbols used to represent experiments, and the center of mass energy [GeV] in parenthesis.

PHENIX 2011 forward W single spin asymmetry analysis

R. Seidl, Y. Fukao, Y. Imazu, T. Mibe,[*1] T. Murakami,[*2] J. Murata,[*3] I. Nakagawa, K. Nakamura,[*2] H. Oide,[*4] S. Park,[*5] J. Seele[*6] N. Saito,[*1] K. Tanida,[*5] K. Watanabe,[*3] and S. Yamashita,[*4]

[nucleon spin, W-boson, polarized parton distribution, Electronics, trigger, cathode chamber]

Using the parity violation of the weak interaction W production in longitudinally polarized proton-proton (pp) collisions allows to access the quark and sea quark polarizations inside the nucleon. In 2011 the first production run with longitudinally polarized pp collisions at $\sqrt{s}$ =500 GeV happened at RHIC. Using the newly commissioned muon trigger system[1)] it was possible to accumulate essentially the full luminosity delivered to PHENIX for W decay muon candidates in the two PHENIX muon arms. The total integrated luminosity is about 18 pb^{-1} within a vertex region of $\pm$30cm which is still just a minor part of the full RHIC spin W program calling for 300 pb^{-1} in total. However, using this data it is possible to obtain a quantitative understating of the $W \to \mu$ cross section, establish the amount of background and obtain the first single spin asymmetries A_L at forward rapidities. As PHENIX is not a hermetic spectrometer, the W kinematics cannot be reconstructed via missing transverse momentum, but one has to rely on inclusive mesurements of the decay muons. As a result a substantial background from muons from other processes as well as falsely identified hadrons remains[2)]. Those background contribuions were mostly obtained using the Pythia event generator and full Geant3 detector simulations and cross checked at various stages in several distributions used to select the signal events. All selection criteria were optimized again to provide a high efficiency for real W decay muons while cutting out as much of the backgrounds as possible. An example can be seen in Fig. 1 for one selection criterium and its Data/MC comparison. The hadronic interactions packages were confirmed to provide reliable results based on the confirmation of Data/MC comparisons for tracks which penetrate all absorbing material and those which get stopped within a last layer of 20cm thick steel. Using those simulations a signal to background ratio of 1/3 or better is expected for muons with transverse momenta above 15-20 GeV. In order to obtain the final W cross section results all efficiency and acceptance corrections need to be finalized. Most of those are finished.The asymmetry calculation, has been prepared and can be finished with the final S/BG values. The W decay muon candidate event yields for each spin state of the two polarized beams are calculated. They are then fit by the following function for each arm and charge:

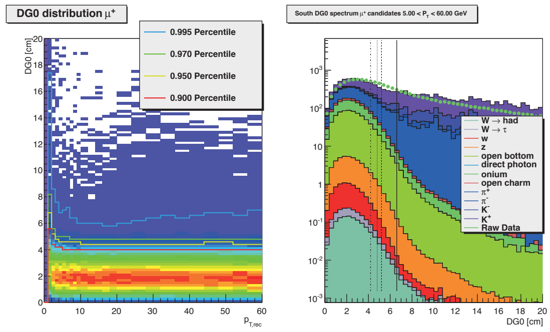

Fig. 1. Left: Muon tracker, Muon Id detector matching distribution DG0 and selection criteria for 99.5,98,95 and 90% efficiency from single muon simulations vs. reconstructed transverse momentum. Right: Data/MC comparison for the same variable where all signal and BG contributions are stacked.

$$
\begin{aligned}
N^{\alpha,\beta} &= \sigma_0 + (-1)^{\alpha}\sigma_L^{Blue} + (-1)^{\beta}\sigma_L^{Yellow} \\
&\quad + (-1)^{\alpha}(-1)^{\beta}\sigma_{LL} \quad , \qquad (1)
\end{aligned}
$$

where α (β) are the two spin states for the blue (yellow) Beam respectively. The corresponding asymmetries are then obtained by normalizing the spin dependent terms by the unpolarized term and the corresponding avarage beam polarization(s). The results' uncertainties are tested by randomizing the spin patters in each running period and extracting the corresponding asymmetries for a large number of iterations. The resulting width in the asymmetry distribution is found to be consistent with the statistical uncertainty. As a last step the single spin asymmetries need to be corrected for the remaining BG, which does not contain any parity violating single spin asymmetries. The analysis is mostly complete and preliminary results are expected soon.

*1 KEK, Tsukuba, Ibaraki, 305-08011 Japan
*2 Kyoto University, Kitashirakawa-Oiwakecho, Kyoto, 606-8502 Japan
*3 Rikkyo University, Rikkyo, 3-34-1, Nishi-Ikebukuro, Tokyo, 171-8501 Japan
*4 The University of Tokyo, Tokyo, Japan
*5 Seoul National University, Seoul, South Korea
*6 RIKEN BNL Research Center, BNL, Upton, NY 11973, U.S.A.

References

1) I. Nakagawa et. al, RIKEN Accel. Prog. Rep. 42 (2009) 216,
M. Grosse-Perdekamp, R. Seidl, RIKEN Accel. Prog. Rep. 42 (2009) 219.
2) R. Seidl, B. Meredith and M. Grosse-Perdekamp, RIKEN Accel. Prog. Rep. 42 (2009) 32.
R. Seidl, et. al, RIKEN Accel. Prog. Rep. 44 (2011) 72.

Analysis works dedicated to PHENIX $W^{\pm} \rightarrow \mu^{\pm}$ measurement

H. Oide,[*4] Y. Fukao, Y. Imazu, T. Mibe,[*1] T. Murakami,[*2] J. Murata,[*3] I. Nakagawa, K. Nakamura,[*2] S. Park,[*5] N. Saito,[*1] J. Seele,[*6] R. Seidl, K. Tanida,[*5] K. Watanabe,[*3] and S. Yamashita,[*4]

[nucleon spin, W-boson, polarized parton distribution, Electronics, trigger, cathode chamber]

The polarization of sea quarks in the proton is one of the major parameters that need to be measured. Production of the W boson in polarized p + p collision is sensitive to sea quark polarization because of the nature of the W boson's parity-violating interaction. The observable of sea quark polarization is longitudinal single spin asymmetry (A_L^W) . Both PHENIX and STAR experiments of RHIC involved the first measurements of A_L^W in the central rapidity region by $W^{\pm} \rightarrow e^{\pm}$ decay channel[1,2]. Meanwhile, measurement of A_L^W in the forward/backward rapidity region is crucial to determine the sea quark polarization separated by quark flavor. The muon spectrometer of PHENIX, covering the rapidity range of $1.2 < |\eta| < 2.2$, is a unique detector for measuring the A_L^W in the forward/backward rapidity region by the $W^{\pm} \rightarrow \mu^{\pm}$ decay channel. In order to trigger only muons with a momentum greater than approximately 8 GeV/c, we introduced a new trigger system called "MuTRG-FEE"[3], and we installed RPC detectors for the determination of the timing of muon tracks. In the runs in 2011, we collected $\sim$18 pb^{-1} integrated luminosity data of $\sqrt{s}$ = 500 GeV p + p collisions with the MuTRG-FEE trigger. The analysis work is currently underway.

$W^{\pm} \rightarrow \mu^{\pm}$ signals in forward/backward rapidity are single muons broadly distributed in the p_T region above 15 GeV/c. W candidate events in PHENIX are identified by selecting a single high momentum muon arriving from the collision vertex, and the missing transverse momentum of ν_μ is not available. The largest background is estimated to be kaons and pions decaying in-flight, reconstructed as "fake high-momentum muons" in addition to real muons from heavy flavors, quarkonia, and Drell-Yan/Z pair production[4]. We performed a simulation to investigate how large the PHENIX calorimeters activities could reject backgrounds. This veto would potentially help to reduce 20% of real muon backgrounds; however, it would not help to reduce fake muons.

Among kinematic variables, the requirement of the small distance closest approach with respect to the beam axis (DCAz) of particle track is the most efficient cut for suppressing fake muons. The collision vertex to be used for DCAz calculation is determined by time-of-flight (TOF) observations with beam-beam counters (BBCs), which are located on both sides of the collision point, surrounding the beam axis. However, the existing reconstruction does not help to solve for vertices in the case of multiple collisions in one beam-bunch crossing, because the event-reconstruction algorithm adopts the average hit timing of all photomultiplier tube channels of BBC according to the TOF from the collision vertex. We developed a new reconstruction algorithm, which partially solves vertices in multiple collisions by making clusters in time. The clustering reconstruction improves the DCAz cut value by making it smaller, whereas the DCAz distribution for fake muons does not change substantially. Figure 1 shows the performance of the new clustering reconstruction.

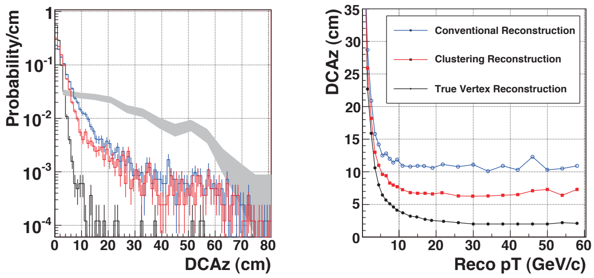

Fig. 1. (Left): Simulated DCAz distribution for $W^+ \rightarrow \mu^+$ signal of reconstructed p_T of 20.0 - 24.0 GeV/c with different vertex reconstructions. Black: true vertex, blue: conventional reco., red: clustering reco, gray band: fake muon from hadrons with clustering reco. Multiple collision Poisson parameter is assumed to be 0.4. (Right): 90% cut plot of DCAz as a function of reconstructed p_T in the simulation of the plot to the left.

Estimation of the signal and backgrounds will follow with this new BBC reconstruction. The preliminary result of $\sigma(pp \rightarrow W^{\pm}) \times \mathcal{B}R(W^{\pm} \rightarrow \mu^{\pm})$ and A_L^W is expected in the first half of 2012.

*1 KEK, Tsukuba, Ibaraki 305-0811, Japan
*2 Kyoto University, Kitashirakawa-Oiwakecho, Kyoto 606-8502, Japan
*3 Rikkyo University, Rikkyo, 3-34-1, Nishi-Ikebukuro, Tokyo 171-8501, Japan
*4 The University of Tokyo, Tokyo, Japan
*5 Seoul National University, Seoul, South Korea
*6 RIKEN BNL Research Center, BNL, Upton, NY 11973, U.S.A.

References
1) A. Adare et al. (PHENIX Collaboration), Phys. Rev. Lett. 106, 062001 (2011).
2) M. M. Aggarwal et al. (STAR Collaboration), Phys. Rev. Lett. 106, 062002 (2011).
3) I. Nakagawa et al., RIKEN Accel. Prog. Rep. 42 (2009).
4) R. Seidl et al., RIKEN Accel. Prog. Rep. 44 (2011).

A Status of π^0 pair A_{LL} analysis in RHIC-PHENIX experiment

K. Hashimoto,[*1] R. Seidl,[*2] Y.Goto,[*2] and PHENIX Collaboration

[nucleon, spin structure of the nucleon, gluon polarization]

A proton has a spin of 1/2, which is attributed to the quarks and gluons in the nucleon. Results from deep inelastic scattering (DIS) experiments show that the quark spin contribution to the proton spin is only about 25%. In PHENIX, the gluon-spin contribution to the proton spin has been studied for the past 10 years. In the recent years, double helicity spin asymmetries, $\mathrm{A_{LL}}$, have been measured in several production channels ($\pi^0, \pi^\pm$ direct photon, etc). One of the highest statistics channels is for the measurement of $\mathrm{A_{LL}}$[1)] for inclusive π^0 production, where the dominant hard sub-processes are quark-gluon and gluon-gluon scattering. Therefore, π^0 production is a good channel for accessing the gluon spin.

In 2009, the STAR collaboration measured single and di-jet A_{LL} in the mid-rapidity region. On the other hand,the PHENIX collaboration measured single π^0 A_{LL} in 2009 and single jet A_{LL} in 2005 in the mid-rapidity region. π^0 pair, single jet , and di-jet A_{LL} measurements are important for PHENIX. In this paper, we on the report status of the π^0 pair A_{LL} analysis.

The status of this analysis is almost preliminary. Hence , in this report, we report a summary of the π^0 pair A_{LL} analysis.

In the comparison with single π^0, π^0 pair A_{LL} analysis involves (1) an extremely different method of combining data and (2) method of background subtraction.

(1) RHIC can store up to 120 polarized proton bunches in each ring for up to 7∼8 hours. RHIC rings are iteratively stored with beams during an experiment, and each store is called "fill". Beam polarization is different in each fill. The follwing equation is the A_{LL} calculation formula.

$$A_{LL} = \frac{1}{P_B P_Y} \frac{N_{++} - RN_{+-}}{N_{++} + RN_{+-}} \tag{1}$$

In this equation, $P_{B,Y}$ is the beam polarization of the RHIC blue and yellow rings. R is the relative luminosity. A_{LL} depends on the beam polarization. For this reason, in a rich statistics channel , for example single π^0, A_{LL} is calculated in each fill with transverse momentum bins (called the "fill-by-fill" method). However, for a low statistics channel, for example, a weak boson, π^0 pair, it is impossible to calculate A_{LL} fill-by-fill in higher transverse momentum bins.

The workaround plan for A_{LL} calculation is very simple, it is to simply integrate all fills and use luminosity weighted beam polarization instead of fill-by-fill beam polarization (called the "sum-up" method.) In π^0 pair analysis, this workaround was used owing the low statistics.

To validate the of sum-up method, π^0 pair A_{LL}s calculated by fill-by-fill and sum-up methods were compared, and the two A_{LL} values were found to match. In this analysis, two parameters were measured in each event. Hence, combinations of π^0 and the background could be used for classifying into three regions, (1)π^0-π^0(signal), (2) the presence of only one π^0(called BGα), and (3) no π^0 in the detector acceptance region(called "BGβ"). The background subtraction formula is as following.

$$A_{LL} = \frac{N^{ALL}}{N^{Signal}} A_{LL}^{ALL} - \frac{N^{BG\alpha}}{N^{Signal}} A_{LL}^{BG\alpha} - \frac{N^{BG\beta}}{N^{Signal}} A_{LL}^{BG\beta} \tag{2}$$

In this equation, A_{LL}^{ALL} is calculated from the signal window (red box in Fig. 1), and BGα and BGβ are included. To subtract BGα and BGβ, we plan to present this analysis result at the JPS meeting scheduled this spring. in the long term, single jet and di-jet measurements are planned in PHENIX and sPHENIX. In particular, if sPHENIX has a full acceptance EM calorimeter, we can obtain higher statistics. If a hadron calorimeter is also available, the best kinematics sensitivity will be achieved in the jet measurement.

This analysis is being performed at CCJ[2)], and we are pleased to announce that the operation has been smith.

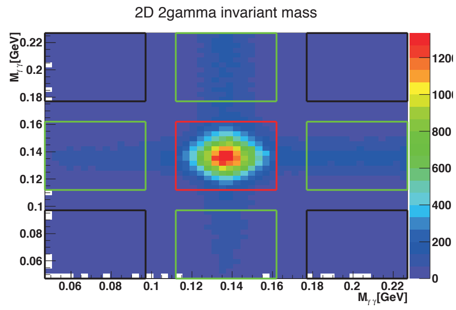

Fig. 1. Mass windows of two-dimensional 2 gamma invariant mass

References
1) A. Adare et.al.: Physical Review Letters 103 (2009) 012003
2) http://ccjsun.riken.jp/ccj/

*1 Department of Physics, Rikkyo University, Japan
*2 Riken, Japan.

Understanding the Relative Luminosity Systematic Uncertainty in Double Helicity Asymmetry Measurements

K. Boyle, and A. Manion,[*1]

[Helicity Structure, Relative Luminosity, Gluon Spin, PHENIX]

Understanding the helicity structure of the proton, and in particular the gluon helicity structure, ΔG, is one of the main goals of the RHIC Spin Program. Double helicity asymmetries (A_{LL}) measured at RHIC are directly related to ΔG. At the PHENIX experiment, π^0 A_{LL} in particular has significant power to constrain ΔG[1] due to the large π^0 cross section and the PHENIX detector design.

Define $A_{LL} = \epsilon_{LL}/(P_1P_2)$, with polarization P and

$$\epsilon_{LL} = \frac{N_{(++,--)} - RN_{(+-,-+)}}{N_{(++,--)} + RN_{(+-,-+)}}, \quad R = \frac{L_{(++,--)}}{L_{(+-,-+)}} \tag{1}$$

where N is the π^0 yield in same ($++$, $--$) or opposite ($+-$, $-+$) helicity proton collisions and R is the relative luminosity. The 2009 π^0 A_{LL} result had a systematic uncertainty due to relative luminosity roughly twice that of the smallest statistical uncertainty[2].

This uncertainty can arise in two ways: miscounting or a measured asymmetry in the luminosity monitor. In PHENIX, we have two luminosity monitors, the Beam-Beam Counters (BBCs) and the Zero Degree Calorimeters (ZDCs). For measuring R, we use the BBCs, while for the determination of the systematic uncertainty, we compare the BBCs and the ZDCs. As was reported earlier[3], a recently developed method to account for miscounting due to rate dependent counting errors varying from bunch to bunch has greatly reduced the uncertainty from miscounting. However, the large uncertainty in 2009 primarily arose from a measured A_{LL} in the BBC-ZDC comparison.

In RHIC, the stable beam polarization is vertical, and must be rotated onto the beam axis for longitudinally polarized collisions. This process is not perfect, and small transverse components remain. We hypothesize that the asymmetry we measure in the BBC-ZDC comparison is not caused by a physical A_{LL}, but instead the result of a known non-zero forward neutron asymmetry[4] measured in the ZDC due to the remaining transverse spin components coupled with misalignments of the beam axis with respect to the detectors.

We can define other double helicity asymmetries such as

$$\epsilon_{LL}^{+-vs-+} = \frac{N_{+-} - RN_{-+}}{N_{+-} + RN_{-+}}, R = \frac{L_{+-}}{L_{-+}} \tag{2}$$

which should be zero as the strong force does not violate parity. Figure 1 shows ϵ_{LL}^{+-vs-+} in 2009 is nonzero.

[*1] Stony Brook University

We have devised a toy Monte Carlo which realistically simulates two beams colliding at different angles and offsets in three dimensions. Particles are produced at each collision vertex according to kinematic distributions measured at RHIC, including an asymmetry in forward neutron production. We then determine if these particles would travel through our BBC and ZDC detector geometries, and calculate the ϵ_{LL}s discussed above assuming a nonzero remaining transverse component. Figure 2 shows that by having the beams offset from the nominal beam axis, we can generate a false ϵ_{LL}^{+-vs-+}, which grows linearly with the offset.

Further studies show that we can also generate other ϵ_{LL}s, including that in Eq. 1, and that the size of ϵ_{LL}^{+-vs-+} is directly related to the size of the nonzero A_{LL} that leads to our large systematic uncertainty. We are planning a beam test at RHIC in 2012 to confirm this effect. We believe that this will allow us to correct for these false asymmetry effects, decreasing systematic uncertainties for our A_{LL} measurements.

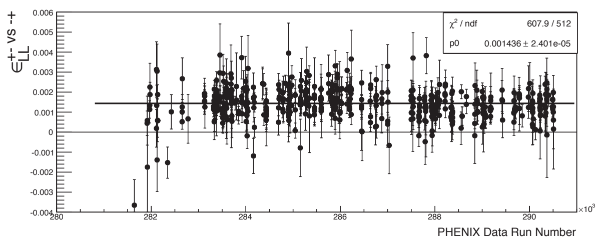

Fig. 1. ϵ_{LL}^{+-vs-+} vs PHENIX run number in 2009.

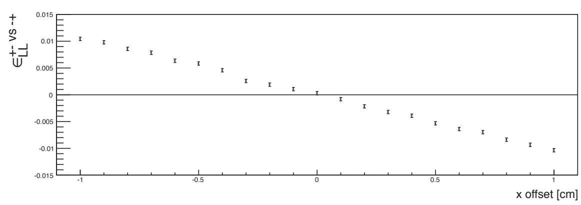

Fig. 2. Simulated ϵ_{LL}^{+-vs-+} vs. beam offset from detector center, with 100% transverse polarization assumed.

References
1) A. Adare, et al. Phys.Rev.Lett. **103**, 012003 (2009)
2) K. Boyle, et al. RIKEN Acc.Prog.Rep. **44**, 64 (2011)
3) A. Manion, et al. RIKEN Acc.Prog.Rep. **42**, 72 (2010)
4) C. Gal, et al., This Journal

PHENIX Local Polarimeter Analysis in Polarized proton-proton collisions at $\sqrt{s}$=200 GeV from RHIC Run 9

C. Gal,*1 K. Boyle,*2 and A. Deshpande,*1

[RHIC, PHENIX, polarized beam, local polarimetry]

Together with the heavy ion programme, one of the main goals of the PHENIX experiment is to shed light on the spin puzzle of nuclear structure using longitudinal and transverse polarized proton beam at $\sqrt{s} = 200$ and 500 GeV[1)]. To this end, the absolute polarization is measured and monitored by the Polarimetry Group for both PHENIX and STAR. The local polarimetry (performed by each of the experiments) measures the direction of a polarized beam by using the forward neutron asymmetry (as defined by equation 1).

$$A_N = \sqrt{A_{LR}^2 + A_{UD}^2} \tag{1}$$

Using the Zero Degree Calorimeter (ZDC) along with the Shower Maximum Detector(SMD)[2)] as a neutron counter one can define left-right, up-down, and phi asymmetries as:

$$A_{LR/UD,b/y} = \frac{1}{P_{b/y}} \cdot \frac{\sqrt{N^{\uparrow}_{L/U} N^{\downarrow}_{R/D}} - \sqrt{N^{\uparrow}_{R/D} N^{\downarrow}_{L/U}}}{\sqrt{N^{\uparrow}_{L/U} N^{\downarrow}_{R/D}} + \sqrt{N^{\uparrow}_{R/D} N^{\downarrow}_{L/U}}} \tag{2}$$

where b/y stands for the blue or yellow beams and $N^{\uparrow}_{R/D}$ is the number of neutrons hitting the right/down part of the detector when the spin direction is up. This asymmetry can be calculated for the north or south detector representing the forward and backward asymmetries. Similarly the phi asymmetries were calculated using a phi segmentation of the face of the SMD.

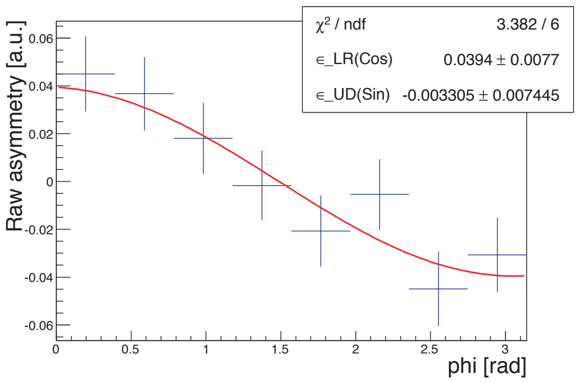

Fig. 1. Phi forward raw asymmetry for the yellow beam as a funtion of phi angle for the transverse running.

In RHIC Run 9 PHENIX ran with longitudinal polarized beams. A calibration measurement was done with the spin rotators off to get a beaseline for the left-right, up-down and phi asymmetries (see figure 1 for an example of forward transverse phi asymmetry). During the longitudinal (physics) running a small bandwidth of the data-acquisition was reserved for the local polarmetry measurement. This data was aggregated for the whole Run and the three asymmetries mentioned above were calculated again.

With the asymmetries measured for both the transverse and the longitudinal periods one can calculate the transverse component as:

$$\frac{P_T}{P} = \sqrt{\left(\frac{A_{LR,long}}{A_{N,trans}}\right)^2 + \left(\frac{A_{UD,long}}{A_{N,trans}}\right)^2} \tag{3}$$

and subsequently the longitudinal component:

$$\frac{P_L}{P} = \sqrt{1 - \left(\sqrt{\left(\frac{A_{LR,long}}{A_{N,trans}}\right)^2 + \left(\frac{A_{UD,long}}{A_{N,trans}}\right)^2}\right)^2} \tag{4}$$

Because the beam can shift it's position on the face of the ZDC when the spin rotators are turned on (and during the course of the whole Run), a study was performed to estimate a systematic error for the longitudinal component of beam. Four points were selected off-center and for each of these points the left-right and up-down asymmetries were calculated for both the transverse and longitudinal running periods, giving a longitudinal component for each. In order to obtain the central value for this measurement it was assummed that the beam was centered on the face of the ZDC, and the spread of the four off-center points gave size of the systematic uncertainty.

The final results for the Blue beam and the Yellow beam during the RHIC Run 9 are as follows:

- $(0.994 \pm ^{+0.006}_{-0.008}(\text{stat}) \pm ^{+0.003}_{-0.010}(\text{syst}))$ Blue Beam
- $(0.974 \pm ^{+0.014}_{-0.018}(\text{stat}) \pm ^{+0.019}_{-0.035}(\text{syst}))$ Yellow Beam

Many thanks to M. Togawa and S. Dairaku for taking the calibration runs during the Run 9 operations.

References

1) G. Bunce et al., Ann. Rev. Nucl. Part. Sci. **50**, 525 (2000)
2) C. Adler et al., Nucl. Instr. And Meth. **A470**, 488 (2001)

*1 SUNY at Stony Brook
*2 RIKEN BNL Research Center

Performance of PHENIX new high momentum muon trigger for Run11

I. Nakagawa, Y. Fukao, Y. Imazu, T. Mibe,[*1] T. Murakami,[*2] J. Murata,[*3] K.R. Nakamura,[*2] H. Oide,[*4] S. Park,[*5] J. Seele[*6], R. Seidl, N. Saito,[*1] K. Tanida,[*5] K. Watanabe,[*3] and S. Yamashita[*4]

[RHIC, PHENIX, nucleon spin, W-boson, Electronics, trigger, cathode chamber]

The PHENIX new high momentum muon trigger system (MuTRG)[1)] was operated as a physics trigger during Run11 polarized proton-proton collision experiment at the collision energy of $\sqrt{s}$ = 500 GeV for the first time. Achieved performance is reported. The new trigger system was impremented to exisiting muon tracker (MuTr) to strengthen the rejection power of conventional muon ID (MUID1D) trigger in order to pursue the asymmetry measurement of high momentum muon from W-boson decay[2)]. The requirements are achieving sufficient rejection power to fit in PHENIX DAQ bandwidth for muon arms of 2kHz with good efficiency.

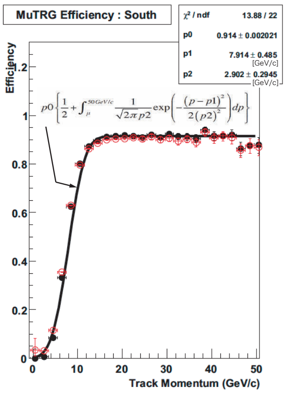

Fig. 1. SG1 Efficiency turn on curve of South MuTRG (black circles). Red circles are prediction by a trigger emulator. Horizontal axis shows the track momenutum.

Since MuTRG parasites on MuTr signal readout, one can define the efficiency by the ratio of reconstructed tracks by MuTRG and MuTr. Failure to reconstruct matching track requiring MuTRG trigger for given reconstructed track in MuTr is thus accounted as the inefficiency of MuTRG. Fig. 1 shows the efficiency of South MuTRG for the track as a function of the track momentum measured by MuTr. The original momentum threshold of $\sim$ 2.4 GeV/c provided by MUID1D trigger is successfully raised to 7.9 GeV/c as indicated by the turn-on-point of the Figure for the track sagitta of $\Delta s \le 1$ (SG1) operation mode. Note the track samples in this plot are mostly "fake high momentum tracks", which originally come from low momentum hadrons decayed into muons in the MuTr tracking volume and happend to be mis-reconstructed as high momentum. We expect the true efficiency for the real high momentum muons are somewhat higher based on the higher efficiency observed in the performance test with cosmic ray.

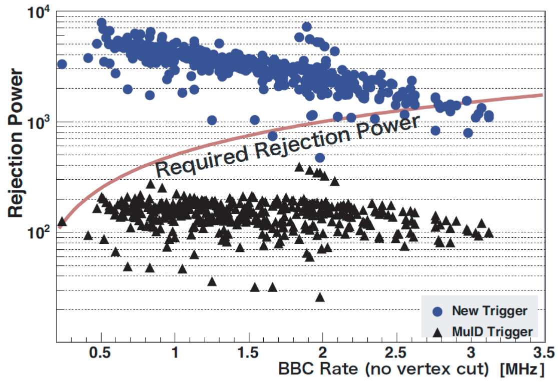

Fig. 2. Rejection powers of MUID1D×BBC (solid triangle) and SG1×MUID1D×BBC.

Fig. 2 shows rejection power of the conventional MUID1D×BBC and the new SG1×MUID1D×BBC triggers as a function of BBC trigger rate. The curve guides the required rejection capability of the high momentum muon trigger in order to fit trigger rate to be in the assigned band width limit of PHENIX DAQ for muon arms (about 2kHz). As can be seen from the plot, the new trigger strengthen the rejection power by factor of 10 to 20 multiplicative to its subset MUID1D×BBC trigger and kept the rejection power sufficiently high 1000 $\sim$ 8000 for the most of the cases except for the very high luminosity period, i.e. BBC rate > 3MHz. Further rejection power (RP) is expected to achieve in future runs with new trigger detectors, i.e. Resistive Plate Chamber (RPC)[3)].

*1 KEK, Tsukuba, Ibaraki, 305-08011 Japan
*2 Kyoto University, Kitashirakawa-Oiwakecho, Kyoto, 606-8502 Japan
*3 Rikkyo University, Rikkyo, 3-34-1, Nishi-Ikebukuro, Tokyo, 171-8501 Japan
*4 University of Tokyo, 7-3-1 Hongo, Bunkyo-ku, Tokyo 113-0033 Japan
*5 Seoul National University, Seoul, South Korea
*6 RIKEN BNL Research Center, BNL, Upton, NY 11973, U.S.A.

References

1) Y. Fukao *et. al.*, RIKEN Accel. Prog. Rep. **43** (2010).
2) H. Oide *et. al.*, RIKEN Accel. Prog. Rep. **45** (2012).
3) Conceptual Design Report for a Fast Muon Trigger (2007), unpublished.

Stability Monitor of PHENIX New High-Momentum Muon Trigger

S. Park,*5 Y. Fukao, Y. Imazu, T. Mibe,*1 T. Murakami,*2 J. Murata,*3 I. Nakagawa, K. Nakamura,*2 H. Oide,*4 N. Saito,*1 J. Seele, R. Seidl,*6 K. Tanida,*5 K. Watanabe,*3 and S. Yamashita,*4

[nucleon spin, W-boson, polarized parton distribution, electronics, trigger, cathode chamber]

A new high-momentum trigger was introduced for the PHENIX experiment, and it was operated to measure the longitudinal single spin asymmetry of W-boson production in polarized proton-proton collision. [1] As a part of the trigger, new front-end electronics (MuTRG-FEE)[2] were added to the existing electronics of muon tracking chambers. The new electronics consist of amplifier and discriminator boards (ADTX), data merger boards (MRG), and interface boards of a data collecting module (DCMIF). A stability monitor system was developed for these new trigger electronics to monitor the performance of the circuit chain. The system monitors the errors committed by the electronics, fake hit rate, signal peak timing, and trigger efficiency.

The MRG receives signals from the ADTX and transmits them to the DCMIF, which is connected to eight MRG boards by eight I/O channels. Information on the errors occurring in the MRG is also sent to the DCMIF and recorded. There can be several reasons for these errors. They mainly occur because of the transmission of corrupted data from ADTX. The error monitor detects frequent errors occurring in select MRG boards. In this way, we can mask the corresponding ADTX board to minimizing the effect of these errors on the data collection.

In addition to the true signal processed in ADTX, noise generated in the analog section of the electronics is also present; this noise may randomly generated spurious hits, termed "fake hits". Fake hits can cause accidental coincidence triggers, and therefore, we need minimize the number of fake hits. The fake hit rate through 2011 runs is small and acceptable, as shown in Fig. 1. Trigger timing is also monitored. The trigger timing should be adjusted with respect to the most probable timing of real hits. It was confirmed that the timing was correct in most of the runs.

The Local Level-1 (LL1) trigger efficiency is defined by the ratio of the number of real events that fired the trigger to the number of events expected to fire the trigger as judged by a trigger emulator. Figure 2 shows the efficiency. Although there are some low efficiency runs in initial period, the efficiency of the runs becomes consistently high toward the end of 2011.

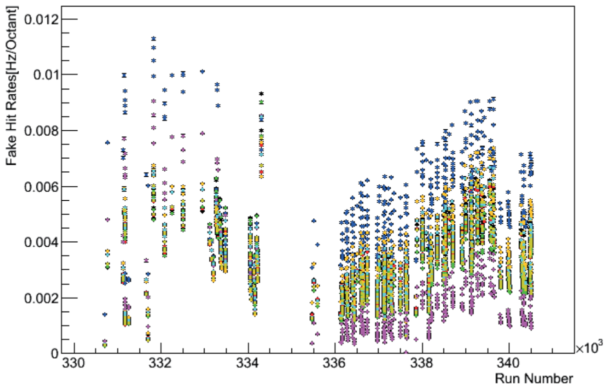

Fig. 1. Fake hit rates in the first station of south muon arm. Each color represents a different octant of the station.

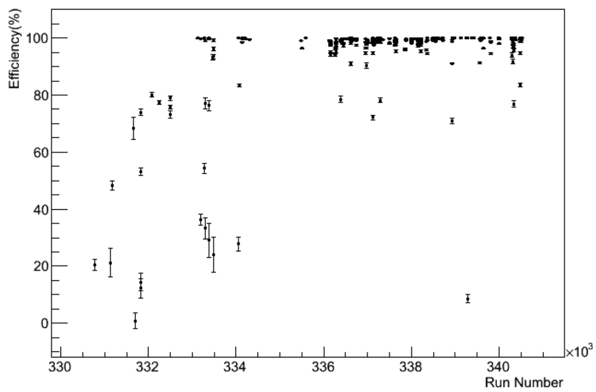

Fig. 2. Results obtained from LL1 efficiency monitor of octant #1 of north muon arm.

The stability monitor provided an overview of trigger operation during 2011 runs during offline analysis. This monitor will be improved and applied to the experiment in 2012, and it is expected provide immediate feedback if the operation mode of the trigger is unsuitable.

*1 KEK, Tsukuba, Ibaraki, 305-08011 Japan
*2 Kyoto University, Kitashirakawa-Oiwakecho, Kyoto, 606-8502 Japan
*3 Rikkyo University, Rikkyo, 3-34-1, Nishi-Ikebukuro, Tokyo, 171-8501 Japan
*4 The University of Tokyo, Tokyo, Japan
*5 Seoul National University, Seoul, South Korea
*6 RIKEN BNL Research Center, BNL, Upton, NY 11973, U.S.A.

References
1) R. Seidl et. al., RIKEN Accel. Prog. Rep. 45 (2012)
2) Y. Fukao et. al., RIKEN Accel. Prog. Rep. 44 (2011)

Impact of circuit restoration on performance of PHENIX muon tracker

Y. Imazu, Y. Fukao,*1 T. Mibe,*1 T. Murakami,*2 J. Murata,*3 I. Nakagawa, K.R. Nakamura,*2 H. Oide,*4 S. Park,*5 J. Seele,*6 R. Seidl, N. Saito,*1 K. Tanida,*5 K. Watanabe,*3 and S. Yamashita,*4

[nucleon spin, W-boson, electronics, trigger, cathode chamber, cross talk]

The investigation of the nucleon spin structure through the measurement of W boson production in proton-proton collision was recently commenced in 2011 in a PHENIX experiment. In the measurement, the PHENIX muon tracker (MuTr) plays a central role both in online and offline analyses to identify the muons decayed from the W boson[1–3].

MuTr is composed of strip-wire gas chambers with a cathode strip read-out. By weighting the read-out charge signals that spread over several cathode strips, we can determine the intersection position of a charged particle. In principle, lower noise, which is equivalent to the stability of the signals in the MuTr, provides better resolution. For effectively distinguishing muons from W bosons, which have a high momentum of >20 GeV, it is required for the MuTr to maintain a resolution on the order of a few hundred micrometers. To achieve this resolution, we need to exhaustively eliminate any possible source of noise/uncertainty in the Mutr that can cause any instability of the signals. Typically, the noise level of the MuTr needs to be limited to a small percentage for the typical size of the signals.

However, an unexpected source of uncertainty was found to affect MuTr signals[4], which was the result of a cross-talk effect over read-out cathode strips through improperly grounded anode wires[5]. This effect created an unwanted, unstable baseline shift of the MuTr signals. By considering the baseline fluctuation, the noise level was found to become twice as bad as expected. The noise level was also expected to become severely high as the collision rate increased.

To address the degradation in the MuTr performance resulting from the cross-talk effect, we first conducted basic studies and R&D studies with test benches in RIKEN[5] to establish practical solutions of circuit restoration in order to ensure proper anode grounding. Then, we partially applied these solutions to the PHENIX MuTr before the 2011 operation.

Through the data collected in the 2011 operation, we were able to confirm that the solutions were effective for the suppression of the cross-talk effect over the entire MuTr acceptance region, as expected from the R&D studies (Fig. 1).

Naive calculations based on the observation of cross-talk relaxation indicate that we can expect an improvement of the resolution by about 50 to 100 μm from the current realistic resolution of 300 μm. In addition, the suppression of the noise rate implies an improvement of the performance of the trigger dedicated for high momentum muons[1]. Encouraged by these findings, we implemented the circuit restoration solutions for more than 60% of the entire MuTr acceptance region before the anticipated operation in 2012. We will soon obtain the results, which will show better performance of the MuTr as a complete system.

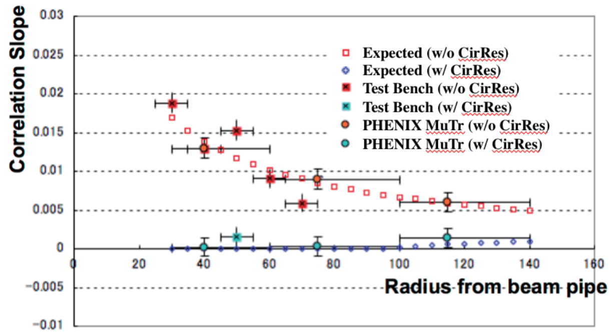

Fig. 1. Measured relaxation of the cross talk effect by circuit restoration. The vertical axis indicates the amplitude of the cross-talk effect signal. The amplitude is plotted as a function of the radius of muon tracking chamber and compared among sections without (w/o, red) or with (w/, blue) the application of circuit restoration (CirRes). Results obtained from the RIKEN test bench are also plotted.

References
1) Y. Fukao et al. *RIKEN Accel. Prog. Rep.*, 44, 2011.
2) R. Seidl et al. *RIKEN Accel. Prog. Rep.*, 45, 2012.
3) H. Oide et al. *RIKEN Accel. Prog. Rep.*, 45, 2012.
4) T. Mibe et al. *RIKEN Accel. Prog. Rep.*, 42, 2009.
5) Y. Imazu et al. *RIKEN Accel. Prog. Rep.*, 44, 2011.

*1 KEK, Tsukuba, Ibaraki 305-08011, Japan
*2 Kyoto University, Kitashirakawa-Oiwakecho, Kyoto 606-8502, Japan
*3 Rikkyo University, Rikkyo, 3-34-1 Nishi-Ikebukuro, Tokyo 171-8501, Japan
*4 The University of Tokyo, Tokyo, Japan
*5 Seoul National University, Seoul, South Korea
*6 RIKEN BNL Research Center, New York, USA

Simulation studies of spallation neutrons for the PHENIX muon arms in GEANT4

K.O. Eyser [*1]

The performance of the PHENIX Muon Tracker Stations (MuTr) with new trigger capabilities is essential for the RHIC W-program and the quality of the data taken with PHENIX at $\sqrt{s}$ = 500 GeV. In previous years signals with large amplitudes and wide cross talk have been observed in the MuTr detectors. Thermal neutrons were suspected to be the source of these large signals with time constants in the range of a few microseconds. Parallel with an effort to reduce the cross talk by grounding anode circuits properly on a large scale, a simulation of spallation neutrons has been developed in order to understand the nature of the background signals and find additional means to reduce them.

The geometrical setup includes the central magnet yoke and coils, one full Muon Arm[1] with the so called lamp shade and muon piston yokes, and two simple models of the Beam-Beam Counters and the Muon Piston Calorimeter (MPC) along with the gas volumes of the three MuTr detectors, see Fig. 1. The simulation was written completely from scratch in GEANT4[2] to provide a complete isotope mix for all used materials in the setup. Physics processes are as complete as needed for the production, scattering, and thermalization of neutrons (as modeled in the QGSP_BERT_HP package used for background studies at the LHC and studies for an ILC). The simulation takes pre-filtered hadrons from PYTHIA[3] generated events for the production of spallation neutrons.

We are comparing the current PHENIX setup from previous years with the addition of a 35 cm thick steel absorber downstream of the central magnet yoke. Further, it has been suggested to include borated polyethylene behind the steel absorber to reduce the thermal neutron flux. The simulation allows to track the spatial origin of the neutron flux through the MuTr detectors. Neutron capture and gamma emission in the MuTr frames which are the physical cause of the big pulses are simply modeled from the thermal neutron part of the energy spectrum. Currently, results for proton-proton collisions at $\sqrt{s}$ = 200 GeV are compared to single bunch measurements in Run10 which will be followed by predictions for the 500 GeV running.

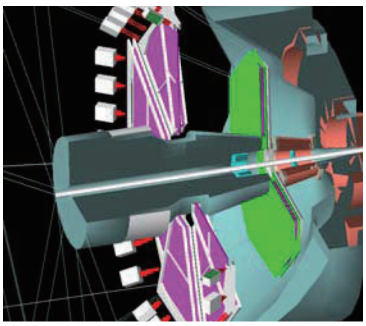

Figure 1: Geometrical description of the PHENIX muon arms in GEANT4. Materials are using complete isotope mixtures of all elements.

The simulation is essential in understanding the nature of neutrons in various energy ranges. Slow neutrons generally behave very much like a gas, which means that a dedicated absorber affects the spatial distribution of neutrons differently from the plain geometry. Also, neutrons can diffuse through large amounts of material, e.g. the muon piston steel. Thermalization times are on the order of ms or longer, the thermalization process is usually slower in heavy materials and faster in material with a high hydrogen content. This is consistent with other measurements and spallation neutron experiments[4]. While the main neutron source from spallation is in the muon piston hole at or around the MPC, compare Fig. 2, the thermalization happens mostly in the volume of the muon tracker. Although we see shadow effects of secondary spallation (e.g. in the outer regions of the central magnet yoke), dedicated neutron absorbers only have a minor effect on the thermal neutron flux. Generally, the area of any absorber wins over its depth due to the gas-like behavior of the slow neutrons. This renders neutron absorbing materials uneconomical when they rely on isotope enriched elements for high cross sections in the thermal energy range without the later emission of high energetic photons.

We conclude that the installation of additional neutron absorbers is not practical at this time. The additional steel absorber behind the central magnet yoke does not increase the thermal neutron flux in the muon trackers, instead it leads to a slightly reduced total neutron flux. Beam related background seems to contribute similarly to the background when we compare the measured time constants with the simulation.

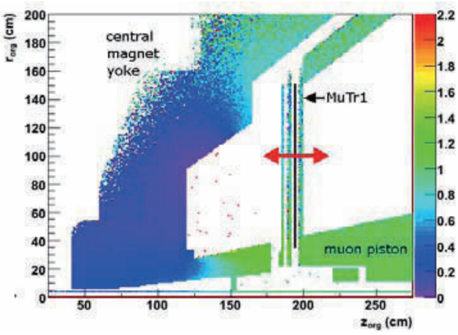

Figure 2: Origins of thermal neutrons in muon tracker station 1 (MuTr1) both coming from up- and downstream of the detector, indicated by the red double arrow. The vertical scale is arbitrary.

References

1) H. Akikawa et al., Nucl. Instr. and Meth. A499, 537-548 (2003)
2) S. Agostinelli et al., Nucl. Instr. and Meth A506, 250-303 (2003)
3) T. Sjöstrand et al., JHEP 05, 026 (2006)
4) http://www.fas.org/sgp/othergov/doe/lanl/lib-www/la-pubs/00326407.pdf

*1 Brookhaven National Laboratory, Upton, NY, USA

Alignment precision for the PHENIX muon tracking chamber

K. Watanabe,[*3] Y. Fukao, Y. Imazu, T. Mibe,[*1] T. Murakami,[*2] J. Murata,[*3] I. Nakagawa, K.R. Nakamura,[*2] H. Oide,[*4] S. Park,[*5] J. Seele[*6], R. Seidl, N. Saito,[*1] K. Tanida,[*5] and S. Yamashita,[*4]

[alignment, nucleon spin, polarized parton distribution, trigger electronics, cathode chamber]

Measurement of sea quark polarization via the single muon decay channel from W boson production is the one of the highlights of RHIC-PHENIX experiment using polarized proton beams at $\sqrt{s} = 500$ GeV. The position (momentum) resolution of the muon tracker (MuTr) detector plays a key role in identifying the high momentum muons from the W delay (signal) from backgrounds, e.g., soft hadrons that have decayed in the magnetic field of the MuTr. The MuTr is composed of 3 tracking stations, namely, stations 1, 2, and 3 from the collision point. Each station is segmented into eight cathode strip chambers for the 2π azimuthal coverage, and we refer to each segment as "octant".

In addition to the intrinsic chamber resolution of 100 μm, the multiple scattering in the station-2 chamber ($X_{\rm rad} = 0.2\%$) and the possible relative misalignment between stations can degrade the momentum resolution of the MuTr. Misalignment has indeed been observed in the past through the use of the zero-magnetic-field data. A misalignment appears in the non-zero peak location of the residual (the difference between the actual hit position at station-2 and the relevant linear interpolation of hit positions between stations 1 and 3) distribution of straight tracks. This information was used to calculate the alignment corrections required for each chamber on a yearly basis. However, the question that arises here is whether the chambers remain exactly at the same locations throughout the experiment period spanning several months.

Here, we introduce two independent approaches for observing the possible chamber movement over three months during Run 9. 1) Track the chamber frame position using the optical alignment system (OASys). OASys consists of a light source at station-1, convex lens at station-2, and CCD camera at station-3. Each octant has 7 sets of these optics mounted on the chamber frames. There are 7 (optics/octant) $\times$ 8 (octant/arm) $\times$ 2 (arm, South and North) = 112 optics in total. OASys performs data acquisition independent of the main DAQ system of PHENIX, and it is able to monitor the real-time relative position of each station. If any chamber moves, its movement is detected as a shift in the position of light spot by the CCD camera of the corresponding octant. 2) Comparison of residual peak positions of straight tracks of zero-field runs measured at three month intervals.

The observed relative movements of South MuTr in the unit of half-octant are plotted in Figure 1 for both OASys and zero-field data. Note that the residual for zero-field data is now defined as the extrapolation at station-3, and not station-2, for a direct comparison with the OASys data. Both measurements show a consistent relative movement of less than $\sim$ 100 μm. However, a weak correlation between them is observed within the error. The relatively large error of the Octant-7 zero-field data point is due to the disabled major HV sections.

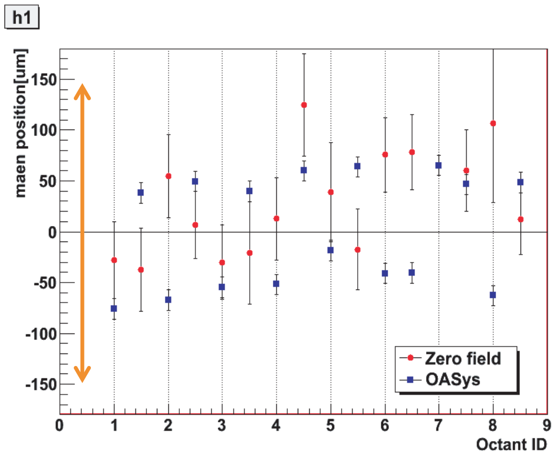

Fig. 1. Chamber movement in the azimuthal direction observed using OASys and zero-field data in the South MuTr during Run 9. The data points of half octant-2 are shifted by 0.5 along the x-axis for better visibility.

As a possible reason for the weak correlation, we consider the zero-field data need to be strictly treated in the acceptance matching between two data sets which are three months a part. Some anode/cathode sections were disabled/enabled over the course of time, and the active area of the detectors did not match. The difference in the active area show movement in the peak position even though there is no physical movement of the chamber during that period because the misalignment has a "position dependence" within the chamber. We found this position dependence is relatively large, i.e., on the order of 100 μm, in many octants, and concluded that this dependence needs to be corrected first.

*1 KEK, Tsukuba, Ibaraki 305-08011, Japan
*2 Kyoto University, Kitashirakawa-Oiwakecho, Kyoto 606-8502, Japan
*3 Rikkyo University, Rikkyo, 3-34-1, Nishi-Ikebukuro, Tokyo 171-8501 Japan
*4 The University of Tokyo, Tokyo, Japan
*5 Seoul National University, Seoul, South Korea
*6 RIKEN BNL Research Center, BNL, Upton, NY 11973, U.S.A.

4. Hadron Physics (Theory)

Chiral magnetic effect from Q-balls†

M. Eto,[*1] K. Hashimoto,[*1] H. Iida,[*1] and A. Miwa,[*2]

[Heavy ion collisions, solitons]

We apply a generic framework of linear sigma models for revealing a mechanism of the mysterious phenomenon, the chiral magnetic effect, in quark-gluon plasma. An electric current arises along a background magnetic field, which is given rise to by Q-balls (non-topological solitons) of the linear sigma model with axial anomaly. We find additional alternating current due to quark mass terms. The mesonic Q-balls, baby boson stars, may be created in heavy-ion collisions.

It is widely believed that QCD has a phase transition between the hadronic phase and the quark-gluon plasma (QGP) phase at finite temperature and density. Experimental searches for QGP in relativistic heavy ion collisions have been revealed that QGP has highly nontrivial properties, such as its perfect fluidity, for example. The chiral magnetic effect (CME)[1,2] would be one of the most striking phenomena in QGP, which has been recently studied from the theoretical and experimental viewpoints. The CME, the separation of electric charge along the axis of an external electromagnetic fields, was predicted as a direct evidence of the (not global but local) strong CP violation under very intense external magnetic fields. Recently, an experimental sign for CME was reported by the STAR Collaboration at RHIC. Since then, CME has been actively studied using non-perturbative techniques in QCD: P-NJL model, holographic QCD, lattice QCD, and so on.

In this short note, in order to understand CME in QGP, we consider a generic linear sigma model (LSM) which is widely used as a key tool to understand the phase transitions. Strictly speaking, the degrees of freedom in LSM would be hadronic. So our analysis using LSM for QGP phase is based on the assumption that LSM captures the physics of corresponding operators in the QGP phase, at least qualitatively. We find a universal mechanism for CME which is given rise to by a stable non-topological solitonic configuration of the (pseudo-)scalar mesons, so-called Q-ball[3]. In the interior of the Q-ball the scalar mesons condense, while it is QGP outside the Q-ball. We find that the electric current along the external magnetic field arises in a similar manner discussed in literature. In addition, as a consequence of the Q-ball, the electric current not only is a direct current but also has a small alternating current from quark mass terms.

The generic LSM of the scalar mesons $\Phi_{ij} = \bar{q}^j_{\rm R} q^i_{\rm L}$ is

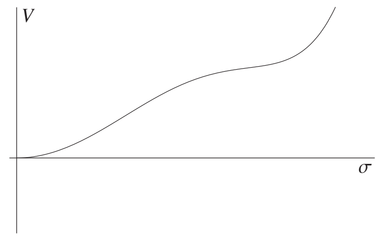

Fig. 1. A typical form of the scalar potential V. There is a true vacuum at $\sigma = 0$ (QGP).

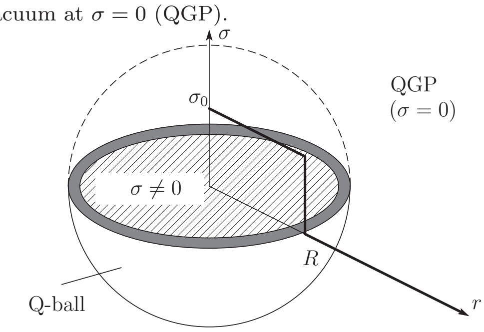

Fig. 2. A schematic picture of the spherical Q-ball.

given by

$$\mathcal{L}_{\rm eff} = {\rm Tr}\left[\partial_\mu \Phi \partial^\mu \Phi^\dagger - M(\Phi + \Phi^\dagger)\right] - V(\Phi\Phi^\dagger) + A\left(\det \Phi + \det \Phi^\dagger\right), \quad (1)$$

where the matrix M is proportional to the quark mass matrix, and the last term is a manifestation of the $U(1)_{\rm A}$ anomaly in QCD. This Lagrangian enjoys the same symmetries as QCD. The chiral $SU(3)_{\rm L} \times SU(3)_{\rm R}$ symmetry and $U(1)_{\rm A}$ acts on the linear sigma model field Φ as $\Phi \to e^{i\alpha} U_{\rm L} \Phi U^\dagger_{\rm R}$.

The existence of Q-balls does not depend on the details of the system[3]. One requirement is that the scalar potential $V(\sigma^2)$ has a true vacuum at $\sigma = 0$ (QGP) as is given in Fig. 1.

With the Q-ball at hand, we can derive that the electric current arises along a constant background magnetic field $\vec{B}$ (the electric field is assumed to be zero)

$$\vec{\mathcal{J}} = \frac{3e^2}{4\pi^2} q^2 \omega \vec{B}. \quad (2)$$

Here, we see that *CME is a consequence of the existence of the Q-ball.*

References

1) D. E. Kharzeev, L. D. McLerran and H. J. Warringa, Nucl. Phys. A **803**, 227 (2008).
2) K. Fukushima, D. E. Kharzeev and H. J. Warringa, Phys. Rev. D **78**, 074033 (2008).
3) S. R. Coleman, Nucl. Phys. B **262**, 263 (1985) [Erratum-ibid. B **269**, 744 (1986)].

† Condensed from the article in Phys. Rev. **D83**, 125033 (2011)

*1 Mathematical Physics Laboratory, RIKEN Nishina Center
*2 Theoretical Physics Laboratory, RIKEN Nishina Center

Anomaly-induced charges in nucleons†

M. Eto*1 K. Hashimoto,*1 H. Iida,*1 T. Ishii,*1 and Y. Maezawa*1

[Baryons, Skyrmions, Anomaly, Magnetic fields]

We show a novel charge structure of baryons in electromagnetic field due to the chiral anomaly. A key connection is to treat baryons as solitons of mesons. We use Skyrmions to calculate the charge distributions in a single nucleon and find an additional charge. We also perform calculations of charge distribution for classical multi-baryons with $B = 2, 3, \cdots, 8$ and 17; they show amusing charge distributions.

Recent advance in observations and experiments explores new effects of strong electromagnetic fields on fundamental particles. Since matter consists of baryons, electromagnetic properties of protons and neutrons are of most importance. Under the strong magnetic fields such as in neutron stars, supernovae and heavy ion collisions, tiny quantum effect of quantum chromo-dynamics may lead to an unveiled and significant consequence.

In this letter, we investigate baryons under external electromagnetic fields. For describing the baryons, we use the Skyrme model[1)] with Wess-Zumino-Witten (WZW) term[2,3)] including electromagnetism. The consequence is amazing: Nucleons in the external electromagnetic fields have anomalous charge distribution due to the chiral anomaly. Nonzero net charge, which is generally non-integer, is induced *even for neutrons*. Correspondingly, we show that the Gell-Mann-Nishijima formula, $Q = I_3 + N_B/2$ (Q: electric charge, I_3: the third component of isospin, N_B: baryon number), has an additional term due to the anomaly.

Figure 1 shows a schematic description of the phenomenon. Due to the anomalous interaction with a quark loop through the WZW term, nucleons (= Skyrmions) have an additional interaction to the electromagnetic field A_μ. Under the external electromagnetic fields, the anomalous coupling induces the additional electric charge.

We focus on the coupling between mesons and photons in the WZW term. In the two-flavor case, this can be given by

$$S_{\rm WZW}[A_\mu] = -\int d^4x\, A_\mu \left(\tfrac{eN_c}{6} j_B^\mu + \tfrac{1}{2} j_{\rm anm}^\mu\right), \quad (1)$$

$$j_B^\mu = \tfrac{1}{24\pi^2}\epsilon^{\mu\nu\rho\sigma}{\rm tr}[R_\nu R_\rho R_\sigma], \quad (2)$$

$$j_{\rm anm}^\mu = -\tfrac{ie^2N_c}{96\pi^2}\epsilon^{\mu\nu\rho\sigma}F_{\nu\rho}{\rm tr}[\tau_3(L_\sigma + R_\sigma)], \quad (3)$$

where j_B^μ is a baryon current giving an integer baryon number, $L_\mu = U^\dagger\partial_\mu U$, $R_\mu = \partial_\mu U U^\dagger$, and $\epsilon^{0123} = -1$, with U being the standard notation for the pion field.

In the presence of background electromagnetic fields, not only the first term but also the second term in

† Condensed from the article in ArXiv:1103.5443 [hep-ph]

*1 Mathematical Physics Laboratory, RIKEN Nishina Center

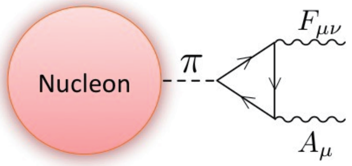

Fig. 1. A schematic figure for electric charge generation of a nucleon. In electromagnetic backgrounds, i.e., $F_{\mu\nu} \neq 0$, the quark-loop diagram generates an additional coupling to the gauge fields A_μ.

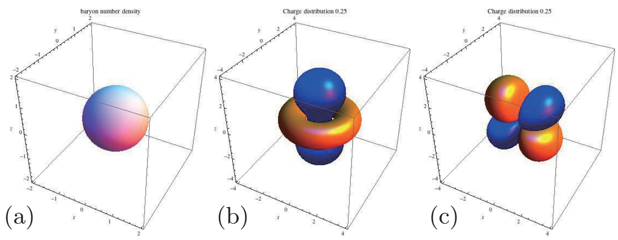

Fig. 2. The constant-height surfaces of (a) density distribution of baryon number, (b) electric charge under magnetic field along the 3rd-axis, and (c) electric charge under magnetic field along the 1st-axis. In (b) and (c), colors stand for positive and negative charge distributions.

Eq. (1) is important. The electric charge Q with the contribution from anomaly ($N_c = 3$) is written as

$$Q = I_3 + \frac{N_B}{2} + \frac{Q_{\rm anm}}{2}, \quad (4)$$

where $N_B = \int d^3x j_B^0$ and $Q_{\rm anm} = \int d^3x j_{\rm anm}^0$. Thus, the Gell-Mann-Nishijima formula is corrected under background electromagnetic fields.

We obtain the anomalous charge for nucleons

$$Q_{\rm anm} = \frac{4e^2N_c}{27\pi} I_3 S_3 \frac{c_0 B_3}{(e_s F_\pi)^2}. \quad (5)$$

Equation (5) shows that an electric charge is actually induced by the anomalous effect *even for a neutron.* We further find that dipole moment vanishes while quadrupole moment appears as a leading multipole.

References

1) T. H. R. Skyrme, Proc. Roy. Soc. Lond. **A260**, 127 (1961).
2) J. Wess and B. Zumino, Phys. Lett. **B37**, 95 (1971).
3) E. Witten, Nucl. Phys. **B223**, 422 (1983a); Nucl. Phys. **B223**, 433 (1983b).

Anomaly-induced charges in baryons†

M. Eto*1 K. Hashimoto,*1 H. Iida,*1 T. Ishii,*1 and Y. Maezawa*1

[Baryons, Skyrmions, Anomaly, Magnetic fields]

We show that quantum chiral anomaly of QCD in magnetic backgrounds induces a novel structure of electric charge inside baryons. To illustrate the anomaly effect, we employ the Skyrme model for baryons, with the anomaly-induced gauged Wess-Zumino term $\sim (\pi_0 + \text{multi-pion})\vec{E}\cdot\vec{B}$. Due to this term, the Skyrmions giving a local pion condensation $\langle(\pi_0 + \text{multi-pion})\rangle \neq 0$ necessarily become a local charge source, in the background magnetic field $\vec{B} \neq 0$. We present detailed evaluation of the anomaly effects, and calculate the total induced charge, for various baryons in the magnetic field.

The chiral anomaly is one of the central concepts in QCD, and it manifests nature of quantum field theories in an explicit way in our hadronic world. As the chiral anomaly is essentially coupled to electromagnetic sector since the electromagnetism is a part of the chiral symmetry, the introduction of nontrivial electromagnetic backgrounds should add a good flavor of physics onto the chiral anomaly. In this paper, we report an interesting new effect induced by the chiral anomaly, for baryons in a background magnetic field.

Our finding is that baryons in a constant magnetic background acquire additional electric charge distribution due to the chiral anomaly. The result that this would generate even a total net charge is quite surprising, but the mechanism is quite simple. It is well-known that Wess-Zumino-Witten (WZW) term[2,3] actually captures the chiral anomaly in terms of the hadronic degrees of freedom. In particular, this term serves as a manifestation of the famous $\pi_0 \to 2\gamma$ decay. Now, any baryon carries a cloud of pions around it, and so it is a source of the pions. Once we replace one of the two γ's in the Wess-Zumino-Witten term by the background magnetic field, we immediately see that the baryon can be a source of the electromagnetism (another γ), *i.e.* the baryon can have an additional charge structure due to the chiral anomaly and the pion cloud.

In this paper, we explicitly demonstrate this mechanism in detail, with a help of a concrete model of the pion-cloud picture of the baryons, the Skyrme model[1] . In the Skyrme model, baryons are given as a solitonic object made of a local pion condensate $\langle\pi(x)\rangle \neq 0$. Plugging the Skyrme solution to the Wess-Zumino-Witten term, it can be shown that the magnetic field background can induce a novel charge structure inside the baryon (Skyrmion).

† Condensed from the article in ArXiv:1109.0020 [hep-ph]

*1 Mathematical Physics Laboratory, RIKEN Nishina Center

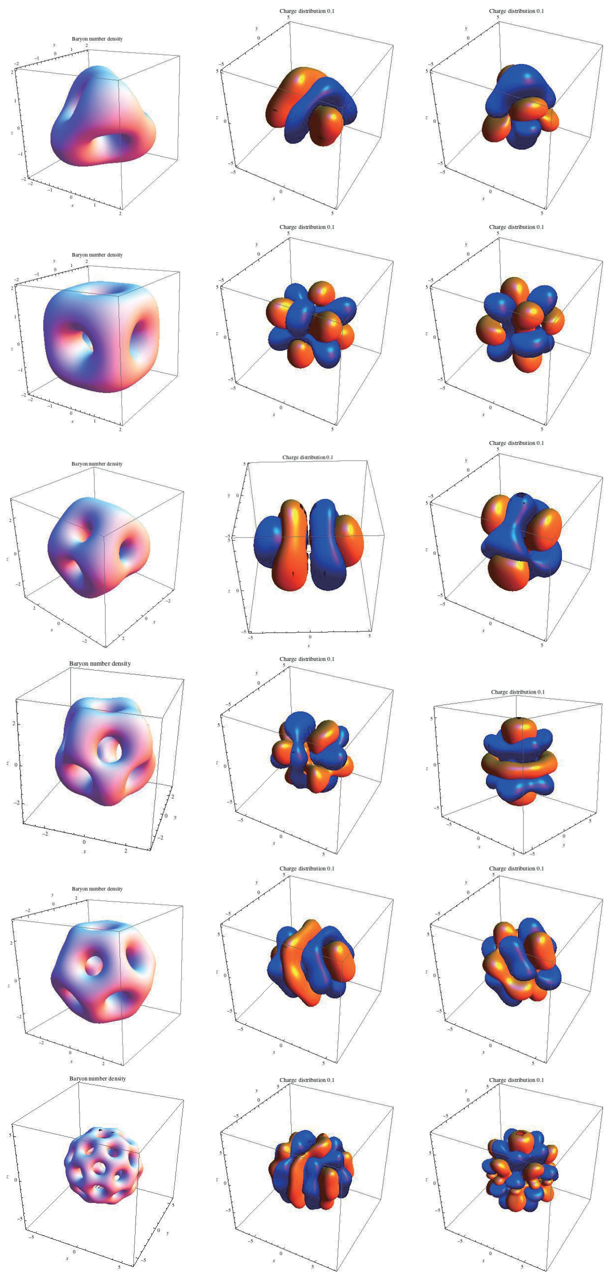

Fig. 1. Higher-charge Skyrmions and their induced charges. From left to right, the baryon number density, induced charge for B_1, and for B_3, respectively. $N_B = 3, 4, \cdots, 7$ and 17 are shown from top to bottom.

References

1) T. H. R. Skyrme, Proc. Roy. Soc. Lond. **A260**, 127 (1961).
2) J. Wess and B. Zumino, Phys. Lett. **B37**, 95 (1971).
3) E. Witten, Nucl. Phys. **B223**, 422 (1983a); Nucl. Phys. **B223**, 433 (1983b).

Towards Understanding Finite Density QCD in the Large N_c Limit†

A. Cherman,[*1] B. C. Tiburzi[*2]

[QCD, finite density, large N_c]

The study of QCD at finite baryon density is severely hampered by the so-called fermion sign problem. As a result, we have no known first principles approach to study nuclear matter, or neutron stars from the theory of colored quarks and gluons. Over the years, it has proven useful to consider QCD, which has three colors ($N_c = 3$), in the limit of a large number of colors. On the surface, the large N_c limit does not seem to simplify matters at finite density—the fermion sign problem persists for all values of N_c. In the limit of a large number of colors, however, one can exploit powerful dualities that exist between strongly coupled gauge theories[2)]. Recent work focused on some rather novel "strong-strong dualities" that have been discovered at finite density[3)]. These dualities relate strongly coupled theories plagued by a fermion sign problem, to strongly coupled theories free of sign problems. Ultimately such dualities give deeper insight into the nature of the sign problem, and possibly provide a way to understand QCD at finite density in the large N_c limit. Already these ideas have lead to a quantitative understanding of the universality of phase diagrams in sign-problem free theories[4)], and rigorous results concerning the existence of the chiral critical point at large N_c[5)].

Provided such strong-strong dualities holds, one can use lattice Monte Carlo techniques to solve numerically the dual theory which is sign-problem free. The difficulty with this proposal concerns the validity of the duality beyond perturbation theory. In particular, the ground state of the dual theory may support the formation of condensates which destroy the large N_c equivalence. Indeed the dual theory to $SU(N_c)$ gauge theory at non-vanishing baryon chemical potential μ_B is $SO(2N_c)$ gauge theory at finite baryon density. The latter theory develops diquark condensation [which is a Bose-Einstein condensate (BEC)] past $\mu_B > m_\pi$. In order to use the gauge theory equivalence for chemical potentials beyond this value, the underlying theory must be modified in such a way to inhibit this condensation[3,6)]. In these works, deformations to accomplish this, $V_\pm$, have been proposed. The validity of the duality then hinges on properties of the ground state of the deformed theory. While such non-perturbative properties are generally difficult to address, the low-density regime ($\mu_B \sim m_\pi$) can be handled with effective field theory methods. Indeed it was shown that the effective field theory supports the validity of the equivalence at the non-perturbative level[6)]. Phase diagrams for the two deformations are depicted in Fig. 1. This promising result encourages us to look at larger densities, $\mu_B \gg m_\pi$, where effective field theory methods cannot be applied. In this regime, lattice QCD computations of the dual theory are needed. Considerable theoretical work is currently underway to understand the nature of baryons in the duality, and eventually to pave the way for large-scale lattice computations.

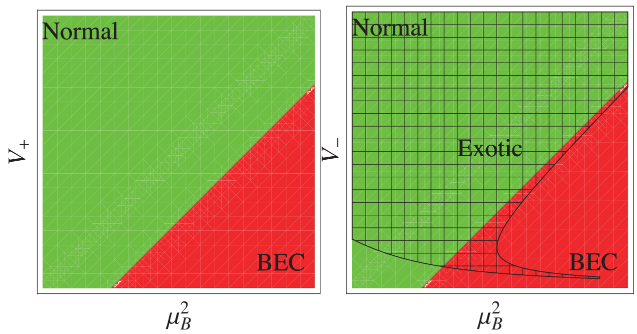

Fig. 1. Schematic phase diagram of deformed $SO(2N_c)$ gauge theory. The x-axis, where $V_\pm = 0$, corresponds to the undeformed theory, and $V_\pm$ represents the strength of the deformation. Regions where diquarks form a BEC correspond to those regions where the equivalence to large N_c QCD breaks down. Notice that one can remain outside the BEC phase for a large enough value of the deformation. There is a large N_c exotic phase characterized by a BEC of diquarks in addition to an η' condensate. Such a phase only exists in the V_--deformed theory (shown in the hatched region), but has been shown to be metastable.

References
1) A. Cherman and B. C. Tiburzi, arXiv:1109.3093 [hep-ph].
2) M. Bershadsky and A. Johansen, Nucl. Phys. B **536**, 141 (1998); M. Schmaltz, Phys. Rev. D **59**, 105018 (1999); M. J. Strassler, hep-th/0104032; P. Kovtun, M. Ünsal and L. G. Yaffe, JHEP **0507**, 008 (2005).
3) A. Cherman, M. Hanada and D. Robles-Llana, Phys. Rev. Lett. **106**, 091603 (2011).
4) M. Hanada and N. Yamamoto, arXiv:1103.5480 [hep-ph].
5) Y. Hidaka and N. Yamamoto, arXiv:1110.3044 [hep-ph].
6) A. Cherman and B. C. Tiburzi, JHEP **1106**, 034 (2011).

† Condensed from Reference[1)]

*1 Department of Applied Mathematics and Theoretical Physics, Cambridge University, UK
*2 Department of Physics, The City College of New York (CUNY), USA; and RIKEN–BNL Research Center, USA

Investigation of phase structure of QCD from imaginary chemical potential†

K. Kashiwa,*1 T. Hell,*2 and W. Weise,*2

[QCD phase diagram, imaginary chemical potential, PNJL model]

The investigation of the phase structure of Quantum chromodynamics (QCD) at finite temperature (T) and real chemical potential ($\mu_{\rm R}$) is an important subject in the particle physics. If we obtain the QCD phase structure from the first principle calculation, there is no problem. The first principle calculation which is the lattice QCD (LQCD) simulation has the sign problem at finite $\mu_{\rm R}$ and is not feasible. If we use several methods and approximations, we can only reach the region $\mu_{\rm R}/T \leq 1$. Therefore, effective model calculations are widely used to investigate the QCD phase diagram. However, the effective model approach has a large ambiguity in its foundation. Because of these reasons, we cannot obtain a reliable phase structure at finite $\mu_{\rm R}$ presently.

To overcome this problem, we considered the imaginary chemical potential ($\mu_{\rm I}$) as a first step. At finite $\mu_{\rm I}$, there is no sign problem, and thus, we can precisely execute the LQCD simulation. Moreover, some characteristic properties are observed at finite $\mu_{\rm I}$ and there is a direct relation between the imaginary and the real chemical potential [1]. This implies that we can obtain some important constraints for a model design and construct a reliable model on the basis of these constraints.

In this work[2], we investigate the phase structure at finite $\mu_{\rm I}$ by using the nonlocal Polyakov-loop extended Nambu–Jona-Lasinio (PNJL) model. The PNJL model can approximately describe the chiral and deconfinement transitions. The nonlocal PNJL model is more reliable model than the local PNJL model which is usually used to investigate the phase diagram at finite $\mu_{\rm R}$. In this study, we also introduce the quark wave function renormalization constant in the nonlocal PNJL model, as described in a previous paper[3]. We show that this nonlocal PNJL model can adequately reproduce the LQCD data[4,5] of transition lines at finite $\mu_{\rm R}$. In this nonlocal PNJL model, the combination of the chemical potential and temporal component of gauge field (A_4) in the distribution function which describe the nonlocality is almost unique. On the other hand, the combination is less clear in the local PMNJL model. Solving this problem is important in order to determined the strength of the vector-type interaction ($G_{\rm v}$). By using the nonlocal PNJL model, we show the possibility that the vector-type interaction which is usually neglected in the model can be determined at finite $\mu_{\rm I}$, and the estimated value of the interaction becomes $G_{\rm v} = 0.4\ G$, where G is the strength of the scalar-type interaction. This value is manifest the reliable range $0.25 \leq G_{\rm v} \leq 0.5$ originating in the effective one-gluon exchange interaction, which can be obtained from QCD with some approximations.

In this work[6], we investigate the system under a strong uniform (electro-) magnetic field at zero chemical potential by using the nonlocal PNJL model. This situation is also calculable by the LQCD simulation, whereby we can obtain some restriction for the model design. We show that the transitions at zero chemical potential at finite T can become first-order if the magnetic field is sufficiently strong in the nonlocal PNJL model. This result is consistent with the recent LQCD prediction[7]. In this study, we do not consider the chemical potential; however, the A_4 field is considered. Therefore, we can determined the A_4-dependence of the model accurately by comparing with LQCD data in the system. If we can clearly identify the dependence, we can also determine the chemical potential dependence because the combination of μ and A_4 in the nonlocal PNJL model is almost unique. Therefore, we can more accurately determine the model parameters by combining the restrictions obtained in the imaginary chemical potential region and the system under the magnetic field.

At the present stage, the available LQCD data are not adequate or sufficiently accurate. However, we can show that several important restrictions for a model design can be obtained for the imaginary chemical potential and the system under the strong magnetic field the present work[2,4].

References

1) A. Roberge, and N. Weiss, Nucl. Phys. **B275**, 734 (1986).
2) K. Kashiwa, T. Hell, W. Weise, Phys. Rev. D **84**, 056010 (2011).
3) T. Hell, K. Kashiwa, W. Weise, Phys. Rev.D **83**, 114008 (2011).
4) P. de Forcrand, and O. Philipsen, Nucl. Phys. **B642**, 290 (2002).
5) L. K. Wu, X. Q. Luo, and H. S. Chen, Phys. Rev. D **76**, 034505 (2007).
6) K. Kashiwa: Phys. Rev. D **83**, 056010 (2011).
7) M. D'Elia, S. Mukherjee, F. Sanfilippo, Phys. Rev. D **82**, 051501 (2010).

† Condensed from the article in Phys. Rev. D **83**, 117901 (2011) and Phys. Rev. D **84**, 056010 (2011)

*1 RIKEN BNL Recearch Center
*2 Physik-Department, Technische Universität München

Thermalization of quark-gluon plasma and the hard probe of initial fluctuations in heavy ion collisions

J. Liao*1,*2

[relativistic heavy ion collisions, quark-gluon plasma, thermalization, jet quenching]

From Saturation to Thermalization. — One of the central theoretical issues in the description of heavy ion collisions is to understand how the partons that are freed by the collisions evolve into a thermalized system amenable to an hydrodynamical description. Recently we've proposed[1)] a possible scenario for the thermalization process during "The First Few Fermi" (/c time) after the "Little Bang". Inherent from saturation in the initial condition, a distinctive feature of the pre-equilibrium matter is the over-population of phase space for the gluons, which we find plays a central role for the thermalization to occur. The over-population will (1) coherently amplify scattering by $1/\alpha_S$ and makes the system behave as a strongly interaction fluid despite non-equilibration and small coupling; (2) lead to the dynamical formation of a Bose condension over the course of thermalization.

We've demonstrated these by developing a transport approach of the thermalization problem. To do that, we've derived in[2)] the transport equation for such a system with elastic $2 \to 2$ gluon scattering as follows:

$$\mathcal{D}_t f(\vec{p}) = \xi\left(\Lambda_s^2 \Lambda\right) \times \vec{\nabla} \cdot \left[\vec{\nabla} f(\vec{p}) + \frac{\vec{p}}{p}\left(\frac{\alpha_S N_c}{\Lambda_s}\right) f(\vec{p})[1+f(\vec{p})]\right] \quad (1)$$

where two important scales Λ and Λ_s are introduced:

$$\Lambda\left(\frac{\Lambda_s}{\alpha_S N_C}\right)^2 \equiv (2\pi^2)\int \frac{d^3p}{(2\pi)^3} f(\vec{p})\left[1+f(\vec{p})\right] \quad (2)$$

$$\Lambda \frac{\Lambda_s}{\alpha_S N_c} \equiv (2\pi^2)\, 2\int \frac{d^3p}{(2\pi)^3}\frac{f(\vec{p})}{p} \quad (3)$$

The two scales are initially both at the saturation scale, but they separates as time evolves and become apart parametrically by the order of $1/\alpha_S$ at thermalization.

One important phenomenological consequence is the electromagnetic emission in such thermalizing glasma. We've recently shown[3)] that such a mechamism may explain the "excess" of electromagnetic production (i.e. photons and dileptons) in the low-mass low-p_t region observed in PHENIX data.

Hard Probe of Geometric Fluctuations in the Initial Condition. — In understanding the mechanism of jet energy loss, the geometric features of jet quenching observables are particularly useful[4)]. In particular the in-plane and out-of-plane difference (v_2 of high P_t hadrons) provides a sensitive tool for differentiating various models. Current data on high-P_t R_{AA} and v_2 from RHIC to LHC appear to favor a physical scenario with strong enhancement of jet-medium interaction near the phase boundary at Tc between the partonic and hadronic matter. An important implication is that the hotter medium at LHC would be "more transparent" to jets as compared with that at RHIC[5,6)].

A new and interesting geometric aspect of jet quenching is the hard probe of the geometric fluctuations (in terms of various harmonics in azimuthal angle) in the initial condition of heavy ion collisions. We've systematically quantified[6)] the response of jet quenching to various harmonic fluctuations. Such results further allow us to show how the hard and soft sectors get mutually correlated through the common event-by-event geometry and how such azimuthal correlation is related to the measured "hard ridge" in hard-soft di-hadron correlations (see Fig.1).

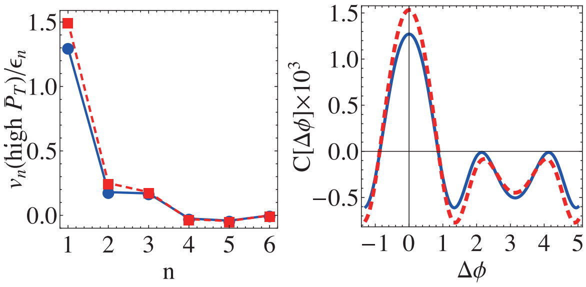

Fig. 1. Jet response to harmonic fluctuation and the resulting hard-soft azimuthal correlation.

*1 Physics Department and Center for Exploration of Energy and Matter, Indiana University, 2401 N Milo B. Sampson Lane, Bloomington, IN 47408, USA.
*2 RIKEN BNL Research Center, Bldg. 510A, Brookhaven National Laboratory, Upton, NY 11973, USA.

References

1) J. -P. Blaizot, F. Gelis, J. Liao, L. McLerran and R. Venugopalan, Nucl. Phys. A **873**, 68 (2012).
2) J. -P. Blaizot, J. Liao and L. McLerran, to appear.
3) M. Chiu, T. Hemmick, V. Khacahtryan, A. Leonidov, J. Liao, L. McLerran, arXiv:1202.3679 [nucl-th].
4) J. Jia, W. A. Horowitz and J. Liao, Phys. Rev. C **84**, 034904 (2011).
5) J. Liao, arXiv:1109.0271 [nucl-th].
6) J. Liao, E. Shuryak, Phys. Rev. Lett. **102**, 202302 (2009).
7) X. Zhang and J. Liao, Phys. Lett. B **713**, 35 (2012).

Initial conditions for dipole evolution beyond the McLerran-Venugopalan model†

A. Dumitru,*1

[QCD, high energy, gluon saturation]

I discuss the dipole scattering amplitude $N(r)$[1)] on a dense target at (moderately) short distances in the semi-classical approximation, including the first sub-leading correction arising from a $\sim\rho^4$ operator in the effective action for the large-x valence charges. This is useful for a better theoretical understanding of the A-dependence of the initial condition for high-energy QCD evolution of $N(r)$.

Following McLerran and Venugopalan (MV)[2)] the "valence" charges with large light-cone momentum fraction x are described as recoilless sources on the light cone with $\rho^a(x_\perp, x^-)$ the classical color charge density per unit transverse area and longitudinal length x^-. In the limit of a very high density of charge ρ the fluctuations of the color charge are described by a Gaussian effective action

$$S_{\rm MV}[\rho] = \int d^2\mathbf{x}_\perp dx^- \; \frac{\rho^a\,\rho^a}{2\mu^2} \; . \tag{1}$$

Here, $\int dx^-\,\mu^2 \sim g^2 A^{1/3}$ is the density of color sources per unit transverse area, proportional to the thickness of the target nucleus. This action can be used to evaluate the expectation value of the dipole operator

$$\begin{aligned} D(r) &\equiv \frac{1}{N_c}\langle {\rm tr}\; V(\mathbf{x}_\perp)V^\dagger(\mathbf{y}_\perp)\rangle \\ &= \exp\left(-\frac{Q_s^2\, r^2}{4}\log\frac{1}{r\Lambda}\right) \; , \end{aligned} \tag{2}$$

where $r \equiv |\mathbf{x}_\perp - \mathbf{y}_\perp|$ and Λ is an infrared cutoff on the order of the inverse nucleon radius. The scale $Q_s \sim \int dx^-\,\mu^2$ denotes the saturation momentum at the initial rapidity.

To go beyond the limit of infinite valence charge density one considers a "random walk" in the space of SU(3) representations constructed from the direct product of a large number of fundamental charges[3)]. The effective action describing color fluctuations then involves a sum of the quadratic, cubic, and quartic Casimirs[4,5)]

$$\begin{aligned} S[\rho] &= \int d^2\mathbf{x}_\perp dx^- \left\{\frac{\rho^a\rho^a}{2\mu^2} - \frac{d^{abc}\rho^a\rho^b\rho^c}{\kappa_3}\right. \\ &\quad \left. + \int dy^- \frac{\rho^a(x^-)\rho^a(x^-)\rho^b(y^-)\rho^b(y^-)}{\kappa_4}\right\} \end{aligned} \tag{3}$$

The coefficients of the higher dimensional operators are $\kappa_3 \sim g^3 A^{2/3}$, $\kappa_4 \sim g^4 A$, and so involve higher powers of $gA^{1/3}$. In what follows we restrict to leading order in $1/\kappa_4$. This leads to the T-matrix[5)]

$$\begin{aligned} N(r) &\equiv 1 - D(r) \\ &= \frac{Q_s^2\, r^2}{4}\log\frac{1}{r\Lambda} - \beta\, Q_s^2\, r^2 \log^3\frac{1}{r\Lambda} \; , \end{aligned} \tag{4}$$

$$\beta \equiv \frac{C_F^2}{6\pi^3}\,\frac{g^8}{Q_s^2\,\kappa_4}\left[\int dx^-\,\mu^4(x^-)\right]^2 . \tag{5}$$

The dipole scattering amplitude for a proton target has been fitted in ref.[6)] to deep-inelastic scattering data. Their initial condition for small-x evolution is

$$N(r) = 1 - \exp\left[-\frac{1}{4}\left(r^2 Q_s^2(x_0)\right)^\gamma \log\frac{1}{r\Lambda}\right] \; , \tag{6}$$

with $\gamma \simeq 1.119$. This model *simultaneously* provides a good description of charged hadron transverse momentum distributions for $p+p$ collisions at 7 TeV center of mass energy[7)]. We can match our result (4) approximately to the AAMQS model by choosing $\beta \simeq 0.01A^{-2/3}$. This matching works in the range $rQ_s \gtrsim 0.04$. Discrepancies appear at very short distances where none of the above can be trusted.

For a nucleus with $A = 200$ nucleons though $\beta \simeq 0$ and so $D(r)$ obtained with the quartic action converges to the MV model expression (2) when the valence charge density is high (i.e., at large $A^{1/3}$). If indeed the ρ^4 term in the action is the correct explanation for the AAMQS model then their modification of the MV model should vanish like $\beta \sim A^{-2/3}$. This should be observable via the "nuclear modification factor" R_{pA} in pA collisions at the LHC.

† Condensed from the article arXiv:1112.4760

*1 Department of Natural Sciences, Baruch College (CUNY), New York and RIKEN BNL Research Center (RIKEN fellow)

References

1) A. H. Mueller, Nucl. Phys. B **415**, 373 (1994).
2) L. D. McLerran and R. Venugopalan, Phys. Rev. D49 (1994) 2233, Phys. Rev. D49 (1994) 3352; Yu. V. Kovchegov, Phys. Rev. D54 (1996) 5463.
3) S. Jeon and R. Venugopalan, Phys. Rev. D **70**, 105012 (2004) [arXiv:hep-ph/0406169]; Phys. Rev. D **71**, 125003 (2005). [arXiv:hep-ph/0503219].
4) A. Dumitru, J. Jalilian-Marian and E. Petreska, Phys. Rev. D **84**, 014018 (2011) [arXiv:1105.4155 [hep-ph]].
5) A. Dumitru and E. Petreska, Nucl. Phys. A **879**, 59 (2012).
6) J. L. Albacete, N. Armesto, J. G. Milhano, P. Quiroga-Arias and C. A. Salgado, Eur. Phys. J. C71, 1705 (2011).
7) A. Dumitru, arXiv:1112.3081

Quark fragmentation process on nucleon target: Transverse momentum dependence†

H. H. Matevosyan,[*1] W. Bentz,[*2] I. C. Cloët,[*1] A. W. Thomas [*1]

[QUARK FRAGMENTATION FUNCTIONS, Semi-inclusive pion production, Deep inelastic scattering, Transverse momentum dependence]

The transverse momentum dependence of semi-inclusive hadron production processes has received considerable attention recently, both for nucleon and nuclear targets[1)]. In this work, we extend our previous studies of quark distribution functions in the proton ($q(x, k_T^2)$) and quark fragmentation functions to pions ($D_q^\pi(z, P_\perp^2)$) to include the dependence on the transverse momenta of the fragmenting quark ($\boldsymbol{k}_T$, relative to the direction of the absorbed photon) and of the produced pion ($\boldsymbol{P}_\perp$, relative to the fragmenting quark). For the elementary distribution and fragmentation functions we use the forms obtained in the Nambu-Jona-Lasinio (NJL) model[2)], and for the multi-fragmentation processes we use a quark-jet description based on the Monte-Carlo method[3)].

To illustrate the transverse momentum dependence, in Fig. 1 we show the results for the ratios $\dfrac{u(x, k_T^2)}{u(x)}$ for $x = 0.8$, and $\dfrac{D_u^{\pi^+}(z, P_\perp^2)}{D_u^{\pi^+}(z)}$ for $z = 0.8$. Here $u(x)$ and $D_u^{\pi^+}(z)$ are the corresponding quantities integrated over the transverse momenta. These results show a considerable deviation from the Gaussian forms which were assumed in most works done so far on the transverse momentum dependence[4)].

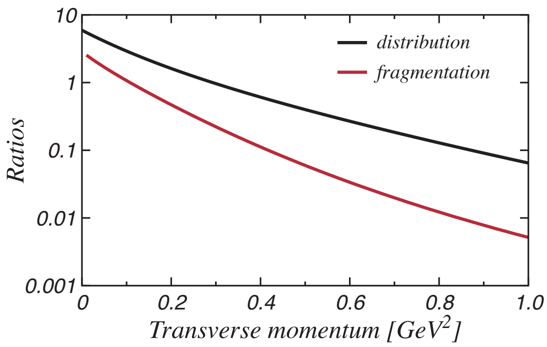

Fig. 1. Ratios of u-quark distribution (for $x = 0.8$) and fragmentation to π^+ (for $z = 0.8$) to their integrated values as functions of the transverse momentum.

The transverse momentum of the produced pion with respect to the direction of the photon is related to the above quantities by $\boldsymbol{P}_T = \boldsymbol{P}_\perp + z\boldsymbol{k}_T$, which leads to the following relation between the average transverse momenta:

$$\langle P_T^2\rangle(x, z) = \langle P_\perp^2\rangle(z) + z^2\langle k_T^2\rangle(x) \tag{1}$$

The results shown in Fig.2 for the case of semi-inclusive pion production have been obtained in the Monte-Carlo method by sampling the transverse momentum of the fragmenting quark according to the distribution function $q(x, k_T^2)$. (The coordinate system is chosen so that the photon has $\boldsymbol{q}_T = 0$, therefore the quark has the same $\boldsymbol{k}_T$ before and after the absorption of the photon.) The average obtained in this direct calculation is defined by $\int d^2P_T\, P_T^2\, \tilde{D}_u^{\pi^+}(x, z, P_T^2)/\tilde{D}_u^{\pi^+}(x, z)$, where the function $\tilde{D}$ is defined so that the cross section for the whole semi-inclusive process is proportional to $\sum_q e_q^2 \tilde{D}_q^{\pi^+}(x, z, P_T^2)$. The result calculated in this way agreed perfectly with the one obtained from Eq.(1).

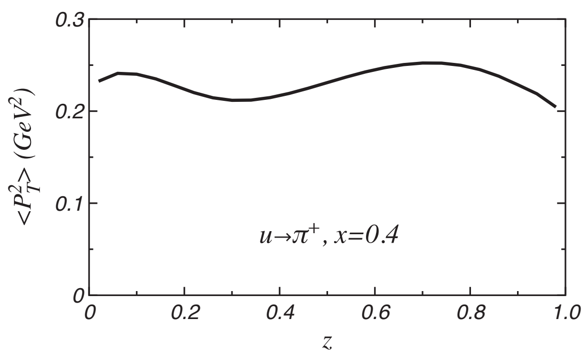

Fig. 2. Average transverse momentum of π^+ (relative to the direction of the absorbed photon) produced by the fragmentation of an up quark in a proton target.

References
1) A. Airapetian et al (HERMES group), Eur. Phys. J. **A 47** (2011) 113.
A. Airapetian et al (HERMES group), Phys. Lett. **B 684** (2010) 114.
2) T. Ito, W. Bentz, I.C. Cloët, A.W. Thomas, K. Yazaki, Phys. Rev. D **80**, 074008 (2009).
3) H. H. Matevosyan, A.W. Thomas, W. Bentz, Phys. Rev. **D 83** (2011) 114010.
4) P. Schweitzer, T. Teckentrup, A. Metz, Phys. Rev. **D 81** (2010) 094019.

† Condensed from an article by H. Matevosyan et al, Phys. Rev. **D 85** (2012) 014021.
*1 University of Adelaide, Adelaide, Australia
*2 Department of Physics, Tokai University, Kanagawa, Japan

Static interactions and stability of matter in Rindler space†

F. Lenz,*1 K. Ohta,*2 and K. Yazaki*3,*4

[Rindler space, static propagator, zero mode]

The study of quantum fields in Rindler space has played an important role in helping us understand quantum fields in nontrivial spacetimes. The importance of these studies derives, to a large extent, from the existence of a horizon in Rindler space. With its close connection to the Minkowski space via the known local relationship between fields in uniformly accelerated and inertial frames, the Rindler space provides the simplest possible context to investigate the kinematics and dynamics of quantum fields close to a horizon.

The kinematics of noninteracting quantum fields in Rindler space[1–3] and their relationship to fields in Minkowski space, together with the interpretation in terms of quantum fields at finite temperature[4,5], are well understood.

In the present research, dynamical issues associated with quantum fields in Rindler space are addressed by studying the interaction between two static sources generated by the exchange of scalar particles, photons, and gravitons. The relevant quantities involved are the corresponding static Rindler space propagators. The time-dependent propagators in Rindler and Minkowski spaces are trivially related to each other by coordinate transformation, but the static propagators obtained by integrating over different time variables are not. The corresponding static interaction potentials in Rindler space are shown to be scale-invariant complex quantities. The imaginary part has its quantum mechanical origin in the presence of an infinity of zero modes in uniformly accelerated frames, which in turn are related to the radiation observed in inertial frames[6–9].

The related effects of uniform acceleration on the stability of matter and the properties of particles are also discussed. In particular, the instability of hydrogen atoms approaching the horizon of a black hole is estimated, and their lifetime is found to be independent of the mass of the black hole; further this lifetime becomes comparable to the age of the universe when the distance from the horizon is about 10^{-4} m. At a shorter distance on the order of 10^{-10} m, the nuclei can be unstable. In connection with dynamical symmetry breaking, a simple model of a self-interacting scalar field, for which the Minkowski vacuum is in the broken phase with a finite expectation value of the field, is studied. Since the coordinate transformation does not change the expectation value, the latter remains unchanged in Rindler space[9], but becomes comparable to the thermal fluctuation of the field near the horizon; thus, it is meaningless to refere to the expectation value as the order parameter for the phase transition.

References

1) S. A. Fulling, Phys. Rev. D **7**, 2850 (1973)
2) D. G. Boulware, Phys. Rev. D **11**, 1404 (1975)
3) P. C. W. Davies, J. Phys. A **8**, 609 (1975)
4) W. G. Unruh, Phys. Rev. D **14**, 870 (1976)
5) W. D. Sciama, P. Candelas and D. Deutsch, Adv. Phys. **30**, 327 (1981)
6) A. Higuchi, G. E. A. Matsas and D. Sudarsky, Phys. Rev. D **45**, R3308 (1992)
7) A. Higuchi, G. E. A. Matsas and D. Sudarsky, Phys. Rev. D **46**, 3450 (1992)
8) H. Ren and E. J. Weinberg, Phys. Rev. D **49**, 6526 (1994)
9) F. Lenz, K. Ohta and K. Yazaki, Phys. Rev. D **78**, 065026 (2008)
10) W. G. Unruh and N. Weiss, Phys. Rev. D **29**, 1656 (1984)

† Condensed from the article in Phys. Rev. D **83**, 064037 (2011)

*1 Institute for Theoretical Physics III, University of Erlangen-Nuernberg, Germany
*2 Institute of Physics, University of Tokyo
*3 Hashimoto Mathematical Physics Laboratory, Nishina Center, RIKEN
*4 Yukawa Institute for Theoretical Physics, Kyoto University

Chiral symmetry breaking in strong QED model with fermion brane

E. Shintani[*1], and T. Onogi[*2]

[Graphene, Monte-Carlo simulation, Chiral symmetry]

In a previous work[1)], we performed the Monte-Carlo simulation of relativistic QED action associated with Graphene lattice[2)]. We will show some updated results in this article.

Our strong QED model is constructed under the concept of local quantum field theory, which has manifest gauge symmetry and scaling of theoretical parameters. In this system, the QED coupling constant becomes effectively strong as $\alpha_e = e^2/(4\pi v_F) \sim \mathcal{O}(1)$, where e denotes the charge of the electron and $v_F \sim \mathcal{O}(10^{-2})$ is introduced as the fermi-velocity in natural units, and therefore the non-perturbative study using the Monte-Carlo simulation plays a crucial role in the study of phase structure. As shown in the perturbative study[3)] on a one-loop order, the fermi-velocity has a logarithmic divergence while gauge coupling has a sub-leading contribution. It is found that this system is mostly controlled by the velocity rather than gauge coupling. Furthermore, renomaliztion group study[3)], study of renormalized velocity used in higher-order perturbative calculation, has indicated the existence of a non-trivial ultraviolet fixed point in a strong coupling region. We hypothesize that such a fixed point involves chiral phase transition corresponding to insulator transition of suspended Graphene. Here, we focus on the search of the critical point in this model.

In our simulation, $N_f = 2$ staggered fermion in the non-compact QED action is employed. The lattice size is $30^2 \times 20$ and $L_z = 8$ which is the same as that used in a previous study[5)]. Here, we have considered anisotropic gauge coupling for electromagnetic interaction, which is realized by rescaling the temporal direction and gauge field by the velocity. This offers the advantage of simultaneously taking v times lower temperature and $1/v$ times larger coupling constant from the original relativistic action. Figure 1 shows the behavior of the chiral condensate (σ) of a quasi-particle and chiral susceptibility (χ_m) as functions of the bare coupling constant $\beta v = v/e^2$. For σ there is no stepping behavior like the first order transition, and σ seems to sequentially approach a discontinuous point in the massless limit. Furthermore, the strong peak of χ_m can be observed, whose peak height increases and whose position moves to a strong coupling region as the mass decreases. This is typical chiral phase transition. Although we have not performed the extrapolation to a massless limit of σ to evaluate the critical point, we roughly estimate α_c =1.45–1.59 at $v = 0.1$. This value is slightly larger than that of the non-relativistic model calculation[5,6)]. Figure 2 shows that α_c moves about 50% in the strong coupling direction by changing from quench to $N_f = 2$ and also α_c increases when changing velocity $v = 0.1$, 0.05, 0.03 (0.03 excepted in quench). These behaviors are mostly consistent with the model estimate in[6)]. Our results suggest a strong evidence of scaling with respect to the velocity parameter because at the tree level, α_c should be constant irrespective of v. To determine the quantitative value of β_c, a detailed scaling study is needed.

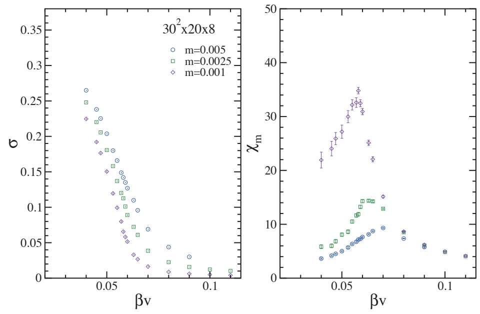

Fig. 1. Chiral condensate (left) and chiral susceptibility (right) at $v = 0.1$ as a function of mass and βv, which is proportional to α_e.

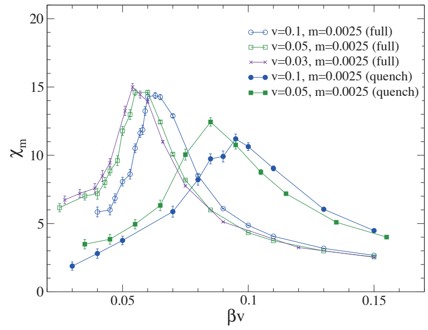

Fig. 2. Comparison of chiral susceptibility with different flavor number (quench and $N_f = 2$) and different velocity parameter at $m = 0.0025$.

*1 RIKEN-BNL Research Center, BNL
*2 Department of Physics, Osaka University

References

1) E. Shintani, T. Onogi, RIKEN Accel. Prog. Rep. Vol. **42** (2010).
2) A. K. Geim and K. S. Novoselov, Nature material Vol.6, 183 (2007).
3) J. González, F. Guinea and M. A. H. Vozmediano, Nucl. Phys. B **424**, 595 (1994).
4) V. N. Kotov, *et al.*, arXiv:1012.3484 [cond-mat.str-el].
5) J. E. Drut and T. A. Lahde, Phys. Rev. B **79**, 165425 (2009).
6) O. V. Gamayun, *et al.*, Phys. Rev. B **81**, 075429 (2010).

Neutral B-meson mixing matrix elements

Y. Aoki,[*1] T. Ishikawa,[*2] T. Izubuchi[*2] (for RBC and UKQCD collaborations)

[Lattice QCD, Standard Model, Flavor Physics]

The neutral B-meson mixing matrix elements in the standard model are defined as

$$\mathcal{M}_q = \langle \bar{B}^0_q | [\bar{b}\gamma^\mu(1-\gamma_5)q][\bar{b}\gamma_\mu(1-\gamma_5)q] | B^0_q \rangle \qquad (1)$$

for B^0 $(q = d)$ and B^0_s $(q = s)$ mesons. Due to the CP violation through Kobayashi-Maskawa mechanism the B^0 and $\overline{B^0}$ mesons acquire different mass. The mass difference in the standard model is expressed using the $\mathcal{M}_q$ and CKM matrix V,

$$\Delta m_q = [\text{known factor}] \cdot |V^*_{tq}V_{tb}|^2 \mathcal{M}_q. \qquad (2)$$

The experimental accuracy of the mass difference observed through the oscillation frequency is sub-percent, thanks to Belle, BaBar and Tevatron experiments. This opens up the opportunity to perform a precision test of the standard model and further to search the new physics beyond the standard model through CKM unitarity.

The highly non-perturbative matrix elements $\mathcal{M}_q$ can be calculated numerically from the first principles using lattice gauge theory. The difference of the matrix element for d and s is only realized by the mass difference between d and s quarks. In lattice calculation the flavor $SU(3)$ breaking ratio $\xi = [\text{kinematic factor}] \cdot \sqrt{\mathcal{M}_s/\mathcal{M}_d}$ can be determined more precisely than the each matrix element, since the large fraction of the statistical and systematic errors cancel in the ratio. Through ξ (theory) and $\Delta m_s/\Delta m_d$ (experiment), the ratio $|V_{td}/V_{ts}|$ is determined. $|V_{td}/V_{ts}|$ provides an important constraint on the unitarity triangle. As the error of the ratio from the experiment is small (sub-percent), the error of the lattice calculation of ξ dominates the width of the allowed range of $|V_{td}/V_{ts}|$.

To achieve the required high precision, the full $2+1$ flavor lattice QCD calculation of ξ is indispensable. The RBC/UKQCD collaborations have been trying to calculate the mixing matrix elements employing static approximation in the heavy quark effective theory (HQET) with the $2+1$ flavor domain wall fermions for the light flavors. The $SU(3)$ breaking ratio ξ calculated with two different heavy quark discretization schemes (APE and HYP2) have been reported[1]. Through this exploratory study, where the resulting precision is not satisfactory, the tasks to improve the precision was made clear. They include a) having smaller quark mass for the extrapolation of the u, d quarks to the physical point, where larger physical volume must be used to make the finite volume effect negligible; b) to have better signal/noise ratio, optimization of quark source smearing parameter should be fine-tuned; c) to control the discretization error, the second lattice spacing is needed for the continuum extrapolation $a \to 0$, where a is the lattice spacing; d) to have less systematic error in c) we need to construct the $O(a)$ improved operator through one-loop lattice perturbation theory[2]. Having accomplished a) and b) a preliminary result have been obtained with impressively better accuracy than the previous study and shown in the same report in the last year.

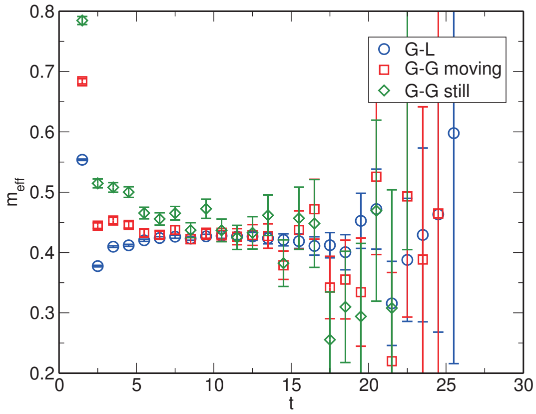

Fig. 1. Effective energy of B_0 as function of operator time separation t for three combinations of quark smearing at source and sink.

This year, a series of calculations at second, finer lattice spacing have been performed. Figure 1 shows the effective energy plot of the B_0 meson at the lightest d quark mass on the fine lattice, where we have used the source smearing parameter tuned in a pilot calculation. We have used this information to set the optimum time separation of the source and sink Euclidean time slice of the three-point functions for the B meson mixing matrix elements, which is now being calculated. The operator improvement will be applied to the results on two lattice spacings. Then the continuum limit will be taken to have the final result.

This project is supported in part by US DOE through USQCD collaboration, JSPS Kakenhi grant No. 21540289, 22224003, 22540301, 23105715, and RIKEN RICC.

References

1) C. Albertus, et al., Phys. Rev. D 82 (2010) 014505.
2) T. Ishikawa, et al., arXiv:1101.1072.

*1 Nagoya University, KMI
*2 RIKEN-BNL Research Center

Full QED+QCD low-energy constants from reweighting method

T. Ishikawa,[*1] T. Blum,[*2] M. Hayakawa,[*3,*4] T. Izubuchi,[*1,*5] C. Jung[*5] and R. Zhou[*6]

[Hadron Physics (Theory)]

The combination of chiral perturbation theory (ChPT) and QED provides a powerful tool for addressing isospin breaking. Partially quenched ChPT (PQChPT) with QED was first derived by Bijnens *et al.* in the $SU(3)$ flavor basis up to next-to-leading order[1)]. In PQChPT, sea and valence quarks are treated separately. Here, we specify the two valence quarks in mesons by the indices 1 and 3 and the three sea quarks (u, d, s) by the indices 4–6, and we introduce quark masses m_i and quark electromagnetic (EM) charges q_i in units of the fundamental EM charge e. The fundamental charge of sea and of valence sectors can be set separately; we represent them as $e_{\rm s}$ and $e_{\rm v}$, respectively. Using these notations, the sea EM charge contribution to the pseudo-scalar (PS) meson mass-squared can be expressed as follows:

$$\Delta(M_{\rm PS}^{SU(3)})^2 = -4e_{\rm s}^2 Y_1 {\rm tr} Q_{{\rm s}(3)}^2 \chi_{13} + \frac{e_{\rm s}e_{\rm v}}{8\pi^2}\frac{C}{F_0^4}\sum_{i=4,5,6}\left(\chi_{1i}\ln\frac{\chi_{1i}}{\mu^2} - \chi_{3i}\ln\frac{\chi_{3i}}{\mu^2}\right) q_i(q_1-q_3), \quad (1)$$

where $\chi_{ij} = B_0(m_i+m_j)$ and $Q_{{\rm s}(3)} = {\rm diag}(q_4, q_5, q_6)$. μ is an arbitrary renormalization scale, and B_0, F_0, C, and Y_1 are low-energy constants (LEC's). Although C can be accessible with $e_{\rm s}=0$ (quenched QED),[2)] the determination of Y_1 requires $e_{\rm s}\neq 0$ (full QED).

So far, most of the lattice QCD simulations neglected the EM charges. While the full QED effect can be incorporated in the Monte Carlo (MC) evolution of the gauge field configuration, the usual gauge ensemble has been generated only with dynamical QCD. However, the full QED effect, in principle, can be included using a reweighting method, which was first proposed and tested by Duncan *et al.*[3)]. Applications of the reweighting to a realistic QED+QCD simulation were recently reported by several groups [4,5)].

An expectation value of some observable O in the full QED+QCD is related to the one in the quenched QED+QED as:

$$\langle O\rangle_{\rm full\ QED+QCD} = \frac{\langle wO\rangle_{\rm quenched\ QED+QCD}}{\langle w\rangle_{\rm quenched\ QED+QCD}}, \quad (2)$$

where w is the reweighting factor, which is basically a ratio of quark determinants [3)]. The configuration set in this work is one of the ensembles used in the quenched QED study on the dynamical domain-wall fermion[2)], whose simulation parameters are $\beta_{\rm QCD} = 2.13$, $L^3\times T\times L_s = 16^3\times 32\times 16$, $(am_{\rm u}, am_{\rm d} and am_{\rm s}) = (0.01, 0.01, 0.04)$. The $U(1)$ photon fields, which have already been generated in the quenched QED study, are combined with the gluon configurations. For the reweighting factors, a stochastic method with random Gaussian noise vectors is used. We break up the quark determinants into many small pieces using a mathematical identity that is called the $n^{\rm th}$-root trick: $w = \det\Omega = \left(\det\Omega^{1/n}\right)^n$. We employ $n=24$ roots and use four complex random noise vectors per root in each configuration to estimate the reweighting factors. Using the reweighting factor in this work and the meson correlators in the quenched QED study[2)], the reweighted meson correlators are obtained by Eq. (2). Examples of effective masses for the π^+ meson are shown in Fig. 1. Using the calculated reweighted data of the meson masses, chiral fits are performed to extract the QED LEC's in Eq. (1) and we obtain

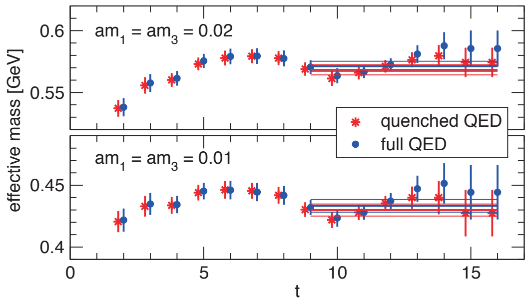

Fig. 1. Effective mass for the π^+ meson in the full QED (blue) and the quenched QED (red).

$$Y_1 = -5.6(3.6)\times 10^{-2}, \quad C = 8.4(4.3)\times 10^{-7}. \quad (3)$$

C determined in this work (full QED) is almost consistent with the one from the quenched QED study[2)], which suggests that the reweighting is well controlled. Study on a larger lattice, $24^3\times 64\times 16$, with further algorithmic improvements to increase statistics, is in progress.

*1 RIKEN BNL Research Center, USA
*2 Physics Department, University of Connecticut, USA
*3 Department of Physics, Nagoya University, Japan
*4 Nishina Center, RIKEN, Japan
*5 Physics Department, Brookhaven National Laboratory, USA
*6 Physics Department, Indiana University, USA

References

1) J. Bijnens *et al.*, Phys. Rev. D **75**, 014505 (2007).
2) T. Blum *et al.*, Phys. Rev. D **82**, 094508 (2010).
3) A. Duncan, *et al.*, Phys. Rev. D **71**, 094509 (2005).
4) A. Portelli *et al.* [BMW], PoS LATTICE **2010**, 121 (2010).
5) N. Ukita [PACS-CS], arXiv:1111.6380 [hep-lat].

Nucleon structure from lattice QCD at nearly physical pion mass

Y. Aoki[1,2], T. Blum[3,2], T. Izubuchi[2,4], C. Jung[4,2], M. Lin[5,2], S. Ohta[6,7,2], S. Sasaki[8,2], and T. Yamazaki[1]

[Nucleon structure, QCD]

Nucleon is an important building block of baryonic matter that makes up ourselves and our environment, carrying the great majority of mass. Quantum chromodynamics (QCD), through its non-perturbative lattice numerical studies using supercomputers, provides a detailed account of how quarks and gluons, confined within nucleon, contribute such large mass despite their own lightness, which is not so different from electron or neutrino. Study of nucleon structures, how its electroweak currents, momentum or angular momentum is distributed, is a major goal of RIKEN-BNL Research Center, both experimentally and theoretically. We provide one of the best theoretical calculations[1–3] distinguished by almost exact chiral and flavor symmetries[4–6] of domain-wall fermions (DWF) quarks, in contrast to many others. Here we summarize the latest of such calculations[7] with an unprecedented large lattice volume, about $(4.6\mathrm{fm})^3$, and nearly physical pion mass values of about 250 and 170 MeV[5,6].

The lattice-QCD ensembles are generated jointly by the RIKEN-BNL-Columbia (RBC) and UKQCD collaborations: the strange-quark mass is set almost exactly at its physical value, and then reweighed to the exact value. The up- and down-quark mass are set degenerate and as light as practical, resulting in pion mass of about 250 and 170 MeV respectively. We refer the details to Refs.[4–6]. We have accumulated about 1,500 gauge configurations for each ensemble, and are using one in eight of them for the present analysis. The nucleon mass is estimated as about 1.05 and 0.98 GeV respectively for the heavy and light ensembles. We are calculating all the form factors of the isovector vector and axialvector currents, some low-moments of the isovector unpolarized and polarized structure functions, and the strangeness content. We refer Refs.[1–3] for details of our analysis methods. Analysis for the heavy, 250-MeV, ensemble has been completed using the RIKEN RICC computers. That for the light, 170-MeV, ensemble is on-going using the US Teragrid/XSEDE computers.

From the calculated isovector vector charge, g_V, we confirm the chiral and flavor symmetries are very well preserved for the ensembles[7]. In Fig. 1 we summarize the calculations of the ratio, g_A/g_V, of the isovector

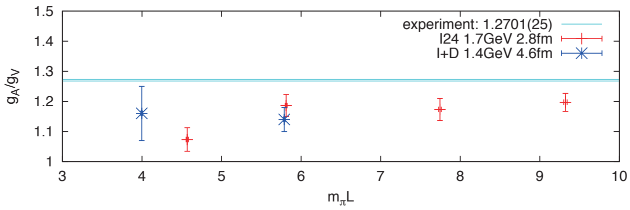

Fig. 1. Ratio g_A/g_V of isovector axial and vector charges, plotted against finite-size scaling parameter, $m_\pi L$, for the present (blue) and published[1)] (red) calculations.

axialvector charge, g_A, and vector charge. The ratio determines neutron life, among other things, and hence nuclear isotope stability. Both the present (blue) and previously published[1)] (red) calculations are plotted against a finite-size scaling parameter, $m_\pi L$, the product of the calculated pion mass, m_π, and the lattice spatial extent, L. The agreement of the present and published results at $m_\pi L \sim 6$, despite significant differences in both m_π and L, confirms the deficit in the lattice calculations and supports our conjecture that the deficit arises from the small finite volume of the lattice that cannot contain virtual pion cloud surrounding the nucleon sufficiently well. We are increasing our statistics to understand this effect better, especially for the light ensemble. Momentum-transfer dependence of all the isovector form factors are being calculated as well.

Some low moments of isovector structure functions are also being calculated. In particular, the quark momentum, $\langle x\rangle_{u-d}$, and helicity, $\langle x\rangle_{\Delta u-\Delta d}$, fractions are showing signs to decrease as the quark mass is set lighter, trending toward the experimental values.

Strange quark content of the nucleon, $\langle N|\bar{s}s|N\rangle$, is also being calculated using strange quark reweighting technique[5)]. It strongly couples with some supersymmetric dark-matter candidates[8)]. Our preliminary analysis suggests small but finite value.

In all these cases reducing the statistical error, especially for the light ensemble at m_π=170 MeV, is essential. We are actively pursuing this goal by improving our algorithms as well as computers.

References
1) T. Yamazaki *et al.*, Phys. Rev. Lett. **100**, 171602 (2008).
2) T. Yamazaki *et al.*, Phys. Rev. D **79**, 114505 (2009).
3) Y. Aoki *et al.*, Phys. Rev. D **82**, 014501 (2010).
4) Y. Aoki *et al.* Phys. Rev. **D83**, 074508 (2011).
5) C. Jung, PoS **LAT2009**, 002 (2009).
6) C. Kelly, PoS **Lattice 2011**, 285.
7) M. Lin and S. Ohta, Prog. Part. Nucl. Phys. in press, arXiv 1112.5489; S. Ohta, PoS **Lattice 2011**, 168.
8) J. R. Ellis *et al.*, Phys. Rev. D **77**, 065026 (2008).

*1 KMI, Nagoya University
*2 RIKEN-BNL Research Center, BNL, USA
*3 University of Connecticut, USA
*4 Brookhaven National Laboratory, USA
*5 Yale University, USA
*6 IPNS, KEK
*7 SOKENDAI
*8 University of Tokyo

5. Particle Physics

Numerical simulation of the $\mathcal{N} = (2, 2)$ Landau–Ginzburg model†

S. Kamata[*1] and H. Suzuki

[Supersymmetry, Non-perturbative dynamics, Landau–Ginzburg model]

A low-energy limit of the two-dimensional $\mathcal{N} = (2, 2)$ Wess–Zumino model (2D $\mathcal{N} = (2, 2)$ WZ model) with a (quasi-)homogeneous superpotential is believed to be a non-trivial $\mathcal{N} = (2, 2)$ superconformal field theory (SCFT).[1–3] This Landau–Ginzburg description[4] of the $\mathcal{N} = (2, 2)$ SCFT is a remarkable non-perturbative phenomenon in the quantum field theory and physically, for example, is considered as appropriate basis for the correlation between the gauged linear sigma model and the Calabi–Yau compactification of the string theory. Although the consistency of this emergence of the SCFT in the low-energy limit has been checked by various analytical methods, it is very difficult to confirm this phenomenon directly because the 2D WZ model is strongly coupled at low energies. Application of conventional numerical techniques (such as the lattice field theory) would not be a straightforward means of confirming the aforementioned phenomenon either because supersymmetry (SUSY) is essential in this non-perturbative dynamics.

Motivated by a recent remarkable study,[5] we carried out a numerical simulation of the 2D $\mathcal{N} = (2, 2)$ WZ model in the present research. We considered the case of a massless cubic superpotential $W(\Phi) = \lambda\Phi^3/3$, which, according to the conjectured correspondence, should become an SCFT in the low-energy limit, where the scaling dimension of a chiral primary field is $1 - h - \bar{h} = 0.666\ldots$ and the central charge is $c = 1$. We employ a non-perturbative formulation[6] that preserves full SUSY, translational invariance, and linear internal symmetries such as the R-symmetry.

Figures 1 and 2 illustrate our main results. The total computational time was 8576.9 CPU · hour at the RIKEN Integrated Cluster of Clusters (RICC) facility. From a finite-size scaling of the susceptibility of the scalar field in Fig. 1, $1 - h - \bar{h} = 0.616(25)(13)$ for the scaling dimension. c was measured to be $c = 1.09(14)(31)$ from a correlation function between the supercurrents. "An effective c" in various energy scales that behaves just like the Zamolodchikov c-function[7] was also measured. These results are consistent with the conjectured emergence of an SCFT, and at the same time, demonstrate that numerical studies can be complementary to analytical investigations for this two-dimensional supersymmetric field theory.

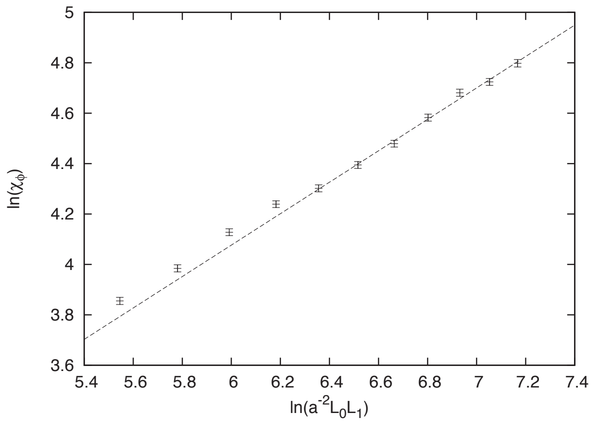

Fig. 1. System volume $a^{-2}L_0L_1$ versus the susceptibility of the scalar field χ_ϕ. The slope of the linear fit (the broken line) gives rise to the scaling dimension $1-h-\bar{h}$.

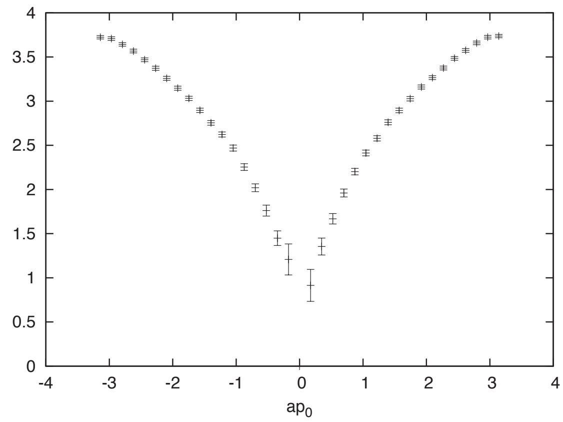

Fig. 2. A correlation function containing the supercurrents normalized by a certain analytic function. The value around the origin $ap_0 \sim 0$ provides the central charge c in the low-energy limit: $c \sim 1$

References
1) E. J. Martinec, Phys. Lett. B **217**, 431 (1989).
2) C. Vafa and N. P. Warner, Phys. Lett. B **218**, 51 (1989).
3) W. Lerche, C. Vafa and N. P. Warner, Nucl. Phys. B **324**, 427 (1989).
4) A. B. Zamolodchikov, Sov. J. Nucl. Phys. **44**, 529 (1986) [Yad. Fiz. **44**, 821 (1986)].
5) H. Kawai and Y. Kikukawa, Phys. Rev. D **83**, 074502 (2011) [arXiv:1005.4671 [hep-lat]].
6) D. Kadoh and H. Suzuki, Phys. Lett. B **684**, 167 (2010) [arXiv:0909.3686 [hep-th]].
7) A. B. Zamolodchikov, JETP Lett. **43**, 730 (1986) [Pisma Zh. Eksp. Teor. Fiz. **43**, 565 (1986)].

† Condensed from the article in Nucl. Phys. B **854**, 552 (2012)
*1 Graduate School of Science, Rikkyo University

Index theorem and overlap formalism with naive and minimally doubled fermions†

T. Kimura,*1,*2 M. Creutz,*3 and T. Misumi*4

It has been recently shown how to identify the would-be zero modes and their chiralities with staggered fermions, and its application to the staggered versions of the overlap and the Wilson fermions.[1,2] This approach is applied by the present authors to other fermions with species doublers, i.e. naive and minimally doubled fermions.[3] In this report we concentrate on the naive fermion theory.

We now investigate the doubler-multiplet for the naive lattice fermion and the corresponding flavored-mass terms. The Dirac operator for the naive fermion in general dimensions is given by $D_{\rm naive}(p) = i\sum_{\mu=1}^{d}\gamma_\mu \sin p_\mu$. For simplicity we here consider the $d=2$ case. Their locations of zeros, chiral charges and transformation matrices for the sets of gamma matrices $\gamma^\mu_{(i)} = \Gamma^\dagger_{(i)}\gamma^\mu\Gamma_{(i)}$, are listed in Table 1.

label	position	χ charge	Γ
1	$(0,0)$	$+$	$\mathbb{1}$
2	$(\pi,0)$	$-$	$i\gamma_1\gamma_5$
3	$(0,\pi)$	$-$	$i\gamma_2\gamma_5$
4	(π,π)	$+$	γ_5

Table 1. Chiral charges for each of zeros in $d=2$ with $\gamma_1=\sigma_1$, $\gamma_2=\sigma_2$ and $\gamma_5=\sigma_3$.

The doubler-multiplet field is given by

$$\Psi(p) = \begin{pmatrix} \psi_{(1)}(p-p_{(1)}) \\ \psi_{(2)}(p-p_{(2)}) \\ \psi_{(3)}(p-p_{(3)}) \\ \psi_{(4)}(p-p_{(4)}) \end{pmatrix}, \qquad (1)$$

and in this case the γ_5 multiplicatioin is expressed as $\gamma_5\psi \to (\gamma_5\otimes(\tau_3\otimes\tau_3))\Psi$, where we express the 4-flavor structure in the doubler-multiplet by two direct products of the Pauli matrix. For our purpose of obtaining the flavored-mass terms to split species, we introduce the following flavor structure in the mass term this time.

$$\bar\Psi(p)(\mathbb{1}\otimes(\tau_3\otimes\tau_3))\Psi(p) = \cos p_1 \cos p_2 \bar\psi(p)\psi(p). \quad (2)$$

Here $\psi(p)$ and $\bar\psi(p)$ are the original Dirac fields in the momentum space for the naive lattice fermion. This flavor structure gives two positive and two negative eigenvalues, which implies there are two species with positive and the others with negative mass. Its position-space expression is given by

$$M_{\tau_3\otimes\tau_3} = m_{\tau_3\otimes\tau_3}\sum_{sym.} C_1C_2 \equiv M_{\rm naive}, \qquad (3)$$

where we define $C_\mu = (T_{+\mu}+T_{-\mu})/2$ with $T_{\pm\mu}$ being the translation operator and $(\sum_{sym.})$ stands for symmetric summation over the order of the factors. $m_{\tau_3\otimes\tau_3}$ is a parameter characterizing magnitude of this mass operator.

To detect the index of the Dirac operator, it is useful to introduce a Hermitean version of the Dirac operator $H(m)=\gamma_5(D-m)$, and its spectral flow. On the other hand, for the lattice fermions with species doublers, the Hermitean versions of the Dirac operator should be in a form of $H_{\rm naive}(m) = \gamma_5(D_{\rm naive} - M_{\rm naive})$. Taking account of the sign of the slope of the crossings, these results satisfies the index theorem for the naive fermion given by

$$\mathrm{Index}(D_{\rm naive}) = 2^d(-1)^{d/2}Q, \qquad (4)$$

where the factor reflects 2^d species.

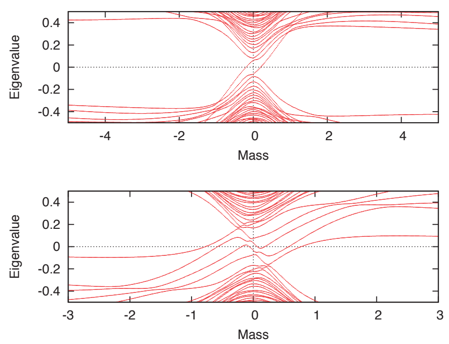

Fig. 1. Spectral flows of the Hermitean operator based on the naive fermion for the 2-dimensional case with a topological charge (top) $Q=1$ and (bottom) $Q=2$.

Fig. 1 shows the numerical result of the spectral flow for the $d=2$ naive fermion with a topological charge $Q=1$ and $Q=2$, respectively. There are doubled crossings around the origin, and the number of crossings counted depending on slopes should be the index related to the topological charge. We can lift this degeneracy by adding other kinds of flavored-mass terms, and thus obtain a single-flavor overlap fermion from the naive fermion kernel.

References
1) D. H. Adams, Phys. Rev. Lett. **104** (2010) 141602.
2) D. H. Adams, Phys. Lett. **B699** (2011) 394.
3) M. Creutz, T. Kimura and T. Misumi, JHEP **12** (2010) 041.

† Condensed from the article in PoS: Lattice 2011 (2011) 106.
*1 Department of Basic Science, University of Tokyo
*2 Mathematical Physics Laboratory, RIKEN Nishina Center
*3 Physics Department, Brookhaven National Laboratory
*4 Yukawa Institute for Theoretical Physics, Kyoto University

Revisiting symmetries of lattice fermions via spin-flavor representation†

T. Kimura,[*1,*2] S. Komatsu,[*3] T. Misumi,[*4] T. Noumi,[*3] S. Torii,[*3] and S. Aoki[*5]

The existence of fermion doublers on the lattice entails the symmetry structure different from that of continuum theory.[1)] Hence, it is important to understand the underlying symmetries in lattice field theory, not only for QCD simulations with these fermion formulations, but also for constructions of other lattice fermion formulations such as overlap, domain-wall, staggered Wilson, staggered overlap and minimally doubled fermions. Moreover fermion doublers could be used to economically simulate QCD-like theories with many flavors, which might be relevant for the construction of techni-color theories.

We show that the kinetic term of the naive fermion has the $U(4) \times U(4)$ symmetry at a finite lattice spacing. In the presence of the mass term or the chiral condensate, this symmetry is explicitly or spontaneously broken down to the diagonal U(4). We verify the existence of Nambu-Goldstone bosons associated with the broken symmetry using the strong coupling analysis.

The kinetic term of the naive fermion action obviously has the vector and axial-vector U(1) symmetry as does the action of the continuum theory, $\psi_n \to \exp(i\theta)\psi_n$, $\psi_n \to \exp(i\theta\gamma_5)\psi_n$. In addition to these well-known symmetries, the lattice kinetic term has other symmetries which include site-dependent prefactors,

$$\begin{aligned} \psi &\to \exp\left[iT^{(+)} + iT^{(-)}\right]\psi, \\ \bar\psi &\to \bar\psi \exp\left[-iT^{(+)} + iT^{(-)}\right]. \end{aligned} \tag{1}$$

Here T (+) and $T^{(-)}$ are site-dependent 4×4 matrices: $T^{(+)} \in \mathcal{M}^+$, $T^{(-)} \in \mathcal{M}^-$ with $\mathcal{M}^+ = \mathrm{span}\{\mathbb{1}_4,\ (-1)^{n_1+\cdots+n_4}\gamma_5,\ (-1)^{\check n_\mu}\gamma_\mu,\ (-1)^{n_\mu} i\gamma_\mu\gamma_5,\ (-1)^{n_{\mu,\nu}} i\left[\gamma_\mu, \gamma_\nu\right]/2\}$, $\mathcal{M}^- = \mathrm{span}\{(-1)^{n_1+\cdots+n_4}\mathbb{1}_4,\ \gamma_5,\ (-1)^{n_\mu}\gamma_\mu,\ (-1)^{\check n_\mu} i\gamma_\mu\gamma_5,\ (-1)^{\check n_{\mu,\nu}} i\left[\gamma_\mu, \gamma_\nu\right]/2\}$, where $\check n_\mu = \sum_{\nu(\neq\mu)} n_\nu$, $n_{\mu,\nu} = n_\mu + n_\nu$ and $\check n_{\mu,\nu} = \sum_{\rho(\neq\mu,\nu)} n_\rho$.

We notice that the elements of $\mathcal{M}^+$ and $\mathcal{M}^-$ are 4×4 Hermitian matrices up to site-dependent signs, and they have the following $\mathbb{Z}_2$-grading structure,

$$\begin{aligned} [\mathcal{M}^+, \mathcal{M}^+] = \mathcal{M}^+, \quad [\mathcal{M}^+, \mathcal{M}^-] = \mathcal{M}^-, \\ [\mathcal{M}^-, \mathcal{M}^-] = \mathcal{M}^+. \end{aligned} \tag{2}$$

These features imply that $\mathcal{M}^+$ generates a U(4) subgroup of the whole symmetry group, we will call $U(4)^+$. By taking linear combinations of $\mathcal{M}^+$ and $\mathcal{M}^-$ appropriately, we can obtain two mutually decoupled U(4) symmetries, which are generated by $\mathcal{M}^R = \mathrm{span}\left\{\frac{1+(-1)^{n_1+\cdots+n_4}}{2}\mathcal{M}\right\}$, $\mathcal{M}^L = \mathrm{span}\left\{\frac{1-(-1)^{n_1+\cdots+n_4}}{2}\mathcal{M}\right\}$, where $\mathcal{M} = \left\{(-1)^{n_1+\cdots+n_4}\mathbb{1}_4,\ \gamma_5,\ (-1)^{n_\mu}\gamma_\mu,\ (-1)^{\check n_\mu} i\gamma_\mu\gamma_5,\ (-1)^{\check n_{\mu,\nu}} i[\gamma_\mu, \gamma_\nu]/2\right\}$. Therefore we conclude that the kinetic term of the naive fermion has $U(4) \times U(4)$ symmetry.

In the presence of the mass term, it is readily seen that the original $U(4) \times U(4)$ symmetry is explicitly broken down to $U(4)^+$ symmetry. Similarly the original $U(4) \times U(4)$ symmetry spontaneously breaks down to $U(4)^+$ symmetry with producing 16 Nambu-Goldstone (NG) bosons, which correspond to 16 generators contained in $\mathcal{M}^-$. One of the notable features of these NG bosons is that they include the site-dependent signs in their definitions, $\bar\psi_n \mathcal{M}^- \psi_n$. These site-dependent signs have the effect of shifting momenta by π. For instance, if we Fourier-transform $\bar\psi_n((-1)^{n_1+\cdots+n_4})\mathbb{1}_4\psi_n$, we obtain a meson with shifted momenta, $(\bar\psi\psi)(p_\mu + \pi)$.

Let us briefly comment on the relation to the "doubling symmetry."[2)] The doubling symmetry in a discrete symmetry generated by the following transformations,

$$\psi_n \longrightarrow (-1)^{n_\mu} i\gamma_5\gamma_\mu\psi_n. \tag{3}$$

We can see that these transformations can be embedded in the following continuous transformations by setting θ to be $\pi/2$,

$$\psi_n \longrightarrow \exp\left(i\theta(-1)^{n_\mu} i\gamma_\mu\gamma_5\right)\exp\left(i\theta\mathbb{1}_4\right)\psi_n. \tag{4}$$

Therefore we conclude that the doubling symmetry is just a discrete subgroup of the $U(4) \times U(4)$ symmetry which we discussed above.

We can apply the same approach to the Wilson fermion action, which is invariant under only the ordinary U(1) vector transformation for general values of the mass parameter m. However an additional U(1) vector symmetry is realized by tuning m and this symmetry is spontaneously broken by pion condensation. Similarly the Karsten-Wilczek and the Boriçi-Creutz minimally-doubled fermions can be investigated, and a similar type of symmetry enhancement and its spontaneous breakdown occurs.

References

1) K. G. Wilson, Phys. Rev. **D10** (1974) 2445.
2) G. P. Lepage, Phys. Rev. **D59** (1999) 074502.

† Condensed from the article in JHEP **01** (2012) 048

*1 Department of Basic Science, University of Tokyo
*2 Mathematical Physics Laboratory, RIKEN Nishina Center
*3 Institute of Physics, University of Tokyo
*4 Yukawa Institute for Theoretical Physics, Kyoto University
*5 Graduate School of Pure and Applied Sciences, University of Tsukuba

Error reduction techniques for Lattice QCD

T. Izubuchi[*1,*2] and E. Shintani,[*2] for RBC and UKQCD Collaborations

More than half of entire computing time in recent lattice QCD have been used for physics measurements. Our understanding of interesting physics are often limited by large statistical errors. Examples include η', $I = 0$ $\pi\pi$ scatterings, $\Delta I = 1/2$ $K \to \pi\pi$, nucleon electric dipole moment, strangeness in nucleon, muon $g-2$ light-by-light, and many chemical potential derivative terms in finite density QCD.

Among the many error reduction techniques, low-mode averaging (LMA)[1] is reviewed here. LMA involves the computation of the lowest eigenvalues and the corresponding eigenvectors of the Dirac operator[a] in order to construct the low-mode part of the quark propagator, S_l. Subsequently the low mode part of the correlation function, $\mathcal{O}_l$, is constructed from S_l. Therefore, the original observable $\mathcal{O}$ is divided into a low-mode part and a part involving high modes (and low modes), $\mathcal{O}_{\rm rest}$:

$$\mathcal{O} = \mathcal{O}_l + \mathcal{O}_{\rm rest} \tag{1}$$

Since the statistical ensemble is invariant under translations G because of the symmetry of the lattice action used and since $\mathcal{O}_l$ is covariant under G, the following equation for the statistical average under the observable $\langle\mathcal{O}\rangle$ holds: $\langle\mathcal{O}_l\rangle = \langle\mathcal{O}_l^G\rangle$, where $\mathcal{O}^G$ is the translated observable under G. Once calculated, the eigenvectors allow the averaging of the correlation function over the entire four-volume (or over many different translations G) of the lattice, increasing the statistics significantly with negligible computing cost:

$$\langle\mathcal{O}\rangle = \langle\mathcal{O}_{\rm LMA}\rangle + \langle\mathcal{O}_{\rm rest}\rangle, \quad \mathcal{O}_{\rm LMA} = \frac{1}{N_G}\sum_G \mathcal{O}_l^G \tag{2}$$

Fig. 1 shows a LMA sample for the small-size problem $16^3\times32\times16$ DWF, for 20 configurations; LMA is done for 32 translations ($N_G = 32$). Blue symbols denote the statistical estimation of full observables, $\langle\mathcal{O}\rangle$, for two point functions of a nucleon (upper plots), pion (middle), and vector (bottom), with source-sink time separations of 6 (left plots), 9 (middle), and 12 (right plots). For each plot, green symbols denote the low-mode contribution, $\langle\mathcal{O}_l\rangle$, for the number of eigenvectors indicated on the x-axis (Orig, 100-600 LOW). The red symbols represent averages of the low-mode contribution, $\mathcal{O}_{\rm LMA}$, and the blue symbols denote the reconstructed observables $\mathcal{O}_{\rm LMA} + \mathcal{O}_{\rm rest}$. One can see that when t is large or the number of eigenvectors is large, the low mode starts to dominate the observables: $\mathcal{O}_l$ (green symbols) are approaches the full quantity $\mathcal{O}$ (blue symbol), so that $\mathcal{O}_{\rm rest}$, and thus its statistical fluctuation, becomes smaller than the original observable $\mathcal{O}$. After reducing the statistical error for $\mathcal{O}_l$ by averaging over G (red symbols), both the low-mode and the full contributions become statistically accurate, and error is reduced by factors close to $\sqrt{N_G} \sim 5$ for large t. Further, the PS meson (middle) is seen to be well approximated by the low-modes even for small t and a small number of eigenvectors. For the examples and statistics considered, there is almost no sign of statistical correlation among $N_G(= 32)$ translated observables, and therefore, in principle, this implies cost-effectiveness by a factor of N_G, without considering for the cost for computing the eigenvectors, which is anyway useful for many other purposes.

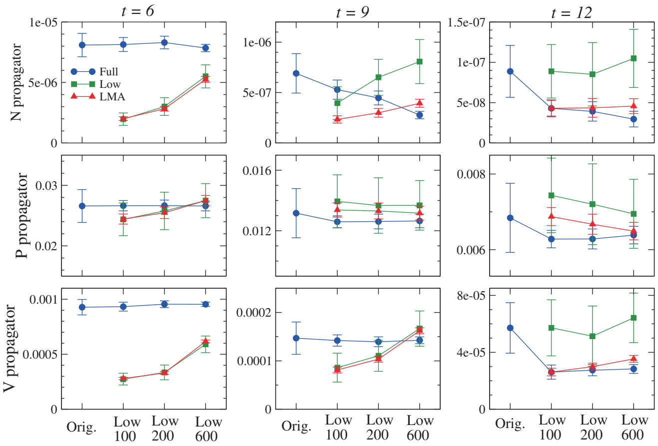

Fig. 1. LMA sample

There continues to be a need for additional error reduction techniques since LMA is primarily work efficiency for low-mode-dominant observables. For instance, the small t regions of the nucleon and vector meson are not improved significantly when LMA is used with a small number of eigenvectors, as seen in Fig. 1. Observables without low-mode dominance include tadpole quark loops ($\langle\bar{q}\Gamma q\rangle, \eta'$, $g-2$ light-by-light , *etc.*), strange/charm quarks, and observables include non-zero spacial momentum. It is also likely that many of the observables measured in the finite temperature/chemical potential studies would not be dominated by low modes. We will address this issue in a future study.

*1 Brookhaven National Laboratory, USA
*2 RIKEN-BNL Research Center, USA
* We thank RIKEN, Brookhaven National Laboratory, and the US DOE. This work is partly supported by KAKENHI Nos. 23105714, 23105715, and 22540301.
a) We have developed and implemented a code for implicitly restarting Lanczos algorithm which involves polynomial acceleration, *eigen spectrum shift*, and *compression/decompression* for eigenvectors of the 4D even/odd preconditioned DWF Dirac operators.

References

1) L. Giusti, P. Hernandez, M. Laine, P. Weisz and H. Wittig: JHEP **0404**, 013 (2004) [hep-lat/0402002].

Matching of ΔS = 1 four-quark operators in RI/SMOM schemes†

C. Lehner*1

[electroweak decays, non-perturbative renormalization]

The study of physical processes which change the strangeness by one unit ($\Delta S = 1$), such as the decay of a kaon into two pions, is important for the understanding of CP violation within the Standard Model (SM) and its possible extensions. Such processes can be used to measure the parameter of direct CP violation ϵ'/ϵ, to study the $\Delta I = 1/2$ rule, and to calculate long-distance contributions to $K_0 - \overline{K}_0$ mixing and the parameter of indirect CP violation ϵ. The weak interaction which mediates these processes can be described by local four-fermion operators at low energy scales. Matrix elements which describe, e.g., two-pion decays of kaons can then be computed with the help of lattice simulations.

In order to perform the renormalization of relevant operators in the lattice computation one can adopt a regularization-independent (RI) renormalization scheme[2)], which allows for the non-perturbative renormalization of lattice operators and the subsequent matching to continuum schemes such as $\overline{\mathrm{MS}}$. Such schemes are defined by subtraction at a specific momentum point (RI/MOM schemes). The original implementation of this method uses an exceptional momentum configuration, where unwanted infrared effects exist and some matching factors exhibit a poor convergence behavior. For these reasons a non-exceptional momentum configuration was proposed in Ref.[3)] and the framework and concepts of new RI/SMOM schemes with a symmetric subtraction point were worked out in Ref.[4)] for the case of bilinear operators and in Ref.[5)] for $\Delta S = 2$ four-quark operators. In Ref.[1)] new RI/SMOM schemes were introduced for the complete SM basis of $\Delta S = 1$ four-quark operators.

Compared to the $\Delta S = 2$ operator basis, the definition of such schemes for the $\Delta S = 1$ operator basis is complicated by the mixing of two-quark operators such as

$$G_1 = \frac{4}{ig^2}\bar{s}\gamma_\nu(1-\gamma_5)[D_\mu,[D^\mu,D^\nu]]d \qquad (1)$$

with four-quark operators such as

$$Q_1 = [\bar{s}_a\gamma_\mu(1-\gamma_5)u_b][\bar{u}_b\gamma^\mu(1-\gamma_5)d_a]\,, \qquad (2)$$

where u, d, s are up, down, and strange quark fields with color indices a and b. For this reason a subtraction point for two-quark operators is provided in addition to the subtraction point for four-quark operators; both are depicted in Fig. 1. The RI/SMOM schemes use the symmetric subtraction point defined by $p_1^2 = p_2^2 = q^2 = -\mu_s^2$, $q = p_1 - p_2$, where μ_s is the subtraction scale.

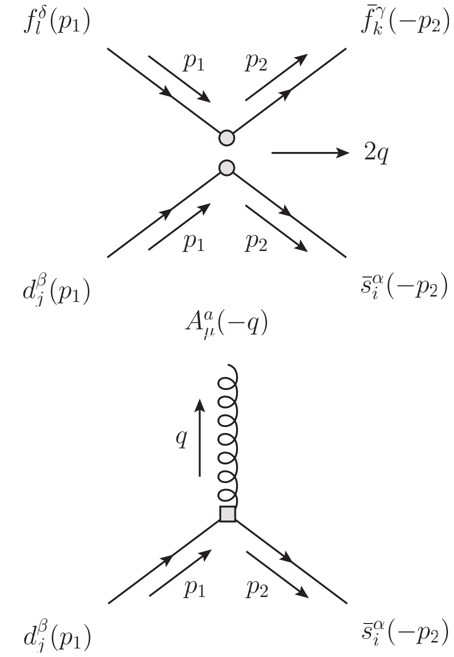

Fig. 1. Four-quark (top) and two-quark (bottom) momentum configuration. Taken from Ref.[1)].

In Ref.[1)] one-loop matching factors for the complete SM operator basis were provided. The results have since been used in Refs.[6,7)] for the non-perturbative renormalization of kaon matrix elements. The authors of Ref.[1)] are currently extending the presented calculation to include active charm quarks, which should allow for a reduction of systematic errors associated with lattice QCD calculations of weak decays.

† Condensed from Ref.[1)]

*1 RIKEN/BNL Research Center, Brookhaven National Laboratory, Upton, NY-11973, USA

References

1) C. Lehner and C. Sturm, Phys.Rev. **D84** (2011) 014001.
2) G. Martinelli, C. Pittori, C. T. Sachrajda, M. Testa and A. Vladikas, Nucl.Phys. **B445** (1995) 81–108.
3) Y. Aoki, P. Boyle, N. Christ, C. Dawson, M. Donnellan *et al.*, Phys.Rev. **D78** (2008) 054510.
4) C. Sturm *et al.*, Phys. Rev. **D80** (2009) 014501.
5) Y. Aoki, R. Arthur, T. Blum, P. Boyle, D. Brommel *et al.*, Phys.Rev. **D84** (2011) 014503.
6) T. Blum, P. Boyle, N. Christ, N. Garron, E. Goode *et al.*, Phys.Rev. **D84** (2011) 114503.
7) T. Blum, P. Boyle, N. Christ, N. Garron, E. Goode *et al.*

The chiral heat effect

T. Kimura[*1,*2] and T. Nishioka[*3]

Recent studies of the chiral anomaly reveal that new types of conductivities are induced in the presence of background fields.[1)] The chiral magnetic effect (CME) is the phenomenon such that an electric current can be parallel to the applied magnetic field provided the asymmetry of the chirality exists between left- and right-handed fermions.

In this paper, we consider a (3+1)-dimensional fermionic theory with the chiral symmetry on a curved space. We let the axial current conserved, but general non-covariant to introduce the chiral chemical potential. The calculation of the stress tensor shows that the heat current flows transverse to a gradient of the temperature which can be encoded to the off-diagonal components of the background metric. We call this new phenomenon a "Chiral Heat Effect" (CHE) that can happen even on a flat space with a thermal gradient. This is a natural counterpart of the CME and a generalization of the surface thermal Hall effect in (2 + 1) dimensions.

Consider a (3+1)-dimensional fermionic theory such as QCD on a curved spacetime. Suppose the Lagrangian enjoys the chiral symmetry at the classical level, but it is broken at the quantum level due to the chiral anomaly. If the theory consists of a massless Dirac fermion, the axial current j^5_μ obeys

$$\nabla_\mu j^{5\mu} = -\frac{1}{756\pi^2}\epsilon^{\mu\nu\rho\sigma}R^{\kappa}{}_{\lambda\mu\nu}R^{\kappa}{}_{\lambda\rho\sigma}. \tag{1}$$

Now we would like to define a conserved axial current to introduce the chiral chemical potential μ_5 even on a curved space. This is achieved by adding the following functional to the original action:

$$\begin{aligned} S &= S_0[\psi,\bar\psi,\mu_5] \\ &+ \frac{1}{3\cdot 2^8\pi^2}\int d^4x\ \sqrt{-g}\theta(t,x)\epsilon^{\mu\nu\rho\sigma}R^{\kappa}{}_{\lambda\mu\nu}R^{\kappa}{}_{\lambda\rho\sigma}, \end{aligned}\tag{2}$$

where $S_0[\psi,\bar\psi,\mu_5]$ is the action for the fermions with the chiral chemical potential, which is introduced as the temporal component of the axial background gauge field, and the total action is invariant under the chiral transformation.[2)] Such an additive contribution is just required for the consistency. Thus this effect is a generic result for CP broken systems. This type of the action is topological (a first Pontryagin class) when the function θ is constant, and the stress-energy tensor is zero. It is, however, no longer topological in general and the stress tensor is given by $T^{\mu\nu} = -\frac{2}{\sqrt{-g}}\frac{\delta S}{\delta g_{\mu\nu}}$:[3)]

$$\begin{aligned} T^{\mu\nu} &= \frac{1}{3\cdot 2^6\pi^2}\Big[2\theta_{;\rho}\left(\epsilon^{\mu\nu\sigma\kappa}R^{\nu}{}_{\sigma;\kappa}+\epsilon^{\nu\rho\sigma\kappa}R^{\mu}{}_{\sigma;\kappa}\right) \\ &+\theta_{;\sigma\rho}\left(\epsilon^{\mu\rho\kappa\lambda}R^{\sigma\nu}{}_{\kappa\lambda}+\epsilon^{\nu\rho\kappa\lambda}R^{\sigma\mu}{}_{\kappa\lambda}\right)\Big], \end{aligned}\tag{3}$$

where $;\kappa$ stands for the covariant derivative with respect to the index κ. In this case, the stress tensor is not conserved

$$\nabla_\mu T^{\mu\nu} = -\frac{1}{3\cdot 2^8\pi^2}\partial^\nu\theta\epsilon^{\kappa\lambda\rho\sigma}R^{\alpha}{}_{\beta\kappa\lambda}R^{\beta}{}_{\alpha\rho\sigma}, \tag{4}$$

unless the θ is constant or the Pontryagin density is zero. In the following discussions, we will consider the situations where the θ is not constant but the Pontryagin density vanishes, so general covariance is not broken.

When the background is flat space, the thermal gradient along j direction gives rise to the fluctuation of the metric $\delta g_{tj} = e^{-i\omega t}\delta g_{tj}(\vec{x})$, and the equation (3) leads the thermal current transverse to the j coordinate

$$\langle J^T_i\rangle = \frac{-i\omega}{3\cdot 2^6\pi^2}\epsilon_{ijk}\partial_j\theta\partial_k^2\delta g_{tk}(x), \tag{5}$$

where we suppress $e^{-i\omega t}$ for simplicity, and let i, j, k be the space coordinates. In this paper we consider the case with zero chemical potential $\mu = 0$, thus the thermal current is equivalent to the energy current. Then, the dependence of θ on the space coorinates gives rise to the thermal Hall effect.

Other interesting situation happens in the presence of a time-dependent θ. If a gradient of the temperature depends on x and y coordinates, one can convert it into the fluctuation of the metric components δg_{tx} and δg_{ty}. Then a heat current is induced by the thermal distribution in the perpendicular plane:

$$\begin{aligned} \langle J^T_i\rangle &= -\frac{1}{3\cdot 2^7\pi^2}\partial_t\theta\Big[\partial_y^3\delta g_{tx}(x,y)-\partial_x\partial_y^2\delta g_{ty}(x,y) \\ &+\partial_x^2\partial_y\delta g_{tx}(x,y)-\partial_x^3\delta g_{ty}(x,y)\Big]. \end{aligned}\tag{6}$$

The time-dependence of θ is related as $\theta = \mu_5 t$ with the chiral chemical potential μ_5 as discussed in the context of the chiral magnetic effect. We would like to call the above the "Chiral Heat Effect" (CHE) with emphasis on the similarity to the CME. The CHE can happen even on a flat space with a thermal gradient in the presence of the time-dependent theta angle or the chiral chemical potential.

References

1) K. Fukushima, D. E. Kharzeev and H. J. Warringa, Phys. Rev. **D78** (2008) 074033.
2) V. A. Rubakov, arXiv:1005.1888 [hep-ph].
3) R. Jackiw and S.-Y. Pi, Phys. Rev. **D68** (2003) 104012.

*1 Department of Basic Science, University of Tokyo
*2 Mathematical Physics Laboratory, RIKEN Nishina Center
*3 Department of Physics, Princeton University, USA

Rapid thermalization by baryon injection in gauge/gravity duality†

K. Hashimoto,*1 N. Iizuka,*2 and T. Oka,*3

[Heavy ion collisions]

Using the AdS/CFT correspondence for strongly coupled gauge theories, we calculate thermalization of mesons caused by a time-dependent change of a baryon number chemical potential. On the gravity side, the thermalization corresponds to a horizon formation on the probe flavor brane in the AdS throat. Since heavy ion collisions are locally approximated by a sudden change of the baryon number chemical potential, we discuss implication of our results to RHIC and LHC experiments, to find a rough estimate of rather rapid thermalization time-scale $t_{\mathrm{th}} < 1\,[\mathrm{fm/c}]$. We also discuss universality of our analysis against varying gauge theories.

The AdS/CFT correspondence[1)], or more broadly, the gauge/gravity duality, is an extremely useful tool to study strongly coupled field theories. Recently, this correspondence has been applied to various field theory settings, and these applications open up many new correspondences between gravity to other branches of physics. Perhaps one of the most surprising things in the success of using gravity to study strongly coupled gauge theories is that it seems to work even for an explanation of heavy-ion collision experiment data at Brookhaven's Relativistic Heavy Ion Collider (RHIC). In RHIC experiments, one of the big surprises was that a quark-gluon plasma (QGP) forms at a very early stage[2)] just after the heavy ion collision, *i.e.* a rapid thermalization occurs. This obviously requires a theoretical explanation, but remains as a challenge, because this requires a calculation of the strongly coupled field theory in non-equilibrium process. In this letter, we study the thermalization in strongly coupled field theories by using the gauge/gravity duality.

The key idea is to approximate the heavy ion collision by a sudden change of a baryon-number chemical potential locally at the collision point. Using the AdS/CFT correspondence, we obtain strongly coupled gauge theory calculations for the thermalization, where a time-dependent confinement/deconfinement transition occurs due to a sudden change of the baryon-number chemical potential, with dynamical degrees of freedom changing from mesons to quark/gluon thermal plasma. We calculate a time-scale for that. Our strategy can be summarized briefly as follows; On the gravity side of the AdS/CFT correspondence, the change in the baryon chemical potential is encoded in how we throw in the baryonically-charged fundamental strings (F-strings) from the boundary to the bulk. Since the F-string endpoint is a source term for the gauge fields on the flavor brane in the AdS bulk, this provides a time-dependent gauge field configuration. This induces a time-dependent effective metric for the degrees of freedom on the flavor brane, which are mesons. As a result, this yields the emergence of an apparent horizon on the flavor brane, which signals, in the dual strongly coupled field theory, the "thermalization of mesons", which we mean that the meson degrees of freedom change into quark and gluon degrees of freedom with thermal equilibrium.

In our framework, the only input is the function which represents how we throw in the baryonically charged F-strings. Therefore, we have small number of parameters, which includes a typical maximum value of the baryon density and the time-scale for changing the chemical potential. With collision parameters at RHIC, we obtain the thermalization time-scale as $t_{\mathrm{th}} < 1$ [fm/c]. Actually this time-scale can be well compared with the known hydrodynamic simulation requirement $t_{\mathrm{th}} < 2$ [fm/c] discussed previously. We also "predict" that heavy-ion collisions at CERN's Large Hadron Collider (LHC) exhibit slightly smaller order of the time-scale for thermalization as $t_{\mathrm{th}} < \mathcal{O}\,(0.1)$ [fm/c].

After solving the equations in the gravity side with a generic time-dependent baryon chemical potential, we compute the apparent horizon and the time-scale for the thermalization. The simplest example offered is $\mathcal{N} = 4$ super Yang-Mills with $\mathcal{N} = 2$ hypermultiplets as "quarks". The computed thermalization time-scale in our formulation is

$$t_{\mathrm{th}} \sim \min_{\{k=0,1,2\}} \left\{ \left(\frac{\lambda}{n_{\mathrm{B}}^2 w^k} \right)^{1/(6+k)} \right\} . \tag{1}$$

Here λ is the QCD 'tHooft coupling constant, w is the typical frequency to change the nuclear density, and n_{B} is the standard nuclear density.

References
1) J. M. Maldacena, Adv. Theor. Math. Phys. **2**, 231 (1998) [Int. J. Theor. Phys. **38**, 1113 (1999)] [arXiv:hep-th/9711200].
2) U. W. Heinz, AIP Conf. Proc. **739**, 163 (2004) [arXiv:nucl-th/0407067].

† Condensed from the article in Phys. Rev. **D86**, 066005 (2011)
*1 Mathematical Physics Laboratory, RIKEN Nishina Center
*2 theory division, CERN
*3 Department of Physics, the University of Tokyo

Multibrane solutions in open string field theory

M. Murata[*1] and M. Schnabl[*2]

[String theory, D-bane, multiple D-brane solution]

We study the properties of a class of solutions of open string field theory, that depend on a single holomorphic function F(z). We show that the energy of these solutions is well defined and given by integer multiples of a single D-brane tension. Potential anomalies are discussed in detail. Some of them can be avoided by imposing suitable regularity conditions on F(z), while the anomaly in the equation of motion seems to require an introduction of the so called phantom term.

One of the hallmark features of open bosonic string field theory[1)] is the existence of a tachyon vacuum state around which there are no perturbative excitations. The perturbative vacuum may describe any consistent D-brane configuration, depending on the choice of boundary conformal field theory (BCFT). As explained by Sen[2)], open bosonic string field theory (OSFT) built upon an arbitrary BCFT always possesses another vacuum that corresponds to a state with no D-branes and hence no open string dynamics. Many solutions have been constructed subsequent to the study of Sen, both numerically or analytically. Some of these solutions describe lower-dimensional D-brane configurations. From the viewpoint of string field theory around the tachyon vacuum, these solutions correspond to various D-branes popping out of the vacuum; however, all solutions found so far have energies lesser than that of the original D-brane. On the one hand this might not appear so surprising as one expects the tachyon condensation to drive the D-brane system to a state with smaller energy. On the other hand, since the final no-D-brane vacuum state is believed to be unique and since string field theory formulated around this vacuum does have solutions with positive energy, it is clear that the apparent impossibility to go higher in the energy is akin to the insuficiency of a particular coordinate system to describe the whole geometry.

Thus a question is, how big is the space of string fields formulated around a given reference BCFT and do solutions with positive energy with respect to the perturbative vacuum exist? This issue has been partially numerically studied in the past by Taylor, Ellwood, and the second author, using level truncation method; however, no conclusive evidence for the existence of such solutions was found. An analytic solution was proposed by Ellwood and the second author, but attempts to compute its energy in level truncation yielded a number that was off by roughly a factor of minus twelve. In this study, we investigate a class of universal solutions of the OSFT equations of motion in the form

$$\Psi = Fc\frac{K}{1-F^2}BcF\,. \tag{1}$$

Here $F = F(K)$, and K, B, and c are well-known string fields. All these solutions are universal, in the sense that their form does not depend on the details of the BCFT.

It turns out that the appropriate conditions can be more conveniently stated in terms of a complex function, which is given by

$$G(z) = 1 - F(z)^2\,. \tag{2}$$

We can easily evaluate the action, and we find for the energy $E = \frac{1}{6}\langle\Psi, Q_B\rangle$ of the solution

$$E = \frac{1}{2\pi^2}\oint\frac{dz}{2\pi i}\frac{G'(z)}{G(z)}\,, \tag{3}$$

where the closed contour C encircles all singularities and branch cuts in the Re $z<0$ half plane. However the contour does not encircle the origin.

One notable example of a family of functions obeying the stronger conditions is

$$G_n(z) = \left(\frac{z}{z+1}\right)^n\,, \tag{4}$$

for which the energy computed either way is

$$E = -\frac{n}{2\pi^2}\,. \tag{5}$$

For $n=1$, this solution represents the tachyon vacuum solution[3)], while for $n=0$, the solution corresponds to the perturbative vacuum $\Psi=0$. Negative values of n indicate states with energies higher than that of the perturbative vacuum. In fact, we conjecture that they indicate configurations of multiple D-branes. Positive values of n would describe "ghost" branes, objects with negative tension. Such objects are not expected to arise in bosonic string, and we showed that they are indeed divergent in the Fock state expansion.

*1 Mathematical Physics Lab., RIKEN Nishina Center
*2 Institute of Physics AS CR, Na Slovance 2, Prague 8, Czech Republic

References
1) E. Witten, Nucl. Phys. B **268** (1986) 253.
2) A. Sen, JHEP **9912** (1999) 027 [arXiv:hep-th/9911116].
3) M. Schnabl, Adv. Theor. Math. Phys. **10** (2006) 433 [arXiv:hep-th/0511286].

β-ensembles for toric orbifold partition function†

T. Kimura[*1,*2]

The instanton counting is extensively applied to various non-perturbative aspects of the four dimensional gauge theory. In particular Nekrasov partition function[1)] plays an essential role in not only the four dimensional Seiberg-Witten theory, but also the two dimensional conformal field theory. The remarkable connection between the four and two dimensional theories through the instanton partition function is called AGT relation.[2)]

In this paper we develop the previous result,[3)] and consider a systematic method to deal with the combinatorial representation of the partition function for the generic four dimensional toric orbifolds $\mathbb{C}^2/\Gamma_{r,s}$, whose boundary is the generic lens space $L(r,s)$. It includes the A_{r-1}-type ALE space as $\mathbb{C}^2/\Gamma_{r,r-1} = \mathbb{C}^2/\mathbb{Z}_r$. The generic four dimensional toric space is given by the quotient $\mathbb{C}^2/\Gamma_{r,s}$ where $\Gamma_{r,s}$ is a $\mathbb{Z}_r$ action labeled by the two coprime integers (r,s) with $0 < s < r$ as $\Gamma_{r,s}$: $(z_1, z_2) \to (\omega_r z_1, \omega_r^s z_2)$ where $\omega_r = \exp(2\pi i/r)$ is the primitive r-th root of unity. Although this orbifold action generates asingularity at the origin of $\mathbb{C}^2$, we can obtain the smooth manifold by resolving the singularity, which is called the Hirzebruch-Jung space.

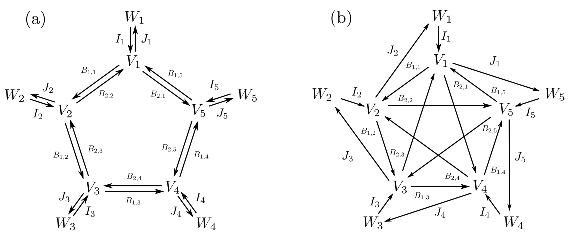

Fig. 1. Quiver diagrams for orbifolding ADHM data: (a) $\mathbb{C}^2/\Gamma_{5,4}$ (the ALE space $\mathbb{C}^2/\mathbb{Z}_5$) and (b) $\mathbb{C}^2/\Gamma_{5,3}$.

We can obtain the orbifold partition function by performing the orbifold projection for the standard one. When we consider the ADHM construction to investigate the instanton moduli space for the toric orbifold, various kinds of quiver structures are appearing as shown in Fig. 1. However it is apparently written in a complicated form, we will show a much simpler method to assign the orbifold projection. To implement that we first lift it up to the q-deformed theory, and then take the root of unity limit of it, as well as the standard orbifold $\mathbb{C}^2/\mathbb{Z}_r$ discussed,[3)]

$$q \longrightarrow \omega_r q, \qquad t \longrightarrow \omega_r^{\bar{s}} q^{\beta}, \tag{1}$$

where $\bar{s} = r - s$. These are related to the Ω-background parameters and the radius of S^1 for the five dimensional theory $\mathbb{R}^4 \times S^1$, $q = e^{R\epsilon_2}$ and $t = e^{-R\epsilon_1}$.

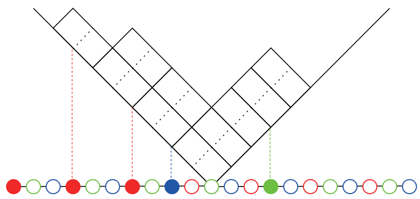

Fig. 2. Decomposition of the partition $\lambda = (5,2,2,1)$ for $\mathbb{C}^2/\Gamma_{3,1}$. A rectangular box is required for obtaining the correspondence between the partition and the particle description with the repulsion parameter $\bar{s} = r - s$.

To obtain the matrix model description, it is natural to decompose the partition as shown in Fig. 2, which corresponds to the irreducible representations of the orbifold action $\Gamma_{r,s}$. In this case, this decomposition is performed with the basis of the one-dimensional particles obeying the generalized fractional exclusive statistics.[4)]

Taking the limit (1), we finally obtain the following matrix measure from the q-deformed Vandermonde determinant,

$$\begin{aligned}\Delta^2(x) &= \prod_{v=0}^{r-1}\prod_{i<j}^{N}\left(x_i^{(v)} - x_j^{(v)}\right)^{2(\beta-\bar{s})/r+2\bar{s}} \\ &\times \prod_{v<w}^{k-1}\prod_{i,j}^{N}\left(x_i^{(v)} - x_j^{(w)}\right)^{2(\beta-\bar{s})/r+2N_{\bar{s}}(v-w)}\end{aligned} \tag{2}$$

where we define $N_{\bar{s}}(x) = \#\{k | x + k \equiv 0 \pmod r), k = 0, \cdots, r-1\}$. Similarly the matrix potential is given by the certain limit of the quantum dilogarithm function,

$$V(x) = \frac{2}{r}\sum_{l=1}^{n}\left[(x-a_l)\log\left(\frac{x-a_l}{\Lambda}\right) - (x-a_l)\right], \tag{3}$$

where a_l is just the Coulomb moduli. Therefore we obtain the following matrix model partition function,

$$Z = \int \prod_{v=0}^{r-1}\prod_{i=1}^{N} dx_i^{(v)} \Delta^2(x) e^{-\frac{1}{\epsilon_2}\sum_{v,i} V(x_i^{(v)})}. \tag{4}$$

The large N limit analysis would extract the gauge theory consequences for the toric orbifold theory.

References

1) N. Nekrasov, Adv. Theor. Math. Phys. 7 (2004) 831–864.
2) L. F. Alday, D. Gaiotto and Y. Tachikawa, Lett. Math. Phys. **91** (2010) 167–197.
3) T. Kimura, JHEP **09** (2011) 015.
4) F. D. M. Haldane, Phys. Rev. Lett. **67** (1991) 937–940.

† Condensed from the article in Prog.Theor.Phys.**127**(2012)271.
*1 Department of Basic Science, University of Tokyo
*2 Mathematical Physics Laboratory, RIKEN Nishina Center

Vortices on orbifolds†

T. Kimura[*1,*2] and M. Nitta[*3]

Vortices, especially in Abelian gauge theory, are essential degrees of freedom in superconductors under the magnetic fields while they also provide a model of strings in relativistic field theories. Other than the flat space $\mathbb{R}^2 \simeq \mathbb{C}$, studies of non-Abelian vortices have been so far restricted to those on regular spaces, such as a cylinder, a torus, Riemann surfaces, and hyperbolic surfaces. In this paper we consider Abelian and non-Abelian vortices on two dimensional singular spaces, namely the orbifolds $\mathbb{C}/\mathbb{Z}_n$.

An orbifold $\mathbb{C}/\mathbb{Z}_n$ is constructed by identifying $z \sim \omega z$, where z is a coordinate of the covering space $\mathbb{C}$ and $\omega = \exp(2\pi i/n)$ is the primitive n-th root of unity. Under this identification the Higgs and gauge field should be transformed as $H(\omega z, \overline{\omega z}) = \Omega H(z,\bar{z})$, $A_z(\omega z, \overline{\omega z}) = \Omega A_z(z,\bar{z})\Omega^{-1}$ where the orbifold transformation matrix Ω, satisfying $\Omega^n = \mathbb{1}$, can be diagonalized without loss of generality due to the gauge symmetry. This implies that (the global part of) the original gauge group $\mathrm{U}(N)$ is broken by the boundary condition, and thus becomes a quiver gauge group, $\prod_m \mathrm{U}(N^{(m)})$.

To investigate the BPS equation in the non-Abelian Higgs model

$$(D_1 + iD_2)H = 0, \quad F_{12} + \frac{g^2}{2}(c\mathbb{1}_N - HH^\dagger) = 0,(1)$$

we now introduce the moduli matrix approach.[1,2] The first equations can be solved as $H(z,\bar{z}) = S^{-1}(z,\bar{z})H_0(z)$, $A_z = A_1 + iA_2 = S^{-1}(z,\bar{z})\partial_z S(z,\bar{z})$, where the holomorphic matrix $H_0(z)$ is called the moduli matrix. It behaves as

$$H_0(\omega z) = \Omega H_0(z), \tag{2}$$

since we have $\Omega H = \Omega S^{-1}(\Omega^{-1}\Omega)H_0$. Note that this construction is invariant under $(H_0(z), S(z,\bar{z})) \to (V(z)H_0(z), V(z)S(z,\bar{z}))$ for $V(z) \in \mathrm{GL}(N,\mathbb{C})$. All we have to do is to find solutions for the moduli matrix to satisfy the condition (2).

In the Abelian case we provide the moduli matrix for generic vortex number $k = ln + m \equiv m \pmod n$,

$$H_{0;n}(z) = z^m \prod_{i=1}^{l}(z^n - z_i^n) = z^m \prod_{i=1}^{l}\prod_{p=0}^{n-1}(z - \omega^p z_i),(3)$$

satisfying the boundary condition $H_0(\omega z) = \omega^m H_0(z)$. Therefore the moduli space for Abelian vortices on the orbifold is given by

$$\mathcal{M}_{N=1,k;n} = (\mathbb{C}/\mathbb{Z}_n)^{[k/n]}/\mathfrak{S}_{[k/n]}, \tag{4}$$

where $[x]$ denotes the floor function, giving the largest integer not greater than x. Similarly we can discuss the non-Abelian theory. When we decompose the winding number as $\{k_i = l_i n + m_i\}_{i=1}^N$, the moduli matrix satisfies

$$\det H_{0;n}(z) = z^{m_1+\cdots+m_N} \prod_{i=1}^{l_1+\cdots+l_N}(z^n - z_i^n). \tag{5}$$

We then investigate collision dynamics of vortices on orbifolds by studying their moduli spaces.[3] For the Abelian vortices with $k = n$ we rewrite the moduli matrix as $H_{0;n}(z,t) = z^n - \xi^n t = \prod_{m=0}^{n-1}(z - \omega\xi t^{1/n})$. After changing $t \to -t$ we have $H_{0;n}(z,-t) = z^n + \xi^n t = \prod_{m=0}^{n-1}(z - \omega e^{\pi i/n}\xi t^{1/n})$. Here we have an extra factor $e^{\pi i/n}$. This means that vortices are colliding at $t = 0$ at the origin with a scattering angle $\theta = \pi/n$. Fig. 1 shows collision of Abelian vortices on the orbifolds $\mathbb{C}/\mathbb{Z}_2$ and $\mathbb{C}/\mathbb{Z}_3$.

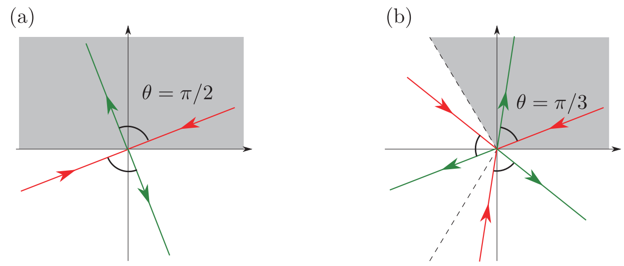

Fig. 1. Collision of vortices on the orbifold (a) $\mathbb{C}/\mathbb{Z}_2$ with $\theta = \pi/2$ and (b) $\mathbb{C}/\mathbb{Z}_3$ with $\theta = \pi/3$. For $\mathbb{Z}_n$ with an odd n, vortices just look passing through the origin of the universal covering space $\mathbb{C}$.

We then discuss the Kähler quotient description of the moduli space,[4] which is given by

$$[B, B^\dagger] + II^\dagger = c\mathbb{1}_k. \tag{6}$$

Here we have $B \in \mathrm{Hom}(V,V)$, $I \in \mathrm{Hom}(V,W)$ for two vector spaces V and W. The winding number and the rank of the gauge group are given by their dimensions, $\dim V = k$ and $\dim W = N$. After decomposing them into irreducible representations of $\mathbb{Z}_n$, the quotient (6) is also decomposed as

$$B_{m-1}B_{m-1}^\dagger - B_m^\dagger B_m + I_m I_m^\dagger = c\mathbb{1}_{k^{(m)}}, \tag{7}$$

for $m = 0, \cdots, n-1$.

References

1) M. Eto *et al*, Phys. Rev. Lett. **96** (2006) 161601.
2) M. Eto *et al*, J. Phys. **A39** (2006) R315–R392.
3) M. Eto *et al*, Phys. Rev. Lett. **98** (2007) 091602.
4) A. Hanany and D. Tong, JHEP **07** (2003) 037.

† Condensed from the article in JHEP **09** (2011) 118

*1 Department of Basic Science, University of Tokyo
*2 Mathematical Physics Lab., RIKEN Nishina Center
*3 Department of Physics, and Research and Education Center for Natural Sciences, Keio University

Novel criticality in matrix models through resonant tunneling

T. Tada

[matrix model, string theory, tunneling]

The tunneling phenomenon is the most salient feature of quantum physics that sometimes appears to be very peculiar even in the eyes of a physicist. One example is the resonant tunneling phenomenon[1]. Consider one-dimensional quantum mechanics with the potential shown in Fig. 1. With the aid of the

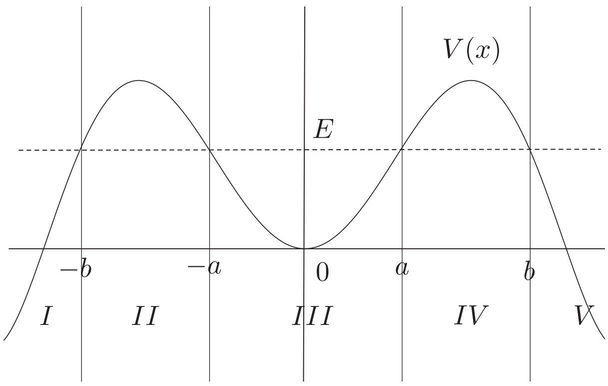

Fig. 1. Potential $V(x)$ and five regions

WKB (Wentzel-Kramers-Brillouin) method, it is fairly straightforward to calculate the transmission coefficient T from region III ($-a \leq x \leq a$) to region V ($a \leq x$) is:

$$T_{III\to V} = \frac{4}{(2\theta + \frac{1}{2\theta})^2}, \theta = \exp(\int_a^b dx\sqrt{2(V-E)}). \quad (1)$$

Here, we set the mass of the particle and $\hbar$ to unity. The transmission coefficient shows that the transmission is suppressed exponentially. The WKB method also allows one to calculate the transmission coefficient from region I ($x \leq -b$) to all the way to region V as follows:

$$T_{I\to V} = \frac{4}{(2\theta + \frac{1}{2\theta})^2 \cos^2 J/2 + 4\sin^2 J/2}, \quad (2)$$

where $J = 2\int_{-a}^{a} dx\sqrt{2(E-V)}$. At first glance, Eq. (2) appears to show exponential suppression again; however, if we set

$$J = 2\pi(n + \frac{1}{2}), \qquad \text{where } n \text{ is an integer}, \quad (3)$$

the transmission coefficient $T_{I\to V}$ becomes exactly one and tunneling transmission through the potential barrier in region II and IV is greatly enhanced. This phenomenon is called resonant tunneling.

The seminal paper of Brezin *et al.*[2] includes an analysis of a set of N^2 coupled one-dimensional anharmonic oscillators, whose variables are arranged in an $N \times N$ Hermitian matrix M. The Hamiltonian in question now looks like

$$H = -\frac{1}{2}\Sigma_{i,j}\frac{\partial^2}{\partial M_{ij}^2} + \mathrm{Tr}V(M), \quad (4)$$

where V can be any potential. For the sake of definiteness, here, we take $V(x) = \frac{1}{2}x^2 + \frac{g}{N}x^4$. Then, owing to its invariance under the unitary transformation $M \to U^\dagger M U$, the above-mentioned system of anharmonic oscillators transforms into N one-dimensional fermion systems with the one-body Hamiltonian

$$h = -\frac{1}{2}\frac{\partial^2}{\partial x^2} + V(x). \quad (5)$$

The ground state is the state where the energy levels are occupied up to the Fermi level ϵ_F with N fermions. This system exhibits critical behavior when ϵ_F exceeds the maximum of V. The behavior is observed at $g_c = -\frac{\sqrt{2}}{3\pi}$. This is the critical point that corresponds to the $c = 1$ non-critical string theory[3].

We believe that if the two above-mentioned topics, resonant tunneling and critical phenomena in $c = 1$ matrix models are "amalgamated", there emerges an interesting possibility[4]. The criticality of $c = 1$ matrix models occurs because of the the degrees of freedom being sufficient for overcoming the potential barrier. When the Fermi level is lower than the nearest peak of the potential, the system is supposed to lie in a stable vacuum. However, if there is another peak beyond the nearest peak and a condition similar to the resonant condition Eq. (3) is met, some of the fermions near the Fermi level may tunnel through the potential barrier. Thus, the system makes a leap and it will cause a certain criticality. We argue that this criticality may correspond to first-order transition since the mechanism of this criticality can accommodate latent heat straightforwardly.

In summary, we have pointed out that there is a new critical phenomenon in matrix quantum mechanics. This phenomenon may shed light on the non-perturbative aspects of string theory.

References

1) See for example; David Bohm, "Quantum Theory," Dover Publications (1989).
2) E. Brezin, C. Itzykson, G. Parisi and J. B. Zuber, Commun. Math. Phys. **59**, 35 (1978).
3) V. A. Kazakov and A. A. Migdal, Nucl. Phys. B **311**, 171 (1988).
4) T. Tada, "Matrix model criticality and resonant tunneling, " RIKEN-TH-207.

Matrix model from $\mathcal{N} = 2$ orbifold partition function†

T. Kimura[*1,*2]

The recent progress on the four dimensional $\mathcal{N} = 2$ supersymmetric gauge theory reveals a remarkable relation to the two dimensional conformal field theory.[1)] This relation provides the explicit interpretation for the partition function of the four dimensional gauge theory[2)] as the conformal block of the two dimensional Liouville field theory, and is naturally regarded as a consequence of the M-brane compactifications.

Now we would like to extend this connection between the two and four dimensional theory to the orbifold theory, $\mathbb{C}^2/\mathbb{Z}_k$. It is shown that the orbifold projection for the gauge theory partition function is naturally performed when one appropriately parametrizes the partition function. This parametrization is just interpreted as the root of unity limit $q \to \omega \equiv \exp(2\pi i/k)$ of the q-deformed partition function while we have to take $q \to 1$ for the usual $\mathbb{R}^4$ space.

Starting with the combinatorial representation and extracting its asymptotic behavior, we derive a new kind of matrix models, and discuss the corresponding gauge theory consequences. We then consider the large N limit of this matrix model, and show Seiberg-Witten curve is arising from the spectral curve of the matrix model.

The partition function for SU(n) gauge theory is represented with n-tuple partition, which can be also expressed by Young diagrams. When we consider its orbifold generalization, it is natural to perform further decomposition as shown in Fig. 1. As a result, we then obtain a multi-matrix model from the combinatorial expression of the partition function by taking its asymptotic limit. The matrix measure part is deeply related to the root of unity limit of the q-Vandermonde determinant,

$$\Delta^2(x) = \prod_{r=0}^{k-1}\prod_{i<j}^{N}(x_i^{(r)} - x_j^{(r)})^{2+2(\beta-1)/k} \times \prod_{r<s}^{k-1}\prod_{i,j}^{N}(x_i^{(r)} - x_j^{(s)})^{2(\beta-1)/k} \tag{1}$$

where β is related to the Ω-background parameters as $\beta = -\epsilon_1/\epsilon_2$.

The matrix potential part is similarty given by the root of unity limit of the quantum dilogarithm function $g(z;q) = \prod_{p=1}^{\infty}\left(1 - \frac{1}{z}q^p\right)$. Parametrizing $q \to \omega e^{\epsilon_2}$, we obtain

$$\log g(z;\omega e^{\epsilon_2}) = \frac{1}{\epsilon_2}\left[\frac{1}{k^2}\mathrm{Li}_2\left(\frac{1}{z^k}\right) + \mathcal{O}(\epsilon_2)\right], \tag{2}$$

† Condensed from the article in JHEP **09** (2011) 015.

*1 Department of Basic Science, University of Tokyo

*2 Mathematical Physics Laboratory, RIKEN Nishina Center

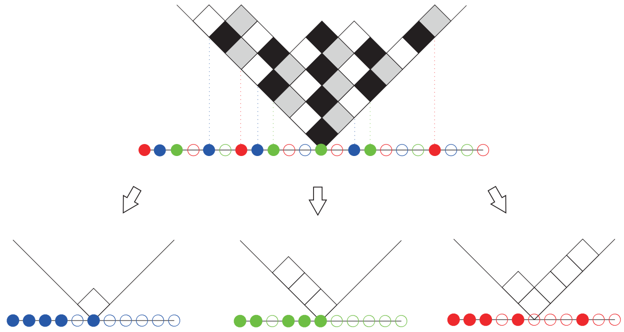

Fig. 1. The decomposition of the partition for $k = 3$.

where $\mathrm{Li}_n(z) = \sum_{p=1}^{\infty}\frac{z^p}{p^n}$ is the n-th polylogarithm function. By restoring the dynamical scale parameter, the matrix potential for the four dimensional theory yields

$$V(x) = \frac{2}{k}\sum_{l=1}^{n}\left[(x-a_l)\log\left(\frac{x-a_l}{\Lambda}\right) - (x-a_l)\right], \tag{3}$$

where a_l is identified with the Coulomb moduli. Then we obtain the matrix model partition function describing the gauge theory on the orbifold,

$$Z = \int \prod_{r=0}^{k-1}\prod_{i=1}^{N} dx_i^{(r)}\Delta^2(x)e^{-\frac{1}{\epsilon_2}\sum_{r,i}V(x_i^{(r)})}. \tag{4}$$

Note that this multi-matrix model is decoupled when we consider the case $\beta = 1$, which is the most desirable situation.

This matrix model is investigated in the 't Hooft limit $N \to \infty$, $\epsilon_2 \to 0$ with $\epsilon_2 N$ being finite. Due to the equation of motion, we obtain the following analytic function (an n-th monic polynomial),

$$P_n(z) = \Lambda^n\left(e^{ky/2} + e^{-ky/2}\right) \equiv \Lambda_n\left(w^k + \frac{1}{w^k}\right) \tag{5}$$

where $y(z) = V'(z) - 2\omega(z)$ is the spectral curve of this matrix model, and $\omega(z)$ is the resolvent. We conclude that this is just the Seiberg-Witten curve for $\mathcal{N} = 2$ Yang-Mills theory on the orbifold $\mathbb{C}^2/\mathbb{Z}_k$. It is also shown that the Seiberg-Witten differential is given by the spectral curve of the matrix model,

$$dS = \frac{1}{2\pi i}z\frac{dw}{w} = \frac{1}{4\pi i}y(z)dz. \tag{6}$$

References

1) L. F. Alday, D. Gaiotto and Y. Tachikawa, Lett. Math. Phys. **91** (2010) 167.
2) N. Nekrasov, Adv. Theor. Math. Phys. **7** (2004) 831.

Spinless basis for spin-singlet FQH states

T. Kimura[*1,*2]

Recently the multi-component quantum Hall state has been featured not only by theorists, but also experimentalists. It is because it would well describe systems with pseudo-spin degrees of freedom, e.g. the multi-layer system, graphene, spinor BEC, etc, which can be realized in a laboratory due to the remarkablre progress on the experimental technology. For such a system, it is natural to consider an invariant state under spin rotation, namely the spin-singlet state.

The trial wavefunction for the multi-component fractional quantum Hall state (FQH state), which is called the Halperin state, is given by

$$\Phi_{\mathrm{H}} = \prod_{i<j}^{N_\uparrow}(z_i - z_j)^m \prod_{i<j}^{N_\downarrow}(w_i - w_j)^m \prod_{i,j}^{N^{\uparrow,\downarrow}}(z_i - w_j)^n . \quad (1)$$

Here z_i and w_i stand for posisions of $\uparrow$ and $\downarrow$ spin particles, respectively. Taking into account the spin-singlet condition, we have to assign the Fock condition for this state,

$$\sum_{j=1}^{N_\uparrow}(1 \mp e(w_i, z_j))\Phi_{\mathrm{H}} = 0, \quad (2)$$

where the operator $e(i,j)$ exchanges w_i and z_j. The sign factor takes *minus* for fermionic and *plus* for bosonic systems. Thus we obtain the condition $m = n+1$. We now extend this condition to arbitrary M-component systems. Although the original Halperin state is just for a two component state, a simple generalization of the Halperin state (1) is also given by

$$\Phi_{\mathrm{H}}^M(\{z_i^{(u)}\}) = \prod_{u=1}^{M}\prod_{i<j}^{N^{(u)}}(z_i^{(u)} - z_j^{(u)})^m \times \prod_{u<v}^{M}\prod_{i,j}^{N^{(u,v)}}(z_i^{(u)} - z_j^{(v)})^n . \quad (3)$$

Again we have to consider the Fock condition (2) to obtain the singlet state. In this case the following condition is required for all the pairs of (v, w),

$$\sum_j (1 \mp e(z_i^{(u)}, z_j^{(v)}))\Phi_{\mathrm{H}}^M(\{z_i^{(u)}\}) = 0. \quad (4)$$

Therefore the singlet condition yields $m = n+1$ as well as the case $M = 2$.

We then show the singlet state (3) is obtained from the corresponding one-component state with the q-Vandermonde determinant,

$$\Delta_{q,t}(z) = \prod_{i<j}\frac{(z_i/z_j;q)_\infty}{(tz_i/z_j;q)_\infty}, \quad (5)$$

where $(z;q)_\infty = \prod_{m=0}^{\infty}(1 - zq^m)$ is the q-Pochhammer symbol. Taking $q \to 1$ with $t = q^r$, we have

$$\Delta_{q,t}(z) \longrightarrow \prod_{i<j}\left(1 - \frac{z_i}{z_j}\right)^r \sim \prod_{i<j}(z_i - z_j)^r . \quad (6)$$

The singular behavior of this function is equivalent to that of the Laughlin state. In other words, they are equivalent in the sense of operator product expansion (OPE). Indeed we obtain the Laughlin state wavefunction by including the zero mode contribution.

The multi-component state is obtained by implementing the Yangian Gelfand-Zetlin basis, which is well investigated for the spin Calogero-Sutherland model.[2] Parametrizing $(q,t) \to (\omega_M q, \omega_M q^r)$ and taking $q \to 1$, we obtain $\Delta_{q,t}(z) \to \prod_{u=1}^M \prod_{I<J}(1 - z_I^{(u)}/z_J^{(u)})(1 - (z_I^{(u)}/z_J^{(u)})^M)^{(r-1)/M} \prod_{u<v}^M \prod_{I,J}(1 - \omega_M^u z_I^{(u)}/\omega_M^v z_J^{(v)})(1 - (z_I^{(u)}/z_J^{(v)})^M)^{(r-1)/M}$, where each particle coordinate is re-defined as $z_i = \omega_M^u z_I^{(u)}$, such that $z_I^{(u)}$ is in the fundamental region of the orbifold $\mathbb{C}/\mathbb{Z}_M$, namely $0 \le \arg(z_I^{(u)}) \le 2\pi/M$. Here $\omega_M = \exp(2\pi i/M)$ is the primitive M-th root of unity. This is not a spin-singlet FQH state yet, but its singular part yields

$$\Delta_{q,t}(z) \sim \prod_{u=1}^{M}\prod_{I<J}\left(z_I^{(u)} - z_J^{(u)}\right)^{(r-1)/M+1} \times \prod_{u<v}^{M}\prod_{I,J}\left(z_I^{(u)} - z_J^{(v)}\right)^{(r-1)/M} . \quad (7)$$

This is just equivalent to the singlet Halperin state (3) because the powers satisfy the singlet condition $(m,n) = ((r-1)/M+1, (r-1)/M)$. This reduction suggests the equivalence between the single-component FQH state obeying (k,r)-admissible condition and the M-component $(k,\tilde{r})$-state where they are related as

$$\tilde{r} = \frac{r-1}{M} + 1. \quad (8)$$

The filling fraction of the $(k,\tilde{r},M)$-state is given by

$$\nu = \frac{kM}{M(\tilde{r}-1)+1} = \frac{kM}{r}. \quad (9)$$

This is obtained from the one-component filling fraction by multiplying a factor M.

*1 Department of Basic Science, University of Tokyo
*2 Mathematical Physics Laboratory, RIKEN Nishina Center

References
1) B. I. Halperin, Helv. Phys. Acta **56** (1983) 75.
2) D. Uglov, Commun. Math. Phys. **193** (1998) 663.

6. Astrophysics

Experimental study of key astrophysical ^{18}Ne(α,p)^{21}Na reaction

L.Y. Zhang,[*1*2*3] J.J. He,[*1] S.W. Xu,[*1] H.Yamaguchi,[*4] S. Kubono,[*4] Y.Wakabayashi,[*5] S.Z. Chen,[*1*2] J. Hu,[*1*4] P. Ma,[*1] Y. Togano,[*6] T. Hashimoto,[*4] D. Kahl,[*4] T. Teranishi,[*7] R.F. Chen,[*1] H.W. Wang,[*8] W.D. Tian,[*8] B. Guo,[*9] S. Hayakawa,[*4] N. Iwasa,[*10] T. Yamada,[*10] T. Komatsubara,[*11]

[Nuclear astrophysics, thick target, resonate reaction]

A nuclear astrophysics experiment was performed at CRIB (CNS low-energy Radioactive-Ion Beam separator) on Mar. 2011. The goal of this experiment was to study the rate of the ^{18}Ne(α,p)^{21}Na reaction, which might be a key breakout reaction from the hot CNO cycle to the *rp*-process in X-ray burst and nova. Yet, the reaction rate is not well understood.

Explosive hydrogen burning is thought to be the main source of energy generation and a source of nucleosynthesis in X-ray burst and nova[1,2]. In X-ray burst, for example, at the typical temperature of 0.4-2 GK, the hydrogen burning occurs in the hot CNO cycle:

$$^{12}\mathrm{C}(p,\gamma)^{13}\mathrm{N}(p,\gamma)^{14}\mathrm{O}(e^{+}\nu)^{14}\mathrm{N}(p,\gamma)^{15}\mathrm{O}(e^{+}\nu)^{15}\mathrm{N}(p,\alpha)^{12}\mathrm{C},$$

while the ^{13}N(e^{+} ν)^{13}C reaction in the CNO cycle is bypassed by the ^{13}N(p, γ)^{14}O reaction. With the progress of compressing and exothermic nuclear reactions, the temperature of the accretion disk increases. When the temperature reaches about 0.4 GK, the second hot CNO cycle becomes dominant:

$$^{12}\mathrm{C}(p,\gamma)^{13}\mathrm{N}(p,\gamma)^{14}\mathrm{O}(\alpha,p)^{17}\mathrm{F}(p,\gamma)^{18}\mathrm{Ne}(e^{+}\nu)^{18}\mathrm{F}(p,\alpha)$$
$$^{15}\mathrm{O}(e^{+}\nu)^{15}\mathrm{N}(p,\alpha)^{12}\mathrm{C}.$$

It is predicted[1,2] that the ^{18}Ne waiting point in the second hot CNO cycle can be bypassed by the ^{18}Ne(α,p)^{21}Na reaction at T ~ 0.6 GK, and subsequently, the reaction chain breaks out to the *rp*-process. Hence it is very important to study this reaction rate.

An 89 MeV ^{21}Na radioactive beam produced by CRIB bombarded a 90-μm-thick polyethylene target, and the cross section data for ^{18}Ne(α,p)^{21}Na could be obtained indirectly by measuring those for the time-reversal reaction of ^{21}Na(p,α)^{18}Ne. The ^{21}Na beam intensity was about 2 × 10^{5} pps, with a purity of about 70% on the CH_2 target.

In this study, we mainly focused on the 8.51 and 8.61 MeV resonate states in the compound ^{22}Mg nucleus. In a previous similar experiment[3], we tentatively made new spin-parity assignments for these states. This new experiment can confirm the assignments with much better statistics. The resonant properties (such as J^{π}, Γ_{α}, and Γ_{p}) of the compound ^{22}Mg nucleus were studied by measuring the ^{21}Na+p resonant elastic/inelastic scattering cross sections. As shown in Fig. 1, we used two PPACs for monitoring beam counts and directions and three sets of ΔE-E silicon telescopes for measuring the energies and scattering angles of the recoiled particles. A NaI array was surrounded for detecting the γ -rays. Several runs with a carbon target were performed for C background subtraction.

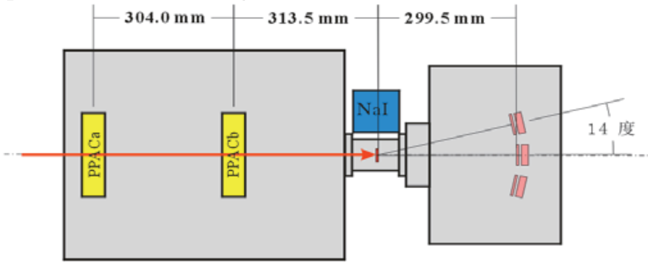

Fig. 1. Schematic view of the detector setup.

In addition, we measured the cross section of the time-reversal reaction ^{21}Na(p,α)^{18}Ne simultaneously. Thus, the forward ^{18}Ne(α,p)^{21}Na cross section could be calculated by using the detailed balance theorem.

Fig. 2 shows a typical particle identification plot. ΔE and E signals are measured by the silicon telescopes; TOF is the time of flight between PPACb and ΔE. The E-TOF method mainly identifies the low-energy particles stopped in the ΔE detector. Further data analysis is on-going.

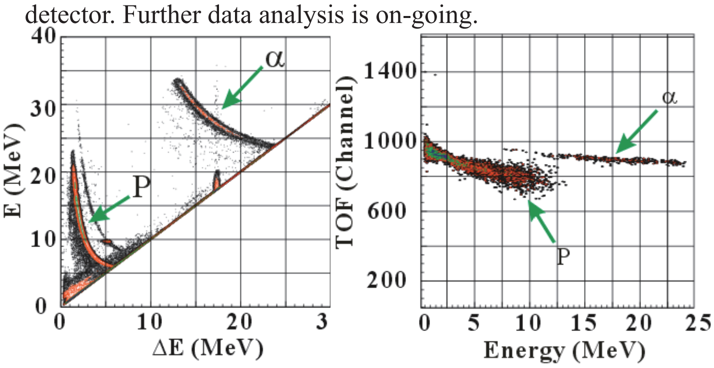

Fig. 2. PID of ΔE-E and E-TOF. The start TOF signal is given by PPACa, and the stop signal is given by PSD.

*1 Institute of Modern Physics, CAS, Lanzhou, China
*2 Graduate University of CAS, Beijing, China
*3 Lanzhou University, Lanzhou, China
*4 Center for Nuclear Study (CNS), University of Tokyo, Japan
*5 Advanced Science Research Center, JAEA, Japan
*6 RIKEN, 2-1 Hirosawa, Wako, Saitama 351-0198, Japan
*7 Department of Physics, University of Kyushu, Japan
*8 Shanghai Institute of Applied Physics, CAS, China
*9 China Institute of Atomic Energy (CIAE), Beijing, China
*10 Department of Physics, University of Tohoku, Japan
*11 Department of Physics, University of Tsukuba, Japan

References

1) A. E. Champage and M. Wiescher, Annu. Rev. Nucl. Part. Sci. 42 (1992) 39.
2) M. Wiescher, et al., J. Phys. G: Nucl. Part. Phys. 25 (1999) R133.
3) J. J. He, et al., Phys. Rev. C 80 (2009) 015801.

7. Accelerator

Deployment of RILAC2 for RIBF experiment

K. Yamada, M. Fujimaki, N. Fukunishi, Y. Higurashi, E. Ikezawa, M. Kase, M. Komiyama, K. Kumagai, T. Maie, T. Nakagawa, J. Ohnishi, H. Okuno, N. Sakamoto, K. Suda, T. Watanabe, Y. Watanabe, and O. Kamigaito

A new linac injector for the RIBF, called RILAC2, was successfully commissioned in 2011. As reported in Ref. 1, the first beam acceleration in RILAC2 was achieved on December 21, 2010, and several studies involving RILAC2 with/without post-accelerators were performed by using xenon and uranium beams in order to increase the transmission efficiency and beam intensity of the RIBF and to test the charge strippers.

Following the studies, the vacuum pumping system on the beam transport line between RILAC2 and the RRC was improved since the vacuum level of the beam line, around 10^{-5} Pa, had been found to be insufficient for the uranium beam. As shown in Fig. 1, beam loss caused by charge exchange reactions was about 10% for the uranium beam in each section between bending magnets. A 220 L/s turbo molecular pump was attached to each chamber placed at C20, C21, C22, and S23 in the beam line. Consequently, the ultimate pressure improved to around 10^{-6} Pa in the section between B7-REB and S23, as seen in Table 1, and the beam loss in the section was suppressed. In the near future, additional pumps will be mounted on S31 and S41, which are in the S3-REB section.

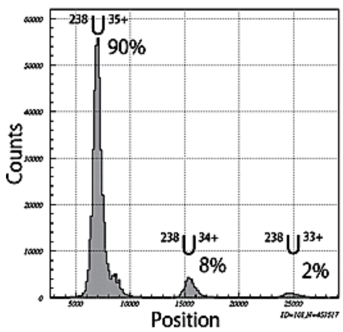

Fig. 1. Charge exchange reaction involving residual gas in the S3-REB section.

The remote control UI for the rf system and vacuum pumps of the RFQ were modified and integrated with the UI of the DTLs by using the FA-Server[2)] and InTouch[3)] in order to shift their rf phases simultaneously. However, there was a specific difference between their phases because of the individual specificities of the auto-phase-control modules.

RILAC2 successfully started supplying uranium beams for the RIBF experiment from October 2011. The rf stability of the RILAC2 resonators during a day is shown in Fig. 2. The upper panel shows the rf voltage stability and the lower panel shows the rf phase stability. The target values are shown by yellow lines in the figure (±0.1% for the voltage, ±0.1° for the phase). The stability of RILAC2 is sufficient to attain the target values. Moreover, the break time in the experiment resulting from the downtime of RILAC2 was less than 0.3% of the total scheduled beam time. The maximum intensity of the uranium beam extracted from the SRC had increased to 330 enA, which is five times higher than that in the previous experiment performed in 2009. A xenon beam with a 13.5 pnA intensity was also used in the RIBF experiment in December 2011.

Owing to the increase in the beam intensity supplied by the ECRIS, beams with a much higher intensity are expected to be accelerated by RILAC2 and in the RIBF accelerator complex.

Table 1. Main vacuum pumps and typical vacuum levels from RILAC2 to the RRC.

Location	Type	Gross pumping speed	Quantity	Vacuum
B12	CRP	750 L/s (N_2)	1	3×10^{-6} Pa
RFQ	CRP	2400 L/s (N_2)	2	5×10^{-6} Pa
B2-REB	CRP	750 L/s (N_2)	1	9×10^{-6} Pa
	TMP	220 L/s (N_2)	1	
DTL1	CRP	2400 L/s (N_2)	1	4×10^{-6} Pa
DTL2	CRP	2400 L/s (N_2)	1	4×10^{-6} Pa
DTL3	CRP	4000 L/s (N_2)	1	4×10^{-6} Pa
B50	TMP	350 L/s (N_2)	1	2×10^{-6} Pa
B61	CRP	750 L/s (N_2)	1	
B7-REB	TMP	1100 L/s (N_2)	1	6×10^{-6} Pa
C20	TMP	220 L/s (N_2)	1	7×10^{-6} Pa
C21	TMP	220 L/s (N_2)	1	8×10^{-7} Pa
C22	TMP	220 L/s (N_2)	1	2×10^{-6} Pa
S23	TMP	220 L/s (N_2)	1	7×10^{-6} Pa
S3-REB	TMP	500 L/s (N_2)	1	3×10^{-5} Pa
S6-REB	TMP	820 L/s (N_2)	1	9×10^{-6} Pa
S64b	TMP	220 L/s (N_2)	1	6×10^{-6} Pa
S71	TMP	220 L/s (N_2)	1	3×10^{-6} Pa

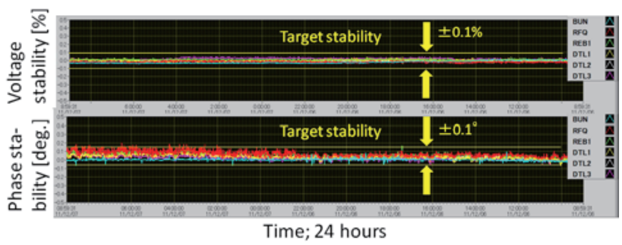

Fig. 2. RF voltage stability and rf phase stability of RILAC2 resonators.

References
1) K. Yamada et al., RIKEN Accel. Prog. Rep. **44**, vii (2011).
2) OPC server software, Roboticsware, FA-Server 4.
3) HMI software for SCADA, Wonderware, InTouch 9.5.

Production of a highly charged uranium ion beam with RIKEN superconducting electron cyclotron resonance ion source†

Y. Higurashi, J. Ohnishi, T. Nakagawa, H. Haba, M. Tamura[*1], T. Aihara[*1], M. Fujimaki, M. Komiyama, A. Uchiyama[*1], and O. Kamigaito

[ECR, uranium, ion source]

Ever since the first heavy-ion beam was obtained at the RIKEN Radioisotope Beam Factory (RIBF) project in 2007 [1)], we have been trying to increase the ion species and the intensity of the ion beams. In 2008, we produced a U^{35+} ion beam using the RIKEN 18 GHz electron cyclotron resonance (ECR) ion source[2)]. The ion beam was accelerated in the accelerator complex of the RIKEN RIBF up to an energy of 345 MeV/u. Even with a weak beam intensity (about 0.4 pnA on the target), we observed the production of more than 40 new isotopes by in-flight fission reactions in only four days of experiments [3)]. This shows that an intense U beam is a strong tool for producing very neutron rich nuclei and for studying the r-process ob nucleosynthesis. Using the RIKEN 18 GHz ECR ion source, we produced a U^{35+} ion beam with an intensity of only 2–4 eμA, which was much lower than the required beam intensity for the RIKEN RIBF. To increase the beam intensity, we constructed a new SC-ECR ion source with an optimum magnetic field strength for 28 GHz, which can produce both classical B_{min} and flat B_{min} [4,5)]. In the autumn of 2009, we obtained the first U^{35+} beam from the RIKEN SC-ECRIS using 18 GHz microwaves. In the spring of 2011, we injected a 28 GHz microwave from a gyrotron into the ion source and produced a highly charged U ion beam. Several test experiments on the production of a U ion beam have been performed.

In this article, we report the results of test experiments on the production of highly charged U ion beams using 18 and 28 GHz microwaves.

Figure 1 shows a photograph of the RF injection side. To produce a U ion beam, we used the sputtering method. As shown in Fig. 1, the U metal was installed on an off-center axis and was supported by a supporting rod. The position of the rod was remotely controlled to within an error of about 0.5 mm. The support rod was water-cooled to reduce the possibility of occurrence of a chemical reaction between the U and the holder material at high temperatures. The rod position and voltage for sputtering were optimized in order to maximize the intensity of highly charged U ion beams.

Figure 2 shows the U^{35+} ion beam intensity as a function of the RF power. Open and closed circles represent the results for 18 and 28 GHz microwave operation, respectively. the values of B_{inj}, B_{min}, B_{ext}, and B_r were 2.3,

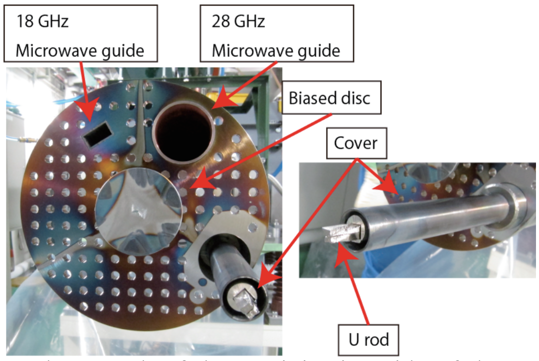

Fig. 1. Photograph of the RF injection side of the RIKEN SC-ECR ion source and the movable rod system used in the sputtering method.

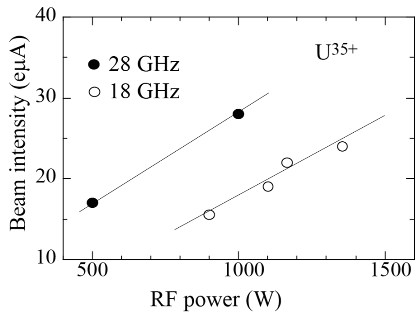

Fig. 2. U^{35+} ion beam intensity as a function of the RF power.

0.5, 1.2, and 1.2 T, respectively for 18 GHz operation. In the case of the 28 GHz operation, B_{inj}, B_{ext}, B_r, and B_{min} were 3.15, 0.62, 1.83, and 1.86 T, respectively.

It appears that the beam intensity produced with the 28 GHz microwaves is always higher than that produced with the 18 GHz microwaves.

We obtained highly charged U ion beams (35+–27+) with an intensity of 0.7–2 pμA from the RIKEN SC-ECRIS by using the sputtering method. It appears that for higher RF powers, we may obtain higher beam intensities, since the beam intensity was not saturated in the test experiments. In the near future, we plan to use a high-temperature oven to produce U vapor for increasing the beam intensity.

References

1)Y. Yano, Nucl. Instrum. Methods B261 (2007) 1009
2)Y. Higurashi et al., Rev. Sci. Instrum 79 (2008) 02C714
3)T. Ohnishi et al., J. Phys. Soc. Jap. 79 (2010) 073201
4)T. Nakagawa et al., Rev. Sci. Instrum. 81 (2010) 02A320
5) G. D. Alton, and D. N. Smithe, Rev. Sci. Instrum. 65(1994)775

† Condensed from a contributed paper published as part of the Proceedings of the 14th International Conference on Ion Source, Giardini-Naxos, Sicily, Italy, September, 2011.

*1 SHI Accelerator Service Ltd.

28-GHz gyrotron for superconducting ECR ion source

J. Ohnishi, Y. Higurashi, and T. Nakagawa

The newly developed 28-GHz superconducting ion source uses a gyrotron microwave source. Figure 1 shows the schematic drawing of this gyrotron. Electron beams produced from a magnetron-type electron gun are injected into an open resonator along solenoid fields, so that they produce 28-GHz microwaves by electron cyclotron resonance in the cavity. The maximum acceleration voltage and current of the electron beams are 22 kV and 1.6 A, respectively. The maximum output power of the microwaves is 10 kW. The gyrotron uses cathode and filament power supplies and two dc power supplies for the solenoid coils, as shown in Fig. 1. The cathode power supply uses a high-voltage transducer and a rectification circuit immersed in a 1000-L oil vessel. Because of the large amount of oil used, we needed to report its storage conditions to the Wako City fire house. Figure 2 shows a drawing of the microwave transmission line. The gyrotron produces TE_{02}-mode microwaves, which are converted into the TE_{01} mode by a mode converter and a mode filter and then transmitted to the ion source. Diode detectors attached to directional couplers are used for the measurement of the forward and reflected powers. The output voltages in the diode detectors have been calibrated to the power obtained from the temperature increase in the cooling water of a dummy load.

The first test on the gyrotron was performed at RIKEN in September 2010 using a dummy load. The ripples in the output power from the gyrotron were as large as approximately 10%, making stable operation in the low-power region (< 1 kW) difficult. The large ripples were due to the ripples (1%) in the cathode voltage. To reduce the voltage ripples, we increased the capacitance of the output regulation circuit tenfold by adding four 7.5-μF paper capacitors with a maximum rated voltage of 37.5 kV. As a result, the ripples in the cathode voltage and those in the microwave power were reduced to approximately one-tenth of the original level. After the power supply modification, the microwave transmitted line was assembled, and the first beam was successfully extracted from the ion source in the 28-GHz operation using the gyrotron, in April 2011. The performance of the ion source is reported in reference 1.

The ECR ion source with the 28-GHz gyrotron was operated from October to December 2011 in order to supply uranium and xenon beams to the RIBF experiments. Figure 3 shows the voltage change in the detector diode attached to the directional coupler, for three days of the machine time. The fluctuation in the diode voltage corresponds to that in the microwave power from 800 W to 1 kW. This fluctuation seems to be correlated with the temperature of the room in which the power supplies are housed, as shown in the figure. We investigated this phenomenon intensively because any

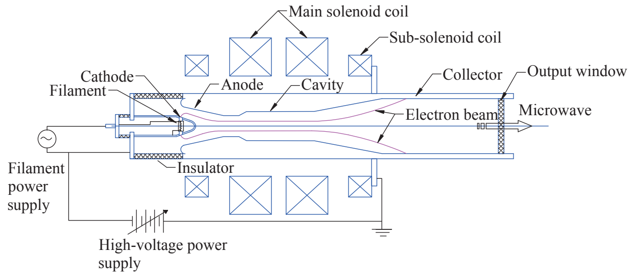

Fig. 1. Schematic drawing of the 28-GHz gyrotron.

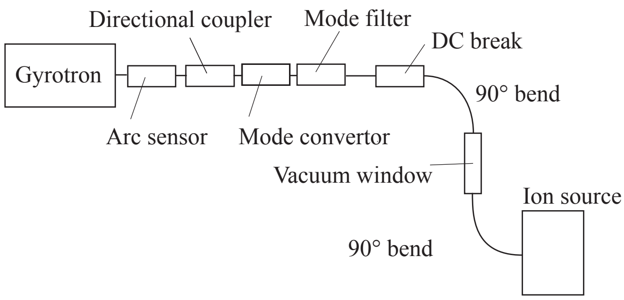

Fig. 2. Microwave transmission line.

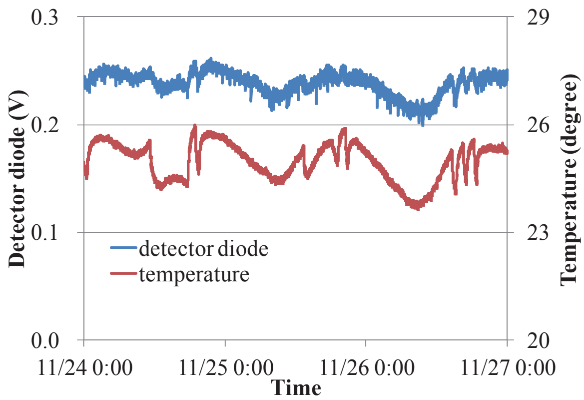

Fig. 3. Diode voltage reflecting the microwave power and room temperature for three days during the uranium machine time.

fluctuation in the microwave power would influence the beam currents. Finally, we found that the microwave power is very sensitive to the current in the main solenoid coil and that the current changes slightly on order of the 1 x 10^{-4}/°C with the temperature of the room. In order to reduce this power fluctuation, we plan to replace the main solenoid power supply with a more stable one in February 2012.

References

1) Y. Higurashi et al.: In this report.

Laser ion source with a double pulse laser system†

*1M. Okamura, *1K. Kondo and *2T. Yamamoto

It has been difficult to obtain a relatively longer ion beam pulse length, using a laser ion source. However, if the laser system is operated in burst mode, a train of the ion beam pulses may be produced. To test the feasibility of this idea, a double pulse laser system was used.

The laser, QUANTEL Brilliant Twin, has two identical oscillators with Q-switches. The transverse polarization directions are perpendicular and the two laser paths are combined by a dielectric polarizing mirror. Each oscillator has its own timing system and can be operated independently. The laser energy, pulse width, and wave length are 850 mJ (maximum), 6 ns (FWHM), and 1064 nm, respectively. In the experiment, a pure iron target was used. The laser energy delivered to the target by each beam was 540 mJ and the laser spot was an ellipse of height 4.1 mm and width 5.2 mm. The estimated laser power density was 5.3 x 10^8 W/cm^2. A collimator of 10 mm diameter was placed before a Faraday cup. The suppression mesh of the cup was biased to -3.5 kV to distinguish ions from the expanded ablation laser plasma. Considering as being transparent the suppression mesh, the effective sensing area was estimated as 59 mm^2. The vacuum was maintained at around a few 10^{-4} Pa. The plasma drift length was 1.89 m.

We scanned the interval between the triggering of the two laser beams from 0.7 μs to 183.7 μs. Both laser beams were adjusted to have almost the same laser energy by changing the Q-switch timings.

Figure 1 shows a typical measured current with a long delay time. The second laser shot was triggered at 183.7 μs after the first shot. The red curve was obtained by superimposing the two individual currents given by each irradiation. The measured current shape exactly matched the superimposed current shape. Once ablation plasma is created, a cloud of neutral gas follows the plasma, since only a portion of the target material is ionized. The second ablation plasma mixed with the neutral gas cloud induced by the previous laser shot, and may recombine with electrons in the gas cloud. However, as shown in Fig.1, the anticipated recombination effect was not observed. When the delay time was above 30 μs, the superimposed currents agreed with the measured double-shot currents with good accuracy.

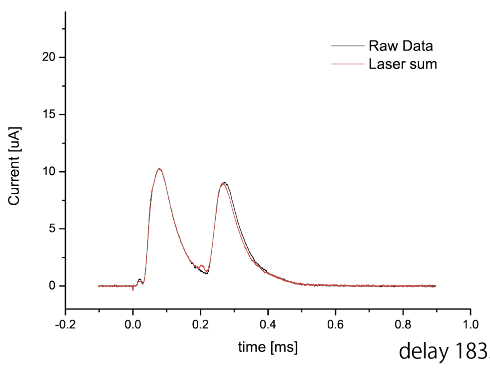

Fig. 1 Double ion pulses with 183.7 ms delay.

Between 10 μs and 30 μs, we observed a small bump at the tail of the main peak. Since the delay time is much smaller than the ion beam current pulse width, the overlapping double pulse was expected to appear as a single peak. Even though the total charge was conserved, the current shape was distorted.

Below 10 μs of delay time, a current reduction was observed and the current shape was distorted severely. The measured peak was split into two peaks, as shown in Fig. 2, which shows the measured current for the 3.7 μs of delay time case.

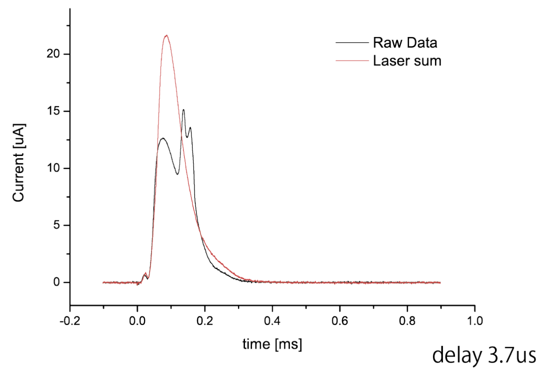

Fig. 2 Double ion pulses with a very short delay.

When we provide low charge state beams from a laser ion source, a typical ion beam pulse length is more than 100 μs[1,2 and 3]. In the present, this technique seems quite useful. We can probably increase the number of laser cavities to more than two if needed. However, if the interval between the two plasmas is less than 10 μs, some current reduction would be observed. More studies are needed to apply this method to high charge state mode operation, which typically provides less than 10 μs of ion beam pulse length.

References

1) M. Okamura, A. Pikin, V. Zajic, T. Kanesue, J. Tamura, Nuclear Instruments and Methods in Physics Research A 606 (2009) 94-96.
2) J. G Alessi, et al., Rev. Sci. Instrum. 81, 02A509 (2010)
3) K. Kondo, T. Kanesue, J. Tamura, M. Okamura, Rev. Sci. Instrum. 81, 02A511 (2010)

† Contributed paper published as part of the Proceedings of the 14th International Conference on Ion Source, Giardini-Naxos, Sicily, Italy, September, 2011.

* Author to whom correspondence should be addressed. Electronic mail: okamura@bnl.gov

Laser ion source with solenoid for Brookhaven National Laboratory-Electron Ion Beam Source†

K. Kondo,*1 T. Yamamoto,*2 M. Sekine, *3 and M. Okamura*1

[Laser ion sorce, Electron beam ion source, Relativistic heavy ion collider]

Laser Ion Source (LIS) is a primary ion source provider for Brookhaven National Laboratory-Electron Beam Ion Source (BNL-EBIS)[1]. LIS needs to fulfill the EBIS requirement of a low peak current of less than 100 μA with a sufficient total charge of 10 nC; however, the adiabatic expansion of the laser ablation plasma causes problems. In order to resolve them, a solenoid that can be expected to confine the plasma transversely is placed at the plasma drift section between the target and the extraction.

For the Nasa Space Radiation Laboratory (NSRL) science program of cosmic ray simulation, a Fe solid flat target was selected as the target. A Nd: YAG laser operating at 1064 nm with a 7 ns pulse length was used to irradiate the target. The estimated laser power density on the target is 7.9×10^8 W/cm^2, which can supply only singly charged ions according to a previous experiment[2]. Our experimental setup consists of two 1 m solenoids with an 11 cm gap between the two solenoids and is used to investigate know plasma behavior in a fringe field. The plasma current inside a solenoid is measured by a new small ion probe with a bias voltage of -100 V. The maximum magnetic field of the solenoid at the center position is 530 G. Figure 1 shows the magnetic distribution, which is normalized by the maximum magnetic field, as well as the working range of the ion probe.

The total charge at the center of the beam axis is shown in Figure 2. Each solid black point is plotted by averaging two data points with the same experimental condition. The red dotted line represents the scaling equation of $N \propto L^{-2}$, which is the expected behavior of the total charge without solenoids. Here, N is the particle number and L is the drift distance. The line crosses the measured value of the most upstream point $L = 93$ mm. All the plotted black points representing the experimental results lie above the expected behavior line of the total charge without solenoids. The charge decreases at the gap between the two solenoids, and the total charge increases again after this gap. At the end of the second solenoid, the total charge is 3 times as large as the charge expected without solenoids. At the center position of the beam axis, the relationship between the total charge and the radial distance from the target, which is 2 cm from the beam axis shows that every measured charge is larger than the charge expected without the solenoids. Moreover, the total charge increases around the fringe field region. At the end of the second solenoid, the total charge is more than five times the magnitude of the charge expected without solenoids in this off-axis condition.

The total charge with the drift distance is measured to be higher than that expected without solenoids because the magnetic field constrains the adiabatic expansion transversely. These results for the two different radial positions indicate that the plasma current around the center of beam axis decays by field divergence and that the current toward the outward region enhances because plasma from the beam center move to the outer region because of the fringe field.

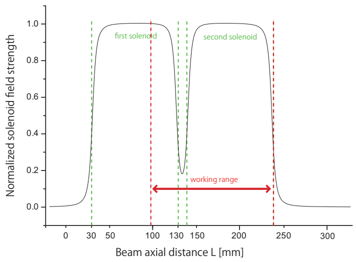

Fig. 1. Normalized magnetic field distribution and the working range of the ion probe.

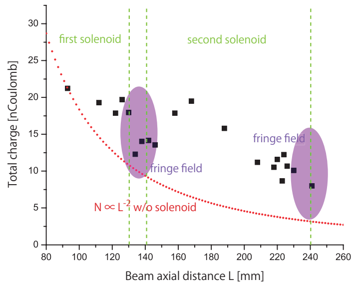

Fig. 2. Total charge vs. beam axial distance at the center of beam axis.

† Condensed from the article in the Proceedings of the 14th International Conference on Ion Source, Giardini-Naxos, Sicily, Italy.

*1 Collider-Accelerator Department, Brookhaven National Laboratory
*2 Cooperative Major in Nuclear Energy, Waseda University
*3 Department of Nuclear Engineering, Tokyo Institute of Technology

References
1) J. Alessi, *et al.,* Rev. Sci. Instrum. **81**, 02A509 (2010).
2) T. Kanesue, *et al.,* Proc. EPAC 08, 2008 p. 421.

Study of H+ production using metal hydride and other compounds by employing laser ion source†

M. Sekine, *1 K. Kondo,*2 M. Okamura*2 and N. Hayashizaki*3

[Laser ion source, proton, metal hydride]

A laser ion source (LIS) can provide a wide variety of highly charged ions with a simple scheme. A laser plasma is created by a pulsed power laser focused on the target surface, and ion beams are extracted from the expanded plasma. By replacing target materials, ion species can be easily changed. We have obtained many types of ions from various targets, including metals, solid compounds, and frozen noble gases except He. We found that in previous experiments also, it was difficult to create a proton beam from a frozen hydrogen target [1, 2]. This is because the sublimation temperature is close to the achievable temperature of a cryo-cooler head and to the temperature attained due to periodic laser exposure. Therefore, in this report, we tested solid materials containing hydrogen at room temperature.

Beeswax ($C_{15}H_{31}COOC_{31}H_{61}$), polyethylene, and metal hydride (MgH_2) were used as the targets. Beeswax and polyethylene are typical carbon hydride compounds. MgH_2 contains protons in its structure. All of them are stable at room temperature and in vacuum.

The target in the vacuum chamber was irradiated using a Nd:YAG laser with a wavelength of 1064 nm and pulse length of 6 ns. The laser light was focused by a convex lens (f = 3000 mm). The incident angle between the laser path and the beam line was 30 degrees. A Faraday cup (FC) with a 10 mm aperture was placed 4.1 m from the targets to measure the beam current. The suppressor voltage of FC was set to -3.5 kV. The plasma was analyzed by an electrostatic ion analyzer (EIA) and the selected ions were detected by a secondary electron multiplier (SEM). The total distance between the detector and target was 5.6 m. Ion species and charge states were determined from the time of flight (TOF) information in the SEM signal and the applied voltage applied to the EIA[3]. The vacuum was below 4×10^{-4} Pa. We used bulk samples of Beeswax and polyethylene. The metal hydrides are supplied as powders, and we prepared compressed targets in shells. The MgH_2 powders in the shells were compressed at a pressure of 39 kg/mm^2 for 5 min by employing an oil hydraulic press.

We determined the amount of hydrogen in these materials by a thermal analysis method[4]. The hydrogen contents of the Mg hydrides were found to correspond to $MgH_{1.78\pm0.02}$. This indicates that the hydrogen of 90% of the hydride did not transform to protons.

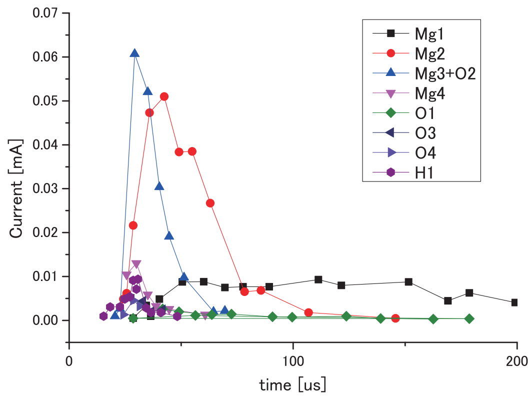

Fig. 1 Analyzed laser plasma of MgH_2 target at FC

Thus, irradiation of Beeswax and polyethylene did not produce plasmas. Laser energy was not concentrated on the surface layers of the target materials, since these targets are transparent to the wavelength of 1064 nm. On the other hand, metal hydrides absorb the laser beam to form ablation plasmas. The metal hydrides are suitable for creating proton beams. However, hydrogen in metal hydrides does not become protons with the expected efficiency. To understand the reason for the low proton production rate, more investigations are needed.

References

1) Jun Tamura, Masahiro Okamura, Proceedings of PAC07, TUPAN064 (2007)
2) J. Tamura, M. Okamura, T. Kanesue, S. Kondrashev. Ion generation from solidified Ne target for a laser ion source. Applied Physics Letters 91, 041504 (2007).
3) Takeshi Kanesue, Jun Tamura, Masahiro Okamura, REVIEW OF SCIENTIFIC INSTRUMENTS 79, 02B102 (2008).
4) J. Reilly and R. H. Wiswall, Reprinted from Inorganic Chemistry, 6, 2220(1967).

† Condensed from the article in the Proceedings of the 14th International Conference on Ion Source, Giardini-Naxos, Sicily, Italy.

*1 Department of Nuclear Engineering, Tokyo Institute of Technology
*2 Collider-Accelerator Department, Brookhaven National Laboratory
*3 Research Laboratory for Nuclear Reactors, Tokyo Institute of Technology

Charge state evolution of ^{238}U and ^{124}Xe beams injected at 50 MeV/u in extremely thick gases

H. Imao,H. Okuno,H. Kuboki,S. Yokouchi,N. Fukunishi,O. Kamigaito,H. Hasebe,T. Watanabe,A. Goto,M. Kase,and Y. Yano

[gas stripper, uranium ion, xenon ion]

The intensity of very heavy ion beam like Xe and U beams at the RIBF has steadily increased mainly because of improvements made to the new injector RILAC2 involving a 28-GHz superconducting ECR ion source. In recent high-intensity runs with Xe and U beams, the fragility of the conventional carbon foil strippers has become obvious, not only for the first thin stripper, but also for the second thick one placed between the two ring cyclotrons fRC and IRC. It is necessary to replace the second stripper every 5-6 h because of thickness degradation.

The use of charge stripping method involving the use of gases is a possible solution to resolve the problem of frequent replacement of the stripper owing to the non-destructive nature of the method. However, the charge state evolution in gas media at 50 MeV/u, which is the energy injected into the second stripper, has never been investigated because of the difficulty in preparing a thick windowless gas target. The thickness required to obtain the equilibrium charge state of the beams increases significantly at higher beam injection energies, e.g., the required thickness of N_2 for a ^{238}U beam at 50 MeV/u is more than 10 mg/cm^2, which is around 100 times the thickness required at 11 MeV/u. The second stripper also functions as an energy degrader to match the beam energy to the injection energy of the subsequent cyclotron IRC. Eventually, for Xe and U beams, the required thickness of the gas targets for the second stripper is more than 15 mg/cm^2.

In the present study, we developed a new charge stripping system that can confine the medium-Z gases, like N_2, with thickness up to 30 mg/cm^2 without using partition windows. The charge state evolution of ^{124}Xe and ^{238}U beams at 50 MeV/u in such extremely thick gases was investigated for the first time.

The new charge stripping system located in the E1 room has two huge differential pumping systems. The design concept of the present differential pumping systems is almost the same as that of a prototype used in the previous study[1]. The length of the new target is short, 50 cm, while the length of the one used in the previous study was 8 m.

In an experiment, $^{124}Xe^{46+}$ and $^{238}U^{71+}$ beams extracted from the fRC with an energy of 50 MeV/u were injected into the gas stripper. The charge distributions of the beams after the stripper were analyzed with the subsequent dipole magnet (DMM1) and the beam intensity was measured with the Faraday cup.

The average charge in the equilibrium state of ^{124}Xe beams at 50 MeV/u for N_2 gas was 51.9^+, which was sufficient for the second stripper. We also observed that the stripping performance of air was equivalent to that of N_2. The air stripper is advantageous since the problem of gas consumption (200 SLM) is not faced.

The average charge in the equilibrium state of ^{238}U beams for N_2 gas was 83.5^+, which was unexpectedly low compared to calculated values[2] and previous data for carbon. The measured charge state evolution of ^{238}U for N_2, He, and Ne is shown in Fig. 1. The fraction of 86^+, which is the required charge for the acceleration of ^{238}U in the subsequent cyclotrons, was only 8% for N_2. This value is significantly smaller than that for carbon ($\approx$ 30%). The nontrivial reduction of the charge for N_2 would indicate that the density of the target material affects the charge changing reactions even in this high energy region around 50 MeV/u[4].

In summary, the charge state evolution of ^{124}Xe and ^{238}U beams in various gases was studied at the injection energy of 50 MeV/u. The use of an air stripper for Xe beams at 50 MeV/u was successfully demonstrated. We also found that the effect of the target density on the reachable charge is not negligible. The use of a high molecular weight gas as a high-density target, e.g., hydrocarbon or fluorocarbon, is a possible way to obtain a higher charge state for ^{238}U.

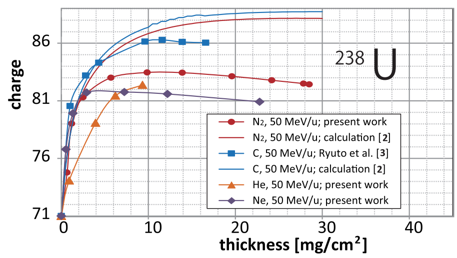

Fig. 1. Measured and calculated charge state evolution.

References
1) H. Imao *et al.*:RIKEN Acc. Prog. Req. **44**, (2011).
2) C. Scheidenberger *et al.*: Nucl. Inst. And Meth. **B142**, 441 (1998).
3) H. Ryuto *et al.*, to be published.
4) H. Kuboki *et al.*: Phys. Rev. ST Acc. Beams **13**, 093501 (2010).

Offline test of plasma window

H. Kuboki, H. Okuno, A. Hershcovitch,*1 T. Dantsuka, H. Hasebe, K. Ikegami, H. Imao, O. Kamigaito, M. Kase, T. Maie, T. Nakagawa, Y. Yano, and S. Yokouchi

A helium (He) gas stripper is one of the leading candidates as a charge stripper for high-intensity uranium beams at RIKEN RI Beam Factory (RIBF)[1]. The construction of a windowless He gas stripper utilizing a strong differential pumping system is now in progress[2,3]. The use of Plasma windows (PWs)[4] in the He gas stripper would afford a differential pumping system that is smaller than a conventional differential pumping system, especially in terms of length. PWs can be used for vacua separation, which they achieve on the basis of two phenomena: 1) High temperature arc plasma and gas (12000 K) can match pressure of the room temperature (300 K) gas with 1/40 the density. 2) The gas flow through a plasma at high temperature is greatly reduced with an increase in viscosity of a plasma.

A PW would be useful especially for the 2nd stripper at RIBF. The thickness required for uranium beams is 17 mg/cm^2, which can be realized by, for example, a 50-cm-long cell filled with He gas at a pressure of 1.8 atm. The current differential pumping system has afforded a He gas stripper of 9.3 mg/cm^2 thickness confined in a 50-cm-long chamber at a pressure of 1 atm using two big pumps with a pumping speed of 4200 m^3/h[3]. Extrapolation from the PW performance in Refs. 5 and 6 has shown the potential that He gas can be confined at up to 2.85 atm in a 30-cm-long gas cell with a 900 m^3/h pumping speed. However, since the PW already developed has a small bore of 2 mm in diameter for beam passing, we have to make a bore diameter as large as 6 mm for actual application to heavy ion beams. We study in advance the possibility of enlarging the bore size and evaluate the differential pumping performance.

An overview of a PW with a differential pumping system used for offline tests is shown in Fig. 1. A PW has three cathodes with tungsten tips, a cathode housing, five cooling plates, and an anode. All copper parts are made of 6N (99.9999%) oxygen-free copper and have channels inside for water cooling. The PW separated the atmosphere from the 1st chamber, which was connected to the 2nd chamber with a pipe having an inner diameter of 8 mm and a length of 10 cm. Both the 1st and 2nd chambers were evacuated by a scroll pump (SP) with a 51 m^3/h pumping speed.

Arc plasma was successfully ignited with Ar gas in September 2011, where the voltage and current were maintained as 90 V and 15 A during operation, respectively. In a series of offline tests, we found that 1) the insulator poly-ether-ether-ketone (PEEK) can

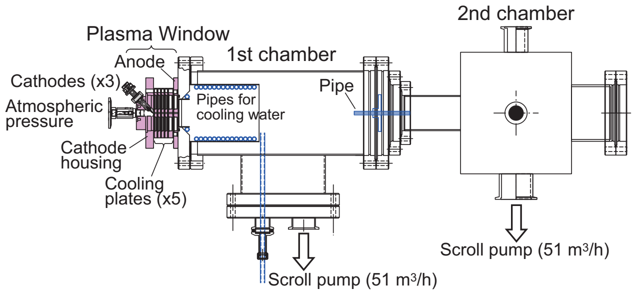

Fig. 1. PW with differential pumping system.

be easily carbonized, 2) tungsten tips should be thoriated (not pure tungsten), and 3) G10 grade glass epoxy laminates are good for insulation but unsuitable for vacuum sealing. The efficiency of differential pumping was worse than that of the PW operated at Brookhaven National Laboratory (PW-BNL)[7]. The pressure in the 1st chamber was 120 Pa, whereas that of PW-BNL was 7 Pa. The base pressure without gas flow was 10 Pa, which was five times worse than that in PW-BNL. This was because of the limited pumping speed of the SPs, whereas the 1st chamber of PW-BNL was evacuated with a 1073 m^3/h pumping speed. In December 2011, we installed a turbomolecular pump with a 792 m^3/h pumping speed to lower the base pressure. However, the base pressure was not improved because of a leak from a space between the cathode and the cathode insulator.

In the near future, we intend to 1) solve the leakage problem and improve the base pressure and 2) perform tests replacing Ar to He gas.

References
1) H. Okuno et al.: Phys. Rev. ST Accel. Beams **14** 033503 (2011).
2) H. Imao et al.: RIKEN Accel. Prog. Rep. **44** 116 (2011).
3) H. Imao et al.: in this report.
4) A. Hershcovitch: J. Appl. Phys. **78** 5283 (1995).
5) A. de Beer et al.: Nucl. Instrm. Meth. **B170** 259 (2000).
6) W. Gerber et al.: Proceedings of the 15th International Conference on Application of Accelerators in Research and Industry (CAARI), Denton, Texas, p. 475 (1998).
7) A. Hershcovitch: private communication (2011).

*1 Brookhaven National Laboratory (BNL), USA

High-Power operation of the rf systems of the superconducting ring cyclotron

N. Sakamaoto, R. Koyama, K. Suda, S. Ishikawa, and K. Yamada

High-power operation of the rf systems of the Superconducting Ring Cyclotron (SRC) was carried out at a frequency of 36.5 MHz for the fist time in October 2011, during the beam service time of the 345 MeV/u ^{238}U beam. The output power of the final rf amplifier was about 100 kW, which generated an acceleration voltage of 530 kV/cavity.

Previously, operation at an rf power of 100 kW was difficult for the following reasons. First, owing to the low touching power of the sliding fingers used to create electric contact between the tuner panel and the cavity wall, the fingers were damaged by the heat load[1)]. Second, because of severe multipacting by a strong stray magnetic field from the superconducting sector magnet[1)], rf breakdown occurred and a few hours elapsed before normalcy was restored. Third, the effect of the stray magnetic field, which was about 120 Gauss, on the power tube (RS2042SK) located outside the magnetic shield of the SRC slightly decreases the efficiency of the power tube and drastically increases the dc current of the screen grid electrode (g2), as shown in Fig.1. Because the output rf power from the amplifier is controlled to maintain the gap voltage constant when the resonant frequency of the cavity varies with the temperature of the cavity, moderate response of the g2 current to the output power is desirable. An increase in the g2 current shortens the lifetime of the power tube; further the maximum rating is easily exceeded, and power supplies are frequently turned off by the automatic interlock system.

The shape of the contact fingers was adjusted so that the fingers fitted the gap between the tuner and the cavity wall. Last year, all the damaged contact fingers attached to the fine tuners that tune the resonant frequency to the operating frequency of the cavity by servo control were replaced. Multipacting is still severe, with a maximum main coil current of 4917 A, for the 345 MeV/u ^{238}U beam. Routine conditioning with a few tens of continuum waves (cw) rf power was effective. Conditioning of each cavity required only one hour, and the process was repeated every fourth or fifth day. For the amplifiers, the impedance of the plate electrode of the power tube were chosen as 180 Ω so as to make the g2 current moderate, by tuning the output capacitor of the amplifier instead of using the standard value of 260 Ω[2)]. This strategy was effective; the operating parameters, I_p, I_{g2}, I_{g1}, diver I_p, rise in the temperature of cooling water, and power efficiency, measured during the ^{238}U beam service are plotted in Fig.2. Note that the voltage applied to the control grid electrode (g1) of the tetrode of the RES2 amplifier is set experimentally at -340 V instead of the normal value of -380 V. Fig.2 clearly shows the efficiency of the RES2 amplifier is better than that of other amplifiers.

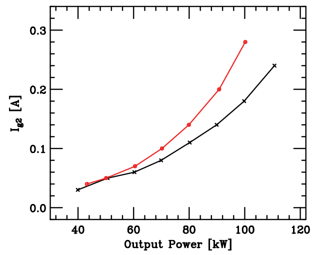

Fig. 1. g2 currents of the power tube in the presence (red line) and absence of a without magnetic field (black line).

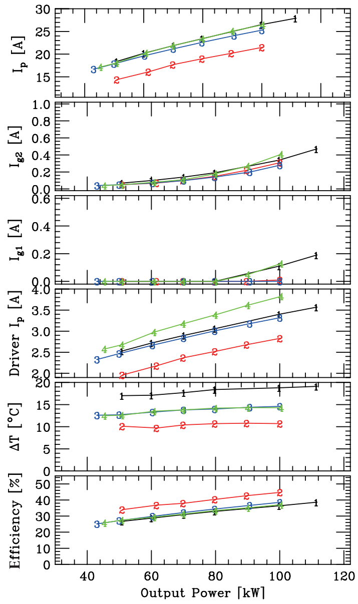

Fig. 2. Operating parameters of the rf amplifier concerning the power tube. The symbols 1∼4 represent the IDs of the rf systems of RES1∼4, respectively. Efficiency is defined as the ratio of the output power to the product of the plate current and the plate voltage.

Table 1. Operating impedance of the power tube

Cavities	RES1	RES2	RES3	RES4
Output Capacitor [pF]	104	102	105	112
Impedance [Ω]	169.6	194.5	177.2	152.2

References

1) N. Sakamoto et. al.: Proc. Cyclotrons'10, (2010)357.
2) N. Sakamoto: RIKEN Accel. Prog. Rep. **44**, p111.

Operation of the RILAC prebuncher at the fourth subharmonic frequency to provide pulsed ^{18}O beams for RIBF

K. Suda, N. Sakamoto, R. Koyama,[*1] T. Ohki,[*1] K. Oyamada,[*1] and K. Yamada

The accelerator group provided pulsed ^{18}O beams with an energy of 250 MeV/u to the RIBF for an experiment involving the SHARAQ spectrograph[1)] from the 2nd to the 12th of July 2011. The acceleration mode used was the variable energy mode (RILAC-RRC-IRC-SRC), in which all the accelerators operated at the same frequency of 32.8 MHz (= 1f). Beam pulsing was suddenly required after a major problem occurred in the AVF cyclotron, leakage of cooling water from a dee electrode, at the end of April[2)]. The AVF cyclotron was to be used as an injector at a frequency of 16.4 MHz. Since an alternative injector, RILAC, operates at the second harmonic frequency, the duration of beam bunches is reduced by half (61.0 → 30.5 ns). However, users are required to have a sufficient time window for the neutron time-of-flight measurement, longer than 120 ns. In order to fulfill this requirement, a prebuncher for RILAC was operated at the fourth subharmonic frequency (f/4 = 8.2 MHz). When beam pulsing is performed by using the fourth subharmonic frequency, ideally, beam ions are expected to exist only in one out of every four bunches. Therefore, a sawtooth wave was thought to be suitable for the buncher; however, equipment for generating a sawtooth wave was not available at RILAC. Therefore, the buncher was operated by using a sinusoidal wave, even though the purity of the pulsed beam became worse. Here, the purity is defined as $I_p/(I_p + I_o)$, where I_p and I_o are the beam intensities for the pulsed and the other three bunches, respectively.

The f/4 signal was generated by a simple frequency divider, which was constructed by using a combination of NIM modules and a bandpass filter, since with only six days left for preparation, suitable equipment could not be obtained. The operation of the frequency divider was as follows. (1) The 1f signal for the accelerators was discriminated and converted into NIM-level logic pulses with a width of 30.5 ns. (2) The pulse rate was divided by 4 using a rate divider. (3) Again, by using a discriminator, logic pulses with a width of 122.0 ns were obtained. (4) The logic pulses were transformed to a sinusoidal wave by using an LC bandpass filter with L = 37.4 μH and C = 10 μF, and the resonant frequency was 8.23 MHz. To set the impedances of the input and output of the filter to about 50 Ω for the purpose of impedance matching, −3 dB and −6 dB attenuators were used, respectively. (5) To remove spurious noise, the output signal was integrated with a time constant of 10 ns by a timing filter amplifier. (6) The obtained signal was divided by a power divider and delivered to low-level circuits of the prebuncher, as well as to each monitoring circuit for the accelerator group and users. The signal was also used to generate local oscillator signals (f − 455 kHz) for the low-level circuits.

The generated subharmonic signal was monitored by an oscilloscope at the RILAC control room; the signal is shown in Fig. 1. By monitoring the time structure of the beam with a phase probe (PP) placed between RILAC tanks #5 and #6 (shown in Fig. 1), the voltage and relative phase of the prebuncher were tuned for maximizing the purity and intensity of the pulsed beam. From the difference between the PP signals with and without beams, the ratio between the beam intensities of the four bunches was obtained as 13:1:1:1, which indicated that the purity was 81%. On the other hand, the purity measured by users was 85% on average during the experiment; the measurement was performed by using a detector at F3 of BigRIPS. Thus, the user's requirement (purity > 70%) was fulfilled.

There was a problem in that the phase of the subharmonic signal was unstable. The fluctuation in the subharmonic phase was measured to be ±10.3° (±3.5 ns) using a lock-in amplifier (LIA). As the reference frequency for the LIA, 1f was chosen instead of f/4 since a stable f/4 signal suitable for this measurement could not be prepared. This instability was attributed to the NIM modules used for the frequency divider. In order to maintain good beam conditions, the relative phase of the rebuncher was tuned once an hour at most.

References
1) K. Yako et al.: In this report.
2) Y. Watanabe and M. Kase et al.: in this report.

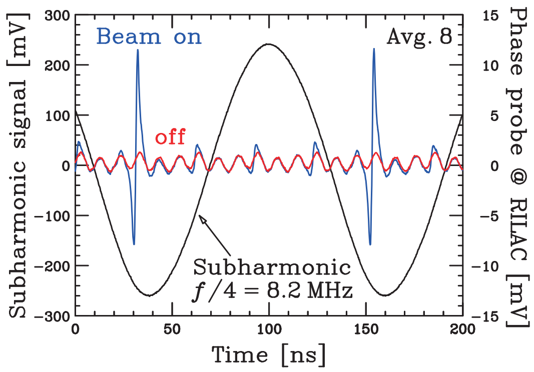

Fig. 1. Fourth subharmonic signal (black line) and time structure of pulsed beams monitored in RILAC (blue line: beam on; red line: beam off).

[*1] SHI Accelerator Service Ltd.

Replacement of new AVF-dee electrodes

Y. Watanabe, N. Sakamoto, K. Suda, T. Maie, M. Kase, T. Kageyama, A. Goto[*1], S. Fukuzawa[*2], M. Hamanaka[*2], S. Ishikawa[*2], K. Kobayashi[*2], Y. Kotaka[*2], R. Koyama[*2], T. Nakamura[*2], M. Nishida[*2], M. Nishimura[*2], J. Shibata[*2], N. Tsukiori[*2] and K. Yadomi[*2]

[AVF cyclotron and dee electrode]

During a 14 MeV proton beam time, a serious vacuum leak occurred in the vacuum chamber of the AVF cyclotron on April 29, 2011, and the beam time was cancelled on April 30. The vacuum chamber of the AVF cyclotron was investigated carefully from May 2 to 6, and in the end, we found that the vacuum leak was occurring at some point along the copper cooling-water pipe, deep inside the second dee electrode (Dee#2), as shown in Fig. 1. Dee#2 was removed from the AVF cyclotron on May 13. The pin hole on the pipe was clearly observed through a 20 mm-diameter viewing hole that was made on the upper electrode plate of Dee#2. The pin hole appears to be as large as 0.2 mm in diameter. We decided to replace both the dee electrodes because we concluded that it would be impossible to repair the pin hole in the narrow isolated section along the pipe.

The new dee electrodes require to be identical to the present ones in order to maintain the performance level inside the rf resonators. However, the following three items were included in the new design to prevent a similar problem in the future: (1) the thickness of the water pipe wall was increased from 0.5 mm to 0.8 mm, (2) the amount of crushing of the water pipe was lessened to some degree, and (3) the bending radius of the water pipe was enlarged from 18 mm to 21 mm or from 21 mm to 40 mm, in order to decrease the maximum amount of stress exerted on it. Because three months were required to fabricate the new dee electrode, some maintenance activities were carried out in the interim. One important maintenance activity was to exchange the old O-ring on the lower side of the vacuum chamber in July as it had been used since 1989 without changing.

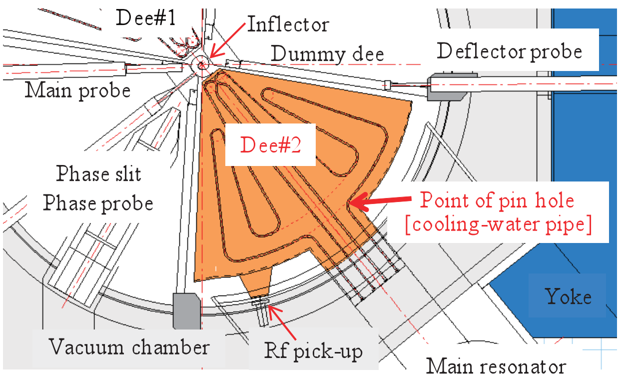

Fig. 1. Layout of AVF-Dee#2

*1 National Institute of Radiological Sciences
*2 SHI Accelerator Service Ltd.

Two sets of new dee electrodes, one for Dee#1 and the other for Dee#2, were delivered to RIKEN at the end of August. This time, Dee#1 and Dee#2 were replaced in early September. First, Dee#2 was installed in Cavity#2 of the AVF cyclotron, as shown in Fig. 2 (a), and the vertical position of the point of Dee#2 was checked with reference to the median plane of the AVF cyclotron at the center. In the first trial, the point of Dee#2 was about 10 mm lower than the median plane of the AVF cyclotron. Then, Dee#2 was removed from the AVF cyclotron and was modified to eliminate this error, on a special surface table, as shown in Fig. 2 (b). Dee#2 was fixed tightly on the special surface table, the top half of Dee#2 was lifted up to adjust the vertical position, and then, Dee#2 was reinstalled in the AVF cyclotron, following which, its vertical position error was measured. This process was repeated until the vertical position error became less than 0.5 mm. Dee#1 was also installed in the same manner. The installation of both Dee electrodes was completed on September 8, 2011.

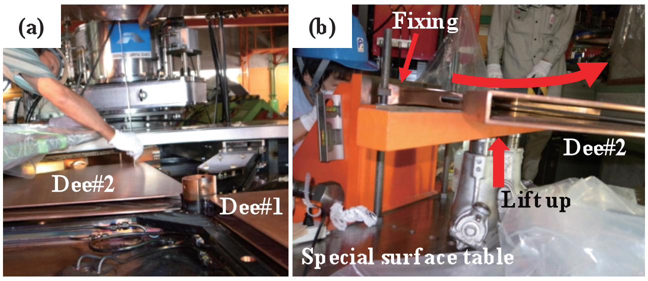

Fig. 2. Installation of Dee#2. (a) Confirmation of a vertical position of the point of Dee#2 that was installed in Cavity#2, (b) Lifting of the top half of Dee#2 on the special surface table.

RF parameters in each resonator were measured, and a rf power test was performed immediately after the installation. Maintenance of the main probe and a vacuum cryo-pump was performed, and a vacuum leak test was completed. Next, the acceleration test of the AVF cyclotron was smoothly carried out on September 22. The present performance of the AVF cyclotron is almost the same as that before the replacement of both the Dee electrodes, although some problems remain to be solved. The calibration of the rf pick-up on the dee electrode appears different from that before the replacement, and a short-time fluctuation of vacuum degree has been observed, whose its source is not clear. These problems need to be solved by early 2012.

Development of the DC plate current detector for the tetrode-based RF amplifier of RILAC

K. Oyamada, N. Sakamoto, M. Hemmi, E. Ikezawa, M. Komiyama, H, Yamauchi*, T. Ohki*, A. Uchiyama*

To improve the reliability of the RF-system of the RILAC, the interlock systems, which detect the over-current of the power tube of the main amplifiers, were renewed. In the last decade, since the start of the experiment of the super heavy element search using RILAC and CSM accelerators, the high power operation of RILAC RF systems had been used freqeunetly for the service of high energy beams. High power operation of the RF system increases the frequency of occurrence of an RF breakdown owing to the following reasons: Spark in the cavity. Overshoots of the maximum ratings of the power tube (tetrode), such as those of the dc current of electrodes of the screen grid and those of the heat load of the plate electrode in the process of auto gain control that makes the acceleration voltage constant by changing the output power of the amplifier. Malfunction of the interlock system caused by the error of the monitor system of the plate current of the power tube on account of the RF noise originating from the amplifiers.

Regarding the RF systems for RILAC, one of the major issues that stop the beam is the malfunction of the current detector of the plate electrode of the power tube built in 1985. A single dc power source for the plate electrode of the power tube supplies a high voltage to two RF systems simultaneously, and therefore, once an over-current is detected, the interlock system turns the power supply off and the two RF systems shut down. It require almost one hour to recover the normalcy of two RF-systems, in other words, 4% reliability is lost per day. Because the beam service schedule had became extremely tight over the years, a minimum beam down time is desired for a reliable operation of the accelerators.

The original current monitors for the No. 1-4 -systems of RILAC built approximately 30 years ago were based on the Hall element, which measured the magnetic field generated by a dc current of the feeder line. The problem with these monitors was that the current was sometimes incorrectly measured as a dc current of 2 to 3A. In the case of a high-power operation, the actual current of 10 to 12A is close to the maximum rating of 15 A and the measured current occasionally exceeds the limit. The failure of the RF-system of RILAC No.1-4 occurred 15 times during the period from January to June 2010.

The new current detector based on DCCT(dc current transformer), is referred to as HCS-20-AP and has been produced by U.R.D. Co., Ltd. The newly designed circuit module utilizes 24 V dc power. A dc-to-dc converter is installed to supply ±15 V power to DCCT module. In order to measure the voltage and the current of the plate electrode of the power tube continuously, monitor output ports are provided on the module. The schematic of the corresponding circuit is shown in Fig. 1.

An off-line feasibility test was performed using a prototype module (Fig.2-a). Five modules have been built, including an auxiliary for amplifiers No. 1-4, and then introduced in amplifiers No.1-3 to check whether the plate current was correctly measured by comparing it with the current meter recording of the dc power supply. After long-term testing, the use of the new current detection module as an interlock was commenced for amplifiers No. 1-4.

The new system has very small noise, which is less than 0.1 A. Since the installation of the new system, that is, over the last 6 months, the RF-system had not failed even once on account of a current over shoot. The measured current values have been logged using a logger (MW100, Yokogawa Electric Corporation) and recorded by the MyDAQ2 [1] system provided by the accelerator control group (Fig. 2-b) which is helpful for the analysis of the stability of the RF-systems.

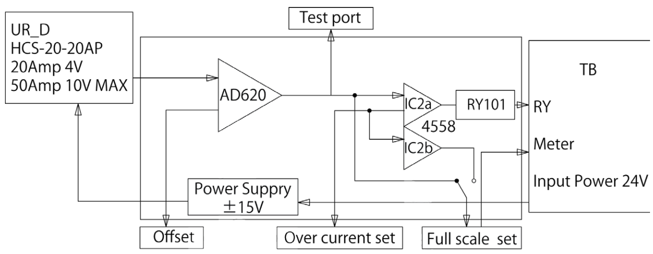

Fig.1 Block diagram of the new plate-current monitor system.

a)

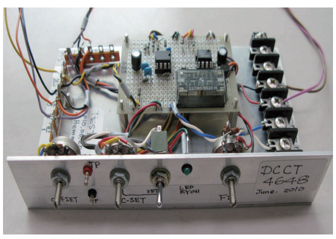

b)

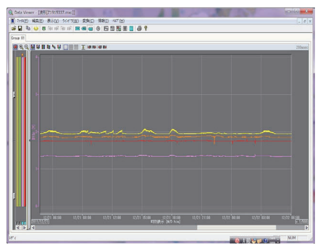

Fig. 2 a) Photo of the prototype. b) Trend graph of the plate current of the tetrode (No. 2 amplifier).

References

1) M. Kobayashi-Komiyama et. al.: Proc. ICALEPCS 2011, Grenoble, France, 2011, p.90.

* SHI Accelerator Service Ltd.

Measurement of magnetic field of fRC-SE sector magnet to realize U^{65+} acceleration

K. Kumagai and N. Fukunishi

The fixed-frequency ring cyclotron (fRC) accelerates uranium beams with a charge state of 71+ from 11 MeV/u to 50 MeV/u during the beam service time. The U^{71+} ions are converted from U^{35+} using a carbon film charge stripper with a thickness of 300 μg/cm^2, located downstream of the RIKEN ring cyclotron (RRC). The carbon film breaks every few hours or tens of hours as a result of the beam bombardment. As the thickness and performance of each film is different, the parameters of the accelerators should be adjusted after changing the carbon film.

A gas stripping system is under development [1)2)]. The gas stripper can be used continuously, and the energy spread of the uranium beam passing through the gas is estimated to be smaller than that in the case of the film charge stripper.

When a He gas stripper was used, the charge state for the maximum yield was around 65+. To accelerate the U^{65+} ions with the fRC, the magnetic field must be increased from 1.69 to 1.86 T at the central region of the sector magnet. Therefore, it was necessary to measure the higher magnetic field of the fRC to confirm that the desired field distribution can be obtained. We used a measuring system for a one-dimensional magnetic field [3)]. The power supply for the beam extraction magnet (MDC1: 1040A-270V) was connected to the SE sector of the fRC main coil. Three other sectors (NE, NW, and SW) were excited at the maximum current (650A) of the original main-coil power supply.

The magnetic fields were measured by Hole Probe at the main-coil current between 622 and 855 A; the current was increased by approximately 30 A for consecutive measurement. The interval between the measurement points along the sector centerline was 50 mm. Since 10 trim coils are all wound toward the outside of the yoke of fRC, a

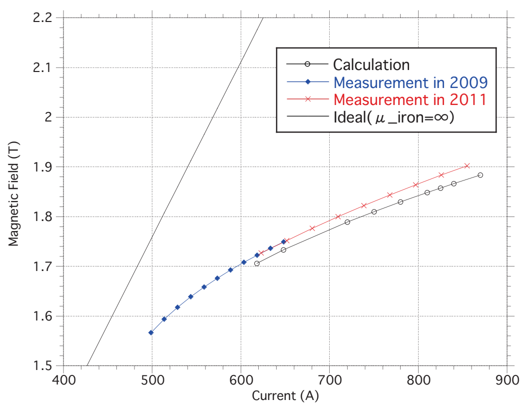

Fig. 1. Excitation curves of the SE sector magnet observed at R = 2600 mm and calculated by TOSCA-3D. The straight line indicates the magnetic field when assuming that the permeability μ of iron yoke is ∞.

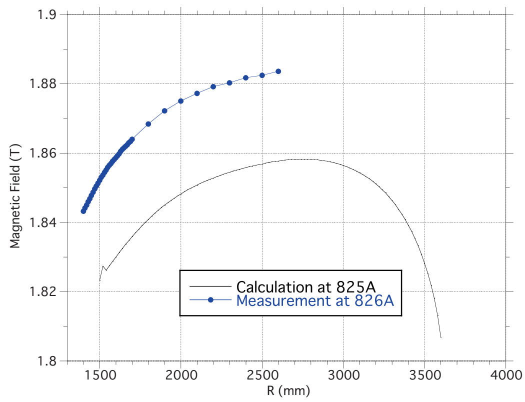

Fig. 2. Difference in the measured and calculated field of the SE sector magnet for the U65+-acceleration.

correction of the magnetic field in the central region of the cyclotron is impossible. For precise measurement of the magnetic field, the interval between the measurement points was 10 mm in the central region.

Excitation curves of the SE sector magnet at a radius of 2600 mm on the sector centerline are shown in Fig. 1. The calculation results obtained using TOSCA-3D are also shown. With the saturation of the magnetic field of the iron yoke, the increase in the magnetic field is reduced as the current increases.

Figure 2 shows the magnetic field distribution along the centerline of the sector magnet at a main coil current of 826 A. The calculated distribution required for the U^{65+} acceleration is also shown. At almost the same current, the measured distribution was larger than the calculated distribution. However, because the coil currents of three other sectors were limited to 650 A, a reverse magnetic field on the SE sector, caused by the other sectors, is supposed to be smaller than the case where all sectors are excited by the same current as that for the SE sector. We estimate that the isochronous field distribution that is required for the U^{65+} acceleration will be obtained at a current of approximately 826 A.

A new main-coil power supply with a maximum current capability of 920 A has been manufacturing. The power supply has been designed to also be used as a spare power supply of the RRC main coil. Injection magnet MIC2 and its power supply, injection magnet BM, and extraction magnet EBM are also being redeveloped with the aim of enhancing the magnetic field.

References

1) H. Okuno et al.: RIKEN Accel. Prog. Rep. **44**, ix (2010).
2) H. Imao et al.: RIKEN Accel. Prog. Rep. **44**, 238 (2010).
3) K. Kumagai et al.: RIKEN Accel. Prog. Rep. **43**, 131 (2009).

Development of current transformer for intensity measurement of ion beam

H. Watanabe, M. Fujimaki, N. Fukunishi, M. Kase

The use of a toroidal beam current transformer for the intensity measurement of charged particle beams has the following advantages [1]. Signal extraction is non-destructive, and therefore, most of the problems associated with the design of Faraday cups can be avoided. Since the ion beam will not be distorted by the measurement, the beam current transformer is well suited for on-line closed-loop feedback to control the ion beam intensity. The most important advantage is the direct proportionality of the output signal to the beam current. Furthermore, precise absolute calibration can be performed by feeding a well-known current pulse from an external current source via dedicated calibration winding.

At GANIL, the development of toroidal current transformers that can be used for accurate measurements was studied beam average current [2]. These transformers are used instead of Faraday cups during operation. The measurement system of GANIL is suitable for beam current measurements at the RIKEN beamline. The system includes a beam chopper, a toroidal current transformer, and a lock-in amplifier. The ion beam from the ion source is chopped by the beam chopper at a certain audio frequency. The chopped ion beam is passing allowed to pass the center hole of the toroidal current transformer. The winding coil of the transformer generates a voltage signal. The spectrum of the generated signal contains the audio frequency signal, whose intensity is proportional to the ion beam current. The lock-in amplifier selectively detects the audio frequency signal.

In this study, a commercial toroidal transformer (Bergoz Instrumentation, FCT-82-05:1-H-INS) is used as the beam detection current transformer. It is installed in the beamline as CT-D13. The output voltage from CT-D13 is measured by a digital lock-in amplifier (NF Corporation, LI5640). The standard electric square pulse current flows through a series resistance (1 MΩ) and is fed to one turn of the calibration winding of the current transformer with a function generator (NF Corporation, WF1973).

The relationship between the CT-D13 output voltage measured by the lock-in amplifier and the standard electric square pulse current fed to the calibration winding is shown in Figure 1. The frequency and duty cycle of the standard current are 3 kHz and 90%, respectively. A linear relationship is seen between these two values.

Then, the actual ion beam current is simultaneously measured by the CT-D13 and Faraday cup (FC-D14) installed downstream of CT-D13. The frequency and duty cycle of the chopped beam current are 3 kHz and 90%, respectively. The output current from FC-D14 is measured by a picoammeter (Keithley Instruments, Inc., Model 6485). The smallest ion beam current is 16 nA. In this case, a linear relationship is seen between standard current and CT-D13 output voltage, with the linearity being about 0.1%.

It is clear that the value of the ion current is calculated from the output voltage of CT-D13. This measurement system is well improved now, and even very small ion beam currents of less than 10 nA can be detected in the future.

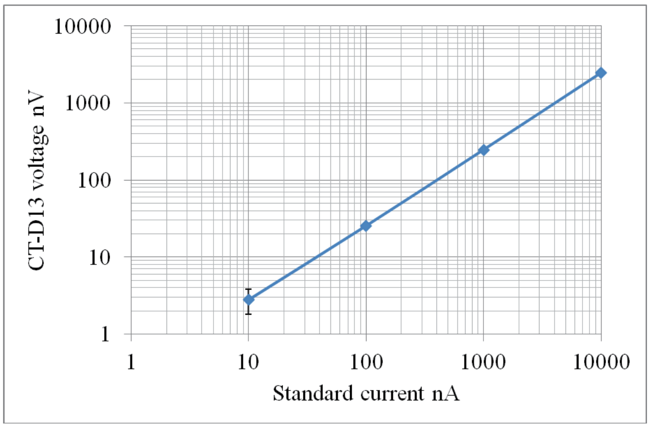

Figure 1. Relationship between standard current and CT-D13 output voltage.

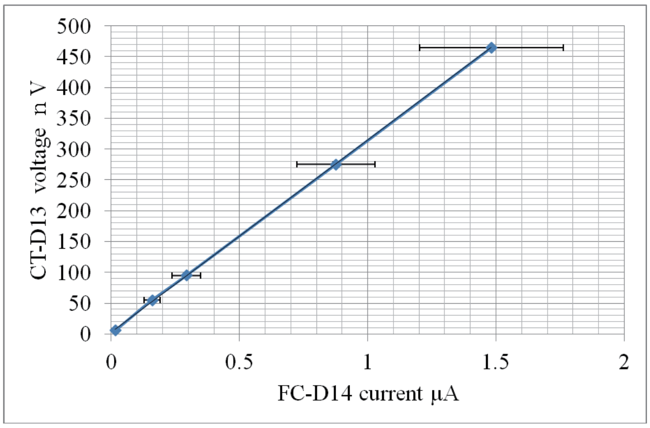

Figure 2. Relationship between FC-D14 output current and CT-D13 output voltage.

References
1) P. Strehl: Beam Instrumentation and Diagnostics (Springer, Berlin Heidelberg New York, 2006).
2) F. Loyer, T. Andre, B. Ducoudret, J. P. Rataud: IEEE Trans. NS-32, No.3 (1985), p. 1938.

Improvement of beam current monitor with high Tc current sensor and SQUID at RIBF†

T. Watanabe,N. Fukunishi Y. Sasaki, M. Kase, and O. Kamigaito

[Beam current monitor, high Tc SQUID]

We have developed a beam current monitor with a high critical temperature (HTc) current sensor and a superconducting quantum interference device (SQUID) for the Radioactive Isotope Beam Factory (RIBF) at RIKEN[1)]. In this study, we have fabricated a new HTc SQUID because the old one was deteriorated. Furthermore, we have improved the HTc current sensor in order to achieve higher current resolution.

The HTc-SQUID monitor was installed in the transport line at RIBF for practical use. However, magnetic flux jumps were observed at the HTc SQUID eventually. If the HTc SQUID captures a frozen flux on the superconducting thin films that can cause a magnetic flux jump, then the frozen flux must be removed by increasing the temperature of the film above Tc. Although we attempted several times to heat the superconducting thin films by using a heater, the flux jumps could not be stopped. As the flux jumps occurred frequently, the HTc-SQUID monitor was disassembled and diagnosed. An electrical test was performed, and the characteristics of the device were found to be significantly different from the original ones. The modulation voltage used in the SQUID decreased from 2.2 V to 0.5 V and the noise increased. Because some visible cracks were also found on the surface of the HTc SQUID, we concluded that the HTc SQUID had clearly deteriorated. However, the HTc current sensor was free from any problems. The deterioration of the HTc SQUID can be attributed to the fact that it had already been used for five years and had undergone a minimum of 100 heat cycles. These elapsed heat cycles are considered as indicative of the life span of the HTc SQUID. Thus, a new HTc SQUID was fabricated[2)].

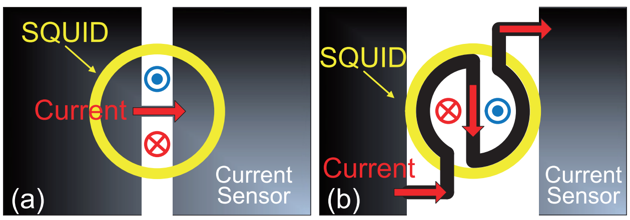

Fig. 1. Schematic drawing of (a) conventional bridge circuit and (b) improved two-coil bridge circuit of the HTc current sensor. Yellow circles indicate schematically drawn positions of the HTc SQUIDs.

† Condensed from the proceedings in 2nd Int. Particle Acc. Conf., 1260 (2010)

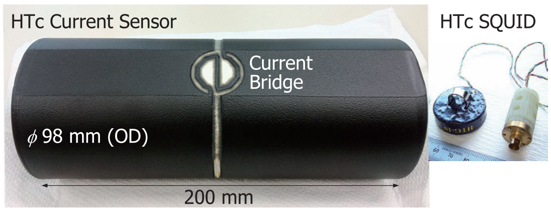

Fig. 2. New HTc current sensor and HTc SQUID.

The noise level of the new HTc SQUID was decreased by using a technology that has advanced steadily in the past five years.

The HTc current sensor was fabricated by dip-coating a thin Bi_2-Sr_2-Ca_2-Cu_3-O_x (Bi-2223) layer onto a 99.9% MgO ceramic substrate. When a charged particle (ion or electron) beam passes along the axis of the HTc current sensor, a shielding current produced by the Meissner effect flows in the opposite direction along the wall of the HTc current sensor to screen the magnetic field generated by the beam. As the outer surface is designed to have a bridge circuit (Fig. 1(a)), the current generated by the charged particle beam is concentrated in the bridge circuit and forms an azimuthal magnetic field around the bridge circuit. The HTc SQUID is set close to the bridge circuit and can detect the azimuthal magnetic field with a high S/N ratio. To further improve the sensitivity of the HTc-SQUID monitor, we designed an HTc current sensor with two coils (Fig. 1(b)). As the two coils covered the input coils of the HTc SQUID effectively, the coupling efficiency between the magnetic field produced by the beam current and the SQUID was expected to improve. The coil and the high permeability core were combined in the HTc SQUID. We measured the sensitivity and found it to be 21 times higher by using a Cu coil with the same shape and a current source. A new coating machine that coats the Bi-2223 material onto the MgO ceramic substrate was designed and fabricated. Fig. 2 shows the completed HTc current sensor. We are reassembling the HTc-SQUID monitor to measure the characteristics of the new HTc SQUID and the current sensor.

References

1) T. Watanabe et al., Proc. 2010 Beam Instrumentation Workshop (BIW10), Santa Fe, New Mexico, US (2010) p. 523.
2) M. I. Faley, Superconductivity - Theory and Applications, ISBN: 978-953-307-167-1, InTech, Vienna, Austria, (2011) p. 148.

New software application for beam profile monitors

M. Kobayashi-Komiyama, A. Uchiyama,*[1] M. Hamanaka,*[1] T. Nakamura,*[1] and N. Fukunishi

In order to measure the transverse beam position and shape, wire-scanner-type beam profile monitors (BPMs) have been installed in the beam transport lines of the RIBF accelerator complex. In the current BPM model, three wires are used to measure the horizontal, vertical, and diagonal components of the spatial beam distribution.[1)] It measures a beam profile by traversing a beam over one second. The BPMs have been used for more than 20 years, and it has become clear that secondary electrons emitted from an upstream wire hit downstream wires, resulting in sizable errors in the beam profile measurement. Therefore, a new BPM model with reduced interference among the three wires is now under consideration.

To operate the BPM and to display data measured by the BPM, we have been using an in-house software application developed in 1999. The present application is designed to control a single BPM, and hence, dozens of copies of the application should be executed during beam tuning since our facility has extended three new cyclotrons, RILAC2, and their beam transport lines over the last decade and the number of BPMs has increased significantly. Thus, there is a need to handle nearly a hundred BPMs in a more efficient way. In addition, the present application has very poor expandability, and therefore, it cannot be used for a future BPM model with a different data I/O interface. To meet the performance requirement, it is better to develop a new program for the BPM from scratch. We have hence developed a new Java-encoded BPM application.

The new BPM application should have the following features:

- It should be capable of the basic functions of the existing BPM application, such as starting the measurement operation, receiving data from a BPM controller, visualizing them on a chart, outputting data to a text file automatically, holding any previous measured data overlaid on real-time measurement data on a chart, and switching a range of amplifiers on a GUI.
- The part of the program pertaining to data acquisition must be easily modifiable, considering that a different data interface could be adopted in a future BPM hardware.
- It should have an operator-friendly GUI to reduce the beam tuning time.

The software application developed in this study starts with a menu panel, where we first choose a beam course. All the BPMs installed in the selected beam course are managed in a grouped way, and we can add or remove BPMs by using selection buttons provided in the menu panel. After selecting the beam course, we move to the actual control panel of the selected BPMs, which is shown in Fig.1. In the control panel, the BPMs are displayed in the order of their position from the upstream end to the downstream end. We can select an upstream/downstream BPM combination sequentially by selecting an indicator on the GUI. This function occupies less space on the monitor of a client PC and will help accelerator operators, who would otherwise have to spend considerable time sorting dozens of BPM data charts, save time. Upon selecting the "START" button, the BPM starts the measurement, and the obtained data are visualized on a chart. One of the merits of the new application is that we can leave any three measured data with the time stamp of measurement on a chart. This feature allows us to compare beam profiles with four different operation parameters directly on a single chart. In addition, we can retrieve any past data on the same chart by selecting the data from lists provided by the software. The existing BPM application cannot retrieve old data, and we have to compare real-time data with a printout of a figure. Now, we can directly compare real-time data with reference data measured in the past by superimposing them on the same chart. Another merit of the new application is that we can present data in two ways on a chart: using either auto-scale or the real scale. This feature helps us know the beam intensity at a glance. We have completed the development of the application and have been using it since December 2011.

Fig. 1. Control panel of BPMs.

References

1) M. Kase et al.: Proc. 11th Int. Conf. on Cyclotrons and their Applications, Tokyo, 1987, p. 443.

*1 SHI Accelerator Service Ltd.

Replacement of Aging Controller GMACS with F3RP61-2L for Power Supplies of Quadrupole Magnets in RILAC

A. Uchiyama,*1 M. Kobayashi-Komiyama, E. Ikezawa, M. Fujimaki, T. Ohki,*1 H. Yamauchi,*1 N. Fukunishi

Front-end controllers, comprised of GMACS manufactured by Taiyo Corp. and I/O devices named data station, were used on the RIKEN heavy-ion linac (RILAC) to control remotely the power supplies for the quadrupole magnets (Q-magnets) located in the drift tubes and injection line. The data station was first implemented in 1979[1)] with a mainframe computer manufactured by Hewlett-Packard Co. From 1988, the data station with GMACS was in operation with Melcom M60 as another mainframe computer.[2)] The controller and Melcom M60 were connected to each other via GPIB. Since 1999, the Experimental Physics and Industrial Control System (EPICS) has been introduced to the RIKEN Accelerator Research Facility (RARF) including RILAC for replacing the existing control system based on Melcom M60.[3)] In the EPICS-based system, the power supplies for Q-magnets were controlled by GMACS and GPIB-LAN converters via a TCP/IP connection. However, the GMACS was not applied to all of the I/O devices in the power supplies. For example, the external interlock status and the on/off-status of the power supplies could not be monitored remotely by EPICS. In addition, for the power supplies of the magnets in the injection line, some hard-wired controllers were used to set the current value without the EPICS, although the current value was monitored with EPICS. This arrangement makes the control system rather complicated to the accelerator operators. In 2003, the controllers in RILAC cavities No.1, No.2, and No.3 as well as the ones in the RIBF magnet control system were replaced with a Network IO (NIO)-based system upon an updated the power supplies of Q-magnets.[4)] The NIO, a commercial product of Hitachi Zosen Corporation, is a VME-based system.[5)] However, the old control system using GMACS for the other magnets, which is in RILAC cavities No.4, No.5, and No.6 and the injection line, was not updated because of limited resources. As a result, the old controllers, constructed more than 20 years ago, remained as a part of the RILAC control system. In order to improve the situation, we replaced GMACS with F3RP61-2L (See Figure.1), which can run EPICS using embedded technology.

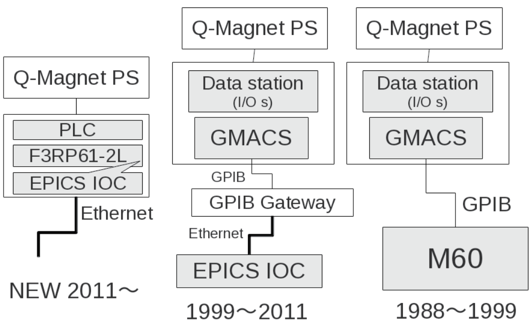

Fig. 1. Comparison system chart of F3RP61-2L-based control system and old ones for Q-magnet power supplies.

*1 SHI Accelerator Service, Ltd.,Tokyo

F3RP61-2L manufactured by Yokogawa Electric Corporation is a CPU module of FA-M3 Programmable Logic Controller (PLC) without a ladder program. As F3RP61-2L runs Linux as its operating system, it can work as an EPICS Input/Output Controller (IOC). It allows us to develop and maintain the software in a highly efficient manner and to cope with limited human resources because various application software is available as a template in the control systems of many accelerator facilities, KEKB, J-PARC, and the Taiwan Photon Source as well as RIBF.[6)7)8)] We adopted a Linux kernel in which a PREEMT_RT patch was applied to improve real-time response and to reduce the latency in the magnet control. For new Q-magnets control in the injection line of RILAC, a hard-wired operator interface is used in favor of a long-standing accustomed method. As a result, it is available to operate the power supplies using both the software GUI-based operator interface and the hard-wired operator interface.

We replaced GMACS and the data station with F3RP61-2L and PLC and upgraded the control system of the Q-magnets power supplies in RILAC. Operation of the upgraded system has already commenced successfully without any serious problems with EPICS.

References

1) T. Kambara et al.: IPCR Cyclotron Prog. Rep. vol.**13**, (1979) p.134-p.135.
2) Y. Miyazawa et al.: RIKEN Accel. Prog. Rep. **22**, (1988) p.4-p.5.
3) M. Komiyama et al.: Proc. Cyclotrons 2004 Tokyo, Japan, (2004).
4) E. Ikezawa et al.: RIKEN Accel. Prog. Rep. **37**, (2004) p.3-p.4.
5) T. Toshiya et al.: Proc. ICALEPCS2003, Gyeongju, Korea, (2003) p.597-p.599.
6) M. Komiyama et al.: Proc. ICALEPCS2009, Kobe, Japan, (2009) p.277-p.279.
7) K. Mikawa et al.: Proc. ICALEPCS2009, Kobe, Japan, (2009) p.558-p.560.
8) C. Y. Wu et al.: Proc. IPAC2010, Kyoto, Japan, (2010) p.2731-p.2733.

RIBF water-cooling system 2011

T. Maie, K. Kusaka, E. Ikezawa, M. Kase

1. RIBF water-cooling system

The setup of the RIBF water-cooling system clearly shows the supply destination of cooling water in each component of the system. Fig.1 and Fig.2 show the overall representation of the RIBF water-cooling system.
The SHARAQ water-cooling system was constructed the SCRIT water-cooling system respectively in 2008 and began operating in 2009 as a cooling installation only for the pilot machine.

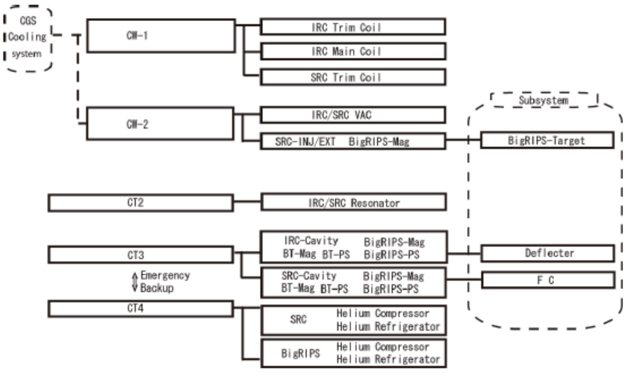

Fig. 1. Schematic of the RIBF water-cooling System

Fig. 2. Photograph of the RIBF water-cooling pump

2. Operation

The operation time of the RIBF water-cooling system of 2011 was approximately 180 days. No major incident occurred, which would hinder the accelerator operation and experiment. However, although there was no prominent failure, there were 2 or 3 instances of issues in the control system of the cooling-water feed system.

3. Maintenance

In the cooling system of the RIBF, various maintenances were performed during the accelerator halt period in summer. Following is the list of components that required maintenance.

1. Cooling tower (cleaning)
2. Chiller for accelerator cooling
3. Plate type heat exchanger
4. Cooling water pump
5. Control air compressor
6. The control device for cooling-water supply

This maintenance is an important process that is required to be completed with a limited budget and in limited time.

4. Conclusion

It is unexpectedly difficult to supply cooling water of a suitable temperature to the accelerator or an experimental device, and was always stabilized.

References
1) T. maie et al: RIKEN Accel. Prog.Rep.44, 93 (2011)

8. Instrumentation

Search for new neutron-rich isotopes of Z~60 with 345MeV/u ^{238}U beam

D. Kameda, T. Kubo, N. Inabe, N. Fukuda, H. Takeda, H. Suzuki, K. Yoshida, K. Kusaka, K. Tanaka, Y. Yanagisawa, M. Ohtake, H. Sato, Y. Shimizu, H. Baba, M. Kurokawa, D. Nishimura, T. Ohnishi, N. Iwasa,[*1] A. Chiba,[*1] T. Yamada,[*1] E. Ideguchi,[*2] S. Go,[*2] R. Yokoyama,[*2] T. Fujii,[*2] H. Nishibata,[*3] K. Ieki,[*4] D. Murai,[*4] S. Momota,[*5] Y. Sato,[*6] J. Hwang,[*6] S. Kim, [*6] O. B. Tarasov,[*7] D. J. Morrissey,[*7] B. M. Sherrill,[*7] and G. Simpson[*8]

[New isotopes, Neutron-rich nuclei, In-flight separator]

Structure of atomic nuclei far from stability has attracted considerable attention owing to the possibility of a drastic change in its shape and shell structure as a function of the neutron and proton numbers. Expansion of the known limit of radioactive isotopes (RI) forms an essential basis for investigating such evolutions of nuclear structure. In-flight fission of uranium allows production of RI beams of neutron-rich nuclei for a wide range of atomic number (Z) values lying beyond the known limit. This was well demonstrated by the discovery of 45 new isotopes of Z in the range of 25-56 at RIBF in 2008.[1)] For further expansion toward the neutron drip line, we conducted a new isotope search for nuclei with Z ranging from 57 to 70 with BigRIPS in October 2011. We have observed several new isotopes during the experiments. The experimental conditions are reported.

The 345 MeV/nucleon $^{238}U^{86+}$ beam was bombarded on a beryllium target at the production target position (F0). Reaction products were separated in the first and second stage of BigRIPS by the two-stage separation method[2)] in which an achromatic energy degrader was used at the first and second dispersive focal planes (F1 and F5). We optimized the spectrometer setting using the code LISE++[4)] to realize an adequate total counting rate at F3 and high transmission to the final focal plane F12. For this purpose, we adopted two BigRIPS settings, targeting new isotopes around $^{159}_{59}$Pr (setting 1) and those around $^{168}_{64}$Gd (setting 2). Each condition was summarized in Table 1. In setting 1, we selected fully stripped ions through the spectrometer. In setting 2, we selected hydrogen-like ions in the first dipole (D1) and fully-stripped ions after the F1 degrader, taking into account the charge-state distribution of fragments and the position of the primary beam at the beam dump after D1. The beam intensity was monitored with a plastic scintillator telescope[3)] by counting light charged particles that were scattered from the target in the backward direction. The RI beam was delivered to a new experimental setup located at F12 for measuring the total kinetic energy (TKE) and isomeric γ-rays of fragments at the same time. The TKE was measured with a silicon stack. The γ-rays were detected with four clover-type Ge detectors surrounding the stack. More detail will be described elsewhere in this progress report. The particle identification was based on the ΔE-TOF-$B\rho$ method combined with the TKE measurement. The energy loss (ΔE), time of light (TOF), and magnetic rigidity ($B\rho$) were used to deduce Z and the mass-to-charge ratio (A/Q). Furthermore, the mass A and charge state Q were deduced separately from the measured TKE, TOF, and $B\rho$ to identify contaminants of hydrogen-like ions. The TOF was measured using plastic scintillators located at F3, F7, and F12. The $B\rho$ measurement was performed using trajectory reconstruction from the measured position and angle of fragments at F3, F5, and F7 with PPACs,[5)] and the transfer matrixes. The ΔE was measured using a part of the Si stack. The total counting rate was several hundred counts per second. The data analysis is currently in progress.

Table 1. Experimental conditions in the BigRIPS settings for search for new isotopes around Z=60 regions.

	Setting 1	Setting 2
^{238}U intensity	0.13 pnA	0.31 pnA
Running time	44 h	58 h
Total dose on target	1.2×10^{14}	3.9×10^{14}
Production target	Be 3.96 mm	Be 4.93 mm
F1 degrader	Al 1.27 mm (curved profile)	
F5 degrader	Al 1.40 mm (wedge)	
$B\rho$(D1)	7.306 Tm	6.950 Tm
Beam dump (mm)	+80/-125	+45/-125
Central particle	^{159}Pr	^{168}Gd
Momentum acceptance	+/- 3%	+/- 3%
Trigger rate (F3)	620cps	260cps
Live time of DAQ	82%	90%

References

1) T. Ohnishi et al.: J. Phys. Soc. Japan **79**, 073201 (2010).
2) N. Fukuda et al.: RIKEN Accel. Prog. Rep. **43**, 165 (2010).
3) Y. Yamaguchi et al.: RIKEN Accel. Prog. Rep. **42,** 161(2009).
4) O.B. Tarasov and D. Bazin: Nucl. Instr. Meth. B **266**, 4657 (2008) and references therein.
5) H. Kumagai et al.: Nucl. Instr. Meth. A **470**, 562 (2001).

*1 Department of Physics, Tohoku University
*2 Center for Nuclear Study (CNS), University of Tokyo
*3 Department of Physics, Osaka University
*4 Department of Physics, Rikkyo University
*5 School of Environmental Science and Engineering, Kochi University of Technology
*6 Department of Physics and Astronomy, Seoul National University
*7 National Superconducting Cyclotron Laboratory / Michigan State University
*8 LPSC-IN2P3

Field map interpolation for superconducting quadrupole magnets

H. Takeda, T. Kubo, K. Kusaka, H. Suzuki, N. Fukuda, D. Kameda, and N. Inabe

The BigRIPS[1)] is characterized by large angular and momentum acceptances and large magnetic rigidity, which are realized by using large-aperture superconducting triplet-quadrupole (STQ) magnets. These magnets have a large pole tip radii of 170 mm (warm bore radii of 120 mm) considering their nominal effective lengths of 500, 800, and 1000 mm. These features enable us to achieve efficient collection and transmission of RI beams; however, the large aperture-to-length ratio leads to a wide fringing field region. The shape of the fringing fields varies according to magnet excitation currents. These effects must be treated correctly to achieve high resolving power in particle identifications.

As described in the previous report[2)], our three-dimensional field map analysis is based on the extraction of the $b_{n,0}(z)$ distribution. Measured field maps are used to obtain the $b_{n,0}$ and all the components, $B_{r,n}, B_{\theta,n}, B_{z,n}$, can be calculated from the $b_{n,0}$. This method has several advantages. One is that Maxwell's equations $\vec{\nabla}\cdot\vec{B} = \vec{\nabla}\times\vec{B} = 0$ are automatically satisfied by the fields calculated from the $b_{n,0}$. Another is that measurement errors in the field maps are averaged out in the integration process to extract the $b_{n,0}$; thus, errors in the computed fields are expected to be small.

Because the excitation currents used in various experiments are not the same as those in our field map measurements, we have to interpolate three-dimensional field maps with respect to the excitation currents. The $b_{n,0}$ is also very useful for the interpolation because it is a function of the z position only. However, it is very hard to interpolate field map data directly because of the large number of data points; fields were measured in three axes (r, θ, z), with 128 steps in the z direction and 40 steps in the θ direction in case of a Q500 magnet; thus, more than 15,000 data were obtained for each excitation current.

In our analysis, the $b_{n,0}(z)$ was extracted for each measured current and was expressed by Enge functions. In the previous measurements performed in 2006, 2008, and 2009, there were marked systematic differences among the measured years in the higher-order Enge coefficients. The differences may come from very small systematic errors such as distortion and misalignment of the field mapping device. This year, we measured quadrupole field maps for all excitation currents in the same setting to avoid the problem mentioned above by using a Q500 magnet in STQ24. Figure 1 shows the extracted $b_{2,0}$ distributions as functions of the z position for all measured currents. Enge coefficients fitted to the $b_{2,0}$ are plotted in Fig. 2 as functions of the excitation currents. The six figures on the left and right correspond to the Enge fitting of the entrance and exit sides, respectively. Results of the previous measurements are also plotted for comparison. Sixth-order polynomials are used to interpolate these coefficients.

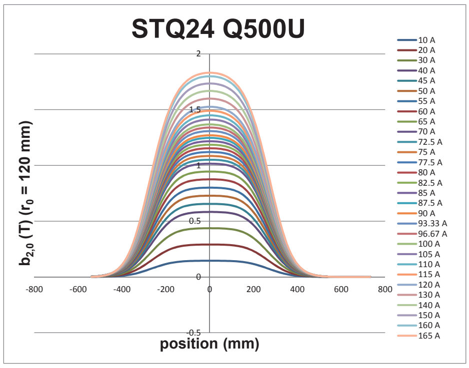

Fig. 1. $b_{2,0}(z)$ distributions extracted from newly measured field maps.

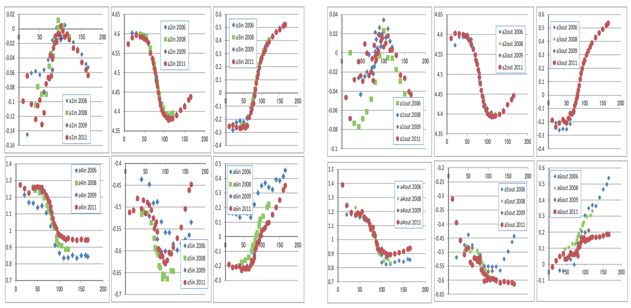

Fig. 2. Enge coefficients are shown as functions of excitation currents. Red symbols are the newly measured results. Previous results are also plotted for comparison in blue (2006), green (2008), and purple (2009).

At this moment, the entrance and exit Enge functions are just connected at the magnet center ($z = 0$). This treatment causes some problems, especially for shorter magnets. Consequently, agreement between the Enge functions and the extracted $b_{n,0}$ becomes worse at the center. Higher order derivatives tend to diverge at $z = 0$, which are required to calculate the three-dimensional fields $B_{r,n}, B_{\theta,n}, B_{z,n}$. Some functions have been proposed to avoid these issues and will be introduced in the COSY optical calculation.

References

1) T. Kubo: Nucl. Instr. and Meth. **B204**, 97 (2003).
2) H. Takeda et al.: RIKEN Acc. Prog. Rep. **44**, 136 (2011).

Development of a device for replacing the scraper at BigRIPS

Y. Yanagisawa, A. Yoshida, K. Yoshida, and T. Kubo

In the course of RI beam production, high-energy light charged particles and neutrons are also produced at the BigRIPS target. These particles cause a radiation heat load on the air-core type superconducting triplet quadropole magnet (STQ1) [1] immediately downstream of the target. To reduce the radiation heat load, a beam collimator, called "scraper", was installed to scrape off the main component of the light particles.[2] Because the optimum geometry of the scraper varies depending on the intensity of the primary beam, target thickness, and so on, several scrapers with different apertures and different lengths should be prepared. We have developed the device to replace the scraper.

The scraper is divided into two parts: an inner scraper and an outer scraper, as shown in Fig.1, and their contact surfaces are tapered for better thermal contact. The overall size of the scraper is the same as that of the prototype described in ref.1. The scraper is made of copper, which has sufficiently high density to stop scattered particles within a short length and is reasonably cheap. From considerations of storage of activation material and ease of the replacement, we decided to replace only the inner scraper, which is designed to be as small as possible. The PHITS[3] simulation helped us evaluate the minimum size of the scraper that can stop the main components of the light particles. As a result, the radius of the inner scraper was modified to half the radius of the prototype, whereas its length of 126 mm remained unchanged.

The requirements for the device are described below. The maximum weight of the inner scraper is 50 kg, assuming that the inner scraper is made of tungsten-, and its length is increased to be 200 mm. The device should be carried by a remote handling maintenance cart in the same manner as device used for the mounting of the BigRIPS target flange unit[4].

The replacing device is shown in Fig.2 along with the scraper. The inner scraper and the outer scraper are attached to the clamp Parts A/B and Parts C shown in Fig. 1, respectively. The installation procedure of the inner scraper is as follows. Firstly, the device along with the inner scraper is mounted the target chamber by the remote handling cart Secondly, the device inserts the inner scraper into the outer scraper. Because the device is clamping the inner scraper with Parts A at the vertical positions, it does not interfere with Parts B/C at the horizontal positions. Finally, Parts B of the inner scraper are rotated so that the inner scraper pushes against the outer scraper until it is locked into Parts C. Thus the inner scraper is firmly attached to the outer scraper.

It is possible to place the dismounted inner scraper in temporary storage by use of the device. Development of the transfer safety method to storage site is currently underway.

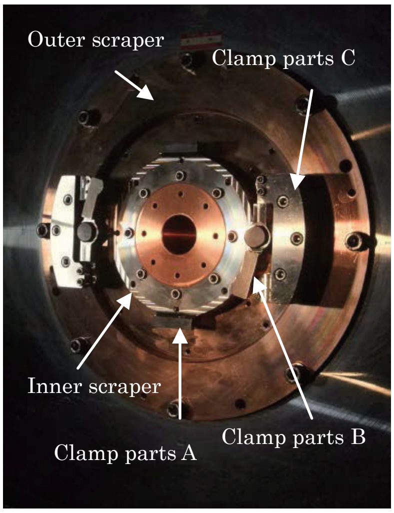

Fig. 1. Photograph of the scraper mounted in the target chamber

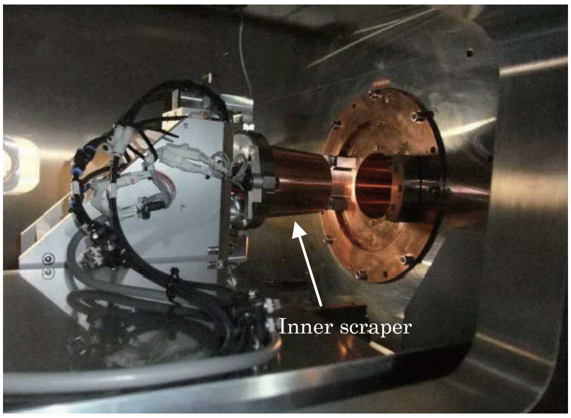

Fig. 2. Photograph of the replacing device with the inner scraper.

References

1) K. Kusaka et al.: RIKEN Accel. Prog. Rep. **37** 297 (2004)
2) A. Yoshida et al.: RIKEN Accel. Prog. Rep. **43** 154 (2011)
3) T. Ohnishi et al.: Prog. in NUCLEAR SCIENCE and TECHNOLOGY, vol.**2** 416 (2011)
4) A. Yoshida et al.: Nucl. Instr. and Meth. A **655** 10 (2011)

Development of new PID setup for measuring total kinetic energy of fragments in the medium- and heavy-mass regions

D. Kameda, T. Kubo, N. Fukuda, M. Kurokawa, N. Iwasa,[*1] A. Chiba,[*1] D. Nishimura, H. Baba, S. Go,[*2] R. Yokoyama,[*2] T. Fujii,[*2] E. Ideguchi,[*2] H. Nishibata,[*3] J. Hwang,[*4] H. Takeda, H. Suzuki, and N. Inabe

[Particle identification, Charge states, Total kinetic energy, Si detectors]

In the production of rare isotopes in the medium- and heavy-mass regions using BigRIPS,[1)] hydrogen-like fragments can be found as significant contaminations because they are hardly separated in BigRIPS. The high-resolution measurement of the mass-to-charge ratio (A/Q) often enable the particle identification (PID) for fully-stripped and hydrogen-like fragments with the difference of the A/Q values.[2)] However, this method is not applicable for isotopes with $A/Q \cong 2$ or 3 owing to the overlap of the A/Q values. In addition, such contamination makes it difficult to identify very rare isotopes, such as new isotopes, since they form a considerable background even if the A/Q values are located between 2 and 3. Recently, we improved this situation by developing a new PID setup for measuring the total kinetic energy (TKE) of fragments. The TKE value is related to the mass of fragments as TKE=$(\gamma\text{-}1)A$, where γ denotes the Lorentz factor. We can thus determine the charge state (Q) from the measured A/Q and A. This method enables a clear identification of the charge states and elimination of hydrogen-like contaminations by software.

We constructed a new setup to search for new isotopes with atomic numbers (Z) ranging from 57 to 70 in 2011. (The experimental condition is described elsewhere in this progress report.) In this neutron-rich region, the hydrogen-like contamination significantly increases and may cause misidentification of new isotopes as fully-stripped fragments, of which A/Q values distribute around 2.7. To separate the charge states, the mass resolution is required to be around 0.3%, which corresponds to a distance of approximated 5σ from peak to peak on the Q plot. Here, the A/Q resolution is expected to be much higher than the mass resolution according to the reported values around 0.04%.[2)] We have adopted a Si stack for this purpose. This setup allows us to detect isomeric γ-rays with high detection efficiency during the search for new isotopes, which realized unambiguous particle identification of new isotopes and provides an opportunity to search for new isomers in this region. One approach involves the use of a thick scintillation counter of a non-organic crystal. However, we did not use such detectors for this purpose because during the γ-ray detection, a significant loss of γ-ray intensity may occur due to γ-ray attenuation in such a large crystal compared to the Si stack. The detailed configuration is reported below.

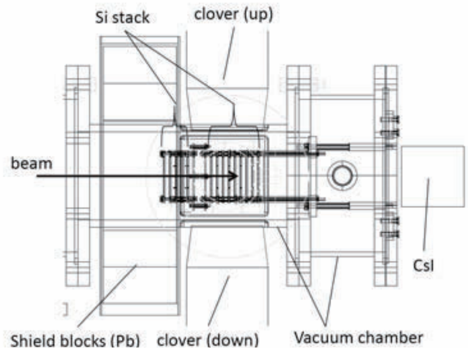

Fig. 1. Schematic layout of the new setup.

The Si stack consisted of 14 layers of a Si detector (Micron) in which thickness of the first two layers is 0.5-mm and that of the others is 1.0 mm; the active area is 50×50 mm^2. The total thickness was determined to cover the stopping ranges of fragments. For example, we first produced fragments of Z~50 with the previously-adopted setting (G3) in 2008[1)] for the calibration of each detector. In this case, most of the fragments were stopped in the last two layers, while some of them penetrated the stack and were stopped in a CsI scintillator located at the end of the beam line. The CsI detector was used for detecting such lighter-mass fragments or light particles produced by a secondary reaction in the Si stack. In the settings for new isotopes of Z=57~70, almost all the fragments were stopped in the 4th and 5th layers numbered from the last layer. The first five layers of the stack were used for deducing the atomic numbers. The Si stack was installed in a vacuum chamber of aluminum, which was connected to the beam line via a gate valve. Four clover-type high-purity Ge detectors were mounted around the chamber for the detection of isomeric γ-rays that were emitted from the Si stack. The chamber has a square shape and 1-mm thick windows between the Si stack and Ge detectors to obtain high detection efficiency. Figure 1 shows the schematic layout of this setup. The data analysis for deducing the mass resolution is currently in progress.

*1 Department of Physics, Tohoku University
*2 Center for Nuclear Study (CNS), University of Tokyo
*3 Department of Physics, Osaka University
*4 Department of Physics and Astronomy, Seoul National University

References

1) T. Kubo et al.: Nucl. Instr. Meth. B **204**, 97 (2003).
2) T. Ohnishi et al.: J. Phys. Soc. Japan **79**, 073201 (2010).

Measurement of neutron dose around BigRIPS

K. Tanaka, N. Inabe, and T. Kubo

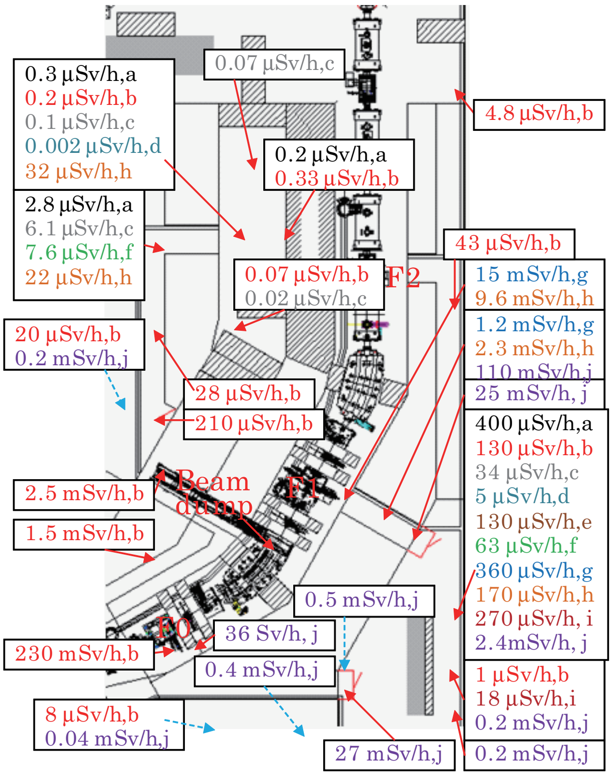

Fig. 1. Measured neutron dose around BigRIPS. The settings at the measurement spots are listed in Table 1. The letters a–j after the dose rate value correspond to the first column of Table 1. The solid arrows indicate spots where measurements were performed using TPS-451, on the same floor of the beam line; the dashed arrows point to spots where measurements were performed using EPD-N2, above the local shield of BigRIPS.

The neutron dose around the BigRIPS-F0 target and beam dump was measured. When an intense beam is provided, a high neutron dose is expected there. Owing to this high neutron dose, setups at BigRIPS can be damaged, and electric circuits can malfunction and give rise to a software error. The beam intensity is increasing with every passing year. Therefore, to cope with the neutron radiation problem, the neutron dose has been measured in several experiments. In this study, dose levels of ^{238}U and ^{124}Xe beams were measured. Dose levels of the ^{48}Ca beam were measured in a previous study[1].

The neutron-survey meter TPS-451C manufactured by Aloka Co. Ltd. and the active personal dosimeter EPD-N2 by Thermo Scientific Co. Ltd. were used for the measurements. The energy range of both detectors is 0.025 eV to 15 MeV.

Figure 1 shows the measured result, and Table 1 lists the beam settings for each measurements. The beam energy on the F0 target in Table 1 is 345 MeV/nucleon for all settings. The neutron-dose levels depend on the beam nuclide, target element, and target thickness. The Bρ value of the D1 magnet (Bρ1) also affects the dose levels because the incident position of the primary beam on the beam dump changes with Bρ1.

As suggested in a previous study[1], neutron doses higher than the designed values have been observed. To apply the high-intensity beam in the future, additional countermeasures will be planned by using this results of the present study.

References

1) K. Tanaka et al.: RIKEN Accel. Prog. Rep. **44**, 132 (2011).

Table 1. List of the BigRIPS settings during the neutron dose measurements. To facilitate easy comparison of the doses, typical values of the beam intensities obtained through the measurement are shown. In addition to the Bρ value of the D1 magnet, and the ratio of the Bρ value of the primary beam to that of the D1 magnet is also shown. If the ratio is less than 1, the primary beam hits the left side of the beam dump in Fig. 1. otherwise, the beam hits the right side.

Setting	Beam	target (element, mm)	Bρ at D1 (T·m)	Bρ ratio	Intensity (particle nA)
a	^{238}U	Be, 4	7.300	0.92	1
b	^{238}U	Be, 5	6.950	0.93	1
c	^{238}U	Be, 5	7.571	0.85	1
d	^{238}U	Pb, 0.95 + Al, 0.3	7.706	0.87	1
e	^{238}U	W, 0.7	7.300	0.90	1
f	^{238}U	no target	10.20	0.79	1
g	^{124}Xe	Be, 4	7.645	0.80	10
h	^{124}Xe	Be, 4	5.255	1.17	10
i	^{124}Xe	no target	8.782	0.79	10
j	^{48}Ca	Be, 15	8.100	0.77	100

Development of ultrathin cryogenic hydrogen target at RIBF

M. Kurata-Nishimura and H. Otsu

[cryogenic hydrogen target]

The cryogenic proton and alpha target system (CRYPTA)[1] is widely used for studying the properties of unstable nuclei. The use of this system along with the missing mass method for inverse-kinematics-reaction studies is expected to provide interesting results at RI Beam Factory (RIBF) . The ultrathin hydrogen target has been investigated in several laboratories in the world[2–5]. To use at the RIBF, the target diameter should be more than 30 mmϕ and the thickness should be less than 1 mg/cm^2, which corresponds to 140 μm for the liquid phase at 20 K. Such an ultrathin hydrogen target with a sufficiently large cross-sectional size and an uniform thickness has not been developed.

The main concern for the thin target is the material of the window foils. The foil should be thin and capable of confining hydrogen gas to the cell even at the cryogenic temperature. Conventionally, a 6-μm Havar foil and a 12-μm alamid film have been used as the window. However, they are not suitable for use as a thin target, since metals such as cobalt and nickel contained in the Havar foil enhance background reactions and the 12 μm alamid film is still too thick and comparable to the total thickness of the proton target itself.

Here, a feasibility study of a mictron film[6] with a thickness of 3.6 μm, which is the thinest nonmetallic foil commercially available, is reported.

Cell window frames with a 20 mmϕ hole were glued with two types of foils: a 3.6-μm mictron foil and a 6-μm Havar foil used as a reference. The expected total thickness of the cell was 2.9 mm. The cell was attached to the second stage of a Gifford-McMahon-cycle refrigerator and surrounded by an aluminum heat shield that was attached to the first stage.

A pressure-resistant test was performed at room temperature. The mictron window bulged out, at the certain values of the inner pressure; however, it withstood pressure difference up to 2 atmosphere. Since the window foil was permanently deformed by high pressure, it was replaced with a new one. Below the temperature of 18 K, hydrogen at the pressure of 423 hPa was confined to the cell and fully liquefied successfully.

For the liquid hydrogen phase, the swelling height was measured with a two-dimensional laser displacement sensor (Keyence, LJ-G200). A sheet-shaped laser light was focused on the mictron window surface, as seen in the photograph in the upper panel of Fig.1. Multi-reflection lines originating from the window layers were obvious at the window because the mictron film was transparent and the Havar foil on the opposite side was refractable. An image formed by diffused reflexes at the surfaces detected by a 2D CMOS imaging sensor is shown in the lower panel of Fig.1. The reflection from the mictron window as well as the Havar window can be observed.

The image was analyzed with a software installed in Keyence LJ-G5000, to trace the most intense point along the horizontal axis, which is indicated by a red solid line. By creating masks on the image, information from a specific surface layer could be extracted. The shape in the diametrical direction at the mictron and Havar window surfaces is presented in Fig.2. The swelling height of the mictron window was 2.5 mm. It is almost equivalent to an estimation value for 12-μm luminor with the same diameter, which has been reported previously[7].

In conclusion, it is confirmed that a 3.6-μm mictron film is suitable for use as the confining wall of an ultrathin hydrogen target. The reduction in the swelling height should be investigated in a future study.

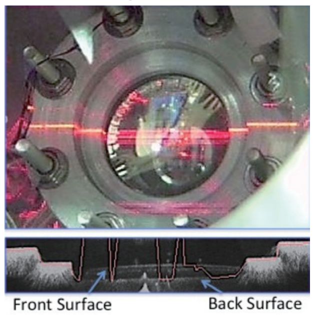

Fig. 1. (TOP) Photograph of the liquid hydrogen cell. (BOTTOM) A diffused-reflexes image of the cell surface obtained by using the 2D laser.

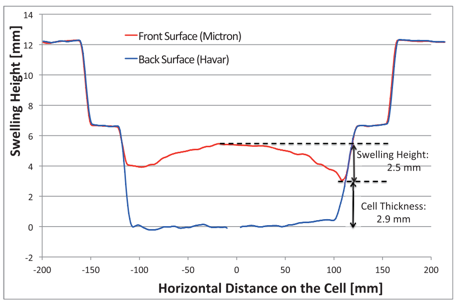

Fig. 2. Swelling height measured in Fig.1.

References

1) H.Ryuto et al., Nucl. Inst. Meth. A555, 1 (2005),
2) S. Ishimoto et al., Nucl. Inst. Meth. A480, 304 (2002)
3) P. Dolegieviez et al., Nucl. Inst. Meth. A564, 32 (2006)
4) P.E. Knowles et al., Nucl. Inst. Meth. A368, 604 (1996)
5) CHYMENE collaboration, private communication.
6) http://www.toray.jp/films/products/pdf/mictron.pdf
7) M. Kurata-Nishimura et. al., RIKEN Accel. Prog. Rep. 44, 218 (2011)

Measurement of residual radiation in the short term around BigRIPS

K. Tanaka, N. Inabe, and T. Kubo

Residual-radiation levels in the short term originating from the irradiation of the high-intensity beam on the BigRIPS setup were measured. The BigRIPS setup is susceptible to problems, especially around the F0 target and the beam dump owing to radiation heating or damage from the high-intensity beam. However, it is possible to access this part for urgent maintenance work immediately after beam irradiation.

The measurement spots are shown in Fig. 1, and the measured dose rates are listed in Table 1. Teletector 6112D GM, a survey meter that can be operated remotely, was used. The γ-ray dose just after irradiation depends on the beam-irradiation dose in recent hours than on total irradiation, because production rates and decay rate of radiation-source nuclides with a short-life are balanced. The irradiation was not stopped for long periods in the 24 h before the first measurements. The residual γ-ray dose after ^{124}Xe and ^{238}U beam irradiation was measured in 2011, and after ^{48}Ca irradiation in 2009. Background levels were measured before beam irradiation and were subtracted from the final measured value. For ^{124}Xe and ^{238}U, it was difficult to measure the dose levels more than several days after irradiation, except at a few spots, because of the high background level. For ^{48}Ca, this time dependence at a few spots was shown in a previous study[1].

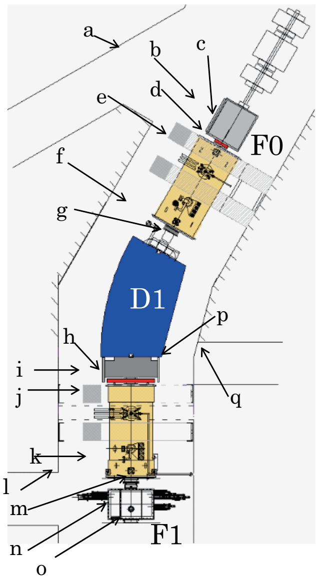

Fig. 1. Layout around F0 and beam-dump chamber of BigRIPS

References

1) K. Tanaka et al.: RIKEN Accel. Prog. Rep. **44**, 134 (2011).

Table 1. Residual doses (μSv/h) measured after beam irradiation was stopped. Beam doses in terms of total irradiation and irradiation in the 24 h before the measurements are shown.

Beam setting	^{48}Ca+Be 15 mm		^{124}Xe+Be 5 mm			^{238}U+Be 5 mm	
Beam stop date	Dec. 28, 2009		Dec. 18, 2011	Dec. 19, 2011		Dec. 8, 2011	
Beam irradiation (particle nA·day) Total/previous 24 hours	7.6/1.9		31.3/5.2	33.0/6.9		16.7/1.8	
Cooling time	20 min.	2 day	40 min	100 min.	1.3 day	20 min.	1.4 day
a	53	4	78	100	18	31	5
b			260	310	60	100	20
c			450	580	110	240	45
d	600	60	600	810	150	330	55
e			250	290	56	75	14
f			65	56	11	39	11
g			1500	1100	410	270	70
h		13	1200		130	300	25
i	94	6	630	310	80	190	17
j	115	6	510	320	70	170	23
k			150	75	12	50	7
l	10	0.7		37	12	28	
m			110		28		
n	20	1		58	26	36	
o	26	0		70	54	59	
p				140	15	220	10
q				72	14	90	8

Installation of radiation shield and pillow seal system around the first STQ of BigRIPS

K. Yoshida, K. Tanaka, N. Inabe, Y. Yanagisawa, A. Yoshida, M. Ohtake, and T. Kubo

The equipment in the first stage of BigRIPS, which consists of the target system, the first superconducting triplet quadrupole magnet (STQ1), the first dipole magnet (D1), STQ2, and the first focus chamber, are exposed to the strong radiation, which arises from the production target and the beam dump. Therefore, radiation shielding and remote maintenance are very important for these equipment. As a part of a series of improvements of the radiation hardness of the first stage of the BigRIPS,[1–3] a radiation shielding block and a pillow seal system were installed upstream and downstream of the STQ1, respectively.

The radiation shielding block, located between the target chamber and STQ1, was designed to reduce neutrons irradiating the STQ1 which arise from the target. As shown in Fig. 1, it neatly fits into the space between the target chamber and STQ1. The shielding block consists of a body part and an insertion part. The body part is made of 11-cm-thcik stainless steel. The insertion part covers the space above the pillow seal system connecting the target chamber and STQ1. It is made of 54-mm-thick tungsten alloy (AMBILOY AN-1800, Mitsubishi Materials C.M.I). This part can be lifted up and removed when target chamber is dismounted from the beamline, whereas the stainless body is attached to the STQ1 and remains fixed to the STQ1. The counterbalance of the radiation shield is also attached to the STQ1 to maintain the weight balance of STQ1. The counterbalance was made of lead covered with a thin stainless steel case.

The pillow seal system that makes it possible to connect and disconnect the vacuum duct remotely has been installed between STQ1 and D1. The system is both-sided and similar to the one downstream of D1.[2] The head of the pillow seal and the facing flanges had the water channels to deal with the radiation heating. The system was designed to be lifted up vertically when it needs to be dismounted from the beamline. All the tubing necessary to operate the pillow seals runs upwards to near the cave ceiling and then connects to the supply line for compressed air and water. Special care was taken in designing the pillow seal system because the D1 chamber is not sufficiently strong to sustain the expansion force of the pillow seal. Because pillow seal maintains a vacuum using diaphragms swollen by compressed air, the flange facing the pillow seal is subjected to a force of about 8000 N. The supporting chamber was inserted between the facing flange of the pillow seal and the D1 chamber. The supporting chamber was fixed on the mounting frame and prevents the force from being transferred to the D1 chamber. The leak rate was found to be about 5×10^{-10} Pa m^3/s, which was similar to that of other pillow seal systems utilizing the BigRIPS beam line.

The pillow seal system together with a previously installed pillow seal systems[1–3] enable the remote mounting and dismounting of target chambers, STQ1, and D1 chamber from the beamline. The installation of a pillow seal at the downstream of the STQ2 is also planned.

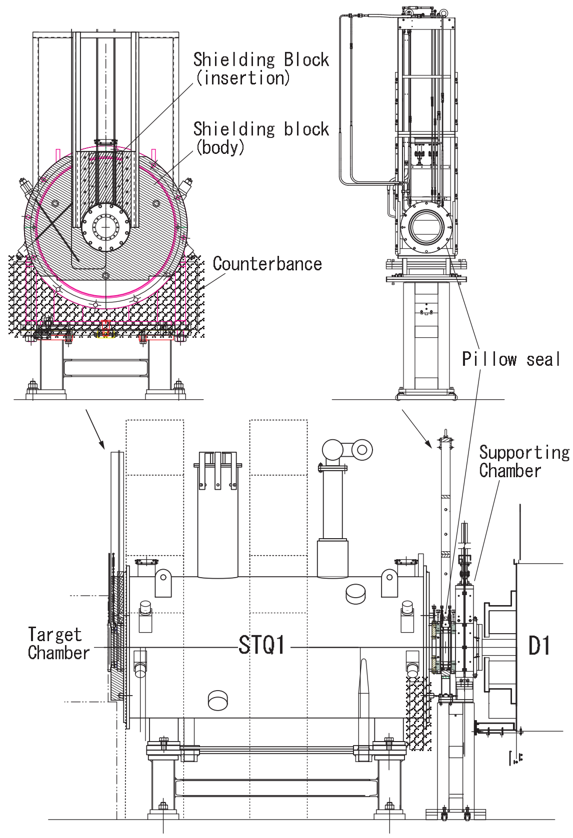

Fig. 1. Schematic drawing of the part of BigRIPS between the target and D1.

References
1) A. Yoshida et al.: RIKEN. Accel. Prog. Rep. **43**, 153 (2010).
2) K. Tanaka et al.: RIKEN. Accel. Prog. Rep. **43**, 161 (2010).
3) N. Inabe et al.: RIKEN. Accel. Prog. Rep. **43**, 150 (2010).

Evaluation of long-term residual radiation around the BigRIPS

K. Tanaka, N. Inabe, and T. Kubo

Residual radiation levels due to the irradiation of the high-intensity beam of ^{48}Ca on the BigRIPS were evaluated. The long-term estimation of residual γ-ray dose is important to make plans for improvement and maintenance tasks in the high-radiation environment. In this study, the long-term dose value was estimated using the data shown in the previous work[1].

The residual γ-ray dose was measured using a GM survey meter, and the source radionuclides were identified from the γ spectra obtained using a Ge detector[1]. Figure 1 shows the time dependences of the residual γ-ray dose at several spots between F0 and the beam dump chamber. To plot these curves, the dose value was measured using the GM survey meter until 90 days after the irradiation was stopped, and then long-term dose rates were deduced by taking into account the decay of the identified radionuclides.

The Ge detector was used only at several high-dose spots, which were close to the beam line. Generated nuclides of the radioactive source were similar, because they are generated in iron or stainless steel materials, which mostly compose the BigRIPS. Therefore, the deduced long-term decay curves are almost same. Short term dose rates depend on local materials and beam irradiations owing to the local differences among the short half-life nuclides produced. The dose rates for more than several weeks of cooling after ^{48}Ca beam irradiation can be estimated using the curves in Fig. 1. Time-dependent dose rates at other spots were also calculated assuming that the radiation at these spots originates from the high-dose area. Figure 2 shows the estimated dose. The irradiation dose is assumed to be 1 particle μA·day of ^{48}Ca beam, and the cooling time is 90 days.

The regular maintenance tasks will be performed from the top, after concrete shield blocks of the ceiling are removed. Therefore, the dose levels around the ceiling are shown in the figure. These were measured in October 2011, when the ceiling was removed for improvement of the BigRIPS[2].

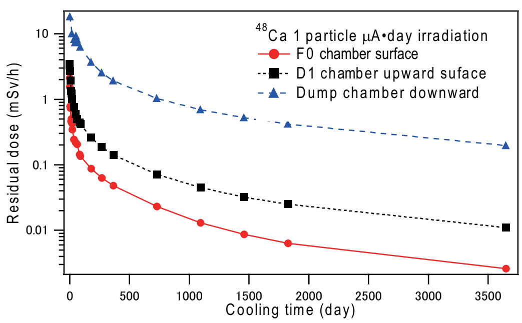

Fig. 1. Time dependence of radiation dose estimated from the measured results using the GM survey meter and Ge detector. The beam is ^{48}Ca, and the irradiation dose is 1 particle μA·day.

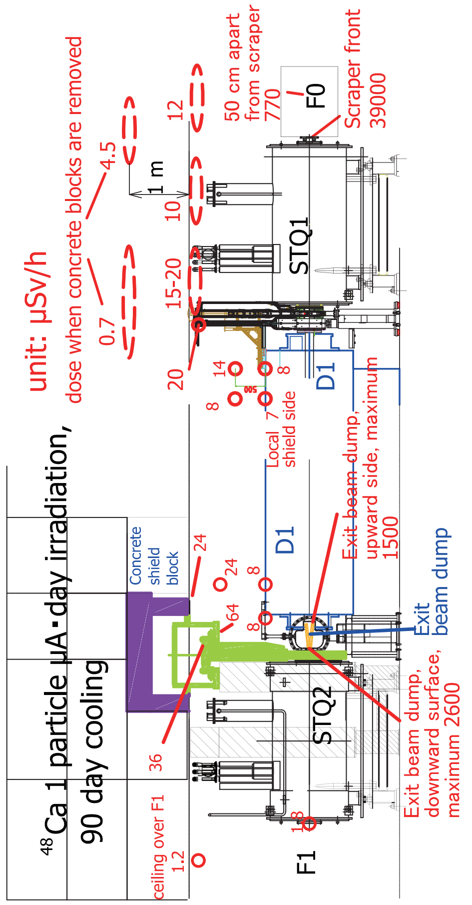

Fig. 2. Estimated residual γ-ray dose rates between F0 and F1 after the irradiation of ^{48}Ca beam of 1 particle μA·day and 90 day cooling.

If this beam irradiation is repeated every year, radiation levels 90 days after the last beam irradiation would be 1.5 (2 year repeat), 1.6 (3 year), 1.7 (5 year), and 1.8 (10 year) times the dose rates shown in Fig. 2. After a cooling time of more than 10 years, more than 95% of the radioactive source would be ^{60}Co ($T_{1/2}$ = 5.3 y).

References

1) K. Tanaka et al.: RIKEN Accel. Prog. Rep. **44**, 134 (2011) and references therein.
2) K. Yoshida et al.: in this RIKEN Accel. Prog. Rep.

Current status of ionization chamber for BigRIPS experiments

D. Nishimura, H. Otsu, J. Zenihiro, N. Fukuda, D. Kameda, H. Suzuki, and H. Takeda

The atomic number (Z) of secondary beams can be identified by the energy loss (ΔE) of ionization chambers (ICs). The manipulation and performance of ICs for BigRIPS[1)] have been reported[2–4)]. In November 2011, experiments were performed with a high counting rate of up to 100 kcps for secondary beams at BigRIPS. To enable it to tolerate a high counting rate, the pre-amplifier for the ionization chamber at F7 (F7IC) was changed to a Mesytec MPR-16 with a short decay time of 10 μs. The shaping-amplifier was also changed to a Mesytec MSCF-16 because it allows us to adjust the pole zero against the output of the pre-amplifier. To take electronic noises into cosideration, the shaping time of the shaping-amplifier was set to 2 μs (σ), which is relatively long.

First, we examined the performance of F7IC at a low counting rate of 1 kcps. Fragments were produced by the in-flight fission of a primary beam of $^{238}U^{86+}$ with an energy of 345 MeV/nucleon on a Be target with a thickness of 5 mm. The magnetic rigidity ($B\rho$) setting of BigRIPS was 7.07 Tm, which implies that the energy of the fragments with $A/Z = 2.5$ was 330 MeV/nucleon. Energy degraders were not set at F1 and F5 of dispersive focal planes. The width of the horizontal slit at F1, narrowly set at ± 2 mm, gave a momentum spread of secondary beams that was as small as $\pm 0.1\%$. The configuration of F7IC was the same as that used for the previous experiment[2)]. The F7IC was filled with P10 (Ar 90% + CH_4 10%) gas at a pressure of 660 Torr. The anode voltage was set at +600 V. The particle identification (PID) was based on the time-of-flight (TOF), ΔE, and $B\rho$ method. Figure 1 shows the PID plot of the TOF between F3 and F7 versus ΔE in F7IC. The start and stop signals for the TOF were measured by a 0.2 mm-thick plastic scintillator at F3 and F7, respectively. Although ΔE was corrected by a factor of the square of the TOF, the vertical unit was arbitrary. The absolute PID was given by detecting gamma rays of the isomer ^{98m}Y ($T_{1/2} = 7.6$ μs) using four HPGe detectors at F12. The Z resolutions for the fragments around $A/Z = 2.5$ in FWHM are deduced from ΔE in F7IC, as shown in Fig. 2. A Z resolution of better than 5σ separation, which is equal to 0.47 in FWHM were achieved for fragments in the entire region of $Z = 31 - 58$.

After performing experiment at a low counting rate, an experiment at a high counting rate of up to 100 kcps was performed. Although the number of pile-up events increased in this experiment, the particles could be identified clearly. The analysis of the Z resolution at a high counting rate is currently underway.

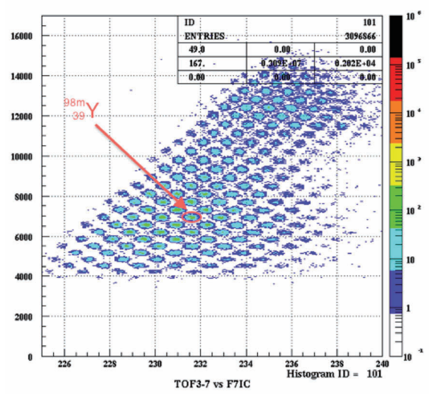

Fig. 1. PID plot of the TOF versus ΔE in F7IC. The horizontal axis is the TOF between F3 and F7 measured by using 0.2-mm thick plastic scintillators in units of ns. Although the vertical axis of ΔE is corrected by a factor of the square of the TOF, the vertical unit is arbitrary.

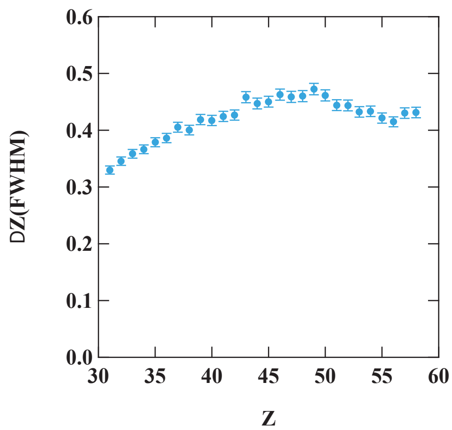

Fig. 2. Z resolution for the fragments around $A/Z = 2.5$ given by ΔE in F7IC at a low counting rate of 1 kcps. A Z resolution of better than 5σ separation which is equal to 0.47 in FWHM were achieved for fragments in the entire region of $Z = 31 - 58$.

References

1) T. Kubo, et al.: Nucl. Instrum. and Methods. **B 204**, 97 (2003).
2) H. Otsu, et al.: RIKEN Accel., Prog. Rep. **42**, 163 (2009).
3) T. Ohnishi, et al.: RIKEN Accel., Prog. Rep. **41**, 123 (2008).
4) K. Kumura, et al.: Nucl. Instrum. and Methods. **A 538**, 608 (2005).

Construction of liquid-nitrogen facility on the north side of RIBF building

M.Ohtake, K. Yoshida, and T. Kubo

A Liquid-nitrogen facility, with a storage tank (internal volume: 5000L) and an evaporator, was constructed on the north side of the Nishina Center RIBF building. These components were obtained from the facility on the north side of the Cooperation Center building in the Wako campus south area, which was shut down a few years ago.

In the facility, there are two withdrawal place of liquid nitrogen. One is the side of the storage tank, and the other is BF3 in the radiation control area, which is 20m below the tank. Vacuum insulated piping was used.

The time required for filling liquid-nitrogen container of 100L is about 30 min per 100L at both places. In addition, the cooling time of the piping is about 5 min at BF3.

The facility is designed for experimental groups and will be used mainly for detector cooling.

Fig.1. Liquid-nitrogen facility on the north side of the Nishina Center RIBF building.

Fig.2. Filling liquid nitrogen place at the side of the tank.

Fig.3. Filling liquid nitrogen place at BF3.

Superconducting dipole magnet of SAMURAI

H. Sato, J. Ohnishi, H. Otsu, Y. Shimizu, K. Yoneda, T. Motobayashi, T. Isobe, K. Kusaka, T. Kubo, T. Kobayashi,*[1] K. Sekiguchi,*[1] T. Nakamura,*[2] Y. Kondo,*[2] Y. Togano,*[3] and T. Murakami*[4]

[SAMURAI, spectrometer, magnetic field, TOSCA]

A large superconducting dipole magnet, which is a main component of a large-acceptance spectrometer "SAMURAI", has 33.2 MJ of stored energy and its total weight is approximately 650 tons.[1)] During an excitation test, a lower coil was once quenched at the current of 561 A, which corresponds to 99.6% of the maximum current given in the specifications (563 A). The quench protection circuit worked correctly and no harm was caused to the coil. In the subsequent excitation test, the current reached 563 A without quenching. A magnetic field of 3.08 T satisfied the given specification. Over excitation to 573 A (102%, 3.11 T) was also performed successfully.

After the excitation test, magnetic field maps were obtained by preliminary measurements on several planes (y = +150, 0, -150, -300 mm) with Hall probes calibrated by NMR.[2)] The obtained excitation curve is shown in Fig. 1. For the center magnetic field on the median plane, the measured values and the calculated values using OPERA-3D/TOSCA were compared. In the calculations, we used a BH curve named "default.bh" for pure iron. In addition, we used two 3-dimensional models: model 1 with only the yoke, and model 2 with the yoke, a rotatable stage, and stud bolts made from steel. The differences between the measured and calculated values for each model are shown in Fig. 2. The calculation performed using model 2 reproduces the measured values better than that performed using model 1, especially for a higher magnetic field. This implies that after the saturation of the iron yoke, some part of the magnetic flux flows into the rotatable stage even though they are magnetically separated. The remaining deviation is presumed to be on account of the difference between the BH curve used in the calculations and that of the actual magnet. Results for other planes show the same trend.

The magnitude of fringe fields along the beam direction (z-axis) was also measured. The result is compared with the values calculated by TOSCA (model 2) in Fig. 3. The fringe fields at a distance of more than 500 mm from the magnet satisfy our requirements (less than 5 mT).

The calculation performed using TOSCA reasonably reproduces the measured center and fringe fields. However, in order to generate accurate magnetic field maps using TOSCA, the calculations need to be confirmed by more precise field maps because the position accuracy of the current data is insufficient due to a small slant of the arm where the Hall probes are attached.

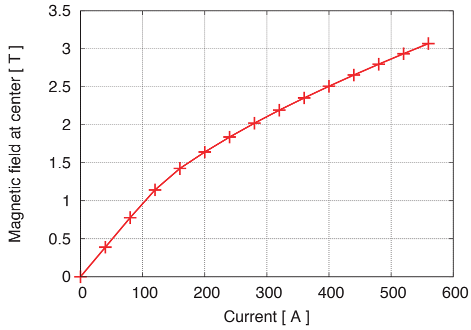

Fig. 1. Excitation curve obtained with NMR.

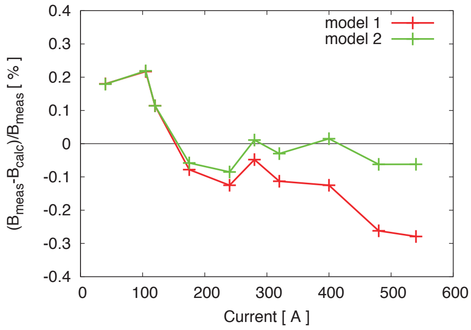

Fig. 2. Difference between the measured and calculated magnetic field at the center position.

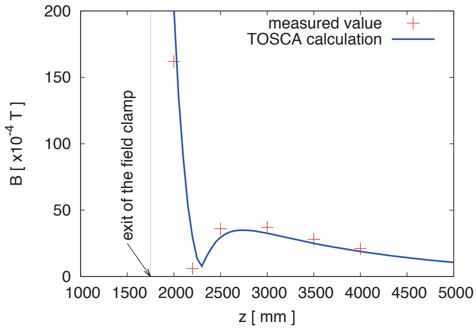

Fig. 3. Fringe field of the magnet along the z-axis.

*1 Department of Physics, Tohoku University
*2 Department of Physics, Tokyo Institute of Technology
*3 Extreme Matter Institute EMMI, GSI, Germany
*4 Department of Physics, Kyoto University

References

1) H. Sato et al.: RIKEN Accl. Prog. Rep. **43**, 180 (2010).
2) J. Ohnishi et al.: In this report.

Magnetic field measurement of the SAMURAI superconducting magnet

J. Ohnishi, H. Sato, and H. Otsu

The SAMURAI spectrometer under construction is one of the main experimental apparatus at RIBF and is equipped with a large superconducting dipole magnet[1] with a weight of approximately 600 t. The magnet was fabricated and excited successfully at the nominal current after one quench in June 2011. Magnetic field maps for determining the rigidity of particles will use results of the magnetic field calculation by Opera-3d.[2] However, magnetic field measurement is required for the following reasons: 1) to acquire absolute values of the magnetic field, which would otherwise be difficult to determine because of the BH-curve of the yoke material, 2) to verify the calculation model geometry and the precision, 3) to confirm that the deformation and displacement of the coil and the yoke are within the assumed range. This measurement was made preliminarily using existing instruments for obtaining significant results within restricted time.

Figure 1 shows the measuring area and coordinate system. The origin of the x-y coordinate is at the center of the magnetic pole. Magnetic field mapping was done by driving a bar to which five Hall probes (Bell Technologies Inc. Model BHT-910) were attached. The driving stage covers 3 m and 0.8 m in the X and Y directions, respectively. The measuring intervals are 20 mm or 40 mm, and the total number of points and measuring time are 3127 and two hours for one map in the case of 40-mm intervals. Coil currents (and magnetic field strengths) were six levels of 52A (0.5T), 105A (1.0T), 175A (1.5T), 280A (2.0T), 400A (2.5T), and 540A (3.0T). The measurement was done at heights of z = 0 mm (median plane), 150 mm, 300 mm, and -150 mm. A total of 27 maps were acquired for 17 days.

The Hall probes were calibrated using a NMR probe at

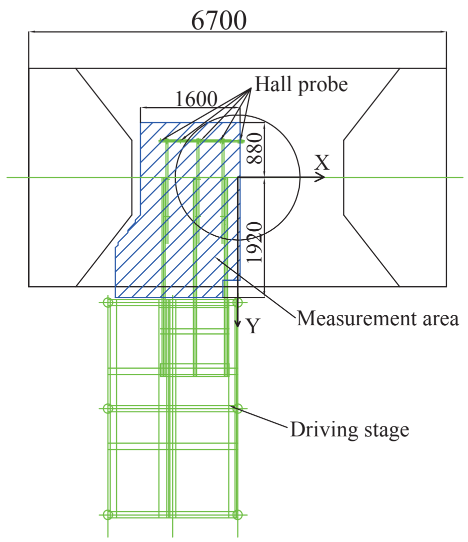

Fig. 1. Measuring area and coordinate system.

the center of the magnet. The shifts from the calibration performed for the measurement of the SRC in 2006 range from -5 G to 10 G. Figure 2(a) and 2(b) shows the magnetic field distributions averaged in y = -880~1640 mm on the median plane and the deviations from the values calculated by Opera-3d in the same region, respectively. The reason for the discontinuous magnetic field distributions, for instance, around -900 mm or -1200 mm, is considered to be the positional error between the Hall probes. In the high magnetic field level, the measured magnetic fields are smaller than the calculated ones by 0.1~0.3%. The reason for this is mainly presumed to be that the BH-curve given as "default" for a pure ion in the Opera-3d calculation differs from that for the real magnet. However, these calculation errors can be reduced by normalizing them using the measured values at the center point. Further, since the divergence of the calculation is roughly uniform, discrepancies are not seen in the calculation model and the real magnet.

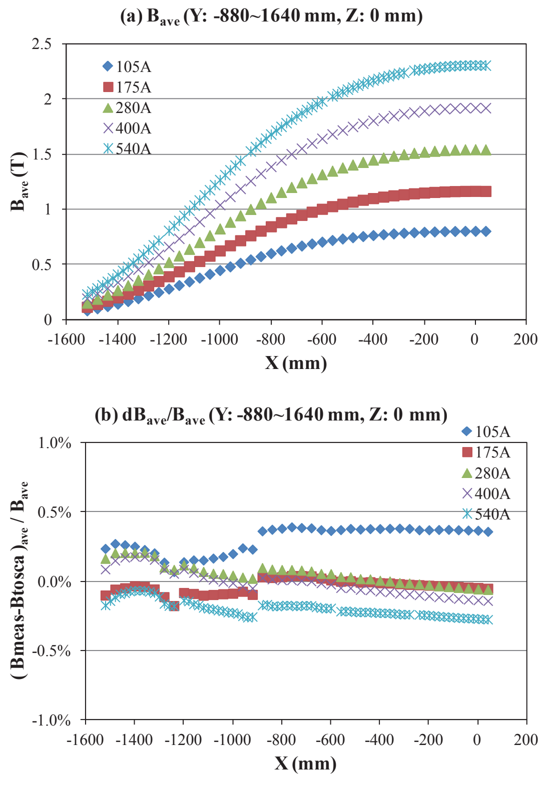

Fig. 2. (a) Magnetic field distributions averaged along the y-direction, and (b) deviations between measurement and calculation.

References
1) H. Sato et al.: In this report.
2) http://www.cobham.com/.

Vacuum system for SAMURAI beam line

Y. Shimizu, H. Otsu, T. Kobayashi,*1 T. Motobayashi, H. Sato, and K. Yoneda

[SAMURAI]

The SAMURAI project is currently underway at RIKEN RI Beam Factory[1,2]. The SAMURAI beam line from the BigRIPS and its vacuum system are under construction to use the SAMURAI spectrometer for RI beam experiment.

Figure 1 and 2 show the layout of the vacuum system for the SAMURAI beam line. The beam stopper and the radiation shutter are placed between the focal plane F12 and the superconducting triplet quadrupole magnet STQ25. The vacuum pumping system with the 1100 l/s TMP is mounted on the beam line. The distance between the exit of the STQ25 and the entrance of the SAMURAI vacuum chamber is about 3.8 ± 1.2 m depending on the place of the STQ25. A target chamber containing beam line detectors and a reaction target will be set in this space. For commissioning experiment, two trigger scintillators (SBTs) and an ion chamber (ICB) will be placed in the air following the STQ25. After them, two drift chambers (BDCs), a reaction target, and a forward drift chamber (FDC1) will be placed in vacuum. In order to measure γ-rays emitted from the excited fragments produced in direct reactions such as Coulomb excitation, a gamma detector array DALI2 will be placed around target.

The SAMURAI vacuum chamber is in the magnet gap and covers the volume inside the magnetic return yokes as shown in Fig. 2. The two 2400 l/s TMP systems are attached to the SAMURAI vacuum chamber from upstream and downstream, respectively. When the SAMURAI vacuum chamber was evacuated by one of them, it took 5 hours to reach 16 Pa, and was finally reached to 8.5×10^{-5} Pa. With the two systems, it is expected to take 3 hours to reach 10^{-3} Pa.

On the exit of the chamber, a flange with two windows with symmetrical configuration is mounted. These two windows are to be used respectively for heavy ions and neutrons or protons, which are spatially separated. The vacuum partition for neutrons was required to minimize the reaction loss and have to support itself. The area to be covered is 2430×800 mm^2. This partition is designed as a sectorial cylinder with a thickness of 3 mm. It is made of stainless steel. The vacuum partition for heavy ions was required to realize lower multiple scattering and lower energy loss. At the same time, it should be strong enough. The vacuum partition is the combination of Kavlar and Mylar. The area to be covered is 2800×800 mm^2. For commissioning experiment, this area is reduced to 2800×400 mm^2, which is the maximum size currently reached to fulfill the requirements. For future experiments measuring heavy fragments and light charged particles in coincidence, systematic studies for a larger partition under the original design are on-going.

The SAMURAI beam line in its first form will be completed in February, 2012 for the first commissioning run planned in March, 2012.

References
1) K. Yoneda *et al.*: In this report.
2) Y. Shimizu *et al.*: J. Phys.: Conf. Ser. **312** 052022 (2011).

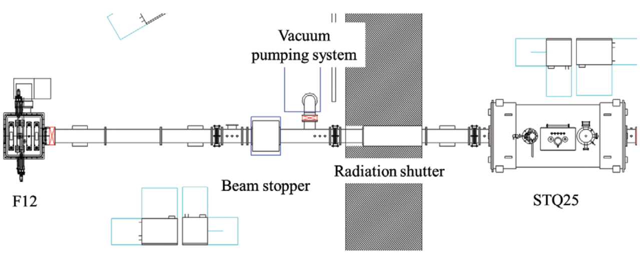

Fig. 1. Layout of the vacuum system (F12∼STQ25).

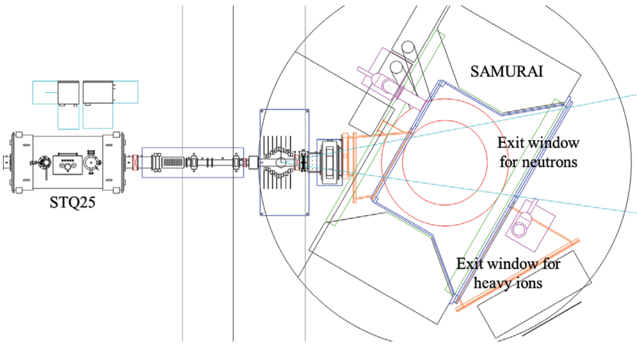

Fig. 2. Layout of the vacuum system (STQ25∼SAMURAI).

*1 Department of Physics, Tohoku University

Calibration methods of the neutron detector array NEBULA

Y. Kondo,*1 T. Nakamura,*1 T. Sako,*1 Y. Kawada,*1 G. S. Lee,*1 N. Kobayashi,*1 R. Minakata,*1 S. Nishi,*1 K. Takahashi,*1 R. Tanaka,*1 N. A. Orr,*2 H. Otsu, Y. Satou,*3 and K. Yoneda

[SAMURAI, NEBULA, neutron detector]

The neutron detector array NEBULA (neutron detection system for breakup of unstable nuclei with large acceptance) is one of the important devices used in SAMURAI at RIBF for measuring four-momentum vectors of fast neutrons at 100–300 MeV emitted in breakup reactions. The specifications of NEBULA have been given in a previous report.[1)] In this report, calibration methods of the light output, position, and time of flight (TOF) are described.

Light output information of the scintillator is important for eliminating γ-ray events through the setting of a threshold value, as well as for defining neutron detection efficiency, which depends on the threshold value. The Compton edge of a 4.4-MeV γ ray emitted from an Am-Be source is an important reference point because the corresponding energy is close to the typical threshold value of 5 MeVee. Since the maximum light output of the secondary proton in the neutron detector is approximately 100 MeVee (electron equivalent), another reference point on the order of several tens of megaelectron volts is necessary for the light output calibration over a wide range. The calibration can be performed by using cosmic-ray muons, which deposit an energy of approximately 30 MeV in the neutron detector.[1)]

The horizontal hit position is determined from the segmentation of scintillator rods, whereas the vertical position is obtained from the time difference between the two photomultiplier tubes attached to the top and the bottom of the neutron detector. Since the vertical position is determined from the timing difference, calibration from the time difference to the vertical position is required. The calibration of the vertical position can be performed using cosmic-ray muons by the coincidence technique with 4m-long horizontal proportional counters, which are mounted in front of and behind each layer of NEBULA.

The zero adjustment of the TOF information can be performed by using high-energy γ rays emitted in heavy-ion collisions. The calibration method was tested by the reaction of an ^{40}Ar beam on a 2-cm thick copper target in the HIMAC facility. Figure 1 shows the two-dimensional histogram of the TOF and light output measured by a neutron detector placed 6-m away from the target at an incident energy of 290 MeV/nucleon, where high-energy γ rays, having an energy of more than 5 MeV, can be seen. High-energy γ-ray events are thus useful for correcting the time-walk effect of leading-edge type discriminators over a wide range. A timing resolution of approximately 200 ps (1σ) was obtained with the 5 MeVee threshold value after excluding the resolution of the TOF start counter. Figure 2 shows the number of γ rays detected with the 5-MeVee threshold as a function of the beam energy. Although the yield of the high-energy γ rays decreases at low incident energy, the calibration method is still feasible at around 250 MeV/nucleon, which is the typical incident energy of RIBF.

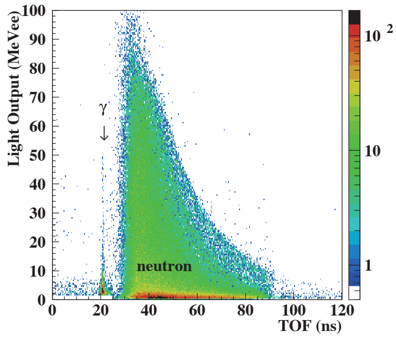

Fig. 1. Two-dimensional plot of the TOF and light output observed in the ^{40}Ar+Cu reaction at 290 MeV/nucleon.

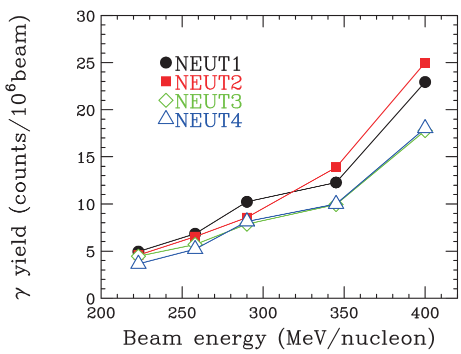

Fig. 2. Yield of high-energy γ rays detected by each neutron detector module placed 6-m away from the target in the ^{40}Ar+Cu reaction as a function of incident energy.

*1 Department of Physics, Tokyo Institute of Technology
*2 LPC Caen, ENSICAEN, Université de Caen, CNRS/IN2P3, Caen France
*3 Department of Physics and Astronomy, Seoul National University

References
1) Y. Kondo et al.: RIKEN Accel. Prog. Rep. **44**, 150 (2011).

Development of SAMURAI-TPC for the Study of the Nuclear Equation of State

T. Isobe, M. Famiano,[*3] A.B. McIntosh,[*4] T. Murakami,[*1] H. Sakurai, R. Shane,[*2] A. Taketani, M.B. Tsang,[*2] W.G. Lynch,[*2] and S.J. Yennello,[*4] for the SAMURAI-TPC Collaboration

[Nuclear equation of state, symmetry energy, unstable nuclei]

The nuclear equation of state (EoS) is a fundamental bulk property of nuclear matter and describes the relationships between the parameters of a nuclear system, such as energy and density. Understanding the nuclear EoS has been one of the major goals of nuclear physics.

Investigation of heavy-ion collision is one of the methods that can be used to study the nuclear EoS. An international collaboration, the Symmetry Energy Project, was formed in FY2009 to study the nuclear EoS over a wide range of nuclear matter densities. The collaboration planned to install a time projection chamber (TPC) in the SAMURAI dipole magnet at the Radioactive Ion Beam Facility (RIBF). By using TPC, experimental observables, such as the flow and yield ratios of charged particles, particularly π^+ and π^- particles, produced in heavy-ion collisions will be measured. At RIBF, a nuclear density of $\rho \sim 2\rho_0$ is expected to be achieved. Experiments using the TPC will allow us to impose constraints on the EoS isospin asymmetry term at high nuclear matter density[1)].

Figure 1 shows an exploded view of the SAMURAI-TPC. The design is based on the EOS-TPC used at the BEVALAC accelerator[2)]. Multi-wire drift chamber (MWDC)-type gas with a cathode-pad readout for the induced signals will be employed for obtaining good position resolution. The target will be located near the TPC entrance. Table 1 lists some specifications of the SAMURAI-TPC.

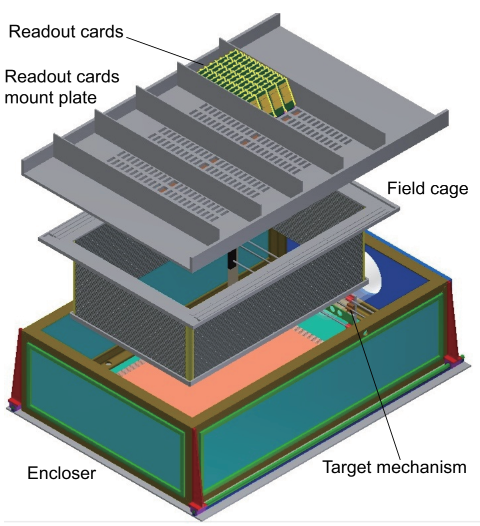

Fig. 1. Exploded view of the SAMURAI-TPC.

Table 1. Specifications of SAMURAI-TPC

pad size	8 mm × 12 mm
number of pads	11664 (108 × 108)
drift length	∼50 cm
chamber gas	P10 (Ar-90% + CH_4-10%)
magnetic field	0.5 T
pressure	∼1 atm
electric field for drift	120 V/cm

This detector is designed to measure ions ranging from pions to oxygen ions, corresponding to a wide range of stopping powers, and consequently, to a wide range of induced signals on the pads. An RHIC-STAR front end electronics (FEE) card[3)] with more than 10k channels will be employed for the first phase experiment with TPC. The dynamic range of the readout is 10 bits, that of the feedback capacitor is 1.6 pF, and a switched capacitor array (SCA)-type analog buffer and Wilkinson ADCs are employed for the digitization of the data.

To determine spatial distortions, and in order to calibrate and monitor the TPC, a laser calibration system will be implemented. We plan to use 16 laser beams for simulating straight particle tracks in the TPC volume. UV-laser beams can produce ionization in gaseous detectors via a two-photon ionization process. We plan to use a Nd-YAG frequency-quadrupled laser ($\lambda = 266$ nm) and to send the laser beams into the TPC field cage through a UV optical fiber system.

The design and construction of the TPC is being performed in the United States. Testing of the TPC by using cosmic rays and UV-laser beams will be commenced after the completion of the construction. After this, the TPC is expected to be shipped to RIBF for first experiment.

*1 Department of Physics, Kyoto University
*2 National Superconducting Cyclotron Laboratory, Michigan State University, United States
*3 Physics Department, Western Michigan University, United States
*4 Cyclotron Institute, Texas A&M University, United States

References
1) L. W. Chen et al.: Phys. Rev. Lett. **94**, 032701 (2005).
2) G. Rai et al.: IEEE Trans. on Nucl. Sci. **37**, 56 (1990).
3) M. Anderson et al.: Nucl. Inst. and Meth. A **499**, 679 (2003).

Design of timing monitoring circuits for time projection chamber readout

K.Urano,[*1] A.Taketani, and H.Baba

A time projection chamber (TPC) will be built for experiments to study equation of state (EOS) of nuclear matter. In order to measure the symmetry-energy term of the EOS, it is necessary to identify the particle species and to measure their momentum vectors simultaneously in the final state of heavy ion collisions over a large phase space.[1] The TPC will be a major detector for experiments and be installed in the SAMURAI magnet. A particle passing through the TPC ionizes gas, and the ions and electrons drift along the applied electric field. Electrons reach the read-out pads and generate electronic signals. The drift time is proportional to the distance between the particle trajectory and the read-out pad. The read-out pad is 8 mm × 12 mm. There are 12000 pads. In addition to the particle trajectory, the deposited energy determines the particle charge. In order to measure the drift time and pulse height, the TPC readout is equipped with the flash ADCs.

The general electronics for the TPC (GET) is currently developed[2] by a collaboration among French, US, and Japanese institutions. The GET includes front-end preamplifiers, analog pipeline buffers, flash ADCs, trigger logic, a digital readout, timing synchronization, and data acquisition. The major specifications of the GET are as follows:

(1) Up to 100 MHz sampling clock.
(2) 12-bit accuracy of AD conversion.
(3) Up to 10 KHz trigger handling without major dead time.
(4) Up to 30,000 channel readout.

In the GET system, 128 channels of preamplifiers, pipeline buffers, and flash ADCs are packed into one printed circuit board (AsAd). Each AsAd board receives the timing signal from a master timing module. Up to 128 AsAd boards form a single GET system, and they are synchronized accurately to run with 100 MHz sampling. A timing monitoring system (SPYBOX) plays an important role for this purpose. The requirements of the SPYBOX are

(1) 128 input channels with differential LVDS from fire wire connectors.[3]
(2) Comparison of the timing between inputs.
(3) A timing resolution of measurement 1 ns.

Figure 1 shows the configuration of the SPYBOX. When the fire wire communication protocol is not employed, each AsAd board sends its reference timing signal to the SPYBOX through fire wires. Each timing signal is received by the LVDS receiver with proper termination in order to isolate the AsAd circuits from multiplexer circuits in the SPYBOX. The LVDS signals are fed into the multiplexers, and two signals are selected and transferred to a time-to-digital converter (TDC) that measures the time difference between two signals. A CPU module controls the multiplexers and reads the data from the TDC. The CPU module also communicates with the rest of the GET system.

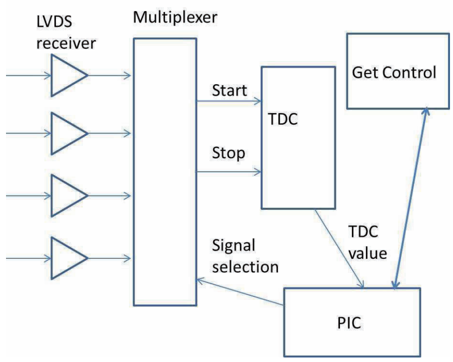

Fig. 1. Block diagram of the SPYBOX

As the LVDS receiver, the ADN4668 from Analog Devices with 200 MHz speed and 100 ps skew time was chosen. The ACAM TDC-GP21 chip with 22 ps resolution, which has 4-wire SPI interface, was selected. The CPU module PIC18F4550 from Microchip was used; it contain a USB interface, digital inputs/outputs, and an SPI interface within a single chip. 74HC251 chips were used for the multiplexers.

When design of the logic diagram and board layout were completed, we realized that the propagation time of 74HC251 is 20 ns. It was too slow for the 100 MHz sampling speed. Therefore, we decided to build a board with 16 channel input boards with slow multiplexers, which was found to be useful for exercising multiplexer control, TDC readout, and communication with the GET systems.

FPGA, which has over 100 I/O pins and programmable logic, is a good candidate of a high speed multiplexer. However, the using FPGA would require careful design to minimize the time timing differences among channels or to calibrate them with respect to the a known timing source.

References
1) T. Isobe et al. in this APR.
2) http://www-actar-get.cea.fr
3) http://www.1394ta.org

*1 Rikkyo University

Development of an amplifier IC with wide dynamic range for Si detector in RIBF SAMURAI spectrometer

A. Takuma*[1], K. Kurita*[1], H. Murakami*[2], A. Taketani*[2], M. Kurokawa*[2], M. Tanaka*[3], H. Negishi*[4]

A large acceptance and high magnetic rigidity spectrometer facility, SAMURAI[1)2)] is under construction at RIBF. We plan to perform a breakup reaction experiment that focuses on a proton rich nuclei structure. The Si tracker needs to detect multiple nuclear fragments from the breakup reaction simultaneously. The atomic number of those fragments is expected to lie between 1 and 50. In the case of Sn and the proton breakup reaction, the difference in the energy deposition is 2500 times larger. In order to realize such measurements, a wide dynamic range of more than 2500 is required.

A dual gain amplifier that satisfies the requirement for this dynamic range has already been developed.[3)] However, it requires twice as many channels for the electronics after the amplifier. We proposed an amplifier, of an integrated circuit, whose output (V_{out}) is proportional to the square root of the input (V_{in}). We call it the square root amplifier.[4)]

Figure 1 shows the diagram of the square root amplifier inside the integrated circuit. This circuit consists of the following three parts; variable feedback, inversion, and sum up. This circuit is an amplifying circuit with negative feedback. The basic objective of the circuit is to increase the feedback according to the input pulse height. The square root function is most suitable for this purpose, because the corresponding energy loss is proportional to Z^2. To realize this nonlinear feedback we approximate it by using a switched resister array. The behavior of this circuit is described using the following three cases.

Case 1 : ($0<V_{AB}<V_{TH1}$) When the applied input voltage is less than the turn-on voltage of comparator1, it behaves as a high resistance device. Thus, $Rf = R1$ because $R2$ and $R3$ are considered to be disconnected.

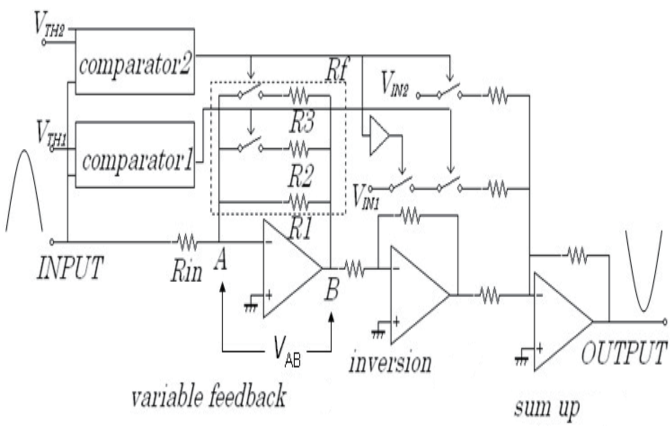

Fig.1. Diagram of square root amplifier

Case 2 : ($V_{TH1}<V_{AB}<V_{TH2}$) When the applied forward voltage is approximately equal to or more than the turn on voltage of compator1, it behaves as a low-resistance device. In case 2, $Rf = R1//R2$ because only $R3$ is considered to be disconnected.

Case 3 : ($V_{TH2}< V_{AB}$) In case 3, $Rf = R1//R2//R3$, because both $R1$ and $R2$ are considered to be connected in parallel.

V_{TH1} is the turn-on voltage of comparator1 and V_{TH2} is the turn-on voltage of comparator2. The symbol "//" indicates a parallel connection. Rf decreases as V_{AB} increases, and the square root shape can be approximated by selecting the proper resisters *R1, R2, and R3*.

The polarity of the input signal is inverted by the variable feedback. It was found that the switching of the resistor array generated discontinuity in the inverted signal. We finally resolved this issue by adding the inversion and the sum up to match the DC the offsets. Output voltage was simulated using Spice® at KEK.

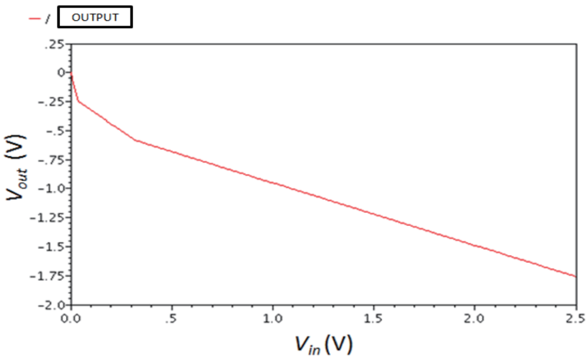

Fig.2. Correlation between V_{in} and V_{out}

Figure 2 shows the input (V_{in}) and (V_{out}) voltage correlation. The curve shown is the simulated curve for the circuit and is similar to line representing of $V_{out} = -\sqrt{V_{in}}$. The curve approximates the square root shape quite well, although it deviates from the function when V_{out} is large. This feature is expected because we designed the function in order to obtain good resolution at low V_{in} for low Z nuclei.

We conclude that our square root circuit will satisfy the requirements of the SAMURAI Si tracker readout. Finally, the data presented herein are simulated values. We need to measure the experimental values after implementing the square root amplifier in an actual integrated circuit.

References
1) K. Yoneda et al.: RIKEN Acc. Prog. Rep. 43, 178 (2010).
2) Y. Togano et al.: RIKEN Acc. Prog. Rep. 44, 146 (2011).
3) M. Kurokawa et al.: RIKEN Acc. Prog. Rep. 43, 182 (2010).
4) S. Yoshida et al.: RIKEN Acc. Prog. Rep. 44, 156 (2011).
®: Simulation Program with Integrated Circuit Emphasis

*[1] Department of Physics, Rikkyo University
*[2] RIKEN
*[3] KEK
*[4] REPIC CORPORATION

Performance evaluation of low-pressure multiwire drift chamber for high-intensity heavy ion beam

H. Miya,[*1,*2] S. Ota,[*1] H. Matsubara,[*1] S. Kawase,[*1] Y. Kikuchi,[*1] K. Kisamori,[*1] M. Takaki,[*1] S. Michimasa,[*1] K. Miki,[*3] S. Noji,[*1] T. Uesaka,[*2] and S. Shimoura,[*1]

[multiwire drift chamber, low pressure gas, high intensity beam]

We have developed low-pressure multiwire drift chambers (LP-MWDCs) for tracking radioactive isotope (RI) beams. The LP-MWDCs are used in BigRIPS and the High-resolution beamline (HRBL) at RI Beam Factory (RIBF). The past developments in the LP-MWDCs has been reported elsewhere[1)].

In the experiments with the SHARAQ[2)] spectrometer, high-resolution spectroscopies are performed with RI beams (mass number: ± 10; beam energy: 100–300 MeV/nucleon; intensity: 1–2 MHz). RI beams are transported to the target position of the SHARAQ by using the dispersion matching technique. The beam tracks on the target have to be measured at an angular resolution of 1 mrad (FWHM) in order to correct the angular spread of the RI beams by using 2 detectors installed at a distance of 500 mm. The position resolution is required to be 500 μm (FWHM). Beam line detectors are required to achieve this resolution on using the high-intensity beam. Here, we report the position resolution and tracking efficiency as a function of the beam intensity (1 kHz–1 MHz) with ^{12}N at the energy of 200 MeV/nucleon.

The LP-MWDCs have 3 anode wire layers and 4 cathode plane layers. The wire in the X plane is stretched in the vertical direction. The wires in the U and V planes are at angles of 30° and −45° with respect to the vertical, respectively. With this configuration, the counting rate per cell can be reduced for the beam with a large width. The cell size and effective area are 9 mm × 9 mm and 216 mm × 144 mm, respectively. The counter gas is pure isobutanem used at a pressure of 10 kPa to diminish the effect of multiple scattering.

The signals are read out from the anode wires for the drift time and energy deposit. The signals are amplified and discriminated by the preamplifier cards (REPIC RPA-132). The leading edge timing and pulse width of discriminated logic signals are recorded with multihit time-to-digital converters (TDCs) (CAEN V1190). The pulse width is the time difference between the leading and trailing edges across the threshold level for amplified signals.

The position resolution was estimated from the residual of $U_{\mathrm{U}} - U_{\mathrm{XV}}$. We considered that errors of the all the planes were of the same value. Here, U_{U} is a hit position in the U layer, and U_{XV} is a hit position along the U axis and is determined from the hit positions in layers X and V. The geometrical configuration of the planes facilitates unambiguous determination of the hit position. Figure 1 (a) shows the position resolutions as a function of the beam intensity at 10 kPa and -1 kV. The position resolution is between 250 and 300 μm (FWHM) for the beam intensity from 1 kHz to 1 MHz. The resolution is sufficient for the required performance.

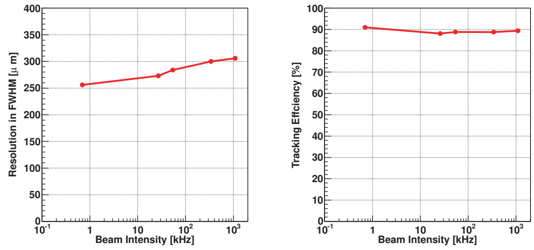

(a) (b)

Fig. 1. Position resolution (a) and tracking efficiencies (b) as a function of beam intensity of ^{12}N at the gas pressure of 10 kPa and applied voltage of -1 kV.

Figure 1 (b) shows tracking efficiencies as a function of the beam intensity at 10 kPa and -1 kV. The tracking efficiency was defined as the ratio of the number of events having the residual within 3 σ to the counted number of beams by using the scintillator at the downstream of the LP-MWDCs. The tracking efficiencies are typically about 90% without the dependence on the beam intensity.

We have developed the LP-MWDC for the tracking detector in the high-resolution experiments with the high intensity heavy ion beam. By using the ^{12}N beam at the intensity between 1 kHz and 1 MHz, the position resolution and tracking efficiency were evaluated. A position resolution was of about 300 μm (FWHM) was achieved at the intensity of 1 MHz; this performance was sufficient for the requirement. The tracking efficiencies are typically 90% without the dependence on the beam intensity.

References

1) H. Miya et al.: RIKEN Prog. Rep. **44** (2011).
2) T. Uesaka et al.: AIP Conf. Proc. **1235** (2010) 308.

*1 Center for Nuclear Study, University of Tokyo
*2 RIKEN Nishina Center
*3 Research Center Nuclear Physics, Osaka University

Development of high-resolution achromatic beam transport for SHARAQ experiments

S. Michimasa,[*1] M. Takaki,[*1] Y. Sasamoto,[*1] H. Baba, M. Dozono, T. Ichihara, N. Inabe, D. Kameda, T. Kawabata,[*2] S. Kawase,[*1] Y. Kikuchi,[*1] K. Kisamori,[*1] T. Kubo, H. Matsubara,[*1] K. Miki,[*3] H. Miya,[*1] S. Noji,[*1] S. Ota,[*1] H. Sakai, S. Shimoura,[*1] H. Suzuki, H. Takeda, H. Tokieda,[*1] K. Yako,[*4] Y. Yanagisawa, and T. Uesaka

[SHARAQ, High resolution beamline, Achromatic optics]

The SHARAQ spectrometer and High-resolution beamline were constructed to realize high-resolution nuclear spectroscopy with RI-induced reactions. The three beam transport option to the SHARAQ spectrometer for each experimental design are as follows: 1. Dispersion matching (DM) transport[2)]; 2. High-resolution achromatic (HRA) transport; and 3. Large-acceptance achromatic (LAA) transport. These transport options mainly differ in the momentum acceptance and momentum resolution of the RI beam. At present, we have successfully developed the ion transport modes of DM and HRA. In the beam study in June 2011, we examined the high-resolution achromatic optics by using a ^{12}Be beam at 200A MeV. We report here the results of the beam study.

The high-resolution achromatic mode is designed to perform event-by-event momentum tagging with a resolution of $\Delta p/p = 1/8500$ and to obtain an achromatic focus at the target position of the SHARAQ spectrometer. Figure 1 shows the designed beam trajectories of the HRA mode. In the figure, the red, green, and blue

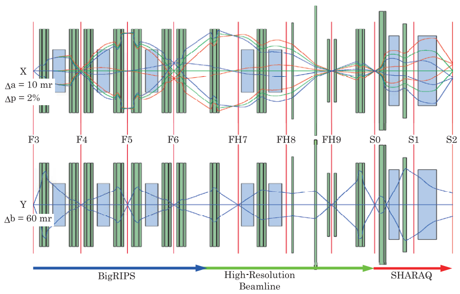

Fig. 1. First-order ion-optical calculation of BigRIPS-SHARAQ beamline. The red, green, and blue lines show the beam trajectories of $\Delta p/p = -1\%$, 0%, and +1%. Angular spreads in X (Y) axis are ±10 (±30) mr.

lines show the beam trajectories of $\Delta p/p = -1\%$, 0%, and +1%, respectively. Angular spreads in the X and Y axes are ±10 mr and ±30 mr, respectively. In the HRA mode, F6 is the dispersive focus for momentum tagging and S0 is the target position of the SHARAQ spectrometer.

*1 CNS, Univ. of Tokyo
*2 Dept. of Physics, Kyoto Univ.
*3 RCNP, Osaka Univ.
*4 Dept. of Physics, Univ. of Tokyo

The tuning of HRA transport started from F3 at BigRIPS, and the beam condition of the secondary beam included a momentum spread of $\Delta p = 2\%$, spot sizes of X: 3.2 mm and Y: 2.9 mm, and angular spreads of X: 10.1 mr and Y: 14.2 mr.

The momentum resolution at the dispersive focus F6 was estimated to be 1/8500 by the measured first-order matrix elements. This value is in good agreement with the designed value, although higher-order components need to be estimated.

Figure 2 shows the beam spots and angular spreads observed from the measurement at S0. From the first-

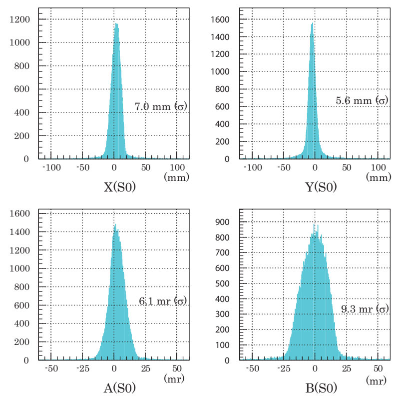

Fig. 2. Distributions of the horizontal position (X), vertical position (Y), horizontal angle (A), and vertical angle (B) at S0.

order optics calculation between F3 and S0, the beam profile at S0 is estimated to be X: 4.8 mm, Y: 4.1 mm, A: 6.7 mr and B: 9.9 mr, respectively.

The observed beam profile was roughly consistent with the estimated profile. However, the spot sizes (X, Y) were slightly large and the angular spreads (A, B) were smaller than the estimated values. The analysis about these difference between observation and evaluation is now on progress. The tuned HRA beam was used in the ^{12}Be(p,n) experiment[3)] performed soon after the present study.

References

1) T. Uesaka *et al.*, J. Phys.: Conf. Ser. **312** (2011) 052028.
2) T. Kawabata *et al.*, Nucl. Instr. Meth. B **266** (2008) 4218.
3) K. Yako *et al.*, *elsewhere in this report.*

Development of WINDS: wide-angle invserse-kinematics neutron detectors for SHARAQ

K. Yako,[*1] H. Sakai,[*2] M. Dozono,[*2] T. Fujii,[*3] S. Kawase,[*3] Y. Kikuchi,[*3] K. Kisamori,[*3] Y. Kubota,[*3] H. Matsubara,[*3] S. Michimasa,[*3] K. Miki,[*4] H. Miya,[*3] S. Noji,[*3] C.S. Lee,[*3] S. Ota,[*2] Y. Sasamoto,[*3] M. Sasano,[*2] S. Shimoura,[*3] M. Takaki,[*3] T.L. Tang,[*3] H. Tokieda,[*3] T. Uesaka,[*2] Z.Y. Xu,[*1] and R. Yokoyama[*3]

[Charge-exchange reaction, inverse kinematics, neutron counter]

The spin-isospin excitations in nuclei provide a good basis for studying a nuclear structure. Although charge-exchange reactions, such as (p,n) and $(^3\mathrm{He},t)$ reactions at intermediate energies, are established probes used to study these excitations in stable nuclei, the charge-exchange study of unstable nuclei is currently only in its early stage. Experiments in inverse kinematics are challenging mainly because the recoils on the probe particle are small. Generally, the detection of recoil particles with kinetic energies below ∼3 MeV is required for the study of Gamow-Teller excitations (See Fig. 1 in Ref. 1 for a specific case of a $^{12}\mathrm{Be}(p,n)$ measurement).

We constructed a facility at SHARAQ where the (p,n) reactions on unstable nuclei can be studied. It consists of a liquid-H_2 (LH_2) target in a scattering chamber made with 1.6 mm-thick aluminum, the magnetic spectrometer SHARAQ, and the wide-angle inverse-kinematics neutron detectors for SHARAQ (WINDS). A schematic view of the facility is shown in Fig. 1. The missing mass spectra of the (p,n) reaction are obtained from the scattering angle of the neutron (θ_{lab}) and its kinetic energy. These spectra are measured by the time-of-flight (TOF) method using WINDS. The timing information of the start of the TOF is obtained from the plastic counter ($1\,\mathrm{mm}^t$) at F-H10, located 2 m upstream of the target position.

WINDS is a set of neutron counters on each (left and right) side of the target, covering the angular region $60° < \theta_{\mathrm{lab}} < 120°$. The distance between the target and the counter wall is 180 cm. The left (right) counter wall consists of 30 (29) plastic scintillators (BC408) of $60 \times 10 \times 3$ cm^3. These scintillators are placed such that the 3-cm-wide planes face the target. Each scintillator is viewed using H7195 PMTs located on both ends through the light guides. The charge information from each PMT is digitized by a CAEN V792 QDC. The timing information is processed by a leading-edge discriminator (LeCroy 4413) and digitized by CAEN V767 TDC.

The efficiency of the neutron counter depends on the energy of neutrons as well as the threshold on light output. The typical efficiency with a counter threshold of 200 keV$_{ee}$ is estimated by using the code NEFF7[2], and it is calculated as 0.36 for 2-MeV neutrons. The efficiency calibration was performed by locating a neutron source of ^{252}Cf at the target position with a "standard" NE213 liquid scintillator at a distance of 80 cm from the source. This allowed us to determine the efficiency of the BC408 counters relative to that of the NE213 counter, whose absolute efficiency as well as energy-/threashold-dependence were well known[2]. The detailed data analysis is currently in progress.

The first (p,n) measurement was performed successfully in June 2011[1].

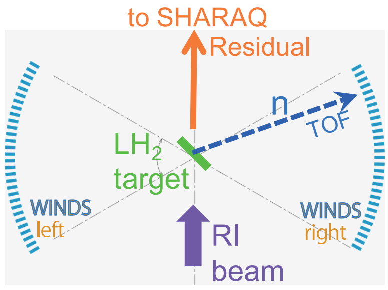

Fig. 1. Schematic view of the setup of the (p,n) measurement in inverse kinematics.

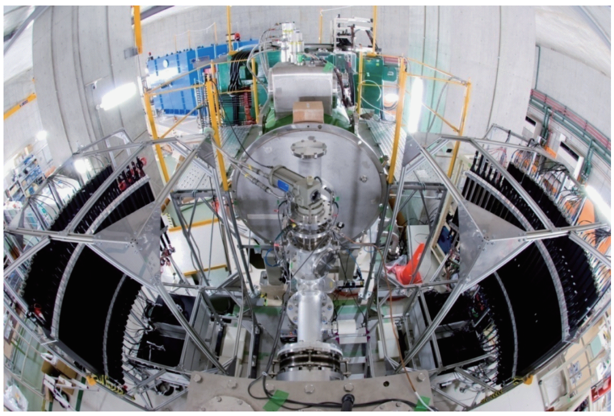

Fig. 2. A Photo of WINDS.

References

1) K. Yako *et al.*: "Measurement of $^{12}\mathrm{Be}(p,n)^{12}\mathrm{B}$ reaction at 200A MeV in inverse kinematics", elsewhere in this Report.
2) G. Dietze and H. Klein: Program NEFF7 (unpublished).

*1 Department of Physics, University of Tokyo
*2 RIKEN Nishina Center
*3 CNS, University of Tokyo
*4 RCNP, Osaka University

Development of CVD Diamond Detector

S. Michimasa,[*1] M. Takaki,[*1] M. Dozono, S. Go,[*1] E. Ideguchi,[*1] K. Kisamori,[*1] H. Matsubara,[*1] H. Miya,[*1] S. Ota,[*1] H. Sakai, S. Shimoura,[*1] A. Stolz,[*2] T.L. Tang,[*1] H. Tokieda,[*1] T. Uesaka, and R.G.T. Zegers[*2]

[CVD diamond detector, Time resolution]

We are developing diamond detectors as a detector with extremely good timing resolution. In FY2010, we fabricated a diamond detector with striped cathodes. A photograph of the diamond detector is shown in Fig. 1. The detector is made of polycrystalline chemical vapor deposition (pCVD) diamond crystal. Its dimensions and thickness are 30 mm×30 mm and 0.2 mm, respectively. The dimensions of the cathode are 28 mm×28 mm. The detector has a pad on one side (Side A) and four strips on the other side (Side B). On Side A, four readout wires are bonded to the corners. On Side B, two readout wires are bonded to both edges of each strip. The width of the four strips are 9 mm, 5 mm, 5 mm, and 9 mm. The detector has a total of 12 readouts for deducing the hit position and timing. During operation, 400 V is applied to the pad (Side A).

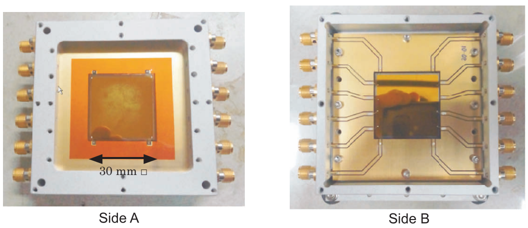

Fig. 1. Photographs and cathode pattern of the diamond detector.

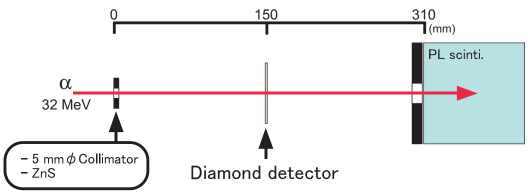

Fig. 2. Setup of the irradiation experiment involving on α beam.

To examine the basic performance of the detector, we performed an irradiation experiment in 2011. The experimental setup is shown in Fig. 2. The experiment was performed in the E7b course at the RIKEN accelerator facility, and a 32-MeV α beam was used. The beam intensity was controlled to be approximately 1000 counts/s and the beam spot was typically 1 cm diameter at the diamond detector.

For processing the signals from the diamond detector, RF preamplifiers were connected to its readouts. We obtained charge information and time of flight (TOF) between the diamond detector and the plastic scintillator. The TOF was measured by using TAC and 13-bit ADC modules.

We determined the detection efficiency of the diamond detector by examining the coincidence ratio between the diamond detector and the plastic scintillator. The detection efficiency of the diamond detector was estimated to be almost 100% for 32-MeV α particles. The energy deposited in the diamond detector corresponded to that of 320A-MeV ^{12}N isotopes. The diamond detector is therefore usable for intermediate-energy light RI beams.

To deduce the timing resolution of the diamond detector, we obtained the time difference spectrum between signal pulses from both edges of a strip of the diamond detector (Fig. 3). The width of the spectrum

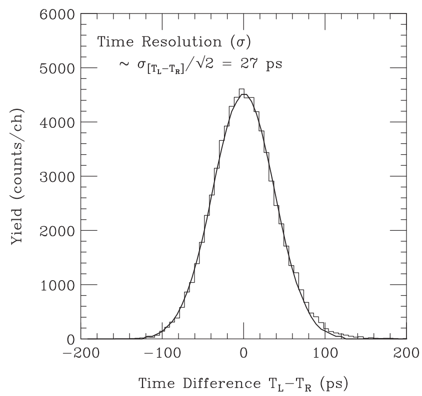

Fig. 3. Time difference spectrum between both edges of a strip of the diamond detector. We deduce the time resolution to be 27 ps from the spectrum.

is equal to the product of $\sqrt{2}$ and the timing resolution for an extremely small beam spot size. Actually, the beam spot size on the diamond detector was estimated to be about 1 cm, and therefore, the main part of the width was considered to be associated with the hit position dependence. However, the upper limit of the time resolution of this diamond detector was estimated to be 27 ps (σ).

As the next step, we are going to install two diamond detectors at the starting point and at the end point of the SHARAQ beamline in order to measure the TOF with extremely good resolution. By combining the precise TOF and the high momentum resolution of the SHARAQ spectrometer, we plan to perform a unique experiment to precisely measure the mass of radioactive nuclei far from stability.

*1 CNS, Univ. of Tokyo
*2 NSCL, MSU, USA

High proton polarization at room temperature by changing the laser pulse structure

T. Kawahara,*1*2 L. T. Tang,*3 A. Shibusawa,*1*2 T. Uesaka,*2 and T. Wakui*4

A polarized solid proton target for RI beam experiments has been developed at the RIKEN and the Center for Nuclear Study, University of Tokyo[1)]. By means of electron polarization in photo-excited triplet states of pentacene, proton polarization of approximately 20% has been achieved in a low magnetic field of 0.1 T and at a high temperature of 100 K and has been applied to RI beam experiments[2,3)]. Recently, we succeeded in increasing the proton polarization at 100 K by changing the pulse structure of laser light[4)].

An Ar ion laser (Coherent TSM25) is used for the optical excitation of pentacene molecules. Continuous wave (CW) light from the laser is mechanically pulsed by using an optical chopper[5)]. The dependences of proton polarization on the duty factor and repetition frequencies are closely related to the properties of the photoexcited triplet states of pentacnene. By changing the settings of the optical chopper, we can scan the duty factor and the repetition frequency in the range of 5–50% and 0.75–10.5 kHz, respectively.

Protons in a single crystal of para-Terphenyl doped with pentacene (0.05 mol%) with a size of 6 ×3 ×2 mm^3 were polarized at room temperature (∼300 K) and in a magnetic field of about 0.3 T. The laser power was set to 0.2 W. Electron polarization in the photoexcited triplet state of pentacene was produced by irradiation of laser light. The electron polarization was transferred to protons with a cross polarization technique.

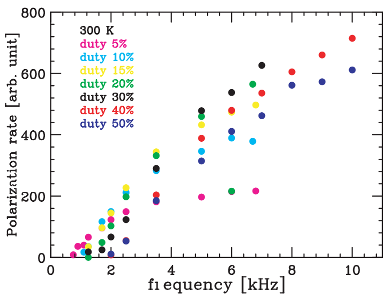

Fig. 1. Polarization rate measured by changing the duty factor and repetition frequency at 300 K.

Figure 1 shows the proton polarization rate as a function of the repetition frequency. Data for different duty factors are plotted. In the present study, we found that the proton polarization rate was maximum when the repetition frequency and the duty factor were 10.5 kHz and 40%, respectively. At low frequencies, the finiteness of triplet-state lifetime bottlenecks the increase of the proton polarization, whereas at the high-frequency limit, the polarization rate is considered to be proportional to the duty factor[4)]. The experimental data at room temperature do not follow the proportionality relation at a high duty factor of 30–50%. For example, the polarization for a 50% duty factor is smaller than that for a 30% duty factor even at 7 kHz. One possible explanation is that, a temperature rise due to the light irradiation leads to an increase in the spin relaxation rate. To confirm the hypothesis, we measured the polarization after changing the lase power (Fig. 2).

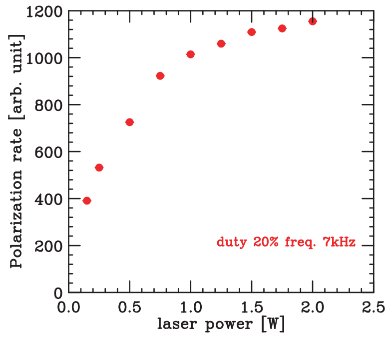

Fig. 2. Polarization rate measured after changing the laser power at 300 K. The duty factor and repitition frequency were 20% and 7 kHz, respectively.

The duty factor and repetition frequency were set to 20% and 7 kHz, respectively. Figure 2 shows a clear trend of saturation of proton polarization at a high laser power. The average laser powers corresponding to 30% and 50% duty factors in the above case are 0.06 W and 0.1 W. The latter condition is already out of the range where proton polarization rate is proportional to the laser power. Thus, it is concluded that cooling of the target is critical for achieving high proton polarization at room temperature.

*1 Department of Physics, Toho University
*2 RIKEN Nishina Center
*3 Center for Nuclear Study, Graduate School of Science, University of Tokyo
*4 Cyclotron and Radioisotope Center, Tohoku University

References

1) T. Uesaka *et al.*: Eur. Phys. J. **150** (2007) 71.
2) T. Uesaka *et al.*: Phys. Rev. C. **82** (2010) 021602.
3) S. Sakaguchi *et al.*: Phys. Rev. C. **84** (2011) 024604..
4) T. Kawahara, *et al.*: RIKEN Accelerator Progress Report vol. 44 (2011).
5) T. Wakui *et al.*: Nucl. Intrum. Methods Phys. Res. A **550** (2005) 521.

Development of a SCRIT luminosity monitor

T. Suda,[*1] T. Adachi[*1] T. Amagai[*1] R. Kitazawa[*1] K. Koizumi[*3] K. Kurita[*3] N. Lundkvist[*1,*4] Y. Miyashita[*2] T. Miyamoto[*1] R. Ogawara,[*3] T. Ohnishi[*2] H. Takehara[*5] T. Tamae[*1] S. Tamaki[*3] M. Wakasugi[*2] and S. Wang[*1]

[SCRIT, electron scattering, bremsstrahlung, luminosity]

A luminosity monitoring system is being constructed for use in electron scattering experiments on short-lived nuclei at the SCRIT electron scattering facility[1)] of the RI Beam Factory. This system monitors the collision luminosity between the stored electron beam and the target short-lived nuclei. The monitoring system measures the number of bremsstrahlung photons produced by the target trapped in the SCRIT device and determines the luminosity online on the basis of the well-established cross section of the bremsstrahlung process[2)].

The system consists of a position detector and a calorimeter for measuring the spatial distribution and energy of the bremsstrahlung photons, respectively, as shown in Fig. 1. It is placed 670 cm downstream from the center of the SCRIT device.

The position detector consists of two identical fiber-scintillation detectors that cross each other and is placed in front of the calorimeter. Each detector has 16 optically isolated fiber scintillators (BFC-10) of 2 x $2\,\mathrm{mm}^2$ cross section with 2 mm-spacing, and they are coupled to a 4 x 4 multi anode PMT (Hamamatsu H6568).

The calorimeter is a Pb-glass Cerenkov detector. The Pb glass has dimension of 100 x 100 x 300 mm^3 and is coupled to a 5 " phototube (Hamamatsu R1250).

Figure 2 shows the spatial distribution of the bremsstrahlung from the target trapped in the SCRIT system. Stable ^{133}Cs ions are employed as targets, and the stored electron energy is 300 MeV. The solid (open) circles show the distributions in the vertical (horizontal) direction.

Since background bremsstrahlung due to collisions with residual gases in the storage ring is inevitable, bremsstrahlung measurements with and without the target Cs ions are alternately repeated for background subtraction.

Although the obtained data are preliminary, it is worth pointing out that the width of both the distributions appears consistent with the typical angular spread of the bremsstrahlung, an order of $\theta \sim m_e/E_e = 1.7$ mrad. for $E_e = 300$ MeV that corresponds to $\sigma_{x,y} \sim 11.4$ mm at 670 cm downstream. Precise measurement of the distribution is essential to determine the accurate acceptance of the system for the bremsstrahlung process.

Detailed data analysis and GEANT4 simulation are underway.

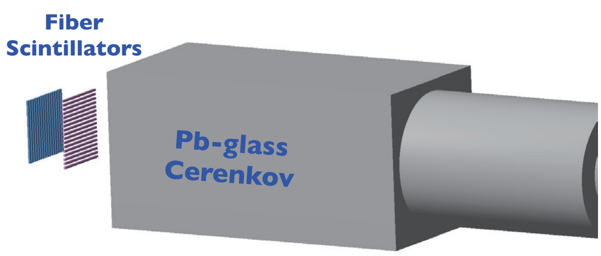

Fig. 1. Bremsstrahlung luminosity monitor.

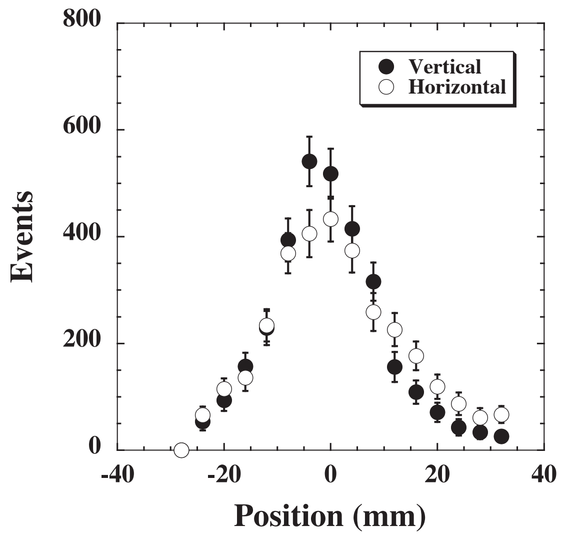

Fig. 2. Spatial distribution of the bremsstrahlung ($E_\gamma \geq$ 100 MeV)

*1 Tohoku University
*2 RIKEN
*3 Rikkyo University
*4 Uppsala University
*5 Nagaoka University of Technology

References
1) M. Wakasugi et. al. :RIKEN Acce. Prog. Rep.**43**, (2009) 1.
2) L. I. Schiff: Phys. Rev.**83**, 252 (1951).

Construction of ISOL system at SCRIT facility

K. Koizumi,[*1] S. Ichikawa, T. Ohnishi, R. Ogawara,[*1] K. Kurita,[*1] Y. Miyashita and M. Wakasugi

[ISOL, SCRIT, unstable nuclei]

To realize electron scattering for short-lived nuclei, the SCRIT (Self-Confining Radioactive isotope Ion Target) technique has been developed[1]. This technique mainly needs an electron storage ring and a low-energy RI (Radioactive Isotope) beam. The electron storage ring has been constructed and developed[2]. This year, the ISOL (Isotope Separator On-Line) system has been constructed at the SCRIT facility to produce a low-energy RI beam, and the commissioning was performed using stable Xe isotopes. Figure 1 shows a schematic layout of the ISOL system. This system consists of an integrated-target-ion source and a beam transport line. In this paper, we present details of this system and results of the commissioning.

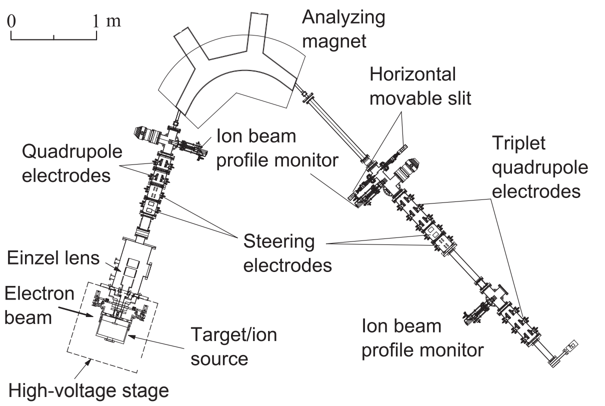

Fig. 1. Schematic layout of the ISOL system.

In the ISOL system, photofission of uranium is induced for RI production. The electron beam is accelerated up to 150 MeV by the RTM[2](Race Track Microtron), and it is focused on a uranium target. On the basis of simulations[3], the total fission rate is expected to be 3×10^{11}fissions/s for a 50g uranium target and a electron beam current of 6.7 μA at an energy of 150 MeV.

For the wide capability of the elements of fission products, we have constructed a FEBIAD (Forced Electron Beam Induced Arc Discharge)-type ion source. This ion source is located on the high-voltage stage, where an ino beam acceleration voltage less than 50 kV is applied. Specifications of the ion source have been presented in Ref. 3.

The beam transport line consists of an einzel lens, eight electrostatic steering devices, eight electrostatic quadrupoles, a 120° analyzing magnet with a radius of 0.8 m, and three ion beam profile monitors. Using the analyzing magnet and two horizontal movable slits positioned after the magnet, the target isotope of interest is separated from the RI beam, which includes many different isotopes. The ion beam profile monitor can simultaneously measure the ion beam current and beam shape. The performance of this monitor has been discussed in Ref. 4.

The commissioning of the ISOL system was performed using stable Xe isotopes. The acceleration voltage was 20 kV. After the optimization of the operating condition of the ion source and beam line, the mass resolution and overall efficiency were measured at the focal point of the analyzing magnet. Here, the overall efficiency included the ionization, extraction, and the transmission efficiencies. Figure 2 shows the measured mass spectrum of Xe isotopes. The rms mass resolution of ^{129}Xe was 1660. The measured current of the ^{129}Xe beam was 61 nA. On the basis of the calibrated Xe production rate, the obtained overall efficiency was about 21%.

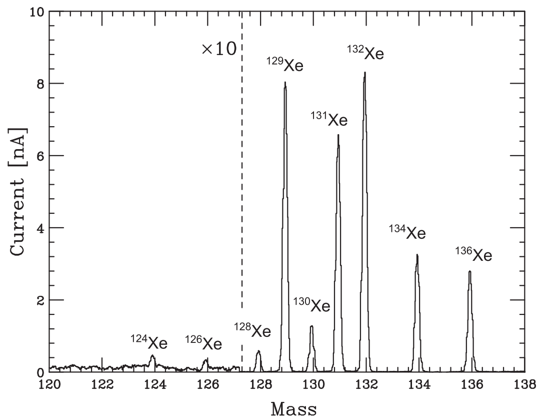

Fig. 2. Mass Spectrum of Xe isotopes.

In summary, we constructed an ISOL system and commissioning was performed. The measured rms mass resolution and overall efficiency in the case of stable Xe isotopes were about 1660 and 21%, respectively. To improve the mass resolution and the overall efficiency, tuning and improvement of the ISOL system are under way.

References
1) M.Wakasugi et al., Nucl. Instr. and Meth. A **532**, 216(2004)
2) M.Wakasugi et al., RIKEN Acc. Prog. Rep. **43**,1(2010)
3) Y.Miyashita et al., RIKEN Acc. Prog. Rep. **44**,171(2011)
4) M.Togasaki et al., RIKEN Acc. Prog. Rep. **44**,173(2011)

*1 Department of Physics, Rikkyo University

Design of Recoil Arm for the SCRIT experiment

R. Ogawara,*1 S. Tamaki,*1 K. Kurita,*1 and M. Wakasugi*2

[SCRIT, Recoil ion, Electron scattering]

The SCRIT (Self-Confining Radioactive Ion Target) electron scattering facility[1,2] is now under construction. Electrons scattered from target ions trapped in the SCRIT device are detected and their angular distribution is obtained. A recoil ion detector referred to as "Recoil Arm" is being designed. It will be used for the determination of the luminosity distribution in the ion trapping region along the beam axis. We shall also try to use the Recoil Arm for estimating the contribution of residual gas ions, which are trapped simultaneously with target ions in scattering events.

Figure 1 shows a schematic of the Recoil Arm. It consists of three main components focus meshes, two quadrupole benders[3], and a channeltron array consisting of 15 channeltrons. Ions that hare recoiled from the trapping region in the SCRIT are accelerated by the electrostatic potential applied to the SCRIT electrode. The meshes consist of two mesh electrodes. The electrostatic potential applied to the first electrode is slightly higher than that applied to the SCRIT. The second electrode which is at earth potential, has a curved structure (radius of curvature : 100 mm) so that the azimuthal angular acceptance is large. Two quadrupole benders are used to deflect transported recoiled ions and reduce the background produced by the synchrotron radiation. The channeltrons are arranged in a line so as to minimize dead space. The aperture of every channeltron is rectangular (15mm×30 mm).

Perpendicularly recoiled ions as a result of forward electron scattering are extracted and parallel transported to the channeltron array. The counting rates of the 15 channneltrons indicate the trapped ion distribution, i.e., luminosity, along the beam axis. We can identify the mass number of the recoil ions in scattering events by measuring the time delay from the instant forward scattered electrons are detected by the plastic scintillator, and estimate the attributable fraction of residual gas ions in scattering events.

The off-line test bench of the Recoil Arm is now under construction. We will be studying the performance of the Recoil Arm before its installation in the SCRIT device.

References

1) M. Wakasugi et al. Nucl. Instr. and Meth. **A 532**, 216 (2004)
2) M. Wakasugi et al RIKEN Acc. Prog. Repo. **43**,1 (2010)
3) H.D.Zemsn et al. Rev. Sci. Instrum. **48**,8 (1977)

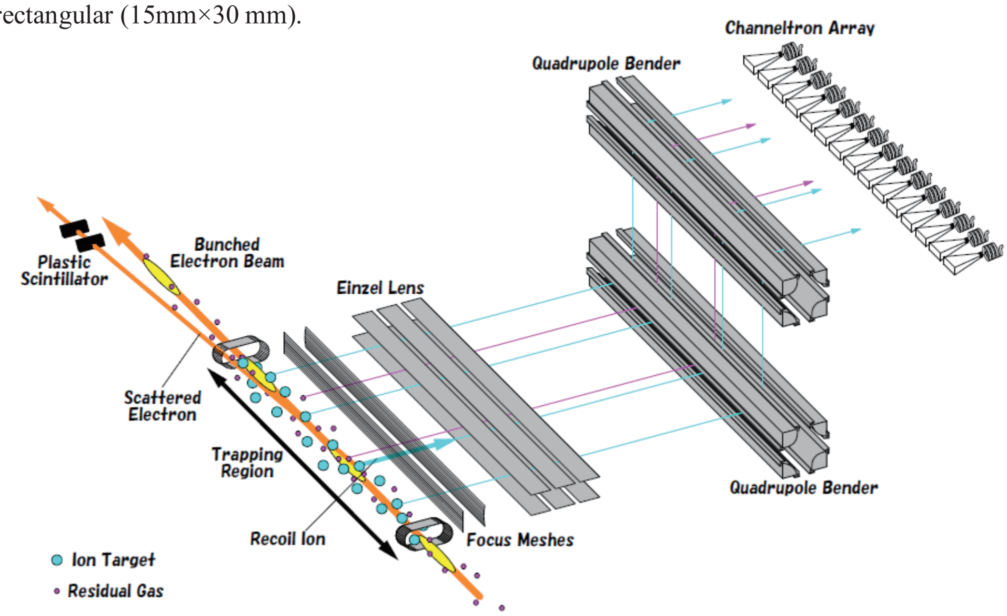

Fig.1. Schematic diagram of the Recoil Arm

*1 Department of Physics, Rikkyo University, Japan
*2 RIKEN Nishina Center, Japan

Improvement of luminosity in the SCRIT electron scattering experiment

S. Tamaki,[*1] T. Adachi,[*2] T. Amagai,[*2] S. Ichikawa, T. Ohnishi, R. Ogawara,[*1] R. Kitazawa,[*2] K. Kurita,[*1] K. Koizumi,[*1] T. Suda,[*2] H. Takehara,[*3] T. Tamae,[*2] M. Togasaki,[*1] M. Hara, T. Hori, Y. Miyashita, T. Miyamoto,[*2] S. Wang,[*2] and M. Wakasugi

[SCRIT, luminosity, electron scattering]

The SCRIT (Self-Confining RI Ion Target)-electron scattering facility was constructed at RIBF in 2009 [1]). An test experiment using stable ^{133}Cs ions was started in 2011, and we succeeded in performing Cs-ion trapping in the SCRIT device and observing elastically scattered electrons from trapped Cs ions[2)]. A tenfold luminosity L of around 10^{27} cm^{-2} sec^{-1}, as compared to that achieved in the R&D study conducted at KSR [3,4)], was obtained in this experiment.

An electron beam loss monitor, which consists of double plastic scintillators (20 × 100 × 10 mm^3), was installed at the downstream end of the SCRIT device in SR2. This monitor detects a part of the electromagnetic showers originating from electron beam losses. It is verified by the luminosity monitor that the counting rate of the loss monitor responds linearly to the luminosity[5)]. The result is shown in Fig. 1. However the luminosity monitor is under construction, and the absolute value of luminosity for this monitor is not calibrated. Hence, the absolute value of the luminosity of the loss monitor is calibrated by the electron detector, which detects elastically scattered electrons from trapped Cs-ions[2)]. Therefore, the beam loss monitor can be used as an online luminosity monitor, and the variations of luminosity, as shown in the figures below, are measured by it.

Time evolution of the luminosity during target-ion trapping was measured at an electron beam current of 200 mA. The result is shown in Fig. 2(a). The luminosity decays with time, and it was maintained over 10^{26} cm^{-2} sec^{-1} for more than 1 sec. We found that the lifetime of the luminosity strongly depends on electron beam stability, and futher details in this regard are now being studied.

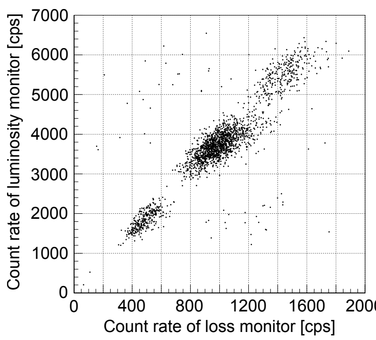

Fig. 1. Correlation chart of the loss monitor and the luminosity monitor.

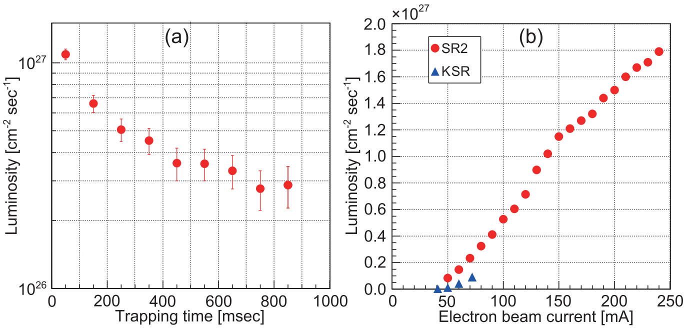

Fig. 2. (a) Time variation of luminosity when electron beam current is about 200 mA. (b) Electron beam current dependence of luminosity for a trapping time of 45 ms.

Figure 2(b) shows the electron beam current dependence of the luminosity for a trapping time of 45 ms, and the corresponding data obtained from the R&D study at KSR are plotted for comparison. The luminosity observed in the present experiment agrees well with that obsereved in the R&D study below 80 mA, and it was extended to 250 mA for SR2. It was found that the luminosity linearly increased with an increasing electron beam current. As a result, a luminosity of 1.8×10^{27} cm^{-2} sec^{-1} was reached at 240 mA.

In summary, we found that the electron beam loss monitor is useful as an online luminosity monitor, and the luminosity measured was about twenty times better than that measured in the R&D study.

*1 Department of Physics, Rikkyo University
*2 Research Center for Electron Photon Science, Tohoku University
*3 Department of Electrical Engineering, Nagaoka University of Technology

References

1) M. Wakasugi et al.: RIKEN Acc. Prog. Rep. **43**, i(2010).
2) S. Wang et al., in this report.
3) M. Wakasugi et al.: Phys. Rev. Lett. **100**, 164801(2008).
4) T. Suda et al.: Phys. Rev. Lett. **102**, 102501(2009).
5) T. Suda et al., in this report.

Design of magnetic spectrometer for the SCRIT project

T. Adachi,[*1] T. Suda,[*1] T. Tamae,[*1] and S. Wang,[*1]

[electron scattering, unstable nuclei, magnetic spectrometer]

The SCRIT electron scattering facility is under construction at the Nishina Center, and the research and development experiments are underway[1)].

In order to identify elastic electron scattering, an energy resolution of at least $\Delta E/E \sim 10^{-3}$ is required. A magnetic spectrometer is needed for this purpose. The large gap is required for this spectrometer, because (1) a large solid angle is needed owing to a low luminosity ($\sim 10^{-27}$ cm^{-2} s^{-1}), (2) a wide scattering angle region has to be covered simultaneously, and (3) the length of the target region is about 40 cm for the SCRIT experiment.

Figure 1 shows the arrangement of the spectrometer system. This system consists of a horizontally bending dipole magnet and front and rear drift chambers. The two detectors sandwich the magnet. Scattered electrons' trajectories are reconstructed from the tracks measured by the drift chambers and the magnetic field distribution of the magnet, and finally, the momenta of the scattered electrons and their scattering positions in the target region are obtained.

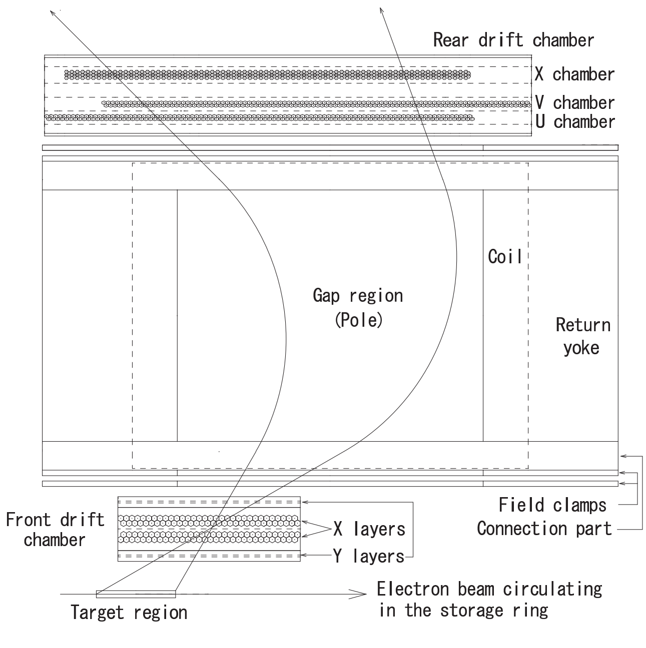

Fig. 1. Arrangement of the spectrometer system. Scattered electron trajectories for the minimum and maximum scattering angles are also shown.

The dipole magnet is rectangular, and its dimensions are 3.20 m (width) × 1.26 m (height) × 1.40 m (length). The total weight of the magnet is about 45 ton. The gap in the magnet is 1.70 m (width) × 0.29 m (height) × 1.40 m (length). The maximum magnetic field B is 0.8 T, and the typical radius of curvature of a scattered electron is 1.25 m for an electron energy of 300 MeV. The electric energy consumption is about 130 kW.

The scattering angle coverage by the spectrometer is $30° \leq \theta \leq 60°$, and the vertical angular acceptance is about $\Delta\phi \sim 10°$. The range of the momentum transfer q measured at electron energies ranging from 150 MeV to 300 MeV is $0.40 \leq q \leq 1.50$ fm^{-1}. In order to obtain a large solid angle, the magnetic spectrometer is placed as close as possible and parallel to the beam line. The solid angle of the spectrometer is about 90 msr.

The pole and the return yoke are composed of pure iron, and the field clamps are composed of carbon steel. The shape of magnet is the so-called window-frame type, which affords homogeneous magnetic fields in the gap. The magnetic field distribution was calculated using the OPERA-3D code[2)]. The inhomogeneity of magnetic field is less than about 0.2% for a 1.4-m wide and 0.28-m high spectrometer gap ; the homogeneity is less than 1.5% even when the gap is up to 1.6 m. Two field clamps are used at each end to minimize the leakage of the magnetic field. The magnetic field at the circulating electron beam line was less than 5 Gauss. It is unlikely to affect the orbit of the circulating electron beam. The installation of this magnet in the SCRIT facility is expected to be finished around the end of February 2013.

The front drift chamber consists of two X layers (wires stretched vertically) and two Y layers (wires stretched horizontally). The rear drift chamber consists of U (wires tilted at an angle of +45°), V (wires tilted at an angle of −45°), and X layers. Except for the Y layers, each layer is composed of hexagonal drift cells, and the length of the sides of the hexagon is 10 mm. For the Y layers, the cells are square with sides measuring 10 mm.

References

1) M. Wakasugi *et. al.*, : RIKEN Accel. Prog. Rep. **44**, 168 (2011).
2) OPERA Vector Field Code, http://www.cobham.com/.

[*1] Electron and Photon Science (ELPH), Tohoku University

Measurement of Electron Beam Profile by Two-Dimensional Interferometer

H. Takehara,[*1] Y. Miyashita, T. Ohnishi, T. Hori, M. Hara, S. Ichikawa, M. Togasaki,[*2] S. Tamaki,[*2] K. Koizumi,[*2] R.Ogawara,[*2] K. Kurita,[*2] and M. Wakasugi

[SCRIT, electron scattering, beam profile monitor, interferometer, luminosity]

We constructed a synchrotron radiation monitor with a two-dimensional interferometer and measured the electron beam profile of an electron storage ring (SR2: SCRIT equipped RIKEN Storage Ring) used for the SCRIT project. In the SCRIT project, which aims to achieve the world's first electron scattering off RIs, it is necessary to achieve a high luminosity (>10^{27}cm^{-2}m^{-1}).[1)] The electron beam profile influences luminosity, and therefore, an electron beam profile monitor is needed for the accelerator operation.

A two-dimensional interferometer can be used for obtaining the beam profile from an interference pattern on the basis of the van Citterut Zernike theorem.[2)] When synchrotron radiation enters through a two-dimensional quad slit, a horizontal and a vertical interference pattern is formed and recorded by a CCD camera. The interference pattern can be denoted by

$$I(x) = I_0 \mathrm{sinc}\left\{\frac{\pi a x}{\lambda L}\right\}^2 \left\{1 + \gamma_x \cos\frac{2\pi D x}{\lambda L}\right\} \quad (1)$$

where $I(x)$ is the intensity of the interference pattern, a is slit width, D is the distance between the pair of slits, L is the distance from quad slit to the CCD camera, λ is the selected wavelength, γ_x is the complex degree of coherence. The van Citterut-Zernike theorem associates the complex degree of coherence and the beam profile. The beam profile is the inverse Fourier transform of the complex degree of coherence:

$$\gamma_x = \int \rho(x) \exp\left\{-i\frac{2\pi D x}{\lambda F}\right\} \mathrm{d}x \quad (2)$$

where $\rho(x)$ is the beam profile of horizontal, and F is distance from synchrotron radiation source to quad slit.

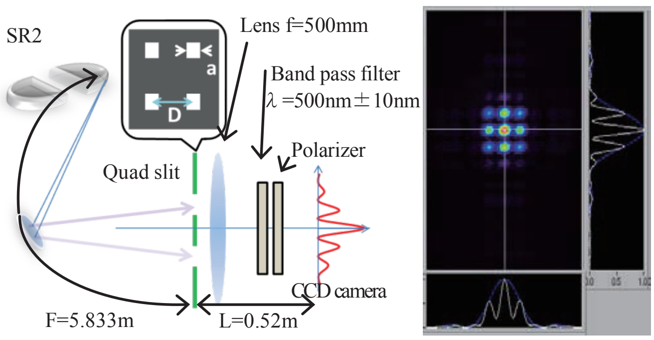

Fig.1 Setup of the two-dimensional interferometer and interference pattern

When the beam profile is assumed to be a Gaussian distribution, the RMS beam size is expressed by

$$\sigma_x = \frac{\lambda F}{\pi D}\sqrt{\frac{1}{2}\ln\frac{1}{\gamma_x}} \quad (3)$$

The best slit distance depends on the beam size. Therefore, we developed a system that could adjust slit distance with a stepping motor. The control of the interferometer and the measurement of the beam profile were executed using LabVIEW.

Figure 1 shows the system setup and an observed interference pattern. The interference pattern was acquired after removing the background from the image observed with the CCD camera. Then, the RMS beam size is calculated. The refresh rate of this system is 100ms.

The typical beam profile for the injection mode was σ_h=1000μm, σ_v=200μm, and that for the SCRIT experimental mode was σ_h=600μm, σ_v=300μm.

Figure 2 shows the luminosity in electron scattering off ^{133}Cs as a function of the beam cross section, which was measured by the present profile monitor. The cross section in Fig.2 was obtained by multiplying the beam profile of σ_h and σ_v. The result showed that the luminosity was inversely proportional to the cross section.

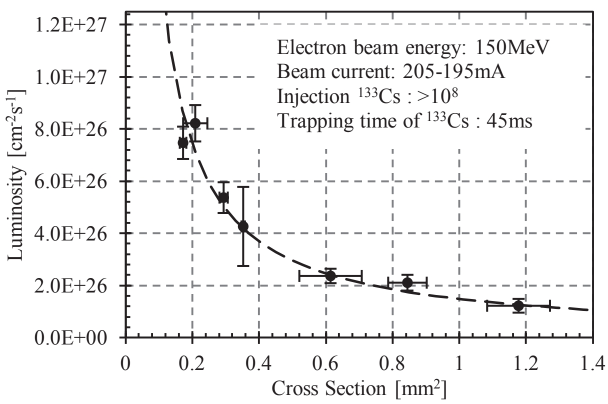

Fig.2 Luminosity as a function of the beam cross section. The dashed line denotes a luminosity of 2.67×10^{27} / (cross section).

References

1) M. Wakasugi et al.: Eur. Phys. J. A42, (2009), p.453–456.
2) M. Masaki and S. Takano: Proc. 5th DIPAC France (2001), p.142

*1 Department of Electrical Engineering, Nagaoka University of Technology
*2 Department of Physics, Rikkyo University

Remodeling of TARN II dipole magnet for the Rare-RI ring

Y. Yamaguchi, H. Suzuki, T. Fujinawa, D. Nagae,*1 A. Ozawa,*1 M. Wakasugi, K. Banba,*2 S. Kimura,*2 T. Yamanaka,*2 and Y. Yano

[Isochronous ring design]

One of the most important topics of study is the isochronous design of the Rare-RI ring. The ring consists of six magnetic sectors, and each magnetic sector consists of four TARN II dipole magnets. The TARN II Dipole (TARN II-D) is a rectangular bending magnet with a radially homogeneous magnetic field. However, it is not acceptable in our isochronous design. Until last year, we considered modifying the pole face of TARN II-D to produce a first-order isochronous field[1]. However, it was found that scraping the TARN II-D would be very costly. Thus, we decided to place a thin laminated iron plate on the pole face of the TARN II-D as the first step, and this can will be done at reasonable cost. Furthermore, we will install trim coils in the TARN II-D to tune the isochronous magnetic field precisely. This remodeling will be performed for the two outer dipoles among the four dipoles in each magnetic sector. Recently, we began remodeling the magnet. In this paper, we report the present status.

The shape of the thin laminated iron plate, which is chosen on the basis of a three-dimensional magnetic field analysis and our simulation program[2], is appropriate for providing a tilted radial magnetic field distribution. The plate has nine layers, and each layer is 0.3 mm thick; however, the widths of the nine layers are different.

Figure 1 shows a simulation result that expresses the relative difference of revolution times (determined from the time taken for 2000 revolutions) inside the ring as a function of momentum. We optimize the shape of the thin laminated iron plate to obtain a field of 1.5 T, and the corresponding simulation result is shown by the black circles. In our measurement technique, the velocity of the particle is fixed. Therefore, it is necessary to change the magnetic field strength of the ring each time we measure the mass of particles with a different m/q. The result denoted by red circles is obtained by assuming 1.0 T, and this magnetic field strength corresponds to a particle with m/q = 2. The result represented by blue circles is for an assumption of 1.6 T, and this magnetic field strength corresponds to a particle with m/q = 3. Consequently, for 1% momentum spaces inside the ring, is achieved an isochronism of 10^{-4} using the ideal shape of the thin laminated iron plate.

On the basis of the consideration mentioned above, the laminated plate was fabricated by using soft magnetic iron sheets (SUYP0). We then glued the laminated plate to the pole face of the TARN II-D with epoxy resin adhesive (EP007 manufactured by Cemedine Co., Ltd.), as shown in Fig. 2. The thickness of the adhesive was about 0.2 mm typically, and the heterogeneity in the thickness did not influence the shape of the magnetic field. The tensile strength of the adhesive was about 10 N/mm^2. This value is considerably larger than the magnetic attraction force for 1.6 T (1.02 N/mm^2).

In order to verify whether the shape of the laminated plate is appropriate, we will soon perform magnetic field measurements for this remodeled magnet.

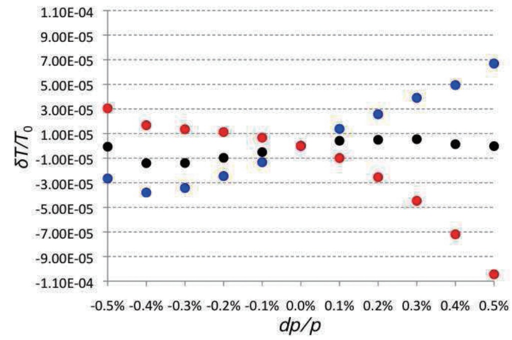

Fig. 1. Simulation results expressing the relative difference of revolution times (determined from the time taken for 2000 revolutions) as a function of momentum. Results indicated by black circles assume 1.5 Tesla, red circles assume 1.0 Tesla, and blue circles assume 1.6 Tesla.

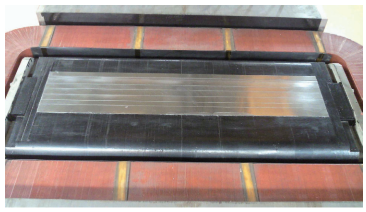

Fig. 2. Photograph of the pole face of the TARN II-D with a thin laminated iron plate. The laminated plate was glued using epoxy resin adhesive.

References
1) Y. Yamaguchi et al.: RIKEN Accel. Prog. Rep. **44**, 1111 (2011).
2) H. Suzuki et al.: RIKEN Accel. Prog. Rep. **43**, 186 (2010).

*1 Institute of Physics, University of Tsukuba
*2 Cemedine Co., Ltd.

Fourth progress report on the development of a portable multi-reflection time-of-flight mass spectrograph for SLOWRI – First separation of (molecular) isobars

P. Schury,*1 Y. Ito,*1 M. Wada, S. Nakamura,*1 S. Naimi, A. Ozawa*1, V. A. Shchepunov.*2, T. Sonoda, A. Takamine, K. Okada, and H. Wollnik*3

[Atomic masses, isobar separator, unstable nuclei]

Development of a multi-reflection time-of-flight (MRTOF) mass spectrometer for use with radioactive ion (RI) beams at the future SLOWRI facility continues to progress. We have previously reported mass resolving powers of $r_m > 100,000$ achieved with short observation times[1]. This should allow the MRTOF to precisely measure masses of very short-lived nuclei.

Prior to entering the MRTOF, ions from a gas cell[2] or thermal source are transported by multipole RF ion guides to a small RF-multipole trap. The trap is filled with low pressure ($P < 10^{-2}$ mbar) He gas, wherein ions can be accumulated and cooled. The center electrodes in the trap can be pulsed to create a dipole electric field which ejects the ions orthogonally with respect to the trap inlet through a 0.6 mm hole in the electrodes. Ions then enter the MRTOF, undergo any number of reflections, and are released to a detector to measure their time-of-flight.

The time-of-flight for any ion species can be given by $t = a + b \cdot n$, where n is the number of laps, b is the circulation time and a is the single-pass (no reflections) time-of-flight. Before a high-resolution mass measurement can be performed with the MRTOF, the approximate b-value for the species of interest, as well as the value of n at which the resolving power is maximum – the so-called time focus – must be known. If the approximate b-value is known for the species of interest, the position of the time focus can be determined simply by scanning over n. The result of such a scan for $A/q \approx 19$ is shown in Fig. 1.

While Fig. 1 is rather busy, a few things are immediately clear. Firstly, the time focus is near $n = 250$ laps. Secondly, by plotting in this way, we can see that the time focus truly appears to be a focus, although it still has some aberrations that could eventually be removed by better tuning of the MRTOF optics. Finally, we see the separation of isobars. The shallow lines running through the plot represent lighter (A=17, 18) ions that were also in the mix. The main peak was identified by comparison with the time-of-flight of a known species, $^{39}K^+$.

Due to a combination of the extremely low rate of the right-most peak (a few per hour) and the contamination from non-isobaric molecules, it was not readily possible determine the identity of the low-yield species by performing peak-fitting to determine the time-of-flight. However, it was possible to determine the circulation time (b-value) using the 2D plot. Being another measure of the time-of-flight, the b-value can be used to determine the identity of an ion species.

Although we do not demonstrate a high resolving power here, we do show that the MRTOF can quickly separate isobars and determine the identity of very low yield species. The capacity to separate isobars and perform precision mass measurements is anticipated be demonstrated online during FY2012/2013.

Table 1. Time-of-flight data used to identify ion species in Fig. 1

Species	m [u]	b-value [ns]	Calc. m [u]
H_3O^+	19.01784	15316.9(1)	–
$^{15}NH_4^+$	19.03086	15322.0(5)	19.0305(9)
$^{14}NDH_3$	19.04010	15326.2(5)	19.0409(9)

*1 Tsukuba University, Ibaraki, Japan
*2 SRL, Manchester, England
*3 University of Gießen, Gießen, Germany
*4 Sophia University

References

1) P. Schury et al., RIKEN Accel. Prog. Rep. 44, 189 (2011)
2) M. Wada et al., Nucl. Instrum. Methods **B204**, 570 (2003)

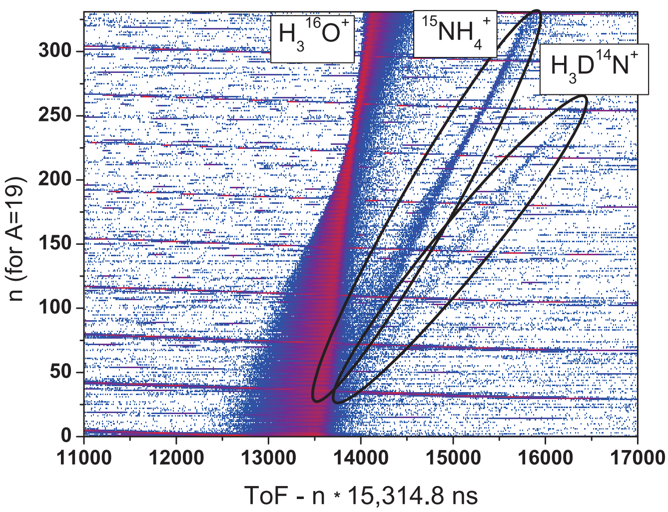

Fig. 1. Separated and uniquely identified $A = 19$ molecular isobars .

ElectroSpray ion source for mass calibration of MR-TOF mass spectrograph used in superheavy element mass measurement

S. Nakamura[*1], Y. Ito[*1], S. Naimi, A. Ozawa[*1], P. Schury[*1], T. Sonoda, A. Takamine[*2], M. Wada, H. Wollnik[*3]

The binding energy is a key observable in the determination of the island of stability in superheavy elements. Since the discovery of these elements, only few masses were measured directly[1)], and most of the other known heavy masses were determined indirectly via the α-decay chain, which is not always reliable. Moreover, the uncertainties increase along the decay chain owing to error propagation. Unambiguous determination of superheavy element masses is planned using the Multireflection Time-of-Flight (MR-TOF) mass spectrograph developed at the SLOWRI facility[3)]. The MR-TOF has shown excellent performance[4)]: a mass resolving power of 100,000 to 200,000 can be easily achieved with a few milliseconds, with a mass precision of 10^{-6} to 10^{-7}, which meets the experimental requirement for mass measurements of superheavy elements. Usually, the mass is determined by comparing the time of flight of the unknown ion with that of known ions having very similar masses, preferably isobars. However, superheavy elements do not have isobars of stable nuclei. Therefore, an ElectroSpray ion source[2)] (ESI) was built to deliver heavy molecules covering the entire mass range required. The ESI will be connected to the MR-TOF mass spectrograph and the Gas-filled Recoil Ion Separator[5)] (GARIS), so that simultaneous mass measurements of superheavy elements and their molecular isobars are possible.

Figure 1 shows the details of the ESI ion source. To produce molecular ions, methanol and water are mixed in 1:1 ratio and then, formic acid is added (0.1% of the total liquid volume). The ionized liquid is transported to the ESI needle, where the ions experience a strong electric field resulting from the voltage difference between the needle and the capillary. This forms the Taylor cone, which forces the liquid to evaporate toward the capillary and allows for the formation of free molecular ions or their clusters. The ions are transported into the capillary by air flow to the RF carpet, where they are stopped near the surface by a radiofrequency pushing field (RF) and driven by a DC field to the exit hole (0.5 mm diameter). The RF carpet consists of a layer of planar printed circuit board with 54 ring electrodes, each 0.15 mm wide and positioned 0.15 mm away from the adjacent electrode (see Fig.1). The RF voltage between neighboring electrodes is typically 100 V at 4.28 MHz, with the DC voltage decreasing by about 1 V for each electrode from the outer ring to the inner one, thereby creating a gradient field.

[*1] Tsukuba University, Ibaraki, Japan
[*2] Aoyama Gakuin, Tokyo, Japan
[*3] University of Gießen, Gießen, Germany

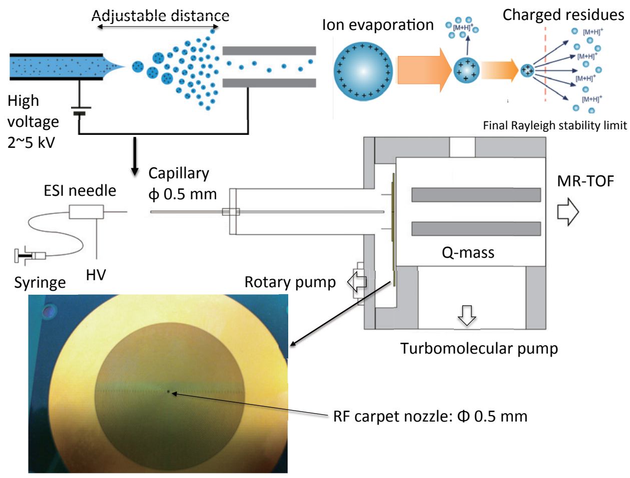

Fig. 1. ElectroSpray ion source and RF carpet experimental setup.

The molecular ions reach the RF carpet exit hole and are then transported to the second chamber, where a quadrupole mass filter (Q-mass) is placed for mass selection. In the first test, a cluster of two methanol molecules could be transported with the RF carpet into the Q-mass. The observed molecular ion current behind the RF carpet is around 15 % of the total ion current observed before the RF carpet. Considering the rough mass selectivity of the RF carpet, the transmission efficiency could be close to unity. The ESI source will soon be installed at the MR-TOF to investigate the wide variety of molecular ions produced by the source.

References
1) M. Block *et al.*, Nature(London) **463**, 785 (2010).
2) I. Manisali *et al.*, TrAC Trends in Analytical Chemistry **24**, 243 (2006).
3) M. Wada *et al.*, Hyperfine Interact. **199**, 269 (2011).
4) P. Schury *et al.*, RIKEN Accel. Prog. Rep. **44**, 166 (2011).
5) K. Morita *et al.*, Eur. Phys. J. **A21**, 257 (2004).

Development of a tapered-RFQ pre-cooler for multi-reflection time-of-flight mass spectrograph

Y. Ito,[*1] M. Wada, P. Schury,[*1] T. Sonoda, S. Naimi, A. Takamine,[*2] S. Nakamura,[*1] H. Mita,[*1] K. Okada,[*3] H. Wollnik,[*4] V. A. Shchepunov,[*5] and A. Ozawa,[*1]

[Mass measurements, unstable nuclei, low energy beam]

A multi-reflection time-of-flight mass spectrograph (MRTOF-MS) has been developed for the precise mass measurement of short-lived radioactive ions (RI). The RI produced at the RIKEN Projectile Fragment Separator (RIPS) with high energy are converted into a low-energy ion beam by a prototype slow RI facility (SLOWRI) and then transported to the preparation trap located before the MRTOF-MS[1–3].

In the He gas filled preparation trap, the continuous low-energy ion beam is accumulated, cooled, and bunched, then injected into the MRTOF-MS where the mass is determined. The tapered-RFQ pre-cooler is at the same pressure as that of the trap and has an effective electric field in the direction of the trap; therefore, it is considered as a part of the trap. Figure 1 shows the typical time sequence in one measurement cycle (left).

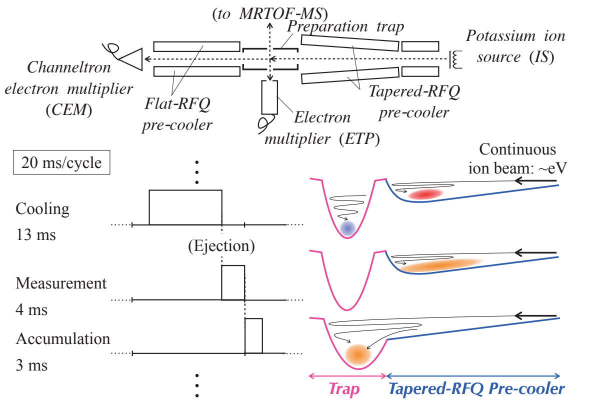

Fig. 1. (Top) A schematic view of the configuration around the preparation trap. (Bottom) The time sequence of the trap and the ion cloud motion for each phase.

As shown in Fig. 1, the ions are blocked before the entrance of the trap during the cooling and measurement phases. To transport them into the trap for the next cycle after blocking, a drag force is necessary. Typically, such drag force is achieved by segmented RFQ rods with axial DC voltages. In the case of the tapered-RFQ, drag force is achieved simply by virtue of the taper shape[4]. This structure can also prevent sharp voltage changes in the axial DC potential.

[*1] University of Tsukuba, Ibaraki, Japan
[*2] Aoyama Gakuin University, Tokyo, Japan
[*3] Sophia University, Tokyo, Japan
[*4] University of Gießen, Gießen, Germany
[*5] SRL, Manchester, England

A tapered-RFQ pre-cooler was built and tested using the present experimental setup[4]. The inner radius of the front end is 0.5 mm smaller than that of rear end. Its efficiency was compared to that of the flat-RFQ pre-cooler built with the same inner radius. Figure 2 shows the efficiency for various values of gas pressure as a function of the trap entrance voltage which probes the ion energy. When the tapered-RFQ pre-cooler is used, the efficiency is found to increase by a factor of 10 during pre-cooling(Fig. 2(b)). This suggests that the ions are accumulated in the tapered-RFQ. In addition, the efficiency from which starts to increase is 2 V smaller compared to the case without pre-cooling. This implies that the ions are cooled by 2 eV in the tapered-RFQ pre-cooler before they enter the trap.

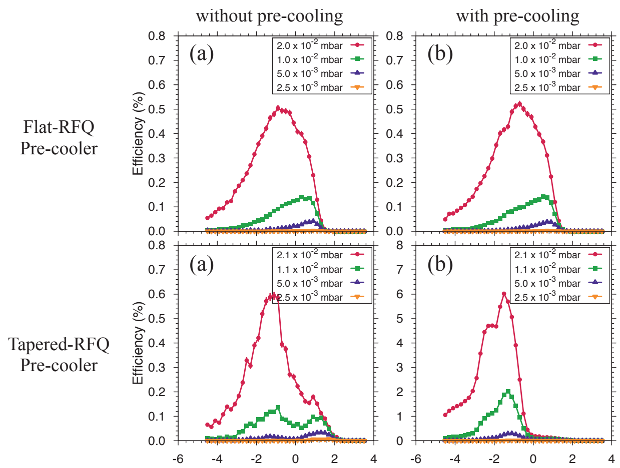

Fig. 2. The efficiency for each type of pre-cooler (a) without pre-cooling and (b) with pre-cooling in the pre-cooler.

The principle of the tapered-RFQ pre-cooler was proven, and as expected it has significantly higher efficiency than the flat-type pre-cooler, as expected. We plan to use this tapered-RFQ pre-cooler for the on-line mass measurement of short-lived RI.

References

1) M. Wada *et al.*: Nucl. Instrum. Meth. B **204**, 570 (2003).
2) Y. Ishida *et al.*: Nucl. Instrum. Meth. B **241**, 983 (2005).
3) P. Schury *et al.*: Eur. Phys. J. A **42**, 343 (2009).
4) Y. Ito *et al.*: RIKEN Accel. Prog. Rep. **44**, 161 (2010).

Status of the resonance ionization laser ion source for SLOWRI PALIS

T. Sonoda, M. Wada, H. Tomita,*1 C. Sakamoto,*1 T. Noto,*1 T. Takatsuka,*1 T. Shinozuka,*2 Y. Matsuo, H. Iimura,*3 T. Furukawa,*4 T. Kubo, P. Schury,*5 S. Naimi, Y. Ito,*5 S. Nakamura,*5 H. Mita,*5 H. Miyatake,*6 S. Jeong,*6 H. Ishiyama,*6 N. Imai,*6 Y. Watanabe,*6 Y. Hirayama,*6 M. Huyse,*7 Yu. Kudryavtsev,*7 P. Van Duppen*7

The proof of principle of a resonance laser ionization gas cell[1)] has been tested. This device is for use of PArasitic Laser Ion-Source (PALIS), which will be implemented at the SLOWRI facility[2)]. We plan to install a laser ionization gas cell near the second focal plane (F2) in the fragment separator (BigRIPS), which can recycle unused RI-beams before removed by F2-slits for beam purification. This scheme will realize two simultaneous experiments involving high- and low-energetic RI-beams in every on-line BigRIPS experiment. Before installing the actual PALIS system in the fragment separator, we developed a prototype laser ionization gas cell with a beam extraction system and achieved following:

(1) Off-line resonance laser ionization test for stable Co, Cu, Fe, Ni, Ti, Nb, Sn, Pd inside the gas cell and its beam extraction to high vacuum region. Fig. 1 (a) shows an example of a detected ion signal for Co in the scan of the first step laser wavelength while the second step laser is fixed to the autoionizing wavelength.

(2) Time profile measurement for evaluating ion behavior inside the gas cell and the SextuPole Ion beam Guide (SPIG)[3)]. We have developed a new differential pumping method for ion transport from high pressure used for gas cell (typically 100 kPa in Ar) with an exit hole of diameter 1 mm, to a high-vacuum region (10^{-4}Pa). We observed that ions can be transported by an assisted force from a gas jet inside the SPIG.

(3) Feasibility study for in gas cell/in gas jet laser spectroscopy[4)]. During the resonance ionization processes, hyperfine splittings as well as isotope shifts can be measured to determine the nuclear spins, moments, and charge radii. We are investigating the resolution for cases of ionization inside the gas cell and inside the supersonic gas jet. Fig. 1 (b) shows an example of an ionization scan by the first step laser for Fe. A reduction in Doppler broadening can be observed in the gas jet spectrum, though this was predominantly attributed to intrinsic broadening caused by laser power and laser linewidth. This spectroscopy technique will also be applied to evaluate the neutron damage to the nuclear reactor through measurement of the abundant ratio of metastable Nb produced by inelastic neutron scattering from stable Nb.[5)]

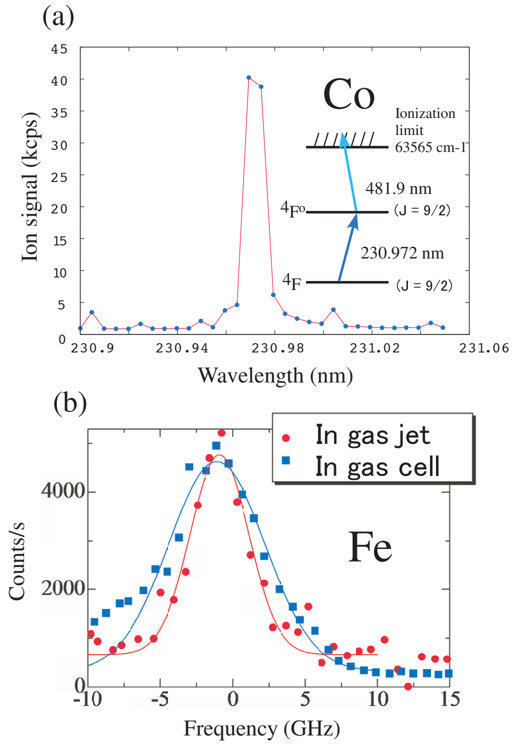

Fig. 1. (a) Scan of the first step laser for Co; the second step laser was tuned to the wavelength of 481.9 nm [1)]. (b) Evaluation of the peak resolution for ionization inside the gas cell and inside the gas jet. The displayed scan is by the first step laser for Fe.

References

1) Yu. Kudryavtsev *et al.*: Nucl. Inst. Meth. B **114** 350 (1996).
2) M. Wada *et al.*: Hyp. Int. **196** 43 (2010).
3) H. J. Xu, et al.,Nucl. Inst. Meth. A333 (1993) 274.
4) T. Sonoda *et al.*: Nucl. Inst. Meth. B **267** 2918 (2009).
5) H. Tomita *et al.*: Hyp. Int. **196** 169 (2010).

*1 Faculty of Engering, Nagoya University
*2 Cyclotron and Radioisotope Center, Tohoku University
*3 Japan Atomic Energy Agency (JAEA)
*4 Department of Physics, Tokyo Metropolitan University
*5 Department of Physics, Tsukuba University
*6 High Energy Accelerator Research Organization (KEK)
*7 Nuclear Spectroscopy group, IKS, K.U. Leuven (Belgium)

Mass separator for KEK isotope separation system (KISS)

H. Ishiyama,[*1] Y. Hirayama,[*1] Y.X. Watanabe,[*1] N. Imai, [*1] M. Oyaizu,[*1] H. Miyatake,[*1] S.C. Jeong,[*1],
K. Niki,[*1] M. Okada,[*1] M. Wada and T. Sonoda,

The β-decay properties of neutron-rich isotopes with neutron numbers $N = 126$, which act as progenitors in the r-process path forming the third peak (A ~ 195) in the r-abundance element distribution, are considered to be critical for understanding astrophysical sites for producing heavy elements such as gold and platinum[1]. A proposal for constructing the KEK Isotope Separation System (KISS) has been accepted, and the installation of the KISS has commenced.

Nuclei around N = 126 such as ^{200}W, ^{201}Re, ^{202}Os could be obtained via the multi-nucleon transfer reaction using a low-energy (~7 MeV/u) ^{136}Xe beam and ^{198}Pt as the target nucleus. The nuclei produced are collected using a gas catcher system and separated using a mass separator with the help of a laser resonance ionization technique. The collected nuclei are transported to the detection system, which consists of a tape transport system and detectors. In 2011, the gas catcher, laser system, and mass separator were installed in E2, E3 and J3. Fig. 1 shows pictures of KISS in E2 and E3 experimental rooms.

The ion-optical configuration of the mass separator is EQD-MD-MQD-F1-EQT-ED, where EQD, MD, MQD, EQT and ED are electrostatic quadrupole doublet, magnetic dipole, magnetic quadrupole doublet, electrostatic quadrupole triplet, and electrostatic deflector for beam switching, respectively. F1 indicates the first focal point of the mass separator, where a slit system is positioned. The basic parameters of the ion-optical elements are listed in Table 1.

Fig. 1. Pictures of the mass separator for KISS in E2 (right panel) and E3 (left panel) experimental rooms.

*1 High Energy Accelerator Research Organization (KEK)

Element	Geometry
EQ	r_{bohr} = 30 mm, L = 100 mm
MD	ρ_D = 1353 mm, θ_D = 45°, Gap = 70 mm
MQ	r_{bohr} = 65 mm, L = 100 mm
ED (parallel plate)	L = 100 mm, Gap = 60 mm

Table 1 Basic parameters of ion-optical elements.

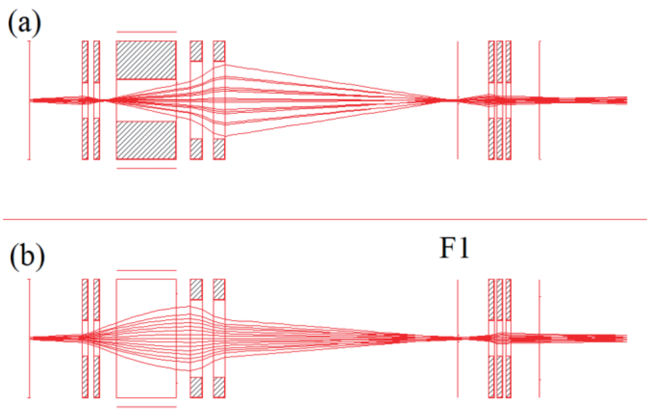

Fig. 2 Ion-beam trajectories at the KISS mass separator. The calculation was performed using GIOS[2] code. Panels (a) and (b) show vertically (y) and horizontally (x) projected trajectories, respectively, of 1^+ ions with A = 210 and E = 60 keV.

Figure 2 shows a result of the ion-optical simulations for 1^+ ions with A = 210 and E = 60 keV. Resultant mass dispersion is 2.06 cm/% and x- and y-magnifications are 0.7 and 0.85, respectively, at F1. An ion beam having an emittance of 10 π・mm・mrad was assumed for the calculation. The expected mass-resolving power is 900, which is sufficient for selecting only ions having mass numbers of interest using a horizontal slit at the focal plane, F1. After mass separation at F1, the beam of interest is transported via EQT and ED to the detection position. The ED is used to switch on/off the beam for β-decay measurement. A beam spot of diameter 10 mm was obtained at the detection position.

The installation of the main components of KISS will be completed in FY2011, and the off line test will start in the beginning of FY2012.

References

1) S.C. Jeong et al.: KEK Report 2010-2
2) H. Wollnik et al.: AIP Conf. Proc. 177 (1988) p. 74.

Differential pumping test of gas cell system for KISS

Y. Hirayama,[*1] S.C. Jeong,[*1] H. Miyatake,[*1] H. Ishiyama,[*1] Y.X. Watanabe,[*1] N. Imai,[*1] M. Oyaizu,[*1] K. Niki,[*1] M. Okada,[*1] M. Wada, T. Sonoda, Y. Matsuo, P. Van Duppen,[*2] Yu. Kudryavtsev,[*2] and M. Huyse[*2]

[gas cell, differential pumping, laser ion source]

We have been constructing the KEK Isotope Separation System (KISS) to study the beta-decay properties of neutron-rich isotopes with neutron number around $N = 126$ from the astrophysical viewpoint[1,2]. In the KISS, a gas cell filled with argon gas at a pressure of 50 kPa, which stops and collects unstable nuclei, is used in conjunction with a laser resonance ionization technique essential for selectively extracting isotopes of interest. For extracting the isotopes as an ion-beam with sufficiently low emittance and high efficiency, the gas-cell system employs differential pumping in order to reduce the pressure in a vacuum chamber from 50 kPa to several 10^{-4} Pa. When the ions leave the gas cell, their transit through the SextuPole Ion Guide (SPIG)[3] is supported by the gas jet, but at the same time, the gas jet makes it difficult to apply the necessary high voltage.

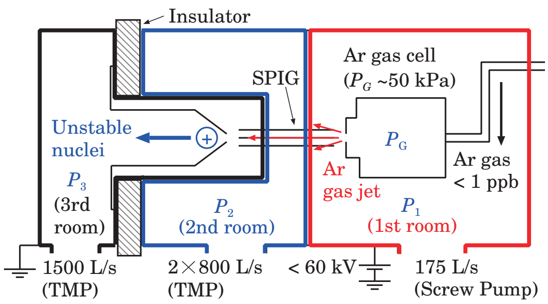

Fig. 1. Schematic view of the gas cell system. The boundaries of first, second, and third rooms are indicated by the red, blue and black thick lines, respectively.

Figure 1 shows a schematic view of the gas-cell system. The vacuum chamber of the gas-cell system is separated into three rooms for differential pumping. The fist, second, and third rooms are pumped down by a 175 l/s screw pump, two 800 l/s turbo molecular pumps (TMP) and a 1500 l/s TMP, respectively. The three neighboring rooms are connected by a SPIG with an aperture diameter 3 mm. The conductance between two adjacent rooms was calculated to be 0.15 l/s. The gas cell filled with argon gas at a pressure of 50 kPa is placed in the first room. The conductance of the gas cell exit, which had an aperture 1 mm in diameter and 0.5 mm long, was calculated to be 0.095 l/s. The second room plays an important role in differential pumping and ensures that the vacuum conditions in the third room are sufficient for applying a high voltage to the first and second rooms (several 10^{-4} Pa).

Pressures P_1, P_2 and P_3 of first, second, and third rooms, respectively, were measured as a function of the pressure, P_G, of the gas-cell and are shown in Fig. 2 together with the calculated values. The calculated values took into account the pumping speed, conductance of the apertures, and spread of the gas jet. The measured P_1 agrees with the calculated value, resulting in a gas-jet spread angle of 3.9°. In contrast, the measured values of P_2 (P_3) were lower (higher) than the calculated values by a factor of 2 (i.e., better (worse) vacuum than expected), which may be due to gas jet formation.

In addition, we observed a large deviation in P_3 around $P_G = 40$ kPa, suggesting that a larger amount of gas arrived into the third room due to the formation of a strong gas jet. The pressure P_3 at $P_G = 50$ kPa was 6.5×10^{-4} Pa, and we successfully applied a voltage as high as 30 kV. The experimental result of the Leuven group indicates that we can expect both good transmission through the SPIG and extraction system and good beam emittance under this condition.

The differential pumping test of the gas-cell system proceeds as scheduled. The laser system for resonant ionization was installed at J3 room under the E2 experimental room. Offline tests for extracting ion beams from the gas-cell system have started and a stable nickel ion-beam ionized using the laser resonance ionization technique was successfully extracted.

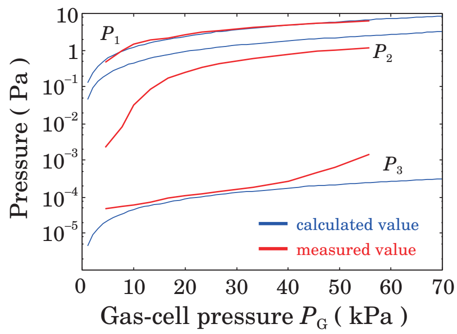

Fig. 2. Pressures of P_1, P_2 and P_3 measured and calculated as a function of the pressure P_G.

References
1) S.C. Jeong et al.: KEK Report 2010-2.
2) Y. Hirayama et al.: RIKEN Accel. Prog. Rep. 44 (2011) 25.
3) H.J. Xu et al.: Nucl. Instru. and Method A333 (1993) 274.

*1 High Energy Accelerator Research Organization (KEK)
*2 Instituut voor Kern-en Stralingsfysica, KU Leuven, Belgium

Development of target system for GARIS

K. Morimoto, D. Kaji, H. Haba, T. Sumita,[*1] A. Yoneda, K. Ozeki, Y. Kudou and K. Morita

[GARIS, super heavy element, target]

The previously used target system[1)] for a gas-filled recoil ion separator (GARIS) has been replaced with a new system. The new target system can operate with three sizes of target wheels. A 60 cm target wheel is newly available for an experiment using GARIS. Figure 1 shows three rotating wheels that can be mounted on the system.

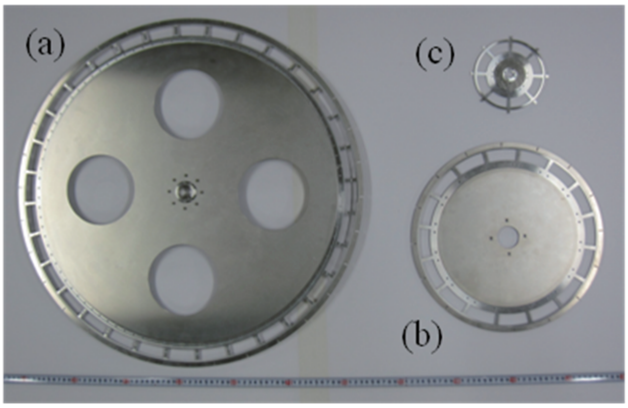

Fig. 1. Photographs of the rotating wheels that can be mounted on the system. (a) 60 cm wheel. (b) 30 cm wheel. (c) 10 cm wheel.

In order to avoid target deterioration from a high intensity primary beam with an intensity higher than 1 pμA, the 60 cm target system was designed. The 60 cm and 30 cm target wheels are driven by an AC-servo motor mounted outside the chamber with a ferrofluidic seal. Steady operation at the maximum target speed 6280 cm/s (2000 rpm) was achieved by using the 60 cm wheel. These wheels were mainly used for metallic materials such as lead or bismuth, which were evaporated onto a carbon foil.

The 10 cm target wheel was designed for use with actinide material, for example, ^{248}Cm. To minimize contamination, the target wheel was mounted in a semi-shielded chamber and installed in the target chamber. The wheel was driven by a stepping motor that could be operated in vacuum.

Table 1 indicates the parameters of the targets, and Figure 2 shows an inside view of the chamber.

The chamber is connected directly to the GARIS. Helium gas filled in the GARIS is introduced into the target chamber and serves the purpose of target cooling. At the upstream of the target chamber, a differential pumping system is installed for connection to the beamline without a separation foil.

Diameter	Number of target sectors	Rotating speed (rpm)	Target speed (cm/s)
60 cm	32	2000	6280
30 cm	16	3000	4710
10 cm	8	1000	523

Table 1. Parameters of the mountable targets.

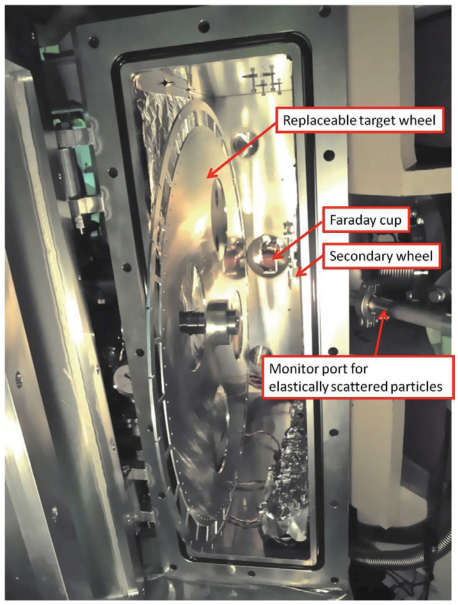

Fig. 2. Photograph of the new target chamber.

The beam is chopped up with proper timing in order to avoid irradiating the target sector frame. The duty cycle of the beam is about 70% - 80%. A Faraday cup and a beam-spot viewer (quartz glass) mounted on the secondary wheel are installed in the chamber. The beam intensity and target condition are monitored by measuring the number of elastically scattered particles. The particles are detected by a PIN diode installed at a 45° forward angle from the target. Beam intensity is determined by counting the rate of scattered particles; and the uniformity of the target thickness is monitored by observing the shape of the energy spectrum.

*1 Faculty of Science and Technology, Tokyo University of Science

References

1) D. Kaji, K. Morimoto, A. Yoneda, H. Hasebe, A. Yoshida, H. Haba, S. Goto, H. Kudo and K. Morita, *Nucl. Instr. Meth.* A, 590, (2008) 198-203.

PHENIX silicon vertex tracker (VTX)

Y. Akiba, R. Akimoto,[*1] H. Asano,[*2] S. Baumgart, M. Bobrek,[*3] K. Boyle,[*4] C-H. Chen,[*4] V. Cianciolo,[*3] A. Deshpande,[*4,*5] L. Ding,[*6] O. Drapier,[*7] A. Enokizono, S. Esumi,[*8] F. Gastaldi,[*7] T. Hachiya, S. Horiuchi,[*8] J. Kanaya, J. Koster,[*4] K. Kurita,[*9] M. Kurosawa,[*4] A. Lebedev,[*6] E. J. Mannel,[*10] M. McCumber,[*11] H. Nakagomi,[*8] R. Nouicer,[*10] C. Ogilvie,[*6] R. Pak,[*10] C. Pancake,[*5] H. Sako,[*12] S. Sato,[*12] E. Shafto,[*5] A. Shaver,[*6] M. Shimomura,[*6] W. Sondheim,[*13] M. Stepanov,[*14] A. Taketani, S. Taneja,[*5] M. Wysocki,[*11] and the PHENIX VTX group

We have constructed a silicon vertex tracker (VTX) for the PHENIX experiment at RHIC. The primary purpose of the detector is to carry out precise measurements of heavy-quark (charm and beauty quarks) production in $A+A$, $p(d)+A$, and polarized $p+p$ collisions. The main topics in physics that can be studied by using the VTX are as follows.

- Probing high-density partonic matter
  - Energy loss of heavy quarks (charm and bottom quarks) in dense matter
  - Elliptic flow of heavy quarks in dense matter
  - Open heavy-quark production
  - Medium-induced modification of jets
- Measurement of the gluon spin polarization $\Delta G(x)$ of the nucleon
  - Determination of $\Delta G(x)$ from heavy-quark measurements
  - Determination of $\Delta G(x)$ from γ-jet measurements
- Nucleon structure in nuclei
  - Gluon shadowing over a broad x range

The above-mentioned measurements are key measurements that are required for future RHIC programs, both for the study of quark-gluon plasma (QGP) in heavy-ion collisions and for the measurement of the nucleon spin-structure functions.

The VTX detector consists of two inner layers of silicon pixel detectors and two outer layers of silicon strip detectors using “stripixel” sensors. The detector covers a pseudorapidity range $|\eta| < 1.2$ and azimuthal angle $\Delta\phi$ about 2 π. The project was funded by RIKEN, the US DOE, and Ecole Polytechnique. The US side of the project commenced in US FY2007. The total budget was US$4.7 million for the four years FY2007-FY2010. RIKEN was responsible for the inner pixel detectors, while the US DOE was responsible for the strip detectors and mechanical structure.

Construction of the detector and its installation in PHENIX was completed in 2010. The detector was then successfully commissioned during the 500 GeV $p+p$ run in RUN11 of RHIC. Details of the commissioning of the pixel subsystem[1)] and the stripixel subsystem[2)] are described in other reports in this volume.

We obtained the first beam data at the end of the $p+p$ run. Subsequently, we collected physics data during Au+Au runs of RHIC at $\sqrt{s_{NN}}$ =19.6 GeV (approx. 5M events), 27 GeV (approx. 13M events), and 200 GeV (approx. 5B events).

Development of the analysis code is currently in progress. A stand-alone tracking code for the VTX is developed[3)]. This code is used to reconstruct the collision vertex with high precision. Simulation studies show that a vertex position resolution of approximately 20 μm can be achieved. One of the most important data analysis tasks is the precise alignment of the detector ladders. Details of detector alignment procedure using the beam data are described in another report[4)] in this volume. A track from the PHENIX central arms is associated with the hits in VTX detectors, and the distance of closest approach (DCA) between the track and the collision vertex is measured. A DCA resolution of approximately 80 μm in the X-Y plane is achieved for $p_T > 1$ GeV/c for real Au+Au data[5)]. This result is consistent with the expected DCA resolution.

References

1) M. Kurosawa et al.: RIKEN Accel. Prog. Rep. **45**,(2012).
2) A. Enokizono et al.: RIKEN Accel. Prog. Rep. **45**,(2012).
3) R. Akimoto et al.: RIKEN Accel. Prog. Rep. **45**,(2012).
4) H. Asano et al.: RIKEN Accel. Prog. Rep. **45**,(2012).
5) T. Hachiya et al.: RIKEN Accel. Prog. Rep. **45**,(2012).

*1 CNS, University of Tokyo, Japan
*2 Kyoto University, Japan
*3 Oak Ridge National Laboratory, USA
*4 RIKEN BNL Research Center, USA
*5 Stony Brook University, USA
*6 Iowa State University, USA
*7 LLR, Ecole Polytechnique, CNRS-IN2P3, France
*8 University of Tsukuba, Japan
*9 Rikkyo University, Japan
*10 Brookhaven National Laboratory, USA
*11 University of Colorado, USA
*12 Japan Atomic Energy Agency, Japan
*13 Los Alamos National Laboratory, USA
*14 University of Massachusetts, USA

Test and development of silicon detector for PHENIX experiment

S. Sato,[*1] Y. Akiba, R. Akimoto,[*2] H. Asano,[*3] S. Bathe,[*4] S. Baumgart, J. Bryslawskyj,[*4] M. Bobrek, [*6] K. Boyle,[*5] C. Chen,[*5] V. Cianciolo,[*6] A. Deshpande,[*5,*7] L. Ding,[*12] O. Drapier,[*8] A. Enokizono, S. Esumi,[*9] F. Gastaldi,[*8] T. Hachiya, S. Horiuchi,[*9] J. Kanaya, J. Koster,[*5] K. Kurita,[*10] M. Kurosawa, A. Lebedev,[*13] E. Mannel,[*11] M. Mccumber,[*15] H. Nakagomi,[*9] R. Nouicer,[*11] C. Ogilvie,[*12] R. Pak,[*11] C. Pancake,[*7] H. Sako,[*1] E. Shaft,[*7] A. Shaver,[*13] M. Shimomura,[*9] W. Sondheim,[*13] M. Stepanov,[*14] A. Taketani, S. Taneja,[*7] M. Wysocki,[*15] and the PHENIX VTX group

[Instrumentation]

For study of particle production containing charm or bottom, like B or D meson, it is key to measure short life time particles. To measure such short life time particles, fine tracking detectors surrounding the collision vertex is an essential technique. PHENIX experiment has developed and installed four layers of the silicon vertex tracking detectors (VTX)[1]; two as the "silicon pixel" detectors and the other two as the "silicon stlip-pixel" detectors. During the beam shutdown period in 2011 summer, the silicon vertex tracking detectors are maintained. In order to have choice to exchange some of the ladders with spares, a spare ladder is pre-checked in RIKEN (Wako, Japan) for the signal readout.

In the summer of 2011, one pair of ladder (consisting of the right and left side parts) of the silicon pixel detector is assembled to have spare for the installed (by 2010) detector[2] in PHENIX-central arm at BNL. Standard checkup procedure[3] is performed prior to shipping to BNL. Figure 1 shows the test bench setup. Firstly by implying test pulse in readout chip, every readout bus line is checked. And secondly by using checking β source (^{90}Sr), discrimination threshold and hot channel is checked to prepare for the real data taking operation. Figure 2 shows hit distribution with β source for each readout chip on the ladder. Due to limited statistics for each chip especially located at edge, lower hit distribution is seen. Also the shadow of the chip itself is seen for every chip at the center of each hit distribution. By exchanging tested ladders, the active area is improved from 69% to 92%. It is observed the coolant called "NOVEC" is evaporated by some 10 liter and some liquid residual (some 30 cm^3) is remained, during some one year of interval for bench test at RIKEN(Wako). Since finite electrical conductance (Fig.3) was observed for the residual coolant in the present setup, it is better to check the resistivity in case of leakage of the coolant.

Fig. 1. Test setup at RIKEN. Pixel detector with coolant "NOVEC" flowpipe is in cooling box, and with SPIRO board on both sides. Beta source scans above box.

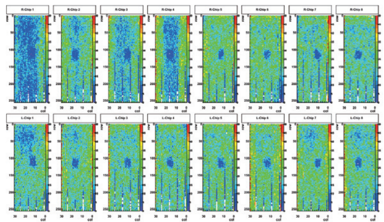

Fig. 2. Test results by checking beta source, for the newly involved set of the silicon pixel ladder in 2011.

Fig. 3. Residual of coolant for the ladder. Some conductance is existing. (The first left digit of tester is MΩ)

References
1) Proposal for a Silicon Vertex Tracker (VTX) for the PHENIX Experiment W. Zajc et al., Brookhaven National Laboratory July, 2004.
2) RIKEN Accel. Prog. Rep. 44, (2011) M. Akimoto et al.: p177 , T. Hachiya et al.: p179, A. Taketani et al.: p181, Y. Akiba et al.: p183, H. Asano et al.:p186,
3) M.Kurosawa et al. RIKEN Acc. Prog.Rep.44,184 (2011)

*1 JAEA, Advanced Science Research Center, Japan
*2 Center for Nuclear Study, Univ. of Tokyo, Japan
*3 Department of Physics, Kyoto Univ., Japan
*4 City University of New York, USA
*5 RIKEN BNL Research Center, USA
*6 Oak Ridge National Laboratory, USA
*7 Stony Brook University, USA
*8 LLR, Ecole Polytechnique, CNRS-IN2P3, France
*9 University of Tsukuba, Japan
*10 Department of physics, Rikkyo University, Japan
*11 Brookhaven National Laboratory, USA
*12 Iowa State University, USA
*13 Los Alamos National Laboratory, USA
*14 University of Massachusetts, USA
*15 University of Colorado, USA

Collision vertex measurement by standalone tracking with PHENIX silicon vertex tracker†

R. Akimoto,*1 Y. Akiba, H. Asano,*2 S. Baumgart, K. Boyle,*3 C. Chen,*4 A. Deshpande,*3,*4 L. Ding,*5 A. Enokizono, S. Esumi,*6 T. Hachiya, S. Horiuchi,*6 K. Kurita,*7 M. Kurosawa, A. Lebedev,*5 M. Mccumber,*8 H. Nakagomi,*6 R. Nouicer,*9 C. Ogilvie,*5 H. Sako,*10 S. Sato,*10 A. Shaver,*5 M. Shimomura,*5 M. Stepanov,*11 A. Taketani, M. Wysocki,*8 and the PHENIX VTX group

Heavy quarks (charm and bottom) form one of the key probes used for studying the properties of quark gluon plasma (QGP). A silicon vertex tracker (VTX) has been developed mainly for the measurement of heavy quarks. This VTX enables the precise measurement of tracks of charged particles, and it is essential to study the behavior of heavy quarks inside QGP.

The VTX used herein is a barrel detector with four barrels surrounding the beam pipe, as shown in Fig. 1. The VTX has been successfully installed for use in the RHIC-PHENIX experiment, and data collection for p + p and Au + Au collisions during the RHIC-RUN11 period has been completed.

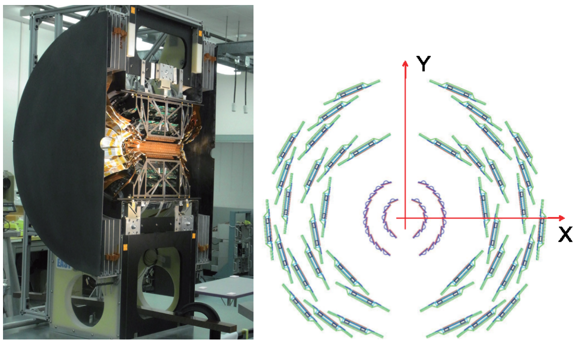

Fig. 1. The left panel shows an overall view of one of the VTX arms. The right panel shows a cross-sectional view of the VTX. The x and y directions used in this study are also defined in this figure.

There are two ways to measure heavy flavored hadrons: reconstruction of all decay products from hadronic decay and measurement of an electron or positron from semi-leptonic decay. Owing to the large hadronic background in central Au + Au collision events, measurements made using semi-leptonic decay makes the systematic error smaller.

Flavor identification is preformed using a distribution of the distance of the closest approach (DCA) from the beam collision vertex. Therefore, the measurement of the track path as well as that of the collision vertex are important for the DCA measurement. The PHENIX central spectrometer[1)] is necessary for the identification of an electron or positron and hence, it is planned that a path of an electron or positron will be reconstructed by using tracks reconstructed by the spectrometer as a seed. In addition, because the acceptance of the spectrometer is extremely small, with a pseudo-rapidity of ±0.35 and an azimuthal angle of 180°, standalone tracking of the VTX is suitable for the collision vertex measurement.

The collision vertex is reconstructed such that the sum of the squares of DCA over the resolution of the DCA is minimum. The resolution of the collision vertex is evaluated with simulation data created with HIJING code[2)] as an event generator and with GEANT3 in a realistic magnetic field. The resolutions in the x, y, and z directions[a)], shown in Fig. 2, are 20.8 μm, 16.0 μm, and 26.1 μm, respectively, which are much smaller than the difference in the lifetimes of the D meson and B meson.

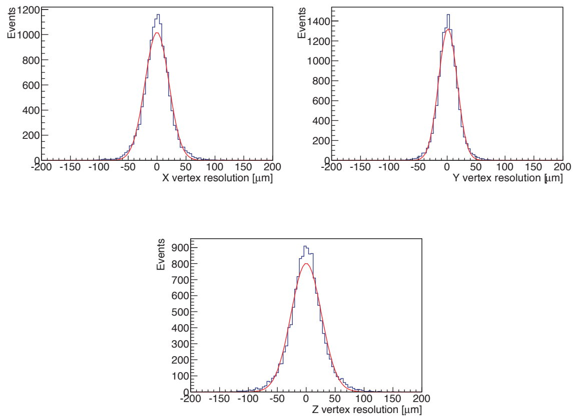

Fig. 2. The top left, top right, and bottom panels show the distribution of the reconstructed collision vertex in the x, y, and z directions, respectively.

*1 Center for Nuclear Study, Univ. of Tokyo, Japan
*2 Department of Physics, Kyoto Univ., Japan
*3 RIKEN BNL Research Center, USA
*4 Stony Brook University, USA
*5 Iowa State University, USA
*6 University of Tsukuba, Japan
*7 Department of Physics, Rikkyo University, Japan
*8 University of Colorado, USA
*9 Brookhaven National Laboratory, USA
*10 JAEA, Advanced Science Research Center, Japan
*11 University of Massachusetts, USA

References
1) K. Adcox et al., Nucl. Instr. and Meth. A **499** (2003) 366
2) http://www-nsdth.lbl.gov/~xnwang/hijing/

a) In this report, the beam direction is defined as z direction and x and y directions are defined in Fig. 1.

DCA measurement with the PHENIX VTX detector

T. Hachiya, Y. Akiba, R. Akimoto,[*1] H. Asano,[*2] S. Bathe,[*3] S. Baumgart, J. Bryslawskyj,[*3] M. Bobrek,[*4] K. Boyle,[*5] C.-H. Chen,[*5] V. Cianciolo,[*4] A. Deshpande,[*5,*6] L. Ding,[*7] O. Drapier,[*8] A. Enokizono, S. Esumi,[*9] F. Gastaldi,[*8] S. Horiuchi,[*9] J. Kanaya, J. Koster, [*5] K. Kurita, [*10] M. Kurosawa, A. Lebedev, [*7] E. Mannel, [*11] M. McCumber, [*14] H. Nakagomi, [*9] R. Nouicer, [*11] C. Ogilvie, [*7] R. Pak, [*11] C. Pancake, [*6] H. Sako, [*13] S. Sato, [*13] E. Shaft, [*6] A. Shaver, [*7] M. Shimomura, [*7] W. Sondheim, [*14] M. Stepanov, [*15] A. Taketani, S. Taneja, [*6] M. Wysocki, [*12] and the PHENIX VTX group

A silicon vertex tracker (VTX)[1–3] was newly constructed in the PHENIX experiment[4]. The primary purpose of the VTX is to measure the production of heavy (charm and bottom) quarks in Au + Au and polarized $p + p$ collisions. These processes are powerful tools for studying the properties of dense partonic matter created in high-energy heavy-ion collisions and for studying the spin structure of the proton in polarized $p + p$ collisions. We took the first VTX data in $p+p$ and Au + Au collisions during the experiment in 2011.

The measurement of the heavy quarks are performed through their semileptonic decay to electrons. The PHENIX central arm (CA) detector can track charged particles by DC and PC and identify electrons by RICH and EMCal[1]. The VTX can measure the distance of the closest approach (DCA) to the primary vertex. By combining the CA detector and the VTX, we can separately measure the charm and bottom production.

We have two track reconstruction methods. One is the standalone tracking (SAT) method using only VTX clusters[5]. The primary vertex is determined as the focal point of the track vectors reconstructed by the SAT method. The other method is the central arm based tracking (CAT) method. In the CAT method, a track vector reconstructed by the CA is extrapolated onto the VTX to search for associated clusters on a layer-by-layer basis. We require at least three associated clusters for track recognition. For each CA track, the DCA is measured using the primary vertex from the SAT method and the track vector reconstructed by the CAT method. The geometrical alignment is very important for the track reconstruction and the DCA measurement. Alignment among the layers of the VTX and between the VTX and the CA detector is performed using both the SAT and CAT methods[6].

Figure 1 shows the DCA distribution with more than 1 GeV/c of transverse momentum (p_T) in 0-20% central Au + Au collisions. The black and red histograms correspond to hadrons and electrons, respectively. The width of the DCA distribution for hadrons is 80 μm, which is almost consistent with the design value obtained by a simulation with the ideal geometry. This indicates that the current alignment works well and that we can separate the charm and bottom contributions. On the other hand, the width of the electrons seems to be broader. If the same result is obtained with higher statistics, then this broadening could indicate the signal of open heavy flavor decays. We have five orders of magnitude larger data than those used in the plot in RUN11. We aim to show the first physics results in 2012.

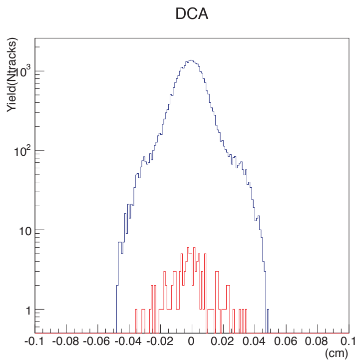

Fig. 1. DCA distribution with $p_T > 1$(GeV/c) in 0-20% central Au+Au collisions. The black and red histograms show the distributions of hadrons and electrons, respectively.

*1 Center for Nuclear Study, The University of Tokyo, Japan
*2 Kyoto University, Japan
*3 City University of New York, USA
*4 Oak Ridge National Laboratory, USA
*5 RIKEN BNL Research Center, USA
*6 Stony Brook University, USA
*7 Iowa State University, USA
*8 LLR, Ecole Polytechnique, CNRS-IN2P3, France
*9 University of Tsukuba, Japan
*10 Rikkyo University, Japan
*11 Brookhaven National Laboratory, USA
*12 University of Colorado, USA
*13 Japan Atomic Energy Agency, Japan
*14 Los Alamos National Laboratory, USA
*15 University of Massachusetts, USA

References

1) Y. Akiba et al.: in this report.
2) R. Nouicer et al., PoS (Vertex 2007) 042 (2007).
3) T. Hachiya et al.: RIKEN Accel. Prog. Rep. **44**, 179 (2011).
4) K. Adcox et al. : Nucl. Instrum. Meth. A **499**, 469 (2003)
5) R. Akimoto et al.: in this report.
6) H. Asano et al.: in this report.

Online Monitoring for the PHENIX VTX Detector

J. Koster[*1] and R. Akimoto[*2]

The PHENIX vertex tracker (VTX), which was installed into the PHENIX experiment at the Relativistic Heavy Ion Collider (RHIC) in late-2010, successfully observed collisions at the collider from early 2011 until the end of the RHIC run in July of 2011. The detector provides precision tracking close to the beamline and will enable measurements of displaced vertices from the decay of charm and bottom, and improve the reconstruction of jets due to its large acceptance. The topic of this report is a software package which was developed to monitor the performance of the VTX detector in near real time.

RHIC provides collisions twenty four hours a day - seven days a week during its operational periods, with exceptions for filling and dumping the beams. During these periods of beam operations, PHENIX collaborators staff the experiment and monitor its data in real time. The software runs a fast analysis on the raw data from each detector system and displays summary plots using the ROOT software framework[1]. This monitoring software is referred to as “Online Monitoring”.

The VTX detector is composed of four barrels of silicon tracking covering the pseudorapidity range $|\eta| < 1.2$ and the full azimuthal angle. The inner two layers are made of pixel sensors and the outer two of “stripixel” sensors. The layers are centered at 2.5, 5, 10 and 14 centimeters from the center of the beamline. The pixel layers are composed of 50 $\mu m \times 450$ μm pixel sensors. The data is provided in binary format, i.e. either a hit or no-hit, and is readout using the ALICE1LHCb chip. The stripixel detector uses a spiral pattern and ADC readout to give good two dimensional position resolution while maintaining a low overall channel count.

There are three basic groups in the online monitoring code. The first checks for errors in the detector readout, i.e. if there were errors in the data transmission. The PHENIX data acquisition system writes data at a large rate (roughly 700 megabytes per second) which requires that data flow through multiple specialized systems each of which may introduce readout errors. If an error is detected, then it taints any analysis done on it. Several checks are done including a checksum comparison between the data which was sent by the detector and the data written to disk, a timestamp check that the data from each sub-component of the detector originated from the same moment in time and other more specialized checks.

The second and third groups perform a simple physics measurements with either the pixel or stripixel layers to verify that its performance matches expectations. The primary tool is the number of hits in each detector sub-unit normalized by the number of events. The pixel detector, which provides only hit or no-hit information for each element, simply counts the number of active elements. However, hits in the stripixel detector, which reads out the charge in each strip, are defined using an ADC threshold. An example plot from physics data taken with the pixel layers is shown in fig. 1.

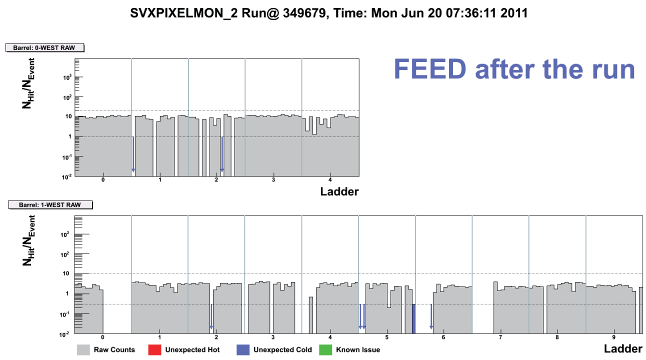

Fig. 1. An example online monitoring plot from the VTX-Pixel detector from Gold-Gold collisions in 2011.

In fig. 1, the top left panel is for the innermost layer and the bottom panel is for the second layer from the beam pipe. Both plots cover only half the detector in the azimuthal angle (West). A similar plot is provided for the other half (East). The horizontal axis denotes a detector sub-unit. The vertical axis is the number of active pixel sensors divided by the number of events. In the event of an error, the top right area of the canvas is reserved for an automatically generated messages for the shift crew to follow.

Using the three types of plots mentioned here, the PHENIX shift crews can generate a complete overview of the VTX detector after only a few mouse clicks. If a problem is identified, then more detailed plots which will not be discussed here are available automatically. Many plots with a narrower focus and more detailed information are available but are not typically viewed unless the more coarse-grained plots identify an issue. This online monitoring system was successfully deployed in 2011 to ensure high quality physics data. Currently, that data is being analyzed for productive physics measurements.

References

1) R. Brun and F. Rademakers: Nucl. Inst. & Meth. in Phys. Res. **A 389**, (1997)

*1 RIKEN BNL Research Center, USA
*2 Center for Nuclear Study, University of Tokyo, Japan

Alignment of PHENIX Silicon Vertex Tracker

H. Asano,*[1] Y. Akiba, R. Akimoto,*[2] K. Boyle,*[4] L. Ding,*[6] A. Enokizono, T. Hachiya, J. Kanaya, J. Koster,*[4] M. Kurosawa,*[4] A. Lebedev,*[6] E. Mannel,*[5] R. Nouicer,*[5] C. Ogilvie,*[6] H. Sako,*[3] S. Sato,*[3] M. Shimomura,*[6] W. Sondheim,*[7] M. Stepanov,*[8] A. Taketani, and the PHENIX VTX group

The PHENIX experiment in the Relativistic Heavy Ion Collider (RHIC) at Brookhaven National Laboratory has been upgraded by installing a silicon vertex tracker (VTX).[1)] The VTX has been developed for heavy flavor (charm and bottom) measurements and dedicated to the precise tracking of primary and secondary vertices; The first set of physics data pertaining to the Au+Au collision in RUN 11 (RHIC experiment performed in 2011) was recorded by the VTX. The first and second layers of the VTX are comprise pixel detectors, and the third and the fourth layer of VTX are comprise stripixel detectors[2)].

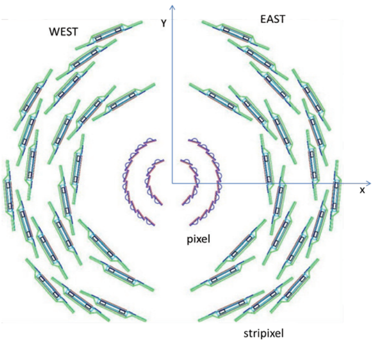

Fig. 1. Cross section of the VTX. The VTX is separated into a west barrel and an east barrel. The first and second layers comprise pixel detectors and the third and forth layers comprise stripixel detectors.

Geometrical calibration is important because precise tracking is required in the VTX to identify primary and secondary vertex reconstruction. The individual sensors in the detector must be calibrated with an accuracy of the intrinsic resolution, which is typically on the order of 10 μm. The position and orientation of each of the 120 pixel sensors and 224 stripixel sensors in space are defined by the translation vector and the rotation matrix. To align each sensor roughly, survey measurements have been carried out, and the translation vector and rotation matrix have been calculated. These data are used as input for the track-based alignment method.

In the track-based alignment for RUN 11, beam data for the peripheral Au+Au collisios are used to limit the hit mulitiplicity on the sensors. Eash sensor is aligned in the VTX internal coordinate by VTX self-tracking (internal alignment) and aligned with respect to the PHENIX central arm detectors located outside the VTX (external alignment). In the internal alignment, each sensor is aligned to adjust the mean of distance of closest approach (DCA) distribution from the beam center to each track reconstructed by the VTX itself. In the external alignment, a drift-chamber-based track with thr VTX cluster is used. The residual from the projected position on each sensor to each VTX cluster are calculated, and then, each sensor is aligned manually to minimize the mean of residual distribution.

The internal and external alignment procedures are repeated iteratively, and each sensor is well aligned within a precision of 2,30 μm precision to the beam center (Fig.2). Even though this is a preliminary result, we obtain a σ(DCA) of approximately 93 μm for the west barrel and $\sim$ 80 μm for the east barrel. These values are very close to our goal, σ(DCA) of 80 μm. A more precise alignment will be achieved in the future.

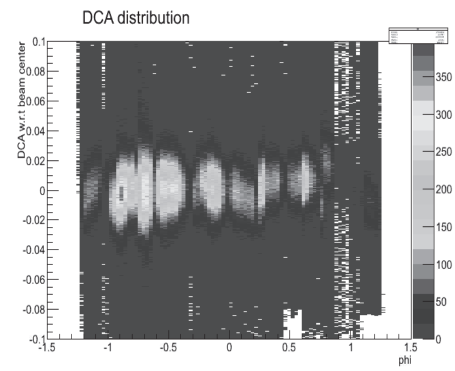

Fig. 2. DCA w.r.t. the beam center vs. phi angle of each track (west barrel). The mean DCA should be zero if the alignment is perfect. The standard deviation of DCA w.r.t. the beam center is 141μm for the west barrel and 132 μm for the east barrel. The DCA resolution can be estimated from these deviations and the beam spot size (σ (beam size) $\sim$ 105μm), which can be calculated from the RHIC beam paramters.

*1 Department of Physics, Kyoto Univ., Japan
*2 Center for Nuclear Study, Univ. of Tokyo, Japan
*3 JAEA, Advanced Science Research Center, Japan
*4 RIKEN BNL Research Center, USA
*5 Brookhaven National Laboratory, USA
*6 Iowa State University, USA
*7 Los Alamos National Laboratory, USA
*8 University of Massachusetts, USA

References

1) Proposal for a Silicon Vertex Tracker (VTX) for PHENIX Experiment, 2006
2) A. Taketani et al., Nucl. Instr. and Meth. A 623 (2010) 374

Spin Physics with a Forward sPHENIX Upgrade

J. Seele,*1

[Transverse Spin physics, Hadronic Physics, Future Upgrades]

The PHENIX experiment is planning an ambitious set of upgrades, sPHENIX, that will largely replace the current detector suite, to pursue new physics goals. A central barrel detector is being developed that will largely focus on jet measurements in high energy heavy ion collisions. Additionally, a forward spectrometer is being designed that will focus on high energy spin physics and cold nuclear matter physics. This report will only cover the forward upgrades and areas related to high energy spin physics.

One of the most interesting and vexing problem in modern high energy spin physics is the source of and description of the measured large transverse single spin asymmetries in polarized proton-proton collisions[1]. These asymmetries have been measured across a wide swath of center of mass energies, from $\sqrt{s} = 4.4$GeV to $\sqrt{s} = 200$GeV, and are roughly equal in magnitude across those energies. Recently, there has been a burst of theoretical progress in this area, where a number of mechanisms have been put forth that have the possibility of describing these large asymmetries. From this burst of progress, two main mechanisms may be the source of these asymmetries. They are called the Sivers mechanism[2] which involves correlations between the spin of the parton and the intrinsic transverse momentum of the parton in the nucleon and the Collins mechanism[3] which involves a correlation between the spin of the scattered parton and the final state transverse momentum that is produced in the fragmentation process.

Based on factorization and universality theorems present in perturbative Quantum ChromoDynamics it is expected that these functions should be process independent and should be able to be measured in another hard process, such as deep-inelastic scattering (DIS), and then be used in the description of proton-proton scattering. But on closer theoretical examination it was found that these processes violated the naive expectations of factorization and universality. For example, it was found that the Sivers function as measured in Drell-Yan (DY) production in polarized proton-proton collisions should have the same magnitude, but opposite sign of the Sivers function measured in DIS. The DIS data for the Sivers function exists from previous experiments, namely HERMES and COMPASS, but there is no data on polarized DY measurements with which to test their theorem. The asymmetries that are of kinematical interest in polarized DY production and that overlap with the DIS kinematics exist at forward rapidities in proton-proton collisions. PHENIX does not currently posses the necessary detectors or kinematical coverage to make these important measurements, thus an upgrade is being pursued which will make it possible for PHENIX to make these important measurements.

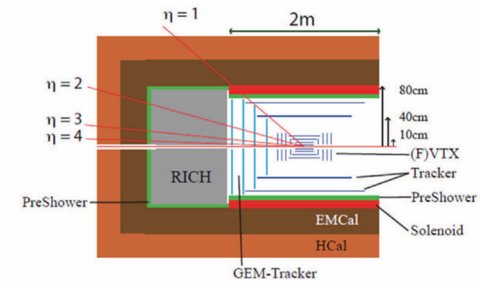

Fig. 1. A strawman design for the sPHENIX detector.

In addition to the DY measurement, there are other measurements of interest that will contribute more and important information to the task of understanding the description of these asymmetries, namely measurements of forward jets and identified hadrons and specifically identified hadrons in jets. It is also one of the mysteries of these asymmetries as to why there is a such a strong dependence on the flavor of the observed hadron[4].

With such a broad array of interesting measurements, it is natural to expect that a general purpose type particle physics detector will the best match to the program. With this in mind, PHENIX has designed a strawman detector, as can be seen in figure 1. The forward region ($-4 \geq \eta \geq -1$) will have calorimetry (both electromagnetic and hadronic) for electron discrimination, electromagnetic energy reconstruction, and hadronic energy reconstruction, tracking for charged particle identification, charge sign measurement and low momentum measurement, and a particle identification or Ring Imaging Cherenkov Detector for discrimination between pions, kaons and protons as well as their anti-particles.

References
1) V. Barone, F. Bradamante and A. Martin, Prog. Part. Nucl. Phys. **65**, 267 (2010) [arXiv:1011.0909 [hep-ph]].
2) D. W. Sivers, Phys. Rev. D **41**, 83 (1990).
3) J. C. Collins, Nucl. Phys. B **396**, 161 (1993) [hep-ph/9208213].
4) J. H. Lee *et al.* [BRAHMS Collaboration], arXiv:0908.4551 [hep-ex].

*1 RIKEN/BNL Research Center

Preparation status of the J-PARC E16 : An experiment to measure the mass modification of vector mesons in nuclei

S. Yokkaichi for the J-PARC E16 Collaboration

We proposed the experiment E16[1)] to measure the vector meson decays in nuclei in order to investigate the chiral symmetry restoration in dense nuclear matter. The experiment will be performed at the J-PARC hadron experimental facility. The proposal of the experiment was granted scientific ("stage 1") approval by the PAC[a)] in March 2007. For the full approval, we need to show not only the experimental feasibility but also the prospects of acquiring sufficient funds and even beam-line construction.

The aim of this experiment is to perform a systematic study of the mass modification of vector mesons, particularly the ϕ meson, in nuclei. The mass modification of vector mesons in hot and/or dense matter is predicted on the basis of the QCD because of the restoration of the chiral symmetry in such matter.

Many experimental studies, including dilepton invariant mass measurements, have been conducted to study the problem, and the mass modifications in hot and/or dense matter have been observed. However, the origin of the modification has not yet been confirmed; in other words, there is no consensus on the interpretations of the phenomena. For example, among heavy-ion experiments, the CERES, NA60, and PHENIX experiments have reported enhancement in their dilepton mass spectra. The CERES and NA60 stated that the spectra can be explained by the broadening of the ρ meson width. However, the PHENIX experiment has been so far unable to explain their spectra by the broadening or by any theoretical calculation yet. Among the photon-induced reactions, the CLAS-g7 experiment reported the width broadening of the ρ meson in the e^+e^- decay channel and explained it by collisional broadening. Further, KEK-PS E325[2)], which was conducted by a collaboration including a part of the authors, measured the e^+e^- invariant mass spectra in 12-GeV p+A reactions and reported enhancements on the low mass sides of ω and ϕ mesons. These enhancements are consistent with the mass decreasing of vector mesons predicted using QCD sum rule[3)]. The mass-shape modification of a narrow resonance, ϕ, can be observed only in E325, because it has the best mass resolution among the above mentioned experiments, better statistics than those of the photon-induced experiment, and better signal-to-noise ratio than that of the heavy-ion experiments.

The aim of this experiment is to measure the ϕ meson decays in the e^+e^- channel with statistics that are two orders larger in magnitude than those of the preceding E325 experiment. In other words, the aim is to accumulate 1×10^5 to 2×10^5 events for each nuclear target (H, C, Cu, and Pb). Thus, we can deduce the dependences of the modification on the matter size and meson momentum, which have never been measured. At the same time, the e^+e^- decays of the ρ, ω, and J/ψ mesons can be measured. For this experiment, we will use a 10^{10}-pps, 30-GeV proton beam in the high-momentum beam line, which will be constructed in the J-PARC hadron experimental facility. In order to increase the statistics by a factor of 100, the beam intensity should be increased by a factor of 10; the acceptance of the spectrometer, by a factor of 5; and the production cross section, by a factor of 2 by increasing the beam energy. In order to cope with the interaction rate at the target that has increased by a factor of 10, to 10^7 Hz, a new spectrometer based on new technology should be built.

Recently, we obtained the MEXT Grant-in-Aid[4)] to develop and construct the spectrometer. Detector development is underway, as reported elsewhere[5–9)]. In short, the two key detectors, basic studies of the GEM Tracker[5)] and HBD[6)] have been performed and detailed mechanical design is required before the production. The studies on LG[7)] and read-out circuits[8,9)] started recently in the JFY 2011.

Our staged goal is to complete construction of one-third of the spectrometer by the end of the JFY 2013 with our limited budget.

[a)] Program Advisory Committee for Nuclear and Particle Physics Experiments at the J-PARC 50-GeV Proton Synchrotron

References

1) S. Yokkaichi *et al.*; J-PARC proposal No. 16 (`http://j-parc.jp/researcher/Hadron/en/pac_0606/pdf/p16-Yokkaichi_2.pdf`), Lect. Notes Phys. **781** 161 (2009).
2) M. Naruki *et al.*; *Phys. Rev. Lett.* **96**, 092301 (2006), R. Muto *et al.*; *Phys. Rev. Lett.* **98**, 042501 (2007).
3) T. Hatsuda and S. H. Lee, *Phys. Rev. C* **46**, R34 (1992), T. Hatsuda, S. H. Lee and H. Shiomi, *Phys. Rev. C* **52**, 3364 (1995).
4) Grant-in-Aid for Scientific Research on Innovative Areas 2104: "Elucidation of New hadrons with a Variety of Flavors", 2009–2013, `http://www.hepl.phys.nagoya-u.ac.jp/public/new_hadron/index-e.html`
5) Y. Komatsu *et al.*; in this report.
6) K. Aoki *et al.*; in this report.
7) Y. Aramaki *et al.*; in this report.
8) T. Takahashi *et al.*; in this report.
9) S. Masumoto *et al.*; in this report.

Readiness of electromagnetic calorimeters for J-PARC E16 experiment

Y. Aramaki, for the J-PARC E16 Collaboration

One of the most essential topics in quantum chromodynamics (QCD) is the origin of hadron mass. The acquisition mechanism of hadron mass is strongly associated with the spontaneous breaking of chiral symmetry in QCD. In hot and/or dense matter, chiral symmetry can be restored and the hadron mass is expected to change. Furthermore, it is predicted that the masses of light vector mesons, such as ρ, ω, and ϕ, even at a normal nuclear density, are reduced[1].

The mass modification of light mesons at a normal nuclear density has been already investigated by the KEK-PS E325 experiment, J-Lab CLAS experiment, and CBELSA/TAPS experiment in Bonn. However, the results from these experiments differ from one another, and thus, the conclusion is still being debated. We proposed that the E16 experiment at J-PARC be performed to provide a decisive conclusion regarding the modification of light vector mesons. More detailed information is given in Ref.[2]. In this report, the preparation status of the lead-glass calorimeters (LGs) used for the J-PARC E16 experiment is described.

The LGs, which were employed in the TOPAZ experiment at KEK-TRISTAN have been reused for the J-PARC E16 experiment. They have been kept in KEK after the deconstruction of the TOPAZ spectrometer.

One LG is composed of five: a lead-glass block, light guide, flange, photomultiplier (PMT), and 2 mm thick magnetic shield case made of PB permalloy. PB is a nickel iron soft-alloy containing 40–50% nickel. All the lead-glass blocks have an identical shape: they are 340 mm in length, 122 mm by 113 mm in the front, and 122 mm by 135 mm at the back. The lead-glass material is SF6W. The radiation length of the block is 1.7 cm (equivalent to 20 radiation lengths). The other physical properties and chemical components of the blocks are described in Ref.[3]. The end face of a block was glued to a flange made of 20 mm thick high manganese steel, and the lead-glass block was supported by the only glue joint. Cherenkov light emitted in the LG is detected by a 3-in. PMT R1652, after passing through the 6 cm long light guide made of lead glass. More detailed information on the LG is available in Ref.[3].

Figure 1 shows the schematic view of the J-PARC E16 spectrometer magnet. The magnet of the KEK-PS E325 spectrometer is reused for the experiment, although the pole piece and coil are modified to fit a larger acceptance than in the KEK-PS E325 spectrometer, and the blue colored parts shown in Fig. 1 were added in the magnet. The LGs are 140–174 cm away from the center of the magnet, and the PMTs are immediately behind the LGs. Even though a strong magnetic flux of approximately 1.7 T at the center of the magnet is returned through the yoke, the magnetic field around the PMTs remains still above 1000 Gauss. Even though a magnetic shield is attached to the PMTs, it is inadequate for reducing the magnetic flux around the PMTs for the setup of the J-PARC E16 spectrometer. Therefore, we need to consider using an additional magnetic shield. The appropriate material, design, and alignment of the additional magnetic shield are currently being determined. The magnetic shield needs to be such that the leakage of magnetic flux is within 150 Gauss because the gain of the PMT in the PB shield is reduced significantly when the leakage is above 150 Gauss. We are currently evaluating the leakage of the magnetic flux with TOSCA, which is a 3-D electromagnetic analysis package and computes by using the finite element method.

Furthermore, we have started an operational check of the PMT at KEK from this year. We need to check whether all the PMTs work properly before the installation of LGs in the J-PARC E16 spectrometer because they have not been used after the TOPAZ experiment was completed. Even though we have already finished checking a few dozen PMTs one by one, the number of PMTs that need to be checked is at least one thousand. Therefore, we need to design a high-voltage system that can simultaneously to operate many PMTs. We are currently manufacturing the power supplies, dividers for applying the high voltages to the PMTs in parallel, and their cables.

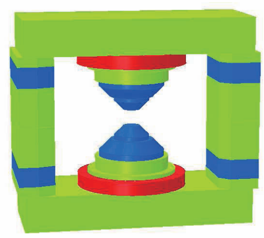

Fig. 1. Magnet of the J-PARC E16 spectrometer drawn with TOSCA. The red parts indicate coils, and the blue parts indicate the additional yokes.

References
1) T. Hatsuda and S.H. Lee: Phys. Rev. C**46**, R34 (1992).
2) S. Yokkaichi *et al.*: in this report.
3) S. Kawabata *et al.*: Nucl. Instr. Meth., A**270**, 11 (1988).

Development of a GEM tracker for J-PARC E16 experiment

Y. Komatsu*1 for the J-PARC E16 Collaboration

[Gas electron multiplier, blind via hole]

The J-PARC E16[1)] experiment is aimed at detecting the modification of the mass spectrum of vector mesons in nuclear matter. In this experiment, a particle tracker that employs a gas electron multiplier[2)] (GEM) is used to measure the momentum of $e^{-(+)}$ in a magnetic field. Ionized electrons are amplified by GEM foils and detected by a readout board. In our configuration, a triple GEM is used to achieve a gain of $\sim 10^4$, and signals are read out by two-dimensional strips, as shown in Fig. 1.

The copper strips are patterned perpendicularly on both sides of a 25-μm-thick polyimide foil. The amount of charge detected by the strips on the far side (called "Y-strips") from the cathode is much less than that on the near side ("X-strips") because the polyimide lacks the structure for charge sharing. To distribute the charge equally, a readout board with blind via holes (BVHs) is manufactured. Island electrodes are fabricated between the X-strips, and they are connected electrically to the Y-strips via the BVHs. The hole is made by chemically etching the Y-strip copper and the foil polyimide, and the island electrode is etched. The copper plating of the hole serves as an electric contact between the Y-strip and the island electrode. These electrodes have the same width as the X-strips, 125 μm. A photograph of the BVH readout is shown in Fig. 2.

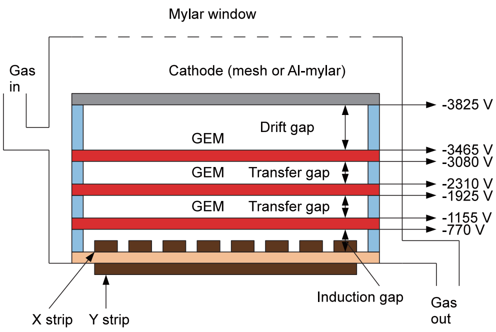

Fig. 1. Shematic of the GEM tracker.

The position resolution, efficiency, and charge sharing are evaluated with the BVH readout at BL33LEP beamline, Spring-8. A photon beam is converted to e^+ and e^- on a Pb target, and the e^+ and e^- are swept by a dipole magnet. We use an e^- beam of 740 MeV. The GEM tracker is set between three silicon strip detectors (SSDs). The position resolution of the GEM tracker is evaluated on the basis of the residual

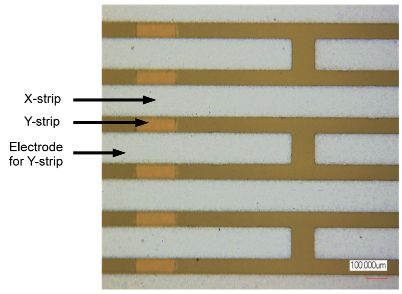

Fig. 2. A photograph of the BVH readout. The strip pitch is 350 μm for the X-strips and 1400 μm for the Y-strips.

of the hit positions determined by the GEM tracker and SSDs. The signals are sampled at 100 MHz using flash ADC modules. Hit strips are selected on the basis of the ADC values, and a charge cluster is defined as a group of hit strips. The position on a tracker is calculated as the weighted mean of the hit strips with the ADC values in the cluster. Collected charge is also calculated as the sum of the ADC values in the cluster.

The position resolution, efficiency and collected charge for X and Y-strips are listed in Table 1. We aim to achieve a resolution of 100 μm for X-strips, and a satisfactory result is obtained with the BVH readout. For comparison, the data obtained using a readout that is not of the BVH type is also considered, and the ratio of the peak value of collected charge is found to be X:Y = 9:1. In contrast, the ratio of collected charge with the BVH readout is X:Y = 5.6:4.4, as shown in Table 1. The efficiency of the Y-strips will be improved by increasing the gain.

Table 1. Position resolution, efficiency, and peak value of collected charge with the BVH readout.

strip pattern	resolution [μm]	efficiency [%]	charge sum [fC]
X	104	98.5	25
Y	285	93.1	20

In summary, expected charge sharing is achieved with the BVH readout, and mass production of the readout has been started for the J-PARC E16 experiment.

References
1) S. Yokkaichi *et al.*; in this report.
2) F. Sauli, Nucl. Instr. and Meth. A 386 (1997) 531.

*1 Department of Physics, University of Tokyo

Performance evaluation of a prototype of Hadron Blind Detector for the J-PARC E16 Experiment

K. Aoki for the J-PARC E16 Collaboration.

[Chiral symmetry, Hadron, Cherenkov detector, CsI]

The J-PARC E16 Experiment aims to study the origin of hadron mass through the mass modification of vector mesons, which decay into e^+e^-[1]. Therefore, electron identification is crucial for the experiment. We chose Hadron Blind Detector (HBD) for the purpose.

HBD is a mirrorless, windowless Cherenkov detector. It was developed and used by the PHENIX experiment[2]. In HBD, CF_4 gas works as both the radiator and the amplification gas for the detector. The radiator length is 500 mm and the bottom surface of the HBD chamber is covered by photocathodes. A schematic drawing of a single photocathode is shown in Fig. 1. Each photocathode comprises a double-stack 100-μm-thick liquid-crystal-polymer GEM on top of which CsI is evaporated. Cherenkov radiation is converted into photoelectrons by the CsI, and the photoelectrons are collected and amplified by the GEMs. The signals are read out with pads. A mesh is placed over the top GEM to manipulate the field above the GEM, which is called a bias field. A reverse bias field is applied so that ionized electrons are swept into the mesh and are not collected by the GEM. On the other hand, the photoelectrons, which are produced near the GEM surface, are collected even in the reverse bias field. Therefore, the photocathode is only sensitive to photoelectrons. For test experiments, a light baffle is prepared over the photocathode to shield it from Cherenkov light. The difference between the signals obtained with and without the baffle is direct evidence of Cherenkov radiation detection. Oxygen and water should be maintained at the ppm level because they absorb ultraviolet light of interest. Since the PHENIX HBD detects 20 photoelectrons for a single electron track and it has the same radiator length, we expected a similar performance.

We constructed a prototype of HBD using CsI-evaporated GEM with a size of 100 $\times$ 100 mm^2. We performed a test experiment at Research Center for Electron Photon Science (ELPH), Tohoku University. We used a positron beam with a momentum of 670 MeV/c. The oxygen and water contamination was about 0.6 ppm and 2 ppm, respectively, as measured using a oxygen meter and a dew point meter. The results are shown in Fig. 2. We successfully observed Cherenkov radiation from positron beams. However, the number of photoelectrons was about 10, less than what we expected. It was insufficient to apply a threshold at 16 photoelectrons so as to obtain a rejection factor of 100, which is required for the experiment.

The quantum efficiency (QE) of the photocathode was measured in the laboratory using a deuterium lamp and a monochrometer. The photocathode has similar QE compared to that in the PHENIX experiment. The QE was measured before and after the test experiment and showed no sign of degradation.

Since it was reported that gas analyzers showed a contamination level lower than the actual level[3] due to the use of CF_4 gas, the gas transparency was directly measured in the laboratory, in a similar way as the QE measurement. The results were compared with the gas analyzer values. The results indicate that the contamination was a few times the analyzer results. However, the loss of Cherenkov photon from the absorption was only 5% and not a source of serious loss.

A study is underway to improve the performance.

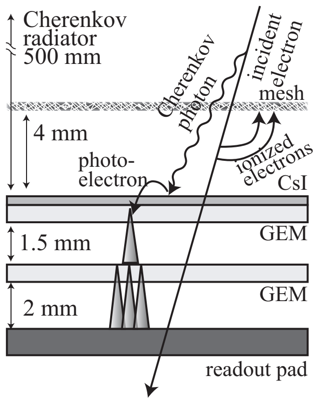

Fig. 1. Schematic drawing of the HBD photocathode.

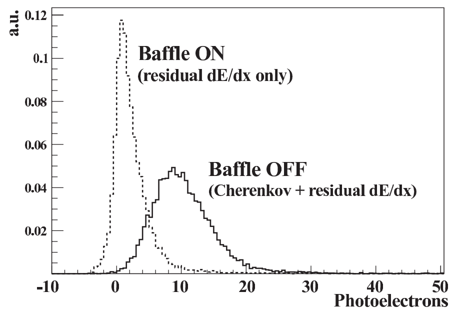

Fig. 2. Charge distribution of HBD with and without the light baffle.

References
1) S. Yokkaichi: RIKEN Acc. Prog. Rep. , in this volume.
2) A. kozolov et al.: Nucl. Instrum. and Meth. **A523**(2004)345.
3) B. Azmoun: private communication.

Design of readout electronics for the J-PARC E16 experiment

T. N. Takahashi for the J-PARC E16 Collaboration

The J-PARC E16 experiment aims to investigate the chiral symmetry restoration in dense matter through the systematic study of the mass modification of vector mesons[1]. The proposed spectrometer system focuses on the invariant mass measurement of e^+e^- pairs decayed from vector mesons. Fig. 1 shows the plan view of the spectrometer system, which consists of gas electron multiplier (GEM) trackers[2] for the momentum reconstruction, hadron blind detectors (HBD)[3] and lead-glass electromagnetic calorimeters (LG)[4] for the electron (positron) identification.

The goal of our data acquisition (DAQ) system is to handle a several kilohertz first-level trigger rate with 90% of live time. The number of readout channels for each detector component is listed in Table 1. As the total number of readout channels amounts to approximately 71000, a dedicated frontend electronics module needs to be developed. For this purpose a design study on readout electronics has recently been commenced.

The GEM tracker needs to have a good position resolution of 100 μm (rms) even for inclined tracks and a high rate capability of ~700 kHz/ch in the severest case. In order to achieve such a level, a readout chip with a fast shaping time of ~50 nanoseconds and a waveform sampler are indispensable for extracting accurate charge and timing information of the signal as well as to reduce pile-ups. Furthermore, the frontend electronics module chips will be mounted near the tracker, and hence, these chips need to be compact, thin, and radiation hard. APV25[5], a 128 channel amplifier-shaper ASIC with an analog pipeline, satisfies the requirements. APV25 offers an additional advantage of a 128:1 analog multiplexed output, which reduces the material budget (e.g., signal cables) for the sensitive area of the spectrometer and provides a cost-effective solution for the digitizer modules. The achieved low power consumption of less than 3 mW/ch leads to a total power consumption of ~180 W, which eliminates the need to install cooling pipes. We are currently developing a APV25-hybrid card and plan to check the performance with a million counts per second beam in the early half of 2012. For the frontend electronics module of the HBD, one of the poential candidates is the electronics that has been successfully used for the PHENIX HBD[6]; it consists of a hybrid preamp (IO-1195-1) followed by a 65 MHz 12 bit FADC. However, the total number of readout pads of the E16 HBD is ~6 times higher as compared to that of the PHENIX HBD, and the component IO-1195-1 would consume ~2.3 kW in the E16 setup (165 mW/ch), which requires the use of cooling pipes in the spectrometer acceptance. We will check the feasibility of applying a readout system with APV25 in the E16 HBD in order to reduce the power consumption.

Table 1. Number of readout channels of E16 detectors.

name	1 module	total (26 modules)
GEM tracker	2160	56160
HBD	540	14040
LG	31–36	846

One 3 inch photomultiplier, Hamamatsu R1652, is attached to every single lead-glass block, each of which is recycled from TRISTAN TOPAZ. The typical width of the PMT output was on the order of several tens of nanoseconds. In order to obtain charge information on such a short pulse with low cost and less dead time, we are considering the use of DRS4[7], which is a switched capacitor array ASIC that operates at a sampling speed in the range of gigaherts. The analog waveform stored in the sampling cells of a DRS4 is read out via a 12 bit FADC at 33 MHz and integrated numerically by the FPGA placed next in the system and in this system DRS4 functions as a time stretcher for short pulses. Although there is some dead time owing to the lack of a pipeline structure in DRS4, it is estimated to be only a few microseconds when only a part of the waveform (e.g., <100 cells) is read out, which is acceptable for our DAQ system.

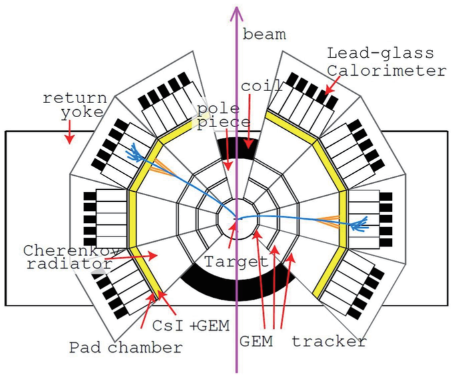

Fig. 1. Plan view of the E16 spectrometer.

References
1) S. Yokkaichi *et al.*; in this report.
2) Y. Komatsu *et al.*; in this report.
3) K. Aoki *et al.*; in this report.
4) Y. Aramaki *et al.*; in this report.
5) M. J. French *et al.*; *Nucl. Instrum. Meth.* A**466** , 359-365 (2001)
6) W. Andersen *et al.*; *Nucl. Instrum. Meth.* A**646**, 35-58 (2011).
7) http://drs.web.psi.ch/

Data acquisition system for the test of GEM tracker for the J-PARC E16 experiment

S. Masumoto[*1,*2] for the J-PARC E16 collaboration

We proposed an E16 experiment at the J-PARC Hadron Experimental Facility to measure the vector meson decays in nuclei with the e^+e^- decay channel, with the aim of investigating the chiral symmetry restoration in dense nuclear matter[1]. An E16 spectrometer consists of three layers of Gas Electron Multiplier (GEM) trackers[2], Hadron Blind Detectors (HBDs), and a lead glass calorimeter.

The GEM trackers are placed in a magnetic field to determine the momenta of electrons and positrons. The incident angle of a particle is expected to be 0°–30°. To achieve the mass resolution of $\sim$5 MeV/c^2, we need to achieve the position resolution of 100 μm for tracks of the incident angle of 0°–30°. The counting rate of the most inner tracker is estimated to be $\sim$5 kHz/mm^2.

A position resolution of the GEM tracker is evaluated with a test experiment at LNS at Tohoku University[3]. A readout board of the GEM tracker has two-dimensional Cartesian projective strips. The strip width is 70 μm and the pitch is 350 μm. Raw signals from the GEM trackers are fed to preamplifiers. The preamplifiers comprise 2 stages of the amplification part. A 1 MΩ resistor and 1 pF capacitance are used as feedback. The second stage amplifies the signal by a factor of 3.2. The total gain of the preamplifiers is 3.2V/pC. The preamplifiers have differential outputs. Flash ADCs (FADCs) are necessary for readouts of the GEM trackers to resolve pileup events and reach less than 100 μm of the position resolution[3]. In the test experiment, RPV-160 modules[4], which are FADCs on the VME system, are used as readouts of the GEM trackers.

However, RPV-160 is not suited for the next step of GEM tracker tests — a tracking test in a magnetic field and a high counting rate test of the GEM trackers. The setup of the tracking test is shown in Fig. 1. Four scintillators and three layers of the GEM trackers are aligned along the beam line. This coincidence of scintillators is used as a beam trigger. The minimum required number of the FADCs for the GEM trackers is 96. Costs of the RPV-160 modules are not reasonable. Furthermore, the maximum DAQ rate of RPV-160 is 100 Hz and is limited by the transfer rate; an improvement in the DAQ rate is required, if possible.

As a candidate for a new GEM DAQ system, we consider the FINESSE FADC board[5] on a COPPER-Lite system[6]. Costs of this system are reasonable for the GEM tracker tests. Furthermore, a maximum DAQ rate of the FADC FINESSE is larger than that of RPV-160.

We attempted to use "FINESSE 65MHz FADC"[5]. We evaluated the new GEM DAQ system using a 9U VME crate, the COPPER-Lite board, and 4 FINESSEs of the FADCs. The sampling rate of the FADCs is set 60 MHz. Inputs of the FADCs and a DAQ trigger are test pulses, which have a counting rate of approximately 1 MHz. To evaluate the maximum DAQ rate of the new DAQ system, DAQ accept signals are counted by a scaler module. The DAQ rate is about 400 Hz. The new DAQ system is more suitable than RPV-160 for the readouts of GEM trackers.

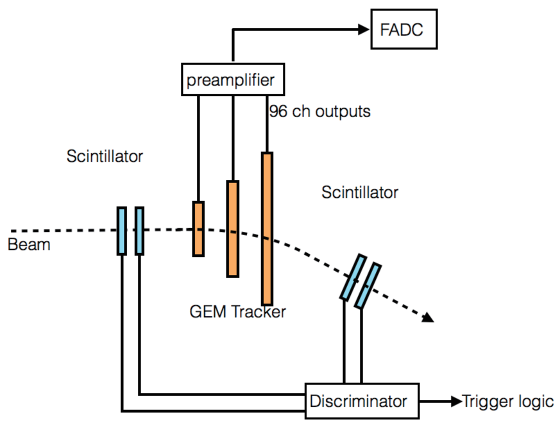

Fig. 1. Setup for the tracking test of the GEM trackers in a magnetic field. Raw signals from the GEM trackers are fed to preamplifiers, and the preamplifier signals are recorded by FADCs.

References

1) S.Yokkaichi, in this report
2) B. Ketzer *et al*, IEEE Trans. Nucl. Sci. vol. 47 No. 5, 2002
3) Y. S. Watanabe *et al.*, Research Report of Lab. of Nucl. Sci., Tohoku Univ. vol. 43, 2010
4) http://www.repic.co.jp/contents/products/repic/maker/rpv_160.html
5) http://kekps.kek.jp/tauchi/finesse/index.html
6) http://www.jahep.org/hepnews/2007/Vol26No3-2007.10.11.12tanaka.pdf
7) T. Uchida, IEEE Trans. Nucl. Sci., vol. 55 No. 3, 2008

*1 RIKEN Nishina Center,
*2 DEpartment of physics, University of Tokyo

Development of a polarized proton target for use in the polarized Drell-Yan experiment

Y. Goto, K. Akasaka,[*1] N. Doshita,[*1] Y. Fukao, S. Ishimoto,[*2] T. Iwata,[*1] H. Kobayashi,[*1] H. Matsuda,[*1] Y. Miyachi,[*1] I. Nakagawa, K. Nakano,[*3] S. Sawada,[*2] T.-A. Shibata,[*3] S. Suzuki,[*2] and Y. Tochigi[*1]

We have been performing the SeaQuest experiment with the aim of detecting muon pairs from the Drell-Yan process with a 120-GeV unpolarized proton beam extracted from the Fermilab Main Injector[1)]. One of the goals of the experiment is to study the flavor symmetry violation of antiquark distributions in the proton.

We have discussed extensions of the SeaQuest experiment with a polarized proton beam or a polarized proton target. In the polarized Drell-Yan experiment, we will be able to study the spin structure of the proton. The single transverse-spin asymmetry of the Drell-Yan process will indicate the transverse-momentum-dependent (TMD) parton distribution functions, which is closely related to the orbital angular momentum in the proton.

Our first topic of interest is the measurement of the TMD quark distribution in the valence region. A simple approach to measuring the valence-quark distribution is to use the polarized proton beam and to detect muon pairs from the Drell-Yan process using existing SeaQuark spectrometer, which covers the forward direction. In this case, we can measure the TMD quark distribution with a large fraction of the momentum in the polarized proton beam. The other approach is to use the polarized proton target, but in this case, we need a backward spectrometer for muon pairs to measure the TMD quark distribution with a large fraction of the momentum in the polarized proton target.

In order to obtain the polarized proton beam in the SeaQuest experiment, a polarized proton ion source needs to be installed, and Siberian snake magnets are necessary in the Booster and the Main Injector to avoid depolarization of the polarized proton beam. Polarimeters are also necessary to monitor the beam polarization in each acceleration stage. We plan to formulate a proposal for the polarized Drell-Yan experiment using the polarized proton beam and the existing spectrometer and submit the proposal in 2012.

In parallel, we are developing a polarized proton target at KEK and Yamagata University[2)]. The target material will be developed using a 5-T magnetic field at 1 K at KEK and using a 2.5-T magnetic field at less than 0.5 K at Yamagata. In the case of using the polarized proton target and detecting muon pairs in the forward direction, we can measure the polarized antiquark distribution with a small fraction of the momentum in the target. If we can extend the SeaQuest spectrometer to cover the forward as well as the backward direction, we can measure the polarized valence-quark distribution in the polarized proton target.

We plan to develop a polarized proton target from irradiated-ammonia at KEK. The target was originally developed by Michigan University[3)] and is presently located in the KEK-PS North Counter Hall. We are rebuilding the target system as a platform for the development. For the polarized Drell-Yan experiment, we require a sufficiently large amount of the target material because of the small cross section of this process. In order to operate the polarized proton target and preserve the polarization, we have to stabilize the target at a low temperature by removing the heat from the injected high-intensity beam. We want to obtain the desired shape of the target material by testing the cooling performance of the target system. The development has been delayed by the earthquake that occurred in 2011. After recovering the facility in the North Counter Hall, we have resumed rebuilding the target system. We are also developing an NMR system and preparing for the detection of the thermal equilibrium signal from the target material.

We are developing different target materials at Yamagata University. One candidate material is an irradiated polyethylene fiber that has a large surface area and high deformation performance and yields a large cooling power. The development will be performed with a new cryostat, which provides an improved stability of the operation. The cooling test of the new cryostat is underway. By adjusting the conductance and suppressing thermal flow from outside of the cryostat, we intend to achieve less than 0.5 K by dilution refrigeration. For the achievement of high polarization, measurement of the electron spin density of the material using electron spin resonance (ESR) is a key process. We are systematically investigating the sensitivity of ESR measurement with targets of different shapes. We will irradiate polyethylene with electron beams and measure the electron spin density precisely with ESR.

This research is supported by the JSPS Grant-in-Aid for Scientific Research (B) 22340070.

*1 Yamagata University
*2 KEK
*3 Tokyo Institute of Technology

References

1) Y. Goto *et al.*: RIKEN. Accel. Prog. Rep. **43**, 80 (2010).
2) Y. Goto *et al.*: RIKEN. Accel. Prog. Rep. **44**, 220 (2011).
3) D. G. Crabb *et al.*: Phys. Rev. Lett. **64**, 2627 (1990).

Micromegas readout for future TPC experiment

T. Isobe, A. Taketani, H. Ando,*1 S. Tamagawa,*1 Y. Kawamo,*2 and H. Miya,*3

[gaseous detector, micro pattern detector]

The Micromegas[1)] readout is one of the most innovative gaseous readouts. It consists of a mesh and plate that are parallel to each other, with a small amplification gap (100 μm). Combined with a conventional drift space, this device makes it possible to remove positive ions produced during avalanche development. This micropattern detector technology offers a substantial advantage in terms of counting rate, energy, spatial and time resolution, granularity on large surface, and simplicity[2–4)]. It is successfully used in many high-energy experiments. This substantial advantage is also expected to be useful for active target TPC experiments at RIBF because of its high counting rate and low angle dependence of spatial resolution. In addition, we expect small crosstalk effect which is important for the simultaneous measurement of small Z (Z$\sim$1) and large Z (Z$\geq$10) particles. One of the critical issues to be addressed in nuclear physics experiments is the deposition of strongly localized charge due to the energy deposition from large Z particles. This would cause sparks and damage the amplification device.

Since no Japanese organization has tried using Micromegas in nuclear physics experiments, we initiated this study by importing the Micromegas board from France, where it was originally invented. The amplification gap in Micromegas is obtained by suspending a mesh over the surface of anode strips or pads. A narrow gap of 128 μm is precisely obtained by printing adequate insulating spacers (pillars) on top of the anode plane via conventional lithography of a photoresistive film. The mesh is stretched and glued onto a frame and then rested on top of the pillars. The challenge to the gluing is with the handling of the mesh to obtain a rather good flatness and parallelism between the anode and cathode, i.e. the mesh. The flatness of the mesh should be accurate to within 10 μm. Recently, a new fabrication method for Micromegas production[5)] has been developed, and we tried to use the Micromegas board fabricated with the new method. Our Micromegas board has 144 pads (6 mm$\times$6 mm) that are designed to be compatible with T2K readout electronics[6)].

Figure 1 shows the setup used for testing Micromegas. A Micromegas board and a plane for making a drift space with a 1 *cm* drift distance are placed in a small gas chamber (20 cm$\times$20 cm$\times$5 cm). P10 (Ar-90% + CH_4-10%) gas is used for gas amplification, and a charge sensitive preamplifier with a 2 pF feedback capacitor is connected to the mesh for reading out the positive signal. Figure 2 shows a ^{90}Sr electron track signal obtained using the Micromegas mesh. We succeeded in obtaining a clear signal with a decay time of 10 μsec by using the Micromegas. After checking the gas gain by using a ^{55}Fe X-ray source, we plan to develop a Japanese version of the Micromegas and to study the response of Micromegas to heavy-ion signals.

*1 Tokyo Metropolitan College of Industrial Technology
*2 Physics Department, Rikkyo University
*3 Center for Nuclear Study (CNS), University of Tokyo

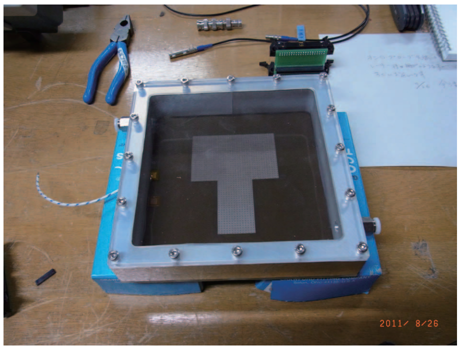

Fig. 1. Setup for Micromegas test contained in a small gas chamber.

Fig. 2. Micromegas electron signal pulse shape.

References

1) Y. Giomataris et al.: Nucl. Inst. and Meth. A **376**, 29 (1996).
2) J. Derre et al.: Nucl. Inst. and Meth. A **449**, 554 (1999).
3) I. Giomataris et al.: Nucl. Inst. and Meth. A **419**, 239 (1998).
4) G. Charpak et al.: Nucl. Inst. and Meth. A **478**, 26 (2002).
5) I. Giomataris al.: Nucl. Inst. and Meth. A **560**, 405 (2006).
6) P. Baron et al.: IEEE Trans. on Nucl. Sci. **55**, 1744 (2008).

Development of the PTFE electrode foil for a gas electron multiplier

M. Wakabayashi,*[1] K. Komiya,*[1] K. Fujiwara,*[1] T. Kobayashi,*[1] H. Hamagaki,*[2] and A. Taketani

The gas electron multiplier (GEM) is a detector that captures X-rays and charged particles on the basis of gas multiplication. The GEM has two problems. It is the first problem that the percentage of good final products is low with about 75%. The second problem is that the GEM foil[1] is easy to break down by the abnormal discharge. Thus, it is necessary to improve both the microfabrication method and the reliability. In this study, we identified materials for the GEM foil and propose a method for the microfabrication of the through-holes in the GEM.

Polyimides (PIs) and liquid-crystal polymers (LCPs) are used as insulator materials for the GEM foil. Copper foils are fixed on both sides of the insulator films to build a flexible printed circuit board. A high voltage of 300V is applied on both sides of the GEM foil, which is 50~100 μm thick. Since the GEM foil would easily rupture if the insulator material is of poor quality, we selected several candidate materials for the insulator. The characteristics of general candidate materials such as polyethylene terephthalate (PET), polyethylene naphthalate (PEN), and polytetrafluoroethylene (PTFE) are summarized in Table 1. Among all the materials, PTFE has the highest arc resistance[2]. Therefore, PTFE is considered the ideal candidate for the insulator of the GEM foil in our evaluation.

Copper was sputtered on the PTFE film by the magnetron sputtering (SX-200, ULVAC, Inc.). A 50-μm-thick PTFE film was chosen for the evaluation. The sputtering conditions were as follows: applied DC power, 1 kW; pressure, 0.67 Pa; and sputtering time, 30 s. The thickness of the copper layer deposited on the PTFE was measured to be 40 ± 3 nm by a stylus profiler (Dektak150, ULVAC, Inc.). The sheet resistance of the film was found to be 4.4 Ω/sq. by the four probe method. Thus, we concluded that the sputtered PTFE film is well suited for use as the GEM foil electrode.

Methods such as chemical etching, plasma etching, and CO_2 laser processing are used for processing through-holes[3) 4)] in commercial GEM foil. Since PTFE has strong chemical resistance, chemical etching was impossible. Furthermore, it was difficult to fabricate through-holes by using CO_2 laser because thermal damage occurred. Consequently, we tried to fabricate through-holes using a femtosecond laser. The advantages of this type of laser are non-heat processing and multiphoton absorption. The copper-sputtered PTFE film discussed in the previous section was used for femtosecond laser processing. The processing conditions were as follows: laser output, 30mW; scanning speed, 0.1 mm/s; and pitch in zigzag arrangement, 200 μm. Figure 1 shows the scanning electron microscope (SEM) images of the PTFE surface and the cross section[5)] of the prototype GEM foil. When using the femtosecond laser, numerous good-quality, defect-free through-holes were formed. The quality of the prototype was confirmed by visual and electrical inspection. Thus, we successfully processed defect-free through-holes.

In summary, we selected PTFE as the insulator material for the GEM foil and fabricate a copper electrode on the PTFE film by magnetron sputtering. We succeeded in fabricating through-holes without short-circuit by using femtosecond laser processing. As the next step, we plan to carry out a high-voltage-application test to study the GEM response to cosmic rays.

*[1] Electronics and Semiconductor Technology Group, Tokyo Metropolitan Industrial Technology Research Institute
*[2] Center for Nuclear Study, University of Tokyo

Table 1. Characteristics of insulator materials.

Materials	PI	LCP	PET	PEN	PTFE
Density [g/cm^3]	1.43	1.35	1.4	1.36	2.13~2.20
Tension strength [MPa]	315	108	48~73	193	20~35
Water absorption [%]	1.3	0.08	0.4	0.3	0
Volume resistivity [Ω•cm]	10^{17}	6×10^{16}	10^{17}	10^{17}	$>10^{18}$
Arc resistance [s]	135	186	117	34	>300
Melting point [deg C]	-	-	258	269	327

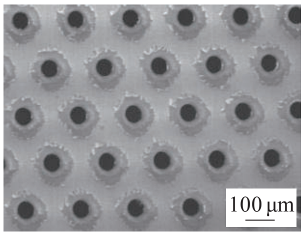

(a)

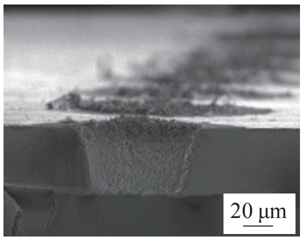

(b)

Fig. 1. SEM images of the prototype GEM foil subject to by femtosecond laser processing. (a) Top view of the GEM foil. (b) Cross section of a hole.

References

1) S.Uno: HIGH ENERGY NEWS, 30, 2, (2011), p.66.
2) JIS K 6911-1995, p.35-36.
3) M. Inuzuka, et al,: Nucl. Instr. and Meth., A 525, (2004), p.529.
4) T. Tamagawa, et al.: Nucl. Instr. and Meth., A 560, (2006), p.418.
5) K. Komiya, et al.: In this report.

Failure analysis methods of GEM

K. Komiya,*1 M. Wakabayashi,*1 K. Fujiwara,*1 T. Kobayashi,*1 A. Taketani, and H. Hamagaki*2

The Gas Electron Multiplier (GEM) is a charged particle detector based on the electron avalanche effect. It was recently used in nuclear and particle physics experiments. A 50-100 um thick Polyimide (PI) or liquid crystal polymer (LCP) film is used as an insulator material for the GEM foil[1]. Copper sheets are laminated on both side of the film to fabricate a flexible printed circuit board. During operation, a high voltage is applied between the copper electrodes. However, the GEM foil tends to break down due to abnormal discharge[2), 3)]. In this report, we describe three methods of obtaining the cross section of a GEM foil in order to analyze the reason for its failure.

The mechanical polishing technique is a commonly used method to obtain the cross section of a material. The GEM foil is filled with an epoxy resin, and then, the foil is polished. Table 1(a) shows a scanning electron microscope (SEM) image of the cross section of a polished GEM foil. Although the cross section is easily observed with this method, the surface of the wall of the through-hole cannot be observed due to the filling of resin.

The ion milling[4)] method is a technique to obtain the cross section surface by irradiation with Ar ions. Table 1(b) shows a SEM image of the cross section of the GEM foil. The removed materials were deposited on the sidewall surface of the through-hole. Thus, the sidewall surface of the through-hole was difficult to observe clearly.

An ultra microtome[5)] can slice a material to obtain a cross-sectional surface. Table 1(c) shows a SEM image of a cross- sectional surface obtained by slicing with an ultra microtome. The sidewall surface of the through-hole was possible to observe.

Next, we tried to analyze the defective GEM foil. Figure 1(a) shows the top view of one of the through-holes in the defective GEM foil. Figure 1(b) shows a SEM image of a cross section obtained using an ultra microtome along the white line in figure 1(a). The contamination at Point (1) in figure 1(b) consisted of copper (24.2 at%) and carbon (44.6 at%) as determined by energy dispersive X-ray spectrometry. The contamination was due to copper being left over from etching process, which suggests that careful cleaning should be done in the manufacturing process.

Consequently, among the three methods, the ultra microtome is the best method for obtaining the cross section of the GEM foil. With the use of the ultra microtome, the sidewall detail of the through-holes was observed without deformation and the compositions of the contaminants could be determined.

*1 Electronics and Semiconductor Technology Group, Tokyo Metropolitan Industrial Technology Research Institute
*2 Center for Nuclear Study, The University of Tokyo

Table 1 The methods to obtain the cross-sectional surface of GEM foil tested in this paper along with the corresponding SEM images.

(a) Mechanical polishing	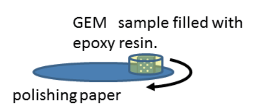	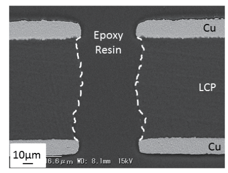
(b) Ion milling	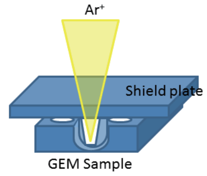	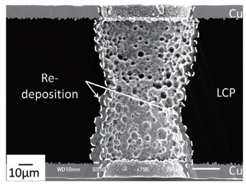
(c) Ultra microtome	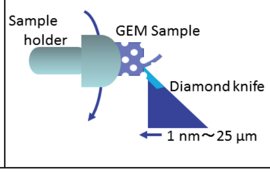	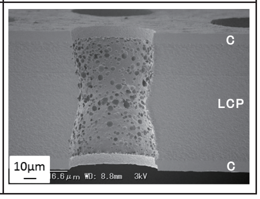

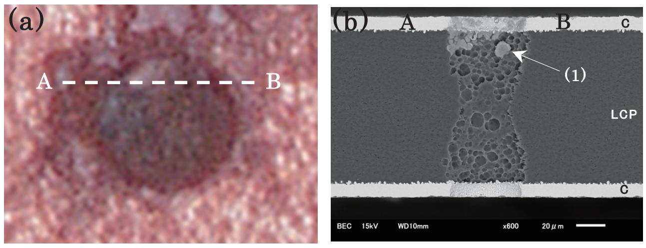

Fig. 1 Images of the defective GEM foil
(a) The Top view of the defective GEM foil
(b)SEM image of the cross section obtained using ultra-microtome

References
1) S. Uno : HIGH ENERGY NEWS, Vol. 30(2011) p66
2) Y.Honma, A Ochi, K Moriya, S. Matsuda, S. Kobayashi : Nuclear Instruments and Methods in Physics Research A 599 (2009) p47–52Physics Research A
3) Alessandro Cardini, IEEE Science symposium Conference Record(2005),p1127-1131
4) The product information, JOEL(http://www.jeol.info/products/ib-09020cp/)
5) The product information, Leica microsystems (http://www.leica-microsystems.com/jp/products/electron-microscope-sample-preparation/biological-specimens/room-temperature-techniques/ultramicrotomy/details/product/leica-em-uc7-1/)

Development of inexpensive radiation detector for educational purpose

I. Y. Kawamo, T. Takahashi,*[1] A. Taketani, H. Murakami*[2], M. Wada, M. Sekimoto,*[3] K. Ninomiya,*[1] H. Ashikaga,*[4] K. Imai,*[5] H. Okura,*[6] S. Kubono,*[7] K. Nakagawa,*[8] T. Fukui,*[9] Y. Maruo,*[10] and Y. Morimoto*[11]

Since the reactor accident at Fukushima, increasingly people concerned about radiation. The group of nuclear physicists and teachers has met and discussed requirements for promoting the education about radiation. In accordance with the discussion, a suitable radiation detector assembly kit is being developed.

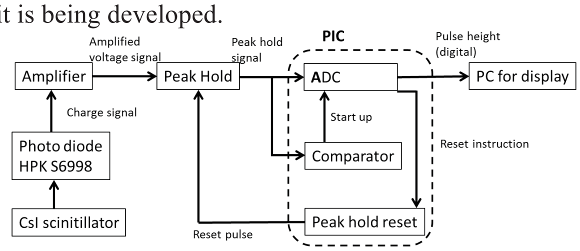

Fig. 1: Conceptual configuration of detector

A conceptual configuration of the detector is shown in Fig. 1. Radiations are injected into CsI crystal and a charge signal is generated at the photo-diode sensor. The signal is fed into a preamplifier and amplified to a level suitable for the analog to digital convertor (ADC). A peak hold circuit holds the integrated signal from the preamplifier to be ready by the ADC. The digitized value is transmitted to the PC and graphically displayed. In this article, we describe the section of the detector upstream from the CsI sensor to the peak hold circuit. The downstream section will be described in another article.[1)]

The amplifier consists of a charge sensitive preamplifier and a shaping amplifier. The photons, which are generated by the radiation in the CsI, excite electron-hole pairs from the valence band in the depletion layer of the photo-diode sensor. The excited electrons and holes drifts toward the voltage biased electrode. The amount of charges generated is proportional to the number of photons and is therefore proportional to the energy of the original radiation. The charges are amplified by the charge sensitive preamplifier and then amplified by the shaping amplifier, which consist of a differential and integrated filter used to reduce the unnecessary noise.

The peak hold circuit holds the peak value of the voltage pulse from the shaping amplifier during A/D conversion. The peak value of the voltage is held by a capacitor. The stored charges leaks, and hence, the voltage drops exponentially according to formula [1)]. After the A/D conversion, the charges are released through a FET switch, which is controlled by the reset pulse.

$$Vo = Vi * \exp\left(-\frac{t}{\tau}\right), \tag{1}$$

When Vo is peak hold output voltage, Vi is input voltage, and τ istime constant.

The noise of the amplifier was evaluated using a multi-channel analyzer SEIKO EG&G MCA 7600. A simulated signal is injected into the preamplifier through the 2 pF capacitor. The amount charge is estimated from the capacitance and applied voltage. The amplifier noise is measured as about 20 keV for FHWM.

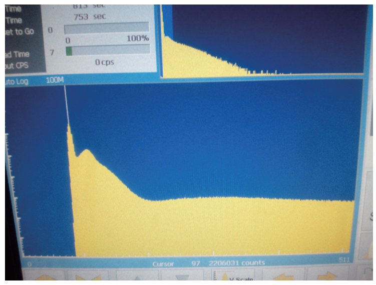

Fig. 2: Pulse height spectrum

The signals from the radiation source Sr-90 are observed by an oscilloscope and MCA. Fig. 2 shows the pulse height spectrum of the shaping amplifier output. The Horizontal axis represents energy with an arbitrary scale. The sharp peak at lower energy is due to the noise, and the wider peak to be due to signals from radiation. The signal to noise ratio is about 2.

The peak hold circuit is tested using voltage pulse input. The input and output are simultaneously observed by an oscilloscope. The peak voltages are held well, and the decay time τ is measured with the oscilloscope. It is 22.5 ms, and the degradation of the output during the 20 μs duration of AD conversion is estimated as 0.09%. This degradation of the pulse height measurement has a negligible effect on the S/N = 2 amplifier system. The output voltage is reset by the turning ON of the FET switch driven by the reset pulse.

We connected all the systems, CsI scintillator, amplifiers, peak hold circuit, and PIC base pulse height analyzer, and tested with the radiation source Cs-137.

Total cost of the parts is about 5000 Yen, which includes the photodiode and locally manufactured multi-channel analyzer[1)], but does not include the cost of the CsI crystal.

In Summary, we have been developing an inexpensive, with easily available parts, radiation detector for an education purpose.

Reference

1) A. Taketani et al. in this report.

*1 Department of Physics, Rikkyo University
*2 RIKEN Wako Institute
*3 KEK
*4 Tottori University of Environmental Studies
*5 Advanced Science Research Center, Japan Atomic Energy Agency
*6 Osaka Science Museum
*7 Center for Nuclear Study, University of Tokyo
*8 Kobe University
*9 Hakuryo junior high, High School
*10 Hyogo Prefectural Kamigoori Senior High School
*11 Hyogo Prefectural Tohban Technical High Schoo

Development of an aerogel Cherenkov detector for spectroscopy of η' mesic nuclei at GSI

Y.K. Tanaka,[*1] H. Fujioka,[*2] H. Geissel,[*3] R.S. Hayano,[*1] K. Itahashi,[*4] S. Itoh,[*1] V. Metag,[*5] M. Nanova,[*5] T. Nishi,[*1] K. Okochi,[*1] H. Outa,[*4] K. Suzuki,[*6] T. Suzuki,[*1] M. Tabata,[*7,*8] and H. Weick,[*3]

[Cherenkov detector, aerogel, exotic nuclei]

In this report, we describe the development of an aerogel Cherenkov detector for spectroscopy of η' mesic nuclei at GSI.[1)] In this experiment, we will inject a $T = 2.5\,\mathrm{GeV}$ proton beam extracted from the synchrotron (SIS) into a ^{12}C target. Then, we will measure the momentum of outgoing deuterons, generated by the $^{12}\mathrm{C(p,d)}\eta'\otimes^{11}\mathrm{C}$ reaction,[2)] using two sets of multiwire drift chambers in the downstream focal plane of the spectrometer (FRS). In addition to the signal deuterons, a large number of background protons (~50 kHz) are expected to reach the focal plane. Therefore, it is necessary to reduce this background rate to the order of 100 Hz at the trigger level. For this purpose, we will use an aerogel Cherenkov detector to identify the background protons. As the background protons have a velocity of $\beta \sim 0.95$ while the deuterons have a velocity of $\beta \sim 0.83$, we can distinguish between them using a Cherenkov radiator with a refractive index of 1.06 − 1.20.

Figure 1 shows an overview of the aerogel Cherenkov detector under development. For the radiator, we use pieces of silica aerogel with a refractive index of about 1.18, developed using a pinhole drying method.[3)] Since aerogel made by this method has a greater transparency length ($> 20\mathrm{mm}$ at $\lambda = 400\,\mathrm{nm}$) than that made by the conventional method, we expect it to serve as an effective Cherenkov radiator. This aerogel can be set in front of the box equipped with eight PMTs. A mirror is also placed inside the box for reflecting the emitted photons in the radiator to facilitate their entry into the PMTs.

To achieve maximum efficiency for identifying the background protons, we have optimized the mirror configuration. By gridding the incident position (x, y) of the background proton on the surface of the aerogel, we simulated the average number μ of photoelectrons observed by the eight PMTs, assuming that the thickness of the aerogel is 2 cm. From this simulation, we determined the optimal angles of the mirror where the minimum value of μ in the region of interest is maximized. Figure 2 is the μ distribution on the (x, y) plane for the optimized angles. In this figure, a minimum of $\mu = 12.7$ photoelectrons and an average of $\mu = 16.6$ photoelectrons are expected. This value is quite sufficient to achieve 99.5% proton rejection capability in the final experiment.

In the near future, we are planning a test experiment of this Cherenkov detector to evaluate its performance. We will inject protons of various velocities into several points on the aerogel and measure the distributions of the total output from the PMTs. Then, we will evaluate the actual performance of this detector by comparing the results with those of the simulation.

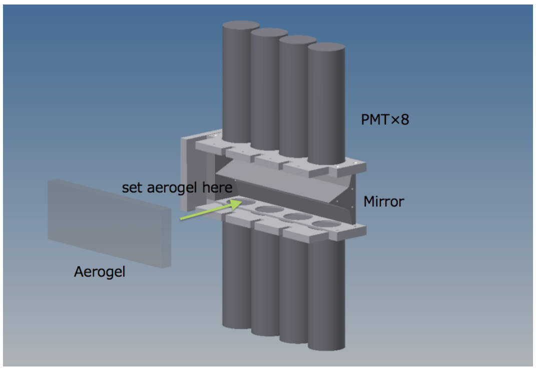

Fig. 1. Overview of the aerogel Cherenkov detector

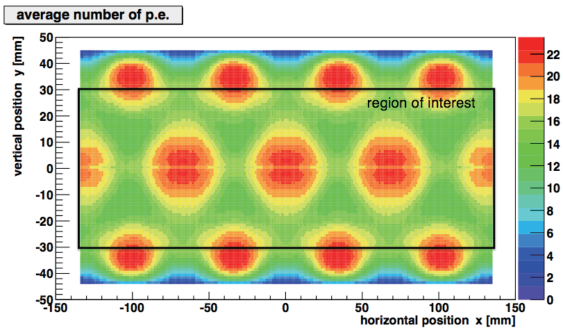

Fig. 2. Average number of photoelectrons for the proton entering the aerogel at a point (x, y)

*1 Department of Physics, University of Tokyo
*2 Division of Physics and Astronomy, Kyoto University
*3 GSI, Germany
*4 RIKEN Nishina Center for Accelerator-Based Science
*5 Universität Gießen, Germany
*6 Stefan Meyer Institut für subatomare Physik, Austria
*7 Japan Aerospace Exploration Agency
*8 Department of Physics, Chiba University

References

1) K. Itahashi et al. : Letter of Intent for GSI-SIS (2011).
2) D. Jido, H. Nagahiro, and S. Hirenzaki : Phys. Rev. C **85**, 032201(R) (2012)
3) M. Tabata et al. : Nucl. Instrum. Methods A **623**, 339-341(2010)

Development of next generation device for NEWTON experiment

K. Ninomiya,[*1,*2] R. Kishi,[*1] H. Nishio,[*1] H. Murakami,[*1] A. Taketani[*2] and J. Murata[*1]

Weakness of the gravitational force as compared to the other three gauge interactions is considered as one of the most severe problems in theoretical physics. It is necessary to resolve this problem in order to unify the three gauge interaction and gravitational force. According to a recent unified theories (super string theory, M-theory, ADD model, etc.), the gravitational field may extend into extra dimensions. In the ADD model[1)], extra dimensions are predicted to exist at below millimeter scale. In such a case, the observation of a deviation from Newton's inverse square law can be expected below millimeter scale. If extra dimensions exist, then the gravitational potential should become modified. Modified gravitational potential is conventionally expressed using the Yukawa interaction form.

$$V(r) = -G\frac{Mm}{r}(1 + \alpha e^{-\frac{r}{\lambda}}) \tag{1}$$

Here, α is the coupling constant and λ is the range of the new interaction. To search for the new Yukawa term, Newton's inverse square law has been experimentally tested. However, the high precision test of the inverse square law is performed at only astronomical scales. Therefore, it is necessary to test the gravitational force below mm scale.

In our experiment, gravitational force is measured using a torsion pendulum (target) and an online image analyzing system. Angular displacements of the torsion pendulum before and after moving the gravity source (attractor) positions are measured as the gravitational signal. The torsion pendulum is twisted toward the balanced position where the restoring force equals the gravitational force from the attractor. Therefore, the strength of the gravitational force can be estimated from the angular displacement of the torsion pendulum[4,5)]. The data recording system was originally developed for the PHENIX experiment at the Relativistic Heavy Ion Collider (RHIC) at Brookhaven National laboratory, as an optical alignment system (OASys)[2)]. By applying this system, we developed a digital image analyzing system using a digital video camera[2,3)]. In the past, we succeeded in testing Newton's inverse square law at the centimeter scale with 5% accuracy in the Newton SC experiment[6)]. In addition, we also succeeded in confirming the weak equivalence principle at the shortest scale in the Newton II experiment[6)]. Based on these results, a next genaration device named Newton IV is developed, which is aimed at achieving the most precise test of the inverse square law below millimeter scale. the Newton IV experiment is a NULL type experiment[7)].

*1 Department of Physics, Rikkyo University, Japan
*2 RIKEN Nishina Center,Japan

A NULL type experiment is advantageous for testing the inverse square law because it is sensitive to deviations from Newtonian gravity. To perform the NULL type experiment, the geometries of the attractor and target selected of the ring type. Using the ring type attractor and ring target, Newtonian gravity can easily be suppressed to determine the layout and the number of holes (fig. 1). Newton IV is designed to be able to move the attractor ring rotating outside the target ring. The attractor is very slow in comparison to the oscillation period of the target ring, the angular displacement of the target coincides with the attractor motion[6)]. Therefore, position dependence between the attractor and the target can be measured.

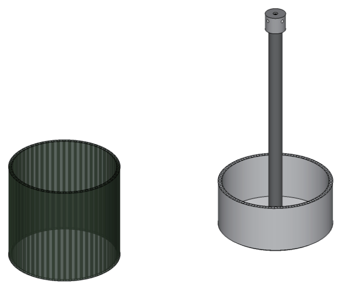

(a) attractor (b) torsion pendulum (target)

Fig. 1. Next generation device. The attractor and the target are made with 60 holes created at equal distances. The target ring is suspended inside the attractor ring using the 40 μm tungsten wire. The gap between the attractor and the target is set to 500 μm.

Now We completed the alignment of the device using a laser displacement sensor and a starting test measurement. Newton IV is designed to be sufficiently sensitive to any deviation from Newtonian gravity. Therefore, this device will enable us to achieve the most precise test of the inverse square law below millimeter scale through the Newton IV experiment.

References

1) Nima Arkani-Hamed, Savas Dimopoulos, Gia Dvali, Phys. Lett. B 429 (1998) 263-272.
2) J. Murata, IEEE Nuclear Science Symposium Conference Record 675 (2005).
3) J. Murata et. al., Nucl. Instrum. Meth. A 500(2003) 309-317.
4) M. Hata et.al., Journal of Physics: Conference Series 189 (2009) 012019
5) K. Ninomiya et.al., Journal of Physics: Conference Series 189 (2009) 012026
6) K. Ninomiya, Master thesis, Rikkyo University (2010)
7) N. Ogawa, Master thesis, Rikkyo University (2011)

Computing and Network Environment at RIKEN Nishina Center

T. Ichihara, Y. Watanabe, and H. Baba

We have been operating Linux/Unix NIS/NFS cluster systems[1,2] at the RIKEN Nishina Center.

Figure 1 shows the current configuration of the Linux/Unix servers at the RIKEN Nishina Center. The host *RIBF.RIKEN.JP* is used as the mail server, NFS server of the user home directory /rarf/u/, and NIS master server. This is a core server for the Linux/Unix cluster. This server and RAID systems were replaced in 2011[2]. Approximately 500 user accounts are registered on this server. The current size of /rarf/u is approximately 16 TB.

Since more than six years have passed since the launch of the /rarf/w RAID system for experimental data analysis and since more than five years have passed since the launch of the *RIBFDATA01.RIKEN.JP* server, we decided to replace them. In addition, the utilization of /rarf/d RAID, which stores the experimental raw data, exceeded more than 80%. Therefore, we have obtained two reliable sets of 52 TB RAID6 with SAS-HDDs for the new /rarf/w data analysis area and a 52 TB RAID6 with SAS-HDDs for the new /rarf/d raw data area.

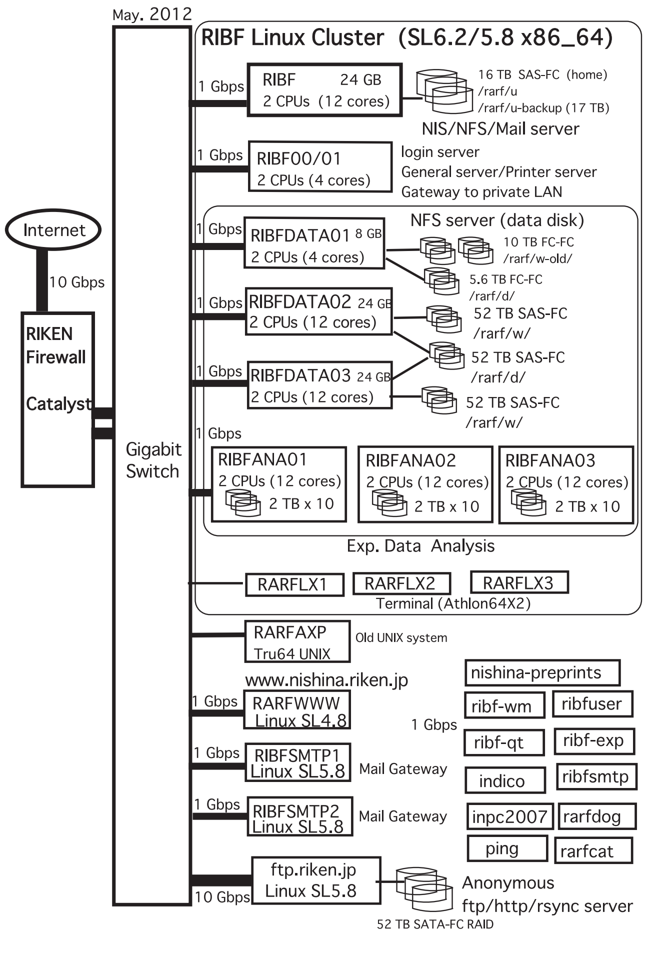

Fig. 1. Configuration of the RIBF Linux cluster.

The planned replacement process is as follows. We will first install new *RIBFDATA02/03* servers and then connect them to the new RAID6 (52 TB SAS-FC each) systems. Then, we will set up the data analysis environment on the new servers. When the new environment is ready, we will copy the contents of /rarf/w in the old RAID to the new RAID systems and then use the new *RIBFDATA02/03* servers and RAID systems. The total size of the new /rarf/w is 104 TB, which is approximately ten times larger than the previous system. Since the experimental data size at the RIBF is increasing with every passing year, this replacement will facilitate the analysis of amounts size of experimental data. We are planning to start using the new *RIBFDATA02/03* servers and the 52 TB + 52 TB RAID system in the spring or summer of 2012. Further, another 52 TB RAID system (/rarf/d) will be connected to *RIBFDATA02/03* to store the new raw data obtained in RIBF experiments. After this replacement, we will stop the operation of the old *RIBFDATA01* system.

In addition, three dedicated data analysis servers, *RIBFANA01/02/03*, have been installed for the analysis of RIBF experiments. These servers are equipped with 10 sets of 2-TB SATA HDD and RAID controller each other for local storage of experimental data. With these local storage devices, experimental data on the servers can be accessed very efficiently without network i/o.

The hosts *RIBF00/01* are used as ssh login servers to provide access to external users; they are used as general-purpose computational servers, printer servers, and a gateways to the RIBF intranet.

The hosts *RIBFSMTP1/2* are mail front-end servers, and they are used for tagging spam mails and isolating virus-infected mails.

An anonymous ftp server, *FTP.RIKEN.JP*, is managed and operated at the RIKEN Nishina Center. Major Linux distributions are mirrored daily at the ftp server for facilitating high-speed access to the users.

The development of the RIBF data acquisition system (DAQ) is described elsewhere[3].

References

1) http://ribf.riken.jp/
2) T. Ichihara et al.: RIKEN Accel. Prog. Rep. 44, 234 (2011).
3) H. Baba et al.: In this report.

CCJ operation in 2011

K. Shoji, H. En'yo, T. Ichihara, Y. Ikeda, T. Nakamura[*1], Y. Watanabe, and S. Yokkaichi

1 Overview

The RIKEN Computing Center in Japan (CCJ)[1)] commenced operations in June 2000 as the largest off-site computing center for the PHENIX[2)] experiment at RHIC[3)]. Since then, CCJ has been providing numerous services as a regional computing center in Asia. We have transferred several hundred TBs of raw data files and nDSTs, which is the term for a type of summary data files at PHENIX, from RHIC Computing Facility (RCF)[4)] to CCJ. The transferred data are first stored in High Performance Storage System (HPSS)[5)] before starting the analysis. CCJ maintains sufficient computing power for simulation and data analysis by operating a PC cluster running a PHENIX compatible environment.

A joint operation with RIKEN Integrated Cluster of Clusters (RICC)[6)] was launched in July 2009. Twenty PC nodes have been assigned to us for dedicated use, sharing the PHENIX computing environment.

Many analysis and simulation projects are being carried out at CCJ, and these projects are listed on the Web page `http://ccjsun.riken.go.jp/ccj/proposals/`. As of December 2011, CCJ has been contributed 29 published papers and more than 33 doctoral theses.

2 Configuration

2.1 Calculation nodes

In our machine room 258/260 in the RIKEN main building, we have 18 PC nodes[a)], which were installed in February 2009, and 10 new PC nodes[b)], which were added in March 2011; these nodes have been used for the analysis of the PHENIX nDST using the local disks. The details of the data-oriented analysis system on the nodes are presented elsewhere[7)]. Numbers of malfunctioned SATA disks in the HP servers (including NFS/AFS servers described in the next section) were 8 out of 190 1-TB disks in Jan–Dec 2011 and 4 out of 120 2-TB disks in Apr–Dec 2011.

We terminated the use of some old nodes, namely, 36 nodes of the IBM server and 18 nodes of the LinuxNetworx server, in March 2011.

The OS on the calculation nodes is Scientific Linux 5.3[8)], and the same OS is run on the 20 nodes used by us at RICC. As a batch-queuing system, LSF 7.0.2[9)] and Condor 7.4.2[10)] were run on the CCJ and RICC nodes, respectively, as of February 2011. Upgrade to LSF 8.0.0 was performed at CCJ in March 2011.

2.2 Data servers

Two data servers (SUN Fire V40 with 10 TB FC-RAID and HP ProLiant DL180 G6 with 20 TB SATA raw disks) are used to manage the RAID disks, which contain the user data and nDST files of PHENIX. The disks are not NFS mounted on the calculation nodes to prevent the performance degradation by the congestion of processes and network. These disks can be accessed only by using the "rcpx" command, which is the wrapper program of "rcp" developed at CCJ and has an adjustable limit for the number of processes on each server. One of the above data servers, a SUN Fire v40, was replaced in March 2012 with a new data server[c)].

The DNS, NIS, NTP, and NFS servers are operated on the server ccjnfs20[d)] with a 10 TB FC-RAID, where users' home and work spaces are located. The home and work spaces are formatted with VxFS 5.0[11)]. Backup of home spaces on ccjnfs20 is saved to another disk server once a day and to HPSS once a week. The backups on HPSS are stored for 3 weeks. In Oct 2011–Mar 2012, a controller of the RAID disk connected to ccjnfs20 frequently committed the "link down" error and stopped the operation of CCJ several times. Replacement of the RAID controller and chassis did not solve the problem, and finally, the I/F card was replaced in March 2012.

2.3 HPSS

Since December 2008, the HPSS servers and the tape robot are located in our machine room, although they are owned and operated by the RIKEN IT division. The specifications of this hardware can be found in literature[12)]. Version upgrade of HPSS from 7.1 to 7.3 was performed in March 2011. The amount of data and the number of files archived in the HPSS were approximately 1.6 PB and 2 million files, respectively, as of January 2012.

2.4 PHENIX software environment

Two PostgreSQL[13)] server nodes are operated for the PHENIX database, whose data size was 56 GB as of January 2012. The data are copied from RCF daily and are made accessible to the users.

In July 2011, one of the two AFS[14)] nodes, which copy the PHENIX software environment from RCF

*1 International Center for Elementary Particle Physics, University of Tokyo

a) HP ProLiant DL180 G5 with dual Xeon E5430 (2.66 GHz, 4 cores), 16 GB memory and 10 TB local SATA data disks for each node

b) HP ProLiant DL180 G6 with dual Xeon X5650 (2.66 GHz, 6 cores), 24 GB / 20 TB as above, for each node

c) HP ProLiant DL180 G6 with 20 TB SATA raw disks

d) SUN Enterprise M4000 with Solaris 10

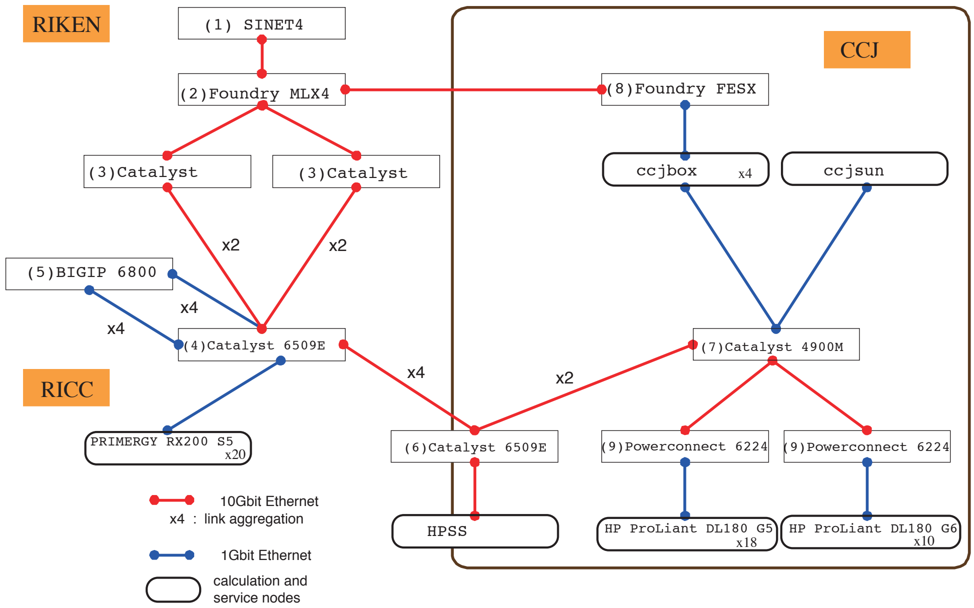

Fig. 1. Schematic view of the network configuration as of January 2012.

and make it accessible to the users, was shutdown and its function was replaced by another one.

2.5 Network configuration

The topology of the network linking CCJ, RICC, and the RIKEN IT division is shown in Fig. 1. We established a link aggregation between Catalyst 6509E and Catalyst 4900M (see 6 and 7 in Fig.1) in December 2011 in order to maintain redundancy, after network suspension in October due to the malfunctioning of the 10GB-LR optical transceiver installed in the 4900M.

2.6 Uninterruptible power-supply system (UPS)

Power consumption of the system, excluding the HPSS, is about 25 kW, and the power is supplied through five UPSs (10.5 kVA each) as of 2011. Two old UPSs were replaced by a new UPS module in March 2012.

3 The earthquake and power cut

In March 11, 2011, “the 2011 off the Pacific coast of Tohoku Earthquake” destroyed a nuclear power plant of Tokyo Electric Power Company (TEPCO). CCJ did not suffer any damage due to the earthquake itself. However, due to the power shotage caused by the disaster, CCJ operation was stopped from the night of March 13 to April 4, although no acutal power outage occured in the Wako Campus.

RIKEN decided to reduce the electric power consumption by 20% of the contracted power at the Wako campus during the summer. But CCJ could continue opperations without any restrictions due to the power-saving measures.

4 Data transfer

Data collected during PHENIX experiment have been transferred from RCF to CCJ using GridFTP[15] through SINET4 (maintained by NII[16]) with a 10 Gbps bandwidth. In 2011, 16 TB of nDSTs of the PHENIX Run-11 were sent from RCF to CCJ, and the data were stored in the HPSS, and also located on local disks on the HP calculation nodes. In 2012, we are expecting additional data transfer from PHENIX Run-11 and Run-12.

References

1) `http://ccjsun.riken.jp/ccj/`, S. Yokkaichi et al., RIKEN Accel. Prog. Rep. **44**, 228 (2011).
2) `http://www.phenix.bnl.gov/`
3) `http://www.bnl.gov/rhic/`
4) `http://www.rhic.bnl.gov/RCF/`
5) `http://www.hpss-collaboration.org/`
6) `http://ricc.riken.jp/`
7) T. Nakamura et al., RIKEN Accel. Prog. Rep. **43**, 167 (2010), J. Phys.: Conf. Ser. **331**, 072025 (2011).
8) `http://www.scientificlinux.org/`
9) `http://platform.com/products/LSF/`
10) `http://www.cs.wisc.edu/condor/description.html`
11) Veritas file system (Symantec Corporation).
12) S. Yokkaichi et al., RIKEN Accel. Prog. Rep. **42**, 223 (2009).
13) `http://www.postgresql.org/`
14) `http://www.openafs.org/`
15) `http://www.globus.org/grid_software/data/gridftp.php`
16) `http://www.nii.ac.jp/`

III. RESEARCH ACTIVITIES II
(Material Science and Biology)

1. Atomic and Solid State Physics (Ion)

Site occupancy of hydrogen in a distorted bcc lattice in niobium alloyed with Mo atoms[†]

E. Yagi,[*1] K. Mori,[*2] K. Miyahara,[*2] S. Fukagai,[*2] S. Koike,[*3] K. Sakuma,[*2] M. Yoshii,[*2] S. Hagiwara,[*2] Y. Okada,[*2] H. Matsuba,[*2] T. Sugawara,[*4] T. Shishido,[*4] and K. Ogiwara

The site occupancy of hydrogen is one of the fundamental problems of the atomistic state of hydrogen in metals. Various types of site occupancy have been observed in group Va bcc metals in the periodic table (i.e.,V, Nb, and Ta) under various conditions. One of the systems suitable for observing various types of site occupancy is Nb alloyed with undersized Mo atoms. Their atomic radii are 1.43 and 1.36 Å, respectively. This alloy system forms a solid solution over the entire Mo concentration (C_{Mo}) range, maintaining a bcc crystal structure, although the lattice parameter changes. Therefore, detailed studies of the C_{Mo} dependence of the site occupancy of hydrogen in the Nb-Mo alloy system are expected to be very useful for understanding the state of hydrogen in bcc metals.

In the present study, to elucidate the origin of the change in the site occupancy of hydrogen, the lattice location of hydrogen dissolved in the single crystals of Nb-Mo alloys containing 39, 48, and 60 at.% Mo atoms has been investigated by the channelling method at room temperature with a tandem accelerator, utilizing a nuclear reaction of $^{1}\mathrm{H}(^{11}\mathrm{B},\alpha)\alpha\alpha$ with a $^{11}\mathrm{B}^{+}$ beam of about 2 MeV to detect hydrogen. This method has been demonstrated to be very useful to locate hydrogen dissolved in metals.[1,2)] In addition, the lattice parameters and half-widths of X-ray reflection lines have been measured at room temperature.

It was observed that, in these alloys, H atoms are distributed over tetrahedral (T) sites and displaced-T (d-T) sites. The d-T site is a site displaced from a T site by about 0.25 Å towards its nearest-neighbour octahedral (O) site. The fractions of the T- and d-T- site occupancies change with a concentration of doped hydrogen C_{H}. In the alloys with C_{Mo}=39 and 48 at.%, the fraction of T-site occupancy decreases with increasing C_{H}. Correspondingly, the fraction of the d-T-site occupancy increases. In each alloy, the concentration of H atoms located at T sites is approximately the same, independently of C_{H}. This result indicates that the concentration of T sites available for occupation of hydrogen, C_{T}, is limited. Therefore, hydrogen preferentially enters T sites, and when the available T sites are exhausted, hydrogen enters d-T sites; the T sites are energetically more favourable than the d-T sites. The C_{H} dependence was not measured in the 60at. %Mo alloy, because hydrogen could not be doped to a concentration higher than 0.3 at.%, probably due to smaller hydrogen solubility at higher C_{Mo}. C_{T} decreases with increasing C_{Mo}. The C_{Mo} dependence of the half-widths of X-ray reflection lines is shown in Fig. 1, together with the site occupancies of hydrogen, including the previously obtained results. There exists a close correlation between such a site change and a change in the half-width. The half-width serves as a measure of lattice distortion averaged over the whole specimen.

At low C_{Mo}, lattice distortion is localized at individual Mo atoms and large around them. Hydrogen is trapped by a Mo atom and occupies the trapped site (T_{tr}), which is displaced by about 0.6 Å from a T site attached to a Mo atom towards that Mo atom, to reduce lattice distortion.[3)] At approximately C_{Mo}=20 at.%, lattice distortion is much reduced due to interference between distortions around individual Mo atoms and, as a result, most of the H atoms occupy T sites and some portion of them occupy O sites.[4)] With increasing C_{Mo}, the distortion again increases, because tetrahedra and octahedra surrounding H atoms consist of Nb and undersized Mo atoms, but the distortion is smaller than that at low C_{Mo}. The O-site occupancy diminishes, and at C_{Mo} higher than about 39 at.% the d-T-site occupancy newly appears. It is concluded that the change in the site occupancy of hydrogen is due to a change in the lattice distortion induced by alloying with undersized Mo atoms, and that the d-T site is a stable site for hydrogen in a bcc lattice distorted at the intermediate level II shown in Fig. 1.

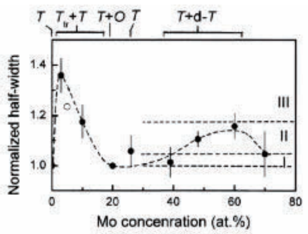

Fig. 1. C_{Mo} dependence of the normalized half-width of the X-ray {321} reflection lines of non-hydrogen-doped Nb-Mo alloys and the site occupancies of hydrogen. The open circle is the result obtained by Matsumoto et al.

References
1) E. Yagi, T. Kobayashi, S. Nakamura, Y. Fukai, and K. Watanabe: J. Phys. Soc. Jpn. **52**, 84 (1983).
2) E. Yagi, T. Kobayashi, S. Nakamura, Y. Fukai, and K. Watanabe: Phys. Rev. B **31**, 1640 (1985).
3) E. Yagi, S. Nakamura, F. Kano, T. Kobayashi, K. Watanabe, Y. Fukai, and T. Matsumoto: Phys. Rev. B **39**, 57 (1989).
4) E. Yagi and S. Koike: J. Phys. Soc. Jpn. **67**, 340 (1998).

† Condensed from the article in J. Phys. Soc. Jpn. **79**, 044602 (2010).

*1 RIKEN and School of Science and Engineering, Waseda University.
*2 School of Science and Engineering, Waseda University.
*3 Department of Physics II, Tokyo University of Science.
*4 Institute for Materials Research, Tohoku University.

Laser-induced reactions between a Ca^+ Coulomb crystal and ammonia molecules

N. Kimura,[*1] K. Okada,[*1] H.A. Schuessler,[*2] M. Wada

[Coulomb crystals, Ca^+, polar molecule, ion-molecule reaction]

In recent decades, several techniques for producing cold atoms, molecules, and their ions have been developed, and they are being applied to the study of cold atomic and molecular processes. In particular, sympathetic cooling of molecular ions by laser-cooled ions can be applied to the study of low-temperature molecular ion-polar molecule reactions[1)], which are very important to understand the chemical evolution of dark interstellar clouds[2)]. Therefore, we plan to measure reaction rates between sympathetically cooled molecular ions and slow polar molecules produced by using a Stark velocity filter. We have previously demonstrated sympathetic Coulomb crystallization of CaH^+ by using laser-cooled Ca^+ ions in a linear Paul trap[3)]. Moreover, we have successfully produced cold polar molecules using a newly developed Stark velocity filter[4)]. In order to measure the reaction rates of cold ion-polar molecule reactions involving sympathetically cooled molecular ions, the reactivity between the polar molecules and the laser-cooled Ca^+ ions must be known. In the present work, we investigated laser-induced reactions between a Ca^+ Coulomb crystal and ammonia molecules and determined the reactivity.

The procedure for the measurement of the state-selected reaction rate was as follows. First, before the reaction rate measurement, we measured the decay rate (γ_{bg}) of a number of Ca^+ ions, associated with background-gas collisions (mainly H_2). Then, ammonia gas was introduced in the vacuum chamber. We measured the decay rate (γ_2) by shining both the cooling lasers; the lasers were used to excite the $^2S_{1/2}$-$^2P_{1/2}$ ($\lambda = 397$ nm) and the $^2D_{3/2}$-$^2P_{1/2}$ ($\lambda =$ 866 nm) transitions. Finally, the reaction rate γ_P of the $Ca^{+*}(^2P_{1/2})$ + NH_3 (ND_3) reaction (P-state reaction) was determined as $\gamma_2 - \gamma_{bg}$. We also measured the decay rate (γ_3) by chopping the 866 nm laser beam to determine the reaction rate γ_D of the $Ca^{+*}(^2D_{3/2})$ + NH_3 (ND_3) reaction (D-state reaction), which can be obtained as $\gamma_3 - \gamma_2$.

Figure 1(a) shows an example of a decay curve for the P-state reaction. The relative numbers of Ca^+ ions were determined from the sizes of Ca^+ fluorescence images[3)]. By fitting an exponential function to the data, we obtained γ_{bg} and the nominal γ_2. Subsequently, a reaction rate (γ_P) of $3.6(0.5) \times 10^{-4}$ s^{-1} was obtained.

We determined γ_P for several NH_3 pressures. Then, the least-squares fitting of γ_P to $\gamma = \sum_i k_i n_i + k_{Low} n$ was carried out in order to obtain the reaction-rate constants; n is the number density of NH_3 and n_i and k_i are the number density and reaction-rate constant of impurity gas i, respectively (Fig. 1(b)). Since the variation of the density of each impurity gas was negligible except for a NH_3 gas, $\sum_i k_i n_i$ was regarded as a constant. As assumed, the residual term $\sum_i k_i n_i$ was negligible. It is to be noted that only the lower limit of the reaction-rate constant was determined in the present experiment because we used a cryogenic linear trap, and the actual NH_3 (ND_3) pressure should be slightly lower than the nominal pressure that was obtained in the vicinity of the cryogenic ion trap region[3)]. The estimated reaction-rate constant is $k_P > 1.3(0.7)$ $\times 10^{-9}$ $(4.1(4.6) \times 10^{-10})$ cm^3/s; the population of the $^2P_{1/2}$ state is calculated to be 4.2×10^{-4} in the present experimental conditions by solving optical Bloch equations for the three-level system[3)]. Similar measurements have previously been carried out for D-state reactions[4)]. We obtain the lower limit of the reaction-rate constant to be $1.1(0.8) \times 10^{-11}$ $(8.5(3.7) \times 10^{-11})$ cm^3/s, where we have assumed that the $^2D_{3/2}$ state population is $\rho_D = 1$.

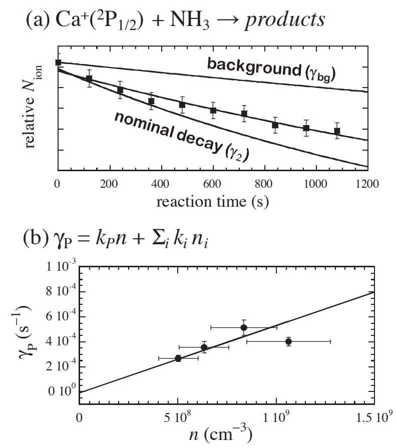

Fig. 1. (a) Reaction-rate measurement for the P-state reaction (NH_3 pressure: $2.6(0.5) \times 10^{-6}$ Pa). (b) A plot of γ_P as a function of the number density of NH_3.

References

1) S. Willitsch*et al.*: Phys. Rev. Lett. **100**, 043203 (2008).
2) V. Wakelam *et al.*: Space Sci. Rev. **156** 13 (2010).
3) N. Kimura *et al.*: Phys. Rev. A **82**, 033422 (2011).
4) K. Okada *et al.*: RIKEN Accel. Prog. Rep. 44, 241(2010); to be appeared in J. Phys. B.

*1 Department of Physics, Sophia University
*2 Department of Physics, Texas A&M University

Enhancement of critical current density by heavy-ion irradiation in FeAs superconductors

T. Tamegai,*[1,*2] Y. Nakajima,*[1,*2] H. Yagyuda,*[1] T. Taen,*[1] T. Kambara, and Y. Kanai

Since the discovery of superconductivity with a high transition temperature, T_c, in LaFeAs(O,F),[1)] iron-based superconductors have attracted much interest from both fundamental and application point of view. One of the most important physical quantities for a superconductor is the critical current density, J_c, below which a superconductor can carry current without dissipation. Unlike T_c, J_c can be improved by introducing defects by various means using chemical or physical methods. Heavy-ion irradiation, which produces columnar defects, is one of the most promising ways for such improvements.[2)]

We have shown that the heavy-ion irradiation is effective in iron-based superconductors by demonstrating five-fold increase of J_c in $Ba(Fe_{0.93}Co_{0.07})_2As_2$ single crystal using 200 MeV Au ions with a dose-equivalent field of B_ϕ = 20 kG.[3)] Similar enhancements of J_c in iron-based superconductors have been reported for other ions with different energies; 1.4 GeV Pb,[4)] 2.6 GeV U,[5)] and 800 MeV Xe.[6)] In addition, proton irradiation has also been demonstrated to be effective to enhance J_c.[7)] In all these irradiation experiments, energetic particles have been introduced along the *c*-axis of the crystal. In anisotropic superconductors, it is well known that the tilting magnetic field produces nontrivial effects. In the case of columnar defects, dispersion of the direction of columnar defects is expected to suppress vortex creep by inducting forced entanglement of vortices.[8)] In the present study, we have studied the angular dependence of the effectiveness of the columnar defects in enhancing J_c.

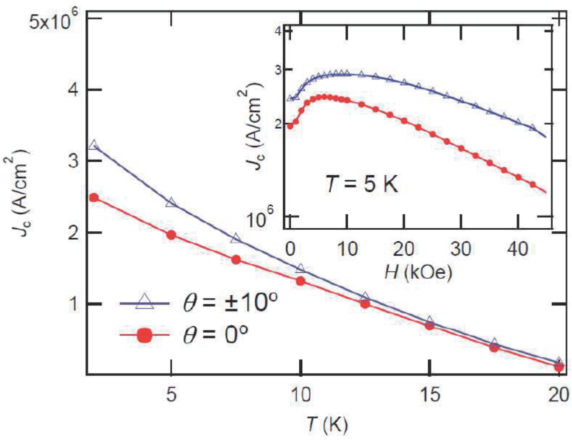

Fig. 1. Temperature dependence of self-field J_c of $Ba(Fe_{0.93}Co_{0.07})_2As_2$ single crystal irradiated by 2.6 GeV U ions at B_ϕ = 80 kG (θ=0°) and B_ϕ = 40 kG (θ=+10°)+B_ϕ = 40 kG (θ=-10°). Inset shows the magnetic field dependence of J_c at 5 K for the same irradiated crystals.

$Ba(Fe_{0.93}Co_{0.07})_2As_2$ single crystals with T_c ~24.5 K have been irradiated by 2.6 GeV U ions with different B_ϕ and different angles from the *c*-axis. In one of the crystals, U ions are irradiated from two directions ±10° from the *c*-axis with a total matching field of 80 kG. J_c is estimated from the magnetization hysteresis loop measured by a SQUID magnetometer based on the extended Bean model. In Fig. 1, temperature dependence of J_c is compared between a sample irradiated along *c*-axis (θ=0°) and another sample irradiated at angles (θ=±10°) from the *c*-axis. At low temperatures, J_c in the sample with θ=±10° is larger by about 30 %. It demonstrates the effect of forced entanglements of vortices.

The broad peak feature of J_c as a function of magnetic field shown in the inset of Fig. 1 is believed to be induced by the self-field effect. When magnetic field is applied along the shortest dimension in a plate-like superconductor, the direction of vortices at low fields close to zero is strongly curved. In such a situation, pinning by columnar defects along the *c*-axis may not be effective. However, once the external field is increased above the self-field value, the direction of vortices is aligned almost parallel to the *c*-axis and the pinning by columnar defects becomes very effective, giving a maximum in J_c as a function of magnetic field. The broad peak feature does not change much by a slight misalignment of the direction of columnar defects. However, when the field is applied at a large angle from the direction of columnar defects, an interesting asymmetry of magnetization hysteresis loop is observed. In the field-decreasing branch, irreversible magnetization is always smaller when the polarity of magnetic field is reversed. When the direction of magnetic field is parallel to the *ab*-plane, enhancement of J_c due to columnar defects is strongly suppressed, and the magnetic hysteresis loop becomes similar to that of unirradiated samples.

References

1) Y. Kamihara *et al.*: J. Am. Chem. Soc. **130**, 3296 (2008).
2) L. Civale *et al.*: Phys. Rev. Lett. **67**, 648 (1991).
3) Y. Nakajima *et al.*: Phys. Rev. B**80**, 012510 (2009).
4) R. Prozorov *et al.*: Phys. Rev. B**81**, 094509 (2010).
5) H. Yagyuda *et al.*: Physica C**471**, 790 (2011).
6) T. Taen *et al.*: doi:10.1016/j.physc.2012.02.040.
7) T. Taen *et al.*: Physica C**471**, 784 (2011).
8) T. Hwa *et al.*: Phys. Rev. Lett. **71**, 3545 (1993).

*1 Department of Physics, University of Tokyo
*2 JST-Transformative Research project on Iron-Pnictides

2. Atomic and Solid State Physics (Muon)

Upgrade of ultra-slow muon beam-line for systematic studies at RIKEN-RAL

D. Tomono, P. Bakule [*1], Y. Ikedo [*2], K. Ishida, M. Iwasaki, T. Kakurai[*2], N. Kawamura[*2], S. Makimura[*2], Y. Matsuda[*3], T. Matsuzaki, T. Mibe[*2], Y. Miyake[*2], K. Nagamine, T. Nagatomo[*2] J. Nakamura[*2], N. Saito[*2], K. Shimomura[*2], P. Strasser[*2], and K. Yokoyama

At the ultra-slow muon beam-line at the RIKEN-RAL Muon Facility, a number of R&D programs were performed to establish a method to generate low-energy muon beam (<100 keV) by laser resonant ionization of thermal muonium[1)]. This method was first applied in near-surface μSR studies[2)]. After the upgrade of the beam-line, we aim to utilize the low-energy muon beam as a source for a new precision measurement of the anomalous magnetic moment of a muon (g-2) using a high intensity muon source at J-PARC MUSE[3)]. This precision measurement requires low-emittance and a highly intense (10^6 muons per second) muon beam. However, the low-energy muon yield is low because the overall conversion efficiency from the surface muon to the low-energy muon is 3×10^{-5} at the maximum. In addition, a low-emittance beam with lower transverse momentum is required for this experiment. Therefore, we are searching for a new muonium production target for these purposes at room temperature[4)]. At RIKEN-RAL, systematic studies on a low-energy muon generation process with lasers will be performed using various targets. Our goal is to increase the low-energy muon yield by two orders of magnitude.

Ongoing works at RIKEN-RAL are (1) upgrade of the Lyman-α (122nm) laser system up to 10 μJ and of the associated setup; this development is reported on separately[5)], (2) modification and automation of the beam-line for systematic studies, and (3) systematic study of the dependence of muonium ionization efficiency on the absolute laser power and position at the muonium target.

In the upgrade, the beam-line magnet power supply units were replaced and their wirings were redone. Further, the data acquisition system was improved. Automation of the power supply control and its read-back control was implemented for stabilizing and fine-tuning the low-energy muon beam. After making these improvements, the beam-line was tested using the previous laser system.

The surface muon beam with a kinetic energy of 4 MeV is stopped at a hot tungsten foil at 2000 K in a vacuum chamber. The muonium is thermally emitted from the foil with a kinetic energy of approximately 0.2 eV in vacuum and then ionized by two lasers with wavelengths of 122 nm (1S→2P) and

[*1] Institute of Physics ASCR, v. v. i. (FZU), Czech Republic
[*2] High Energy Accelerator Research Organization (KEK)
[*3] University of Tokyo

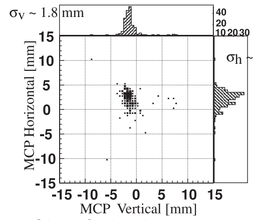

Fig. 1. Beam profile of the low-energy muon at the MCP.

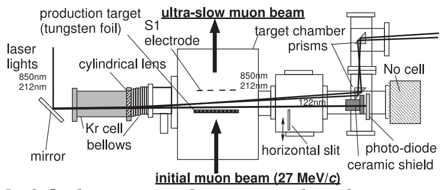

Fig. 2. Modified setup in the target chamber to ionize muonium with laser lights. The 355 nm laser light (omitted in this figure) is introduced from the top at 30° from the Lyman-α laser light.

355 nm (2P→unbound). The muons from ionized muoniums are accelerated with an electric field to the desired kinetic energy from 1 to 10 kV. The beam was observed using a multi-channel plate (MCP, RoentDek DLD40) located downstream. Figure 1 shows a beam profile at the MCP, where the muons are accelerated to 9 kV. The profile is consistent with the profile before the upgrade. The beam-line is ready for new systematic studies.

In the next step, muonium ionization efficiency will be evaluated as a function of the absolute laser power and position per unit area using the muonium evaporated from the tungsten target. We will measure the Lyman-α emission with a photo-diode and the low-energy muon yield in the established beam-line. Figure 2 shows a modified setup in a target chamber in a horizontal direction. The Lyman-α emission is generated through a Kr gas cell with 212 nm and 850 nm laser lights by the process of the two-photon resonant sum-difference frequency mixing scheme. A cylindrical lens (MgF_2) separates the three laser lights: Lyman-α emission is observed with the photo-diode (IRD AXUV300) and two other laser lights are deflected to the outside of the chamber in order to reduce huge background light in the photo-diode. We plan to start this measurement at the next beam-time in 2012.

References
1) P. Bakule et al.: Nucl. Inst. Meth. **B266**, 355(2008).
2) Y. Matsuda et al.: RIKEN Accel. Rep. **40**, 238(2007).
3) N. Saito et al.: E34 Proposal at J-PARC.
4) Y. Fujiwara et al.: RIKEN Accel. Rep. **44**, 260(2011).
5) K. Yokoyama et al.: In this report.

SLM-OPA for the Lyman-α laser system in the RIKEN-RAL muon facility

K. Yokoyama, P. Bakule, M. Iwasaki, O. A. Louchev, N. Saito and S. Wada

The positively charged, pulsed low energy muon (LE-μ^+) is an experimental probe, which has excellent features such as a narrow energy spectrum, short pulse, and small beam size. It enables muon spin rotation (μSR) experiments to be carried out with depth control, and it makes the conventional μSR possible in the surface and sub-surface regions. The LE-μ^+ also has a potential application in measuring the muon anomalous magnetic momentum, which is one of the fundamental physical constants that can be used to test the widely accepted standard theory. The RIKEN-RAL muon facility has developed the LE-μ^+ source and has established its feasibility and its above-mentioned features. However, the low and unstable yield of this source makes it unsuitable for practical use. One of the reasons for the low and unstable yield is the weak light source that photoionizes the muonium atoms (Mu) that have evaporated from the Mu generation target[1]. In this method, the Mu Lyman-α (Ly-α) laser light (122 nm in wavelength) excites the Mu atoms from the ground state to the 2p state, and subsequently, another UV light (355 nm) dissociates the electron from the muon. The difficulty lies in determining how stable and intense Ly-α laser light can be generated.

The Ly-α laser system requires two wavelengths, 212.55 nm (ω_1) and 820 nm (ω_2), to generate the Ly-α wavelength ($\omega_{Ly\text{-}\alpha}$) by two-photon resonant four-wave difference frequency mixing in a Krypton gas cell. Considering that the wave-mixing takes advantage of the resonantly enhanced third-order susceptibility $\chi^{(3)}$ in the Kr energy state, the bandwidth of ω_1 needs to be extremely narrow (on the order of picometers), which requires single longitudinal mode (SLM) operation. Further, the ω_1 power strongly affects the $\omega_{Ly\text{-}\alpha}$ output power, which is proportional to $\chi^{(3)}P_1{}^2P_2$, where P_x denotes the laser power of ω_x. Therefore, it is a key to generate an intense ω_1 in the stable SLM. To generate ω_1, the laser system first generates 850-nm laser light, which is amplified by four Ti:Sapphire amplification stages and then converted into ω_1 as the fourth harmonic.

In the previous Ly-α laser system, an optical parametric oscillator (OPO) was used to supply the 850-nm laser light. However, the problem with this system was that the ω_1 center wavelength did not continue to overlap the Kr two-photon absorption spectrum because of the thermal vibration of the OPO optical cavity. As a result, $\omega_{Ly\text{-}\alpha}$ was not stable in power, even when ω_1 was in the SLM. Therefore, we recently developed an SLM optical parametric amplifier (OPA) to achieve better control over ω_1 and to improve the overall laser performance[2].

The newly developed SLM-OPA system uses an SLM CW laser as a seed source, which is specifically designed for atomic excitation, and amplifies the seed light by the optical parametric process for achieving high gain. This allows the SLM optical cavity to be spatially isolated in a temperature-controlled housing, and as a result, the ω_1 wavelength becomes morestable. As shown in Fig. 1, the SLM-OPA system is constituted of three KTP crystals in the walk-off compensated configuration, wherein each crystal contained in an oven to maintain the temperature at 90 ℃ to avoid optical damage (so-called gray track formation). The seed 850-nm CW laser light is collimated with the 532-nm pump pulse and passes through the crystals for OPA. The crystals are not anti-reflection coated because the damage threshold of the coating is lower than that of the crystal; this limits the maximum pulse energy. As a result, each surface of the crystals partially reflects and attenuates the laser beams. In addition, to prevent recursive oscillation between the crystal faces, the crystal surfaces are wedged at an angle of 1°, which results in the deviation of the beams due to the dispersion. To avoid excessive attenuation and deviation, the pump beam is evenly split into two in terms of power and collimated with the 850-nm beam again after it passes the first two crystals. The amplified pulse then enters the Ti:Sapphire stages for further amplification.

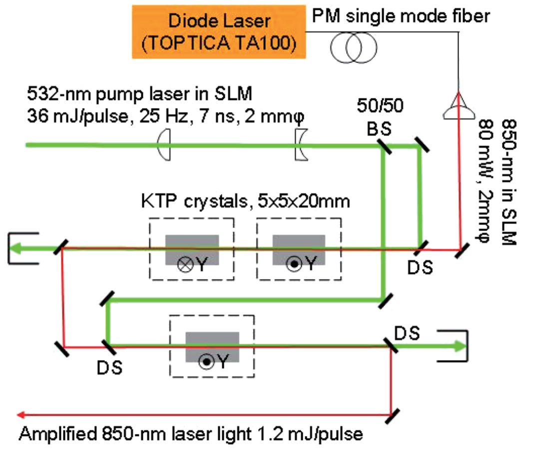

Fig. 1 SLM-OPA layout. "Y" indicates the direction of the crystal axis either pointing out of or into the paper

Thus far, we have achieved a 1.2 mJ/pulse and a 4 ns (FWHM) pulse duration, which are comparable with the output of the previously used OPO. To obtain a higher gain from the OPA, we attempted the installation of a fourth KTP crystal. However, the excessive intensity at 850 nm induces the up-conversion (850 + 1422 → 532 nm) and saturation of the power. We can possibly suppress the up-conversion and expect higher gain by enlarging the mode volume. The SLM-OPA has already been used in the most recent LE-μ^+ generation experiment, which proved that the central wavelength and bandwidth of ω_1 were stable and sufficiently narrow (2.4 GHz at 425 nm) for Kr two-photon absorption.

References

1) P. Bakule et al., Nucl. Instr. Meth. B **266**, 335 (2008)
2) K. Yokoyama et al., RIKEN Accel. Prog. Rep. **44**, 244 (2011)

Development of the high-pressure transport measurement system by using the gas-pressurized system at the RIKEN-RAL Muon Facility

I. Watanabe, Y. Ishii[1)], M.A. Jawad, C. Offer[2)], R. Done[2)], C. Goodway[3)], R. Down[4)], M. Kibble[2)], J. Keeping[2)], M. Jura[5)], K. Oleg[5)], J. Lord[6)], A. Hillier[6)], F.L. Pratt[6)], N. Tajima[7)], I. Kawasaki, T. Matsuzaki, and R. Kato,

The high pressure is important to explore new electronic states of materials. A crystal structure of material can be squeezed by the pressure causing a decrease or a change of the distance between neighboring atoms. Such a change of the electronic state could lead to new interesting phenomena. For instance, the pressure changes the electronic conductivity from insulating to conducting, or from conducting to insulating. Especially, the effect of the pressure is quite large in case of organic molecules. The crystal structure of organic molecules generally has the low density of atoms and lots of vacancies. Ligand electrons which mainly rule the magnetism, transportation and other general related behavior spread inside the crystal. This spread state of frontier electron orbitals also causes a big effect of the pressure on lots of electronic behavior. The transfer integral among ligand electrons can be easily changed as the atomic distance is slightly changed even by a weak pressure. Therefore, it is very interesting to apply the pressure to organic molecules in order to explore new electronic states, new phenomena, new magnetism, new transport properties and so on.

In this article, we report our new project to develop a pressure system to measure transport properties in high magnetic field. Transport properties are generally important to understand the basic electronic state of the material, so that lots of pressure studies have been conducted on lots of organic molecules with applying magnetic fields. Almost all of high-pressure transport measurements have been done by using Bridgman type high-pressure cells which use liquid pressure mediums. Thus, the control of the pressure, especially with changing the temperature, is fairly difficult because all of liquid pressure mediums are frozen below some temperature points like 100 K or so. Those frozen pressure mediums sometimes lose the homogeneity of the pressure causing the misunderstanding of experimental results of physical properties. Also, it is quite difficult to know about the absolute pressure value in the high-pressure cell because we have no sensor which can be used in a high-pressure cell. Those technical difficulties can be solved out when the gas is used as the pressure medium. We can monitor the pressure value by using a pressure gauge at any temperatures. We can carefully control the pressure value by operating a gas intensifier with a fine accuracy.

[1)] Department of Physics, Tokyo Medical University.
[2)] Design Group, ISIS, RAL
[3)] High Pressure Group, ISIS, RAL
[4)] Cryogenic Group, ISIS, RAL
[5)] Sample Environmental Group, ISIS, RAL
[6)] Muon Group, ISIS, RAL
[7)] Department of Physics, Toho U.

Fig. 1: High-pressure center stick (left) and the high-pressure cell for transportation measurements (right). The stick is used with the existing cryostat for HiFi. The gas pressure is applied from the top of the cell through a capillary with the 0.4 mm inner diameter.

The gas comes into any tiny spaces around the sample to make the pressure homogeneous even if the gas is frozen at low temperatures. From this view point, the gas He is ideal as the pressure medium which satisfies all requirements to make the ideal pressure condition.

However, there has not been developed any gas-pressurized system to measure transport properties in the past due to some technical difficulties and law restrictions on gas-pressurized equipment. Besides, transport measurements well require high magnetic fields of the order of a couple of Tesla to achieve deeper understanding of physical properties. This point also makes the gas-pressurized system complicate.

At Rutherford-Appleton Laboratory, there is a high-pressure group and a design group. They have lots of experiences to make and arrange gas-pressurized high-pressure systems for neutron scattering experiments. By collaborating with those groups, we have already established a gas-pressurized high-pressure system for μSR at the RIKEN-RAL Muon Facility. We have got a gas intensifier which can compress the gas He up to 7 kbar. By making use of this high-pressure system, we have built up a high-pressure system for transport measurements (Fig. 1). The base temperature is around 2 K by using an existing cryostat. In conjunction with a high-field magnet, named HiFi, we can apply magnetic fields up to 5 T. The high-pressure cell is made by CuBe and pressurized by our gas intensifier. A test operation of the system is planned in order to make sure the performance of the system as designed and some organic molecules will be tested.

Development of the high-pressure SQUID system by using the gas-pressurized system at the RIKEN-RAL Muon Facility

I. Watanabe, Y. Ishii[1)], H. Taniguchi[2)], Y. Onodera[2)], T. Uehara[2)], M. Ito[2)], C. Offer[3)], R. Done[3)], C. Goodway[4)], R. Down[5)], M. Kibble[3)], J. Keeping[3)], M. Jura[6)], K. Oleg[5)], J. Lord[7)], A. Hillier[7)], F.L. Pratt[7)], N. Tajima[8)], I. Kawasaki, T. Matsuzaki, and R. Kato,

The high pressure is an important parameter to study electronic properties of materials without any changes of their chemical compositions. Especially for organic materials, like molecular magnets and conductors, the high pressure can create lots of new physical properties which appear under the pressure. That is because that organic materials are very soft and easily compressed. The overlap between molecular orbitals inside the crystal can be drastically changed as the distance between them is slightly changed by the pressure. For instance, some molecular based system changes its electronic property from insulating to conducting as increasing the pressure, and finally the superconducting state appears. Thus, the pressure dependence study of electronic properties is quite interesting to find out new physics and new electronic properties in variety of molecular systems.

Despite everybody agrees with the importance of the pressure, high-pressure equipments which can apply well-controlled hydrostatic pressure have not been well developed. As a simple high-pressure setup in a laboratory level, piston cylinder cells made by CuBe are widely used for the pressure study. Such systems typically use oil as the pressure medium. The pressure medium is frozen with decreasing temperature reducing the pressure to the sample. This frozen state of the pressure medium also well affects the direction of the pressure. Thus, as long as the oil is used as the pressure medium, it is quite hard to produce the homogenized pressure to the sample. In order to avoid these problems, it is better to use a gas like He as the pressure medium. However, it is not allowed for research purposes to increase the gas pressure above 3 kbar in Japan. Thus, there is no chance to make any gas-pressurized systems for physics studies.

On the other hand, the regulation of the gas pressure in the UK is well established and we can develop gas-pressurized systems to carry our physics studies of materials under the pressure. At the Rutherford-Appleton Laboratory (RAL), a high-pressure group has been organized to support high-pressure tasks and high-pressure experiments. This group has a lot of experiences to operate gas-pressurized systems for neutron scattering experiments. In addition to this high-pressure group, RAL has a design group to realize high-pressure systems which satisfy required experimental high-pressure conditions. We have been working with those groups to establish a gas-pressurized high-pressure SQUID system at RAL. Figure shows the picture of the setup of the high-pressure SQUID which has been developed and installed by our groups at RAL.

Figure: A setup of the high-pressure SQUID.

The standard Quantum-Design SQUID magnetometer has been sent from RIKEN to RAL. This SQUID can apply the magnetic field up to 7 T and can cool the sample down to 2 K. A high-pressure cell for this SQUID has been designed by the RAL design group to be fit to this magnetometer. The high-pressure cell was designed to stand against the gas pressure up to 5 kbar. The material of the cell is CuBe. The gas pressure medium is He. The He gas is compressed by a gas intensifier which is being used for high-pressure μSR at RIKEN-RAL. By using this system, we can measure the magnetic susceptibility under the pressure up to 5 kabr. The strongest advantage of this system is to apply the very homogeneous and accurate pressure to the sample at any temperature below 300 K down to 2 K. This system is the first gas-pressurized high-pressure SQUID system in the world.

A cooling down test of the pressure cell has been finished and no leak at the base temperature has been confirmed. From now on, test experiments by using some organic magnets will be conducted in order to get the first data. This high-pressure SQUID system will be open to researchers from the world to explore new fields of molecular based systems.

[1)] Department of Physics, Tokyo Medical University.
[2)]Department of Physics, Saitama University.
[3)]Design Group, ISIS, RAL
[4)]High Pressure Group, ISIS, RAL
[5)]Cryogenic Group, ISIS, RAL
[6)]Sample Environmental Group, ISIS, RAL
[7)]Muon Group, ISIS, RAL
[8)]Department of Physics, Toho U.

μSR study of superconductivity in iron-based superconductor $Ba_{1-x}K_xFe_2As_2$

K. Ohishi,[*1,5] Y. Ishii,[*2,5] I. Watanabe,[*5] T. Saito,[*3] H. Fukazawa,[*3,5] Y. Kohori,[*3,5] K. Kihou,[*4,5] C. H. Lee,[*4,5] H. Kito,[*4,5] A. Iyo,[*4,5] and H. Eisaki[*4,5]

The discovery of superconductivity in $LaFeAsO_{1-x}F_x$ [1)] has stimulated a tremendous research effort toward elucidating the superconducting pairing mechanism. In the hole-doped system $Ba_{1-x}K_xFe_2As_2$, it is suggested that the superconducting gap structure changes with increasing K concentration. For example, in optimally doped $Ba_{1-x}K_xFe_2As_2$ ($x \sim 0.4$), many experimental and theoretical results suggest a multiple full gap with sign change, namely, the $s_{\pm}$-wave. On the other hand, recent studies including our μSR result[2)] have suggested that the superconducting gap in KFe_2As_2 has line nodes[3–5)], in contrast to the nodeless gap suggested in $Ba_{0.6}K_{0.4}Fe_2As_2$. It is also suggested that the superconducting gap structure changes at $x \sim 0.7$, where there is a steep decrease in T_c. Resolving how such different gap structures evolve as a function of K-doping will likely be the key to understanding these intriguing phenomena.

In order to elucidate the superconducting gap structure in the middle range of K concentration, we performed zero-field (ZF) μSR measurements at RIKEN-RAL Muon Facility in the Rutherford Appleton Laboratory, Didcot, UK. This experiment was approved by J-PARC as proposal no. 2011A0032; however, it was performed at RIKEN-RAL because J-PARC was damaged by the Great East Japan Earthquake.

Figure 1 shows the ZF-μSR time spectra of $Ba_{0.06}K_{0.94}Fe_2As_2$ at various temperatures. These ZF-μSR spectra exhibit almost no temperature dependence below 120 K. The data were fitted by a simple exponential function, $AP_z(t) = A_s \exp(-\lambda t) + A_{\rm Ag}$, where A_s and $A_{\rm Ag}$ are the μ-e decay asymmetries for the sample and Ag sample holder, respectively, and λ is the muon spin relaxation rate. The temperature dependence of λ is shown in Fig. 2. It is considered that the observed small relaxation rate $\lambda \sim 0.023\ \mu s^{-1}$ is due to a tiny amount of iron impurity, which is not detected by magnetization measurement. Generally, muon spin relaxation in ZF can be due to (1) a random static field (nuclear dipolar field), which causes dephasing of muon spins, and (2) dynamic fields originating from spin fluctuations or spin waves, resulting in energy dissipative $1/T_1$ processes. These two factors can be distinguished by their different responses to a longitudinal field (LF). We have performed LF-μSR measurements and confirmed that the observed relaxation is static and is completely decoupled by $H = 5$ mT, suggesting that the internal field at the muon site is consistent with that from the nuclear fields.

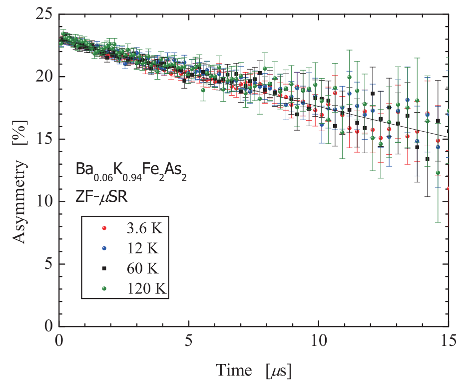

Fig. 1. ZF-μSR time spectra in $Ba_{0.06}K_{0.94}Fe_2As_2$ at various temperatures.

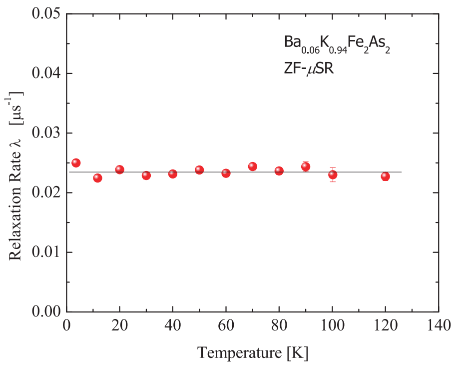

Fig. 2. Temperature dependence of relaxation rate λ in $Ba_{0.06}K_{0.94}Fe_2As_2$.

We have also performed similar measurements for $Ba_{1-x}K_xFe_2As_2$ ($x = 0.8, 1.0$) and found that there is no temperature dependence in the muon spin relaxation rate, suggesting that time reversal symmetry breaking is not possible in these materials.

*1 Research Center for Neutron Science and Technology, CROSS
*2 Department of Physics, Tokyo Medical University
*3 Department of Physics, Chiba University
*4 AIST
*5 JST-TRIP

References

1) Y. Kamihara *et al.*, J. Am. Chem. Soc. **130** (2008) 3296.
2) K. Ohishi *et al.*, submitted to J. Phys. Soc. Jpn.
3) H. Fukazawa *et al.*, J. Phys. Soc. Jpn. **78** (2009) 083712.
4) J. K. Dong *et al.*, Phys. Rev. Lett. **104** (2010) 087005.
5) K. Hashimoto *et al.*, Phys. Rev. B **82** (2010) 014526.

Precise investigation of superconductivity of single crystals of $Ba_{1-x}K_xFe_2As_2$

H. Fukazawa,[*1,5] T. Saito,[*1] Y. Kohori,[*1,5] K. Ohishi,[*2,5] Y. Ishii,[*3,5] I. Watanabe[*5], K. Kihou,[*4,5] C. H. Lee,[*4,5] H. Kito,[*4,5] A. Iyo,[*4,5] and H. Eisaki,[*4,5]

The discovery of superconductivity in $LaFeAsO_{1-x}F_x$ [1)] has stimulated a tremendous research effort toward elucidating the superconducting pairing mechanism. In the hole-doped system $Ba_{1-x}K_xFe_2As_2$, an important features is that superconductivity occurs even for $x = 1$, although T_c itself is much lower ($T_c \sim 3.5$ K) than the optimum T_c ($\sim$38 K). Moreover, it is suggested that the superconducting gap structure changes with increasing K concentration in $Ba_{1-x}K_xFe_2As_2$ because a multiple full gap was observed in an optimally doped sample, whereas a nodal gap was observed in KFe_2As_2. It is also suggested that the superconducting gap structure changes at $x \sim 0.7$, where there is a steep decrease in T_c.

In order to elucidate the superconducting gap structure in the middle range of K concentration, we performed transverse-field (TF) μSR measurements at RIKEN-RAL Muon Facility in the Rutherford Appleton Laboratory, Didcot, UK. RIKEN-RAL is developing the sample environment and equipment considerations, and recently, an Oxford Instruments Heliox cryostat (Temperature range: 0.3 $\sim$ 70 K) was modified to allow for "fly-past" operation. In the fly-past mode, a small sample is suspended in the beam, and any muons not stopping in the sample ideally pass through a hole in the back detector bank and out to the end of the fly-past tank, where their positrons are not detected; hence, they do not contributing to statistical noise or background. This enables us to obtain a good S/N ratio with a small sample. In this study, we used this new setup, Heliox with fly-past mode, and performed TF-μSR measurements for a single crystalline sample of $Ba_{0.06}K_{0.94}Fe_2As_2$ at temperatures between 0.3 K and 10 K. A magnetic field of 15 mT was applied perpendicular to the c-axis. The sample was field-cooled at the measured magnetic field in order to eliminate the effect of flux pinning. The TF-μSR spectra were fitted by a two-component function, $AP(t) = A_s \exp\left(-\frac{\sigma^2 t^2}{2}\right) \exp(i\omega t + \phi) + A_{\mathrm{Ag}} \exp(i\omega_{\mathrm{Ag}} t + \phi)$, where A ($= A_s + A_{\mathrm{Ag}}$) is the total μ-e decay asymmetry; A_s and A_{Ag} are the partial asymmetries for $Ba_{0.06}K_{0.94}Fe_2As_2$, respectively; and ω and ω_{Ag} and the central frequencies for $Ba_{0.06}K_{0.94}Fe_2As_2$ and the Ag sample holder, respectively. σ is the muon spin depolarization rate, and ϕ is the initial phase. A Gaussian relaxation function gives a good approximation of description of the lineshape for the flux-line lattice (FLL) state.

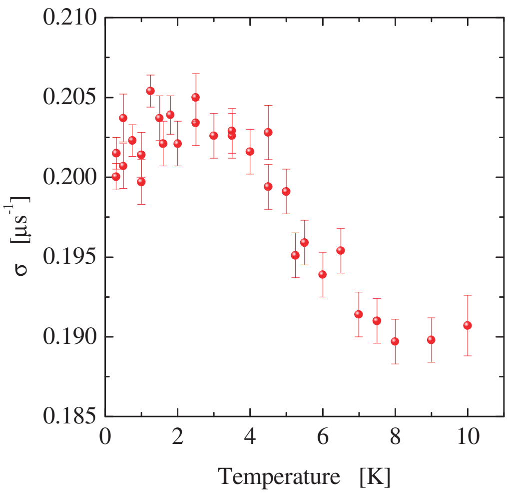

Fig. 1. Temperature dependence of muon spin relaxation rate σ in $Ba_{0.06}K_{0.94}Fe_2As_2$ at $H = 15$ mT.

Figure 1 shows the temperature dependence of muon spin relaxation rate σ. As seen in this figure, below T_c = 8 K, σ increases with decreasing temperature due to the formation of the FLL. Although a detailed analysis is underway, we have found that the absolute values of obtained σ are small compared with the data obtained at TRIUMF, Vancouver, Canada. It is considered that some of muons do not stop at the sample but stop near the sample and that this is caused by the difference in the sample holder size. We usually use a sample holder that is 30 $\times$ 50 mm^2, but this time the holder size was about 10 $\times$ 15 mm^2 for the new fly-past setup. In principle, muons that do not stop at the sample pass through the the hole in the back detector bank. However, in practice, some of muons not stopping at the sample may stop at another part of cryostat, namely, the aluminum radiation shield.

This is the current status of the development of Heliox with the fly-past mode of TF-μSR. In order to obtain a better S/N ratio, we have to improve upon the above problem and then discuss the superconducting gap structure in the middle range of K concentration in $Ba_{1-x}K_xFe_2As_2$.

*1 Department of Physics, Chiba University
*2 Research Center for Neutron Science and Technology, CROSS
*3 Department of Physics, Tokyo Medical University
*4 AIST
*5 JST-TRIP

References

1) Y. Kamihara *et al.*, J. Am. Chem. Soc. **130** (2008) 3296.

μSR study of Heusler compounds $Ru_{2-x}Fe_xCrSi$

M. Hiroi,[*1] T. Suzuki,[*2] and I. Watanabe

Recently, magnetic properties of the Heusler compounds $Ru_{2-x}Fe_xCrSi$ have been studied.[1)] The Fe-rich compounds were found to be ferromagnetic. In addition, it was recently revealed that the Ru-rich compound Ru_2CrSi shows an antiferromagnetic transition at $T_N = 14$ K.[2)] Although the Ru-rich compound $Ru_{1.9}Fe_{0.1}CrSi$ was found to show a peak in magnetic susceptibility at $T_N^* \sim 30$ K, which seemed to indicate an antiferromagnetic transition, in the specific heat measurement, no phase transition was found around T_N^* or at any other temperatures.[3,4)] Instead, below a T_g of $\sim$15 K, the difference between the magnetic susceptibilities observed in a zero-field-cooling process and a field-cooling process increased.[3)] This observation suggests the formation of a spin-glass (SG) state. We performed μSR measurements of $Ru_{1.9}Fe_{0.1}CrSi$ to investigate these anomalies and magnetic states microscopically. In zero-field (ZF) μSR measurements, the peak of the relaxation rate was observed at a T_g of $\sim$15 K, and this suggests the onset of spin freezing at this temperature. Furthermore, the longitudinal-field (LF) μSR measurement was performed at 0.265 K, and this measurement confirmed the presence of a static internal magnetic field. The internal field was estimated to be approximately 0.1308 ± 0.005 T. From these results we concluded that SG transition occurs at a T_g of $\sim$15 K. On the other hand, an anomaly in the relaxation rate of the ZF-μSR, indicating a phase transition, appeared to be absent around T_N^*, whereas with decreasing temperature a large decrease in the initial asymmetry and a gradual increase in the relaxation rates were observed starting at $\sim$40 K, which is slightly higher than T_N^*. Although no anomaly clearly indicating a phase transition was found around T_N^* in the μSR measurements, the loss of the initial asymmetry may have been caused by a static internal field. In this case, there is a possibility that successive SG transitions occur in this compound. Therefore, in order to investigate magnetic states below $\sim T_N^*$, we performed LF-μSR measurements for polycrystalline $Ru_{1.9}Fe_{0.1}CrSi$.

The measurements were carried out at the RIKEN-RAL Muon Facility using a spin-polarized single-pulse positive surface muon beam. LF-μSR time spectra were measured at various temperatures between 8 K and 40 K for longitudinal magnetic fields of up to 0.395 T.

Figure 1 shows the μSR time spectra of $Ru_{1.9}Fe_{0.1}CrSi$ for different values of the longitudinal magnetic field at 25 K. The spectra are not corrected for the magnetic field dependence of the instrumental background. The spectra consist of two components, and the asymmetry parameter $A(t)$ can be expressed as

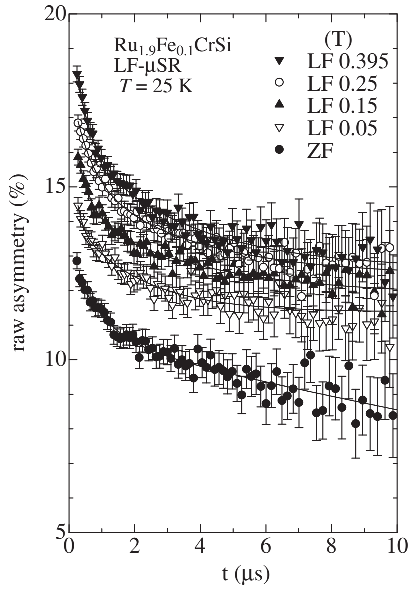

Fig. 1. LF-μSR spectra of $Ru_{1.9}Fe_{0.1}CrSi$ at various longitudinal magnetic fields at 25 K. The spectra are not corrected for the magnetic field dependence of the instrumental background. Solid lines represent the fit for $A_1 \exp(-\lambda_1 t) + A_2 \exp(-\lambda_2 t)$.

$$A(t) = A_1 \exp(-\lambda_1 t) + A_2 \exp(-\lambda_2 t), \quad (1)$$

where A_i and λ_i ($\lambda_1 > \lambda_2$) are the initial asymmetry and muon spin relaxation rate, respectively, for each component. As shown in Fig. 1, the time spectra are fitted well using Eq. (1). All the time spectra that were recorded below $\sim$30 K are fitted by Eq. (1), whereas the time spectra at 40 K are fitted well using a single exponential function. From the results of the fit, A_2 appears to increase at around 0.2 T rather rapidly with increasing magnetic field. This behavior is also observed at lower temperatures. This may imply that an internal field is present below $\sim$30 K. However, to draw conclusions we need to perform a more detailed analysis.

*1 Department of Physics and Astronomy, Kagoshima University
*2 Graduate School of Arts and Sciences, International Christian University

References
1) M. Hiroi et al.: Phys. Rev. B. **76** 132401 (2007).
2) M. Hiroi et al.: to be published in J. Phys.: Conf. Series
3) M. Hiroi et al.: Phys. Rev. B. **79** 224423 (2009).
4) M. Ito et al.: Phys. Rev. B **82** 024406 (2010)

Griffiths singularity in the diluted Ising antiferromagnet $Ho_xY_{1-x}Ru_2Si_2$

Y. Tabata,*1 K. Matsuda,*1 T. Waki,*1 H. Nakamura,*1 and I. Watanabe

Random magnets such as randomly diluted (anti)ferromagnets have been the focus of considerable attention in the field of statistical physics for many years because their inherent randomness and frustration can suppress the development of long-range magnetic orders and cause intriguing phenomena[1]. Among of them, the Griffiths phase was proposed in a famous theoretical study by Griffiths[2]; magnetic clusters, in which the spins are locally ordered, develop in diluted ferromagnets for all concentrations below the Curie temperature of the pure system, T_C^{pure}, and the so-called Griffiths phase, being neither the conventional ordered states nor the paramagnetic disordered state, is formed as a result of slowly fluctuating large magnetic clusters. The Griffiths phase was discovered theoretically in very early days, however, the experimental verification has not made much progress. One of the reasons for the lack of the progress is the weakness of the Grifftihs singularity at $T_G = T_C^{pure}$.

Against this background, we are trying to capture signs of the Griffiths singularity in the diluted Ising antiferromagnet $Ho_xY_{1-x}Ru_2Si_2$ by using the μSR technique. A dynamics measurement technique such as the μSR technique is appropriate to observe the Griffiths singularity because the singularity in dynamics is considered to be more prominent than that in statics. In this report, our preliminary μSR results for $Ho_xY_{1-x}Ru_2Si_2$ are presented. The pure compound $HoRu_2Si_2$ is an antiferromagent with a Neel temperature T_N^{pure} of 18.6 K[3], and T_N is linearly suppressed by nonmagnetic Y-substitution as $T_N(x) \propto x$. We conducted zero-field (ZF) and longitudinal-field (LF) μSR experiments at the RIKEN-RAL Muon Facility at the Rutherford-Appleton Laboratory in the UK in the temperature (T) range of 7−100 K for LFs in the range of 0−3950 G. All experiments were performed by using single-crystal samples of the $x = 0.18$ compound. The μ-on spin polarization of the incident beam was parallel to the magnetically easy c-axis of the compound.

The ZF μSR curves at low temperatures below 30 K show a peculiar relaxation consists of two relaxation components, fast Lorentzian-type and slow Gaussian-type components, whereas those at higher temperatures show only the simple Lorentzian-type component. The slow Gaussian-type relaxation is decoupled by a LF of 3950 G, indicating that the relaxation originates from the quasi-static internal field. On the other hand, the fast Lorentzian-type relaxation is dynamic and is not affected by the LF of 3950 G, indicating that the time scale of the fluctuations is shorter than 10^{-9} s.

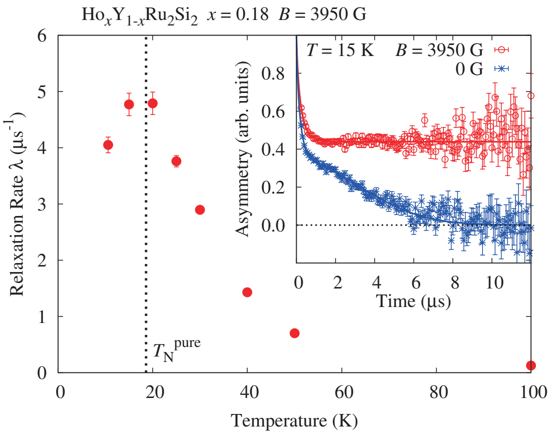

Fig. 1. T-dependence of the relaxation rate λ at a LF of 3950 G. The vertical dotted line represents the Néel temperature of the pure compound, T_N^{pure}. The inset shows the μ-on relaxation curves at $T = 15$ K for LF values of 0 and 3950 G.

To reveal the dynamic feature of this diluted magnet, we show the T-dependence of the relaxation rate of the fast component, λ, at the LF of 3950 G in Fig. 1. λ is obtained by fitting the relaxation data to the stretched exponential function $A\exp[-(\lambda t)^\beta]$. The relaxation rate clearly shows a divergent behavior to T_N^{pure}, not to the Néel temperature of the $x = 0.18$ compound $T_N(x = 0.18)$, which is 2.69 K. Moreover, despite of the number of data not being large, a cusp-like anomaly is found at T_N^{pure}. These results are striking signs of the Griffiths singularity at $T_G = T_N^{pure}$.

References

1) A. P. Young: *Spin Glasses and Random Fields* (World Scientific, 1998); R. Folk et al.: Physics Uspekhi 46, 169 (2003); T. Vojta et al.: Phys. Stat. Sol. (B) 241, 2118 (2004).
2) R. B. Griffiths: Phys. Rev. Lett. 23, 17 (1969).
3) T. Shigeoka et al.: J. Phys. Soc. Jpn. 70, Suppl. A 206 (2001).

*1 Department of Materials Science and Engineering, Kyoto University, Japan

μSR studies on strongly correlated cubic Tm and Pr compounds with orbital degrees of freedom in the crystal-field ground state

H.S. Suzuki,[*1] D. Kuno,[*2] S. Takagi,[*2] T. Suzuki, I. Watanabe and T. Matsuzaki

Cubic non-Kramers rare earth compounds of $PrMg_3$ and $TmAg_2In$ exhibit strongly correlated electron behavior characterized by a huge broad anomaly in the T-dependence of specific heat below 1 K[1]. The crystal field ground states (CFGS) in both have orbital degrees of freedom, suggesting that multipoles in CFGS possibly are related to their strongly correlated electron behaviors. In particular, the non-Kramers CFGS doublet Γ_3 in $PrMg_3$ has no magnetic dipoles, but electric quadrupoles and a magnetic octupole. Here, we report the experimental results to extend the findings of a previous study (R328) in order to uncover the ground state and the low-T properties of $PrMg_3$ down to the dilution refrigerator temperature range. μSR measurements were carried out using the AUGUS spectrometer at RIKEN-RAL Muon Facility. The ZF and LF spin relaxation function $G_Z(t)$ was measured on the single crystals with the initial μ^+ spin polarization P_{μ^+} along the cubic [001] axis.

Figure 1 shows the temperature variations of μSR time spectra under zero field. The muon spin relaxation rate of ZF-μSR gradually increases with the decrease in the temperature. In order to roughly extract a trend in the temperature dependence of the relaxation rate, $G_Z(t)$ is fitted using the power exponential function $G_Z(t) = exp(-(\lambda t)^\beta)$, and the obtained parameters are plotted in Fig. 2. The increase in λ continues below 20 K, where the magnetic susceptibility becomes almost independent of the temperature. In this experiment, we found that the increase stopped around $T^* \sim 0.2$ K, as shown in Fig. 2. Note that the temperature dependence of the elastic constant $(C_{11}\text{-}C_{12})/2$, *i.e.*, the quadrupole susceptibility, shows a shoulder anomaly around T^*[2].

As reported in our previous work, the time spectra for ZF and LF at low temperatures can be described well in terms of the dynamical Kubo-Toyabe model, in which the resultant local fields are enhanced. Thus, as seen in the case of the non-magnetic ground state[3], μ^+ relaxation in $PrMg_3$ is probably dominated by dipolar coupling near nuclear magnetic moments in the presence of strong hyperfine enhancement of the ^{141}Pr nuclear magnetism. On the other hand, the T^* is too high for the nuclear magnetic ordering temperature[4]. Multipole fluctuations in electrons can reflect on the μ^+ relaxation through possible on-site couplings between the multipoles of the electron and the nucleus. In order to reveal the contributions from the multipole moments and the nuclear magnetic moments, we are currently continuing the investigation using TF-μSR and are also conducting a comparative study on $PrAg_2In$.

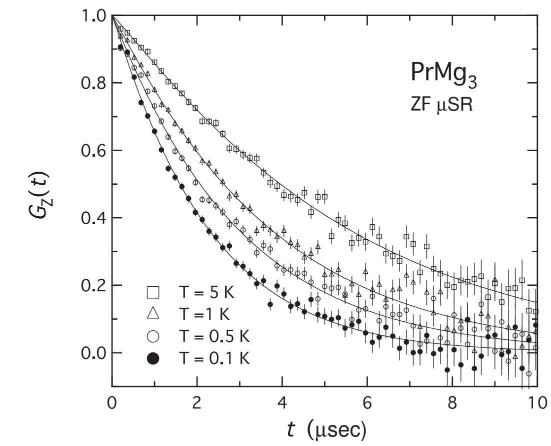

Fig. 1. Temperature variation in the ZF μSR time spectra of $PrMg_3$.

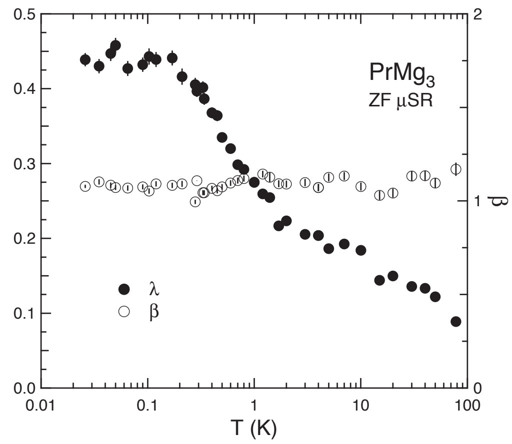

Fig. 2. Temperature dependence of the ZF-μSR rate λ and exponent β from the fitting function $G_Z(t) = exp(-(\lambda t)^\beta)$

References
1) H. Tanida et al. : J. Phys. Soc. Jpn. **75**, 073705 (2006)
2) K. Araki, et al. : Physica B **44**, 3187 (2009)
3) D.E. MacLaughlin, et al.: Phys. Rev. B **61**, 555 (2000)
4) J. Yoshida, et al.: J. Phys. Conf. Series **150**, 042241 (2009)

*1 National Institute for Materials Science
*2 Physics Department, Graduate School of Science, Tohoku University

Toward the understanding of slow spin relaxation in $Nd_2Ti_2O_7$ with μSR

H. Guo[*1], H. Xing[*1], I. Watanabe[*2], G. Cao[*1], and Z. Xu[*1]

Rare earth titanates with the chemical formula $R_2Ti_2O_7$ have drawn much attention. Compounds with smaller rare earth ions (Sm^{3+}-Lu^{3+}) have a cubic pyrochlore structure, and exotic magnetic phases such as spin ice were observed due to geometrical frustration[1]. On the other hand, magnetic properties of monoclinic $R_2Ti_2O_7$ with larger rare earth ions (La^{3+}-Nd^{3+}) have received less attention because of the absence of geometrical frustration. We have identified the paramagnetic anisotropy of $Nd_2Ti_2O_7$ (NTO)[2], and examined its magnetic-field-induced slow spin relaxation using dc and ac susceptibility measurements. NTO shows paramagnetic behavior down to 0.58 K and exhibits a magnetic transition during specific heat measurement. In order to clarify the magnetic ground state and the field effect in the slow spin process, we performed zero-field (ZF) and longitudinal-field (LF) μSR measurement at ISIS.

As can be seen from Fig. 1, the muon spin relaxation showed an oscillation in ZF at 0.3 K, which is consistent with the specific heat result and indicats an ordered magnetic state. The asymmetry can be well fitted by $A(t) = A_1\cos(\gamma_\mu Bt+\varphi)e^{-\lambda_1 t} + A_2 e^{-\lambda_2 t}$, where $\gamma_\mu/2\pi = 13.55$ kHz/G is the gyromagnetic ratio of muon. The extracted internal field

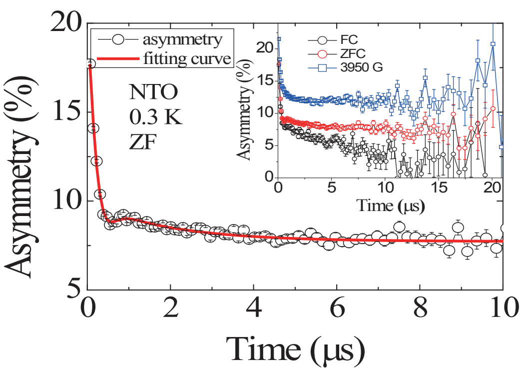

Fig. 1. The muon spin polarization shows oscillation at 0.3 K in the NTO sample. The inset shows the magnetic field history effect below the transition temperature (at 0.3 K), and the rapid initial depolarization in LF (3590 G) indicates the existence of fluctuating fields.

B = 53.7±5.5 G. Considering the effective moment of Nd^{3+} (3.54 μ_B) and the negative Curie-Weiss temperature θ_{CW} = -42 K, it is reasonable to conclude that the magnetic ground state is antiferromagnetic. However, the sample showed field history dependence when we measured the relaxation at zero field after cooling the sample in zero field (ZFC), in a longitudinal field of 3950 G, and quenching the field (FC), as shown in the inset of Fig.1. Therefore, the most probable magnetic structure of NTO would be canted AFM.

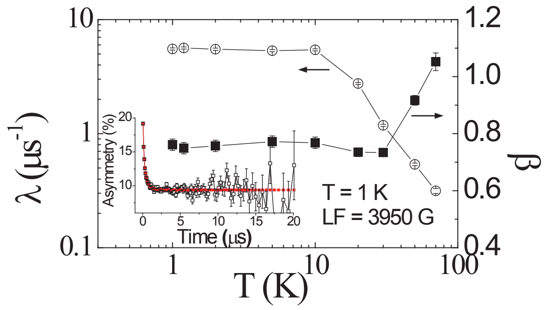

Fig. 2. Temperature dependence of muon spin depolarization rate and β. The inset shows the fitting using a stretched exponential function at 1 K.

Another important feature is the rapid initial decay of moun spin polarization. If this results from a distribution of the static field, a longitudinal field with $H_{ext} > 5H_{int}$ will effectively decouple the moun spin from the static field. However, as seen from the inset of Fig. 1, a LF of 3950 G only has a tiny influence. Therefore, in addition to the static field, there would be a coexistence of dynamic fields.

The asymmetry in the LF above 1 K is fitted using the stretched exponential function $A(t) = e^{-(\lambda t)^\beta}$, the fitting results are shown in Fig. 2. In the fast fluctuating limit, $1/\lambda$ is proportional to the fluctuating rate; therefore, Nd^{3+} spin slows gradually as the temperature approaches 10 K. Below 10 K, λ is almost temperature independent, which is common in frustrated systems, indicating that the density of state is appreciable for low energy magnetic excitations[3]. Though NTO is not geometrically frustrated, the frustration index $\theta_W/T_c = 72$ is quite large, which might be the origin of the observed $\lambda(T)$ behavior. On the other hand, β gradually dropped from 1 to 0.7 with decreasing temperature. According to previous study[4], if β is 0.5, the system should be inhomogenous. However, even in the single crystalline sample, there may be an oxygen deficiency and therefore chemical inhomogeneity, this should be temperature independent, thus, the $\beta(T)$ behavior must have some other origin. Considering the 8 unequal sites of Nd^{3+}, the $\beta(T)$ behavior might be a reflection of different local fields at different sites.

[*1] Department of Physics, Zhejiang University, Hangzhou, China
[*2] Advanced Meson Science Laboratory, Nishina Center for Accelerator-Based Science, RIKEN, Wako, Japan

References

1) J. Gardner et al: Rev. Mod. Phys.: **82**, 53 (2010).
2) H. Xing et al.: J. Phys.: Condens. Matter: **23**, 216005 (2011).
3) F. Bert et al: Phys. Rev. Lett.: **97**, 117203 (2006)
4) Y. Uemura et al: Phys. Rev. B: **31**, 546 (1985)

RIKEN Accel. Prog. Rep. 45 (2012)

μSR study of spin-liquid state in equilateral triangular spin tubes

H. Manaka,[*1] T. Suzuki,[*2] and I. Watanabe[*3]

Triangular spin tubes belong to a new category of one-dimensional Heisenberg antiferromagnets along the tubes coexisting with geometrically frustrated spin systems in the triangular plane. Recently, we discovered that chromium fluoride ($CsCrF_4$) forms ideal equilateral triangular spin tubes with spin 3/2[1)]. All Cr ions are at equivalent sites, and each Cr-Cr-Cr bond angle in the triangular plane is 60°[2)]. Because superexchange interactions through the three Cr-F-Cr paths in each equilateral triangle may be maintained at equilibrium at 0 K, we suspect resonating spin-singlet pairs in each equilateral triangle. From the magnetic susceptibility and heat capacity data above 1.5 K, we concluded that $CsCrF_4$ consists of a gapless spin-liquid ground state that encompasses resonating spin-singlet pairs not only in each equilateral triangle but also along the tubes[2)]. To determine the spin dynamics of the spin-liquid ground state, μSR measurements were performed on $CsCrF_4$ at the RIKEN-RAL Muon Facility in the U.K, and polycrystalline samples of $CsCrF_4$ were prepared.

In fluorides, low-frequency oscillations due to the dipole-dipole coupling of F-μ^+-F states are generally observed. The observation of μSR time spectra under a zero magnetic field at various temperatures revealed that typical F-μ^+-F states appeared above 4 K; however, below 4 K, these states disappeared because an internal magnetic field developed. Figure 1 shows the

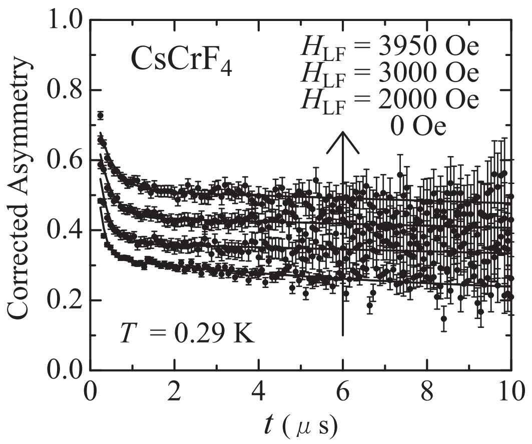

Fig. 1. μSR time spectra of $CsCrF_4$ for various longitudinal magnetic fields ($H_{\rm LF}$) up to 3950 Oe at 0.29 K. The solid lines are the best-fit line given by Eq. (1).

*1 Graduate School of Science and Engineering, Kagoshima University
*2 International Christian University
*3 Advanced Meson Science Laboratory, RIKEN Nishina Center

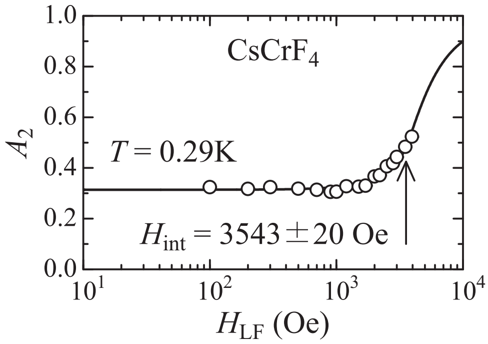

Fig. 2. Variation of A_2 under $H_{\rm LF}$ up to 3950 Oe at 0.29 K. The solid line is the best-fit line given by Eq. (2).

μSR time spectra under various longitudinal magnetic fields ($H_{\rm LF}$) at 0.29 K. As can be seen in this figure, the time spectra could be fitted well by the two components of muon spin relaxation, expressed by

$$A(t) = A_1 \exp(-\lambda_1 t) + A_2 \exp(-\lambda_2 t), \tag{1}$$

where A_1 and A_2 are the initial asymmetry, and λ_1 and λ_2 ($\lambda_1 > \lambda_2$) are the muon spin relaxation rates for fast and slow components, respectively. The decoupling behaviors, i.e., the upward shift of the time spectra with increasing $H_{\rm LF}$, may indicate the existence of a static internal magnetic field ($H_{\rm int}$) at 0.29 K. This result does not agree with the spin-liquid ground state model, as discussed in Refs. [1, 2]. At present, we are trying to estimate the value of $H_{\rm int}$, although the ground state is obscure. Figure 2 shows dependence of A_2 on $H_{\rm LF}$. When we assume that the internal magnetic field at each muon site has a unique magnitude but a random direction, we can estimate $H_{\rm int}$ as

$$A_2 = \frac{3}{4} - \frac{1}{4x^2} + \frac{(x^2-1)^2}{16x^3} \ln\frac{(x+1)^2}{(x-1)^2}, \tag{2}$$

where $x = H_{\rm LF}/H_{\rm int}$. As a result, we obtain $H_{\rm int}$ =3543 ± 20 Oe at 0.29 K and 3506 ± 20 Oe at 1.0 K. On the other hand, at 4.0 K, no decoupling behaviors are observed up to $H_{\rm LF}$ = 3950 Oe. This result suggests that magnetic long-range order occurs below 4.0 K owing to the development of a fluctuating internal magnetic field. Further analyses of the μSR time spectra at various temperatures and longitudinal magnetic fields are necessary to determine the ground state.

References

1) H. Manaka *et al.*, J. Phys. Soc. Jpn. **78**, 093701 (2009).
2) H. Manaka *et al.*, J. Phys. Soc. Jpn. **80**, 084714 (2011).

μSR study of quasi two-dimensional $S = 1/2$ triangular antiferromagnet, $EtMe_3Sb[Pd(dmit)_2]_2$

Y. Ishii[*1], I. Watanabe, T. Suzuki[*2], T. Matsuzaki and R. Kato

The magnetic ground states of two-dimensional triangular antiferromagnetic systems are of great interest to the research community. Magnetic frustration arising from the triangular lattice structure suppresses the long-range magnetic ordering (LRMO). This kind of quantum spin states without either LRMO or lattice symmetry breaking is referred to as the quantum spin liquid (QSL) state. Many experimentalists have sought real model materials exhibiting the QSL state; however, only a few candidates are known. One of the well-known QSL candidates is an organic material, κ-(BEDT-TTF)$_2$Cu$_2$(CN)$_3$[1)]. This compound has a 2D triangular lattice structure of $S = 1/2$ dimeric units of BEDT-TTF molecules and shows no LRMO down to 35 mK. However, at low temperatures, a field-induced NMR line-width broadening was observed, indicating an appearance of a field-induced weak magnetic moment[2)]. Recently, TF-μSR studies have revealed that as a ground state, a small gap exists in the spin excitation spectrum and there is a field-induced weak antiferromagnetic (WAF) phase[3)]. Another QSL candidate is the salt of a metal complex molecule, $EtMe_3Sb[Pd(dmit)_2]_2$. This material has an almost regular triangular structure of $S = \frac{1}{2}$ dimeric units with exchange interaction J of 200 $\sim$ 300 K and shows no LRMO or lattice symmetry breaking down to 20 mK ($\leq$0.01 % of J)[4,5)]. Thus, this compound is a strong QSL candidate. However, its ground state nature is still a controversial issue[5,6)]. In order to reveal the group state and the spin dynamics of this material, we have performed magnetic-field-dependent μSR measurements of this $EtMe_3Sb$ salt.

Field-dependent μSR experiments had been performed with the ARGUS spectrometer installed at the RIKEN-RAL Muon Facility. Single crystals which were used in this study, were synthesized by means of the air oxidation method.

The obtained μSR spectra are well described by the expression

$$P(t) = A\exp(-\lambda t) \times G_{\mathrm{KT}}(\Delta, t, H_{\mathrm{ext}})$$

where λ is the muon depolarization rate associated with the electron spin fluctuation and G_{KT} is the Kubo-Toyabe function that indicates the existence of randomly oriented nuclear magnetic moments. At zero field, the overall shapes of the temperature-dependent μSR time spectra were almost identical and the Δ and λ values were almost constant below 100 K: $\Delta \simeq$ 0.15 μs^{-1} and $\lambda \simeq 0.15\ \mu s^{-1}$. Thus, there was no sign of any kind of magnetic ordering down to 28 mK. This result also suggests that the effect of electron spin fluctuation may be strong in the temperature range 28 mK $\leq T \leq$ 100 K as the value of $\lambda \simeq 0.15\ \mu s^{-1}$ at zero fields is significantly large considering that it is in a paramagnetic state. The field-dependent λ observed at 28 mK is proportional to the root of the external field, H, as shown in fig. 1. This root-H behavior can be recognized to be a diffusive motion of some spin-excited state along the 1D direction, although the system has a 2D layered crystal structure. The most possible origin of this spin-excited state is an unpaired spin that is excited from the sea of the expected QSL state. Assuming this possibility is natural, we can suggest a model to explain our observed 1D diffusive motion. With the consideration that the lattice distortion in this system is substantially anisotropic, the singlet pairs should be realized along the molecular stacking direction, which is 1D. This kind of 1D spin-Peierls-like singlet formation can be seen in a real material, $EtMe_3P[Pd(dmit)_2]_2$, which also has an almost regular triangular structure and shows a Valence Bond Solid (VBS) ground state.[7)].

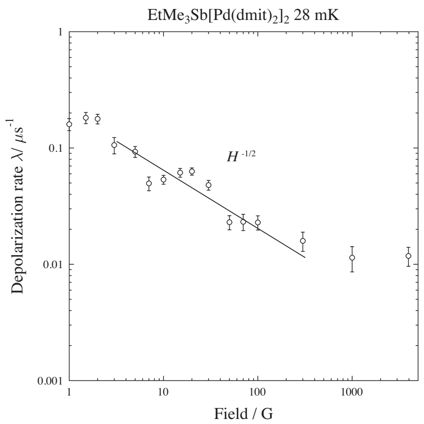

Fig. 1. Magnetic-field-dependent muon depolarization rate λ of $EtMe_3Sb[Pd(dmit)_2]_2$ measured at 28 mK.

*1 Department of Physics, Tokyo Medical University.
*2 Graduate School of Arts and Sciences, International Christian University.

References
1) Y. Shimizu et al., Phys. Rev. Lett., **91**, 107001 (2003)
2) Y. Shimizu et al., Phys. Rev. B **73**, 140407(R) (2006)
3) F. L. Pratt et al., Nature, **471**, 612 (2011)
4) T. Itou et al., Phys. Rev. B, **77**, 104413 (2008)
5) T. Itou et al., Nature Physics, **6**, 673 (2010)
6) M. Yamashita et al., Science **328**, 1246 (2010)
7) M. Tamura et al., J. Phys. Soc. Jpn., **75**, 093701 (2006)

Study of magnetic orderings in organic-inorganic hybrid of $(C_6H_5CH_2CH_2NH_3)_2CuCl_4$

A. A. Nugroho,*1 A. Polyakov,*2 T. T. M. Palstra,*2 and I. Watanabe,*3

[Magnetic hybrid, long-range order]

The flexibility to manipulate the organic-inorganic hybrids has attracted much attention to explore the functionality of this class of materials. These materials offer large possibilities for tailoring the material functionalities and physical properties such as electrical, optical and magnetic properties by adjusting its organic and inorganic building block[1]. The organic component in the hybrids can be used not only to bind the inorganic components but also to control the connectivity between the inorganic components as well as to manipulate their dimensionality. One of the interesting series of the organic-inorganic hybrids is the magnetic hybrids with perovskite type transition-metal salt $(C_6H_5CH_2CH_2NH_3)_2CuCl_4$. The interlayer spacing between the transition metal salt, $CuCl_4$ is of the order of nm, which gives rise to the compounds two dimensional properties[2]. Nevertheless the magnetic susceptibility measurement of this compound shows the magnetic transition temperature around 10 K, which is much higher than those found in magnetic organic materials, and signifying a 3D long range order. The establishment of 3D interaction is not only important for understanding a long distance magnetic interaction but also for finding parameters to develop hybrid material with higher transition temperature.

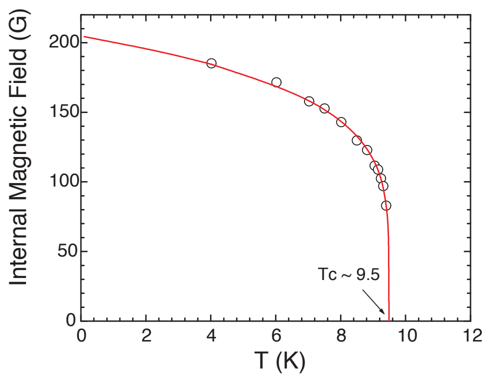

Fig. 1. Temperature dependence of the internal field of $(C_6H_5CH_2CH_2NH_3)_2CuCl_4$. The line is obtained by fitting the data with formula discussed in the text.

We have carried out the Zero Field (ZF)- and Longitudinal Field (LF)-muSR on $(C_6H_5CH_2CH_2NH_3)_2CuCl_4$. Figure 1 shows the temperature dependence of internal field obtained from the muon spin rotation frequency. The data is fitted by $B(T) = B_0(1 - T/T_c)^{\beta}$, resulted in the value of $\beta = 0.2$ with the corresponding value of T_c =9.5 K and B_0 = 205 G. This result confirms the magnetization data that the Cu-hybrid orders ferromagnetically below 9 K.

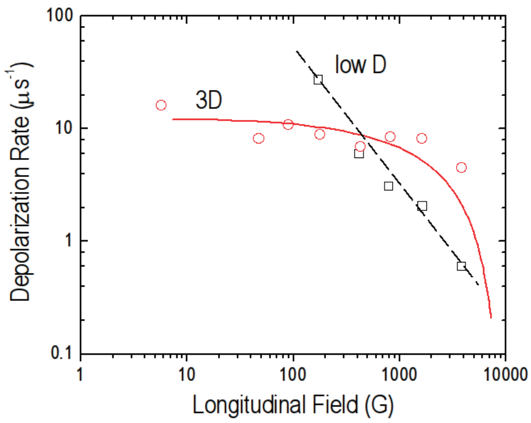

Fig. 2. LF-μSR spectra of $(C_6H_5CH_2CH_2NH_3)_2CuCl_4$ at 30 K (○) and 4 K (□), eyes guided by lines.

Figure 2 shows the longitudinal-field of depolarization rate above and below the 3D magnetic ordering of Cu-hybrids. Above the magnetic transition, the depolarization rate can be fitted better by the red field model rather that the diffusion model. This indicates that the magnetic moment of Cu fluctuate freely and the 2D character does not seem to show a dominant effect. However below the magnetic ordering temperature, a diffusion model seems to work. Based on the available data, we can not distinguish between the 2D and 1D diffusion model. Having the limitation of magnetic field strength, the interpretation of the low field data need to be confirmed, especially for the low temperature regime to explain the mechanism of the 3D long-range ordering with a long distance separation of the 2D magnetic layer. In order to describe the general mechanism for the organic-inorganic hybrid, the μSR measurement in high magnetic field should be performed in the same hybrid structure with different transition metal ion such as Mn and a longer chain organic components separating the 2D layers.

*1 FMIPA, Institut Teknologi Bandung, Indonesia
*2 Solid State Chemistry, Rijkuniversiteit Groningen, The Netherlands
*3 The Institute of Physical and Chemical Research (RIKEN)

References

1) C. N. R Rao et al.: J. Phys.: Condens. Matter 20, 083202 (2008)
2) Anne Arkenbout: Organic-inorganic Hybrids, Ph.D Thesis RuG (2010)

Study of spin-equilibrium and succeeding magnetic phase transitions in iron(III) complex by μSR spectroscopy

N. Kojima,*1 K. Kagesawa,*1 A. Okazawa,*1 and I. Watanabe

Recently, we synthesized novel mixed-valence or heterometal monothiooxalate-bridged iron complexes, $A[M^{II}Fe^{III}(mto)_3]$ (A = $(n\text{-}C_nH_{2n+1})_4N$, $(C_6H_5)_4P$; M = Fe[1], Mn, Zn[2], Cd[3]; mto = C_2O_3S), having a spin equilibrium between the high-spin (HS) (S = 5/2) and low-spin (LS) (S = 1/2) states at the $Fe^{III}O_3S_3$ site. The observation of spin equilibrium in $A[M^{II}Fe^{III}(mto)_3]$ is the first such example among assembled metal complexes, and therefore mto-bridged iron(III) complexes have the potential to show intriguing physical properties. For instance, $(C_6H_5)_4P[Mn^{II}Fe^{III}(mto)_3]$ shows anomalous multistep magnetic phase transitions at 23 and 30 K owing to the spin equilibrium at the iron(III) site, which were confirmed by means of magnetic and ^{57}Fe Mössbauer spectroscopic analyses. However, the details of the magnetic ordering behavior and the dynamics of the spin equilibrium have not yet been clarified.

The muon-spin relaxation (μSR) tequnique can be employed to probe into the multistep magnetic ordering in $(C_6H_5)_4P[Mn^{II}Fe^{III}(mto)_3]$ because of the wide time window afforded by the technique (10^{-6} to 10^{-11} s). Therefore, we investigated the dynamical property of the spin states of $(C_6H_5)_4P[Mn^{II}Fe^{III}(mto)_3]$ by μSR.

Polycrystalline samples were wrapped in aluminum foils and stuck to a silver plate with Scotch tape. We used a minicryostat in the temperature range between 7 and 100 K. The μSR time spectra were obtained in zero (ZF) and longitudinal magnetic field (LF) applied along the direction of initial muon-spin polarization. The ZF- and LF-μSR were analyzed using

$$A(t) = A_0 \exp(-\lambda_0 t) + A_1 \exp(-\lambda_1 t), \qquad (1)$$

where A_0 and A_1 are the corrected initial asymmetries of the slow and fast relaxation components, respectively, and λ_0 and λ_1 are the respective muon-spin relaxation rates. For the spectra above 23 K in ZF, the Kubo-Toyabe function was applied to the first term.

Figure 1 shows the temperature dependence of λ_0. The λ_0 of ZF-μSR shows a divergent peak around 23 K, which is attributed to the critical slowing down toward the magnetic ordering. This result is consistent with the ^{57}Fe Mössbauer spectra[4], where a magnetically split sextet grows below 23 K. On the other hand, no peak of λ_0 could be found around 30 K, where the magnetic ordering surely occures. It is most likely that the spin equilibrium at the iron(III) site remains and its magnetic fluctuation disturbes the critical slowing down toward the magnetic ordering at 30 K.

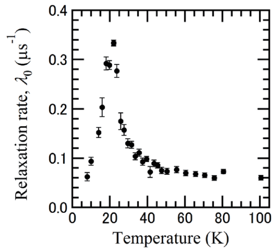

Fig. 1. Temperature dependence of the relaxation rate, λ_0, in ZF for the slow relaxation component.

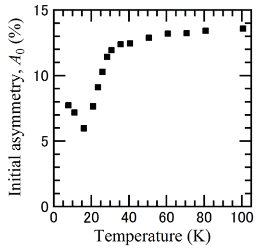

Fig. 2. Temperature dependence of the corrected initial asymmetry, A_0, in LF = 3950 Oe for the slow relaxation component.

Figure 2 shows the temperature dependence of A_0 in LF = 3950 Oe. The muon spin was not decoupled up to 3950 Oe. This result may be caused by the spin fluctuation derived from the spin equilibrium at the iron site. The monotonic decrement of A_0 from 100 to 30 K indicates the temperature dependence of the ratio between the LS and HS states in the spin equilibrium, which is consistent with the temperature dependence of the magnetic susceptibility. An abrupt decrease in A_0 around 30 K implies the occurrence of the magnetic phase transition that corresponds to the ordering of only the manganese(II) spins.

In conclusion, we confirmed the magnetic ordering in $(C_6H_5)_4P[Mn^{II}Fe^{III}(mto)_3]$ at 23 K and the strong spin fluctuation above the magnetic phase transition. In addition to LF-μSR, X-ray magnetic circular dichroism measurement is necessary to clarify the magnetically ordered state between 23 and 30 K.

References

1) K. Kagesawa et al.: Polyhedron **28**, 1822 (2009).
2) K. Kagesawa et al.: Chem. Lett. **39**, 872 (2010).
3) N. Kojima et al.: Materials **3**, 3141 (2010).
4) K. Kagesawa: Doctoral Thesis, Univ. of Tokyo (2010)

*1 Department of Basic Science, Graduate School of Arts and Sciences, The University of Tokyo

Muon study of pre-martensitic phenomena associated with thermoelastic martensitic transformation in NiTi alloys

M. Mihara,[*1] K. Shimomura,[*2] Y. Ninomiya,[*3] H. Araki,[*3] M. Mizuno,[*3] Y. Shirai,[*4] I. Watanabe, K. Inoue,[*4] S. Yamamoto,[*3] T. Nagatomo,[*2] K. M. Kubo,[*5] T. Nakano,[*1] R. Kadono[*2] and K. Nishiyama[*2]

Near-equiatomic NiTi alloys are extensively used in consumer appliances because they exhibit pseudoelastic and/or shape-memory effects. The mechanism underlying this exotic behavior is the so-called thermoelastic martensitic transformation. An anomalous behavior has been found in positron lifetime measurements of the $Ni_{51}Ti_{49}$ alloy: an anomalous increase in the positron lifetime with lowering temperature, prior to the martensitic transformation[1]. This phenomenon might be related to phonon softening, which occurs prior to the martensitic transformation[2]. In this situation, a positively charged particle such as a positron, upon introduction into the softened lattice, is expected to be trapped selectively at vacant sites with low atomic density, and therefore, the annihilation probability of positrons with inner-shell electrons decreases and the positron lifetime increases (self-trapping model). Muon spin relaxation (μSR) using positive muons is a good complementary study to verify this hypothesis because a similar phenomenon is expected when a positive muon is injected into the lattice. In this report, we present the results of zero-field muon spin relaxation (ZF-μSR) of $Ni_{50}Ti_{50}$ and $Ni_{51}Ti_{49}$ alloys, which have different martensitic transformation start temperatures $T_{\rm Ms}$ of 344 K and 223 K, respectively.

The experiment was performed at J-PARC and the RIKEN-RAL muon facility. The ZF-μSR spectra of $Ni_{50}Ti_{50}$ and $Ni_{51}Ti_{49}$ indicate slow Gaussian-like relaxation. The muon spin relaxation rate Δ was deduced by fitting the data with a static Kubo-Toyabe function, as shown in Fig. 1 and Fig. 2. For both $Ni_{50}Ti_{50}$ and $Ni_{51}Ti_{49}$, the values of Δ drastically change by about three times, from $\sim$0.01 μs^{-1} to $\sim$0.025 μs^{-1}, with decreasing temperature. The temperature range over which Δ changes is lower for $Ni_{51}Ti_{49}$ than for $Ni_{50}Ti_{50}$, and this seems to be correlated with the martensitic transformation temperature. The present experimental value of $\Delta = \sim 0.025$ μs^{-1} at the lower temperature limit is close to the predicted value of $\Delta = 0.03$ μs^{-1}, when muons are assumed to be located at octahedral interstitial sites surrounded by two Ni atoms and four Ti atoms.

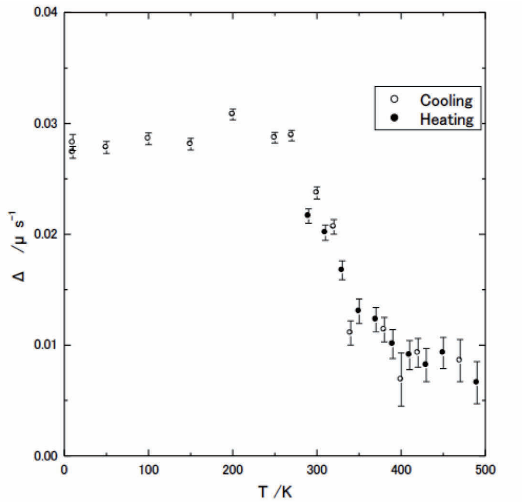

Fig. 1. Temperature dependence of muon spin relaxation rate Δ for $Ni_{50}Ti_{50}$.

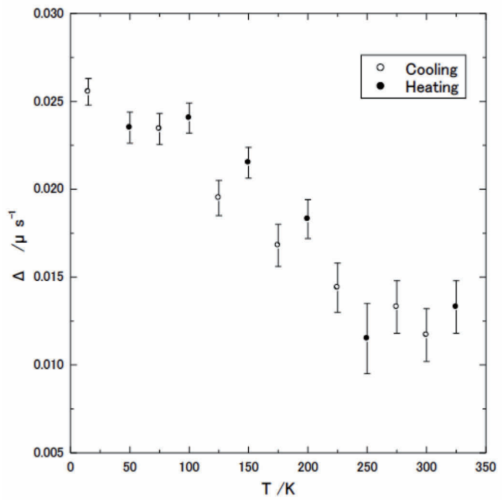

Fig. 2. Temperature dependence of muon spin relaxation rate Δ for $Ni_{51}Ti_{49}$.

References
1) H. Araki et al., Mater. Sci. Forum **327-328**, 437 (2000).
2) S.K. Satija et al,. Phys. Rev. **B 29**, 6031 (1984).

*1 Department of Physics, Osaka University
*2 Institute of Materials Structure Science, KEK
*3 ASFM, Osaka University
*4 Deprtment of Materical Science and Engineering, Kyoto University
*5 International Christian University

Lithium-ion diffusion in novel battery materials

J. Sugiyama,[*1] H. Nozaki,[*1] M. Harada,[*1] K. Mukai,[*1] M. Månsson,[*2] K. Ohishi, and I. Watanabe

[Lithium diffusion, positive electrode, battery]

Diffusion of Li^+ ions in solids is an important factor controlling the charge-discharge rate of Li-ion batteries. Although a self-diffusion coefficient of Li^+ ions ($D_{\rm Li}$) in solids is usually evaluated by ^{7}Li-NMR, experimental difficulties arise for materials that contain magnetic ions. This is because the magnetic ions contribute additional spin-lattice relaxation processes that are considerably larger than the $1/T_1$ expected from only Li diffusion[1]. On the other hand, muons do not feel fluctuating magnetic moments at high temperatures, but instead sense the change in nuclear dipole field due to Li diffusion[2]. Even if magnetic moment of the magnetic ions still affects the muon-spin depolarization rate, such an effect is, in principle, distinguishable from that of nuclear dipole fields. In particular, application of a weak longitudinal field can decouple the magnetic and nuclear dipole interactions[3].

Recently, the mixed metal oxides of the form $\rm Li(Co_{1-x-y}Ni_xMn_y)O_2$ have become the focus of attention. In particular, the $\rm Li(Co_{1/3}Ni_{1/3}Mn_{1/3})O_2$ compound has been put forward as one of the most promising candidates for a novel battery electrode material[4]. The structure of these compounds is the same as that of $\rm LiCoO_2$, i.e. a rhomohedral lattice (space group $R\bar{3}m$), where the $\rm (Co/Ni/Mn)O_2$ planes are stacked between nonmagnetic Li layers in the c-direction. However, despite a large number of electrochemical studies, there is no systematic research on $D_{\rm Li}$ as a function of x and y. We have, thus, initiated a μ^+SR work on $\rm Li(Co_{1-x-y}Ni_xMn_y)O_2$ in order to find an optimal composition from a viewpoint of $D_{\rm Li}$.

First, we have concentrated upon the $\rm LiCo_{1-x}Ni_xO_2$ system in 2011. Figure 1 shows the temperature (T) dependences of the field distribution width (Δ) and filed fluctuation rate (ν) for $\rm LiCo_{1-x}Ni_xO_2$. As T increases from 50 K, Δ decreases with increasing slope ($d\Delta/dT$) and finally levels off at a constant value above $\sim$ 400 K for $\rm LiCoO_2$. On the contrary, ν starts to increase above $\sim$ 200 K with increasing T for the four compounds and reaches the maximum value at $\sim$ 300 K for $\rm LiCoO_2$ ($\sim$ 400 K for $\rm LiNiO_2$). Here, since the increase in ν above 200 K is mainly induced by Li diffusion, we can estimate $D_{\rm Li}$ at 300 K and its activation energy (E_a) from the $\nu(T)$ curve (Fig. 2), where we assumed that $D_{\rm Li} = D_0 \exp(-E_a/k_{\rm B}T)$. This could suggest that the optimal x is located between 0.5 and 0.8. We, hence, plan to accumulate the data on these x regions in 2012.

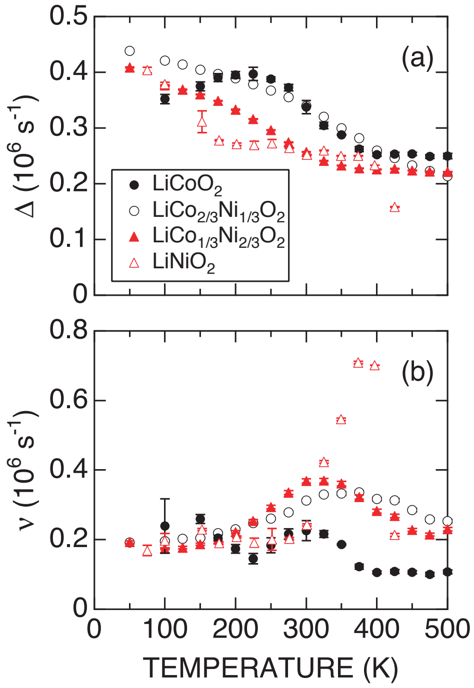

Fig. 1. Temperature dependences of Δ and ν for $\rm LiCo_{1-x}Ni_xO_2$ with $x = 0$, 1/3, 2/3, and 1.

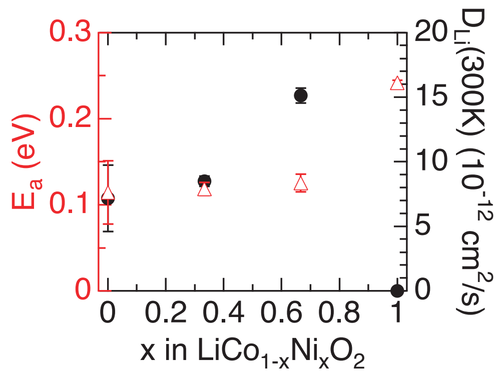

Fig. 2. Activation energy, E_a (open triangles) and $D_{\rm Li}$ at 300 K (solid circles) as a function of x in $\rm LiCo_{1-x}Ni_xO_2$.

References
1) K. Nakamura, Solid State Ionics **121**, 301 (1999).
2) J. Sugiyama *et al.*, Phys. Rev. Lett. **103**, 147601 (2009); Phys. Rev. B **82**, 224412 (2010).
3) R. S. Hayano *et al.*, PRB **20**, 850 (1979).
4) B. J. Hwang *et al.*, Chem. Mater. **15**, 3676 (2003), and references cited therein.

[*1] Toyota Central Research and Development Labs., Inc.
[*2] ETH Zürich, Switzerland

Na-dynamics in quasi-one-dimensional ionic conductors, NaM_2O$_4$ (M =Ti, V, Cr, and Mn)

J. Sugiyama,[*1] H. Nozaki,[*1] M. Harada,[*1] M. Månsson,[*2] H. Sakurai,[*3] K. Ohishi, and I. Watanabe

[Sodium diffusion, solid electrolyte, battery]

For future solid-state batteries, an electrolyte material requires both high ionic conductivity and low electric conductivity. In this context, $CaFe_2O_4$-type one-dimensional (1D) compounds containing Na ions would be a good candidate for an electrolyte material (Fig. 1), because of their 1D channel structure, in which Na are located, and a strong electron-electron interaction between d electrons of a transition-metal in the 1D chain. Particularly, considering the limited amount of natural resources of Li, a technology to manage Na dynamics would be a key factor for realizing the future batteries.

According to our previous study on Na_xCoO_2[1)], it was found that μ^+SR provides unique information on Na dynamics in magnetic materials. This is because the implanted muons in oxides are usually located in the vicinity of O^{2-} ions so as to make a stable μ^+-O^{2-} bond. Indeed, muons are known to be stable until 500 K for $LiCrO_2$[2)]. Therefore, muons do not feel fluctuating magnetic moments at high T, but instead sense the change in nuclear dipole field due to Na diffusion. Even if magnetic moments still affect the muon-spin depolarization rate, such an effect is, in principle, distinguishable from that of nuclear dipole fields. In addition, a weak longitudinal field decouples the magnetic and nuclear dipole interactions.

Figure 2 shows the zero field (ZF-) and longitudinal field (LF-) spectra for NaV_2O_4 at 200 K and 450 K. At 200 K, *i.e.* above its T_N = 140 K, the spectra exhibit a typical static Kubo-Toyabe relaxation due to nuclear magnetic field of Na and V. However, a dynamic behavior is clearly observed at 450 K. In fact, as T increases from 200 K, the field fluctuation rate (ν) increases with increasing slope ($d\nu/dt$), and reaches a maximum around 450 K, around which the field distribution width (Δ) decreases slightly with T. Although there are no NMR and electrochemical studies for NaV_2O_4 at high T, such behavior strongly suggests the occurance of Na diffusion above ~ 300 K. We plan to measure the μ^+SR spectra for NaV_2O_4 at higher T and for the other NaM_2O$_4$ compounds in 2012.

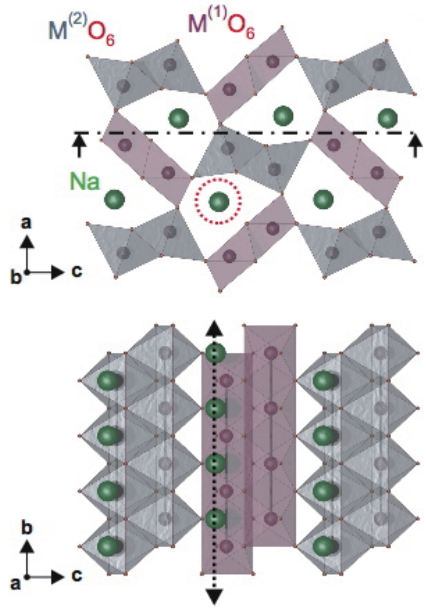

Fig. 1. Crystal structure of NaM_2O$_4$.

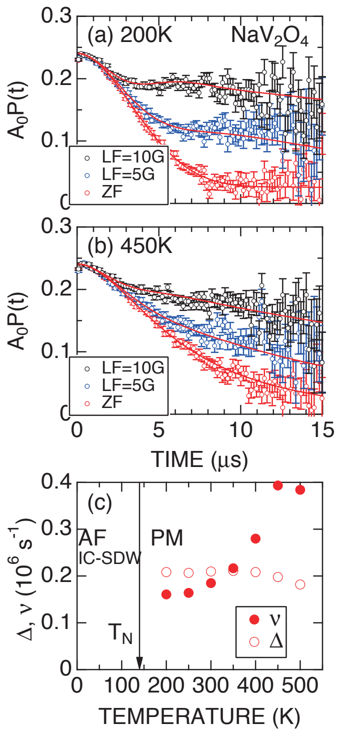

Fig. 2. ZF- and LF-spectra at (a) 200 K and (b) 450 K for NaV_2O_4, (c) T dependences of the field distribution width (Δ) and the filed fluctuation rate (ν).

References
1) M. Månsson, in the μSR2011 conference (2011).
2) J. Sugiyama *et al.*, Phys. Rev. B **82**, 224412 (2010).

*1 Toyota Central Research and Development Labs., Inc.
*2 ETH Zürich, Switzerland
*3 National Institute for Materials Science (NIMS)

Search for a muonium-emitting material as a source of an ultracold muon beam for a new J-PARC muon g-2 experiment

Y. Fujiwara,[*1,11] P. Bakule,[*6] G. Beer,[*12] D. Contreras,[*12] M. Esashi,[*7] Y. Fukao,[*4] S. Hirota,[*11] H. Iinuma,[*4] K. Ishida,[*1] M. Iwasaki,[*1,8] T. Kakurai,[*11] S. Kanda,[*11] H. Kawai,[*3] N. Kawamura,[*4] G. Marshall,[*2] H. Masuda,[*9] Y. Matsuda,[*10] T. Mibe,[*4] Y. Miyake,[*4] K. Ohishi,[*1] H. Ohnishi,[*1] A. Olin,[*2] N. Saito,[*4,11] K. Shimomura,[*4] P. Strasser,[*4] M. Tabata,[*3,5] D. Tomono,[*1] K. Tsukada,[*1] K. Ueno,[*1] K. Yokoyama,[*1] S. Yoshida[*7]

A High-intensity low-energy muon beam is a key requirement for the precise measurement of the anomalous muon g-factor (g-2), proposed to be carried out at J-PARC[1)]. It is known that when 4-MeV muons are stopped by targets made of certain materials, some of the muons are thermally evaporated into vacuum from the surface as muoniums. Low-energy muons, produced by laser ionization of thermal muoniums, are accelerated and are stored in a magnetic storage ring for g-2 measurement. We are studying silica aerogel at TRIUMF as a part of our search for efficient thermal-muonium-emitting materials[2)] by using a method presented in another report[3)]. Fig.1 shows the experimental setup inside the vacuum chamber.

In 2011, we obtained new data by using four types of silica aerogels. The densities of the silica aerogels were 27, 49, 99, and 180 mg/cc, and thicknesses were 7.8, 4.2, 2.3, and 2.4 mm, respectively. We also carried outbackground measurements for a silica glass plate with a density of 2.0 g/cc and a thickness of 0.096 mm.

The beam momentum was adjusted for each target so that approximately half of the incident muons were stopped by the target. Thus, the distribution of muon stopping positions showed a maximum at the target surface on the downstream side for every target.

We aim to achieve the following from measurements of each target: To obtain the diffusion constant by determining the fraction of muoniums exiting the target volume and to estimate the emission parameters such as emission angle and energy distribution from the time evolution of the muonium distribution in vacuum.

Fig.2 shows preliminary data for the space-time distribution of a decayed muonium candidate; the horizontal axis (Z) represents the distance from the target surface and the vertical axis denotes the time elapsed after the muon beam was stopped. The muonium signal was selected by requesting a coincidence of two decay products[3)], an electron and a positron, for a time window of 30 ns and a spatial window of 10 mm. While movement of muoniums in vacuum was clearly observed in the case of the aerogel with a density of 27 mg/cc sample, it was not observed for the glass plate.

Detailed analysis to obtain the muonium emission rate, the detailed muonium distribution and the dependence of the distribution on the target materials is in progress.

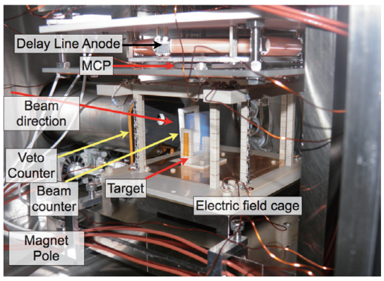

Fig. 1. Experimental setup inside the vacuum chamber.

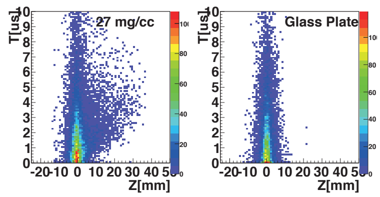

Fig. 2. Space-time distribution of Mu candidate decay points for the 27 mg/cc silica aerogel target (left) and the glass plate (right).

*1 RIKEN Nishina Center, Japan
*2 Canada's National Laboratory for Particle and Nuclear Physics (TRIUMF), Canada
*3 Department of Physics, Chiba University, Japan
*4 High Energy Accelerator Research Organization (KEK), Japan
*5 Japan Aerospace Exploration Agency (JAXA), Japan
*6 Institute of Physics, ASCR, v. v. i., Czech Republic
*7 Advanced Institute for Materials Research (WPI-AIMR), Tohoku University, Japan
*8 Department of Physics, Tokyo Institute of Technology, Japan
*9 Division of Applied Chemistry, Tokyo Metropolitan University, Japan
*10 College of Arts and Sciences, The University of Tokyo, Japan
*11 Department of Physics, The University of Tokyo, Japan
*12 Department of Physics, University of Victoria, Canada

References

1) N. Saito, M. Iwasaki et al.:P34 Proposal at J-PARC
2) Y. Fujiwara et al.:RIKEN Accel. Prog. Rep, **44** 260 (2011)
3) K. Ueno et al.:in this report.

Development of a three-dimensional imager for investigation of muonium distribution in vacuum

K. Ueno,[*1] P. Bakule,[*2] G. Beer,[*3] D. Contreras,[*4] M. Esashi,[*5] Y. Fujiwara,[*1,*6] Y. Fukao,[*7] S. Hirota,[*6] H. Iinuma,[*7] K. Ishida,[*1] M. Iwasaki,[*1,*8] T. Kakurai,[*6] S. Kanda,[*6] H. Kawai,[*9] N. Kawamura,[*7] G. Marshall,[*4] H. Masuda,[*10] Y. Matsuda,[*11] T. Mibe,[*7] Y. Miyake,[*7] K. Ohishi,[*1] H. Ohnishi,[*1] A. Olin,[*7] N. Saito,[*6,*7] K. Shimomura,[*7] P. Strasser,[*7] M. Tabata,[*9,*12] D. Tomono,[*1] K. Tsukada,[*1] K. Yokoyama,[*1] S. Yoshida[*5]

We plan a new muon g-2 experiment having a precision of 0.1 ppm by using a high-intensity ultracold muon beam in a highly uniform magnetic field at the J-PARC[1)]. In order to produce the ultracold muon beam, the method of laser ionization of thermal Mu, which was developed at the KEK Muon Science Laboratory and RIKEN-RAL[2)3)], is used. To optimize the Mu target material and the laser spot position for the new experiment, we have investigated the space-time distribution of emitted Mu from silica aerogel targets at TRIUMF by using a three-dimensional imager[4)]. In this article, we report the setup and performance of the three-dimensional imager and a new detector calibration method having an ultra violet (UV) system.

In the most recent calculation of the Mu distribution, a two-dimensional imager, which had a position resolution of 6 mm (FWHM)[5)], was used. In order to effectively determine the laser spot position for the new experiment, more precise information about the Mu distribution is needed because the laser spot size is a few mm in diameter. Hence, we developed a new three-dimensional imager with the position resolution of a few mm. Figure 1 shows the schematic view of the three-dimensional imager. The imager mainly consists of three components: a multi-wire drift chamber (MWDC)[6)], an NaI detector, and a multi-channel plate (MCP). The MCP and the target were placed in a vacuum chamber, and the other components were placed outside the chamber. The three-dimensional track and energy of the positrons produced by the muon decay were detected by the MWDC and NaI, respectively. The electron remaining after the muon decay was guided by the electric and magnetic fields, and its two-dimensional position was detected by the MCP. Using these position data and time information, the decay vertex and time evolution of Mu, which escaped from the target into the vacuum region, were calculated. The position resolutions of the MWDC and MCP were 0.5 mm and 1 mm (RMS), respectively. The vertex resolution at the target region was 2 mm (RMS) because of the parallax effect and positron scattering at the chamber window. Detailed analysis is in progress to evaluate the Mu distribution[7)].

We are developing a new position calibration system for the MCP because the electric field could be distorted near the target. A thin copper wire is placed in vacuum and irradiated with UV light, and the photoelectrons emitted from the wire are detected, as shown in Fig. 2 (left). Figure 2 (right) shows the preliminary image obtained when the wire is placed near the center of the imager. We are planning to develop a precise response function for position reconstruction using the new calibration system.

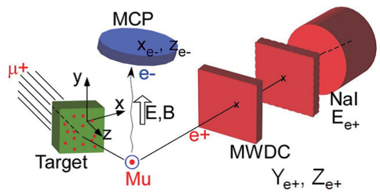

Fig. 1. Schematic view of the three-dimensional imager.

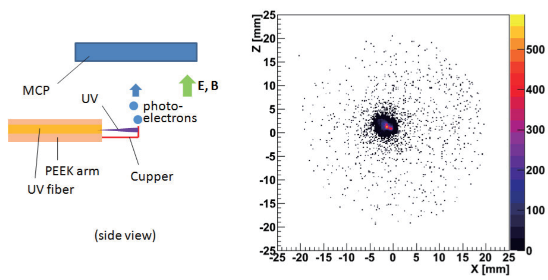

Fig. 2. Schematic view of the setup of the UV system (left) and the image of photoelectrons obtained(right).

*1 RIKEN Nishina Center
*2 Rutherford Appleton Laboratory
*3 Dept. of Physics and Astronomy, Univ. of Victoria
*4 Canada's National Laboratory for Particle and Nuclear Physics (TRIUMF)
*5 Advanced Institute for Materials Research (WPI-AIMR), Tohoku University
*6 Dept. of Physics, The University of Tokyo
*7 High Energy Accelerator Research Organization (KEK)
*8 Dept. of Physics, Tokyo Institute of Technology
*9 Dept. of Physics, Chiba University
*10 Div. of Appl. Chem., Tokyo Metropolitan Univ.
*11 College of Arts and Sciences, The Univ. of Tokyo
*12 Japan Aerospace Exploration Agency (JAXA)

References
1) N. Saito, M. Iwasaki et al.: P34 proposal at J-PARC.
2) K. Nagamine et al.: Phys. Rev. Lett. **74** (1995) 4811.
3) P. Bakule et al.: NIM. B **266**, (2008) 355.
4) Y. Fujiwara et al.: RIKEN Accel. Rep. **44** (2010) 260.
5) G. A. Beer et al.: Phys. Rev. Lett. **57** (1986) 671.
6) R. S. Henderson et al.: NIM A **548** (2005) 306.
7) Y. Fujiwara et al.: RIKEN Accel. Rep. **45** (2011).

3. Radiochemistry and Nuclear Chemistry

Preparation of ^{99}Mo and ^{181}W radiotracers

A. Wada,[*1] Y. Oura,[*1] H. Haba, and J. Kanaya

In chemical studies of element 106, Sg, it is important to compare the chemical properties of Sg with those of its lighter homologues, Mo and W. The preparation of no-carrier-added radiotracers, ^{99}Mo ($T_{1/2}$ = 2.74 d) and ^{181}W ($T_{1/2}$ = 121.2 d), was investigated in this research.

^{99}Mo was prepared from Al foils on which the fission products of ^{252}Cf were implanted. Five Al foils (12.5 μm thick each) were stacked on a 2.7 MBq ^{252}Cf source for 19 h. From the activity of ^{99}Mo implanted on each foil, it was confirmed that a 25-μm-thick Al foil was sufficient to trap ^{99}Mo. Using ^{99}Mo produced by the (n, γ) reaction, the chemical procedure for separating ^{99}Mo from the Al foils was evaluated. The evaluated procedure, adsorption of ^{99}Mo in 6 M HCl including Al on an anion-exchange resin and elution with 5 M HNO_3/1 M HF, was applied to the Al foils covered on the ^{252}Cf source. The final Mo fraction contained 2.8 kBq ^{99}Mo, and the chemical yield of ^{99}Mo was 96%.

^{181}W was produced by the ^{181}Ta (p, n)^{181}W reaction using 14-MeV protons supplied from the RIKEN AVF Cyclotron. First, the excitation function of this reaction was determined. A stack consisting of some ^{nat}Ta (10 μm thick) and ^{nat}Cu (10 or 50 μm thick) foils was irradiated by 0.5-0.6 μA protons for 1 h. After irradiation, characteristic X-rays associated with the EC decay of ^{181}W in Ta foils and γ-rays from Cu foils were measured non-destructively by a Ge detector (GMX type) at the appropriate cooling times. The proton energy in each foil was calculated by the OSCAR code[1)], and the proton flux was determined from the activity of ^{65}Zn produced by the ^{65}Cu (p, n) reaction, whose cross section was referred to the Experimental Nuclear Reaction Data (EXFOR) provided by Brookhaven National Laboratory.

The cross sections determined by two different irradiations are shown in Fig. 1 with the theoretical values calculated by the TALYS code[2)] and the experimental values[3–5)] cited in EXFOR. Hansen et al.[5)] measured characteristic X-rays of ^{181}W using a NaI scintillation detector. Chodil et al.[3)] and Thomas et al.[4)] measured the neutrons emitted by proton-induced reactions and reported the sum of (p, n) and (p, pn) cross sections. Chodil et al.[3)] estimated that the contribution of the (p, pn) reaction was much smaller than that of the (p, n) reaction, on the basis of the (p, pn) cross section determined by Cohen et al.[6)] Our study is the first to focus on the determination of the ^{181}Ta(p, n)^{181}W cross sections using the Ge detector; in this study, cross section values with a smaller error than that in the previous ones were obtained. The peak position obtained in this study was consistent with the literature values, but the cross section values around the peak energy were about 30% smaller than the literature values. Further, the values at an energy of 12-14 MeV were inconsistent with the minimum values at about 13 MeV reported by Thomas et al.[4)] but consistent with those reported by Chodil et al.[3)] The values calculated by TALYS showed a good agreement with the experimental values at energies lower than 9 MeV and higher than 12 MeV. Between 9 MeV and 12 MeV, TALYS underestimated the experimental cross sections, and the peak position obtained by TALYS was about 1 MeV lower than the experimental value.

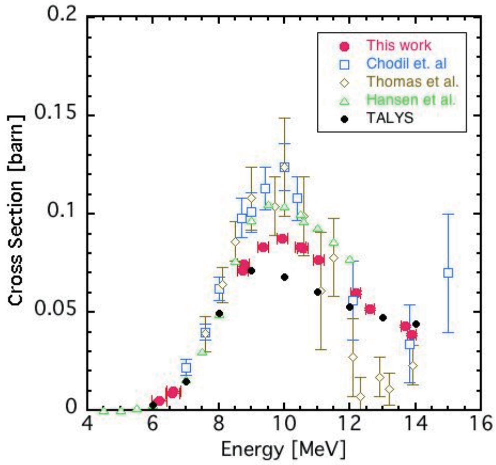

Fig. 1. Excitation function of the ^{181}Ta(p, n)^{181}W reaction.

The chemical procedure for separating ^{181}W from the Ta foil was examined using ^{187}W and ^{182}Ta produced by the (n, γ) reaction, on the basis of a procedure that involved anion exchange with HNO_3/HF, as reported by Liang et al.[7)] . Since trace amount of F^- contaminants in the ^{181}W fraction seemed to interfere with the study of the ion-exchange behavior of W, we are improving the procedure to obtain a ^{181}W solution that does not contain even trace amount of F^-.

[*1] Department of Chemistry, Tokyo Metropolitan University

References

1) K.Hata, et al.: JAERI-M 5558 (1974).
2) A.J. Koning, et al.: in *Proceedings of the International Conference on Nuclear Data for Science and Technology*, edited by O.Bersillon et al. (EDP Sciences, 2008), p.211.
3) G. Chodil, et al.: Nucl. Phys. **A93**, 648 (1967).
4) R. G. Thomas, et al.: Phys. Rev. **159**, 1022 (1967).
5) L.F.Hansen, et al.: Nucl. Phys. **30**, 389 (1962).
6) B.L.Cohen, et al.: Phys. Rev. **94**, 620 (1954).
7) X. Liang, et al.: J. Nucl. Radiochem. Sci. **11**, Suppl. 70 (2010).

Excitation functions of Rf isotopes produced in ^{248}Cm + ^{18}O reaction

M. Murakami,[*1] S. Goto,[*2] H. Murayama,[*1] T. Kojima,[*1] D. Kaji, K. Morimoto, H. Haba, Y. Kudou, T. Sumita, R. Sakai, A. Yoneda, K. Morita, H. Kikunaga,[*3] Y. Kasamatsu,[*4] T. K. Sato,[*5] and H. Kudo[*6]

[Superheavy elements, ^{261,262}Rf, GARIS, excitation function]

^{261}Rf (^{261}Rf^{a}; $T_{1/2}$ = 68 s) has been used in chemical studies of Rf. In recent years, it was reported that there exists a spontaneously fissioning (SF) isomer (^{261}Rf^{b}; $T_{1/2}$ = 1.9 s) in ^{261}Rf.[1,2] On the other hand, a SF isomer with the similar half-life of 2.1 s was also reported for ^{262}Rf ($T_{1/2}$ = 47 ms).[3,4] It is possible that these two SF isomers are the same nuclide and one of these isomers is incorrectly assigned. To clarify this ambiguity, we measured the excitation functions of Rf isotopes in the ^{248}Cm + ^{18}O reaction.[5]

A ^{248}Cm$_2$O$_3$ target with a thickness of 230 μg/cm^2 was preparerd by electrodeposition onto a Ti backing foil with a thickness of 0.91 mg/cm^2. Rf isotopes were produced by bombarding the Cm target with an ^{18}O beam supplied from RIKEN Linear Accelerator (RILAC). The beam energies were 88.2, 90.2, 94.8, and 101.3 MeV at the center of the target. The typical beam intensity was 6 pμA. GARIS was used to separate the evaporation residues (ERs) in-flight from the incident particles and majority of by-products. ERs were implanted into a position-sensitive Si strip detector mounted at the focal plane of GARIS. The beam ON/OFF method was applied to measure the decay events of Rf isotopes under low background conditions. At each beam energy, beam ON/OFF periods were set to 6 s/6 s and 0.1 s/0.1 s.

The characteristic α-lines of ^{261}Rf^{a} and its daughter nuclide ^{257}No were clearly observed. By normalizing the cross section of ^{261}Rf^{a} as 13 nb[6] at a beam energy of 94.8 MeV, the excitation function of ^{261}Rf^{a} was obtained as shown in Fig 1 (a). This excitation function of ^{261}Rf^{a} is in agreement with the previously reported one.[6]

At 94.8 MeV, the decay component of SF events was observed in 6 s/6 s measurement. The obtained half-life was 4.2 ± 1.2 s. On the other hand, short-lived decay was not observed in 0.1 s/0.1 s measurement. The number of observed SF events in 0.1 s/0.1 s measurement were well explained by 4.2-s SF and the long-lived background of ^{256}Fm. The excitation function of 4.2-s SF nuclide is shown in Fig. 1 (b). This excitation function exhibited the maximum cross section at 94.8 MeV, and the shape of the excitation function is almost the same as that of ^{261}Rf^{a}. This result indicates that the 4.2-s SF nuclide is ^{261}Rf^{b}.

Short-lived SF decay components were observed at 88.2 MeV and 101.3 MeV in 0.1 s/0.1 s measurement. The half-lives were 23.5 ± 14.0 ms and 11.3 ± 7.3 ms for 88.2 MeV and 101.3 MeV, respectively. Since short-lived SF decay components were not observed at 94.8 MeV, these SF decay components was considered to originate from different nuclides. Judging from the observed beam energies and half-lives, we assigned these nuclides observed at 88.2 MeV and 101.3 MeV to ^{262}Rf and ^{260}Rf, respectively. The excitation functions of ^{262}Rf and ^{260}Rf are shown in Fig 1 (c) and (d), respectively. The excitation function of 4.2-s SF nuclide is clearly different from those of ^{262}Rf and ^{260}Rf. We concluded that the few-seconds SF nuclide previously assigned to ^{261}Rf^{b} and ^{262}Rf is not ^{262}Rf but ^{261}Rf^{b}.

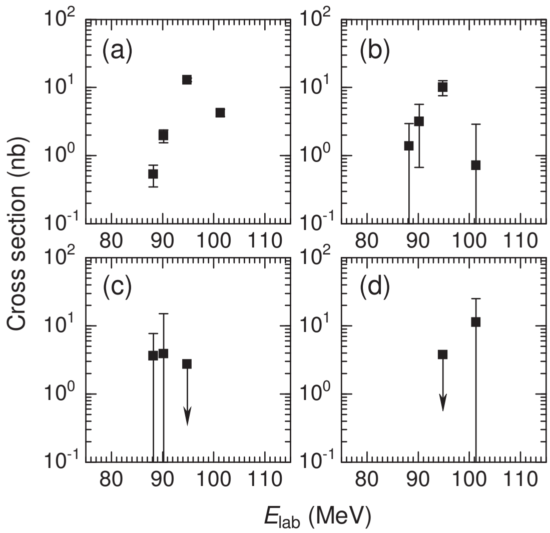

Fig. 1. Excitation functions of (a) ^{261}Rf^{a}, (b) 4.2-s spontaneously fissioning nuclide, (c) ^{262}Rf, and (d) ^{260}Rf.

References
1) S. Hofmann et al.: Eur. Phys. J. A **14**, 147 (2002).
2) H. Haba et al.: Phys. Rev. C **83**, 034602 (2011).
3) L. P. Somerville et al.: Phys. Rev. C **31**, 1801 (1985).
4) M. R. Lane et al.: Phys. Rev. C **53**, 2893 (1996).
5) S. Goto et al.: RIKEN Accel. Prog. Rep. **44**, 261 (2011).
6) Y. Nagame et al.: J. Nucl. Radiochem. Sci. **3**, 85 (2002).

*1 Graduate School of Science and Technology, Niigata University
*2 Center for Instrumental Analysis, Niigata University
*3 Research Center for Electron Photon Science, Tohoku University
*4 Graduate School of Science, Osaka University
*5 Advanced Science Research Center, JAEA
*6 Faculty of Science, Niigata University

Production and quality estimation of ^{109}Cd for fee-based distribution

J. Kanaya, H. Haba, Y. Wakitani,* S. Yamamoto,* A. Ohtsubo,* and K. Takahashi

Cadmium-109, with a half-life of $T_{1/2}$ = 462.6 d, decays by electron capture to ^{109m}Ag ($T_{1/2}$ = 39.6 s), which decays to stable ^{109}Ag by the emission of an 88.0-keV γ-ray. Thus, ^{109}Cd has been used as a calibration source in X-ray and/or γ-ray detectors and as a radiotracers in environmental studies of Cd contamination.[1,2] This radioisotope can be also employed in nuclear medicine as a ^{109}Cd/^{109m}Ag generator.[3,4] Since October 2007, we have distributed purified ^{109}Cd solutions to the general public in collaboration with the Japan Radioisotope Association.[5] In this paper, we describe our production method and the quality estimation of ^{109}Cd by using a recently conducted typical experiment as an example.

Cadmium-109 was produced by irradiating a silver plate in a natural isotopic abundance (chemical purity: >99.99%; thickness: 263 mg cm^{-2}) *via* the ^{109}Ag(*p,n*)^{109}Cd reaction using a 13.7-MeV proton beam from the RIKEN AVF Cyclotron. The irradiation time was 45.6 h, and the average beam intensity was 11.6 µA. During the irradiation, the target was continuously cooled by circulating helium gas and water. After the irradiation, ^{109}Cd was chemically separated from the Ag target according to the procedure shown in Fig. 1. The Ag plate was first dissolved with 10 mL of concentrated nitric acid and several drops of hydrogen peroxide solution. The solution was evaporated to dryness, and the residue was dissolved with 200 mL of H_2O.

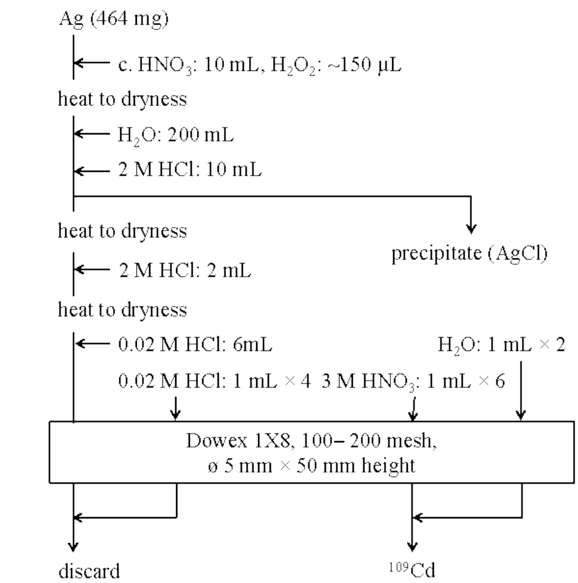

Fig. 1. Chemical separation procedure of ^{109}Cd from the Ag target.

Ten mL of 2 M HCl was added dropwise to the solution to precipitate AgCl. A major portion of the target material was eliminated by filtration, and the filtrate was evaporated to dryness. The residue was dissolved with 2 M HCl and evaporated to dryness again. Then, it was dissolved with 0.02 M HCl and loaded onto the anion-exchange column (ø5 mm × 50-mm height) packed with an anion-exchange resin (Dowex 1X8, 100–200 mesh, Cl$^-$ form). The column was then washed with 0.02 M HCl by referring to the procedures in Refs.,[6,7] where ^{109}Cd was adsorbed on the resin and unwanted byproducts such as ^{57}Co and ^{65}Zn were eluted. Finally, ^{109}Cd was eluted with 3 M HNO_3 and H_2O. The radioactivities of ^{109}Cd at each step were measured by γ-ray spectrometry using a Ge detector. The chemical impurity in the final solution was estimated by ICP-MS for a control sample that had been treated with the same chemical procedure as the irradiated target and was adjusted to 3 mL of 0.1 M HNO_3 for the ICP-MS measurement.

The γ-ray spectrum of the purified ^{109}Cd is shown in Fig. 2. In this work, 40 MBq of ^{109}Cd was produced at the end of the bombardment. The production yield of ^{109}Cd was 76 kBq µA^{-1}h^{-1} under the present experimental condition. The chemical yield was 80%. The chemical impurities were below 1 ppm for all detectable elements other than Na (3.0 ppm). A separation factor of 5×10^6 was achieved for the Ag target material. The specific activity of ^{109}Cd was 91 MBq µg^{-1}.

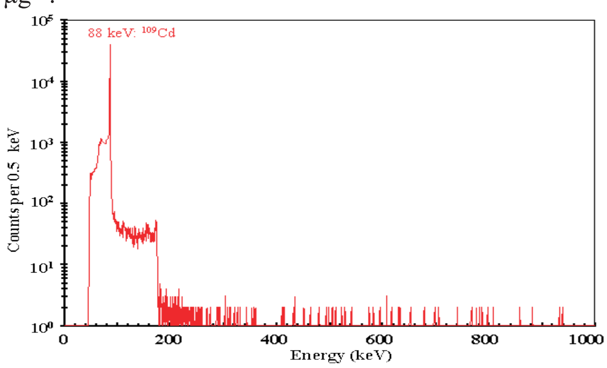

Fig. 2. γ-ray spectrum of the purified ^{109}Cd for fee-based distribution.

References

1) L. Landini and J. A. Osso Jr.: J. Radioanal. Nucl. Chem. **250**, 429 (2001).
2) L. Goetz et al.: Radiochem. Radioanal. Lett. **45**, 51 (1980).
3) M. Fassbender et al.: Radiochim. Acta **92**, 237 (2004).
4) M. S. Mansur et al.: J. Radioanal. Nucl. Chem. **201**, 205 (1995).
5) T. Kambara et al.: RIKEN Accel. Prog. Rep. **42**, 295 (2008).
6) M. Sadeghi et al.: J. Radioanal. Nucl. Chem. **281,** 619 (2009).
7) M. Sadeghi et al.: Radiochim. Acta **97**, 113 (2009).

* Japan Radioisotope Association

Automated rapid α/SF detection system for studying aqueous chemistry of superheavy elements at RIKEN

H. Haba, Y. Kasamatsu,[*1] H. Kikunaga,[*2] A. Yoneda, J. Kanaya, and K. Morita

The extremely low production yields and short half-lives of superheavy element (SHE, atomic numbers $Z \geq 104$) nuclei force us to perform rapid, efficient, and repetitive experiments with single atoms. The ion-exchange behavior of element 104, $^{261}Rf^{a}$ ($T_{1/2}$ = 68 s), has successfully been studied at the Japan Atomic Energy Agency in HNO_3, HCl, HF, and HF/HNO_3 by using the Automated Ion-exchange separation apparatus coupled with the Detection system for Alpha spectroscopy (AIDA).[1–3] The AIDA has enabled us to perform thousands of cyclic discontinuous chromatographic separations of short-lived $^{261}Rf^{a}$ in aqueous solutions and the automated detection of α-particles within a typical cycle of 2 min. At RIKEN, we plan to start the study of the aqueous chemistry of SHEs such as $^{261}Rf^{a}$, ^{262}Db (element 105, $T_{1/2}$ = 34 s), and $^{265}Sg^{b}$ (element 106, $T_{1/2}$ = 14.4 s) using the RIKEN AVF Cyclotron. In this work, we have developed an automated α/spontaneous fission (SF) detection system that can be coupled to various aqueous chemistry apparatuses.

Figure 1 shows a top view of the automated α/SF detection system. Figure 2 shows a bird's-eye view. This system consists of a storage column of tantalum dishes for holding sample solutions, a round table for sixteen Ta dishes, i.e., a sample collection port, and sixteen detector chambers for the detection of α-particles and/or SF fragments. Beside the round table, we set up the appropriate aqueous chemistry apparatus. A Selective Compliance Assembly Robot Arm (SCARA) robot (Yamaha YK500XG) picks up a Ta dish from the storage column through suction and positions it on the round table. The table is rotated to position the dish at the desired port for sample collection, and the solution, typically ~200 μL for each dish, is rapidly dried by using hot helium gas and a halogen heat lamp. After drying, the robot transfers the sample dish to the detector chamber, which is equipped with a Si PIN photodiode detector (Hamamatsu S3204-09) and a preamplifier (Hamamatsu H4083). The detector chamber is closed promptly and evacuated, and a voltage of –50 V is applied to the detector from a complex module comprising a power source and a gate generator (Vacuum Products GG-10001). The whole system is controlled by a programmable logic controller (Keyence KV-3000), and each action is triggered by relay contact signals from a separate controller used for the chemistry apparatus. The time required to start the measurement after drying the sample is about 5 s. Each Si PIN photodiode has a counting efficiency of 36%. The α-energy resolution is about 50 keV full width at half-maximum (FWHM) at 5.486 MeV. Event signals are amplified with a 16-channel spectroscopy amplifier (Clear-Pulse 4066) and recorded in an event-by-event mode using a 16-channel PHA & LIST VME module (Niki Glass A3100).

The present system will be coupled to various chemistry apparatuses such as the ion-exchange unit of the AIDA (JAEA-ARCA),[1)] a solvent extraction apparatus with a micro-chemical chip,[4)] and an apparatus used for the rapid preparation of precipitate samples.[5)]

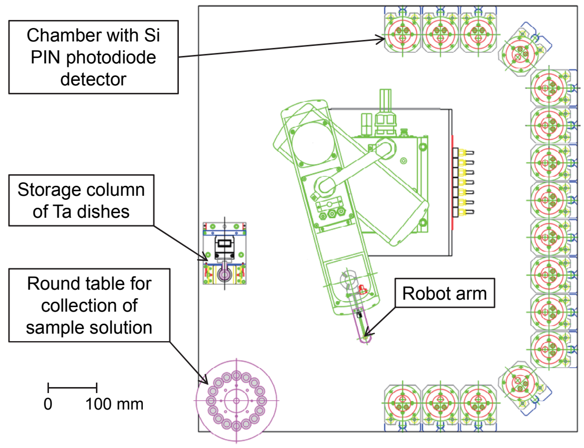

Fig. 1. Top view of the automated rapid α/SF detection system for studying aqueous chemistry of SHEs.

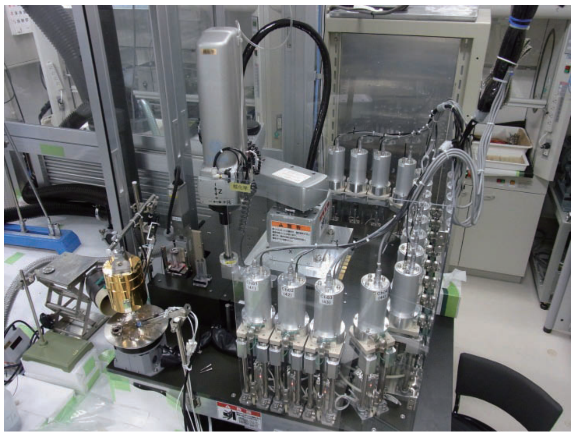

Fig. 2. Bird's-eye view of the automated rapid α/SF detection system.

References
1) Y. Nagame et al.: Radiochim. Acta **93**, 519 (2005).
2) A. Toyoshima et al.: Radiochim. Acta **96**, 125 (2008).
3) Y. Ishii et al.: Bull. Chem. Soc. Jpn. **84**, 903 (2011).
4) K. Ooe et al.: J. Nucl. Radiochem. Sci. **8**, 59 (2004).
5) Y. Kasamatsu et al.: The 92nd Annual Meeting of the Chemical Society of Japan, Yokohama, March 26, 2012.

*1 Graduate School of Science, Osaka University
*2 Research Center for Electron Photon Science, Tohoku University

4. Radiation Chemistry and Biology

Diffusion suppression in gel dosimetry by addition of nanoclay

T. Maeyama, N. Fukunishi, K. L. Ishikawa,[*1,*2,*3] K. Fukasaku,[*1,*4] T. Furuta,[*1] S. Takagi,[*1*5] S. Noda,[*6] and R. Himeno[*1,*6]

To advance heavy-ion cancer therapy, it is essential to precisely predict the dose distribution in a patient's body during treatment planning. Introducing the Monte Carlo (MC) simulation technique into treatment planning is expected to be fruitful because it is a more precise method than currently used deterministic codes, such as the ones based on the pencil beam method.[1)] We have hence started developing a MC simulation system dedicated to heavy-ion cancer therapy based on the particle transport code PHITS.[2)] Strict validation tests of the dose distribution calculated from PHITS are also required before MC simulation is put to clinical use. We have also performed validation tests of dose distribution of a carbon beam calculated from PHITS by using three-dimensional (3D) gel dosimeters, and here we report improvements related to the gel dosimeters.

Gel dosimeters, including radiation sensitive chemicals, are nearly tissue-equivalent and are capable of 3D dose imaging using MRI because radiation-induced chemical products shift the relaxation time of protons in gels. Two kinds of gel dosimeters have been widely used. Fricke Xylenol Gel (FXG) utilizes radiation-induced oxidation of Fe^{2+} ion to Fe^{3+}. The color of FXG, xylenol orange (XO), also changes with increasing Fe^{3+}. However, this gel has a poor spatial resolution due to the diffusion of Fe^{3+}. Polymer gels, based on radiation-induced polymerization, require careful treatment because the polymerization process is inhibited by oxygen.[3)] The accuracy of gel dosimeters depends on these factors. We have started improving FXG and developing a dichromate gel (DCG) in the form of nanocomposite gels (NC gels) that include inorganic clay, the effectiveness of which was recently reported in the field of soft matter science. Nanoclay is expected to suppress diffusion by absorbing chemical compounds.[4)]

The nanoclay used here is a synthetic hectorite named Laponite XLG (Rockwood). Details of the chemical compositions of gel dosimeters are summarized in Table 1. Irradiations were done with 250-keV X-rays (3.4 Gy/min) or $^{12}C^{6+}$ 135-MeV/nucleon accelerated by the RIKEN Ring Cyclotron (RRC). Measurement of the relaxation rates ($R_1 = 1/T_1$) were done using a 1.5-T MRI (Philips).

Table 1 Chemical composition.

	Composition	Agar	Laponite
FXG	1 mM $FeSO_4$, 50 mM H_2SO_4, 0.1 mM XO	2%	0.5–1.5%
DCG	1mM $K_2Cr_2O_7$, 25 mM $HClO_4$	2%	1%

*1 RIKEN Computational Science Research Program
*2 Dept. of Nucl. Eng. & Management, Grad. Sch. Eng., Univ. of Tokyo
*3 Photon Science Center, Grad. Sch. Eng., Univ. of Tokyo
*4 Dept. of neurosurgery, Himon'ya Hosapital
*5 Dept. of Mech. Eng., Sch. Eng., Univ. of Tokyo
*6 RIKEN Advanced Center for Computing and Communication

Spatial dose distributions were estimated from the R_1 maps. Diffusion coefficients of FXG were measured using a CCD.

FXG with 1.5% nanoclay exhibited one-fourth the diffusion coefficient of FXG without clay. The present additive amount of nanoclay affords almost the maximum possible because nanoclay induces auto oxidation of FXG. Complete suppression of diffusion was observed in the case of DCG with 1% nanoclay. Moreover, the DCG showed excellent properties such as good chemical stability and no oxygen inhibition. Increases in R_1 with increasing dose were observed for DCG with both X-ray and carbon beam irradiation in the dose range of 0.3–1 kGy. An example of an R_1 map obtained for DCG is shown in the upper panel of Fig. 1. The DCG was irradiated uniformly with $^{12}C^{6+}$ 135-MeV/nucleon at a dose rate of about 40 Gy/min, and the total dose was 1 kGy at the entrance surface. The lower panel shows the increase R_1, which is basically proportional to the dose, as a function of the penetration depth. DCG exhibited chemically stable characteristics for 5 days after heavy ion irradiation. We found that these NC gels do not suffer from the disadvantages of conventional gel dosimeters such as poor spatial resolution caused by diffusion and oxygen inhibition. In addition, DCG has a desirable property as a dosimeter in that the dose response of DCG exhibits a weaker LET dependence than other gel dosimeters such as FXG and polymer gels. The present method utilizing nanoclay can also be applied to various liquid chemical dosimeters. One possibility is to apply NC gels to highly sensitive liquid dosimeters such as coumarin chemical dosimeter.[5)]

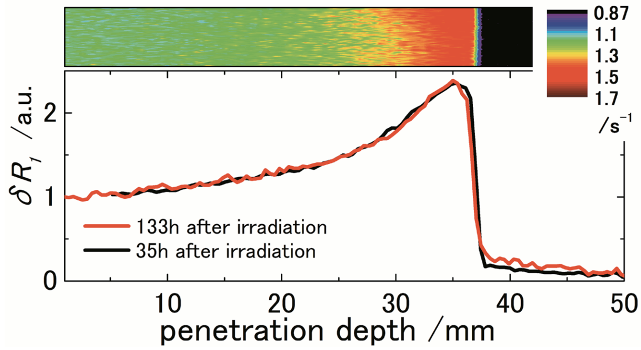

Fig. 1. R_1 distribution of DCG after irradiation with $^{12}C^{6+}$ 135-MeV/nucleon accelerated by RRC.

References

1) B. Shaffner et al.: Phys. Med. Biol. **44,** 27 (1999).
2) K. Niita et al.: JAEA-Data/Code 2010-022 (2010).
3) C. Baldock et al.: Phys. Med. Biol. **55,** R1 (2010).
4) Q. Wang et al.: Nature **463,** 339 (2010).
5) T. Maeyama et al.: Radiat. Phys. Chem. **80,** 535 (2011).

Effects of trichostatin A on radiosensitivity to heavy ions are dependent on the irradiation dose in human cancer cells

M. Izumi, T. Tsukada, and T. Abe

Histone deacetylase inhibitors are promising antitumor drugs that act through reactivation of silenced tumor suppressor genes. Several histone deacetylase inhibitors are currently undergoing clinical trials for hematological cancer as well as solid tumors[1]. In addition to intrinsic anticancer activity, histone deacetylase inhibitors are additive to or synergistic with radiotherapy,[2)3)] although the mechanism by which histone deacetylase inhibitors enhance radiation sensitivity in human cells remains unknown. To investigate the roles of chromatin structure in DNA repair after heavy-ion irradiation and to examine the possibility of chemotherapy with histone deacetylase inhibitors in combination with the radiotherapy, we have been focusing on the damage response after cells are treated with a potent histone deacetylase inhibitor, trichostatin A (TSA).

In the previous report, we observed that TSA enhanced the sensitivity of human HeLa cells to x-rays as well as carbon ions[4]. However, TSA exhibited different effects on sensitivity to x-rays and carbon ions. The treatment with TSA resulted in an increase in radiosensitivity to x-rays up to 5 Gy. In contrast, TSA enhanced radiosensitivity to carbon ions at doses lower than 3 Gy, whereas the cells showed almost the same sensitivity at 5 Gy. Therefore, in this study, we tried to irradiate cells with a higher dose of various heavy ions as well as x-rays.

HeLa cells were trypsinized and plated as single cells in TSA-free media. After allowing 24 h for attachment, the cells were pre-treated with TSA (0.1 μM) for 10 h and irradiated with x-rays, carbon ions at 80 keV/μm, or argon ions at 300 keV/μm. Then, the cells were cultured for additional 14 h in the presence of TSA, and the radiosensitivity was estimated by the colony-forming efficiency 14 days later. First, we irradiated the cells with x-rays up to 10 Gy after TSA treatment to investigate if the enhancement of radiosensitivity was only observed at a lower dose (Fig. 1). The treatment with TSA enhanced the sensitivity to x-rays up to 10 Gy, which was equivalent to 5 Gy of carbon-ion or 3 Gy of argon-ion irradiation in the survival rate. Therefore, the effect of TSA seemed to be dependent on the radiation quality, and not on the survival rate.

Next we examined the radiosensitivity to carbon ions up to 7 Gy to examine if TSA enhanced the radiosensitivity at doses higher than 5 Gy. We also examined the radiosensitivity to argon ions to investigate if TSA showed the same effect as that observed after carbon–ion irradiation. The treatment with TSA enhanced radiosensitivity to carbon ions at doses lower than 3 Gy. However, TSA enhanced resistance to carbon ions at doses higher than 7 Gy. The effect of TSA on the sensitivity to argon ions was similar to that on the sensitivity to carbon ions. TSA enhanced radiosensitivity to argon ions at doses lower than 2 Gy, whereas TSA enhanced resistance to argon ions at doses higher than 4 Gy. Therefore, the enhancement of sensitivity was not observed at higher doses of heavy-ion irradiation. In addition, the survival rate did not change at doses higher than 3 Gy of carbon ions or 2 Gy of argon ions.

On the basis of these results, we speculate that the DNA damage response induced by heavy ions depends on the irradiation dose. Currently, we are investigating whether TSA affects on the behavior of repair proteins and checkpoint proteins after heavy-ion irradiation at different doses. We also plan to examine the effects of TSA on the radiosensitivity of genetically modified cell lines that have defects in the DNA repair pathway.

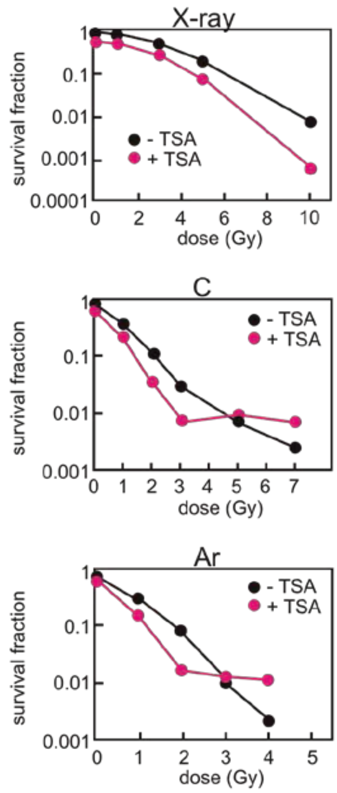

Fig. 1 The effects of trichostatin A (TSA) on HeLa cell radiosensitivity. The black and red circles indicate survival in the absence and presence of TSA, respectively.

References

1) R. L. Piekarz et al: Blood **103,** 4636 (2004).
2) Y. Zhang, et al: Radiat. Res. **161,** 667 (2004).
3) K. Camphausen et al: Clin. Cancer Res. **10,** 6066 (2004).
4) M. Izumi: RIKEN Accel. Prog. Rep. **44,** 264 (2011)

Cell-killing effect of low dose of high-LET heavy ions (IV)

M. Tomita,[*1] T. Tsukada, and M. Izumi

The heterogeneity of the absorbed dose within the targeted tissues is more relevant with high-LET particle radiation than with low-LET photons. In space, astronauts are exposed to low fluencies of high-LET radiation. In addition, normal cells surrounding a tumor are also exposed to heavy ions in heavy-ion cancer therapy. Over the past two decades, non-DNA-targeted effects, which are not a direct consequence of radiation-induced initial lesions produced in cellular DNA, have been evaluated and are defining a new paradigm in radiation biology. These effects include low-dose hyper-radiosensitivity (HRS), radiation-induced bystander response, and so on.[1)] Radiation-induced bystander response is defined as a response in cells that have not been directly targeted by radiation, but are in the neighborhood of cells that have been directly exposed.[1,2)] Therefore, the bystander response induced by low doses of high-LET radiation is an important problem in radiation biology. In this study, we aim to clarify the molecular mechanisms and biological implications of bystander responses induced by low doses of high-LET radiation. Previously, we had reported that normal human fibroblasts that were irradiated with low doses of high-LET iron (Fe) ions induced HRS, suggesting that bystander cell killing was induced.[3,4)] In addition, nitric oxide (NO) was found to be involved in this process.[4)] Here, we report that high-LET argon (Ar) ions also induced HRS in the low-dose region.

Figure 1 shows the clonogenic survival curve of normal human lung embryonic fibroblast WI-38 cells irradiated with 95 MeV/u Ar ions at 310 keV/μm. Cells were plated in a 25-cm^2 cell-culture flask for one week in order to form confluent monolayers. The surviving fraction was determined by a colony forming assay. The relationship between the surviving fraction and irradiated dose was linear at doses higher than 0.2 Gy (Fig. 1A), and the dose resulting in 10% cell survival (D_{10}) was 1.4 Gy. The cell killing efficiency per unit dose of Ar ions was higher than that of Fe ions (D_{10} = 3.3 Gy). As shown in Fig. 1B, HRS could be observed in the cells irradiated with Ar ions, as was the case for Fe ions,[3,4)] at doses lower than 0.1 Gy. Carboxy-PTIO (c-PTIO), which is a scavenger of NO, was added to the culture medium. The surviving fractions of the cells that were pretreated with c-PTIO at doses of over 0.2 Gy were not significantly different from those of the cells that were not pretreated with c-PTIO (Fig. 1A). The decrease in cell survival at low doses was partly suppressed by pretreatment with c-PTIO (Fig. 1B). These results suggest that NO-mediated bystander response is also involved in the process of HRS induced by low doses of Ar ions.

For a bystander response to occur, at least two signaling pathways should be functional: one pathway is through the direct physical interaction between cells, such as in the case of gap-junction intercellular communication (GJIC), and the other is through the interaction between the cells and the culture medium.[4)] The incomplete suppression of the HRS by c-PTIO indicates that other molecules are involved in bystander signaling. We are examining the role of GJIC and reactive oxygen species in the HRS induced by high-LET radiations.

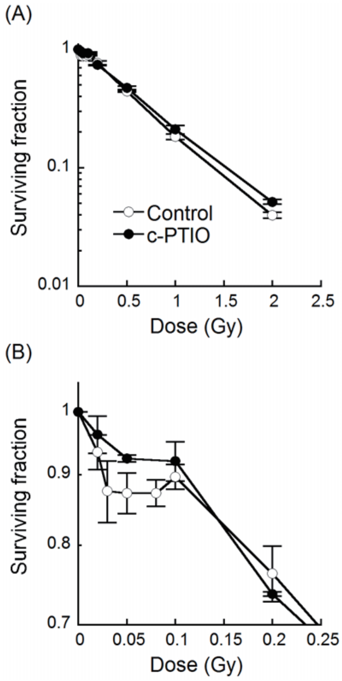

Fig. 1. Cell-survival curves of WI-38 cells. Confluent monolayers of WI-38 cells were irradiated with 95 MeV/u Ar ions (310 keV/μm) and some of them were pretreated with c-PTIO with 20 μM. Panel A shows all data obtained in this study. Panel B shows surviving fractions at doses under 0.25 Gy. The error bars of the *SFs* represent the standard errors of the means.

References
1) K. M. Prise et al.: Radiat. Prot. Dosimetry **99**, 223 (2002).
2) H. Matsumoto et al.: Curr. Mol. Pharmacol **4**, 126 (2011).
3) M. Tomita et al.: RIKEN Accel. Prog. Rep. **42**, 276 (2009).
4) M. Tomita et al.: RIKEN Accel. Prog. Rep. **43**, 276 (2010).

*1 Central Research Institute of Electric Power Industry

Identification of V-ATPase-independent candidate pathways that control cell expansion in *Arabidopsis*

K. Hanai,*[1] Y. Kazama, T. Hirano,*[2] T. Abe, and A. Ferjani*[1]

Plant cells expand to a huge size, and in extreme cases, they expand to a size that is several hundred-fold larger than their original size during proliferative growth. Turgor pressure exerted by the vacuole against the cell wall is also required for cellular expansion. While the cell wall hinders cell expansion, coordinated cell-wall loosening associated with synthesis *de novo* and trafficking of cell-wall components is a prerequisite for proper organogenesis.

Recent studies have highlighted several pathways that affect cell expansion in developing leaves, either directly or indirectly. For example, compensated cell expansion (CCE), triggered by decrease in leaf-cell number, has been reported to occur in aerial lateral organs such as cotyledons and leaves.[1,2] Furthermore, endoreduplication is now widely recognized to affect cell size in a positive manner. Nevertheless, recent efforts by using developmental genetic tools have identified several mutants that do not necessarily obey the above mentioned rules. For example, some *extra small sisters* (*xs*) mutants with specific defects in cell expansion can inhibit CCE in a particular compensation-exhibiting mutant background, but not in others.[3] Interestingly, the endopolyploidy levels in these *xs* mutants were either decreased, unaffected, or increased, in comparison with those in the wild-type (WT), suggesting that CCE could be mediated, at least in part, by ploidy-independent mechanisms. Therefore, these findings indicate the complex network underlying the regulation of cell expansion.

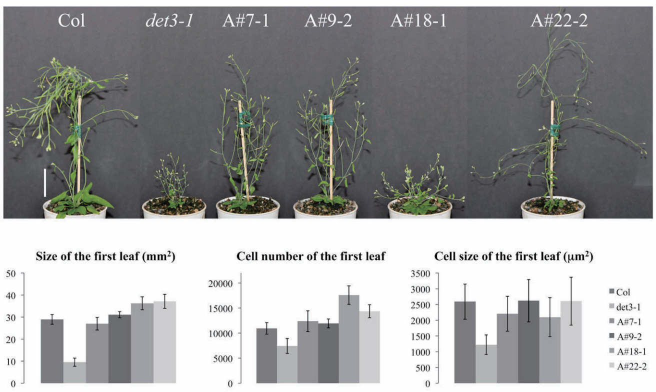

Fig. 1. Gross morphology at 41 DAS (top panels) and cellular phenotypes (bottom panels) at 25 DAS of the newly isolated mutants. The overall plant size of the mutants increased to a greater extent than that of the *det3-1* mutant. In addition, the area, cell number, and cell size of the first leaf have either totally or significantly recovered in the 4 representative mutant lines. Scale bar indicates 3 cm. DAS, days after sowing.

V-ATPase is a multimeric complex composed of 28 subunits. Interestingly, the partial dysfunction of V-ATPase in *de-etiolated3* mutant (*det3-1*; with a defect in the V-ATPase C subunit) causes defects in cell elongation, resulting in severe plant dwarfism (Fig. 1).[4]

In normal cell expansion, V-ATPase plays an important role in the trans-golgi network (TGN), which functions in the trafficking of proteins involved in the biosynthesis of cell-wall components, such as cellulose.[5] Here, to unravel the contribution of V-ATPase to cellular expansion, we mutagenized *det3-1* seeds by using a $^{12}C^{6+}$ heavy-ion beam (linear energy transfer, 30 keV/μm; 400 Gy) and screened mutants that show significant recovery in their final leaf-cell size.

Large-scale screening of mutants with enhanced cell expansion was performed for 4280 M_1 seeds, and this allowed the collection of 135 pools (where M_2 seeds from 11 M_1 plants were gathered in each pool). Among them, 110 M_2 seeds from each pool (total, 68 pools) were sown, and 56 lines of interest in the M_2 population were collected. Further evaluation of the mutant line phenotype in the M_3 generation yielded 48 lines, among which 32 lines were analyzed in detail. Finally, an additional screening, in which total plant height and main stem-node length were measured, allowed the identification of 14 lines of interest. These lines were subjected to a histological analysis in which first leaf area, cell number, and cell size were determined (Fig. 1). We isolated several lines in which cell expansion had shown significant (A#7-1 and A#18-1) or total recovery (A#9-2 and A#22-2). Interestingly, while most lines exhibited a "BIG *det3-1*" phenotype, the A#22-2 plants were rather similar to WT (Fig. 1). An allelism test will be conducted soon to evaluate whether these mutations occurred in independent loci. Together, our results strongly suggest that cell expansion can recover to WT levels, even in the absence of a fully active V-ATPase complex. Cloning of the genes mutated in the lines mentioned above would shed light on a yet unknown genetic pathway that functions independently of V-ATPase to regulate cell expansion. In our future study, mutants such as A#9-2 and A#22-2 will be given the highest priority, provided they have a strong potential to enhance cell expansion in *det3-1* mutant.

References
1) A. Ferjani et al.: Plant Physiol. 144, 988-999 (2007).
2) A. Ferjani et al.: Plant Cell 23, 2895-2908 (2011).
3) U. Fujikura et al.: Plant Cell Physiol. 48, 278-286 (2007).
4) Y. Fukao et al.: Plant Signaling & Behavior 6, 1-3 (2011).
5) A. Brüx et al.: Plant Cell 20, 1088-1100 (2008).

*1 Department of Biology, Tokyo Gakugei University
*2 RIKEN, Innovation Center

Characterization of DNAs mutated by C-ion beam with highly efficient LET in mutagenesis of *Arabidopsis thaliana*†

Y. Kazama, T. Hirano, H. Saito, Y. Liu, S. Ohbu, Y. Hayashi and T. Abe

Heavy-ion beams show high linear energy transfer (LET) and thus more effectively induce DNA double-strand breaks than other mutagenic techniques. Previously, we determined the most effective heavy-ion LET (LETmax: 30.0 keV μm^{-1}) for *Arabidopsis* mutagenesis by analyzing the effect of LET on mutation induction.[1] The mutation rates obtained by C-ion irradiation with LETmax were two to three times those obtained by C-ion irradiation with other LET. Because mutagens such as EMS, γ-rays, and heavy-ion beams should be chosen appropriately depending on the experimental purpose, it is important to know the nature of mutations induced by C ions with LETmax. However, the molecular structure of DNA mutated by heavy ions with LETmax remains unclear. Knowledge of the structure of mutated DNA will contribute not only to the effective exploitation of heavy-ion beam mutagenesis but also to the selection of a suitable detection system for induced DNA mutations.

To characterize the structure of DNA mutated by C-ion beam with LETmax, we screened the well-characterized mutants elongated *hypocotyls* (*hy*) and *glabrous* (*gl*) from the M_2 generation after C-ion irradiation with 30.0 keV μm^{-1} at a dose of 400 Gy. Mutants were also screened from the M_2 generation after irradiation with LET of 22.5 keV μm^{-1} at a dose of 250 Gy and at a dose of 450 Gy. Genomic DNA was purified from the isolated mutant and wild-type plants four weeks after germination. The purified DNAs were subjected to high-resolution melting curve (HRM) analysis using primers specific to the putative mutated genes (*HY1*, *HY2*, *HY3*, and *HY4* for the *hy* mutants; *GL1*, *GL2*, and *TTG1* for the *gl* mutants). When a positive signal was identified, the amplified fragment was sequenced with the same primers as those used for HRM analysis. When the whole or a part of the coding region could not be amplified, flanking sequence analysis using TAIL-PCR was performed to determine the structures of the mutated DNAs. Because the number of identified mutant lines was limited, the following mutants were also included in the characterization of the DNA mutations: *altered meristem program* (*amp*) *1*,[2] *pinoid* (*pid*) *1*,[3] and *yellow variegated* (*var*) *2*.[4]

In total, 22 mutations were identified. Mutations of 17 of the 18 independent *hy* and *gl* mutant lines were determined successfully. In addition, two mutations in the *AMP1* gene, two mutations in the *PID1* gene, and one mutation in the *VAR2* gene were identified. The size and type of mutations induced by 22.5 keV μm^{-1} and 30.0 keV μm^{-1} LET did not show a marked difference (Table 1). The C-ion-induced mutations consisted of base substitutions, deletions, reciprocal translocations, and a complex rearrangement. Of the 22 alleles, four showed large rearrangements, including translocations and a large deletion; these were detected in high-dose irradiated mutants (400 Gy and 450 Gy). Fourteen mutants had deletions less than 100 bp and four mutants had base substitutions. Of the four alleles with a base substitution, three had transversions and had was a transition. Among the four alleles, only one allele (C-27-gl1) had a missense mutation (D→N), whereas the other alleles had nonsense mutations that resulted in the production of C-terminally truncated proteins. In total, 21 alleles were null mutants. Whether the C-27-gl1 allele was a null mutation was not elucidated, although the phenotype of the C-27-gl1 mutant was similar to that of a null mutant of *GL1* (data not shown). These results indicated that C ions with LETs of 22.5 or 30.0 keV μm^{-1} mainly caused small DNA alterations and that most of the induced mutants were null mutants. These small DNA alterations can be detected by detection systems for single nucleotide polymorphism (SNP), such as HRM analysis. It is concluded that C ions with an LET of 30.0 keV μm^{-1} might be suitable as a powerful reverse-genetics technology in conjunction with an SNP detection system to produce null mutants.

References
1) Y. Kazama: Plant Biotech. 25, 115 (2008).
2) C.A. Helliwell: Plant Cell 13, 2115 (2001)
3) S.K. Christensen: Cell 100, 469 (2000)
4) K. Takechi: Plant Cell Physiol. 41:1334 (2000)

Table 1. Mutations detected in this study

LET (keV/μm)	Dose	Type of mutation			
		BS	Del (<10 bp)	Del (10–100 bp)	Others
22.5	250	2	3	1	-
22.5	450	1	2	1	Del (32,355 bp), RTL
30.0	400	1	6	1	CR, RTL

BS: Base substitution, Del: Deletion, RTL: Reciprocal translocation, CR: Complex rearrangement

† Condensed from an article in BMC Plant Biology. **11**, 161 (2011)

A novel method of utilizing heavy-ion beams for efficient induction of large deletions in *Arabidopsis thaliana*

T. Hirano, Y. Kazama, S. Ohbu, Y. Shirakawa, Y. Liu, T. Kambara, N. Fukunishi, and T. Abe

Linear energy transfer (LET) is an important parameter to be considered in heavy-ion mutagenesis of plants. Detailed analyses of the molecular nature of DNA alterations have been reported as an LET-dependant effect for induced mutation. When dry seeds of *Arabidopsis thaliana* were irradiated with C-ions irradiation at 101–124 keV/μm, large deletions and/or rearrangements, including insertions, inversions, and translocations, were detected in the germline mutations.[1] Since these results are different from the mutation spectra obtained after C-ion irradiation at 22.5 keV/μm and 30.0 keV/μm[2], it is predicted that the nature of DNA alterations changes with the LET values. However, no quantitative data are available on the molecular nature of the mutations induced with high LET irradiation above 101–124 keV/μm. Therefore, we irradiated dry seeds of *A. thaliana* with Ar- and C-ions at 290 keV/μm and characterized the effects of the high LET irradiation on DNA alterations in plants.

Dry seeds of *A. thaliana* ecotype Columbia were placed in a plastic bag and arranged in a single layer. The seeds were then irradiated with 290 keV/μm of Ar- and C-ions irradiation at a dose of 50 Gy. Growth conditions and screening methods for *hy* and *gl* mutants were as described previously.[2] After the Ar-ion irradiation, the total number of *hy* and *gl* mutants obtained from 51,686 M_2 plants were 16 and 11, respectively. After 57,771 M_2 plants from the C-ion irradiated seeds had been screened, 14 *hy* mutants and 9 *gl* mutants were obtained. In addition to the *hy* and *gl* mutants, we also obtained the following morphological mutants: *brassinosteroid insensitive 2*, *ethylene-dependent gravitropism-deficient yellow-green 1*, and *yellow variegated 2*. The M_3 seeds of the mutants were harvested and the phenotype of the M_3 plants was analyzed to confirm whether the phenotype of the mutants was inherited.

In total, 14 and 13 mutated genes were identified in the plants derived after Ar- and C-ion irradiations, respectively. In both mutants, deletion mutations were observed most frequently (>90%). We focused on the deletion sizes of germline mutations and compared them to previously reported data. Among the deletions, the proportion of large deletions (>100 bp) was about 54% for Ar-ion irradiation and about 64% for C-ion irradiation, and the proportions after 290 keV/μm of Ar- and C-ion irradiations were larger than that observed after 22.5–30 keV/μm of C-ion irradiation (Fig. 1). Moreover, the proportion after 101–124 keV/μm of C-ion irradiation was about 27%.[1] Therefore, we concluded that the size of the deletions generated by irradiation with heavy-ion beams increased with increase in LET. In *Arabidopsis*, many genes (>10%) form tandem arrays.[3, 4] For knockout of the tandemly arrayed genes, large deletions are required, and the appropriate deletion-size is estimated to be around 5–10 kbp, according to the gene density in *Arabidopsis*.[3] Therefore, the Ar- and C-ions at 290 keV/μm will prove useful as novel mutagens for the analysis of the tandemly arrayed genes.

In the mutations identified in this study, 8 out of a total of 27 loci contained deletions with some rearrangements such as large insertions (>80 kbp), inversions, or translocations. Complex rearrangements were also observed in *A. thaliana* irradiated with C ions at 101–124 keV/μm, at almost the same frequency (8 loci/28 loci)[1], and these frequencies were higher than that at 22.5 keV/μm and 30.0 keV/μm (2 loci/14 loci).[2] This phenomenon of LET-dependent increase in complex rearrangements has also been reported in human TK6 lymphoblastoid cells.[5, 6] Taken together, it is suggested that higher LET irradiation frequently induces complex rearrangements, in addition to large deletions.

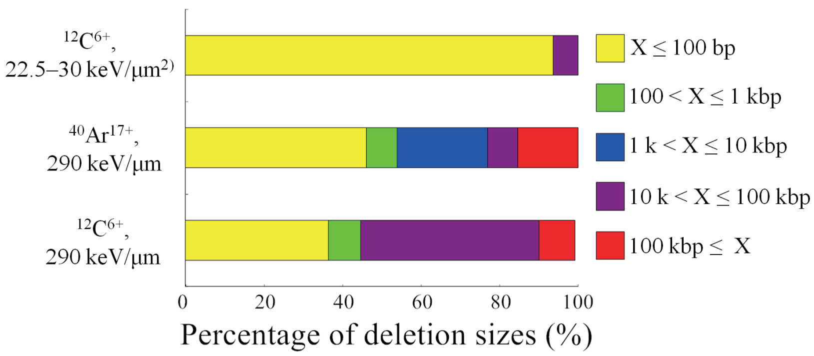

Fig. 1 Comparison of the deletion sizes induced by heavy-ion irradiation with different LETs. The deletions generated in the mutants were grouped according to size.

References

1) Shikazono et al.: J. Exp. Bot. **56**, 587 (2005).
2) Y. Kazama et al.: BMC Plant Biol. **11**, 161 (2011).
3) The Arabidopsis Genome Initiative: Nature **408**, 796 (2000).
4) Rizzon et al.: PLoS Comput. Biol. **2**, e115 (2006).
5) Kagawa et al.: Mutagenesis **14**, 199 (1999).
6) Yatagai: Biol. Sci. Space **18**, 224 (2004).

Effects of X-rays on phosphorylation of AtH2AX and DNA replication in root tips of *Arabidopsis* seedlings

K.Takagi[*1], T.Hirano, Y. Kazama, T.Tsukada, Y. Hayashi, and T. Abe

To investigate the relationship between the DNA damage sensing mechanism and the DNA replication in plant meristem, phosphorylation of histone H2AX (AtH2AX) and incorporation of the nucleotide analog ethynyl deoxyuridine (EdU) into the nucleus were examined in the root tip of *Arabidopsis* seedlings after their X-ray irradiation.

Seeds of *Arabidopsis thaliana* (ecotype Columbia) were sown on the solid medium composed of 1/2 MS, 2% sucrose, and 0.3% gellan gum. After 4 days from the sowing, the seedlings were irradiated with 80 Gy X-rays (150 kVp). They were fixed 6 hours after the irradiation. One hour before fixation, they were incubated in the medium containing 10 μM EdU. After the fixation, phosphorylated AtH2AX (γ-AtH2AX) was detected by indirect whole-mount immunofluorescence, according to the method of Sauer et al.[1)], with modifications, using a polyclonal antibody raised against γ -AtH2AX. As the nuclear marker, a monoclonal antibody raised against histone H3 dimethylated at lysine 4 (H3K4me2) was used. For detecting EdU, a Click-iT EdU cell proliferation assay kit (Molecular probes) was used. All three markers were detected simultaneously in the same samples. The signals were acquired as an optical section of 5 μm thickness by using a confocal scanning laser microscopy (Olympus FV-300). Terminology from Péret et al.[2)] was used for describing the parts of a root structure.

In the root tip of an unirradiated seedling, there was almost no detection of γ-AtH2AX signals (Fig. 1A,G). EdU incorporated nuclei were distributed throughout the root tip, especially apparent in the stele (Fig. 1B,H).

At 6 hours after 80 Gy X-ray irradiation, γ-AtH2AX signals could be detected from the root tip. Prominent γ-AtH2AX foci were observed in some cells either in the apical or basal meristem (Fig. 1D,J). Nuclei with EdU incorporation in the apical meristem almost disappeared (Fig. 1E), indicating that the cell cycle in this area was arrested. The number of EdU incorporating cells in this part was 10.2% of that in the unirradiated control. In contrast, some nuclei in the basal meristem continued to incorporate EdU (Fig. 1K), indicating that they were replicating DNA. The number of EdU incorporating cells in this part was 64.0% of that in the unirradiated control. At 1 day after the irradiation, the length of the proliferation zone of the root was shortened, and the disappearance of the elongation zone was observed (data not shown). Other investigators[3)4)] noted the occurrence of endoreduplication for differentiation in the basal meristem after irradiation. These data suggest that endoreduplication occurs in this part after irradiation, rather than the normal cell cycle proceeds.

*1 The Wakasa Wan Energy Research Center

In many cells, the EdU signal was colocalized with γ-AtH2AX signals in the same nucleus (Fig. 1 M). This result suggests that DNA replication started without the completion of DNA repair.

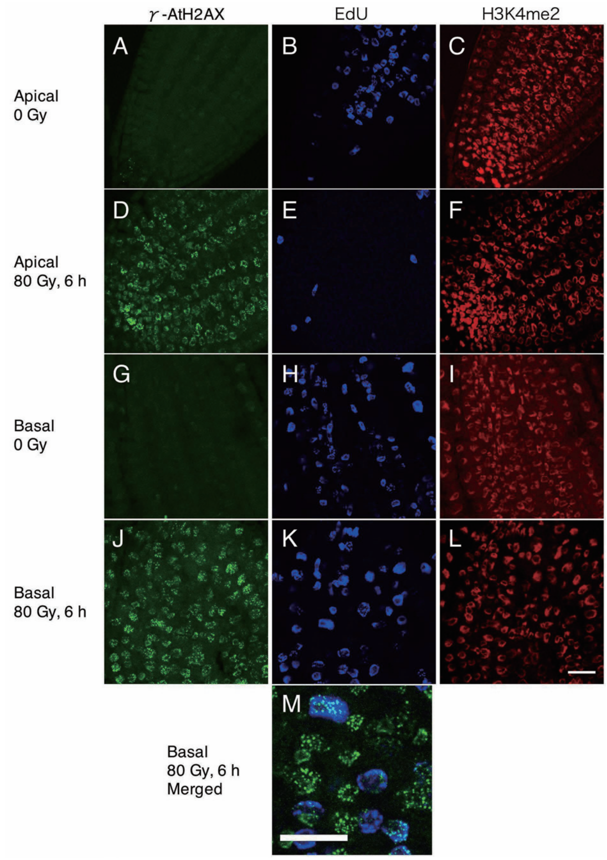

Fig. 1. Localization of γ-AtH2AX and EdU signals after the X-ray irradiation.
A-C and G-I indicate the apical and basal meristem of an unirradiated root, respectively. D-F and J-L respectively indicate the apical and basal meristem of an 80 Gy X-ray irradiated root. M shows a merged and enlarged image of J and K. Scale bars in L and M represent 20 μm.

Our present results indicate that different regulation of DNA replication in the apical and basal root meristem occurs after X-ray irradiation and suggests that cells in the basal meristem start DNA replication to differentiate without the completion of DNA repair.

References

1) Sauer et al.: Nature Protocols 1(1), 99 (2006).
2) Péret et al.: Trends in Plant Sci. 14(7), 399 (2009).
3) Ricaud et al: PLoS One 5, e430 (2007).
4) Adachi et al.: PNAS 108(24), 10004 (2011).

Molecular characterization of *OsHY2* mutation induced by heavy-ion beam in rice

R. Morita, Y. Hayashi, S. Kogure, T. Wakana, H. Tokairin, T. Sato,[*1] and T. Abe

Flowering time is thought to be one of the most important characteristics associated with the regional adaptability of plants. Floral bud development is dependent on specific environmental signals such as temperature and photoperiod. In the short-day plant rice (*Oryza sativa* L.), floral bud formation is promoted in the short-day condition. To clarify the regulation mechanism underlying flowering time in rice, a lot of mutants for flowering time are required. Therefore, we screened mutants for flowering time from a mutant population generated by ion-beam irradiation.

We screened an extremely early heading mutant line (6-67) from a mutant population generated by Ne-ion irradiation (15 Gy, LET 63 keV/μm) in 2010. Compared to the original variety Nipponbare, 6-67 formed pale green leaves and exhibited an early heading phenotype (about 1 month). To investigate the days to heading (DH), we started to grow both 6-67 mutant lines and Nipponbare (4 progenies each) in a greenhouse since June 17, 2011. Nipponbare exhibited 90.0 DH, whereas 6-67 mutant lines exhibited 47.3 DH (Fig. 1). This result indicated that 6-67 mutant lines exhibited early heading phenotype in a long-day condition. Two mutant lines *se5* and X61, which exhibited early heading phenotype in both long-day and short-day conditions have been reported previously[1,2]. *se5* exhibited 46.0 DH in a long-day condition, whereas the original variety, Norin8, exhibited 100.8 DH[1]. Similarly, X61 exhibited 49.0 DH in a long-day condition, whereas the original variety, Gimbozu, exhibited 78.2 DH[2]. *se5* harbors a 1-bp deletion in the first exon of the *OsHY1* gene, whereas X61 harbors a 1-bp insertion in the first exon of the *OsHY2* gene. Because of the similarity in the phenotypes of 6-67 and *OsHY* mutants, we performed sequencing analysis to clarify whether 6-67 harbored mutations in *OsHY1* (Os06g0603000) or *OsHY2* (Os01g0949400). The sequencing analysis revealed that there was no mutation in the *OsHY1* gene, whereas 6-67 harbored a 2-bp deletion in exon 4 of the *OsHY2* gene; this induced a frame-shift mutation and produced an immature stop codon (Fig. 2).

Saito et al. (2010) concluded that the mutation induced in the *OsHY2* gene caused early flowering in rice plants[2]. They performed genetic analysis with only a single null allele. In this study, we detected a new null allele induced in *OsHY2* gene. Our findings supported the data of Saito et al. (2010), because both early flowering mutant X61 and 6-67 harbored the mutation in the *OsHY2* gene.

Flowering time is an important agronomic trait in rice. We possessed both early- and late-flowering time mutants. The identification of the responsible genes in the mutants will allow us to understand the mechanism for the control of flowering time in rice plants. Studies of the flowering time mutants are currently in progress.

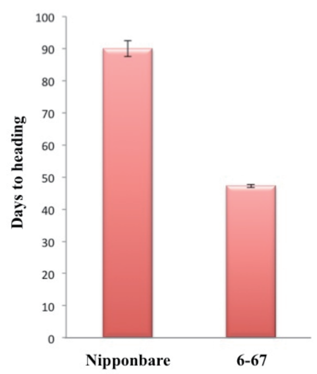

Fig. 1 Days to heading for Nipponbare and 6-67.
Bar indicates standard deviation (n = 4).

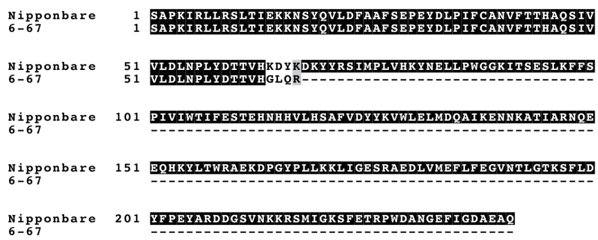

Fig. 2 Alignments of the deduced amino acid sequence of OsHY2.
The amino acid sequence of OsHY2 in both Nipponbare and 6-67 is shown. Sequence alignments were performed using ClustalW and BOXSHADE programs.

References

1) T. Izawa et al.: Plant J. **22**. 391 (2000).

2) H. Saito et al.: Theor. Appl. Genet. **122**. 109 (2010).

*1 Graduate School of Life Sciences, Tohoku University.

Identification of mutated gene in rice dwarf mutant for mutation induced by heavy ion beam

S. Kogure, R. Morita, Y. Hayashi, T. Wakana, H. Tokairin, T. Sato*[1], and T. Abe

Our team has studied the mutation induction in rice and *Arabidopsis* as an effect of heavy-ion beam irradiation. Each of these is a model plant of monocots and dicots. They are useful for searching mutation sites because their entire genome sequences are available. In this study, we report the identification of the mutated gene of a dwarf mutant in rice. In a previous study, we obtained the semi-dwarf mutant 3-58 by irradiating the imbibed seeds of rice (*Oryza sativa* L. cv. Nipponbare) with a C-ion beam (15 Gy, LET 50 keV/μm)[1]. 3-58 exhibited a reduced plant height and increased branching. The phenotype is different from known rice-gibberellin-related mutants, which show severe dwarfness with wide leaf blades and dark green leaves[2].

To determine the position of the mutated gene in 3-58, we performed map-based cloning. We grew F_2 population from a cross between 3-58 (japonica rice cultivar) and Kasalath (indica rice cultivar) in a greenhouse at 28°C for 5 weeks, and we selected 24 mutant type individuals that exhibited reduced plant height from 125 F_2 plants (Fig. 1, 2). When we used an SSR (simple sequence repeat) marker 01-04 (F: tggtctcgggttttcagttt, R: acaatgacacgccatagcaa) located on chromosome 1, a linkage between the marker 01-04 and the mutated phenotype was observed. 19 individuals showed the Nipponbare genotype, and 5 were heterozygotes. None showed the Kasalath genotype. Near the position of 01-04, there are two genes, Os01g0701400 (890kb from 01-04) and Os01g0746400 (1300kb from 01-04), which are orthologs of *MORE AXILLARY BRANCHING* (*MAX*) *1* and *MAX4*, respectively. In *Arabidopsis*, a series of the branching mutants is identified as *max*[3), 4)], and the mutants also show the dwarf phenotype. Os01g0746400 is already reported as a causative gene of a branching mutant, *DWARF10* (*D10*)[5] (Fig. 3). A sequence analysis revealed that 3-58 contained 3-bp deletion in the 4th exon of Os01g0746400, which caused 1-amino acid deletion. No mutation was detected in Os01g0701400. Our finding suggested that the mutation induced in 3-58 is a new allele of the *D10* gene. Another possibility remains that an unknown dwarf causative gene(s) results (result) in mutation, because the contribution of the 3-bp deletion in the mutant phenotype remains ascertained.

It is necessary to identify more mutated regions of rice mutants for characterizing the mutations induced by heavy-ion beam irradiation. We have isolated various rice mutants and the research continues.

References
1) Y. Hayashi et al.: RIKEN Accel. Prog. Rep. **43**, 282 (2010).
2) A. Sakai et al.: Science **299**, 1896 (2003).
3) P. Strinberg et al.: Development **129**, 1131 (2002).
4) K. Sorefan et al.: Genes Dev. **17**, 1469 (2003).
5) T. Arite et al.: Plant J. **51**, 1019 (2007)

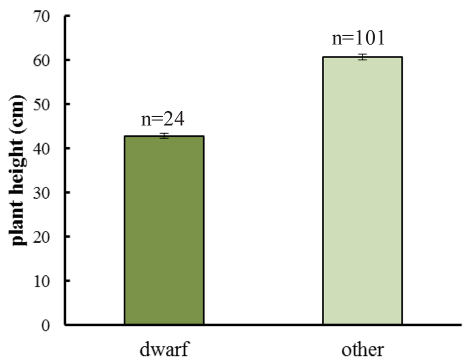

Fig. 1. Plant height of F_2 mutants 5weeks after germination. Bar=SD

Fig. 2. Photograph of F_2 plants 3 months after germination. F_2 dwarf plants (left) showed shorter plant height and more branches than Nipponbare wild type plants (right).

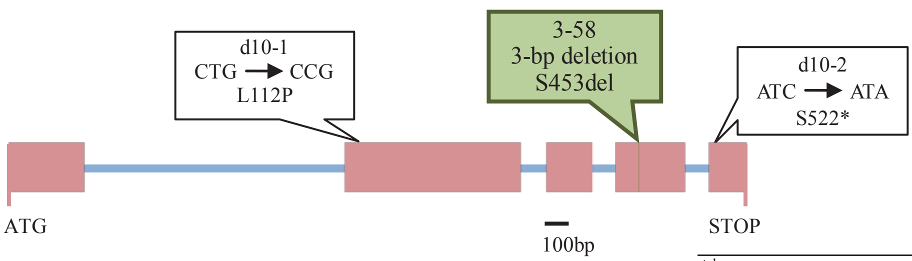

Fig. 3. Exon-intron structure of Os01g0746400 (*D10*). The mutations of 3-58, d10-1[5], and d10-2[5] are shown. 3-58 has a 3-bp deletion at exon4.

*1 Graduate School of Life Sciences, Tohoku University

Effect of water content on sensitivity to heavy-ion beams in rice seeds

Y. Hayashi, R. Morita, S. Kogure and T. Abe

The water content in rice, wheat, and barley seeds affects their radio sensitivity to X-rays and gamma rays. Radio sensitivity to X-rays is minimal at intermediate water content (14% to 16%) in rice, and it increases rapidly above and below this range[1)]. The water content in seeds has also been found to influence the damage caused during the storage period after irradiation (storage effect). Rice seeds with 6% water content show a remarkable storage effect, while the seeds with 12% or more water content show no storage effect after gamma irradiation[2)]. In contrast, some studies have reported that no storage effect or difference in the damage to seedlings according to water content in the seeds was detected with high LET radiation such as thermal neutrons[3), 4)]. We examined the effect of water content in rice seeds on radio sensitivity to heavy-ion beams (high LET radiation) and storage effect after irradiation.

The dry seeds of rice (*Oryza sativa* L. cv. Nipponbare) were equilibrated to 9.3, 11.1, and 12.3% water content through storage at various constant humidity. The seeds were packed in plastic bags and irradiated with $^{12}C^{+6}$ at a dose of 75, 100, and 125 Gy. The seeds were soaked in water 4 days after irradiation for 3 days at 28℃ for germination. The seeds were sown in the soil in pots and grown in a greenhouse. Germination rate, seedling height, and root length were measured 14 days after sowing. The germination rate was remarkably affected in seeds with 9.3% water content at 100-Gy and 125-Gy irradiation (Fig. 1). Surviving plants from the seeds with 9.3% water content showed a significant reduction in seedling height and root length at 75-Gy and 100-Gy irradiation (Fig. 2)

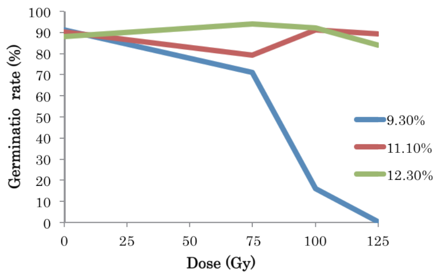

Fig. 1. Germination rate of seeds with different water contents after irradiation with C-ion beams.

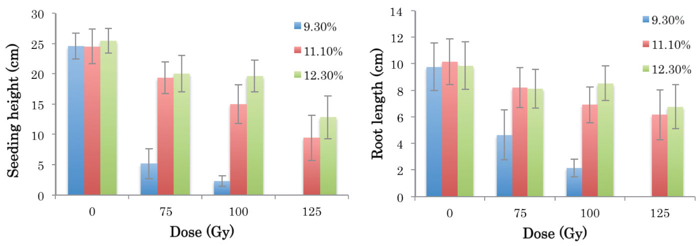

Fig. 2. Seedling height and root length after irradiation with C-ion beams.

To examine the storage effects in dry seeds after irradiation with heavy-ion beams, the seeds were equilibrated to 9.3, 10.8, and 13.0% water content and then irradiated with $^{12}C^{+6}$ at a dose of 125 Gy. The irradiated seeds were divided into 3 groups. One group was soaked in water immediately; one, after 1 day; and one, after 14 days. Then, all the seeds were grown as described above. The germination rate was measured 14 days after sowing. While the seeds with more than 10.8% water content showed no change in the germination rate during the 14-day storage period, the seeds with 9.3% water content showed rapid reduction within the first 24h after irradiation and then exhibited significant reduction up to 4 days (Table 1). This result suggested that the seeds with 9.3% water content showed different dose response from that shown in Fig. 1 after no storage period.

Our findings indicate that the water content of seeds affects radio sensitivity and storage effects after irradiation with heavy-ion beams such as X-rays and gamma rays. The water content of dry seeds is an important consideration while determining the optimum condition for irradiation with heavy-ion beams. Further investigation is required to reveal the relationship between water content and mutation induction in dry seed of rice after irradiation with heavy-ion beams.

Table 1. Germination rate of seeds with different water contents in storage periods of 0 day to 14 days after irradiation with C-ion beams.

Storage	Water content (%)					
period	Control*	C-ion beam				
(days)	9.4	9.3	10.8	11.1	12.3	13.0
0	95	98	95			96
1	95	20	99			97
4**	90	0		89	85	
14	97	0	99			99

* Non-irradiated seeds
** Data from the experiment shown in Fig. 1

References
1) C. Myttenaere et al.: Radiat. Bot., **5**, 443 (1965)
2) M. J. Conatantin et al.: Radiat. Bot., **10**, 539 (1970)
3) Y. Kawyama et al.: Japan J. Breed. **37** 299 (1987)
4) Y. Ukai et al.: Breeding Sci., **59** 129 (2009).

Effect of linear energy transfer on deletion induction by irradiation with heavy-ion beams in the apomictic plant *Panicum maximum*

M. Takahara*[1], M. Ebina*[1], R. Morita, Y. Kazama, T. Abe, T. Takamizo*[1], and H. Nakagawa*[2]

Apomixis is a form of asexual reproduction through seeds. It is widely observed among wild plant species but is almost completely absent among major crop species. Apomixis has the potential to benefit the field of agriculture greatly. Therefore, we aimed to isolate the gene(s) controlling apomixis for application in major crops. Guinea grass (*Panicum maximum* Jacq.), a major tropical forage grass, has some characteristics suitable for the study of apomixis. For example, it has both facultative apomictic lines and obligate sexual lines. However, recent studies have suggested that recombination is suppressed at the apomixis-controlling locus in guinea grass. To narrow down the apomixis-controlling genomic region, we tried to develop deletion mutants for this region by using irradiation with heavy-ion beams. In the present study, to assess the effect of linear energy transfer (LET) on deletion induction, seeds of guinea grass were irradiated with 3 different types of heavy-ion beams.

Dry seeds of guinea grass (an apomictic cultivar 'Natsukaze') were irradiated with $^{12}C^{6+}$ (23 keV/μm) ions at 300 and 400 Gy, $^{20}Ne^{10+}$ (63 keV/μm) ions at 150 and 200 Gy, and $^{56}Fe^{24+}$ (624 keV/μm) ions at 20 and 40 Gy. The doses were determined by referring to previous results that showed that the LD_{50} value for Natsukaze was 550 Gy for C, 270 Gy for Ne, and 55 Gy for Fe.[1] The M_1 plants generated from the irradiated seeds were grown in a field. Panicles were collected from 3 independent ears for each mutant, and DNA was extracted and purified using the cetyltrimethylammonium bromide (CTAB) method. Then, screening with polymerase chain reaction (PCR) was performed using apomixis-specific sequence-tagged site (STS) markers, which were expected to be located in the apomixis-controlling genomic region.

To date, a total of 237 M_1 plants (711 samples) were screened, and 118 deletion lines were obtained (Table 1). Previously, it has been reported that higher LET irradiation induced larger deletions.[2), 3)] Nevertheless, LET-dependent effect on deletion-size was not observed in this study. The number of lost markers was widely ranged for every type of heavy-ion beam, suggesting that both relatively smaller and larger deletions were induced in every level of LET irradiation. A higher dose of irradiation tended to induce more mutants and larger deletions for every type of heavy-ion beam. Among the mutants that had lost 2~20 STS markers (40 mutants), the deletion common to all 3 samples (ears) was detected in only 13 mutants. In the other 27 mutants, the deletion was detected in only 1~2 samples. These results suggested that many of the mutants had chimeric original and mutated tissues.

To determine the exact deletion-size for each mutant, we need to obtain whole sequences of the apomixis-controlling genomic region. Whole sequencing of this region by using a next-generation sequencer is currently in progress.

Reference
1) M. Takahara et al.: RIKEN Accel. Prog. Rep. **44,** 273 (2011).
2) Y. Kazama et al.: RIKEN Accel. Prog. Rep. **43**, 284 (2010).
3) H. Ichida et al.: Mutation Res. **639**, 101 (2008).

Table 1 The number of deletion mutants that lost STS marker(s) in the apomixis-controlling genomic region.

Ion	Dose (Gy)	No. of plants analyzed	No. of lost marker(s) 1		2~5		6~10		11~20		Almost all		Average of lost markers[a]	Max. lost markers[a]
C	300	25	8	(32.0%)[b]	1	(4.0%)	1	(4.0%)	0	(0%)	1	(4.0%)	4.5	6
C	400	48	17	(35.4%)	7	(14.6%)	0	(0%)	3	(6.3%)	0	(0%)	6.9	19
Ne	150	31	11	(35.5%)	2	(6.5%)	0	(0%)	0	(0%)	1	(3.2%)	2.0	2
Ne	200	91	21	(23.1%)	13	(14.3%)	1	(1.1%)	3	(3.3%)	3	(3.3%)	5.4	13
Fe	20	23	9	(39.1%)	1	(4.3%)	1	(4.3%)	0	(0%)	1	(4.3%)	5.5	8
Fe	40	19	6	(31.6%)	6	(31.6%)	0	(0%)	1	(5.3%)	0	(0%)	3.3	10
Total		237	72	(30.4%)	30	(12.7%)	3	(1.3%)	7	(3.0%)	6	(2.5%)	5.2	19

[a] Average or maximum number of lost markers among the mutants that had lost 2~20 STS markers.
[b] Relative rate in the plants analyzed (No. of mutants that lost STS marker(s)/ No. of plants analyzed).

*1 National Agriculture and Food Research Organization (NARO) Institute of Livestock and Grassland Science
*2 Biomass Research & Development Center, NARO

Analysis of DNA damage response in male gametes of *Cyrtanthus mackenii* during pollen tube growth

T. Hirano, K. Takagi, [*1] Y. Hoshino, [*2] and T. Abe

Pollen grains are exposed to environmental mutagenic agents such as UV light and ionizing radiation. Therefore, DNA damage could be induced in the male gametophytes during the processes of pollination, pollen tube growth, and double fertilization. It is presumed that the male gametes are required to repair the DNA damage for transmitting accurate genome information to the next generation. It has been reported that unscheduled DNA synthesis occurs during pollen tube growth, following mutagen treatments.[1] Moreover, DNA repair-related genes are expressed in the male gametes.[2, 3] However, no detailed data are available on the response to DNA damage in the male gametes. In the present study, therefore, we irradiated the pollen grains of *Cyrtanthus mackenii* with heavy-ion beam, which can induce DNA double strand breaks (DSBs), and analyzed the response to DNA damage in the male gametes during pollen tube growth by using *in vitro* culture system.

Anthers of *C. mackenii* in 1.5-ml tubes were irradiated with C ions (22.5 keV/μm) at a dose of 10–80 Gy and then stored at -20°C. For pollen germination, pollen grains from the anthers were sown in 2 ml of liquid pollen culture medium[4] and cultured at 25°C in the dark. Male-gamete isolation from the pollen tube and immunocytochemical analysis were performed according to the protocol described previously.[5]

At first, we measured the germination rate and pollen tube length after 24 h of culture. In the pollen grains irradiated with 80 Gy, the germination rate and pollen tube length were 50% and 2.5 mm, respectively. Compared to the non-irradiated pollen grains, the irradiated pollen grains showed no decrease in the germination rate and pollen tube growth.

Since *C. mackenii* forms bicellular pollen, we focused onsperm formation during the pollen tube growth. In the non-irradiated pollen grains, the sperm formation rate at 24 h was 78%. The sperm formation rates decreased with increase in the irradiated dose: when the pollen grains were irradiated at 40 Gy and 80 Gy, the sperm formation rates were 55% and 23%, respectively. Since the sperm formation in *C. mackenii* occurs after around 9–12 h of culture[5], we investigated the cell cycle phase in pollen mitosis II (PM II) after 12 h of culture. In non-irradiated pollen grains, 76% of the generative cells completed metaphase. However, most of the generative cells irradiated at 40 Gy and 80 Gy stopped at metaphase, and the generative cells that completed metaphase were 42% and 2% after irradiation with 40 Gy and 80Gy, respectively. Therefore, we supposed that DNA damage in the generative cells irradiated with a high dose were not completely repaired after 12 h of culture. To elucidate this assumption, we attempted to detect the phosphorylated histone H2AX (γH2AX) in the male gametes during PM II as an indicator for DSB. In the male gametes derived from the pollen grains irradiated at 40 Gy and 80 Gy, γH2AX foci were not detected in the anaphase, telophase, and sperm cells. However, the generative cells and metaphase cells formed γH2AX foci (Fig. 1), and the proportion of cells with the focus in the metaphase cells was 79% and 80% after irradiation with 40 Gy and 80 Gy, respectively. These results suggest that one of the reasons for the increase in metaphase cells in PMII is the unrepaired DSBs that remain in the metaphase cells, and spindle assembly check point might be working in PM II.

References

1) Jackson: Mutat. Res. **181**, 17 (1987).
2) Xu et al.: Plant J. **13**, 823 (1998).
3) Borges et al.: Plant Physiol. **148**, 1168 (2008).
4) Hirano and Hoshino: J. Plant Res. **122**: 225 (2009).
5) Hirano and Hoshino: Sex. Plant Reprod. **23**: 153 (2010).

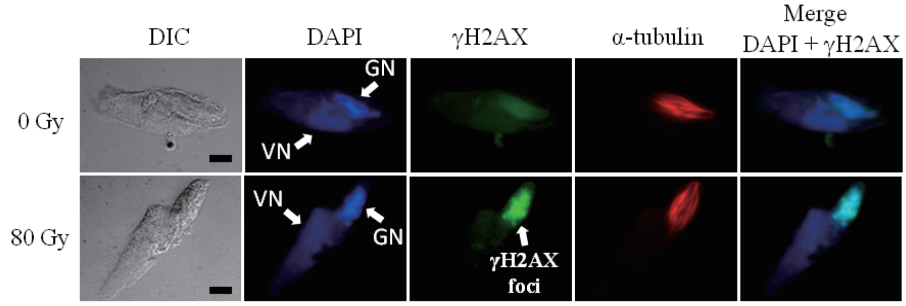

Fig. 1 γH2AX foci in the metaphase cells. The non-irradiated and irradiated pollen grains were cultured for 12 h. GN; generative nucleus, VN; vegetative nucleus. Bars = 10 μm.

*1 Wakasa Wan Energy Research Center
*2 Field Science Center for Northern Biosphere, Hokkaido University

Imbalanced functional disorders between pollen germination and seed formation after irradiation with heavy-ion beams and γ-rays

W. Aonuma,[*1] K. Ishii, [*1] N. Fujita,[*1] Y. Shimizu,[*1] Y. Kazama, T. Abe, S. Kawano[*1]

Irradiation with heavy-ion beams, which is used to isolate Y-chromosome deletion mutants from the dioecious plant *Silene latifolia*, is indispensable for studying the plant sex chromosome.[1] Although the germination rate of the pollen irradiated with a high dose of heavy-ion beams did not decrease, the seed obtained by pollinating such irradiated pollen was unusually small and showed an extremely low germination rate.[2] To confirm these imbalanced functional disorders between pollen germination and seed formation, pollen was irradiated with γ-rays and C-ion beams within dose ranges of 10 – 120 Gy, and then the pollen germination rate on the stigma and the seed formation rate obtained from the irradiated pollen were investigated.

Pollen grains were irradiated with γ-rays by using Gammacell® 3000 Elan at doses of 10 – 120 Gy. Doses of C-ion beams ($^{12}C^{6+}$; energy: 135 MeV/nucleon, LET: 23 keV/μm) used were the same as those of γ-rays. The irradiated pollen was pollinated onto female flowers, and then the germination rate of 300 pollen grains on the stigma was measured using aniline blue staining. A pollen grain was scored as germinated when the length of the pollen tube exceeded the diameter of the pollen grain (Fig. 1).

The irradiated pollen was used to fertilize female flowers, and then the number of seeds in the capsules were shown in C-ion beams (B) and γ-rays (C) of Fig. 2. Remarkable difference between irradiation with γ-rays and C-ion beams was observed in the size of the capsule and the number of seeds, even at 40 Gy of irradiation.

There was little difference between irradiation with γ-rays and C-ion beams with respect to the decrease in the germination rate of the irradiated pollen even at 120-Gy irradiation (Fig. 3). However, a remarkable difference was observed in the number of seeds obtained from the irradiated pollen. The average number of seeds obtained from non-irradiated pollen was approximately 200 grains. The seed formation rate decreased to 38% with 40 Gy of C-ion-beam irradiation, whereas it decreased to 10% with 40 Gy of γ-ray irradiation (Fig. 3).

The difference in the seed formation rate after irradiation with C-ion beams and γ-rays was larger when a low-dose range of irradiation was used rather than a high-dose range. The seed formation rates were 83% at 10 Gy and 70% at 20 Gy of C-ion beams. However, in the case of γ-rays,the seed formation rates were 40% and 18% at 10 Gy and 20 Gy, respectively. The seed formation rate with C-ion beams was twice as that with high as γ-rays irradiation at both the doses. This tendency was observed even at doses greater than 80 Gy. Few seeds were formed with 120 Gy of γ-rays, whereas the seed formation rate was 7% with 120 Gy of C-ion beams (Fig. 3).

Fertile pollen grains are required for successful seed formation. The decrease in the imbalance between the pollen germination rate and the seed formation rate suggests that the germinated pollen is not necessarily fertile.

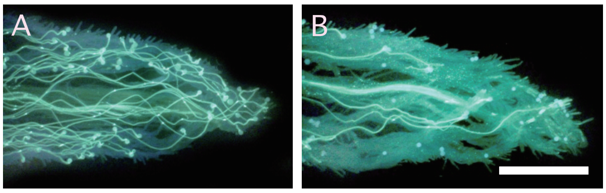

Fig. 1. Effect of irradiation with heavy-ion beams on the pollen germination visualized by aniline blue staining. (A) Non-irradiated pollen. (B) Pollen irradiated with 120 Gy of C-ion beams. Bar = 500 μm

Fig. 2. Radiation effect on the number of seeds and the size of the capsule. (A) A capsule obtained from non-irradiated pollen. (B) A capsule obtained from pollens irradiated with C-ion beams, at a dose of 40 Gy. (C) A capsule obtained from pollens irradiated with γ-rays, at a dose of 40 Gy. Bar = 1 cm

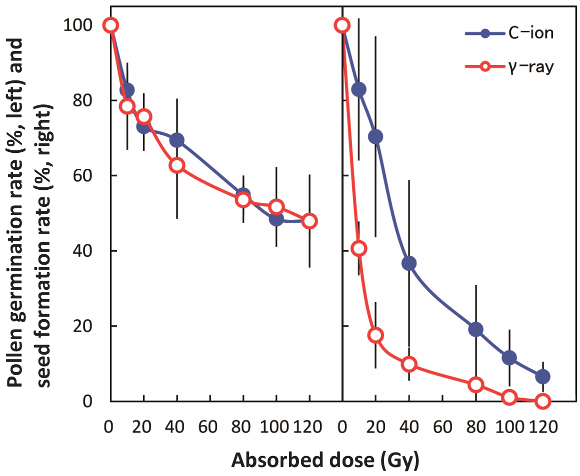

Fig. 3. Effect on the pollen germination rate (left) and the seed formation rate (right) after irradiation with C-ion beams (●) and γ-rays (○). The relative rate to non-irradiation is defined as the germination rate or the seed formation rate of 100%. Bars show standard deviation (n = 300 pollen grains and 7 capsules)

References

1) Ishii, K., et al.: RIKEN Accel. Prog. Rep. **43**, 279 (2010).
2) Aonuma, W., et al.: RIKEN Accel. Prog. Rep. **44**, 271 (2011).

*1 Department of Integrated Biosciences, The University of Tokyo

Heavy-ion beam irradiation is an effective technique to reduce major allergens in peanut seeds†

C. Cabanos,*1 H. Katayama,*1 H. Urabe,*1 C. Kuwata,*2 Y. Murota,*2 T. Hirano, Y. Hayashi, T. Abe, Y. Okumoto,*1 and N. Maruyama*1

Peanut allergy, with a worldwide prevalence of 0.5 to 2%, has long been a health problem as it causes mild to severe anaphylactic shock in some cases and death in severe cases.[1] Currently, there are 13 allergens identified in peanut seeds according to Allergome. Three of the 13 allergens, namely, Ara h 1 (7S globulin), Ara h 2 (2S albumin), and Ara h 3 (11S globulin), are considered as the immunodominant allergens. The advent of recombinant DNA technology has made possible the means to alleviate the problem of food allergy through genetic modifications of the plant itself by suppressing and silencing the genes responsible for producing allergens. Although the approach has been successful in reducing the expression of some allergenic proteins, these cannot result in a complete suppression of production or knockout of a particular allergen in the plant.[2] The regulatory obstacles in the use of transgenic crops and their derivatives also present another difficulty in mass production of hypoallergenic peanuts. One approach that may achieve the ultimate goal of producing peanut seeds with complete knockout of allergen isoforms is a technique known as heavy-ion beam irradiation. Here, we report our attempt to develop a new hypoallergenic Japanese peanut variety by heavy-ion beam irradiation (the E5 beam line in the RIKEN RI-beam factory).

Table 1. Percent normal germination of the seeds of 5 Japanese peanut varieties after C ion irradiation.

Beam dose (Gy)	Nakate yutaka	Tachi masari	Chibahan dachi	Omasa ri	Sato noka	Average of all varieties (on the basis of the beam dose)
0	90 (36)	100 (40)	77.5 (31)	90 (36)	97.5 (35)	**91.0**
12.5	100 (40)	97.5 (39)	82.5 (33)	97.5 (35)	97.5 (35)	**95.0**
25	100 (40)	87.5 (35)	75 (30)	90 (36)	97.5 (35)	**90**
50	100 (40)	97.5 (39)	80 (32)	90 (36)	97.5 (35)	**93**
75	97.5 (39)	95 (38)	85 (34)	95 (38)	97.5 (35)	**94**
100	95 (38)	92.5 (37)	80 (32)	90 (36)	96 (35)	**90.7**
150	0 (0)	0 (0)	2.5 (1)	0 (0)	0 (0)	**0.5**

Parentheses, the number of germinated seeds out of 40 seeds.

Table 1 shows the percent normal germination rate at increasing dose of C ion of the 5 Japanese peanut varieties.

As shown, a maximum dose of 100 Gy, beyond which the germination rate starts to significantly decrease, was found to retain seed germination rate (80% up to 100%) comparable to non-irradiated controls (0 Gy) in all varieties. We determined the maximum dose of heavy-ion beam (100 Gy) that was used in the irradiation experiment.

A total of 2,000 peanut seeds of Nakateyutaka variety were irradiated with 100 Gy of either C or N ions. A total of 1,509 lines were obtained from both C- and N-ion irradiated lines and were screened for knockout mutations. Overall, a total of 11,335 harvested seeds from both N- and C-ion irradiated parent plants were screened using sodium dodecyl sulphate-polyacrylamide gel electrophoresis (SDS-PAGE) analysis. A total of 17 seeds showed knockout mutation, 8 of which were observed as lacking either 1 of the 2 isoforms of Ara h 2 and the others were observed as lacking 1 of the isoforms of Ara h 3 (a part of the data is shown in Fig. 1). In Ara h 2 mutants, 5 of the mutant lines lacked the high molecular weight isoform and 3 lacked the low molecular weight isoform of the allergen. These results indicate that heavy-ion beam irradiation is a powerful means in producing knockout hypoallergenic peanuts.

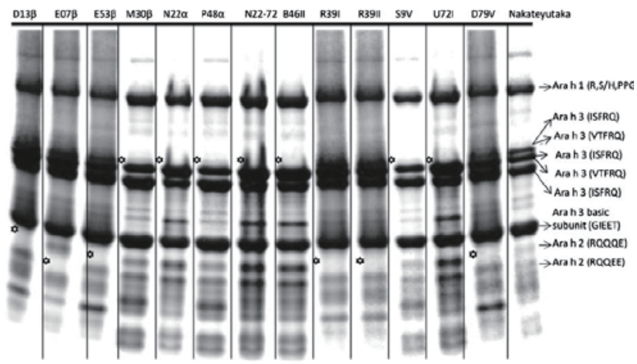

Fig. 1 Protein phenotype of the M_2 knockout mutants.
Asterisks indicate the missing allergen isoforms after heavy-ion beam irradiation. N-terminal sequences of the major protein bands are shown in parentheses.

References
1) A.H. Liu, R. Jaramillo, S.H. Sicherer, R.A. Wood, S.A. Bock, A.W. Burks, M. Massing, R.D. Cohn, and D.C. Zeldin: J. Allergy Clin. Immunol. **126**, 798-806 (2010)
2) H.W. Dodo, K.N. Konan, F.C. Chen, M. Egnin, and O.M. Viquez: Plant Biotechnol. J., **6**, 135-145 (2008)

† Condensed from the article in Molecular Breeding (2012) in press

*1 Graduate School of Agriculture, Kyoto University
*2 Chiba Prefectural Agriculture and Forestry Research Center

Effect of heavy-ion beam irradiation on the survival and growth of in vitro cultured nodal segments of *Artemisia annua* L.

P. Inthima,*[1,*2] K. Supaibulwatana,*[2] M. Otani,*[1] T. Hirano,*[3] Y. Hayashi,*[4] T. Abe,*[3,4] and M. Nakano*[1]

Artemisia annua L. is known as a medicinal plant that produces an antimalarial compound, artemisinin. World Health Organization has been recommended the use of artemisinin as artemisinin-based combination therapies for treatment of diseases caused by the drug-resistant parasite, *Plasmodium falciparum*[1]. However, artemisinin production is relatively low, varying about 0.01−0.8% in dry weight[2]. Therefore, induction and screening of high artemisinin-producing plants is necessary. Heavy-ion beam radiation has recently been shown to be one of the effective means of broadening the genetic variability because of its higher relative biological effectiveness than that of other radiations such as gamma rays, X-rays, and electrons[3]. Consequently, the application of heavy-ion beam irradiation to generate high artemisinin-producing mutants of *A. annua* was examined.

Nodal segments with an axillary bud (0.5 cm long) were excised from in vitro-grown plantlets of *A. annua* and precultured on a solid medium supplemented with 0.1 mg/L α-naphthaleneacetic acid and 1 mg/L 6-benzylaminopurine in plastic Petri dishes (6 cm in diameter) for 5 days prior to irradiation with $^{12}C^{+6}$ ions [135 MeV/nucleon; Linear Energy Transfer (LET): 23 keV/μm] at 0, 2.5, 5, 10, 20, and 50 Gy. Thirty nodal segments were placed per dish. Irradiated segments were transferred to test tubes (2.5 × 15 cm) containing a plant growth regulator-free medium for shoot induction.

As shown in Fig. 1, compared with the non-irradiated control (0 Gy), the ^{12}C-ion beam irradiation at 2.5 and 5 Gy had no effect on the survival of nodal segments, whereas a slight lethal effect was observed 30 days after irradiation at 10 Gy. However, at higher doses, remarkable reductions in the survival percentage were observed. More than 50% of nodal segments irradiated at 20 and 50 Gy died within 10 days after irradiation. All the nodal segments irradiated at 50 Gy died, and only about 5% of those irradiated at 20 Gy survived 50 days after irradiation. Growth of axillary bud-derived shoots after irradiation is shown in Fig. 2. Retarded shoot growth was observed when ^{12}C ion dose increased. No axillary bud-derived shoots were obtained after 50 Gy irradiation.

Acclimatization and cultivation of plantlets derived from ^{12}C-ion beam irradiated nodal segments, mutant screening by random amplified polymorphic DNA analysis, and morphological characterization are now in progress.

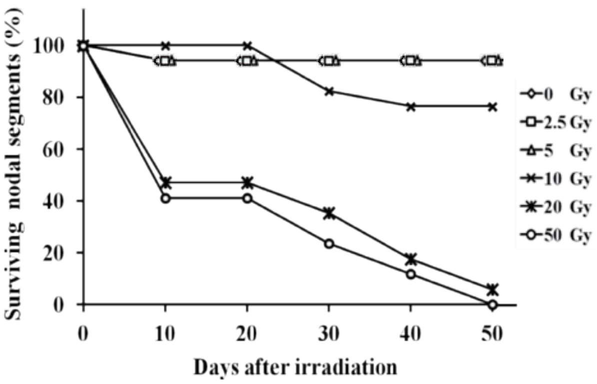

Fig. 1. Survival time course of the percentage of nodal segments of *Artemisia annua* after various doses of ^{12}C-ion beam irradiation.

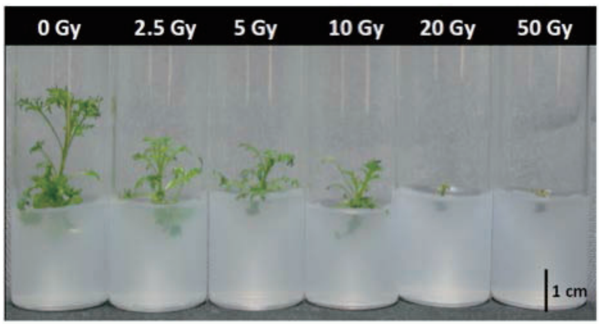

Fig. 2. Effect of different doses of ^{12}C-ion beam irradiation on the growth of axillary bud-derived shoots of *Artemisia annua*, 30 days after irradiation.

*1 Faculty of Agriculture, Niigata University
*2 Faculty of Science, Mahidol University, Thailand
*3 Ion beam Breeding Laboratory, RIKEN Innovation Center
*4 Radiation Biology Team, RIKEN Nishina Accelerator Research Center

References
1) T. K. Mutabingwa. 2005. Acta Trop. **95**:305–315.
2) M.Z. Abdin et al. 2003. Planta Med. **69**:289−299.
3) M. Nakano et al. 2010. Plant Biotechnol. **27**:155-160.

Characteristics of early-flowering mutant line of strawberry cultivar Satsumaotome induced by C-ion irradiation

Y. Takenoshita*, M. Takemure*, M. Ooe*, H. Saito and T. Abe

In recent Japan, the demand for strawberries increases sometime around Christmas. Although the strawberry cultivar Satsumaotome, which was developed in Kagoshima Prefecture, has large fruits and good quality, it is classified as a late-harvesting cultivar and cannot be harvested during the period of high demand. Therefore, we aimed to develop early-flowering mutants derived from Satsumaotome by ion-beam irradiation. We estimated suitable doses of C-ion beams for irradiation to multiple-shoot cultures[1), and we selected an early-flowering mutant line B0518[2) 3)]. In this study, we investigated the flowering and fruiting habits and yield of B0518 for 3 years, from 2008 to 2010.

During the 3 years observation, in a greenhouse at Minamisatsuma in Kagoshima, the terminal inflorescence of B0518 flowered 1 to 4 days earlier than that of Satsumaotome, and the primary axillary inflorescence flowered 14 to 31 days earlier than that of Satsumaotome (Table 1). These characteristics of flowering showed similar trends over the 3 years; therefore we concluded that the early flowering characteristics of B0518 were stable.

In addition, B0518 had approximately 1.4 less leaves between the terminal inflorescence and the primary axillary inflorescence than Satsumaotome (Table 2). These results indicated that early flower-bud initiation of the primary axillary inflorescence of B0518 was caused by mutation as a result of ion-beam irradiation.

The terminal inflorescence and the primary axillary inflorescence of B0518 were harvested earlier than Satsumaotome during the 3 years; as a result, the fruit yield by December 31 of B0518 increased by 2-18kg/a, and the fruit yield by February 28 increased 11-45kg/a than that of Satsumaotome respectively (Table 1, 3).

In terms of the shape of the fruit, color of the peel, and color of the flesh, B0518 was identical to Satsumaotome (data not shown).

From the results of this study, we confirmed that B0518 was an early-flowering line whose fruits retained the excellent characteristics of Satsumaotome. We also confirmed that B0518 was a high-yielding line, compared to the original cultivar Satsumaotome.

Currently, we are conducting a performance test for the commercial production of B0518 in the production regions. Furthermore, we are investigating the characteristics of a promising new line obtained after B0518.

References

1) M.Ooe et al.:RIKEN Accel.Prog.Rep.**42**, 286 (2009)
2) Y.Takenoshita et al.:RIKEN Accel.Prog.Rep.**42**, 287 (2009)
3) Y.Takenoshita et al.:RIKEN Accel.Prog.Rep.**43**, 288 (2010)

Table 1. Flowering and harvest dates of B0518 in 2008-2010

Line・Cultivar	Terminal inflorescence						Primary axillary inflorescence					
	Flowering date			Harvest date			Flowering date			Harvest date		
	2008	2009	2010	2008	2009	2010	2008	2009	2010	2008	2009	2010
B0518	Nov. 10	Nov. 8	Nov. 13	Dec. 24	Dec. 15	Dec. 24	Dec. 22	Dec. 2	Dec. 20	Feb. 1	Jan. 17	Feb. 14
Satsumaotome	Nov. 11	Nov. 10	Nov. 17	Dec. 26	Dec. 16	Dec. 27	Jan. 8	Jan. 1	Jan. 18	Feb. 23	Feb. 17	Feb. 28

Flowering date: 50% of the plants (n = 20) at first flower   Harvest date: 20% of the plants (n = 20) at first harvest

Table 2. Number of leaves between terminal inflorescence and primary axillary inflorescence of B0518 in 2008-2010

Line・Cultivar	Number of leaves		
	2008	2009	2010
B0518	—	2.8	2.8
Satsumaotome	—	4.2	4.1

Date represent the mean values (n = 20)

Table 3. Fruit yield of B0518 by December 31 and by February 28 in 2008-2010

Line・Cultivar	Fruit yield by December 31 (kg/a)			Fruit yield by February 28 (kg/a)		
	2008	2009	2010	2008	2009	2010
B0518	31	41	36	201	229	166
Satsumaotome	24	39	18	190	184	147

Date represent the mean values (n = 20)

* Kagoshima Prefectural Institute for Agricultural Development

Salt-resistant rice grown in paddy fields affected by the tsunami

T. Abe, Y. Hayashi, R. Morita, T. Endo[*1] and T. Sato[*2]

The world is facing a serious food and energy crisis. Plant mutation breeding has played an important role in overcoming this crisis and maintaining world stability. The breeding of new mutant varieties provides higher yield potential, more productive biomass-energy use, better adaptation to climate change and variability, and a nutrient composition that is more beneficial to human health. In areas of Japan affected by the recent tsunami, where saline paddy fields have spread, there is a particular need for breeding techniques to produce new rice varieties with saline resistance. New techniques are also required to achieve faster and more effective breeding

At RIKEN, we have developed a unique technology for mutation induction by using heavy-ion beams from particle accelerators at the RI Beam Factory (RIBF). This development was achieved through an efficient synergistic link between agricultural science and accelerator physics. The use of ion beams for mutagenesis has a number of advantages: the approach has low exposure levels and high survival rates, it achieves high mutation rates, and it creates a wide variety of different mutations. Because heavy-ion beams provide a very high amount of energy, even a single ion is enough to significantly damage a gene – in fact, the beams have enough energy to break the double strand of the DNA. The technique is also very useful in producing mutants that lack just a single gene; multiple propagation technology can be used to convert these mutants into new cultivars. Examples of such breeds include 'Safinia Rose' (petunia), 'Temari Bright Pink' (vervena) [1, 2], and 'Olivia Pure White' (dianthus) [3]. The development period for producing new varieties is only 3 years.

When applied to rice, the ion-beam technique produced dwarf, early-, late-flowering, and high-yield mutants. In addition, we successfully isolated 4 salt-resistant lines (6-99, 19-74, 14-45 and 18-36) from 325 progeny lines between 2003 and 2009 [4, 5]. We cultivated salt-resistant rice in the paddy fields (Hebita, Ishinomaki-shi) affected by the recent tsunami (Fig. 1). Compared to the yields of the control plants (Nipponbare), the 6-99 and 18-36 plants were 1.05- and 1.20- fold higher, respectively. This area has undergone numerous improvements for salt removal since April 2011. Therefore, the yields of the original cultivars in Miyagi Prefecture have not decreased.

In the next stage of our work, we plan to breed salt-resistant lines of tastier commercial rice varieties from Miyagi Prefecture. For this purpose, imbibed seeds of rice ('Hitomebore' and 'Manamusume') were irradiated with the C ions at maximum linear energy transfer (LETmax, 50 keV/μm, 15Gy) [6, 7], the most effective LET for mutation induction. The seedlings were grown in a paddy field at the Miyagi Prefectural Furukawa Agricultural Experiment Station. We obtained 368 M_2 lines for 'Hitomebore' and 349 for 'Manamusume'. We will select salt-resistant lines in the saline paddy field in Tohoku University in 2012.

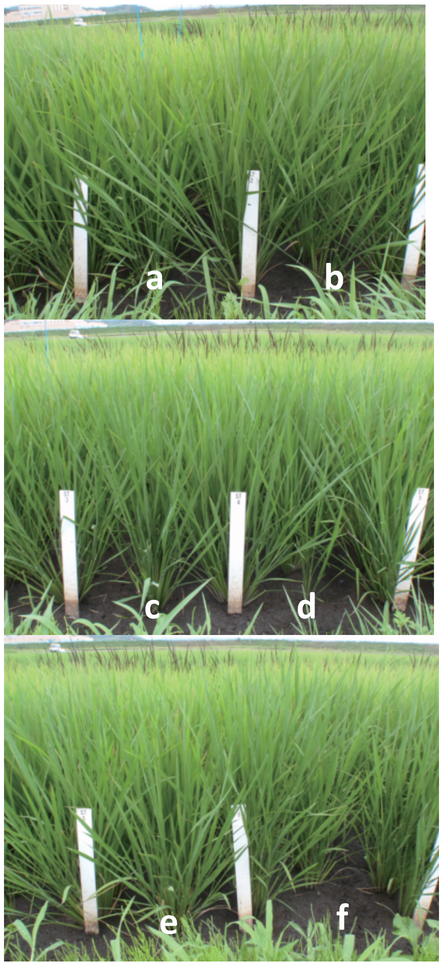

Fig. Salt-resistant rice grown in paddy fields in Ishinomaki on 4 Aug. a, Nipponbare; b, 6-99; c, 19-74; d, 14-45; e, 18-36; f, Hitomebore.

References
1) K. Suzuki et al.: RIKEN Accel.Prog. Rep. **35**, 129 (2002).
2) T. Kanaya et al.: Plant Biotech. **25**, 91-96 (2008).
3) M. Sugiyama et al.: RIKEN Accel.Prog. Rep. **41**, 229 (2008).
4) Y. Hayashi et al.: RIKEN Accel.Prog. Rep. **40**, 253 (2007).
5) Y. Hayashi et al.: RIKEN Accel.Prog. Rep. **41**, 234 (2008).
6) Y. Kazama et al.: Plant Biotech. **25**, 113-117 (2008).
7) Y.Hayashi et al:Cyclotoron and their applications 2007, pp.237-239 (2008)

[*1] Miyagi Prefectural Furukawa Agricultural Experiment Station

IV. OPERATION RECORDS

1. Operation of RIBF

Operations of RIBF ring cyclotrons (RRC, fRC, IRC, and SRC)

S. Ishikawa,[*1] M. Kase, T. Aihara,[*1] M. Fujimaki, N. Fukunishi, S. Fukuzawa,[*1] A. Goto, M. Hamanaka,[*1] H. Hasebe, Y. Higurashi, E. Ikezawa, H. Imao, T. Kageyama, O. Kamigaito, M. Kidera, K. Kobayashi,[*1] M. Komiyama, Y. Kotaka,[*1] R. Koyama,[*1] H. Kuboki, K. Kumagai, T. Maie, M. Nagase, T. Nakagawa, T. Nakamura,[*1] M. Nishida,[*1] M. Nishimura,[*1] T. Ohki,[*1] Y. Ohshiro,[*2] H. Okuno, K. Oyamada,[*1] N. Sakamoto, J. Shibata,[*1] K. Suda, M. Tamura,[*1] N. Tsukiori,[*1] A. Uchiyama,[*1] T. Watanabe, Y. Watanabe, K. Yadomi,[*1] K. Yamada, S. Yamaka,[*2] H. Yamauchi,[*1] and S. Yokouchi

The 2011 operations of the four RIBF ring cyclotrons (RRC, fRC, IRC, and SRC) are reported. The list of beams accelerated by these cyclotrons is shown in table 1.

The experiments in the RIBF building could not be arranged because of the construction of the SAMURAI during January to March 2011. On March 11, the East-Japan earthquake occurred. Although the direct damage by the earthquake was apparently small, the operations of accelerators were limited owing to the resulting shortage of electric power till September 2011. In June and July, only a 345 MeV/nucleon ^{18}O beam was accelerated and delivered to the BigRIPS and the SHARAQ to ensure that the performances of the RIBF stayed the same as before.

The RILAC2 system together with a 28GHz gyrotron -driven ECR ion source became ready in the summer of 2011, producing a $^{238}U^{35+}$ beam with an intensity of around 30 eμA. From November to December 2011, U and Xe beams were scheduled for the first time in the acceleration mode of 28GHzECR-RILAC2-RRC-fRC-IRC-SRC. A 345 MeV/nucleon ^{238}U beam with an intensity of 3.7 pnA at FC-G01 and a 345 MeV/ nucleon ^{124}Xe beam with an intensity of 7.7 pnA were obtained.

In 2011, the RRC standalone operation for the ordinary experiments in the Nishina Building was very limited, because the AVF was out of service from April to September owing to issues in its D-electrode. The seasonal biology experiment was carried out in the mode RILAC-RRC (h=7) mode, generating a 85MeV/ nucleon ^{12}C beam.

It was found in May 2011 that the RRC main coil in the East-sector magnet had a layer short, which has since been causing fluctuation as high as ±20ppm in the RRC magnetic field. In summer 2012, a newly fabricated one t will be replaced by the main coil.

In early 2012, the new gas stripper system with a large differential pumping will be installed just after the RRC (A02), as the first stripper in the case of uranium acceleration. An intense beam of more than 10 pnA will be expected with this new charge-stripper system.

*1 SHI Accelerator Service Ltd.
*2 Center for Nuclear Study, the University of Tokyo

Table 1. Beams accelerated by RRC, fRC, IRC, or SRC in 2011.

Accelerators	Particle	Experiment Course	Energy (MeV/u)	Beam intensity (pnA)	Beam tuning (hr)	Experiment (hr)	Allocation frequency
AVF-RRC	^{12}C	E5B	135	< 1	67	46	3
	^{14}N	E3B	135	486	25	50	1
	^{22}Ne	RIPS	110	310	79	117	3
	^{22}Ne	E5B	135	< 1	13	6	1
	^{40}Ar	E5B	95	< 1	22	9	3
	^{56}Fe	E5B	90	< 1	22	12	1
RILAC-RRC	^{12}C	E5B	85	<1, (112)	18	11	1
	^{23}Na	RIPS	63	1050	14	60	1
	^{70}Zn	RIPS	63	94	21	166	1
RILAC2-RRC	^{238}U	E5A	10.8	< 2 (10)	35	12	1
RILAC-RRC-IRC-SRC	^{18}O	SHARAQ	250	181	146	303	1
RILAC2-RRC-fRC - IRC- SRC	^{124}Xe	BigRIPS	345	7.7	96	166	1
	^{238}U	BigRIPS	345	3.5	271	1191	1
	^{124}Xe	MS	345	—	51	0	1
RILAC2-RRC-(fRC)	^{124}Xe	MS	10.8	—	40	0	1
	^{238}U	MS	51	—	346	0	1
	^{238}U	MS	10.8	—	91	0	2

RILAC operation

E. Ikezawa, T. Ohki,* M. Kase, T. Nakagawa, N. Sakamoto, H. Okuno, N. Fukunishi, M. Fujimaki, M. Nagase, T. Kageyama, S. Yokouchi, M. Kobayashi-Komiyama, M. Kidera, Y. Higurashi, T. Watanabe, K. Yamada, T. Maie, H. Hasebe, H. Kuboki, K. Suda, Y. Watanabe, T. Aihara,* H. Yamauchi,* A. Uchiyama,* K. Oyamada,* M. Tamura,* and O. Kamigaito

The RIKEN heavy-ion linac (RILAC) has been operating steadily throughout the reporting period and has been supplying various ion beams for various experiments. However, the operation was suspended for 21 days because of the 2011 off the Pacific coast of Tohoku Earthquake on March 11th. Some statistics on the RILAC operation from January 1 to December 31, 2011, are given in Table 1. The total beam service time of the RILAC accounted for 92.7% of its operation time. The two operation modes of the RILAC, namely, the stand-alone mode and the injection mode, in which the beam is injected into the RIKEN Ring Cyclotron (RRC), accounted for 88.5% and 11.5% of the total beam service time of the RILAC, respectively. ^{12}C, ^{18}O, ^{19}F, ^{23}Na, ^{70}Zn, and ^{82}Kr ions produced with an 18-GHz ECR ion source (18G-ECRIS) were accelerated by the RILAC. Among them, for the beam experiments at the RI Beam Factory (RIBF), a 2.185-MeV/nucleon ^{18}O-ion beam accelerated by the RILAC was injected into the RRC between May and June 2011. The e3 beam course in target room No. 1 was used for 5065.5 h for research experiments involving the heaviest elements and the study of the physical and chemical properties of these elements with the GARIS. The other beam courses in target rooms No. 1 and No. 2 were not used. In 2011, research experiments on the heaviest elements were carried out for 49 days from January through March, 51 days from April through May, 64 days from June through August, 29 days in September, and 48 days from November through December.

We carried out the following improvements and overhauls during the reporting period. A control system for power supplies of quadrupole magnets embedded in drift tubes of RILAC cavities, and plate current detector sensors of the final stage of the RILAC RF power amplifier were improved. Details are reported elsewhere in this issue.[1), 2)] A beam profile monitor was newly installed at the beam course just before the installation of the dipole magnet in target room No. 1. In the RF systems, the power supplies that were in their final and intermediate stages of operation were subjected to annual inspection. In addition, the major components of mechanical parts were subjected to simple inspection. In the water-cooling systems used for the 18G-ECRIS, vacuum pumps, and the RILAC cooling tower circuit, three water pumps were overhauled. The other water pumps were subjected to simple inspection. Two heat exchangers of the water-cooling system used for the CSM RF system and drift tubes in the RILAC cavities were overhauled. All cooling towers were subjected to monthly inspection and annual cleaning. In addition, a fan motor and diffuser panels of the cooling tower used for the FC-RFQ RF system were replaced with new ones. An internal pump, a fan motor, and rotor blades of the closed circuit cooling tower used for vacuum pumps were replaced with new ones. All turbomolecular pumps were subjected to annual inspection. Four cryogenic pumps used for the CSM and the RILAC cavities were overhauled.

Table 1. Statistics on the RILAC operation from January 1 to December 31, 2011.

Operation time of RILAC	6171.0	h
Mechanical trouble	295.5	h
Stand-alone RILAC	5065.5	h
Injection into RRC	655.5	h
Total beam service time of RILAC	5721.0	h

We experienced the following mechanical problems during the reporting period. A beam pipe with an external diameter of 80 mm in target room No. 1 had a vacuum leak caused by the earthquake. The leaky part was soldered. A part of the wall of the RILAC building was also damaged by the earthquake. Part of the cooling pipe of the RF power feeder for the FC-RFQ cavity had a vacuum leak; we repaired the pipe with a repair material as a stopgap measure. In addition, the faulty part was newly fabricated. Later, we replaced the faulty part with the new one. The RILAC RF power amplifier No. 1 had a problem because water leaked from a water joint inside the grid stub; we repaired the joint. A microwave amplifier used for the 18G-ECRIS had a problem because the klystron was worn out after many years of operation; we replaced it with a substitute as a stopgap measure. A water chiller used for the 18G-ECRIS had a problem; we therefore switched to the backup unit. There were problems in the RILAC RF and the CSM RF systems, the DC power supplies, the low-level controllers, and the air-cooling fans; we replaced each component with a spare one. A cryogenic vacuum pump used for the RILAC No. 1 cavity had a problem; we replaced it with a new one.

References
1) A. Uchiyama et al.: in this issue.
2) K. Oyamada et al.: in this issue.

* SHI Accelerator Service Ltd.

AVF Operation

M. Nishimura,*[1] M. Kase, M. Fujimaki, N. Fukunishi, S. Fukuzawa,*[1] A. Goto, M. Hamanaka,*[1] H. Hasebe, Y. Higurashi, E. Ikezawa, H. Imao, S. Ishikawa,*[1] T. Kageyama, O. Kamigaito, M. Kidera, K. Kobayashi,*[1] M. Komiyama, Y. Kotaka,*[1] R. Koyama,*[1] H. Kuboki, K. Kumagai, T. Maie, M. Nagase, T. Nakagawa, T. Nakamura,*[1] M. Nishida,*[1] Y. Ohshiro,*[2] H. Okuno, N. Sakamoto, J. Shibata,*[1] K. Suda, N. Tsukiori,*[1] T. Watanabe, Y. Watanabe, K. Yadomi,*[1] K. Yamada, S. Yamaka,*[2] and S. Yokouchi

In 2011, the total annual operation hours of the K70 AVF cyclotron (denoted as AVF hereafter) decreased by 23% as compared to those in the preceding years. This was attributed to the troubles related vacuum in the AVF as well as the governmental limitation on the usage of electric power as a consequence of the East-JAPAN earthquake of March 11.

The AVF did not suffer any apparent damage by the earthquake. The AVF operation was restarted in April after carefully checking each individual part of the AVF in the off-line mode for a month. However, in late April, a serious water leak occurred inside the AVF, the vacuum in the chamber became much worse and the beam time for RI production was cancelled midway.

It was found, after the investigation, that the water-leak originated from the cooling-water pipe deep inside one of the acceleration electrodes (the so-called D-electrode) connected to cavity#2. The AVF was out of service until the end of August, when both D electrodes were replaced by newly fabricated ones. This trouble was probably due to wearing after very long-term operations of 23 years and was probably not directly related to the earthquake of March 11.

As shown in table 1, the beam time of the injection to AVF-RRC-SRC was not scheduled in 2011. Six beam times of AVF-RRC were scheduled in early 2011; the operation time was only 270 hours, which is almost half of that in a normal year.

All the beams accelerated by the AVF in 2011 were listed in table 2. The acceleration of ^{7}Li was tested in order to estimate the beam intensity of ^{6}Li using a new type of crucible to produce the Lithium vapor into the plasma of the Hyper ECR ion source.

In 2011, beam times related to the RI production were carried out frequently. A 12 MeV/nucleon deuteron beam was used for this purpose for the first time. In autumn 2011, four sets of one-day beam times of a 5.5 MeV/nucleon He beam were carried as usual for a student experiment.

*1 SHI Accelerator Service Ltd.
*2 Center for Nuclear Study, the University of Tokyo

Table 1. The statistics of AVF operation in 2010.

	2010	2011
Total operation time	3339 hr	2570 hr
Beam tuning	1016 hr	880 hr
Injection to RRC	511 hr	270 hr
injection to RRC-SRC	507 hr	0 hr
AVF standalone	1304 hr	1419 hr
Beam course (AVF standalone)		
E7a	734 hr	876 hr
E7b	74 hr	60 hr
C03	385 hr	357 hr
Machine study	110 hr	124 hr

Table2. AVF Beam List of 2011.

Particle	E(MeV/u)	Course
p	12, 14	RI Production
p	14, 15.4	MS
d	12.0	RI Production
d	5.5	MS
α	6.5	Student Ex
α	8.8	CRIB
^{7}Li	8.6	MS
^{12}C	7.0	RRC－E5
^{14}N	7.0	RRC－E5
^{15}N	5.0	CRIB
^{18}O	6.1	CRIB
^{20}Ne	6.2	CRIB
^{20}Ne	7.0	RRC－E5
^{22}Ne	5.8	RRC－RIPS
^{24}Mg	7.5	CRIB
^{40}Ar	5.2	RRC－E5
^{56}Fe	5.0	RRC－E5

Radiation safety management at RIBF

Y. Uwamino, H. Sakamoto, R. Hirunuma-Higurashi, H. Mukai[*1], A. Akashio, H. Fukuda, S. Hashiguchi[*2], T. Okayasu, S. Fujita, T. Yamaki, K. Nakano, H. Aiso, K. Igarashi and S. Iizuka

Residual radioactivity at the deflectors of cyclotrons has been measured regularly during maintenance since 1986; the variations in the dose rates of the cyclotrons are shown in Fig. 1. Since 2006, the beam intensity of the AVF cyclotron has been increased for radioisotope production, causing the dose rate to also increase. The dose rate at the RRC has not shown any significant change since 1990, and its value has usually been around 20 mSv/h, except in 2007 and 2009. The dose rate at the SRC rose in 2011, and the value became similar to those at the AVF and RRC. This increase is attributed to a 150-pnA 345-MeV/nucleon ^{48}Ca beam that was used toward the end of 2010. We did not get an opportunity to measure the dose rates at the fRC and IRC in 2011.

The residual radioactivity was measured along the beam lines after almost every experiment. In Fig. 2, spots 1–30, marked with solid circles, denote the locations where high dose rates were observed. Table 1 lists these dose rates and the dates of measurement, beam conditions, and decay periods after the end of operation. The maximum dose rate was found to be 25 mSv/h at point 28, which was observed on the surface of the BigRIPS target chamber.

We continuously monitored the radiation in and around the RIBF by using neutron and gamma area monitors. In 2011, it was very difficult to measure the gamma-ray dose outside the facility, because it was hard to distinguish between the dose due to the fallout of the accident at the Fukushima Daiichi power station and the dose due to the accelerator operation. Therefore, in this report, only neutron dose is discussed.

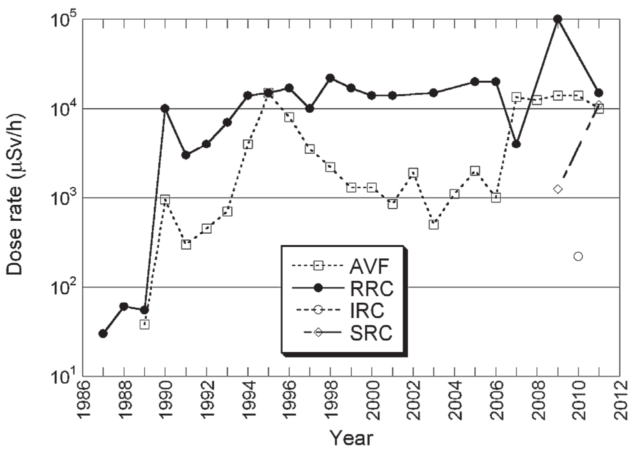

Fig. 1. Dose rates at the deflectors of four cyclotrons.

*1 Japan Environment Research Corporation
*2 Daiwa Atomic Engineering Corporation

No accelerator was operated during the period from August 19 to 25 and August 30 to September 1, and the dose rates during these periods were assumed the result from natural background radiation. The net accumulated neutron dose, i.e., the neutron dose excluding that due to the background radiation, at the site boundary was less than the detection limit, which was assumed to be 2 μSv/y. The gamma-ray dose was always less than the detection limit, which was about 8 μSv/y, if the neutron dose was not detected. The annual neutron dose in 2011 was assumed to be lower than 10 μSv/y, which is considerably lower than the legal limit (1 mSv/y).

Three radiation monitors were placed at the boundary of the radiation-controlled area. One was placed in the computer room of the Nishina building, and the other two were placed on the roofs of the IRC and BigRIPS vaults in the RIBF accelerator building. The highest value of dose rate was observed on the IRC roof; this value, 5.3 μSv/y for neutrons, could be attributed to beam loss in the transport

Table 1. Dose rates measured at beam lines in 2011. Points 1−30 indicate measurement locations shown in Fig. 2.

Point	Dose rate (μSv/h)	Date (M/D)	Particle	Energy (MeV/nucleon)	Intensity (pnA)	Decay period (h)
1	160	7/13	Ne-20	7	570	2088
2	900	7/13	Ne-20	7	570	2088
3	270	7/13	p	14	15000	3753
4	1200	3/1	Fe-56	95	1	135
5	90	3/1	Fe-56	95	1	135
6	130	1/7	Fe-58	63	150	42
7	130	1/7	Fe-58	63	150	42
8	300	1/7	Fe-58	63	150	42
9	1500	7/13	Ne-22	110	360	3437
10	500	2/18	C-12	135	1	22
11	90	2/25	N-14	135	500	284
12	700	2/25	N-14	135	500	284
13	190	12/9	U-238	345	7	32
14	500	12/9	U-238	345	7	32
15	860	12/9	U-238	345	7	32
16	140	6/15	O-18	250	180	78
17	420	6/15	O-18	250	180	78
18	4500	1/18	Ca-48	345	150	480
19	95	6/15	O-18	88	325	77
20	130	6/15	O-18	88	325	77
21	350	6/15	O-18	88	325	77
22	650	6/15	O-18	88	325	77
23	170	6/15	O-18	88	325	77
24	110	6/20	O-18	250	180	197
25	750	6/20	O-18	250	180	197
26	150	6/20	O-18	250	180	197
27	170	6/20	O-18	250	180	197
28	25000	6/20	O-18	250	180	197
29	400	6/20	O-18	250	180	197
30	240	6/20	O-18	250	180	197

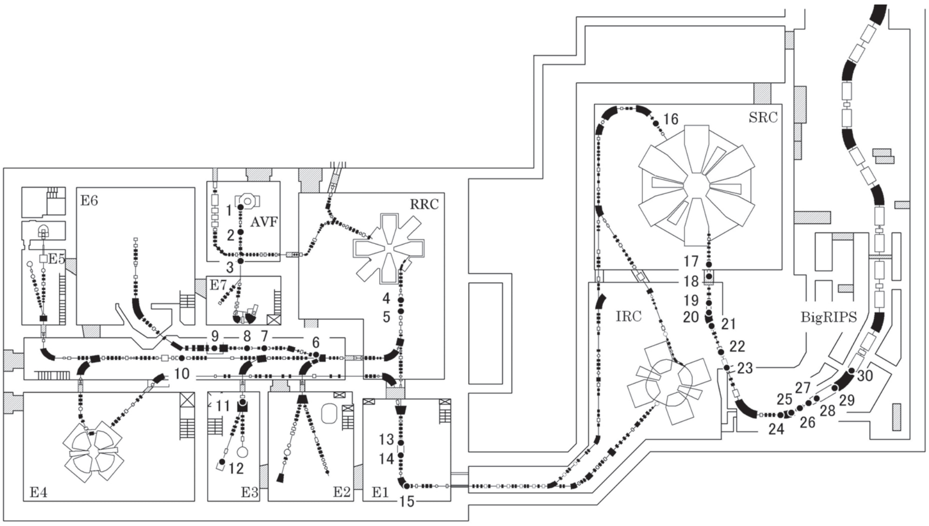

Fig. 2. Layout of beam lines at RIBF. Locations where high dose rate was observed are indicated by solid circles (1–30).

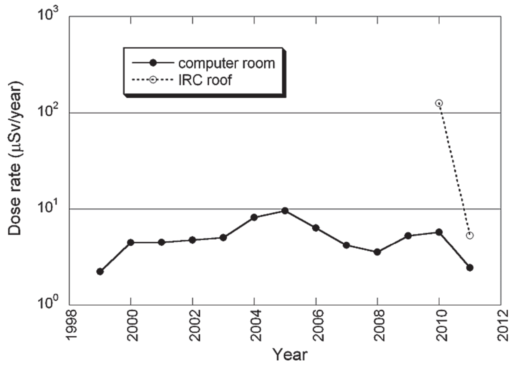

Fig. 3. Accumulated leakage radiation at the boundary of radiation-controlled area.

line between SRC and BigRIPS. The neutron dose in the computer room was 2.4 μSv/y and that on the BigRIPS roof was lower than the detection limit (3 μSv/y). The annual neutron dose at these locations since 1999 is shown in Fig. 3.

Water from the closed cooling systems at the BigRIPS and at the IRC and SRC cyclotrons was sampled after operation involving a 345-MeV/nucleon 150-pnA ^{48}Ca beam in December 2010, and radionuclide concentrations were measured using a liquid-scintillation counter and a Ge detector. The results are listed in Table 2. The sum of the ratios of the concentrations to the legal concentration limits for the drain water of all radionuclides in the BigRIPS exit beam dump was greater than 1/10, and the water was dumped into a drain tank to prevent room contamination in the case of any leakage. The water in the drain tank, which contains drain water from other places too, is released after confirming that the concentration of radionuclides is lower than the legal limit. This confirmation is required by law.

We are also responsible for ensuring safety at the Radioisotope Center, which is used not only by the researchers at the Nishina Center for Accelerator-Based Science but also by researchers from the of Wako campus. We will soon have new researchers from the Brain Science Institute (BSI) since the radioisotope handling facility in the BSI east building will be closed down. Damaged parts of the walls and floors of the evacuated rooms have been repaired, and the wall paper and the linoleum floor sheet have been replaced.

On March 15, 2011, the environment around the RIBF and the Radioisotope Center was contaminated by the fallout of the accident at the Fukushima Daiichi nuclear power station caused by a gigantic earthquake and a subsequent tsunami on March 11. Hence, the radiation-controlled areas in these facilities were much cleaner than the outside and we stopped the ventilation systems and limited personnel access in order to minimize the contamination inside. Owing to these efforts, the contamination on the floors of the facilities was almost negligible. Moreover, the high-sensitivity Ge gamma-ray detectors were protected from contamination.

Table 2. Radionuclide concentration in cooling water of BigRIPS as on June 27, 2011, and SRC as on February 14, 2011, legal limits for drain water, and ratio of concentration to legal concentration limit.

Cooling water	Nuclide	Concentration [a] (Bq/cm^3)	Limit [b] (Bq/cm^3)	Ratio to limit [a/b]
BigRIPS F0 target	H-3	2.0	60	3.3e-2[1)]
	Be-7	1.7e-2	30	5.7e-4
			sum	3.3e-2
BigRIPS exit beam dump	H-3	6.7	60	1.1e-1
	Co-57	1.3e-3	4	3.2e-4
	Mn-54	2.4e-3	1	2.4e-3
			sum	1.2e-1
BigRIPS side-wall beam dump	H-3	3.6	60	6.0e-2
	Be-7	4.3e-2	30	1.4e-3
			sum	6.2e-2
SRC	H-3	0.68	60	1.1e-2
	Be-7	4.3e-3	30	1.4e-4
	Sc-46	8.8e-4	0.6	1.5e-3
			sum	1.3e-2

1) read as 3.3×10^{-2}

Radiation monitoring in the RIBF using ionization chambers

M. Nakamura, H. Watanabe, K. Yamada, H. Okuno and M. Kase

In recent years, we have attempted to monitor the radiation at SRC, RRC, and the beam lines in the beam distribution corridor by using self-made ionization chambers (ICs) for detecting the beam loss at several important components at the RIBF[1-4]. In these experiments, we were able to perform simultaneous measurements of beam loss at each component. Furthermore, we were able to confirm that these results reflected the conditions of accelerator operations such as ion beam extraction, transport, focusing, and other controls[2-4].

For the next stage, we attempted to incorporate the signals from these ICs into the accelerator control system, because in the case of the increase in beam loss, the operation must be ceased to protect the important components from serious damages. For this purpose, we first input an alarm signal from the IC near the electrostatic deflection channel (EDC) of SRC to the beam interlock system (BIS). This is because the EDC is quite an important part of SRC and we frequently experience troubles at the EDC during the acceleration.

The positions, sizes, and experimental conditions of the ICs were described in the previous report[4]. We monitored the radiation during the operation of SRC from October 12 to December 8, 2011. During this period, $^{238}U^{86+}$ was accelerated at 345 MeV/nucleon. We investigated the beam loss at the EDC of SRC using the same method as that described in the previous reports[3, 4]. Based on this result, we calibrated the signal of the IC near the EDC and converted the signal intensity to beam loss, even if the ion beam intensity changed.

We input the alarm signal from the IC to the BIS after the beam intensity became stable. On November 14, the adjustment of accelerator was generally completed and the beam intensity became around 150 enA. Consequently, on November 15, we set the alarm level at 2.5 V. This level corresponded to a beam loss of approximately 93% at the EDC. After a few days, the ion beam current as well as the signal intensity of the IC increased. At 8:47 on November 25, the signal intensity from the IC exceeded 2.5 V, and consequently, an alarm signal was sent to the BIS and the accelerator operation was stopped, as shown in Fig. 1. After the operation was restarted, the ion beam intensity increased further, we disconnected the IC alarm signal from the BIS for a few minutes and continued to monitor the conditions of accelerator operations. After a few days, the ion beam intensity increased to around 260 enA. Therefore, on November 29, to allow the beam intensity to reach up to 300 enA, the alarm level was set at 5 V. This signal intensity corresponded to the beam loss of approximately 93% at the EDC at the beam intensity of 300 enA. After this change, the beam intensity increased to a maximum of 290-320 enA. However, the alarm signal did not reach the BIS and the accelerator operation was not stopped until the end of the $^{238}U^{86+}$ ion beam experiment. This result suggested that the adjustment of SRC was more suitable than at the beginning.

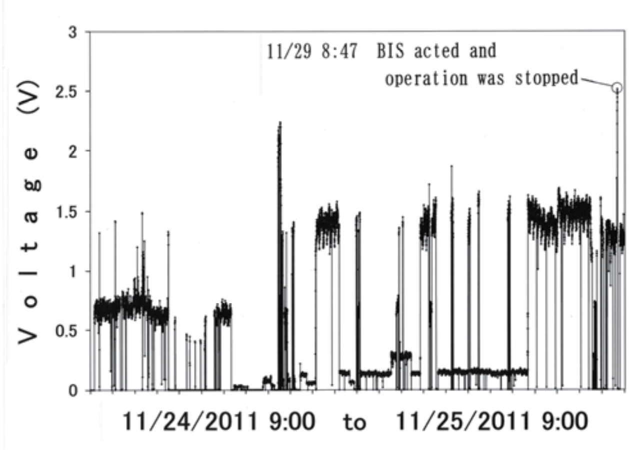

Fig. 1 Signal from the IC near EDC of SRC

After the beam was changed to the $^{48}Ca^{20+}$ ion beam, we set the alarm level at above 90% beam loss at the EDC. This is because in the case of the $^{48}Ca^{20+}$ ion beam acceleration, the thermometer attached to the EDC of SRC generated an acceleration stop signal when a sudden rise of temperature, corresponding to more than 90% beam loss, was detected [4]. From these results, we can state that the IC system can contribute to the safety operation of accelerators. The next issue for study is the decision of the alarm level, which would facilitate more effective accelerator operations. When the alarm level is set too low, the IC system frequently stops the beam acceleration and disturbs the accelerator operation. On the other hand, when the level is set too high, it has no significance to the safety accelerator operation. For this purpose, we have to accumulate the data from the ICs for all the ion beams used in RIBF and to investigate the suitable alarm level for each beam.

References

1) M. Nakamura et al.: RIKEN Accel. Prog. Rep. 42, 141 (2009)
2) M. Nakamura et al.: RIKEN Accel. Prog. Rep. 43, 138 (2010)
3) M. Nakamura et al.: Proc. 7th Annual Meeting of Particle Accelerator Society of Japan, WEPS135, Himeji, Japan.
4) M. Nakamura et al.: RIKEN Accel. Prog. Rep. 44, 293 (2011)

Beam-time statistics of RIBF experiments

H. Ueno and H. Sakai

This report describes the statistics of beam times (BTs) utilized at the RIBF facility. In the following discussion, they are categorized into two groups: high-energy and low-energy mode BTs. In the former, beams were delivered in the acceleration scheme of AVF, RILAC, or RILAC2 → RRC → (fRC → IRC →) SRC, where the accelerators in parentheses can be skipped in the cascade acceleration, depending on the beam used. In the latter, the acceleration scheme is AVF or RILAC (→ RRC).

Immediately after the earthquake that occurred on March 11, 2011, all high-energy mode BTs scheduled for the first half of FY2011 were canceled. The electric power supplied to the Wako campus was placed under the supervision of the Committee for Power Saving Measures at Wako Campus (CPSMWC), established under the RIKEN Emergency Headquarters. In accordance with the decision arrived at by the CPSMWC, the BT in this period was conducted as follows:

i) BTs for which power could be supplied by the CGS were performed, and this included the BTs of the super heavy element (SHE) research and radiation biology researches scheduled in April–September. In the latter BTs, RILAC was used as an injector in lieu of AVF due to a serious problem identified in the AVF cyclotron system in May. All BTs that could not be conducted without AVF were, therefore, canceled until the repair of AVF was completed in September.

ii) Performance tests of the overall accelerator facility, including BigRIPS, ZD, and SHARAQ, under optimized combinations of cyclotrons to achieve the minimum power consumption, were conducted from May to the end of June. Fortunately, no serious damage was reported, although the accelerators up to RRC suffered to a greater or lesser extent.

iii) The accelerators were shut down for three months immediately after ii) except for the SHE and the radiation biology BTs, as mentioned in i).

In the second half of FY2011, under the approval of a power-use plan by the CPSMWC, high-energy mode BTs, which use ^{238}U and ^{124}Xe beams, were scheduled from October to the middle of December after the cooling system of SRC/BigRIPS was started in early September. For these BTs, RILAC2, as well as the 28-GHz Superconducting ECR Ion Source, were first operated for beam deliveries to users. With reference to the restriction of utility-power use, high-energy mode BTs in the scheme of AVF-RRC-SRC were scheduled from the middle of February to the end of March, and these BTs include the first SAMURAI and EURICA commissioning BTs.

The data summary of high-energy mode BTs utilized in FY2011 is shown in Fig. 1 as a bar chart, where the total BTs provided for the experiments to users and those provided for the experiments in the machine-study category are indicated by blue and orange bars, respectively. Further, the BT that was regarded to be effectively used for users' PAC approved experiments, taking into account beam currents and other conditions is shown by solid black lines. The data summary of FY2011 BTs conducted in the low-energy mode is shown in Fig. 2. BTs are classified by the accelerator operation modes AVF, RILAC, and RRC, with their injections. Experiments in which AVF or RILAC was operated in the stand-alone mode were conducted in parallel with the high-energy mode BTs when their cyclotron cascade acceleration did not include such an accelerator as an injector.

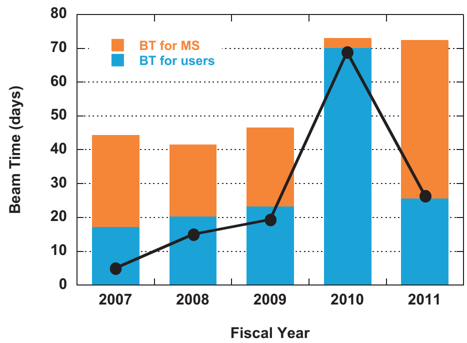

Fig. 1. A bar chart showing the BT statistics for high-energy mode experiments from FY2007 to FY2011. For details, see the text. Note that statistics of both the on-line and off-line operation times for the accelerator conditioning and the BTs during which the accelerators up to IRC were used, are not included.

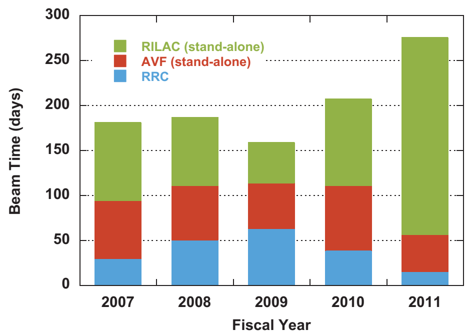

Fig. 2. A bar chart showing the BT statistics for low-energy mode experiments from FY2007 to FY2011.

Program Advisory Committee meetings for nuclear physics, and material and life science

H. Ueno, K. Ishida, Y. Kobayashi, and H. Sakai

Two Program Advisory Committees (PACs) are responsible for reviewing submitted proposals in the fields of nuclear physics (NP-PAC) and material and life science (ML-PAC). The NP-PAC is co-organized by RIKEN Nishina Center and CNS, Univ. of Tokyo. The ML-PAC reviews experimental programs at RAL and RIBF.

NP-PAC

The 9th and 10th NP-PAC meetings were held on June 24 and 25 and on December 9 and 10, 2011, respectively[1]. The acceptance of proposals to use CRIB has been suspended since the 9th NP-PAC meeting. The EURICA project (Euroball RIKEN Cluster Array) will be launched fully in FY2012. The proposals requesting the use of EURICA were first reviewed at the 10th NP-PAC meeting. The new grading scale, introduced at the 7th NP-PAC meeting, was adopted in both these NP-PAC meetings to rank approved proposals as S, A, or B. Table 1 summarizes the outcomes of these two NP-PAC meetings.

ML-PAC

The 8th ML-PAC meeting was held on September 5 and 6, 2011[2], at which seventeen RAL proposals were submitted and reviewed and no RIBF experiments were proposed. The summary of the outcome of meeting is given in Table 2.

PAC members

NP-PAC: R. Tribble (Texas A&M, the chair), R.F. Casten (Yale Univ.), B. Fulton (Univ. of York), T. Glasmacher (MSU), M.N. Harakeh (KVI), M. Huyse (KU Leuven), T. Kishimoto (RCNP), A. Korsheninnikov (Kurchatov Institute), M. Lewitowicz (GANIL), C.J. (Kim) Lister (ANL), T. Nakamura (Tokyo Tech.), A. Ono (Tohoku Univ.), C. Scheidenberger (GSI), T. Shimoda (Osaka Univ.), F.-K. Thielemann (Univ. of Basel), M. Yahiro (Kyushu Univ.), Y. Ye (Peking Univ.)

ML-PAC: J.-M. Poutissou (TRIUMF, the chair), A. Amato (PSI), G.A. Beer (Univ. Victoria), F. Hanaoka (Gakushuin Univ.), R. Kato (RIKEN), K. Komaki (Univ. of Tokyo), K. Kubo (ICU), D.E. MacLaughlin (UC Riverside), S. Maekawa (JAEA), K. Nagamine (UC Riverside, RIKEN, KEK), N. Nishida (Tokyo Tech.), K. Nishiyama (KEK), F.L. Pratt (RAL), I. Yamaguchi (Tokyo Univ. of Agri.), J. Zmeskal (SMI)

Table 2. Summary of the outcome of the 8th ML-PAC meeting.

	8th ML-PAC (September 5–6, 2011)			
	proposal number		beam time (days)	
	requested	approved	requested	approved
RAL	17	17	96	54
RIBF	0	0	0	0
Total	17	17	96	54

References
1) http://www.nishina.riken.jp/RIBF/NP-PAC/index.html
2) http://www.nishina.riken.jp/RIBF/ML-PAC/index.html

Table 1. Summary of outcomes of the 9th and 10th NP-PAC meetings. The sum of the proposals ranked with S, A, and B is listed in the "approved" columns.

	9th NP-PAC (June 24–25, 2011)				10th NP-PAC (December 9–10, 2011)			
	proposal number		beam time (days)		proposal number		beam time (days)	
	requested	approved	requested	approved	requested	approved	requested	approved
GARIS (RILAC)	0	0	0	0	1	0	23	23
RIPS (RRC)	1	0	10.5	0	1	1	9.5	9.5
BigRIPS/ZDS	7	5	42.25	18	22	20	191	166.5
SHARAQ	1	1	4	4	0	0	0	0
SAMURAI	3	3	34.2	15.5	4	2	41.25	15.5
Construction	1	1	–	–	2	2	–	–
Total	13	10	90.95	37.5	30	25	264.75	214.5

Industrial application of RIBF and fee-based distribution of radioisotopes

T. Kambara, A. Nakao, A. Yoshida, H. Haba, J. Kanaya, Y. Wakitani,[*1] S. Yamamoto,[*1] and A. Ohtsubo[*1]

The non academic activities managed by the Industrial Cooperation team of RIKEN Nishina Center (RNC) are described below.

Since 2009, RNC has been running a project named "Promotion of applications of high-energy heavy ions and RI beams" for fee-based use of its accelerator facility. In this project, the old part of the RIBF, including the AVF cyclotron, RILAC, RIKEN Ring Cyclotron, and some experimental instruments such as RIPS, have been made available for non academic proposals from domestic users, including private companies. Beam times are allocated to the proposals approved by a dedicated program advisory committee, Industrial PAC, and the users pay the beam time fee to RIKEN. The users have exclusive ownership of the results and the intellectual properties obtained by the use of RIBF and are not required to publish them. In order to encourage the use of RIBF by those who are not familiar with the utilization of ion beams, the first two beam times in each proposal can be assigned free of charge, i.e., they would be trial uses. To date, the Industrial PAC has met twice and approved five proposals as trial uses, and four beam times have been executed.
In 2011, a proposal titled "Development of wear analysis technique of industrial materials with radioactive beam (Na-22)," had a successful 2.5-day beam time with a ^{22}Na beam of about 25 MeV/nucleon and 1.5×10^8 particle/s produced at RIPS. In October 2011, a new price list that specified the beam-time fee for various acceleration modes was issued. In December 2011, the project website (http://ribf.riken.jp/sisetu-kyoyo/, in Japanese) was updated to provide on overview of the project, the procedure to use the facility, and the reports of the past trial-use results. For inquiries, please contact the team through E-mail (sisetu-kyoyo@ribf.riken.jp).

The team also handles fee-based distribution of radioisotopes (RIs) produced at RIBF to users in Japan. The project was started in October 2007 in collaboration with the Japan Radioisotope Association[1)] (JRIA), which is an organization to support the utilization of RI in Japan. According to a Material Transfer Agreement between JRIA and RIKEN, JRIA mediates the transaction of the RIs and distributes them for a fixed fee to users. The distributed RIs are ^{65}Zn ($T_{1/2}$ = 244 days), ^{109}Cd ($T_{1/2}$ = 463 days), and ^{88}Y($T_{1/2}$ = 107 days) produced by the RI Applications Team with a 14-MeV proton beam from the AVF cyclotron. Although ^{65}Zn and ^{109}Cd have a small but continuous demand in Japan, their commercial supply terminated in 2007, and RIKEN was expected to fill the gap. We also commenced the distribution of ^{88}Y in 2010, expecting that it would be useful in development of nuclear medicine with ^{90}Y.
In 2011, we delivered six shipments of ^{109}Cd with a total activity of 41 MBq and 12 shipments of ^{65}Zn with a total activity of 62.1 MBq. The final recipients of the RIs were six universities and three research institutes. Compared with 2010, the amount of ^{109}Cd distributed in 2011 was higher by about 35% (30 MBq in 2010) and the amount of ^{65}Zn was lower by about 54% (136.1 MBq in 2010). The RI production at the AVF cyclotron was suspended after the earthquake on March 11 until the end of September. Due to the shortage of stock, the distribution of ^{65}Zn was suspended from the middle of August and that of ^{109}Cd from the middle of September, until the beginning of November when they were resumed. The three months of suspension may have contributed to the decrease in the amount of distributed ^{65}Zn. Figure 1 shows the yearly trends of the amounts of the distributed RIs. Data about ^{88}Y is not included because we have not yet accepted any order for it.

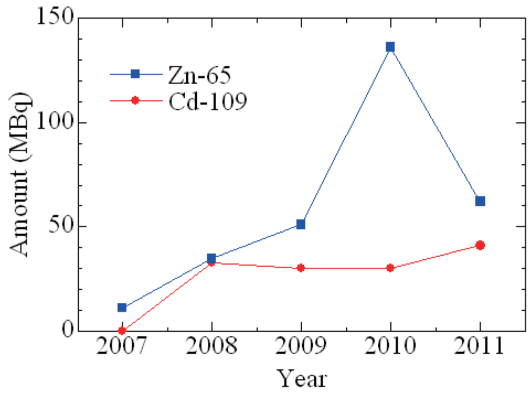

Fig. 1. Amounts of ^{65}Zn and ^{109}Cd distributed yearly from 2007 to 2011.

Information on the RIs can be obtained from JRIA through its dedicated website (https://www.j-ram.net/jram/DispatchTopPage.do; in Japanese), FAX (03-5395-8055), or E-mail (gyomu1@jrias.or.jp).

References
1) http://www.jrias.or.jp/index.cfm/1,html (Japanese), http://www.jrias.or.jp/index.cfm/11,html (English).

*1 Japan Radioisotope Association

Electricity situation of Wako campus in 2011

T. Fujinawa, E. Ikezawa and M. Kase

The monthly power consumption data for RNC (RIKEN Nishina Center) and the enology supply by CGS[1] (Co-Generation System) table are shown in Fig.1 for 2011 and in Fig. 2 for 2010. The total annual data are listed in Tabe1. The total power consumption of RIKEN Wako campus in 2011 was 115,552 MWh, which is lower than that in 2010 by 14%. On the other hand, the total power consumption of RNC in 2011 was 67,176 MWh, which was almost the same as that in 2010.

The electrical power stipulated in the FY2011 electricity contract between RIKEN and TEPCO (Tokyo Electric Power Co.) was reduced from 22.5 to 22 MW, considering the power consumption from TEPCO in the previous year. The maximum power supply to Wako campus from TEPCO had reached 21 MW with the CGS output of 6.46 MW on July 28, 2010, when the RIBF experiments using the oxygen (^{18}O) beam were conducted.

When discussing the power situation in 2011, it is imperative to mention the serious consequences of the Fukushima Daiichi nuclear disaster, which led to a serious power shortage not only affecting TEPCO but also the entire country, particularly during summer In summer 2011, RIKEN was officially required to save electricity by 15% （equivalent to 3.3 MW） of that in the contract for the Wako campus.

Since RIKEN's Energy Saving Committee decided to reduce power consumption by 25% (an additional 10%) almost full time, it became extremely difficult to operate the accelerators in RIBF.

According to the Special offer by TEPCO, which aimed for reduce power consumption by not less than 30% between 13:00 to 17:00 on specific days, when the general power consumption is predicted to be very high, RIKEN successfully managed to reduce power consumption by 49% on average in the corresponding slots. The number of these specific days was 68 in 2011 (usually around 16), resulting in a large profit for RIKEN.

After March 11, the day of the earthquake, CGS continued (its unhindered operation). The periodic inspection of 8,000 hours scheduled in August was postponed to January, 2012. As a result, the output power of CGS increased in 2011 by more than 50% as compared to that in 2010. Due to many difficulties, the operation of the accelerators was reduced to a minimum during the first half of the year. However, with the commencement of the RIBF experiments in early October, the power consumption increased in autumn, as shown in Fig. 1.

Reference

1) T.Fujinawa and Y. Yano: J. Particle Accelerator Society of Japan Vol.8,No.1,2011(18-25)

2) T.Fujinawa: RIKEN Accel.Prog.Rep.44(2011)

Table 1 Energy particular in 2011

2011	Total	Unit	Note
Wako ele.	115,552	MWh	All Wako-campus electric power from TEPCO
RNC ele.	32,088	MWh	RNC electric power from TEPCO
CGS e-output	35,089	MWh	CGS electrical power output
RNC e total	67,176	MWh	RNC total electric power
CGS thermal	45,205	tons	RNC thermal power

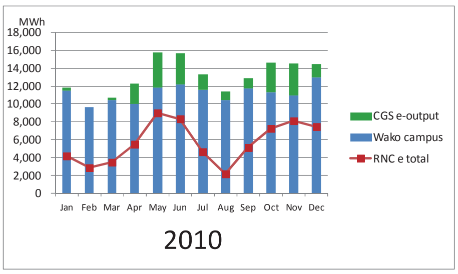

Fig.1 Electrical consumption in 2010

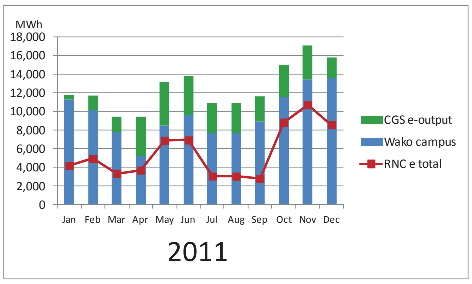

Fig.2 Electrical consumption in 2011

Construction plan for new co-generation systems

T. Fujinawa

1. RIKEN Wako campus

After the Fukushima Daiichi nuclear disaster, RIKEN Nishina Center (hereinafter referred to as RNC) promptly came up with a plan for the construction of a new co-generation system[1)] (CGS) with a capacity of 5 to 10 MW of electrical output. In the end, we came to the conclusion that by setting up a 6 MW-class gas engine (GE) in the No.2 high-voltage substation of the 2nd bank, the existing facilities will be effectively utilized (Fig.1). The plan called for the operation of the system to commence next summer. However, the Facilities and Utility department rejected the plan and instead a contract to set up two units of GE with a capacity of 1.5 MW each, to be commissioned in the fall of 2012. The new system will be set up in the south area of Wako campus.

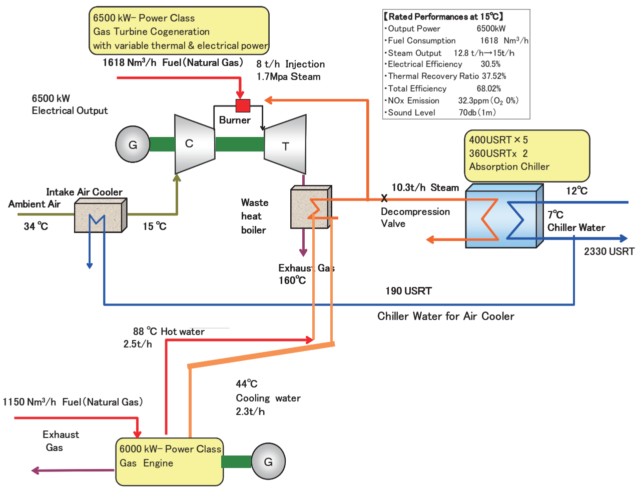

Fig.1 New CGS plan by RNC

2. National Institute of Radiological Science (NIRS)

At the request of NIRS, RNC cooperated in preparing CGS plan to construct a GE with a capacity equivalent to 6 MW, on the roof of HIMAC Apparently; NIRS needs RNC's know-how and experience about CGS operation in an accelerator facility.

Moreover, the plan requires that all refrigerating machines showing age-related degradation to be replaced with absorption chillers and that a CGS be used as an uninterruptible power supply system (UPS).

Regrettably, this plan had to be cancelled since it was not approved by the Ministry of Education, Culture, Sports, Science and Technology.

3. International Linear Collider project (ILC)

High Energy Accelerator Research Organization (KEK) requested RNC to draft a power supply plan for using CGS for the ILC. The primary plan is as follows:

There are two proposed sites for ILC, one in Iwate Prefecture with 50-Hz and 154-kV power supply and another in Saga Prefecture with 60- Hz and 220- kV.

Five sets of transformers with a capacity of 50 MVA each and medium voltage of 11 kV class will be set up. For low voltage, single-phase 220/105 V, three-phase 220 V, and 415 V four-wire systems will be provided. MV/LV transformers are dry-type 2-MVA, and by alternating the star-delta and delta-delta windings, harmonic currents will be reduced.

The gas turbine generator for a CGS with a capacity of 27 MW and air-compression ratio of 0.21 MPa is selected. Two CGS plants are scheduled to be constructed as UPS.

Reference

1) T.Fujinawa and Y. Yano: J. Particle Accelerator Society of Japan Vol.8,No.1,2011(18-25)

Operation of SRC Cryogenic System

H. Okuno, T. Dantsuka, Y. Mori,[*1], A. Mikami,[*1], M. Ohshima,[*1], R. Ise,[*1], T. Suzuki,[*1], K. Yamamoto,[*1] Y. Teduka,[*1] and S. Watanabe[*1]

[Superconducting ring cyclotron, cryogenic, He refrigerator]

The SRC cryogenic system, which consists of three compressors, a He refrigerator, and four He buffer tanks for cooling the 240-MJ superconducting magnets used for the SRC, has a cooling capacity of about 1 kW and an inventory of 5000 l liquid He. The cooling system was operated for around 6 months in 2011, with a 2-month maintenance shutdown in summer (July–August) and two shutdowns due to unforeseen issues, as shown in Fig. 1. The trend observed for the main coil current of the SRC sector magnet is also shown in this figure.

The first unforeseen issue was the earthquake that occurred on 3/11. Figure 2 shows the liquid helium level in the control dewar for the SRC when the earthquakes occurred. Obviously, liquid helium is shaking with the width of 1% , although the cooling system itself showed no damage due to the earthquake. It corresponds to about 20 l. We started the recovery of the liquid helium from the superconducting magnet immediately after the earthquake. The liquid helium level was recovered to the operational level on 5/11.

The other issue was the breaking of a controller of the cryogenic valve. Unfortunately, the valve was located at the inlet of the first turbine that defines the total flow rate through the helium refrigerator. Consequently, the entire cooling system became unstable, as shown in Fig. 3; finally, three of the four turbines were tripped.

Presently, we are suffering from a small continuous leak of He gas from the closed cycle of the cooling system. The leak rate is about 1 m^3/day. Subsequently, we need to refill about 300 m^3 of He gas in the system once every two months. We are continuously searching the point of the leak but have not found it yet.

*1 Nippon Kucho Service Co., Ltd

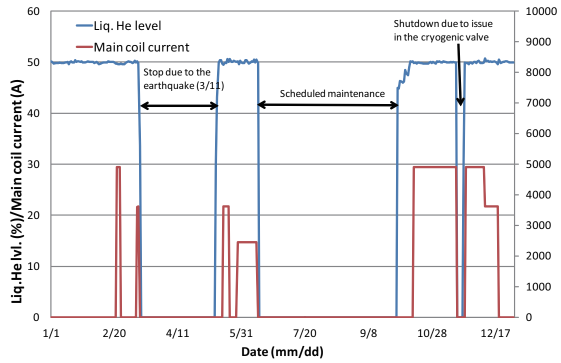

Fig. 1. Trend observed in liquid He level in the dewar and main coil current for the SRC superconducting sector magnet.

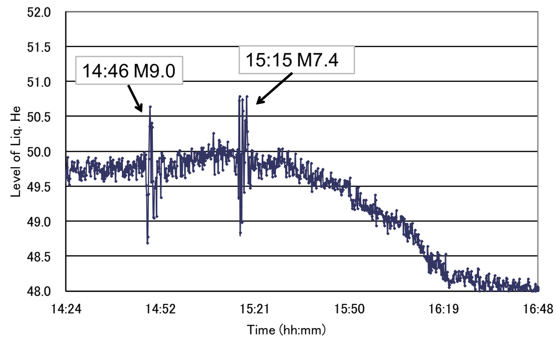

Fig. 2. Liquid helium level during the earthquake on 3/11/2011.

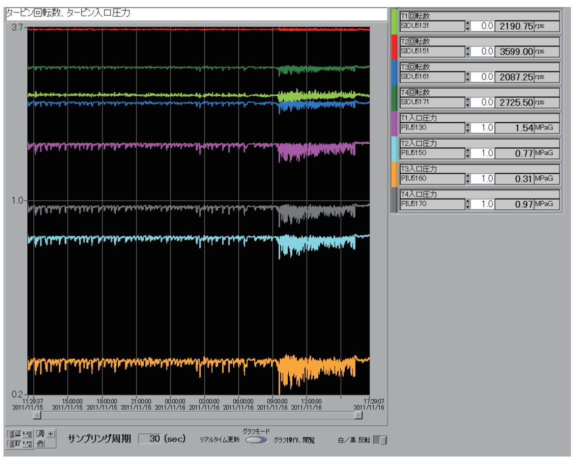

Fig. 3. Fluctuation of the rotation speed and inlet/outlet pressure of the expansion turbines in the He refrigerator at the time of the issue with controller of the cryogenic valve.

Present status of STQ system in BigRIPS and RI-beam delivery line

K. Kusaka, M. Ohtake, T. Kubo, K. Yoshida, T. Ohnishi, Y. Mori[*1], R. Ise[*1], M. Ohshima[*1], T. Suzuki[*1], K. Yamamoto[*1], S. Watanabe[*1], Y. Tezuka[*1], A. Mikami[*1], H. Ito[*2] and T. Tsuchihasi[*2]

The BigRIPS separator and the RI-Beam delivery line are characterized by the superconducting triplet quadrupoles (STQs).[1)] While the five STQs (STQ1-STQ5) in the first stage of the BigRIPS are cooled by a liquid helium cryogenic plant[1)], all the STQs in the second stage of the BigRIPS (STQ6-STQ14) and the RI-beam delivery line (STQ15-STQ23) are cooled by a stand-alone refrigeration system with small cryocoolers on their cryostat.[1,2)]

STQs with small cryocoolers are characterized by their large cold mass and small 4 K heat-load. Each STQ consists of three cold-iron quadrupoles with pole-tip radius of 170 mm and yoke radius of 480 mm. The nominal effective lengths of the quadrupoles are 500 (Q500), 800/1000 (Q800/Q1000), and 500 (Q500) mm, respectively. They are rigidly connected and installed in the helium (He) vessel to ensure that the total 4 K cold mass weighs more than 8 t. The superconducting coils together with iron yokes are cooled by liquid helium bath method in the He vessel and the total 4 K heat load of the system is less than 2 W.[3)]

Two small cryocoolers are mounted on the STQ cryostat. One is a Gifford-McMahon cooler that uses a Joule-Thomson expansion (GM/JT) to cool the He vessel with a cooling capacity of 2.5 W at 4.3 K. It liquefies He gas that evaporates in the He vessel with the recondensing heat exchanger unit. The other is a Gifford-McMahon (GM) cooler, which cools high-T_c superconducting power leads (PL) and a shield surrounding the He vessel. Detail on the cryostat design can be found in ref. 3.

After the precooling operation, which is performed by transferring 3000~5000 L of liquid nitrogen and ~2000 L of liquid helium into the He vessels for each STQ,[4)] two small cryocoolers maintain the liquid helium level in the He vessel, in order that the superconducting coils are well cooled in the liquid helium bath. All the STQs are successfully operated in the beam time periods.

Most of the cryocoolers have been continuously operated since 2006 to maintain the liquid helium levels in the STQ cryostats. The operation time of the cryocoolers is longer than 60,000 h for STQ6-STQ15, and 45,000 h for STQ16-STQ23. A regular maintenance of the GM/JT and GM coolers is indispensable for continuous long-term operations. JT-line flushing, which is performed every year, is one of the most important maintenance tasks for the GM/JT cooler and it reduces impurity concentrations in the JT circuit. Until 2009, JT-line flushing was performed by dismounting the GM/JT cooler from the STQ cryostat to warm up the helium circuit in the cooler. In 2010, a "heater-bar" maintenance method was introduced, in which the JT line is flushed without dismounting the cooler from the cryostat. The heater bar, installed in the displacer-cylinder, warms up the JT line in this method. This method greatly reduces the helium loss from the He vessel during the maintenance period. In addition to JT-flushing, all the displacers of the GM/JT and GM coolers are replaced every year.

Figure 1 shows a long-term trend of the GM head temperature and that of the power lead (PL1) in the STQ13 cryostat as an example. Blue arrows indicate when the scheduled regular maintenances of the GM cooler were carried out. The coolant gas charge to the GM compressor is also shown by the green arrows, and the discharge (P_H) and suction (P_L) pressures of the compressor are also plotted. A gradual increase of the GM head temperature between the maintenances indicates the importance of the periodic maintenances. From January to May in 2011, the GM head temperature increased rapidly and the coolant gas charge did not work, and consequently, we were forced to perform an unscheduled maintenance (shown as a red arrow) on May 24, 2011. We have not been able to determine the reason for the degradation of the cooling capacity yet.

References
1) T. Kubo et al: IEEE Transactions on Appl. Supercond., Vol. 17, 1069 (2007).
2) K. Kusaka et al.: IEEE Transactions on Appl. Supercond., Vol. 14, 310 (2004).
3) K. Kusaka et al.: RIKEN Accel. Prog. Rep. 41, 246 (2008).

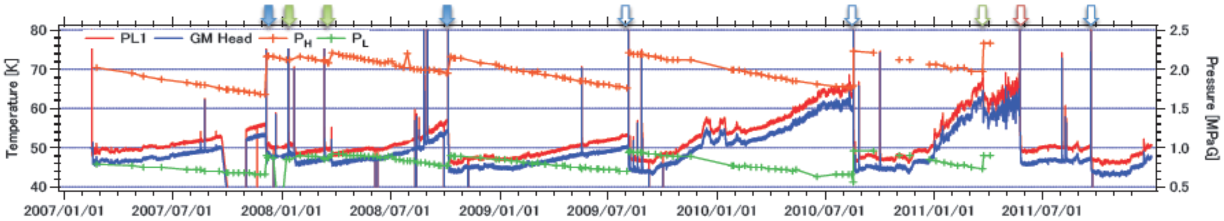

Fig. 1 A long-term trend of the GM head and the power lead (PL1) temperature of STQ13. The discharge and suction pressures of the GM compressor, denoted by P_H and P_L, respectively, are plotted using the pressure axis, shown to the right.

*1 Nippon Kucho Service Co., Ltd.
*2 Toshiba Corporation

Present status of liquid-Helium supply and recovery system

T. Dantsuka, H. Okuno, Y. Odashima, M. Nakamura, T. Maie, K. Kato, K. Ikegami, M. Kase, S. Tsuruma, M. Ohshima*, R. Ise*

The liquid-helium supply and recovery system[1], which can produce liquid helium at a rate of 200 L/h from pure helium gas, has been stably operated since the beginning of April 2001. The volumes of liquid helium that were supplied each year from 2001-2010 are shown in Fig. 1. The volume gradually increased from 2001 to 2008 but sharply decreased in 2009, before again increasing sharply in 2010.. In particular, the Surface Chemistry Laboratory had stopped using liquid helium by the end of September 2009, but instead the Surface and Interface Science Laboratory had started using it.

We extended the recovery pipe at one location. A new recovery pipe was connected to the existing pipe at the Nishina Building at B2F.

The control system of the compressor for liquefying helium gas tripped several times between December 2009 and February 2010. This tripping may have been caused by the temperature of the cooling water; we are investigating the cause presently.

The purity of helium gas recovered from laboratories gradually improved once the construction of the system was completed. The volume of helium gas recovered from each building in the Wako campus and the volume transported to the liquid-helium supply and recovery system were measured. The recovery efficiency, which is defined as the ratio of the amount of recovered helium gas to the amount of supplied liquid helium, was calculated. The recovery efficiency for the buildings on the south side of the Wako campus, such as the Cooperation Center building of the Advanced Device Laboratory, the Chemistry and Material Physics building, and the Nanoscience Joint Laboratory building, increased to a value above 90%. The average recovery efficiency from January 2008 to July 2011 is shown in Fig. 2. It also increased to a value above 90%.

References

1) K. Ikegami et al.: RIKEN Accel. Prog. Rep. 34, 349 (2001).

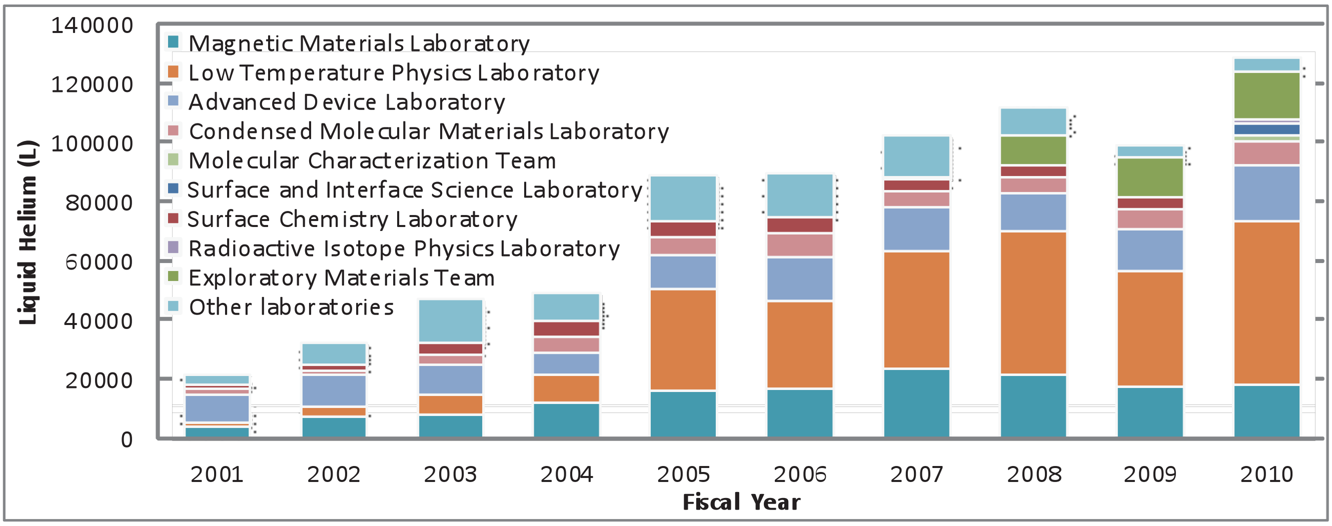

Fig.1. Volumes of liquid helium supplied to laboratories for each fiscal year from 2001 to 2010

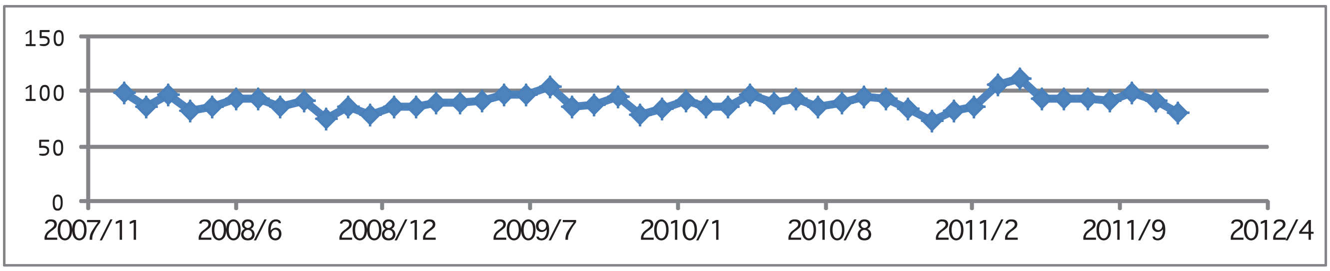

Fig.2. Average recovery efficiency measured from January 2008 to July 2011

* Nippon Air Conditioning Service K.K.

V. FUKUSHIMA SURVEY
& RELATED RESEARCH

Preface to Special Section

Our Mission as Nuclear Physicists

On March 15th, 2011 at 10:00 am, high radiation level shown on the monitor prevented a radiation worker to leave the controlled area of the Nishina RI Beam Factory (RIBF), followed by many others who encountered the same problem. We soon realized that a high level of radioactivity did not originate from anything indoors but already existed outdoors (the radioactivity inspection is usually performed only at an exit). Ironically, the fallout from the Fukushima Dai-ichi Nuclear Power Plant made the controlled area of our accelerator facility the least contaminated place in the Wako campus of RIKEN.

For older generation, this situation wasn't new. Many years ago, atmospheric nuclear-bomb tests that took place overseas caused fallout to drift over to Japan that led to the similar radioactive situation observed in the Japanese accelerator facilities. This time, however, the fallout was due to the nuclear power plant disaster.

We gathered in the radiation proof control room of RIBF, and watched the monitoring posts to assess the situation. Then, we decided to upload the logged data to RIKEN's public website, and began taking several other measurements to determine the radioactive nuclear species of the fallout. While desperately hoping that the situation would not worsen, we convened special meetings every week to exchange latest knowledge and information.

The Nishina Center also functioned as the base to send radiation surveyors to Fukushima's affected area to measure the dosage of bodies, clothes, furniture, cars and any items that the refugees had with them. At the beginning, it was tough since no public transportation was available. Even in such dire situation however, it was very remarkable that many nuclear physicists from all over Japan joined to conduct this survey. Later as a follow-up, we joined the large-area soil survey initiated by the Research Center of Nuclear Physics of Osaka University and the Center of Nuclear Study of the University of Tokyo.

This special section of the Accelerator Progress Report records the works we were involved in 2011 in the aftermath of the Fukushima nuclear disaster. The Nishina Center is the largest Japanese research institute for nuclear physics, and our RIBF was built to study the nuclear synthesis at the beginning of the universe. Nuclear fuel is a gift from the nuclear synthesis, and atomic energy is the most important social application born from nuclear physics. As nuclear physicists, many of us feel that we could not escape from original sin for creating the world that led to the Fukushima nuclear accident. We have therefore done whatever we could as radiation workers with expertise in nuclear physics to deal with the aftermath of the disaster.

Yet what we were able to do and achieve were very limited in the face of nuclear crisis of such magnitude, we hope from the bottom of our hearts a swift recovery from the tragedy and that this kind of tragedy will never happen again.

Hideto En'yo
Director,
RIKEN Nishina Center for Accelerator-Based Science

Diffusion of radioactive materials from Fukushima Daiichi Nuclear Power Plant detected by gamma-ray measurements on expressways†

H. Matsumura[*1], K. Saito[*1], J. Ishioka[*2] and Y. Uwamino

The accident at the Fukushima Daiichi Nuclear Power Plant caused by the enormous earthquake and subsequent tsunami on March 11, 2011, scattered a large amount of radionuclides in the Tohoku and Kanto areas. On the request of the Ministry of Education, Culture, Sports, Science and Technology, we visited Fukushima city on March 14, and we were asked by the Fukushima prefectural government to measure the dose rates along expressways in Fukushima prefecture.

By using an NaI(Tl) scintillation survey meter and a $LaBr_3$ γ-ray spectrometer, whose energy resolution is significantly superior to that of NaI(Tl), we measured γ-rays along the roads, shown as thick lines in Fig. 1, on March 15−17 and April 8.

As an example, the measured data on the Tohoku expressway are shown in Fig. 2. As indicated by the open squares, when we started measurements in Fukushima city at 1:33 p.m. on March 15, the dose rate was less than 0.1 μSv/h, which was the dose rate of the natural background. A radioactive plume that contained ^{133}Xe, ^{132}Te, ^{132}I, ^{131}I, ^{134}Cs, and ^{136}Cs was first observed at the Koriyama-Higashi interchange at 3:25 p.m. We measured dose rates in Iwaki city, and found them to be approximately 2 to 3 μSv/h. However, when we returned to Fukushima city at 8 p.m., we found the city to already be polluted by as much as approximately 10 μSv/h.

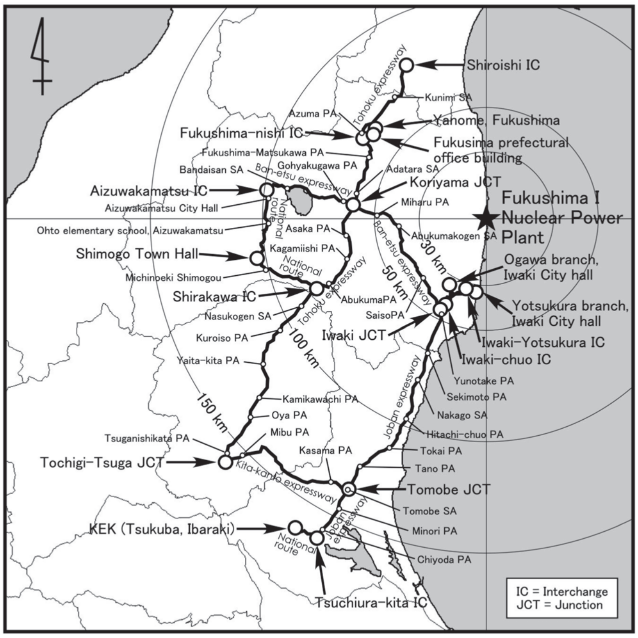

Fig. 1. Route map of the gamma-ray measurements.

On March 16, the dose distributions in south Fukushima and the Aizu area were measured. The dose rate at Shirakawa interchange, which is the southern end of Fukushima, was 4.6 μSv/h at 2 p.m.; however, it was lower than the 1 μSv/h dose rate measured in southern Aizu. In Aizuwakamatsu city, the dose rate was approximately 1−2 μSv/h.

The dose distribution till the Ibaraki prefecture was measured on March 17. The dose rate in Fukushima prefecture was similar to that measured on March 15 and 16. The dose rate remained high outside Fukushima prefecture and was higher than 1 μSv/h up to the Yaita-Kita parking area in Tochigi prefecture.

The dose rate distribution was measured again on April 8 from Ibaraki prefecture to Miyagi prefecture, and it was found that the relative distribution had not changed. The attenuation of the absolute value was explained as the decay of radionuclides that were detected by the γ-ray spectroscopy. This implied that for the measured area, most of the radioactive material was deposited with the rain on March 15, that it did not move from the initial location, and that there was effectively no additional deposition of radioactive material after March 15.

Although the dose rate distributions of ^{132}Te, ^{132}I, ^{134}Cs, ^{136}Cs, and ^{137}Cs were similar, the distribution of ^{131}I was different from those of the others. The dominant nuclides in terms of the dose rate were ^{132}Te and ^{132}I for the March 15 to 17 measurements and ^{134}Cs and ^{137}Cs for the April 8 measurements.

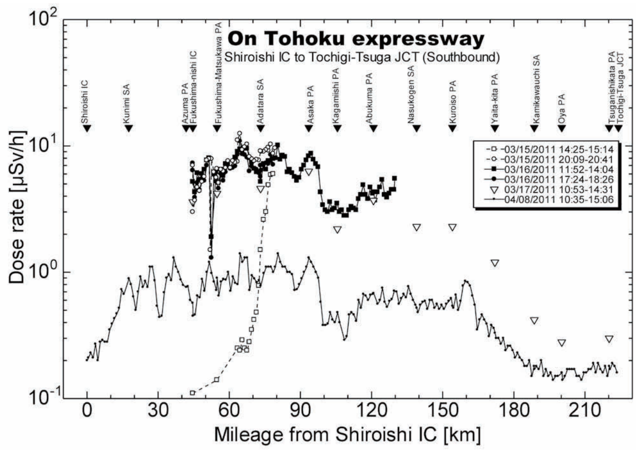

Fig. 2. Comparison of distributions of the dose rate measured along Tohoku expressway, from the complete measurement series.

† Condensed from the article in Transactions of the Atomic Energy Society of Japan **10**, 152 (2011), in Japanese.

*1 High Energy Accelerator Research Organization
*2 Safety Division, RIKEN

Radiation screening of evacuated people in Fukushima

N. Aoi, H. En'yo, T. Fujinawa, H. Hasebe, K. Ikegami, T. Kambara, Y. Kanai, M. Kase, I. Nakagawa, H. Onishi, H. Otsu, H. Sakai, A. Taketani, H. Ueno, M. Wada, Yu. Watanabe

Immediately after the accidents of the Fukushima Daiichi nuclear power plant in March 2011, the experimental nuclear physics society organized a collaborative effort to aid evacuated people in Fukushima. The joint action was initiated by RNC together with RCNP, Osaka University, and was supported by the crisis management team of RIKEN and the MEXT. In the early stages, RNC served as a logistics base for the detachments from west Japan. Since public transportation to Fukushima was disrupted and gas supply was limited, we could only access Fukushima using automobiles with special permission from the police. The effort commenced on 21st March and was conducted continuously till May end and intermittently till early August. In total, RNC contributed 103 man-day to the effort, which was about 28% of the total contribution from the nuclear physics society team.

The team worked together with many other teams from different organizations such as universities and local autonomous bodies under the medical team of Fukushima prefectural government, which was supported by the Radiation Emergency Medical Assistance Team (REMAT) from National Institute for Radiological Science. All teams would assemble at the temporary Fukushima prefectural office in Fukushima city and were assigned the next day's tasks. The screening center for the evacuated people were scattered throughout the Fukushima prefecture, and the participants from RNC visited the centers in Koriyama-city, Kawamata-town, Yamakiya-chiku in Kawamata, Nakoso in Iwaki-city, and Tamura-city for the early emergency screening. Since late May, we have also contributed to the screening of residents within 20 km of the power plant who temporarily visited their home town. The base stations for the temporary visits were Bajikoen in Minamisouma-city, Hirono-town, and Hurumichi in Tamura-city.

In the end of April, the nuclear physics society team submitted a written proposal to the Fukushima prefectural government, outlining their suggestions on how best to conduct the screening activity.

Fig. 1. Screening of local citizens at Kawamata public health center on 24th March.

Many in the RNC staff were also very supportive of our efforts, in particular, the members of the administration office of RNC led by Mr. S. Asakawa. Some participants from RNC reported their experiences during the support work in Ref. 1, and in the following.

T. Fujinawa: I participated in the screening over three separated periods: late March to early April, May, and late July to early August. In late March, I had to drive a car from Wako to Fukushima to transport colleagues from Osaka and Kyushu. The highway was damaged by the earthquake, which made it difficult to drive a car. Access to Fukushima improved drastically once the Tohoku Shinkansen restarted operation on 29th April.

I participated in the emergency screening of evacuees at Big-palette in Koriyama but none of them exceeded the official reference level of 13 kcpm; however, I advised the residents to wash their hands and shoes, and gargle frequently, because many of them showed more than our standard level. In the early stages, the food supply at the hotel was limited and the temporary office would run short of copy paper. We brought many boxes of paper, batteries for survey meters, disposable body warmers, as well as our own food. The situation there changed with every visit I made. In August, only a few volunteers from our team remained, but much work had yet be done; I was even asked to stay longer. All of us hoped that the lives of those in the stricken area would soon return to normalcy.

H. Otsu: On March 28, I visited Kawamata public health center, where our team was conducting an emergency survey as well as thyroid gland screening for children. The radiation dose rate outside the building was 3 μSv/h, and ^{131}I had been found to be the main component. The radiation dose rate inside the building at 9:30, the beginning of the screening was 0.1 μSv/h and gradually increased as people entered and exited. About 500 people underwent surface screening and 230 children underwent thyroid gland screening. Almost the same number of people visited on March 29. Kawamata is located between Fukushima Dai'ichi nuclear power plant and Fukushima city. Hence, a variety of people, not only residents from towns near the power plant, such as Namie, but also prefecture officials, self-defense personnel, police, and radiation inspectors, passed through this screening center.

Surface survey were performed on the upper body, lower body, stomach, back, arms, legs; and soles of shoes using a GM survey meter. If the count rate was more than 100 kcpm, we asked the self-defense personnel to wash the entire body, while if the count rate was more than 13 kcpm, we cleaned the contaminated part with a wet tissue or flowing water.

Even with high radiation doses outside, the surface of the cloths were not so contaminated. The count rates were 200∼500 cpm, almost equivalent to the room background in that area. High contamination was sometimes found on the soles of shoes. In one instance, the backs of a lady's shoes showed a count rate exceeding the reference level. We accompanied her while she washed them under flowing water, but this was in vain, because even after washing, the counting rate was not significantly reduced. We advised her to let us dispose of them. The self-defense office gave her a pair of sandals, which the Crocs company provided. Subsequently, we noticed that the adhesion of contaminants to polyvinyl acetate was much lower than that for other materials such as polyvinyl chloride.

In an exception, high count rate of 4 kcpm was detected on the upper body of a fire fighter in Namie town. He continued to work and provide water and treat the bodily wastes of people who had been evacuated from towns near Namie. He had to handle water hoses with his hands, and his upper jacket was contaminated. We advised him to take off the jacket outside the entrance of his house and not wear it indoors to reduce the contamination in residential spaces.

As mentioned above, one of the key points we focused on was the soles of shoes. We had the choice of recommending that they be disposed of. However, a girl of the same age as my daughter told me before being surveyed that her shoes were a birthday present from her grandmother. I held my breath while surveying her from top to her shoes. The count rate of her shoe soles was about 1 kcpm, much lower than the first reference level. I could just advise her mother to keep them outside the entrance and to wash hands every time when she came back to home.

During that time, I read a local newspaper every morning in order to gauge residents' mood as well. The anger of the people of Fukushima was evident there. However, although many would express their anger, there were also many who kept calm and tried to keep themselves informed about the radiation situation as much as possible. I admire their behavior.

M. Wada: An important task in the first weeks after the explosion was to investigate the radioactive iodine concentration in the thyroid gland, in particular for children. Together with other teams, we surveyed several hundred people and found that no one exceeded the official limit. The survey was performed in a relatively low background environment in the center with a NaI(Tl) scintillation survey meter. However, the background level was much higher than ordinary and the statistical treatment in the survey meter was not sufficient to avoid criticism afterwards. We could have taken more precautions during the measurements. For example, using a simple metal tube to cover the sides of the detector could have reduced the background rate significantly and the use of a simple scaler, which can count the number of pulses, could have afforded the results with much higher statistical accuracy.

In the later stages, we encountered few cases where the contamination of the body surface exceeded the reference levels, which coincided with increased demands to survey food, drinking water, soil in rice fields. However, screening of such materials was not an official mission and there were no suitable detectors for such purposes at the screening center. Occasionally, we received some samples and performed measurements at RIKEN with HPGe spectrometers. We found that the drinking water in the wells, including a well in Nagadoro-chiku of Iitate-mura which was known as a highly contaminated area, were clean from radioactive iodine or cesium at all. The soil in the rice filed was highly contaminated, but the water in the rice fields was also as clean as drinkable level. However, we did not have an official channel through which we could convey such information. We could only inform prefectural officers on the next visit. When the surfaces of vegetables were highly contaminated, we could detect using a GM survey meter, however, the sensitivity was much lower than the reference level of 500 Bq/kg. If we could have taught the residents a simple ashing method[2], they could have prepared the concentrated samples at home, which could have been easily tested at the screening center. Unfortunately, we were not aware of this simple and sensitive method at that time.

Overall, we did contribute some extent; however, we served more as radiation workers. As researchers, we could have worked towards finding better solutions to the problems and contributed in a more organized way.

Fig. 2. Screening of thyroid of local children at Yamakiya community center on 24th March.

References
1) H. Hasebe, J. Particle Accelerator Society of Japan, **8**, No. 3, (2011) 132-136.
2) M. Wada et al., Acc. Prog. Rep. 45 (2012).

Gamma-ray dose resulting from the accident at Fukushima Daiichi Nuclear Power Plant, as measured by the radiation monitoring posts in Wako campus

H. Mukai, S. Hashiguchi, H. Sakamoto, A. Akashio, R. Higurashi-Hirunuma and Y. Uwamino

A large heavy-ion accelerator complex, RIBF, and the Radioisotope Center are used in the RIKEN Wako campus, and the dose rates at the site boundary are continuously measured by six radiation monitoring posts, as shown in Fig. 1.

In March 2011, a magnitude-9.0 earthquake and a subsequent severe tsunami occurred, and huge amounts of radionuclides were released from the Fukushima Daiichi Nuclear Power Plant. Plumes containing radionuclides from the power plant passed over the Wako campus several times in March, and some amounts of radionuclides were deposited.

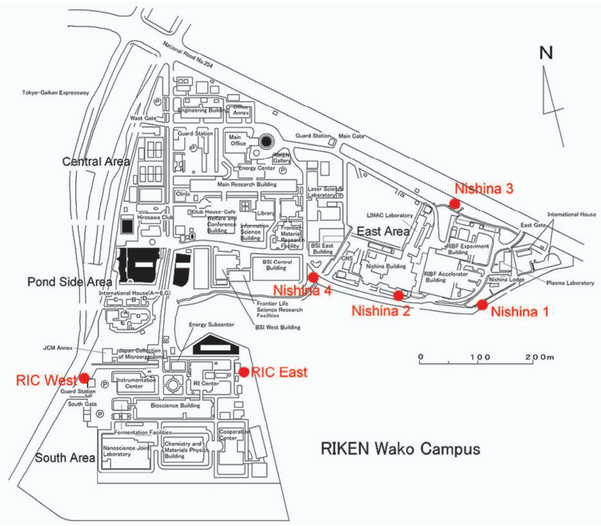

Fig. 1. Locations of radiation monitoring posts.

As shown in Fig. 2, a strong spike of dose rate was observed at 10 a.m. on March 15. This spike was mostly due to the γ-rays from ^{133}Xe gas[1], and the dose rate quickly decreased again because the radionuclide deposit on the ground was small. However, a second big plume came on March 21, and the rain on that day caused the deposition of ^{132}Te, ^{131}I, ^{134}Cs, and ^{137}Cs.[1] This deposit has been keeping the environmental dose rate high, as shown in Fig. 3.

In Fig. 2, small spikes occurring simultaneously with the rainfall are seen. These spikes are not due to the accident but due to the deposit of natural descendant radionuclides of uranium and thorium. Spikes are also seen in Fig. 3. The longer-term fluctuations in Fig. 3 are thought to be due to changes in the conditions around the monitors, that is, heavy rainfall, pileup of fallen leaves, etc.

The dose rate due to the accident was estimated to be 0.1 μSv/h on March 30. The contributions due to individual radionuclides were estimated on the basis of the radionuclide concentration in the soil: ^{132}Te, 22%; ^{131}I, 25%; ^{134}Cs, 38%; and ^{137}Cs, 15%. From the half-lives of these nuclides, the accumulated dose during a year from March 15, 2011, was estimated to be about 0.5 mSv. The internal dose due to the inhalation of the airborne radionuclides, which was measured by Haba *et al.*[2], was also calculated, and the total annual dose due to the accident was estimated to be 0.55 mSv.

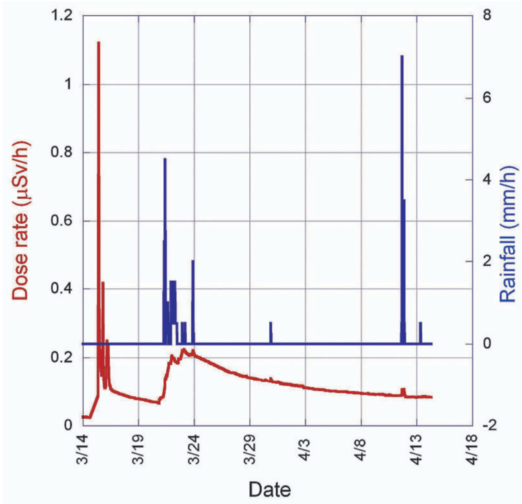

Fig. 2. Hourly averaged dose rate measured by RIC West post, along with the rainfall amount.

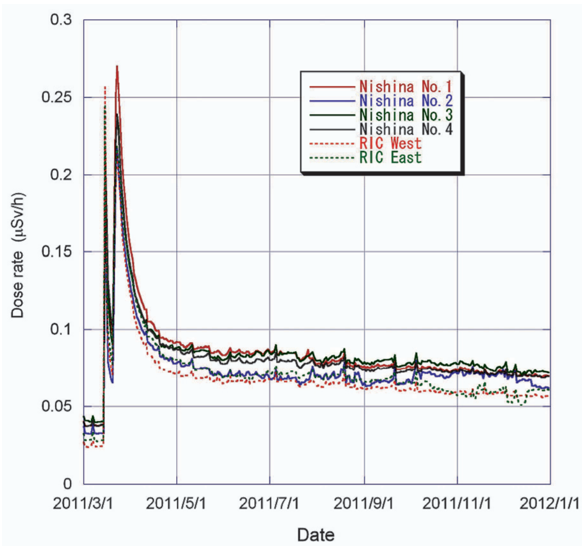

Fig. 3. Daily averaged dose rates measured at six posts.

References

1) H. Otsu *et al.*, elsewhere in this issue.
2) H. Haba *et al.*, elsewhere in this issue.

Measurement of radioactivity concentrations of airborne radionuclides in Wako after the Fukushima Dai-ichi nuclear power plant accident

H. Haba, J. Kanaya, H. Mukai, T. Kambara, and M. Kase

On Mar. 11, 2011, an earthquake of magnitude 9.0 occurred near the east coast of Honshu, Japan, and was followed by a large tsunami. The disasters caused damage to the Fukushima Dai-ichi nuclear power plant (FDNPP), resulting in the release of radionuclides into the environment. On Mar. 15, at a monitoring post of the RIKEN Wako Institute, located about 220 km to the southwest of FDNPP, we observed a rapid increase of dose rate from the usual 0.03 μSv h^{-1} at 4:00 (JST) to 1.2 μSv h^{-1} at 10:00. Hence, we initiated an urgent measurement of the radioactivity concentrations of airborne radionuclides.

Air dust was collected using a commercially available air dust sampler (M&F Enterprise SP-30) installed at the RIKEN Wako Institute (35°46'32" N, 139°37'04" E). The sampling flow rate was 30 L min^{-1}. A cellulose glass-fiber filter (ADVANTEC HE-40T) was used. No activated carbon filter was used; hence, our measurements were not sensitive to gaseous radioiodine. Dust was collected for 30 min for the first two samples in the period Mar. 15 11:15–11:45 and Mar. 16 13:15–13:45. After the third sample (Mar. 16 18:32–Mar. 17 9:00), dust was continuously collected for about one year, except for short interruptions due to the filter change. The filter samples were subjected to γ-ray spectrometry using a Ge detector. The detector efficiency was calibrated to an accuracy of 2%–10% using a multiple γ-ray standard source with the same size as the sample. A calibrated ^{134g}Cs source was also used to correct for the coincidence summing for ^{134g}Cs.

In this work, radionuclides of ^{140}La, ^{140}Ba, ^{137}Cs, ^{136g}Cs, ^{134g}Cs, ^{133g}I, ^{132g}I, ^{132}Te, ^{131}I, ^{131m}Te, ^{131g}Te, ^{129m}Te, ^{129g}Te, ^{110m}Ag, ^{99m}Tc, ^{99}Mo, and ^{95g}Nb were identified. Figure 1 shows a typical γ-ray spectrum of the sample collected in the period Mar. 29 9:40–Mar. 30 11:15. The peaks of volatile ^{131}I, ^{137}Cs, and ^{134g}Cs are very intense since they have a high release probability. In Fig. 2, the time variations of the activity concentrations of ^{131}I, ^{137}Cs, and ^{134g}Cs are shown at the end of sampling as reference time. In the first sample, the maximum activity concentrations of ^{131}I, ^{137}Cs, and ^{134g}Cs were 35 ± 1, 8.8 ± 0.2, and 8.5 ± 0.2 Bq m^{-3}, respectively. Although the activity concentrations decrease with time, one can see two prominent peaks corresponding to Mar. 20 10:05–Mar. 21 10:00 and Mar. 29 9:40–Mar. 31 10:00 as indicated by arrows in Fig. 2. It is interesting to note that a distinct peak corresponding to Mar. 22 10:05–Mar. 23 10:00 is observed only for ^{131}I, indicating that the behavior of radioiodine is different from the behaviors of ^{137}Cs and ^{134g}Cs. These time variations are very similar to those measured at Japan Chemical Analysis Center, Chiba, located about 220 km to the south-southeast of FDNPP.[1] Amano et al.[1] measured the ratios of gaseous iodine to total iodine to be 0.52–0.71, using the cellulose glass-fiber filter in combination with an activated charcoal cartridge. Thus, the total activity concentrations of ^{131}I measured at the RIKEN Wako Institute are estimated to be 2.1–3.4 times those presented in Fig. 2. The activity concentrations of ^{137}Cs and ^{134g}Cs are almost equal for all samples. The ^{134g}Cs/^{137}Cs ratio is calculated to be 1.0 ± 0.1 for Mar. 15, and this value is consistent with other observations related to the FDNPP accident.[1]

We also determined the activity concentrations for other radionuclides such as ^{140}Ba, ^{136g}Cs, ^{133g}I, ^{132}Te, ^{129m}Te, ^{110m}Ag, ^{99}Mo, and ^{95g}Nb.[2] Our data, together with the measurements from other monitoring stations, will help provide further information on the characteristics of the fuel, release mechanism, and the transport of the radionuclides.

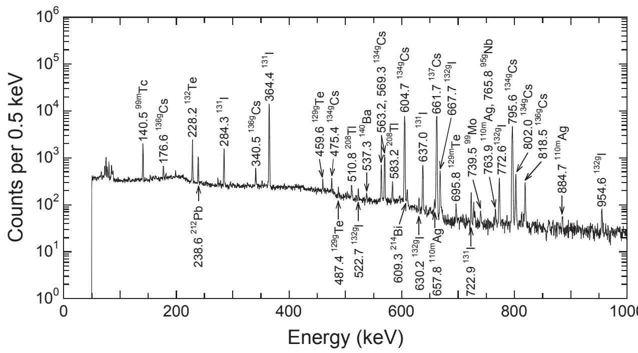

Fig. 1. The γ-ray spectrum for the air dust sample collected in the period Mar. 29 9:40–Mar. 30 11:15 (JST). The filter sample was measured for 35866 s, 1353 s after the end of the sampling.

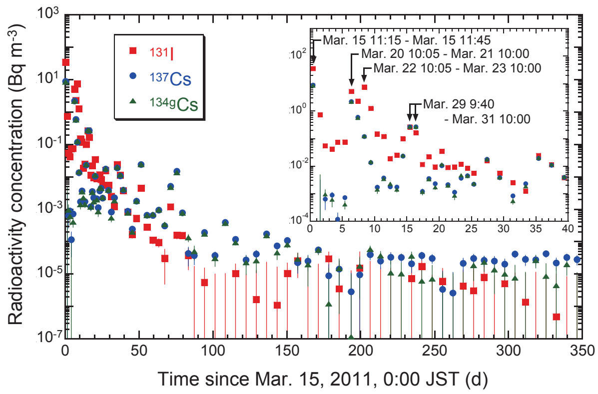

Fig. 2. Time variation of the activity concentrations of ^{131}I, ^{137}Cs, and ^{134g}Cs, as observed at the RIKEN Wako Institute. Inset shows the time variation for 0–40 days.

References

1) H. Amano et al.: J. Environ. Radioact. (in press).
2) H. Haba et al.: submitted to Geochemical Journal.

RIKEN Accel. Prog. Rep. 45 (2012)

Environmental radioactivity at Wako from Fukushima Daiichi Nuclear Power Plant

H. Otsu, N. Aoi, [*2] H. Baba, R.J.Chen, H. En'yo, T. Fujinawa, S. Go, [*1] H. Hasebe, T. Hashimoto, [*1,*2] H. Watanabe, T. Ichihara, E. Ideguchi, [*1] T. Isobe, J. Lee, K. Ozeki, K. Kisamori, [*1] S. Kubono, [*1] M. Kurokawa, G. Lorusso, K. Miki, [*2] S. Michimasa, [*1] H. Miya, [*1] T. Motobayashi, S. Ota, [*1] P. Doornenbal, M. Sako, H. Sakurai, S. Sakaguchi, D. Steppenbeck, M. Takaki, [*1] M. Takechi, [*3] S. Takeuchi, A. Taketani, Y. Togano, [*3] H. Tokieda, [*1] Y. Wakabayashi, [*1] K. Yoshinaga, T. Kawahara, [*1] H. Imao, Y. Ito, and N. Sakamoto (fGamma collaboration)[*]

After the severe accident at the Fukushima Daiichi Nuclear Power Plant, we started monitoring the environmental radioactivity at Wako campus in order to detect a possible increase in the radioactive elements dispersed from the plant.

We set a germanium detector with volume of 146 cm^3 outside the RIBF building, next to the entrance facing the open space with a lawn. Gamma rays could be measured directly in the environment for 23 days, from March 15 to April 8. Initially, the data were collected by a multi-channel analyzer at 15-min intervals. On March 19, we installed an automatic data acquisition system that continuously processed the signals and generated histograms from the data every 15 minutes. Data accumulation continued with 24h a day except during the intervals when liquid nitrogen was supplied for cooling the germanium crystal and preamplifier.

Energy spectra obtained on March 24 and April 1 are shown in Fig. 1. Many of the observed peaks correspond to gamma-ray radiations, which would originate from the Fukushima Daiichi Nuclear Power Plant. Among them, ^{132}Te, ^{131}I, ^{132}I, ^{134}Cs, and ^{137}Cs isotopes are observed as prominent peaks. Gain shift and offset deviation in the detector or electronics caused by fluctuations in environmental parameters such as temperature or humidity were corrected by referring to each gamma ray peak.

The time dependence of the radiation is shown in Fig. 2. Before March 21 (6th day on the horizontal axis in the figure), the main contributions were from ^{131}I, ^{132}Te, and its daughter ^{132}I. March 21 and 22 were rainy. During these two days, the radiation from these four isotopes increased very significantly. However, after the 22nd, we did not observe such increases associated with the rain.

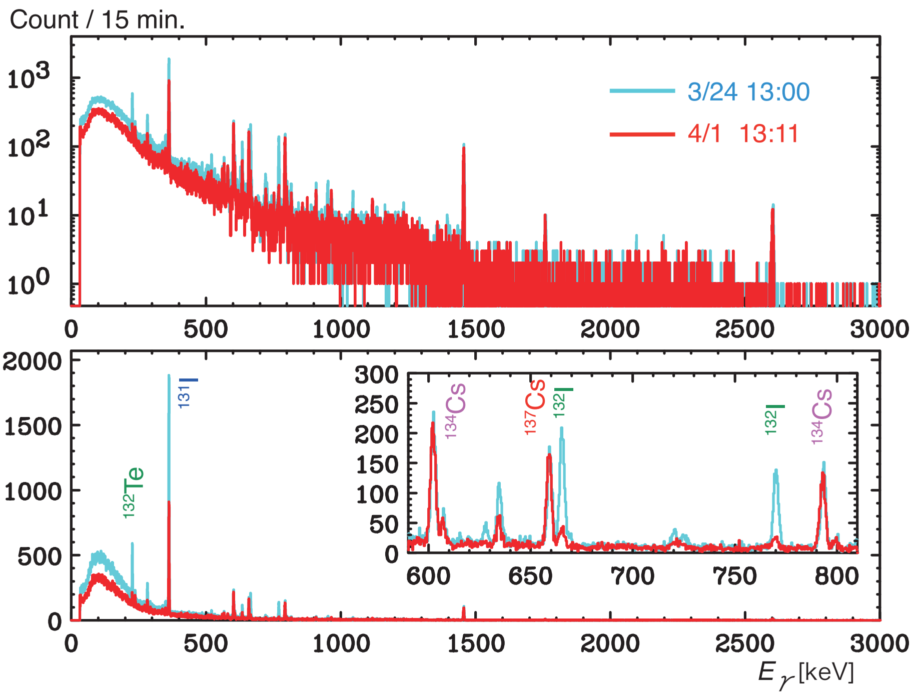

Fig. 1. Gamma-ray energy spectra obtained using the Ge detector on March 24 (cyan) and April 1 (red). Top frame shows energy spectra with logarithmic vertical axis, whereas bottom frame shows the same spectra with linear axis. Inset of the bottom frame shows spectra from 600 to 800 keV region.

*1 CNS, The University of Tokyo
*2 Present affiliation: RCNP, Osaka University
*3 Present affiliation: GSI

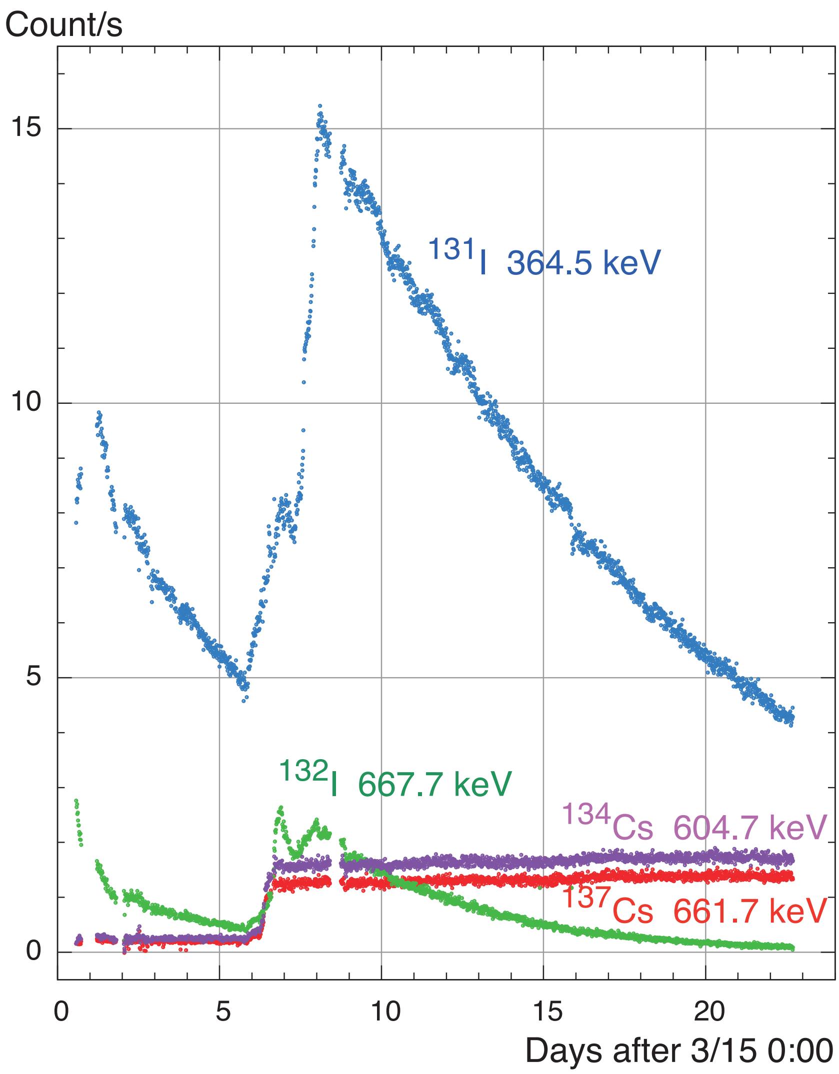

Fig. 2.
Time dependence of observed radiation.

Horizontal axis corresponds to days after March 15 at 0:00 A.M. and vertical axis indicates the counts per second.

March 21 and 22 were rainy. A drastic difference of trends occurred before and after these days. Before March 21 (6th day on the horizontal axis in the figure) the main contributions were from ^{131}I, ^{132}Te, and its daughter ^{132}I. During rain, the radiation from the isotopes indicated increased very significantly.

However, we did not observe such increases associated with rain after the 22nd. After the rains, iodine isotopes decreased with their decay half lives or on the same order. Cesium isotopes did not decrease in this period. In fact, they seemed to increase slightly.

These tendencies indicate that most of the radioactive elements in the air were fell down to the ground by the rain around the 21st. Subsequently the cesium 134 and 137 isotopes exhibited a small but continuous increase during the measurement because of the further deposition of these isotopes.

In order to evaluate the amount of radioactive elements accumulated on the ground, we performed a Monte Carlo simulation with the GEANT4[1] toolkit by taking into account the area (ΔS) corresponding to the scoping angular acceptance, detection efficiency ($\varepsilon(E_\gamma)$), and absorption effects ($f(E_\gamma, \boldsymbol{r})$) by air and other materials. We obtained the coupled parameters $f\varepsilon\Delta S$ as:

$$f\epsilon\Delta S = \epsilon(E_\gamma)\int_S f(E_\gamma,\vec{r})\frac{dS}{\cos(\theta)}.$$

The obtained values were 6.2×10^{-4} and 5.0×10^{-4} [m^2] at 364.5 keV and 660 keV, respectively. By taking the branching ratios into account, we evaluated the surface density of radioisotopes on the grass in the Wako Campus as 26 kBq/m^2 for ^{131}I and 2.8~3.0 kBq/m^2 for each of the other three isotopes on March 25. In these analyses, we assumed for simplicity that all radioactive elements remained on the ground surface and did not penetrate or sank into the soil. Further analyses are needed for quantitative estimation, especially for the consideration of depth distribution inside the soil. Systematic errors are estimated to be about 20%, mainly due to ambiguity in the simplified model employed for the simulation.

In summary, we measured the environmental radioactivity in the Wako area in the period following the Fukushima Daiichi Nuclear Power Plant accident and evaluated the results.

References
1) http://geant4.cern.ch/

Radioactive Xe arriving in and passing through Wako area

H. Otsu, fGamma collaboration[*1]

Immediately after the severe accident that occurred at the Fukushima Daiichi Nuclear Power Plant, we started the spatial radiation dose measurement in Wako campus[1)]. In this article, we report on the evidence of gaseous xenon isotopes arriving in and passing over the Wako area. The major components were ^{133}Xe, ^{133m}Xe, and ^{135}Xe, as identified by our Ge detector measurements. Experimental details can be found in Ref. 1 of this volume.

From March 15 to 16, abrupt changes in the environmental dose were observed at three instances[2)] by area monitors at the RIKEN Nishina center as burst-like phenomena. The equipment was not ready for the first and second abrupt changes. In the early morning on the 16th, the third abrupt change occurred, although the scale of the burst was smaller than those of the previous two events. At that occasion, we successfully observed gamma-ray peaks originating from the burst.

Figure 1 shows gamma-ray energy spectra recorded between 5:09 and 8:50. Representative spectra are shown in red, with a maximum at 6:15, and in cyan, as passing over the period at 8:39. The spectrum at 13:50 on the 15th is also shown by solid green line for comparison. Magnitudes of the three peaks at 81, 233, and 250 keV had already increased at 5:09. They rapidly reduced at 8:50 while those of other peaks stayed almost in constant during these 4 hours. From gamma-ray energies of 81, 233, and 250 keV,

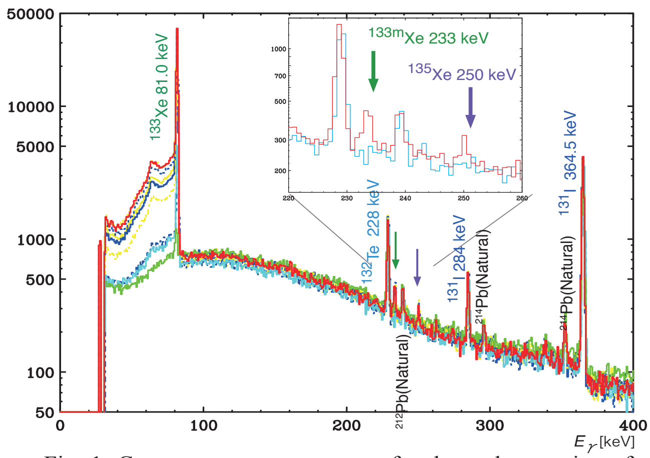

Fig. 1. Gamma-ray energy spectra for the early morning of the 16th of March with green indicating a reference, which corresponds to the spectrum at 13:50 on March 15. Horizontal axis indicates gamma-ray energy. Vertical axis shows detection counts within 15 minutes. In the inset, spectra are enlarged for the range between 220 and 260 keV. Here, data are limited for 6:15 (Red), 8:39 (Cyan), and reference (Green). Peaks related to ^{133}Xe, ^{133m}Xe, and ^{135}Xe were observed during the burst.

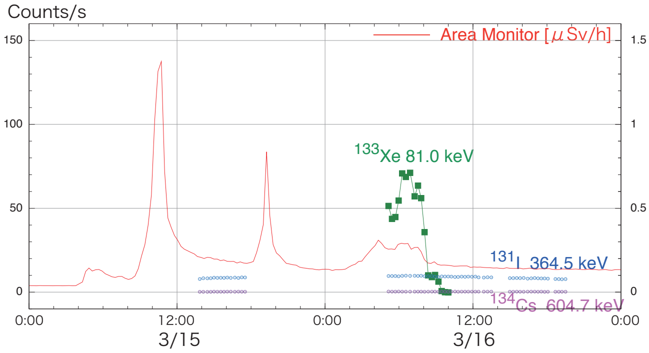

Fig. 2. Time dependence of Xe 81.0 keV peaks (left vertical axis) with dose read out by area monitor in μSv/h unit (right vertical axis). The 81 keV peak is not very prominent during daytime on the 15th.

we identified ^{133}Xe, ^{133m}Xe, and ^{135}Xe, respectively. Other possibilities for the origin of the 81 keV peak, for example, 80 keV from ^{131}I, are rejected because no lines corresponding to their branches were observed. The bump-like structure below the 81 keV peak is interpreted as corresponding to the Compton scattering component.

Figure 2 shows the time dependence of the 81 keV peak in counts per second and the radiation dose measured by the area monitor in μSv/h unit for comparison. The ^{133}Xe yield varied on the morning of the 16th in a manner similar to the area monitor dose, whereas the peak yields for ^{131}I and ^{134}Cs remained almost constant.

These comparisons indicate that rapid increases in the dose were caused by gaseous Xe activities. Another observation is the more rapid decrease of the yield than any of the lifetime of the Xe isotopes: 5.25 d for ^{133}Xe, 2.19 d for ^{133m}Xe, and 9.14 h for ^{135}Xe. This suggests that gaseous Xe passed through the area as a cloud without causing a large amount of activity accumulation on the ground.

The efficiency of the germanium detector with the same geometry (56.8 mmφ × 61.7 mm) was calibrated using several checking sources with a facially distribution. Detection efficiency at 81 keV was calculated with the extrapolation as 0.11. From these properties og the detector, we estimate the gamma-radiation flux density as 2.5×10^5 [$m^{-2}s^{-1}$] at the observed burst maximum (70 Counts/s).

In summary, we observed a rapid increase and decrease in radiation on March 16 at the Wako campus. We conclude from our gamma-ray measurements that they originate from radioactive Xe gases. The Xe isotopes were considered to have passed over the Wako area.

References

1) H. Otsu, fGamma collaboration, this volume.
2) Y. Uwamino, this volume, private communication.

*1 Gamma collaboration members are listed in the previous report in this volume.

Measurement of ^{137}Cs and ^{90}Sr in a Surface Soil Sample Obtained from Namie, Fukushima

Y. Kobayashi, Y. Saito*1, M. Iwasaki, and R. Hayano*2

An enormous quantity of the radionuclides has been discharged owing to the hydrogen explosion of the nuclear reactor in the Fukushima Daiichi Nuclear Power Plant in March 2011. We performed γ-ray spectroscopy for detecting ^{137}Cs and the liquid scintillation technique for detecting ^{90}Sr with the rapid chemical separation of the soil obtained from Namie, Fukushima Pref., to evaluate the distribution and deposition of the radioactive fallout from the accident[1]. A soil sample with 2-cm thickness was collected from the surface and from an area of 200 cm^2 in Namie on April 29, 2011. The sampling point, at the latitude 37º 35’ 34.77” North and the longitude 140º 45’ 12.85” East, is located approximately 30 km northwest from the site of the explosion. The spatial dose rate was 25~30 μSv/h at the sampling time. The total wet weight of the sample was 19.8 g.

The complete sample was placed in a plastic bottle for the γ-ray spectrometry that was performed using a Ge detector. The γ-ray spectrum of the soil sample obtained from Namie is shown in Fig. 1. Most γ-peaks could be assigned to long-lived radioactive ^{137}Cs ($T_{1/2}$ = 30.1 y) and ^{134}Cs ($T_{1/2}$ = 2.06 y). The concentration of ^{137}Cs was estimated from the peak area of a typical 661.9-keV γ-ray. The activity of ^{137}Cs was estimated to be 63,400 Bq/kg (wet soil) by a calculation performed using the counting rate of 20.4 cps, the counting efficiency of the Ge detector, and the branching ratio of the 661.9 keV γ-ray.

^{90}Sr can achieve a secular equilibrium with the high-energy β-emitter ^{90}Y in a few weeks. ^{90}Sr concentration was determined by means of the low-background liquid scintillation technique with rapid chemical separation through oxalate coprecipitation[2]. The soil was heat-treated at 450 ºC for 24 h and dissolved in aqua regia. Then, the Y and Sr carrier solution was added to it. ^{90}Y was extracted from bis(2-ethyl-hexyl) phosphoric acid (HDEHP) and toluene solution after the radioactive equilibrium of $^{90}Sr/^{90}Y$ was reached. Yttrium was separated as a hydroxide, and then, oxalate salt was precipitated with the condition for which the pH was ~1.5. The chemical yield was estimated to be 70%. The sample for the β-ray measurement was prepared by adding a liquid scintillator (Perkin Elmer Ultima Gold AB). The measurement was performed in a Packard low-background detector. Figure 2 shows the β-spectra of a soil sample prepared by rapid chemical separation, a blank test, and a hydroxide as reference including $^{90}Sr/^{90}Y$ with 160 Bq activity. The end point (E_{max} = 2.2 MeV for ^{90}Y) could not be detected in the spectrum of the soil sample, and the line shape in its case differed visibly from that of the reference precipitation. It was concluded that the activity of ^{90}Sr in the soil sample was below the detection limit. The detection limit of the present method was estimated to be 35 Bq/kg from the counting efficiency and counting rate of the reference sample. The $^{90}Sr/^{137}Cs$ ratio caluculated in this study was consistent with the analytical report published by MEXT on May 31, 2011.

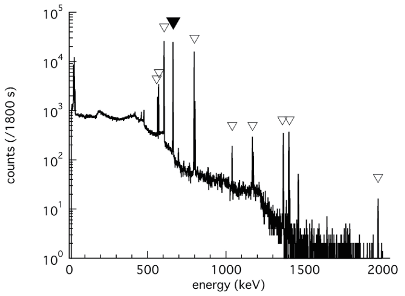

Fig. 1. γ-ray spectrum of the soil sample obtained from Namie, Fukushima.▼ and ▽ indicate the 661.9-keV γ peak of ^{137}Cs and the γ-rays of ^{134}Cs, respectively. The measuring time was 1800 s.

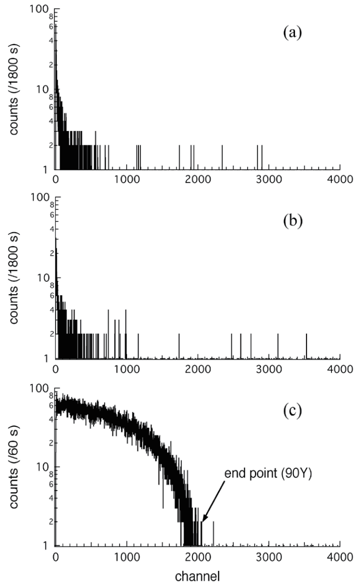

Fig. 2. β-ray spectra of (a) a oxalate salt extracted after chemical separation, (b) the blank test, and (c) the reference which was a precipitation of $Y(OH)_3$ obtained using a $^{90}Sr/^{90}Y$ tracer with 160 Bq activity.

*1 College of Science and Engineering, Aoyama Gakuin Univ.
*2 Department of Physics, University of Tokyo

References
1) *http://www.radiochem.org/kinkyu/index.html*
2) *http://www.kankyo-hosyano.go.jp/series/lib/No2.pdf*
3) *http://radioactivity.mext.go.jp/ja*

Measurement of β-ray emitting isotopes from the Fukushima Daiichi nuclear power plant accident

F. Sakuma, M. Tokuda[*1], Y. Sada[*2] and T. Hashimoto[*3]

[Fukushima reactor accident, β-ray isotopes]

The Fukushima Daiichi nuclear power plant accident, caused by the earthquake that occurred on March 11, 2011, resulted in the release of large amounts of radioactive materials into the atmosphere. Emissions from γ-ray emitting isotopes such as ^{137}Cs and ^{131}I were observed and reported immediately after the accident. However, the isotopes that emitted only β-rays, such as ^{90}Sr, were not detected owing to the difficulty in the measurement of β-rays. As it is known that the ^{90}Sr/^{137}Cs activity ratio was observed to be up to 1.5 at the Chernobyl accident[1)], we attempted to measure the β-ray emitters using plastic scintillators and photomultiplier tubes (PMTs) in March and April 2011. The experimental setup is shown in Fig. 1. We wiped the roof of a car ($\sim$1.5 m^2) with a cleaning tissue (Nippon Paper Crecia, Kimwipe S-200) on March 23 at around 17:00: the car was parked in the RIKEN Wako campus from before the earthquake to the time of wiping. In order to measure the spectra of β-rays with a few MeV of energy, a thin (t1 mm, PMT1) and a thick (t50 mm, PMT2) plastic scintillator were used. A sample was set on the thin scintillator, and an event trigger was generated by a coincidence signal of the PMT1 and the PMT2. The ADC spectrum of the β-rays was obtained using the thick scintillator. In addition, two large plastic scintillators (PMT3 and PMT4) that covered the complete system were used as cosmic-ray veto counters.

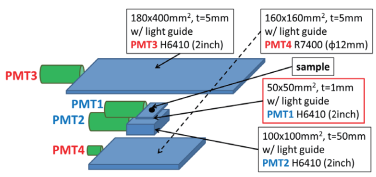

Fig. 1. Schematic drawing of the setup.

The ADC spectra obtained from the sample are shown in Fig. 2; these spectra were obtained with the same setup but on a different days: April 1, 21:30 to April 2, 4:36, and April 20, 16:22 to April 21, 16:26. Each ADC spectrum was fitted with the background cosmic-ray spectrum and referenced ^{90}Sr spectrum in the ADC range between 500 ch and 800 ch. The cosmic-ray and ^{90}Sr spectra were obtained with an empty sample and ^{90}Sr source of $\sim$0.9 MBq, respectively. The endpoint energy of ^{90}Sr is 2.280 MeV, and its half-life is 28.79 y, i.e., $^{90}_{38}\mathrm{Sr} \rightarrow (^{\beta^-0.5459\mathrm{MeV}}_{28.79\mathrm{y}}) \rightarrow {}^{90}_{39}\mathrm{Y} \rightarrow (^{\beta^-2.280\mathrm{MeV}}_{64.053\mathrm{h}}) \rightarrow {}^{90}_{40}\mathrm{Zr}$. In the figures, the spectrum shape can be seen to obviously change, i.e., the count rate in the range over 500 ch decreased with time. As the half-life of ^{90}Sr is very long, this decreasing radioactivity indicates that we could not have observed the β-rays emitted by ^{90}Sr. In this case, what isotope had been observed that emitted β-rays similar to ^{90}Sr? Figure 3 shows the count rate in the ADC range between 500 ch and 800 ch after subtracting the background, in which each data point is obtained on a different day and the start time corresponds to April 1, 21:30. The fitting result of a half-life is 3.20 $\pm$ 0.23 d, which is consistent with the half life of ^{132}Te, i.e., $^{132}\mathrm{Te} \rightarrow (^{\beta^-2.137\mathrm{MeV}}_{3.20\mathrm{d}}) \rightarrow {}^{132}\mathrm{I}$. In fact, a radiation monitor group in KEK reported the observation of ^{132}Te in March 2011[2)].

In conclusion, we could not observe β-rays emitted by ^{90}Sr, although we observed a β-ray emitting isotope, ^{132}Te, which was released from the Fukushima reactor after the accident in March 2011.

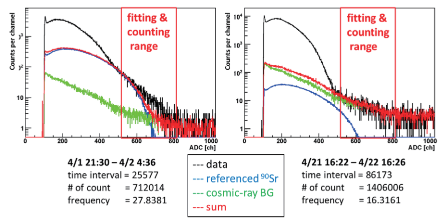

Fig. 2. ADC spectra obtained from the sample. (see text)

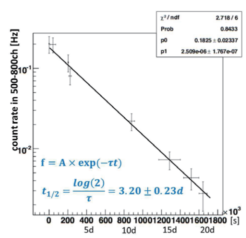

Fig. 3. Count rate in the ADC range between 500 ch and 800 ch after subtracting the background.

*1 Department of Physics, Tokyo Institute of Technology
*2 Department of Physics, Kyoto University
*3 Department of Physics, The University of Tokyo

References
1) Environmental Consequences of the Chernobyl Accident and their Remediation (IAEA, 2006)
2) http://www.kek.jp/quake/radmonitor/

Pilot survey of feral cattle in the vicinity of Fukushima Daiichi Nuclear power plant

M. Wada, H. Haba, S. Sato,[*1] S. Roh,[*1] and M. Toyomizu[*1]

A pilot survey of radioactive contamination of feral cattle in Minamisoma city was performed in late August 2011. After the accident of Fukushima Daiichi nuclear power plant, many cattle left their enclosures and survived by consuming plants and water in a ditch that may have been radioactively contaminated. Therefore, it is worth surveying the radioactive contamination in the muscles, organs, blood, urine, and feces of cattle before slaughter disposition.

Increasing internal radiation dose in human body because of contaminated food became a sensitive problem especially after contaminated beef was found in the market. The beaf cattle consumed contaminated straw immediately before being butchered, and the meat contained more than 2 kBq/kg of radioactive cesium. The transfer rate of cesium from the contaminated food to the body and the metabolism rate have been previously studied[1,2]. If the specific radioactivities in cattle muscle could be evaluated from that in the blood or urine when the cattle are alive, it might aid in assessing the use of those cattle.

In the first sampling, we evaluated 5 cows captured at Long. 140.929E, Lat. 37.572N, about 19 km NNW from the nuclear power plant. Samples of blood, urine, feces, and amniotic fluid were taken in 20 cc vial bottles, and samples of muscles and other organs were taken in 100 cc bottles at the location. The 5 cows that were evaluated inhabited a trench with abundant availability of water. We observed that the urine color of these cows was clearer than that of cows in a stock farm. One cow was pregnant and we sampled both the fetus and amnionic fluid.

The radioactivity levels of samples were measured using a well shielded HPGe detector with a relative efficiency of 20%. The absolute efficiency for each sample bottle was calibrated using a mixed standard source in a water matrix. The sum correction factors for the γ-rays from ^{134}Cs were evaluated with a sample itself but placed at 10 cm apart from the detector.

The specific activities of the sum of ^{134,137}Cs were plotted for individual cattle (Fig. 1). Cs activity did not show a uniform distribution even within the muscles, and the internal organs showed much lower radioactivity level than that in the muscles. The specific activities were also plotted as a function of the blood activity (Fig. 2). Positive correlations were found, for example, ratios of the fillet and tongue to the blood were approximately 33 and 12, respectively. Since evaluation of the total amount of urine per day was difficult for such feral cattle, we could not use urine samples for quantitative evaluation of whole body activities. In a liver sample, some amounts of ^{110m}Ag 148(5)Bq/kg) and ^{129m}Te 20(1) Bq/kg) were found. These radionuclides were also detected in the soil of the area inhabited by the cattle; further, we speculated that the cattle consumed contaminated soil when drinking the water in the ditch, which resulted in the heavy metals to concentrate in the liver.

Although we planned to continue the survey, because of an organization issue, only the first pilot survey was conducted, and the number of samples was limited because of the allowed sampling time at the location. However, we consider our limited data worth reporting, because our data may be used in combination with other surveys.

References

1) J.E. Johnson, et al.: J. of Nutrition, **94**, 282 (1968).
2) G. Voigt et al.: Science of Total Environment, **85**, 329 (1989). S. Ambe et al.: Chem. Lett. **2001**, 149.

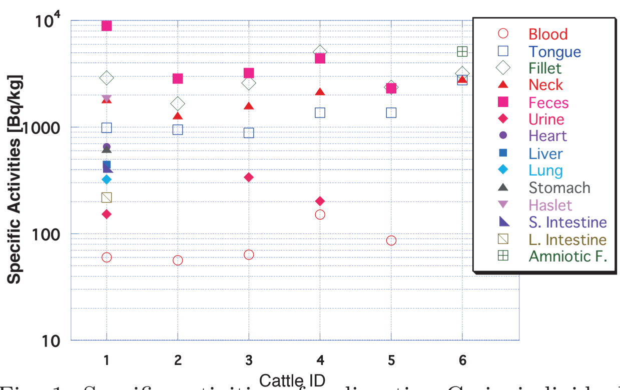

Fig. 1. Specific activities of radioactive Cs in individual cattle samples. #6 is the fetus of #5.

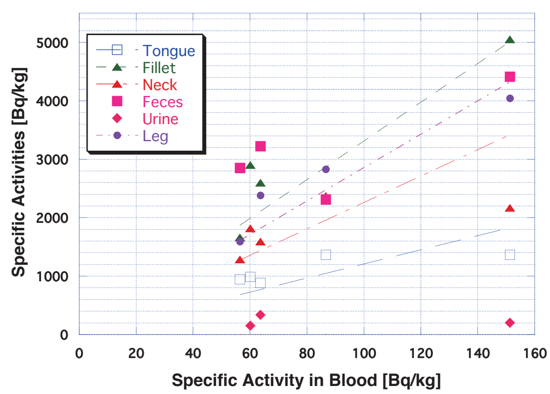

Fig. 2. Specific activities of radioactive Cs as functions of the specific activity of blood.

[*1] Graduate School of Agricultural Science, Tohoku University

Gamma ray spectroscopic analysis of underwater environmental samples from ocean near Fukushima Daiichi Nuclear Power Plant

S. Moriya and H. Otsu

Radioactive materials have been released into the nearby ocean from Fukushima Daiichi nuclear power plant after severe accidents in March, 2011. Here, we discuss a series of analyses that we performed to access the incorporation of such radioactivity into members of the coastal eco-system.

Oceanic biomasses and environmental samples were collected at the Fishery port of Hisanohama and the surrounding coastal regions (figure 1). Sample collection was done through self contained underwater breathing apparatus (SCUBA) diving. The SCUBA sampling was done in collaboration with the Japanese Association of Underwater Science. We collected 10 litter of sea water and filtrated it using a 0.22 μm Omuni pore filter (Millipore) until the filter was clogged, after which we obtained microbial biomass. The filtrated water was then evaporated to obtain sea salts. We also collected biofilm materials from the surfaces of rocks and macro benthos (Ascidiacea, Sponge, Sea urchin, Starfish and Shellfish) from seabed.

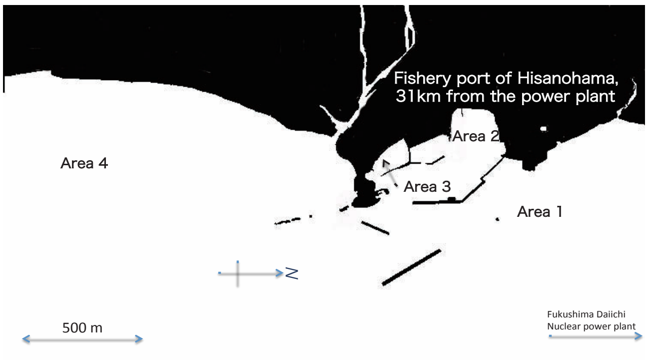

Fig.1 : Sampling spots in Hisanohama.

Biofilm on the rock was collected using a wire brush with distilled water. The samples of biofilm and macro benthos were dried at 120 ℃ in a drying oven, then milled using a food mixer. The obtained samples were analyzed with gamma ray spectroscopy.

Results of the gamma ray spectroscopic analysis using a Germanium detector are shown in table 1. According to these results, the environmental water and primary producers (oceanic microbes and biofilms) contain ^{134}Cs and ^{137}Cs. However, the macro benthos on the sea floor contain not only radioactive Cs but ^{110m}Ag in their body.

To estimate the source of ^{110m}Ag in such the organisms, we performed additional sampling to obtain bottom mud using a short piston core sampler operated by the SCUBA divers. The core sampler is assembled with an end cap and a PVC tube of 40 mm diameter and approximately 25 cm length. The piston of the core sampler is made from craft resin with the same PVC tube as that in the template (40 mm diameter and approx. 5 cm length) and is inserted into

Table 1. Detected radioactive elements from each sample. Corrections are needed for ^{134}Cs and ^{110m}Ag for sum effects. Error(RMS) indicates statistical only.

		Radiation [Bq/kg(Dry)], or [Bq/m^3] for Microbes, evaluated on 2012/03/11					
Area	Material	^{134}Cs	Error	^{137}Cs	Error	^{110m}Ag	Error
1	Sea salt	4.4	0.2	6.1	0.3	–	
2011/12/10	Microbes	15	3	15	3	–	
Lat. 37.151N	Biofilm	874	36	1431	53	–	
Long. 41.005E	Sponge	221	4	381	7	39	2
	Ascidiacea	181	2	293	3	128	2
	Star fish	7.2	0.4	10.1	0.6	29	1
	Sea Urchin	110	17	205	29	125	29
2	Sea salt	4.0	0.5	6.1	0.6	–	
2011/11/20	Microbes	109	9	176	9	–	
Lat. 37.150N	Biofilm	611	45	926	47	–	
Long. 41.001E	Sponge	245	4	422	5	4.6	1.1
	Ascidiacea	134	2	215	3	82	2
	Sea Urchin	101	1	156	2	81	6
3	Sea salt	2.7	0.2	4.7	0.2	–	
2011/12/3	Microbes	31	2	51	3	–	
Lat. 37.147N	Biofilm	1416	67	2343	85	–	
Long. 41.002E	Ascidiacea	295	5	465	2	64	1
	Shell fish	107	1	160	1	45	1
4	Sea salt	2.7	0.1	4.6	0.2	–	
2011/11/26	Microbes	6.9	1.3	9.1	3.8	–	
Lat. 37.136N	Biofilm	284	20	427	25	–	
Long. 41.003E	Sponge	260	5	431	6	131	12
	Shell fish	95	1	146	1	34	1
	Sea Urchin	30	1	47	1	10.8	0.5
2	Mud(Surface)	819	11	1341	9	13	1
2011/12/17	Mud(Bottom)	500	9	819	8	–	

the PVC tube during the operation. Core samples from the depth of 15-20 cm have been analyzed by sectioning depth of 5 cm each by using the Ge detector. The results (Table 1) show that the materials on surface of the seabed contain ^{110m}Ag and both of $^{134, 137}$Cs but bottom mud from deeper position contain only radioactive Cs.

These results suggest that the once-precipitated radioactive Ag is possibly re-suspended into the oceanic water by the swell of the ocean and is fed by macro benthos. The mechanism for ^{110m}Ag precipitation is still unclear. Further analyses of the seawater contents by fine fractionation and its relationship with land-originated compounds are needed to understand the entry of ^{110m}Ag into the coastal eco-system.

Note that the gamma ray analyses are ongoing especially on the correction of the sum peaks from ^{134}Cs and ^{110m}Ag because of the relative geometry between a sample and the Ge detector. These are planned to be corrected using the GEANT4 code by considering the sample height information.

In summary, we determined the radioactivity absorbed by oceanic plants and animals not only for Cs isotopes but also for Ag isotopes released from the power plant accident. These results will be utilized to understand the future eco-system situation around these areas.

Analysis of Gamma-ray Emitters in Soils for Obtaining Maps of Deposited Radioactive Substances around Fukushima Daiichi Nuclear Power Plant

S. Shimoura[*1]

In order to prepare maps of radioactive substances deposited on the ground surface, soil samples from the 5-cm surface layer were collected for about 2,200 locations within approximately 100 km from the Fukushima Daiichi Nuclear Power Plant (NPP) from June 6 to 14 and from June 27 to July 8, 2011. About 10,000 samples in total, corresponding to five or three different points for each location, were analyzed by the Japan Chemical Analysis Center (JCAC) (40%) and by a collaboration (60%) among universities and institutes, including Center for Nuclear Study (CNS), RIKEN Nishina Center (RNC), Research Center for Nuclear Physics (RCNP), and other organizations. CNS acted as a hub of the collaboration, where tasks such as receiving and checking about 6000 samples from Fukushima; sending them to 22 analysis groups depending on their capacities; and collecting, checking, and summarizing the results were performed. About 120 samples, collected from within 20 km of NPP, were analyzed by CNS and RNC.

The activities of Cs-134, Cs-137, and I-131 were analyzed by measuring γ-rays emitted by all the samples using the germanium detectors of each analysis group. Activities of other substances such as Te-129m, Ag-110m were also analyzed for about 2000 samples. Each analysis group calibrated the absolute magnitudes of the activities by using the IAEA-444 standard samples[1)] filled in the same U8 type containers (5 cm$^{\phi}$ $\times$ 5 cm^{H}) as the soil samples that were circulated among the collaboration. Since Cs-134 and Cs-137 are involved in the IAEA-444 standard, their absolute activities were determined by the relative yields from the IAEA-444 sample and each soil sample.

Measurement time for a sample was basically one hour, whereas long runs with around 10 hours were also performed for some samples to measure the radiation from I-131. However, large portion of the samples have no significant value for I-131 because of decay out through more than 10 half lives and of Compton backgrounds from the radiation of Cs-134 and Cs-137.

The same $\sim$300 samples were analyzed by multiple groups, one of which is either CNS or JCAC, for the purpose of a cross checking. Results from these different groups were consistent within 30% for each sample and within 15% for an average of five samples for each location. The deviation is considered to be due to the inhomogeneity of the activities in soil samples, since it was found that for some samples, counting rates depended on the direction of the sample relative to the detector.

The maps based on the resultant activities (Cs-137, Cs-134, I-131, Te-129m, and Ag-110m) are found from the Web pages of MEXT[2)], JAEA[3)], and RCNP.[4)]

As shown in ref.[2)], the ratios of the activities of Cs-134 to Cs-137 were independent of the locations about 0.9–1.0 . On the other hand, activity ratios of I-131 to Cs-137 of the soils in the southern coastal areas are about 4 times larger than those in the northern areas. The present results are expected to be used as a basis for assessing the radiation dose in the concerned areas, further investigations in the environmental research works, and other such purposes.

The measurements at RNC and CNS were performed by H. En'yo, Y. Watanabe, S. Yokkaichi, H. Watanabe, M. Nishimura, T. Kishida, H. Otsu, H. Ohnishi, T. Tada, K. Ozeki, K. Morita, D. Kaji, H. Haba, J. Kanaya, E. Ikezawa, T. Maeyama, M. Nabase, K. Ikegami, A. Yoshida, T. Hori, Y. Yamaguchi, S. Sonoda, Y. Ito, Y. Uwamino, H. Mukai, S. Fujita, M. Fujinawa, H. Sakata, T. Kambara, K. Yamada, T. Otsuka, E. Ideguchi, S. Ota, D. Nakajima, M.-H. Tanaka, R. Yoshino, Y. Sasamoto, S. Noji, S. Go, M. Takaki, K. Kisamori, R. Yokoyama, T. Fujii, Y. Kubota, R. Saito, and S. Shimoura.

The present work was in the course of the project under the 2011 Strategic Funds for the Promotion of Science and Technology, entitled "Establishment of the Base for Taking Measures for Environmental Impact of Radioactive Substances – Study on Distribution of Radioactive Substances" of MEXT.

References

1) http://nucleus.iaea.org/rpst/Documents/rs_iaea_444.pdf
2) various reports can be found at http://radioactivity.mext.go.jp/en/; http://radioactivity.mext.go.jp/ja/ (in Japanese)
3) http://ramap.jaea.go.jp/map/
4) http://www.rcnp.osaka-u.ac.jp/dojo/ (in Japanese)

Appendix:

The participants of the soil sampling from RNC and CNS are as follows: S. Fujita, K. Ikegami, Y. Ito, T. Kageyama, S. Kubono, K. Morimoto, H. Mukai, S. Nishimura, K. Ogawa, T. Sonoda, and M. Wada.

*1 Center for Nuclear Study (CNS), The University of Tokyo

Simple screening method for radioactively contaminated food using ashing method with Geiger-Müller counter

M. Wada and H. Haba

After the accident of the Fukushima Daiichi nuclear power plant in the middle of March, 2011, radioactive contamination of food has become a serious concern, especially for those who live in the area where the soil is highly contaminated. It is worth developing a simple screening method, which can be used at home.

In general, β-rays can be detected with a much higher efficiency than γ-rays, and the shielding of β-rays is considerably easier than that of γ-rays. However, β-rays can be shielded by the sample itself. Only surface contamination can be detected by a thin-window Gaiger-Müller (GM) counter. If the radioactivity could be concentrated into a thin sample, the total β radiation detection method would be a significantly sensitive method for contamination surveys.

Most foods consist of water, carbohydrates, proteins, lipids and ash. The concerned radionuclides, such as Cs or Sr, belong to the ash that can be extracted from the sample by an ashing process. The content of ash in food is on the order of 1%, which implies 100 times concentration can be achieved.

First, we tested this method at home using a kitchen grill for fish in order to ash the food samples without contamination. This required approximately 20 min under a medium flame, and the temperature of the samples was less than 500 °C. The weight of ash was less than 1 g. The ashes were flattened and covered with a 10 μm kitchen film (polyvinylidene chloride). The β-rays from the ash were detected using a 5 cmϕ aperture GM survey meter (TCS146B). The amount of potassium (K) in foods was noted from an ingredients table and the specific activity of them could be calculated from the natural abundance of ^{40}K (0.0117%) and the half-life (1.28×10^9 y). The calculated counting rate ΔI_{cal} from the table, with a branching ratio of 90% and a detection efficiency of 25%, was compared with the measured counting rate ΔI_{exp} after subtracting the background (Tab. 1). They agreed well within the limits of a statistical error.

Next, samples that were radioactively contaminated were tested at laboratory (Tab. 2). The specific activities of ^{134,137}Cs and ^{40}K were determined with a HPGe detector before ashing. The expected β-ray count rate I_{cal} was evaluated with the cover area of this setup (75%); the efficiencies of β-rays (14.1%, 12.5% and 22.5% for ^{137}Cs, ^{134}Cs and ^{40}K, respectively), which were evaluated by accounting for the self absorption with a typical thickness (30 mg/cm^2) and for the mean β-energies and branching ratios. When the amount of ash was less than 1 g, the experimentally measured β-ray counting rates ΔI_{exp} agreed with the calculated values.

Table 1. Specific activities of ^{40}K in foods and the counting rates (I_{cal} and I_{exp}) obtained with a GM counter.

spices	ash %	K %	*S.A.* Bq/kg	m g	ΔI_{cal} cpm	ΔI_{exp} cpm
Spinach	1.7	0.69	219	59	174	169(19)
Soy bean	1.4	0.49	155	33	70	72(14)
W. mellon	0.2	0.12	38	100	51	67(11)
Onion	0.4	0.15	48	114	73	70(9)
Milk	0.7	0.11	35	76	36	34(19)

Table 2. Measurements of contaminated samples.

sample	Cs Bq/kg	K40 Bq/kg	mass g	ash g	ΔI_{cal} cpm	ΔI_{exp} cpm
Berry1	135	76.7	21.1	0.53	33	38(4)
Berry2	135	76.7	22.6	2.1	36	22(3)
Urine1	1727	532	23.9	4.0	378	217(5)
Urine2	549	377	21.0	0.9	149	158(5)
Milk1	145	48.8	20.2	0.2	28	24(3)
Milk2	268	47	20.0	$<$0.1	42	44(3)

In the Milk1 measurement, the background count N_{B} was 350 in 10 min and the count from the sample N was 592 in 10 min. The detection limit in this case was $N_{\mathrm{m}} = 84$ counts (8.4 cpm) with a decision criteria of 3. It roughly corresponded to a total activity of 1.2 Bq in the sample. The maximum amount of the sample was limited by the amount of ash. Considering the self shielding of β-rays, the amount of ash should be less than 1 g. If a 50 g sample is used, the detection limit, in terms of the total specific activity including ^{40}K, reaches 24 Bq/kg.

The contribution from ^{40}K is an important concern. For most foods, the approximate amount of K can be determined from an ingredients table, or, if an exact value is needed, a commercial K ion meter, such as C131K, can be used. We tested many samples with a widely varying K concentration and the values determined showed good agreement with the activity measurements recorded with a HPGe detector.

Although the total β radiation measurement method has unavoidable drawbacks in the identification of radionuclides and in the efficiency evaluation, it is still a useful method for screening with a reference level of 100 Bq/kg. It should also be noted that this method is sensitive to radionuclides that do not exhibit γ-ray radiation, such as ^{90}Sr, even though Sr is not considered a major radionuclide in the presently discussed accident.

NaI scintillation detectors for quantitative measurement of radioactive cesium in milk, blood, urine, and soil

M. Wada

After the accident of the Fukushima Daiichi nuclear power plant in mid-March in 2011, radioactive contamination of soil, food, and human's body became a serious concern in Japan. An HPGe semiconductor detector is the best device to measure the specific activity of weakly contaminated samples, however, it is worth evaluating a possibility of using NaI(Tl) scintillation spectrometers for this purpose, as they are available within a reasonable price range and are relatively easy to operate. Several months after the accident, most short-lived nuclei disappeared, and major radionuclides that remained in the environment are ^{134,137}Cs. This implies that we can use low-resolution spectrometers without identification problems.

Statistically, the detection limit, in units of the count number, according to the Cooper's method[1] is

$$N_{\rm m} = (A_{\rm m}^2 + A_{\rm m}\sqrt{A^2+8B})/2 \approx A_{\rm m}\sqrt{2B}, \qquad (1)$$

where $A_{\rm m}$ is the decision criteria, and typically, $A_{\rm m} = 3$ is used. B denotes background counts. The minimum detectable specific activity is then,

$$D_{\rm m} = N_{\rm m}/(\epsilon f T m) \approx A_{\rm m}\sqrt{2B}/(\epsilon f T m), \qquad (2)$$

where ϵ is the efficiency, f is the branching ratio, T is the measurement time, and m is the weight of the sample. B and ϵ, T, and m are strongly correlated, and hence, the actual dependence of $D_{\rm m}$ is

$$D_{\rm m} \propto A_{\rm m}\sqrt{w}/(f\epsilon^{\alpha} m^{\beta}\sqrt{T}), \qquad (3)$$

where α and β are approximately 0.5, but are variable due to the background and the sample condition, and w is the peak width. If we compare $D_{\rm m}$ for a typical HPGe and a 3 in. NaI detector, $w_{\rm Ge}/w_{\rm NaI} \approx 1/50$ and $\epsilon_{\rm Ge}/\epsilon_{\rm NaI} \approx 1/5$. In such a naive evaluation, NaI shows only $\sqrt{10}$ times less sensitivity as long as disturbing γ-ray peaks are not present in the region of interest.

A typical spectrum of ^{134,137}Cs consists of three peaks (Fig. 1): the one on the right at 800 keV is a mixture of peaks at 795 keV ($f = 85.44\%$) and 801 keV (8.73%) for ^{134}Cs; the one in the center is a 662 keV γ-ray from ^{137}Cs; the one on the left at 600 keV is a mixture of peaks at 605 keV (97.56%), 569 keV(15.43%), and 563 keV (8.38%) for ^{134}Cs. The specific activities (D) and the statistical errors (σ_D) can be deduced from the net counts of these peaks (N_i) and the standard deviation (σ_{Ni}) using the mixed branching ratios ($f_{600} = 121.73\%, f_{662} = 85.1\%, f_{800} = 94.17\%$), and the detection efficiencies ϵ_i, including the sum corrections. For example,

$$D_{134} = N_{800}/(f_{800}\epsilon_{800}Tm), \sigma_{D134} = \sigma_{800}/(f_{800}\epsilon_{800}Tm). \qquad (4)$$

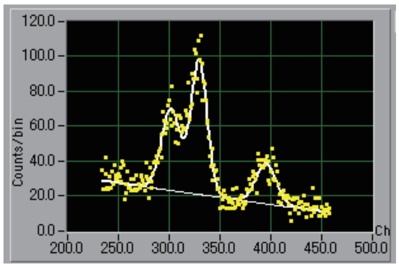

Fig. 1. γ-rays from ^{134,137}Cs of 2.8(1), 3.4(1) Bq measured with 3 in. well-type NaI spectrometer.

The net counts and their standard deviations can be obtained by the least-square fitting of the spectrum with three Gaussian peaks and a linear background (Fig. 1). Alternatively, the classical Covell's method, which determines the background line from the gross counts in specified regions on both sides of the peak, can be used to evaluate the net counts. Although this method cannot separate overlapped peaks, stable values of the sum counts N_L and the standard deviation σ_{NL} can be obtained. The contribution from ^{134}Cs can be subtracted with N_{800} using the ratio, $\alpha = f_{600}\epsilon_{600}/(f_{800}\epsilon_{800})$. The specific activities of ^{137}Cs and the statistical error are

$$D_{137} = (N_L - \alpha N_{800})/(f_{662}\epsilon_{662}Tm), \qquad (5)$$

$$\sigma_{D137} = \sqrt{\sigma_{NL}^2 + \alpha^2\sigma_{800}^2}/(f_{662}\epsilon_{662}Tm). \qquad (6)$$

A 3 in. well-type NaI scintillation spectrometer with an auto sample changer (Perkin Elmer) has been used to measure milk, blood, and urine from cattle, and soil samples. Although the volume of the sample is limited to 20 cm^3, the 4π solid angle provides a 15% photo-peak efficiency for 662 keV γ-rays. The detection limit for each radioisotope reached 0.15 Bq (7.5 Bq/kg) with a low potassium abundance sample for a one-hour measurement. The limit depends on the level of the continuum background, which is mainly caused by the Compton scattering of 1461 keV γ-rays from ^{40}K. In less contaminated samples, particularly for soil samples, peaks from environmental radioactivities such as ^{214}Bi and ^{214}Pb can cause misidentification problems. The annihilation peak at 511 keV also causes a problem in the background determination.

Well-shielded NaI spectrometers are indeed a useful tool for conducting radioactive contamination surveys.

References
1) J.A. Cooper, Nucl. Instr. Meth, **82**, 273 (1970).

Development of Pulse Height Analyzer for Education about Radiation

A. Taketani, T. Takahashi,*1 I.Y. Kawamo,*1 H. Murakami, M. Wada, M. Sekimoto,*2 K. Ninomiya,*1 Y. Ashikaga,*3 K. Imai,*4 H. Okura,*5 S. Kubono,*6 K. Nakagawa,*7 T. Fukui,*8 Y. Maruo,*9 and Y. Morimoto*10

The first prototype radiation detector for educational purposes was developed with the peripheral interface controller (PIC). After the Fukushima atomic reactor accidents, people inadequate knowledge abou radiations and radio activities bocame worried about their health and reacted improperly. We as physicists, can contribute to addressing their concern by helping them understand radiation and training them to take suitable actions. We are a group consisting of teachers, a curator, and physicists, and we have been discussing on how to develop a good education system for this puropose and have identified important items "experience of radiation measurement", "understand of radiation detection principle," and "assembling of radiation detector." The feature requirements for a radiation detector kit are

(1) Easy to assemble without a soldering iron.
(2) Inexpensive, with easily procurable parts.
(3) Ablity to detect environmental radiation.
(4) Tunable detection threshold.

The complete design of the first trial detector is described in Kawamo's article[1]. The detector consits of two main items, a sensor component and a pulse height analyzer (PHA). Radiations are injected into the sensor component and converted readable voltage signals. The sensor component consists of a sensor, a preamplifier, a shaping amplifier and a peak hold circuit.[1] Then, the PHA converts the voltage signal into digital values and displays their energy spectrum. The PHA consists of a comparator, an ADC, a pulse generator, and a display. The function diagram is shown in Fig. 1. When the signal from the peak hold circuit of the sensor component is fed into the comparator and ADC, only the signals exceeding the threshold are converted into a digital pulse height value by the ADC. Then, the digital values are transmitted to the PC for displaying the energy spectrum. The PHA was made from PIC18F4550[2] by Microchip; it is an 8-bit CPU with an ADC, comparators, digital inputs, digital outputs (DO), and a USB interface within a single chip. The chip has flash ROM for programing, which can be written into by a dedicated writer or a USB interface. The program for the PIC is written in C language[3]. The board with the PIC and other necessary parts costs 1100 yen. The typical AD conversion time required after signal rises in the peak hold circuit is 10μs. After AD conversion, the digitized pulse height values are stored in the PIC memory and transferred periodically to the PC through the USB interface. This chip can measure up to 100 KCPS radiation with adequate PIC memory. However, this value is extreamly high radiation to handle in a classroom. The data acquisition program on the PC was developed by using Microsoft Visual C#.[4] The program is event driven. When the PIC transmits the pulse height data, the PC receives them and updates the histogram display. Transmission requires about the 5 ms inclusive of the USB interrupt process. Fig. 2 shows the obtained histogram of ^{137}Cs the checking source.

The prototype of the PHA for the radiation detector was developed for educational purposes. It satisfied the functional requiements. We will produce 200 radiation detector assembly kits for supplying to classrooms.

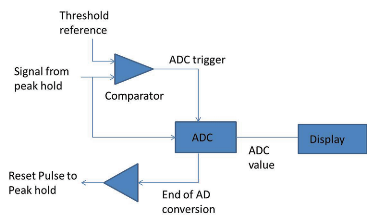

Fig. 1. Functional block diagram of pulse height analyzer.

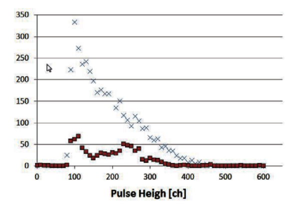

Fig. 2. Histogram of the pulse peight for ^{137}Cs. Squares and crosses represent backgrounds and signals respectively.

*1 Rikkyo University, Japan
*2 KEK, Japan
*3 Tottori University of Environmental Studies
*4 Japan Atomic Energy Agency
*5 Osaka Science Museum
*6 University of Tokyo
*7 Kobe University
*8 Hakuryo Junior High/Senior High School
*9 Hyogo Prefectural Kamigori High School
*10 Hyogo Prefectural Tobban High School

References
1) Y. Kawamo in this APR.
2) PIC18F2455/2550/4455/4550 Data sheet.
3) MPLAB C18 C Compiler User's Guide.
4) www.microsoft.com/visualstudio

Alternative method to evaluate internal dose using simple γ-ray spectrometer

M. Wada

Internal dose has been a critical topic of concern after the accident at the Fukushima Daiichi nuclear power plant. A significant amount of radionuclides released from the power plant has been spread over a wide area in Japan. After the such incident the human body may take radioactive substances directly from the plume in the initial days and indirectly from contaminated foods afterward. In order to evaluate the internal dose, the concentration of radioactive substances in the whole body should be measured. A so-called Whole Body Counter (WBC) has been exclusively used for such a purpose. However, popularly used WBCs have not been designed for low-level contamination and cannot be aimed for use in a high background environment. Furthermore, the number of WBCs for public use is limited compared to the demand. Hence, an alternative way to evaluate the concentration of radioactive substance in the human body is worth considering.

The main radioactive substances of concern are ^{137}Cs and ^{134}Cs. From a survey conducted on animals, it is known that radioactive Cs is mainly distributed in the muscles and not in the internal organs or bones[1). It would be more effective to measure the "muscle-rich" parts of a human body with a well-shielded γ-ray detector. A good candidate for such a part is the leg. A "U"-form shielding can be placed on top of the leg and a detector with a cylindrical shielding block can be placed at the bottom. Although the palm would not be muscle-rich, we evaluated the measurement of specific activity in the palm using standard γ-ray spectrometers used for food screening, without any modification to the shielding.

A phantom sample was made using a globe filled with 173 g contaminated rice with specific activities of 62.2(1.9) Bq/kg and 50.5(2.0) Bq/kg for ^{137}Cs and ^{134}Cs, respectively. The phantom was placed on top of the standard HPGe spectrometer to mimic a palm is grasping the head of the detector. At first, the detection efficiency, including the sum correction, was calibrated with a long measurement time. Then, the same phantom and an actual hand were measured with a realistic measurement time of 10 min. The net counts and their statistical error σ_N, the deduced activities, and the detection limits D_m in case of the decision criteria of 3 were listed in Table 1. The detection limits reached $\approx$2 Bq, which correspond to specific activities of $\approx$11 Bq/kg.

Table 1. γ-ray measurement of phantom palm (173 g) (top) and human hand (bottom) for 10 min measurements using a HPGe spectrometer.

γ-ray keV	efficiency %	count (σ_N)	Activity Bq	D_m Bq
662	1.40(5)	73.7(9.0)	10.3(1.3)	1.87
604	1.28(2)	68.3(9.0)	9.1(1.2)	2.18
795	1.05(2)	51.0(7.1)	9.45(1.3)	1.55
1460	0.63(9)	8(2.8)	16.5(7.0)	26
662	1.40(5)	3.8(2.8)	0.53(0.39)	1.68
604	1.28(2)	1.5(3.5)	0.20(0.47)	2.05
795	1.05(2)	1.8(2.5)	0.33(0.47)	2.28
1460	0.63(9)	19(4)	43.9(9.9)	19.0

A similar test was also performed with a 3" $\phi\times$3" NaI(Tl) scintillation spectrometer used for food screening (OKEN FNF-401). The efficiency, including the sum correction, for the mixed peaks of 795 keV and 801 keV γ-rays (branching ratio is 0.942) from ^{134}Cs was 3.1%, and the detection limit was 6.0 Bq for the same 172 g sample with a 10 min measurement. The result corresponds to a specific activity of 36 Bq/kg.

These two test measurements showed promising results. With a slight modification of the shielding block, γ-ray spectrometers for food samples can be used to evaluate the concentration of radioactive substances in a human palm.

Another problem in the WBC involves determining the detection efficiencies. Usually, phantom human bodies are used for the efficiency calibrations. However, the geometry of the human body is quite different for each individual, and the different distributions of radioactive substances within the body can cause large ambiguities in the efficiency evaluation. We propose here a simple way to evaluate the concentration of radioactive substances in the whole body as a ratio to that of potassium. Although the actual distributions of potassium and cesium are not equivalent[2), we can approximate that the two alkali elements are equally distributed to some extent. Under such an approximation, the ratio of the specific activities can be

$$\frac{A_{137\mathrm{Cs}}}{A_{40\mathrm{K}}} = \frac{N_{661}}{N_{1460}} \frac{\epsilon_{1460}}{\epsilon_{661}} \frac{b_{1460}}{b_{661}} \approx 0.056 \frac{N_{661}}{N_{1460}}, \qquad (1)$$

where N_x are the net counts, ϵ_x are the efficiencies, and b_x are the branching ratios. It should be noted that 1) N_{1460} is usually too small for a short-time measurement with a small HPGe spectrometer; 2) a sum peak of ^{134}Cs at 1401 keV can be overlapped with the ^{40}K peak in NaI measurements; and 3) the internal absorptions of different γ-rays can be slightly different.

References
1) M. Wada et al., In this report.
2) N. Yamagata, J. Radiation Research, **3**, 9 (1962).

VI. ORGANIZATION AND ACTIVITIES OF RIKEN NISHINA CENTER

(Activities and Members)

Organization Chart of Nishina Center for Accelerator-Based Science

As of March 31, 2012

- President RIKEN Ryoji Noyori
  - Nishina Center Advisory Council
    - RBRC Scientific Review Committee (SRC) Meeting
    - Advisory Committee for the RIKEN-RAL Muon Facility
  - RBRC Management Steering Committee(MSC)
- Director RIKEN WAKO Institute
  Tomoya Ogawa
  - Advanced Research Promotion Division
    - Accelerator-based Research Promotion Section
- Nishina Center for Accelerator-Based Science
  Director:Hideto En'yo (D.Sci)

  RIBF Research
  Deputy Director:Walter F. Henning (Ph.D)

  RIBF synergetic-use coordinator:
  Tohru Motobayashi (D.Sci)

  Senior Advisor:Yasushige Yano (D.Sci)
  Senior Advisor:Masayasu Ishihara (D.Sci)

  - Scientific Policy Committee
  - Program Advisory Committee
  - Coordination Committee
  - Safety Review Committee
  - Machine Time Committee
  - Public Relations Committee

Theoretical Research Division

- Quantum Hadron Physics Laboratory — Tetsuo Hatsuda (D.Sci)
- Theoretical Nuclear Physics Laboratory — Takashi Nakatsukasa (D.Sci)
- Strangeness Nuclear Physics Laboratory — Emiko Hiyama (D.Sci)
- Mathematical Physics Laboratory — Koji Hashimoto (D.Sci)

Sub Nuclear System Research Division

- Radiation Laboratory — Hideto En'yo (D.Sci)
- Advanced Meson Science Laboratory — Masahiko Iwasaki (D.Sci)
- RIKEN BNL Research Center — Nicholas P. Samios (Ph.D)
  - Theory Group — Larry McLerran (Ph.D)
  - Computing Group — Taku Izubuchi (D. Sci)
  - Experimental Group — Yasuyuki Akiba (D.Sci)
- RIKEN Facility Office at RAL — Teiichiro Matsuzaki (D.Sci)

RIBF Research Division

- Radioactive Isotope Physics Laboratory — Hiroyoshi Sakurai (D.Sci)
- Spin isospin Laboratory — Tomohiro Uesaka (D.Sci)
- Superheavy Element Laboratory — Kosuke Morita (D.Sci)
- High Energy Astrophysics Laboratory — Toru Tamagawa (D.Sci)
- Astro-Glaciology Research Unit — Yuko Motizuki (D.Sci)
- Accelerator Group — Osamu Kamigaito (D.Sci)
  - Accelerator R&D Team — Hiroki Okuno (D.Sci)
  - Ion Source Team — Takahide Nakagawa (D.Sci)
  - RILAC Team — Eiji Ikezawa
  - Cyclotron Team — Naruhiko Sakamoto (D.Sci)
  - Beam Dynamics & Diagnostics Team — Nobuhisa Fukunishi (D.Sci)
  - Cryogenic Technology Team — Hiroki Okuno (D.Sci)
  - Infrastructure Management Team — Masayuki Kase
- Instrumentation Development Group — Masanori Wakasugi (D.Sci)
  - SLOWRI Team — Michiharu Wada (D.Sci)
  - Polarized RI Beam Team — Hideki Ueno (D.Sci)
  - Rare RI-ring Team — Masanori Wakasugi (D.Sci)
  - SCRIT Team — Masanori Wakasugi (D.Sci)
- Research Instruments Group — Toshiyuki Kubo (D.Sci)
  - GARIS Team — Kouji Morimoto (D.Sci)
  - BigRIPS Team — Koichi Yoshida (D.Sci)
  - SAMURAI Team — Tohru Motobayashi (D.Sci)
  - Computing and Network Team — Takashi Ichihara (D.Sci)
  - Detector Team — Atsushi Taketani (D.Sci)
- Accelerator Applications Research Group — Tomoko Abe (D.Agr)
  - Radiation Biology Team — Tomoko Abe (D.Agr)
  - RI Applications Team — Hiromitsu Haba (D.Sci)
- User Liaison and Industrial Cooperation Group — Hideyuki Sakai (D.Sci)
  - User Support Office — Hideki Ueno (D.Sci)
  - Industrial Cooperation Team — Atsushi Yoshida (D.Sci)
- Safety Management Group — Yoshitomo Uwamino (D.Eng)

Members of Nishina Center for Accelerator-based Science

Executive Members

Hideto EN'YO (Director)
Walter F. HENNING (Deputy Director)
Tohru MOTOBAYASHI (RIBF synergetic-use coordinator)
Yasushige YANO (Senior Advisor)
Masayasu ISHIHARA (Senior Advisor)
Minami IMANISHI (Secretary)

Research Promotion Section Members

Shigeki ASAKAWA (Manager, Head of Accelerator-based Research Promotion Section)
Kyoji YAMADA
Takamori SHIMANA (until December 31, 2011)
Hayato NISHIMURA (since January 1, 2012)
Mari AOKI (until May 31, 2011)
Yukari ONISHI (since June 1, 2011)
Masatoshi MORIYAMA
Yukiko SATO
Rie KUWANA
Yuko OKADA

Nishina Center's Committee Members

Nishina Center Advisory Council (NCAC) Members

May, 2011

(Chair) Sydney GALES (GANIL, FRANCE)
Angela BRACCO (University of Milan, ITALY)
Wit BUSZA (MIT, USA)
Makoto INOUE (Kyoto University Research Reactor Institute)
Alexey KORSHENINNIKOV (Kurchatov Institute, RUSSIA)
Karlheinz LANGANKE (GSI, GERMANY)
Richard MILNER (MIT, USA)
Shoji NAGAMIYA (J-PARC Center)
Jean-Michel POUTISSOU (TRIUMF, CANADA)
WenQing SHEN (SINAP, P. R. CHINA)
Bradley SHERRILL (MSU, USA)
Tadashi SHIMODA (Osaka University)
Andrew TAYLOR (ISIS, UK)
Hiroshi TOKI (RCNP of Osaka University)
Robert TRIBBLE (Texas A & M University, USA)

Scientific Policy Committee Members

August, 2011

(Chair) Shoji NAGAMIYA (J-PARC Center)
Yasuhiko FUJII (Comprehensive Research Organization for Science and Society)
Yoshiyuki FUJII (National Institute of Polar Research)
Shoji FUTATSUGAWA (Japan Radioisotope Association)
Osamu HASHIMOTO (Tohoku University)
Ryutaro HIMENO (RIKEN)
Ryosuke KADONO (KEK)
Tadafumi KISHIMOTO (RCNP of Osaka University)
Hitoshi NAKAGAWA (National Agriculture and Food Research Organization)
Mitsuaki NOZAKI (KEK)
Hideo OHNO (JASRI)
Takaharu OTSUKA (CNS)
Osamu SHIMOMURA (KEK)
Kazuo SHINOZAKI (RIKEN)
Kohei TAMAO (RIKEN)
Hirokazu TAMURA (Tohoku University)
Hirohiko TSUJII (NIRS)
Akira UKAWA (University of Tsukuba)

Program Advisory Committee meeting for Nuclear Physics Experiments at RI Beam Factory (NP-PAC) Members

June, 2011 / December, 2011

(Chair) Robert TRIBBLE (Texas A & M University, USA)
Rick F. CASTEN (Yale University, USA)
Brian FULTON (University of York, ENGLAND)
Thomas GLASMACHER (NSCL, MSU, USA)
Muhsin N. HARAKEH (KVI, NETHERLANDS)
Mark HUYSE (Instituut voor Kern- en Stralingsfysica, BELGIUM)
Tadafumi KISHIMOTO (RCNP, Osaka University, JAPAN)
Alexey KORSHENINNIKOV (RRC Kurchatov Institute, RUSSIA)
Marek LEWITOWICZ (GANIL, FRANCE)
Christopher J. (KIM) LISTER (ANL, USA)
Takashi NAKAMURA (Tokyo Institute of Technology, JAPAN)
Akira ONO (Tohoku University, JAPAN)
Christoph SCHEIDENBERGER (GSI, GERMANY)
Tadashi SHIMODA (Osaka University, JAPAN)
Friedrich-K. THIELEMANN (University of Basel, SWITZERLAND)
Masanobu YAHIRO (Kyushu University, JAPAN)
Yanlin YE (Peking University, P. R. CHINA)

Program Advisory Committee meeting for Materials and Life Science Researches at RIKEN Nishina Center (ML-PAC) Members

September, 2011

(Chair) Jean-Michel POUTISSOU (TRIUMF, CANADA)
Alex AMATO (PSI, SWITZERLAND)
George A. BEER (University of Victoria, CANADA)
Fumio HANAOKA (Gakushuin University, JAPAN)
Reizo KATO (RIKEN, JAPAN)
Kenichiro KOMAKI (University of Tokyo, JAPAN)
Kenya KUBO (International Christian University, JAPAN)
Douglas E. MACLAUGHLIN (University of California, Riverside, USA)
Sadamichi MAEKAWA (JAEA, JAPAN)
Kanetada NAGAMINE (University of California, Riverside, USA)
Nobuhiko NISHIDA (Tokyo Institute of Technology, JAPAN)
Kusuo NISHIYAMA (KEK, JAPAN)
Francis L. PRATT (RAL, STFC, UK)
Isamu YAMAGUCHI (Tokyo University of Agriculture, JAPAN)
Johann ZMESKAL (Stefan Meyer Institute For Subatomic Physics, AUSTRIA)

Industrial Program Advisory Committee (In-PAC) Members

(not held)

(Chair) Akihiro IWASE (Osaka Prefecture University)
Toshiyuki AZUMA (RIKEN)
Kenya KUBO (International Christian University)
Toshinori MITSUMOTO (Sumitomo Heavy Industries, Ltd.)
Hitoshi NAKAGAWA (National Agriculture and Food Research Organization)
Nobuhiko NISHIDA (Tokyo Institute of Technology)

Theoretical Research Division
Quantum Hadron Physics Laboratory

1. Abstract

Atomic nuclei are made of protons and neutrons bound by the exchange of Yukawa's pion and other mesons. Also, protons and neutrons are made of quarks bound by the exchange of gluons. These strong interactions are governed by the non-Abelian gauge theory called the quantum chromodynamics (QCD). On the basis of theoretical and numerical analyses of QCD, we study the interactions between the nucleons, properties of the dense quark matter realized at the center of neutron stars, and properties of the hot quark-gluon plasma realized in the early Universe. Strong correlations common in QCD, graphene and cold fermionic atoms are also studied theoretically.

2. Major Research Subjects

(1) Origin of the nuclear force
(2) Quark-gluon plasma at high temperature and at high baryon density
(3) Lattice gauge theory
(4) Strongly correlated many-body systems
(5) High precision QED

3. Summary of Research Activity

(1) Lattice Nuclear Force

1-1. Hyperon Interaction and the H-dibaryon
The flavor-singlet H dibaryon, which has strangeness -2 and baryon number 2, is studied by the approach recently developed for the baryon-baryon interactions in lattice QCD. The flavor-singlet central potential is derived from the spatial and imaginary-time dependence of the Nambu-Bethe-Salpeter wave function measured in Nf=3 full QCD simulations with the lattice size of L =2, 3, 4 fm. The potential is found to be insensitive to the volume, and it leads to a bound H dibaryon with the binding energy of 30–40 MeV for the pseudoscalar meson mass of 673–1015 MeV.
1-2. Three-Nucleon Forces from Lattice QCD
It has been realized that three-nucleon forces (3NF) play an important role in various phenomena in nuclear physics and astrophysics. We performed an exploratory study to determine 3NF from first-principle lattice QCD simulations. Repulsive 3NF is found at short distance in the triton channel.

(2) Heavy-quark potential in hot QCD

We calculate for the first time the complex potential between a heavy quark and antiquark at finite temperature across the deconfinement transition in lattice QCD. The real and imaginary part of the potential at each separation distance r is obtained from the spectral function of the thermal Wilson loop. We confirm the existence of an imaginary part above the critical temperature Tc, which grows as a function of r and underscores the importance of collisions with the gluonic environment for the melting of heavy quarkonia in the Quark-Gluon-Plasma.

(3) Study concerning non-perturbative study of supersymmetric quantum field theories

3-1. Numerical test of the N=2 Landau-Ginzburg description
By some analytic arguments, it is widely considered that the low-energy limit of the two-dimensional N=2 Wess-Zumino model (2D N=2 WZ model) is a non-trivial supersymmetric conformal field theory (SUSY CFT). To test this conjecture from the completely different view point, we carried out a numerical simulation of the 2D N=2 WZ model by using a momentum-cutoff regularization that we had been proposed. We measured the scaling dimension of the scale field and the central charge of the system in the lowe-energy limit and obtained encouraging results that are consistent with the emergence of SUSY CFT.

3-2. Algebraic proof of the supersymmetric limit in lattice formulations of the four-dimensional N=1 supersymmetric Yang-Mills theory
All the current numerical simulations of the four-dimensional N=1 supersymmetric Yang-Mills theory (4D N=1 SYM) are based on the idea that, in the continuum limit, the chiral symmetric limit lead to the restoration of the supersymmetry (SUSY) Ward-Takahashi identity. Although this is naturally expected from the view point of the corresponding effective field theory, there has been no rigorous proof of this coincidence of the chiral symmetric limit and the supersymmetric limit. By

formulating a generalized BRS transformation that treats the gauge, SUSY, translation and U(1) axial transformations in a unified way, we gave an algebraic proof of this fundamental fact.

3-3. Supersymmetric Yang-Mills theory on the lattice
Supersymmetry is one of interesting subjects in elementary particle physics. Non-perturbative effects of supersymmetric theories can be extracted from numerical simulations of lattice theory. We performed a numerical simulation of two dimensional N=(2,2) lattice supersymmetric Yang-Mills theory with periodic boundary condition. Our results are consistent with the supersymmetry restoration in the continuum limit.

(4) Lattice Monte Carlo simulations for unitary fermions in a box and a trap
We used a recently developed lattice Monte Carlo method to study systems of two-component nonrelativistic fermions at infinite scattering length and vanishing interaction range (e.g., "unitary fermions"). In the process of these studies, we also developed an unconventional method for extracting energies from multi-fermion correlation function distributions with heavy tails, allowing us to performed studies of up to 66 fermions confined to a finite box, and 70 fermions confined to a harmonic trap. We compared our few-body results for the energy of these systems with previously published benchmarks, finding agreement within statistical errors. We also performed two independent many-body calculations of the Bertsch parameter, defined as the ground state energy of untrapped unitary fermions in units of the free gas energy at the same density.

(5) QED calculation of the lepton anomalous magnetic moments.
The anomalous magnetic moments of electron and muon have been studied in view of the perturbation theory of the quantum electrodynamics(QED). The eighth-order contributions have been completely determined. The tenth-order contributions that involve at least one fermion loop have been obtained. The more accurate value of the fine-structure constant thus becomes available.

Head
Tetsuo HATSUDA

Members
Hiroshi SUZUKI
Takumi DOI

Postdoctoral Researchers
Daisuke KADOH
Michael ENDRES

Contract Researchers
Makiko MATSUKAWA

Visiting Scientists
Motoi TACHIBANA (Fac. of Sci. and Eng., Saga Univ.)
Toichiro KINOSHITA (Phys. Dep., Cornell Univ.)
Sinya AOKI (Grad. Sch. of Sci., Univ. Tsukuba)
Taichi KAWANAI (Grad. Sch. of Sci., Univ. Tokyo)
Ryoichi SEKI (Phys. Dep., California State Univ.)
Masahito UEDA (Grad. Sch. of Sci., Univ. Tokyo)

Research Consultants
Hiroshi TOKI (RCNP, Osaka Univ.)

Internarional Program Assiciate
Nino BRATVIC (Phys. Dep., Technical Univ. Munich)
Fukun XU (Chinese Academy of Science)

Student Trainee

Bruno CHARRON (Grad. Sch. of Sci., Univ. Tokyo)

Intern

Yuji HIRONO (Grad. Sch. of Sci., Univ. Tokyo)

Secretariy

Yoko FUJITA
Yuri TSUBURAI

Theoretical Research Division
Theoretical Nuclear Physics Laboratory

1. Abstract

Nuclei are finite many-particle systems composed of protons and neutrons. They are self-bound in femto-scale (10^{-15}m) by the strong interaction (nuclear force) whose study was pioneered by Hideki Yukawa. Uncommon properties of the nuclear force (repulsive core, spin-isospin dependence, tensor force, etc.) prevent complete microscopic studies of nuclear structure. There exist number of unsolved problems even at present. In addition, radioactive beam facilities reveal novel aspects of unstable nuclei. We are tackling these old problems and new issues in theoretical nuclear physics, developing new models and pursuing large-scale calculations of quantum many-body systems. We are also strongly involved in research on other quantum many-body systems, to resolve mysteries in the quantum physics

2. Major Research Subjects

(1) Nuclear structure and quantum reaction theories
(2) First-principle calculations with the density functional theory for many Fermion systems
(3) Computational nuclear physics

3. Summary of Research Activity

(1) Correlation between the pygmy dipole strength and neutron skin thickness
We have been studying the low-lying electric dipole mode, so-called the pygmy dipole resonances (PDR) in neutron-rich isotopes, with systematic calculation of the electric dipole responses up to mass A=110 region. In this year, we investigate correlation between the PDR and the neutron skin thickness. The PDR distributions show a remarkable linear correlation with the neutron skin thickness for each isotopic chain with N=28-34 and N>50, with a universal slope of 0.18-0.20 fm^{-1}. On the other hand, the correlation is weak outside of these regions. We also discussed parameter dependence of such correlation and found same conclusion.

(2) Finite amplitude method for evaluation of the RPA matrix
The explicit evaluation of the matrix of random-phase approximation (RPA) is known to be very demanding task in realistic nuclear energy functionals. We have developed a new methodology to do this using the finite amplitude method (FAM). The method was tested with a code we developed last year using an existing spherically symmetric Hartree-Fock-Bogoliubov code (HFBRAD) in the coordinate-space representation. It turns out to be very efficient with a capability to turn an existing HF(B) code into the (Q)RPA code, very easily.

(3) Properties of the giant resonances in spherical and deformed nuclei
Roles of deformation on the giant resonance were systematically investigated by means of the deformed QRPA employing the Skyrme and the local pairing energy-density functionals. Particularly, deformation effects, the mixing of the giant resonances with different multipolarities, and dependence on the effective mass are discussed and clarified.

(4) Studies of nuclear responses in heavy deformed nuclei using the canonical-basis TDHFB method
The canonical-basis TDHFB method is suitable for studies of dynamical properties of nuclei with superfluidity. The computer program with the Skyrme functional was developed and used for the systematic linear response calculations of heavy deformed nuclei. We have calculated the photoabsorption cross sections in nuclei along the r-process path and have found significant increase of low-energy E1 strength in isotopes with N>82. This may give a great impact on the nucleosynthesis in supernovae explosions.

(5) Microscopic description of large-amplitude quadrupole collective dynamics in low-lying states
In this study, we have studied large-amplitude quadrupole deformation dynamics using the five-dimensional quadrupole collevtive Hamiltonian. We determine the collective potential and inertial functions with the constrained Hartree-Fock-Bogoliubov plus local quasiparticle random-phase-approximation method. We have applied this method to low-lying states in neutron-rich isotopes around ^{64}Cr, where the recent experimental data suggest the onset of deformation. The calculated results are in good agreement with the available data and indicate that the shape transition from spherical and prolate may occur from ^{60}Cr to ^{64}Cr. With this method, we also have studied ^{110}Mo, whose new excited states have been observed in the experiment at RIKEN. In this region of Mo isotopes, a shape transition from prolate, via gamma-soft (unstable against axially asymmetric deformation), to oblate was predicted theoretically. Our calculation has reproduced the experimental data for ^{110}Mo well and showed that the low-lying states in ^{110}Mo are rather gamma-soft.

(6) Mean-field calculation including proton-neutron mixing

Proton-neutron (p-n) pairing is one of the open problems in nuclear physics and expected to play some role in various phenomena in medium and heavy mass region. In spite of the recent experimental progress, it is still unclear what the fingerprint of the p-n pairing is and how like-particle and p-n correlations interplay in the p-h and p-p channels. The aim of this study is to elucidate the role of p-n pairing on basis of the nuclear energy density functional theory. As a first step toward the calculation based on the density functional theory including p-n pairing, we have developed a numerical code for the Hartree-Fock calculation based on the Skyrme energy density functional which incorporates an arbitrary proton-neutron mixing in the p-h channel. In this calculation, the single-particle states are described as a mixture of protons and neutrons and the energy density functional is generalized to the form with the p-n mixed density. We are now performing test calculations for nuclei around the N=Z line in the light and medium-mass regions.

(7) Extra-push energy in heavy-ion fusion reaction studied with the TDHF simulation
We have studied extra push dynamics in heavy ion fusion reactions. Our purpose is to investigate whether the microscopic time-dependent Hartree-Fock (TDHF) calculation quantitatively reproduces the extra-push energy for the fusion reaction, including the criterion for the mass combination of projectile and target above which the extra push is needed, and how much the extra push energy is. We study these issues in heavy-ion fusion reactions with TDHF theory employing the full Skyrme energy functional and without any geometric symmetry restrictions. We performed a systematic investigation with a variety of projectile-target combinations and found that for light systems the TDHF fusion threshold, interaction barrier with frozen-density energy density functional (FD-EDF) method and experimental Coulomb barrier have a quite good agreement, which imply extra push is not needed for light systems. However for heavy system, the TDHF fusion threshold is higher than the interaction barrier with FD-EDF method. This is consistent with empirical law of the necessity of the extra-push energy for heavy systems.

(8) Enhancement of ^{16}O+^{18}O sub-barrier fusion cross sections by distortion of valence neutrons in ^{18}O
Effects of valence neutrons in ^{16}O+^{18}O sub-barrier fusions are investigated in a potential model using adiabatic potentials obtained by a method of anti-symmetrized molecular dynamics (AMD) with a constraint on internuclear distance. We found that the sub-barrier fusion cross sections of ^{16}O+^{18}O are enhanced because of distortion of valence neutrons in ^{18}O.

(9) Separation of a Slater determinant wave function with a neck structure into spatially localized subsystems
A method to separate a Slater determinant wave function with a two-center neck structure into spatially localized subsystems is proposed. An orthonormal set of spatially localized single-particle wave functions is obtained by diagonalizing the coordinate operator for the major axis of a necked system. Using the localized single-particle wave functions, the wave function of each subsystem is defined. Therefore, defined subsystem wave functions are used to obtain density distributions and mass centers of subsystems. The present method is applied to the separation of Margenau-Brink cluster wave functions of alpha + alpha, ^{16}O + ^{16}O, and alpha + ^{16}O into their subsystems, and also to the separation of anti-symmetrized molecular dynamics (AMD) wave functions of ^{10}Be into alpha + ^{6}He subsystems.

(10) Coexistence of various rotational bands and alpha clustering in ^{42}Ca
Coexistence of various low-lying rotational bands in ^{42}Ca have been investigated using the deformed-basis AMD. The parity and angular momentum projections and the generator coordinate method (GCM) obtained low-lying states. Energy variations with constraints on quadrupole deformation parameter and intercluster distance between alpha and ^{38}Ar clusters obtained the GCM basis. The rotational band built on the second 0+ (1.84 MeV) state was reproduced, and coexistence of two more 0+ rotational bands and side bands of them due to triaxial deformation was predicted. Variety of combinations of particle-hole configurations for protons and neutrons develops rich structures in ^{42}Ca.

(11) Ab initio calculation for photoabsorption reaction in 4He in collaboration
There are some discrepancies in the low energy data on the photoabsorption cross section of ^{4}He. In order to resolve this controversy, we calculate the cross section with realistic nuclear forces and explicitly correlated Gaussian functions. Final state interactions and two- and three-body decay channels are taken into account. The cross section is evaluated in two methods: With the complex scaling method and the microscopic R-matrix method. Both methods give virtually the same result. The cross section rises sharply from the 3H+p threshold, reaching a giant resonance peak at 26–27MeV. Our calculation reproduces almost all the data above 30MeV. We stress the importance of ^{3}H+p and ^{3}He+n cluster configurations on the cross section as well as the effect of the one-pion exchange potential on the photonuclear sum rule.

(12) Systematic analysis of total reaction cross sections in unstable nuclei
Exploring nuclei has been making rapid progresses beyond the p-, sd-shell region. Recently, the total reaction and interaction cross sections, which are closely related to the nuclear size properties, are measured in neutron-rich Ne and Mg region. They exhibit some exotic structures, for example, halos, skins deformations etc. and motivate us to make a

systematic analysis of the total reaction cross sections. We employ the Glauber model which is widely used for analyzing high energy nuclear reactions. In order to describe exotic deformations, input densities are generated from the wave functions obtained by the Skyrme-Hartree-Fock Method in a fully three-dimensional coordinate space. The calculated total reaction cross sections of Ne isotopes consistently agree with the very recent measurement and imply importance of deformations for reproducing a large increase of the cross section as increasing a neutron number. Predictions for Mg and Si isotopes are made. A detail analysis is underway and will be reported soon.

(13) Thermal nuclear pairing within the self-consistent quasiparticle RPA
The self-consistent quasiparticle RPA (SCQRPA) is constructed to study the effects of fluctuations on pairing properties in nuclei at finite temperature and z-projection M of angular momentum. Particle-number projection (PNP) is taken into account within the Lipkin-Nogami method. Several issues such as the smoothing of superfluid-normal phase transition, thermally assisted pairing in hot rotating nuclei, extraction of the nuclear pairing gap using an improved odd-even mass difference are discussed. A novel approach of embedding the PNP SCQRPA eigenvalues in the canonical and microcanonical ensembles is proposed and applied to describe the recent empirical thermodynamic quantities for iron, molybdenum, dysprosium, and ytterbium isotopes.

(14) Shear-viscosity to entropy-density ratio from giant dipole resonances in hot nuclei
The Green-Kubo relation and fluctuation-dissipation theorem are employed to calculate the shear viscosity η of a finite hot nucleus directly from the width and energy of the giant dipole resonance (GDR) of this nucleus. The ratio η/s of shear viscosity η to entropy density s is extracted from the experimental systematics of the GDR in copper, tin, and lead isotopes at finite temperature T . These empirical results are then compared with the predictions by several independent models as well as with almost model-independent estimations. Based on these results, it is concluded that the ratio η/s in medium and heavy nuclei decreases with increasing temperature T to reach (1.3–4) x $1/(4\pi)$ (in the units of hbar by k_B) at T = 5 MeV.

(15) Pairing reentrance in hot rotating nuclei
The pairing gaps, heat capacities, and level densities are calculated within the BCS-based quasiparticle approach, including the effect of thermal fluctuations on the pairing field within the pairing model plus non-collective rotation along the z axis for 60Ni and 72Ge nuclei. The analysis of the numerical results obtained shows that, in addition to the pairing gap, the heat capacity can also serve as a good observable to detect the appearance of the pairing reentrance in hot rotating nuclei, whereas such a signature in the level density is rather weak. The test calculations by using the same single-particle configuration as that used in the recent calculations within the Shell-Model Monte Carlo (SMMC) approach, but obtained within the Woods-Saxon potential, reveal that the neutron pairing reentrance in 72Ge is an artifact, which is caused by the use of the same single-particle spectrum for both protons and neutrons, whereas the irregularity on the curve for the logarithm of level density, reported in the SMMC calculations, is caused by unphysically large values of the heat capacity at low T within the SMMC approach.

(16) Black-sphere-model study on energy dependence of nucleon-nucleon total cross section
In the framework of the contemporary black-sphere model, we examined the energy dependence of nucleon-nucleon total cross section. We have found that the new parameterization by Bertulani and De Conti is precise enough to calculate total reaction cross sections, which deffers from the standard one in the proton-proton total cross section for the energies less than 300 MeV. This is due to the lack of precise data in this energy region. We calculate total reaction cross section of carbon-carbon reaction in the black-sphere model with two different parameterizations, one is given by Bertulani and De Conti and the other is the one by the SAID program of the version "SP07". The difference between the two curves appears clearly, and the curve obtained by the one by Bertulani and De Conti reproduces the precise data very good. It is hard to distinguish one from the other if we would use proton-carbon reactions.

(17) Size of excited states
We systematically derive a length scale characterizing the size of a low-lying, beta-stable nucleus from empirical data for the diffraction peak angle in the proton inelastic differential cross section of incident energy around 1 GeV. We have found that for ^{12}C, $^{58,60,62,64}Ni$, and ^{208}Pb, the value of a_l, the black-sphere radius of spin l, obtained from the inelastic channel is generally larger than the value obtained from the elastic channel and tends to increase with E_x, with a few exceptions in which case the black sphere radius decreases with E_x in its central value but can be regarded as unchanged allowing for the error bars. This is consistent with the behavior of the transition radii obtained systematically from electron inelastic scattering off ^{208}Pb. The increase is remarkable for the Hoyle state, a feature consistent with the alpha clustering picture. We hope that the present analysis could develop into a systematic drawing of the black-sphere radii of isomers and nuclei in other characteristic excited states over a chart of the nuclides.

Head

Takashi NAKATSUKASA

Members

Akihisa KOHAMA

Special Postdoctoral Researchers

Yasutaka TANIGUCHI
Nobuo HINOHARA
Tsunenori INAKURA
Wataru HORIUCHI

Postdoctoral Researcher

Koichi SATO

Contract Researchers

NguyenDinh DANG

Research Associate

Guo LU

Senior Visiting Scientists

Kenichi MATSUYANAGI
Hiroyuki SAKURAGI

Research Consultants

Kiyomi IKEDA
Syuhei YAMAJI
Kosai TANABE

Visiting Scientists

Takashi ABE (Univ of Tokyo)
Yasuhisa ABE (RCNP)
Anatolijs AFANASJEVS (Mississippi State Univ.)
Yoshihiro ARITOMO (JINR)
Paolo AVOGADRO (Univ. of Milan)
Simone BARONI (Univ. of Washington)
Carlos BERTULIANI (Texas A&M Univ.)
Satoshi CHIBA (Japan Atomic Energy Agency.)
TiebKhoa DAO (Inst. Nucl. Scie. Tech.)
Elisabeth ELSTER (Ohio Univ.)
Yoshiko ENYO (Kyoto Univ.)
Shuichiro EBATA (Univ. of Tokyo)
Hubert FLOCARD (INP-Orsay)
Yasuro FUNAKI (Univ. Tsukuba)
Shinichiro FUJII (CNS)
Koichi HAGINO (Tohoku Univ.)
Ikuko HAMAMOTO (Lund Univ.)

Koji HIGASHIYAMA (Chiba Institute of Technology)
Michio HONMA (Aizu Univ.)
Takatoshi HORIBATA (Aomori Univ.)
Munetake ICHIMURA (The Open Univ of Japan)
Kei IIDA (Kochi Univ.)
Akitsu IKEDA (Shizuoka Inst. Scie. Tech.)
Naoyuki ITAGAKI (YITP)
Makoto ITO (Kansai Univ.)
Akira IWAMOTO (Japan Atomic Energy Agency)
Jie MENG (Peking Univ.)
Kaori KAKI (Shizuoka Univ.)
Kiyoshi KATO (Hokkaido Univ.)
Toshitaka KAJINO (NAOJ)
Masaaki KIMURA (Hokkaido Univ.)
Wenhui LONG (Peking Univ.)
Takuma MATSUMOTO (Kyushu Univ.)
Peter MOLLER (Los Alamos National Lab.)
Kazuo MUTO (Tokyo Institute of Technology)
Kazuyuki OGATA (RCNP)
Makito OI (Senshu Univ.)
Akira ONO (Tohoku Univ.)
Masahisa OTA (Konan Univ.)
Kazuhiro OYAMATSU (Aichi Shukutoku Univ.)
Hiroyuki SAGAWA (Aizu Univ.)
Badawy SARHAN (Cairo Univ.)
Ryoichi SEKI (California Univ.)
Noritaka SHIMIZU (Univ of Tokyo)
Yoshifumi SHIMIZU (Kyushu Univ.)
Kosuke SUMIYOSHI (Numazu National College of Technology)
Akihiro SUZUKI (Suzuki Corporation)
Yasuyuki SUZUKI (Niigata Univ.)
Toshio SUZUKI (Fukui Univ.)
Naoki TAJIMA (Univ of Fukui)
Masatoshi TAKANO (Waseda Univ.)
Masaaki TAKASHINA (RCNP)
Kazuo TAKAYANAGI (Sophia Univ.)
Noboru TAKIGAWA (Tohoku Univ.)
Kazuko TANABE (Otsuma Women's Univ.)
Jun TERASAKI (Univ. North Carolina)
Yutaka UTSUNO (Japan Atomic Energy Agency.)
Takahiro WADA (Kansai Univ.)
Kazuhiro YABANA (Grad. Sch. of Pure and Applied Sci., Univ. Tsukuba)
Taiichi YAMADA (Kanto Gakuin Univ.)
Masayuki YAMAGAMI (Aizu Univ.)
Kenichi YOSHIDA (Niigata Univ.)
Naotaka YOSHINAGA (Saitama Univ.)
Yumin ZHAO (Shanghai Jiao Tong Univ.)

Students

International Program Associate

Jia-Jie SHEN (Shanghai Jiao Tong Univ.)

Secretaries

Noriko KIYAMA

Keiko SUZUKI

Theoretical Research Division
Strangeness nuclear physics Laboratory

1. Abstract

We proposed accurate few-body calculational method called “Infinitesimally shifted Gaussian lobe method”. Recently, we developed this method to four-body systems and five-body systems. This method is applicable for various three- and four-body systems. For example, we applied it to hypernuclear physics and clarified what is important and impressed. In fact, we applied this method to three kinds of hypernuclear experiments (KEK-E419, BNL-E930, and -E929) in the past, and we contributed to these experiments by discussing with experimentalists, analyzing the data, and interpreting the data.

2. Major Research Subjects

(1) Hypernuclear structure from the view point of few-body problem
(2) Ultra clod atom
(3) Baryon-baryon interaction based on lattice QCD
(4) Clustering structure for ^{12}C and ^{16}O

3. Summary of Research Activity

(1) The binding energies of the ground state and the excited state of ^4He trimer and ^4He tetramer were performed using Gaussian Expansion Method. From the binding energies of the

excited state of these systems, and behavior of the wavefunction, we propose a model which predicts the binding energy of the first excited state of ^4He_N (N>3) measured from the $^4He_{N-1}$ ground state to be nearly $n/(2(N-1))B_2$ where B_2 is the dimmer binding energy.
(2) By the quenched lattice QCD simulation for two nucleons with finite scattering energy, validity of the derivative expansion of the general nucleon-nucleon potential is studied. The leading-order potentials obtained at different energies (E ～0 MeV and 45 MeV) show no difference within statistical errors, which validated the local approximation of the potential up to E=45 MeV for the central and tensor potentials.

Head
Emiko HIYAMA

Special Postdoctoral Researchers
Pascal NAIDON

Contract Researchers
Yasuro FUNAKI
Takahisa KOIKE
Keiko MURANO
Ying ZHANG
Jinju HU

Visiting Scientists
Takayuki MYO (Osaka Institute of Technology)
Taiichi YAMADA (Kanto Gakuin University)
Tetsuo HYODO (Tokyo Institute of Technology)
Makoto OKA (Tokyo Institute of Technology)
Tomokazu FUKUDA (Osaka Electro-Communication University)
Daisuke JIDO (YITP, Kyoto University)
Hidekatsu NEMURA (University of Tsukuba)
Soichi ISHIKAWA (Hosei University)
Takenori FURUMOTO (YITP, Kyoto University)
Atsushi HOSAKA (RCNP, Osaka University)
Shoji SHINMURA (Gifu University)

Akinobu DOTE (High Energy Accelerator Research Organization, KEK)
Thomas RIJKEN (Radboud University Nijmegen)
Kazuma NAKAZAWA (Gifu University)
Atsushi UMEYA (Nihon Institute of technology)
Yoichi IKEDA (Tokyo Institute of technology)
Toru SATO (Osaka University)
Satoru HIRENZAKI (Nara Women's University)
Masayuki ASAKAWA (Osaka University)
Masakiyo KITAZAWA (Osaka Univeristy)

Research Consultants
Yasuo YAMAMOTO
Kiyomi IKEDA

Student Trainees
Simpei ENDO (Grad. Sch. Sci., University of Tokyo)

Secretary
Makiko OHISHI
Yoko FUJITA
Yuri TSUBURAI

Theoretical Research Division
Mathematical Physics Laboratory

1. Abstract

The aim of mathematical physics laboratory is to apply mathematical scheme to resolve long-standing issues in various subjects of physics. Mathematics, in particular that originates in superstring theory, has universal feature which is common to wide range of physics. This covers elementary particle physics, hadron physics, nuclear physics, cosmology, general relativity and condensed matter physics. We apply mathematical scheme such as superstring theory, D-branes, AdS/CFT correspondence, solitons, statistical mechanics and integrable systems. Topics which the laboratory covers currently include non-perturbative analysis of quantum chromo-dynamics, superstrings, and models beyond the standard model of particle physics, and soliton physics.

2. Major Research Subjects

(1) Application of Superstring Theory
(2) Non-perturbative analyses of strongly-coupled gauge theories
(3) Physics of Black Holes and Cosmology
(4) Solitons physics
(5) Condensed matter theory
(6) Transport phenomena

3. Summary of Research Activity

Interplay between mathematics and physics is indispensable, as any physics law is described in terms of mathematics. However, the present status of various theoretical physics does not fully appreciate the usefulness of mathematics, as each topics goes into details and has less interaction with other subjects even nearby. We integrate various subjects of physics, by applying recent development of mathematics and mathematical physics, to solve long-standing issues in physics. In particular, mathematical methods in superstring theory has been developed and is mature enough to be applied to other physics. We put efforts on the application as described below, in addition to some other mathematical techniques such as numerical simulations, solitons and integrable systems.

(1) Application of superstring theory

AdS/CFT correspondence and nuclear physics

The renowned AdS/CFT correspondence, which was initiated in superstring theory, is a useful and powerful tool for analyzing strongly-coupled gauge theories. This has been applied to QCD, the dynamics of quarks. We studied how this powerful tool can have an impact on nuclear physics. We computed an effective action of multi-baryon systems, which should serve as a basic quantum action for nuclear physics. This turned out to reproduce nicely nuclear forces and baryon spectrum. In addition, three-body nuclear force was computed.

AdS/CFT correspondence and hadron mass

In generic holographic QCD, we find that baryons are bound to form a nucleus, and that its radius obeys the empirically-known mass number (A) dependence r $A^{1/3}$ for large A. Our result is robust, since we use only a generic property of D-brane actions in string theory. We also show that nucleons are bound completely in a finite volume. Furthermore, employing a concrete holographic model (derived by Hashimoto, Iizuka, and Yi, describing a multi-baryon system in the Sakai-Sugimoto model), the nuclear radius is evaluated as $O(1)\times A^{1/3}$ [fm], which is consistent with experiments.

(2) Lattice QCD

1) Charmonium spectral functions with the variational method in zero and finite temperature lattice QCD
   We propose a method to evaluate spectral functions on the lattice based on a variational method. On a lattice with a finite spatial extent, spectral functions consist of discrete spectra only. Adopting a variational method, we calculate the locations and the heights of spectral functions at low-lying discrete spectra. We first test the method in the case of analytically solvable free Wilson quarks at zero and finite temperatures and confirm that the method well reproduces the analytic results for low-lying spectra.

2) Phase structure of finite temperature QCD in the heavy quark region
   We study the quark mass dependence of the finite temperature QCD phase transition in the heavy quark region using an

effective potential defined through the probability distribution function of the average plaquette.

(3) Transport phenomena

1) Ultrasoft Fermionic Mode in Yukawa Theory at High Temperature
We explore whether an ultrasoft fermionic mode exists at extremely high temperature in Yukawa theory with massless fermion.

2) Hadron properties at finite temperature and density with two-flavor Wilson fermions
Meson properties at finite temperature and density were studied in lattice QCD simulations with two-flavor Wilson fermions. For this purpose, we investigate screening masses of mesons in pseudo-scalar (PS) and vector (V) channels. We found that the temperature dependence of the screening masses normalized by temperature, shows notable structure, and approach 2π at high temperature in both channels, which is consistent with twice the thermal mass of a free quark in high temperature limit.

(4) String theory and field theory

1) Matrix model from N=2 orbifold partition function
The orbifold generalization of the partition function, which would describe the gauge theory on the ALE space, is investigated from the combinatorial perspective. It is shown that the root of unity limit of the q-deformed partition function plays a crucial role on the orbifold projection. Then starting from the combinatorial representation of the partition function, a new type of multi-matrix model is derived by considering its asymptotic behavior. It is also shown that Seiberg-Witten curve for the corresponding gauge theory arises from the spectral curve of this multi-matrix model.

2) Β-ensembles for toric orbifold partition function
We investigate combinatorics of the instanton partition function for the generic four dimensional toric orbifolds. It is shown that the orbifold projection can be implemented by taking the inhomogeneous root of unity limit of the q-deformed partition function. The asymptotics of the combinatorial partition function yields the multi-matrix model for a generic β.

(5) Soliton physics

1) Vortices on Orbifolds
The Abelian and non-Abelian vortices on orbifolds are investigated based on the moduli matrix approach, which is a powerful method to deal with the BPS equation. The moduli space and the vortex collision are discussed through the moduli matrix as well as the regular space. It is also shown that a quiver structure is found in the Kahler quotient, and a half of ADHM is obtained for the vortex theory on the orbifolds as the case before orbifolding.

Head
Koji HASHIMOTO

Postdoctoral Researchers
Masaki MURATA
Yoshimasa HIDAKA

Contract Researcher
Yu MAEZAWA
Hideaki IIDA
Tetsutaro HIGAKI

Rsearch Consultant
Keiji IGI
Yoshio YAMAGUCHI

Senior Visiting Scientist

Koichi YAZAKI

Visiting Scientists

Tatsumi AOYAMA (Nagoya Univ.)
Kazuo FUJIKAWA (Nihon Univ.)
Masanori HAYAKAWA (University of Washington)
Norihiro IIZUKA (CERN)
Nobuyuki ISHIBASHI (Univ. of Tsukuba)
Hiroshi ITOYAMA (Osaka City Univ.)
Shoichi MIDORIKAWA (Aomori Univ.)
Muneto NITTA (Keio Univ.)
Kazutoshi OHTA (Meiji Gakuin Univ.)
Makoto SAKAGUCHI (Keio Univ.)
Norisuke SAKAI (Tokyo Women's Christian Univ.)
Yuuichirou SHIBUSA (Nagasaki Inst. Of Applied Science)
Asato TSUCHIYA (Shizuoka Univ.)
Yoshio YAMAGUCHI (Univ. of Tokyo)
Tamiaki YONEDA (The Open Univ. of Japan)

Students

Student Trainee

Taro KIMURA (Univ. of Tokyo)

Secretary

Noriko KIYAMA
Keiko SUZUKI

Sub Nuclear System Research Division
Radiation Laboratory

1. Abstract

Nucleons, such as protons and neutrons, are a bound state of constituent quarks glued together with gluons. The detail structure of nucleons, however, is not well understood yet. Especially the mechanism to build up the spin of proton, which is 1/2, is a major problem in physics of the strong force. The research goal of Radiation Laboratory is to solve this fundamental question using the world first polarized-proton collider, realized at RHIC in Brookhaven National Laboratory (BNL) in USA. RHIC stands for Relativistic Heavy Ion Collider, aiming also to create Quark Gluon Plasma, the state of Universe just after the Big Bang. RIKEN-BNL Research Center (RBRC) directed by N. Samios carries our core team at BNL for those exciting researches using the PHENIX detector. We have found that the proton spin carried by gluons is indeed small, which is a very striking finding beyond our expectations. Recently we successfully identified W boson in the electron/positron decay channel, with which we established the method to determine how much anti-quarks carry the proton spin. Other than the activities at RHIC we are preparing new experiments at SPring-8, J-PARC and Fermilab to study the nature of hadron. We are also performing technical developments such as novel ion sources, fine pitch pixel detectors and neutron optical devices.

2. Major Research subjects

1) Spin physics with relativistic polarized-proton collisions at RHIC
2) Study of nuclear matter at high temperature and/or at high density
3) Technical developments on radiation detectors and accelerators

3. Summary of Research Activity

(1) Experimental study of spin structure of proton using RHIC polarized proton collider

[See also RIKEN-BNL Research Center Experimental Group for the activities at BNL]

In order to understand the spin-structure of the proton, we are currently studying the contributions from antiquark spin and orbital angular motion of quarks and gluons to the nucleon. We have been measuring quark and antiquark spin contributions to the proton with W bosons produced in polarized-proton collisions by observing decay electrons in the central detector and decay muons in the forward detector of the RHIC-PHENIX experiment. The majority of the data is expected to be taken in the next few years for this program. To study orbital motion of quarks and gluons in the proton, one of the key measurements is the Drell-Yan process (quark-antiquark annihilation) with polarized beams and/or targets. We are considering to perform such measurements at RHIC by upgrading the PHENIX detector with forward-going electron/positron detection capability. As a pilot for the fixed-target experiment, some of us are participating in the SeaQuest experiment using 120-GeV unpolarized protons at Fermilab. One of the goals of the experiment is to measure the flavor asymmetry of the antiquark distributions in unexplored kinematic regions. Furthermore, measurements of azimuthal distribution of muon pairs with respect to the transverse vector of virtual photon allow us to study the orbital motion of quarks in the nucleon with unpolarized beam and target.

(2) Experimental study of quark-gluon plasma using RHIC heavy ion collider

[See also RIKEN-BNL Research Center Experimental Group for the activities at BNL]

In Wako we are operating a cluster computer system specialized to analyze huge data sets taken with the PHENIX detector. We newly introduced 10 calculation nodes of dual hexa-core CPUs and 10 sets of 2TB local disk for data repository, in addition to the current system (18 nodes, dual quad-core CPUS, 10 sets of 1TB disks) introduced two years ago. In the cluster, 380 jobs can run simultaneously reading out 380 TB of data parallelly with use of the house-made job control system. The system was forced to stop for 21 days due to the power saving caused by the Tohoku Earthquake, although the system itself did not damaged.

(3) Study of properties of mesons and exotic hadrons with domestic accelerators

Preparation of the experiment E16 at J-PARC Hadron Experimental Hall is underway with the Grant -in-Aid for Scientific Research on Innovative Areas (MEXT, No. 21105004) . The experiment aims to perform the systematic study of the mass modification of low-mass vector mesons in nuclei to explore the chiral symmetry in nuclear matter, i.e. the mechanism to create the mass of hadrons. The development of Gas Electron Multiplier (GEM) tracker was completed and a detailed mechanical design for the installation is ongoing. For the Hadron-blind Cherenkov detector (HBD: CsI coated GEM with CF4 gas radiator) we have achieved good quantum efficiency in CsI photocathode, and are investigating to improve the collection efficiency of the photoelectrons by optimizing the high-voltage configuration for the GEMs. We have started to design the arrangement of lead-glass calorimeters and the read-out electronics. The additional poles and yokes for the existing magnet were fabricated to enlarge the spectrometer acceptance. The magnet will be installed at J-PARC in JFY2012, and the spectrometer construction is to be completed by the end of JFY 2013.

(4) Detector development for PHENIX experiment

The silicon vertex tracker (VTX) which was installed in December 2010, has demonstrated excellent performance in determining the track information around a collision point. We found, however, several ladders of silicon detectors malfunctioned due to the electric contact problem. Through the summer 2011, we have reworked on those ladder and successfully fixed them on time for the data taking in 2012. We have also completed the momentum-sensitive trigger system for the PHENIX forward muon arms under the collaboration with KEK, Kyoto and Rikkyo University. The new trigger system has demonstrated a satisfactory performance in taking data of polarized proton collisions at energy of 500GeV, providing the first sea-quark polarization measurements via W-boson production at forward rapidity. The new trigger system will be further upgraded by adding the timing information from the newly-installed resistive plate chambers.

(5) Neutron optics

Cold or thermal neutron beam is a high-sensitivity probe to study not only the structure of condensed matter, but also fundamental physics. We have been successful in developing of an interferometer using multilayer mirrors, which is useful to test quantum mechanics and other fundamental physics, and of differential phase imaging to to see an internal structure of a bulk materials. This year some of these activities were transferred to Social Infrastructure Technology Development Program in RIKEN Innovation Center, and the construction of the compact neutron source with a proton accelerator of 7MeV has started at the K1 space in the RIBF building.

(6) Development of beam source

Under the collaboration with BNL and KEK, we are developing laser ion sources (LIS) to produce a high current heavy-ion beam, which are useful for the next generation accelerators. We have demonstrated the instantaneous intensity of more than 70 mA for highly charged carbon and aluminum beams. This is the highest current heavy ion beam produced by any methods. This year, we have started to fabricate a new LIS using a sub nano second laser system to provide various heavy ions to an induction based synchrotron in KEK.

Head

Hideto EN’YO

Members

Yasuyuki AKIBA
Yuji GOTO
Itaru NAKAGAWA
Yoshie OTAKE
Yasushi WATANABE
Satoshi YOKKAICHI
Ralf SEIDL

Special Postdoctoral Researchers

Kazuya AOKI
Yoshichika SEKI

Foreign Postdoctoral Researcher

Stephen BAUMGART

Contract Researchers

Yoshinori FUKAO
Tomohiro NISHITANI
Takashi HACHIYA

Postdoctoral Researcher

Yoki ARAMAKI
Yoshimitsu IMAZU
Kohei SHOJI
Tomonori TAKAHASHI

Contract Technical Scientist

Yohei NAKATSUGAWA

Senior Visiting Scientists

Toshiaki SHIBATA (Grad. Sch. of Sci. and Eng., Tokyo Inst. of Tech. Sch. of Sci.)
Hirohiko SHIMIZU (Inst. of Materials Structure Sci., KEK)
Ken-ichi AOKI (Grad. Sch. of Sci., Kanazawa Univ.)
Takashi NAKANO (RCNP, Osaka Univ.)

Visiting Scientists

Tomohiro ADACHI (DAI-ICHI KIDEN CO.,LTD)
Christine A.AIDALA (Univ. Massachusetts, Amherst, USA)
Ryoji AKIMOTO (CNS, Univ. Tokyo)
Alexander BAZILEVSKY (BNL, USA)
Wolfgang BENTZ (Tokai Univ.)
Mickey CHIU (Univ. of Illinois at Urbana, USA)
Ondrej CHVALA (Univ. of California at Riverside)
Takumi DOI (University of Kentucky)
Dipanwita DUTTA (Nuclear Physics Division, Bhabha Atomic Research Centre)
Hirotsugu FUJII (Grad. Sch./College of Arts and Sciences, Univ. of Tokyo)
Kenji FUKUSHIMA (YITP, Kyoto Univ.)
Haruhiko FUNAHASHI (Grad. Sch. of Sci., Kyoto Univ.)
Yuji HASEGAWA (Wien Inst. Tech.)
Tetsuo HATSUDA (Grad. Sch. of Sci., Univ. of Tokyo)
Toshiyuki HATTORI (Res. Lab. for Nuclear Reactors, Tokyo Inst. of Tech. Sch. of Sci.)
Masanori HIRAI (Grad. Sch. of Sci. and Eng., Tokyo Inst. of Tech.)
Kensuke HOMMA (Grad. Sch. of Sci., Hiroshima Univ.)
Takuma HORAGUCHI (Grad. Sch. of Sci., Hiroshima Univ.)
Ryo ICHIMIYA (KEK)
Katsuya ISHIGURO (Grad. Sch. of Natural Sci. & Tech., Kanazawa Univ.)
Noriyoshi ISHII (Grad. Sch. of Pure and Applied Sci., Univ. of Tsukuba)
Hirokazu ISHINO (Tokyo Inst.Tech.)
Robert JAMESON (Goethe Universitat Frankfurt, Germany)
Takeshi KANESUE (Kyushu Univ.)
Hirotsugu KASHIWAGI (Takasaki Advanced Radiation Res. Inst., JAEA)
Hiroyuki KAWAMURA (The Univ.of Liverpool)
Yuji KOIKE (Grad. Sch. of Sci. & Tech., Niigata Univ.)
Yoshiaki KOMA (Numazu National College of Technology)
Kotaro KONDO (Grad. Sch. of Sci. and Eng., Tokyo Inst. of Tech.)
Shunzo KUMANO (Inst. of Particle and Nuclear Studies, KEK)
Teiji KUNIHIRO (Grad. Sch. of Sci., Kyoto Univ.)
Makoto KUWAHARA (Nagoya Univ.)

Yoshikazu MAEDA (RCNP , Osaka Univ.)
Yajun MAO (Peking Univ., China)
Tsutomu MIBE (KEK)
Liu MING (LANL)
Kenji MISHIMA (KEK)
Yoshiyuki MIYACHI (Tokyo Inst. Tech.)
Yoshihiro MORI (Grad. Sch. of Sci., Kanazawa Univ.)
Norihito MURAMATSU (RCNP, Osaka Univ.)
Ryotaro MUTO (KEK)
Katsuro NAKAMURA (Grad. Sch. of Sci., Kyoto Univ.)
Yoshifumi NAKAMURA (DESY, Germany)
Atsushi NAKAMURA (Information Media Center, Hiroshima Univ.)
kenichi NAKANO (Tokyo Inst. Tech.)
Megumi NARUKI (KEK)
Masayuki NIIYAMA (Grad. Sch. of Sci., Kyoto Univ.)
Munehisa OHTANI (Inst. fuer Theoretische Physik, Universitact Regensburg, Germany)
Hiromi OKADA (KEK)
Masahiro OKAMURA (BNL, USA)
Kyoichiro OZAWA (Grad. Sch. of Sci., Univ. of Tokyo)
Petra RIEDLER (CERN, Switzerland)
Naohito SAITO (J-PARC, KEK)
Hiroyuki SAKO (JAEA)
Murad SARSOUR (Georgia State University)
Shoichi SASAKI (Grad. Sch. of Sci., Univ. of Tokyo)
Susumu SATO (JAEA)
Shin-ya SAWADA (Inst. of Particle and Nuclear Studies, KEK)
Michiko SEKIMOTO (Inst. of Particle and Nuclear Studies, KEK)
Kenta SHIGAKI (Grad. Sch. of Sci., Hiroshima Univ.)
Prashant SHUKLA (Nuclear Physics Division, Bhabha Atomic Research Centre)
Kazutaka SUDO (Inst. of Particle and Nuclear Studies, KEK)
Toru SUGITATE (Grad. Sch. of Sci., Hiroshima Univ.)
Mizuki SUMIHAMA (RCNP , Osaka Univ.)
Tsuneo SUZUKI (Grad. Sch. of Sci., Kanazawa Univ.)
Taneja SWADHIN (SUNY at Stony Brook)
Masao TABUCHI (Nagoya Univ.)
Junpei TAKANO (KEK)
Kiyoshi TANIDA (Seoul National Univ.)
Hisayuki TORII (Grad. Sch. of Sci., Hiroshima Univ.)
Xiaorong WANG (New Mexico State University)
Shizui WATANABE (Tokyo Metropolitan College of Aeronautical Engineering)
Imuran YOUNUS (Univ. of New Mexico, USA)

Students

Junior Research Associate

Hidemitsu ASANO (Fac. of Sci., Kyoto Univ.)
Yuya KOMATSU (Fac. Sci. , Univ. Tokyo)
Shinichi MASUMOTO (Fac. Sci. , Univ. Tokyo)
Masaya NIHASHI (Grad. Sch. of Sci., Hiroshima Univ.)

Megumi SEKINE (Tokyo Inst. Tech.)
Dosatsu SAKATA (Univ. Tsukuba)
Takahito TODOROKI (Univ. Tsukuba)

International Program Associate

Sunyoung RYU (RCNP,Osaka Univ.)

Student Trainees

Atsushi ERA (Nagoya Univ.)
Ciprian GAL (Dept. of Physics , SUNY at Stony Brook)
Masayasu HASEGAWA (Grad. Sch. of Sci., Kanazawa Univ.)
Kimiaki HASHIMOTO (Fac. of Sci., Rikkyo Univ.)
Kazuya HAYASE (Tokyo Univ. of Science)
Seiko HIROTA (Fac. Sci. , Univ. Tokyo)
Shouyang HU (China Inst. Atom. Energy)
Sotaro KANDA (Fac. Sci. , Univ. Tokyo)
Kouki KANNO (Fac. Sci. , Univ. Tokyo)
Paul KLINE (Dept. of Physics , SUNY at Stony Brook)
Yukiyoshi KON (RCNP , Osaka Univ.)
Andrew MANION (Dept. of Physics , SUNY at Stony Brook)
Shou MIYASAKA (Tokyo Inst. Tech.)
Shinji MOTOKI (Grad. Sch. of Biosphere Sci., Hiroshima Univ.)
Yoshihide NAKAMIYA (Grad. Sch. of Sci., Hiroshima Univ.)
Wataru NAKAI (Fac. Sci. , Univ. Tokyo)
Takahiro SAWADA (RCNP, Osaka Univ.)
Atsuko TAKAGI (Fac. Sci. , Univ. Tokyo)
Yuki WATANABE (Tokyo Univ. of Science)
Yosuke WATANABE (Fac. Sci. , Univ. Tokyo)
Ruizhe YANG (UIUC)

Intern

Inseok YOON (Seoul National Univ.)
Park SANGHWA (Seoul National Univ.)
Takayuki YAMAMOTO (Waseda Univ.)

Part-time Staff (Research Assistance)

Ryota MATSUBARA (Rikkyo Univ.)
Haruna MURAKAMI (Rikkyo Univ.)
Kentaro WATANABE (Rikkyo Univ.)

Secretaries

Noriko KIYAMA
Keiko SUZUKI

Sub Nuclear System Research Division
Advanced Meson Science Laboratory

1. Abstract

Particles like muons, pions, and kaons have finite lifetimes, so they do not exist in natural nuclei or matters. Implanting these particles into nuclei/matters, exotic phenomena in varieties of objects can be studied from a new point of view.

Kaon is the second lightest meson which has strange-quark as a constituent quark. It is expected that if one embed a kaon into nuclei, the sizes of the nuclei become smaller and forms a high density object beyond the normal nuclear density. Study of this object could lead to better understanding of the origin of the mass of the matter, and may reveal the quark degree of freedom beyond the quark-confinement. Those properties can be studied by precise heavy pionic atom research in different angle. The other example is the weak interaction in nuclear matter. It can only be studied by the weak decay of hypernuclei, which have lambda particle in the nuclei.

Muon provides even wider variety of study ranging from particle physics to condensed matter and life sciences. For instance, stopping positively charged muon in a material, we obtain information on the magnetic properties or the local field at the trapped site. Injecting negatively charged muon to mixture of deuterium and tritium, muon attracts surrounding atoms and is known to cause d-t fusions.

As is already clear, in our research we introduce different kind of impurities into nuclei/matters, and study new states of matter, new phenomena, or the object properties.

2. Major Research Subjects

(1) Study of meson property and interaction in nuclei
(2) Origin of matter mass / quark degree of freedom in nuclei
(3) Condensed matter and material studies with muon
(4) Nuclear and particle physics studies via muon catalyzed fusion and ultra cold muon beam
(5) Materials science using Mössbauer spectroscopy

3. Summary of Research Activity

Hadron physics at J-PARC and RIKEN-RIBF

Kaon and pion will shed a new insight to the nuclear physics. The recent discovery of deeply bound pionic atom enables us to investigate the properties of mesons in nuclear matter. At RIKEN-RIBF, we are preparing precise experimental study of the pionic atom. We are intensively preparing another next generation kaon experiments (E15, E17 and E31) at J-PARC as day-one experiments. In these experiments, we are aiming at precise determination of the KN interaction, and clarify the nature of kaon in nuclei and $\Lambda(1405)$. By these experiments, we aim to be a world-leading scientific research group using these light meta-stable particles.

1) Deeply bound kaonic nuclei

We have performed experimental exploration of theoretically predicted deeply bound kaonic nuclear states in ^{3}He nucleus K^-ppn and K^-pnn. Akaishi and Yamazaki first calculated large binding energy and narrow width for the K^-ppn state. One of the most interesting features of the kaonic nucleus is that the strong attraction of the kaon is expected to contract the surrounding nucleons resulting in extremely high density of several times larger than normal nuclear density. Measurement of the kaon properties at such high energy density will provide precious information on the origin of hadron masses and the chiral symmetry breaking and its partial restoration.

The experimental principle adopted uses stopped K^- on suprefluid helium target, and we focus on emitted nucleon momenta measurement by Time-of-Flight (TOF) method. The last orbit of kaonic ^{4}He atom is 2p and the branching ratio from the last orbit to the nuclear kaon bound state accompanied with a nucleon emission was estimated to be 1 % at minimum.

The exploration was performed from 2002/September till 2005/December as series of experiments at the KEK-PS (E471, E549, E570) with almost common experimental setup. The obtained spectral shape was rather smooth and elaborate analysis showed upper limit of the kaonic nucleus formation for both K^-ppn and K^-pnn states.

After the completion of above series of experiments, the KEK-PS was shut down to switch to a new facility J-PARC. Presently, we are starting for an experiment to search for K^-pp nuclear system at the K1.8BR beamline of the J-PARC.

2) Deeply bound pionic atoms

We have made precision spectroscopy of pionic lead and tin atoms, and extracted information on the in-medium interaction between pion and nucleus, which leads to the exclusive quantitative evaluation of the chiral symmetry restoration in the nuclear matter.

Our collaboration which mainly consists of the RIKEN and the University of Tokyo group conducted throughout the experiments starting from R&D of pionic atom formation in nuclear reactions to its application to the precision spectroscopy.

The experiment was carried out in GSI, Darmstadt. Our first discovery was pionic 2p state in the lead 207 nucleus where the negative pion is accommodated in a delicate balance between the Coulomb attraction and the strong repulsion.

Following the discovery, we have performed experiments to measure 1s pionic lead 205 and ^{115}Sn, ^{119}Sn and ^{123}Sn isotopes.

We have analyzed the experimental spectra elaborately and extracted in-medium isovector interaction between pion and nucleus. In combination with experimental information on the pionic hydrogen and deuterium which gives the interaction in vacuum, we have accomplished evalution of the in-medium interaction modification. The modification is originating in the partial restoration of the chiral symmetry in the nucleus, and we have quantitatively evaluated for the first time the reduction of the chiral order parameter in the nuclear matter to be 33 %, which is consistent with theoretical prediction of 30 %.

Presently, we have been preparing for a sophisticated experimental setup of the pionic atom spectroscopy at the RIBF in the RIKEN and recently performed the first experiment to measure pionic ^{121} Sn stom. We expect about twice better experimental resolution with much smaller systematic errors.

3) Precision X-ray measurement of kaonic atom

Simultaneously with the above experiment (1), we have performed an X-ray spectroscopy of atomic $3d \rightarrow 2p$ transition of negatively charged K mesons captured by helium atoms. Many Kaonic atoms are known to be measured with various elements, however, there are very large deviations in the measured energy levels for the helium (and the oxygen) from the systematic expectations. The deviation originates in technical issues in old experiments, and new and high precision data have been long awaited for. Also, wave functions of the Kaonic atoms are expected to reflect the information on the existence of the inner structure, namely deeply bound Kaonic states. As a result of the experiment, we have succeeded in performing the spectroscopy and achieved the shift of 2 ± 2(stat.) ± 2(syst.) eV. The obtained results reject older data without any doubt, and the above deviation is dissolved. Presently, aiming at the determination of the level width and yield, we are analyzing the data. To clarify the KN interaction strength, we are preparing another x-ray measurement of the kaonic helium-3 atom, which is another day-one experiment at J-PARC.

Muon science at RIKEN-RAL branch

The research area ranges over particle physics to condensed matter studies and life science. Our core activities are based on the RIKEN-RAL Muon Facility located at the Rutherford Appleton Laboratory (UK), which provides intense pulsed-muon beam. We have variety of important research activities such as muon-catalyzed fusion (μ CF) and condensed matter physics by muon spin rotation / relaxation / resonance (⌈ΣP).

(A) Condensed matter/materials studies with μ SR

A new experimental area named Port-4 is now being arranged for general purpose μ SR studies. A new spectrometer CHRONUS is available for advanced μ SR experiments in Port-4. A new platform covering the whole area of Port-4 has been completed and preparations of cryostats are going on. Two brand new cryostats which can cool the sample temperature down to 2 K in the He-has atmosphere. A new DAQ system is also going to be arranged and some test experiments are planned to be carried out in April-May by using real muon beams. In parallel with this installation work of Port-4, we are carrying on μ SR experiments on variable materials in Port-2 which has been used for ordinal μ SR experiments. We especially have concentrated on organic materials in 2011 in order to investigate novel ground states of molecule magnets. Our topics μ SR investigations for material sciences are as follows.

1) The one-dimensional motion of spin excited states was observed in the ground state of $EtMe_3Sb[Pd(dmit)_2]_2$ organic magnet in which the spin-liquid state is formed. This one-dimensional diffusion behavior is expected to be an evidence of the appearance a resonating state of spins like the RVB state.

2) A new quantum phase transition of the spin liquid state caused by weak magnetic fields has been found in a triangular organic magnet. This effect can be explained by a theoretical VISON model which is on the basis of the coupling between spins and phonon vibrations.

3) Magnetic and non-magnetic impurity effects on the magnetic correlation in Cu-based high-T_C superconducting oxides have been in found to trap holes in the CuO_2 plane destructing the superconducting state.

(B) Nuclear and particle physics studies via muon catalyzed fusion and ultra cold muon beam

1) Muon catalyzed fusion (μ CF)

We are studying the muon catalyzed fusion (μ CF) processes in a wide range of hydrogen target conditions such as isotope mixture, temperature, density and phase. We constructed and tested a new high pressure and high density solid D_2 target system. We confirmed the formation of solid D_2 at 30 K and 550 bar. We plan a further test up to 36 K and 1000 bar.

2) Generation of ultra slow positive muon beam

Low energy muon beam, whose kinetic energy is variable from a few keV to a few tens of keV, will be useful for μ SR as well as for the source of a very sharp beam for precision measurement of muon's anomalous gyro-magnetic ratio (g-2). Progresses were made in several key techniques to produce low energy muons. We finished the measurement of muonium emission from material surface of several silica aerogel samples in collaboration with TRIUMF. Present laser system and slow muon beam line is being upgraded at RIKEN-RAL to study the laser ionization process of the muonium. A new laser system is developed at RIKEN Wako campus to increase the laser intensity and the ionization efficiency by 100 times. Final amplifier of the laser system is under construction and the Lyman-alpha generation test is planned in 2012.

Mössbauer spectroscopy at RIKEN-RIBF and HIMAC

^{57}Fe Mössbauer spectroscopy following ion implantation of radioactive ^{57}Mn ($T_{1/2}$ = 1.45 min) has been applied to investigate the site positions and atomic jump processes of Fe impurity atoms in semiconductors under light illuminations. ^{57}Mn is one of the useful nuclear probes to study the dynamic behavior and chemical states of dilute Fe atoms in solid. Iron impurities are known to degrade seriously electronic properties of silicon-based devices as well as solar cells. Generally, Fe atoms are thought to occupy only on interstitial sites in Si leading to a fast diffusion. In addition, substitutional Fe atoms were not found experimentally by standard evaluation techniques. Our investigation is to clarify the impurity diffusion of Fe atoms and the formation processes of "*substitutional Fe atoms*" in Si at high temperatures. The relaxation behaviors observed in our experiments can be interpreted in terms of a diffusion-reaction process of interstitial Fe atoms with vacancies, leading to the formation of *substitutional Fe atoms* in the Si matrix. The process must be related to the recovery processes from non-equilibrium to the equilibrium states of the Si lattice around the ^{57}Fe nuclear probes. In this period, ^{57}Mn implanation Mössbauer spectra in a solar cell were measured under light illumination at RIKEN-RIBF. Comparing with the spectrum of p-type multi-crystalline-Si, the broad spectra of the solar cell can be analyzed as a superposition of interstitial and substitutional Fe components with different charge states.

^{57}Mn/^{57}Fe Mössbauer studies have been performed to study the formation and recovery processes of the defects induced by the implantation in α-Al_2O_3, MgO, and LiH at HIMAC. We succeeded in measuring ^{57}Fe Mössbauer spectra obtained after ^{57}Mn implantation in α-Al_2O_3 with an adequate ratio of the resonance peak against the background by applying the anticoincidence measurement in spite of the extremely low ^{57}Mn implantation dose. The Mössbauer spectra measured at various temperatures could be analyzed by three components of symmetrical doublets. There was not any significant magnetic splitting in this temperature region. On the basis of the density functional calculation, these components were assigned to Fe^{3+} at the substitutional Al^{3+} sites in α-Al_2O_3, to interstitial Fe atoms surrounded with octahedral O_6 symmetry, and to Fe atoms at a substitutional Al^{3+} sites with an oxygen deficiency.

Theoretical Researches

1)Non-perturbative aspects of string theory

One of the most promising approach toward the understanding of the non-perturbative aspects of string theory is that through matrix models. We have found a new dynamics in one of those matrix models. We have shown that one of matrix models which related to non-critical string theory with the central charge one exhibits a novel critical behavior through the phenomenon stems from the very quantum nature of the system, the tunneling phenomenon. We have pointed out that if the potential of the model is set properly, there should occur certain tunneling called resonant tunneling put the system to certain singular behavior, before the system reached the well-known criticality, where the fermi surface reached the ridge of the potential valley. The precise nature of this novel critical behavior is yet to be uncovered but this phenomenon will likely to shed lights on non-perturbative aspects of string theory through its matrix model dynamics.

2)Physics of Quantum Hall system

We have investigated the interlayer phase coherence and the Josephson currents in the bilayer quantum Hall system based on the noncommutative geometrical approach. We have demonstrated that the Josephson inplane current provokes anomalous behaviors in the Hall resistance in counterflow and drag experiments. Furthermore, we investigate the condition on the input current for the tunneling current to be coherent and dissipationless. Our results explain quite well the experimental report on the input current due to the von Klitzing group [Phys. Rev. Lett. 104 (2010) 116802]. We have predicted also how the condition changes when the sample is tilted in the magnetic field.

Head
Masahiko IWASAKI

Members
Katsuhiko ISHIDA
Kenta ITAHASHI
Yoshio KOBAYASHI
Teiichiro MATSUZAKI
Hiroaki OHNISHI
Haruhiko OUTA
Fuminori SAKUMA
Tsukasa TADA
Isao WATANABE

Special Postdoctoral Researcher
Kazuki UENO

Contract Researchers
Ikuto KAWASAKI
Shinji OKADA
Dai TOMONO
Koji YOKOYAMA

Senior Visiting Scientist
Kazuhiro TANAKA (IPNS, KEK)

Visiting Scientists
Tadashi ADACHI (Grad. Sch. Eng., Tohoku Univ.)
Jun AKIMITSU (Coll. Sci. Eng., Aoyama Gakuin Univ.)
Kunio AWAGA (Grad. Sch. Sci., Nagoya Univ.)
Pavel BAKULE (RAL, UK)
George BEER (Univ. of Victoria, Canada)
HyoungChan BHANG (Seoul National Univ., Korea)
N. Ludmila BOGDANOVA (ITEP, Russia)
Catalina CURCEANU (INFN, Italy)
Prasad Tara DAS (SUNY, USA)
Irwan DHARMAWAN (UNPAD, Indonesia)
Yasuaki EINAGA (Fac. Sci & Tech., Keio. Univ.)
Zyun Francis EZAWA (Grad. Sch. Sci., Tohoku Univ.)
Donald FLEMING (Univ. of British Columbia/TRIUMF)
Masaya ENOMOTO (Fac. Sci., Tokyo Univ. of Sci.)
Mark FAYFMAN (Kurchatov Inst., Russia)
Yutaka FUJII (Fac. Eng., Fukui Univ.)
Hiroyuki FUJIOKA (Grad. Sch. Sci., Univ. of Tokyo)
Masaki FUJITA (IMR, Tohoku Univ.)
Hideto FUKAZAWA (Grad. Sch. Sci., Chiba Univ.)
Nobumasa FUNAMORI (Grad. Sch. Sci., Univ.of Tokyo)

Yukio FURUKAWA (Fac. Sci. & Eng., Waseda Univ.)
Takayuki GOTO (Fac. Sci. & Tech., Sophia Univ.)
Masashi HARADA (Toyota Central R&D Labs.)
Kazuo HAYAKAWA (Fac of Sci. & Tech., Shizuoka Inst. Sci. & Tech.)
Ryugo, S. HAYANO (Grad. Sch. Sci., Univ.of Tokyo)
Wataru HIGEMOTO (ASRC, JAEA)
Satoru HIRENZAKI (Fac. Sci., Nara Women's Univ.)
Masahiko HIROI (Fac. Sci., Kagoshima Univ.)
Hiromi IINUMA (IPNS, KEK)
Masami IIO (CSC, KEK)
Susumu IKEDA (IMSS, KEK)
Yutaka IKEDO (IMSS, KEK)
Rintaro INOUE (ICR, Kyoto Univ.)
Takayuki ISHIDA (Grad. Sch. Infor. & Eng., Univ. Elect. Commu.)
Yasuyuki ISHII (Dept. Phys., Tokyo Medical Univ.)
Fumihiro ISHIKAWA (Grad. Sch. Sci. & Tech., Niigata Univ.)
Shigeru ISHIMOTO (IPNS, KEK)
Tomoichi ISHIWATARI (SMI, Austria)
Takashi ITO (ASRC, JAEA)
Ryosuke KADONO (IMSS, KEK)
Koichi KAGESAWA (Grad. Sch. Arts and Sci., Univ of Tokyo)
Kazuya KAMAZAWA (Toyota Central R&D Labs.)
Toshiji KANAYA (ICR, Kyoto Univ.)
Motomi KATADA (Grad. Sch. Sci. & Eng., Tokyo Met. Univ.)
Mineo KATO (IMSS, KEK)
Roland KAWAKAMI (UC Riverside, USA)
Takayuki KAWAMATA (Grad. Sch. Sci., Nagoya Univ.)
Naritoshi KAWAMURA (IMSS, KEK)
Seiko KAWAMURA (J-PARC, JAEA)
Hikomitsu KIKUCHI (Grad. Sch. Eng., Univ. of Fukui)
Yasushi KINO (Fac. Sci., Tohoku Univ.)
Wataru KOBAYASHI (Grad. Sch. Pure & Applied Sci., Univ. of Tsukuba)
Akihiro KODA (IMSS, KEK)
Masahito KODERA (Fac. Sci. & Eng., Doshisha Univ.)
Yoh KOHORI (Fac. Sci., Chiba Univ.)
Yoji KOIKE (Grad. Sch. Eng., Tohoku Univ.)
Kenji KOJIMA (IMSS, KEK)
Norimichi KOJIMA (Grad. Sch. Arts and Sci., Univ of Tokyo)
Kenya KUBO (Grad. Sch. Sci., ICU)
Shoko KUME (Grad. Sch. Sci., Univ.of Tokyo)
Yoshitaka KUNO (Grad. Sch. Sci., Osaka Univ.)
Takuya KURAHASHI (IMS)
Haruhiko KUROE (Fac. Sci. & Tech., Sophia Univ.)
Guido LANGOUCHE (NVAO, Netherlands)
Chow LEE (UCF, USA)
Shunsuke MAKIMURA (IMSS, KEK)
Hirotaka MANAKA (Grad. Sch. Sci. & Eng., Kagoshima Univ.)
Yasuyuki MATSUDA (Grad. Sch. Arts and Sci., Univ. of Tokyo)

Tsutomu MIBE (IPNS, KEK)
Mototsugu MIHARA (Grad. Sch. Sci., Osaka Univ.)
Yasuhiro MIYAKE (IMSS, KEK)
Hitoshi MIYASAKA (Grad. Sch. Sci., Tohoku Univ.)
Jun MIYAZAKI (Fac. Sci. Div., Nihon Univ.)
Soichiro MIZUSAKI (Coll.Sci. & Eng., Aoyama Gakuin Univ.)
Tomoyuki MOCHIDA (Grad. Sch. Sci., Kobe Univ.)
Kazuhiko MUKAI (Toyota Central R&D Labs.)
Yujiro NAGATA (Coll. Sci. Eng., Aoyama Gakuin Univ.)
Takashi NAGATOMO (Grad. Sch. Sci., ICU)
Hiroyuki NAKAMURA (Grad. Sch. Eng., Kyoto Univ.)
Jin NAKAMURA (Grad. Sch. Infor. & Eng., Univ. Elect. Commu.)
Kazutaka NAKAHARA (Univ. of Maryland. USA)
Satoshi NAKAMURA (Grad. Sch. Sci., Tohoku Univ.)
Takashi NAKAMURA (Grad. Sch. Sci. & Eng., Tokyo Tech.)
Takayoshi NAKAMURA (RIES, Hokkaido Univ.)
Takehito NAKANO (Grad. Sch. Sci., Osaka Univ.)
Saburou NASU (Grad, Sch. Eng. & Sci., Osaka Univ.)
Kazuhiko NINOMIYA (Advanced Sci. Res. Center, JAEA)
Nobuhiko NISHIDA (Fac. Sci., Tokyo Tech.)
Kusuo NISHIYAMA (IMSS, KEK)
Tatsuo NORITAKE (Toyota Central R&D Labs.)
Hiroyuki NOUMI (RCNP, Osaka Univ.)
Hiroshi NOZAKI (Toyota Central R&D Labs.)
Yasuo NOZUE (Grad. Sch. Sci., Osaka Univ.)
Agung NUGROHO (ITB, Indonesia)
Kazuki OHISHI (CROSS Tokai)
Yoshitaka OHKUBO (KURRI, Kyoto Univ.)
Atsushi OKAZAWA (Grad. Sch. Arts and Sci., Univ of Tokyo)
Vassili PEREVOZCHIKO (VNIEF, Russia)
Leonid PONOMAREV (Kurchatov Institute, Russia)
Francis PRATT (RAL, UK)
Risdiana (Padjadjarn Univ., Indonesia)
Lusy SAFRIANI (UNPAD, Indonesia)
Shin-ichi SAKAMOTO (J-PARC, JAEA)
Naohito SAITO (IPNS, KEK)
Tobat SARAGI (Univ. of Kassel, Germany)
Kazuhiko SATO (Grad. Sch. Sci. & Eng., Saitama Univ.)
Masaharu SATO (Grad. Sch. Sci., Univ.of Tokyo)
Tomoko SATO (Grad. Sci., Hiroshima Univ.)
Wataru SATO (Grad. Sch. Na Sci. & Tech., Kanazawa Univ.)
Ralph SCHEICHER (Michigan Tech. Univ., USA)
Ryoichi SEKI (California State Univ., Northridge, USA)
Kouichirou SHIMOMURA (IMSS, KEK)
Ichiro SHIRAKI (Grad. Sch. Medi. & Eng. Sci., Univ. of Yamanashi)
Patrick STRASSER (IMSS, KEK)
Hiroyuki SUGAI (Advanced Sci. Res. Center, JAEA)
Jun SUGIYAMA (Toyota Central R&D Labs.)

Ken SUZUKI (SMI, Austria)
Hiroyuki SUZUKI (NIMS)
Soh SUZUKI (CRC, KEK)
Takao SUZUKI (Grad. Sch. Sci., ICU)
Takatoshi SUZUKI (Grad. Sch. Sci., Univ.of Tokyo)
Yoshikazu TABATA (Grad, Sch. Eng. & Sci., Kyoto Univ.)
Shigeru TAKAGI (Grad, Sch. Sci., Tohoku Univ.)
Kazuyuki TAKAI (Grad. Sch. Sci. & Eng., Tokyo Tech.)
Nao TAKESHITA (NeRI, AIST)
Yoichi TANABE (WPI, Tohoku Univ.)
Manobu TANAKA (IPNS, KEK)
Hiroshi TANIDA (Grad. Sch. Adv. Sci. Matter, Hiroshima Univ.)
Akihiro TANIGUCHI (KURRI, Kyoto Univ.)
Harry TOM (UC Riverside, USA)
Eiko TORIKAI (Grad. Sch. Medi. & Eng. Sci., Univ. of Yamanashi)
Akihisa TOYODA (IPNS, KEK)
Kyo TSUKADA (Grad. Sch. Sci., Tohoku Univ.)
Satoshi TSUTSUI (JASRI)
Masatomo UEHARA (Grad. Sch. Eng., Yokohama Natl.Univ.)
Helmut WEICK (GSI, Germany)
Zhuan XU (Zhejiang Univ. China)
Eiichi YAGI (Fac. Sci. & Eng., Waseda Univ.)
Yasuhiro YAMADA (Fac. Sci., Tokyo Univ. of Sci.)
Toshimitsu YAMAZAKI (Grad. Sch. Sci., Univ.of Tokyo)
Yutaka YOSHIDA (Fac of Sci. & Tech., Shizuoka Inst. Sci. & Tech.)
Arkady YUKHINCHUK (VNIIEF, Russia)
Johann ZMESKAL (SMI, Austria)

Visting Technicians

Shinji KAI (Tanaka Kikinzoku Kogyo K.K.)
Jumpei NAKAMURA (IMSS, KEK)
Kazuo OOYAMA (JOHO Com.)
Kunihiro SHIMA (Tanaka Kikinzoku Kogyo K.K.)

Research Consultants

Yoshinori AKAISHI
Atsuko ITO
Masayasu KAMIMURA
Hironari MIYAZAWA

Students

Junior Reserch Associates

Yuya FUJIWARA (Grad. Sch. Sci., Univ. of Tokyo)
Yuta SADA (Grad. Sch. Sci., Kyoto Univ.)
Makoto TOKUDA (Grad. Sch. Sci. & Eng., Tokyo Tech.)
Tadashi HASHIMOTO (Grad. Sch. Sci., Univ. of Tokyo)

International Program Associate

Budi ADIPERDANA (UNPAD, Indonesia)
Guo HANJIE (Zhejiang Univ., China)

Student Trainees

Yuki AKIYAMA (Grad. Sch.Sci. & Eng., Shizuoka Inst. Sci. & Tech.)
Ryo DEGAWA (Fac. Sci., Tokyo Univ. of Sci.)
Shun ENOMOTO (Grad, Sch. Sci., Osaka Univ.)
Jafar ESMAILI (Isfahan Univ. Tech., Iran)
Tadashi HASHIMOTO (Grad. Sch. Sci., Univ. of Tokyo)
Maryam HASSANVAND (Isfahan Univ. Tech., Iran)
Masatoshi HIRAISHI (Sch. High Enegy Acce. Sci., Sokendai)
Kentaro INOUE (Grad. Sch. Sci., Osaka Univ.)
Miho ITO (Grad. Sch. Sci. & Eng., Saitama Univ.)
Satoshi ITOH (Grad. Sch. Sci., Univ. of Tokyo)
Takuya KAKURAI (Grad. Sch. Sci., Univ.of Tokyo)
Yu KAWAHARA (Grad. Sch. Sci., Tokyo Univ. Sci.)
Akio KAWASAKI (MIT, USA)
Jun KOBAYASHI (Fac. Sci., Saitama Univ.)
Hiroshi KOU (Grad. Sch. Sci. & Eng., Tokyo Tech.)
Hiroto KUMABE (Grad. Sch.Sci. & Eng., Shizuoka Inst. Sci. & Tech.)
Daisuke KUNO (Grad. Sch. Sci., Tohoku Univ.)
Kazuya MAE (Grad. Sch. Sci, ICU)
Tatsuya MATSUE (Fac. Sci., Tokyo Univ. Sci.)
Masanori MIYAZAKI (Sch. Phys. Sci.,Sokendai)
Masaki NAKAMURA (Grad. Sch. Sci. & Eng., Tokyo Tech.)
Yugo NINOMIYA (Grad, Sch. Eng. & Sci., Osaka Univ.)
Takahiro NISHI (Grad. Sch. Sci., Univ. of Tokyo)
Yuki NOZAWA (Grad. Sch. Sci., Kyoto Univ.)
Noriaki OKABE (Grad. Sch. Sci. & Eng., Saitama Univ.)
Kota OKOCHI (Grad. Sch. Sci., Univ.of Tokyo)
Yusuke ONODERA (Grad. Sch. Sci. & Eng., Saitama Univ.)
ROGER PINK (SUNY at Albany, USA)
Manami SATAKE (Grad. Sch. Sci. & Eng., Tokyo Tech.)
Ryo SHIMIZU (Fac. Sci., Tokyo Univ. of Sci.)
Takaaki SHINKAWA (Grad. Sch. Sci. & Eng., Saitama Univ.)
Wayan Gede SUHARTA (ITSNS, Indonesia)
Kensuke SUZUKI (Grad. Sch. Eng., Tohoku Univ.)
Yoshiki TANAKA (Grad. Sch. Sci., Univ.of Tokyo)
Kazuhiro TAKAHASHI (Grad. Sch. Sci., Univ. of Tokyo)
Koichi TODOROKI (Grad. Sch. Sci., Univ. of Tokyo)
Natsuki TOMIDA (Grad. Sch. Sci., Kyoto Univ.)
Yoshinori TSUKAMOTO (Fac. Sci. & Eng., Shizuoka Inst. Sci. & Tech.)
Yoshiko TSUKIYAMA (Grad. Sch. Sci. & Eng., Saitama Univ.)
Tomotaka UEHARA (Fac. Sci., Saitama Univ.)
Ryo USUI (Fac. Sci., Tokyo Univ. of Sci.)
Riku YAMAGUCHI (Fac. Sci., Tokyo Univ. Sci.)
Noyuri YAMAMURA (Grad. Sch. Sci, ICU)

Mamoru YASUIKE (Fac. Sci., Tokyo Univ. Sci.)
Tomohiro YASUNAGA (Fac. Sci. & Eng., Doshisha Univ.)
Junya YOSHIDA (Grad. Sch. Arts and Sci., Univ of Tokyo)

Part-time Staff

Toshihiko HIRAIWA (Grad. Sch. Sci., Kyoto Univ.)

Assistants

Yoko FUJITA
Yuri TSUBURAI

Sub Nuclear System Research Division
RIKEN-BNL Research Center

1. Abstract

The RIKEN BNL Research Center was established in April 1997 at Brookhaven National Laboratory. The Center is dedicated to the study of strong interactions, including spin physics, lattice QCD and RHIC physics through the nurturing of a new generation of young physicists. The Center has three research groups: Theory Group led by L. McLerran, Experimental Group led by Y. Akiba, and Computing Group led by T. Izubuchi. In addition to the strong research program in these three groups, we have a joint-fellowship program with other Universities. The fellowship program enables a talented researcher to maintain a tenure track position at his/her university as well as a Fellow position at RBRC for a certain period of time.

2. Major Research Subjects

Major research subjects of the theory group are
(1) Perturbative QCD
(2) Phenomenological QCD

Major research subject of the experimental group are
(1) Experimental Studies of the Spin Structure of the Nucleon
(2) Study of Quark-Gluon Plasma at RHIC
(3) PHENIX detector upgrades

Major research subject of the computing group is
(1)Lattice QCD numerical research

3. Summary of Research Activity

Summary of Research Activities of the three groups of the Center are given in the sections of each group.

Director

Nicholas P. SAMIOS (Ph.D)

Administrative Staff / RIKEN Japan

Shigeki ASAKAWA (Administration Manager, Accelerator-based Research Promotion Section)
Kazunori MABUCHI (Deputy Administration Manager, RBRC)
Keiko SUZUKI (Japan)

Sub Nuclear System Research Division
RIKEN-BNL Research Center
Theory Group

1. Abstract

The RIKEN BNL Research Center (RBRC) was established in April 1997 at Brookhaven National Laboratory in New York, USA. The Center is dedicated to study of strong interactions, including hard QCD/spin physics, lattice QCD and RHIC physics through nurturing of a new generation of young physicists. The Theory Group activities are closely and intimately related to those of the Nuclear Theory, High Energy Theory and Lattice Gauge Theory Groups at BNL. The RBRC theory group carries out research in three areas: numerical lattice QCD, perturbative QCD and phenomenological QCD. It pioneered the use of the domain-wall fermion method in lattice QCD and has investigated various aspects of hadron physics including the calculation of neutral Kaon CP-violations that is relevant for checking the Cabibbo-Kobayashi-Maskawa theory. The perturbative QCD effort has developed various new methods required for studying hadron structures, especially in spin physics research. The group has pioneered phenomenological QCD researches of color superconductivity, isospin density, and small-x phenomena in extreme hadronic matters.

2. Major Research Subjects

(1) Perturbative QCD
(2) Phenomenological QCD
(3) Lattice QCD numerical research (From 2011, also at RBRC's Computing group)

3. Summary of Research Activity

The RIKENBNL Research Center (RBRC) was established in 1997 to support the RIKEN activities at RHIC in BNL, and also to promote theoretical studies related to RHIC, i.e. theories of strong interaction. The center's first director was T. D. Lee (Columbia University), and in October 2003, the former director of BNL, N. P. Samios, succeeded to the post of director. H. En'yo, Chief scientist of RIKEN in Wako, is also associate director of RBRC. The center consists of a theory group lead by L. Mclerran (BNL), an experimental group lead by Y. Akiba of RIKEN, currently resident at BNL, and a computing group lead by T. Izubuchi (BNL&RBRC).

Research in the RBRC theory group focuses on a wide variety of phenomena caused by the strong interaction, one of the four fundamental interactions in nature. The strong interaction is described theoretically by Quantum Chromodynamics (QCD), and the research projects in the RBRC theory group aim to elucidate various phenomena brought about by the strong interaction from the principles of QCD. Major subjects of our research include studies (a) based on lattice QCD, (b) on spin physics based on perturbative QCD, and (c) on QCD in extreme conditions such as high temperature, high density or high energy. RBRC offers RHIC Physics Fellowships, allowing joint appointments with universities. These Fellowships enable a talented researcher to maintain a tenure track position at his/her university as well as a Fellow position at RBRC for a certain period of time. This system was established in order to increase the research potential of RBRC and to disseminate its research activities and results.

At present, RBRC has cooperative agreements with Arizona State University, the City University of New York, University of Connecticut, Pennsylvania State University, the State University of New York at Stony Brook, Texas A&M University, as well as with BNL and with Lawrence Berkeley National Laboratory.

(1) Perturbative QCD and spin physics

The ongoing RHIC spin experiments have motivated much of the parallel theoretical developments at RBRC. In the area of transverse spin physics, novel predictions have been obtained for the single transverse-spin asymmetry in open charm production in pp collisions at RHIC. This asymmetry probes three gluon correlations in polarized proton. In addition, radiative QCD corrections to single-spin observables were investigated, providing the relevant evolution equations. Further work focused on hyperon production at RHIC, and on azimuthal asymmetries in the Drell-Yan process.

In the spin and perturbative QCD program, a major contribution from the hadronization process to the single transverse spin asymmetry in inclusive hadron production was obtained, which is likely to explain the recent experimental anomaly between the eta and pi mesons. In addition, the evolution and the universality properties of the so-called naive time-reversal odd fragmentation function has been obtained. Other work includes the investigation of the universality properties of the unintegrated gluon distribution a small x .

(2) Phenomenological QCD -- QCD under extreme conditions --

To establish a detailed picture of relativistic heavy ion collisions, QCD-based theoretical approaches are in progress. Especially the idea of "color glass condensation (CGC)" can be a key to understand the initial condition of the heavy ion collision. Other phenomenological approaches are in progress to understand the characteristics of strongly interacting quark gluon plasma. A recent effort has been initiated to understand heavy ion elliptic flow in term s of viscous hydrodynamics. A new finite temperature effective field theory is being developed for the strongly interacting quark gluon plasma to explain the suppression of sheer viscosity in the region of the phase transition.

Efforts on RHIC phenomenology proceed on a broad front. Recent efforts include improving hydrodynamic computations using state of the art equations of state derived from lattice gauge theory. Understanding the nature of matter at high baryon number density has generated the idea of Quarkyonic Matter, that may have implications for an upcoming low energy run at RHIC and eventual experiments in the future at FAIR and NICA. An issue being studied is the nature of mass generation and the breaking of translational invariance. A central focus of work at RBRC, the Color Glass Condensate and the Glasma, matter that controls the high energy limit of QCD, is being realized in experiments at RHIC. A workshop held in May 2010 summarized activity in this field, and proceedings will come out as a special edition of Nuclear Physics A. Much activity focuses on the relation between observations at LHC and the implications made at RHIC.

Group Leader

Larry McLERRAN

Deputy Group Leader

Robert PISARSKI

Members

Derek TEANEY *2
Adrian DUMITRU *2
Cecilia LUNARDINI *2
Anna STASTO *2
Jinfeng LIAO *2
Fedor BEZRUKOV *2
Zhongbo KANG *3
Adam BZDAK *3
Koji KASHIWA *4

Visiting Members

Miklos GYULASSY (Columbia Univ., USA)
Robert L. JAFFE (Massachusetts Inst. Technol., USA)
Edward SHURYAK (State Univ. New York, Stony Brook, USA)
Testufumi HIRANO (U. Tokyo)
Feng YUAN (LBNL)

Secretarial Staff

Kerry ZENDZIAN (Secretary to Director N. P. Samios)
Pamela ESPOSITO (Theory Group Secretary)
Taeko ITO (Assistant to Account Manager for Administration)
Susan FOSTER (Experimental Group Secretary)

****1 RIKEN BNL Fellow *2 RHIC Physics Fellow,***
****3 Research Associate, *4 Special Postdoctoral Researcher,***
****5 RHIC visiting Fellow***

Sub Nuclear System Research Division
RIKEN BNL Research Center
Computing Group

1. Abstract

The Computing Group at the RIKEN BNL Research Center (RBRC) was split from the Theory Group at the RBRC in October 2011.

The main mission of the group is to provide important numerical information that is indispensable for theoretical interpretation of experimental data using the theories of particle and nuclear physics. Their primary area of research is lattice quantum chromodynamics (QCD), in which the strong interactions between quarks and gluons are simulated from first principles on large-scale computers.

A unique feature of their studies is the use of quark fields on lattices with *chiral symmetry*, called domain-wall quarks, which has been extensively developed in the RBRC since 1996. The Computing Group has strong ties to the High Energy Theory, Nuclear Theory, and Lattice Gauge Theory Groups at BNL as well as with theory groups at other US universities such as Columbia University and the University of Connecticut. As part of their activities, they form one of the largest lattice QCD collaborations, the RIKEN BNL Columbia (RBC) Collaboration, which began in 2000 and was extended in 2005 to include another active collaboration, the UKQCD collaboration, based primarily at the University of Edinburgh and the University of Southampton.

2. Major Research Subjects

(1) Tests for Standard Model of particle and nuclear physics, especially in the framework of the Cabibbo–Kobayashi–Maskawa (CKM) theory
(2) Dynamics of QCD and related theories
(3) Theoretical and algorithmic development for lattice field theories

3. Summary of Research Activity

In 2011, QCD with Chiral Quarks (QCDCQ), a third-generation lattice QCD computer that is a pre-commercial version of IBM's Blue Gene/Q, was installed as an in-house computing resource at the RBRC. The computer was developed by a collaboration among RBRC, Columbia University, the University of Edinburgh, and IBM. Two racks of QCDCQ having a peak computing power of 2 × 200 TFLOPS are in operation at the RBRC. In addition to the RBRC machine, one rack of QCDCQ is owned by BNL for wider use for scientific computing. The group has also used the IBM Blue Gene supercomputers located at Argonne National Laboratory and BNL (NY Blue), and the cluster computers at RIKEN (Japan), Fermi National Accelerator Laboratory , the Jefferson Lab, and others.

Such computing power enables the group to perform precise calculations using up, down, and strange quark flavors with proper handling of the important symmetry, called chiral symmetry, that quarks have. Several projects are ongoing: flavor physics in the framework of the CKM theory for kaons and B mesons; the electromagnetic properties of hadrons; hadronic contributions to the muon's anomalous magnetic moment; the proton's and neutron's electric dipole moments; proton decay; nucleon form factors, which are related to the proton spin problem; and QCD thermodynamics in finite temperature/density systems such as those produced in heavy-ion collisions at the Relativistic Heavy Ion Collider. Major breakthroughs on important problems such as the direct CP violation process ($K \rightarrow \pi\pi$, ε'/ε) will be attempted using this computer.

Group Leader

Taku IZUBUCHI *1

Members

Tomomi ISHIKAWA *1
Brian TIBURZI *2
Eigo SHINTANI *3
Christoph LEHNER *3(RIKEN FPR)

Visiting Members

Yasumichi AOKI (Nagoya Univ.)
Robert MAWHINNEY (Columbia Univ., USA)

Shigemi OHTA (KEK)
Thomas BLUM (University of Connecticut)
Chulwoo JUNG (BNL)
Meifeng LIN (Yale Univ.)
Yusuke TANIGUCHI (Tsukuba Univ.)
Takeshi YAMAZAKI (Nagoya Univ.)

Secretarial Staff

Kerry ZENDZIAN (Secretary to Director N. P. SAMIOS)
Pamela ESPOSITO (Theory Group Secretary)
Taeko ITO (Assistant to Account Manager for Administration)
Susan FOSTER (Experimental Group Secretary)

****1 RIKEN BNL Fellow *2 RHIC Physics Fellow,***
****3 Research Associate, *4 Special Postdoctoral Researcher,***
****5 RHIC visiting Fellow***

Sub Nuclear System Research Division
RIKEN-BNL Research Center
Experimental Group

1. Abstract

RIKEN BNL Research Center (RBRC) Experimental Group studies the strong interactions (QCD) using RHIC accelerator at Brookhaven National Laboratory, the world first heavy ion collider and polarized p+p collider. We have three major activities: Spin Physics at RHIC, Heavy ion physics at RHIC, and detector upgrades of PHENIX experiment at RHIC.

We study the spin structure of the proton using the polarized proton-proton collisions at RHIC. This program has been promoted by RIKEN's leadership. The first focus of the research is to measure the gluon spin contribution to the proton spin. Our recent data analysis has shown that the proton spin carried by the gluons is small, which is a very striking finding beyond our expectations.

The aim of Heavy ion physics at RHIC is to re-create Quark Gluon Plasma (QGP), the state of Universe just after the Big Bang. Two important discoveries, jet quenching effect and strong elliptic flows, have established that new state of dense matter is indeed produced in heavy ion collisions at RHIC. We are proceeding to understand the nature of the matter. Recently, we have measured direct photons in Au+Au collisions for $1<p_T<3$ GeV/c , where thermal radiation from hot QGP is expected to dominate. The comparison between the data and theory calculations indicates that the initial temperature of 300 MeV to 600 MeV is achieved. These values are well above the transition temperature to QGP, which is calculated to be approximately 170 MeV by lattice QCD calculations.

We has major roles in detector upgrades of PHENIX experiment, namely, the silicon vertex tracker (VTX) and muon trigger upgrades. Both of these two upgrade projects have been completed recently and we took the first data using the upgrade detectors.

2. Major Research Subjects

(1) Experimental Studies of the Spin Structure of the Nucleon
(2) Study of Quark-Gluon Plasma at RHIC
(3) PHENIX detector upgrades

3. Summary of Research Activity

The RIKEN-BNL Research Center was established in 1997 to support the RIKEN activities at RHIC in BNL, and also to promote theoretical studies related to RHIC, i.e. theories of strong interaction. The center's first director was T. D. Lee (Columbia University), and in October 2003, the former director of BNL, N.P. Samios, succeeded to the post of the director. The center consists of a theory group lead by L. Mclerran (BNL) and an experimental group lead by Y. Akiba, a vice chief scientist of RIKEN in Wako.

We study the strong interactions (QCD) using the RHIC accelerator at Brookhaven National Laboratory, the world first heavy ion collider and polarized p+p collider. We have three major activities: Spin Physics at RHIC, Heavy ion physics at RHIC, and detector upgrades of PHENIX experiment.

(1) Experimental study of spin structure of proton using RHIC polarized proton collider

How is the spin of proton formed with 3 quarks and gluons? This is a very fundamental question in Quantum Chromodynamics (QCD), the theory of the strong nuclear forces. The RHIC Spin Project has been established as an international collaboration between RIKEN and Brookhaven National Laboratory (BNL) to solve this problem by colliding two polarized protons for the first time in history. This project also has extended the physics capabilities of RHIC.

The first goal of the RHIC spin physics program is to elucidate a contribution of the gluon spin in the proton spin. We have measured double-helicity asymmetries of neutral pions to study gluon polarization in proton. Our most recent publication from 2006 run have shown that the gluon polarization in the proton is small, and only about half of proton spin can be accounted by gluon spin in the measured region of gluon momentum in proton. The remaining part must be carried by gluons in lower momentum region where the measurement is not sensitive, and/or reside in the orbital-angular momentum of quarks and gluons.

To finalize the smallness of the gluon-spin contribution, we need to measure double helicitiy asymmetry in direct photon production. This process is dominated by a single and the simplest process, gluon Compton scattering, in perturbative QCD, and is the golden channel to determine the gluon density and the gluon polarization in the proton. We published a paper on direct photon cross section in p+p collisions at RHIC. Preliminary results on double-helicity asymmetry of direct photon from the 2006 run have been obtained.

We have also accumulating transversely-polarized proton collision data to measure single transverse-spin asymmetries of processes which are predicted to be sensitive to the orbital-angular momentum of quarks and gluons. In 2006 and 2008, PHENIX recorded 2.7/pb and 4.5/pb, respectively, of transversely-polarized proton collisions data at 200 GeV to investigate single transverse-spin asymmetries. Several transverse spin analyses of these high statistics data are on going.

The 2009 run of RHIC is a major spin run. We had the first 500 GeV p+p run and a long p+p run at 200 GeV. The main purpose of the 500 GeV run is to measure anit-quark polarization from the single longitudinal asymmetry A_L in the W boson production. Approximately 14/pb of data were recorded in PHENIX in the 5 weeks of 500 GeV data taking period. From this data we have observed the first signal of W→e decays in p+p collisions in PHENIX central arm. We measured the production cross section of the W boson and a large spin asymmetry A_L in the W production. These results have been recently published in Physical Review Letters.

We have the second 500 GeV polarized p+p run in 2011. New steel absorber and new muon trigger system have been installed in PHENIX before the run to improve our capability to measure muons from the W decays. Approximately 25/pb of data were recorded during the run. Recently we had preliminary results of single spin asymmetry A_L of $W\rightarrow\mu$ in the 2011 run.

In addition to the study of polarized p+p collisions at RHIC, we study quark fragmentation function. With collaboration with the BELLE experiment at High Energy Accelerator Research Organization (KEK), we discovered that the spin direction of a quark can be determined from its hadronic fragments. Precise data of the quark fragmentation function can be used to understand the cross sections and the spin dependences of particle production in polarized p+p collisions at RHIC. We continue the study of the quark fragmentation function at BELLE.

(2) Experimental study of Quark-Gluon Plasma using RHIC heavy-ion collider

The goal of high energy heavy ion physics at RHIC is study of QCD in extreme conditions i.e. at very high temperature and at very high energy density. Experimental results from RHIC have established that dense partonic matter is formed in Au+Au collisions at RHIC. The matter is very dense and opaque, and it has almost no viscosity and behaves like a perfect fluid. These conclusions are primarily based on the following two discoveries:

- Strong suppression of high transverse momentum hadrons in central Au+Au collisions (jet quenching)
- Strong elliptic flow

The focus of the research in heavy ion physics at RHIC is now to investigate the properties of the matter. RBRC have played the leading roles in some of the most important results from PHENIX in the study of the matter properties. These include (1) measurements of heavy quark production from the single electrons from heavy flavor decay (2) measurements of J/y production (3) measurements of di-electron continuum and (4) measurements of direct photons.

The most important recent result is the measurement of direct photons for $1<p_T<5$ GeV/c in p+p and Au+Au through their internal conversion to e^+e^- pairs. If the dense partonic matter formed at RHIC is thermalized, it should emit thermal photons. Observation of thermal photon is direct evidence of early thermalization, and we can determine the initial temperature of the matter. It is predicted that thermal photons from QGP phase is the dominant source of direct photons for $1<p_T<3$ GeV/c at the RHIC energy. We measured the direct photon in this pT region from measurements of quasi-real virtual photons that decays into low-mass e^+e^- pairs. Strong enhancement of direct photon yield in Au+Au over the scaled p+p data has been observed. Several hydrodynamical models can reproduce the central Au+A data within a factor of two. These models assume formation of a hot system with initial temperature of T_{init} = 300 MeV to 600 MeV. This is the first measurement of initial temperature of quark gluon plasma formed at RHIC. These results are recently published in Physical Review Letters. Y. Akiba received 2011 Nishina Memorial Prize for this work.

Recently, we have constructed and installed a silicon vertex tracker VTX as written in the next section. Measurements of heavy quark production in p+p and A+A collisions using the new detector is the main focus of the group in the coming years. We are now working on the data analysis of the 2011 Au+Au data.

(3) PHENIX detector upgrade

The group has major roles in several PHENIX detector upgrades, namely, the silicon vertex tracker (VTX) and muon trigger upgrades.

VTX is 4 layers of silicon tracker, jointly funded by RIKEN and the US DOE. The inner two layers are silicon pixel detectors and the outer two layers are silicon strip detectors. The detector has been completed in November 2010 and has been installed in PHENIX IR. With this new detector we can measure heavy quark (charm and bottom) production in p+p and heavy ion collisions. We took the first data with the new detector in 2011.

Muon trigger upgrades are needed for W→ mu measurement at 500 GeV. New trigger electronics (Muon Trigger FEE) have been installed in the muon arms. New muon trigger detectors based on RPC technology have been also installed. With these new trigger-systems, we started measuring the W production in forward and backward direction in 2011 and recorded approximately 25/pb of polarized p+p collision data.

Group Leader
Yasuyuki AKIBA

Deputy Group Leader
Abhay DESHPANDE

Members
Yuji GOTO
Itaru NAKAGAWA
Takashi ICHIHARA
Atsushi TAKETANI
Yasushi WATANABE
Satoru YOKKAICHI
Ralf-Christian SEIDL
Kensuke OKADA *1
Stefan BATHE *2
Kieran BOYLE *1
Josef SEELE *1
John KOSTER *3 (RIKEN FPR)
Chin-Hao CHEN *3
Maki KUROSAWA *4
Akihisa TAKAHARA (CNS-U-Tokyo)*5
Hidemitsu ASANO (Kyoto Univ.)*5
Masaya NIHASHI (Hiroshima Univ.)*5
Takahito TODOROKI (Tsukuba Univ.)*5
Megumi SEKINE (TiTech)*5

Visiting Members
Naohito SAITO (KEK)
Zheng LEE (BNL)
Kiyoshi TANIDA (Seoul Univ.)
Akio OGAWA (BNL)
Masahiro OKAMURA (BNL)
Rachid NOUICER (BNL)
Kotaro KONDO (BNL)
Ady HERSHCOVITCH (BNL)
Kohei SHOJI (RIKEN, Radiation Lab.)
Takashi HACHIYA (RIKEN, Radiation Lab.)
Yoshimitsu IMAZU (RIKEN, Radiation Lab.)
Yoshinori FUKAO (KEK)
Katsuro NAKAMURA (Kyoto Univ.)*6
Ryoji AKIMOTO (CNS-U-Tokyo)*6

****1RIKEN BNL Fellow, *2 RHIC Physics Fellow,***
****3 Research Associate, *4 Special Postdoctoral Researcher,***
****5 Junior Research Associate, *6 JSPS Student, *7 Student trainee***

RIBF Research Division
Radioactive Isotope Physics Laboratory

1. Abstract

This laboratory explores exotic nuclear structures and dynamics in exotic nuclei that have never been investigated before, such as those with largely imbalanced proton and neutron numbers. Our aim is to discover new phenomena and properties in exotic nuclei by developments of new experimental techniques utilizing fast RI beams. Another important subject is the equation-of-state in asymmetric nuclear matter, and its association with the origin of elements and with neutron stars. For instance, we are making attempts to the better understand underlying mechanism for exotic stability-enhancements of very neutron-rich fluorine isotopes, the large deformation of the nucleus Mg-34 with N=22 in spite of its vicinity to the N=20 magic neutron number and anomalous collectivity in C-16. We are further extending these studies to medium- and heavy-mass regions by developing facilities, detectors and unique methods at RIBF, thereby leading on the challenging task to find new exotic phenomena. We also perform numerical simulations of nucleosynthesis under the environment of core-collapse supernovae, and moreover quest for footprints of supernovae and solar activities in the past, embedded in Antarctic ice core.

2. Major Research Subjects

(1) Study of structure and dynamics of exotic nuclei through developments of new tools in terms of reaction- and technique-based methodology
(2) Research on EOS in asymmetric nuclear matter via heavy-ion induced reactions
(3) Promotion of nuclear astrophysics in an interdisciplinary organization
(4) Detector developments for spectroscopy and reaction studies

3. Summary of Research Activity

(1) Missing mass method

Missing mass technique is promising for programs at RIBF. Detection of recoil particles from target is essential in excitation energy determination of particle unbound states without any assumption of particle- and gamma-decay processes, and also giving transfer angular momentum from the angular distribution measurement. We have developed a solid hydrogen target as well as a detector system called ESPRI for proton-(in)elastic scattering. In 2010, the first missing mass spectroscopy was performed at RIBF, where the start-of-art detector MUST2 was invited from France to investigate matter distributions and unbound excited states for O-24 and its neighboring nuclei via proton elastic and inelastic scatterings. The data is now in progress.

At the RIPS facility, a missing mass program under the PKU-RIKEN collaboration was carried out in 2009, and two papers were published in 2011. In this program, (p,p alpha) reaction was employed to investigate molecular structure in He-6 and -8, as well as H-7 structure.

(2) In-beam gamma spectroscopy

In the medium and heavy mass region explored at RIBF, collective natures of nuclei are one of important subjects, which are obtained through production and observation of high excited and high spin states. To populate such states, heavy-ion induced reactions such as fragmentation, fission are useful. So far, we have developed two-step fragmentation method as an efficient method to identify and populate excited states, and lifetime measurements to deduce transition strength. At the end of 2008, the first spectroscopy on nuclei island-of-inversion region was performed and the result on the first excited state in Ne-32 was published in PRL in 2009. At the end of 2009, the second campaign of in-beam gamma spectroscopy was organized and backgrounds originating from atomic processes in heavy target were investigated. At the end of 2010, the island-of-inversion region was revisited and the region at N=28 was also investigated. A multitude of data via inelastic, nucleon knock-out, fragmentation channels were obtained.

In 2011, preliminary results obtained from the 2010 data were presented in the ARIS11 conference. October and November, in-beam gamma spectroscopy for a Ni-78 region and the vicinity of Sn-132 was carried out.

(3) Decay spectroscopy

Beta- and isomer-spectroscopy is one of the most efficient methods for studying nuclear structure, especially for non-yrast levels. We had accumulated experimental techniques at the RIPS facility to investigate nuclear structure in light mass region via beta-gamma and beta-p coincidence. Concerning the medium and heavy mass region available at RIBF, we have developed two position-sensitive active-stoppers to achieve low-background via position correlation; strip-silicon detectors and a cylindrical active stopper called CAITEN. At the end of 2009, the first decay spectroscopy on neutron-rich nuclei with A~100 was performed at the new facility of RIBF. Half-lives for 18 neutron-rich nuclei were determined for the first time, and the results were published in PRL, where we discussed in comparison with theoretical predictions as well as in terms of the r-process path. At the same time, the CAITEN detector was successfully tested with fragments produced with a Ca-48 beam.

In 2011, the 2009 data set produced two more letter papers on a new deformed magic number N=64 in the Zr isotopes (PRL) and development of axial symmetry in Mo-110 (PLB). To promote decay spectroscopy further, EUROBALL-RIKEN Cluster Array (EURICA) collaboration has been started. A few workshops were organized to discuss physics cases. Under the EU-RIKEN collaboration, 12 Euro Cluster arrays have been installed at the RIBF. At the end of March, the EURICA was commissioned and found to have performances expected.

(4) Equation-of-state via heavy-ion central collisions

Equation-of-state in asymmetric nuclear matter is one of major subjects in physics of exotic nuclei. Concerning RIBF programs, a detector for pions produced in heavy-ion collisions is being tested at the HIMAC. A TPC for the SAMURAI spectrometer (SAMURAI-TPC) is being designed under the collaboration with MSU, which will be installed in 2014.

(5) Interdisciplinary study for nuclear astrophysics

To understand the origin of elements beyond ion, interdisciplinary works are important in linking data from nuclear physics program. We are promoting simulation of nucleosynthesis in the r-process path, and investigation of Antarctic ice core to search for footprints of supernovae as well as solar activity in the past via mass spectrometer, to link data obtained from nuclear physics program. In July, 2011, a new research unit to cover these activities has been created in Nishina Center, and has become independent of this laboratory.

Head

Hiroyoshi SAKURAI

Members

Takashi ICHIHARA
Takashi KISHIDA
Yoichi NAKAI
Shunji NISHIMURA
Hideaki OTSU
Hiu Ching LEE
Tadaaki ISOBE

Research Associate

Hiroshi WATANABE
Satoshi TAKEUCHI
Mizuki NISHIMURA

Contract Researcher

Taro NAKAO

Special Postdoctoral Researcher

Juzo ZENIHIRO
Daiki NISHIMURA

Foreign Postdoctoral Researcher

David STEPPENBECK
Zhihuan LI
Pieter DOORNENBAL

Senior Visiting Scientist

Kengo OGAWA (Chiba Univ.)

Visiting Scientists

Nori AOI (RCNP)

Dam Nguyen BINH (Institue of Physicks, Vietnam Academy of Science and Technology)
Silivio CHERUBINI (University of Catania, Italy)
Mitsunori FUKUDA (Osaka University)
Adrian GELBERG (Universitat zu Koeln, Germany)
Atsushi HATAKEYAMA (Tokyo University of Agriculture and Technology)
Chuangye HE (China Institute of Atomic Energy)
Kazuo IEKI (Rikkyo University)
Le Hong KHIEM (Institue of Physicks, Vietnam Academy of Science and Technology)
Ivan KOJOUHAROV (GSI)
Yosuke KONDO (Tokyo Institute of Technology)
Nikolaus Ludwig KURZ (GSI)
Indranil MAZUMDAR (GSI)
Takamasa MOMOSE (The University of British Columbia, Canada)
Takashi NAKAMURA(Tokyo Institute of Technology)
Evgueni NIKOLSKI (RRC Kurchatov Institute, Institute of General and Nuclear Physics, Russia)
Hooi Jing ONG (RCNP)
Naohiko OTSUKA (International Atomic Energy Agency, Austria)
Kimiko SEKIGUCHI (Tohoku Univ.)
Henning SCHAFFNER (GSI)
Maya TAKECHI (GSI)
Xiaolong WANG (Kyoto Univ.)

Contract Researcher

Yasuyuki GONO
Yasuo AOKI
Tateaki TORII

Junior Research Associate

Shintaro GO
Masami SAKO
Kenta YOSHINAGA
Masafumi MATSUSHITA

Student Trainees

Kunihiko TAJIRI (Osaka Univ.)
Nobuyuki KOBAYASHI (Tokyo Institute of Technology)
Shinji SUZUKI (Nigata Univ.)
Yo KENMOKU (Osaka Univ.)
Masayuki NAGASHIMA (Nigata Univ.)
Yuki KATO (Meiji Univ.)
Takayuki SAKO (Tokyo Institute of Technology)
Duy NGUYEN (Academy of Science and Technology)
Jongwon HWANG (Seoul National Univ.)
Kenichi SUGIMOTO (The Tokyo University of Science)
Tomoki ASAKA (Tohoku Univ.)
Kouki KAMEI (Tohoku Univ.)
Giseung LEE (Tokyo Institute of Technology)
Ryuki TANAKA (Tokyo Institute of Technology)

Yasuhiro YAMAGUCHI (Meiji Univ.)
Kei IMAMURA (Meiji Univ.)
Sunji KIM (Soul Univ., Korea)
Kota KOBAYASHI (Rikkyo Univ.)
Hiroyuki MIYASAKO (Miyazaki Univ.)
ZhengYu XU (Tokyo Univ.)
Hirotaka FURUKI (Saitama Univ.)
Fumi SUZUKI (Saitama Univ)
Kanae SATO (Saitama Univ.)
Syuu MIYAZAWA (Saitama Univ.)
Takahiro NIWA (Tsukuba Univ.)
Hidekazu UENISHI (Osaka Univ.)
Masaki YAGUCHI (Osaka Univ.)
Koudai IWAMOTO (Osaka Univ.)
Toshiyuki OGURA (Niigata Univ.)
Takeshi ITO (Niigata Univ.)
Takahiro MASHIKO (Tohoku Univ.)
Jun TAKATSU (Osaka Univ.)
Junpei MIYAZAKI (Tohoku Univ.)
Kento TAKAHASHII (Tohoku Univ.)
Hiroki TETSUKA (Tokyo Gakugei Univ.)
Yoshiki TSUTSUI (Tokyo Gakugei Univ.)
Masaharu IZAWA (Meiji Univ.)
Ryogo MINAKATA (Tokyo Institute of Technology)
Yosuke MITSUYA (Meiji Univ.)
Yoshiaki SHIGA (Rikkyo Univ.)
Daiki TOMITA (Rikkyo Univ.)
Yosuke MORITA (Osaka Univ.)
Junichi OHNO (Osaka Univ.)
Masaru WAKABAYASHI (Osaka Univ.)
Yasuto KAMISHOU (Osaka Univ.)
Hiroki NISHIBATA (Osaka Univ.)
Sho KUBOTA (Tokyo University of Agriculture and Technology)
Kosuke ABE (Nigata Univ.)
Taku SAKAI (Nigata Univ.)
Yoshihiro NAKAMURA (Nigata Univ.)
Daishiro SERA (Nigata Univ.)
Naotaka ICHIHASHI (Saitama Univ.)
Yifan ZHU (The Tokyo University of Science)
Hisaya HOTAKA (Tohoku Univ.)
Kotomi MUTO (Tohoku Unv.)
Yasunori WADA (Tohoko Univ.)
Takahiro TAGUCHI (Tohoku Univ.)
Tetsuya YAMAMOTO (Osaka Univ.)
Seijiro NISHI (Tokyo Institute of Technology)

IPA

Ruijiu CHEN (Peking Univ., China)

Xiaofei YANG (Peking Univ., China)
He WANG (Peking Univ., China)
Hongna LIU (Peking Univ., China)

Visiting Rsearcher
Giuseppe LORUSSO (JSPS)
Paer-Anders SOEDERSTROEM (JSPS)

Secretary
Tomoko FUJII
Yu NAYA

RIBF Research Division
Spin isospin Laboratory

1. Abstract

A nucleus is a finite-body quantum system of hadrons and is a self-organizing system governed by the strong interaction. How do "variety" and "regularity" develop and coexist in the nuclear world? We are aiming at clarifying its mechanism through experimental studies of radio-active nuclei produced at the RI Beam Factory.
In particular, the Spin-Isospin Laboratory pursues research activities putting focus on interplay of spin and isospin which are manifestations of symmetry of nature.
We are, at present, performing experiments with spin-polarized protons to solve the magicity-loss problem appearing far from the beta-stability line.

2. Major Research Subjects

(1) Experimental studies of radioactive nuclei via direct reactions
(2) Search for undiscovered states through RI-beam induced reactions
(3) Production of spin-polarized nuclei
(4) Study of nucleo-systhesis with heavy-ion storage ring

3. Summary of Research Activity

(1) Experimental studies of radioactive nuclei via direct reactions

Direct reactions induced by light-ions serve as powerful spectroscopic tools to investigate various aspects of nuclei. We are advancing experimental programs with the light-ion induced reactions with RI-beams in inverse kinematics, by developing new detector systems and advanced target systems. Spin asymmetry measurements for the proton elastic scattering from neutron-rich ^{6,8}He nuclei were performed at 71 MeV/u with a spin-polarized solid proton target. Results of the experiment indicate drastic weakening of the spin-orbit coupling in ^{6,8}He. In 2011, a missing-mass technique was brought into the (p,n) reaction studies in the inverse-kinematics with a newly-developed neutron detector array WINDS. The first experiment for ^{12}Be at 200 MeV/u was highly successful and provided us with rich information on Gamow-Teller strength in the nucleus.

(2) Search for yet-to-be-discovered states through RI-beam induced reactions

RI-beam induced charge exchange reactions have unique properties which are missing in stable-beam induced reactions and can be used to reach yet-to-be-discovered states. The capabilities of RI-beam induced charge exchange reactions are based on availabilities of

- A variety of selectivities in transferred quantum numbers, ΔS, ΔT, $\Delta T\mathbf{z}$, ΔL etc, and
- Kinematical conditions which can not be reached via the stable-beam induced reactions.

Several experiments have been done or are planned with the SHARAQ spectrometer at RIBF. In 2009, the first (t, ^{3}He) experiment with the SHARAQ spectrometer was performed for ^{90}Zr and ^{208}Pb targets and the results clearly shows a bump structure identified to be β^{+}-type isovector spin monopole resonances. A series of experiments to search for other isovector monopole resonances were conducted in 2010.

(3) Production of spin-polarized nuclei

A spin-polarized solid proton target is developed for use in RI-beam experiments. The polarization principle based on electron spin alignment in photo-excited triplet states in aromatic molecule enables the target operation in a low magnetic field of 0.1 T, which makes the polarized target unique for use in RI-beam experiments.

(4) Study of nucleo-systhesis with heavy-ion storage ring

The r-process of nucleo-synthesis is essentially important in accounting abundances of elements heavier than iron. Despite of its importance, not so much is known about the r-process. Determination of masses of neutron-rich nuclei with mass numbers of 60 or higher is crucial in pinning down the r-process path, which in turn lead us to a deeper understanding of the nucleo-sythesis. A new isochronous storage ring, called “Rare RI ring” is planned to be constructed to determine masses of very rare isotopes with a precision of $\Delta m/m = 10^{-6}$.

Head
Tomohiro UESAKA

Members
Masaki SASANO
Juzo ZENIHIRO

Contract Researcher
Masanori DOZONO

Senior Visiting Scientists
Hiroyuki SAGAWA (Aizu University)

Visiting Scientists
Takashi WAKUI (Tohoku University)
Satoshi SAKAGUCHI (Kyusyu University)
Kenjiro MIKI (Osaka University)

Student Trainees
Tomomi KAWAHARA (Toho University)
Tatsuo BABA (Kyoto University)
Taku FUKUNAGA (Kyusyu University)
Tomosuke KADOYA (Kyoto University)
Megumi TAKAHASHI (Tohoku University)
Miho TSUMURA (Kyoto University)
Hidetomo WATANABE (Kyoto University)
Junpei YASUDA (Kyusyu University)

Secretary
Tomoko FUJII
Yu NAYA

RIBF Research Division
Superheavy Element Laboratory

1. Abstract

The elements with their atomic number Z>103 are called as trans-actinide or superheavy elements. The chemical properties of those elements have not yet been studied in detail. Those elements does not exist in nature therefore, they must be produced artificially for scientific studies. In our laboratory, we have been studying the physical and chemical properties of the superheavy elements utilizing the accelerators in RIKEN and various methods of efficient production for the superheavy elements.

2. Major Research Subjects

(1) Search for new superheavy elements
(2) Decay spectroscopy of the heaviest nuclei
(3) Study of the chemical properties of the heaviest elements
(4) Study of the reaction mechanism of the fusion process

3. Summary of Research Activity

(1) Searching for new elements
To expand the periodic table of elements and the nuclear chart, we will search for new elements.
(2) Spectroscopic study of the nucleus of heavy elements
Using the high sensitivity system for detecting the heaviest element, we plan to perform a spectroscopic study of nuclei of the heavy elements.
(3) Chemistry of superheavy elements
Study of chemistry of the trans-actinide (superheavy element) has just started world-wide, making it a new frontier in the field of chemistry. Relativistic effects in chemical property are predicted by many theoretical studies. We will try to develop this new field.
(4) Study of a reaction mechanism for fusion process
Superheavy elements have been produced by complete fusion reaction of two heavy nuclei. However, the reaction mechanism of the fusion process is still not well understood. When we design an experiment to synthesize nuclei of the superheavy elements, we need to determine a beam-target combination and the most appropriate reaction energy. This is when assists of the theory becomes important. We will try to develop a reaction theory useful in designing an experiment by collaborating with the theorists.

Head
Kosuke MORITA

Members
Kouji MORIMOTO

Nishina Center Research Scientist
Daiya KAJI

Nishina Center Technical Scientist
Akira YONEDA

Postdoctoral Researcher
Yasuo WAKABAYASHI

Contract Researcher
Yuki KUDOU
Kazutaka OHZEKI

Visiting Technician

Yuichiro WAKITANI
Shinichi YAMAMOTO

Visiting Scientists

Kazuhiko AKIYAMA (Tokyo Metropolitan Univ.)
Shin-ichi GOTO (Niigata Univ.)
Kentaro HIROSE (Tohoku Univ.)
Takatoshi ICHIKAWA (Yukawa Institute for Theotetical Physics, Kyoto Univ.)
Yoshitaka KASAMATU (Osaka Univ.)
Tsutomu OHTUKI (Tohoku Univ.)
Yasuji OURA
Minoru SAKAMA (Tokushima Univ.)
Atsushi SHINOHARA (Osaka Univ.)
Keisuke SUEKI (Grad. Sch. Pure Appl. Sci., Univ. Tsukuba)
Koichi TAKAMIYA (Kyoto Univ Research Reactor Institute)
Fuyuki TOKANAI (Dept. Phys., Yamagata Univ.)
Akihiko YOKOYAMA (Dept. Chemi., Kanazawa Univ.)
Takashi YOSHIMURA (Osaka Univ.)

Research Consultants

Kenji KATORI
Toru NOMURA

Students

Junior Research Associate

Takayuki SUMITA (Tokyo Univ. of Science)

Student Trainees

Shota KIMURA (Tohoku Univ.)
Aiko KINO (Osaka Uiv.)
Yukiko KOMORI (Osaka Univ.)
Ai KURIYAMA (Osaka Univ.)
Yuki KIKUTANI (Osaka Univ.)
Hideki KAIYA (Kanazawa Univ.)
Yuuka KOGAMA (Osaka Univ.)
Yuki TAKEDA (Kanazawa Univ.)
Reona TAKAYAMA (Osaka Univ.)
Kousuke TODA (Kanazawa Univ.)
Ryutaro SAKAI (Saitama Univ.)
Keita MAYAMA (Yamagata Univ.)
Mirei TAKEYAMA (Yamagata Univ.)
Saori NAMAI (Yamagata Univ.)
Masaki NISHIO (Kanazawa Univ.)
Megumi NISHIKAWA (Kanazawa Univ.)
Takahiro MASHIKO (Yamagata Univ.)
Masashi MURAKAMI (Niigata Univ.)
Norihiro YAMADA (Kanazawa Univ.)

Takuya YOKOKITA (Osaka Uiv.)
Ayaka WADA (Tokyo Metropolitan Univ.)

Secretary
Shinko ODAI

RIBF Research Division
High Energy Astrophysics Laboratory

1. Abstract

In the immediate aftermath of the Big Bang, the beginning of the universe, only hydrogen and helium existed. However, nuclear fusion in the interior of stars and the explosion of supernovae in the universe over the course of 13.7 billion years led to the evolution of a world brimming with the many different elements we have today. By using man-made satellites to observe X-rays and gamma-rays emitted from celestial objects, we are observing the synthesis of the elements at their actual source. Our goal is to comprehensively elucidate the scenarios for the formation of the elements in the universe, together with our research on sub-atomic physics through the use of an accelerator.

2. Major Research Subjects

(1) Nucleosynthesis in Stars and Supernovae
(2) Particle Acceleration Mechanism in Astronomical Objects
(3) Physics in Extremely Strong Magnetism and Gravity
(4) Research and Development of Innovative X-ray and Gamma-ray detectors

3. Summary of Research Activity

High Energy Astrophysics Laboratory started on April 2010. The goal of our research is to reveal the mechanism of nucleosynthesis in the universe, and to observe exotic physical phenomena in extremely strong magnetic and/or gravitational field. We have observed supernova remnants, strongly magnetized neutron stars, pulsars, black holes and galaxies with X-ray astronomical satellites.

We continue to construct the Gravity and Extreme Magnetism Small Explorer (GEMS) under the collaboration with NASA Goddard Space Flight Center (USA). GEMS is the first dedicated satellite for the X-ray polarimetry, which is opening a new field in Astrophysics and Astronomy. To estimate the lifetime of the X-ray polarimeter detector (a gas time projection chamber) in space, we developed the monitoring method of impurity in drift gas and estimated lifetime as a function of the amount of impurity. We have developed a Monte-Carlo simulator based on the Geant4 toolkit. The simulator helped us to estimate the particle background (mainly protons and electrons/positrons) in orbit, and to estimate the detector response when X-rays were injected.

We continue to survey the gamma-ray emission from thundercloud. In this year, we placed two identical gamma-ray detectors apart from 700 m each other at the Kashiwazaki nuclear plant. We detected gamma-ray emission for 4 minutes from thundercloud, followed by the sudden stop of the emission as coincident with lightning. We also revealed that the emission of gamma-ray was limited in a cone region and it moved as thunder cloud moved. With the RIKEN neutron monitor placed in Tibet, we observed very long-lived gamma-ray emission from thundercloud lasted in 40 minutes. We did not know at this moment whether the emission mechanism of the long-lived one was the same as we have observed in Japan.

We continue to observe the supernova remnants with the Japanese X-ray satellite Suzaku and European XMM-Newton. We discovered the charge exchange (CX) emission in Puppis A Supernova Remnant. Nobody expected the emission mechanism, in which X-ray is emitted when ionized atoms collide to neutral ones, has realized in Supernova Remnants. We have observed a black-hole binary Cygnus X-1 with Suzaku and performed timing analyses to measure the variation timescale of several parameters, which characterize the black-hole binary system.

Head
Toru TAMAGAWA

Special Postdoctoral Researchers
Satoru KATSUDA
Shin'ya YAMADA

Postdoctral Researchers
Harufumi TSUCHIYA
Takao KITAGUCHI

Visiting Scientists

Yukikatsu TERADA (Saitama Univ.)
Yujin NAKAGAWA (Waseda Univ.)
Madoka KAWAHARADA (ISAS/JAXA)
Aya BAMBA (ISAS/JAXA)
Asami HAYATO (NASA/GSFC)
Atsushi SENDA (JST)
Poshak GANDHI (ISAS/JAXA)
Ken OHSUGA (NAOJ)
Naohisa INADA (Univ. of Tokyo)
Rohta TAKAHASHI (Tomakomai Nat'l College of
Toru MISAWA (Shinshu Univ.)
Hiroya YAMAGUCHI (CfA/Harvard Univ.)
Teruaki ENOTO (Stanford Univ.)

Support Scientist / Technical Support Staff

Hiroshi KATO

Students

Junior Research Associates

Atsushi HARAYAMA (Saitama Univ.)

Student Trainees

Takanori IWAHASHI (Tokyo Univ. of Science)
Saori KONAMI (Tokyo Univ. of Science)
Wataru IWAKIRI (Saitama Univ.)
Fumi ASAMI (Tokyo Univ. of Science)
Rie YOSHII (Tokyo Univ. of Science)
Akifumi YOSHIKAWA (Tokyo Univ. of Science)
Yoko TAKEUCHI (Tokyo Univ. of Science)
Kenichi IWATA (Shibaura Institute of Technology)
Kenta KANEKO (Kogakuin Univ.)

Secretary

Yu NAYA

RIBF Research Division
Astro-Glaciology Research Unit

Our Astro-Glaciology Research Unit, just organized in July 2011, promotes both theoretical and experimental studies to open up a new interdisciplinary research field between astrophysics and glaciology. On the theoretical side, we numerically simulate:

(1) Changes in the chemical composition of the stratosphere induced by high-energy photons and/or particles emitted from explosive astronomical phenomena, such as solar proton events and galactic supernovae, and

(2) Explosive nucleosynthesis, including that of elements heavier than iron, arising in the environment of core-collapse supernova explosions.

Subjects (1) and (2) themselves are very important in solar–terrestrial research and nuclear astrophysics, respectively; furthermore, they are intended to be coupled with experimental studies.

On the experimental side, we analyze the ice cores drilled at the Dome Fuji station in Antarctica in collaboration with the National Institute of Polar Research, Tokyo. These ice cores correspond to time capsules of the past. In particular, the ice cores obtained at Dome Fuji are known to be unique because they contain much more information on conditions in the stratosphere than any other cores recovered from other locations in either hemisphere. This means that astronomical information can be obtained using the Dome Fuji ice cores. Accordingly, we measure:

(3) Variations in the ion concentrations in the ice cores, in order to seek the proxy of past solar activity and the footprints of supernovae in our galaxy, and

(4) Variations in the water isotopes (^{18}O and ^{2}H) in the ice cores, in order to study past atmospheric temperature variability on the earth.

Here, the basis for item (4) is already established in glaciology. By comparing the experimental results for items (3) and (4), we aim to understand the relationship between solar activity and climate change in the past on the millennium scale. Theoretical studies related to items (1) and (2) will provide a background for distinguishing the characteristics of the astronomical events that can be recorded in the ice cores.

Head

Yuko MOTIZUKI

Members

Kazuya TAKAHASHI (Concurrent)
Yoichi NAKAI (Concurrent)

Contract Researcher

Kentaro SEKIGUCHI

Visiting Scientists

Bradley MEYER (Clemson Univ., USA)
Sachiko AMARI (Washington Univ.,USA)
Akira HORI (Kitami Institute of Technology)
Hiroyuki KOURA (Japan Atomic Energy Agency)
Hideki MADOKORO (Mitsubishi Heavy Industries, Ltd.)
Takahiro TACHIBANA (Waseda High Sch., Waseda Univ.)
Kohji TAKAHASHI (Universite Libre de Bruxelles)

Student Trainees

Satomi KIKUCHI (Saimata University)

Part-time Staff

Ai SHIMADA
Keiko FUKUSHIMA

Secretary

Yu KAWAMURA
Yuri TSUBURAI
Yoko FUJITA

RIBF Research Division
Accelerator Group

1. Abstract

The accelerator group, consisting of seven teams, pursues various upgrades programs involving the next-generation heavy-ion accelerator facility, the Radioisotope Beam Factory (RIBF), to improve the accelerator performance and operation efficiency. The programs include research and development of a superconducting electron cyclotron resonance ion source, charge stripping systems, beam diagnostic devices, radiofrequency systems, control systems, and beam simulation studies. We also maintain the large infrastructure necessary to realize effective operation of the RIBF and are actively promoting the application of the facility to a variety of research fields.
Our primary mission is to supply intense, stable heavy-ion beams to users through effective operation, maintenance, and upgrading of the RIBF accelerators and related infrastructure. The director members listed below govern the development programs that are not dealt with by a single group, such as intensity upgrades and effective operation. They, along with other laboratories belonging to the RIBF research division, also explore future plans for the RIBF accelerators.

2. Major Research Subjects

(1) Intensity upgrade of RIBF accelerators (Okuno)
(2) Effective and stable operation of RIBF accelerators (Fukunishi)
(3) Commissioning of RILAC2 injector (Kase, Kamigaito)
(4) Investigation of future projects (Kamigaito, Fukunishi, Okuno)

3. Summary of Activity

(1) The new injector system, RILAC2, was successfully commissioned.
(2) High-intensity ^{18}O, ^{124}Xe, and ^{238}U beams were supplied to users.
(3) A gas stripper system based on helium gas was developed and installed for the uranium beam.
(4) Possible future plans were explored by considering the potential performance of RIBF accelerators and activities at rare-isotope beam facilities worldwide.
(5) Operation of the RIBF accelerators was restored after the 2011 Tōhoku earthquake.

Group Director
Osamu KAMIGAITO

Deputy Group Director
Hiroki OKUNO (Intensity Upgrade)
Nobuhisa FUKUNISHI (Stable and Efficient Operation)

Members
Masayuki KASE

Secretary
Yoko SAKUMA

RIBF Research Division
Accelerator Group
Accelerator R&D Team

1. Abstract
We are developing the key hardware in the upgrade of the Radioisotope Beam Factory (RIBF) accelerator complex. Our primary focus is the charge stripper, which plays an essential role in the accelerator complex. Charge strippers remove many electrons from ions and realize efficient acceleration of heavy ions by greatly enhancing the charge state. The intensity of uranium beams is limited by the lifetime of the carbon foil stripper conventionally installed in the acceleration chain. Improving the stripper lifetime is essential to increasing the beam power toward the final goal of the RIBF in the future. We are developing the low-Z gas stripper. Gas strippers are generally free from lifetime-related problems but produce a low equilibrium charge state because of the absence of density effects. A low-Z gas stripper, however, can produce an equilibrium charge state as high as that in carbon foil because the electron capture process is suppressed. Another focus is the upgrade of the world's first superconducting ring cyclotron.

2. Major Research Subjects
(1) Development of charge strippers for high-power beams (foil, low-Z gas)
(2) Upgrade of the superconducting ring cyclotron
(3) Maintenance and R&D of the electrostatic deflection/inflection channels for beam extraction/injection

3. Summary of Research Activity
(1) Development of charge strippers for high-power beams (foil, low-Z gas)
Okuno, H., Imao, H., Hasebe, H., Kuboki, H.
(2) Upgrade of the superconducting ring cyclotron
Okuno, H., Ohnishi, J.
(3) Maintenance and R&D of the electrostatic deflection/inflection channels for beam extraction/injection
Okuno, H., Ohnishi, J.

Team Leader
Hiroki OKUNO

Members
Jun-ichi OHNISHI
Hiroshi IMAO

Nishina center engineer
Hiroo HASEBE

Special Postdoctoral Researcher
Hironori KUBOKI

Visiting Scientists
Noriyosu HAYASHIZAKI (Tokyo Institute of Technology)
Mitsuhiro FUKUDA (RCNP, Osaka Univ.)
Andreas ADELMANN (PSI, Switzerland)

Research Consultants
Yoshiaki CHIBA
Isao YAMANE

RIBF Research Division
Accelerator Group
Ion Source Team

1. Abstract

Our aim is to operate and develop the ECR ion sources for the accelerator-complex system of the RI Beam Factory. We focus on further upgrading the performance of the RI Beam Factory through the design and fabrication of a superconducting ECR heavy-ion source for production of high-intensity uranium ions.

2. Major Research Subjects

(1) Operation and development of the ECR ion sources
(2) Development of a superconducting ECR heavy-ion source for production of high-intensity uranium ions

3. Summary of Research Activity

(1) Operation and development of ECR ion sources

T. Nakagawa, M. Kidera, Y. Higurashi, T. Ozeki, H. Haba, T. Urabe, and T. Kageyama

We routinely produce and supply various kinds of heavy ions such as zinc and neon ions for the super-heavy element serach experiment as well as uranium ions for RIBF experiments. We also perform R&D's to meet the requirements for stable supply of high-intensity heavy ion beams.

(2) Development of a superconducting ECR ion source for use in production of a high-intensity uranium beam

T. Nakagawa, J. Ohnishi, M. Kidera, Y. Higurashi, T. Ozeki, and H. Haba

The RIBF is required to supply uranium beams with very high intensity so as to produce RI's. We have designed and are fabricating an ECR ion source with high magnetic field and high microwave-frequency, since the existing ECR ion sources have their limits in beam intensity. The coils of this ion source are designed to be superconducting for the production of high magnetic field. We are also designing the low-energy beam transport line of the superconducting ECR ion source.

Team Leader
Takahide NAKAGAWA

Nishina center csientist
Masanori KIDERA
Yoshihide HIGURASHI

Special temporary employee
Tadashi KAGEYAMA

Special postdoctral reseracher
Takakazu OHZEKI
Tatsuya URABE

Visiting Scientists
Takehiro MATSUSE (Fac.Text. Sci. Technol.,Shinshu Univ.)

RIBF Research Division
Accelerator Group
RILAC Team

1. Abstract

The operation and maintenance of the RIKEN Heavy-ion Linac (RILAC) have been carried out. There are two operation modes: one is the stand-alone mode operation and the other is the injection mode operation. The RILAC has been used especially as an injector for the RIKEN RI- Beam Factory accelerator complex. The RILAC is composed of the ECR ion source, the frequency-variable RFQ linac, six frequency-variable main linac cavities, and six energy booster cavities (CSM).

2. Major Research Subjects

(1) The long term high stability of the RILAC operation.
(2) Improvement of high efficiency of the RILAC operation.

3. Summary of Research Activity

The RILAC was started to supply ion beams for experiments in 1981. Thousands hours are spent in a year for delivering many kinds of heavy-ion beams to various experiments.

The RILAC has two operation modes: one is the stand-alone mode operation delivering low-energy beams directly to experiments and the other is the injection mode operation injecting beams into the RRC. In the first mode, the RILAC supplies a very important beam to the nuclear physics experiment of "the research of super heavy elements". In the second mode, the RILAC plays a very important role as upstream end of the RIBF accelerator complex.

The maintenance of these devices is extremely important in order to keep the log-term high stability and high efficiency of the RILAC beams. Therefore, improvements are always carried out for the purpose of more stable and more efficient operation.

Team Leader
Eiji IKEZAWA

Member
Yutaka WATANABE

Research Consultants
Toshiya CHIBA
Masatake HEMMI
Yoshitoshi MIYAZAWA

RIBF Research Division
Accelerator Group
Cyclotron Team

1. Abstract

Together with other teams of Nishina Center accelerator division, maintaining and improving the RIBF cyclotron complex. The accelerator provides high intensity heavy ions. Our mission is to have stable operation of cyclotrons for high power beam operation. Recently stabilization of the rf system is a key issue to provide 10 kW heavy ion beam.

2. Major Research Subjects

(1) RF technology for Cyclotrons
(2) Operation of RIBF cyclotron complex
(3) Maintenance and improvement of RIBF cyclotrons
(4) Single turn operation for polarized deuteron beams
(5) Development of superconducting cavity for the rebuncher system

3. Summary of Research Activity

Development of the rf system for a reliable operation
Development of highly stabilized low level rf system
Development of superconducting rebuncher cavity
Development of the intermediate-energy polarized deuteron beams.

Team Leader
Naruhiko SAKAMOTO

Nishina Center Research Scientist
Kenji SUDA

Foreign Postdoctoral Researcher
Lu LIANG

RIBF Research Division
Accelerator Group
Beam Dynamics and Diagnostics Team

1. Abstract

In order to realize stable and efficient operations of RIBF accelerator complex, various improvements including beam diagnosis, computer control, power supplies have been performed. Our final goal is to extract the full performance of RIBF accelerator complex.

2. Major Research Subjects

(1) Establishing higher beam transmission efficiency of our multi-stage accelerator system.
(2) Development of beam diagnosis.
(3) Development of computer control.
(4) Bending power upgrade of fRC.

3. Summary of Research Activity

(1) Development of the beam diagnostic technology
Two kinds of non-destructive beam intensity monitors including the world first HTC-SQUID monitor have been developed.
(2) Development of the computer control system of accelerators
EPICS-based control system and a homemade beam interlock system have been stably operated. Control system of a new injector system RILAC2 has started its operation. A Java-based data archive system has been also developed.
(3) New power supplies
Two kinds of new power supplies have been introduced in order to realize bending-power upgrade of fRC. These new power supplies are also designed to work as substitutes of aging power supplies used for RRC.
(4) New injector system RILAC2 has been successfully commissioned.

Team Leader
Nobuhisa FUKUNISHI

Members
Masaki FUJIMAKI
Keiko KUMAGAI
Tamaki WATANABE
Kazunari YAMADA

Contract Technical Scientist
Misaki KOBAYASHI-KOMIYAMA
Hiroshi WATANABE
Makoto NAGASE

Postdoctral Researcher
Takuya MAEYAMA

Visiting Scientists
Hiromichi RYUTO (Photonics and Electronics Science and Engineering Center, Kyoto University)
Jun-ichi ODAGIRI (Accelerator Laboratory, High Energy Accelerator Research Organization (KEK))
Yuichiro SASAKI

Research Consultants
Jiro FUJITA

RIBF Research Division
Accelerator Group
Cryogenic Technology Team

1. Abstract

We operate the cryogenic system for the superconducting ring cyclotron at the Radioisotope Beam Factory (RIBF). We also operate the helium cryogenic system in the southern part of the RIKEN Wako campus and deliver liquid helium to users at RIKEN. Our goal is to collect 100% of the helium gas after liquid helium usage on the Wako campus.

2. Major Research Subjects

(1) Operation of the cryogenic system for the superconducting ring cyclotron at the RIBF
(2) Operation of the helium cryogenic plant in the southern part of the Wako campus and delivering liquid helium to users on the Wako campus

3. Summary of Research Activity

(1) Operation of the cryogenic system for the superconducting ring cyclotron at the RIBF
Okuno, H., Dantsuka, T.
(2) Operation of the helium cryogenic plant in the southern part of the Wako campus and delivering liquid helium to users on the Wako campus
Dantsuka, T., Nakamura, M., Maie, T., Ikegami, K., Tsuruma, S., Okuno., H.

Team Leader
Hiroki OKUNO

Members
Masato NAKAMURA

Nishina Center Engineer
Takeshi MAIE

Technical Staff-I
Tomoyuki DANTSUKA

Research Consultant
Kumio IKEGAMI

Part timer
Shizuho TSURUMA

RIBF Research Division
Accelerator Group
Infrastructure Management Team

1. Abstract

The RIBF accelerators are an incomparable multi-stage accelerator complex. For the long and stable operations of these accelerators, their infrastructures become very important. Our team supports their infrastructure; buildings, electric facilities, cooling system, vacuum system and so on. It also concerns the regular operation and maintenance of all the accelerators, and improves or renews the old parts of the accelerators.

2. Major Research Subjects

Management of the RIBF accelerator infrastructure; buildings, electric facilities, cooling system, vacuum system and so on.

3. Summary of Research Activity

The current research subjects are summarized as follows:

(1) Operation and maintenance of infrastructure for RIBF accelerators.
(2) Improvement or renewal of the, especially old, accelerators.
(3) Support of accelerator operations.

Team Leader

Masayuki KASE

Members

Hiromi YAMASAWA

Temporary Employee

Tadashi FUJINAWA

Visiting Scientists

Hideshi MUTO (Tokyo Univ. of Sci. Suwa)

RIBF Research Division
Instrumentations Development Group

1. Abstract

This group develops experimental installations for the RI Beam factory. Experimental installations currently planned include designs containing common elements enabling multiple use, as well as others that are highly program specific. All are designed to maximize the research potential of the world's most intense RI beams, made possible by the exclusive equipment available at the RI Beam Factory.

2. Major Research Subjects

(1) SCRIT Project
(2) SLOWRI Project
(3) Polarized RI Beam Project
(4) Rear RI Ring Project

3. Summary of Research Activity

We are developing beam manipulation technology in carrying out above listed project. They are the high-quality slow RI beam production (SCRIT and SLOWRI), the beam cooling and stopping (SCRIT and SLOWRI), the polarized and aligned RI beam production (Pol. RI Beam), and the beam accumulation technology (Rare RI Ring). The technological knowhow accumulated in our projects will play a significant role in the next generation RIBF. Future Plan for each project is described in subsections. SCRIT is now under construction and partially tested using stable isotopes. Rare RI Ring construction has been started in this year. Design studies of SLOWRI have been almost finished and it ready for construction. A new technique to efficiently align nuclear spin of RI produced by Big RIPS has been developed by Pol. RI Beam project team. This will be powerful tool for nuclear structure study for short-lived unstable nuclei.

Group Leader
Masanori WAKASUGI

Secretary
Minami IMANISHI

RIBF Research Division
Instrumenttation Development Group
SLOWRI Team

1. Abstract

A next-generation slow radioactive nuclear ion beam facility (SLOWRI) which provides slow, high-purity and small emittance ion beams of all elements is being build as one of the principal facilities at the RIKEN RI-beam factory (RIBF). High energy radioactive ion beams from the projectile fragment separator BigRIPS are thermalized in a large gas catcher cell. The thermalized ions in the gas cell are guided and extracted to a vacuum environment by a combination of dc electric fields and inhomogeneous rf fields (rf carpet ion guide). From there the slow ion beam is delivered via a mass separator and a switchyard to various devices: such as an ion trap, a collinear fast beam apparatus, and a multi-reflection time of flight mass spectrometer. In the R&D works at the present RIKEN facility, an overall efficiency of 5% for a 100A MeV ^{8}Li ion beam from the present projectile fragment separator RIPS was achieved and the dependence of the efficiency on the ion beam intensity was investigated.

First spectroscopy experiment at the prototype SLOWI was performed on Be isotopes. Energetic ions of ^{7,10,11}Be from the RIPS were trapped and laser cooled in a linear rf trap and precision spectroscopy was performed. The evaluated ion temperature of <10 mK demonstrates that a reduction of more than 15 orders of magnitude for the kinetic energy of radioactive Be was achieved online. Precise investigation of the hyperfine structure will confirm the anomalous mean radius of the valence neutron of the so called neutron halo nucleus.

Other spectroscopy experiments using the slow RI-beams are also under progress in off-line setups. A collinear fast beam apparatus for nuclear charge radii measurements was build and tested with stable Ar+ ion beams. A multi-reflection time-of-flight mass spectrograph (MRTOF-MS) was build for precise and fast measurements of short-lived radioactive nuclei. A high mass resolving power of 140,000 for K and Rb ions has been achieved with a 5 ms measurement period. This new mass spectrograph is best suited for very heavy ions such as super heavy elements. Using a compact rf-carpet gas catcher at GARIS facility, we will perform direct mass measurements of nuclei heavier than uranium with the MRTOF-MS.

An advanced SLOWRI facility is also proposed. The expected number of nuclides which can be investigated at SLOWRI is more than 3000, however, the realistic beam time for each experiment would be very limited. The advanced facility will parasitically provide slow RI-beams everyday as long as the fragment separator BigRIPS is operated. The parasitic beam can be produced from those nuclei dumped at the first focal plane slits of BigRIPS by placing a compact gas catcher cell. The thermalized and neutralized RI in the cell can be re-ionized at the exit of the cell by resonance laser ionization. Development the new method, named PALIS, is underway.

2. Major Research Subjects

(1) Development and construction of the next-generation slow RI-beam facility
(2) Laser spectroscopy of trapped radioactive Beryllium isotopes.
(3) Development of a multi-reflection time-of-flight mass spectrograph for precision mass measurements of short-lived nuclei.
(4) Development of collinear fast beam apparatus for isotope shift measurements.
(5) Development of parasitic slow RI-beam production method using resonance laser ionization.

3. Summary of Research Activity

(1) Development of universal slow RI-beam facility

WADA, Michiharu, SCHURY Peter, SONODA, Tetsu, ITO, Yuta, TAKAMINE, Aiko, OKADA, Kunihiro, KUBO, Toshiyuki, WOLLNIK, Hermann, SCHUESSLER, Hans, KATAYAMA Ichiro

A next-generation slow radioactive nuclear ion beam facility (SLOWRI) which provides slow, high-purity and small emittance ion beams of all elements is being build as one of the principal facilities at the RIKEN RI-beam factory (RIBF). High energy radioactive ion beams from the projectile fragment separator BigRIPS are thermalized in a large gas catcher cell. The thermalized ions in the gas cell are guided and extracted to a vacuum environment by a combination of dc electric fields and inhomogeneous rf fields (rf carpet ion guide). From there the slow ion beam is delivered via a mass separator and a switchyard to various devices: such as an ion trap, a collinear fast beam apparatus, and a multi-reflection time of flight mass spectrometer. In the R&D works at the present RIKEN facility, an overall efficiency of 5% for a 100*A* MeV ^{8}Li ion beam from the present projectile fragment separator RIPS was achieved and the dependence of the efficiency on the ion beam intensity was investigated.

(2) Laser spectroscopy of trapped radioactive beryllium isotope ions

WADA, Michiharu, TAKAMINE, Aiko, SCHURY Peter, SONODA Tetsu, OKADA, Kunihiro, KANAI, Yasuyuki, YOSHIDA, Atsushi, KUBO, Toshiyuki, YAMAZAKI, Yasunori, WOLLNIK, Hermann, SCHUESSLER, Hans, NODA, Koji, OHTANI, Shunsuke, KATAYAMA Ichiro

As a first application of the prototype SLOWRI setup, we applied hyperfine structure spectroscopy to the beryllium isotopes to determine in particular the anomalous radius of the valence neutron of the neutron halo nucleus ^{11}Be, and to determine the charge radii of these beryllium isotopes through laser-laser double resonance spectroscopy of laser-cooled ions. Laser cooling is an essential prerequisite for these planned experiments. The first laser spectroscopy experiments for beryllium isotopes were performed to measure the resonance frequencies of 2s $^2S_{1/2}$ - 2p $^2P_{3/2}$ transition of ^{7}Be+, ^{9}Be+, $^{10}Be^+$ and ^{10}Be+ ions and the nuclear charge radii of these isotopes were determined. The hyperfine structure of $^{11}Be^+$ and $^7Be^+$ ions using the laser-microwave double resonance spectroscopy were also performed and the magnetic hyperfine constants of $^7Be^+$ and $^{11}Be^+$ ions were determined with an accuracy of 10^{-7}

(3) Development of a multi-reflection TOF mass spectrograph for short-lived nuclei

WADA, Michiharu, SCHURY Peter, ITO, Yuta, NAIMI, Sarah, NAKAMURA, Sousuke, TAKAMINE, Aiko, SONODA Tetsu, OKADA, Kunihiro, WOLLNIK, Hermann,

The atomic mass is one of the most important quantity of a nucleus and has been studied in various methods since the early days of physics. Among many methods we chose a multi-reflection time-of-flight (MR-TOF) mass spectrometer. Slow RI beams extracted from the RF ion-guide are bunch injected into the spectrometer with a repetition rate of ~500 Hz. The spectrometer consists of two electrostatic mirrors between which the ions travel back and forth repeatedly. These mirrors are designed such that energy-isochrononicity in the flight time is guaranteed during the multiple reflections while the flight time varies with the masses of ions. A mass-resolving power of 140,000 has been obtained with a 5 ms flight time for K and Rb isotopes. It is equivalent to use a 90 T magnet for a Penning trap mass spectrometer. This mass-resolving power should allow us to determine ion masses with an accuracy of 10^{-7}. The advantages of the MR-TOF spectrometer are: 1) short measurement periods, typically 2 ms, which allows all neutron rich nuclei to be investigated, 2) the device is compact and its operation is simple, especially, it is independent from the all upstream devices, accelerators and fragment separators, 3) ions of more than isobars can be measured simultaneously, so that mass reference can easily be established in the mass spectra. In total, the number of measurable nuclides within a limited beam time would be larger than that can be achieved by other methods. It should be noted here also that this method can be used even during a low-duty parasite beam time. Online mass measurements of short-lived radioactive nuclei are planned in FY2011.

This new mass spectrograph is best suited for direct mass measurements of very heavy nuclei, such as super heavy elements. We start a project, SHE-MASS, aiming at comprehensive mass measurements of many nuclei heavier than uranium at GARIS facility. For any time-of-flight mass spectrometers, mass references are indispensable. We developed an electro-spray ion source for molecular ions, which can produce a variety of molecular ions in a wide mass range. We used a compact rf-carpet for accumulating molecular ions with low abundant isotopes and found that there are isobaric molecules in many mass numbers. We have also confirmed that the accuracy of mass determination is always within the precision of the mass measurements in tests with isobaric triplets

(4) Development of collinear fast beam apparatus for nuclear charge radii measurements

WADA, Michiharu, SCHUESSLER, Hans, IIMURA, Hideki, SONODA, Tetsu, SCHURY, Peter, TAKAMINE, Aiko, OKADA, Kunihiro, WOLLNIK, Hermann,

The root-mean-square charge radii of unstable nuclei have been determined exclusively by isotope shift measurements of the optical transitions of singly-charged ions or neutral atoms by laser spectroscopy. Many isotopes of alkaline, alkaline-earth, noble-gases and several other elements have been measured by collinear laser spectroscopy since these ions have all good optical transitions and are available at conventional ISOL facilities. However, isotopes of other elements especially refractory and short-lived ones have not been investigated so far.

In SLOWRI, isotopes of all atomic elements will be provided as well collimated mono-energetic beams. This should expand the range of applicable nuclides of laser spectroscopy. In the first years of the RIBF project, Ni and its vicinities, such as Ni, Co, Fe, Cr, Cu, Ga, Ge are planned to be investigated. They all have possible optical transitions in the ground states of neutral atoms with presently available laser systems. Some of them have so called recycle transitions which enhance the detection probabilities noticeably. Also the multistep resonance ionization (RIS) method can be applied to the isotopes of Ni as well as those of some other elements. The required minimum intensity for this method can be as low as 10 atoms per second.

We have built an off-line mass separator and a collinear fast beam apparatus with a large solid-angle fluorescence detector. A 617 nm transition of the metastable Ar+ ion at 20 keV was measured with both collinear and anti-collinear geometry that allowed us to determine the absolute resonant frequency of the transition at rest with more than 10^{-8} accuracy. Such high accuracy measurements for Ti and Ni isotopes are in progress.

(5) Development of parasitic slow RI-beam production scheme using resonance laser ionization

WADA, Michiharu, SONODA Tetsu, MITA, Hiroki, TAKAMINE, Aiko, OKADA, K., MATSUO Yukari, FURUKAWA, Takeshi, TIMITA, Hideki, KOBAYASHI T., MIYATAKE Hiroari, JEONG Sun Chan, ISHIYAMA, H., IMAI, N., HIRAYAMA Y., KATAYAMA I., TOMITA, H., IIMURA, H., SHINOZUKA T., WAKUI, T., HUYSE, M., VAN DUPPEN, P., KUDRYAVTSEV, Yu., SCHUESSLER, H., WOLLNIK, H.

More than 99.9% of RI ions produced in projectile fission or fragmentation are simply dumped in the first dipole magnet and the slits. A new scheme, named PALIS, to rescue such dumped precious RI using a compact gas catcher cell and resonance laser ionization was proposed. The thermalized RI ions in a cell filled with Ar gas can be quickly neutralized and transported to the exit of the cell by gas flow. Irradiation of resonance lasers at the exit ionizes neutral RI atoms efficiently and selectively. The ionized RI ions can be further selected by a magnetic mass separator and transported to SLOWRI experimental area for spectroscopy experiment. The resonance ionization scheme itself can also be a useful method to perform precision optical spectroscopy of RI of many elements.

An off-line setup for resonance ionization in gas cell is prepared. Extraction from 500 mbar Ar gas cell by resonance ionization method for Ni and Cu ions were demonstrated. A differential pumping from 500 mbar to 10-5 mbar using multiple small pumps and an rf sextupole ion beam guide (SPIG) has been achieved. Design of a gas cell which will be placed at the second focal plane (F2) of BigRIPS is in progress.

Head

Michiharu WADA

Members

Tetsu SONODA
Peter SCHURY
Sarah NAIMI
Yuta ITO
Sousuke NAKAMURA
Hiroki MITA
Shigeaki ARAI
Aiko TAKAMINE
Kunihiro OKADA
Ichiro KATAYAMA
Hideki IIMURA
Hideo TOMITA
Hans SCHUESSLER
Hermann WOLLNIK
Hirokane KAWAKAMI

RIBF Research Division
Instrumentation Development Group
Polarized RI Beam Team

1. Abstract

The team conducts research and development studies of a technique for the production of spin-oriented radioactive-isotope beams (RIBs) and applies it to research in nuclear physics, fundamental physics, and materials science. Microscopic investigation of physical and chemical processes is performed on the basis of nuclear physics techniques that take advantage of intrinsic nuclear properties and phenomena (e.g., spins, electromagnetic nuclear moments, decay modes). In particular, the precession/resonance of an oriented nuclear spin under an external field is observed via a change in the angular distribution of radiation in the study of nuclear structures through nuclear moments. Experimental methods and devices for fundamental physics research with polarized nuclei have also been developed. The same methods are used to investigate condensed matter, such as semiconductors, ferromagnets, fullerenes, and systems with dilute magnetic impurities, by exploiting radioactive nuclei as microscopic probes into them. All these research activities are to be extended to a wide variety of unstable nuclei provided by the Radioisotope Beam Factory (RIBF). A method of producing beams of highly polarized radioactive nuclei, taking full advantage of the RIBF, is being developed.

2. Major Research Subjects

(1) Nuclear moment measurements of unstable nuclei
(2) RIKEN Projectile Fragment Separator (RIPS) upgrade and the development of highly polarized slow RI beams
(3) Fundamental physics: Study of symmetry
(4) Condensed matter studies using radioactive nuclear probes

3. Summary of Research Activity

(1) Nuclear-moment measurements of unstable nuclei

Our earlier work revealed that spin-oriented RIBs can be produced as a function of their outgoing momenta and emission angles in the projectile fragmentation reaction. With the obtained spin-polarized nuclei, ground- and excited-state nuclear moments can be determined by means of the β-ray-detected nuclear magnetic resonance (β-NMR) and time differential perturbed angular distribution (TDPAD) methods, respectively. The sub-themes are the following:

- Development of a new method of producing highly spin-aligned RIBs by two-step projectile fragmentation combined with the momentum dispersion matching technique and the magnetic moment measurement of isomeric states in ^{32}Al by the TDPAD method
- Nuclear structure study of neutron-rich aluminum isotopes $^{30\text{–}32}$Al on the border of the *island of inversion* and $^{33\text{–}34}$Al on/beyond it
- Investigation of a new *island of inversion* around $N = 28$ and nuclear moment measurements of neutron-rich isotopes
- Ground-state electric quadrupole moment measurements of ^{23}Al for the study of the $T = 3/2$ mirror symmetry
- Study of nuclei around the Fe region: isospin symmetry study by means of the magnetic moment of the 10^+ isomer in ^{54}Ni, and study of magicity in the vicinity of ^{68}Ni through the quadrupole moment of the $13/2^+$ isomeric state in ^{69}Cu and the isomeric state in ^{65}Fe

(2) RIPS upgrade and the development of highly polarized slow RI beams

The upgrade of the RIPS was proposed in the phase II programs. In the cyclotron-cascade acceleration scheme, beams are accelerated to an energy of E/A = 115 MeV by an intermediate-stage ring cyclotron (IRC). In this upgrade, the former fragment separator RIPS was equipped with a new beam line that delivers beams of heavy ions of E/A = 115 MeV from the IRC cyclotron. RI beams produced by the primary beams at this intermediate energy are energetic enough to produce RIBs via projectile fragmentation reactions and suitably low in energy to be stopped in a sample material of limited thickness. Compared with the production yield of RIBs in the present azimuthally varying field (AVF) Riken Ring Accelerator (RRC) acceleration scheme, the yield is dramatically increased. Our team is conducting a design study of the upgrade program. We noted that RIBs produced at E/A = 115 MeV can be spin-oriented so that further nuclear moment measurements can be conducted. Further, the addition of a new atomic beam resonance method combined with fragmentation-based RIBs to this program, which is under development, will enable the production of highly spin-polarized RIBs in a low beam energy region. Thus, they could be useful not only for nuclear moment measurements but also for spin-related subjects in nuclear physics, fundamental physics, and materials science.

(3) Fundamental physics: Study of symmetry

The nuclear spins of stable and unstable isotopes sometimes play important roles in fundamental physics research. New experimental methods and devices have been developed for studies of the violation of time reversal symmetry (T-violation) using spin-polarized nuclei. These experiments aim to detect the small frequency shift in the spin precession or measure the *T*-odd angular correlation in β decay as *T*-violating signals arising from new mechanisms beyond the Standard Model. The sub-themes are the following:

- Precise measurement of spin-precession frequency with a new type of nuclear spin maser for atomic electric dipole moment (EDM) search
- Development of highly sensitive atomic magnetometer for EDM experiments
- Development of a new Mott polarimeter for *T*-violation experiment using β decay of polarized unstable nuclei

(4) Condensed matter studies using radioactive nuclear probes
Online time differential perturbed angular correlation experiments have been conducted through γ-ray measurements by using RIBs as a probe. The microscopic structures and dynamics of ferromagnets and the properties of semiconductors have been investigated using the deduced internal local fields and the spin relaxation of the probe in materials. The β-NMR/nuclear quadrupole resonance (NQR) method is also used for these condensed matter studies. The methods and apparatus for these studies have been developed. In addition, basic studies of the probe nuclei have been conducted. The sub-themes are the following:

- Study of Fe impurities in silicon solar cells with online Mössbauer spectroscopy of implanted ^{57}Fe
- Development of an on-line perturbed angular-correlation method with ^{19}O beams as a new probe
- Study of the fast diffusion of Cu impurity atoms in Si through β-NMR/NQR with implanted ^{58}Cu
- Study of the superconductivity of diamond by heavy ion implantation

Team Leader
Hideki UENO

Members
Yoshio KOBAYASHI

Research Consultant
Takuya OKADA

Visiting Scientists
Hisazumi AKAI (Osaka Univ.)
Koichiro ASAHI (Tokyo Tech)
Dimiter BALABANSKI (Bulgarian Academy of Sciences)
Takeshi FURUKAWA (Tokyo Metropolitan Univ.)
Yuichi ICHIKAWA (Tokyo Tech)
Radomira LOZEVA (CNRS/IN2P3)
Kensaku MATSUTA (Osaka Univ.)
Jiro MURATA (Rikkyo Univ.)
Akihiro YOSHIMI (Okayama Univ.)
Makoto UCHIDA (Tokyo Tech)

Junior Research Associate
Yoko ISHIBASHI (Univ. of Tsukuba)

Student Trainees
Masatoshi CHIKAMORI (Tokyo Tech)
Hironori HAYASHI (Tokyo Tech)
Takeshi INOUE (Tokyo Tech)
Yuji ISHII (Tokyo Tech)
Hirokazu MIYATAKE (Tokyo Tech)

Tsubasa NANAO (Tokyo Tech)
Hazuki SHIRAI (Tokyo Tech)
Masato TSUCHIYA (Tokyo Tech)
Keisyun YAMAMURA (Fukui Univ. of Tech.)
Naoki YOSHIDA (Tokyo Tech)

RIBF Research Division
Instrumentation Development Group
Rare RI-ring Team

1. Abstract

We are developing the isochronous storage ring to measure the mass for rare radioactive isotopes (Rare RI ring). It is assumed that uranium is synthesized by neutron capture process after the supernovae explosion (r-process). To prove r-process, mass measurements for the rare RI are indispensable. To deduce the mass, we measure the circulation time (cyclotron frequency) for the rare RI inside the ring. RI beams produce in RIBF have some energy spread. To compensate the spread, isochronicity inside the ring is indispensable (isochronous storage ring). We will inject the rare RI one by one to the ring (individual injection) to identify the RI event-by-event.

2. Major Research Subjects

Developments of isochronous storage ring to measure mass of rare RI.

3. Summary of Research Activity

Developments of isochronous storage ring to measure mass of rare RI.
The conceptual design for an isochronous storage ring has been finalized, and the construction has been started in this year. To minimize construction cost, we re-use TARN-II bending magnets with additional trim coils as main components of the ring. A quick activated kicker magnet system required for one by one injection will be installed. Design study of another important item schottoki beam monitor has also been finalized and it will be manufactured soon. Fundamental ring system will be completed with in this fiscal year.

Team Leader
Masanori WAKASUGI

Research Associate
Yoshitaka YAMAGUCHI

Visiting Scientists
Akira OZAWA (Inst. Phys., Univ.of Tsukuba)
Takeshi SUZUKI (Saitama University)
Takayuki YAMAGUCHI (Saitama University)
Takashi KIKUCHI (Nagaoka University of Technology)
Daisuke NAGAE (Inst. Phys., Univ.of Tsukuba)

Junior Research Associate
Yasushi ABE (University of Tsukuba)

RIBF Research Division
Instrumentation Development Group
SCRIT Team

1. Abstract

We aim at the investigation of internal nuclear structure of short-lived radioactive nuclei (RI) by means of electron scattering. Electron scattering for RI's has never been performed duo to inability to make target of these nuclei. An electron-RI collider system, which requires a huge accelerator complex, has so far been unique solution to overcome the difficulty. We have developed a novel internal target system named SCRIT (Self-Confining RI Ion Target) in an electron storage ring to make the experiment easier with much compact experimental system.

2. Major Research Subjects

Development of the SCRIT technology and electron scattering for unstable nuclei.

3. Summary of Research Activity

Development of a novel internal target of unstable nuclei (SCRIT) in an electron storage ring for electron scattering experiment.
(Wakasugi, Ohnishi, Ichikawa, Kurita, Suda, Tamae, Adachi, Wang, Hori, Hara)
We have finished the installation of a SCRIT device into the SR2 in last year. Test experiment of SCRIT electron scattering using stable Cs isotope has been performed, and it was found that collision luminosity between electron beam and target Cs ions trapped in the SCRIT device exceeds 10^{27} /(cm^{2}s) at the electron beam current of 200 mA. An RI ion source and an ISOL system has been constructed and they have been tested using stable Xe isotopes. Overall extraction efficiency was found to be 21 % and mass resolution (M/ΔM) of ISOL system was achieved to be 1660. We plan to start RI production at the ISOL system in 2012.

Team Leader
Masanori WAKASUGI

Special Postdoctoral Researcher
Tetsuya OHNISHI

Research Consultant
Shin-ichi ICHIKAWA
Masahiro HARA
Toshitada HORI

Visiting Scientists
Toshimi SUDA (Research Center of Electron Photon Science, Tohoku Univ.)
Tadaaki TAMAE (Research Center of Electron Photon Science, Tohoku Univ.)
Kazuyoshi KURITA (Inst. Phys., Rikkyo Univ.)
Tatsuya ADACHI (Research Center of Electron Photon Science, Tohoku Univ.)
Shuo WANG (Research Center of Electron Photon Science, Tohoku Univ.)

RIBF Research Division
Research Instruments Group

1. Abstract

The research instruments group is the driving force at RI Beam Factory (RIBF) for continuous enhancement of activities and competitiveness of experimental research. Consisting of five teams, we are in charge of the design, construction, operation and improvement of the core research instruments at RIBF, such as BigRIPS separator, ZeroDegree spectrometer, GARIS spectrometer and SAMURAI spectrometer, and the related infrastructure and equipments. The group also conducts related experimental research as well as R&D studies on the research instruments.

2. Major Research Subjects

Design, construction, operation and improvement of the core research instruments at RIBF and related R&D studies. Experimental studies on exotic nuclei.

3. Summary of Research Activity

The current research subjects are summarized as follows:

(1) Design, construction, operation, and improvement of the core research instruments at RIBF and their related infrastructure and equipments for continuous enhancement of activities and competitiveness of experimental research
(2) R&D studies on technical issues of the core research instruments and related equipments at RIBF
(3) Experimental research on exotic nuclei using the core research instruments at RIBF

Group Director
Toshiyuki KUBO

Senior Visiting Scientist
Toshio KOBAYASHI (Tohoku University)

RIBF Research Division
Research Instruments Group
GARIS Team

1. Abstract

Development and maintenance of devices related to the study of superheavy elements

2. Major Research Subjects

(1) Maintenance and development of a recoil separator and related devices
(2) Development of rapid chemistry devices

3. Summary of Research Activity

(1) Maintenance and development of recoil separator

A gas-filled recoil separator has been used as the main experimental device for the study of superheavy elements. We will develop and maintain the related devices. We will also offer user support if a researcher wishes to use the devices for his/her own research program.

(2) Development of devices for fast chemistry

We research and develop devices for fast chemistry of superheavy elements. We also offer user support to potential users.

Team Leader
Kouji MORIMOTO

Nishina Center Research Scientist
Daiya KAJI

Nishina Center Technical Scientist
Akira YONEDA

RIBF Research Division
Research Instruments Group
BigRIPS Team

1. Abstract

This team is in charge of design, construction, development and operation of BigRIPS in-flight separator and its related research instruments at RI beam factory (RIBF). They are employed not only for the production of RI beams but also the experimental studies using RI beams.

2. Major Research Subjects

Design, construction, development and operation of BigRIPS in-flight separator, RI-beam transport lines, and their related research instruments

3. Summary of Research Activity

This team is in charge of design, construction, development and operation of BigRIPS in-flight separator, RI-beam transport lines, and their related research instruments such as ZeroDegree spectrometer at RI beam factory (RIBF). They are employed not only for the production of RI beams but also various kinds of experimental studies using RI beams.

The research subjects may be summarized as follows:

(1) General studies on RI-beam production using in-flight scheme.
(2) Studies on ion-optics of in-flight separators, including particle identification of RI beams
(3) Simulation and optimization of RI-beam production.
(4) Development of beam-line detectors and their data acquisition system.
(5) Experimental studies on production reactions and unstable nuclei.
(6) Experimental studies of the limits of nuclear binding.
(7) Development of superconducting magnets and their helium cryogenic systems.
(8) Development of a high-power production target system.
(9) Development of a high-power beam dump system.
(10) Development of a remote maintenance and remote handling systems.
(11) Operation, maintenance and improvement of BigRIPS separator system, RI-beam transport lines, and their related research instruments such as ZeroDegree spectrometer and so on.
(12) Experimental research using RI beams.

Team Leader

Koichi YOSHIDA

Members

Naohito INABE
Masao OHTAKE
Yoshiyuki YANAGISAWA

Contract Researchers

Kensuke KUSAKA
Naoki FUKUDA
Hiroyuki TAKEDA

Research Associates

Daisuke KAMEDA
Kanenobu TANAKA
Hiroshi SUZUKI

Part-time Staff

Hidekazu KUMAGAI

Visiting Scientist

Bradley SHERRILL (NSCL, Michigan State Univ., USA)
Daniel BAZIN (NSCL, Michigan State Univ., USA)
Anthony NETTLETON (NSCL, Michigan State Univ., USA)
Laura BANDURA (NSCL, Michigan State Univ., USA)
Oleg TARASOV (NSCL, Michigan State Univ., USA)
David MORRISSEY (NSCL, Michigan State Univ., USA)
Hans GEISSEL (GSI, Germany)
Martin WINKLER (GSI, Germany)
Michael FAMIANO (Western Michigan Univ., USA)
Jerry NOLEN (Argonne National Lab., USA)
Shashikant MANIKONDA (Argonne National Lab., USA)
Yutaka MIZOI (Osaka Electro-Commnication Univ.)
Kazuo IEKI (Rikkyo Univ.)
Naohito IWASA (Tohoku Univ.)
Sadao MOMOTA (Kochi University of Technology)
Le Hong KHIEM (IOP, Vietnamese Academy for Science and Technology)
Viet Cuong PHAN (IOP, Vietnamese Academy for Science and Technology)

Students

Student Trainees

Daichi MURAI (Rikkyo Univ.)
Taku YAMADA (Tohoku Univ.)
Ayuko CHIBA (Tohoku Univ.)
Yohei OKODA (Tohoku Univ.)

RIBF Research Division
Research Instruments Group
SAMURAI Team

1. Abstract

In collaboration with research groups in and outside RIKEN, the team designs, develops and constructs the SAMURAI spectrometer and relevant equipment that are and will be used for reaction experiments using RI beams at RI Beam Factory. SAMURAI consists of a large superconducting dipole magnet and a variety of detectors to measure charged particles and neutrons. Based on the outcome from the commissioning experiment in March 2012, the team prepares for first experiments with SAMURAI planned in the year 2012. The team also provides basis for research activities by, for example, organizing workshops and forming a "collaboration" platform among researchers interested in studies with SAMURAI.

2. Major Research Subjects

Design, development and construction of the SAMURAI spectrometer and its related research instruments. Help and management for SAMURAI-based research programs.

3. Summary of Research Activity

The current research activities are summarized as follows:

(1) Operation, maintenance and improvement of a large superconducting dipole magnet that will be the main component of the SAMURAI spectrometer.
(2) Design, development and construction of various detectors that are used for nuclear reaction experiments at SAMURAI.
(3) Preparation for starting experiments using SAMURAI planned in 2012.
(4) Formation of a collaboration platform called “SAMURAI collaboration”.

Team Leader
Tohru MOTOBAYASHI

Members
Hiromi SATO
Ken-ichiro YONEDA
Yohei SIMIZU

Senior Visiting Scientist
Toshio KOBAYASHI (Tohoku University)

Visiting Scientist
Nobuyuki CHIGA (Tohoku University)
Piotr BEDNARCZYK (IFJ PAN, Krakow, Poland)

RIBF Research Division
Research Instruments Group
Computing and Network Team

1. Abstract

This team is in charge of development, management and operation of the computing and network environment, mail and information servers and data acquisition system and management of the information security of the RIKEN Nishina Center.

2. Major Research Subjects

(1) Development, management and operation of the general computing servers
(2) Development, management and operation of the mail and information servers
(3) Development, management and operation of the data acquisition system
(4) Development, management and operation of the network environment
(5) Management of the information security

3. Summary of Research Activity

This team is in charge of development, management and operation of the computing and network environment, mail and information servers and data acquisition system and management of the information security. The details are described elsewhere in this progress report.

(1) Development, management and operation of the general computing servers

We are operating Linux/Unix NIS/NFS cluster system for the data analysis of the experiments and general computing. This cluster system consists of eight computing servers with 28 CPU cores and totally 40 TB RAID of highly-reliable Fibre-channel HDD. Approximately 500 user accounts are registered on this cluster system. We are planning to replace the data analyses servers and RAID file systems for the experimental data in the spring of 2012. Details are described elsewhere in this volume. We are adopting the latest version of the Scientific Linux (X86_64) as the primary operating system, which is widely used in the accelerator research facilities, nuclear physics and high-energy physics communities in the world.

(2) Development, management and operation of the mail and information servers

We are operating RIBF.RIKEN.JP server as a mail/NFS/NIS server. This server is a core server of RIBF Linux/Unix cluster system. We have replaced this server and RAID file systems in the summer of 2011. This Postfix is used for mail transport software and dovecot is used for imap and pop mail services. These software packages enable secure and reliable mail delivery. Sophos Email Security and Control (PMX) installed on the mail front-end servers tags spam mails and isolates virus-infected mails. The probability to identify the spam is approximately 95-99%.We are operating several information servers such as WWW servers, Wiki servers, Groupware servers, Windows-Media and Quick-Time streaming servers, and an anonymous FTP server (FTP.RIKEN.JP).

(3) Development, management and operation of the data acquisition system

We are developing a data-acquisition system for the RIBF. This system has functions of network-distributed data processing, hierarchical event building and parallel readout. To get better readout speed, we have developed the tiny VME readout system based on FPGA. It can achieve the best readout speed of the VME bus. In collaboration with CEA Saclay and GANIL, the development of the multi-detector data-base system is in progress. This system merges data taken by different DAQ systems based on the time stamp.

(4) Development, management and operation of the network environment

We have been managing the network environment collaborating with Advanced Center for Computing and Communications (ACCC). All the Ethernet ports of the information wall sockets are capable of the Gigabit Ethernet connection (10/100/1000BT). Many wireless LAN access points have been installed to cover the almost entire area of Nishina Center including the radiation control area.

(5) Management of the information security

It is essential to take proper information security measures for information assets.
We are managing the information security of Nishina Center collaborating with ACCC.

Team Leader

Takashi ICHIHARA

Member

Yasushi WATANABE
Hidetada BABA

RIBF Research Division
Research Instruments Group
Detector Team

1. Abstract

This team is in charge of development, fabrication, and operation of various detector for nuclear physics experiment in RIKEN Nishina center. Also the team organizes collaboration work for detector technology among related research groups in order to improve mutual share of knowledge and experience.

2. Major Research Subjects

(1) Development of the detector with high position resolution and high counting rate
(2) Development of high dynamic range preamplifier for silicon strip detector
(3) Development of time projection chamber
(4) Construction of silicon pixel detector.
(5) Search for extra dimensions by measuring short-range gravity
(6) Radiation detector for education

3. Summary of Research Activity

(1) Development of the detector with high position resolution and high counting rate
RIBF experiment must have high rate capability to explore low cross section events. We would like to develop such detector by using MICROMEGAS or GEM technology. RIKEN and Tokyo Met. Indust. Res. Institute was collaborated for low cross talk pad readout. We designed it and fabricated the trial readout pad and compared with simulation results. Various type MICROMEGAS sensors was built and tested.

(2) Development of high dynamic range preamplifier
Coulomb break up experiment at RIBF needs high dynamic range silicon strip detector in order to identify the charged particle from proton to Sn. We have two solutions for analog amplifiers. One is dual gain preamplifier and other is square root response amplifier. Dual hybrid preamplifiers of application specific integrated circuit has been designed and fabricated by collaboration with KEK. It was confirmed having expected dynamic range on first trial. Second turn of design was fabricated and tested. The design for connection to readout electronics was proceed with collaboration with Washington University and Texas A&M.

(3) Development of time projection chamber
A time projection chamber will be used for SAMURAI spectrometer. RIKEN, Kyoto and MSU are building TPC.
For the electronics development, we designed the timing monitor board and fabricated.

(4) Development of silicon pixel detector.
RIKEN, Rikkyo, KEK, and JAEA group is responsible for the pixel ladder fabrications for the RHIC PHENIX detector upgrade. The ladder is a module which is composed of pixel sensor modules, support frame, and readout bus. We completed the fabrication of ladders and installed them into the PHENIX apparatus in December 2010 and started commissioning with stripixel detector part. We confirmed the tracking resolutions are good enough to identify the heavy quark productions.
Due to differences in CTE between the pixel stave and the silicone encapsulant, thermal cycling promoted the breaking of wire bonds during 2011 operation. They are under repairing.

(5) Search for extra dimensions by measuring short-range gravity
Short range gravity force is measured by using torsion pendulum. If the gravity force is deviated from the inverse square law, it will be the indication of the new physics. We are measuring the movement of the torsion pendulum by using CCD with online fashion analysis tools.

(6) Radiation detector for education
After Fukushima reactor accident, people are so worried about the radiation. The detector team has collaboration with University professors and high school teaches, for developing an educational system for knowledge of radiation. We concluded it is necessary to have radiation detector assemble kit with reasonable price. Our team started the kit development.

Team Leader
Atsushi TAKETANI

Visiting Scientist
Meiko UESAKA (Rikkyo University)
Kohei FUJIWARA (Tokyo Metropolitan Industrial Tehcnology Research Institute)

Research Consultant
Hiroyuki MURAKAMI

Students
Junior Research Associate
Kazufumi NINOMIYA
Hiroyuki MIYA

Student Trainees
Akira TAKUMA (Fac. of Sci., Rikkyo Univ.)
Yuijyun KAWAMO (Fac. of Sci., Rikkyo Univ.)
Kyousule URANO (Fac. of Sci., Rikkyo Univ.)
Tatsuya TAKAHASHI (Fac. of Sci., Rikkyo Univ.)
Syuhei YOSHIDA (Fac. of Sci., Rikkyo Univ.)
Yuki KAMATA (Fac. of Sci., Rikkyo Univ.)
Ryusuke SAITO (Fac. of Sci., Rikkyo Univ.)

RIBF Research Division
Accelerator Applications Research Group

1. Abstract

Accelerator Applications Research Group promotes various applications of ion beams from RI Beam Factory. Radiation Biology Team studies biological effects of fast heavy ions and develops heavy-ion breeding. RI Applications Team studies production and application of radioisotopes and develops new technologies of accelerator mass spectrometry for the trace-element analyses. Details of these activities are described by each team elsewhere. The group has also collaborated with research groups in and outside RIKEN in research and applications of heavy-ion irradiation effects on materials.

2. Major Research Subjects

Research and development in biology, chemistry and materials science utilizing heavy-ion beams from RI Beam Factory.

3. Summary of Research Activity

(1) Biological effects of fast heavy ions.
(2) Development of heavy-ion breeding.
(3) Production and application of radioisotopes.
(4) Developments of trace elements analyses.

Group Director
Tomoko ABE

Secretary
Yoshiko SAKATA

RIBF Research Division
Accelerator Applications Research Group
Radiation Biology Team

1. Abstract

The radiation biology team conducts studies of various biological effects of fast heavy ions. It is also involved in the development of a new technique for breeding plants by heavy-ion irradiation. Fast heavy ions can cause dense, localized ionization of matter along their tracks, in contrast to photons (e.g., X-rays and g-rays), which cause randomly distributed isolated ionization. The localized, dense ionization can cause double-strand DNA breaks in cells induced by; these breaks are not easily repaired, and they are more effective at inducing mutations than single-strand DNA breaks. A unique feature of our experimental facility at the RIKEN Ring Cyclotron (RRC) is that living bodies in helps them the atmosphere or bottles can be irradiated because the delivered heavy-ion beams have sufficiently high energy to penetrate matter to a significant depth. The radiation biology team uses a dedicated beam line (E5B) of the RRC to irradiate microbes, plants, and animals with a wide variety of ion beams, ranging from C to Fe. The research subjects include physiological studies of DNA repair, genome analyses of mutation, and mutation breeding of plants by heavy-ion irradiation. Some new cultivars have already been introduced to the market.

2. Major Research Subjects

(1) Biological effects of heavy-ion irradiation
(2) Ion-beam breeding and genome analysis
(3) Innovative applications of heavy-ion beams

3. Summary of Research Activity

The radiation biology team focuses on the biological effects of fast heavy ions from the RRC by using 135 MeV/u C, N, and Ne ions, 95 MeV/u Ar ions, and 90 MeV/u Fe ions. It is also involved in the development of a breeding technique for microbes and plants. The main topics covered are as follows:

(1) Biological effects of heavy-ion irradiation

A uniform dose distribution is the key to systematic studies and thus to improvement of the mutation efficiency. Therefore, plants and microbes are treated using ions with a stable linear energy transfer (LET). The deletion size appears to depend on the LET: Almost 90% of deletions are less than 53 bp in *Arabidopsis* when using C ions (22.5~30 keV/μm). This type of irradiation is suitable for examining breeding and reverse genetics systems in conjunction with single-nucleotide polymorphism detection systems, for example, targeting induced local lesions in genomes. Among the deletions, the proportion of large deletions (>100 bp) was about 54% for Ar-ion irradiation and about 64% for C-ion irradiation. Heavy-ion beams of 290 keV/μm are efficient inducers of large deletions.

(2) Ion-beam breeding and genome analysis

An LET of 30 keV/μm with C and N ions is the most effective for inducing mutations in *Arabidopsis*. In rice, the highest number of mutations is observed with C and Ne ions in the LET range of 61 to 74 keV/μm. Thus, the LET of the ion beam is an important factor affecting mutagenesis. Many types of mutations that produce variegated, dwarf, early- or late-flowering, high-yielding, and salt-tolerant phenotypes are found in M_2 plants. Over the last decade, molecular biology has made great advances through technological innovation. We use high-throughput DNA sequencing techniques such as next-generation sequencing instruments and microarray technologies to analyze gene mutations. Mutants have become more and more useful and important in modern genetic studies, enabling the discovery of genes that control important traits, and revealing the functions and mechanisms underlying their operations. The discovery of genes using mutants may lead to the emergence of a new field in biology, 'mutagenomics'.

(3) Innovative applications of heavy-ion beams

An international heavy-ion breeding research consortium has been organized, with 156 national user groups and 15 international institutes in 2011. The consortium includes agricultural experimental stations, universities, and seed and horticulture companies. The radiation biology team irradiated about 1500 different samples for a total beam time of 45 hours in one year. The advantages of heavy-ion mutagenesis include, a low dose with high survival rates, induction of high mutation rates, and a wide range of variation. The ion beam used often changes only a single characteristic. Thus, a new variety can be obtained by selecting a mutant that exhibits modification to a target trait while retaining the existing valuable traits. This approach has been particularly successful in flower breeding. The consortium has introduced 20 new cultivars of plants and 2 of microbes to the market in Japan, the USA, Canada, and the EU since 2001. The development period for these new varieties was only three years.

Team Leader
Tomoko ABE

Members
Masako IZUMI
Teruyo TSUKADA

Special Postdoctoral Researcher
Yusuke KAZAMA

Technical Staff I
Yoriko HAYASHI
Sachiko KOGURE

Technical Staff II
Sumie OHBU

Part-time Staffs
Wataru AONUMA
Yuko HAYASHI
Koutaro ISHII
Yuki SHIRAKAWA
Hideo TOKAIRIN
Taeko WAKANA

Visiting Scientists
Ryutaro AIDA (Natl. Inst. Floricult. Sci.)
Mari AMINO (Tokai University Hospital)
Chang-Hyu BAE (Sunchon Natl. Univ., Korea)
Hiroyuki DAIMON (Osaka Pref. Univ.)
Ali FERJANI (Tokyo Gakugei Univ.)
Makoto FUJIWARA (Grad. Sch., Col. Arts Sci., Univ. of Tokyo)
Eitaro FUKATSU (Forest tree beeding Cet.)
Yoshiya FURUSAWA (Natl. Inst. Radiol. Sci.)
Toshinari GODO (Botanic Gardens Toyama)
Misako HAMATANI (Hiroshima City Agric. Forest. Promot. Cen.)
Yasuhide HARA (Kanagawa Inst. Agric. Sci.)
Masanori HATASHITA (Wakasa Wan Energy Res. Cen.)
Atsushi HIGASHITANI (Grad. Sch. Life Sci., Tohoku Univ.)
Ryoichi HIRAYAMA (Natl. Inst. Radiol. Sci.)
Akiko HOKURA (Tokyo Denki Univ.)
Ichiro HONDA (Natl. Agric. Res. Cen.)
Mitsugu HORITA (Hokuren Agri. Res. Inst.)
Hiroyuki ICHIDA (Meiji Univ.)
Yuji ITO (Natl. Agric. Res. Cen., Hokkaido Region)
Akihiro IWASE (Grad. Sch. Engin., Osaka Pref. Univ.)
Hiroshi KAGAMI (Shizuoka Citrus Exp. Station)
Tetsuya KAKO (Suntory Flowers, Ltd.)

Takeshi KANAYA (Suntory Flowers, Ltd.)
Si-Yong KANG (Dep. Rad. Plant Breed. Genet., KAERI, Korea)
Tomojirou KOIDE (Riken Vitamin Co., Ltd.)
Tsutomu KUBOYAMA (Ibaraki Univ.)
Norihiko MISHIMA (Fukuda Denshi Co., Ltd.)
Yutaka MIYAZAWA (Grad. Sch. Life Sci., Tohoku Univ.)
Kazumitsu MIYOSHI (Fac. Bioresour. Sci., Akita Pref. Univ.)
Toshikazu MORISHITA (Inst. Rad. Breeding, Natl. Inst. Agric. Res.)
Koji MURAI (Fukui Pref. Univ.)
Francesco MUSUMECI (Catania Univ.)
Daisuke NAKADA (Ela Medical Japan Co., Ltd.)
Koichiro NISHIKAWA (FLORSAIKA CIA. LTDA.)
Norihiro OHTSUBO (Natl. Inst. Floricult. Sci.)
Tomo OOMIYA (Hokkaido Ornamental Plants Veg. Res. Cen.)
Kenji OSAWA (Nagano Agric. Res. Cen.)
Masaya SAKAI (Fukuda Denshi Co., Ltd.)
Kouichi SAKAMOTO (YUKIGUNI AGURI Co., Ltd.)
Tadashi SATO (Grad. Sch. Life Sci., Tohoku Univ.)
Yoichi SATO (Riken Food Co., Ltd.)
Mikio SHIMADA (Kyoto Univ.)
Fumio SUGAWARA (Tokyo Univ. of Sci.)
Masao SUGIYAMA (Hokko Chem. Ind. Co., Ltd.)
Keita SUGIYAMA (Nat. Inst. Veg.Tea Sci.)
Ryuji SUGIYAMA (Ajinomoto, Co., INC.)
Kazunori SUZUKI (Plant Biotech. Inst. Ibaraki Agric. Cen.)
Masao SUZUKI (Natl. Inst. Radiol. Sci.)
Kenichi SUZUKI (Suntory Flowers, Ltd.)
Kunio SUZUKI (Technoflora, Co., Ltd.)
Hinako TAKEHISA (Natl. Inst. Agric. Sci.)
Sachie TANAKA (Tokai Univ.)
Teruhiko TERAKAWA (Hokko Chem. Ind. Co., Ltd.)
Ken TOKUHARA (Dogashima Orchid Cen.)
Masanori TOMITA (CRIEPI)
Hisashi TSUJIMOTO (Fac. Agri., Tottori Univ.)
Kozo TSUKADA (Nippon Veterinary and Life-sci. Univ.)
Makoto UBUKATA (Hokkaido Univ.)
Masao WATANABE (Fac. Agri., Tohoku Univ.)
Takuji YOSHIDA (Takii Seed Co., Ltd.)
Yasuko YOSHIHARA(Japan Atomic Energy Agency)
Koichiro YOSHIOKA (Tokai University Hospital)

Research Fellows

Hideki ASAUMI (Ehime Agricultural Experiment Station)
Masataka CHAYA (Nagasaki Agr. Forest. Exp. Station)
Fumiko HIDAKA (Kagoshima Pref. Inst. for Agric. Dev.)
Shunsuke IMANISHI (Natl. Inst.Veg. and Tea Sci.)
Hiroaki KISAKA (Ajinomoto, Co., INC.)
Yuri KURUMATANI (Chiba Pref. Agr. Res. Cent.)

Chikara KUWATA (Chiba Pref. Agr. Res. Cent.)
Tadanori MINO (Wadomari Cho Agr. Exp. Station)
Miyuki NISHI (Saga Agricultural Experiment Station)
Kyousuke NIWA (Hyogo Pref. Res. Inst.)
Tadahito OOTUBO (Wadomari Cho Agr. Exp. Station)
Eikou OOYABU (Saga Pref. Agr. Res. Cen.)
Takenori SAITO (Shizuoka Tea Exp. Station)
Yoshihide SAKITA (Wadomari Cho Agr. Exp. Station)
Tsukasa SHIRAO (Kagoshima Biotechnology Inst.)
Keiichi TAKAGI (Wakasa-wan Energy Research Center)
Kei-ichiro UENO (Kagoshima Biotechnology Inst.)
Naoji WAKITA (Wadomari Cho Agr. Exp. Station)

Consultant
Hiroyuki SAITO

Students
Junior Research Associate
Liqiu MA (Grad. Sch. Sci. & Engin., Saitama Univ.)

Student trainees
Hiroki HANASHIMA (Tokyo Denki Univ.)
Fumihiro MASUYAMA (Tokyo Denki Univ.)
Takuma NAGANO (Tokyo Denki Univ.)
Naoko ODA (Fac. Sci., Tokyo Univ. of Sci.)
Tetsuya OKABE (Fac. Sci., Tokyo Univ. of Sci.)
Hiroki TAOKA (Fac. Sci., Tokyo Univ. of Sci.)

RIBF Research Division
Accelerator Applications Research Group
RI Applications Team

1. Abstract

The RI Applications Team develops production technologies for radioisotopes (RIs) at the RIKEN RI Beam Factory (RIBF) for application studies in physics, chemistry, biology, medicine, and pharmaceutical and environmental sciences. Purified RIs such as ^{65}Zn and ^{109}Cd are delivered to universities and institutes for fee-based distribution through the Japan Radioisotope Association. Furthermore, we develop new mass spectrometry technologies for trace element analyses using accelerator technology and apply them to scientific research fields such as cosmochemistry, environmental science, and archaeology. We also develop chemical materials for electron cyclotron resonance (ECR) ion sources for acceleration of heavy ion such as ^{48}Ca, ^{70}Zn, and ^{238}U at the RIBF.

2. Major Research Subjects

(1) Research and development of RI production technology at the RIBF
(2) RI application research
(3) Development of trace element analysis using accelerator techniques and its application to geoscience and environmental science
(4) Research and development of chemical materials for ECR ion sources at the RIBF

3. Summary of Research Activity

(1) Research and development of RI production technology at the RIBF

Using heavy-ion accelerators at the RIBF, we are developing RI production technologies for application studies in physics, chemistry, biology, medicine, and pharmaceutical and environmental sciences. With proton and deuteron beams from the azimuthally varying field cyclotron (AVF), we produce about 20 long-lived radiotracers. Among them, ^{65}Zn, ^{109}Cd, and ^{88}Y are delivered to the Japan Radioisotope Association for fee-based distribution to the general public in Japan. Since 2007, we have accepted 56 orders for ^{65}Zn with a total activity of 319.5 MBq and 22 orders for ^{109}Cd with 154.0 MBq of activity. On the other hand, radionuclides of a large number of elements are simultaneously produced from metallic targets such as ^{nat}Ti, ^{nat}Ag, ^{nat}Hf, and ^{197}Au irradiated with a 135 MeV nucl.$^{-1}$ ^{14}N beam from the RIKEN Ring Cyclotron (RRC). This multitracer is also provided to universities and institutes for collaborative research.

(2) RI application research

The chemistry of newly discovered superheavy elements (SHEs, atomic numbers $Z \geq 104$) is an interesting and challenging research subject in nuclear and radiochemistry. We are developing SHE production systems as well as rapid chemistry apparatuses at the RIKEN Linear Accelerator (RILAC) and AVF. At the RILAC, a gas-jet transport system has been coupled to the gas-filled recoil ion separator (GARIS). We are developing a gas chromatograph apparatus directly coupled to the GARIS that enables in-situ complexation and gas chromatographic separation of a large variety of volatile SHE compounds. We have also installed a gas-jet-coupled SHE production system on the AVF beam line. Aqueous chemistry apparatuses for ion exchange and solvent extraction are under development together with automated rapid α particle and spontaneous fission detection systems. Using intense heavy-ion beams from the RILAC and AVF, SHEs such as ^{261}Rf, ^{262}Db, and ^{265}Sg are produced, and their chemical properties are investigated on a single-atom scale.

(3) Development of trace element analysis using accelerator techniques and its application to geoscience and environmental science

We developed two new mass spectrometry technologies for trace element analyses as an application of accelerator technology to various fields such as cosmochemistry, environmental science, and archaeology. One is a new type of accelerator mass spectrometry at the RILAC equipped with an ECR ion source. This system is available for measuring trace elements (10^{-14}–10^{-15} level) and is expected to be especially effective for measurements of low-electron-affinity elements such as ^{26}Al, ^{41}Ca, and ^{53}Mn. As a preliminary study, the ECR ion source system was evaluated and the basic data were obtained for the detection and quantitative analysis of trace nuclides in archaeological samples (cinnabar) and functional metals. We attempted to develop another technology by customizing a mass spectrometer equipped with a stand-alone ECR ion source for analyses of elemental and isotopic abundances. In 2011, we examined the Mo isotope measurements of metal samples using sputtering methods. Furthermore, we equipped a mini-ECR ion source with Q-type mass spectrometry so that trace analyses of chemical warfare agents can be applied on site.

(4) Research and development of chemical materials for ECR ion sources at the RIBF

We prepared CaO, TiO_2, ZnO, and metallic U for ECR ion sources at the RIBF for acceleration of ^{48}Ca, ^{50}Ti, ^{70}Zn, and ^{238}U ions, respectively, in collaboration with Ion Source Team at the RIKEN Nishina Center.

Team Leader
Hiromitsu HABA

Members
Kazuya TAKAHASHI
Jumpei KANAYA

Visiting Scientists
Hiroshi HIDAKA (Fac. Sci., Hiroshima Univ.)
Hidetoshi KIKUNAGA (Res. Center Elec. Photon Sci., Tohoku Univ.)
Tatsuo OKANO (Inst. Industrial Sci., Univ. Tokyo)
Hiroshi SHIMIZU (Fac. Sci., Hiroshima Univ.)
Miho TAKAHASHI (Tokyo Univ. Marine Sci. and Tech.)
Masayoshi TODA (Tokyo Univ. Marine Sci. and Tech.)
Tokuko WATANABE (Aoyama Gakuin Women's Junior College)
Shigekazu YONEDA (Natl. Sci. Museum)

Visiting Technicias
Ai OHTSUBO (Japan Radiation Association)
Yuichiro WAKITANI (Japan Radiation Association)
Shinichi YAMAMOTO (Japan Radiation Association)

RIBF Research Division
User Liaison and Industrial Cooperation Group

Abstract

The essential mission of the "User Liaison and Industrial Cooperation(ULIC) Group" is to maximize the research activities of RIBF by attracting users in various fields with a wide scope.

The ULIC Group consists of two teams.

The User Support Team provides various supports to visiting RIBF users through the User's Office. The Industrial Cooperation Team supports potential users in industries who use the beams for application purposes or for accelerator related technologies other than basic research. Production of various radioisotopes by the AVF cyclotron is also one of the important mission. The produced radioisotopes are distributed to researchers in Japan for a charge through the Japan Radioisotope Association.

Group Director

Hideyuki SAKAI

Deputy Group Director

Hideki UENO (User Support)

Members

Mieko KOGURE

Special Temporary Employee

Tadashi KAMBARA

Senior Visiting Scientists

Ikuko HAMAMOTO
Munetake ICHIMURA

Secretary

Yoshiko SAKATA
Tomoko IWANAMI
Emiko ISOGAI
Katsura IWAI

RIBF Research Division
User Liaison and Industrial Cooperation Group
User Support Office

1. Abstract

To enhance synergetic common use of the world-class accelerator facility, the Radioisotope Beam Factory (RIBF), it is necessary to promote a broad range of applications and to maximize the facility's importance. The facilitation and promotion of the RIBF are important missions charged to the team. Important operational activities of the team include: i) the organization of international Program Advisory Committee (PAC) meetings to review experimental proposals submitted by RIBF users, ii) RIBF beam-time operation management, and iii) promotion of facility use by hosting outside users through the RIBF Independent Users program, which is a new-user registration program begun in FY2010 at the RIKEN Nishina Center (RNC) to enhance the synergetic common use of the RIBF. The team opened the RIBF Users Office in the RIBF building in 2010, which is the main point of contact for Independent Users and provides a wide range of services and information.

2. Major Research Subjects

(1) Facilitation of the use of the RIBF
(2) Promotion of the RIBF to interested researchers

3. Summary of Research Activity

(1) Facilitation of the use of the RIBF

The RIBF Users Office, formed by the team in 2010, is a point of contact for user registration through the RIBF Independent User program. This activity includes:

- registration of users as RIBF Independent Users,
- registration of radiation workers at the RIKEN Wako Institute,
- provision of an RIBF User Card (a regular entry permit) and an optically stimulated luminescence dosimeter for each RIBF Independent User, and
- provision of safety training for new registrants regarding working around radiation, accelerator use at the RIBF facility, and information security, which must be completed before they begin RIBF research.

The RIBF Users Office is also a point of contact for users regarding RIBF beam-time-related paperwork, which includes:

- contact for beam-time scheduling and safety review of experiments by the In-House Safety Committee,
- preparation of annual Accelerator Progress Reports, and
- maintaining the above information in a beam-time record database.

In addition, the RIBF Users Office assists RIBF Independent Users with matters related to their visit, such as invitation procedures, visa applications, and the reservation of on-campus accommodation.

(2) Promotion of the RIBF to interested researchers

- The team has organized an international PAC for RIBF experiments; it consists of leading scientists worldwide and reviews proposals in the field of nuclear physics (NP) purely on the basis of their scientific merit and feasibility. The team also assists another PAC meeting for material and life sciences (ML) organized by the RNC Advanced Meson Laboratory. The NP and ML PAC meetings are organized twice a year.
- The team coordinates beam times for PAC-approved experiments and other development activities. It manages the operating schedule of the RIBF accelerator complex according to the decisions arrived at by the RIBF Machine Time Committee.
- To promote research activities at RIBF, proposals for User Liaison and Industrial Cooperation Group symposia/mini-workshops are solicited broadly both inside and outside of the RNC. The RIBF Users Office assists in the related paperwork.
- The team is the point of contact for the RIBF users' association. It arranges meetings at RNC headquarters for the RIBF User Executive Committee of the users' association.
- The Team conducts publicity activities, such as arranging for RIBF tours, development and improvement of the RNC official web site, and delivery of RNC news via email and the web.

Team Leader
Hideki UENO

Vice Team Leader
Yasushi WATANABE

Technical Staff I
Narumasa MIYAUCHI

RIBF Research Division
User Liaison and Industrial Cooperation Group
Industrial Cooperation Team

1. Abstract

The scope of the industrial cooperation team includes industrial application of RIBF facility and research and development for industrial application of accelerator associated technologies.

2. Major Subjects

Distribution of radioisotopes Zn-65, Cd-109 and Y-88 produced at RIKEN AVF Cyclotron and investigation of novel industrial applications of the accelerator beam and its related technologies

3. Summary of Research Activity

(1) Fee-based distribution of radioisotopes
At RIBF, various specific radioisotopes for research have been produced with the cyclotrons and used for research projects. This team handles fee-based distribution of radioisotopes Zn-65, Y-88 and Cd-109, which are produced by the RI application team at the AVF cyclotron, to non-affiliated users under a Material Transfer Agreement between Japan Radioisotope Association and RIKEN. In 2011, total amount of 62MBq of Zn-65 and 41MBq of Cd-109 were distributed. In addition, we started distribution of Y-88 in February 2010.
(2) Industrial application of RIBF
This team manages and supports the non-academic applications of heavy ion and RI beams at the RIBF facility. Until 2010, three private companies utilized the heavy-ion and RI beams. A development of a wear analysis technique using RI-beam, a heavy-ion irradiation test for semi-conductors of space use was carried out.

Team Leader
Atsushi YOSHIDA

Members
Aiko NAKAO
Hiroshige TAKEICHI

Visiting Scientists
Shuhei TATEMICHI (Fuji Electric Systems)
Masanori INOUE (Fuji Electric Systems)

RIBF Research Division
Safety Management Group

1. Abstract
The RIKEN Nishina Center for Accelerator-Based Science possesses one of the largest accelerator facilities in the world, which consists of two heavy-ion linear accelerators and five cyclotrons. This is the only site in Japan where uranium ions are accelerated. The center also has electron accelerators of microtron and synchrotron storage ring. Our function is to keep the radiation level in and around the facility below the allowable limit and to keep the exposure of workers as low as reasonably achievable. We are also involved in the safety management of the Radioisotope Center, where many types of experiments are performed with sealed and unsealed radioisotopes.

2. Major Research Subjects
（１） Safety management at radiation facilities of Nishina Center for Accelerator-Based Science
（２） Safety management at Radioisotope Center
（３） Radiation shielding design and development of accelerator safety systems

3. Summary of Research Activity
Our most important task is to keep the personnel exposure as low as reasonably achievable and to prevent accidents. Therefore, we patrol the facility daily; measure the ambient dose rates; maintain the survey meters, shield doors, and exhaust air and wastewater facilities; replenish the protective supplies; and manage radioactive waste. We also provide advice, supervision, and assistance for major accelerator maintenance work.
The radiation safety interlock system of the RIBF building has been extended in conjunction with the constructions of new experimental facilities; the last alteration was done for the SAMURAI and EURICA detectors early in 2012. To contribute to the restoration of eastern Japan after contamination by the accident at the Fukushima nuclear power plant, we measured many soil samples and air filters sent by Fukushima prefecture and measured gamma rays with a portable Ge detector in situ.

Head
Yoshitomo UWAMINO

Members
Hisao SAKAMOTO
Rieko HIGURASHI HIRUNUMA

Technical Staff I
Atsuko AKASHIO

Assistant
Tomomi OKAYASU

Contract Officer
Satoshi HASHIGUCHI
Hiroyuki FUKUDA
Hiroki MUKAI

Special Temporary Employee
Shin FUJITA

Temporary Employee
Masaharu OKANO

Visiting Scientists

Takashi NAKAMURA
Koji OHISHI
Noriaki NAKAO

Secretary

Tsutomu YAMAKI
Kazushiro NAKANO
Hiroko AISO
Kimie IGARASHI
Satomi IIZUKA

Center for Nuclear Study, Graduate School of Science, University of Tokyo.

1. Abstract

The Center for Nuclear Study (CNS) aims to elucidate the nature of nuclear system by producing the characteristic states where the Isospin, Spin and Quark degrees of freedom play central roles. These researches in CNS lead to the understanding of the matter based on common natures of many-body systems in various phases. We also aim at elucidating the explosion phenomena and the evolution of the universe by the direct measurements simulating nuclear reactions in the universe. In order to advance the nuclear science with heavy-ion reactions, we develop AVF upgrade, CRIB and SHARAQ facilities in the large-scale accelerators laboratories RIBF. We promote collaboration programs at RIBF as well as RHIC-PHENIX and ALICE-LHC with scientists in the world, and host international meetings and conferences. We also provide educational opportunities to young scientists in the heavy-ion science through the graduate course as a member of the department of physics in the University of Tokyo and through hosting the international summer school.

2. Major Research Subjects

(1) Accelerator Physics
(2) Nuclear Astrophysics
(3) Nuclear spectroscopy of exotic nuclei
(4) Quark physics
(5) Nuclear Theory
(6) SHARAQ project
(7) Active Target Development

3. Summary of Research Activity

(1) Accelerator Physics

One of the Major tasks of the accelerator group is the AVF upgrade project that includes development of ion sources, upgrading the AVF cyclotron of RIKEN and the beam line to CRIB. Development of ECR heavy ion sources is to provide a new HI beams, higher and stable beams of metallic ions, and to improve the control system. Two CNS ECR sources now provide all the beams for the AVF cyclotron and support not only CRIB experiments but also a large number of RIBF experiments. Three major developments were performed for upgrading the AVF cyclotron. The first is a design study of the central region of the cyclotron with harmonic number of 1. The second is installation of a new central module to increase the beam energy up to K78. The third is installation of a new beam deflector monitor to improve the transmission efficiency. Injection beam monitoring and control are being studied. New ion-source beam diagnosis and monitoring system (ISDM) was designed. This new beam monitor will become a powerful tool for all the RIBF facility.

(2) Nuclear Astrophysics

The nuclear astrophysics group studies relevant astrophysical reactions and special nuclear structures using a low-energy RI beam separator, CRIB. CRIB is good at producing low-mass, low-energy, and proton-rich RI beams with good intensities. Using proton-rich beams, we study stellar thermonuclear reaction processes at high temperatures, such as hot p-p chain, hot CNO cycle, rp-process, and α*p*-process.

One of the major interests is on (α,*p*) reactions. Recently, ^{30}S(α,*p*) and ^{22}Mg(α,*p*) reactions were directly measured using an active target with GEM (GEM-MSTPC). They are particularly important reactions in the nucleosynthesis in X-ray bursters. Several measurements of proton resonant scattering were recently performed on ^{21}Na, ^{26}Si, and ^{22}Na, to study resonances in the compound nuclei. The information of the resonances is important for the evaluation of possible enhancements of (*p*,γ) and (*p*,α) reaction rates. Developments of new beams have also been carried out, and ^{16}N and ^{22}Na beams became available. An improvement project of the Wien filter by redesigning insulators for the high voltages is on going.

(3) Nuclear structure of exotic nuclei

The NUSPEQ (NUclear SPectroscopy for Extreme Quantum system) group studies exotic structures in high-isospin and/or high-spin states in nuclei. The CNS GRAPE (Gamma-Ray detector Array with Position and Energy sensitivity) is a major apparatus for high-resolution in-beam gamma-ray spectroscopy. Missing mass spectroscopy using the SHARAQ is going to start as another approach on exotic nuclei. In 2011, the following progress has been made.

Analysis of α inelastic scattering data from nuclei in the island of inversion, which was taken by using GRAPE, has progressed. Experiments of searching new isomers by using ^{238}U and ^{124}Xe primary beams from SRC were performed and the analysis of the obtained data is in progress.

A plunger system for recoil distance method was developed for the approved experiments of the lifetime measurements of neutron-rich fp-shell nuclei. The readout system of 12 detectors of the CNS GRAPE was upgraded, where digital pulse data taken by sampling ADCs are analyzed by FPGAs on boards.

Experimental setup of studying tetra neutron system using the double-charge exchange reaction $^{4}He(^{8}He,^{8}Be)4n$ at 200 A MeV was prepared for the measurement in April 2012.

(4) Quark Physics

Main goal of the quark physics group is to understand the properties of hot and dense nuclear matter created by colliding heavy nuclei at relativistic energies. The group has been involved in the PHENIX experiment at Relativistic Heavy Ion Collider (RHIC) at Brookhaven National Laboratory, and the ALICE experiment at Large Hadron Collider (LHC) at CERN.

As for PHENIX, the group has been concentrating on the physics analysis involving leptons and photons; direct photon production at low transverse momentum using the virtual-gamma method, J/ψ production in ultra-peripheral Au+Au collisions, and electron measurement from semi-leptonic decay of heavy flavor mesons which uses the Si VTX detector subsystem.

As for ALICE, the group has involved in the data analyses, which include production of multi-strangeness baryons in p+p collisions, multi-particle correlation in Pb+Pb collisions, nuclear modification of energetic neutral pions in Pb+Pb collisions, and measurement of low-mass lepton pairs. The group has also been playing a leading role in the development of forward calorimeter for future upgrade.

R&D of gas electron multiplier (GEM) and related techniques has been continuing. Development of resistive GEM with resistive anodes and GEM with glass insulator have been progressing in collaboration with the Tamagawa group of RIKEN.

(5) Nuclear Theory

The nuclear theory group has been promoting the RIKEN-CNS collaboration project on large-scale nuclear structure calculations since 2001 and maintaining its parallel computing cluster. Based on this experience and its achievements, we participated in activities of HPCI Strategic Programs for Innovative Research (SPIRE) Field 5 “The origin of matter and the universe” in 2011. The SPIRE project aims at an integral understanding of the origin and structure of matter and the Universe utilizing the K computer, which is the world's fastest supercomputer in 2011.

In the SPIRE project, we are in charge of the elucidation of nuclear properties using ultra large-scale simulations of quantum many-body systems and its applications. In order to perform large-scale shell-model calculations, we developed an efficient computer program of the Monte Carlo Shell Model (MCSM) method for massive parallel computation, and performed benchmark calculations at the K computer. We plan a production run at the K computer in 2012 and later. In parallel, we studied the effective interaction of medium-heavy nuclei which is essential for the large-scale shell-model calculations.

(6) SHARAQ project

The SHARAQ group promoted the (p,n) charge exchange reaction measurement in the unstable nucleus ^{12}Be, a search for the four neutron system by using the exothermic double charge exchange reaction ($^{8}He,2^{8}He$),and a (polp,2p)/(polp,pn) reaction measurement in unstable oxygen isotopes $^{14,22,24}O$ with a polarized proton target.

For these experiments, we developed the achromatic ion optics of High-resolution beamline, named high-resolution achromatic mode. This mode has a momentum tagging focus with $\Delta p/p = 1/7500$ at BigRIPS F6, and the momentum acceptance is ±1%.

We have been developing detectors with high efficiency, high resolution and high detection rate to adopt upcoming experiments with High-resolution beamline and SHARAQ spectrometer. A plastic scintillator array for low-energy neutrons was constructed for the (p,n) reaction measurement with inverse kinematics, was successfully operated in the $^{12}Be(p,n)$ experiment. The scheme of pulse processing and data acquisition at final focal plane of SHARAQ spectrometer was upgraded for two particle detection in the ($^{8}He,2^{4}He$) reaction. For a development of the diamond detector, we performed an irradiation test with a 32-MeV alpha beam, and achieved the time resolution of 30 ps for light particles.

(7) Active Target Development

The aim of the active target project is to utilize the missing-mass spectroscopy in inverse kinematics by developing the active targets. We have developed two types of active targets for high-energy (100-300MeV/u) beam experiments, where β+-type Gamow-Teller transition and inelastic scattering are studied, and for low-energy (a few MeV/u) beam experiments, where the (α,p) reactions are studied from the viewpoint of astrophysical interest.

The active target for high-energy beam is under developed and the test experiment using 250-MeV/u ^{56}Fe beam was performed at HIMAC. The active target was operated with 1-atm deuterium gas and a stack of three GEMs for the first time and successfully measured the recoiled particles from reaction. We first plan to measure the inelastic scattering on the

unstable nuclei using this active target.
The other active target for low-energy beam was used for some experiments to study the (α,p) reactions on 18Ne, 22Mg, and 30S at CRIB, which is relevant to the r-process nucleosynthesis. In the experiment the active target was operated with 0.2-atm He+CO_2 and two (or three) layers of thick GEM, and was very stable in whole period of each experiment which was more than 1 week. We plan to measure the decay of 16N after upgrading of the active target, in which the gating grid operation will be adopted.

Director

Takaharu OTSUKA

Scientific Staff

Susumu SHIMOURA (Professor)
Shigeru KUBONO (Professor)
Hideki HAMAGAKI (Associate Professor)
Noritak SHIMIZU (Project Associate Professor)
Eiji IDEGUCHI (Lecturer)
Hidetoshi YAMAGUCHI (Research Associate)
Shin'ichiro MICHIMASA (Research Associate)
Taku GUNJI (Research Associate)
Shinsuke OTA (Research Associate)

Guest Scientists

Toshinori MITSUMOTO (Guest Associate Professor, Sumitomo Heavy Industries, Ltd.)
Toshio SUZUKI (Guest Professor, Nihon Univ.)

Technical Staff

Norio YAMAZAKI
Yukimitsu OHSHIRO

Techinical Assistants

Shin-ichi WATANABE
Hiroshi KUREI
Hideaki NINOMIYA
Akira YOSHINO
Shoichi YAMAKA

Project Research Associates

Hisayuki TORII
Koshiroh TUKIYAMA
Takahumi DOI (Apr.-Dec., 2011)
Takashi ABE

Post Doctoral Associates

Toru YOSHIDA
Hideaki MATSUBARA
Masanori DOZONO (-30. Apr. 2011, JSPS fellow)
Yorito YAMAGUCHI
Yoshiko SASAMOTO
Shunpei NOJI

Shuichiro EBATA (Apr. 1, 2011-)

Graduate Students

Satoshi SANO
Seiya HAYAKAWA (-27 Oct., 2011)
David. M KAHL
Akihisa TAKAHARA
Hiroyuki MIYA
Ryoji AKIMOTO
Yasuto HORI
Hiroshi TOKIEDA
Tomoya TSUJI
Shintaro GO
Shoichiro KAWASE
ShinIchi HAYASHI
KeiIchi KISAMORI
Motonobu TAKAKI
Atsushi NUKARIYA
Yosuke KIKUCHI
Tang T. LEUNG
Yuko SEKIGUCHI
Toshihiko FUJII
Rin YOKOYAMA
Yuki KUBOTA
CheongSoo LEE

Administration Staff

Midori HIRANO
Ikuko YAMAMOTO
Takako ENDO
Yukino KISHI
Toshiko ITAGAKI
Yuko SOMA

Radioactive nuclear beam R&D group, IPNS (Institute for Particle and Nuclear Studies), KEK (High Energy Accelerator Research Organization)

1. Abstract

We have been constructing the KEK Isotope Separation System (KISS) at RIKEN to investigate the β-decay properties of neutron-rich nuclei with neutron numbers of N = 126 relevant to the r-process of heavy element nucleosynthesis in cosmos. The main components of the KISS have been installed in FY 2011, and its off-line test is under progress.

2. Major Research Subjects

(1) Radioactive isotope beam production and manipulation for nuclear experiments.
(2) Explosive nucleosyhnthesis (rp- and r-process).
(3) Heavy ion reaction mechanism for producing heavy neutron-rich nuclei.
(4) Single particle states of neutron-rich nuclei by isobaric analog resonances.

3. Summary of Research Activity

Several nuclei around A ≈ 200 with N = 126 and nearby nuclei can be produced through the multi-nucleon transfer (MNT) reaction using a stable ^{136}Xe beam on ^{198}Pt target from RIKEN Ring Cyclotron (RRC). The MNT reactions are considered as a promising tool for producing heavy neuron rich nuclei, especially below ^{208}Pb in the nuclear chart. The cross section measurement to estimate the yields of those nuclei was performed using VAMOS spectrometer at GANIL. The analysis is under progress.

The KISS would separate a single species of radioactive nuclei among target like fragments (TLF) produced via MNT by using a gas catcher cell combined with a laser induced resonant ionization and a mass separator, and allows us to study the β-decay properties of the nuclei of rare reaction channels. The installation of main components such as the gas cell, the laser system and the mass separator were completed. At the first off-line test, the neutral Ni atoms evaporated in the gas cell were ionized by the resonant ionization. They were successfully extracted as an ion beam and mass-analyzed by the mass separator installed downstream of the gas cell. More detailed performance test (off-line test experiments) of the KISS is under progress. The commissioning of the KISS by injecting energetic beams from RRC will be performed in FY2012. (Related to the subjects (1)-(3)).

For direct measurements of the reaction cross section of ^{44}Ti(α, p)^{47}V, which is one of key reactions to evaluate ^{44}Ti yield in supernova nucleosynthesis, we proposed an experiment and the ^{44}Ti beam development at CRIB will be performed next year. (Related to the subjects (1) and (2))

For investigating the nature of the single particle states of light neutron rich-nuclei around N=20, we performed an experiment using the beam of ^{34}Si from RIPS. In the experiment, neutron single-particle states in the neutron-rich nucleus ^{35}Si, which is located beside the N=20 shell breaking nucleus ^{32}Mg, were investigated through their isobaric analog resonances (IARs). The excitation function for ^{34}Si+p elastic scattering was measured around 0° in the laboratory frame by the thick target inverse kinematics (TTIK) method with a ^{34}Si beam around 5 MeV/nucleon and a thick polyethylene target. Eight resonances were successfully observed. Angular momenta and proton and total widths of the resonances were assigned using R-matrix analysis. With the help of information of the β decay study, six isobaric analog resonances were identified. Spectroscopic factors and spin-parities of the corresponding parent states in ^{35}Si were also deduced. The present work demonstrates that the proton resonance elastic scattering with TTIK method for IARs can be used as a powerful tool for studying neutron single-particle states in neutron-rich nuclei. (Related to the subject (4))

Group Leader

Sunchan JEONG
Hiroshi MIYATAKE

Members

Yutaka WATANABE
Yoshikazu HIRAYAMA
Nobuaki IMAI
Michihiro OYAIZU
Hironobu ISHIYAMA

TORIJIN (Todai-RIKEN Joint International Program for Nuclear Physics)

1. Abstract

University of Tokyo and RIKEN have agreed to corporate with each other in the field of nuclear physics and have established Todai-RIKEN Joint International Program for Nuclear Physics (TORIJIN) in June 2006. The aim of this organization is to promote the international collaborations, such as JUSTIPEN (Japan-US Theory Institute for Physics with Exotic Nuclei). JUSTIPEN was launched in June 2006 in order to facilitate collaborations between U.S. and Japanese scientists whose main research thrust is in the area of the physics of exotic nuclei.

2. Main activities

Promote the international collaborations of both theoretical and experimental nuclear physicists under JUSTIPEN.

3. Summary of Research Activity

Under the JUSTIPEN program, 12 nuclear scientists in the U.S. have visited Japan in this fiscal year (Apr. 2011-Mar. 2012). Theoretical Nuclear Physics Laboratory and User Liaison and Industrial Cooperation Group were mainly responsible for the US visitors' accommodation and other arrangements. Under this project, a number of collaborations have been established. We also organized a joint workshop at Oak Ridge National Laboratory in March 2011, and will have the next joint meeting in October-November, 2012 in Oak Ridge. The JUSTIPEN sent US scientists to the international long-term workshop "Dynamics and correlations in exotic nuclei" held at Yukawa Institute in Sep-Oct, 2011, recognizing it as one of US-Japan collaboration activities. Many US scientists attended the workshop and we had fruitful discussions. In addition, the 10^{th} CNS international summer school was organized in August, 2011, for which we invited eight lecturers, three of them from abroad.

Chair

Takaharu OTSUKA (University of Tokyo)

Vice chair

Hiroyoshi SAKURAI (University of Tokyo/RIKEN)

Steering board members

Susumu SHIMOURA (University of Tokyo)
Takashi NAKATSUKASA (RIKEN)
Tohru MOTOBAYASHI (RIKEN)

Events from April 2011 to March 2012

2011	Apr. 1	Quantum Hadron Physics Laboratory and Spin isospin Laboratory, new research Labratorys launched at RNC
	Apr. 12	"Newcomers of Nishina Center 2011" Apr. 12
	Apr. 23	RIKEN Wako Institute's Open House
	Apr. 27	The memorandum of understanding (MOU) among RIKEN and Indonesian universities (Bandung Institute of Technology, Surabaya Institute of Technology and Padjadjaran University) has been renewed
	May 9	A joint press release was held by Tokyo University of Science and RIKEN on the measurement of the energy levels of the excited states of Zr isotopes and the discovery of the deformation magic number 64
	May 26-28	The Nishina Center Advisory Committee (NCAC 2011)
	Jun. 21	17th Meeting of the Management Steering Committee
	Jun. 24-25	The 9th Program Advisory Committee for Nuclear Physics experiments at RI Beam Factory
	Jul. 1	Astro-Glaciology Research Unit, a new research unit launched at RNC
	Aug. 5	Scientific Policy Committee
	Sep. 5-6	The 8th Program Advisory Committee for Materials and Life Science Experiments at RIKEN Nishina Center
	Sep. 26-Oct.01	The 10th CNS Summer School (CNSSS11)
	Oct. 1	RBRC Computing Group established
	Oct. 4-14	Peking University-Nishina School
	Oct. 18	KEK isotope separator system (KISS) joint research" between IPNS(KEK) and RNC(RIKEN)
	Dec. 9-10	The 10th Program Advisory Committee for Nuclear Physics experiments at RI Beam Factory
2012	Feb. 29	Interim Review of Superheavy Element Laboratory
	Mar. 28	Euroball-RIKEN Cluster Array (EURICA) Project unveiled
	Mar. 31	The Foyer of the RIBF bldg. "CYCLOPEDIA" was completed

Awards from April 2011 to March 2012

Awardee & Laboratory	Tetsuya Ohnishi (Research Instruments Group)
Name of award	The Commendation for Science and Technology by the Minister of Education, Culture, Sports, Science and Technology The Young Scientists' Prize
Sponsoring organization	Ministry of Education, Culture, Sports, Science and Technology (MEXT)
Date of award	Apr. 20, 2011

Awardee & Laboratory	Yasushige Yano (RBRC)
Name of award	Gersh Budker Prize
Sponsoring organization	European Physical Society Accelerator Group
Date of award	Sep. 8, 2011

Awardee & Laboratory	Ryouhei Morita (Ion Beam Breeding Laboratory) Yoriko Hayashi, Sachiko Kogure, Hideo Tokairin, Tomoko Abe, Tadashi Sato, Hinako Takehisa (Radiation Biology Team)
Name of award	Outstanding Presentation Award
Sponsoring organization	Japanese Society of Breeding
Date of award	Oct. 24, 2011

Awardee & Laboratory	Yasuyuki Akiba (Radiation Laboratory/RIKEN BNL Research Center)
Name of award	Nishina Memorial Prize 2011
Sponsoring organization	Nishina Memorial Foundation
Date of award	Dec. 6, 2011

Awardee & Laboratory	Atsuko Akashio, Rieko Higurashi, Yoshitomo Uwamino (Safety Management Group)
Name of award	Good Poster Presentation Award
Sponsoring organization	Japan Radioisotope Association
Date of award	Nov. 1, 2011

Awardee & Laboratory	Syunsuke Imanishi (Accelerator Applications Research Group Radiation Biology Team)
Laboratory	Accelerator Applications Research Group Radiation Biology Team
Name of award	Young Investigator Award in the Strategic Promotion Program for Basic Nuclear Research
Sponsoring organization	Japan Science and Technology Agency
Date of award	Feb. 6, 2012

Awardee & Laboratory	Hiroki Okuno (Accelerator Group, Accelerator R&D Team and Cryogenic Technology Team), Nobuhisa Fukunishi (Accelerator Group, Beam Dynamics & Diagnostics Team), Jun-ichi Ohnishi (Accelerator R&D Team), Naruhiko Sakamoto (Cyclotron Team)
Name of award	The Suwa Award for 2011
Sponsoring organization	Foundation for High Energy Accerelator Science
Date of award	Feb. 20, 2012

Awardee & Laboratory	Satoshi Katsuta (High-Energy Astrophysics Laboratory)
Name of award	The 4th Space Science Encouragement Prize
Sponsoring organization	Society for Promotion of Space Science
Date of award	Mar. 6, 2012

Awardee & Laboratory	Nobuo Hinohara (Theoretical Nuclear Physics Laboratory)
Name of award	The Young Scientist Award
Sponsoring organization	The Physical Society of Japan
Date of award	Mar. 24, 2012

Awardee & Laboratory	Noriyoshi Ishii (Radiation Laboratory)
	Tetsuo Hatsuda, Shinya Aoki (Quantum Hadron Physics Laboratory)
Name of award	Award for Academic Papers on Physics
Sponsoring organization	The Physical Society of Japan
Date of award	Mar. 24, 2012

VII. LIST OF PUBLICATIONS
& PRESENTATIONS

RIKEN Nishina Center for Accelerator-Based Science

Publications

[Journal]

(Original Papers) *Subject to Peer Review

Afanasiev S., Akiba Y., Aoki K., Asai J., Bathe S., Boyle K., Deshpande A., Enyo H., Fukao Y., Goto Y., Hachiya T., Ichihara T., Ishihara M., Miyachi Y., Nakagawa I., Shibata T., Shoji K., Taketani A., Tanida K., Torii H., Watanabe Y., Yokkaichi S., Okada K., Saito N., and PHENIX C.: "Photoproduction of J/ψ and of high mass e^+e^- in ultra-peripheral Au+Au collisions at $\sqrt{s_{NN}}$ = 200 GeV", Phys. Lett. B **679**, No. 4, pp. 321–329 (2009). *

Adare A., Akiba Y., Aoki K., Asai J., Bathe S., Boyle K., Deshpande A., Enyo H., Fukao Y., Goto Y., Hachiya T., Ichihara T., Ichimiya R., Ikeda Y., Ishihara M., Mao Y., Nakagawa I., Nakano K., Ralf S., Shibata T., Shoji K., Taketani A., Tanida K., Torii H., Watanabe Y., Yokkaichi S., Kurosawa M., Okada K., Saito N., and PHENIX C.: "Photon-hadron jet correlations in $p + p$ and $Au + Au$ collisions at $\sqrt{s_{NN}}$ = 200 GeV", Phys. Rev. C **80**, 024908-1–024908-14 (2009). *

Afanasiev S., Akiba Y., Aoki K., Bathe S., Boyle K., Deshpande A., Enyo H., Fukao Y., Goto Y., Hachiya T., Ichihara T., Ishihara M., Shibata T., Shoji K., Taketani A., Tanida K., Torii H., Watanabe Y., Yokkaichi S., Okada K., Saito N., and PHENIX C.: "Systematic studies of elliptic flow measurements in Au+Au collisions at $\sqrt{s_{NN}}$ = 200 GeV", Phys. Rev. C **80**, 024909-1–024909-25 (2009). *

Afanasiev S., Akiba Y., Aoki K., Bathe S., Boyle K., Deshpande A., Enyo H., Fukao Y., Goto Y., Hachiya T., Ichihara T., Ishihara M., Shibata T., Shoji K., Taketani A., Tanida K., Torii H., Watanabe Y., Yokkaichi S., Okada K., Saito N., and PHENIX C.: "High-pT π^0 production with respect to the reaction plane in $Au + Au$ collisions at $\sqrt{s_{NN}}$ = 200 GeV", Phys. Rev. C **80**, 054907-1–054907-29 (2009). *

Adare A., Akiba Y., Aoki K., Asai J., Bathe S., Boyle K., Deshpande A., Enyo H., Fukao Y., Goto Y., Ichihara T., Ichimiya R., Ikeda Y., Ishihara M., Mao Y., Nakagawa I., Nakano K., Ralf S., Shibata T., Shoji K., Taketani A., Tanida K., Torii H., Watanabe Y., Yokkaichi S., Kurosawa M., Okada K., Saito N., and PHENIX C.: "Gluon-spin contribution to the proton spin from the double-helicity asymmetry in inclusive π^0 production in polarized $p+p$ collisions at $\sqrt{s}$ = 200 GeV", Phys. Rev. Lett. **103**, 012003-1–012003-6 (2009). *

Adare A., Akiba Y., Aoki K., Asai J., Bathe S., Boyle K., Deshpande A., Enyo H., Fukao Y., Goto Y., Hachiya T., Ichihara T., Ichimiya R., Ikeda Y., Ishihara M., Mao Y., Nakagawa I., Nakano K., Ralf S., Shibata T., Shoji K., Taketani A., Tanida K., Torii H., Watanabe Y., Yokkaichi S., Kurosawa M., Okada K., Saito N., and PHENIX C.: "Measurement of bottom versus charm as a function of transverse momentum with electron-hadron correlations in $p + p$ collisions at $\sqrt{s}$ = 200 GeV", Phys. Rev. Lett. **103**, 082002-1–082002-7 (2009). *

Afanasiev S., Akiba Y., Aoki K., Bathe S., Boyle K., Deshpande A., Enyo H., Fukao Y., Goto Y., Hachiya T., Ichihara T., Ishihara M., Shibata T., Shoji K., Taketani A., Tanida K., Torii H., Watanabe Y., Yokkaichi S., Okada K., and PHENIX C.: "Charged kaon interferometric probes of space-time evolution in $Au + Au$ collisions at $\sqrt{s_{NN}}$ = 200 GeV", Phys. Rev. Lett. **103**, 142301-1–142301-6 (2009). *

Kuboki H., Okuno H., Hasebe H., Yokouchi S., Ryuto H., Fukunishi N., Kamigaito O., Kase M., Goto A., and Yano Y.: "Charge strippers for high intensity uranium beams in the RIKEN RI beam factory", Nucl. Instrum. Methods Phys. Res. A **613**, No. 3, pp. 436–438 (2010). *

Adare A., Akiba Y., Aoki K., Asai J., Bathe S., Boyle K., Deshpande A., Enyo H., Fukao Y., Goto Y., Hachiya T., Ichihara T., Ishihara M., Mao Y., Nakagawa I., Nakamura K., Nakano K., Ralf S., Shibata T., Shoji K., Taketani A., Tanida K., Torii H., Watanabe Y., Yokkaichi S., Okada K., Saito N., and PHENIX C.: "Detailed measurement of the e^+e^- pair continuum in $p+p$ and Au+Au collisions at $\sqrt{s_{NN}}$ = 200 GeV and implications for direct photon production", Phys. Rev. C **81**, No. 3, pp. 034911-1–034911-56 (2010). *

Adare A., Akiba Y., Aoki K., Asai J., Bathe S., Boyle K., Deshpande A., Enyo H., Fukao Y., Goto Y., Hachiya T., Ichihara T., Ichimiya R., Ikeda Y., Ishihara M., Mao Y., Nakagawa I., Nakano K., Ralf S., Shibata T., Shoji K., Taketani A., Tanida K., Torii H., Watanabe Y., Yokkaichi S., Kurosawa M., Okada K., Saito N., and PHENIX C.: "Transverse momentum dependence of η meson suppression in Au+Au collisions at $\sqrt{s_{NN}}$ = 200 GeV", Phys. Rev. C **82**, No. 1, pp. 011902-1–011902-7 (2010). *

Adare A., Akiba Y., Aoki K., Asai J., Bathe S., Boyle K., Deshpande A., Enyo H., Fukao Y., Goto Y., Hachiya T., Ichihara T., Ichimiya R., Ikeda Y., Ishihara M., Mao Y., Nakagawa I., Nakano K., Ralf S., Shibata T., Shoji K., Taketani A., Tanida K., Torii H., Watanabe Y., Yokkaichi S., Kurosawa M., Okada K., Saito N., and PHENIX C.: "Double-helicity dependence of jet properties from dihadrons in longitudinally polarized $p + p$ collisions at $\sqrt{s}$ = 200 GeV", Phys. Rev. D **81**, No. 1, pp. 012002-1–012002-11 (2010). *

Adare A., Akiba Y., Aoki K., Asai J., Bathe S., Boyle K., Deshpande A., Enyo H., Fukao Y., Goto Y., Ichihara T., Ichimiya R., Ikeda Y., Ishihara M., Mao Y., Nakagawa I., Nakano K., Ralf S., Shibata T., Shoji K., Taketani A., Tanida K., Torii H., Watanabe Y., Yokkaichi S., Kurosawa M., Okada K., Saito N., and PHENIX C.:

"Transverse momentum dependence of J/ψ polarization at midrapidity in $p+p$ collisions at $\sqrt{s}=200$ GeV", Phys. Rev. D **82**, No. 1, pp. 012001-1–012001-10 (2010). *

Adare A., Akiba Y., Aoki K., Asai J., Bathe S., Boyle K., Deshpande A., Enyo H., Fukao Y., Goto Y., Hachiya T., Ichihara T., Ichimiya R., Ikeda Y., Ishihara M., Mao Y., Nakagawa I., Nakano K., Ralf S., Shibata T., Shoji K., Taketani A., Tanida K., Torii H., Watanabe Y., Yokkaichi S., Kurosawa M., Okada K., Saito N., and PHENIX C.: "High p_T direct photon and π^0 triggered azimuthal jet correlations and measurement of k_T for isolated direct photons in $p+p$ collisions at $\sqrt{s}=200$ GeV", Phys. Rev. D **82**, No. 7, pp. 072001-1–072001-18 (2010). *

Adare A., Akiba Y., Aoki K., Asai J., Bathe S., Boyle K., Deshpande A., Enyo H., Fukao Y., Goto Y., Ichihara T., Ichimiya R., Ikeda Y., Ishihara M., Mao Y., Nakagawa I., Nakamura K., Nakano K., Ralf S., Shibata T., Shoji K., Taketani A., Tanida K., Torii H., Watanabe Y., Yokkaichi S., Kurosawa M., Okada K., Saito N., Nakamura T., and PHENIX C.: "Measurement of transverse single-spin asymmetries for J/ψ production in polarized $p+p$ collisions at $\sqrt{s}=200$ GeV", Phys. Rev. D **82**, No. 11, pp. 112008-1–112008-13 (2010). *

Adare A., Akiba Y., Aoki K., Asai J., Bathe S., Boyle K., Deshpande A., Enyo H., Fukao Y., Goto Y., Hachiya T., Ichihara T., Ishihara M., Mao Y., Nakagawa I., Nakano K., Ralf S., Shibata T., Shoji K., Taketani A., Tanida K., Torii H., Watanabe Y., Yokkaichi S., Okada K., Saito N., and PHENIX C.: "Enhanced Production of Direct Photons in Au+Au Collisions at $\sqrt{s_{NN}}=200$ GeV and Implications for the Initial Temperature", Phys. Rev. Lett. **104**, 132301-1–132301-6 (2010). *

Adare A., Akiba Y., Aoki K., Asai J., Bathe S., Boyle K., Deshpande A., Enyo H., Fukao Y., Goto Y., Hachiya T., Ichihara T., Ichimiya R., Ikeda Y., Ishihara M., Mao Y., Nakagawa I., Nakano K., Ralf S., Shibata T., Shoji K., Taketani A., Tanida K., Torii H., Watanabe Y., Yokkaichi S., Kurosawa M., Okada K., Saito N., and PHENIX C.: "Transition in Yield and Azimuthal Shape Modification in Dihadron Correlations in Relativistic Heavy Ion Collisions", Phys. Rev. Lett. **104**, 252301-1–252301-7 (2010). *

Adare A., Akiba Y., Aoki K., Bathe S., Boyle K., Deshpande A., Enyo H., Fukao Y., Goto Y., Hashimoto K., Ichihara T., Ichimiya R., Ikeda Y., Ishihara M., Mao Y., Nakagawa I., Nakano K., Ralf S., Shibata T., Shoji K., Taketani A., Tanida K., Torii H., Watanabe Y., Yokkaichi S., Kurosawa M., Okada K., Saito N., and PHENIX C.: "Elliptic and Hexadecapole Flow of Charged Hadrons in Au+Au Collisions at $\sqrt{s_{NN}}=200$ GeV", Phys. Rev. Lett. **105**, 062301-1–062301-6 (2010). *

Adare A., Akiba Y., Aoki K., Bathe S., Boyle K., Deshpande A., Enyo H., Fukao Y., Goto Y., Ichihara T., Ichimiya R., Ikeda Y., Ishihara M., Mao Y., Nakagawa I., Nakano K., Ralf S., Shibata T., Shoji K., Taketani A., Tanida K., Torii H., Watanabe Y., Yokkaichi S., Kurosawa M., Okada K., Saito N., and PHENIX C.: "Azimuthal Anisotropy of π^0 Production in Au+Au Collisions at $\sqrt{s_{NN}}=200$ GeV: Path-Length Dependence of Jet Quenching and the Role of Initial Geometry", Phys. Rev. Lett. **105**, 142301-1–142301-7 (2010). *

Kuboki H., Okuno H., Yokouchi S., Hasebe H., Kishida T., Fukunishi N., Kamigaito O., Goto A., Kase M., and Yano Y.: "Charge-state distribution measurements of ^{238}U and ^{136}Xe at 11 MeV/nucleon using gas charge stripper", Phys. Rev. Spec. Top.: Accel. Beams **13**, No. 9, pp. 093501-1–093501-9 (2010). *

Kuboki H., Okuno H., Yokouchi S., Hasebe H., Kishida T., Fukunishi N., Kamigaito O., Goto A., Kase M., and Yano Y.: "Charge-state distribution measurements using gas charge stripper toward ^{238}U and ^{136}Xe acceleration at RIKEN RIBF", Nucl. Instrum. Methods Phys. Res. A **655**, No. 1, pp. 17–20 (2011). *

Adare A., Akiba Y., Aoki K., Asai J., Bathe S., Boyle K., Deshpande A., Enyo H., Fukao Y., Goto Y., Hachiya T., Ichihara T., Ichimiya R., Ikeda Y., Ishihara M., Mao Y., Nakagawa I., Nakamura K., Nakano K., Ralf S., Shibata T., Shoji K., Taketani A., Tanida K., Torii H., Watanabe Y., Yokkaichi S., Kurosawa M., Okada K., Saito N., Nakamura T., and PHENIX C.: "Nuclear modification factors of ϕ mesons in d+Au, Cu+Cu, and Au+Au collisions at $\sqrt{s_{NN}}=200$ GeV", Phys. Rev. C **83**, No. 2, pp. 024909-1–024909-10 (2011). *

Adare A., Akiba Y., Aoki K., Asai J., Bathe S., Boyle K., Deshpande A., Enyo H., Fukao Y., Goto Y., Ichihara T., Ichimiya R., Ikeda Y., Ishihara M., Mao Y., Nakagawa I., Nakano K., Ralf S., Shibata T., Shoji K., Taketani A., Tanida K., Torii H., Watanabe Y., Yokkaichi S., Kurosawa M., Okada K., Saito N., and PHENIX C.: "Azimuthal correlations of electrons from heavy-flavor decay with hadrons in $p+p$ and Au+Au collisions at $\sqrt{s_{NN}}=200$ GeV", Phys. Rev. C **83**, No. 4, pp. 044912-1–044912-16 (2011). *

Adare A., Akiba Y., Aoki K., Asai J., Bathe S., Boyle K., Deshpande A., Enyo H., Fukao Y., Goto Y., Hachiya T., Hashimoto K., Ichihara T., Ichimiya R., Ikeda Y., Ishihara M., Mao Y., Miyachi Y., Nakagawa I., Nakamura K., Nakano K., Ralf S., Shibata T., Shoji K., Taketani A., Tanida K., Torii H., Watanabe Y., Yokkaichi S., Kurosawa M., Okada K., Saito N., and PHENIX C.: "Cross section and double helicity asymmetry for η mesons and their comparison to π^0 production in $p+p$ collisions at $\sqrt{s}=200$ GeV", Phys. Rev. D **83**, No. 3, pp. 032001-1–032001-11 (2011). *

Adare A., Akiba Y., Aoki K., Asai J., Bathe S., Boyle K., Deshpande A., Enyo H., Fukao Y., Goto Y., Hachiya T., Ichihara T., Ichimiya R., Ikeda Y., Ishihara M., Mao Y., Nakagawa I., Nakano K., Ralf S., Shibata T., Shoji K., Taketani A., Tanida K., Torii H., Watanabe Y., Yokkaichi S., Kurosawa M., Okada K., Saito N., and PHENIX C.: "Measurement of neutral mesons in $p+p$ collisions at $\sqrt{s}=200$ GeV and scaling properties of hadron production", Phys. Rev. D **83**, No. 5, pp. 052004-1–052004-26 (2011). ∗

Adare A., Akiba Y., Aoki K., Bathe S., Boyle K., Deshpande A., Enyo H., Fukao Y., Goto Y., Hashimoto K., Ichihara T., Ichimiya R., Ikeda Y., Ishihara M., Mao Y., Miyachi Y., Nakagawa I., Nakamura K., Nakano K., Ralf S., Shibata T., Shoji K., Taketani A., Tanida K., Torii H., Watanabe Y., Yokkaichi S., Kurosawa M., Okada K., Saito N., Nakamura T., and PHENIX C.: "Cross Section and Parity-Violating Spin Asymmetries of $W^{\pm}$ Boson Production in Polarized $p+p$ Collisions at $\sqrt{s}=500$ GeV", Phys. Rev. Lett. **106**, No. 6, pp. 062001-1–062001-6 (2011). ∗

Okuno H., Fukunishi N., Goto A., Hasebe H., Imao H., Kamigaito O., Kase M., Kuboki H., Yano Y., and Yokouchi S.: "Low-Z gas stripper as an alternative to carbon foils for the acceleration of high-power uranium beams", Phys. Rev. Spec. Top.: Accel. Beams **14**, No. 3, pp. 033503-1–033503-8 (2011). ∗

Kuboki H., Okuno H., Hasebe H., Yokouchi S., Fukunishi N., Higurashi Y., Ohnishi J., Nakagawa T., Imao H., Kamigaito O., Goto A., Kase M., and Yano Y.: "Charge-state distribution of ^{238}U in nitrogen gas and carbon foil at 14 and 15 MeV/nucleon", Phys. Rev. Spec. Top.: Accel. Beams **14**, No. 5, pp. 053502-1–053502-7 (2011). ∗

Oral Presentations

(International Conference etc.)

Imai N., Ong H., Aoi N., Sakurai H., Demichi K., Kawasaki H., Baba H., Dombradi Z., Elekes Z., Fukuda N., Fulop Z., Gelberg A., Gomi T., Hasegawa H., Ishikawa K., Iwasaki H., Kaneko E., Kanno S., Kishida T., Kondo Y., Kubo T., Kurita K., Michimasa S., Minemura T., Miura M., Motobayashi T., Nakamura T., Notani M., Onishi T., Saito A., Shimoura S., Sugimoto T., Suzuki M., Takeshita E., Takeuchi S., Tamaki M., Yamada K., Yoneda K., Watanabe H., and Ishihara M.: "Anomalously small B(E2) value of ^{16}C", International Nuclear Physics Conference (INPC2004), Goteborg, Sweden, June–July (2004).

Watanabe T., Sasaki Y., Kase M., Watanabe S., Ikeda T., Kawaguchi T., and Yano Y.: "Development of new HTS current sensor and HTS magnetic shields for HTS-SQUID beam current monitor", 8th European Conference on Applied Superconductivity (EUCAS '07), Brussels, Belgium, Sept. (2007).

Kuboki H., Okuno H., Hasebe H., Yokouchi S., Ryuto H., Fukunishi N., Kamigaito O., Kase M., Goto A., and Yano Y.: "Charge strippers for high intensity uranium beams in the RIKEN RI beam factory", 24th World Conference of the International Nuclear Target Development Society, (GANIL), Caen, France, Sept. (2008).

Watanabe T., Fukunishi N., Kase M., Sasaki Y., and Yano Y.: "Development of beam current monitor with HTS SQUID and HTS current sensor", 11th International Conference on HEAVY ION ACCELERATOR TECHNOLOGY (HIAT09), Venezia, Italy, June (2009).

Kuboki H., Okuno H., Hasebe H., Yokouchi S., Fukunishi N., Kamigaito O., Imao H., Goto A., Kase M., and Yano Y.: "Charge-state distribution measurements of ^{238}U using nitrogen gas and carbon foil charge strippers at 11, 14, and 15 MeV/nucleon", 25th World Conference of the International Nuclear Target Development Society, (TRIUMF), Vancouver, Canada, Sept. (2010).

Kuboki H., Okuno H., Hasebe H., Yokouchi S., Kishida T., Fukunishi N., Kamigaito O., Goto A., Kase M., and Yano Y.: "Charge-state distribution measurements using gas charge stripper toward ^{238}U and ^{136}Xe acceleration at RIKEN RIBF", 25th World Conference of the International Nuclear Target Development Society, (TRIUMF), Vancouver, Canada, Sept. (2010).

Enyo H.: "Nuclear Physics in Japan and RIKEN Nishina Center", French-Japanese Symposium on Nuclear Structure Problems, Wako, Jan. (2011).

Komatsu Y., Aoki K., Enyo H., Kanaya J., Kannno K., Masumoto S., Nakai W., Ozawa K., Sekimoto M., Takagi A., Watanabe Y., and Yokkaichi S.: "GEM spectrometer for J-PARC E16 experiment", 2nd international conference on micro pattern gaseous detectors (MPGD2011), (International organizing committee for MPGD2011), Kobe, Aug.–Sept. (2011).

Yamaguchi Y., Wakasugi M., Suzuki H., Fujinawa T., Uesaka T., Yano Y., Ozawa A., Nagae D., Yamaguchi T., Suzuki T., Kikuchi T., Jiang W., Sasaki T., and Tokuchi A.: "Present status of rare-RI ring project in RIKEN RI beam factory", 8th International Conference on Nuclear Physics at Storage Rings (STORI-11), (INFN-LNF), Frascati, Italy, Oct. (2011).

(Domestic Conference)

延與秀人: "理研 J-PARC 連携センター構想", 研究会「ハドロンホールの拡張によって展開する物理」, (高エネルギー加速器研究機構), つくば, 3 月 (2010).

Quantum Hadron Physics Laboratory

Publications

[Journal]

(Original Papers) *Subject to Peer Review

Aoki S., Ishikawa K., Ishizuka N., Izubuchi T., Kadoh D., Kanaya K., Kuramashi Y., Namekawa Y., Okawa M., Taniguchi Y., Ukawa A., Ukita N., Yamazaki T., and Yoshie T.: "Physical Point Simulation in 2 + 1 Flavor Lattice QCD", Phys. Rev. D **81**, No. 7, pp. 074503-1–074503-12 (2010). *

Kimura T., Komatsu S., Misumi T., Noumi T., Torii S., and Aoki S.: "Revisiting symmetries of lattice fermions via spin-flavor representation", J. High Energy Phys. **2012**, No. 01, pp. 048-1–048-20 (2012). *

Kamata S. and Suzuki H.: "Numerical simulation of the $\mathcal{N} = (2,2)$ Landau–Ginzburg model", Nucl. Phys. B **854**, No. 3, pp. 552–574 (2012). *

Aoyama T., Hayakawa M., Kinoshita T., and Nio M.: "Tenth-order QED lepton anomalous magnetic moment: Eighth-order vertices containing a second-order vacuum polarization", Phys. Rev. D **85**, No. 3, pp. 033007-1–033007-17 (2012). *

Oral Presentations

(Domestic Conference)

Endres M. G.: "Lattice Supersymmetry", Seminar, (KITP), 金沢, 1 月 (2011).

土井 琢身, HAL QCD C.: "Exploring three-nucleon forces in lattice QCD", 大規模計算による原子核研究の展開：核子多体系を中心に, (HPCI 戦略プログラム), 和光, 1 月 (2012).

Endres M. G.: "Monte Carlo Simulations for Unitary Fermions in a Box and in a Trap", Seminar, Kobe, 2 月 (2012).

土井琢身, 青木慎也, 初田哲男, 池田陽一, 井上貴史, 石井理修, 村野啓子, 根村英克, 佐々木健志: "Cutoff effects on Three-Nucleon Forces in Lattice QCD", 日本物理学会第 67 回年次大会, (日本物理学会), 西宮市, 3 月 (2012).

Theoretical Nuclear Physics Laboratory

Publications

[Journal]

(Original Papers) *Subject to Peer Review

Matsuo M. and Nakatsukasa T.: "Open problems in nuclear structure near drip lines", J. Phys. G **37**, No. 6, pp. 064017-1–064017-10 (2010). *

Hashimoto K., Iizuka N., and Nakatsukasa T.: "N-body nuclear forces at short distances in holographic QCD", Phys. Rev. D **81**, 106003-1–106003-5 (2010). *

Tanaka K., Yamaguchi T., Suzuki T., Ohtsubo T., Fukuda M., Nishimura D., Takechi M., Ogata K., Ozawa A., Izumikawa T., Aiba T., Aoi N., Baba H., Hashizume Y., Inafuku K., Iwasa N., Kobayashi K., Komuro M., Kondo Y., Kubo T., Matsuyama T., Michimasa S., Motobayashi T., Nakabayashi T., Nakazima S., Nakamura T., Sakurai H., Shinoda R., Shinohara M., Suzuki H., Takeshita E., Takeuchi S., Togano Y., Yamada K., Yasuno T., and Yhoshitake M.: "Observation of a large reaction cross-section in the drip-line nucleus ^{22}C", Phys. Rev. Lett. **104**, No. 6, pp. 062701-1–062701-4 (2010). *

Hinohara N., Sato K., Nakatsukasa T., and Matsuo M.: "Local QRPA vibrational and rotational inertial functions for large-amplitude quadrupole collective dynamics", Acta Phys. Pol. B **42**, 443–446 (2011). *

Nakatsukasa T., Avogadro P., Ebata S., Inakura T., and Yoshida K.: "Self-consistent description of nuclear photoabsorption cross-sections", Acta Phys. Pol. B **42**, 609–618 (2011). *

Nomura K., Otsuka T., Shimizu N., and Guo L.: "Derivation of IBM Hamiltonian for deformed nuclei", J. Phys.: Con. Ser. **267**, No. 1, pp. 012050-1–012050-6 (2011). *

Nakatsukasa T.: "Density functional approaches to atomic nuclei", J. Phys.: Con. Ser. **302**, 012050-1–012050-6 (2011). *

Ebata S., Nakatsukasa T., and Yabana K.: "Linear response calculation using the canonical-basis TDHFB with a schematic pairing functional", J. Phys.: Con. Ser. **312**, 092023-1–092023-6 (2011). *

Pinilla E. C., Baye D., Descouvemont P., Horiuchi W., and Suzuki Y.: "Tests of the discretized-continuum method in three-body dipole strengths", Nucl. Phys. A **865**, 43–56 (2011). *

Kosuke N., Takaharu O., Shimizu N., and Guo L.: "Microscopic formulation of the interacting boson model for rotational nuclei", Phys. Rev. C **83**, No. 4, pp. 041302-1–041302-5 (2011). *

Yoshida K. and Hinohara N.: "Shape changes and large-amplitude collective dynamics in neutron-rich Cr isotopes", Phys. Rev. C **83**, No. 6, pp. 061302-1–061302-5 (2011). *

Inakura T., Nakatsukasa T., and Yabana K.: "Emergence of pygmy dipole resonances: Magic numbers and neutron skins", Phys. Rev. C **84**, No. 2, pp. 021302-1–021302-4 (2011). *

Nguyen D. D.: "Shear-viscosity to entropy-density ratio from giant dipole resonances in hot nuclei", Phys. Rev. C **84**, No. 3, pp. 034309-1–034309-12 (2011). *

Nguyen H. Q. and Nguyen D. D.: "Pairing reentrance in hot rotating nuclei", Phys. Rev. C **84**, No. 5, pp. 054324-1–054324-8 (2011). *

Hinohara N., Sato K., Yoshida K., Nakatsukasa T., Matsuo M., and Matuyanagi K.: "Shape fluctuations in the ground and excited 0+ states of ^{30,32,34}Mg", Phys. Rev. C **84**, No. 6, pp. 061302-1–061302-5 (2011). *

Avogadro P. and Nakatsukasa T.: "Finite amplitude method for the quasi-particle-random-phase approximation", Phys. Rev. C **84**, 014314-1–014314-7 (2011). *

Waldecker S. J., Barbieri C., and Dickhoff W. H.: "Microscopic self-energy calculations and dispersive optical-model potentials", Phys. Rev. C **84**, 034616-1–034616-11 (2011). *

Stoitsov M., Kortelainen M., Nakatsukasa T., Losa C., and Nazarewicz W.: "Monopole strength function of deformed superfluid nuclei", Phys. Rev. C **84**, 041305-1–041305-5 (2011). *

Feldmeier H., Horiuchi W., Neff T., and Suzuki Y.: "Universality of short-range nucleon-nucleon correlations", Phys. Rev. C **84**, 054003-1–054003-13 (2011). *

Watanabe H., Yamakuchi K., Odahara A., Sumikama T., Nishimura S., Yoshinaga K., Li Z., Miyashita Y., Sato K., Prochniak L., Baba H., Berryman J. S., Blasi N., Bracco A., Camera F., Chiba J., Doornenbal P. C., Go S., Hashimoto T., Hayakawa S., Hinke C., Hinohara N., Ideguchi E., Isobe T., Ito Y., Jenkins D. G., Kawada Y., Kobayashi N., Kondo Y., Krucken R., Lorusso G., Nakano T., Nakatsukasa T., Kurata-Nishimura M., Ong H. J., Ota S., Podolyak Z., Sakurai H., Scheit H., Steiger K., Steppenbeck D., Sugimoto K., Tajiri K., Takano S., Takashima A., Teranishi T., Wakabayashi Y., Walker P. M., Wieland O., and Yamaguchi H.: "Development of axial asymmetry in the neutron-rich nucleus 110Mo", Physics Letter B **704**, 270–275 (2011). *

Iida K., Oyamatsu K., Sarhan B. A., and Kohama A.: "Proton-nucleus total reaction cross sections in the optical limit Glauber theory: subtle dependence on the equation of state of nuclear matter", Prog. Theor. Phys. **126**, No. 6, pp. 1091–1100 (2011). *

Iida K., Koide S., Kohama A., and Oyamatsu K.: "Proton inelastic diffraction by a black nucleus and the size of excited nuclei", Mod. Phys. Lett. A **27**, No. 3, pp. 1250020-1–1250020-9 (2012). *

Watanabe G. and Makela H.: "Dissipation-induced squeezing", Phys. Rev. A **85**, 023604-1–023604-6 (2012). *

Hinohara N., Li Z., Nakatsukasa T., Niksic T., and Vretenar D.: "Effect of time-odd mean fields on inertial parameters of the quadrupole collective Hamiltonian", Phys. Rev. C **85**, No. 2, pp. 024323-1–024323-14 (2012). ∗

(Others)

Horiuchi W., Suzuki Y., and Baye D.: "Strength function in continuum with a square integrable basis", Few Body Syst. **50**, 455–458 (2010).

Horiuchi W., Suzuki Y., and Sato T.: "Electro-weak responses of ^{4}He using realistic nuclear interactions", Proceedings of Science **NC10**, No. 150, pp. 1–5 (2010).

Kohama A., Iida K., and Oyamatsu K.: "Study of nuclear matter density distributions using hadronic probes", AIP Conf. Proc. **1355**, 115–118 (2011).

Hinohara N., Sato K., Yoshida K., Nakatsukasa T., and Matsuo M.: "Microscopic description of large-amplitude shape-mixing dynamics with local QRPA inertial functions", AIP Conf. Proc. **1355**, 200–205 (2011).

Horiuchi W., Suzuki Y., and Sato T.: "Electro-weak transitions of ^{4}He using realistic nuclear interactions", Int. J. Mod. Phys. E **20**, No. 4, pp. 781–784 (2011).

Taniguchi Y., Kimura M., Enyo Y., and Horiuchi H.: "Clustering correlations and triaxiality in sd-shell region", Int. J. Mod. Phys. E **20**, No. 4, pp. 1046–1049 (2011).

Sato K. and Hinohara N.: "Microscopic analysis of shape mixing in low-lying states of proton-rich nuclei in the Se-Kr region", J. Phys.: Con. Ser. **312**, No. 9, pp. 092054-1–092054-6 (2011).

Yoshida K., Hinohara N., and Nakatsukasa T.: "Skyrme energy-density functional approach to collective dynamics", J. Phys.: Con. Ser. **321**, No. 1, pp. 012017-1–012017-4 (2011).

Horiuchi W., Feldmeier H., Neff T., and Suzuki Y.: "Universality of short-range correlations in light nuclei", J. Phys.: Con. Ser. **321**, No. 1, pp. 012043-1–012043-4 (2011).

Sihver L., Lantz M. J., Takechi M., Kohama A., Ferrari A., Cerutti F., and Sato T.: "A comparison of total reaction cross section models used in particle and heavy ion transport codes", Adv. Space Res. **49**, 812–819 (2012).

[Book · Proceedings]

(Others)

Hinohara N., Sato K., Nakatsukasa T., and Matsuo M.: "Large-amplitude quadrupole collective dynamics in Se and Kr isotopes", Workshop on Hadron and Nuclear Physics 09 (HNP09), Suita, 2009–11, World Scientific, Singapore, pp. 331–339 (2010).

Oral Presentations

(International Conference etc.)

Ebata S., Nakatsukasa T., Inakura T., Hashimoto Y., and Yabana K.: "Linear Response Calculation using Canonical-basis TDHFB with a schematic pairing functional", ICHOR-EFES International Symposium on New Facet of Spin-Isospin Responses (SIR2010), (Department of Physics, School of Science, University of Tokyo), Hongo, Feb. (2010).

Ebata S., Nakatsukasa T., Inakura T., Hashimoto Y., and Yabana K.: "Linear Response Calculation using Canonical-basis TDHFB with a schematic pairing functional", The 10th International Symposium on Origin of Matter and Evolution of the Galaxies (OMEG10), (Research Center for Nuclear Physics, Osaka University), Ibaraki, Osaka, Mar. (2010).

Nakatsukasa T.: "Recent theoretical investigations on properties of low-energy dipole states", 1st Topical Workshop on Modern Aspects in Nuclear Structure: Advances in Nuclear Structure with arrays including new scintillator detectors, (University of Milano), Bormio, Italy, Feb. (2011).

Nakatsukasa T.: "Finite amplitude method for RPA and QRPA calculations", 5th LACM-EFES-JUSTIPEN Workshop, (Oak Ridge National Laboratory), Oak Ridge, USA, Mar. (2011).

Hinohara N.: "Large-amplitude shape dynamics around the island of inversion", 5th LACM-EFES-JUSTIPEN Workshop, (ORNL/UT, RIKEN, University of Tokyo, EFES), Oak Ridge, USA, Mar. (2011).

Kohama A.: "Systematic studies of nuclear reactions using EXFOR - from a viewpoint of a database user -", Workshop on Data Compilation of the Multinationally-maintained Experimental Nuclear Reaction Database (EXFOR), (IAEA), Vienna, Austria, Apr. (2011).

Nakatsukasa T.: "Systematic calculation of photo-response with the Skyrme functional", 3rd Workshop on Level Density and Gamma Strength, (Oslo University), Oslo, Norway, May (2011).

Nguyen D. D.: "Thermal pairing and nuclear thermodynamics", INT Special Seminar, (INT, University of Washington), Seattle, USA, May–May (2011).

Nguyen D. D.: "Thermal pairing and nuclear viscosity", Physics Colloquium of Department of Physics, College of Science, University of Idaho, (Department of Physics, University of Idaho), Moscow, USA, May–May (2011).

Ebata S., Nakatsukasa T., and Inakura T.: "Canonical-basis TDHFB calculation for E1 mode of heavy nuclei (A¿100)", ARIS 2011, (University of Leuven), Leuven, Belgium, May–June (2011).

Nakatsukasa T.: "Microscopic theory of large-amplitude collective motion", ARIS 2011, (University of Leuven), Leuven, Belgium, May–June (2011).

Inakura T., Nakatsukasa T., and Yabana K.: "Systematic claculation of E1 mode with Skyrme-RPA", ARIS 2011, (the universities of Leuven (K.U.Leuven) and Brussels (ULB)), Leuven, Belgium, May–June (2011).

Nakatsukasa T.: "Finite amplitude method for nuclear response function", Advances in Nuclear Many-Body Theory, (University of Zagreb), Primosten, Croatia, June (2011).

Hinohara N.: "Microscopic description of shape coexistence and shape transition", Advances in Nuclear Many-Body Theory, (University of Zagreb), Primosten, Croatia, June (2011).

Horiuchi W., Suzuki Y., and Arai K.: "Description of Nuclear reactions with realistic interactions using a square integrable basis", ETC Workshop on Continuum and correlations in light nuclei, (The European Center for Theoretical Studies in Nuclear Physics and Related Areas), Trento, Italy, June (2011).

Hinohara N.: "Large-amplitude deformation dynamics in low-lying states of magnesium isotopes around island of inversion", RIBF ULIC and CNS Symposium on Frontier of Gamma-ray Spectroscopy (Gamma11), Wako, June–July (2011).

Sato K., Hinohara N., Nakatsukasa T., Matsuo M., and Matuyanagi K.: "Microscopic analysis of development of deformation in neutron-rich Cr isotopes", RIBF ULIC and CNS Symposium on Frontier of Gamma-ray Spectroscopy (Gamma11), Wako, June–July (2011).

Inakura T., Nakatsukasa T., and Yabana K.: "Pygmy dipole resonance within fully self-consistent Skyrme-RPA", RIBF ULIC and CNS Symposium on Frontier of Gamma-ray Spectroscopy (Gamma11), Wako, June–July (2011).

Horiuchi W., Suzuki Y., and Koji A.: "Correlated basis approach to $A > 4$ systems", ECT Workshop on Not so few, but not too Many, (The European Center for Theoretical Studies in Nuclear Physics and Related Areas), Trento, Italy, July (2011).

Horiuchi W., Feldmeier H., Neff T., and Suzuki Y.: "Universality of short-range nucleon-nucleon correlations in nuclei", 5th Asia-Pacific Coneferene on Few-Body Problems in Physics 2011 (APFB2011), (Sungkyunkwan University), Seoul, Korea, Aug. (2011).

Nakatsukasa T.: "Single-particle and collective motions in nuclei", International Summer School on Subatomic Physics (ISSSP 2011), (Peking Universiyt), Beijing, China, Aug. (2011).

Sato K., Hinohara N., Nakatsukasa T., Matsuo M., and Matuyanagi K.: "Microscopic approach to large-amplitude deformation dynamics with local QRPA inertial masses", Rutherford Centennial Conference on Nuclear Physics 2011, (University of Manchester), Manchester, UK, Aug. (2011).

Ebata S., Nakatsukasa T., and Inakura T.: "Study of pygmy dipole resonance with a new time-dependent mean field theory", Rutherford Centennial Conference on Nuclear Physics 2011, (Institute of Physics Nuclear Physics Group), Manchester, UK, Aug. (2011).

Nakatsukasa T.: "Time-dependent mean-field approaches to nuclear response and reactio", INT workshop on Interfaces between structure and reactions for rare isotopes and nuclear astrophysics 2011, (INT), Seattle, USA, Aug.–Sept. (2011).

Nguyen D. D.: "Viscosity of hot nuclei", 19th International School on Nuclear Physics, Neutron Physics and Applications, (Institute for Nuclear Research and Nuclear Energy (Bulgarian Academy of Sciences) and Bulgarian Nuclear Regulatory Agency), Varna, Bulgaria, Sept. (2011).

Hinohara N.: "On the microscopic theory of large-amplitude collective motion", Restoring broken symmetries within the nuclear Energy Density Functional method, (CEA/SPhN), Saclay, France, Sept. (2011).

Hinohara N.: "Extraction of collective coordinates by means of adiabatic theory of large-amplitude collective motion", YIPQS Long-term workshop Dynamics and Correlations in Exotic Nuclei (DCEN2011), (YITP, Kyoto University), Kyoto, Sept.–Oct. (2011).

Nakatsukasa T.: "Finite amplitude method for TDDFT", YIPQS Long-term workshop Dynamics and Correlations in Exotic Nuclei (DCEN2011), (YITP), Kyoto, Sept.–Oct. (2011).

Sato K., Hinohara N., Nakatsukasa T., Matsuo M., and Matuyanagi K.: "Microscopic approach to large-amplitude deformation dynamics with local QRPA inertial functions", YIPQS Long-term workshop Dynamics and Correlations in Exotic Nuclei (DCEN2011), (Yukawa Institute for Theoretical Physics), Kyoto, Sept.–Oct. (2011).

Horiuchi W., Feldmeier H., Neff T., and Suzuki Y.: "Short-range and tensor correlations in nuclei", YIPQS Long-term workshop Dynamics and Correlations in Exotic Nuclei (DCEN2011), (Yukawa Institute for Theoretical Physics), Kyoto, Sept.–Oct. (2011).

Hinohara N.: "Microscopic analysis of shape coexistence/mixing and shape phase transition in neutron-rich nuclei around ^{32}Mg", Frontier Issues in Physics of Exotic Nuclei (YKIS2011), (YITP, Kyoto University), Kyoto, Oct. (2011).

Sato K., Hinohara N., Nakatsukasa T., Matsuo M., and Matuyanagi K.: "Microscopic study of shape transition in neutron-rich Cr isotopes around $N = 40$", Frontier Issues in Physics of Exotic Nuclei (YKIS2011), (Yukawa Institute for Theoretical Physics), Kyoto, Oct. (2011).

Horiuchi W., Suzuki Y., and Arai K.: "Nuclear reactions with a realistic nuclear interaction using a square integrable basis", Frontier Issues in Physics of Exotic Nuclei (YKIS2011), (Yukawa Institute for Theoretical Physics), Kyoto, Oct. (2011).

Inakura T., Nakatsukasa T., and Yabana K.: "Shell and neutron-skin effects on pygmy dipole resonaces", Frontier Issues in Physics of Exotic Nuclei (YKIS2011), (Yukawa Institute for Theoretical Physics), Kyoto, Oct. (2011).

Nakatsukasa T.: "Time-dependent density functional theory for nuclear dynamics", The Korean Physical Society Autumn Meeting 2011, (The Korean Physical Society), Busan, Korea, Oct. (2011).

Nakatsukasa T.: "Real-time calculations of many-body dynamics in quantum systems", Conference on Computational Physics (CCP2011), (Oak Ridge National Laboratory), Gatlinburg, USA, Oct.–Nov. (2011).

Nakatsukasa T.: "Recent developments in linear response calculations with the time-dependent density-functional theory", 11th International Symposium on Origin of Matter and Evolution of Galaxies (OMEG11), (University of Tokyo), Wako, Nov. (2011).

Horiuchi W., Feldmeier H., Neff T., and Suzuki Y.: "Tensor correlations in light nuclei", International symposium on frontiers in nuclear physics: Tensor interaction in nuclear and hadron physics, (Beihang University), Beijing, China, Nov. (2011).

Sato K., Hinohara N., Nakatsukasa T., Matsuo M., and Matuyanagi K.: "Microscopic approach to collective dynamics in neutron-rich nuclei around ^{64}Cr", ISPUN11, (Institute for Nuclear Science and Technique), Hanoi, Viet Nam, Nov. (2011).

Inakura T., Nakatsukasa T., and Yabana K.: "shell and neutron-skin effects on pygmy dipole resonances", ISPUN11, (GANiL, HIC for FAIR, NAFOSTED), Hanoi, Vietnam, Nov. (2011).

Nguyen D. D.: "Viscosity of hot nuclei", ISPUN11, (Institute for Nuclear Science and Technique), Hanoi, Vietnam, Nov. (2011).

Nguyen D. D.: "Viscosity: From air to a hot nucleus", International Workshop on Theoretical Approaches to Correlations in Nuclei at the Limits of Stability 2011, (TanTao University), Long An, Vietnam, Nov. (2011).

Nakatsukasa T.: "Low-energy E1 strength, skin thickness, and reaction cross section in neutron-rich nuclei", Physics Division Seminar (2011), (Oak Ridge National Laboratory), Oak Ridge, USA, Nov. (2011).

Kohama A., Iida K., and Oyamatsu K.: "Total reaction cross section and nuclear symmetry energy", YITP-KoRIA Workshop on Nuclear Symmetry Energy, (Yukawa Institute for Theoretical Physics, Kyoto University), Kyoto, Nov. (2011).

Nakatsukasa T.: "Density functional approaches to atomic nuclei", 35th Symposium on Nuclear Physics, (University of Mexico), Cocoyok, Mexico, Jan. (2012).

Horiuchi W., Navratil P., Quaglioni S., Suzuki Y., and Arai K.: "Ab initio description of reactions in light nuclei", 2nd Workshop on Perspectives of the Ab Initio No-Core Shell Model, (TRIUMF), Vancouver, Canada, Feb. (2012).

(Domestic Conference)

中務 孝: "Pairing and collective motions in nuclei", 3rd Todai-RIKEN workshop on the BEC and QCD, (University of Tokyo), 東京, 2 月 (2011).

小濱洋央, 飯田圭, 親松和浩: "核子 - 核子全断面積とくろたま模型", 日本物理学会第 66 回年次大会, (日本物理学会), 新潟, 3 月 (2011).

小濱洋央, 飯田圭, 親松和浩: "Importance of proton-proton total cross sections and proton-nucleus total reaction cross sections at 100-300 MeV", RCNP 研究会「RCNP での核データ研究戦略検討会」, (大阪大学核物理研究センター), 大阪, 6 月 (2011).

日野原伸生: "集団 Hamiltonian を用いた四重極大振幅集団運動の微視的記述", 千葉大学原子核理論セミナー, (千葉大学), 千葉, 7 月 (2011).

中務孝: "核内核子の 1 粒子運動の基礎と密度汎関数理論", サマースクール「クォークから超新星爆発まで」, (基礎物理学研究所), 京都, 8 月 (2011).

谷口億宇, 延輿佳子: "余剰中性子による亜障壁核融合断面積の増大", 基研研究会「微視的核反応理論による物理」, (京都大学), 京都, 8 月 (2011).

堀内渉, 稲倉恒法, 中務孝, 鈴木宜之: "グラウバー理論を用いた全反応断面積の系統解析", 基研研究会「微視的核反応理論による物理」, (京都大学基礎物理学研究所), 京都, 8 月 (2011).

稲倉恒法: "ピグミー双極子共鳴と中性子スキンの相関について", 日本物理学会 2011 年秋季大会, (日本物理学会), 弘前 , 9 月 (2011).

中務孝: "原子核における核子相関", 日本物理学会 2011 年秋季大会, (日本物理学会), 弘前, 9 月 (2011).

小濱洋央, 飯田圭, 親松和浩: "核子 - 核子全断面積と核子 - 原子核全反応断面積のエネルギー依存性", 日本物理学会 2011 年秋季大会, (日本物理学会), 弘前, 9 月 (2011).

日野原伸生, Vretenar D.: "Xe, Ba 同位体における変形相転移の微視的記述", 日本物理学会 2011 年秋季大会, (日本物理学会), 弘前, 9 月 (2011).

堀内渉, 鈴木宜之, 新井好司: "現実的核力を用いたヘリウム 4 の光吸収断面積の解析", 日本物理学会 2011 年秋季大会, (日本物理学会), 弘前, 9 月 (2011).

谷口億宇: "酸素同位体の低エネルギー核融合断面積における余剰中性子の効果", 日本物理学会 2011 年秋季大会, (日本物理学会), 弘前, 9 月 (2011).

佐藤弘一, 日野原伸生, 中務孝, 松尾正之, 松柳研一: "N=40 付近の中性子過剰 Cr 核における変形転移の研究", 日本物理学会 2011 年秋季大会, (日本物理学会), 弘前, 9 月 (2011).

江幡修一郎, 中務孝, 稲倉恒法: "Cb-TDHFB による重い核 (100¿A) に対する低エネルギー双極子振動の系統的研究", 日本物理学会 2011 年秋季大会, (日本物理学会), 弘前, 9 月 (2011).

堀内渉, Feldmeier H., Neff T., 鈴木宜之: "原子核における短距離相関の普遍性", 日本物理学会 2011 年秋季大会, (日本物理学会), 弘前, 9 月 (2011).

堀内渉, 鈴木宜之: "少数体手法にクラスター状態の記述", RCNP 研究会「クラスターガス状態探索のための研究戦略会議」, (大阪大学核物理研究センター), 茨木, 大阪, 9 月 (2011).

小濱 洋央: "Estimating initial reaction rates using σ_R: Kurotama and other formulae", 理化学研究所仁科加速器研究センター共用促進・産業連携部ミニワークショップ：PHITS 講習会, 和光, 11 月 (2011).

小濱洋央: "RIBF データの系統的提供と課題", RIBF 共用促進・産業連携部ミニワークショップ 「不安定核ビーム

反応実験データ採録の課題と将来」, 和光, 12 月 (2011).

谷口億宇: “^{42}Ca の励起状態のクラスタ相関と E0 遷移”, 京都大学基礎物理学研究所研究会「E0, E1 励起を通じて探る原子核の低い励起エネルギーのエキゾチックな構造」, (京都大学), 京都, 12 月 (2011).

堀内渉, 鈴木宜之, 新井好司, 佐藤透: “現実的核力を用いたヘリウム 4 の励起スペクトルと電弱応答”, 京都大学基礎物理学研究所研究会「E0, E1 励起を通じて探る原子核の低い励起エネルギーのエキゾチックな構造」, (京都大学基礎物理学研究所), 京都, 12 月 (2011).

稲倉恒法: “ピグミー共鳴状態に対する中性子殻構造とスキンの影響”, 京都大学基礎物理学研究所研究会「E0, E1 励起を通じて探る原子核の低い励起エネルギーのエキゾチックな構造」, (京都大学基礎物理学研究所), 京都, 12 月 (2011).

江幡修一郎, 中務孝, 稲倉恒法: “Cb-TDHFB による低エネルギー E1 分布の系統的計算”, 京都大学基礎物理学研究所研究会「E0, E1 励起を通じて探る原子核の低い励起エネルギーのエキゾチックな構造」, (京都大学基礎物理学研究所), 京都, 12 月 (2011).

佐藤弘一, 中務孝, Dobaczewski J.: “p-n 混合を入れた原子核の平均場計算”, 素核宇融合による計算基礎物理学の進展, (新学術領域研究「素核宇宙融合による計算科学に基づいた重層的物質構造の解明」), 志摩, 12 月 (2011).

中務孝: “密度汎関数理論による核構造・核反応の大規模数値計算”, 大規模計算による原子核研究の展開：核子多体系を中心に, (計算基礎科学連携拠点), 和光, 1 月 (2012).

中務孝: “計算機で見る原子核”, 第 10 回 HSS ワークショップ, (北海道大学), 札幌, 2 月 (2012).

谷口億宇: “sd 及び pf 殻領域の低励起変形状態におけるクラスタ相関”, 第 2 回実証的原子核物理学研究会, (大阪大学), 茨木, 2 月 (2012).

谷口億宇, 延與佳子: “空間的相関の強い系における部分系波動関数の定義とその応用”, 日本物理学会第 67 回年次大会, (日本物理学会), 西宮, 3 月 (2012).

堀内渉: “軽い核におけるテンソル相関の重要性とその効果”, 日本物理学会第 67 回年次大会, (日本物理学会), 西宮, 3 月 (2012).

堀内渉, 稲倉恒法, 中務孝, 鈴木宜之: “全反応断面積の系統解析から見る不安定核の構造変化”, 日本物理学会第 67 回年次大会, (日本物理学会), 西宮, 3 月 (2012).

稲倉恒法: “低エネルギー E1 強度で見る中性子スキン”, 日本物理学会第 67 回年次大会, (日本物理学会), 西宮, 3 月 (2012).

佐藤弘一, 中務孝, Dobaczewski J.: “陽子―中性子混合を入れた平均場計算”, 日本物理学会第 67 回年次大会, (日本物理学会), 西宮, 3 月 (2012).

Strangeness Nuclear Physics Laboratory

Publications

[Journal]

(Original Papers) *Subject to Peer Review

Nemura H., Ishii N., Aoki S., and Hatsuda T.: "Study of Hyperon-Nucleon Potential from Lattice QCD", Int. J. Mod. Phys. E **19**, No. 12, pp. 2442–2447 (2010). *

Hiyama E., Kamimura M., Yamamoto Y., and Motoba T.: "Five-body cluster structure of the double-Λ hypernucleus $^{11}_{\Lambda\Lambda}$Be", Phys. Rev. Lett. **104**, 212502-1–212502-4 (2010). *

Hiyama E., Kamimura M., Yamamoto Y., Motoba T., and Rijken T. A.: "S = -1 hypernuclear structure", Prog. Theor. Phys. Suppl. **185**, 106–151 (2010). *

Hiyama E., Kamimura M., Yamamoto Y., Motoba T., and Rijken T. A.: "S = -2 hypernuclear structure", Prog. Theor. Phys. Suppl. **185**, 152–196 (2010). *

Oral Presentations

(International Conference etc.)

Hiyama E.: "S=-1 and S=-2 hypernuclei from view points of few-body problem", Hadron Physics Meeting strangeness physics at J-PARC, (Asia Pacific Center for Theoretical Physics), Pohang, Korea, May (2011).

Hiyama E.: "Five-body calculation of systems including strange quark", ECT Workshop on Not so few, but not too Many, (European Centre for Theoretical Studies in Nuclear Physics and Related Areas), Trento, Italy, July (2011).

Hiyama E.: "S=-1 and S=-2 few body systems", 5th Asia-Pacific Coneferene on Few-Body Problems in Physics 2011 (APFB2011), (Asia Pacific Center for Theoretical Physics), Seoul, Korea, Aug. (2011).

Hiyama E.: "Clustering aspects of light nuclei", ECT Workshop on Strange Hadronic Matter, (European Centre for Theoretical Studies in Nuclear Physics and Related Areas), Trento, Italy, Sept. (2011).

Hiyama E.: "Structure of 10LBe and 10LB hypernuclei studied with the four-body cluster model", Korea-Japan workshop on nuclear and hadron physics at J-PARC, (Seoul National University), Seoul, Korea, Sept. (2011).

Zhang Y.: "Continuum Skyrme Hartree-Fock-Bogoliubov theory with Green's function method for exotic nuclei", YIPQS Long-term workshop Dynamics and Correlations in Exotic Nuclei (DCEN2011), (YITP), Kyoto, Sept.–Oct. (2011).

Hiyama E.: "Few-body aspects of hypernuclear physics", 3rd International Conference on Nuclear Fragmentation (NUFRA 2011), (Frankfurt Institut for Advanced Studies), Kemer, Turkey, Oct. (2011).

Hiyama E.: "Four-body calculations of 4He tetramer and light hypernuclei using realistic two-body potentials", Critical Stability 2011, Erice, Italy, Oct. (2011).

(Domestic Conference)

飯尾雅実, 板橋健太, 岩崎雅彦, 應田治彦, 大西宏明, 佐久間史典, 佐藤将春, 塚田暁, 友野大, 藤岡宏之, 山崎敏光, 石元茂, 岩井正明, 鈴木祥二, 関本美知子, 豊田晃久, 石川隆, 竜野秀行, 鈴木隆敏, 早野龍五, 松田恭幸, 永江知文, 平岩聡彦, 味村周平, 野海博之, 阪口篤志, 藤原裕也, 徳田真, 千葉順成, 福田共和, 溝井浩, Beer G. A., 方享燦, Choi S., 林熙重, 石渡智一, Buehler P., Cargnelli M., Hirtl A., Kienle P., Marton J., Widmann E., Zmeskal J., 岡田信二, Curceanu C. O., Guaraldo C., Iliescu M., Pietreanu D., Sirghi D., Sirghi F., Faso D., Morra O., Busso L.: "K中間子原子核探査実験のための液体ヘリウム3標的の開発III", 日本物理学会2008年秋季大会, (日本物理学会), 盛岡, 9月 (2008).

味村周平, Beer G., 方享燦, Bragadireanu M. A., Buehler P., Busso L., Cargnelli M., Choi S., Curceanu C. O., 榎本瞬, Faso D., 藤原裕也, 藤岡宏之, 福田共和, Guaraldo C., 橋本直, 早野龍五, 平岩聡彦, 飯尾雅実, 井上謙太郎, 石川隆, 石元茂, 石渡智一, 板橋健太, 岩井正明, 岩崎雅彦, Kikenle P., 康寛史, Marton J., 松田恭幸, 溝井浩, Morra O., 永江知文, 野海博之, 岡田信二, 大西宏明, 應田治彦, 佐田優太, 阪口篤志, 佐久間史典, 佐藤将春, 関本美知子, Shi H., Sirghi D., Sirghi F., 鈴木謙, 鈴木祥仁, 鈴木隆敏, 竜野秀行, 徳田真, 友野大, 豊田晃久, 塚田暁, Widmann E., 山崎敏光, Yim H., Zmeskal J.: "J-PARCにおけるK中間子深束縛核探索実験のためのTGEM-TPC開発", 日本物理学会第65回年次大会, (日本物理学会), 岡山, 3月 (2010).

佐田優太, 味村周平, Beer G., 方享燦, Bragadireanu M. A., Buehler P., Busso L., Cargnelli M., Choi S., Curceanu C. O., 榎本瞬, Faso D., 藤岡宏之, 藤原裕也, 福田共和, Guaraldo C., 橋本直, 早野龍五, 平岩聡彦, 飯尾雅実, 井上謙太郎, 石黒洋輔, 石川隆, 石元茂, 石渡智一, 板橋健太, 岩井正明, 岩崎雅彦, 川崎信吾, Kikenle P., 康寛史, Marton J., 松田恭幸, 溝井浩, Morra O., 永江知文, 野海博之, 大西宏明, 岡田信二, 應田治彦, 阪口篤志, 佐久間史典, 佐藤将春, 関本美知子, Shi H., Sirghi D., Sirghi F., 鈴木謙, 鈴木祥仁, 鈴木隆敏, 竜野秀行, 徳田真, 友野大, 豊田晃久, 塚田暁, Widmann E., 山崎敏光, Yim H., Zmeskal J.: "J-PARC E15実験に用いる円筒形検出器群のコミッショニング", 日本物理学会2010年秋季大会, (日本物理学会), 北九州市, 9月 (2010).

飯尾雅実, 板橋健太, 岩崎雅彦, 應田治彦, 大西宏明, 佐久間史典, 友野大, 塚田暁, 山崎敏光, 榎本瞬, 石橋直哉, 井上謙太郎, 阪口篤志, 吉田幸太郎, 味村周平, 野海博之, 石元茂, 岩井正明, 鈴木祥二, 関本美知子, 豊田晃久, 石川隆, 佐藤将春, 鈴木隆敏, 施赫將, 竜野秀行, 橋本直, 早野龍五, 藤原裕也, 松田恭幸, 康寛史, 徳田真, 永江知文, 平岩聡彦, 藤岡宏之, 佐田優太, 福田共和, 溝井浩, Faso D., Morra O., Bragadireanu M., Curceanu C. O., Guaraldo C., Iliescu M., 岡田信二, Pietreanu D., Sirghi D., Sirghi F., Buehler P., Cargnelli M., 石渡智一, Marton J., Widmann E., Zmeskal J., 鈴木謙, 方享燦, Choi S., 林熙重, Kienle P., Busso L., Beer G. A.: "Λ (1405)精密分光のための重水素標的の開発(1)", 日本物理学会2010年秋季大会, (日本物理学会), 北九州, 9月 (2010).

佐田優太, 味村周平, Beer G., 方享燦, Bragadireanu M. A., Buehler P., Busso L., Cargnelli M., Choi S., Curceanu C. O., 榎本瞬, Faso D., 藤岡宏之, 藤原裕也, 福田共和, Guaraldo C., 橋本直, 早野龍五, 平岩聡彦, 飯尾雅実, 井上謙太郎, 石黒洋輔, 石川隆, 石元茂, 石渡智一, 板橋健太, 岩井正明, 岩崎雅彦, 川崎信吾, Kikenle P., 康寛史, Marton J., 松田恭幸, 溝井浩, Morra O., 永江知文, 野海博之, 大西宏明, 岡田信二, 應田治彦, 阪口篤志, 佐久間史典, 佐藤将春, 関本美知子, Shi H., Sirghi D., Sirghi F., 鈴木謙, 鈴木祥仁, 鈴木隆敏, 竜野秀行, 徳田真, 友野大, 豊田晃久, 塚田暁, Widmann E., 山崎敏光, Yim H., Zmeskal J.: “K1.8BR beamline の円筒型検出器群 (CDS) の commissioning について”, KEK 理論センター研究会「ストレンジネス核物理 2010」, (高エネルギー加速器研究機構　素粒子原子核研究所), つくば市, 12 月 (2010).

佐田優太, 味村周平, Beer G., 方享燦, Bragadireanu M. A., Buehler P., Busso L., Cargnelli M., Choi S., Curceanu C. O., 榎本瞬, Faso D., 藤岡宏之, 藤原裕也, 福田共和, Guaraldo C., 橋本直, 早野龍五, 平岩聡彦, 飯尾雅実, 井上謙太郎, 石黒洋輔, 石川隆, 石元茂, 石渡智一, 板橋健太, 岩井正明, 岩崎雅彦, 川崎信吾, Kikenle P., 康寛史, Marton J., 松田恭幸, 溝井浩, Morra O., 永江知文, 野海博之, 大西宏明, 岡田信二, 應田治彦, 阪口篤志, 佐久間史典, 佐藤将春, 関本美知子, Shi H., Sirghi D., Sirghi F., 鈴木謙, 鈴木祥仁, 鈴木隆敏, 竜野秀行, 徳田真, 友野大, 豊田晃久, 塚田暁, Widmann E., 山崎敏光, Yim H., Zmeskal J.: “J-PARC E15 実験に用いる円筒形検出器群のコミッショニング（2）”, 日本物理学会第 66 回年次大会, (日本物理学会), 新潟, 3 月 (2011).

徳田真, 味村周平, Beer G., 方享燦, Bragadireanu M. A., Buehler P., Busso L., Cargnelli M., Choi S., Curceanu C. O., 榎本瞬, Faso D., 藤岡宏之, 藤原裕也, 福田共和, Guaraldo C., 橋本直, 早野龍五, 平岩聡彦, 飯尾雅実, 井上謙太郎, 石黒洋輔, 石川隆, 石元茂, 石渡智一, 板橋健太, 岩井正明, 岩崎雅彦, 川崎信吾, Kikenle P., 康寛史, Marton J., 松田恭幸, 溝井浩, Morra O., 永江知文, 野海博之, 大西宏明, 岡田信二, 應田治彦, 阪口篤志, 佐田優太, 佐久間史典, 佐藤将春, 関本美知子, Shi H., Sirghi D., Sirghi F., 鈴木謙, 鈴木祥仁, 鈴木隆敏, 竜野秀行, 友野大, 豊田晃久, 塚田暁, Widmann E., 山崎敏光, Yim H., Zmeskal J.: “J-PARC における K 中間子深束縛核探索実験（E15 実験）のための TGEM-TPC の開発 II”, 日本物理学会第 66 回年次大会, (日本物理学会), 新潟, 3 月 (2011).

Zhang Y.: “Continuum Skyrme Hartree-Fock-Bogoliubov theory with Green’s function method for exotic nuclei”, 日本物理学会 2011 年秋季大会, (JPS), 弘前, 9 月 (2011).

小池貴久: “(K^{-},K^{+}) 反応による軽い Ξ^{-} ハイパー核の生成”, 日本物理学会 2011 年秋季大会, (日本物理学会), 弘前 , 9 月 (2011).

小池 貴久: “Kbar-(NN) equivalent local potential from Kbar(NN)-pi(Sigma N) coupled channel model”, Future Prospects of Hadron Physics at J-PARC and Large Scale Computational Physics, (J-PARC 分室、KEK 理論センター), 東海村, 2 月 (2012).

土井琢身, 青木慎也, 初田哲男, 池田陽一, 井上貴史, 石井理修, 村野啓子, 根村英克, 佐々木健志: “Cutoff effects on Three-Nucleon Forces in Lattice QCD”, 日本物理学会第 67 回年次大会, (日本物理学会), 西宮市, 3 月 (2012).

小池貴久: “(K^{-},K^{+}) 反応による軽い Ξ^{-} ハイパー核の生成 II”, 日本物理学会第 67 回年次大会, (日本物理学会), 西宮, 3 月 (2012).

Mathematical Physics Laboratory

Publications

[Journal]

(Original Papers) *Subject to Peer Review

Chen H., Hashimoto K., and Matsuura S.: "Towards a holographic model of color-flavor locking phase", J. High Energy Phys. **1002**, 104-1–104-34 (2010). *

Hashimoto K., Iizuka N., and Yi P.: "A matrix model for baryons and nuclear forces", J. High Energy Phys. **1010**, 003-1–003-28 (2010). *

Hashimoto K. and Iizuka N.: "Three-body nuclear forces from a matrix model", J. High Energy Phys. **1011**, 058-1–058-23 (2010). *

Hashimoto K.: "Nuclear force from string theory", Nucl. Phys. A **835**, 192–198 (2010). *

Hashimoto K., Hirayama T., and Hong D.: "Quark mass dependence of hadron spectrum in holographic QCD", Phys. Rev. D **81**, 045016-1–045016-10 (2010). *

Hashimoto K., Iizuka N., and Nakatsukasa T.: "N-body nuclear forces at short distances in holographic QCD", Phys. Rev. D **81**, 106003-1–106003-5 (2010). *

Hashimoto K. and Iizuka N.: "Nucleon statistics in holographic QCD: Aharonov-Bohm effect in a matrix model", Phys. Rev. D **82**, 105023-1–105023-2 (2010). *

Hashimoto K.: "Hadron spectra and quark mass dependence in holographic QCD", Prog. Theor. Phys. Suppl. **186**, 211–215 (2010).

Kimura T.: "Matrix model from $\mathcal{N}=2$ orbifold partition function", J. High Energy Phys. **2011**, No. 9, pp. 015-1–015-34 (2011). *

Kimura T. and Nitta M.: "Vortices on orbifolds", J. High Energy Phys. **2011**, No. 9, pp. 118-1–118-21 (2011). *

Kanada-En'yo Y. and Hidaka Y.: "Alpha-cluster structure and density waves in oblate nuclei", Phys. Rev. C **84**, 014313-1–014313-16 (2011). *

Cho S., Furumoto T., Hyodo T., Jido D., Ko C. M., Lee S. H., Nielsen M., Ohnishi A., Sekihara T., Yasui S., Yazaki K., and ExHIC C.: "Studying exotic hadrons in heavy ion collisions", Phys. Rev. C **84**, 064910-1–064910-17 (2011). *

Eto M., Hashimoto K., Iida H., and Miwa A.: "Chiral magnetic effect from Q-balls", Phys. Rev. D **83**, 125033-1–125033-5 (2011). *

Hashimoto K. and Morita T.: "Nucleus from String Theory", Phys. Rev. D **84**, No. 4, pp. 046004-1–046004-5 (2011). *

Hashimoto K., Iizuka N., and Oka T.: "Rapid thermalization by baryon injection in gauge/gravity duality", Phys. Rev. D **84**, No. 6, pp. 066005-1–066005-9 (2011). *

Jittoh T., Kohri K., Koike M., Sato J., Sugai K., and Yazaki K.: "Big-bang nucleosynthesis with a long-lived charged massive particle including ^{4}He spallation processes", Phys. Rev. D **84**, 035008-1–035008-11 (2011). *

Kimura T., Komatsu S., Misumi T., Noumi T., Torii S., and Aoki S.: "Revisiting symmetries of lattice fermions via spin-flavor representation", J. High Energy Phys. **2012**, No. 01, pp. 048-1–048-20 (2012). *

Kojo T., Hidaka Y., Fukushima K., McLerran L., and Pisarski R.: "Interweaving chiral spirals", Nucl. Phys. A **875**, 94–138 (2012). *

Hidaka Y., Satow D., and Kunihiro T.: "Ultrasoft fermionic modes at high temperature", Nucl. Phys. A **876**, 93–108 (2012). *

Aoyama T., Hayakawa M., Kinoshita T., and Nio M.: "Tenth-order QED lepton anomalous magnetic moment: Eighth-order vertices containing a second-order vacuum polarization", Phys. Rev. D **85**, No. 3, pp. 033007-1–033007-17 (2012). *

Kimura T.: "β-Ensembles for Toric Orbifold Partition Function", Prog. Theor. Phys. **127**, No. 2, pp. 271–285 (2012). *

(Review)

橋本幸士: "時空の創生：超弦理論から原子核へ 1. 超弦理論と素粒子", 日本原子力学会誌 **52**, No. 11, pp. 737–741 (2010).

橋本幸士: "時空の創生：超弦理論から原子核へ 2. 超弦理論と宇宙論：極小素粒子と極大の関係", 日本原子力学会誌 **52**, No. 12, pp. 791–795 (2010).

橋本幸士: "時空の創生：超弦理論から原子核へ 3. 陽子・中性子＝仮想高次元重力", 日本原子力学会誌 **53**, No. 1, pp. 31–35 (2011).

Oral Presentations

(International Conference etc.)

Hashimoto K.: "D-Brane Engineering of solitons in metastable vacua and QCD strings", National Taiwan University, Physics Department Seminar, Taipei, Taiwan, Dec. (2007).

Hashimoto K.: "Hadron spectra and quark mass dependence in holographic QCD", New Frontiers in QCD 2010, (Yukawa institute, Kyoto university), Kyoto, Jan.–Mar. (2010).

Hashimoto K.: "Holography and nuclear physics", IPMU Focus Week: Condensed matter physics meets high energy physics, (IPMU, the university of Tokyo), Kashiwa, Feb. (2010).

Hashimoto K.: "Nuclear physics from string theory I", APCTP-WCU Focus Program: From dense matter to compact stars in QCD and in hQCD, (APCTP), Pohang, Korea, May–June (2010).

Hashimoto K.: "Gravity dual of heavy nuclei", Workshop: Gravity and Cosmology 2010, (Yukawa institute for theoretical physics), Kyoto, May–July (2010).

Hashimoto K.: "Holographic QCD and beyond", 22nd Rencontres de Blois "Particle Physics and Cosmology: first results from the LHC", (CEA, CNRS), Blois, France, July (2010).

Hashimoto K.: "Nuclear force from string theory", ECT*–EMMI International Workshop on: Chiral Symmetry and Confinement in Cold, Dense Quark Matter, (ECT*), Tronto, Italy, July (2010).

Hashimoto K.: "Nuclear matrix model: a path to nuclear physics from superstrings", International Conference on the Structure of Baryons (BARYONS' 10), (RCNP), Osaka, Dec. (2010).

Hashimoto K.: "Rapid theralization by baryon injection in gauge/gravity duality", 11th workshop on non-perturbative QCD, (Brown university), paris, france, June (2011).

Misumi T., Creutz M., Kimura T., Nakano T., and Ohnishi A.: "Aoki phases in staggered-Wilson fermions", 29th International Symposium on Lattice Field Theory (Lattice 2011), Squaw Valley, USA, July (2011).

Kimura T., Creutz M., and Misumi T.: "Index theorem and overlap formalism with naive and minimally doubled fermions", 29th International Symposium on Lattice Field Theory (Lattice 2011), Squaw Valley, USA, July (2011).

Hashimoto K.: "Holographic nuclei and nuclear matter", 2nd Year of APCTP-WCU Focus program: From dense matter to compact stars in QCD and in hQCD, (APCTP), Pohang, Korea, Aug. (2011).

Hashimoto K.: "Nucleus from string theory", 2nd International Workshop on Quarks and Hadrons under Extreme Conditions-Lattice QCD, Holography, Topology, and Physics at RHIC/LHC-, (Keio university), Tokyo, Nov. (2011).

Hashimoto K.: "Superstring theory and its spacetime", Cold Antimatter and High Precision Physics (Pbar11), Matsue, Nov. (2011).

Hidaka Y.: "Ultrasoft fermionic modes at high temperature", Facets of Strong-Interaction Physics, (Darmstadt University), Hirschegg, Australia, Jan. (2012).

(Domestic Conference)

木村太郎: "組合せ論的オービフォルド分配関数の漸近挙動と行列模型", 千葉大セミナー, (千葉大学), 千葉, 6 月 (2011).

村田仁樹: "開弦の場の理論における多重Dブレイン解について", 日本大学セミナー 2011, (日本大学), 東京, 6 月 (2011).

村田仁樹: "On Multiple-brane Solutions in Open Bosonic String Field Theory", 基研研究会「場の理論と弦理論」, (基礎物理学研究所), 京都, 7 月 (2011).

中野嵩士, 三角樹弘, 木村太郎, 大西明: "Staggered-Wilson fermion における Aoki phase の強結合解析", 熱場の量子論とその応用, (京都大学　基礎物理学研究所), 京都, 8 月 (2011).

橋本幸士: "超弦理論と原子核", 日本物理学会 2011 年秋季大会, (日本物理学会), 弘前, 9 月 (2011).

木村太郎: "組合せ論的オービフォルド分配関数の漸近挙動と行列模型", 日本物理学会 2011 年秋季大会, (日本物理学会), 富山, 9 月 (2011).

木村太郎: "Beta-ensemble matrix models for orbifold partition function", 京都大学素粒子論研究室セミナー, (京都大学素粒子論研究室), 京都, 10 月 (2011).

木村太郎: "Beta-ensemble matrix models for orbifold partition function", 東工大素粒子論研究室セミナー, (東京工業大学素粒子論研究室), 東京, 10 月 (2011).

村田仁樹: "開弦の場の理論における多重Dブレイン解について", 理論物理素粒子コロキウム, (立教大学), 東京, 10 月 (2011).

木村太郎: "組合せ論と行列模型", 行列模型とその周辺, 東京, 2 月 (2012).

村田仁樹: "弦の場の理論における多重 D ブレイン解について", 第 5 回超弦理論と宇宙, (基礎物理学研究所), 別府, 2 月 (2012).

中野嵩士, 三角樹弘, 木村太郎, 大西明: "スタッガードウィルソンフェルミオンを用いた強結合解析とカイラル極限", 日本物理学会第 67 回年次大会, (日本物理学会), 西宮, 3 月 (2012).

Radiation Laboratory

Publications

[Journal]

(Original Papers) *Subject to Peer Review

Fukao Y. and Local Pol Collabor .: "Measurement of single transverse-spin asymmetry in forward production of photons and neutrons in pp collisions at $\sqrt{s}=200$ GeV", AIP Conf. Proc., pp. 584–588 (2003).

Nishitani T., Tabuchi M., Takeda Y., Suzuki Y., Motoki K., and Meguro T.: "Superlattice Photocathode with High Brightness and Long NEA-Surface Lifetime", Am. inst. phys. **1149**, 1047–1051 (2009). *

Afanasiev S., Akiba Y., Aoki K., Asai J., Bathe S., Boyle K., Deshpande A., Enyo H., Fukao Y., Goto Y., Hachiya T., Ichihara T., Ishihara M., Miyachi Y., Nakagawa I., Shibata T., Shoji K., Taketani A., Tanida K., Torii H., Watanabe Y., Yokkaichi S., Okada K., Saito N., and PHENIX C.: "Photoproduction of J/ψ and of high mass e^+e^- in ultra-peripheral Au+Au collisions at $\sqrt{s_{NN}}=200$ GeV", Phys. Lett. B **679**, No. 4, pp. 321–329 (2009). *

Tamae T., Sato Y., Yokokawa T., Asano Y., Kawabata M., Konno O., Nakagawa I., Nishikawa I., Hirota K., Yamazaki H., Kimura R., Miyase H., Tsubota H., Giusti C., and Meucci A.: "Comparison of the C-12 (e, e′ p) cross section at low momentum transfer with a relativistic calculation", Phys. Rev. C **80**, No. 6, pp. 064601-1–064601-7 (2009). *

Adare A., Akiba Y., Aoki K., Asai J., Bathe S., Boyle K., Deshpande A., Enyo H., Fukao Y., Goto Y., Hachiya T., Ichihara T., Ichimiya R., Ikeda Y., Ishihara M., Mao Y., Nakagawa I., Nakano K., Ralf S., Shibata T., Shoji K., Taketani A., Tanida K., Torii H., Watanabe Y., Yokkaichi S., Kurosawa M., Okada K., Saito N., and PHENIX C.: "Photon-hadron jet correlations in $p+p$ and $Au+Au$ collisions at $\sqrt{s_{NN}}=200$ GeV", Phys. Rev. C **80**, 024908-1–024908-14 (2009). *

Afanasiev S., Akiba Y., Aoki K., Bathe S., Boyle K., Deshpande A., Enyo H., Fukao Y., Goto Y., Hachiya T., Ichihara T., Ishihara M., Shibata T., Shoji K., Taketani A., Tanida K., Torii H., Watanabe Y., Yokkaichi S., Okada K., Saito N., and PHENIX C.: "Systematic studies of elliptic flow measurements in Au+Au collisions at $\sqrt{s_{NN}}=200$ GeV", Phys. Rev. C **80**, 024909-1–024909-25 (2009). *

Afanasiev S., Akiba Y., Aoki K., Bathe S., Boyle K., Deshpande A., Enyo H., Fukao Y., Goto Y., Hachiya T., Ichihara T., Ishihara M., Shibata T., Shoji K., Taketani A., Tanida K., Torii H., Watanabe Y., Yokkaichi S., Okada K., Saito N., and PHENIX C.: "High-pT π^0 production with respect to the reaction plane in $Au+Au$ collisions at $\sqrt{s_{NN}}=200$ GeV", Phys. Rev. C **80**, 054907-1–054907-29 (2009). *

Adare A., Akiba Y., Aoki K., Asai J., Bathe S., Boyle K., Deshpande A., Enyo H., Fukao Y., Goto Y., Ichihara T., Ichimiya R., Ikeda Y., Ishihara M., Mao Y., Nakagawa I., Nakano K., Ralf S., Shibata T., Shoji K., Taketani A., Tanida K., Torii H., Watanabe Y., Yokkaichi S., Kurosawa M., Okada K., Saito N., and PHENIX C.: "Gluon-spin contribution to the proton spin from the double-helicity asymmetry in inclusive π^0 production in polarized $p+p$ collisions at $\sqrt{s}=200$ GeV", Phys. Rev. Lett. **103**, 012003-1–012003-6 (2009). *

Adare A., Akiba Y., Aoki K., Asai J., Bathe S., Boyle K., Deshpande A., Enyo H., Fukao Y., Goto Y., Hachiya T., Ichihara T., Ichimiya R., Ikeda Y., Ishihara M., Mao Y., Nakagawa I., Nakano K., Ralf S., Shibata T., Shoji K., Taketani A., Tanida K., Torii H., Watanabe Y., Yokkaichi S., Kurosawa M., Okada K., Saito N., and PHENIX C.: "Measurement of bottom versus charm as a function of transverse momentum with electron-hadron correlations in $p+p$ collisions at $\sqrt{s}=200$ GeV", Phys. Rev. Lett. **103**, 082002-1–082002-7 (2009). *

Afanasiev S., Akiba Y., Aoki K., Bathe S., Boyle K., Deshpande A., Enyo H., Fukao Y., Goto Y., Hachiya T., Ichihara T., Ishihara M., Shibata T., Shoji K., Taketani A., Tanida K., Torii H., Watanabe Y., Yokkaichi S., Okada K., and PHENIX C.: "Charged kaon interferometric probes of space-time evolution in $Au+Au$ collisions at $\sqrt{s_{NN}}=200$ GeV", Phys. Rev. Lett. **103**, 142301-1–142301-6 (2009). *

Nakagawa I.: "Muon trigger upgrade at PHENIX", J. Phys.: Con. Ser. **230**, No. 1, pp. 012038-1–012038-6 (2010).

Adare A., Akiba Y., Aoki K., Asai J., Bathe S., Boyle K., Deshpande A., Enyo H., Fukao Y., Goto Y., Hachiya T., Ichihara T., Ishihara M., Mao Y., Nakagawa I., Nakamura K., Nakano K., Ralf S., Shibata T., Shoji K., Taketani A., Tanida K., Torii H., Watanabe Y., Yokkaichi S., Okada K., Saito N., and PHENIX C.: "Detailed measurement of the e^+e^- pair continuum in $p+p$ and Au+Au collisions at $\sqrt{s_{NN}}=200$ GeV and implications for direct photon production", Phys. Rev. C **81**, No. 3, pp. 034911-1–034911-56 (2010). *

Adare A., Akiba Y., Aoki K., Asai J., Bathe S., Boyle K., Deshpande A., Enyo H., Fukao Y., Goto Y., Hachiya T., Ichihara T., Ichimiya R., Ikeda Y., Ishihara M., Mao Y., Nakagawa I., Nakano K., Ralf S., Shibata T., Shoji K., Taketani A., Tanida K., Torii H., Watanabe Y., Yokkaichi S., Kurosawa M., Okada K., Saito N., and PHENIX C.: "Transverse momentum dependence of η meson suppression in Au+Au collisions at $\sqrt{s_{NN}}=200$ GeV", Phys. Rev. C **82**, No. 1, pp. 011902-1–011902-7 (2010). *

Adare A., Akiba Y., Aoki K., Asai J., Bathe S., Boyle K., Deshpande A., Enyo H., Fukao Y., Goto Y., Hachiya T., Ichihara T., Ichimiya R., Ikeda Y., Ishihara M., Mao Y., Nakagawa I., Nakano K., Ralf S., Shibata T.,

Shoji K., Taketani A., Tanida K., Torii H., Watanabe Y., Yokkaichi S., Kurosawa M., Okada K., Saito N., and PHENIX C.: "Double-helicity dependence of jet properties from dihadrons in longitudinally polarized $p+p$ collisions at $\sqrt{s}=200$ GeV", Phys. Rev. D **81**, No. 1, pp. 012002-1–012002-11 (2010). *

Adare A., Akiba Y., Aoki K., Asai J., Bathe S., Boyle K., Deshpande A., Enyo H., Fukao Y., Goto Y., Ichihara T., Ichimiya R., Ikeda Y., Ishihara M., Mao Y., Nakagawa I., Nakano K., Ralf S., Shibata T., Shoji K., Taketani A., Tanida K., Torii H., Watanabe Y., Yokkaichi S., Kurosawa M., Okada K., Saito N., and PHENIX C.: "Transverse momentum dependence of J/ψ polarization at midrapidity in $p+p$ collisions at $\sqrt{s}=200$ GeV", Phys. Rev. D **82**, No. 1, pp. 012001-1–012001-10 (2010). *

Adare A., Akiba Y., Aoki K., Asai J., Bathe S., Boyle K., Deshpande A., Enyo H., Fukao Y., Goto Y., Hachiya T., Ichihara T., Ichimiya R., Ikeda Y., Ishihara M., Mao Y., Nakagawa I., Nakano K., Ralf S., Shibata T., Shoji K., Taketani A., Tanida K., Torii H., Watanabe Y., Yokkaichi S., Kurosawa M., Okada K., Saito N., and PHENIX C.: "High p_T direct photon and π^0 triggered azimuthal jet correlations and measurement of k_T for isolated direct photons in $p+p$ collisions at $\sqrt{s}=200$ GeV", Phys. Rev. D **82**, No. 7, pp. 072001-1–072001-18 (2010). *

Adare A., Akiba Y., Aoki K., Asai J., Bathe S., Boyle K., Deshpande A., Enyo H., Fukao Y., Goto Y., Ichihara T., Ichimiya R., Ikeda Y., Ishihara M., Mao Y., Nakagawa I., Nakamura K., Nakano K., Ralf S., Shibata T., Shoji K., Taketani A., Tanida K., Torii H., Watanabe Y., Yokkaichi S., Kurosawa M., Okada K., Saito N., Nakamura T., and PHENIX C.: "Measurement of transverse single-spin asymmetries for J/ψ production in polarized $p+p$ collisions at $\sqrt{s}=200$ GeV", Phys. Rev. D **82**, No. 11, pp. 112008-1–112008-13 (2010). *

Adare A., Akiba Y., Aoki K., Asai J., Bathe S., Boyle K., Deshpande A., Enyo H., Fukao Y., Goto Y., Hachiya T., Ichihara T., Ishihara M., Mao Y., Nakagawa I., Nakano K., Ralf S., Shibata T., Shoji K., Taketani A., Tanida K., Torii H., Watanabe Y., Yokkaichi S., Okada K., Saito N., and PHENIX C.: "Enhanced Production of Direct Photons in Au+Au Collisions at $\sqrt{s_{NN}}=200$ GeV and Implications for the Initial Temperature", Phys. Rev. Lett. **104**, 132301-1–132301-6 (2010). *

Adare A., Akiba Y., Aoki K., Asai J., Bathe S., Boyle K., Deshpande A., Enyo H., Fukao Y., Goto Y., Hachiya T., Ichihara T., Ichimiya R., Ikeda Y., Ishihara M., Mao Y., Nakagawa I., Nakano K., Ralf S., Shibata T., Shoji K., Taketani A., Tanida K., Torii H., Watanabe Y., Yokkaichi S., Kurosawa M., Okada K., Saito N., and PHENIX C.: "Transition in Yield and Azimuthal Shape Modification in Dihadron Correlations in Relativistic Heavy Ion Collisions", Phys. Rev. Lett. **104**, 252301-1–252301-7 (2010). *

Adare A., Akiba Y., Aoki K., Bathe S., Boyle K., Deshpande A., Enyo H., Fukao Y., Goto Y., Hashimoto K., Ichihara T., Ichimiya R., Ikeda Y., Ishihara M., Mao Y., Nakagawa I., Nakano K., Ralf S., Shibata T., Shoji K., Taketani A., Tanida K., Torii H., Watanabe Y., Yokkaichi S., Kurosawa M., Okada K., Saito N., and PHENIX C.: "Elliptic and Hexadecapole Flow of Charged Hadrons in Au+Au Collisions at $\sqrt{s_{NN}}=200$ GeV", Phys. Rev. Lett. **105**, 062301-1–062301-6 (2010). *

Adare A., Akiba Y., Aoki K., Bathe S., Boyle K., Deshpande A., Enyo H., Fukao Y., Goto Y., Ichihara T., Ichimiya R., Ikeda Y., Ishihara M., Mao Y., Nakagawa I., Nakano K., Ralf S., Shibata T., Shoji K., Taketani A., Tanida K., Torii H., Watanabe Y., Yokkaichi S., Kurosawa M., Okada K., Saito N., and PHENIX C.: "Azimuthal Anisotropy of π^0 Production in Au+Au Collisions at $\sqrt{s_{NN}}=200$ GeV: Path-Length Dependence of Jet Quenching and the Role of Initial Geometry", Phys. Rev. Lett. **105**, 142301-1–142301-7 (2010). *

Fukao Y. and PHENIX C.: "Forward upgrade for W physics at RHIC-PHENIX experiment", J. Phys.: Con. Ser. **295**, 1–5 (2011).

Nakamura T., Enyo H., Ichihara T., Watanabe Y., and Yokkaichi S.: "Data oriented job submission scheme or the PHENIX user analysis in CCJ", J. Phys.: Con. Ser. **331**, 1–6 (2011). *

Adare A., Akiba Y., Aoki K., Asai J., Bathe S., Boyle K., Deshpande A., Enyo H., Fukao Y., Goto Y., Hachiya T., Ichihara T., Ichimiya R., Ikeda Y., Ishihara M., Mao Y., Nakagawa I., Nakamura K., Nakano K., Ralf S., Shibata T., Shoji K., Taketani A., Tanida K., Torii H., Watanabe Y., Yokkaichi S., Kurosawa M., Okada K., Saito N., Nakamura T., and PHENIX C.: "Nuclear modification factors of ϕ mesons in d+Au, Cu+Cu, and Au+Au collisions at $\sqrt{s_{NN}}=200$ GeV", Phys. Rev. C **83**, No. 2, pp. 024909-1–024909-10 (2011). *

Adare A., Akiba Y., Aoki K., Asai J., Bathe S., Boyle K., Deshpande A., Enyo H., Fukao Y., Goto Y., Ichihara T., Ichimiya R., Ikeda Y., Ishihara M., Mao Y., Nakagawa I., Nakano K., Ralf S., Shibata T., Shoji K., Taketani A., Tanida K., Torii H., Watanabe Y., Yokkaichi S., Kurosawa M., Okada K., Saito N., and PHENIX C.: "Azimuthal correlations of electrons from heavy-flavor decay with hadrons in $p+p$ and Au+Au collisions at $\sqrt{s_{NN}}=200$ GeV", Phys. Rev. C **83**, No. 4, pp. 044912-1–044912-16 (2011). *

Adare A., Akiba Y., Aoki K., Asai J., Bathe S., Boyle K., Deshpande A., Enyo H., Fukao Y., Goto Y., Hachiya T., Hashimoto K., Ichihara T., Ichimiya R., Ikeda Y., Ishihara M., Mao Y., Miyachi Y., Nakagawa I., Nakamura K., Nakano K., Ralf S., Shibata T., Shoji K., Taketani A., Tanida K., Torii H., Watanabe Y., Yokkaichi S., Kurosawa M., Okada K., Saito N.,

and PHENIX C.: "Cross section and double helicity asymmetry for η mesons and their comparison to π^0 production in $p+p$ collisions at $\sqrt{s}=200$ GeV", Phys. Rev. D **83**, No. 3, pp. 032001-1–032001-11 (2011). *

Adare A., Akiba Y., Aoki K., Asai J., Bathe S., Boyle K., Deshpande A., Enyo H., Fukao Y., Goto Y., Hachiya T., Ichihara T., Ichimiya R., Ikeda Y., Ishihara M., Mao Y., Nakagawa I., Nakano K., Ralf S., Shibata T., Shoji K., Taketani A., Tanida K., Torii H., Watanabe Y., Yokkaichi S., Kurosawa M., Okada K., Saito N., and PHENIX C.: "Measurement of neutral mesons in $p+p$ collisions at $\sqrt{s}=200$ GeV and scaling properties of hadron production", Phys. Rev. D **83**, No. 5, pp. 052004-1–052004-26 (2011). *

Adare A., Akiba Y., Aoki K., Bathe S., Boyle K., Deshpande A., Enyo H., Fukao Y., Goto Y., Hashimoto K., Ichihara T., Ichimiya R., Ikeda Y., Ishihara M., Mao Y., Miyachi Y., Nakagawa I., Nakamura K., Nakano K., Ralf S., Shibata T., Shoji K., Taketani A., Tanida K., Torii H., Watanabe Y., Yokkaichi S., Kurosawa M., Okada K., Saito N., Nakamura T., and PHENIX C.: "Cross Section and Parity-Violating Spin Asymmetries of $W^{\pm}$ Boson Production in Polarized $p+p$ Collisions at $\sqrt{s}=500$ GeV", Phys. Rev. Lett. **106**, No. 6, pp. 062001-1–062001-6 (2011). *

Larin I., McNulty D., Clinton E., Ambrozewicz P., Lawrence D., Nakagawa I., Prok Y., Teymurazyan A., and PrimEx C.: "New Measurement of the π^0 Radiative Decay Width", Phys. Rev. Lett. **106**, No. 16, pp. 162303-1–162303-5 (2011). *

Nakagawa I.: "Experimental Opportunities of ChPT at J-PARC", Proceedings of Science **CD09**, No. 012, pp. 1–8 (2011).

Kojo T., Hidaka Y., Fukushima K., McLerran L., and Pisarski R.: "Interweaving chiral spirals", Nucl. Phys. A **875**, 94–138 (2012). *

(Review)

深尾祥紀: "π^0 粒子生成における Double Helicity Asymmetry 測定による陽子内グルーオン偏極度の研究", 原子核研究 **54**, No. 1, pp. 43–53 (2009).

[Book・Proceedings]

(Original Papers) *Subject to Peer Review

Fukao Y. and PHENIX C.: "Δg measurement at PHENIX", Deep Inelastic Scattering 2006: Proceedings of the 14th International Workshop, Tsukuba, 2006–4, World Scientific Publishing Co Pte Ltd, Toh Tuck Link, pp. 739–742 (2007).

Fukao Y. and PHENIX C.: "Forward upgrade for W physics at RHIC-PHENIX experiment", Proceedings of the XVII International Workshop on Deep-Inelastic Scattering and Related Topics, Madrid, Spain, 2009–4, Science Wise Publishing, , pp. 1–5 (2009).

Oral Presentations

(International Conference etc.)

Fukao Y. and Local Polarimeter .: "Measurement of single transverse-spin asymmetries in forward production of photons and neutrons in pp collisions at $\sqrt{s}$=200 GeV", 15th International Spin Physics Symposium (SPIN 2002), (Brookhaven National Laboratory), New York, USA, Sept. (2002).

Fukao Y. and PHENIX C.: "Probing gluon polarization with π^0's in longitudinally polarized proton collisions at the RHIC-PHENIX experiment", 16th International Spin Physics Symposium (SPIN 2004), (SPIN2004 Committee), Trieste, Italy, Oct. (2004).

Fukao Y. and PHENIX C.: "The overview of the spin physics at RHIC-PHENIX experiment", Particles and Nuclei International Conference (PANIC05), (PANIC05 Committees), Santa Fe, USA, Oct. (2005).

Fukao Y. and PHENIX C.: "Δg measurements at PHENIX", 14th International Workshop on Deep Inelastic Scattering (DIS2006), (DIS2006 Committees), Tsukuba, Apr. (2006).

Fukao Y. and PHENIX C.: "The Phenix forward muon trigger upgrade project for the study of the proton spin", 17th International Workshop on Deep-Inelastic Scattering and Related Subjects (DIS2009), (Universidad Autonoma), Madrid, Spain, Apr. (2009).

Nakagawa I.: "Experimental opportunities of ChPT at J-PARC", 6th International Workshop on Chiral Dynamics, (Bern University), Bern, Switzerland, July (2009).

Fukao Y. and PHENIX C.: "Development and performance evaluation of front-end electronics for forward W trigger at RHIC-PHENIX experiment", 3rd Joint Meeting of the Nuclear Physics Divisions of the APS and JPS (Hawaii 2009), (APS/JPS), Hawaii, USA, Oct. (2009).

Sakata D. and Horaguchi T.: "Optimization of jet finding algorithm in high energy heavy ion collisions with ALICE at LHC", 3rd Joint Meeting of the Nuclear Physics Divisions of the APS and JPS (Hawaii 2009), (APS JPS), Hawaii, USA, Oct. (2009).

Nakagawa I.: "Muon trigger upgrade at PHENIX", 26th Winter Workshop on Nuclear Dynamics, (Michigan State University), Ocho Rios, Jamaica, Jan. (2010).

Akiba Y.: "Experimental Study of Quark Gluon Plasma at RHIC", One-day School and Three+Half-day Symposium on High Energy Strong Interactions (HESI2010),, (YITP, Kyoto University), Kyoto, Aug. (2010).

Fukao Y. and PHENIX C.: "Forward upgrade for W physics at RHIC-PHENIX experiment", 19th International Spin Physics Symposium (SPIN 2010), (Forschungszentrum), Juelich, Germany, Sept.–Oct. (2010).

Yokkaichi S.: "Vector meson measurements from KEK and JPARC", Heavy Ion Meeting 2010-12, (Yonsei Univ and APCTP), Seoul, Korea, Dec. (2010).

Enomoto S., Kou H., Tokuda M., Iwasaki M., Iio M., Itahashi K., Outa H., Onishi H., Sakuma F., Tomono D., Tsukada K., Yamazaki T., Ishimoto S., iwai m., suzuki s., Sekimoto M., Toyoda A., ishikawa t., Sato M., Suzuki T., Hexi s., Tatsuno H., Hashimoto T., Hayano R., fujiwara y., Matsuda Y., Sada Y., Nagae T., Hiraiwa T., Fujioka H., ajimura s., inoue k., Noumi H., sakaguchi a., fukuda t., Mizoi Y., Faso D., Morra O., bragadireanu M., Curceanu C. O., guaraldo c., iliescu M., Okada S., shrghi d., sirghi F., Buehler p., Cargnell M., Ishiwatari T., marton J., Suzuki K., widmann E., Zmeskal J., Bhang H., choi S., yim H., kienle p., busso L., Beer G., and Tanida K.: “Spectroscopic study of Lambda(1405) via the (K-,n) reaction on deuteron”, 2010/12 Osaka Japan, (RCNP), Osaka, Dec. (2010).

Aramaki Y.: “Direct photon production at RHIC”, 19th Particles and Nuclei International Conference (PANIC11), (Laboratory for Nuclear Science (LNS) at the Massachusetts Institute of Technology (MIT)), Cambridge, USA, July (2011).

Komatsu Y., Aoki K., Enyo H., Kanaya J., Kannno K., Masumoto S., Nakai W., Ozawa K., Sekimoto M., Takagi A., Watanabe Y., and Yokkaichi S.: “GEM spectrometer for J-PARC E16 experiment”, 2nd international conference on micro pattern gaseous detectors (MPGD2011), (International organizing committee for MPGD2011), Kobe, Aug.–Sept. (2011).

Yokkaichi S.: “J-PARC E16 experiment and the hadron modification in nuclear matter”, Korea-Japan workshop on nuclear and hadron physics at J-PARC, (Seoul National University), Seoul, Korea, Sept. (2011).

Akiba Y.: “Experimental Summary”, ISMD2011, (Hiroshima University), Miyajima, Hiroshima, JAPAN, Sept. (2011).

Nakamura K.: “Double Spin Asymmetry of Single Electron Production at PHENIX Experiment”, Lake Louise Winter Institute, (University of Alberta), Lake Louise, Canada, Feb. (2012).

(Domestic Conference)

深尾祥紀, Local　Polarimeter .: “RHIC-PHENIX 実験のための Local Polarimeter の開発および Local Polarimeter を用いた光子、中性子生成における single transverse-spin asymmetry の測定”, 日本物理学会第 58 回年次大会, (日本物理学会), 仙台, 3 月 (2003).

深尾祥紀, PHENIX C.: “偏極陽子-陽子衝突における PHENIX Central Arm を用いた π^0 A_{LL} の測定”, 日本物理学会 2003 年秋季大会, (日本物理学会), 宮崎, 9 月 (2003).

深尾祥紀, PHENIX C.: “RHIC-PHENIX 実験における π^0 粒子の double spin asymmetry A_{LL} とイベント構造の研究”, 日本物理学会第 59 回年次大会, (日本物理学会), 福岡, 3 月 (2004).

深尾祥紀, PHENIX C.: “RHIC-PHENIX 実験における π^0 粒子の double helicity asymmetry の系統的研究”, 日本物理学会 2004 年秋季大会, (日本物理学会), 高知, 9 月 (2004).

深尾祥紀, PHENIX C.: “RHIC-PHENIX 実験における π^0 粒子の double helicity asymmetry A_{LL} の測定と陽子内グルーオン偏極度の研究”, 日本物理学会第 61 回年次大会, (日本物理学会), 松山, 3 月 (2006).

黒澤真城, 秋葉康之, 浅井淳吉, Deepak B., 藤原康平, 延與秀人, 狩野博之, 大西宏明, 小貫良行, Charles P., Eugene S., 竹谷篤, 山本義博: “PHENIX シリコンピクセル検出器の宇宙線によるテスト実験”, 日本物理学会 2007 年春季大会, (首都大学東京), 東京, 3 月 (2007).

深尾祥紀, PHENIX C.: “RHIC-PHENIX 実験のための高運動量ミュー粒子トリガー回路の既存読み出し回路への影響と今後の開発”, 日本物理学会第 63 回年次大会, (日本物理学会), 東大阪, 3 月 (2008).

黒澤真城, 秋葉康之, 一宮亮, 延與秀人, 大西宏明, 奥村真樹, 小貫良行, 川嶋基敬, 河西実希, 金谷淳平, 栗田和好, 関本美知子, 竹谷 篤, 藤原 康平, Deepak B., Mannel E. J., Riedler P., PHENIX C.: “PHENIX 実験シリコンピクセル検出器のためのハイブリッドセンサーおよび PILOT チップの品質検査”, 日本物理学会第 63 回年次大会, (近畿大学), 東大阪, 3 月 (2008).

荒巻陽紀, PHENIX C.: “Measurement of neutral pion production at $\sqrt{s_{NN}} = 200$ GeV Au+Au collisions at RHIC-PHENIX”, 日本物理学会 2008 年秋季大会, (山形大学), 盛岡, 9 月 (2008).

飯尾雅実, 板橋健太, 岩崎雅彦, 應田治彦, 大西宏明, 佐久間史典, 佐藤将春, 塚田暁, 友野大, 藤岡宏之, 山崎敏光, 石元茂, 岩井正明, 鈴木祥二, 関本美知子, 豊田晃久, 石川隆, 竜野秀行, 鈴木隆敏, 早野龍五, 松田恭幸, 永江知文, 平岩聡彦, 味村周平, 野海博之, 阪口篤志, 藤原裕也, 徳田真, 千葉順成, 福田共和, 溝井浩, Beer G. A., 方享燦, Choi S., 林熙重, 石渡智一, Buehler P., Cargnelli M., Hirtl A., Kienle P., Marton J., Widmann E., Zmeskal J., 岡田信二, Curceanu C. O., Guaraldo C., Iliescu M., Pietreanu D., Sirghi D., Sirghi F., Faso D., Morra O., Busso L.: “K 中間子原子核探査実験のための液体ヘリウム 3 標的の開発 III”, 日本物理学会 2008 年秋季大会, (日本物理学会), 盛岡 , 9 月 (2008).

羽木洋介, 河西実希, 延與秀人, 秋葉康之, 黒澤真城, 金谷淳平, 栗田和好, 橋本公瑛, 藤原康平, 関本美知子: “PHENIX 用シリコンピクセル検出器の高エネルギー陽子ビームを用いた性能評価”, 日本物理学会第 64 回年次大会, (日本物理学会), 東京, 3 月 (2009).

黒澤真城, PHENIX C.: “PHENIX 実験シリコンバーテックス検出器を用いたスピン物理”, 日本物理学会第 64 回年次大会, (立教大学), 東京, 3 月 (2009).

大竹淑恵: “ULS における干渉実験と微分位相イメージング法の開発の現状”, 第 2 回 C1-3 連携重点課題研究会, (東京大学　物性研究所　中性子科学研究施設), 東海村, 7 月 (2009).

大竹淑恵: “完全結晶を用いた冷中性子実験”, 中性子デバイスとその応用　ワークショップ, (京都大学　原子炉実験所), 京都, 2 月 (2010).

深尾祥紀: “Double helicity asymmetry for π^0 production in polarized p+p collisions at $\sqrt{s} = 200$ GeV”, 日本物理学会第 65 回年次大会, (日本物理学会), 岡山, 3 月 (2010).

坂田洞察, ALICE C.: “LHC-ALICE 実験におけるジェット測定のジェット抑制効果による影響”, 日本物理学会第 65 回年次大会, (日本物理学会), 岡山, 3 月 (2010).

羽木洋介, 河西実希, 延與秀人, 秋葉康之, 黒澤真城, 金谷淳平,

栗田和好, 橋本公瑛, 藤原康平, 関本美知子: "PHENIX シリコンピクセル検出器組み立て後の品質検査", 日本物理学会第 65 回年次大会, (日本物理学会), 岡山, 3 月 (2010).

Baumgart S. L.: "Separation of Charm and Beauty Using the PHENIX-VTX Detector in Simulation", 日本物理学会第 65 回年次大会, (岡山大学), 岡山, 3 月 (2010).

味村周平, Beer G., 方享燦, Bragadireanu M. A., Buehler P., Busso L., Cargnelli M., Choi S., Curceanu C. O., 榎本瞬, Faso D., 藤原裕也, 藤岡宏之, 福田共和, Guaraldo C., 橋本直, 早野龍五, 平岩聡彦, 飯尾雅実, 井上謙太郎, 石川隆, 石元茂, 石渡智一, 板橋健太, 岩井正明, 岩崎雅彦, Kikenle P., 康寛史, Marton J., 松田恭幸, 溝井浩, Morra O., 永江知文, 野海博之, 岡田信二, 大西宏明, 應田治彦, 佐田優太, 阪口篤志, 佐久間史典, 佐藤将春, 関本美知子, Shi H., Sirghi D., Sirghi F., 鈴木謙, 鈴木祥仁, 鈴木隆敏, 竜野秀行, 徳田真, 友野大, 豊田晃久, 塚田暁, Widmann E., 山崎敏光, Yim H., Zmeskal J.: "J-PARC における K 中間子深束縛核探索実験のための TGEM-TPC 開発", 日本物理学会第 65 回年次大会, (日本物理学会), 岡山, 3 月 (2010).

後藤雄二: "PHENIX 実験での $\sqrt{s}$=500GeV 偏極陽子衝突による前方中性子の横スピン非対称度測定", 日本物理学会第 65 回年次大会, (日本物理学会), 岡山, 3 月 (2010).

Baumgart S. L.: "Recent Progress in Open Heavy Flavor in Heavy-Ion Collisions", Heavy Ion Cafe at Tokyo, CNS, (東京大学原子核科学研究センター), 東京, 6 月 (2010).

青木和也: "J-PARC E16 experiment", Workshop "Dielectron experiments at GSI and KEK/J-PARC", (新学術領域「多彩なフレーバーで探る新しいハドロン存在形態の包括的研究」総括班), 東海村, 6 月 (2010).

大竹淑恵: "結晶モノクロメータによる中性子干渉計の開発研究", 第 5 回先進原子力科学技術に関する連携重点研究討論会, (日本原子力研究開発機構, 東京大学大学院原子力専攻), 東海村, 8 月 (2010).

Baumgart S. L.: "Recent Progress in Open Heavy-Flavor Studies at RHIC and Future Prospects at RHIC and LHC", Heavy Ion Pub at Nagoya University, (名古屋大学), 名古屋, 8–8 月 (2010).

榎本瞬, 康寛史, 徳田真, 岩崎雅彦, 飯尾雅実, 板橋健太, 應田治彦, 大西宏明, 佐久間史典, 友野大, 塚田暁, 山崎敏光, 石元茂, 関本美知子, 豊田晃久, 佐藤将春, 鈴木隆敏, 竜野秀行, 橋本直, 早野龍五, 松田恭幸, 佐田優太, 永江知文, 平岩聡彦, 藤岡宏之, 野海博之, 溝井浩, Curceanu C. O., 岡田信二, 石渡智一, 鈴木謙, Zmeskal J., 方享燦, Beer G., 谷田聖, J-PARC E15/E17/E31 C.: "d(K-,n) 反応を用いた Lambda(1405) 分光実験のための陽子検出器の開発 (2)", 日本物理学会 2010 年秋季大会, (日本物理学会), 北九州, 9 月 (2010).

青木和也, 四日市悟, 金谷淳平, 桝本新一, 小松雄哉: "J-PARC E16 実験の為の、ハドロン・ブラインド検出器の開発", 日本物理学会 2010 年秋季大会, (九州工業大学), 北九州, 9 月 (2010).

康寛史, 徳田真, 岩崎雅彦, 飯尾雅実, 板橋健太, 應田治彦, 大西宏明, 佐久間史典, 友野大, 塚田暁, 山崎敏光, 石元茂, 関本美知子, 豊田晃久, 佐藤将春, 鈴木隆敏, 竜野秀行, 橋本直, 早野龍五, 松田恭幸, 佐田優太, 永江知文, 平岩聡彦, 藤岡宏之, 榎本瞬, 野海博之, 溝井浩, Curceanu C. O., 岡田信二, 石渡智一, 鈴木謙, Zmeskal J., 方享燦, Beer G., 谷田聖, J-PARC E15/E17/E31 C.: "J-PARC K1.8BR ビームラインにおける K ビーム調整 (2)", 日本物理学会 2010 年秋季大会, (日本物理学会), 北九州, 9 月 (2010).

深尾祥紀, 今津義充, 庄司幸平, 竹谷篤, 中川格, Ralf S., 中村克朗, 齊藤直人, 三部勉, 谷田聖, 廣田誠子, PHENIX Collaboration .: "PHENIX muon arm trigger upgrade (II) ビーム、宇宙線を用いた性能評価", 日本物理学会 2010 年秋季大会, (日本物理学会), 北九州, 9 月 (2010).

中川格: "PHENIX Muon Trigger Upgrade (III) ューオントラッカーの性能改善", 日本物理学会 2010 年秋季大会, (日本物理学会), 北九州, 9 月 (2010).

荒巻陽紀, PHENIX C.: "Study of parton energy loss with high-pT pi0 in Au+Au collisions at PHENIX", 日本物理学会 2010 年秋季大会, (九州工業大学), 北九州, 9 月 (2010).

後藤雄二, 澤田真也, 柴田利明, 中野健一, 宮坂翔, 宮地義之, 竹谷篤: "Fermilab-E906/SeaQuest 実験の立ち上げの現状", 日本物理学会 2010 年秋季大会, (日本物理学会), 北九州, 9 月 (2010).

佐田優太, 味村周平, Beer G., 方享燦, Bragadireanu M. A., Buehler P., Busso L., Cargnelli M., Choi S., Curceanu C. O., 榎本瞬, Faso D., 藤岡宏之, 藤原裕也, 福田共和, Guaraldo C., 橋本直, 早野龍五, 平岩聡彦, 飯尾雅実, 井上謙太郎, 石黒洋輔, 石川隆, 石元茂, 石渡智一, 板橋健太, 岩井正明, 岩崎雅彦, 川崎信吾, Kikenle P., 康寛史, Marton J., 松田恭幸, 溝井浩, Morra O., 永江知文, 野海博之, 大西宏明, 岡田信二, 應田治彦, 阪口篤志, 佐久間史典, 佐藤将春, 関本美知子, Shi H., Sirghi D., Sirghi F., 鈴木謙, 鈴木祥仁, 鈴木隆敏, 竜野秀行, 徳田真, 友野大, 豊田晃久, 塚田暁, Widmann E., 山崎敏光, Yim H., Zmeskal J.: "J-PARC E15 実験に用いる円筒形検出器群のコミッショニング", 日本物理学会 2010 年秋季大会, (日本物理学会), 北九州市, 9 月 (2010).

飯尾雅実, 板橋健太, 岩崎雅彦, 應田治彦, 大西宏明, 佐久間史典, 友野大, 塚田暁, 山崎敏光, 榎本瞬, 石橋直哉, 井上謙太郎, 阪口篤志, 吉田幸太郎, 味村周平, 野海博之, 石元茂, 岩井正明, 鈴木祥二, 関本美知子, 豊田晃久, 石川隆, 佐藤将春, 鈴木隆敏, 施赫將, 竜野秀行, 橋本直, 早野龍五, 藤原裕也, 松田恭幸, 康寛史, 徳田真, 永江知文, 平岩聡彦, 藤岡宏之, 佐田優太, 福田共和, 溝井浩, Faso D., Morra O., Bragadireanu M., Curceanu C. O., Guaraldo C., Iliescu M., 岡田信二, Pietreanu D., Sirghi D., Sirghi F., Buehler P., Cargnelli M., 石渡智一, Marton J., Widmann E., Zmeskal J., 鈴木謙, 方享燦, Choi S., 林熙重, Kienle P., Busso L., Beer G. A.: "Λ (1405) 精密分光のための重水素標的の開発 (1)", 日本物理学会 2010 年秋季大会, (日本物理学会), 北九州, 9 月 (2010).

佐田優太, 味村周平, Beer G., 方享燦, Bragadireanu M. A., Buehler P., Busso L., Cargnelli M., Choi S., Curceanu C. O., 榎本瞬, Faso D., 藤岡宏之, 藤原裕也, 福田共和,

Guaraldo C., 橋本直, 早野龍五, 平岩聡彦, 飯尾雅実, 井上謙太郎, 石黒洋輔, 石川隆, 石元茂, 石渡智一, 板橋健太, 岩井正明, 岩崎雅彦, 川崎信吾, Kikenle P., 康寛史, Marton J., 松田恭幸, 溝井浩, Morra O., 永江知文, 野海博之, 大西宏明, 岡田信二, 應田治彦, 阪口篤志, 佐久間史典, 佐藤将春, 関本美知子, Shi H., Sirghi D., Sirghi F., 鈴木謙, 鈴木祥仁, 鈴木隆敏, 竜野秀行, 徳田真, 友野大, 豊田晃久, 塚田暁, Widmann E., 山崎敏光, Yim H., Zmeskal J.: "K1.8BR beamline の円筒型検出器群 (CDS) の commissioning について", KEK 理論センター研究会「ストレンジネス核物理 2010」, (高エネルギー加速器研究機構 素粒子原子核研究所), つくば市, 12 月 (2010).

關義親, 宇田純郎, 舟橋春彦, 日野正裕, 北口雅暁, 大竹淑恵, 清水裕彦, 竹谷薫: "2 経路を完全分離した多層膜冷中性子干渉計の開発", 日本中性子科学会第 10 回年会, (日本中性子科学会), 仙台, 12 月 (2010).

關義親: "2 経路完全分離型多層膜冷中性子干渉計の開発", 中性子制御デバイスとその応用 IV, (京都大学原子炉実験所), 大阪府熊取町, 2 月 (2011).

大竹淑恵: "中性子干渉イメージング", 中性子制御デバイスとその応用 IV, (京都大学 原子炉実験所), 大阪府熊取町, 2 月 (2011).

轟木貴人: "Long range rapidity correlations in high energy nucleus collisions at RHIC and LHC", 第 11 回 Heavy Ion Pub, (大阪大学, 広島大学, 名古屋大学), 豊中, 2 月 (2011).

關義親: "2 経路完全分離型多層膜中性子干渉計の開発", 小角・反射率・高分解能装置研究会, (東京大学物性研究所), 柏, 2 月 (2011).

四日市悟: "Project C01 and J-PARC E16 spectrometer", 2010 年度「多彩なフレーバーで探る新しいハドロン存在形態の包括的研究」領域研究会, (新学術領域「多彩なフレーバーで探る新しいハドロン存在形態の包括的研究」総括班), 和光, 2–3 月 (2011).

蜂谷崇, 黒澤真城, 竹谷篤, 藤原康平, 二宮一史, 秋葉康之, 金谷淳平, Baumgart S. L., 秋元亮二, 浅野秀光, 栗田和好, 西尾悠法, 渡邉健太郎, 今井憲一, 佐藤進, 佐甲博之, 関本美知子, Pancaker C., Shafto E., Apadula N., Mannel E. J., Gastaldi F., Deapier O., Sahlmuller B., Lewis B., Koster J., Stepanov M., Shaver A., Bowen J., Bryslawskyj J.: "PHENIX シリコン崩壊点飛跡検出器 (VTX) の組立と設置", 日本物理学会第 66 回年次大会, (日本物理学会), 新潟, 3 月 (2011).

浅野秀光, 黒澤真城, 竹谷篤, 藤原康平, 二宮一史, 秋葉康之, 金谷淳平, 蜂谷崇, Baumgart S. L., 秋元亮二, 栗田和好, 西尾悠法, 渡邉健太郎, 今井憲一, 佐藤進, 佐甲博之, 関本美知子, Pancaker C., Shafto E., Apadula N., Mannel E. J., Gastaldi F., Deapier O., Sahlmuller B., Lewis B., Koster J., Stepanov M., Shaver A., Bowen J., Bryslawskyj J.: "偏極陽子衝突ビームを用いた PHENIX 崩壊点飛跡検出器 (VTX) のコミッショニング", 日本物理学会第 66 回年次大会, (日本物理学会), 新潟, 3 月 (2011).

浅野秀光, 秋葉康之, 金谷淳平, 黒澤真城, 竹谷篤, 蜂谷崇, Koster J., 秋元亮二, Stephen B., 栗田和好, 今井憲一, 佐甲博之, 佐藤進, 関本美知子, 藤原康平, Baldo S., Benji L., Chuck P., Eugene S., Nicole A., Eric .., Franck G., Olivier D., Mikhail S., Alexander S., James B., Jason B.: "偏極陽子衝突ビームを用いた PHENIX 崩壊点飛跡検出器 VTX) のコ ミッショニング", 日本物理学会第 66 回年次大会, (社団法人 日本物理学会), 新潟, 3 月 (2011).

黒澤真城, 竹谷篤, 藤原康平, 二宮一史, 秋葉康之, 金谷淳平, 蜂谷崇, Baumgart S. L., 秋元亮二, 浅野秀光, 栗田和好, 西尾悠法, 渡邉健太郎, 今井憲一, 佐藤進, 佐甲博之, 関本美知子, Pancaker C., Shafto E., Apadula N., Mannel E. J., Gastaldi F., Deapier O.: "PHENIX シリコン崩壊点飛跡測定器（VTX）ピクセル検出器モジュールの量産完成報告", 日本物理学会第 66 回年次大会, (日本物理学会), 新潟, 3 月 (2011).

蜂谷崇, 秋葉康之, 黒澤真城, 竹谷篤, Baumgart S. L., 浅野秀光, 秋元亮二, 佐藤進, 佐甲博之, 関本美知子, 藤原康平, 金谷淳平, 栗田和好, 二ノ宮一史, 西尾悠法, 今井憲一, Pancake C., Shafto E., Apadula N., Lewis B., Sahlmuller B., Mannel E. J., Gastaldi F., Drapier O., Koster J., Stepanov M.: "PHENIX シリコン崩壊点飛跡検出器 (VTX) の組立と設置", 日本物理学会第 66 回年次大会, (日本物理学会), 新潟, 3 月 (2011).

井上謙太郎, 康寛史, 徳田真, 岩崎雅彦, 飯尾雅実, 板橋健太, 應田治彦, 大西宏明, 佐久間史典, 友野大, 塚田暁, 山崎敏光, 石元茂, 岩井正明, 鈴木祥仁, 関本美知子, 豊田晃久, 石川隆, 佐藤将春, 鈴木隆敏, Hexi s., 竜野秀行, 橋本直, 早野龍五, 藤原裕也, 松田恭幸, 佐田優太, 永江知文, 平岩聡彦, 藤岡宏之, 味村周平, 榎本瞬, 野海博之, 阪口篤志, 福田共和, 溝井浩, Faso D., Morra O., bragadireanu M., Curceanu C. O., guaraldo c., iliescu M., 岡田信二, shrghi d., sirghi F., Buehler p., Cargnell M., 石渡智一, marton J., 鈴木謙, widmann E., Zmeskal J., 方享燦, choi S., yim H., kienle p., busso L., Beer G., 谷田聖: "J-PARC E-31 実験における後方散乱陽子飛跡検出 の設計開発と Geant4 Simulation", 日本物理学会第 66 回年次大会, (日本物理学会), 新潟, 3 月 (2011).

榎本瞬, 康寛史, 徳田真, 岩崎雅彦, 飯尾雅実, 板橋健太, 應田治彦, 大西宏明, 佐久間史典, 友野大, 塚田暁, 山崎敏光, 石元茂, 岩井正明, 鈴木祥仁, 関本美知子, 豊田晃久, 石川隆, 佐藤将春, 鈴木隆敏, Hexi s., 竜野秀行, 橋本直, 早野龍五, 藤原裕也, 松田恭幸, 佐田優太, 永江知文, 平岩聡彦, 藤岡宏之, 味村周平, 井上謙太郎, 野海博之, 阪口篤志, 福田共和, 溝井浩, Faso D., Morra O., bragadireanu M., Curceanu C. O., guaraldo c., iliescu M., 岡田信二, shrghi d., sirghi F., Buehler p., Cargnell M., 石渡智一, marton J., 鈴木謙, widmann E., Zmeskal J., 方享燦, choi S., yim H., kienle p., busso L., Beer G., 谷田聖: "d(K-,n) 反応を用いた Lambda(1405) 分光実験のための陽子検出器の開発 (3)", 日本物理学会第 66 回年次大会, (日本物理学会), 新潟, 3 月 (2011).

今津義充, 深尾祥紀, 唐津謙一, 栗田和好, 齊藤直人, 庄司幸平, 竹谷篤, 谷田聖, 中川格, 中村克朗, 廣田誠子, 三部勉, 村上哲也, 村田次郎, Ralf S., 渡邉健太郎: "PHENIX Muon Arm Upgrade(2) PHENIX 実験における μ 粒子飛跡検出器の性能改善策とその評価", 日本物理学会第 66 回年次大会, (日本物理学会), 新潟, 3 月 (2011).

二宮一史, 竹谷篤, 西尾悠法, 渡邉健太郎, 秋山岳伸, 小川就也,

川村広和, 岸礼子, 秦麻記, 村田次郎: “ピコ精度画像処理型変位計を用いた近距離重力実験 IV”, 日本物理学会第 66 回年次大会, (日本物理学会), 新潟, 3 月 (2011).

佐田優太, 味村周平, Beer G., 方享燦, Bragadireanu M. A., Buehler P., Busso L., Cargnelli M., Choi S., Curceanu C. O., 榎本瞬, Faso D., 藤岡宏之, 藤原裕也, 福田共和, Guaraldo C., 橋本直, 早野龍五, 平岩聡彦, 飯尾雅実, 井上謙太郎, 石黒洋輔, 石川隆, 石元茂, 石渡智一, 板橋健太, 岩井正明, 岩崎雅彦, 川崎信吾, Kikenle P., 康寛史, Marton J., 松田恭幸, 溝井浩, Morra O., 永江知文, 野海博之, 大西宏明, 岡田信二, 應田治彦, 阪口篤志, 佐久間史典, 佐藤将春, 関本美知子, Shi H., Sirghi D., Sirghi F., 鈴木謙, 鈴木祥仁, 鈴木隆敏, 竜野秀行, 徳田真, 友野大, 豊田晃久, 塚田暁, Widmann E., 山崎敏光, Yim H., Zmeskal J.: “J-PARC E15 実験に用いる円筒形検出器群のコミッショニング（2）”, 日本物理学会第 66 回年次大会, (日本物理学会), 新潟, 3 月 (2011).

徳田真, 味村周平, Beer G., 方享燦, Bragadireanu M. A., Buehler P., Busso L., Cargnelli M., Choi S., Curceanu C. O., 榎本瞬, Faso D., 藤岡宏之, 藤原裕也, 福田共和, Guaraldo C., 橋本直, 早野龍五, 平岩聡彦, 飯尾雅実, 井上謙太郎, 石黒洋輔, 石川隆, 石元茂, 石渡智一, 板橋健太, 岩井正明, 岩崎雅彦, 川崎信吾, Kikenle P., 康寛史, Marton J., 松田恭幸, 溝井浩, Morra O., 永江知文, 野海博之, 大西宏明, 岡田信二, 應田治彦, 阪口篤志, 佐田優太, 佐久間史典, 佐藤将春, 関本美知子, Shi H., Sirghi D., Sirghi F., 鈴木謙, 鈴木祥仁, 鈴木隆敏, 竜野秀行, 友野大, 豊田晃久, 塚田暁, Widmann E., 山崎敏光, Yim H., Zmeskal J.: “J-PARC における K 中間子深束縛核探索実験（E15 実験）のための TGEM-TPC の開発 II”, 日本物理学会第 66 回年次大会, (日本物理学会), 新潟, 3 月 (2011).

關義親, 大竹淑恵, 広田克也, 安達智宏, 山形豊, 朱正明, 森田晋也, 岩下芳久, 市川雅浩, 北口雅暁, 日野正裕, 高橋敏男, 吉沢英樹, Lee S. W., Olbinado M. P., 矢代航, 百生敦: “中性子微分位相コントラストイメージング法の開発”, 日本物理学会第 66 回年次大会, (日本物理学会), 新潟, 3 月 (2011).

四日市悟: “Hadron modification at finite density”, 新学術領域 「素核宇宙融合」×「新ハドロン」クロスオーバー研究会, (新学術領域 「素核宇宙融合」&「新ハドロン」), 神戸, 6 月 (2011).

黒澤真城, 秋葉康之, 秋元亮二, 浅野秀光, 榎園昭智, 蜂谷崇, 佐甲博之, 佐藤進, 竹谷篤, Bathe S., Boyle K., Koster J., Mannel E. J., Nouicer R., Pancake C., Sondheim W.: “RHIC-PHENIX 実験のためのシリコン崩壊点検出器完成設置報告”, 日本物理学会 2011 年秋季大会, (社団法人　日本物理学会), 弘前, 9 月 (2011).

今津義充, 深尾祥紀, 庄司幸平, 竹谷篤, 中川格, Ralf S., PHENIX Collaboration .: “PHENIX Muon Tracking Chamber の性能改善 (I)”, 日本物理学会 2011 年秋季大会, (日本物理学会), 弘前, 9 月 (2011).

秋元亮二, 秋葉康之, 浅野秀光, 蜂谷崇, 佐甲博之, 佐藤進, 竹谷篤, 黒澤真城, Koster J., Baumgart S. L., PHENIX C.: “PHENIX 崩壊点飛跡検出器の性能評価”, 日本物理学会 2011 年秋季大会, (社団法人　日本物理学会), 弘前, 9 月 (2011).

秋葉康之: “Recent Results from RHIC and future plans”, 日本物理学会 2011 年秋季大会, (日本物理学会), 弘前, 9 月 (2011).

蜂谷崇, the　PHENIX c.: “RHIC-PHENIX 実験におけるシリコン崩壊点検出器 (VTX) による飛跡検出と粒子識別”, 日本物理学会 2011 年秋季大会, (日本物理学会), 弘前, 9 月 (2011).

轟木貴人: “Two particle correlations with higher harmonic reaction plane in Au+Au 200 GeV collisions at RHIC-PHENIX”, 日本物理学会 2011 年秋季大会, (日本物理学会), 弘前, 9 月 (2011).

坂田洞察: “Jet measurements with ALICE experiment at the LHC”, 日本物理学会 2011 年秋季大会, (日本物理学会), 弘前, 9 月 (2011).

浅野秀光, PHENIX　collaboratio .: “RHIC-PHENIX 実験におけるシリコン崩壊点検出器 (VTX) のアライメント”, 日本物理学会 2011 年秋季大会, (一般社団法人　日本物理学会), 弘前, 9 月 (2011).

後藤雄二: “核子構造の物理の将来”, 日本物理学会 2011 年秋季大会, (日本物理学会), 弘前, 9 月 (2011).

四日市悟: “E16 and High Momentum Beam Line”, HUA Workshop for the Future of the Hadron Hall, (J-PARC ハドロンホールユーザー会), Tsukuba, 10 月 (2011).

後藤雄二: “核子スピン構造の研究の進展”, 第 2 回総合スピン科学シンポジウム, (山形大学), 山形, 10 月 (2011).

小松雄哉, 青木和也, 荒巻陽紀, 桝本新一,　木敦子, 高橋智則, 四日市悟, 小沢恭一郎, 中井恒, 菅野光樹, 関本美知子: “J-PARC E16 実験のための GEM Tracker 開発の現状”, 第 8 回「マイクロパターンガス検出器 (MPGD) 研究会」, (近畿大学、高エネルギー加速器研究機構　測定器開発室), 東大阪, 12 月 (2011).

青木和也, 荒巻陽紀, 菅野光樹, 小松雄哉, 桝本新一, 小沢恭一郎, 関本美知子,　木敦子, 高橋智則, 四日市悟: “J-PARC E16 実験の為のハドロンブラインド検出器の開発”, 第 8 回「マイクロパターンガス検出器 (MPGD) 研究会」, (近畿大学), 東大阪, 12 月 (2011).

四日市悟: “project C01:Vector meson measurements in nuclei”, 2011 年度「多彩なフレーバーで探る新しいハドロン存在形態の包括的研究」領域研究会, (新学術領域「新ハドロン」総括班), 吹田, 2 月 (2012).

蜂谷崇: “RHIC-PHENIX 実験におけるシリコン崩壊点検出器 (VTX) による飛跡検出”, 日本物理学会第 67 回年次大会, (日本物理学会), 西宮, 3 月 (2012).

土井琢身, 青木慎也, 初田哲男, 池田陽一, 井上貴史, 石井理修, 村野啓子, 根村英克, 佐々木健志: “Cutoff effects on Three-Nucleon Forces in Lattice QCD”, 日本物理学会第 67 回年次大会, (日本物理学会), 西宮市, 3 月 (2012).

今津　義充,　生出　秀行,　庄司　幸平,　中川　格,　Ralf S., PHENIX　Collaboratio .: “RHIC-PHENIX 実験における W ボゾン生成非対称性の測定 (I) W ボソン測定に係る μ 粒子飛跡検出器の性能向上〜”, 日本物理学会第 67 回年次大会, (日本物理学会), 西宮, 3 月 (2012).

浅野秀光, PHENIX　collaboratio .: “RHIC-PHENIX 実験におけるシリコン崩壊点検出器 (VTX) のアライメン

ト", 日本物理学会第 67 回年次大会, (一般社団法人日本物理学会), 西宮市, 3 月 (2012).

Advanced Meson Science Laboratory

Publications

[**Journal**]

(Original Papers) *Subject to Peer Review

Mihara M., Izumikawa T., Ueno H., Matsuta K., Nishimura D., Nagatomo T., Moriguchi T., Ito Y., Nagae D., Fukuda M., Yoshimi A., Yamada K., Takechi M., Ichikawa Y., Momota S., Hirayama Y., Ohtsubo T., Suzuki S., Ozawa A., Ishibashi Y., Kubo T., Ooishi H., Namiki Y., Hachiuma K., Namihira K., Horikawa D., Minamisono T., Yamaguchi T., Kuboki T., Suzuki T., Sato K., Kobayashi Y., and Asahi K.: "Beta-NMR measurement of 58Cu in Si", Hyperfine Interact. **197**, 143–147 (2010). *

Nagatomo T., Ueno H., Mihara M., Matsuta K., Yoshimi A., Ichikawa Y., Yamada K., Kawamura H., Ozawa A., Moriguchi T., Ishibashi Y., Asahi K., Uchida M., Suzuki K., Inoue T., Hasama Y., Iijima H., Sumikama T., Fukuda M., and Minamisono T.: "Precise nuclear moments of extremely proton-rich nuclus 23Al", Hyperfine Interact. **198**, 103–107 (2010). *

Hiyama E., Kamimura M., Yamamoto Y., and Motoba T.: "Five-body cluster structure of the double-Λ hypernucleus $^{11}_{\Lambda\Lambda}$Be", Phys. Rev. Lett. **104**, 212502-1–212502-4 (2010). *

Hiyama E., Kamimura M., Yamamoto Y., Motoba T., and Rijken T. A.: "S = -1 hypernuclear structure", Prog. Theor. Phys. Suppl. **185**, 106–151 (2010). *

Hiyama E., Kamimura M., Yamamoto Y., Motoba T., and Rijken T. A.: "S = -2 hypernuclear structure", Prog. Theor. Phys. Suppl. **185**, 152–196 (2010). *

Koike T. and Harada T.: "Formation of the Essential Kaonic Nucleus, $K^{-}pp$", Prog. Theor. Phys. Suppl., No. 186, pp. 367–372 (2010). *

Matsuba H., Yagi E., Sugi C., Okada Y., Hirabayashi K., Iida T., Koike S., Hayashi T., Higami N., Murakami Y., Takebayashi A., Yoshida T., Sugawara T., Shishido T., and Ogiwara K.: "Site occupancies of hydrogen in Nb alloyed with oversized Ta atoms or undersized Mo atoms", J. Phys. Soc. Jpn. **80**, 104602-1–104602-8 (2011). *

Andresen G. B., Ashkezari M. D., Baquero-Ruiz M., Bowe P. D., Butler E., Cesar C., Charlton M., Deller A., Eriksson S., Fujiwara M., Hayano R., Hayden M. E., Humphries A. J., Hydomako R., Jonsell S., Kemp S. L., Robicheaux F., Sarid E., Silveira D. D., Storey J. W., Thompson R. I., van der Werf D. P., and Yamazaki Y.: "Confinement of antihydrogen for 1,000 seconds", Nat. Phys. **7**, 558–564 (2011). *

Yoshimi K., Naya Y., Mitani N., Kato T., Inoue M., Natori S., Takahashi T., Weitemier A. Z., Nishikawa N., McHugh T. J., Einaga Y., and Kitazawa S.: "Phasic reward responses in the monkey striatum as detected by voltammetry with diamond microelectrodes", Neurosci. Res. **71**, No. 1, pp. 49–62 (2011). *

Skuma K., Higami N., and Yagi E.: "Atomistic state of hydrogen trapped by vacancies and formation of H-associated vacancy clusters in Nb as observed by the channelling method", ISIJ Int. **52**, No. 2, pp. 187–197 (2012). *

(Review)

多田司: "素粒子概論 1", Radioisotopes **60**, No. 6, pp. 241–248 (2011).

多田司: "素粒子概論 2", Radioisotopes **60**, No. 10, pp. 417–431 (2011).

多田司: "素粒子概論 3", Radioisotopes **60**, No. 12, pp. 527–532 (2011).

佐久間史典, 鈴木隆敏: "J-PARC における反 K 中間子原子核の研究", 原子核研究 **55**, No. 2, pp. 47–59 (2011).

Oral Presentations

(International Conference etc.)

Iwasaki M.: "Experimental study to search for kaonic nuclear states", 10th International Workshop on Meson Production, Properties and Interaction (MESON2008), (Jagiellonian University, Cracow), Krakow, Poland, June (2008).

Iwasaki M.: "ϕ mass shift in nuclei", International Conference on Exotic Atoms (EXA2008), (Stefan Meyer Institute for Subatomic Physics), Vienna, Austria, Sept. (2008).

Iwasaki M.: "RIKEN J-PARC center and its physics objectives", ECT International Workshop on Hadronic Atoms and Kaonic Nuclei Solved Puzzles, Open Problems and Future Challenges in Theory and Experiment, (Laboratori Nazionali di Frascati), Trento, Italy, Oct. (2009).

Iwasaki M.: "Development of new muon source for muon g-2 measurement and muon magnetic microscope", Advanced Science Research Symposium 2009 (ASR2009): Positron, Muon and other exotic particle beams for materials and atomic/molecular sciences, (Japan Atomic Energy Agency), Tokai, Nov. (2009).

Sakuma F. and Tokuda M.: "Development of Thick-GEMs for GEM-TPC Tracker", 1st International Workshop towards the Giant Liquid Argon Charge Imaging Experiment (GLA2010), (KEK), Tsukuba, Mar. (2010).

Sakuma F.: "A search for double anti-kaon production in antiproton-3He annihilation at J-PARC", Germany, Munich, 2010/5, (Technical University Munich), Munich, Germany, May (2010).

Sakuma F.: "Current status of the thick-GEM TPC for the J-PARC E15 experiment", Germany, Munich, 2010/5, (Technical University Munich), Munich, Germany, May (2010).

Iwasaki M.: "R&D of Laser resonant ionization at RIKEN-RAL", 1st g-2/EDM collaboration meeting, (High Energy Accelerator Research Organization), Tsukuba, June (2010).

Iwasaki M.: "g-2@J-PARC", 1st workshop on Intensity

Frontier of Muon Fundamental Science, (High Energy Accelerator Research Organization), Tsukuba, June (2010).

Sakuma F.: "A search for double anti-kaon production in antiproton 3He annihilation at J-PARC", ECT*, (ECT*), Trento, Italy, Oct. (2010).

Enomoto S., Kou H., Tokuda M., Iwasaki M., Iio M., Itahashi K., Outa H., Onishi H., Sakuma F., Tomono D., Tsukada K., Yamazaki T., Ishimoto S., iwai m., suzuki s., Sekimoto M., Toyoda A., ishikawa t., Sato M., Suzuki T., Hexi s., Tatsuno H., Hashimoto T., Hayano R., fujiwara y., Matsuda Y., Sada Y., Nagae T., Hiraiwa T., Fujioka H., ajimura s., inoue k., Noumi H., sakaguchi a., fukuda t., Mizoi Y., Faso D., Morra O., bragadireanu M., Curceanu C. O., guaraldo c., iliescu M., Okada S., shrghi d., sirghi F., Buehler p., Cargnell M., Ishiwatari T., marton J., Suzuki K., widmann E., Zmeskal J., Bhang H., choi S., yim H., kienle p., busso L., Beer G., and Tanida K.: "Spectroscopic study of Lambda(1405) via the (K-,n) reaction on deuteron", 2010/12 Osaka Japan, (RCNP), Osaka, Dec. (2010).

Sakuma F., Curceanu C. O., Iwasaki M., Kienle P., Onishi H., Tokuda M., Tsukada K., Widmann E., Yamazaki T., and Zmeskal J.: "Double antikaonic nuclear clusters in antiproton-3He annihilation at J-PARC", 10th International Conference on Low Energy Antiproton Physics (LEAP2011), (TRIUMF), Vancouver, Canada, Apr.–May (2011).

(Domestic Conference)

黒澤真城, 秋葉康之, 浅井淳吉, Deepak B., 藤原康平, 延與秀人, 狩野博之, 大西宏明, 小貫良行, Charles P., Eugene S., 竹谷篤, 山本義博: "PHENIX シリコンピクセル検出器の宇宙線によるテスト実験", 日本物理学会 2007 年春季大会, (首都大学東京), 東京, 3 月 (2007).

黒澤真城, 秋葉康之, 一宮亮, 延與秀人, 大西宏明, 奥村真樹, 小貫良行, 川嶋基敬, 河西実希, 金谷淳平, 栗田和好, 関本美知子, 竹谷 篤, 藤原 康平, Deepak B., Mannel E. J., Riedler P., PHENIX C.: "PHENIX 実験シリコンピクセル検出器のためのハイブリッドセンサーおよび PILOT チップの品質検査", 日本物理学会第 63 回年次大会, (近畿大学), 東大阪, 3 月 (2008).

飯尾雅実, 板橋健太, 岩崎雅彦, 應田治彦, 大西宏明, 佐久間史典, 佐藤将春, 塚田暁, 友野大, 藤岡宏之, 山崎敏光, 石元茂, 岩井正明, 鈴木祥二, 関本美知子, 豊田晃久, 石川隆, 竜野秀行, 鈴木隆敏, 早野龍五, 松田恭幸, 永江知文, 平岩聡彦, 味村周平, 野海博之, 阪口篤志, 藤原裕也, 徳田真, 千葉順成, 福田共和, 溝井浩, Beer G. A., 方享燦, Choi S., 林熙重, 石渡智一, Buehler P., Cargnelli M., Hirtl A., Kienle P., Marton J., Widmann E., Zmeskal J., 岡田信二, Curceanu C. O., Guaraldo C., Iliescu M., Pietreanu D., Sirghi D., Sirghi F., Faso D., Morra O., Busso L.: "K 中間子原子核探査実験のための液体ヘリウム 3 標的の開発 III", 日本物理学会 2008 年秋季大会, (日本物理学会), 盛岡, 9 月 (2008).

佐久間史典: "E16 実験における KK 対測定の検討", 新学術領域「多彩なフレーバーで探る新しいハドロン存在形態の包括的研究」2009 年度領域研究会, (名古屋大学), 名古屋, 11 月 (2009).

徳田真, 佐久間史典, 岩崎雅彦: "J-PARC E15 実験における TPC のための TGEM 開発 2009", 第 6 回「マイクロパターンガス検出器 (MPGD) 研究会」, (神戸大学、KEK 測定器開発室), 神戸, 12 月 (2009).

味村周平, Beer G., 方享燦, Bragadireanu M. A., Buehler P., Busso L., Cargnelli M., Choi S., Curceanu C. O., 榎本瞬, Faso D., 藤原裕也, 藤岡宏之, 福田共和, Guaraldo C., 橋本直, 早野龍五, 平岩聡彦, 飯尾雅実, 井上謙太郎, 石川隆, 石元茂, 石渡智一, 板橋健太, 岩井正明, 岩崎雅彦, Kikenle P., 康寛史, Marton J., 松田恭幸, 溝井浩, Morra O., 永江知文, 野海博之, 岡田信二, 大西宏明, 應田治彦, 佐田優太, 阪口篤志, 佐久間史典, 佐藤将春, 関本美知子, Shi H., Sirghi D., Sirghi F., 鈴木謙, 鈴木祥仁, 鈴木隆敏, 竜野秀行, 徳田真, 友野大, 豊田晃久, 塚田暁, Widmann E., 山崎敏光, Yim H., Zmeskal J.: "J-PARC における K 中間子深束縛核探索実験のための TGEM-TPC 開発", 日本物理学会第 65 回年次大会, (日本物理学会), 岡山, 3 月 (2010).

佐久間史典: "Results of KEK-PS E325 experiment", 第 3 回「ハドロン・スクエア」, 東海村, 6 月 (2010).

佐久間史典: "A search for double anti-kaon production in antiproton-3He annihilation at J-PARC", Workshop on Strangeness in Nuclei, 和光, 6 月 (2010).

榎本瞬, 康寛史, 徳田真, 岩崎雅彦, 飯尾雅実, 板橋健太, 應田治彦, 大西宏明, 佐久間史典, 友野大, 塚田暁, 山崎敏光, 石元茂, 関本美知子, 豊田晃久, 佐藤将春, 鈴木隆敏, 竜野秀行, 橋本直, 早野龍五, 松田恭幸, 佐田優太, 永江知文, 平岩聡彦, 藤岡宏之, 野海博之, 溝井浩, Curceanu C. O., 岡田信二, 石渡智一, 鈴木謙, Zmeskal J., 方享燦, Beer G., 谷田聖, J-PARC E15/E17/E31 C.: "d(K-,n) 反応を用いた Lambda(1405) 分光実験のための陽子検出器の開発 (2)", 日本物理学会 2010 年秋季大会, (日本物理学会), 北九州, 9 月 (2010).

康寛史, 徳田真, 岩崎雅彦, 飯尾雅実, 板橋健太, 應田治彦, 大西宏明, 佐久間史典, 友野大, 塚田暁, 山崎敏光, 石元茂, 関本美知子, 豊田晃久, 佐藤将春, 鈴木隆敏, 竜野秀行, 橋本直, 早野龍五, 松田恭幸, 佐田優太, 永江知文, 平岩聡彦, 藤岡宏之, 榎本瞬, 野海博之, 溝井浩, Curceanu C. O., 岡田信二, 石渡智一, 鈴木謙, Zmeskal J., 方享燦, Beer G., 谷田聖, J-PARC E15/E17/E31 C.: "J-PARC K1.8BR ビームラインにおける K ビーム調整 (2)", 日本物理学会 2010 年秋季大会, (日本物理学会), 北九州, 9 月 (2010).

橋本直, 榎本瞬, 藤原裕也, 藤岡宏之, 早野龍五, 平岩聡彦, 飯尾雅実, 石元茂, 石渡智一, 板橋健太, 岩崎雅彦, 康寛史, 松田恭幸, 野海博之, 岡田信二, 大西宏明, 應田治彦, 佐田優太, 佐久間史典, 佐藤将春, 鈴木隆敏, 竜野秀行, 徳田真, 友野大, 塚田暁, 山崎敏光, Zmeskal J., Curceanu C. O., 施 (シ) 赫, 関本美知子, 豊田晃久, 井上謙太郎, 谷田聖, Bhang H., Choi S., Calgnelli M., Kienle P., Marton J., Widmann E., Wunschek B., Guaraldo C., Vazquez Doce O., Sirghi F., Sirghi D., Romero Vidal A.: "K 中間子 ^{3}He 原子の X 線精密分光実験に用いるシリコンドリフト検出器の性

能評価 (II)", 日本物理学会 2010 年秋季大会, (日本物理学会), 北九州, 9 月 (2010).

深尾 祥紀, 今津 義充, 庄司 幸平, 竹谷 篤, 中川 格, Ralf S., 中村 克朗, 齊藤 直人, 三部 勉, 谷田 聖, 廣田 誠子, PHENIX Collaboration .: "PHENIX muon arm trigger upgrade (II) ビーム、宇宙線を用いた性能評価", 日本物理学会 2010 年秋季大会, (日本物理学会), 北九州, 9 月 (2010).

佐田優太, 味村周平, Beer G., 方享燦, Bragadireanu M. A., Buehler P., Busso L., Cargnelli M., Choi S., Curceanu C. O., 榎本瞬, Faso D., 藤岡宏之, 藤原裕也, 福田共和, Guaraldo C., 橋本直, 早野龍五, 平岩聡彦, 飯尾雅実, 井上謙太郎, 石黒洋輔, 石川隆, 石元茂, 石渡智一, 板橋健太, 岩井正明, 岩崎雅彦, 川崎信吾, Kikenle P., 康寛史, Marton J., 松田恭幸, 溝井浩, Morra O., 永江知文, 野海博之, 大西宏明, 岡田信二, 應田治彦, 阪口篤志, 佐久間史典, 佐藤将春, 関本美知子, Shi H., Sirghi D., Sirghi F., 鈴木謙, 鈴木祥仁, 鈴木隆敏, 竜野秀行, 徳田真, 友野大, 豊田晃久, 塚田暁, Widmann E., 山崎敏光, Yim H., Zmeskal J.: "J-PARC E15 実験に用いる円筒形検出器群のコミッショニング", 日本物理学会 2010 年秋季大会, (日本物理学会), 北九州市, 9 月 (2010).

飯尾雅実, 板橋健太, 岩崎雅彦, 應田治彦, 大西宏明, 佐久間史典, 友野大, 塚田暁, 山崎敏光, 榎本瞬, 石橋直哉, 井上謙太郎, 阪口篤志, 吉田幸太郎, 味村周平, 野海博之, 石元茂, 岩井正明, 鈴木祥二, 関本美知子, 豊田晃久, 石川隆, 佐藤将春, 鈴木隆敏, 施赫將, 竜野秀行, 橋本直, 早野龍五, 藤原裕也, 松田恭幸, 康寛史, 徳田真, 永江知文, 平岩聡彦, 藤岡宏之, 佐田優太, 福田共和, 溝井浩, Faso D., Morra O., Bragadireanu M., Curceanu C. O., Guaraldo C., Iliescu M., 岡田信二, Pietreanu D., Sirghi D., Sirghi F., Buehler P., Cargnelli M., 石渡 智一, Marton J., Widmann E., Zmeskal J., 鈴木謙, 方享燦, Choi S., 林熙重, Kienle P., Busso L., Beer G. A.: "Λ (1405) 精密分光のための重水素標的の開発 (1)", 日本物理学会 2010 年秋季大会, (日本物理学会), 北九州, 9 月 (2010).

岩崎雅彦: "超低速ミュオンが拓く素粒子物理", 中間子科学研究会「超低速ミュオン：その無限の可能性を探る」, (日本中間子科学学会), 甲府, 10 月 (2010).

徳田真, 佐久間史典, 岩崎雅彦: "J-PARC E15 実験における TPC のための TGEM 開発 2010", 第 7 回「マイクロパターンガス検出器 (MPGD) 研究会」, (山形大学、KEK 測定器開発室), 山形, 11 月 (2010).

佐田優太, 味村周平, Beer G., 方享燦, Bragadireanu M. A., Buehler P., Busso L., Cargnelli M., Choi S., Curceanu C. O., 榎本瞬, Faso D., 藤岡宏之, 藤原裕也, 福田共和, Guaraldo C., 橋本直, 早野龍五, 平岩聡彦, 飯尾雅実, 井上謙太郎, 石黒洋輔, 石川隆, 石元茂, 石渡智一, 板橋健太, 岩井正明, 岩崎雅彦, 川崎信吾, Kikenle P., 康寛史, Marton J., 松田恭幸, 溝井浩, Morra O., 永江知文, 野海博之, 大西宏明, 岡田信二, 應田治彦, 阪口篤志, 佐久間史典, 佐藤将春, 関本美知子, Shi H., Sirghi D., Sirghi F., 鈴木謙, 鈴木祥仁, 鈴木隆敏, 竜野秀行, 徳田真, 友野大, 豊田晃久, 塚田暁, Widmann E., 山崎敏光, Yim H., Zmeskal J.: "K1.8BR beamline の円筒型検出器群 (CDS) の commissioning について", KEK 理論センター研究会「ストレンジネス核物理 2010」, (高エネルギー加速器研究機構　素粒子原子核研究所), つくば市, 12 月 (2010).

橋本直, 榎本瞬, 藤原裕也, 藤岡宏之, 早野龍五, 平岩聡彦, 飯尾雅実, 石元茂, 石渡智一, 板橋健太, 岩崎雅彦, 康寛史, 松田恭幸, 野海博之, 岡田信二, 大西宏明, 應田治彦, 佐田優太, 佐久間史典, 佐藤将春, 鈴木隆敏, 竜野秀行, 徳田真, 友野大, 塚田暁, 山崎敏光, Zmeskal J., Curceanu C. O., 施 (シ) 赫, 関本美知子, 豊田晃久, 井上謙太郎, 谷田聖, Bhang H., Choi S., Calgnelli M., Kienle P., Marton J., Widmann E., Wunschek B., Guaraldo C., Vazquez　Doce O., Sirghi F., Sirghi D., Romero　Vidal A.: "K 中間子ヘリウム 3 X 線精密分光実験の準備状況", KEK 理論センター研究会「ストレンジネス核物理 2010」, (KEK 理論センター), つくば, 12 月 (2010).

佐久間史典, 中村祐喜, 河合秀幸, 大西宏明, 田端誠, 徳田真: "Development of an Aerogel Cherenkov Counter for the J-PARC E16 Upgrade", 2010 年度「多彩なフレーバーで探る新しいハドロン存在形態の包括的研究」領域研究会, 和光, 2–3 月 (2011).

井上謙太郎, 康寛史, 徳田真, 岩崎雅彦, 飯尾雅実, 板橋健太, 應田治彦, 大西宏明, 佐久間史典, 友野大, 塚田暁, 山崎敏光, 石元茂, 岩井正明, 鈴木祥仁, 関本美知子, 豊田晃久, 石川隆, 佐藤将春, 鈴木隆敏, Hexi s., 竜野秀行, 橋本直, 早野龍五, 藤原裕也, 松田恭幸, 佐田優太, 永江知文, 平岩聡彦, 藤岡宏之, 味村周平, 榎本瞬, 野海博之, 阪口篤志, 福田共和, 溝井浩, Faso D., Morra O., bragadireanu M., Curceanu C. O., guaraldo c., iliescu M., 岡田信二, shrghi d., sirghi F., Buehler p., Cargnell M., 石渡智一, marton J., 鈴木謙, widmann E., Zmeskal J., 方享燦, choi S., yim H., kienle p., busso L., Beer G., 谷田聖: "J-PARC E-31 実験における後方散乱陽子飛跡検出 の設計開発と Geant4 Simulation", 日本物理学会第 66 回年次大会, (日本物理学会), 新潟, 3 月 (2011).

榎本瞬, 康寛史, 徳田真, 岩崎雅彦, 飯尾雅実, 板橋健太, 應田治彦, 大西宏明, 佐久間史典, 友野大, 塚田暁, 山崎敏光, 石元茂, 岩井正明, 鈴木祥仁, 関本美知子, 豊田晃久, 石川隆, 佐藤将春, 鈴木隆敏, Hexi s., 竜野秀行, 橋本直, 早野龍五, 藤原裕也, 松田恭幸, 佐田優太, 永江知文, 平岩聡彦, 藤岡宏之, 味村周平, 井上謙太郎, 野海博之, 阪口篤志, 福田共和, 溝井浩, Faso D., Morra O., bragadireanu M., Curceanu C. O., guaraldo c., iliescu M., 岡田信二, shrghi d., sirghi F., Buehler p., Cargnell M., 石渡智一, marton J., 鈴木謙, widmann E., Zmeskal J., 方享燦, choi S., yim H., kienle p., busso L., Beer G., 谷田聖: "d(K-,n) 反応を用いた Lambda(1405) 分光実験のための陽子検出器の開発 (3)", 日本物理学会第 66 回年次大会, (日本物理学会), 新潟, 3 月 (2011).

橋本直, 榎本瞬, 藤原裕也, 藤岡宏之, 早野龍五, 平岩聡彦, 飯尾雅実, 石元茂, 石渡智一, 板橋健太, 岩崎雅彦, 康寛史, 松田恭幸, 野海博之, 岡田信二, 大西宏明, 應田治彦, 佐田優太, 佐久間史典, 佐藤将春, 鈴木隆敏, 竜野秀行, 徳田真, 友野大, 塚田暁, 山崎敏光, Zmeskal J., Curceanu C. O., 施 (シ) 赫, 関本美知子, 豊田晃久, 井上謙太郎, 谷田聖, Bhang H., Choi S., Calgnelli M., Kienle P., Marton J., Widmann E., Wunschek B., Guaraldo C., Vazquez Doce O., Sirghi F., Sirghi D., Romero Vidal A.: “K 中間子 ^{3}He 原子の X 線精密分光実験に用いるシリコンドリフト検出器の性能評価 (III)”, 日本物理学会第 66 回年次大会, (日本物理学会), 新潟, 3 月 (2011).

佐田優太, 味村周平, Beer G., 方享燦, Bragadireanu M. A., Buehler P., Busso L., Cargnelli M., Choi S., Curceanu C. O., 榎本瞬, Faso D., 藤岡宏之, 藤原裕也, 福田共和, Guaraldo C., 橋本直, 早野龍五, 平岩聡彦, 飯尾雅実, 井上謙太郎, 石黒洋輔, 石川隆, 石元茂, 石渡智一, 板橋健太, 岩井正明, 岩崎雅彦, 川崎信吾, Kikenle P., 康寛史, Marton J., 松田恭幸, 溝井浩, Morra O., 永江知文, 野海博之, 大西宏明, 岡田信二, 應田治彦, 阪口篤志, 佐久間史典, 佐藤将春, 関本美知子, Shi H., Sirghi D., Sirghi F., 鈴木謙, 鈴木祥仁, 鈴木隆敏, 竜野秀行, 徳田真, 友野大, 豊田晃久, 塚田暁, Widmann E., 山崎敏光, Yim H., Zmeskal J.: “J-PARC E15 実験に用いる円筒形検出器群のコミッショニング（2）”, 日本物理学会第 66 回年次大会, (日本物理学会), 新潟, 3 月 (2011).

徳田真, 味村周平, Beer G., 方享燦, Bragadireanu M. A., Buehler P., Busso L., Cargnelli M., Choi S., Curceanu C. O., 榎本瞬, Faso D., 藤岡宏之, 藤原裕也, 福田共和, Guaraldo C., 橋本直, 早野龍五, 平岩聡彦, 飯尾雅実, 井上謙太郎, 石黒洋輔, 石川隆, 石元茂, 石渡智一, 板橋健太, 岩井正明, 岩崎雅彦, 川崎信吾, Kikenle P., 康寛史, Marton J., 松田恭幸, 溝井浩, Morra O., 永江知文, 野海博之, 大西宏明, 岡田信二, 應田治彦, 阪口篤志, 佐田優太, 佐久間史典, 佐藤将春, 関本美知子, Shi H., Sirghi D., Sirghi F., 鈴木謙, 鈴木祥仁, 鈴木隆敏, 竜野秀行, 友野大, 豊田晃久, 塚田暁, Widmann E., 山崎敏光, Yim H., Zmeskal J.: “J-PARC における K 中間子深束縛核探索実験（E15 実験）のための TGEM-TPC の開発 II”, 日本物理学会第 66 回年次大会, (日本物理学会), 新潟, 3 月 (2011).

斎藤徳人, Loutchev O. A., 和田智之, 横山幸司, 石田勝彦, 岩崎雅彦: “大強度ライマン α レーザーの開発”, ワークショップ 超低速ミュオン顕微鏡, (日本中間子学会他), 東京, 5 月 (2011).

岩崎雅彦: “超低速ミュオン顕微鏡：その限りない可能性を探る”, 日本物理学会 2011 年秋季大会, (日本物理学会), 富山 , 9 月 (2011).

石井康之, 鈴木栄男, 渡邊功雄, 松崎禎市郎, 加藤礼三: “量子スピン液体 $EtMe_3Sb[Pd(dmit)_2]_2$ の極低温スピンダイナミクス”, 日本物理学会 2011 年秋季大会, 富山, 9 月 (2011).

斎藤徳人, Loutchev O. A., Pavel B., 横山幸司, 石田勝彦, 岩崎雅彦, 和田智之: “2 光子共鳴 4 波混合によるライマン α 共鳴放射線の発生効率の評価”, レーザー学会学術講演会第 32 回年次大会, (社団法人レーザー学会), 仙台市, 1–2 月 (2012).

斎藤徳人, 岡村幸太郎, 浦田佳治, 丸山真幸, 月花智博, 横山幸司, Loutchev O. A., 石田勝彦, 岩崎雅彦, 和田智之: “ミュオニウム励起用コヒーレントライマン α 共鳴放射線源の開発”, レーザー学会学術講演会第 32 回年次大会, (社団法人レーザー学会), 仙台市, 1–2 月 (2012).

小林義男, 伊藤幹直, 松尾司, 森雅樹, 中村仁, 岡澤厚, 小島憲道, 玉尾皓平: “直線二配位 Fe 錯体の巨大内部磁場 (2)”, 日本化学会第 92 春季年会, (日本化学会), 横浜, 3 月 (2012).

Theory Group

Publications

[Journal]

(Original Papers) *Subject to Peer Review

Kojo T., Hidaka Y., McLerran L., and Pisarski R. D.: "Quarkyonic Chiral Spirals", Nucl. Phys. A **843**, No. 1-4, pp. 37–58 (2010). *

Rodriguez R., Fries R., and Ramirez E.: "Event-by-Event Jet Quenching", Phys. Lett. B **693**, No. 2, pp. 108–113 (2010). *

Gamberg L. and Kang Z.: "Process Dependent Sivers Function and Implication for Single Spin Asymmetry in Inclusive Hadron Production", Phys. Lett. B **696**, No. 1-2, pp. 109–118 (2010). *

Lacey R. A., Taranenko A., Wei R., Ajitanand N. N., Alexander J. M., Jia J., Pak R., Rischke D. H., Teaney D., and Dusling K.: "Azimuthal Anisotropy: Transition from Hydrodynamic Flow to Jet Suppression", Phys. Rev. C **82**, No. 3, pp. 034910-1–034910-4 (2010). *

Xiao B. and Yuan F.: "Initial and Final State Interaction Effects in Small-x Quark Distributions", Phys. Rev. D **82**, No. 11, pp. 114009-1–114009-13 (2010). *

Fries R.: "High Energy Nuclear Collisions: Theory Overview", Pramana J. Phys. **75**, No. 2, pp. 235–245 (2010). *

Liu J., Kang Z., and Wang E.: "Recursive Method for Opacity Expansion at Finite Temperature", Chin. Phys. C **35**, No. 1, pp. 44–49 (2011). *

Kojo T.: "Quarkyonic Matter and Chiral Spirals", J. Phys.: Con. Ser. **270**, 012049-1–012049-4 (2011). *

Stasto A. M.: "High Energy Limit in QCD", Mod. Phys. Lett. A **26**, No. 9, pp. 603–623 (2011). *

Hidaka Y., Kojo T., McLerran L., and Pisarski R. D.: "The Dichotomous Nucleon: Some Radical Conjectures for the Large Nc Limit", Nucl. Phys. A **852**, No. 1, pp. 155–174 (2011). *

Stasto A. M.: "Limiting Fragmentation in Hadronic Collisions", Nucl. Phys. A **854**, No. 1, pp. 64–70 (2011). *

Dumitru A.: "Initial Conditions and Global Event Properties from Color Glass Condensate", Nucl. Phys. A **854**, No. 1, pp. 71–75 (2011). *

Xiao B. and Yuan F.: "Two Particle Correlations: Saturation and Issues with Universality", Nucl. Phys. A **854**, No. 1, pp. 180–186 (2011). *

Nardi M., Kharzeev D., Levin E., and Tuchin K. L.: "Initial State Effects on J/psi Production at RHIC Energy: From d+Au to Au+Au", Nucl. Phys. A **855**, No. 1, pp. 392–395 (2011). *

Fries R. and Rodriguez R.: "Event-by-Event Jet Quenching and Higher Fourier Moments of Hard Probes", Nucl. Phys. A **855**, No. 1, pp. 424–427 (2011). *

Kojo T.: "A (1 + 1)-Dimensional Example of Quarkyonic Matter", Nucl. Phys. A **877**, No. 7, pp. 70–94 (2011). *

Kang Z., Qiu J., and Sterman G.: "Factorization and Quarkonium Production", Nucl. Phys. B (Proc. Suppl.) **214**, 39–43 (2011). *

Kang Z. and Soffer J.: "Positivity Bounds for Sivers Functions", Phys. Lett. B **695**, No. 1-4, pp. 275–278 (2011). *

Dumitru A., Jalilian-Marian J., Lappi T., Schenke B., and Venugopalan R.: "Renormalization Group Evolution of Multi-Gluon Correlators in High Energy QCD", Phys. Lett. B **706**, No. 2/3, pp. 219–224 (2011). *

Berger J. and Stasto A. M.: "Numerical Solution of the Nonlinear Evolution Equation at Small x with Impact Parameter and Beyond the Leading Logarithmic Approximation", Phys. Rev. D **83**, No. 3, pp. 034015-1–034015-21 (2011). *

Kang Z.: "QCD Evolution of Naive-Time-Reversal-Odd Fragmentation Functions", Phys. Rev. D **83**, No. 3, pp. 036006-1–036006-7 (2011). *

Kang Z., Qiu J., Vogelsang W., and Yuan F.: "Observation Concerning the Process Dependence of the Sivers Functions", Phys. Rev. D **83**, No. 9, pp. 094001-1–094001-9 (2011). *

Dominguez F., Marquet C., Xiao B., and Yuan F.: "Universality of Unintegrated Gluon Distributions at Small x", Phys. Rev. D **83**, No. 10, pp. 105005-1–105005-27 (2011). *

Kashiwa K.: "Entanglement between chiral and deconfinement transitions under strong uniform magnetic background field", Phys. Rev. D **83**, 117901-1–117901-4 (2011). *

Dumitru A., Jalilian-Marian J., and Petreska E.: "Two-Gluon Correlations and Initial Conditions for Small x Evolution", Phys. Rev. D **84**, No. 1, pp. 014018-1–014018-9 (2011). *

Kang Z. and Vitev I.: "Photon-Tagged Heavy Meson Production in High Energy Nuclear Collisions", Phys. Rev. D **84**, No. 1, pp. 014034-1–014034-10 (2011). *

Kang Z. and Yuan F.: "Single Spin Asymmetry Scaling in the Forward Rapidity Region at RHIC", Phys. Rev. D **84**, No. 3, pp. 034019-1–034019-8 (2011). *

Kang Z., Metz A., Qiu J., and Zhou J.: "Exploring the Structure of the Proton Through Polarization Observables in lp -¿ jet X", Phys. Rev. D **84**, No. 3, pp. 034046-1–034046-10 (2011). *

Yang L. and Lunardini C.: "Revealing Local Failed Supernovae with Neutrino Telescopes", Phys. Rev. D **84**, No. 6, pp. 063002-1–063002-5 (2011). *

Kashiwa K., Thomas H., and Weise W.: "Nonlocal Polyakov-Nambu-Jona-Lasinio model and imaginary chemical potential", Phys. Rev. D **84**, 056010-1–056010-13 (2011). *

Dominguez F., Xiao B., and Yuan F.: "k(t) Factorization for Hard Processes in Nuclei", Phys. Rev. Lett. **106**, No. 2, pp. 022301-01–022301-4 (2011). *

Kang Z. and Kharzeev D. E.: "Quark Fragmentation in the Theta Vacuum", Phys. Rev. Lett. **106**, 042001-1–042001-4 (2011). *

Fries R. and Nonaka C.: "Evaluating Results from the Relativistic Heavy Ion Collider with Perturbative QCD and Hydrodynamics", Prog. Part. Nucl. Phys. **66**, No. 3, pp. 607–660 (2011). *

Dumitru A.: "Quarkonium in a Non-Ideal Hot QCD Plasma", Prog. Theor. Phys. Suppl. **2011**, No. 187, pp. 87–95 (2011). *

Kojo T., Hidaka Y., Fukushima K., McLerran L., and Pisarski R.: "Interweaving chiral spirals", Nucl. Phys. A **875**, 94–138 (2012). *

Oral Presentations

(International Conference etc.)

McLerran L.: "Strongly Interacting Matter Matter at Very High Energy Density: 3 Lectures in Zakopane", 50th Crakow School of Theoretical Physics, (Michal Praszalowicz), Zakopane, Poland, June (2010).

McLerran L.: "Quark Gluon Plasma, Color Glass Condensate and Glasma: 3 Lectures at Lake Baikal", Baikal Summer School, (Baikal Summer School on Physics of Elementary Particles and Astrophysics), Bolshie Koty, Irkutsk, Russia, July (2010).

McLerran L.: "The CGC and the Glasma: Two Lectures at the Yukawa Institute", Symposium of the YIPQS International Workshop "High Energy Strong Interactions 2010 - Parton Distributions and Dense QCD Matter" (HESI 2010), (Yukawa Institute for Theoretical Physics (YITP)), Kyoto, Aug. (2010).

Kojo T., Hidaka Y., McLerran L., Pisarski R. D., and Tsvelik A. M.: "Quarkyonic phase", Dense QCD Phases in Heavy-lon Collisions(Dense matter10), (JINR), Dubna, Russia, Aug.–Sept. (2010).

Kojo T., McLerran L., Hidaka Y., Tsvelik A. M., and Pisarski R. D.: "Quarkyonic Chiral Spirals", Quark Confinement and the Hadron Spectrum2010(QCHS), (Madrid University), Madrid, Spain, Aug.–Sept. (2010).

McLerran L.: "FAQs about Quarkyonic Matter", Excited QCD 2011, (Les Houches Physics School), Les Houches, France, Feb. (2011).

Kojo T., McLerran L., Hidaka Y., Pisarski R. D., and Tsvelik A. M.: "Quarkyonic Matter", Quarks, Gluons, and Hadronic Matter under Extreme Conditions, (Darmstadt University of Technology), St. Goar, Germany, Mar. (2011).

McLerran L.: "Strongly Interacting Matter at Very High Energy Density", Brazilian Workshop on Nuclear Physics, Foz do Iguacu, Brazil, June (2011).

Tiburzi B.: "Lattice QCD with Classical and Quantum Electrodynamics", 29th International Symposium on Lattice Field Theory (Lattice 2011), (Lawrence Livermore National Laboratory), Squaw Valley, USA, July (2011).

Ohta S.: "Nucleon structure from 2+1f dynamical DWF lattice QCD at nearly physical pion mass", 29th International Symposium on Lattice Field Theory (Lattice 2011), Squaw Valley, USA, July (2011).

Cherman A. and Tiburzi B.: "The Fermion Sign Problem at Finite Density, and Large Nc Orbifold Equivalence", 2011 Meeting of the Division of Particles and Fields of the American Physical Society (DPF-2011), (Brown University), Providence, RI, USA, Aug. (2011).

Computing Group

Publications

[**Journal**]

(Original Papers) *Subject to Peer Review

Aoki S., Ishikawa K., Ishizuka N., Izubuchi T., Kanaya K., Kuramashi Y., Murano K., Namekawa Y., Okawa M., Taniguchi Y., Ukawa A., Ukita N., and Yoshie T.: "Non-Perturbative Renormalization of Quark Mass in Nf = 2 + 1 QCD with the Schrodinger Functional Scheme", J. High Energy Phys. **1008**, 101-1–101-27 (2010). *

Aoki S., Ishikawa K., Ishizuka N., Izubuchi T., Kadoh D., Kanaya K., Kuramashi Y., Namekawa Y., Okawa M., Taniguchi Y., Ukawa A., Ukita N., Yamazaki T., and Yoshie T.: "Physical Point Simulation in 2 + 1 Flavor Lattice QCD", Phys. Rev. D **81**, No. 7, pp. 074503-1–074503-12 (2010). *

Ishikawa T., Aoki Y., Flynn J. M., Izubuchi T., and Loktik O.: "One-Loop Operator Matching in the Static Heavy and Domain-Wall Light Quark System with O(a) Improvement", J. High Energy Phys. **1105**, 040-1–040-79 (2011). *

Aoki Y., Arthur R., Blum T., Boyle P. A., Brommel D., Christ N. H., Dawson C., Flynn J. M., Izubuchi T., Jin X., Jung C., Kelly C., Li M., Lichtl A., Lightman M., Lin M. F., Mawhinney R. D., Maynard C. M., Ohta S., Pendleton B. J., Sachrajda C. T., Scholz E. E., Soni A., Wennekers J., Zanotti J. M., and Zhou R.: "Continuum Limit Physics from 2 + 1 Flavor Domain Wall QCD", Phys. Rev. D **83**, No. 7, pp. 074508-1–074508-72 (2011). *

Lehner C. and Sturm C.: "Matching Factors for Delta S = 1 Four-Quark Operators in RI/SMOM Schemes", Phys. Rev. D **84**, No. 1, pp. 014001-1–014001-24 (2011). *

Aoki Y., Arthur R., Blum T., Boyle P. A., Brommel D., Christ N. H., Dawson C., Izubuchi T., Jung C., Kelly C., Kenway R. D., Lightman M., Mawhinney R. D., Ohta S., Sachrajda C. T., Scholz E. E., Soni A., Sturm C., Wennekers J., and Zhou R.: "Continuum Limit of BK from 2 + 1 Flavor Domain Wall QCD", Phys. Rev. D **84**, No. 1, pp. 014503-1–014503-32 (2011). *

Experimental Group

Publications

[Journal]

(Original Papers) *Subject to Peer Review

Afanasiev S., Akiba Y., Aoki K., Asai J., Bathe S., Boyle K., Deshpande A., Enyo H., Fukao Y., Goto Y., Hachiya T., Ichihara T., Ishihara M., Miyachi Y., Nakagawa I., Shibata T., Shoji K., Taketani A., Tanida K., Torii H., Watanabe Y., Yokkaichi S., Okada K., Saito N., and PHENIX C.: "Photoproduction of J/ψ and of high mass e^+e^- in ultra-peripheral Au+Au collisions at $\sqrt{s_{NN}}$ = 200 GeV", Phys. Lett. B **679**, No. 4, pp. 321–329 (2009). *

Adare A., Akiba Y., Aoki K., Asai J., Bathe S., Boyle K., Deshpande A., Enyo H., Fukao Y., Goto Y., Hachiya T., Ichihara T., Ichimiya R., Ikeda Y., Ishihara M., Mao Y., Nakagawa I., Nakano K., Ralf S., Shibata T., Shoji K., Taketani A., Tanida K., Torii H., Watanabe Y., Yokkaichi S., Kurosawa M., Okada K., Saito N., and PHENIX C.: "Photon-hadron jet correlations in $p + p$ and $Au + Au$ collisions at $\sqrt{s_{NN}}$ = 200 GeV", Phys. Rev. C **80**, 024908-1–024908-14 (2009). *

Afanasiev S., Akiba Y., Aoki K., Bathe S., Boyle K., Deshpande A., Enyo H., Fukao Y., Goto Y., Hachiya T., Ichihara T., Ishihara M., Shibata T., Shoji K., Taketani A., Tanida K., Torii H., Watanabe Y., Yokkaichi S., Okada K., Saito N., and PHENIX C.: "Systematic studies of elliptic flow measurements in Au+Au collisions at $\sqrt{s_{NN}}$ = 200 GeV", Phys. Rev. C **80**, 024909-1–024909-25 (2009). *

Afanasiev S., Akiba Y., Aoki K., Bathe S., Boyle K., Deshpande A., Enyo H., Fukao Y., Goto Y., Hachiya T., Ichihara T., Ishihara M., Shibata T., Shoji K., Taketani A., Tanida K., Torii H., Watanabe Y., Yokkaichi S., Okada K., Saito N., and PHENIX C.: "High-pT π^0 production with respect to the reaction plane in $Au + Au$ collisions at $\sqrt{s_{NN}}$ = 200 GeV", Phys. Rev. C **80**, 054907-1–054907-29 (2009). *

Adare A., Akiba Y., Aoki K., Asai J., Bathe S., Boyle K., Deshpande A., Enyo H., Fukao Y., Goto Y., Ichihara T., Ichimiya R., Ikeda Y., Ishihara M., Mao Y., Nakagawa I., Nakano K., Ralf S., Shibata T., Shoji K., Taketani A., Tanida K., Torii H., Watanabe Y., Yokkaichi S., Kurosawa M., Okada K., Saito N., and PHENIX C.: "Gluon-spin contribution to the proton spin from the double-helicity asymmetry in inclusive π^0 production in polarized $p+p$ collisions at $\sqrt{s}$ = 200 GeV", Phys. Rev. Lett. **103**, 012003-1–012003-6 (2009). *

Adare A., Akiba Y., Aoki K., Asai J., Bathe S., Boyle K., Deshpande A., Enyo H., Fukao Y., Goto Y., Hachiya T., Ichihara T., Ichimiya R., Ikeda Y., Ishihara M., Mao Y., Nakagawa I., Nakano K., Ralf S., Shibata T., Shoji K., Taketani A., Tanida K., Torii H., Watanabe Y., Yokkaichi S., Kurosawa M., Okada K., Saito N., and PHENIX C.: "Measurement of bottom versus charm as a function of transverse momentum with electron-hadron correlations in $p + p$ collisions at $\sqrt{s}$ = 200 GeV", Phys. Rev. Lett. **103**, 082002-1–082002-7 (2009). *

Afanasiev S., Akiba Y., Aoki K., Bathe S., Boyle K., Deshpande A., Enyo H., Fukao Y., Goto Y., Hachiya T., Ichihara T., Ishihara M., Shibata T., Shoji K., Taketani A., Tanida K., Torii H., Watanabe Y., Yokkaichi S., Okada K., and PHENIX C.: "Charged kaon interferometric probes of space-time evolution in $Au + Au$ collisions at $\sqrt{s_{NN}}$ = 200 GeV", Phys. Rev. Lett. **103**, 142301-1–142301-6 (2009). *

Adare A., Akiba Y., Aoki K., Asai J., Bathe S., Boyle K., Deshpande A., Enyo H., Fukao Y., Goto Y., Hachiya T., Ichihara T., Ishihara M., Mao Y., Nakagawa I., Nakamura K., Nakano K., Ralf S., Shibata T., Shoji K., Taketani A., Tanida K., Torii H., Watanabe Y., Yokkaichi S., Okada K., Saito N., and PHENIX C.: "Detailed measurement of the e^+e^- pair continuum in $p+p$ and Au+Au collisions at $\sqrt{s_{NN}}$ = 200 GeV and implications for direct photon production", Phys. Rev. C **81**, No. 3, pp. 034911-1–034911-56 (2010). *

Adare A., Akiba Y., Aoki K., Asai J., Bathe S., Boyle K., Deshpande A., Enyo H., Fukao Y., Goto Y., Hachiya T., Ichihara T., Ichimiya R., Ikeda Y., Ishihara M., Mao Y., Nakagawa I., Nakano K., Ralf S., Shibata T., Shoji K., Taketani A., Tanida K., Torii H., Watanabe Y., Yokkaichi S., Kurosawa M., Okada K., Saito N., and PHENIX C.: "Transverse momentum dependence of η meson suppression in Au+Au collisions at $\sqrt{s_{NN}}$ = 200 GeV", Phys. Rev. C **82**, No. 1, pp. 011902-1–011902-7 (2010). *

Adare A., Akiba Y., Aoki K., Asai J., Bathe S., Boyle K., Deshpande A., Enyo H., Fukao Y., Goto Y., Hachiya T., Ichihara T., Ichimiya R., Ikeda Y., Ishihara M., Mao Y., Nakagawa I., Nakano K., Ralf S., Shibata T., Shoji K., Taketani A., Tanida K., Torii H., Watanabe Y., Yokkaichi S., Kurosawa M., Okada K., Saito N., and PHENIX C.: "Double-helicity dependence of jet properties from dihadrons in longitudinally polarized $p + p$ collisions at $\sqrt{s}$ = 200 GeV", Phys. Rev. D **81**, No. 1, pp. 012002-1–012002-11 (2010). *

Adare A., Akiba Y., Aoki K., Asai J., Bathe S., Boyle K., Deshpande A., Enyo H., Fukao Y., Goto Y., Ichihara T., Ichimiya R., Ikeda Y., Ishihara M., Mao Y., Nakagawa I., Nakano K., Ralf S., Shibata T., Shoji K., Taketani A., Tanida K., Torii H., Watanabe Y., Yokkaichi S., Kurosawa M., Okada K., Saito N., and PHENIX C.: "Transverse momentum dependence of J/ψ polarization at midrapidity in $p + p$ collisions at $\sqrt{s}$ = 200 GeV", Phys. Rev. D **82**, No. 1, pp. 012001-1–012001-10 (2010). *

Adare A., Akiba Y., Aoki K., Asai J., Bathe S., Boyle K., Deshpande A., Enyo H., Fukao Y., Goto Y., Hachiya

T., Ichihara T., Ichimiya R., Ikeda Y., Ishihara M., Mao Y., Nakagawa I., Nakano K., Ralf S., Shibata T., Shoji K., Taketani A., Tanida K., Torii H., Watanabe Y., Yokkaichi S., Kurosawa M., Okada K., Saito N., and PHENIX C.: "High p_T direct photon and π^0 triggered azimuthal jet correlations and measurement of k_T for isolated direct photons in $p+p$ collisions at $\sqrt{s} = 200$ GeV", Phys. Rev. D **82**, No. 7, pp. 072001-1–072001-18 (2010). ∗

Adare A., Akiba Y., Aoki K., Asai J., Bathe S., Boyle K., Deshpande A., Enyo H., Fukao Y., Goto Y., Ichihara T., Ichimiya R., Ikeda Y., Ishihara M., Mao Y., Nakagawa I., Nakamura K., Nakano K., Ralf S., Shibata T., Shoji K., Taketani A., Tanida K., Torii H., Watanabe Y., Yokkaichi S., Kurosawa M., Okada K., Saito N., Nakamura T., and PHENIX C.: "Measurement of transverse single-spin asymmetries for J/ψ production in polarized $p + p$ collisions at $\sqrt{s} = 200$ GeV", Phys. Rev. D **82**, No. 11, pp. 112008-1–112008-13 (2010). ∗

Adare A., Akiba Y., Aoki K., Asai J., Bathe S., Boyle K., Deshpande A., Enyo H., Fukao Y., Goto Y., Hachiya T., Ichihara T., Ishihara M., Mao Y., Nakagawa I., Nakano K., Ralf S., Shibata T., Shoji K., Taketani A., Tanida K., Torii H., Watanabe Y., Yokkaichi S., Okada K., Saito N., and PHENIX C.: "Enhanced Production of Direct Photons in Au+Au Collisions at $\sqrt{s_{NN}} = 200$ GeV and Implications for the Initial Temperature", Phys. Rev. Lett. **104**, 132301-1–132301-6 (2010). ∗

Adare A., Akiba Y., Aoki K., Asai J., Bathe S., Boyle K., Deshpande A., Enyo H., Fukao Y., Goto Y., Hachiya T., Ichihara T., Ichimiya R., Ikeda Y., Ishihara M., Mao Y., Nakagawa I., Nakano K., Ralf S., Shibata T., Shoji K., Taketani A., Tanida K., Torii H., Watanabe Y., Yokkaichi S., Kurosawa M., Okada K., Saito N., and PHENIX C.: "Transition in Yield and Azimuthal Shape Modification in Dihadron Correlations in Relativistic Heavy Ion Collisions", Phys. Rev. Lett. **104**, 252301-1–252301-7 (2010). ∗

Adare A., Akiba Y., Aoki K., Bathe S., Boyle K., Deshpande A., Enyo H., Fukao Y., Goto Y., Hashimoto K., Ichihara T., Ichimiya R., Ikeda Y., Ishihara M., Mao Y., Nakagawa I., Nakano K., Ralf S., Shibata T., Shoji K., Taketani A., Tanida K., Torii H., Watanabe Y., Yokkaichi S., Kurosawa M., Okada K., Saito N., and PHENIX C.: "Elliptic and Hexadecapole Flow of Charged Hadrons in Au+Au Collisions at $\sqrt{s_{NN}} = 200$ GeV", Phys. Rev. Lett. **105**, 062301-1–062301-6 (2010). ∗

Adare A., Akiba Y., Aoki K., Bathe S., Boyle K., Deshpande A., Enyo H., Fukao Y., Goto Y., Ichihara T., Ichimiya R., Ikeda Y., Ishihara M., Mao Y., Nakagawa I., Nakano K., Ralf S., Shibata T., Shoji K., Taketani A., Tanida K., Torii H., Watanabe Y., Yokkaichi S., Kurosawa M., Okada K., Saito N., and PHENIX C.: "Azimuthal Anisotropy of π^0 Production in Au+Au Collisions at $\sqrt{s_{NN}} = 200$ GeV: Path-Length Dependence of Jet Quenching and the Role of Initial Geometry", Phys. Rev. Lett. **105**, 142301-1–142301-7 (2010). ∗

Okada K. and PHENIX c.: "Delta G and Delta qbar measurements at PHENIX", AIP Conf. Proc. **1418**, 21–28 (2011).

Nakamura T., Enyo H., Ichihara T., Watanabe Y., and Yokkaichi S.: "Data oriented job submission scheme or the PHENIX user analysis in CCJ", J. Phys.: Con. Ser. **331**, 1–6 (2011). ∗

Adare A., Akiba Y., Aoki K., Asai J., Bathe S., Boyle K., Deshpande A., Enyo H., Fukao Y., Goto Y., Hachiya T., Ichihara T., Ichimiya R., Ikeda Y., Ishihara M., Mao Y., Nakagawa I., Nakamura K., Nakano K., Ralf S., Shibata T., Shoji K., Taketani A., Tanida K., Torii H., Watanabe Y., Yokkaichi S., Kurosawa M., Okada K., Saito N., Nakamura T., and PHENIX C.: "Nuclear modification factors of ϕ mesons in d+Au, Cu+Cu, and Au+Au collisions at $\sqrt{s_{NN}} = 200$ GeV", Phys. Rev. C **83**, No. 2, pp. 024909-1–024909-10 (2011). ∗

Adare A., Akiba Y., Aoki K., Asai J., Bathe S., Boyle K., Deshpande A., Enyo H., Fukao Y., Goto Y., Ichihara T., Ichimiya R., Ikeda Y., Ishihara M., Mao Y., Nakagawa I., Nakano K., Ralf S., Shibata T., Shoji K., Taketani A., Tanida K., Torii H., Watanabe Y., Yokkaichi S., Kurosawa M., Okada K., Saito N., and PHENIX C.: "Azimuthal correlations of electrons from heavy-flavor decay with hadrons in $p + p$ and Au+Au collisions at $\sqrt{s_{NN}} = 200$ GeV", Phys. Rev. C **83**, No. 4, pp. 044912-1–044912-16 (2011). ∗

Adare A., Akiba Y., Aoki K., Asai J., Bathe S., Boyle K., Deshpande A., Enyo H., Fukao Y., Goto Y., Hachiya T., Hashimoto K., Ichihara T., Ichimiya R., Ikeda Y., Ishihara M., Mao Y., Miyachi Y., Nakagawa I., Nakamura K., Nakano K., Ralf S., Shibata T., Shoji K., Taketani A., Tanida K., Torii H., Watanabe Y., Yokkaichi S., Kurosawa M., Okada K., Saito N., and PHENIX C.: "Cross section and double helicity asymmetry for η mesons and their comparison to π^0 production in $p+p$ collisions at $\sqrt{s} = 200$ GeV", Phys. Rev. D **83**, No. 3, pp. 032001-1–032001-11 (2011). ∗

Adare A., Akiba Y., Aoki K., Asai J., Bathe S., Boyle K., Deshpande A., Enyo H., Fukao Y., Goto Y., Hachiya T., Ichihara T., Ichimiya R., Ikeda Y., Ishihara M., Mao Y., Nakagawa I., Nakano K., Ralf S., Shibata T., Shoji K., Taketani A., Tanida K., Torii H., Watanabe Y., Yokkaichi S., Kurosawa M., Okada K., Saito N., and PHENIX C.: "Measurement of neutral mesons in $p + p$ collisions at $\sqrt{s} = 200$ GeV and scaling properties of hadron production", Phys. Rev. D **83**, No. 5, pp. 052004-1–052004-26 (2011). ∗

Adare A., Akiba Y., Aoki K., Bathe S., Boyle K., Deshpande A., Enyo H., Fukao Y., Goto Y., Hashimoto K., Ichihara T., Ichimiya R., Ikeda Y., Ishihara M., Mao Y., Miyachi Y., Nakagawa I., Nakamura K., Nakano

K., Ralf S., Shibata T., Shoji K., Taketani A., Tanida K., Torii H., Watanabe Y., Yokkaichi S., Kurosawa M., Okada K., Saito N., Nakamura T., and PHENIX C.: "Cross Section and Parity-Violating Spin Asymmetries of $W^{\pm}$ Boson Production in Polarized $p + p$ Collisions at $\sqrt{s} = 500$ GeV", Phys. Rev. Lett. **106**, No. 6, pp. 062001-1–062001-6 (2011). ∗

Nakagawa I.: "Sea Quark Polarization Measurement Via W-Boson in Forward Rapidity at PHENIX", AIP Conf. Proc. **1418**, 122–129 (2012).

Oral Presentations

(International Conference etc.)

Boyle K.: "Recent PHENIX Results for A_{LL} and Current Constraints on ΔG", Gluon Polarization in the Nucleon, (University of Illinois, Urbana-Champaign), Urbana, USA, June (2008).

Boyle K.: "Recent Results and Future Prospects for the PHENIX Spin Program", 18th International Symposium on Spin Physics (SPIN 2008), (University of Virginia), Charlottesville, USA, Oct. (2008).

Boyle K.: "Current Results and Future Prospects from PHENIX", Berkeley Summer Program on Nucleon Spin Physics, (Lawrence Berkeley National Laboratory), Berkeley, USA, June (2009).

Boyle K.: "Studying the Helicity Structure of the Proton at PHENIX", Advanced Studies Institute: Symmetries and Spin (SPIN-Praha-2009), (Charles University in Prague), Prague, Czech, July–Aug. (2009).

Boyle K.: "Nucleon Structure from High-Energy Polarized Proton-Proton Collisions", 8th European Research Conference on Electromagnetic Interactions with Nucleons and Nuclei (EINN 2009), (Institute of Accelerating Systems and Applications (IASA)), Mylos, Greece, Sept. (2009).

Boyle K.: "Quark and Gluon Polarization measurements with PHENIX", Brookhaven Summer Program on Nucleon Spin Physics, Upton, NY, USA, July (2010).

Boyle K.: "Extraction of ΔG from progected EIC deta", Electron-Ion Collider Collaboration Meeting, (Catholic University), Washington DC, USA, July (2010).

Boyle K.: "Overview of Spin Physics at RHIC", Excited QCD 2011, (Ecole de Physique des Houches), Les Houches, France, Feb. (2011).

Boyle K.: "Nucleon Spin Structure", APS April Meeting 2011, (American Physical Society), Anaheim, USA, Apr.–May (2011).

Koster J.: "Status of the PHENIX VTX Detector Upgrade", APS April Meeting 2011, Anaheim, USA, Apr.–May (2011).

Okada K. and PHENIX c.: "Delta G and Delta qbar at PHENIX", 8th Circum-Pan-Pacific Symposium on High Energy Spin Physics (PacSPIN 2011), (University of Adelaide, Australia 5005), Cairns, Australia, June (2011).

Koster J.: "Current and Near-term Transverse Spin Measurements at PHENIX", RHIC and AGS Annual User's Meeting, (Brookhaven National Laboratory), Upton, USA, June (2011).

Komatsu Y., Aoki K., Enyo H., Kanaya J., Kannno K., Masumoto S., Nakai W., Ozawa K., Sekimoto M., Takagi A., Watanabe Y., and Yokkaichi S.: "GEM spectrometer for J-PARC E16 experiment", 2nd international conference on micro pattern gaseous detectors (MPGD2011), (International organizing committee for MPGD2011), Kobe, Aug.–Sept. (2011).

Koster J.: "PHENIX results and perspectives on transverse spin asymmetries", Third International Workshop on Transverse Polarization Phenomena in Hard Scattering(Transversity 2011), Veli Losinj, Croatia, Aug.–Sept. (2011).

Seele J.: "Future Plans for PHENIX", 4th International Workshlop on High Energy Physics in the LHC Era, (University Technico Federico Santa Maria), Valparaiso, Chile, Jan. (2012).

Chen C.: "Higher-Order Flow Harmonics in Heavy Ion Collisions Measured by PHENIX", 4th International Workshlop on High Energy Physics in the LHC Era, (Universidad Tecnica Federico Santa Maria), Valparaiso, Chile, Jan. (2012).

(Domestic Conference)

黒澤真城, 秋葉康之, 浅井淳吉, Deepak B., 藤原康平, 延與秀人, 狩野博之, 大西宏明, 小貫良行, Charles P., Eugene S., 竹谷篤, 山本義博: "PHENIX シリコンピクセル検出器の宇宙線によるテスト実験", 日本物理学会 2007 年春季大会, (首都大学東京), 東京, 3 月 (2007).

羽木洋介, 河西実希, 延與秀人, 秋葉康之, 黒澤真城, 金谷淳平, 栗田和好, 橋本公瑛, 藤原康平, 関本美知子: "PHENIX 用シリコンピクセル検出器の高エネルギー陽子ビームを用いた性能評価", 日本物理学会第 64 回年次大会, (日本物理学会), 東京, 3 月 (2009).

上坂明子, 竹谷篤, 栂野泰宏, 村上浩之, 本林透, 米田健一郎: "シリコン検出器用電荷有感型前置増幅器のダイナミックンジの拡大", 日本物理学会第 65 回年次大会, (日本物理学会), 岡山, 3 月 (2010).

羽木洋介, 河西実希, 延與秀人, 秋葉康之, 黒澤真城, 金谷淳平, 栗田和好, 橋本公瑛, 藤原康平, 関本美知子: "PHENIX シリコンピクセル検出器組み立て後の品質検査", 日本物理学会第 65 回年次大会, (日本物理学会), 岡山, 3 月 (2010).

高原 明久: "Study of J/ψ photoproduction in ultra-peripheral Au+Au collisions at the PHENIX experiment", 日本物理学会第 65 回年次大会, (日本物理学会), 岡山, 3 月 (2010).

青木 和也, 四日市 悟, 金谷 淳平, 桝本 新一, 小松 雄哉: "J-PARC E16 実験の為の、ハドロン・ブラインド検出器の開発", 日本物理学会 2010 年秋季大会, (九州工業大学), 北九州, 9 月 (2010).

高原 明久: "J/ψ photoproduct on in ultra-peripheral Au+Au collisions at $\sqrt{s_{NN}} = 200$ GeV using the PHENIX detector", 日本物理学会 2010 年秋季大会,

(日本物理学会), 北九州, 9 月 (2010).

岡田謙介, PHENIX C.: “偏極陽子衝突における W ボゾン生成の電子崩壊過程を用いたスピン非対称度の測定”, 日本物理学会 2010 年秋季大会, (九州工業大学), 北九州, 9 月 (2010).

深尾 祥紀, 今津 義充, 庄司 幸平, 竹谷 篤, 中川 格, Ralf S., 中村 克朗, 齊藤 直人, 三部 勉, 谷田 聖, 廣田 誠子, PHENIX Collaboration .: “PHENIX muon arm trigger upgrade (II) ビーム、宇宙線を用いた性能評価”, 日本物理学会 2010 年秋季大会, (日本物理学会), 北九州, 9 月 (2010).

蜂谷崇, 黒澤真城, 竹谷篤, 藤原康平, 二宮一史, 秋葉康之, 金谷 淳平, Baumgart S. L., 秋元 亮二, 浅野 秀光, 栗田 和好, 西尾 悠法, 渡邉 健太郎, 今井 憲一, 佐藤 進, 佐甲博之, 関本美知子, Pancaker C., Shafto E., Apadula N., Mannel E. J., Gastaldi F., Deapier O., Sahlmuller B., Lewis B., Koster J., Stepanov M., Shaver A., Bowen J., Bryslawskyj J.: “PHENIX シリコン崩壊点飛跡検出器 (VTX) の組立と設置”, 日本物理学会第 66 回年次大会, (日本物理学会), 新潟, 3 月 (2011).

浅野 秀光, 黒澤 真城, 竹谷 篤, 藤原 康平, 二宮 一史, 秋葉康之, 金谷淳平, 蜂谷崇, Baumgart S. L., 秋元亮二, 栗田和好, 西尾 悠法, 渡邉 健太郎, 今井 憲一, 佐藤 進, 佐甲博之, 関本美知子, Pancaker C., Shafto E., Apadula N., Mannel E. J., Gastaldi F., Deapier O., Sahlmuller B., Lewis B., Koster J., Stepanov M., Shaver A., Bowen J., Bryslawskyj J.: “偏極陽子衝突ビームを用いた PHENIX 崩壊点飛跡検出器 (VTX) のコミッショニング”, 日本物理学会第 66 回年次大会, (日本物理学会), 新潟, 3 月 (2011).

浅野秀光, 秋葉康之, 金谷淳平, 黒澤真城, 竹谷篤, 蜂谷崇, Koster J., 秋元亮二, Stephen B., 栗田和好, 今井憲一, 佐甲博之, 佐藤進, 関本美知子, 藤原康平, Baldo S., Benji L., Chuck P., Eugene S., Nicole A., Eric .., Franck G., Olivier D., Mikhail S., Alexander S., James B., Jason B.: “偏極陽子衝突ビームを用いた PHENIX 崩壊点飛跡検出器 VTX) のコ ミッショニング”, 日本物理学会第 66 回年次大会, (社団法人　日本物理学会), 新潟, 3 月 (2011).

黒澤真城, 竹谷篤, 藤原康平, 二宮一史, 秋葉康之, 金谷淳平, 蜂谷崇, Baumgart S. L., 秋元亮二, 浅野秀光, 栗田和好, 西尾悠法, 渡邉健太郎, 今井憲一, 佐藤進, 佐甲博之, 関本美知子, Pancaker C., Shafto E., Apadula N., Mannel E. J., Gastaldi F., Deapier O.: “PHENIX シリコン崩壊点飛跡測定器（VTX）ピクセル検出器モジュールの量産完成報告”, 日本物理学会第 66 回年次大会, (日本物理学会), 新潟, 3 月 (2011).

蜂谷崇, 秋葉康之, 黒澤真城, 竹谷篤, Baumgart S. L., 浅野秀光, 秋元亮二, 佐藤進, 佐甲博之, 関本美知子, 藤原康平, 金谷 淳平, 栗田 和好, 二ノ宮 一史, 西尾 悠法, 今井 憲一, Pancake C., Shafto E., Apadula N., Lewis B., Sahlmuller B., Mannel E. J., Gastaldi F., Drapier O., Koster J., Stepanov M.: “PHENIX シリコン崩壊点飛跡検出器 (VTX) の組立と設置”, 日本物理学会第 66 回年次大会, (日本物理学会), 新潟, 3 月 (2011).

岡田謙介: “偏極陽子衝突実験で探る陽子スピンの謎”, EPP セミナー, (九州大学), 福岡, 7 月 (2011).

黒澤真城, 秋葉康之, 秋元亮二, 浅野秀光, 榎園昭智, 蜂谷崇, 佐甲博之, 佐藤進, 竹谷篤, Bathe S., Boyle K., Koster J., Mannel E. J., Nouicer R., Pancake C., Sondheim W.: “RHIC-PHENIX 実験のためのシリコン崩壊点検出器完成設置報告”, 日本物理学会 2011 年秋季大会, (社団法人　日本物理学会), 弘前, 9 月 (2011).

高原 明久: “Study of J/ψ photoproduction in ultra-peripheral Au+Au collisions at$\sqrt{s_{NN}}$=200GeV using the PHENIX detector”, 日本物理学会 2011 年秋季大会, (日本物理学会), 弘前, 9 月 (2011).

Boyle K.: “Experimental status and outlook of spin physics at RHIC”, High-Energy QCD Workshop, 和光, 10 月 (2011).

小松雄哉, 青木和也, 荒巻陽紀, 桝本新一, 　木敦子, 高橋智則, 四日市悟, 小沢恭一郎, 中井恒, 菅野光樹, 関本美知子: “J-PARC E16 実験のための GEM Tracker 開発の現状”, 第 8 回「マイクロパターンガス検出器 (MPGD) 研究会」, (近畿大学、高エネルギー加速器研究機構　測定器開発室), 東大阪, 12 月 (2011).

黒澤真城, PHENIX C.: “RHIC-PHENIX 実験のためのシリコン崩壊点検出器 (VTX) の動作状況”, 日本物理学会第 67 回年次大会, (社団法人日本物理学会), 西宮市, 3–3 月 (2012).

Radioactive Isotope Physics Laboratory

Publications

[Journal]

(Original Papers) *Subject to Peer Review

Nishimura S.: "First Decay Spectroscopy Experiment at RIBF", AIP Conf. Proc. **1269**, No. 1, pp. 91–97 (2010). *

Mihara M., Izumikawa T., Ueno H., Matsuta K., Nishimura D., Nagatomo T., Moriguchi T., Ito Y., Nagae D., Fukuda M., Yoshimi A., Yamada K., Takechi M., Ichikawa Y., Momota S., Hirayama Y., Ohtsubo T., Suzuki S., Ozawa A., Ishibashi Y., Kubo T., Ooishi H., Namiki Y., Hachiuma K., Namihira K., Horikawa D., Minamisono T., Yamaguchi T., Kuboki T., Suzuki T., Sato K., Kobayashi Y., and Asahi K.: "Beta-NMR measurement of 58Cu in Si", Hyperfine Interact. **197**, 143–147 (2010). *

Nagatomo T., Ueno H., Mihara M., Matsuta K., Yoshimi A., Ichikawa Y., Yamada K., Kawamura H., Ozawa A., Moriguchi T., Ishibashi Y., Asahi K., Uchida M., Suzuki K., Inoue T., Hasama Y., Iijima H., Sumikama T., Fukuda M., and Minamisono T.: "Precise nuclear moments of extremely proton-rich nuclus 23Al", Hyperfine Interact. **198**, 103–107 (2010). *

Ohnishi T., Kubo T., Kusaka K., Yoshida A., Yoshida K., Ohtake M., Fukuda N., Takeda H., Kameda D., Tanaka K., Inabe N., Yanagisawa Y., Gono Y., Watanabe H., Otsu H., Baba H., Ichihara T., Yamaguchi Y., Takechi M., Nishimura S., Ueno H., Yoshimi A., Sakurai H., Motobayashi T., Nakao T., Mizoi Y., Matsushita M., Ieki K., Kobayashi N., Tanaka K., Kawada Y., Tanaka N., Deguchi S., Sato Y., Kondo Y., Nakamura T., Yoshinaga K., Ishii c., Yoshii h., Miyashita Y., Uematsu N., Shiraki Y., Sumikama T., Chiba J., Ideguchi E., Saito A., Yamaguchi T., Hachiuma I., Suzuki T., Moriguchi T., Ozawa A., Ohtsubo T., Famiano M. A., Geissel H., Nettleton A. S., Tarasov O. B., Bazin D. P., Sherrill B. M., Manikonda S. L., and Nolen J. A.: "Identification of 45 New Neutron-Rich Isotopes Produced by In-Flight Fission of a ^{238}U Beam at 345 MeV/nucleon", J. Phys. Soc. Jpn. **79**, No. 7, pp. 073201-1–073201-5 (2010). *

Mizuno T., Yamada T., Tsuchida H., Nakai Y., and Itoh A.: "Kinetic-energy release in N_2 fragmentation by charge-changing collisions of 2-MeV C^+ ions", Phys. Rev. A **82**, No. 5, pp. 054702-1–054702-3 (2010). *

Tanaka K., Fukuda M., Mihara M., Takechi M., Nishimura D., Chinda T., Sumikama T., Kudo S., Matsuta K., Minamisono T., Suzuki T., Ohtsubo T., Izumikawa T., Momota S., Yamaguchi T., Oonish T., Ozawa A., Tanihata I., and Zheng T.: "Density distribution of ^{17}Ne and possible shell-structure change in the proton-rich sd-shell nuclei", Phys. Rev. C **82**, No. 4, pp. 044309-1–044309-11 (2010). *

Tanaka K., Yamaguchi T., Suzuki T., Ohtsubo T., Fukuda M., Nishimura D., Takechi M., Ogata K., Ozawa A., Izumikawa T., Aiba T., Aoi N., Baba H., Hashizume Y., Inafuku K., Iwasa N., Kobayashi K., Komuro M., Kondo Y., Kubo T., Matsuyama T., Michimasa S., Motobayashi T., Nakabayashi T., Nakazima S., Nakamura T., Sakurai H., Shinoda R., Shinohara M., Suzuki H., Takeshita E., Takeuchi S., Togano Y., Yamada K., Yasuno T., and Yhoshitake M.: "Observation of a large reaction cross-section in the drip-line nucleus ^{22}C", Phys. Rev. Lett. **104**, No. 6, pp. 062701-1–062701-4 (2010). *

Kuboki H., Okuno H., Yokouchi S., Hasebe H., Kishida T., Fukunishi N., Kamigaito O., Goto A., Kase M., and Yano Y.: "Charge-state distribution measurements of ^{238}U and ^{136}Xe at 11 MeV/nucleon using gas charge stripper", Phys. Rev. Spec. Top.: Accel. Beams **13**, No. 9, pp. 093501-1–093501-9 (2010). *

Kobayashi T. and Matsuo Y.: "Hydrogenation of fragment cations produced by femtosecond laser ablation of boron nitride", J. Chem. Phys. **135**, No. 20, pp. 204504-1–204504-5 (2011). *

Asahi K., Furukawa T., Inoue T., Yoshimi A., Nanao T., Chikamori M., Suzuki K., Tsuchiya M., Hayashi H., Uchida M., Ueno H., Matsuo Y., and Fukuyama T.: "Search for an electric dipole moment in 129Xe atom with nuclear spin oscillator technique", J. Phys.: Con. Ser. **302**, No. 012039, pp. 1–6 (2011). *

Ichikawa Y., Onishi T., Suzuki D., Iwasaki H., Kubo T., Banerjee S. R., Chakrabarti A., Aoi N., Brown A. B., Fukuda N., Kubono S., Motobayashi T., Nakabayashi T., Nakamura T., Nakao T., Okumura T., Ong H., Suzuki H., Suzuki M., Teranishi T., Yamada K., Yamaguchi H., and Sakurai H.: "Proton-rich nuclear structure and mirror asymmetry investigated by β-decay spectroscopy of ^{24}Si", J. Phys.: Con. Ser. **312**, No. 092031, pp. 1–6 (2011). *

Kuboki H., Okuno H., Yokouchi S., Hasebe H., Kishida T., Fukunishi N., Kamigaito O., Goto A., Kase M., and Yano Y.: "Charge-state distribution measurements using gas charge stripper toward ^{238}U and ^{136}Xe acceleration at RIKEN RIBF", Nucl. Instrum. Methods Phys. Res. A **655**, No. 1, pp. 17–20 (2011). *

Nakai Y., Majima T., Mizuno T., Tsuchida H., and Itoh A.: "C_{60} fragmentation in charge-changing collisions with slow Au^+ ions", Phys. Rev. A **83**, No. 5, pp. 053201-1–053201-6 (2011). *

Deacon A. N., Steppenbeck D., Zhu S., Freeman S. J., Janssens R. V., Carpenter M. P., Fornal B., Honma M., Kay B. P., Kondev F. G., Kozemczak J., Larabee A., Lauritsen T., Lister C. J., Robinson A. P., Seweryniak D., Smith J. F., Sun Y., Wang X., Xu F., and Yang Y.: "Single-particle and collective structures in ^{55}Cr and ^{55}V", Phys. Rev. C **83**, No. 6, pp. 064305-1–064305-15 (2011). *

Nishimura S., Li Z., Watanabe H., Yoshinaga K., Sumikama T., Tachibana T., Yamaguchi K., Nishimura M., Lorusso G., Miyashita Y., Odahara A., Baba H., Berryman J. S., Blasi N., Bracco A., Camera F., Chiba J., Doornenbal P. C., Go S., Ideguchi E., Isobe T., Jenkins D. G., Kawada Y., Kobayashi N., Kondo Y., Kruecken R., Kubono S., Nakano T., Ong H., Ota S., Podolyak Z. F., Sakurai H., Scheit H., Steppenbeck D., Sugimoto K., Takano S., Takashima A., Tajiri K., Teranishi T., Wakabayashi Y., Walker P. M., and Wieland O.: "β-Decay Half-Lives of Very Neutron-Rich Kr to Tc Isotopes on the Boundary of the r-Process Path: An Indication of Fast r-Matter Flow", Phys. Rev. Lett. **106**, 052502-1–052502-5 (2011). *

Inoue T., Tsuchiya M., Furukawa T., Hayashi H., Nanao T., Yoshimi A., Uchida M., Matsuo Y., and Asahi K.: "Frequency characteristics of a nuclear spin maser for the search for the electric dipole moment of 129Xe atom", Physica E **43**, No. 3, pp. 847–850 (2011). *

Watanabe H., Yamakuchi K., Odahara A., Sumikama T., Nishimura S., Yoshinaga K., Li Z., Miyashita Y., Sato K., Prochniak L., Baba H., Berryman J. S., Blasi N., Bracco A., Camera F., Chiba J., Doornenbal P. C., Go S., Hashimoto T., Hayakawa S., Hinke C., Hinohara N., Ideguchi E., Isobe T., Ito Y., Jenkins D. G., Kawada Y., Kobayashi N., Kondo Y., Krucken R., Lorusso G., Nakano T., Nakatsukasa T., Kurata-Nishimura M., Ong H. J., Ota S., Podolyak Z., Sakurai H., Scheit H., Steiger K., Steppenbeck D., Sugimoto K., Tajiri K., Takano S., Takashima A., Teranishi T., Wakabayashi Y., Walker P. M., Wieland O., and Yamaguchi H.: "Development of axial asymmetry in the neutron-rich nucleus 110Mo", Physics Letter B **704**, 270–275 (2011). *

(Others)

Nakano Y., Inoue T., Azuma T., Hatakeyama A., Nakai Y., Komaki K., Yamazaki Y., Takada E., and Murakami T.: "Resonant Coherent Excitation of Li-like Ar15+ Ions in a Thin Si Crystal", J. Phys.: Con. Ser. **163**, No. 1, pp. 012094-1–012094-4 (2009).

Sihver L., Lantz M. J., Takechi M., Kohama A., Ferrari A., Cerutti F., and Sato T.: "A comparison of total reaction cross section models used in particle and heavy ion transport codes", Adv. Space Res. **49**, 812–819 (2012).

[Book・Proceedings]

(Original Papers) *Subject to Peer Review

Asahi K., Inoue T., Nanao T., Tsuchiya M., Hayashi H., Furukawa T., Yoshimi A., Uchida M., Ueno H., Matsuo Y., and Fukuyama T.: "Search for Electric Dipole Moment in 129Xe Atom Using a Nuclear Spin Oscillator", Proceedings of 4th International Workshop on Fundamental Physics Using Atoms 2010, Osaka, 2010–8, , Osaka, pp. 24–28 (2010). *

Oral Presentations

(International Conference etc.)

Imai N., Ong H., Aoi N., Sakurai H., Demichi K., Kawasaki H., Baba H., Dombradi Z., Elekes Z., Fukuda N., Fulop Z., Gelberg A., Gomi T., Hasegawa H., Ishikawa K., Iwasaki H., Kaneko E., Kanno S., Kishida T., Kondo Y., Kubo T., Kurita K., Michimasa S., Minemura T., Miura M., Motobayashi T., Nakamura T., Notani M., Onishi T., Saito A., Shimoura S., Sugimoto T., Suzuki M., Takeshita E., Takeuchi S., Tamaki M., Yamada K., Yoneda K., Watanabe H., and Ishihara M.: "Anomalously small B(E2) value of ^{16}C", International Nuclear Physics Conference (INPC2004), Goteborg, Sweden, June–July (2004).

Tanaka K., Yamaguchi T., Suzuki T., Ozawa A., Aiba T., Aoi N., Baba H., Fukuda M., Hashizume Y., Inafuku K., Iwasa N., Izumikawa T., Kobayashi K., Komuro M., Kondo Y., Uesaka M., Matsuyama T., Michimasa S., Nakabayashi T., Nakajima S., Ohtsubo T., Shinoda R., Shinohara M., Suzuki H., Takechi M., Takeshita E., Takeuchi S., Togano Y., Yamada K., Yasuno T., Yoshitake M., Kubo T., Nakamura T., Sakurai H., and Motobayashi T.: "Measurement of reaction cross section for ^{22}C", 5th International Workshop on Direct Reaction with Exotic Beams (DREB2007), Wako, May–June (2007).

Tanaka K., Yamaguchi T., Suzuki T., Ozawa A., Aiba T., Aoi N., Baba H., Fukuda M., Hashizume Y., Inafuku K., Iwasa N., Izumikawa T., Kobayashi K., Komuro M., Kondo Y., Uesaka M., Matsuyama T., Michimasa S., Nakabayashi T., Nakajima S., Ohtsubo T., Shinoda R., Shinohara M., Suzuki H., Takechi M., Takeshita E., Takeuchi S., Togano Y., Yamada K., Yasuno T., Yoshitake M., Kubo T., Nakamura T., Sakurai H., and Motobayashi T.: "Giant neutron halo in ^{22}C studied via reaction cross sections at intermediate energy", International Nuclear Physics Conference (INPC2007), (Science Council of Japan, RIKEN and others), Tokyo, June (2007).

Sato H., Iwasa N., Kawabata T., Kobayashi T., Kondo Y., Kubo T., Kusaka K., Motobayashi T., Murakami T., Nakamura T., Ohnishi J., Ohnishi T., Okuno H., Otsu H., Sakurai H., Satou Y., Sakaguchi-Sekiguchi K., Togano Y., and Yoneda K.: "SAMURAI spectrometer at RIKEN RI beam factory", Advanced Studies Institute: Symmetries and Spin (SPIN-Praha-2009), (Charles University), Prague, Czech, July–Aug. (2009).

Morimoto K., Morita K., Kaji D., Haba H., Ohzeki K., Kudou Y., Sato N., Sumita T., Yoneda A., Ichikawa T., Goto S., Fujimori Y., Ideguchi E., Kasamatsu Y., Katori K., Komori Y., Koura H., Kudo H., Ooe K., Ozawa A., Tokanai F., Tsukada K., Yamaguchi T., and Yoshida A.: "Production and Decay Properties of ^{266}Bh and its daughter nuclei by using the ^{248}Cm(^{23}Na,5n) Reaction", Seventh Workshop on the Chemistry of the Heaviest elements, Mainz, Germany, Oct. (2009).

Asahi K., Inoue T., Furukawa T., Tsuchiya M., Hayashi H., Nanao T., Uchida M., and Yoshimi A.: "Experimental search for an EDM in 129Xe atom", International Workshop on UCN and Fundamental Neutron Physics (UCN2010), (RCNP), Osaka, Apr. (2010).

Tsuchiya M., Inoue T., Hayashi H., Nanao T., Furukawa T., Yoshimi A., Uchida M., and Asahi K.: "A Test Bench for the Polarization Study of 129Xe for an EDM Search Experiment", International Nuclear Physics Conference (INPC2010), (TRIUMF), Vancouver, Canada, July (2010).

Nanao T., Yoshimi A., Inoue T., Furukawa T., Tsuchiya M., Hayashi H., Uchida M., and Asahi K.: "Development of High-Sensitivity NMOR Magnetometry for an EDM Experiment", International Nuclear Physics Conference (INPC2010), (TRIUMF), Vancouver, Canada, July (2010).

Furukawa T., Inoue T., Nanao T., Yoshimi A., Tsuchiya M., Hayashi H., Uchida M., and Asahi K.: "Magnetic Field Stabilization for 129Xe EDM Search Experiment", International Nuclear Physics Conference (INPC2010), (TRIUMF), Vancouver, Canada, July (2010).

Inoue T., Yoshimi A., Furukawa T., Tsuchiya M., Hayashi H., Nanao T., Uchida M., and Asahi K.: "Search for an EDM in Diamagnetic Atom 129Xe with Nuclear Spin Maser Technique", International Nuclear Physics Conference (INPC2010), (TRIUMF), Vancouver, Canada, July (2010).

Asahi K., Nanao T., Tsuchiya M., Hayashi H., Furukawa T., Yoshimi A., Uchida M., Ueno H., and Matsuo Y.: "Search for an electric dipole moment in 129Xe atom using a nuclear spin oscillator", International conference on Fundamental Physics Using Atoms, Osaka, Aug. (2010).

Suda S., Nakano Y., Metoki K., Azuma T., Takano Y., Hatakeyama A., Nakai Y., Komaki K., Takada E., and Murakami T.: "Electron emission from fast heavy ions associated with resonant coherent excitation", 15th International Conference on the Physics of Highly Charged Ions (HCI2010), (Fudan University), Shanghai, China, Aug.–Sept. (2010).

Kuboki H., Okuno H., Hasebe H., Yokouchi S., Kishida T., Fukunishi N., Kamigaito O., Goto A., Kase M., and Yano Y.: "Charge-state distribution measurements using gas charge stripper toward ^{238}U and ^{136}Xe acceleration at RIKEN RIBF", 25th World Conference of the International Nuclear Target Development Society, (TRIUMF), Vancouver, Canada, Sept. (2010).

Inoue T., Furukawa T., Nanao T., Yoshimi A., Suzuki K., Tsuchiya M., Hayashi H., Uchida M., and Asahi K.: "Development of the nuclear spin maser toward the atomic EDM search", 19th International Spin Physics Symposium (SPIN 2010), Julich, Germany, Sept.–Oct. (2010).

Yoshimi A., Nanao T., Inoue T., Furukawa T., Tsuchiya M., Hayashi H., Chikamori M., Uchida M., and Asahi K.: "Development of NMOR magnetometer for spin-maser EDM experiment", Villigen, Switzerland 2010/10, (PSI), Villigen, Switzerland, Oct. (2010).

Inoue T., Furukawa T., Nanao T., Yoshimi A., Suzuki K., Chikamori M., Hayashi H., Uchida M., and Asahi K.: "Experimental search for 129Xe atomic EDM with nuclear spin maser technique", Villigen, Switzerland 2010/10, (PSI), Villigen, Switzerland, Oct. (2010).

Ichikawa Y., Ueno H., Ishii Y., Furukawa T., Yoshimi A., Kameda D., Aoi N., Watanabe H., Asahi K., Iijima H., Suzuki K., Inoue T., Tsuchiya M., Hayashi H., Nanao T., Kubo T., Inabe N., Ohnishi T., Takeda H., Fukuda N., Ishihara M., Daugas J., Chevrier R., Georgiev G., Rajabali M. M., and Balabanski D. L.: "Production of spin-aligned RI beam via two-step fragmentation reaction with dispersion matching", University of Aizu-JUSTIPEN-EFES Symposium on "Cutting-Edge Physics of Unstable Nuclei", (University of Aizu), Aizuwakamatsu, Nov. (2010).

Morimoto K., Morita K., Kaji D., Haba H., Ohzeki K., Kudou Y., Sato N., Sumita T., Yoneda A., Ichikawa T., Fujimori Y., Goto S., Huang T., Ideguchi E., Kasamatsu Y., Katori K., Komori Y., Koura H., Kudo H., Murakami M., Ozawa A., Sakai R., Tokanai F., Tsukada K., Yamaguchi T., and Yoshida A.: "Confirmations of the synthesis of ^{278}113 produced by the ^{209}Bi(^{70}Zn,n)^{278}113 reaction", International Chemical Congress of Pacific Basin Societies (PACIFICHEM 2010), Honolulu, USA, Dec. (2010).

Asahi K., Inoue T., Nanao T., Tsuchiya M., Hayashi H., Furukawa T., Uchida M., Yoshimi A., Ueno H., and Matsuo Y.: "Search for Electric Dipole Moment in 129Xe atom Using a Nuclear Spin Oscillator", International Symposium Nanoscience and Quantum Physics (nanoPHYS'11), Tokyo, Jan. (2011).

Isobe T.: "SAMURAI TPC", Workshop on advanced detector technology for nuclear physics, Wako, Jan. (2011).

Ichikawa Y., Ueno H., Ishii Y., Furukawa T., Yoshimi A., Kameda D., Aoi N., Watanabe H., Asahi K., Iijima H., Suzuki K., Inoue T., Tsuchiya M., Hayashi H., Nanao T., Kubo T., Inabe N., Ohnishi T., Takeda H., Fukuda N., Ishihara M., Daugas J., Chevrier R., Georgiev G., Rajabali M. M., and Balabanski D. L.: "g-factor measurements for highly spin-aligned isomeric states", RIBF-ULIC-Symposium-007: E(U)RICA International Workshop, Saitama, May (2011).

Ichikawa Y., Ueno H., Ishii Y., Furukawa T., Yoshimi A., Kameda D., Aoi N., Watanabe H., Asahi K., Iijima H., Suzuki K., Inoue T., Tsuchiya M., Hayashi H., Nanao T., Kubo T., Inabe N., Ohnishi T., Takeda H., Fukuda N., Ishihara M., Daugas J., Chevrier R., Georgiev G., Rajabali M. M., and Balabanski D. L.: "Production of spin-aligned RI beam via two-step fragmentation with dispersion matching", ARIS 2011, (Katholieke Universiteit Leuven), Leuven, Belgium, May–June (2011).

Chevrier R., Daugas J., Gaudefroy L., Ichikawa Y., Ueno H., Haas M., Haas H., Cottenier S., Aoi N., Asahi K., Balabanski D. L., Fukuda N., Furukawa T., Georgiev G., Hayashi H., Iijima H., Inabe N., Inoue T., Ishihara M., Ishii Y., Kameda D., Kubo T., Nanao T., Neyence G., Ohnishi T., Rajabali M. M., Suzuki K., Takeda H., Tsuchiya M., Vermeulen N., Watanabe H., and Yoshimi A.: "Quadrupole moment measurement of the $N = 27$ nucleus $43m$S", ARIS 2011, (Katholieke Universiteit Leuven), Leuven, Belgium, May–June (2011).

Ichikawa Y., Ueno H., Ishii Y., Furukawa T., Yoshimi A., Kameda D., Aoi N., Watanabe H., Asahi K., Iijima H., Suzuki K., Inoue T., Tsuchiya M., Hayashi H., Nanao T., Kubo T., Inabe N., Ohnishi T., Takeda H., Fukuda N., Ishihara M., Daugas J., Chevrier R., Georgiev G., Rajabali M. M., and Balabanski D. L.: "g-factor measurement for highly spin-aligned isomeric state of ^{32}Al", RIBF ULIC and CNS Symposium on Frontier of Gamma-ray Spectroscopy (Gamma11), (CNS, The University of Tokyo and RIKEN Nishina Center), Saitama, June–July (2011).

Suda S., Nakano Y., Metoki K., Shindo D., Ohtsuki S., Azuma T., Hatakeyama A., Komaki K., Nakai Y., Takada E., and Murakami K.: "Convey electron emission following ionization of highly-charged ions excited by resonant coherent excitation", ICPEAC, (ICPEAC Committees), Belfast, UK, July (2011).

Matsuo Y.: "Laser spectroscopy of atoms in superfluid helium", MATRIX2011 Research of Chemistry and Physics of Matrix Isolated Species, (University of British Columbia), Vancouver, Canada, July (2011).

Ichikawa Y., Ueno H., Ishii Y., Furukawa T., Yoshimi A., Kameda D., Aoi N., Watanabe H., Asahi K., Iijima H., Suzuki K., Inoue T., Tsuchiya M., Hayashi H., Nanao T., Kubo T., Inabe N., Ohnishi T., Takeda H., Fukuda N., Ishihara M., Daugas J., Chevrier R., Georgiev G., Rajabali M. M., and Balabanski D. L.: "Production of spin-aligned RI beam via two-step fragmentation with dispersion matching", Rutherford Centennial Conference on Nuclear Physics 2011, (The University of Machester), Manchester, United Kingdom, Aug. (2011).

Chevrier R., Daugas J., Gaudefroy L., Ichikawa Y., Ueno H., Haas M., Haas H., Cottenier S., Aoi N., Asahi K., Balabanski D. L., Fukuda N., Furukawa T., Georgiev G., Hayashi H., Iijima H., Inabe N., Inoue T., Ishihara M., Ishii Y., Kameda D., Kubo T., Nanao T., Neyence G., Ohnishi T., Rajabali M. M., Suzuki K., Takeda H., Tsuchiya M., Vermeulen N., Watanabe H., and Yoshimi A.: "Quadrupole moment measurement of the $N = 27$ nucleus ^{43}S^{m}", Colloque GANIL 2011, (GANIL), Corsica, France, Sept. (2011).

Yoshimi A., Nanao T., Inoue T., Chikamori M., Furukawa T., Ichikawa Y., Hayashi H., Tsuchiya M., Miyatake H., Ishii Y., Yoshida N., Shirai H., Uchida M., Ueno H., Matsuo Y., Fukuyama T., and Asahi K.: "Development of high-sensitivity magnetometer for EDM experiment with ^{129}Xe spin ocsillator", 5th International conference on "Fundamental Physics Using Atoms - Towards better understanding of our matter universe -", (Okayama University), Okayama, Oct. (2011).

Chikamori M., Miyatake H., Inoue T., Nanao T., Furukawa T., Yoshimi A., Ichikawa Y., Tsuchiya M., Hayashi H., Ishii Y., Yoshida N., Shirai H., Uchida M., Ueno H., Matsuo Y., Fukuyama T., and Asahi K.: "Development of Xe SEOP cells for an experiment searching or an atomic electric dipole moment in ^{129}Xe", 5th International conference on "Fundamental Physics Using Atoms - Towards better understanding of our matter universe -", (Okayama University), Okayama, Oct. (2011).

Nanao T., Furukawa T., Inoue T., Chikamori M., Yoshimi A., Ichikawa Y., Tsuchiya M., Hayashi H., Miyatake H., Ishii Y., Yoshida N., Shirai H., Uchida M., Ueno H., Matsuo Y., Fukuyama T., and Asahi K.: "Stabilization of environmental magnetic fields in the Tokyo Tech ^{129}Xe atomic DM experiment", 5th International conference on "Fundamental Physics Using Atoms - Towards better understanding of our matter universe -", (Okayama University), Okayama, Oct. (2011).

Inoue T., Nanao T., Chikamori M., Furukawa T., Yoshimi A., Ichikawa Y., Hayashi H., Tsuchiya M., Miyatake H., Ishii Y., Yoshida N., Shirai H., Uchida M., Ueno H., Matsuo Y., Fukuyama T., and Asahi K.: "^{129}Xe atomic EDM search with nuclear spin maser technique", 5th International conference on "Fundamental Physics Using Atoms" - Towards better understanding of our matter universe -, (Okayama University), Okayama, Oct. (2011).

Matsuo Y.: "Electron spin polarization of optically pumped atoms in superfluid helium", RIKEN-Kazan Federal University (KFU) Joint Symposium: Spins, Wako, Oct. (2011).

Ichikawa Y., Ueno H., Ishii Y., Furukawa T., Yoshimi A., Kameda D., Aoi N., Watanabe H., Asahi K., Iijima H., Suzuki K., Inoue T., Tsuchiya M., Hayashi H., Nanao T., Kubo T., Inabe N., Ohnishi T., Takeda H., Fukuda N., Ishihara M., Daugas J., Chevrier R., Georgiev G., Rajabali M. M., and Balabanski D. L.: "Spin-aligned RI beam produced by two-step projectile fragmentation", ISPUN11, (Institute for Nuclear Science and Technique), Hanoi, Vietnam, Nov. (2011).

Nakai Y., Hidaka H., Watanabe N., and Kojima T.: "Equipment for ionic cluster formation based on ion drift-tube with selected-ion injection", 18th Symposium on Atomic, Cluster, and Surface Physics (SASP2012), (Institut de Planetologie et d'Astrophysique de Grenoble (IPAG)), Alpe d'Huez, France, Jan. (2012).

(Domestic Conference)

飯尾雅実, 板橋健太, 岩崎雅彦, 應田治彦, 大西宏明, 佐久間

史典, 佐藤将春, 塚田暁, 友野大, 藤岡宏之, 山崎敏光, 石元茂, 岩井正明, 鈴木祥二, 関本美知子, 豊田晃久, 石川隆, 竜野秀行, 鈴木隆敏, 早野龍五, 松田恭幸, 永江知文, 平岩聡彦, 味村周平, 野海博之, 阪口篤志, 藤原裕也, 徳田真, 千葉順成, 福田共和, 溝井浩, Beer G. A., 方享燦, Choi S., 林熙重, 石渡智一, Buehler P., Cargnelli M., Hirtl A., Kienle P., Marton J., Widmann E., Zmeskal J., 岡田信二, Curceanu C. O., Guaraldo C., Iliescu M., Pietreanu D., Sirghi D., Sirghi F., Faso D., Morra O., Busso L.: “K 中間子原子核探査実験のための液体ヘリウム 3 標的の開発 III”, 日本物理学会 2008 年秋季大会, (日本物理学会), 盛岡 , 9 月 (2008).

飯島裕章, 吉見彰洋, 市川雄一, 石井裕司, 吉田直貴, 古川武, 内田誠, 鈴木都文, 井上壮志, 土屋真人, 林宏憲, 七尾翼, 近森正敏, 上野秀樹, 旭耕一郎: “中性子過剰核 41,43S の磁気モーメント測定のための磁場回転装置の開発”, 平成 22 年度 KUR 専門研究会「短寿命核および放射線を用いた物性研究（III)」, 大阪, 2 月 (2010).

上坂明子, 竹谷篤, 馬場秀忠, 本林透, 村上浩之, 栂野泰宏, 米田健一郎: “広いダイナミックレンジを持った電荷有感型前置増幅器開発”, 日本物理学会第 65 回年次大会, (日本物理学会), 岡山, 3 月 (2010).

上坂明子, 竹谷篤, 栂野泰宏, 村上浩之, 本林透, 米田健一郎: “シリコン検出器用電荷有感型前置増幅器のダイナミックレンジの拡大”, 日本物理学会第 65 回年次大会, (日本物理学会), 岡山, 3 月 (2010).

松浦佑一, 古川武, 小林徹, 畠山温, 加藤裕樹, 立川真樹, 松尾由賀利: “超流動ヘリウム中での Au 原子の励起スペクトルと偏極生成”, 第 7 回 AMO 討論会, つくば, 6 月 (2010).

七尾翼, 吉見彰洋, 井上壮志, 古川武, 土屋真人, 林宏憲, 内田誠, 旭耕一郎: “EDM 実験のための NMOR を用いた高感度磁力計の開発”, 日本物理学会 2010 年秋季大会, 北九州, 9 月 (2010).

石井裕司, 市川雄一, 上野秀樹, 古川武, 吉見彰洋, 亀田大輔, 青井考, 渡邉寛, 旭耕一郎, 飯島裕章, 鈴木都文, 井上壮志, 土屋真人, 林宏憲, 七尾翼, 久保敏幸, 稲辺尚人, 大西哲哉, 竹田浩之, 福田直樹, 石原正泰, Daugas J., Chevrier R., Georgiev G., Rajabali M. M., Balabanski D. L.: “TD-PAD 法を用いた ^{32}Al アイソマーの磁気モーメント測定”, 日本物理学会 2010 年秋季大会, (日本物理学会), 北九州, 9 月 (2010).

園田哲, 和田道治, 富田英生, 岡田邦宏, 伊藤由太, 飯村秀紀, 中村聡佑, Schuessler H. A., 高峰愛子, 松尾由賀利, 久保敏幸, 古川武, 片山一郎, 涌井崇志, 篠塚勉, Huyse M., Kudryavtsev. Y., Duppen P. V.: “理研における共鳴イオン化レーザーイオン源の開発”, 日本物理学会 2010 年秋季大会, (日本物理学会), 北九州市, 9 月 (2010).

上坂明子, 竹谷篤, 馬場秀忠, 本林透, 村上浩之, 栂野泰宏, 米田健一郎, 郡司卓, 浜垣秀樹, 林真一, 田中真伸: “広いダイナミックレンジを持った電荷有感型前置増幅器の開発”, 日本物理学会第 66 回年次大会, (日本物理学会), 新潟, 3 月 (2011).

藤原康平, 竹谷篤, 磯部忠昭, 小林丈士: “重イオン衝突実験用広ダイナミックレンジ TPC 用読出しパッドの開発”, 日本物理学会第 66 回年次大会, (日本物理学会), 新潟, 3 月 (2011).

石井裕司, 市川雄一, 上野秀樹, 古川武, 吉見彰洋, 亀田大輔, 青井考, 渡邉寛, 旭耕一郎, 飯島裕章, 鈴木都文, 井上壮志, 土屋真人, 林宏憲, 七尾翼, 久保敏幸, 稲辺尚人, 大西哲哉, 竹田浩之, 福田直樹, 石原正泰, Daugas J., Chevrier R., Georgiev G., Rajabali M. M., Balabanski D. L.: “TD-PAD 法を用いた ^{32}Al アイソマーの磁気モーメント測定 II”, 日本物理学会第 66 回年次大会, (日本物理学会), 新潟, 3 月 (2011).

松浦佑一, 古川武, 小林徹, 畠山温, 加藤裕樹, 山口康広, 今村慧, 幕田将宏, 立川真樹, 松尾由賀利: “超流動ヘリウム環境を用いた Au 原子の光ポンピングと二重共鳴”, 日本物理学会第 66 回年次大会, 新潟, 3 月 (2011).

古川武, 涌井崇志, 佐々木彩子, 泉さやか, 市川雄一, 吉見彰洋, 田尻邦彦, 石井裕司, 吉田直貴, 松浦佑一, 加藤裕樹, 山口康広, 今村慧, 幕田将宏, 畠山温, 和田道治, 園田哲, 伊藤由太, 七尾翼, 小林徹, 西村俊二, 西村美月, 近藤洋介, 青井考, 米田健一郎, 久保野茂, 大城幸光, 上野秀樹, 篠塚勉, 下田正, 旭耕一郎, 松尾由賀利: “^{87}Rb ビームを用いた超流動ヘリウム中でのレーザー核分光法開発実験”, 日本物理学会第 66 回年次大会, 新潟, 3 月 (2011).

市川雄一, 上野秀樹, 石井裕司, 古川武, 吉見彰洋, 亀田大輔, 青井考, 渡邉寛, 旭耕一郎, 飯島裕章, 鈴木都文, 井上壮志, 土屋真人, 林宏憲, 七尾翼, 久保敏幸, 稲辺尚人, 大西哲哉, 竹田浩之, 福田直樹, 石原正泰, Daugas J., Chevrier R., Georgiev G., Rajabali M. M., Balabanski D. L.: “分散整合二回散乱法による核スピン整列 RI ビームの生成 II”, 日本物理学会第 66 回年次大会, (日本物理学会), 新潟, 3 月 (2011).

松尾由賀利: “超流動ヘリウム中における 13 族原子 (Al, Ga, In) の励起スペクトル”, Chemistry and Fundamental Science, (新学術領域「原子が切り拓く極限量子の世界」総括班), 東京, 5 月 (2011).

小林徹, 松尾由賀利: “窒化ホウ素基板のレーザーアブレーションで生成するフラグメント正イオンの水素化反応性”, 第 27 回化学反応討論会, (化学反応討論会事務局), 東京, 6 月 (2011).

加藤裕樹, 古川武, 今村慧, 山口康広, 小林徹, 畠山温, 立川真樹, 松尾由賀利: “超流動ヘリウム中に埋め込まれた 13 族原子 In, Ga の励起スペクトル”, 第 8 回 AMO 討論会, (原子・分子・光科学 (AMO) 討論会実行委員会), 東京, 6 月 (2011).

松浦佑一, 古川武, 小林徹, 畠山温, 加藤裕樹, 山口康広, 今村慧, 幕田将宏, 立川真樹, 松尾由賀利: “超流動ヘリウム環境を用いた Au 原子の光ポンピングと二重共鳴”, 第 8 回 AMO 討論会, (原子・分子・光科学 (AMO) 討論会実行委員会), 東京, 6 月 (2011).

中井陽一, 日高宏, 渡部直樹, 小島隆夫: “イオン打ち込み型移動管を用いた水和クラスターイオンの生成実験の現状”, 日本物理学会 2011 年秋季大会, (日本物理学会), 富山, 9 月 (2011).

今村慧, 古川武, 山口康広, Yang X., 加藤裕樹, 小林徹, 幕田将宏, 畠山温, 小田島仁司, 松尾由賀利: “超流動 He 環境におけるアルカリ原子の超微細構造間隔測定”, 日本物理学会 2011 年秋季大会, (日本物理学会), 富山, 9 月 (2011).

古川武, 涌井崇志, 佐々木彩子, 泉さやか, 市川雄一, 吉見彰洋, 田尻邦彦, 石井裕司, 吉田直貴, 松浦佑一, 加藤裕樹, 山口康広, 今村慧, 幕田将宏, 畠山温, 和田道治, 園田哲, 伊藤由太, 七尾翼, 小林徹, 西村俊二, 西村美月, 近藤洋介, 青井考, 米田健一郎, 久保野茂, 上野秀樹, 下田正, 篠塚勉, 旭耕一郎, 松尾由賀利: “超流動ヘリウム中に打ち込まれた ^{87}Rb ビームのレーザー誘起蛍光観測と光ポンピング”, 日本物理学会 2011 年秋季大会, (日本物理学会), 弘前, 9 月 (2011).

市川雄一, 上野秀樹, 石井裕司, 古川武, 吉見彰洋, 亀田大輔, 青井考, 渡邉寛, 旭耕一郎, 飯島裕章, 鈴木都文, 井上壮志, 土屋真人, 林宏憲, 七尾翼, 久保敏幸, 稲辺尚人, 大西哲哉, 竹田浩之, 福田直樹, 石原正泰, Daugas J., Chevrier R., Georgiev G., Rajabali M. M., Balabanski D. L.: “分散整合二回散乱法による核スピン整列 RI ビームの生成 III”, 日本物理学会 2011 年秋季大会, (日本物理学会), 弘前, 9 月 (2011).

舟田周平, 谷川英臣, 笹公和, 小原ひとみ, 中井陽一, Pedersen J. O., Hvelplund P., 冨田成夫: “$N_2/H_2O/SO_2$ 中での 20MeV 陽子線による液滴生成過程における SO_2 濃度依存性”, 日本物理学会 2011 年秋季大会, (日本物理学会), 富山, 9 月 (2011).

須田慎太郎, 中野祐司, 目時健一, 畠山温, 中井陽一, 東俊行, 小牧研一郎, 高田栄一, 村上健: “コヒーレント共鳴励起にともなう電子放出の観測 5”, 日本物理学会 2011 年秋季大会, (日本物理学会), 富山, 9 月 (2011).

磯部忠昭: “重イオン衝突におけるフローの測定を通した EoS の研究”, RIBF-ULIC-miniWS Nuclear Matter in Neutron Stars, 和光, 9 月 (2011).

松尾由賀利: “レーザーでつくるスピン偏極と原子・原子核物理への応用”, 「核スピン研究とその応用」研究会, (東京工業大学), 東京, 11 月 (2011).

中野祐司, 須田慎太郎, 畠山温, 中井陽一, 小牧研一郎, 東俊行, 高田栄一, 村上健: “薄膜結晶におけるコヒーレント共鳴励起：空イオンの選択的生成”, 第 12 回「イオンビームによる表面・界面解析」特別研究会, (応用物理学会・薄膜表面物理分科会), 東京, 12 月 (2011).

石井裕司, Georgiev G., 市川雄一, 白井葉月, 上野秀樹, 石橋陽子, 吉田直貴, 古川武, Sotty C., Chevrier R., Daugas J., Ljungvall J., Lozeva R. L., 新倉潤, Yordanov D., 渡邉寛, 西村太樹, 西畑洸希, 近森正敏, 宮武裕和, 七尾翼, 丹羽崇博, 岡田俊祐, 齋藤佑多, 旭耕一郎, Balabanski D. L.: “Production of a spin-aligned ^{69}Cu beam by one-nucleon-removal reactions and measurement of its nuclear moments”, 日本物理学会第 67 回年次大会, (日本物理学会), 西宮, 3 月 (2012).

加藤裕樹, 古川武, 小林徹, 今村慧, 山口康広, Yang X., 畠山温, 立川真樹, 松尾由賀利: “超流動ヘリウム環境下における In 原子の電子スピン緩和”, 日本物理学会第 67 回年次大会, (日本物理学会), 西宮, 3 月 (2012).

松浦佑一, 古川武, 小林徹, 畠山温, 加藤裕樹, 山口康広, 今村慧, 幕田将宏, 立川真樹, 松尾由賀利: “超流動ヘリウム環境を用いた Au 原子のスピン偏極と核スピンの導出”, 日本物理学会第 67 回年次大会, (日本物理学会), 西宮, 3 月 (2012).

Spin isospin Laboratory

Oral Presentations

(International Conference etc.)

Yamaguchi Y., Wakasugi M., Suzuki H., Fujinawa T., Uesaka T., Yano Y., Ozawa A., Nagae D., Yamaguchi T., Suzuki T., Kikuchi T., Jiang W., Sasaki T., and Tokuchi A.: "Present status of rare-RI ring project in RIKEN RI beam factory", 8th International Conference on Nuclear Physics at Storage Rings (STORI-11), (INFN-LNF), Frascati, Italy, Oct. (2011).

(Domestic Conference)

古川武, 涌井崇志, 佐々木彩子, 泉さやか, 市川雄一, 吉見彰洋, 田尻邦彦, 石井裕司, 吉田直貴, 松浦佑一, 加藤裕樹, 山口康広, 今村慧, 幕田将宏, 畠山温, 和田道治, 園田哲, 伊藤由太, 七尾翼, 小林徹, 西村俊二, 西村美月, 近藤洋介, 青井考, 米田健一郎, 久保野茂, 上野秀樹, 下田正, 篠塚勉, 旭耕一郎, 松尾由賀利: "超流動ヘリウム中に打ち込まれた ^{87}Rb ビームのレーザー誘起蛍光観測と光ポンピング", 日本物理学会 2011 年秋季大会, (日本物理学会), 弘前, 9 月 (2011).

Superheavy Element Laboratory

Publications

[Journal]

(Original Papers) *Subject to Peer Review

Haba H., Kaji D., Kikunaga H., Kudou Y., Morimoto K., Morita K., Ohzeki K., Sumita T., and Yoneda A.: "Production and decay properties of the 1.9-s isomeric state in 261Rf", Phys. Rev. C **83**, No. 3, pp. 034602-1–034602-7 (2011). *

Ooe K., Yahagi W., Komori Y., Fujisawa H., Takayama L., Kikunaga H., Yoshimura T., Takahashi N., Haba H., Kudou Y., Ezaki Y., and Shinohara A.: "Extraction behavior of carrier-free and macro amounts of molybdenum and tungsten from HCl solution", Proc.Radiochim **1**, 127–129 (2011). *

Takayama L., Ooe K., Yahagi W., Fujisawa H., Komori Y., Kikunaga H., Yoshimura T., Takahashi N., Takahisa K., Haba H., Kudou Y., Ezaki Y., Toyoshima A., Asai M., Nagame Y., Saito T., Mitsugashira T., and Shinohara A.: "Solvent extraction of trivalent actinides with di(2-ethylhexyl) phosphoric acid", Proc.Radiochim **1**, 157–160 (2011). *

Haba H., Kaji D., Kudou Y., Morimoto K., Morita K., Ohzeki K., Sakai R., Sumita T., Yoneda A., Kasamatsu Y., Komori Y., Shinohara A., Kikunaga H., Kudo H., Nishio K., Ooe K., Sato N., and Tsukada K.: "Production of 265Sg in the 248Cm(22Ne,5n)265Sg reaction and decay properties of two isomeric states in 265Sg", Phys. Rev. C **85**, 024611-1–024611-11 (2012). *

Oral Presentations

(International Conference etc.)

Tanaka K., Yamaguchi T., Suzuki T., Ozawa A., Aiba T., Aoi N., Baba H., Fukuda M., Hashizume Y., Inafuku K., Iwasa N., Izumikawa T., Kobayashi K., Komuro M., Kondo Y., Uesaka M., Matsuyama T., Michimasa S., Nakabayashi T., Nakajima S., Ohtsubo T., Shinoda R., Shinohara M., Suzuki H., Takechi M., Takeshita E., Takeuchi S., Togano Y., Yamada K., Yasuno T., Yoshitake M., Kubo T., Nakamura T., Sakurai H., and Motobayashi T.: "Measurement of reaction cross section for ^{22}C", 5th International Workshop on Direct Reaction with Exotic Beams (DREB2007), Wako, May–June (2007).

Tanaka K., Yamaguchi T., Suzuki T., Ozawa A., Aiba T., Aoi N., Baba H., Fukuda M., Hashizume Y., Inafuku K., Iwasa N., Izumikawa T., Kobayashi K., Komuro M., Kondo Y., Uesaka M., Matsuyama T., Michimasa S., Nakabayashi T., Nakajima S., Ohtsubo T., Shinoda R., Shinohara M., Suzuki H., Takechi M., Takeshita E., Takeuchi S., Togano Y., Yamada K., Yasuno T., Yoshitake M., Kubo T., Nakamura T., Sakurai H., and Motobayashi T.: "Giant neutron halo in ^{22}C studied via reaction cross sections at intermediate energy", International Nuclear Physics Conference (INPC2007), (Science Council of Japan, RIKEN and others), Tokyo, June (2007).

Morimoto K., Morita K., Kaji D., Haba H., Ohzeki K., Kudou Y., Sato N., Sumita T., Yoneda A., Ichikawa T., Goto S., Fujimori Y., Ideguchi E., Kasamatsu Y., Katori K., Komori Y., Koura H., Kudo H., Ooe K., Ozawa A., Tokanai F., Tsukada K., Yamaguchi T., and Yoshida A.: "Production and Decay Properties of ^{266}Bh and its daughter nuclei by using the ^{248}Cm(^{23}Na,5n) Reaction", Seventh Workshop on the Chemistry of the Heaviest elements, Mainz, Germany, Oct. (2009).

Morimoto K., Morita K., Kaji D., Haba H., Ohzeki K., Kudou Y., Sato N., Sumita T., Yoneda A., Ichikawa T., Fujimori Y., Goto S., Huang T., Ideguchi E., Kasamatsu Y., Katori K., Komori Y., Koura H., Kudo H., Murakami M., Ozawa A., Sakai R., Tokanai F., Tsukada K., Yamaguchi T., and Yoshida A.: "Confirmations of the synthesis of ^{278}113 produced by the ^{209}Bi(^{70}Zn,n)^{278}113 reaction", International Chemical Congress of Pacific Basin Societies (PACIFICHEM 2010), Honolulu, USA, Dec. (2010).

Asai M., Haba H., Tsukada K., Sato N., Kasamatsu Y., Kaji D., Morimoto K., Morita K., Sato T., Toyoshima A., Ishii Y., Takahashi R., Nagame Y., Ishii T., Nishinaka I., Kojima Y., and Ichikawa T.: "Alpha-gamma and high-resolution alpha fine-structure spectroscopy for the heaviest nuclei", 4th International Conference on the Chemistry and Physics of the Transactinide Elements (TAN11), (Joint Institute for Nuclear Research), Sochi, Russia, Sept. (2011).

Kasamatsu Y., Komori Y., Kikutani Y., Yokokita T., Kino A., Yoshimura T., Takahashi N., Haba H., Kudou Y., Kikunaga H., Otsuki T., Mitsugashira T., and Shinohara A.: "Application of the rapid preparation method of hydroxide coprecipitate with Sm to superheavy element chemistry -Model experiment for Rf chemistry-", 4th International Conference on the Chemistry and Physics of the Transactinide Elements (TAN11), (Joint Institute for Nuclear Research), Sochi, Russia, Sept. (2011).

Haba H., Kaji D., Kasamatsu Y., Kikunaga H., Komori Y., Kudo H., Kudou Y., Morimoto K., Morita K., Ooe K., Ohzeki K., Sakai R., Sato N., Shinohara A., Sumita T., Tsukada K., and Yoneda A.: "Production of 265Sg for chemical studies using the gas-jet transport system coupled to the RIKEN gas-filled recoil ion separator", 4th International Conference on the Chemistry and Physics of the Transactinide Elements (TAN11), (Joint Institute for Nuclear Research), Sochi, Russia, Sept. (2011).

(Domestic Conference)

小嶋貴幸, 村山裕史, 村上昌史, 後藤真一, 羽場宏光, 加治大哉, 森本幸司, 工藤祐生, 森田浩介, 菊永英寿, 佐藤哲也, 塚田和明, 工藤久昭: "理研 GARIS/gas-jet システムを利用した気相化学の基礎研究", 2011 日本放射化学会年会・第

55 回放射化学討論会, (日本放射化学会年会), 長野, 9 月 (2011).

浅井雅人, 羽場宏光, 佐藤望, 笠松良崇, 加治大哉, 森本幸司, 森田浩介, 嶋洋佑, 柴田理尋, 塚田和明, 佐藤哲也, 豊嶋厚史, 石井哲郎, 永目諭一郎: “高分解能 α 線微細構造測定による重核の核構造研究”, 2011 日本放射化学会年会・第 55 回放射化学討論会, (日本放射化学会年会), 長野, 9 月 (2011).

村上昌史, 後藤真一, 村山裕史, 小嶋貴幸, 加治大哉, 森本幸司, 羽場宏光, 住田貴之, 酒井隆太郎, 工藤祐生, 米田晃, 森田浩介, 菊永英寿, 笠松良崇, 佐藤哲也, 工藤久昭: “248Cm + 18O 反応による Rf 同位体の励起関数の測定”, 2011 日本放射化学会年会・第 55 回放射化学討論会, (日本放射化学会年会), 長野, 9 月 (2011).

High Energy Astrophysics Laboratory

Publications

[Journal]

(Original Papers) *Subject to Peer Review

Gandhi P., Dhillon V. S., Durant M., Fabian A. C., Kubota A., Makishima K., Malzac J., Marsh T. R., Miller J. M., Shahbaz T., Spruit H. C., and Casella P.: "Rapid optical and X-ray timing observations of GX339-4: multicomponent optical variability in the low/hard state", Mon. Not. R. Astron. Soc. **407**, No. 4, pp. 2166–2192 (2010). *

Tsuchiya H. and ASγ .: "Cosmic-ray energy spectrum around the knee obtained by the Tibet experiment and future prospects", Adv. Space Res. **47**, 629–639 (2011). *

Tsuchiya H. and ASγ .: "Cosmic-ray energy spectrum around the knee observed with the Tibet air-shower experiment", Astrophys. Space Sci. Trans. **7**, 15–20 (2011). *

Tsuchiya H. and ASγ .: "Observation of the Fermi pulsar catalog at TeV energies with the Tibet air shower experiment", Astrophys. Space Sci. Trans. **7**, 211–215 (2011). *

Tsuchiya H., Enoto T., Yamada S., Yuasa T., Nakazawa K., Kitaguchi T., Kawaharada M., Kokubun M., Kato H., Okano M., and Makishima K.: "Long-duration γ ray emissions from 2007 and 2008 winter thunderstorms", J. Geophys. Res. **116**, D09113-1–D09113-14 (2011). *

Enoto T., Makishima K., Nakazawa K., Kokubun M., Kawaharada M., Kotoku J., and Shibazaki N.: "Soft and Hard X-Ray Emissions from the Anomalous X-Ray Pulsar 4U 0142+61 Observed with Suzaku", Publ. Astron. Soc. Jpn. **63**, No. 2, pp. 387–396 (2011). *

Noda H., Makishima K., Uehara Y., Nakazawa K., and Yamada S.: "Suzaku Discovery of a Hard Component Varying Independently of the Power-Law Emission in MCG -6-30-15", Publ. Astron. Soc. Jpn. **63**, No. 2, pp. 449–458 (2011). *

Torii S., Yamada S., Makishima K., Sakurai S., Nakazawa K., Noda H., Done C., Takahashi H., and Gandhi P.: "Spectral and Timing Studies of Cyg X-1 in the Low/Hard State with Suzaku", Publ. Astron. Soc. Jpn. **63**, S771–S783 (2011). *

Serino M., Yoshida A., Kawai N., Nakagawa Y., Ueda Y., Mihara T., Nakahira S., Eguchi S., Hiroi K., Ishikawa M., Isobe N., Kimura M., Kitayama H., Kohama M., Matsumura T., Matsuoka M., Morii M., Nakajima M., Negoro H., Shidatsu M., Sootome T., Sugimori K., Sugizaki M., Suwa F., Toizumi T., Tomida H., Tsuboi Y., Tsunemi H., Ueno S., Usui R., Yamamoto T., Yamaoka K., Yamauchi M., and Yamazaki K.: "Peculiarly narrow SED of GRB 090926B with MAXI and Fermi/GBM", Publ. Astron. Soc. Jpn. **63**, S1035–S1040 (2011). *

[Book・Proceedings]

(Original Papers) *Subject to Peer Review

Tsuchiya H. and ASγ .: "Heliospheric signatures seen in the sidereal anisotropy of high-energy galactic cosmic ray intensity", Proceedings of the 9th Annual International Astrophysics Conference, Maui, USA, 2010–3, American Institute of Physics, NY, pp. 285–290 (2010). *

Oral Presentations

(International Conference etc.)

Tsuchiya H.: "Non-thermal radiation processes in lightning and thunderclouds", International workshop on lightning physics, Suita, Dec. (2011).

(Domestic Conference)

土屋晴文, 榎戸輝揚, 鳥居建男, 岡野眞治, 加藤博, 牧島一夫: "地球大気内の雷や雷雲による粒子加速", 日本地球惑星科学連合 2010 年度大会, (日本地球惑星科学連合), 千葉, 5 月 (2010).

玉川徹, 岩橋孝典, 阿佐美ふみ, Jean S., Keith J., 早藤麻美, 田原譲, 高橋忠幸, 牧島一夫: "X 線偏光観測衛星 GEMS の現状と偏光計テストユニット試験", 日本天文学会 2010 年秋季年会, (日本天文学会), 金沢, 9 月 (2010).

松原豊, 永井雄也, さこ隆志, 伊藤好孝, 三塚岳, 柴田祥一, 宗像一起, 加藤千尋, 小島浩司, 土屋晴文, 渡邊恭子: "SciBar 検出器を用いた太陽中性子観測計画 III-計画の進行状況-", 日本物理学会 2010 年秋季大会, (日本物理学会), 北九州, 9 月 (2010).

岩橋 孝典, 玉川 徹, 阿佐美 ふみ, 小波 さおり, 吉川 瑛文, 早藤 麻美, 牧島 一夫, Swank J., Jahoda K., GEMS Collaboration .: "宇宙 X 線偏光観測衛星 GEMS 搭載用偏光計のバックグラウンドシミュレーション", 日本物理学会 2010 年秋季大会, (日本物理学会), 北九州, 9 月 (2010).

吉川瑛文, 玉川徹, 早藤麻美, 岩橋孝典, 阿佐美ふみ, 浜垣秀樹, 郡司卓, 秋元亮二, 忽滑谷淳史, 林真一, 上野一樹, 越智敦彦, Oliveira R. D.: "レジスティブ電極 GEM(RE-GEM) の開発状況", 第 7 回「マイクロパターンガス検出器 (MPGD) 研究会」, (山形大学), 山形, 11 月 (2010).

玉川徹: "GEM-TPC 偏光計の開発と DME 中での GEM の振る舞い", 第 7 回「マイクロパターンガス検出器 (MPGD) 研究会」, (山形大学), 山形, 11 月 (2010).

武内陽子, 玉川徹, 阿佐美ふみ, 吉川瑛文, 岩橋孝典, 小波さおり, 岩切渉: "GEM 両極板およびパッドからの信号読み出し", 第 7 回「マイクロパターンガス検出器 (MPGD) 研究会」, (山形大学), 山形, 11 月 (2010).

土屋晴文, 榎戸輝揚, 鳥居建男, 岡野眞治, 加藤博, 牧島一夫: "雷や雷雲からの X 線・γ 線を利用しての電場による粒子加速の検証", 平成 22 年度 ICRR 共同利用研究成果発表会 , (東京大学宇宙線研究所), 東京, 12 月 (2010).

吉川瑛文, 玉川徹, 早藤麻美, 岩橋孝典, 阿佐美ふみ, 浜垣秀樹, 郡司卓, 秋元亮二, 忽滑谷淳史, 林真一, 上野一樹, 越智敦彦, Oliveira R. D.: "レジスティブ電極 GEM(RE-GEM) の製作と電子増幅度調査", 日本物理学会第 66 回年次大会, (新潟大学), 新潟, 3 月 (2011).

永井雄也, さこ隆志, 松原豊, 伊藤好孝, 三塚岳, ディエゴロペス, 宗像一起, 加藤千尋, 小財正義, 中野義丈, 安江新一, 鶴指眞李, 柴田祥一, 小島浩司, 土屋晴文, 渡邊恭子, 小井辰巳: "SciBar 検出器を用いた太陽中性子観測計画Ⅴ：小型試験機の結果を用いた検出効率の見積もり", 日本物理学会第 66 回年次大会, (日本物理学会), 新潟, 3 月 (2011).

武内陽子, 玉川徹, 岩橋孝典, 阿佐美ふみ, 吉川瑛文, 小波さおり, 岩切渉: "ジメチルエーテル中での GEM の両極板およびパッドからの信号読み出し", 日本物理学会第 66 回年次大会, (日本物理学会), 新潟, 3 月 (2011).

日比野欣也, 土屋晴文, チベット ASγコラボレーション: "チベットでの雷や雷雲に由来する放射線の観測 I", 日本物理学会第 66 回年次大会, (日本物理学会), 新潟, 3 月 (2011).

土屋晴文, 日比野欣也, 川田和正, 堀田直紀, 立山暢人, 大西宗博, 瀧田正人, 陳鼎, 黄晶, 宮坂浩正, 近藤一郎, 高橋恵美子, 霜田進, 山田豊, 宗像一起, 牧島一夫: "チベットでの雷や雷雲に由来する放射線の観測 II", 日本物理学会第 66 回年次大会, (日本物理学会), 新潟, 3 月 (2011).

西澤正己, 土屋晴文, チベット ASγコラボレーション: "チベット空気シャワーアレイによる太陽の影の変動", 日本物理学会第 66 回年次大会, (日本物理学会), 新潟, 3 月 (2011).

土屋晴文, 川田和正, チベット ASγコラボレーション: "チベット水チェレンコフミューオン観測装置 16：建設報告 2", 日本物理学会第 66 回年次大会, (日本物理学会), 新潟, 3 月 (2011).

郷昌樹, 土屋晴文, チベット ASγコラボレーション: "空気シャワーコアーアレイ（YAC）による空気シャワー相互作用モデルの検証（II)", 日本物理学会第 66 回年次大会, (日本物理学会), 新潟, 3 月 (2011).

山田真也: "X 線観測によるブラックホール観測の現状と今度の進展", 首都大学東京大橋研究室セミナー 2011, 東京, 5 月 (2011).

山田真也: "X 線観測によるブラックホール研究の進展と将来展望", 早稲田大学理論宇宙物理学研究室セミナー 2011, 東京, 5 月 (2011).

山田真也, 牧島一夫: "「すざく」衛星によるブラックホール連星 Cygnus X-1 の最新成果", 日本物理学会 2011 年秋季大会, 弘前, 9 月 (2011).

武内陽子, 玉川徹, 阿佐美ふみ, 吉川瑛文, 岩橋孝典, 小波さおり, 岩切渉, 山田真也, 早藤麻美: "液晶ポリマー GEM の両極板およびパッド電極からの信号読み出し", 日本物理学会 2011 年秋季大会, (日本物理学会), 弘前, 9 月 (2011).

山田真也: "ブラックホール連星の X 線観測の最先端", 第 124 回「高エネルギー宇宙物理研究室 知の共有ゼミ」, 和光, 11 月 (2011).

土屋晴文: "非熱的な観測で探る雷や雷雲のなかでの高エネルギー粒子加速", 高エネルギー宇宙物理学研究会, (大阪大学理学研究科高原研究室), 豊中, 12 月 (2011).

玉川徹, 早藤麻美, 北口貴雄, 山田真也, 岩橋孝典, 阿佐美ふみ, 吉川瑛文, 武内陽子, 岩切渉, 幸村孝由, 金子健太, 田原譲, 高橋忠幸, 牧島一夫, Swank J., Jahoda K.: "X 線観測衛星 GEMS", 第 12 回宇宙科学シンポジウム, (宇宙科学研究所), 相模原市, 1 月 (2012).

Astro-Glaciology Research Unit

Publications

[Journal]

(Original Papers) *Subject to Peer Review

Igarashi M., Nakai Y., Motizuki Y., Takahashi K., Motoyama H., and Makishima K.: "Dating of the Dome Fuji shallow ice core based on a record of volcanic eruptions from AD 1260 to AD 2001", Polar Science **5**, No. 4, pp. 411–420 (2011). *

Boyd R. N., Famiano M. A., Meyer B. S., Motizuki Y., Kajino T., and Roederer I. U.: "The r-process in metal-poor stars and black hole formation", Astrophys. J. Lett. **744**, No. 1, pp. 1–4 (2012). *

(Others)

望月優子: "「氷床コアを用いた天文学」の構築へ向けて", JGL **7**, No. 1, pp. 7–9 (2011).

[Book・Proceedings]

(Original Papers) *Subject to Peer Review

Nociforo C., Farinon F., Musumarra A., Boutin D., Zoppo A. D., Figuera P., Geissel H., Hagino K., Knobel R., Kojouharov I., Kuboki T., Kurcewicz J., Litvinov Y. A., Mazzocco M., Motizuki Y., Ohtsubo T., Okuma Y., Patyak Z., Pellegrini M. G., Pietri S., Podolyak Z., Prochazka A., Scheidenberger C., Scuderi V., Sun B., Suzuki T., Torresi D., Weick H., Winfield J. S., Winckler N., Winkler M., Wollersheim H. J., and Yamaguchi T.: "Measurements of alfa-decay half-lives at GSI", The Proceeding of The Nordic Conference on Nuclear Physics 2011, Stockholm, Sweden, 2011–6, Physica Scripta, Stockholm, pp. 1–4 (2012). *

Boyd R. N., Famiano M. A., Meyer B. S., Motizuki Y., Kajino T., and Roederer I. U.: "The r-process in metal-poor stars and black hole formation", The Proceedings of the 11th International Symposium on Origin of Matter and Evolution of Galaxies, wako, 2011–12, CNS, Wako, pp. 1–6 (2012). *

(Others)

Tanabe K. and Motizuki Y.: "Symbiotic nova eruption of R Aquarii; A geological remnant?", The Proceedings of Palermo Workshop 2011 on the Golden Age of Cataclysmic Variables and Related Objects, Palermo, Italy, 2012–9, MACRO MEM. S.A.IT, Palermo, pp. 282–285 (2012).

望月優子: "銀河系内超新星爆発の痕跡", アイスコアー地球環境のタイムカプセル, 成山堂書店, 東京, pp. 185–202 (2011).

Oral Presentations

(International Conference etc.)

Tanabe K. and Motizuki Y.: "Symbiotic Nova eruption of R Aquarii; A Geological Remnant?", Int. conf. on the Golden Age of Cataclysmic Variables and Related Objects, (Istituto di Astrofisica Spaziale e Fisica Cosmica), Palermo, Italy, Sept. (2011).

Sekiguchi K., Nakai Y., Motizuki Y., Imamura T., and Akiyoshi H.: "A simulation study of stratospheric chemical reactions induced by astronomical ionizing events", The 2nd Int. Nagoya Workshop on the Relationship between Solar Activity and Climate Changes, (STEL, Nagoya University), Nagoya, Jan. (2012).

Motizuki Y., Nakai Y., and Takahashi K.: "Nitrate ion concentrations observed in an Antarctic Dome-Fuji ice core and its implications for the solar activity cycles", The 2nd Int. Nagoya Workshop on the Relationship between Solar Activity and Climate Changes, (STEL, Nagoya University), Nagoya, Jan. (2012).

Nakai Y., Kikuchi S., Takahashi K., and Motizuki Y.: "Verification of significance for solar cycles in ^{14}C concentration variation by consideration of measurement uncertainty", The 2nd Int. Nagoya Workshop on the Relationship between Solar Activity and Climate Changes, (STEL, Nagoya University), Nagoya, Jan. (2012).

(Domestic Conference)

菊地里実, 望月優子, 中井陽一, 高橋和也: "測定誤差を考慮した放射性炭素 14 濃度測定による過去の太陽周期", 日本天文学会 2011 年春季年会, (日本天文学会), つくば, 3 月 (2011).

望月優子, 中井陽一, 高橋和也, 五十嵐誠, 本山秀明, 鈴木啓助: "ドローニングモードランド氷床コア中の火山噴火シグナルとの同期から決定した新しいドームふじ浅層コア年代", 日本地球惑星科学連合 2011 年度大会, (日本地球惑星科学連合), 千葉, 5 月 (2011).

望月優子: "わたしたちは星のこども：宇宙と生命とのつながり", 第 3 回全国同時七夕講演会（NEXT プログラム「国民と科学・技術対話」）, (日本天文学会), 二本松, 7 月 (2011).

望月優子: "南極氷床コアからさぐる過去 2 千年の太陽活動探索プロジェクト", 日本天文学会 2011 年秋季年会, (日本天文学会), 鹿児島, 9 月 (2011).

望月優子, 本山秀明, 飯塚芳徳, 藤田秀二, 藤田耕史, 保科優: "ドームふじ地域の積雪に太陽プロトン現象の痕跡はあるか？", 北海道大学低温研究所シンポジウム「ドームふじコアを用いた新しい古環境復元法」, (北海道大学低温研究所), 札幌, 12 月 (2011).

望月優子: "南極氷床コアからさぐる過去 2000 年の太陽活動に関する分野横断的研究—プロジェクト紹介", 北海道大学低温研究所シンポジウム「ドームふじコアを用いた新しい古環境復元法」, (北海道大学低温研究所), 札幌, 12 月 (2011).

中井陽一, 望月優子, 高橋和也: "DF2001 コアの硝酸イオン周期解析", 北海道大学低温研究所シンポジウム「ドームふじコアを用いた新しい古環境復元法」, (北海道大学低温研究所), 札幌, 12 月 (2011).

高橋和也, 中井陽一, 望月優子: "ドームふじ DF2001 浅層コアの陽・陰イオン分析のまとめ", 北海道大学低温研究所シンポジウム「ドームふじコアを用いた新しい古環境復元法」, (北海道大学低温研究所), 札幌, 12 月 (2011).

望月優子: "雪や氷の成分は宇宙のどこで、いつ生まれたのか？", 日本雪氷学会雪氷化学分科会 2012 年雪合宿, (日本雪氷学会雪氷化学分科会), 松本, 2 月 (2012).

望月優子: “雪氷コアからさぐる天文・宇宙のサイエンス”, 分野別職業講話（NEXT プログラム「国民との科学・技術対話」）, (神奈川県立横浜翠嵐高等学校), 横浜, 3 月 (2012).

Accelerator Group

Publications

[Journal]

(Original Papers) *Subject to Peer Review

Kuboki H., Okuno H., Hasebe H., Yokouchi S., Ryuto H., Fukunishi N., Kamigaito O., Kase M., Goto A., and Yano Y.: "Charge strippers for high intensity uranium beams in the RIKEN RI beam factory", Nucl. Instrum. Methods Phys. Res. A **613**, No. 3, pp. 436–438 (2010). *

Hasebe H., Okuno H., Kuboki H., Ryuto H., Fukunishi N., Kamigaito O., Goto A., Kase M., and Yano Y.: "Development of long-life carbon stripper foils for uranium ion beams", Nucl. Instrum. Methods Phys. Res. A **613**, No. 3, pp. 453–456 (2010). *

Kuboki H., Okuno H., Yokouchi S., Hasebe H., Kishida T., Fukunishi N., Kamigaito O., Goto A., Kase M., and Yano Y.: "Charge-state distribution measurements of ^{238}U and ^{136}Xe at 11 MeV/nucleon using gas charge stripper", Phys. Rev. Spec. Top.: Accel. Beams **13**, No. 9, pp. 093501-1–093501-9 (2010). *

Kuboki H., Okuno H., Yokouchi S., Hasebe H., Kishida T., Fukunishi N., Kamigaito O., Goto A., Kase M., and Yano Y.: "Charge-state distribution measurements using gas charge stripper toward ^{238}U and ^{136}Xe acceleration at RIKEN RIBF", Nucl. Instrum. Methods Phys. Res. A **655**, No. 1, pp. 17–20 (2011). *

Okuno H., Fukunishi N., Goto A., Hasebe H., Imao H., Kamigaito O., Kase M., Kuboki H., Yano Y., and Yokouchi S.: "Low-Z gas stripper as an alternative to carbon foils for the acceleration of high-power uranium beams", Phys. Rev. Spec. Top.: Accel. Beams **14**, No. 3, pp. 033503-1–033503-8 (2011). *

Kuboki H., Okuno H., Hasebe H., Yokouchi S., Fukunishi N., Higurashi Y., Ohnishi J., Nakagawa T., Imao H., Kamigaito O., Goto A., Kase M., and Yano Y.: "Charge-state distribution of ^{238}U in nitrogen gas and carbon foil at 14 and 15 MeV/nucleon", Phys. Rev. Spec. Top.: Accel. Beams **14**, No. 5, pp. 053502-1–053502-7 (2011). *

[Book・Proceedings]

(Original Papers) *Subject to Peer Review

Ohnishi J., Higurashi Y., Nakagawa T., and Kamigaito O.: "Extraction system and beam qualities of the RIKEN full superconducting ECR ion source", Proceedings of of the 1st International Particle Accelerator Conference (IPAC'10), Kyoto, 2010–5, the IPAC'10 OC/ACFA, , pp. 4194–4196 (2010).

渡邉裕, 池沢英二, 佐藤洋一, 奥野広樹, 中川孝秀, 日暮祥英, 大西純一, 藤巻正樹, 福西暢尚, 横内茂, 熊谷桂子, 込山美咲, 渡辺博, 加瀬昌之, 後藤彰, 上垣外修一: "理研リニアック（RILAC）新入射 BT 系建設状況", 第 6 回日本加速器学会年会プロシーディングス, 東海村, 2009– 日本加速器学会, 東海村, pp. 608–610 (2010).

大西純一, 奥野広樹, 福西暢尚, 山田一成, 後藤彰, 上垣外修一: "超伝導リングサイクロトロンの磁場設定とその分析", 第 6 回日本加速器学会年会プロシーディングス, 東海, 2009–8, 日本加速器学会, 東京, pp. 598–600 (2010).

(Others)

Suda K., Fujimaki M., Fukunishi N., Hemmi M., Kamigaito O., Kase M., Koyama R., Kumagai K., Sakamoto N., and Yamada K.: "Stable Operation of RF Systems for RIBF", CYCLOTRONS'10, Lanzhou, China, 2010–9, edited by Watanabe T., The CYCLOTRONS'10 Organizing Committee, Lanzhou, pp. 198–200 (2010).

須田健嗣, 山田一成, 坂本成彦, 新井重昭, 千葉好明, 上垣外修一, 加瀬昌之, 渡邉裕: "新入射器 RILAC2 の Drift Tube Linac 空洞の設計・製作・試験", 第 8 回日本加速器学会年会プロシーディングス, つくば市, 2011–8, 日本加速器学会, 豊島区, pp. MOPS105-1–MOPS105-6 (2011).

Oral Presentations

(International Conference etc.)

Kuboki H., Okuno H., Hasebe H., Yokouchi S., Ryuto H., Fukunishi N., Kamigaito O., Kase M., Goto A., and Yano Y.: "Charge strippers for high intensity uranium beams in the RIKEN RI beam factory", 24th World Conference of the International Nuclear Target Development Society, (GANIL), Caen, France, Sept. (2008).

Watanabe T., Fukunishi N., Kase M., Sasaki Y., and Yano Y.: "Development of beam current monitor with HTS SQUID and HTS current sensor", 11th International Conference on HEAVY ION ACCELERATOR TECHNOLOGY (HIAT09), Venezia, Italy, June (2009).

Sato H., Iwasa N., Kawabata T., Kobayashi T., Kondo Y., Kubo T., Kusaka K., Motobayashi T., Murakami T., Nakamura T., Ohnishi J., Ohnishi T., Okuno H., Otsu H., Sakurai H., Satou Y., Sakaguchi-Sekiguchi K., Togano Y., and Yoneda K.: "SAMURAI spectrometer at RIKEN RI beam factory", Advanced Studies Institute: Symmetries and Spin (SPIN-Praha-2009), (Charles University), Prague, Czech, July–Aug. (2009).

Kuboki H., Okuno H., Hasebe H., Yokouchi S., Fukunishi N., Kamigaito O., Imao H., Goto A., Kase M., and Yano Y.: "Charge-state distribution measurements of ^{238}U using nitrogen gas and carbon foil charge strippers at 11, 14, and 15 MeV/nucleon", 25th World Conference of the International Nuclear Target Development Society, (TRIUMF), Vancouver, Canada, Sept. (2010).

Kuboki H., Okuno H., Hasebe H., Yokouchi S., Kishida T., Fukunishi N., Kamigaito O., Goto A., Kase M., and Yano Y.: "Charge-state distribution measurements using gas charge stripper toward ^{238}U and ^{136}Xe acceleration at RIKEN RIBF", 25th World Conference of the International Nuclear Target Development Society, (TRIUMF), Vancouver, Canada, Sept. (2010).

Watanabe T., Fukunishi N., Sasaki Y., Kase M., and Kamigaito O.: "Improvement of beam current monitor with high Tc current sensor and SQUID at the RIBF", IPAC 2011, (CERN), Kursaal, San Sebastian, Spain, Sept. (2011).

(Domestic Conference)

長谷部裕雄, 久保木浩功, 奥野広樹, 福西暢尚, 上垣外修一, 今尾浩士, 加瀬昌之: "大強度ウランビーム用炭素薄膜の開発", 第 7 回日本加速器学会年会, (日本加速器学会), 姫路, 8 月 (2010).

渡邉環, 福西暢尚, 加瀬昌之, 若杉昌徳, 藤巻正樹, 山田一成, 坂本成彦, 須田健嗣, 今尾浩士, 込山美咲, 上垣外修一: "RIBF における LabVIEW を用いたビームエネルギー測定システム", 第 8 回日本加速器学会年会, (高エネルギー加速器研究機構), つくば市, 8 月 (2011).

須田健嗣, 山田一成, 坂本成彦, 新井重昭, 千葉好明, 上垣外修一, 加瀬昌之, 渡邉裕: "新入射器 RILAC2 の Drift Tube Linac 空洞の設計・製作・試験", 第 8 回日本加速器学会年会, (日本加速器学会), つくば, 8 月 (2011).

Accelerator R&D Team

Publications

[Journal]

(Original Papers) *Subject to Peer Review

Kuboki H., Okuno H., Hasebe H., Yokouchi S., Ryuto H., Fukunishi N., Kamigaito O., Kase M., Goto A., and Yano Y.: "Charge strippers for high intensity uranium beams in the RIKEN RI beam factory", Nucl. Instrum. Methods Phys. Res. A **613**, No. 3, pp. 436–438 (2010). *

Hasebe H., Okuno H., Kuboki H., Ryuto H., Fukunishi N., Kamigaito O., Goto A., Kase M., and Yano Y.: "Development of long-life carbon stripper foils for uranium ion beams", Nucl. Instrum. Methods Phys. Res. A **613**, No. 3, pp. 453–456 (2010). *

Kuboki H., Okuno H., Yokouchi S., Hasebe H., Kishida T., Fukunishi N., Kamigaito O., Goto A., Kase M., and Yano Y.: "Charge-state distribution measurements of ^{238}U and ^{136}Xe at 11 MeV/nucleon using gas charge stripper", Phys. Rev. Spec. Top.: Accel. Beams **13**, No. 9, pp. 093501-1–093501-9 (2010). *

Matsuba H., Yagi E., Sugi C., Okada Y., Hirabayashi K., Iida T., Koike S., Hayashi T., Higami N., Murakami Y., Takebayashi A., Yoshida T., Sugawara T., Shishido T., and Ogiwara K.: "Site occupancies of hydrogen in Nb alloyed with oversized Ta atoms or undersized Mo atoms", J. Phys. Soc. Jpn. **80**, 104602-1–104602-8 (2011). *

Kuboki H., Okuno H., Yokouchi S., Hasebe H., Kishida T., Fukunishi N., Kamigaito O., Goto A., Kase M., and Yano Y.: "Charge-state distribution measurements using gas charge stripper toward ^{238}U and ^{136}Xe acceleration at RIKEN RIBF", Nucl. Instrum. Methods Phys. Res. A **655**, No. 1, pp. 17–20 (2011). *

Hassan T. A., Imao H., Oshima N., Mohri A., and Yamazaki Y.: "Fast electron accumulation and its mechanism in a harmonic trap under ultrahigh vacuum conditions", Phys. Plasmas **18**, No. 032507, pp. 032507-1–032507-5 (2011). *

Okuno H., Fukunishi N., Goto A., Hasebe H., Imao H., Kamigaito O., Kase M., Kuboki H., Yano Y., and Yokouchi S.: "Low-Z gas stripper as an alternative to carbon foils for the acceleration of high-power uranium beams", Phys. Rev. Spec. Top.: Accel. Beams **14**, No. 3, pp. 033503-1–033503-8 (2011). *

Kuboki H., Okuno H., Hasebe H., Yokouchi S., Fukunishi N., Higurashi Y., Ohnishi J., Nakagawa T., Imao H., Kamigaito O., Goto A., Kase M., and Yano Y.: "Charge-state distribution of ^{238}U in nitrogen gas and carbon foil at 14 and 15 MeV/nucleon", Phys. Rev. Spec. Top.: Accel. Beams **14**, No. 5, pp. 053502-1–053502-7 (2011). *

(Review)

渡邉裕, 池沢英二, 大西純一, 熊谷桂子, 込山美咲, 藤縄雅, 藤巻正樹, 眞家武士, 山澤秀行, 横内茂, 渡邉環, 渡辺博: "理研 RIBF 新入射器 RILAC2 の建設", 加速器 **7**, No. 4, pp. 285–293 (2010).

[Book・Proceedings]

(Original Papers) *Subject to Peer Review

Ohnishi J., Higurashi Y., Nakagawa T., and Kamigaito O.: "Extraction system and beam qualities of the RIKEN full superconducting ECR ion source", Proceedings of of the 1st International Particle Accelerator Conference (IPAC'10), Kyoto, 2010–5, the IPAC'10 OC/ACFA, , pp. 4194–4196 (2010).

大西純一, 中川孝秀, 湊恒明, 奥野広樹, 日暮祥英, 日下健祐, 後藤彰: "28 GHz ECR イオン源用超伝導コイルの製作と励磁試験", 第 5 回加速器学会年会・第 33 回リニアック技術研究会プロシーディングス, 東広島市, 2008–8, 日本加速器学会, 東京, pp. 406–408 (2008).

渡邉裕, 池沢英二, 佐藤洋一, 奥野広樹, 中川孝秀, 日暮祥英, 大西純一, 藤巻正樹, 福西暢尚, 横内茂, 熊谷桂子, 込山美咲, 渡辺博, 加瀬昌之, 後藤彰, 上垣外修一: "理研リニアック（RILAC）新入射 BT 系建設状況", 第 6 回日本加速器学会年会プロシーディングス, 東海村, 2009– 日本加速器学会, 東海村, pp. 608–610 (2010).

大西純一, 奥野広樹, 福西暢尚, 山田一成, 後藤彰, 上垣外修一: "超伝導リングサイクロトロンの磁場設定とその分析", 第 6 回日本加速器学会年会プロシーディングス, 東海, 2009–8, 日本加速器学会, 東京, pp. 598–600 (2010).

大西純一, 中川孝秀, 日暮祥英, Minato T.: "28 GHz ECR イオン源用超伝導磁石の完成と運転", 第 6 回日本加速器学会年会プロシーディングス, 東海, 2009–8, 日本加速器学会, 東京, pp. 635–637 (2010).

(Others)

須田健嗣, 山田一成, 坂本成彦, 新井重昭, 千葉好明, 上垣外修一, 加瀬昌之, 渡邉裕: "新入射器 RILAC2 の Drift Tube Linac 空洞の設計・製作・試験", 第 8 回日本加速器学会年会プロシーディングス, つくば市, 2011–8, 日本加速器学会, 豊島区, pp. MOPS105-1–MOPS105-6 (2011).

Oral Presentations

(International Conference etc.)

Kuboki H., Okuno H., Hasebe H., Yokouchi S., Ryuto H., Fukunishi N., Kamigaito O., Kase M., Goto A., and Yano Y.: "Charge strippers for high intensity uranium beams in the RIKEN RI beam factory", 24th World Conference of the International Nuclear Target Development Society, (GANIL), Caen, France, Sept. (2008).

Sato H., Iwasa N., Kawabata T., Kobayashi T., Kondo Y., Kubo T., Kusaka K., Motobayashi T., Murakami T., Nakamura T., Ohnishi J., Ohnishi T., Okuno H., Otsu H., Sakurai H., Satou Y., Sakaguchi-Sekiguchi K., Togano Y., and Yoneda K.: "SAMURAI spectrometer at RIKEN RI beam factory", Advanced Studies Institute: Symmetries and Spin (SPIN-Praha-2009), (Charles University), Prague, Czech, July–Aug. (2009).

Higaki H., Kuroda N., Imao H., Nagata Y., Enomoto

Y., Michishio K., Kira K., Kim C., Okamoto H., Hori M., Kanai Y., Mohri A., Torii H., Matsuda Y., and Yamazaki Y.: "A Tank Circuit Monitoring a Large Number of Antiprotons in MUSASHI", 1st International Particle Accelerator Conference (IPAC'10), (High Energy Accelerator Research Organization (KEK)), Kyoto, May (2010).

Kuboki H., Okuno H., Hasebe H., Yokouchi S., Fukunishi N., Kamigaito O., Imao H., Goto A., Kase M., and Yano Y.: "Charge-state distribution measurements of ^{238}U using nitrogen gas and carbon foil charge strippers at 11, 14, and 15 MeV/nucleon", 25th World Conference of the International Nuclear Target Development Society, (TRIUMF), Vancouver, Canada, Sept. (2010).

Kuboki H., Okuno H., Hasebe H., Yokouchi S., Kishida T., Fukunishi N., Kamigaito O., Goto A., Kase M., and Yano Y.: "Charge-state distribution measurements using gas charge stripper toward ^{238}U and ^{136}Xe acceleration at RIKEN RIBF", 25th World Conference of the International Nuclear Target Development Society, (TRIUMF), Vancouver, Canada, Sept. (2010).

Enomoto Y., Kuroda N., Michishio K., Kim C., Higaki H., Nagata Y., Kanai Y., Torii H., Corradini M., Leali M., Lodi-Rizzini E., Vascagna V., Venturelli L., Zurlo N., Fujii K., Ohtsuka M., Tanaka K., Imao H., Nagashima Y., Matsuda Y., Juhasz B., Mohri A., and Yamazaki Y.: "Synthesis of antihydrogen atoms in a cusp trap", 22nd International Symposium on Ion Atom Collisions (ISIAC 2011), (University of caen), Caen, France, July (2011).

(Domestic Conference)

長谷部裕雄, 久保木浩功, 奥野広樹, 福西暢尚, 上垣外修一, 今尾浩士, 加瀬昌之: "大強度ウランビーム用炭素薄膜の開発", 第 7 回日本加速器学会年会, (日本加速器学会), 姫路, 8 月 (2010).

渡邉環, 福西暢尚, 加瀬昌之, 若杉昌徳, 藤巻正樹, 山田一成, 坂本成彦, 須田健嗣, 今尾浩士, 込山美咲, 上垣外修一: "RIBF における LabVIEW を用いたビームエネルギー測定システム", 第 8 回日本加速器学会年会, (高エネルギー加速器研究機構), つくば市, 8 月 (2011).

須田健嗣, 山田一成, 坂本成彦, 新井重昭, 千葉好明, 上垣外修一, 加瀬昌之, 渡邉裕: "新入射器 RILAC2 の Drift Tube Linac 空洞の設計・製作・試験", 第 8 回日本加速器学会年会, (日本加速器学会), つくば, 8 月 (2011).

Ion Source Team

Publications

[**Journal**]

(Original Papers) *Subject to Peer Review

Kuboki H., Okuno H., Hasebe H., Yokouchi S., Fukunishi N., Higurashi Y., Ohnishi J., Nakagawa T., Imao H., Kamigaito O., Goto A., Kase M., and Yano Y.: "Charge-state distribution of ^{238}U in nitrogen gas and carbon foil at 14 and 15 MeV/nucleon", Phys. Rev. Spec. Top.: Accel. Beams **14**, No. 5, pp. 053502-1–053502-7 (2011). *

[**Book・Proceedings**]

(Original Papers) *Subject to Peer Review

Ohnishi J., Higurashi Y., Nakagawa T., and Kamigaito O.: "Extraction system and beam qualities of the RIKEN full superconducting ECR ion source", Proceedings of of the 1st International Particle Accelerator Conference (IPAC'10), Kyoto, 2010–5, the IPAC'10 OC/ACFA, , pp. 4194–4196 (2010).

大西純一, 中川孝秀, 湊恒明, 奥野広樹, 日暮祥英, 日下健祐, 後藤彰: "28 GHz ECR イオン源用超伝導コイルの製作と励磁試験", 第 5 回加速器学会年会・第 33 回リニアック技術研究会プロシーディングス, 東広島市, 2008–8, 日本加速器学会, 東京, pp. 406–408 (2008).

渡邉裕, 池沢英二, 佐藤洋一, 奥野広樹, 中川孝秀, 日暮祥英, 大西純一, 藤巻正樹, 福西暢尚, 横内茂, 熊谷桂子, 込山美咲, 渡辺博, 加瀬昌之, 後藤彰, 上垣外修一: "理研リニアック（RILAC）新入射 BT 系建設状況", 第 6 回日本加速器学会年会プロシーディングス, 東海村, 2009– 日本加速器学会, 東海村, pp. 608–610 (2010).

大西純一, 中川孝秀, 日暮祥英, Minato T.: "28 GHz ECR イオン源用超伝導磁石の完成と運転", 第 6 回日本加速器学会年会プロシーディングス, 東海, 2009–8, 日本加速器学会, 東京, pp. 635–637 (2010).

RILAC Team

Publications

[Journal]

(Review)

渡邉裕, 池沢英二, 大西純一, 熊谷桂子, 込山美咲, 藤縄雅, 藤巻正樹, 眞家武士, 山澤秀行, 横内茂, 渡邉環, 渡辺博: “理研 RIBF 新入射器 RILAC2 の建設”, 加速器 **7**, No. 4, pp. 285–293 (2010).

[Book · Proceedings]

(Original Papers) *Subject to Peer Review

渡邉裕, 池沢英二, 佐藤洋一, 奥野広樹, 中川孝秀, 日暮祥英, 大西純一, 藤巻正樹, 福西暢尚, 横内茂, 熊谷桂子, 込山美咲, 渡辺博, 加瀬昌之, 後藤彰, 上垣外修一: “理研リニアック（RILAC）新入射 BT 系建設状況”, 第 6 回日本加速器学会年会プロシーディングス, 東海村, 2009– 日本加速器学会, 東海村, pp. 608–610 (2010).

(Others)

Suda K., Fujimaki M., Fukunishi N., Hemmi M., Kamigaito O., Kase M., Koyama R., Kumagai K., Sakamoto N., and Yamada K.: “Stable Operation of RF Systems for RIBF”, CYCLOTRONS’10, Lanzhou, China, 2010–9, edited by Watanabe T., The CYCLOTRONS’10 Organizing Committee, Lanzhou, pp. 198–200 (2010).

須田健嗣, 山田一成, 坂本成彦, 新井重昭, 千葉好明, 上垣外修一, 加瀬昌之, 渡邉裕: “新入射器 RILAC2 の Drift Tube Linac 空洞の設計・製作・試験”, 第 8 回日本加速器学会年会プロシーディングス, つくば市, 2011–8, 日本加速器学会, 豊島区, pp. MOPS105-1–MOPS105-6 (2011).

Oral Presentations

(Domestic Conference)

須田健嗣, 山田一成, 坂本成彦, 新井重昭, 千葉好明, 上垣外修一, 加瀬昌之, 渡邉裕: “新入射器 RILAC2 の Drift Tube Linac 空洞の設計・製作・試験”, 第 8 回日本加速器学会年会, (日本加速器学会), つくば, 8 月 (2011).

Cyclotron Team

Publications

[Book・Proceedings]

(Others)

Suda K., Fujimaki M., Fukunishi N., Hemmi M., Kamigaito O., Kase M., Koyama R., Kumagai K., Sakamoto N., and Yamada K.: "Stable Operation of RF Systems for RIBF", CYCLOTRONS'10, Lanzhou, China, 2010–9, edited by Watanabe T., The CYCLOTRONS'10 Organizing Committee, Lanzhou, pp. 198–200 (2010).

須田健嗣, 山田一成, 坂本成彦, 新井重昭, 千葉好明, 上垣外修一, 加瀬昌之, 渡邉裕: "新入射器 RILAC2 の Drift Tube Linac 空洞の設計・製作・試験", 第 8 回日本加速器学会年会プロシーディングス, つくば市, 2011–8, 日本加速器学会, 豊島区, pp. MOPS105-1–MOPS105-6 (2011).

Oral Presentations

(Domestic Conference)

渡邉環, 福西暢尚, 加瀬昌之, 若杉昌徳, 藤巻正樹, 山田一成, 坂本成彦, 須田健嗣, 今尾浩士, 込山美咲, 上垣外修一: "RIBF における LabVIEW を用いたビームエネルギー測定システム", 第 8 回日本加速器学会年会, (高エネルギー加速器研究機構), つくば市, 8 月 (2011).

須田健嗣, 山田一成, 坂本成彦, 新井重昭, 千葉好明, 上垣外修一, 加瀬昌之, 渡邉裕: "新入射器 RILAC2 の Drift Tube Linac 空洞の設計・製作・試験", 第 8 回日本加速器学会年会, (日本加速器学会), つくば, 8 月 (2011).

Beam Dynamics & Diagnostics Team

Publications

[Journal]

(Original Papers) *Subject to Peer Review

Mihara M., Izumikawa T., Ueno H., Matsuta K., Nishimura D., Nagatomo T., Moriguchi T., Ito Y., Nagae D., Fukuda M., Yoshimi A., Yamada K., Takechi M., Ichikawa Y., Momota S., Hirayama Y., Ohtsubo T., Suzuki S., Ozawa A., Ishibashi Y., Kubo T., Ooishi H., Namiki Y., Hachiuma K., Namihira K., Horikawa D., Minamisono T., Yamaguchi T., Kuboki T., Suzuki T., Sato K., Kobayashi Y., and Asahi K.: "Beta-NMR measurement of 58Cu in Si", Hyperfine Interact. **197**, 143–147 (2010). *

Nagatomo T., Ueno H., Mihara M., Matsuta K., Yoshimi A., Ichikawa Y., Yamada K., Kawamura H., Ozawa A., Moriguchi T., Ishibashi Y., Asahi K., Uchida M., Suzuki K., Inoue T., Hasama Y., Iijima H., Sumikama T., Fukuda M., and Minamisono T.: "Precise nuclear moments of extremely proton-rich nuclus 23Al", Hyperfine Interact. **198**, 103–107 (2010). *

Kuboki H., Okuno H., Hasebe H., Yokouchi S., Ryuto H., Fukunishi N., Kamigaito O., Kase M., Goto A., and Yano Y.: "Charge strippers for high intensity uranium beams in the RIKEN RI beam factory", Nucl. Instrum. Methods Phys. Res. A **613**, No. 3, pp. 436–438 (2010). *

Hasebe H., Okuno H., Kuboki H., Ryuto H., Fukunishi N., Kamigaito O., Goto A., Kase M., and Yano Y.: "Development of long-life carbon stripper foils for uranium ion beams", Nucl. Instrum. Methods Phys. Res. A **613**, No. 3, pp. 453–456 (2010). *

Tanaka K., Yamaguchi T., Suzuki T., Ohtsubo T., Fukuda M., Nishimura D., Takechi M., Ogata K., Ozawa A., Izumikawa T., Aiba T., Aoi N., Baba H., Hashizume Y., Inafuku K., Iwasa N., Kobayashi K., Komuro M., Kondo Y., Kubo T., Matsuyama T., Michimasa S., Motobayashi T., Nakabayashi T., Nakazima S., Nakamura T., Sakurai H., Shinoda R., Shinohara M., Suzuki H., Takeshita E., Takeuchi S., Togano Y., Yamada K., Yasuno T., and Yhoshitake M.: "Observation of a large reaction cross-section in the drip-line nucleus ^{22}C", Phys. Rev. Lett. **104**, No. 6, pp. 062701-1–062701-4 (2010). *

Kuboki H., Okuno H., Yokouchi S., Hasebe H., Kishida T., Fukunishi N., Kamigaito O., Goto A., Kase M., and Yano Y.: "Charge-state distribution measurements using gas charge stripper toward ^{238}U and ^{136}Xe acceleration at RIKEN RIBF", Nucl. Instrum. Methods Phys. Res. A **655**, No. 1, pp. 17–20 (2011). *

(Review)

渡邉裕, 池沢英二, 大西純一, 熊谷桂子, 込山美咲, 藤縄雅, 藤巻正樹, 眞家武士, 山澤秀行, 横内茂, 渡邉環, 渡辺博: "理研 RIBF 新入射器 RILAC2 の建設", 加速器 **7**, No. 4, pp. 285–293 (2010).

[Book · Proceedings]

(Original Papers) *Subject to Peer Review

渡邉裕, 池沢英二, 佐藤洋一, 奥野広樹, 中川孝秀, 日暮祥英, 大西純一, 藤巻正樹, 福西暢尚, 横内茂, 熊谷桂子, 込山美咲, 渡辺博, 加瀬昌之, 後藤彰, 上垣外修一: "理研リニアック（RILAC）新入射 BT 系建設状況", 第 6 回日本加速器学会年会プロシーディングス, 東海村, 2009– 日本加速器学会, 東海村, pp. 608–610 (2010).

大西純一, 奥野広樹, 福西暢尚, 山田一成, 後藤彰, 上垣外修一: "超伝導リングサイクロトロンの磁場設定とその分析", 第 6 回日本加速器学会年会プロシーディングス, 東海, 2009–8, 日本加速器学会, 東京, pp. 598–600 (2010).

(Others)

Suda K., Fujimaki M., Fukunishi N., Hemmi M., Kamigaito O., Kase M., Koyama R., Kumagai K., Sakamoto N., and Yamada K.: "Stable Operation of RF Systems for RIBF", CYCLOTRONS'10, Lanzhou, China, 2010–9, edited by Watanabe T., The CYCLOTRONS'10 Organizing Committee, Lanzhou, pp. 198–200 (2010).

須田健嗣, 山田一成, 坂本成彦, 新井重昭, 千葉好明, 上垣外修一, 加瀬昌之, 渡邉裕: "新入射器 RILAC2 の Drift Tube Linac 空洞の設計・製作・試験", 第 8 回日本加速器学会年会プロシーディングス, つくば市, 2011–8, 日本加速器学会, 豊島区, pp. MOPS105-1–MOPS105-6 (2011).

Oral Presentations

(International Conference etc.)

Kuboki H., Okuno H., Hasebe H., Yokouchi S., Ryuto H., Fukunishi N., Kamigaito O., Kase M., Goto A., and Yano Y.: "Charge strippers for high intensity uranium beams in the RIKEN RI beam factory", 24th World Conference of the International Nuclear Target Development Society, (GANIL), Caen, France, Sept. (2008).

Watanabe T., Fukunishi N., Kase M., Sasaki Y., and Yano Y.: "Development of beam current monitor with HTS SQUID and HTS current sensor", 11th International Conference on HEAVY ION ACCELERATOR TECHNOLOGY (HIAT09), Venezia, Italy, June (2009).

Watanabe T., Fukunishi N., Sasaki Y., Kase M., and Kamigaito O.: "Improvement of beam current monitor with high Tc current sensor and SQUID at the RIBF", IPAC 2011, (CERN), Kursaal, San Sebastian, Spain, Sept. (2011).

(Domestic Conference)

渡邉環, 福西暢尚, 加瀬昌之, 若杉昌徳, 藤巻正樹, 山田一成, 坂本成彦, 須田健嗣, 今尾浩士, 込山美咲, 上垣外修一: "RIBF における LabVIEW を用いたビームエネルギー測定システム", 第 8 回日本加速器学会年会, (高エネルギー加速器研究機構), つくば市, 8 月 (2011).

須田健嗣, 山田一成, 坂本成彦, 新井重昭, 千葉好明, 上垣外修一, 加瀬昌之, 渡邉裕: "新入射器 RILAC2 の Drift Tube Linac 空洞の設計・製作・試験", 第 8 回日本加速器学会年

会, (日本加速器学会), つくば, 8 月 (2011).

古田琢哉, 石川顕一, 福西暢尚, 野田茂穂, 高木周, 前山拓哉, 深作和明, 姫野龍太郎: “PHITS への OpenMP を用いたメモリ共有型並列計算の導入”, 第 7 回 PHITS 研究会, (日本原子力研究開発機構), 茨城県東海村, 8 月 (2011).

前山拓哉, 福西暢尚, 石川顕一, 深作和明, 高木周, 古田琢哉, 野田茂穂, 姫野龍太郎: “フリッケゲル線量計による炭素線の線量分布測定”, 第 54 回放射線化学討論会, (日本放射線化学会), 吹田, 9 月 (2011).

古田琢哉, 石川顕一, 福西暢尚, 前山拓哉, 高木周, 深作和明, 姫野龍太郎: “重粒子線治療のための PHITS コードを用いた線量計算手法の開発”, 次世代ナノ統合シミュレーションソフトウェアの研究開発（ナノ）次世代生命体統合シミュレーションソフトウェアの研究開発（ライフ）公開シンポジウム, (文部科学省次世代スーパーコンピュータプロジェクト・ナノ分野グランドチャレンジ研究開発・ナノ統合拠点、次世代生命体統合シミュレーションソフトウェアの研究開発), 神戸市, 3 月 (2012).

Cryogenic Technology Team

Publications

[Journal]

(Review)

渡邉裕, 池沢英二, 大西純一, 熊谷桂子, 込山美咲, 藤縄雅, 藤巻正樹, 眞家武士, 山澤秀行, 横内茂, 渡邉環, 渡辺博: "理研 RIBF 新入射器 RILAC2 の建設", 加速器 **7**, No. 4, pp. 285–293 (2010).

Oral Presentations

(International Conference etc.)

Ikeda S., Kubota T., Yanagisawa H., Yuki M., Tsuruma S., and Okamoto A.: "Hybridization-sensitive fluorescent probes for sequence-specific detection of nucleic acids", 37th International Symposium on Nucleic Acids Chemistry 2010 (ISNAC 2010), Yokohama, Nov. (2010).

Infrastructure Management Team

Publications

[Journal]

(Review)

渡邉裕, 池沢英二, 大西純一, 熊谷桂子, 込山美咲, 藤縄雅, 藤巻正樹, 眞家武士, 山澤秀行, 横内茂, 渡邉環, 渡辺博: "理研 RIBF 新入射器 RILAC2 の建設", 加速器 **7**, No. 4, pp. 285–293 (2010).

(Technical Document)

藤縄雅: "大型加速器施設用無停電電源としての熱電併給装置の実績と考察", 加速器 **8**, No. 1, pp. 18–25 (2011).

[Book・Proceedings]

(Original Papers)　*Subject to Peer Review

渡邉裕, 池沢英二, 佐藤洋一, 奥野広樹, 中川孝秀, 日暮祥英, 大西純一, 藤巻正樹, 福西暢尚, 横内茂, 熊谷桂子, 込山美咲, 渡辺博, 加瀬昌之, 後藤彰, 上垣外修一: "理研リニアック（RILAC）新入射 BT 系建設状況", 第 6 回日本加速器学会年会プロシーディングス, 東海村, 2009– 日本加速器学会, 東海村, pp. 608–610 (2010).

Oral Presentations

(International Conference etc.)

Fujinawa T.: "Design,installation and operation of the electrical power supply system for RIBF, the super-size accelerator facility, RIKEN", 9th International Workshop on IEIEJ, (The institute of Electrical Installation Engineers of Japan), Miyazaki, Sept. (2011).

Yamaguchi Y., Wakasugi M., Suzuki H., Fujinawa T., Uesaka T., Yano Y., Ozawa A., Nagae D., Yamaguchi T., Suzuki T., Kikuchi T., Jiang W., Sasaki T., and Tokuchi A.: "Present status of rare-RI ring project in RIKEN RI beam factory", 8th International Conference on Nuclear Physics at Storage Rings (STORI-11), (INFN-LNF), Frascati, Italy, Oct. (2011).

(Domestic Conference)

藤縄雅: "世界を冠絶する理研 RI ビームファクトリー用クレーン", 第 44 回日本大学生産工学部学術講演会, (日本大学　生産工学部), 習志野, 12 月 (2011).

Instrumentation Development Group

Publications

[**Journal**]

(Original Papers) *Subject to Peer Review

Mihara M., Izumikawa T., Ueno H., Matsuta K., Nishimura D., Nagatomo T., Moriguchi T., Ito Y., Nagae D., Fukuda M., Yoshimi A., Yamada K., Takechi M., Ichikawa Y., Momota S., Hirayama Y., Ohtsubo T., Suzuki S., Ozawa A., Ishibashi Y., Kubo T., Ooishi H., Namiki Y., Hachiuma K., Namihira K., Horikawa D., Minamisono T., Yamaguchi T., Kuboki T., Suzuki T., Sato K., Kobayashi Y., and Asahi K.: "Beta-NMR measurement of 58Cu in Si", Hyperfine Interact. **197**, 143–147 (2010). *

Nagatomo T., Ueno H., Mihara M., Matsuta K., Yoshimi A., Ichikawa Y., Yamada K., Kawamura H., Ozawa A., Moriguchi T., Ishibashi Y., Asahi K., Uchida M., Suzuki K., Inoue T., Hasama Y., Iijima H., Sumikama T., Fukuda M., and Minamisono T.: "Precise nuclear moments of extremely proton-rich nuclus 23Al", Hyperfine Interact. **198**, 103–107 (2010). *

Tanaka K., Fukuda M., Mihara M., Takechi M., Nishimura D., Chinda T., Sumikama T., Kudo S., Matsuta K., Minamisono T., Suzuki T., Ohtsubo T., Izumikawa T., Momota S., Yamaguchi T., Oonish T., Ozawa A., Tanihata I., and Zheng T.: "Density distribution of ^{17}Ne and possible shell-structure change in the proton-rich sd-shell nuclei", Phys. Rev. C **82**, No. 4, pp. 044309-1–044309-11 (2010). *

Tanaka K., Yamaguchi T., Suzuki T., Ohtsubo T., Fukuda M., Nishimura D., Takechi M., Ogata K., Ozawa A., Izumikawa T., Aiba T., Aoi N., Baba H., Hashizume Y., Inafuku K., Iwasa N., Kobayashi K., Komuro M., Kondo Y., Kubo T., Matsuyama T., Michimasa S., Motobayashi T., Nakabayashi T., Nakazima S., Nakamura T., Sakurai H., Shinoda R., Shinohara M., Suzuki H., Takeshita E., Takeuchi S., Togano Y., Yamada K., Yasuno T., and Yhoshitake M.: "Observation of a large reaction cross-section in the drip-line nucleus ^{22}C", Phys. Rev. Lett. **104**, No. 6, pp. 062701-1–062701-4 (2010). *

Oral Presentations

(International Conference etc.)

Morimoto K., Morita K., Kaji D., Haba H., Ohzeki K., Kudou Y., Sato N., Sumita T., Yoneda A., Ichikawa T., Goto S., Fujimori Y., Ideguchi E., Kasamatsu Y., Katori K., Komori Y., Koura H., Kudo H., Ooe K., Ozawa A., Tokanai F., Tsukada K., Yamaguchi T., and Yoshida A.: "Production and Decay Properties of ^{266}Bh and its daughter nuclei by using the ^{248}Cm(^{23}Na,5n) Reaction", Seventh Workshop on the Chemistry of the Heaviest elements, Mainz, Germany, Oct. (2009).

Morimoto K., Morita K., Kaji D., Haba H., Ohzeki K., Kudou Y., Sato N., Sumita T., Yoneda A., Ichikawa T., Fujimori Y., Goto S., Huang T., Ideguchi E., Kasamatsu Y., Katori K., Komori Y., Koura H., Kudo H., Murakami M., Ozawa A., Sakai R., Tokanai F., Tsukada K., Yamaguchi T., and Yoshida A.: "Confirmations of the synthesis of ^{278}113 produced by the ^{209}Bi(^{70}Zn,n)^{278}113 reaction", International Chemical Congress of Pacific Basin Societies (PACIFICHEM 2010), Honolulu, USA, Dec. (2010).

Yamaguchi Y., Wakasugi M., Suzuki H., Fujinawa T., Uesaka T., Yano Y., Ozawa A., Nagae D., Yamaguchi T., Suzuki T., Kikuchi T., Jiang W., Sasaki T., and Tokuchi A.: "Present status of rare-RI ring project in RIKEN RI beam factory", 8th International Conference on Nuclear Physics at Storage Rings (STORI-11), (INFN-LNF), Frascati, Italy, Oct. (2011).

(Domestic Conference)

渡邉環, 福西暢尚, 加瀬昌之, 若杉昌徳, 藤巻正樹, 山田一成, 坂本成彦, 須田健嗣, 今尾浩士, 込山美咲, 上垣外修一: "RI-BF における LabVIEW を用いたビームエネルギー測定システム", 第 8 回日本加速器学会年会, (高エネルギー加速器研究機構), つくば市, 8 月 (2011).

阿部康志, 長江大輔, 小沢顕, 森口哲朗, 石橋陽子, 伊藤由太, 奥村公威, 金沢光隆, 佐藤眞二, 鈴木宏, 錦織良, 福岡翔太, 山口貴之, 山口由高: "理研稀少 RI リングのための飛行時間検出器の開発", 日本物理学会 2011 年秋季大会, (日本物理学会), 弘前, 9 月 (2011).

小沢 顕: "Overview of rare-RI ring and mass measurements", 仁科センター研究会「稀少 RI リングの物理」, 和光, 11 月 (2011).

SLOWRI Team

Publications

[**Journal**]

(Original Papers)　*Subject to Peer Review

Mihara M., Izumikawa T., Ueno H., Matsuta K., Nishimura D., Nagatomo T., Moriguchi T., Ito Y., Nagae D., Fukuda M., Yoshimi A., Yamada K., Takechi M., Ichikawa Y., Momota S., Hirayama Y., Ohtsubo T., Suzuki S., Ozawa A., Ishibashi Y., Kubo T., Ooishi H., Namiki Y., Hachiuma K., Namihira K., Horikawa D., Minamisono T., Yamaguchi T., Kuboki T., Suzuki T., Sato K., Kobayashi Y., and Asahi K.: "Beta-NMR measurement of 58Cu in Si", Hyperfine Interact. **197**, 143–147 (2010). *

[**Book・Proceedings**]

(Others)

須田健嗣, 山田一成, 坂本成彦, 新井重昭, 千葉好明, 上垣外修一, 加瀬昌之, 渡邉裕: "新入射器 RILAC2 の Drift Tube Linac 空洞の設計・製作・試験", 第 8 回日本加速器学会年会プロシーディングス, つくば市, 2011–8, 日本加速器学会, 豊島区, pp. MOPS105-1–MOPS105-6 (2011).

Oral Presentations

(Domestic Conference)

園田哲: "レーザー共鳴イオン化イオンガイドによるパラサイト低速 RI 生成法", 第 5 回停止・低速不安定核ビームを用いた核分光研究会, (大阪大学), 豊中, 12 月 (2008).

園田哲: "理研 SLOWRI 共鳴イオン化用新レーザーシステムの開発", 第 6 回停止・低速不安定核ビームを用いた核分光研究会, (東京工業大学), 東京, 3 月 (2010).

園田哲, 和田道治, 富田英生, 岡田邦宏, 伊藤由太, 飯村秀紀, 中村聡佑, Schuessler H. A., 高峰愛子, 松尾由賀利, 久保敏幸, 古川武, 片山一郎, 涌井崇志, 篠塚勉, Huyse M., Kudryavtsev. Y., Duppen P. V.: "理研における共鳴イオン化レーザーイオン源の開発", 日本物理学会 2010 年秋季大会, (日本物理学会), 北九州市, 9 月 (2010).

古川武, 涌井崇志, 佐々木彩子, 泉さやか, 市川雄一, 吉見彰洋, 田尻邦彦, 石井裕司, 吉田直貴, 松浦佑一, 加藤裕樹, 山口康広, 今村慧, 幕田将宏, 畠山温, 和田道治, 園田哲, 伊藤由太, 七尾翼, 小林徹, 西村俊二, 西村美月, 近藤洋介, 青井考, 米田健一郎, 久保野茂, 大城幸光, 上野秀樹, 篠塚勉, 下田正, 旭耕一郎, 松尾由賀利: "^{87}Rb ビームを用いた超流動ヘリウム中でのレーザー核分光法開発実験", 日本物理学会第 66 回年次大会, 新潟, 3 月 (2011).

須田健嗣, 山田一成, 坂本成彦, 新井重昭, 千葉好明, 上垣外修一, 加瀬昌之, 渡邉裕: "新入射器 RILAC2 の Drift Tube Linac 空洞の設計・製作・試験", 第 8 回日本加速器学会年会, (日本加速器学会), つくば, 8 月 (2011).

阿部康志, 長江大輔, 小沢顕, 森口哲朗, 石橋陽子, 伊藤由太, 奥村公威, 金沢光隆, 佐藤眞二, 鈴木宏, 錦織良, 福岡翔太, 山口貴之, 山口由高: "理研稀少 RI リングのための飛行時間検出器の開発", 日本物理学会 2011 年秋季大会, (日本物理学会), 弘前, 9 月 (2011).

古川武, 涌井崇志, 佐々木彩子, 泉さやか, 市川雄一, 吉見彰洋, 田尻邦彦, 石井裕司, 吉田直貴, 松浦佑一, 加藤裕樹, 山口康広, 今村慧, 幕田将宏, 畠山温, 和田道治, 園田哲, 伊藤由太, 七尾翼, 小林徹, 西村俊二, 西村美月, 近藤洋介, 青井考, 米田健一郎, 久保野茂, 上野秀樹, 下田正, 篠塚勉, 旭耕一郎, 松尾由賀利: "超流動ヘリウム中に打ち込まれた ^{87}Rb ビームのレーザー誘起蛍光観測と光ポンピング", 日本物理学会 2011 年秋季大会, (日本物理学会), 弘前, 9 月 (2011).

Polarized RI Beam Team

Publications

[**Journal**]

(Original Papers) *Subject to Peer Review

Mihara M., Izumikawa T., Ueno H., Matsuta K., Nishimura D., Nagatomo T., Moriguchi T., Ito Y., Nagae D., Fukuda M., Yoshimi A., Yamada K., Takechi M., Ichikawa Y., Momota S., Hirayama Y., Ohtsubo T., Suzuki S., Ozawa A., Ishibashi Y., Kubo T., Ooishi H., Namiki Y., Hachiuma K., Namihira K., Horikawa D., Minamisono T., Yamaguchi T., Kuboki T., Suzuki T., Sato K., Kobayashi Y., and Asahi K.: "Beta-NMR measurement of 58Cu in Si", Hyperfine Interact. **197**, 143–147 (2010). *

Nagatomo T., Ueno H., Mihara M., Matsuta K., Yoshimi A., Ichikawa Y., Yamada K., Kawamura H., Ozawa A., Moriguchi T., Ishibashi Y., Asahi K., Uchida M., Suzuki K., Inoue T., Hasama Y., Iijima H., Sumikama T., Fukuda M., and Minamisono T.: "Precise nuclear moments of extremely proton-rich nuclus 23Al", Hyperfine Interact. **198**, 103–107 (2010). *

Ohnishi T., Kubo T., Kusaka K., Yoshida A., Yoshida K., Ohtake M., Fukuda N., Takeda H., Kameda D., Tanaka K., Inabe N., Yanagisawa Y., Gono Y., Watanabe H., Otsu H., Baba H., Ichihara T., Yamaguchi Y., Takechi M., Nishimura S., Ueno H., Yoshimi A., Sakurai H., Motobayashi T., Nakao T., Mizoi Y., Matsushita M., Ieki K., Kobayashi N., Tanaka K., Kawada Y., Tanaka N., Deguchi S., Sato Y., Kondo Y., Nakamura T., Yoshinaga K., Ishii c., Yoshii h., Miyashita Y., Uematsu N., Shiraki Y., Sumikama T., Chiba J., Ideguchi E., Saito A., Yamaguchi T., Hachiuma I., Suzuki T., Moriguchi T., Ozawa A., Ohtsubo T., Famiano M. A., Geissel H., Nettleton A. S., Tarasov O. B., Bazin D. P., Sherrill B. M., Manikonda S. L., and Nolen J. A.: "Identification of 45 New Neutron-Rich Isotopes Produced by In-Flight Fission of a ^{238}U Beam at 345 MeV/nucleon", J. Phys. Soc. Jpn. **79**, No. 7, pp. 073201-1–073201-5 (2010). *

Asahi K., Furukawa T., Inoue T., Yoshimi A., Nanao T., Chikamori M., Suzuki K., Tsuchiya M., Hayashi H., Uchida M., Ueno H., Matsuo Y., and Fukuyama T.: "Search for an electric dipole moment in 129Xe atom with nuclear spin oscillator technique", J. Phys.: Con. Ser. **302**, No. 012039, pp. 1–6 (2011). *

Ichikawa Y., Onishi T., Suzuki D., Iwasaki H., Kubo T., Banerjee S. R., Chakrabarti A., Aoi N., Brown A. B., Fukuda N., Kubono S., Motobayashi T., Nakabayashi T., Nakamura T., Nakao T., Okumura T., Ong H., Suzuki H., Suzuki M., Teranishi T., Yamada K., Yamaguchi H., and Sakurai H.: "Proton-rich nuclear structure and mirror asymmetry investigated by β-decay spectroscopy of ^{24}Si", J. Phys.: Con. Ser. **312**, No. 092031, pp. 1–6 (2011). *

Furukawa T., Inoue T., Nanao T., Yoshimi A., Tsuchiya M., Hayashi H., Uchida M., and Asahi K.: "Magnetic Field Stabilization for ^{129}Xe EDM Search Experiment", J. Phys.: Con. Ser. **312**, No. 102005, pp. 1–5 (2011). *

Nanao T., Yoshimi A., Inoue T., Furukawa T., Tsuchiya M., Hayashi H., Uchida M., and Asahi K.: "Development of high-sensitivity NMOR magnetometry for an EDM experiment", J. Phys.: Con. Ser. **312**, No. 102015, pp. 1–5 (2011). *

Inoue T., Furukawa T., Nanao T., Yoshimi A., Suzuki K., Chikamori M., Tsuchiya M., Hayashi H., Uchida M., and Asahi K.: "Experimental search for ^{129}Xe atomic EDM with nuclear spin maser technique", Phys. Procedia **17**, 100–103 (2011). *

Yoshimi A., Nanao T., Inoue T., Furukawa T., Uchida M., Tsuchiya M., Hayashi H., Chikamori M., and Asahi K.: "Development of NMOR magnetometer for spin-maser EDM experiment", Phys. Procedia **17**, 245–250 (2011). *

Inoue T., Tsuchiya M., Furukawa T., Hayashi H., Nanao T., Yoshimi A., Uchida M., Matsuo Y., and Asahi K.: "Frequency characteristics of a nuclear spin maser for the search for the electric dipole moment of 129Xe atom", Physica E **43**, No. 3, pp. 847–850 (2011). *

[**Book · Proceedings**]

(Original Papers) *Subject to Peer Review

Asahi K., Inoue T., Nanao T., Tsuchiya M., Hayashi H., Furukawa T., Yoshimi A., Uchida M., Ueno H., Matsuo Y., and Fukuyama T.: "Search for Electric Dipole Moment in 129Xe Atom Using a Nuclear Spin Oscillator", Proceedings of 4th International Workshop on Fundamental Physics Using Atoms 2010, Osaka, 2010–8, , Osaka, pp. 24–28 (2010). *

Oral Presentations

(International Conference etc.)

Imai N., Ong H., Aoi N., Sakurai H., Demichi K., Kawasaki H., Baba H., Dombradi Z., Elekes Z., Fukuda N., Fulop Z., Gelberg A., Gomi T., Hasegawa H., Ishikawa K., Iwasaki H., Kaneko E., Kanno S., Kishida T., Kondo Y., Kubo T., Kurita K., Michimasa S., Minemura T., Miura M., Motobayashi T., Nakamura T., Notani M., Onishi T., Saito A., Shimoura S., Sugimoto T., Suzuki M., Takeshita E., Takeuchi S., Tamaki M., Yamada K., Yoneda K., Watanabe H., and Ishihara M.: "Anomalously small B(E2) value of ^{16}C", International Nuclear Physics Conference (INPC2004), Goteborg, Sweden, June–July (2004).

Asahi K., Inoue T., Furukawa T., Tsuchiya M., Hayashi H., Nanao T., Uchida M., and Yoshimi A.: "Experimental search for an EDM in 129Xe atom", International Workshop on UCN and Fundamental Neutron Physics (UCN2010), (RCNP), Osaka, Apr. (2010).

Tsuchiya M., Inoue T., Hayashi H., Nanao T., Furukawa T., Yoshimi A., Uchida M., and Asahi K.: "A Test

Bench for the Polarization Study of 129Xe for an EDM Search Experiment", International Nuclear Physics Conference (INPC2010), (TRIUMF), Vancouver, Canada, July (2010).

Nanao T., Yoshimi A., Inoue T., Furukawa T., Tsuchiya M., Hayashi H., Uchida M., and Asahi K.: "Development of High-Sensitivity NMOR Magnetometry for an EDM Experiment", International Nuclear Physics Conference (INPC2010), (TRIUMF), Vancouver, Canada, July (2010).

Furukawa T., Inoue T., Nanao T., Yoshimi A., Tsuchiya M., Hayashi H., Uchida M., and Asahi K.: "Magnetic Field Stabilization for 129Xe EDM Search Experiment", International Nuclear Physics Conference (INPC2010), (TRIUMF), Vancouver, Canada, July (2010).

Inoue T., Yoshimi A., Furukawa T., Tsuchiya M., Hayashi H., Nanao T., Uchida M., and Asahi K.: "Search for an EDM in Diamagnetic Atom 129Xe with Nuclear Spin Maser Technique", International Nuclear Physics Conference (INPC2010), (TRIUMF), Vancouver, Canada, July (2010).

Asahi K., Nanao T., Tsuchiya M., Hayashi H., Furukawa T., Yoshimi A., Uchida M., Ueno H., and Matsuo Y.: "Search for an electric dipole moment in 129Xe atom using a nuclear spin oscillator", International conference on Fundamental Physics Using Atoms, Osaka, Aug. (2010).

Inoue T., Furukawa T., Nanao T., Yoshimi A., Suzuki K., Tsuchiya M., Hayashi H., Uchida M., and Asahi K.: "Development of the nuclear spin maser toward the atomic EDM search", 19th International Spin Physics Symposium (SPIN 2010), Julich, Germany, Sept.–Oct. (2010).

Yoshimi A., Nanao T., Inoue T., Furukawa T., Tsuchiya M., Hayashi H., Chikamori M., Uchida M., and Asahi K.: "Development of NMOR magnetometer for spin-maser EDM experiment", Villigen, Switzerland 2010/10, (PSI), Villigen, Switzerland, Oct. (2010).

Inoue T., Furukawa T., Nanao T., Yoshimi A., Suzuki K., Chikamori M., Hayashi H., Uchida M., and Asahi K.: "Experimental search for 129Xe atomic EDM with nuclear spin maser technique", Villigen, Switzerland 2010/10, (PSI), Villigen, Switzerland, Oct. (2010).

Ueno H.: "Spin polarization phenonema of unstable exotic beam experiment", 11th Asia Pacific Physics Conference (APPC11), (Association of Asia Pacific Physical Societies (AAPPS) and the Chinese Physical Society (CPS)), Shanghai, China, Nov. (2010).

Ichikawa Y., Ueno H., Ishii Y., Furukawa T., Yoshimi A., Kameda D., Aoi N., Watanabe H., Asahi K., Iijima H., Suzuki K., Inoue T., Tsuchiya M., Hayashi H., Nanao T., Kubo T., Inabe N., Ohnishi T., Takeda H., Fukuda N., Ishihara M., Daugas J., Chevrier R., Georgiev G., Rajabali M. M., and Balabanski D. L.: "Production of spin-aligned RI beam via two-step fragmentation reaction with dispersion matching", University of Aizu-JUSTIPEN-EFES Symposium on "Cutting-Edge Physics of Unstable Nuclei", (University of Aizu), Aizuwakamatsu, Nov. (2010).

Ueno H.: "Production of spin-aligned RI beams via the two-step fragmentation reaction", French Japanese Symposium on Nuclear Structure Problems, Wako, Jan. (2011).

Asahi K., Inoue T., Nanao T., Tsuchiya M., Hayashi H., Furukawa T., Uchida M., Yoshimi A., Ueno H., and Matsuo Y.: "Search for Electric Dipole Moment in 129Xe atom Using a Nuclear Spin Oscillator", International Symposium Nanoscience and Quantum Physics (nanoPHYS'11), Tokyo, Jan. (2011).

Ueno H.: "Overview of Nishina Center & RIBF", ISFMS 2011, Bali, Indonesia, Apr. (2011).

Ichikawa Y., Ueno H., Ishii Y., Furukawa T., Yoshimi A., Kameda D., Aoi N., Watanabe H., Asahi K., Iijima H., Suzuki K., Inoue T., Tsuchiya M., Hayashi H., Nanao T., Kubo T., Inabe N., Ohnishi T., Takeda H., Fukuda N., Ishihara M., Daugas J., Chevrier R., Georgiev G., Rajabali M. M., and Balabanski D. L.: "g-factor measurements for highly spin-aligned isomeric states", RIBF-ULIC-Symposium-007: E(U)RICA International Workshop, Saitama, May (2011).

Ichikawa Y., Ueno H., Ishii Y., Furukawa T., Yoshimi A., Kameda D., Aoi N., Watanabe H., Asahi K., Iijima H., Suzuki K., Inoue T., Tsuchiya M., Hayashi H., Nanao T., Kubo T., Inabe N., Ohnishi T., Takeda H., Fukuda N., Ishihara M., Daugas J., Chevrier R., Georgiev G., Rajabali M. M., and Balabanski D. L.: "Production of spin-aligned RI beam via two-step fragmentation with dispersion matching", ARIS 2011, (Katholieke Universiteit Leuven), Leuven, Belgium, May–June (2011).

Chevrier R., Daugas J., Gaudefroy L., Ichikawa Y., Ueno H., Haas M., Haas H., Cottenier S., Aoi N., Asahi K., Balabanski D. L., Fukuda N., Furukawa T., Georgiev G., Hayashi H., Iijima H., Inabe N., Inoue T., Ishihara M., Ishii Y., Kameda D., Kubo T., Nanao T., Neyence G., Ohnishi T., Rajabali M. M., Suzuki K., Takeda H., Tsuchiya M., Vermeulen N., Watanabe H., and Yoshimi A.: "Quadrupole moment measurement of the $N = 27$ nucleus $43m$S", ARIS 2011, (Katholieke Universiteit Leuven), Leuven, Belgium, May–June (2011).

Ichikawa Y., Ueno H., Ishii Y., Furukawa T., Yoshimi A., Kameda D., Aoi N., Watanabe H., Asahi K., Iijima H., Suzuki K., Inoue T., Tsuchiya M., Hayashi H., Nanao T., Kubo T., Inabe N., Ohnishi T., Takeda H., Fukuda N., Ishihara M., Daugas J., Chevrier R., Georgiev G., Rajabali M. M., and Balabanski D. L.: "g-factor measurement for highly spin-aligned isomeric state of ^{32}Al", RIBF ULIC and CNS Symposium on Frontier of Gamma-ray Spectroscopy (Gamma11), (CNS, The University of Tokyo and RIKEN Nishina Center), Saitama, June–July (2011).

Ichikawa Y., Ueno H., Ishii Y., Furukawa T., Yoshimi A., Kameda D., Aoi N., Watanabe H., Asahi K., Iijima H., Suzuki K., Inoue T., Tsuchiya M., Hayashi H., Nanao T., Kubo T., Inabe N., Ohnishi T., Takeda H., Fukuda N., Ishihara M., Daugas J., Chevrier R., Georgiev G., Rajabali M. M., and Balabanski D. L.: "Production of spin-aligned RI beam via two-step fragmentation with dispersion matching", Rutherford Centennial Conference on Nuclear Physics 2011, (The University of Machester), Manchester, United Kingdom, Aug. (2011).

Ueno H.: "Nuclear-moment measurements around $N = 20$ neutron-rich nuclei", Colloque GANIL 2011, (GANIL), Corsica, France, Sept. (2011).

Chevrier R., Daugas J., Gaudefroy L., Ichikawa Y., Ueno H., Haas M., Haas H., Cottenier S., Aoi N., Asahi K., Balabanski D. L., Fukuda N., Furukawa T., Georgiev G., Hayashi H., Iijima H., Inabe N., Inoue T., Ishihara M., Ishii Y., Kameda D., Kubo T., Nanao T., Neyence G., Ohnishi T., Rajabali M. M., Suzuki K., Takeda H., Tsuchiya M., Vermeulen N., Watanabe H., and Yoshimi A.: "Quadrupole moment measurement of the $N = 27$ nucleus $^{43}S^{m}$", Colloque GANIL 2011, (GANIL), Corsica, France, Sept. (2011).

Yoshimi A., Nanao T., Inoue T., Chikamori M., Furukawa T., Ichikawa Y., Hayashi H., Tsuchiya M., Miyatake H., Ishii Y., Yoshida N., Shirai H., Uchida M., Ueno H., Matsuo Y., Fukuyama T., and Asahi K.: "Development of high-sensitivity magnetometer for EDM experiment with ^{129}Xe spin ocsillator", 5th International conference on "Fundamental Physics Using Atoms - Towards better understanding of our matter universe -", (Okayama University), Okayama, Oct. (2011).

Chikamori M., Miyatake H., Inoue T., Nanao T., Furukawa T., Yoshimi A., Ichikawa Y., Tsuchiya M., Hayashi H., Ishii Y., Yoshida N., Shirai H., Uchida M., Ueno H., Matsuo Y., Fukuyama T., and Asahi K.: "Development of Xe SEOP cells for an experiment searching or an atomic electric dipole moment in ^{129}Xe", 5th International conference on "Fundamental Physics Using Atoms - Towards better understanding of our matter universe -", (Okayama University), Okayama, Oct. (2011).

Nanao T., Furukawa T., Inoue T., Chikamori M., Yoshimi A., Ichikawa Y., Tsuchiya M., Hayashi H., Miyatake H., Ishii Y., Yoshida N., Shirai H., Uchida M., Ueno H., Matsuo Y., Fukuyama T., and Asahi K.: "Stabilization of environmental magnetic fields in the Tokyo Tech ^{129}Xe atomic DM experiment", 5th International conference on "Fundamental Physics Using Atoms - Towards better understanding of our matter universe -", (Okayama University), Okayama, Oct. (2011).

Inoue T., Nanao T., Chikamori M., Furukawa T., Yoshimi A., Ichikawa Y., Hayashi H., Tsuchiya M., Miyatake H., Ishii Y., Yoshida N., Shirai H., Uchida M., Ueno H., Matsuo Y., Fukuyama T., and Asahi K.: "^{129}Xe atomic EDM search with nuclear spin maser technique", 5th International conference on "Fundamental Physics Using Atoms" - Towards better understanding of our matter universe -, (Okayama University), Okayama, Oct. (2011).

Ueno H.: "Spin-aligned radioactive-isotope beams through the two-step fragmentation and nuclear moments of aluminum isotopes", Frontier Issues in Physics of Exotic Nuclei (YKIS2011), (Kyoto University), Kyoto, Oct. (2011).

Ichikawa Y., Ueno H., Ishii Y., Furukawa T., Yoshimi A., Kameda D., Aoi N., Watanabe H., Asahi K., Iijima H., Suzuki K., Inoue T., Tsuchiya M., Hayashi H., Nanao T., Kubo T., Inabe N., Ohnishi T., Takeda H., Fukuda N., Ishihara M., Daugas J., Chevrier R., Georgiev G., Rajabali M. M., and Balabanski D. L.: "Spin-aligned RI beam produced by two-step projectile fragmentation", ISPUN11, (Institute for Nuclear Science and Technique), Hanoi, Vietnam, Nov. (2011).

(Domestic Conference)

飯島裕章, 吉見彰洋, 市川雄一, 石井裕司, 吉田直貴, 古川武, 内田誠, 鈴木都文, 井上壮志, 土屋真人, 林宏憲, 七尾翼, 近森正敏, 上野秀樹, 旭耕一郎: "中性子過剰核 41,43S の磁気モーメント測定のための磁場回転装置の開発", 平成 22 年度 KUR 専門研究会「短寿命核および放射線を用いた物性研究（III）」, 大阪, 2 月 (2010).

松浦佑一, 古川武, 小林徹, 畠山温, 加藤裕樹, 立川真樹, 松尾由賀利: "超流動ヘリウム中での Au 原子の励起スペクトルと偏極生成", 第 7 回 AMO 討論会, つくば, 6 月 (2010).

七尾翼, 吉見彰洋, 井上壮志, 古川武, 土屋真人, 林宏憲, 内田誠, 旭耕一郎: "EDM 実験のための NMOR を用いた高感度磁力計の開発", 日本物理学会 2010 年秋季大会, 北九州, 9 月 (2010).

石井裕司, 市川雄一, 上野秀樹, 古川武, 吉見彰洋, 亀田大輔, 青井考, 渡邉寛, 旭耕一郎, 飯島裕章, 鈴木都文, 井上壮志, 土屋真人, 林宏憲, 七尾翼, 久保敏幸, 稲辺尚人, 大西哲哉, 竹田浩之, 福田直樹, 石原正泰, Daugas J., Chevrier R., Georgiev G., Rajabali M. M., Balabanski D. L.: "TDPAD 法を用いた ^{32}Al アイソマーの磁気モーメント測定", 日本物理学会 2010 年秋季大会, (日本物理学会), 北九州, 9 月 (2010).

園田哲, 和田道治, 富田英生, 岡田邦宏, 伊藤由太, 飯村秀紀, 中村聡佑, Schuessler H. A., 高峰愛子, 松尾由賀利, 久保敏幸, 古川 武, 片山 一郎, 涌井 崇志, 篠塚 勉, Huyse M., Kudryavtsev. Y., Duppen P. V.: "理研における共鳴イオン化レーザーイオン源の開発", 日本物理学会 2010 年秋季大会, (日本物理学会), 北九州市, 9 月 (2010).

吉見彰洋: "EDM 探索実験の現状", 日本大学原子核理論コロキウム, 東京, 9 月 (2010).

上野 秀樹: "Study of the island of inversion through nuclear-moment measurements", 仁科センター研究会「電磁気モーメント・核力反応による Island of Inversion の理解にむけて」, 和光, 12 月 (2010).

七尾 翼: "Current status for magnetometer development", Atomic Magnetometry and Fundamental Physics, Tokyo, 1 月 (2011).

井上壮志: “EDM search in a 129Xe atom”, Atomic Magnetometry and Fundamental Physics, Tokyo, 1 月 (2011).

吉見彰洋: “Magnetometer for EDM experiments”, Atomic Magnetometry and Fundamental Physics, Tokyo, 1 月 (2011).

吉見彰洋: “EDM 測定における磁力計について”, 中性子制御デバイスとその応用 IV, 大阪府熊取町, 2 月 (2011).

石井裕司, 市川雄一, 上野秀樹, 古川武, 吉見彰洋, 亀田大輔, 青井考, 渡邉寛, 旭耕一郎, 飯島裕章, 鈴木都文, 井上壮志, 土屋真人, 林宏憲, 七尾翼, 久保敏幸, 稲辺尚人, 大西哲哉, 竹田浩之, 福田直樹, 石原正泰, Daugas J., Chevrier R., Georgiev G., Rajabali M. M., Balabanski D. L.: “TDPAD 法を用いた ^{32}Al アイソマーの磁気モーメント測定 II”, 日本物理学会第 66 回年次大会, (日本物理学会), 新潟, 3 月 (2011).

松浦佑一, 古川武, 小林徹, 畠山温, 加藤裕樹, 山口康広, 今村慧, 幕田将宏, 立川真樹, 松尾由賀利: “超流動ヘリウム環境を用いた Au 原子の光ポンピングと二重共鳴”, 日本物理学会第 66 回年次大会, 新潟, 3 月 (2011).

古川武, 涌井崇志, 佐々木彩子, 泉さやか, 市川雄一, 吉見彰洋, 田尻邦彦, 石井裕司, 吉田直貴, 松浦佑一, 加藤裕樹, 山口康広, 今村慧, 幕田将宏, 畠山温, 和田道治, 園田哲, 伊藤由太, 七尾翼, 小林徹, 西村俊二, 西村美月, 近藤洋介, 青井考, 米田健一郎, 久保野茂, 大城幸光, 上野秀樹, 篠塚勉, 下田正, 旭耕一郎, 松尾由賀利: “^{87}Rb ビームを用いた超流動ヘリウム中でのレーザー核分光法開発実験”, 日本物理学会第 66 回年次大会, 新潟, 3 月 (2011).

市川雄一, 上野秀樹, 石井裕司, 古川武, 吉見彰洋, 亀田大輔, 青井考, 渡邉寛, 旭耕一郎, 飯島裕章, 鈴木都文, 井上壮志, 土屋真人, 林宏憲, 七尾翼, 久保敏幸, 稲辺尚人, 大西哲哉, 竹田浩之, 福田直樹, 石原正泰, Daugas J., Chevrier R., Georgiev G., Rajabali M. M., Balabanski D. L.: “分散整合二回散乱法による核スピン整列 RI ビームの生成 II”, 日本物理学会第 66 回年次大会, (日本物理学会), 新潟, 3 月 (2011).

加藤裕樹, 古川武, 今村慧, 山口康広, 小林徹, 畠山温, 立川真樹, 松尾由賀利: “超流動ヘリウム中に埋め込まれた 13 族原子 In, Ga の励起スペクトル”, 第 8 回 AMO 討論会, (原子・分子・光科学 (AMO) 討論会実行委員会), 東京, 6 月 (2011).

松浦佑一, 古川武, 小林徹, 畠山温, 加藤裕樹, 山口康広, 今村慧, 幕田将宏, 立川真樹, 松尾由賀利: “超流動ヘリウム環境を用いた Au 原子の光ポンピングと二重共鳴”, 第 8 回 AMO 討論会, (原子・分子・光科学 (AMO) 討論会実行委員会), 東京, 6 月 (2011).

七尾翼, 古川武, 井上壮志, 吉見彰洋, 近森正敏, 土屋真人, 林宏憲, 石井裕司, 吉田直貴, 内田誠, 旭耕一郎: “EDM 測定のための環境磁場安定化システムの構築”, 日本物理学会 2011 年秋季大会, (日本物理学会), 弘前, 9 月 (2011).

吉田直貴, 吉見彰洋, 上野秀樹, 市川雄一, 石井裕司, 井上壮志, 土屋真人, 林宏憲, 七尾翼, 近森正敏, 内田誠, 旭耕一郎: “β-NMR 実験のための新型制御系・データ収集系の開発”, 日本物理学会 2011 年秋季大会, (日本物理学会), 弘前, 9 月 (2011).

近森正敏, 井上壮志, 七尾翼, 古川武, 吉見彰洋, 土屋真人, 林宏憲, 石井裕司, 吉田直貴, 内田誠, 旭耕一郎: “EDM 測定のための ^{129}Xe 核スピン偏極セルの製作”, 日本物理学会 2011 年秋季大会, (日本物理学会), 弘前, 9 月 (2011).

阿部康志, 長江大輔, 小沢顕, 森口哲朗, 石橋陽子, 伊藤由太, 奥村公威, 金沢光隆, 佐藤眞二, 鈴木宏, 錦織良, 福岡翔太, 山口貴之, 山口由高: “理研稀少 RI リングのための飛行時間検出器の開発”, 日本物理学会 2011 年秋季大会, (日本物理学会), 弘前, 9 月 (2011).

井上壮志, 七尾翼, 近森正敏, 古川武, 吉見彰洋, 土屋真人, 林宏憲, 石井裕司, 吉田直貴, 内田誠, 旭耕一郎: “能動帰還型核スピンメーザーの周波数特性”, 日本物理学会 2011 年秋季大会, (日本物理学会), 弘前, 9 月 (2011).

今村慧, 古川武, 山口康広, Yang X., 加藤裕樹, 小林徹, 幕田将宏, 畠山温, 小田島仁司, 松尾由賀利: “超流動 He 環境におけるアルカリ原子の超微細構造間隔測定”, 日本物理学会 2011 年秋季大会, (日本物理学会), 富山, 9 月 (2011).

古川武, 涌井崇志, 佐々木彩子, 泉さやか, 市川雄一, 吉見彰洋, 田尻邦彦, 石井裕司, 吉田直貴, 松浦佑一, 加藤裕樹, 山口康広, 今村慧, 幕田将宏, 畠山温, 和田道治, 園田哲, 伊藤由太, 七尾翼, 小林徹, 西村俊二, 西村美月, 近藤洋介, 青井考, 米田健一郎, 久保野茂, 上野秀樹, 下田正, 篠塚勉, 旭耕一郎, 松尾由賀利: “超流動ヘリウム中に打ち込まれた ^{87}Rb ビームのレーザー誘起蛍光観測と光ポンピング”, 日本物理学会 2011 年秋季大会, (日本物理学会), 弘前, 9 月 (2011).

市川雄一, 上野秀樹, 石井裕司, 古川武, 吉見彰洋, 亀田大輔, 青井考, 渡邉寛, 旭耕一郎, 飯島裕章, 鈴木都文, 井上壮志, 土屋真人, 林宏憲, 七尾翼, 久保敏幸, 稲辺尚人, 大西哲哉, 竹田浩之, 福田直樹, 石原正泰, Daugas J., Chevrier R., Georgiev G., Rajabali M. M., Balabanski D. L.: “分散整合二回散乱法による核スピン整列 RI ビームの生成 III”, 日本物理学会 2011 年秋季大会, (日本物理学会), 弘前, 9 月 (2011).

七尾翼, 井上壮志, 近森正敏, 宮武裕和, 吉見彰洋, 古川武, 市川雄一, 林宏憲, 土屋真人, 石井裕司, 吉田直貴, 白井葉月, 内田誠, 旭耕一郎: “Development of atomic magnetometer based on NMOR for an EDM experiment”, 日本物理学会第 67 回年次大会, (日本物理学会), 西宮, 3 月 (2012).

井上壮志, 七尾翼, 近森正敏, 宮武裕和, 古川武, 吉見彰洋, 市川雄一, 土屋真人, 林宏憲, 石井裕司, 吉田直貴, 白井葉月, 内田誠, 旭耕一郎: “Frequency character of active spin maser II”, 日本物理学会第 67 回年次大会, (日本物理学会), 西宮, 3 月 (2012).

宮武裕和, 近森正敏, 井上壮志, 七尾翼, 吉見彰洋, 古川武, 市川雄一, 林宏憲, 土屋真人, 石井裕司, 吉田直貴, 白井葉月, 猪野隆, 内田誠, 旭耕一郎: “Production of ^{3}He Polarization for a ^{3}He co-magnetometer”, 日本物理学会第 67 回年次大会, (日本物理学会), 西宮, 3 月 (2012).

石井裕司, Georgiev G., 市川雄一, 白井葉月, 上野秀樹, 石橋陽子, 吉田直貴, 古川武, Sotty C., Chevrier R., Daugas J., Ljungvall J., Lozeva R. L., 新倉潤, Yordanov D., 渡邉寛, 西村太樹, 西畑洸希, 近森正敏, 宮武裕和, 七尾翼, 丹羽崇博, 岡田俊祐, 齋藤佑多, 旭耕一郎, Balabanski D. L.: “Production of a spin-aligned ^{69}Cu beam by one-nucleon-removal reactions and measurement of its nuclear moments", 日本物理学会第 67 回年次大会, (日本物理学会), 西宮, 3 月 (2012).

加藤裕樹, 古川武, 小林徹, 今村慧, 山口康広, Yang X., 畠山温, 立川真樹, 松尾由賀利: "超流動ヘリウム環境下における In 原子の電子スピン緩和", 日本物理学会第 67 回年次大会, (日本物理学会), 西宮, 3 月 (2012).

松浦佑一, 古川武, 小林徹, 畠山温, 加藤裕樹, 山口康広, 今村慧, 幕田将宏, 立川真樹, 松尾由賀利: "超流動ヘリウム環境を用いた Au 原子のスピン偏極と核スピンの導出", 日本物理学会第 67 回年次大会, (日本物理学会), 西宮, 3 月 (2012).

Rare RI-ring Team

Publications

[Journal]

(Original Papers) *Subject to Peer Review

Mihara M., Izumikawa T., Ueno H., Matsuta K., Nishimura D., Nagatomo T., Moriguchi T., Ito Y., Nagae D., Fukuda M., Yoshimi A., Yamada K., Takechi M., Ichikawa Y., Momota S., Hirayama Y., Ohtsubo T., Suzuki S., Ozawa A., Ishibashi Y., Kubo T., Ooishi H., Namiki Y., Hachiuma K., Namihira K., Horikawa D., Minamisono T., Yamaguchi T., Kuboki T., Suzuki T., Sato K., Kobayashi Y., and Asahi K.: "Beta-NMR measurement of 58Cu in Si", Hyperfine Interact. **197**, 143–147 (2010). *

Nagatomo T., Ueno H., Mihara M., Matsuta K., Yoshimi A., Ichikawa Y., Yamada K., Kawamura H., Ozawa A., Moriguchi T., Ishibashi Y., Asahi K., Uchida M., Suzuki K., Inoue T., Hasama Y., Iijima H., Sumikama T., Fukuda M., and Minamisono T.: "Precise nuclear moments of extremely proton-rich nuclus 23Al", Hyperfine Interact. **198**, 103–107 (2010). *

Ohnishi T., Kubo T., Kusaka K., Yoshida A., Yoshida K., Ohtake M., Fukuda N., Takeda H., Kameda D., Tanaka K., Inabe N., Yanagisawa Y., Gono Y., Watanabe H., Otsu H., Baba H., Ichihara T., Yamaguchi Y., Takechi M., Nishimura S., Ueno H., Yoshimi A., Sakurai H., Motobayashi T., Nakao T., Mizoi Y., Matsushita M., Ieki K., Kobayashi N., Tanaka K., Kawada Y., Tanaka N., Deguchi S., Sato Y., Kondo Y., Nakamura T., Yoshinaga K., Ishii c., Yoshii h., Miyashita Y., Uematsu N., Shiraki Y., Sumikama T., Chiba J., Ideguchi E., Saito A., Yamaguchi T., Hachiuma I., Suzuki T., Moriguchi T., Ozawa A., Ohtsubo T., Famiano M. A., Geissel H., Nettleton A. S., Tarasov O. B., Bazin D. P., Sherrill B. M., Manikonda S. L., and Nolen J. A.: "Identification of 45 New Neutron-Rich Isotopes Produced by In-Flight Fission of a ^{238}U Beam at 345 MeV/nucleon", J. Phys. Soc. Jpn. **79**, No. 7, pp. 073201-1–073201-5 (2010). *

Oral Presentations

(International Conference etc.)

Yamaguchi Y., Wakasugi M., Suzuki H., Fujinawa T., Uesaka T., Yano Y., Ozawa A., Nagae D., Yamaguchi T., Suzuki T., Kikuchi T., Jiang W., Sasaki T., and Tokuchi A.: "Present status of rare-RI ring project in RIKEN RI beam factory", 8th International Conference on Nuclear Physics at Storage Rings (STORI-11), (INFN-LNF), Frascati, Italy, Oct. (2011).

(Domestic Conference)

阿部康志, 長江大輔, 小沢顕, 森口哲朗, 石橋陽子, 伊藤由太, 奥村公威, 金沢光隆, 佐藤眞二, 鈴木宏, 錦織良, 福岡翔太, 山口貴之, 山口由高: "理研稀少 RI リングのための飛行時間検出器の開発", 日本物理学会 2011 年秋季大会, (日本物理学会), 弘前, 9 月 (2011).

山口由高: "Design of rare-RI ring", 仁科センター研究会「稀少 RI リングの物理」, 和光, 11 月 (2011).

長江大輔: "TOF detector for RIKEN rare-RI ring", 仁科センター研究会「稀少 RI リングの物理」, 和光, 11 月 (2011).

石井裕司, Georgiev G., 市川雄一, 白井葉月, 上野秀樹, 石橋陽子, 吉田直貴, 古川武, Sotty C., Chevrier R., Daugas J., Ljungvall J., Lozeva R. L., 新倉潤, Yordanov D., 渡邉寛, 西村太樹, 西畑洸希, 近森正敏, 宮武裕和, 七尾翼, 丹羽崇博, 岡田俊祐, 齋藤佑多, 旭耕一郎, Balabanski D. L.: "Production of a spin-aligned ^{69}Cu beam by one-nucleon-removal reactions and measurement of its nuclear moments", 日本物理学会第 67 回年次大会, (日本物理学会), 西宮, 3 月 (2012).

SCRIT Team

Publications

[Journal]

(Original Papers)　*Subject to Peer Review

Tamae T., Sato Y., Yokokawa T., Asano Y., Kawabata M., Konno O., Nakagawa I., Nishikawa I., Hirota K., Yamazaki H., Kimura R., Miyase H., Tsubota H., Giusti C., and Meucci A.: "Comparison of the C-12 (e, e′ p) cross section at low momentum transfer with a relativistic calculation", Phys. Rev. C **80**, No. 6, pp. 064601-1–064601-7 (2009). *

Oral Presentations

(International Conference etc.)

Sato H., Iwasa N., Kawabata T., Kobayashi T., Kondo Y., Kubo T., Kusaka K., Motobayashi T., Murakami T., Nakamura T., Ohnishi J., Ohnishi T., Okuno H., Otsu H., Sakurai H., Satou Y., Sakaguchi-Sekiguchi K., Togano Y., and Yoneda K.: "SAMURAI spectrometer at RIKEN RI beam factory", Advanced Studies Institute: Symmetries and Spin (SPIN-Praha-2009), (Charles University), Prague, Czech, July–Aug. (2009).

Kambara T., Yoshida A., Yanagisawa Y., Kameda D., Fukuda N., Ohnishi T., Kubo T., Uemoto R., Nagano A., and Uno H.: "Industrial Application of Radioactive Ion Beam at RIKEN RI Beam Factory", 11th International Conference on Applications of Nuclear Techniques, Crete, Greece, June (2011).

(Domestic Conference)

上本龍二, 鵜野浩行, 永野章, 大西哲哉, 亀田大輔, 福田直樹, 柳澤善行, 吉田敦, 久保敏幸, 神原正: "RI ビームの連続磨耗測定法への適用", 自動車技術会 2011 年春季大会, (公益社団法人自動車技術会), 横浜, 5 月 (2011).

Research Instruments Group

Publications

[Journal]

(Original Papers) *Subject to Peer Review

Tanaka K., Yamaguchi T., Suzuki T., Ohtsubo T., Fukuda M., Nishimura D., Takechi M., Ogata K., Ozawa A., Izumikawa T., Aiba T., Aoi N., Baba H., Hashizume Y., Inafuku K., Iwasa N., Kobayashi K., Komuro M., Kondo Y., Kubo T., Matsuyama T., Michimasa S., Motobayashi T., Nakabayashi T., Nakazima S., Nakamura T., Sakurai H., Shinoda R., Shinohara M., Suzuki H., Takeshita E., Takeuchi S., Togano Y., Yamada K., Yasuno T., and Yhoshitake M.: "Observation of a large reaction cross-section in the drip-line nucleus ^{22}C", Phys. Rev. Lett. **104**, No. 6, pp. 062701-1–062701-4 (2010). *

Yoshida A., Yanagisawa Y., and Kubo T.: "Beam-spot temperature monitoring on the production target at the BigRIPS separator", Nucl. Instrum. Methods Phys. Res. A **655**, 10–16 (2011). *

Oral Presentations

(International Conference etc.)

Sato H., Iwasa N., Kawabata T., Kobayashi T., Kondo Y., Kubo T., Kusaka K., Motobayashi T., Murakami T., Nakamura T., Ohnishi J., Ohnishi T., Okuno H., Otsu H., Sakurai H., Satou Y., Sakaguchi-Sekiguchi K., Togano Y., and Yoneda K.: "SAMURAI spectrometer at RIKEN RI beam factory", Advanced Studies Institute: Symmetries and Spin (SPIN-Praha-2009), (Charles University), Prague, Czech, July–Aug. (2009).

Ohnishi T., Kusaka K., and Kubo T.: "Radiation transport calculation using PHITS code for radiation heat load and damage to superconducting radioactive isotope beam separator BigRIPS at RIKEN", 7th Supercomputing in Nuclear Application and the 3rd Monte Carlo (SNA+MC2010), (Japan Atomic Energy Agency), Tokyo, Oct. (2010).

Tanaka K., Inabe N., Ohnishi T., and Kubo T.: "Radiation transport calculation using PHITS code for the activation of BigRIPS separator at RIKEN radioactive isotope beam factory and comparison with the measurement", 7th Supercomputing in Nuclear Application and the 3rd Monte Carlo (SNA+MC2010), (Japan Atomic Energy Agency), Tokyo, Oct. (2010).

Ichikawa Y., Ueno H., Ishii Y., Furukawa T., Yoshimi A., Kameda D., Aoi N., Watanabe H., Asahi K., Iijima H., Suzuki K., Inoue T., Tsuchiya M., Hayashi H., Nanao T., Kubo T., Inabe N., Ohnishi T., Takeda H., Fukuda N., Ishihara M., Daugas J., Chevrier R., Georgiev G., Rajabali M. M., and Balabanski D. L.: "Production of spin-aligned RI beam via two-step fragmentation reaction with dispersion matching", University of Aizu-JUSTIPEN-EFES Symposium on "Cutting-Edge Physics of Unstable Nuclei", (University of Aizu), Aizuwakamatsu, Nov. (2010).

Tanaka K., Inabe N., and Kubo T.: "Pillow seal system at BigRIPS", Darmstadt, Germany, 2010/12, (GSI), Darmstadt, Germany, Dec. (2010).

Tanaka K., Ohnishi T., Inabe N., and Kubo T.: "Radiation transport calculations for BigRIPS and comparison with measurements", Darmstadt, Germany, 2010/12, (GSI), Darmstadt, Germany, Dec. (2010).

Yoshida A., Yanagisawa Y., Yoshida K., and Kubo T.: "Operational experience of the target system for BigRIPS in-flight RI beam separator", 4th High Power Targetry Workshop, (European Spallation Source, Lund), Malmo, Sweden, May (2011).

Ichikawa Y., Ueno H., Ishii Y., Furukawa T., Yoshimi A., Kameda D., Aoi N., Watanabe H., Asahi K., Iijima H., Suzuki K., Inoue T., Tsuchiya M., Hayashi H., Nanao T., Kubo T., Inabe N., Ohnishi T., Takeda H., Fukuda N., Ishihara M., Daugas J., Chevrier R., Georgiev G., Rajabali M. M., and Balabanski D. L.: "g-factor measurements for highly spin-aligned isomeric states", RIBF-ULIC-Symposium-007: E(U)RICA International Workshop, Saitama, May (2011).

Ichikawa Y., Ueno H., Ishii Y., Furukawa T., Yoshimi A., Kameda D., Aoi N., Watanabe H., Asahi K., Iijima H., Suzuki K., Inoue T., Tsuchiya M., Hayashi H., Nanao T., Kubo T., Inabe N., Ohnishi T., Takeda H., Fukuda N., Ishihara M., Daugas J., Chevrier R., Georgiev G., Rajabali M. M., and Balabanski D. L.: "Production of spin-aligned RI beam via two-step fragmentation with dispersion matching", ARIS 2011, (Katholieke Universiteit Leuven), Leuven, Belgium, May–June (2011).

Chevrier R., Daugas J., Gaudefroy L., Ichikawa Y., Ueno H., Haas M., Haas H., Cottenier S., Aoi N., Asahi K., Balabanski D. L., Fukuda N., Furukawa T., Georgiev G., Hayashi H., Iijima H., Inabe N., Inoue T., Ishihara M., Ishii Y., Kameda D., Kubo T., Nanao T., Neyence G., Ohnishi T., Rajabali M. M., Suzuki K., Takeda H., Tsuchiya M., Vermeulen N., Watanabe H., and Yoshimi A.: "Quadrupole moment measurement of the $N = 27$ nucleus 43mS", ARIS 2011, (Katholieke Universiteit Leuven), Leuven, Belgium, May–June (2011).

Kambara T., Yoshida A., Yanagisawa Y., Kameda D., Fukuda N., Ohnishi T., Kubo T., Uemoto R., Nagano A., and Uno H.: "Industrial Application of Radioactive Ion Beam at RIKEN RI Beam Factory", 11th International Conference on Applications of Nuclear Techniques, Crete, Greece, June (2011).

Ichikawa Y., Ueno H., Ishii Y., Furukawa T., Yoshimi A., Kameda D., Aoi N., Watanabe H., Asahi K., Iijima H., Suzuki K., Inoue T., Tsuchiya M., Hayashi H., Nanao T., Kubo T., Inabe N., Ohnishi T., Takeda H., Fukuda N., Ishihara M., Daugas J., Chevrier R., Georgiev G., Rajabali M. M., and Balabanski D. L.: "g-factor measurement for highly spin-aligned isomeric state of

^{32}Al", RIBF ULIC and CNS Symposium on Frontier of Gamma-ray Spectroscopy (Gamma11), (CNS, The University of Tokyo and RIKEN Nishina Center), Saitama, June–July (2011).

Ichikawa Y., Ueno H., Ishii Y., Furukawa T., Yoshimi A., Kameda D., Aoi N., Watanabe H., Asahi K., Iijima H., Suzuki K., Inoue T., Tsuchiya M., Hayashi H., Nanao T., Kubo T., Inabe N., Ohnishi T., Takeda H., Fukuda N., Ishihara M., Daugas J., Chevrier R., Georgiev G., Rajabali M. M., and Balabanski D. L.: "Production of spin-aligned RI beam via two-step fragmentation with dispersion matching", Rutherford Centennial Conference on Nuclear Physics 2011, (The University of Machester), Manchester, United Kingdom, Aug. (2011).

Chevrier R., Daugas J., Gaudefroy L., Ichikawa Y., Ueno H., Haas M., Haas H., Cottenier S., Aoi N., Asahi K., Balabanski D. L., Fukuda N., Furukawa T., Georgiev G., Hayashi H., Iijima H., Inabe N., Inoue T., Ishihara M., Ishii Y., Kameda D., Kubo T., Nanao T., Neyence G., Ohnishi T., Rajabali M. M., Suzuki K., Takeda H., Tsuchiya M., Vermeulen N., Watanabe H., and Yoshimi A.: "Quadrupole moment measurement of the $N = 27$ nucleus ^{43}S^{m}", Colloque GANIL 2011, (GANIL), Corsica, France, Sept. (2011).

Ichikawa Y., Ueno H., Ishii Y., Furukawa T., Yoshimi A., Kameda D., Aoi N., Watanabe H., Asahi K., Iijima H., Suzuki K., Inoue T., Tsuchiya M., Hayashi H., Nanao T., Kubo T., Inabe N., Ohnishi T., Takeda H., Fukuda N., Ishihara M., Daugas J., Chevrier R., Georgiev G., Rajabali M. M., and Balabanski D. L.: "Spin-aligned RI beam produced by two-step projectile fragmentation", ISPUN11, (Institute for Nuclear Science and Technique), Hanoi, Vietnam, Nov. (2011).

(Domestic Conference)

石井裕司, 市川雄一, 上野秀樹, 古川武, 吉見彰洋, 亀田大輔, 青井考, 渡邉寛, 旭耕一郎, 飯島裕章, 鈴木都文, 井上壮志, 土屋真人, 林宏憲, 七尾翼, 久保敏幸, 稲辺尚人, 大西哲哉, 竹田浩之, 福田直樹, 石原正泰, Daugas J., Chevrier R., Georgiev G., Rajabali M. M., Balabanski D. L.: "TDPAD 法を用いた ^{32}Al アイソマーの磁気モーメント測定", 日本物理学会 2010 年秋季大会, (日本物理学会), 北九州, 9 月 (2010).

園田哲, 和田道治, 富田英生, 岡田邦宏, 伊藤由太, 飯村秀紀, 中村聡佑, Schuessler H. A., 高峰愛子, 松尾由賀利, 久保敏幸, 古川 武, 片山一郎, 涌井崇志, 篠塚勉, Huyse M., Kudryavtsev. Y., Duppen P. V.: "理研における共鳴イオン化レーザーイオン源の開発", 日本物理学会 2010 年秋季大会, (日本物理学会), 北九州市, 9 月 (2010).

石井裕司, 市川雄一, 上野秀樹, 古川武, 吉見彰洋, 亀田大輔, 青井考, 渡邉寛, 旭耕一郎, 飯島裕章, 鈴木都文, 井上壮志, 土屋真人, 林宏憲, 七尾翼, 久保敏幸, 稲辺尚人, 大西哲哉, 竹田浩之, 福田直樹, 石原正泰, Daugas J., Chevrier R., Georgiev G., Rajabali M. M., Balabanski D. L.: "TDPAD 法を用いた ^{32}Al アイソマーの磁気モーメント測定 II", 日本物理学会第 66 回年次大会, (日本物理学会), 新潟, 3 月 (2011).

市川雄一, 上野秀樹, 石井裕司, 古川武, 吉見彰洋, 亀田大輔, 青井考, 渡邉寛, 旭耕一郎, 飯島裕章, 鈴木都文, 井上壮志, 土屋真人, 林宏憲, 七尾翼, 久保敏幸, 稲辺尚人, 大西哲哉, 竹田浩之, 福田直樹, 石原正泰, Daugas J., Chevrier R., Georgiev G., Rajabali M. M., Balabanski D. L.: "分散整合二回散乱法による核スピン整列 RI ビームの生成 II", 日本物理学会第 66 回年次大会, (日本物理学会), 新潟, 3 月 (2011).

上本龍二, 鵜野浩行, 永野章, 大西哲哉, 亀田大輔, 福田直樹, 柳澤善行, 吉田敦, 久保敏幸, 神原正: "RI ビームの連続磨耗測定法への適用", 自動車技術会 2011 年春季大会, (公益社団法人自動車技術会), 横浜, 5 月 (2011).

市川雄一, 上野秀樹, 石井裕司, 古川武, 吉見彰洋, 亀田大輔, 青井考, 渡邉寛, 旭耕一郎, 飯島裕章, 鈴木都文, 井上壮志, 土屋真人, 林宏憲, 七尾翼, 久保敏幸, 稲辺尚人, 大西哲哉, 竹田浩之, 福田直樹, 石原正泰, Daugas J., Chevrier R., Georgiev G., Rajabali M. M., Balabanski D. L.: "分散整合二回散乱法による核スピン整列 RI ビームの生成 III", 日本物理学会 2011 年秋季大会, (日本物理学会), 弘前, 9 月 (2011).

GARIS Team

Oral Presentations

(International Conference etc.)

Morimoto K., Morita K., Kaji D., Haba H., Ohzeki K., Kudou Y., Sato N., Sumita T., Yoneda A., Ichikawa T., Goto S., Fujimori Y., Ideguchi E., Kasamatsu Y., Katori K., Komori Y., Koura H., Kudo H., Ooe K., Ozawa A., Tokanai F., Tsukada K., Yamaguchi T., and Yoshida A.: "Production and Decay Properties of ^{266}Bh and its daughter nuclei by using the ^{248}Cm(^{23}Na,5n) Reaction", Seventh Workshop on the Chemistry of the Heaviest elements, Mainz, Germany, Oct. (2009).

Morimoto K., Morita K., Kaji D., Haba H., Ohzeki K., Kudou Y., Sato N., Sumita T., Yoneda A., Ichikawa T., Fujimori Y., Goto S., Huang T., Ideguchi E., Kasamatsu Y., Katori K., Komori Y., Koura H., Kudo H., Murakami M., Ozawa A., Sakai R., Tokanai F., Tsukada K., Yamaguchi T., and Yoshida A.: "Confirmations of the synthesis of ^{278}113 produced by the ^{209}Bi(^{70}Zn,n)^{278}113 reaction", International Chemical Congress of Pacific Basin Societies (PACIFICHEM 2010), Honolulu, USA, Dec. (2010).

BigRIPS Team

Publications

[Journal]

(Original Papers) *Subject to Peer Review

Ohnishi T., Kubo T., Kusaka K., Yoshida A., Yoshida K., Ohtake M., Fukuda N., Takeda H., Kameda D., Tanaka K., Inabe N., Yanagisawa Y., Gono Y., Watanabe H., Otsu H., Baba H., Ichihara T., Yamaguchi Y., Takechi M., Nishimura S., Ueno H., Yoshimi A., Sakurai H., Motobayashi T., Nakao T., Mizoi Y., Matsushita M., Ieki K., Kobayashi N., Tanaka K., Kawada Y., Tanaka N., Deguchi S., Sato Y., Kondo Y., Nakamura T., Yoshinaga K., Ishii c., Yoshii h., Miyashita Y., Uematsu N., Shiraki Y., Sumikama T., Chiba J., Ideguchi E., Saito A., Yamaguchi T., Hachiuma I., Suzuki T., Moriguchi T., Ozawa A., Ohtsubo T., Famiano M. A., Geissel H., Nettleton A. S., Tarasov O. B., Bazin D. P., Sherrill B. M., Manikonda S. L., and Nolen J. A.: "Identification of 45 New Neutron-Rich Isotopes Produced by In-Flight Fission of a ^{238}U Beam at 345 MeV/nucleon", J. Phys. Soc. Jpn. **79**, No. 7, pp. 073201-1–073201-5 (2010). *

Tanaka K., Fukuda M., Mihara M., Takechi M., Nishimura D., Chinda T., Sumikama T., Kudo S., Matsuta K., Minamisono T., Suzuki T., Ohtsubo T., Izumikawa T., Momota S., Yamaguchi T., Oonish T., Ozawa A., Tanihata I., and Zheng T.: "Density distribution of ^{17}Ne and possible shell-structure change in the proton-rich sd-shell nuclei", Phys. Rev. C **82**, No. 4, pp. 044309-1–044309-11 (2010). *

Tanaka K., Yamaguchi T., Suzuki T., Ohtsubo T., Fukuda M., Nishimura D., Takechi M., Ogata K., Ozawa A., Izumikawa T., Aiba T., Aoi N., Baba H., Hashizume Y., Inafuku K., Iwasa N., Kobayashi K., Komuro M., Kondo Y., Kubo T., Matsuyama T., Michimasa S., Motobayashi T., Nakabayashi T., Nakazima S., Nakamura T., Sakurai H., Shinoda R., Shinohara M., Suzuki H., Takeshita E., Takeuchi S., Togano Y., Yamada K., Yasuno T., and Yhoshitake M.: "Observation of a large reaction cross-section in the drip-line nucleus ^{22}C", Phys. Rev. Lett. **104**, No. 6, pp. 062701-1–062701-4 (2010). *

Ichikawa Y., Onishi T., Suzuki D., Iwasaki H., Kubo T., Banerjee S. R., Chakrabarti A., Aoi N., Brown A. B., Fukuda N., Kubono S., Motobayashi T., Nakabayashi T., Nakamura T., Nakao T., Okumura T., Ong H., Suzuki H., Suzuki M., Teranishi T., Yamada K., Yamaguchi H., and Sakurai H.: "Proton-rich nuclear structure and mirror asymmetry investigated by β-decay spectroscopy of ^{24}Si", J. Phys.: Con. Ser. **312**, No. 092031, pp. 1–6 (2011). *

Yoshida A., Yanagisawa Y., and Kubo T.: "Beam-spot temperature monitoring on the production target at the BigRIPS separator", Nucl. Instrum. Methods Phys. Res. A **655**, 10–16 (2011). *

[Book · Proceedings]

(Original Papers) *Subject to Peer Review

大西純一, 中川孝秀, 湊恒明, 奥野広樹, 日暮祥英, 日下健祐, 後藤彰: "28 GHz ECR イオン源用超伝導コイルの製作と励磁試験", 第 5 回加速器学会年会・第 33 回リニアック技術研究会プロシーディングス, 東広島市, 2008–8, 日本加速器学会, 東京, pp. 406–408 (2008).

Oral Presentations

(International Conference etc.)

Sato H., Iwasa N., Kawabata T., Kobayashi T., Kondo Y., Kubo T., Kusaka K., Motobayashi T., Murakami T., Nakamura T., Ohnishi J., Ohnishi T., Okuno H., Otsu H., Sakurai H., Satou Y., Sakaguchi-Sekiguchi K., Togano Y., and Yoneda K.: "SAMURAI spectrometer at RIKEN RI beam factory", Advanced Studies Institute: Symmetries and Spin (SPIN-Praha-2009), (Charles University), Prague, Czech, July–Aug. (2009).

Morimoto K., Morita K., Kaji D., Haba H., Ohzeki K., Kudou Y., Sato N., Sumita T., Yoneda A., Ichikawa T., Goto S., Fujimori Y., Ideguchi E., Kasamatsu Y., Katori K., Komori Y., Koura H., Kudo H., Ooe K., Ozawa A., Tokanai F., Tsukada K., Yamaguchi T., and Yoshida A.: "Production and Decay Properties of ^{266}Bh and its daughter nuclei by using the ^{248}Cm(^{23}Na,5n) Reaction", Seventh Workshop on the Chemistry of the Heaviest elements, Mainz, Germany, Oct. (2009).

Yoshida A.: "Beam spot temperature monitoring on production target of BigRIPS separator", 25th World Conference of the International Nuclear Target Development Society, (TRIUMF), Vancouver, Canada, Sept. (2010).

Ohnishi T., Kusaka K., and Kubo T.: "Radiation transport calculation using PHITS code for radiation heat load and damage to superconducting radioactive isotope beam separator BigRIPS at RIKEN", 7th Supercomputing in Nuclear Application and the 3rd Monte Carlo (SNA+MC2010), (Japan Atomic Energy Agency), Tokyo, Oct. (2010).

Tanaka K., Inabe N., Ohnishi T., and Kubo T.: "Radiation transport calculation using PHITS code for the activation of BigRIPS separator at RIKEN radioactive isotope beam factory and comparison with the measurement", 7th Supercomputing in Nuclear Application and the 3rd Monte Carlo (SNA+MC2010), (Japan Atomic Energy Agency), Tokyo, Oct. (2010).

Ichikawa Y., Ueno H., Ishii Y., Furukawa T., Yoshimi A., Kameda D., Aoi N., Watanabe H., Asahi K., Iijima H., Suzuki K., Inoue T., Tsuchiya M., Hayashi H., Nanao T., Kubo T., Inabe N., Ohnishi T., Takeda H., Fukuda N., Ishihara M., Daugas J., Chevrier R., Georgiev G., Rajabali M. M., and Balabanski D. L.: "Production of spin-aligned RI beam via two-step fragmentation reaction with dispersion matching", University of Aizu-JUSTIPEN-EFES Symposium on "Cutting-

Edge Physics of Unstable Nuclei", (University of Aizu), Aizuwakamatsu, Nov. (2010).

Tanaka K., Inabe N., and Kubo T.: "Pillow seal system at BigRIPS", Darmstadt, Germany, 2010/12, (GSI), Darmstadt, Germany, Dec. (2010).

Yoshida A.: "Progress in BigRIPS high-power target", Darmstadt, Germany, 2010/12, (GSI), Darmstadt, Germany, Dec. (2010).

Tanaka K., Ohnishi T., Inabe N., and Kubo T.: "Radiation transport calculations for BigRIPS and comparison with measurements", Darmstadt, Germany, 2010/12, (GSI), Darmstadt, Germany, Dec. (2010).

Morimoto K., Morita K., Kaji D., Haba H., Ohzeki K., Kudou Y., Sato N., Sumita T., Yoneda A., Ichikawa T., Fujimori Y., Goto S., Huang T., Ideguchi E., Kasamatsu Y., Katori K., Komori Y., Koura H., Kudo H., Murakami M., Ozawa A., Sakai R., Tokanai F., Tsukada K., Yamaguchi T., and Yoshida A.: "Confirmations of the synthesis of ^{278}113 produced by the ^{209}Bi(^{70}Zn,n)^{278}113 reaction", International Chemical Congress of Pacific Basin Societies (PACIFICHEM 2010), Honolulu, USA, Dec. (2010).

Enomoto S., Kou H., Tokuda M., Iwasaki M., Iio M., Itahashi K., Outa H., Onishi H., Sakuma F., Tomono D., Tsukada K., Yamazaki T., Ishimoto S., iwai m., suzuki s., Sekimoto M., Toyoda A., ishikawa t., Sato M., Suzuki T., Hexi s., Tatsuno H., Hashimoto T., Hayano R., fujiwara y., Matsuda Y., Sada Y., Nagae T., Hiraiwa T., Fujioka H., ajimura s., inoue k., Noumi H., sakaguchi a., fukuda t., Mizoi Y., Faso D., Morra O., bragadireanu M., Curceanu C. O., guaraldo c., iliescu M., Okada S., shrghi d., sirghi F., Buehler p., Cargnell M., Ishiwatari T., marton J., Suzuki K., widmann E., Zmeskal J., Bhang H., choi S., yim H., kienle p., busso L., Beer G., and Tanida K.: "Spectroscopic study of Lambda(1405) via the (K-,n) reaction on deuteron", 2010/12 Osaka Japan, (RCNP), Osaka, Dec. (2010).

Yoshida A., Yanagisawa Y., Yoshida K., and Kubo T.: "Operational experience of the target system for BigRIPS in-flight RI beam separator", 4th High Power Targetry Workshop, (European Spallation Source, Lund), Malmo, Sweden, May (2011).

Ichikawa Y., Ueno H., Ishii Y., Furukawa T., Yoshimi A., Kameda D., Aoi N., Watanabe H., Asahi K., Iijima H., Suzuki K., Inoue T., Tsuchiya M., Hayashi H., Nanao T., Kubo T., Inabe N., Ohnishi T., Takeda H., Fukuda N., Ishihara M., Daugas J., Chevrier R., Georgiev G., Rajabali M. M., and Balabanski D. L.: "g-factor measurements for highly spin-aligned isomeric states", RIBF-ULIC-Symposium-007: E(U)RICA International Workshop, Saitama, May (2011).

Ichikawa Y., Ueno H., Ishii Y., Furukawa T., Yoshimi A., Kameda D., Aoi N., Watanabe H., Asahi K., Iijima H., Suzuki K., Inoue T., Tsuchiya M., Hayashi H., Nanao T., Kubo T., Inabe N., Ohnishi T., Takeda H., Fukuda N., Ishihara M., Daugas J., Chevrier R., Georgiev G., Rajabali M. M., and Balabanski D. L.: "Production of spin-aligned RI beam via two-step fragmentation with dispersion matching", ARIS 2011, (Katholieke Universiteit Leuven), Leuven, Belgium, May–June (2011).

Chevrier R., Daugas J., Gaudefroy L., Ichikawa Y., Ueno H., Haas M., Haas H., Cottenier S., Aoi N., Asahi K., Balabanski D. L., Fukuda N., Furukawa T., Georgiev G., Hayashi H., Iijima H., Inabe N., Inoue T., Ishihara M., Ishii Y., Kameda D., Kubo T., Nanao T., Neyence G., Ohnishi T., Rajabali M. M., Suzuki K., Takeda H., Tsuchiya M., Vermeulen N., Watanabe H., and Yoshimi A.: "Quadrupole moment measurement of the $N = 27$ nucleus $43m$S", ARIS 2011, (Katholieke Universiteit Leuven), Leuven, Belgium, May–June (2011).

Kambara T., Yoshida A., Yanagisawa Y., Kameda D., Fukuda N., Ohnishi T., Kubo T., Uemoto R., Nagano A., and Uno H.: "Industrial Application of Radioactive Ion Beam at RIKEN RI Beam Factory", 11th International Conference on Applications of Nuclear Techniques, Crete, Greece, June (2011).

Ichikawa Y., Ueno H., Ishii Y., Furukawa T., Yoshimi A., Kameda D., Aoi N., Watanabe H., Asahi K., Iijima H., Suzuki K., Inoue T., Tsuchiya M., Hayashi H., Nanao T., Kubo T., Inabe N., Ohnishi T., Takeda H., Fukuda N., Ishihara M., Daugas J., Chevrier R., Georgiev G., Rajabali M. M., and Balabanski D. L.: "g-factor measurement for highly spin-aligned isomeric state of ^{32}Al", RIBF ULIC and CNS Symposium on Frontier of Gamma-ray Spectroscopy (Gamma11), (CNS, The University of Tokyo and RIKEN Nishina Center), Saitama, June–July (2011).

Ichikawa Y., Ueno H., Ishii Y., Furukawa T., Yoshimi A., Kameda D., Aoi N., Watanabe H., Asahi K., Iijima H., Suzuki K., Inoue T., Tsuchiya M., Hayashi H., Nanao T., Kubo T., Inabe N., Ohnishi T., Takeda H., Fukuda N., Ishihara M., Daugas J., Chevrier R., Georgiev G., Rajabali M. M., and Balabanski D. L.: "Production of spin-aligned RI beam via two-step fragmentation with dispersion matching", Rutherford Centennial Conference on Nuclear Physics 2011, (The University of Machester), Manchester, United Kingdom, Aug. (2011).

Chevrier R., Daugas J., Gaudefroy L., Ichikawa Y., Ueno H., Haas M., Haas H., Cottenier S., Aoi N., Asahi K., Balabanski D. L., Fukuda N., Furukawa T., Georgiev G., Hayashi H., Iijima H., Inabe N., Inoue T., Ishihara M., Ishii Y., Kameda D., Kubo T., Nanao T., Neyence G., Ohnishi T., Rajabali M. M., Suzuki K., Takeda H., Tsuchiya M., Vermeulen N., Watanabe H., and Yoshimi A.: "Quadrupole moment measurement of the $N = 27$ nucleus ^{43}S^{m}", Colloque GANIL 2011, (GANIL), Corsica, France, Sept. (2011).

Yamaguchi Y., Wakasugi M., Suzuki H., Fujinawa T., Uesaka T., Yano Y., Ozawa A., Nagae D., Yamaguchi T., Suzuki T., Kikuchi T., Jiang W., Sasaki T., and Tokuchi

A.: “Present status of rare-RI ring project in RIKEN RI beam factory”, 8th International Conference on Nuclear Physics at Storage Rings (STORI-11), (INFN-LNF), Frascati, Italy, Oct. (2011).

Ichikawa Y., Ueno H., Ishii Y., Furukawa T., Yoshimi A., Kameda D., Aoi N., Watanabe H., Asahi K., Iijima H., Suzuki K., Inoue T., Tsuchiya M., Hayashi H., Nanao T., Kubo T., Inabe N., Ohnishi T., Takeda H., Fukuda N., Ishihara M., Daugas J., Chevrier R., Georgiev G., Rajabali M. M., and Balabanski D. L.: “Spin-aligned RI beam produced by two-step projectile fragmentation”, ISPUN11, (Institute for Nuclear Science and Technique), Hanoi, Vietnam, Nov. (2011).

(Domestic Conference)

飯尾雅実, 板橋健太, 岩崎雅彦, 應田治彦, 大西宏明, 佐久間史典, 佐藤将春, 塚田暁, 友野大, 藤岡宏之, 山崎敏光, 石元茂, 岩井正明, 鈴木祥二, 関本美知子, 豊田晃久, 石川隆, 竜野秀行, 鈴木隆敏, 早野龍五, 松田恭幸, 永江知文, 平岩聡彦, 味村周平, 野海博之, 阪口篤志, 藤原裕也, 徳田真, 千葉順成, 福田共和, 溝井浩, Beer G. A., 方享燦, Choi S., 林熙重, 石渡智一, Buehler P., Cargnelli M., Hirtl A., Kienle P., Marton J., Widmann E., Zmeskal J., 岡田信二, Curceanu C. O., Guaraldo C., Iliescu M., Pietreanu D., Sirghi D., Sirghi F., Faso D., Morra O., Busso L.: “K 中間子原子核探査実験のための液体ヘリウム 3 標的の開発 III”, 日本物理学会 2008 年秋季大会, (日本物理学会), 盛岡, 9 月 (2008).

榎本瞬, 康寛史, 徳田真, 岩崎雅彦, 飯尾雅実, 板橋健太, 應田治彦, 大西宏明, 佐久間史典, 友野大, 塚田暁, 山崎敏光, 石元茂, 関本美知子, 豊田晃久, 佐藤将春, 鈴木隆敏, 竜野秀行, 橋本直, 早野龍五, 松田恭幸, 佐田優太, 永江知文, 平岩聡彦, 藤岡宏之, 野海博之, 溝井浩, Curceanu C. O., 岡田信二, 石渡智一, 鈴木謙, Zmeskal J., 方享燦, Beer G., 谷田聖, J-PARC E15/E17/E31 C.: “d(K-,n) 反応を用いた Lambda(1405) 分光実験のための陽子検出器の開発 (2)”, 日本物理学会 2010 年秋季大会, (日本物理学会), 北九州, 9 月 (2010).

康寛史, 徳田真, 岩崎雅彦, 飯尾雅実, 板橋健太, 應田治彦, 大西宏明, 佐久間史典, 友野大, 塚田暁, 山崎敏光, 石元茂, 関本美知子, 豊田晃久, 佐藤将春, 鈴木隆敏, 竜野秀行, 橋本直, 早野龍五, 松田恭幸, 佐田優太, 永江知文, 平岩聡彦, 藤岡宏之, 榎本瞬, 野海博之, 溝井浩, Curceanu C. O., 岡田信二, 石渡智一, 鈴木謙, Zmeskal J., 方享燦, Beer G., 谷田聖, J-PARC E15/E17/E31 C.: “J-PARC K1.8BR ビームラインにおける K ビーム調整 (2)”, 日本物理学会 2010 年秋季大会, (日本物理学会), 北九州, 9 月 (2010).

石井裕司, 市川雄一, 上野秀樹, 古川武, 吉見彰洋, 亀田大輔, 青井考, 渡邉寛, 旭耕一郎, 飯島裕章, 鈴木都文, 井上壮志, 土屋真人, 林宏憲, 七尾翼, 久保敏幸, 稲辺尚人, 大西哲哉, 竹田浩之, 福田直樹, 石原正泰, Daugas J., Chevrier R., Georgiev G., Rajabali M. M., Balabanski D. L.: “TD-PAD 法を用いた ^{32}Al アイソマーの磁気モーメント測定”, 日本物理学会 2010 年秋季大会, (日本物理学会), 北九州, 9 月 (2010).

飯尾雅実, 板橋健太, 岩崎雅彦, 應田治彦, 大西宏明, 佐久間史典, 友野大, 塚田暁, 山崎敏光, 榎本瞬, 石橋直哉, 井上謙太郎, 阪口篤志, 吉田幸太郎, 味村周平, 野海博之, 石元茂, 岩井正明, 鈴木祥二, 関本美知子, 豊田晃久, 石川隆, 佐藤将春, 鈴木隆敏, 施赫將, 竜野秀行, 橋本直, 早野龍五, 藤原裕也, 松田恭幸, 康寛史, 徳田真, 永江知文, 平岩聡彦, 藤岡宏之, 佐田優太, 福田共和, 溝井浩, Faso D., Morra O., Bragadireanu M., Curceanu C. O., Guaraldo C., Iliescu M., 岡田信二, Pietreanu D., Sirghi D., Sirghi F., Buehler P., Cargnelli M., 石渡 智一, Marton J., Widmann E., Zmeskal J., 鈴木謙, 方享燦, Choi S., 林熙重, Kienle P., Busso L., Beer G. A.: “Λ (1405) 精密分光のための重水素標的の開発 (1)”, 日本物理学会 2010 年秋季大会, (日本物理学会), 北九州, 9 月 (2010).

井上謙太郎, 康寛史, 徳田真, 岩崎雅彦, 飯尾雅実, 板橋健太, 應田治彦, 大西宏明, 佐久間史典, 友野大, 塚田暁, 山崎敏光, 石元茂, 岩井正明, 鈴木祥仁, 関本美知子, 豊田晃久, 石川隆, 佐藤将春, 鈴木隆敏, Hexi s., 竜野秀行, 橋本直, 早野龍五, 藤原裕也, 松田恭幸, 佐田優太, 永江知文, 平岩聡彦, 藤岡宏之, 味村周平, 榎本瞬, 野海博之, 阪口篤志, 福田共和, 溝井浩, Faso D., Morra O., bragadireanu M., Curceanu C. O., guaraldo c., iliescu M., 岡田信二, shrghi d., sirghi F., Buehler p., Cargnell M., 石渡智一, marton J., 鈴木謙, widmann E., Zmeskal J., 方享燦, choi S., yim H., kienle p., busso L., Beer G., 谷田聖: “J-PARC E-31 実験における後方散乱陽子飛跡検出 の設計開発と Geant4 Simulation”, 日本物理学会第 66 回年次大会, (日本物理学会), 新潟, 3 月 (2011).

榎本瞬, 康寛史, 徳田真, 岩崎雅彦, 飯尾雅実, 板橋健太, 應田治彦, 大西宏明, 佐久間史典, 友野大, 塚田暁, 山崎敏光, 石元茂, 岩井正明, 鈴木祥仁, 関本美知子, 豊田晃久, 石川隆, 佐藤将春, 鈴木隆敏, Hexi s., 竜野秀行, 橋本直, 早野龍五, 藤原裕也, 松田恭幸, 佐田優太, 永江知文, 平岩聡彦, 藤岡 宏之, 味村 周平, 井上 謙太郎, 野海 博之, 阪口 篤志, 福田共和, 溝井浩, Faso D., Morra O., bragadireanu M., Curceanu C. O., guaraldo c., iliescu M., 岡田信二, shrghi d., sirghi F., Buehler p., Cargnell M., 石渡智一, marton J., 鈴木謙, widmann E., Zmeskal J., 方享燦, choi S., yim H., kienle p., busso L., Beer G., 谷田聖: “d(K-,n) 反応を用いた Lambda(1405) 分光実験のための陽子検出器の開発 (3)”, 日本物理学会第 66 回年次大会, (日本物理学会), 新潟, 3 月 (2011).

石井裕司, 市川雄一, 上野秀樹, 古川武, 吉見彰洋, 亀田大輔, 青井考, 渡邉寛, 旭耕一郎, 飯島裕章, 鈴木都文, 井上壮志, 土屋真人, 林宏憲, 七尾翼, 久保敏幸, 稲辺尚人, 大西哲哉, 竹田浩之, 福田直樹, 石原正泰, Daugas J., Chevrier R., Georgiev G., Rajabali M. M., Balabanski D. L.: “TD-PAD 法を用いた ^{32}Al アイソマーの磁気モーメント測定 II”, 日本物理学会第 66 回年次大会, (日本物理学会), 新潟, 3 月 (2011).

市川雄一, 上野秀樹, 石井裕司, 古川武, 吉見彰洋, 亀田大輔, 青井考, 渡邉寛, 旭耕一郎, 飯島裕章, 鈴木都文, 井上壮志, 土屋真人, 林宏憲, 七尾翼, 久保敏幸, 稲辺尚人, 大西哲哉, 竹田浩之, 福田直樹, 石原正泰, Daugas J., Chevrier R., Georgiev G., Rajabali M. M., Balabanski D. L.: “分散整合二回散乱法による核スピン整列 RI ビームの生成 II”,

日本物理学会第 66 回年次大会, (日本物理学会), 新潟, 3 月 (2011).

上本龍二, 鵜野浩行, 永野章, 大西哲哉, 亀田大輔, 福田直樹, 柳澤善行, 吉田敦, 久保敏幸, 神原正: “RI ビームの連続磨耗測定法への適用”, 自動車技術会 2011 年春季大会, (公益社団法人自動車技術会), 横浜, 5 月 (2011).

阿部康志, 長江大輔, 小沢顕, 森口哲朗, 石橋陽子, 伊藤由太, 奥村公威, 金沢光隆, 佐藤眞二, 鈴木宏, 錦織良, 福岡翔太, 山口貴之, 山口由高: “理研稀少 RI リングのための飛行時間検出器の開発”, 日本物理学会 2011 年秋季大会, (日本物理学会), 弘前, 9 月 (2011).

市川雄一, 上野秀樹, 石井裕司, 古川武, 吉見彰洋, 亀田大輔, 青井考, 渡邉寛, 旭耕一郎, 飯島裕章, 鈴木都文, 井上壮志, 土屋真人, 林宏憲, 七尾翼, 久保敏幸, 稲辺尚人, 大西哲哉, 竹田浩之, 福田直樹, 石原正泰, Daugas J., Chevrier R., Georgiev G., Rajabali M. M., Balabanski D. L.: “分散整合二回散乱法による核スピン整列 RI ビームの生成 III”, 日本物理学会 2011 年秋季大会, (日本物理学会), 弘前, 9 月 (2011).

鈴木宏: “Simulation of particle trajectories for RIKEN rare-RI ring”, 仁科センター研究会「稀少 RI リングの物理」, 和光, 11 月 (2011).

SAMURAI Team

Publications

[Journal]

(Original Papers) *Subject to Peer Review

Tanaka K., Yamaguchi T., Suzuki T., Ohtsubo T., Fukuda M., Nishimura D., Takechi M., Ogata K., Ozawa A., Izumikawa T., Aiba T., Aoi N., Baba H., Hashizume Y., Inafuku K., Iwasa N., Kobayashi K., Komuro M., Kondo Y., Kubo T., Matsuyama T., Michimasa S., Motobayashi T., Nakabayashi T., Nakazima S., Nakamura T., Sakurai H., Shinoda R., Shinohara M., Suzuki H., Takeshita E., Takeuchi S., Togano Y., Yamada K., Yasuno T., and Yhoshitake M.: "Observation of a large reaction cross-section in the drip-line nucleus ^{22}C", Phys. Rev. Lett. **104**, No. 6, pp. 062701-1–062701-4 (2010). *

Oral Presentations

(International Conference etc.)

Sato H., Iwasa N., Kawabata T., Kobayashi T., Kondo Y., Kubo T., Kusaka K., Motobayashi T., Murakami T., Nakamura T., Ohnishi J., Ohnishi T., Okuno H., Otsu H., Sakurai H., Satou Y., Sakaguchi-Sekiguchi K., Togano Y., and Yoneda K.: "SAMURAI spectrometer at RIKEN RI beam factory", Advanced Studies Institute: Symmetries and Spin (SPIN-Praha-2009), (Charles University), Prague, Czech, July–Aug. (2009).

Sato H.: "Status of the SAMURAI project", Darmstadt, Germany, 2010/12, (GSI), Darmstadt, Germany, Dec. (2010).

Taketani A., Takuma A., Uesaka M., Motobayashi T., Yoneda K., Togano Y., and Murakami H.: "Wide Dynamic range readout preamplifier for Silicon Strip Sensor", Advanced School and Workshop on Nuclear Physics Signal Processing (ANSiP 2011), Acireale, Italy, Nov. (2011).

(Domestic Conference)

上坂明子, 竹谷篤, 馬場秀忠, 本林透, 村上浩之, 栂野泰宏, 米田健一郎: "広いダイナミックレンジを持った電荷有感型前置増幅器開発", 日本物理学会第 65 回年次大会, (日本物理学会), 岡山, 3 月 (2010).

上坂明子, 竹谷篤, 栂野泰宏, 村上浩之, 本林透, 米田健一郎: "シリコン検出器用電荷有感型前置増幅器のダイナミックレンジの拡大", 日本物理学会第 65 回年次大会, (日本物理学会), 岡山, 3 月 (2010).

上坂明子, 竹谷篤, 馬場秀忠, 本林透, 村上浩之, 栂野泰宏, 米田健一郎, 郡司卓, 浜垣秀樹, 林真一, 田中真伸: "広いダイナミックレンジを持った電荷有感型前置増幅器の開発", 日本物理学会第 66 回年次大会, (日本物理学会), 新潟, 3 月 (2011).

古川武, 涌井崇志, 佐々木彩子, 泉さやか, 市川雄一, 吉見彰洋, 田尻邦彦, 石井裕司, 吉田直貴, 松浦佑一, 加藤裕樹, 山口康広, 今村慧, 幕田将宏, 畠山温, 和田道治, 園田哲, 伊藤由太, 七尾翼, 小林徹, 西村俊二, 西村美月, 近藤洋介, 青井考, 米田健一郎, 久保野茂, 大城幸光, 上野秀樹, 篠塚勉, 下田正, 旭耕一郎, 松尾由賀利: "^{87}Rb ビームを用いた超流動ヘリウム中でのレーザー核分光法開発実験", 日本物理学会第 66 回年次大会, 新潟, 3 月 (2011).

佐藤広海: "Superconducting dipole magnet for SAMURAI", SAMURAI International Workshop 2011, 和光, 3 月 (2011).

古川武, 涌井崇志, 佐々木彩子, 泉さやか, 市川雄一, 吉見彰洋, 田尻邦彦, 石井裕司, 吉田直貴, 松浦佑一, 加藤裕樹, 山口康広, 今村慧, 幕田将宏, 畠山温, 和田道治, 園田哲, 伊藤由太, 七尾翼, 小林徹, 西村俊二, 西村美月, 近藤洋介, 青井考, 米田健一郎, 久保野茂, 上野秀樹, 下田正, 篠塚勉, 旭耕一郎, 松尾由賀利: "超流動ヘリウム中に打ち込まれた ^{87}Rb ビームのレーザー誘起蛍光観測と光ポンピング", 日本物理学会 2011 年秋季大会, (日本物理学会), 弘前, 9 月 (2011).

Computing and Network Team

Publications

[Journal]

(Original Papers) *Subject to Peer Review

Ohnishi T., Kubo T., Kusaka K., Yoshida A., Yoshida K., Ohtake M., Fukuda N., Takeda H., Kameda D., Tanaka K., Inabe N., Yanagisawa Y., Gono Y., Watanabe H., Otsu H., Baba H., Ichihara T., Yamaguchi Y., Takechi M., Nishimura S., Ueno H., Yoshimi A., Sakurai H., Motobayashi T., Nakao T., Mizoi Y., Matsushita M., Ieki K., Kobayashi N., Tanaka K., Kawada Y., Tanaka N., Deguchi S., Sato Y., Kondo Y., Nakamura T., Yoshinaga K., Ishii c., Yoshii h., Miyashita Y., Uematsu N., Shiraki Y., Sumikama T., Chiba J., Ideguchi E., Saito A., Yamaguchi T., Hachiuma I., Suzuki T., Moriguchi T., Ozawa A., Ohtsubo T., Famiano M. A., Geissel H., Nettleton A. S., Tarasov O. B., Bazin D. P., Sherrill B. M., Manikonda S. L., and Nolen J. A.: "Identification of 45 New Neutron-Rich Isotopes Produced by In-Flight Fission of a ^{238}U Beam at 345 MeV/nucleon", J. Phys. Soc. Jpn. **79**, No. 7, pp. 073201-1–073201-5 (2010). *

Tanaka K., Yamaguchi T., Suzuki T., Ohtsubo T., Fukuda M., Nishimura D., Takechi M., Ogata K., Ozawa A., Izumikawa T., Aiba T., Aoi N., Baba H., Hashizume Y., Inafuku K., Iwasa N., Kobayashi K., Komuro M., Kondo Y., Kubo T., Matsuyama T., Michimasa S., Motobayashi T., Nakabayashi T., Nakazima S., Nakamura T., Sakurai H., Shinoda R., Shinohara M., Suzuki H., Takeshita E., Takeuchi S., Togano Y., Yamada K., Yasuno T., and Yhoshitake M.: "Observation of a large reaction cross-section in the drip-line nucleus ^{22}C", Phys. Rev. Lett. **104**, No. 6, pp. 062701-1–062701-4 (2010). *

Nishimura S., Li Z., Watanabe H., Yoshinaga K., Sumikama T., Tachibana T., Yamaguchi K., Nishimura M., Lorusso G., Miyashita Y., Odahara A., Baba H., Berryman J. S., Blasi N., Bracco A., Camera F., Chiba J., Doornenbal P. C., Go S., Ideguchi E., Isobe T., Jenkins D. G., Kawada Y., Kobayashi N., Kondo Y., Kruecken R., Kubono S., Nakano T., Ong H., Ota S., Podolyak Z. F., Sakurai H., Scheit H., Steppenbeck D., Sugimoto K., Takano S., Takashima A., Tajiri K., Teranishi T., Wakabayashi Y., Walker P. M., and Wieland O.: "β-Decay Half-Lives of Very Neutron-Rich Kr to Tc Isotopes on the Boundary of the r-Process Path: An Indication of Fast r-Matter Flow", Phys. Rev. Lett. **106**, 052502-1–052502-5 (2011). *

Watanabe H., Yamakuchi K., Odahara A., Sumikama T., Nishimura S., Yoshinaga K., Li Z., Miyashita Y., Sato K., Prochniak L., Baba H., Berryman J. S., Blasi N., Bracco A., Camera F., Chiba J., Doornenbal P. C., Go S., Hashimoto T., Hayakawa S., Hinke C., Hinohara N., Ideguchi E., Isobe T., Ito Y., Jenkins D. G., Kawada Y., Kobayashi N., Kondo Y., Krucken R., Lorusso G., Nakano T., Nakatsukasa T., Kurata-Nishimura M., Ong H. J., Ota S., Podolyak Z., Sakurai H., Scheit H., Steiger K., Steppenbeck D., Sugimoto K., Tajiri K., Takano S., Takashima A., Teranishi T., Wakabayashi Y., Walker P. M., Wieland O., and Yamaguchi H.: "Development of axial asymmetry in the neutron-rich nucleus 110Mo", Physics Letter B **704**, 270–275 (2011). *

Oral Presentations

(Domestic Conference)

上坂明子, 竹谷篤, 馬場秀忠, 本林透, 村上浩之, 椨野泰宏, 米田健一郎: "広いダイナミックレンジを持った電荷有感型前置増幅器開発", 日本物理学会第 65 回年次大会, (日本物理学会), 岡山, 3 月 (2010).

上坂明子, 竹谷篤, 馬場秀忠, 本林透, 村上浩之, 椨野泰宏, 米田健一郎, 郡司卓, 浜垣秀樹, 林真一, 田中真伸: "広いダイナミックレンジを持った電荷有感型前置増幅器の開発", 日本物理学会第 66 回年次大会, (日本物理学会), 新潟, 3 月 (2011).

小林峰, 戸田新之輔, 馬場秀忠, 霜田進, 上田一之, 桑原裕司: "三次元中エネルギーイオン散乱装置を用いた新しい軽元素の分析方法", 第 12 回「イオンビームによる表面・界面解析」特別研究会, (応用物理学会・薄膜表面物理分科会), 東京, 12 月 (2011).

Computing and Network Team

Publications

[Journal]

(Original Papers) *Subject to Peer Review

Ohnishi T., Kubo T., Kusaka K., Yoshida A., Yoshida K., Ohtake M., Fukuda N., Takeda H., Kameda D., Tanaka K., Inabe N., Yanagisawa Y., Gono Y., Watanabe H., Otsu H., Baba H., Ichihara T., Yamaguchi Y., Takechi M., Nishimura S., Ueno H., Yoshimi A., Sakurai H., Motobayashi T., Nakao T., Mizoi Y., Matsushita M., Ieki K., Kobayashi N., Tanaka K., Kawada Y., Tanaka N., Deguchi S., Sato Y., Kondo Y., Nakamura T., Yoshinaga K., Ishii c., Yoshii h., Miyashita Y., Uematsu N., Shiraki Y., Sumikama T., Chiba J., Ideguchi E., Saito A., Yamaguchi T., Hachiuma I., Suzuki T., Moriguchi T., Ozawa A., Ohtsubo T., Famiano M. A., Geissel H., Nettleton A. S., Tarasov O. B., Bazin D. P., Sherrill B. M., Manikonda S. L., and Nolen J. A.: "Identification of 45 New Neutron-Rich Isotopes Produced by In-Flight Fission of a ^{238}U Beam at 345 MeV/nucleon", J. Phys. Soc. Jpn. **79**, No. 7, pp. 073201-1–073201-5 (2010). *

Tanaka K., Yamaguchi T., Suzuki T., Ohtsubo T., Fukuda M., Nishimura D., Takechi M., Ogata K., Ozawa A., Izumikawa T., Aiba T., Aoi N., Baba H., Hashizume Y., Inafuku K., Iwasa N., Kobayashi K., Komuro M., Kondo Y., Kubo T., Matsuyama T., Michimasa S., Motobayashi T., Nakabayashi T., Nakazima S., Nakamura T., Sakurai H., Shinoda R., Shinohara M., Suzuki H., Takeshita E., Takeuchi S., Togano Y., Yamada K., Yasuno T., and Yhoshitake M.: "Observation of a large reaction cross-section in the drip-line nucleus ^{22}C", Phys. Rev. Lett. **104**, No. 6, pp. 062701-1–062701-4 (2010). *

Nishimura S., Li Z., Watanabe H., Yoshinaga K., Sumikama T., Tachibana T., Yamaguchi K., Nishimura M., Lorusso G., Miyashita Y., Odahara A., Baba H., Berryman J. S., Blasi N., Bracco A., Camera F., Chiba J., Doornenbal P. C., Go S., Ideguchi E., Isobe T., Jenkins D. G., Kawada Y., Kobayashi N., Kondo Y., Kruecken R., Kubono S., Nakano T., Ong H., Ota S., Podolyak Z. F., Sakurai H., Scheit H., Steppenbeck D., Sugimoto K., Takano S., Takashima A., Tajiri K., Teranishi T., Wakabayashi Y., Walker P. M., and Wieland O.: "β-Decay Half-Lives of Very Neutron-Rich Kr to Tc Isotopes on the Boundary of the r-Process Path: An Indication of Fast r-Matter Flow", Phys. Rev. Lett. **106**, 052502-1–052502-5 (2011). *

Watanabe H., Yamakuchi K., Odahara A., Sumikama T., Nishimura S., Yoshinaga K., Li Z., Miyashita Y., Sato K., Prochniak L., Baba H., Berryman J. S., Blasi N., Bracco A., Camera F., Chiba J., Doornenbal P. C., Go S., Hashimoto T., Hayakawa S., Hinke C., Hinohara N., Ideguchi E., Isobe T., Ito Y., Jenkins D. G., Kawada Y., Kobayashi N., Kondo Y., Krucken R., Lorusso G., Nakano T., Nakatsukasa T., Kurata-Nishimura M., Ong H. J., Ota S., Podolyak Z., Sakurai H., Scheit H., Steiger K., Steppenbeck D., Sugimoto K., Tajiri K., Takano S., Takashima A., Teranishi T., Wakabayashi Y., Walker P. M., Wieland O., and Yamaguchi H.: "Development of axial asymmetry in the neutron-rich nucleus 110Mo", Physics Letter B **704**, 270–275 (2011). *

Oral Presentations

(Domestic Conference)

上坂明子, 竹谷篤, 馬場秀忠, 本林透, 村上浩之, 栂野泰宏, 米田健一郎: "広いダイナミックレンジを持った電荷有感型前置増幅器開発", 日本物理学会第 65 回年次大会, (日本物理学会), 岡山, 3 月 (2010).

上坂明子, 竹谷篤, 馬場秀忠, 本林透, 村上浩之, 栂野泰宏, 米田健一郎, 郡司卓, 浜垣秀樹, 林真一, 田中真伸: "広いダイナミックレンジを持った電荷有感型前置増幅器の開発", 日本物理学会第 66 回年次大会, (日本物理学会), 新潟, 3 月 (2011).

小林峰, 戸田新之輔, 馬場秀忠, 霜田進, 上田一之, 桑原裕司: "三次元中エネルギーイオン散乱装置を用いた新しい軽元素の分析方法", 第 12 回「イオンビームによる表面・界面解析」特別研究会, (応用物理学会・薄膜表面物理分科会), 東京, 12 月 (2011).

Accelerator Applications Research Group

Publications

[Journal]

(Original Papers) *Subject to Peer Review

Kanai Y., Hoshino M., Kambara T., Ikeda T., Hellhammer R., Stolterfoht N., and Yamazaki Y.: "Guiding of Slow Highly Charged Ions through Nanocapillaries - Dynamic Aspect-", J. Phys.: Con. Ser. **194**, 012068-1–012068-8 (2009). *

Tanaka T., Yamada A., Suzuki Y., Kobayashi T., Takahashi K., Kambara T., Saito F., Okamura K., Uchikoshi S., Nakano N., Hamago S., Takenaka M., Mano D., Morisaki S., and Ogura A.: "Improvement of gas sensitivity for a polymer membrane electrode by high-energy ion beam irradiation", Trans. Mater. Res. Soc. Jpn. **36**, No. 3, pp. 321–324 (2011). *

Oral Presentations

(International Conference etc.)

Tanaka T., Suzuki Y., Kobayashi T., Takahashi K., Kambara T., Saito F., Hyodo T., Nagashima Y., Okamura K., Uchikoshi S., Nakano N., Iwase A., Hamago S., Takenaka M., Mano D., and Morisaki S.: "Sensitivity of high energy nitrogen irradiated ePTFE equipped sensors for H2 and toxic gases", 20th Academic Symposium of MRS-Japan 2010, Yokohama, Dec. (2010).

Hayashi Y., Morita R., Tokairin H., Sato T., and Abe T.: "Effect of heavy-ion beam irradiation on mutation induction in Rice", 18th International Botanical Congress (IBC2011), (International Botanical Congress Comittee), Melbourne, Australia, July (2011).

Abe T., Kazama Y., Hirano T., Morita R., and Hayashi Y.: "Ion beam mutagenesis: new innovative technology for mutation breeding", 18th International Botanical Congress (IBC2011), (International Botanical Congress Comittee), Melbourne, Australia, July (2011).

Nakano T., Hirohama E., Tanigaki F., Ogawa S., Abe T., Hayashi Y., Nitasaka E., Akashi R., Hashiguchi M., and Aoki T.: "ISS Education Program "JAXA Seeds in Space I"", 62nd International Astronautical Congress, (International Astronautical Federation), Cape Town, South Africa, Oct. (2011).

(Domestic Conference)

林依子, 森田竜平, 森島友美, 永野拓馬, 東海林英夫, 小暮祥子, 保倉明子, 佐藤雅志, 阿部知子: "重イオンビーム照射によって誘発したイネ耐塩性突然変異系統の特性比較", 日本育種学会第 119 回講演会, (日本育種学会), 横浜, 3 月 (2011).

古川浩二, 岩澤洋樹, 阿部知子, 田畑哲之, 松山知樹: "DNA マーキングによるシンビジウムの品種内判別（第 5 報）", 園芸学会平成 23 年度秋季大会, (園芸学会), 岡山, 9 月 (2011).

古川浩二, 岩澤洋樹, 阿部知子, 田畑哲之, 松山知樹: "シンビジウム品種内系統判別のための DNA マーク作出と増殖個体での保存性の確認", 日本 DNA 多型学会第 20 回学術集会, (日本 DNA 多型学会), 横浜, 12 月 (2011).

永田祐吾, 毛利明博, 黒田直史, 大塚未来, 櫻井翔太, 高木聡, 田中香津生, 藤居甲基, 満汐孝治, Murtagh D. J., Ulmer S., 鳥居寛之, 金井保之, 長嶋泰之, 檜垣浩之, 松田恭幸, 山崎泰規: "基底状態反水素原子の偏極ビーム生成の計算", 日本物理学会第 67 回年次大会, (日本物理学会), 西宮, 3 月 (2012).

Radiation Biology Team

Publications

[Journal]

(Original Papers) *Subject to Peer Review

Fujiwara M., Hashimoto H., Kazama Y., Abe T., Yoshida S., Sato N., and Itoh R. D.: "The assembly of the FtsZ ring at the mid-chloroplast division site depends on a balance between the activities of AtMinE1 and ARC11/AtMinD1", Plant Cell Physiol. **49**, No. 3, pp. 345–361 (2008). *

Kanai Y., Hoshino M., Kambara T., Ikeda T., Hellhammer R., Stolterfoht N., and Yamazaki Y.: "Guiding of Slow Highly Charged Ions through Nanocapillaries - Dynamic Aspect-", J. Phys.: Con. Ser. **194**, 012068-1–012068-8 (2009). *

Niwa K., Yamamoto T., Furuita H., and Abe T.: "Mutation breeding in the marine crop Porphyra yezoensis (Bangiales, Rhodophyta): Cultivation experiment of the artificial red mutant isolated by heavy-ion beam mutagenesis", Aquaculture **314**, 182–187 (2011). *

Kazama Y., Hirano T., Saito H., Liu Y., Ohbu S., Hayashi Y., and Abe T.: "Characterization of highly efficient heavy-ion utagenesis in *Arabidopsis thaliana*", BMC Plant Biol. **11**, 161-1–161-10 (2011). *

Hirano T., Yukawa T., Miyoshi K., and Mii M.: "Wide applicability of cryopreservation with vitrification method for seeds of some Cymbidium species", Plant Biotechnol. **28**, No. 1, pp. 99–102 (2011). *

Yatagai F., Honma M., Takahashi A., Omori K., Suzuki H., Shimazu T., Seki M., Hashizume T., Ukai A., Sugawara K., Abe T., Dohmae N., Enomoto S., Ohnishi T., Gordon A., and Ishioka N.: "Frozen human cells can record radiation damage accumulated during space flight: mutation induction and radioadaptation", Radiat. Environ. Biophys. **50**, 125–134 (2011). *

Fujita N., Torii C., Ishii K., Aonuma W., Shimizu Y., Kazama Y., Abe T., and Kawano S.: "Narrowing Down the Mapping of Plant Sex-determination regions using new Y-chromosome-specific markers and heavy-ion Beam irradiation-induced Y-deletion mutants in *Silene latifolia", G3: Genes, Genomes, Genetics* **2**, *No. 2, pp. 271–278 (2012).* *

古川浩二, 岩澤洋樹, 阿部知子, 松山知樹: *"シンビジウム品種内系統判別のための DNA マーク開発", DNA 多型* **19**, *93–96 (2011).* *

吉井雄一, 保倉明子, 阿部知子, 井藤賀操, 榊原均, 寺田靖子, 中井泉: *"放射光マイクロビーム蛍光 X 線分析と XAFS 解析によるホンモンジゴケ (Scopelophila cataractae) 体内における銅と鉛の蓄積に関する研究", X 線分析の進歩* **42**, *347–358 (2011).* *

(Review)

泉雅子: "放射線の生物への影響", ぶんせき, No. 9, pp. 527–531 (2011).

[Book · Proceedings]

(Original Papers) *Subject to Peer Review

Mizuno T., Izumi M., and Eichinger C. S.: "Quality Control of DNA Polymerase alpha", Fundamental Aspects of DNA replication, 2011–9, InTech, Croatia, pp. 205–218 (2011). *

(Review)

阿部知子, 林依子, 石井重久: "重イオンビームで日本のサクラが変わる", 第 3 回智のシンポジウム：文明・文化と科学技術 論文集, 東京, 2010–11, 「智のシンポジウム」組織委員会, 東京, pp. 27–30 (2010).

Oral Presentations

(International Conference etc.)

Yoshida S. and Abe T.: "An innovative method for mutation breeding using swift heavy ions", 2nd Joint Asian Accelerator Workshop (JAAWS), (Pohang Accelerator Laboratory), Pohang, Korea, Nov. (2010).

Tanaka T., Suzuki Y., Kobayashi T., Takahashi K., Kambara T., Saito F., Hyodo T., Nagashima Y., Okamura K., Uchikoshi S., Nakano N., Iwase A., Hamago S., Takenaka M., Mano D., and Morisaki S.: "Sensitivity of high energy nitrogen irradiated ePTFE equipped sensors for H2 and toxic gases", 20th Academic Symposium of MRS-Japan 2010, Yokohama, Dec. (2010).

Hirano T., Takagi K., Hoshino Y., and Abe T.: "Analysis of DNA damage response in male gametes of Cyrtanthus mackenii during pollen tube growth", 18th International Botanical Congress (IBC2011), (International Botanical Congress Committee), Melbourne, Australia, July (2011).

Hayashi Y., Morita R., Tokairin H., Sato T., and Abe T.: "Effect of heavy-ion beam irradiation on mutation induction in Rice", 18th International Botanical Congress (IBC2011), (International Botanical Congress Comittee), Melbourne, Australia, July (2011).

Abe T., Kazama Y., Hirano T., Morita R., and Hayashi Y.: "Ion beam mutagenesis: new innovative technology for mutation breeding", 18th International Botanical Congress (IBC2011), (International Botanical Congress Comittee), Melbourne, Australia, July (2011).

Kazama Y., Hirano T., Nishihara K., Ohbu S., Shirakawa Y., Hayashi Y., and Abe T.: "Ion-beam mutagenesis: New technology for the control of deletion-size by heavy-ion beam irradiation", 18th International Botanical Congress (IBC2011), (The international botanical congress committee), Melbourne, Australia, July (2011).

Morita R., Hayashi Y., Shibukawa T., Takehisa H., Nishimura M., and Abe T.: "Radiation Mutagenesis: Molecular characterization of mutations induced by gamma irradiation and heavy-ion beam in rice", 18th International Botanical Congress (IBC2011), Melbourne, Australia, July (2011).

Ma L., Kazama Y., Abe T., Tanaka S., and Hatakeyama S.: "Examination of the Relationship between the

Killing Effect and Induced Mutation by Irradiation with Different Heavy-ion Beams in Neurospora crassa", BIT's 1st Annual World Congress of Microbes-2011, (Information Research Center of International Talent, China State Administration of Foreign Experts Affairs; China Medicinal Biotech Association), Beijing, China, July–Aug. (2011).

Morita R., Hayashi Y., Kogure S., Tokairin H., Takehisa H., Hanzawa E., Sato T., and Abe T.: "Isolation of salt-tolerant mutants of rice inducedby heavy-ion irradiation", 7th Asian Crop Science Association Conference, (The Asian Crop Science Association), Bogor, West Java, Indonesia, Sept. (2011).

Nakano T., Hirohama E., Tanigaki F., Ogawa S., Abe T., Hayashi Y., Nitasaka E., Akashi R., Hashiguchi M., and Aoki T.: "ISS Education Program "JAXA Seeds in Space I"", 62nd International Astronautical Congress, (International Astronautical Federation), Cape Town, South Africa, Oct. (2011).

(Domestic Conference)

石井公太郎, 天内康人, 風間裕介, 河野重行: "染色体末端特異的サテライトの FISH で明らかにされたヒロハノマンテマ異形性染色体の起源", 日本植物形態学会第 21 回総会・大会, (日本植物形態学会), 山形, 9 月 (2009).

阿部知子: "重イオンビームによる DNA 破壊と品種改良", 第 51 回仁科加速器センター月例コロキウム, 和光, 1 月 (2010).

阿部知子, 風間裕介, 平野智也, 森田竜平, 林依子: "花だとの品種改良への重イオンビームの利用と今後の展開", 第 47 回アイソトープ・放射線研究発表会, (日本アイソトープ協会), 東京, 7 月 (2010).

阿部知子: "巨大加速器で新しい植物を創る", 文部科学省情報ひろば「サイエンスカフェ」, (日本学術会議、文部科学省), 東京, 7 月 (2010).

玉木克知, 石川順也, 水谷祐一郎, 山中正仁, 林依子, 阿部知子: "イオンビームを利用したハボタンの突然変異誘発効果について", 第 15 回園芸学会近畿支部兵庫大会, (園芸学会近畿支部), 神戸, 8 月 (2010).

阿部知子, 風間裕介, 平野智也, 森田竜平, 林依子: "GeV 重イオンビームによる DNA 破壊と品種改良", 原子衝突研究協会第 35 回年会, (原子衝突研究協会), 奈良, 8 月 (2010).

阿部知子: "世界で一つだけの花をつくる", 第 27 回みんなのくらしと放射線展, (『みんなのくらしと放射線」知識普及実行委員会), 大阪, 8 月 (2010).

二羽恭介, 山本剛史, 古板博文, 阿部知子: "養殖ノリの突然変異育種 1 :重イオンビーム照射で分離された赤色型変異体の野外養殖試験", 平成 22 年度日本水産学会秋季大会, (日本水産学会), 京都, 9 月 (2010).

佐々木克友, 山口博康, 間竜太郎, 四方雅仁, 阿部知子, 大坪憲弘: "第 2 ウォールが蕚化したトレニア変異表現型の原因は TfUFO 機能欠損に由来する", 第 28 回日本植物細胞分子生物学会大会・シンポジウム, (日本植物細胞分子生物学会), 仙台, 9 月 (2010).

阿部知子: "重イオンビームで植物の新品種をつくる", 第 3 回彩の国未来創造フェア, 大宮, 9 月 (2010).

森田竜平, 西村実, 阿部知子: "突然変異を利用した品種改良:作物のポテンシャルを引き出す", 第 3 回智のシンポジウム: 文明・文化と科学技術, (第 3 回智のシンポジウム ー文明・文化と科学技術ー 組織委員会), 東京, 11 月 (2010).

阿部知子: "原子物理学 X バイオテクノロジー=食料・環境問題解決への貢献", 寺小屋フォーラム, (テクノ未来塾), 東京, 12 月 (2010).

保倉明子, 原田紗希, 平野智也, 阿部知子, 原田英美子, 矢崎一史, 佐野俊夫, 中井泉, 寺田靖子: "タバコ培養細胞 BY-2 高エネルギーμ-XRF 分析", 第 24 回日本放射光学会年会・放射光科学合同シンポジウム, (日本放射光学会), つくば, 1 月 (2011).

林依子, 森田竜平, 森島友美, 永野拓馬, 東海林英夫, 小暮祥子, 保倉明子, 佐藤雅志, 阿部知子: "重イオンビーム照射によって誘発したイネ耐塩性突然変異系統の特性比較", 日本育種学会第 119 回講演会, (日本育種学会), 横浜, 3 月 (2011).

平野智也, 高城啓一, 星野洋一郎, 阿部知子: "重イオンビームを用いたキルタンサス雄性配偶子の DNA 損傷応答解析", 園芸学会平成 23 年度春季大会, (園芸学会), 宇都宮, 3 月 (2011).

中村薫, 宇藤山裕美, 阿部知子, 林依子, 福元孝一, 郡司定雄: "重イオンビームを用いたスイートピーの突然変異", 園芸学会平成 23 年度春季大会, (園芸学会), 宇都宮, 3 月 (2011).

古川浩二, 岩澤洋樹, 阿部知子, 田畑哲之, 松山知樹: "DNA マーキングによるシンビジウムの品種判別技術の開発 (第 4 報)", 園芸学会平成 23 年度春季大会, (園芸学会), 宇都宮, 3 月 (2011).

二羽恭介, 阿部知子: "養殖ノリの単胞子由来の葉状体に出現したモザイク状キメラ", 平成 23 年度日本水産学会春季大会, (日本水産学会), 東京, 3 月 (2011).

森田竜平, 中川繭, 林依子, 竹久妃奈子, 東海林英夫, 佐藤雅志, 阿部知子: "イネ温度感受性葉緑素合成不全突然変異体の解析", 日本育種学会第 119 回講演会, (日本育種学会), 横浜, 3–3 月 (2011).

風間裕介, 馬立秋, 平野智也, 大部澄江, 白川侑希, 林祐子, 阿部知子: "シロイヌナズナの M1 世代での迅速な突然変異検出系を用いた LET 効果の解析", 日本育種学会第 120 回講演会, (日本育種学会), 福井, 9 月 (2011).

平野智也, 風間裕介, 大部澄江, 白川侑希, 林祐子, 阿部知子: "シロイヌナズナを用いた DNA 突然変異への LET 効果の解析 (2)", 日本育種学会第 120 回講演会, (日本育種学会), 福井, 9 月 (2011).

風間裕介, 馬立秋, 平野智也, 大部澄江, 白川侑希, 林祐子, 畠山晋, 阿部知子: "アルビノ変異セクターを指標とした重イオンビーム変異迅速検出系の確立", 日本植物形態学会第 23 回総会・大会, (日本植物形態学会), 東京, 9 月 (2011).

森田竜平, 中川繭, 林依子, 竹久妃奈子, 東海林英夫, 佐藤雅志, 小暮祥子, 阿部知子: "葉緑素合成不全イネ変異体の解析", 第 29 回日本植物細胞分子生物学会大会, (日本植物細胞分子生物学会), 福岡, 9 月 (2011).

平野智也, 風間裕介, 大部澄江, 白川侑希, 阿部知子: "重イオンビーム誘発突然変異に対する LET 効果の解析", 第 29 回日本植物細胞分子生物学会大会, (日本植物細胞分子生物学会), 福岡, 9 月 (2011).

風間裕介, 西原潔, 阿部知子, 河野重行: "ヒロハノマンテマ

X 染色体連鎖遺伝子 *SlWUS1* は性染色体進化の過程で Y 染色体から消失した？”, 日本植物学会第 75 回大会, (日本植物学会), 東京, 9 月 (2011).

片野真奈, 風間裕介, 平野智也, 阿部知子, 堀口吾朗, Ferjani A., 塚谷裕一: “*fugu5* 変異体に対する重イオンビーム照射で作出した変異体—補償作用によって昂進される細胞伸長制御系の遺伝学的解析—”, 日本植物学会第 75 回大会, (日本植物学会), 東京, 9 月 (2011).

馬立秋, 風間裕介, 阿部知子, 田中秀逸, 畠山晋: “アカパンカビにおける炭素、鉄、アルゴンイオンビームの致死効果と ad-3 遺伝子座での前方向突然変異の解析”, 日本遺伝学会第 83 回大会, (日本遺伝学会), 京都, 9 月 (2011).

森田竜平, 中川繭, 林依子, 小暮祥子, 竹久妃奈子, 東海林英夫, 佐藤雅志, 阿部知子: “イネ温度感受性 virescent 変異体の解析”, 日本育種学会第 120 回講演会, (日本育種学会), 福井, 9–9 月 (2011).

泉雅子, 柳憲一郎, 水野武, 今本尚子, 花岡文雄: “Identification of the Mcm2-7 binding sequence of human Mcm10”, 第 34 回日本分子生物学会年会, (日本分子生物学会、日本生化学会), 横浜, 12 月 (2011).

RI Applications Team

Publications

[Journal]

(Original Papers) *Subject to Peer Review

Kanai Y., Hoshino M., Kambara T., Ikeda T., Hellhammer R., Stolterfoht N., and Yamazaki Y.: "Guiding of Slow Highly Charged Ions through Nanocapillaries - Dynamic Aspect-", J. Phys.: Con. Ser. **194**, 012068-1–012068-8 (2009). *

Ishii Y., Toyoshima A., Tsukada K., Asai M., Li Z., Nagame Y., Miyashita S., Mori T., Suganuma H., Haba H., Goto S., Kudo H., Akiyama K., Oura Y., Shinohara A., Schaedel M., Pershina V., and Kratz J. V.: "Fluorido Complex Formation of Element 104, Rutherfordium (Rf)", Bull. Chem. Soc. Jpn. **84**, No. 9, pp. 903–911 (2011). *

Haba H., Kaji D., Kikunaga H., Kudou Y., Morimoto K., Morita K., Ohzeki K., Sumita T., and Yoneda A.: "Production and decay properties of the 1.9-s isomeric state in 261Rf", Phys. Rev. C **83**, No. 3, pp. 034602-1–034602-7 (2011). *

Kikunaga H., Fujisawa H., Ooe K., Takayama L., Shinohara A., Takamiya K., Kasamatsu Y., Ezaki Y., Haba H., Nakanishi T., Mitsugashira T., Hirose K., and Otsuki T.: "Precision measurement of the half-life of 90mNb and 99mTc", Proc.Radiochim **1**, 113–116 (2011). *

Ooe K., Yahagi W., Komori Y., Fujisawa H., Takayama L., Kikunaga H., Yoshimura T., Takahashi N., Haba H., Kudou Y., Ezaki Y., and Shinohara A.: "Extraction behavior of carrier-free and macro amounts of molybdenum and tungsten from HCl solution", Proc.Radiochim **1**, 127–129 (2011). *

Takayama L., Ooe K., Yahagi W., Fujisawa H., Komori Y., Kikunaga H., Yoshimura T., Takahashi N., Takahisa K., Haba H., Kudou Y., Ezaki Y., Toyoshima A., Asai M., Nagame Y., Saito T., Mitsugashira T., and Shinohara A.: "Solvent extraction of trivalent actinides with di(2-ethylhexyl) phosphoric acid", Proc.Radiochim **1**, 157–160 (2011). *

Kikunaga H., Yoshimura T., Kuribayashi T., Kitamoto Y., Takahashi N., Haba H., Ezaki Y., Enomoto S., Mitsugashira T., and Shinohara A.: "Separation of Am(III), Cm(III), and Cf(III) using capillary electrophoresis", Proc.Radiochim **1**, 167–171 (2011). *

Haba H., Kaji D., Kudou Y., Morimoto K., Morita K., Ohzeki K., Sakai R., Sumita T., Yoneda A., Kasamatsu Y., Komori Y., Shinohara A., Kikunaga H., Kudo H., Nishio K., Ooe K., Sato N., and Tsukada K.: "Production of 265Sg in the 248Cm(22Ne,5n)265Sg reaction and decay properties of two isomeric states in 265Sg", Phys. Rev. C **85**, 024611-1–024611-11 (2012). *

(Review)

羽場宏光: "新元素の合成と化学", 放射化学ニュース **24**, 34–40 (2011).

(Others)

Toyoshima A., Asai M., Li Z., Sato N., Sato T., Ooe K., Kikuchi T., Kaneya Y., Kitatsuji Y., Tsukada K., Nagame Y., Schaedel M., Kasamatsu Y., Kogama Y., Shinohara A., Haba H., and Even J.: "Determination of the reduction potential of mendelevium between 2+ and 3+ states using an electrochemistry apparatus", JAEA-Review **2011-040**, 39–40 (2011).

Oral Presentations

(International Conference etc.)

Kambara T.: "Research and Application of Radiation Biology with Fast Heavy Ions at RIKEN RI Beam Factory", The Korean Physical Society 2010 Autumn Meeting, (The Korean Physical Society), Bongpyeong, Korea, Oct. (2010).

Akada N., Hiromura M., Kanayama Y., Igarashi K., Haba H., and Enomoto S.: "Metabolic interaction of bittern and various trace elements in mice by using multi-tracer technology and Gamma-ray emission imaging system (GREI)", METALLOMICS 2011, (ISM), Munster, Germany, June (2011).

Komatsu Y., Aoki K., Enyo H., Kanaya J., Kannno K., Masumoto S., Nakai W., Ozawa K., Sekimoto M., Takagi A., Watanabe Y., and Yokkaichi S.: "GEM spectrometer for J-PARC E16 experiment", 2nd international conference on micro pattern gaseous detectors (MPGD2011), (International organizing committee for MPGD2011), Kobe, Aug.–Sept. (2011).

Asai M., Haba H., Tsukada K., Sato N., Kasamatsu Y., Kaji D., Morimoto K., Morita K., Sato T., Toyoshima A., Ishii Y., Takahashi R., Nagame Y., Ishii T., Nishinaka I., Kojima Y., and Ichikawa T.: "Alpha-gamma and high-resolution alpha fine-structure spectroscopy for the heaviest nuclei", 4th International Conference on the Chemistry and Physics of the Transactinide Elements (TAN11), (Joint Institute for Nuclear Research), Sochi, Russia, Sept. (2011).

Kasamatsu Y., Komori Y., Kikutani Y., Yokokita T., Kino A., Yoshimura T., Takahashi N., Haba H., Kudou Y., Kikunaga H., Otsuki T., Mitsugashira T., and Shinohara A.: "Application of the rapid preparation method of hydroxide coprecipitate with Sm to superheavy element chemistry -Model experiment for Rf chemistry-", 4th International Conference on the Chemistry and Physics of the Transactinide Elements (TAN11), (Joint Institute for Nuclear Research), Sochi, Russia, Sept. (2011).

Toyoshima A., Ooe K., Li Z., Asai M., Sato N., Sato T., Kikuchi T., Kaneya Y., Kitatsuji Y., Tsukada K., Nagame Y., Schaedel M., Kasamatsu Y., Kogama Y., Shinohara A., Haba H., and Even J.: "Electrochemical reduction of mendelevium in HCl solution", 4th International Conference on the Chemistry and Physics of the Transactinide Elements (TAN11), (Joint Institute for Nuclear Research), Sochi, Russia, Sept. (2011).

Haba H., Kaji D., Kasamatsu Y., Kikunaga H., Komori Y., Kudo H., Kudou Y., Morimoto K., Morita K., Ooe K., Ohzeki K., Sakai R., Sato N., Shinohara A., Sumita T., Tsukada K., and Yoneda A.: "Production of 265Sg for chemical studies using the gas-jet transport system coupled to the RIKEN gas-filled recoil ion separator", 4th International Conference on the Chemistry and Physics of the Transactinide Elements (TAN11), (Joint Institute for Nuclear Research), Sochi, Russia, Sept. (2011).

Akada N., Hiromura M., Kanayama Y., Igarashi K., Haba H., and Enomoto S.: "Intravital interactions of trace elements and bittern in diabetes and cardiac disease model mice", ICMG 2011, (ICMG), Kobe, Sept. (2011).

Wakitani Y., Yamamoto S., Yamada T., Kanaya J., Haba H., Takahashi K., and Kambara T.: "Production and distribution of radioisotopes via the JRIA-RIKEN collaboration", 7th International Conference on Isotopes, (ROSATOM), Moscow, Russia, Sept. (2011).

(Domestic Conference)

羽木洋介, 河西実希, 延與秀人, 秋葉康之, 黒澤真城, 金谷淳平, 栗田和好, 橋本公瑛, 藤原康平, 関本美知子: "PHENIX 用シリコンピクセル検出器の高エネルギー陽子ビームを用いた性能評価", 日本物理学会第 64 回年次大会, (日本物理学会), 東京, 3 月 (2009).

羽木洋介, 河西実希, 延與秀人, 秋葉康之, 黒澤真城, 金谷淳平, 栗田和好, 橋本公瑛, 藤原康平, 関本美知子: "PHENIX シリコンピクセル検出器組み立て後の品質検査", 日本物理学会第 65 回年次大会, (日本物理学会), 岡山, 3 月 (2010).

青木 和也, 四日市 悟, 金谷 淳平, 桝本 新一, 小松 雄哉: "J-PARC E16 実験の為の、ハドロン・ブラインド検出器の開発", 日本物理学会 2010 年秋季大会, (九州工業大学), 北九州, 9 月 (2010).

浅野 秀光, 秋葉 康之, 金谷 淳平, 黒澤 真城, 竹谷 篤, 蜂谷 崇, Koster J., 秋元 亮二, Stephen B., 栗田 和好, 今井 憲一, 佐甲博之, 佐藤進, 関本美知子, 藤原康平, Baldo S., Benji L., Chuck P., Eugene S., Nicole A., Eric .., Franck G., Olivier D., Mikhail S., Alexander S., James B., Jason B.: "偏極陽子衝突ビームを用いた PHENIX 崩壊点飛跡検出器 VTX) のコ ミッショニング", 日本物理学会第 66 回年次大会, (社団法人　日本物理学会), 新潟, 3 月 (2011).

福地知則, 本村信治, 武田伸一郎, 羽場宏光, 渡辺恭良, 榎本秀一: "コンプトンカメラ/PET デュアルモダリティの利点", 第 6 回日本分子イメージング学会総会・学術集会, (日本分子イメージング学会), 神戸, 5 月 (2011).

脇谷雄一郎, 山元真一, 山田崇裕, 神原正, 羽場宏光, 金谷淳平, 高橋和也: "理研 AVF サイクロトロンを用いた RI 製造", 第 48 回アイソトープ・放射線研究発表会, (日本アイソトープ協会), 東京, 7 月 (2011).

羽場宏光: "新元素の化学：気体充填型反跳核分離装置を用いた新展開", 第 72 回応用物理学会学術講演会, (応用物理学会), 山形, 8–9 月 (2011).

小嶋貴幸, 村山裕史, 村上昌史, 後藤真一, 羽場宏光, 加治大哉, 森本幸司, 工藤祐生, 森田浩介, 菊永英寿, 佐藤哲也, 塚田和明, 工藤久昭: "理研 GARIS/gas-jet システムを利用した気相化学の基礎研究", 2011 日本放射化学会年会・第 55 回放射化学討論会, (日本放射化学会年会), 長野, 9 月 (2011).

豊嶋厚史, Li Z., 浅井雅人, 佐藤望, 佐藤哲也, 大江一弘, 菊池貴宏, 金谷佑亮, 北辻章浩, 塚田和明, 永目諭一郎, Schaedel M., 笠松良崇, こがま優香, 篠原厚, 羽場宏光, Even J.: "メンデレビウム (Md) の還元電位測定", 2011 日本放射化学会年会・第 55 回放射化学討論会, (日本放射化学会年会), 長野, 9 月 (2011).

浅井雅人, 羽場宏光, 佐藤望, 笠松良崇, 加治大哉, 森本幸司, 森田浩介, 嶋洋佑, 柴田理尋, 塚田和明, 佐藤哲也, 豊嶋厚史, 石井哲郎, 永目諭一郎: "高分解能 α 線微細構造測定による重核の核構造研究", 2011 日本放射化学会年会・第 55 回放射化学討論会, (日本放射化学会年会), 長野, 9 月 (2011).

村上昌史, 後藤真一, 村山裕史, 小嶋貴幸, 加治大哉, 森本幸司, 羽場宏光, 住田貴之, 酒井隆太郎, 工藤祐生, 米田晃, 森田浩介, 菊永英寿, 笠松良崇, 佐藤哲也, 工藤久昭: "248Cm + 18O 反応による Rf 同位体の励起関数の測定", 2011 日本放射化学会年会・第 55 回放射化学討論会, (日本放射化学会年会), 長野, 9 月 (2011).

和田彩佳, 大浦泰嗣, 羽場宏光, 金谷淳平: "99Mo ならびに 181W トレーサーの調製と陰イオン交換研究での利用", 2011 日本放射化学会年会・第 55 回放射化学討論会, (日本放射化学会), 長野, 9 月 (2011).

金谷淳平, 神原正, 羽場宏光, 高橋和也, 山田崇裕, 脇谷雄一郎, 山元真一: "理研 AVF サイクロトロンを用いた RI 製造と有償頒布", 2011 日本放射化学会年会・第 55 回放射化学討論会, (日本放射化学会), 長野, 9 月 (2011).

User Liaison and Industrial Cooperation Group

Publications

[Journal]

(Original Papers) *Subject to Peer Review

Kanai Y., Hoshino M., Kambara T., Ikeda T., Hellhammer R., Stolterfoht N., and Yamazaki Y.: "Guiding of Slow Highly Charged Ions through Nanocapillaries - Dynamic Aspect-", J. Phys.: Con. Ser. **194**, 012068-1–012068-8 (2009). *

Mihara M., Izumikawa T., Ueno H., Matsuta K., Nishimura D., Nagatomo T., Moriguchi T., Ito Y., Nagae D., Fukuda M., Yoshimi A., Yamada K., Takechi M., Ichikawa Y., Momota S., Hirayama Y., Ohtsubo T., Suzuki S., Ozawa A., Ishibashi Y., Kubo T., Ooishi H., Namiki Y., Hachiuma K., Namihira K., Horikawa D., Minamisono T., Yamaguchi T., Kuboki T., Suzuki T., Sato K., Kobayashi Y., and Asahi K.: "Beta-NMR measurement of 58Cu in Si", Hyperfine Interact. **197**, 143–147 (2010). *

Ohnishi T., Kubo T., Kusaka K., Yoshida A., Yoshida K., Ohtake M., Fukuda N., Takeda H., Kameda D., Tanaka K., Inabe N., Yanagisawa Y., Gono Y., Watanabe H., Otsu H., Baba H., Ichihara T., Yamaguchi Y., Takechi M., Nishimura S., Ueno H., Yoshimi A., Sakurai H., Motobayashi T., Nakao T., Mizoi Y., Matsushita M., Ieki K., Kobayashi N., Tanaka K., Kawada Y., Tanaka N., Deguchi S., Sato Y., Kondo Y., Nakamura T., Yoshinaga K., Ishii c., Yoshii h., Miyashita Y., Uematsu N., Shiraki Y., Sumikama T., Chiba J., Ideguchi E., Saito A., Yamaguchi T., Hachiuma I., Suzuki T., Moriguchi T., Ozawa A., Ohtsubo T., Famiano M. A., Geissel H., Nettleton A. S., Tarasov O. B., Bazin D. P., Sherrill B. M., Manikonda S. L., and Nolen J. A.: "Identification of 45 New Neutron-Rich Isotopes Produced by In-Flight Fission of a ^{238}U Beam at 345 MeV/nucleon", J. Phys. Soc. Jpn. **79**, No. 7, pp. 073201-1–073201-5 (2010). *

Tanaka T., Yamada A., Suzuki Y., Kobayashi T., Takahashi K., Kambara T., Saito F., Okamura K., Uchikoshi S., Nakano N., Hamago S., Takenaka M., Mano D., Morisaki S., and Ogura A.: "Improvement of gas sensitivity for a polymer membrane electrode by high-energy ion beam irradiation", Trans. Mater. Res. Soc. Jpn. **36**, No. 3, pp. 321–324 (2011). *

Oral Presentations

(International Conference etc.)

Asahi K., Nanao T., Tsuchiya M., Hayashi H., Furukawa T., Yoshimi A., Uchida M., Ueno H., and Matsuo Y.: "Search for an electric dipole moment in 129Xe atom using a nuclear spin oscillator", International conference on Fundamental Physics Using Atoms, Osaka, Aug. (2010).

Kambara T.: "Industrial applications of the RIKEN cyclotron", 2nd Joint Asian Accelerator Workshop (JAAWS), (Pohang Accelerator Laboratory (PAL)), Pohang, Korea, Nov.–Dec. (2010).

Kambara T., Yoshida A., Yanagisawa Y., Kameda D., Fukuda N., Ohnishi T., Kubo T., Uemoto R., Nagano A., and Uno H.: "Industrial Application of Radioactive Ion Beam at RIKEN RI Beam Factory", 11th International Conference on Applications of Nuclear Techniques, Crete, Greece, June (2011).

Wakitani Y., Yamamoto S., Yamada T., Kanaya J., Haba H., Takahashi K., and Kambara T.: "Production and distribution of radioisotopes via the JRIA-RIKEN collaboration", 7th International Conference on Isotopes, (ROSATOM), Moscow, Russia, Sept. (2011).

(Domestic Conference)

上本龍二, 鵜野浩行, 永野章, 大西哲哉, 亀田大輔, 福田直樹, 柳澤善行, 吉田敦, 久保敏幸, 神原正: "RI ビームの連続磨耗測定法への適用", 自動車技術会 2011 年春季大会, (公益社団法人自動車技術会), 横浜, 5 月 (2011).

脇谷雄一郎, 山元真一, 山田崇裕, 神原正, 羽場宏光, 金谷淳平, 高橋和也: "理研 AVF サイクロトロンを用いた RI 製造", 第 48 回アイソトープ・放射線研究発表会, (日本アイソトープ協会), 東京, 7 月 (2011).

金谷淳平, 神原正, 羽場宏光, 高橋和也, 山田崇裕, 脇谷雄一郎, 山元真一: "理研 AVF サイクロトロンを用いた RI 製造と有償頒布", 2011 日本放射化学会年会・第 55 回放射化学討論会, (日本放射化学会), 長野, 9 月 (2011).

User Support Office

Publications

[Journal]

(Original Papers) *Subject to Peer Review

Mihara M., Izumikawa T., Ueno H., Matsuta K., Nishimura D., Nagatomo T., Moriguchi T., Ito Y., Nagae D., Fukuda M., Yoshimi A., Yamada K., Takechi M., Ichikawa Y., Momota S., Hirayama Y., Ohtsubo T., Suzuki S., Ozawa A., Ishibashi Y., Kubo T., Ooishi H., Namiki Y., Hachiuma K., Namihira K., Horikawa D., Minamisono T., Yamaguchi T., Kuboki T., Suzuki T., Sato K., Kobayashi Y., and Asahi K.: "Beta-NMR measurement of 58Cu in Si", Hyperfine Interact. **197**, 143–147 (2010). *

Nagatomo T., Ueno H., Mihara M., Matsuta K., Yoshimi A., Ichikawa Y., Yamada K., Kawamura H., Ozawa A., Moriguchi T., Ishibashi Y., Asahi K., Uchida M., Suzuki K., Inoue T., Hasama Y., Iijima H., Sumikama T., Fukuda M., and Minamisono T.: "Precise nuclear moments of extremely proton-rich nuclus 23Al", Hyperfine Interact. **198**, 103–107 (2010). *

Ohnishi T., Kubo T., Kusaka K., Yoshida A., Yoshida K., Ohtake M., Fukuda N., Takeda H., Kameda D., Tanaka K., Inabe N., Yanagisawa Y., Gono Y., Watanabe H., Otsu H., Baba H., Ichihara T., Yamaguchi Y., Takechi M., Nishimura S., Ueno H., Yoshimi A., Sakurai H., Motobayashi T., Nakao T., Mizoi Y., Matsushita M., Ieki K., Kobayashi N., Tanaka K., Kawada Y., Tanaka N., Deguchi S., Sato Y., Kondo Y., Nakamura T., Yoshinaga K., Ishii c., Yoshii h., Miyashita Y., Uematsu N., Shiraki Y., Sumikama T., Chiba J., Ideguchi E., Saito A., Yamaguchi T., Hachiuma I., Suzuki T., Moriguchi T., Ozawa A., Ohtsubo T., Famiano M. A., Geissel H., Nettleton A. S., Tarasov O. B., Bazin D. P., Sherrill B. M., Manikonda S. L., and Nolen J. A.: "Identification of 45 New Neutron-Rich Isotopes Produced by In-Flight Fission of a ^{238}U Beam at 345 MeV/nucleon", J. Phys. Soc. Jpn. **79**, No. 7, pp. 073201-1–073201-5 (2010). *

Tanaka K., Fukuda M., Mihara M., Takechi M., Nishimura D., Chinda T., Sumikama T., Kudo S., Matsuta K., Minamisono T., Suzuki T., Ohtsubo T., Izumikawa T., Momota S., Yamaguchi T., Oonish T., Ozawa A., Tanihata I., and Zheng T.: "Density distribution of ^{17}Ne and possible shell-structure change in the proton-rich sd-shell nuclei", Phys. Rev. C **82**, No. 4, pp. 044309-1–044309-11 (2010). *

Tanaka K., Yamaguchi T., Suzuki T., Ohtsubo T., Fukuda M., Nishimura D., Takechi M., Ogata K., Ozawa A., Izumikawa T., Aiba T., Aoi N., Baba H., Hashizume Y., Inafuku K., Iwasa N., Kobayashi K., Komuro M., Kondo Y., Kubo T., Matsuyama T., Michimasa S., Motobayashi T., Nakabayashi T., Nakazima S., Nakamura T., Sakurai H., Shinoda R., Shinohara M., Suzuki H., Takeshita E., Takeuchi S., Togano Y., Yamada K., Yasuno T., and Yhoshitake M.: "Observation of a large reaction cross-section in the drip-line nucleus ^{22}C", Phys. Rev. Lett. **104**, No. 6, pp. 062701-1–062701-4 (2010). *

Asahi K., Furukawa T., Inoue T., Yoshimi A., Nanao T., Chikamori M., Suzuki K., Tsuchiya M., Hayashi H., Uchida M., Ueno H., Matsuo Y., and Fukuyama T.: "Search for an electric dipole moment in 129Xe atom with nuclear spin oscillator technique", J. Phys.: Con. Ser. **302**, No. 012039, pp. 1–6 (2011). *

Inoue T., Furukawa T., Nanao T., Yoshimi A., Suzuki K., Chikamori M., Tsuchiya M., Hayashi H., Uchida M., and Asahi K.: "Experimental search for ^{129}Xe atomic EDM with nuclear spin maser technique", Phys. Procedia **17**, 100–103 (2011). *

Nishimura S., Li Z., Watanabe H., Yoshinaga K., Sumikama T., Tachibana T., Yamaguchi K., Nishimura M., Lorusso G., Miyashita Y., Odahara A., Baba H., Berryman J. S., Blasi N., Bracco A., Camera F., Chiba J., Doornenbal P. C., Go S., Ideguchi E., Isobe T., Jenkins D. G., Kawada Y., Kobayashi N., Kondo Y., Kruecken R., Kubono S., Nakano T., Ong H., Ota S., Podolyak Z. F., Sakurai H., Scheit H., Steppenbeck D., Sugimoto K., Takano S., Takashima A., Tajiri K., Teranishi T., Wakabayashi Y., Walker P. M., and Wieland O.: "β-Decay Half-Lives of Very Neutron-Rich Kr to Tc Isotopes on the Boundary of the r-Process Path: An Indication of Fast r-Matter Flow", Phys. Rev. Lett. **106**, 052502-1–052502-5 (2011). *

Oral Presentations

(International Conference etc.)

Inoue T., Furukawa T., Nanao T., Yoshimi A., Suzuki K., Tsuchiya M., Hayashi H., Uchida M., and Asahi K.: "Development of the nuclear spin maser toward the atomic EDM search", 19th International Spin Physics Symposium (SPIN 2010), Julich, Germany, Sept.–Oct. (2010).

Yoshimi A., Nanao T., Inoue T., Furukawa T., Tsuchiya M., Hayashi H., Chikamori M., Uchida M., and Asahi K.: "Development of NMOR magnetometer for spin-maser EDM experiment", Villigen, Switzerland 2010/10, (PSI), Villigen, Switzerland, Oct. (2010).

Inoue T., Furukawa T., Nanao T., Yoshimi A., Suzuki K., Chikamori M., Hayashi H., Uchida M., and Asahi K.: "Experimental search for 129Xe atomic EDM with nuclear spin maser technique", Villigen, Switzerland 2010/10, (PSI), Villigen, Switzerland, Oct. (2010).

Ichikawa Y., Ueno H., Ishii Y., Furukawa T., Yoshimi A., Kameda D., Aoi N., Watanabe H., Asahi K., Iijima H., Suzuki K., Inoue T., Tsuchiya M., Hayashi H., Nanao T., Kubo T., Inabe N., Ohnishi T., Takeda H., Fukuda N., Ishihara M., Daugas J., Chevrier R., Georgiev G., Rajabali M. M., and Balabanski D. L.:

"Production of spin-aligned RI beam via two-step fragmentation reaction with dispersion matching", University of Aizu-JUSTIPEN-EFES Symposium on "Cutting-Edge Physics of Unstable Nuclei", (University of Aizu), Aizuwakamatsu, Nov. (2010).

Ichikawa Y., Ueno H., Ishii Y., Furukawa T., Yoshimi A., Kameda D., Aoi N., Watanabe H., Asahi K., Iijima H., Suzuki K., Inoue T., Tsuchiya M., Hayashi H., Nanao T., Kubo T., Inabe N., Ohnishi T., Takeda H., Fukuda N., Ishihara M., Daugas J., Chevrier R., Georgiev G., Rajabali M. M., and Balabanski D. L.: "g-factor measurements for highly spin-aligned isomeric states", RIBF-ULIC-Symposium-007: E(U)RICA International Workshop, Saitama, May (2011).

Ichikawa Y., Ueno H., Ishii Y., Furukawa T., Yoshimi A., Kameda D., Aoi N., Watanabe H., Asahi K., Iijima H., Suzuki K., Inoue T., Tsuchiya M., Hayashi H., Nanao T., Kubo T., Inabe N., Ohnishi T., Takeda H., Fukuda N., Ishihara M., Daugas J., Chevrier R., Georgiev G., Rajabali M. M., and Balabanski D. L.: "Production of spin-aligned RI beam via two-step fragmentation with dispersion matching", ARIS 2011, (Katholieke Universiteit Leuven), Leuven, Belgium, May–June (2011).

Chevrier R., Daugas J., Gaudefroy L., Ichikawa Y., Ueno H., Haas M., Haas H., Cottenier S., Aoi N., Asahi K., Balabanski D. L., Fukuda N., Furukawa T., Georgiev G., Hayashi H., Iijima H., Inabe N., Inoue T., Ishihara M., Ishii Y., Kameda D., Kubo T., Nanao T., Neyence G., Ohnishi T., Rajabali M. M., Suzuki K., Takeda H., Tsuchiya M., Vermeulen N., Watanabe H., and Yoshimi A.: "Quadrupole moment measurement of the $N = 27$ nucleus $43m$S", ARIS 2011, (Katholieke Universiteit Leuven), Leuven, Belgium, May–June (2011).

Ichikawa Y., Ueno H., Ishii Y., Furukawa T., Yoshimi A., Kameda D., Aoi N., Watanabe H., Asahi K., Iijima H., Suzuki K., Inoue T., Tsuchiya M., Hayashi H., Nanao T., Kubo T., Inabe N., Ohnishi T., Takeda H., Fukuda N., Ishihara M., Daugas J., Chevrier R., Georgiev G., Rajabali M. M., and Balabanski D. L.: "g-factor measurement for highly spin-aligned isomeric state of ^{32}Al", RIBF ULIC and CNS Symposium on Frontier of Gamma-ray Spectroscopy (Gamma11), (CNS, The University of Tokyo and RIKEN Nishina Center), Saitama, June–July (2011).

Ichikawa Y., Ueno H., Ishii Y., Furukawa T., Yoshimi A., Kameda D., Aoi N., Watanabe H., Asahi K., Iijima H., Suzuki K., Inoue T., Tsuchiya M., Hayashi H., Nanao T., Kubo T., Inabe N., Ohnishi T., Takeda H., Fukuda N., Ishihara M., Daugas J., Chevrier R., Georgiev G., Rajabali M. M., and Balabanski D. L.: "Production of spin-aligned RI beam via two-step fragmentation with dispersion matching", Rutherford Centennial Conference on Nuclear Physics 2011, (The University of Machester), Manchester, United Kingdom, Aug. (2011).

Chevrier R., Daugas J., Gaudefroy L., Ichikawa Y., Ueno H., Haas M., Haas H., Cottenier S., Aoi N., Asahi K., Balabanski D. L., Fukuda N., Furukawa T., Georgiev G., Hayashi H., Iijima H., Inabe N., Inoue T., Ishihara M., Ishii Y., Kameda D., Kubo T., Nanao T., Neyence G., Ohnishi T., Rajabali M. M., Suzuki K., Takeda H., Tsuchiya M., Vermeulen N., Watanabe H., and Yoshimi A.: "Quadrupole moment measurement of the $N = 27$ nucleus ^{43}S^m", Colloque GANIL 2011, (GANIL), Corsica, France, Sept. (2011).

Ichikawa Y., Ueno H., Ishii Y., Furukawa T., Yoshimi A., Kameda D., Aoi N., Watanabe H., Asahi K., Iijima H., Suzuki K., Inoue T., Tsuchiya M., Hayashi H., Nanao T., Kubo T., Inabe N., Ohnishi T., Takeda H., Fukuda N., Ishihara M., Daugas J., Chevrier R., Georgiev G., Rajabali M. M., and Balabanski D. L.: "Spin-aligned RI beam produced by two-step projectile fragmentation", ISPUN11, (Institute for Nuclear Science and Technique), Hanoi, Vietnam, Nov. (2011).

(Domestic Conference)

飯島裕章, 吉見彰洋, 市川雄一, 石井裕司, 吉田直貴, 古川武, 内田誠, 鈴木都文, 井上壮志, 土屋真人, 林宏憲, 七尾翼, 近森正敏, 上野秀樹, 旭耕一郎: "中性子過剰核 41,43S の磁気モーメント測定のための磁場回転装置の開発", 平成 22 年度 KUR 専門研究会「短寿命核および放射線を用いた物性研究（III）」, 大阪, 2 月 (2010).

石井裕司, 市川雄一, 上野秀樹, 古川武, 吉見彰洋, 亀田大輔, 青井考, 渡邉寛, 旭耕一郎, 飯島裕章, 鈴木都文, 井上壮志, 土屋真人, 林宏憲, 七尾翼, 久保敏幸, 稲辺尚人, 大西哲哉, 竹田浩之, 福田直樹, 石原正泰, Daugas J., Chevrier R., Georgiev G., Rajabali M. M., Balabanski D. L.: "TDPAD 法を用いた ^{32}Al アイソマーの磁気モーメント測定", 日本物理学会 2010 年秋季大会, (日本物理学会), 北九州, 9 月 (2010).

蜂谷崇, 黒澤真城, 竹谷篤, 藤原康平, 二宮一史, 秋葉康之, 金谷 淳平, Baumgart S. L., 秋元 亮二, 浅野 秀光, 栗田和好, 西尾 悠法, 渡邉 健太郎, 今井 憲一, 佐藤 進, 佐甲博之, 関本美知子, Pancaker C., Shafto E., Apadula N., Mannel E. J., Gastaldi F., Deapier O., Sahlmuller B., Lewis B., Koster J., Stepanov M., Shaver A., Bowen J., Bryslawskyj J.: "PHENIX シリコン崩壊点飛跡検出器 (VTX) の組立と設置", 日本物理学会第 66 回年次大会, (日本物理学会), 新潟, 3 月 (2011).

浅野 秀光, 黒澤 真城, 竹谷 篤, 藤原 康平, 二宮 一史, 秋葉康之, 金谷淳平, 蜂谷崇, Baumgart S. L., 秋元亮二, 栗田和好, 西尾 悠法, 渡邉 健太郎, 今井 憲一, 佐藤 進, 佐甲博之, 関本美知子, Pancaker C., Shafto E., Apadula N., Mannel E. J., Gastaldi F., Deapier O., Sahlmuller B., Lewis B., Koster J., Stepanov M., Shaver A., Bowen J., Bryslawskyj J.: "偏極陽子衝突ビームを用いた PHENIX 崩壊点飛跡検出器 (VTX) のコミッショニング", 日本物理学会第 66 回年次大会, (日本物理学会), 新潟, 3 月 (2011).

黒澤真城, 竹谷篤, 藤原康平, 二宮一史, 秋葉康之, 金谷淳平, 蜂谷崇, Baumgart S. L., 秋元亮二, 浅野秀光, 栗田和好, 西尾悠法, 渡邉健太郎, 今井憲一, 佐藤進, 佐甲博之, 関本美知子, Pancaker C., Shafto E., Apadula N., Mannel E.

J., Gastaldi F., Deapier O.: "PHENIX シリコン崩壊点飛跡測定器（VTX）ピクセル検出器モジュールの量産完成報告", 日本物理学会第 66 回年次大会, (日本物理学会), 新潟, 3 月 (2011).

石井裕司, 市川雄一, 上野秀樹, 古川武, 吉見彰洋, 亀田大輔, 青井考, 渡邉寛, 旭耕一郎, 飯島裕章, 鈴木都文, 井上壮志, 土屋真人, 林宏憲, 七尾翼, 久保敏幸, 稲辺尚人, 大西哲哉, 竹田浩之, 福田直樹, 石原正泰, Daugas J., Chevrier R., Georgiev G., Rajabali M. M., Balabanski D. L.: "TDPAD 法を用いた ^{32}Al アイソマーの磁気モーメント測定 II", 日本物理学会第 66 回年次大会, (日本物理学会), 新潟, 3 月 (2011).

古川武, 涌井崇志, 佐々木彩子, 泉さやか, 市川雄一, 吉見彰洋, 田尻邦彦, 石井裕司, 吉田直貴, 松浦佑一, 加藤裕樹, 山口康広, 今村慧, 幕田将宏, 畠山温, 和田道治, 園田哲, 伊藤由太, 七尾翼, 小林徹, 西村俊二, 西村美月, 近藤洋介, 青井考, 米田健一郎, 久保野茂, 大城幸光, 上野秀樹, 篠塚勉, 下田正, 旭耕一郎, 松尾由賀利: "^{87}Rb ビームを用いた超流動ヘリウム中でのレーザー核分光法開発実験", 日本物理学会第 66 回年次大会, 新潟, 3 月 (2011).

市川雄一, 上野秀樹, 石井裕司, 古川武, 吉見彰洋, 亀田大輔, 青井考, 渡邉寛, 旭耕一郎, 飯島裕章, 鈴木都文, 井上壮志, 土屋真人, 林宏憲, 七尾翼, 久保敏幸, 稲辺尚人, 大西哲哉, 竹田浩之, 福田直樹, 石原正泰, Daugas J., Chevrier R., Georgiev G., Rajabali M. M., Balabanski D. L.: "分散整合二回散乱法による核スピン整列 RI ビームの生成 II", 日本物理学会第 66 回年次大会, (日本物理学会), 新潟, 3 月 (2011).

古川武, 涌井崇志, 佐々木彩子, 泉さやか, 市川雄一, 吉見彰洋, 田尻邦彦, 石井裕司, 吉田直貴, 松浦佑一, 加藤裕樹, 山口康広, 今村慧, 幕田将宏, 畠山温, 和田道治, 園田哲, 伊藤由太, 七尾翼, 小林徹, 西村俊二, 西村美月, 近藤洋介, 青井考, 米田健一郎, 久保野茂, 上野秀樹, 下田正, 篠塚勉, 旭耕一郎, 松尾由賀利: "超流動ヘリウム中に打ち込まれた ^{87}Rb ビームのレーザー誘起蛍光観測と光ポンピング", 日本物理学会 2011 年秋季大会, (日本物理学会), 弘前, 9 月 (2011).

市川雄一, 上野秀樹, 石井裕司, 古川武, 吉見彰洋, 亀田大輔, 青井考, 渡邉寛, 旭耕一郎, 飯島裕章, 鈴木都文, 井上壮志, 土屋真人, 林宏憲, 七尾翼, 久保敏幸, 稲辺尚人, 大西哲哉, 竹田浩之, 福田直樹, 石原正泰, Daugas J., Chevrier R., Georgiev G., Rajabali M. M., Balabanski D. L.: "分散整合二回散乱法による核スピン整列 RI ビームの生成 III", 日本物理学会 2011 年秋季大会, (日本物理学会), 弘前, 9 月 (2011).

石井裕司, Georgiev G., 市川雄一, 白井葉月, 上野秀樹, 石橋陽子, 吉田直貴, 古川武, Sotty C., Chevrier R., Daugas J., Ljungvall J., Lozeva R. L., 新倉潤, Yordanov D., 渡邉寛, 西村太樹, 西畑洸希, 近森正敏, 宮武裕和, 七尾翼, 丹羽崇博, 岡田俊祐, 齋藤佑多, 旭耕一郎, Balabanski D. L.: "Production of a spin-aligned ^{69}Cu beam by one-nucleon-removal reactions and measurement of its nuclear moments", 日本物理学会第 67 回年次大会, (日本物理学会), 西宮, 3 月 (2012).

Industrial Cooperation Team

Publications

[Journal]

(Original Papers) *Subject to Peer Review

Kanai Y., Hoshino M., Kambara T., Ikeda T., Hellhammer R., Stolterfoht N., and Yamazaki Y.: "Guiding of Slow Highly Charged Ions through Nanocapillaries - Dynamic Aspect-", J. Phys.: Con. Ser. **194**, 012068-1–012068-8 (2009). *

Luo S., Zhu B., Nakao A., Nakatomi R., and Yu H.: "Functionalized conducting polymer nano-networks from controlled oxidation polymerization toward cell engineering", Adv. Eng. Mater. **13**, No. 10, pp. B423–B427 (2011). *

Nakajima Y. and Takeichi H.: "Human processing of short temporal intervals as revealed by an ERP waveform analysis", Frontiers in Integrative Neuroscience **5**, No. 74, pp. 1–10 (2011). *

Aoki Y., Habazaki H., Nagata S., Nakao A., Kunitake T., and Yamaguchi S.: "Finite Size Effect of Proton-Conductivity of Amorphous Silicate Thin Films Based on Mesoscopic Fluctuation of Glass Network", J. Am. Chem. Soc. **133**, No. 10, pp. 3471–3479 (2011). *

Akamatsu K., Maruyama K., Chen W., Nakao A., and Shin-ichi N.: "Drastic difference in porous structure of calcium alginate microspheres prepared with fresh or hydrolyzed sodium alginate", J. Colloid Interface Sci. **363**, 707–710 (2011). *

Sato H., Nakao A., and Yamagishi A.: "Formation of chiral heterometallic oligomers by combination of inert Ru(III) tectons and labile Ni(II) connectors", New J. Chem. **35**, 1823–1828 (2011). *

Mitsudo T., Gagnon C., Takeichi H., and Grondin S.: "An electroencephalographic investigation of the filled-duration illusion", Frontiers in Integrative Neuroscience **5**, No. 84, pp. 1–13 (2012). *

[Book · Proceedings]

(Others)

竹市博臣: "心理実験技術", ブレインコミュニケーション：脳と社会の通信手段, （社）電子情報通信学会, 東京, pp. 46–79 (2011).

Oral Presentations

(International Conference etc.)

Kamijo M., Takeichi H., Okada H., and Omori T.: "An electroencephalogram step to language aptitude evaluation: a case study on Japanese EFL understanding", 15th STEM Conference, (The Society for Teaching English through Media (STEM)), Busan, Korea, Apr. (2011).

Mitsudo T., Gagnon C., Takeichi H., and Grondin S.: "An electroencephalographic investigation of the filled-duration illusion", 17th Annual Meeting of the Organization on Human Brain Mapping (HBM2011), Quebec City, Canada, June (2011).

Takeichi H., Nakajima Y., Mitsudo T., and Tobimatsu S.: "Processing and representing temporal patterns in the brain: a classifier and scaling analysis", 13th International Rhythm Perception and Production Workshop, Leipzig, Germany, July (2011).

Aoyama T., Fujihara T., Muto T., Takaishi K., Nakao A., Watanabe S., Matsumoto M., Matsumoto S., Inoue S., Muranaka A., Hashizume D., Uchiyama M., and Ribierre J. M.: "Reversible p-n conversion and logic gates based on a solution-processible thienoquinoid semiconductor", 11th European Conference on Molecular Electronics (ECME2011), (European Conference on Molecular Electronics), Barcelona, Spain, Sept. (2011).

Takeichi H., Gunji A., and Inagaki M.: "Development of an Efficient Method for Evaluation of Pervasive Developmental Disorders", International Neuropsychological Society 40th Annual Meeting, Montreal, Canada, Feb. (2012).

(Domestic Conference)

上條美和子, 竹市博臣, 岡田浩之, 大森隆司: "脳波（EEG）による言語能力の検証：日本語と英語聴取を比較したケーススタディ", 日本英語音声学会（EPSJ）関東支部第 11 回研究大会, 東京, 6 月 (2011).

Safety Management Group

Publications

[Journal]

(Original Papers) *Subject to Peer Review

Hagiwara M., Sanami T., Masumoto K., Iwamoto Y., Matsuda N., Sakamoto Y., Nakane Y., Nakashima H., and Uwamino Y.: "Spectrum measurement of neutrons and gamma-rays from thick H218O target bombarded with 18 MeV protons", J. Korean Phys. Soc. **59**, No. 2, pp. 2035–2038 (2011). *

松村宏, 斎藤究, 石岡純, 上蓑義朋: "高速道路上のガンマ線測定により得られた福島第一原子力発電所から飛散した放射性物質の拡散状況", 日本原子力学会和文論文誌 **10**, No. 3, pp. 152–162 (2011). *

[Book・Proceedings]

(Original Papers) *Subject to Peer Review

Hagiwara M., Sanami T., Iwamoto Y., Matsuda N., Sakamoto Y., Nakane Y., Nakashima H., Masumoto K., and Uwamino Y.: "Systematic measurement of neutron and gamma-ray yields on thick targets bombarded with 18 MeV protons", JAEA-Conf 2011-002, Fukuoka, 2010–11, Japan Atomic Energy Agency, Ibaraki, pp. 119–124 (2011). *

Oral Presentations

(Domestic Conference)

赤塩敦子, 日暮利江子, 上蓑義朋: "実務マニュアルに基づく遮蔽計算プログラムの作成", 平成 23 年度主任者部会年次大会（第 52 回放射線管理研修会）, (日本アイソトープ協会放射線取扱主任者部会), 山形, 11 月 (2011).

CNS (Center for Nuclear Study, Graduate School of Science, University of Tokyo)

Publications

[Journal]

(Original Papers) *Subject to Peer Review

K. Admodt *et al.* for the ALICE Collaboration: "Rapidity and transverse momentum dependence of inclusive J/ψ production in pp collisions at $\sqrt{s} = 7$ TeV", Phys.Lett. B704 (2011) 442-455 *

K. Admodt *et al.* for the ALICE Collaboration: "Higher Harmonic Anisotropic Flow Measurements of Charged Particles in Pb-Pb Collisions at $\sqrt{s_{NN}} = 2.76$ TeV", Phys. Rev. Lett. 107, 032301 (2011) *

K. Admodt *et al.* for the ALICE Collaboration: "Production of pions, kaons and protons in pp collisions at $\sqrt{s} =$ 900 GeV with ALICE at the LHC", Eur.Phys.J.C 71(6): 1655, 2011*

B. Abelev *et al.* for the ALICE Collaboration: "Heavy flavour decay muon production at forward rapidity in proton?proton collisions at $\sqrt{s} = 7$ TeV", Phys. Lett. B 708 (2012) 265*

B. Abelev *et al.* for the ALICE Collaboration: "Measurement of Event Background Fluctuations for Charged Particle Jet Reconstruction in Pb-Pb collisions at $\sqrt{s_{NN}}$ = 2.76 TeV", JHEP 03 (2012) 053*

K. Admodt *et al.* for the ALICE Collaboration: "Femtoscopy of pp collisions at $\sqrt{s}$=0.9 and 7 TeV at the LHC with two-pion Bose-Einstein correlations", Phys. Rev. D 84, 112004 (2011)*

B.Abelev *et al.* for the ALICE Collaboration: "Measurement of charm production at central rapidity in proton-proton collisions at $\sqrt{s} = 7$ TeV", JHEP 01 (2012) 128*

B.Abelev *et al.* for the ALICE Collaboration: "J/ψ polarization in pp collisions at $\sqrt{s}$=7 TeV", Phys.Rev.Lett. 108 (2012) 082001*

K. Admodt *et al.* for the ALICE Collaboration: "Particle-Yield Modification in Jetlike Azimuthal Dihadron Correlations in Pb-Pb Collisions at $\sqrt{s_{NN}}$=2.76 TeV", Phys. Rev. Lett. 108, 092301 (2012)*

K. Admodt *et al.* for the ALICE Collaboration: "Harmonic decomposition of two particle angular correlations in Pb-Pb collisions at $\sqrt{s_{NN}} = 2.76$ TeV", Phys.Lett. B708 (2012) 249-264*

A. Adare *et al.* for the PHENIX Collaboration: "Azimuthal correlations of electrons from heavy-flavor decay with hadrons in p+p and Au+Au collisions at $\sqrt{s} =$ 200 GeV", Phys. Rev. C 83, 044912 (2011)*

A. Adare *et al.* for the PHENIX Collaboration: "Identified charged hadron production in p+p collisions at $\sqrt{s} = 200$ and 62.4 GeV", Phys. Rev. C 83, 064903 (2011)*

A. Adare *et al.* for the PHENIX Collaboration: "Event structure and double helicity asymmetry in jet production from polarized $p + p$ collisions at $\sqrt{s} = 200GeV$", Phys. Rev. D 84, 012006 (2011)*

A. Adare *et al.* for the PHENIX Collaboration: "Suppression of away-side jet fragments with respect to the reaction plane in Au + Au collisions at $\sqrt{s_{NN}} = 200$ GeV", Phys. Rev. C 84, 024904 (2011)*

A. Adare *et al.* for the PHENIX Collaboration: "Cold Nuclear Matter Effects on J/ψ Yields as a Function of Rapidity and Nuclear Geometry in $d + A$ Collisions at $\sqrt{s_{NN}} = 200$ GeV", Phys. Rev. Lett. 107, 142301 (2011)*

A. Adare *et al.* for the PHENIX Collaboration: "Production of ω mesons in $p + p$, d + Au, Cu + Cu, and Au + Au collisions at $\sqrt{s_{NN}} = 200$ GeV", Phys. Rev. C 84, 044902 (2011)*

A. Adare *et al.* for the PHENIX Collaboration: "Heavy-quark production in $p + p$ and energy loss and flow of heavy quarks in Au + Au collisions at $\sqrt{s_{NN}} = 200$ GeV", Phys. Rev. C 84, 044905 (2011)*

A. Adare *et al.* for the PHENIX Collaboration: "Suppression of Back-to-Back Hadron Pairs at Forward Rapidity in d + Au Collisions at $\sqrt{s_{NN}} = 200$ GeV", Phys. Rev. Lett. 107, 172301 (2011)*

A. Adare *et al.* for the PHENIX Collaboration: "J/ψ suppression at forward rapidity in Au + Au collisions at $\sqrt{s_{NN}} = 200$ GeV", Phys. Rev. C 84, 054912 (2011)*

A. Adare *et al.* for the PHENIX Collaboration: "Measurements of Higher Order Flow Harmonics in Au + Au Collisions at $\sqrt{s_{NN}} = 200$ GeV", Phys. Rev. Lett. 107, 252301 (2011)*

Ozawa A., Hashizume Y., Aoki Y., Tanaka K., Aiba T., Aoi N., Baba H., A.Brown B., Fukuda M., Inafuku K., Iwasa N., Izumikawa T., Kobayashi K., Komuro M., Kondo Y., Kubo T., Kurokawa M., Matsuyama T., Michimasa S., Motobayashi T., Nakabayashi T., Nakajima S., Nakamura T., Ohtsubo T., Sakurai H., Shinoda R., Shinohara M., Suzuki H., Suzuki T., Takechi M., Takeshita E., Takeuchi S., Togano Y., Yamada K., Yamaguchi T., Yasuno T., Yoshitake M., "One- and two-neutron removal reactions from ^{19,20}C with a proton target", Phys. Rev. C **84**, (2011) 064315,*

S. Watanabe, S. Kubono, Y. Ohshiro, H.Yamaguchi, M. Kase, M. Wada, and R. Koyama, "Simple, High-Sensitive, and Non-Destructive Beam Monitor for RI Beam Facilities", Nucl. Instr. Meth. A **633** 8–14 (2011).*

J. Chen, A.A. Chen, G. Amadio, S. Cherubini, H. Fujikawa, S. Hayakawa, J.J. He, N. Iwasa, D. Kahl, L.H. Khiem, S. Kubono, S. Kurihara, Y.K. Kwon, M. La Cognata, J.Y. Moon, M. Niikura,S. Nishimura, J. Pearson, R.G. Pizzone, T. Teranishi, Y. Togano, Y. Wakabayashi, and H. Yamaguchi, "Strong 25Al+p resonances via elastic proton scattering with a radioactive 25Al beam" Phys. Rev. C **85** 015805 (2012).*

N. Imai, Y. Hirayama, Y.X. Watanabe, T. Teranishi, T. Hashimoto, S. Hayakawa, Y. Ichikawa, H. Ishiyama, S.C. Jeong, D. Kahl, S. Kubono, H. Miyatake, H. Ueno, H.

Yamaguchi, K. Yoneda, A. Yoshimi, “Isobaric analog resonances of the $N = 21$ nucleus ^{35}Si”, Phys. Rev. C **85**, 034313 (2012). *

H.S. Jung, C.S. Lee, Y.K. Kwon, J.Y. Moon, J.H. Lee, C.C. Yun, S. Kubono, H. Yamaguchi, T. Hashimoto, D. Kahl, S. Hayakawa, Choi Seonho, M.J. Kim, Y.H. Kim, Y.K. Kim, J.S. Park, E.J. Kim, C.B. Moon, T. Teranishi, Y. Wakabayashi, N. Iwasa, N.T. Yamada, Y. Togano, S. Kato, S. Cherubini, G.G. Rapisarda, “Experimental study of resonant states in ^{27}P via elastic scattering of ^{26}Si+p”, Phys. Rev. C. **85**, 045802 (2012)*

Y. Togano, Y. Yamada, N. Iwasa, K. Yamaga, T Modobayashi, N. Aoi, H. Baba, S. Bishop, X. Cai, P. Doornenbal, D. Fang, T. Furukawa, K. Ieki, T. Kawabata, S. Kanno, N. Kobayashi, Y. Kondo, T. Kuboki, N. Kume, K. Kurita, M. Kurokawa, Y.G. Ma, Y. Matsuo, H. Murakami, M. Matsushita, T. Nakamura, K. Okada, S. Ota, Y. Satou, S. Shimoura, R. Shinoda, K.N. Tanaka, S. Takeuchi, W. Tian, H. Wang, J. Wang, K .Yoneda, “Hindered Proton Collectivity i S-28(16)12: Possible Magic Number at Z=16”, Phys. Rev. Lett. 21 (2012) 22501*

H. Watanabe, K. Yamaguchi, A. Odahara, T. Sumikama, S. Nishimura, K. Yoshinaga, Z. Li, Y. Miyashita, K. Sato, L. Prochniak, H. Baba, J.S. Berryman, N. Blasi, A. Bracco, F. Camera, J. Chiba, P. Doornenbal, S. Go, T. Hashimoto, S. Hayakawa, C. Hinke, N. Hinohara, E. Ideguchi, T. Isobe, Y. Ito, D.G. Jenkins, Y. Kawada, N. Kobayashi, Y. Kondo, R. Krucken, S. Kubono, G. lorusso, T. Nakao, T. Nakatsukasa, M. Kurata-Nishimura, H.J. Ong, S. Ota, Z. Podolyak, H. Sakurai, H. Sheit, K. Steiger, D. Steppenbeck, K. Sugimoto, K. Tajiri, S. Takano, A. Takashima, T. Teranishi, Y. Wakabayashi, P.M. Walker, O. Wieland, H. Yamaguchi “Development of axial asymmetry in the neutron-rich nucleus Mo-110” Phys. Lett. B 704 (2011) 270–275*

H. Watanabe, T. Sumikama, S. Nishimura, K. Yoshinaga, Z. Li, Y. Miyashita, K. Yamaguchi, H. Baba, J.S. Berryman, N. Blasi, A. Bracco, F. Camera, J. Chiba, P. Doornenbal, S. Go, T. Hashimoto, S. Hayakawa, C. Hinke, E. Ideguchi, T. Isobe, Y. Ito, D.G. Jenkins, Y. Kawada, N. Kobayashi, Y. Kondo, R. Krucken, S. Kubono, G. Lorusso, T. Nakao, M. Kurata-Nishimura, A. Odahara, H.J. Ong, S. Ota, Z. Podolyak, H. Sakurai, H. Sheit, Y. Shi, K. Steiger, D. Steppenbeck, K. Sugimoto, K. Tajiri, S. Takano, A. Takashima, T. Teranishi, Y. Wakabayashi, P.M. Walker, O. Wieland, F.R. Xu, H. Yamaguchi “Low-lying level structure of the neutron-rich nucleus Nb-109: A possible oblate-shape isomer” Phys. Lett. B 696 (2011) 186-190*

T. Sumikama, K. Yoshinaga, H. Watanabe, S. Nishimura, Y. Miyashita, K. Yamaguchi, K. Sugimoto, J. Chiba, H. Baba, J.S. Berryman, N. Blasi, A. Bracco, F. Camera, P. Doornenbal, S. Go, T. Hashimoto, S. Hayakawa, C. Hinke, E. Ideguchi, T. Isobe, Y. Ito, D.G. Jenkins, Y. Kawada, N. Kobayashi, Y. Kondo, R. Krucken, S. Kubono, G. Lorusso, T. Nakao, M. Kurata-Nishimura, A. Odahara, H.J. Ong, S. Ota, Z. Podolyak, H. Sakurai, H. Sheit, K. Steiger, D. Steppenbeck, S. Takano, A. Takashima, K. Tajiri, T. Teranishi, Y. Wakabayashi, P.M. Walker, O. Wieland, H. Yamaguchi “Structural Evolution in the Neutron-Rich Nuclei Zr-106 and Zr-108” Phys. Rev. Lett. 106 (2011) 202501*

S. Nishimura, Z. Li, H. Watanabe, K. Yoshinaga, T. Sumikama, T. Tatibana, K. Yamaguchi, M. Kurata-Nishimura, G. Lorusso, Y. Miyashita, A. Odahara, H. Baba, J.S. Berryman, N. Blasi, A. Bracco, F. Camera, J. Chiba, P. Doornenbal, S. Go, T. Hashimoto, S. Hayakawa, C. Hinke, E. Ideguchi, T. Isobe, Y. Ito, D.G. Jenkins, Y. Kawada, N. Kobayashi, Y. Kondo, R. Krucken, S. Kubono, T. Nakao, H.J. Ong, S. Ota, Z. Podolyak, H. Sakurai, H. Sheit, K. Steiger, D. Steppenbeck, K. Sugimoto, K. Tajiri, S. Takano, A. Takashima, T. Teranishi, Y. Wakabayashi, P.M. Walker, O. Wieland, H. Yamaguchi “beta-Decay Half-Lives of Very Neutron-Rich Kr to Tc Isotopes on the Boundary of the r-Process Path: An Indication of Fast r-Matter Flow” Phys. Rev. Lett. 106 (2011) 052502*

Y. Togano, T. Gomi, T. Motobayashi, Y. Ando, N. Aoi, H. Baba, K. Demichi, Z. Elekes, N. Fukuda, Z. Fulop, U. Futakami, H. Hasegawa, Y. Higurashi, K. Ieki, N. Imai, M. Ishihara, K. Ishikawa, N. Iwasa, H. Iwasaki, S. Kanno, Y. Kondo, T. Kubo, S. Kubono, M. Kunibu, K. Kurita, Y.U. Matsuyama, S. Michimasa, T. Minemura, M. Miura, H. Murakami, T. Nakamura, M. Notani, S. Ota, A. Saito, H. Sakurai, M. Serata, S. Shimoura, T. Sugimoto, E. Takeshita, S. Takeuchi, K. Ue, K. Yamada, Y. Yanagisawa, K. Yoneda, A. Yoshida “Resonance states in P-27 using Coulomb dissociation and their effect on the stellar reaction Si-26(p,gamma)P-27 Phys. Rev. C84 (2011) 035808*

H. Matsubara, A. Tamii, Y. Shimizu, K. Suda, Y. Tameshige, J. Zenihiro: “Wide-window gas target system for high resolution experiment with magnetic spectrometer”, Nucl. Instrum. Methods A 678 (2012) 122-129.*

Yamaguchi T., Tanaka K., Suzuki T., Ozawa A., Ohtsubo T., Aiba T., Aoi N., Baba H., Fukuda M., Hashizume Y., Inafuku K., Iwasa N., Izumikawa T., Kobayashi K., Komuro M., Kondo Y., Kubo T., Kurokawa M., Matsuyama T., Michimasa S., Motobayashi T., Nakabayashi T., Nakajima S., Nakamura T., Sakurai H., Shinoda R., Shinohara M., Suzuki H., Takechi M., Takeshita E., Takeuchi S., Togano Y., Yamada K., Yasuno T., Yoshitake M., “Nuclear reactions of ^{19,20}C on a liquid hydrogen target measured with the superconducting TOF spectrometer”, Nucl. Phys. **A864** (2011) 1–37.,*

Satou Y., Nakamura T., Kondo Y., Matsui N., Hashimoto Y., Nakabayashi T., Okumura T., Shinohara M., Fukuda

N., Sugimoto T., Otsu H., Togano Y., Motobayashi T., Sakurai H., Yanagisawa Y., Aoi N., Takeuchi S., Gomi T., Ishihara M., Kawai S., Ong H.J., Onishi T.K., Shimoura S., Tamaki M., Kobayashi T., Matsuda Y., Endo N., Kitayama M., "^{14}Be(p,n)^{14}B reaction at 69 MeV in inverse kinematics", Phys. Lett. B **697** (2011) 459-462.,*

Back T., Qi C., Moradi F.Ghazi, Cederwall B., Johnson A., Liotta R., Wyss R., Al-Azri H., Bloor D., Brock T., Wadsworth R., Grahn T., Greenlees P.T., Hauschild K., Herzan A., Jacobsson U., Jones P.M., Julin R., Juutinen S., Ketelhut S., Leino M., Lopez-Martens A., Nieminen P., Peura P., Rahkila P., Rinta-Antila S., Ruotsalainen P., Sandzelius M., Saren J., Scholey C., Sorri J., Uusitalo J., Go S., Ideguchi E., Cullen D.M., Procter M.G., Braunroth T., Dewald A., Fransen C., Hackstein M., Litzinger J., Rother W., "Lifetime measurement of the first excited 2^+ state in ^{108}Te", Phys. Rev. C **84** (2011) 041306.,*

Sato N., Haba H., Ichikawa T., Kaji D., Kudou Y., Morimoto K., Morita K., Ozeki K., Sumita T., Yoneda A., Ideguchi E., Koura H., Ozawa A., Shinozuka T., Yamaguchi T., Yoshida A., "Production and Decay Properties of ^{264}Hs and ^{265}Hs", J. Phys. Soc. Jpn. **80** (2011) 094201.,*

[Book・ Proceedings]

(Original Papers) *Subject to Peer Review

H. Yamaguchi,T. Hashimoto, S. Hayakawa, D.N. Binh, D. Kahl, S. Kubono, "Alpha-induced astrophysical reactions studied at CRIB", Proceedings of the International Symposium on Nuclear Astrophysics "Nuclei in the Cosmos - XI", Heidelberg, Germany, July 19–23 2010, Proceedings of Science, PoS(NIC-XI)214, (2011).*

Y. Akamatsu, H. Hamagaki, T. Hatsuda, T. Hirano "Can transport peak explain the low-mass enhancement of dileptons at RHIC?", Proceedings of the 22nd INTERNATIONAL CONFERENCE ON ULTRA RELATIVISTIC NUCLEUS-NUCLEUS COLLISIONS, 23-28 May 2011. Annecy, France; J. Phys. G 38 (2011) 124184.

Hideki Hamagaki, "First results from the ALICE experiment at LHC" Proceedings of the 25th Nishinomiya-Yukawa Memorial International Workshop on High Energy Strong Interactions 2010: Parton Distributions and Dense QCD Matter (HESI10); Prog. Theor. Phys. Suppl. 187 (2011) 237-249.

Y. Hori, H. Hamagaki, T. Gunji, "Simulation study for forward calorimater in LHC-ALICE experiment" Proceedings of the 14th International Conference on Calorimetry in High Energy Physics (CALOR 2010), 10-14 May 2010. Beijing, China; J. Phys. Conf. Ser. 293 (2011) 012029.

K. Aoki, H. Enyo, T. Gunji, H. Hamagaki, J. Kanaya, Y. Komatsu, S. Masumoto, K. Ozawa, T. Sato, M. Sekimoto, T. Tsuji, K. Utsunomiya, Y. Watanabe, S. Yokkaichi "A development of HBD for the J-PARC E16 experiment." Proceedings of the 12th Vienna Conference on Instrumentation, 15-20 Feb, 2010, Vienna, Austria; Nucl. Instrum. Meth. A628 (2011) 300-303.

Itahashi K., Berg G.P.A., Fujioka H., Geissel H., Hayano R.S., Hirenzaki S., Ikeno N., Inabe N., Itoh S., Kameda D., Kubo T., Matsubara H., Michimasa S., Miki K., Miya H., Nakamura M., Nishi T., Noji S., Ota S., Suzuki K., Takeda H., Todoroki K., Tsukada K., Uesaka T., Weick H., Yoshida K., " Measurement of Pionic ^{121}Sn atoms at the RI beam factory", Hyperfine Interact. **209** (2012) 51–56.

Oral Presentations

(International Conference etc.)

H. Hamagaki, "Experimental Overview of High Energy Density QCD", Presented in the XLI International Symposium on Multiparticle Dynamics (ISMD2011) 25 - 30 Sep. 2011, Miyajima, Hiroshima, Japan.

T. Gunji: "Experimental studies of gluon shadowing/saturation (initial condition) in p+A/A+A collisions at RHIC and LHC" at the 20th Heavy Ion Cafe, Jan. 21, 2012, University of Tokyo, Komaba Campus, Japan

Hisayuki Torii for the ALICE Collaboration (Poster), "Neutral Meson Identified by ALICE-PHOS in Pb+Pb Collisions at sqrt(s)$_{NN}$=2.76TeV" , at Quark Matter 2011, May 26, 2011, Annecy, France

Yorito Yamaguchi for the PHENIX collaboration (Poster), "Low pT direct photon production in 200GeV d+Au collisions measured by the PHENIX detector" at the 22nd International conference on ultra-relativistic nucleus-nucleus collisions (QM2011), May 23–28, 2011, Annecy, France

Yorito Yamaguchi, "Photons at RHIC" at the High-pT Probes of High-Density QCD at the LHC (HPHD2011), May 30–June 1, 2011, Ecole Polytechnique, Paris, France

Yorito Yamaguchi, "Photon Measurements in Heavy Ion Collisions" at the XLI International Symposium of Multiparticle Dynamics (ISMD2011), Sep. 26–30, 2011, Miyajima, Hiroshima, Japan

Yorito Yamaguchi for the PHENIX collaboration, "Direct Photon Production in the Thermal Region from PHENIX" at the 27th Lake Louise Winter Institute, Feb. 19–25, 2012, Lake Louise, Alberta, Canada

TAKAHARA, Akihisae for the PHENIX Collaboration "J/ψ Photoproduction in ultra-peripheral Au+Au collisions measured by RHIC-PHENIX", QXX International Workshop on Deep-Inelastic Scattering and Related Subjects, March, 2012, Bonn, Germany

Matsubara H., Takaki M., Uesaka T., Aoi N., Dozono M., Fujii T., Hashimoto T., Hatanaka K., Kikuchi Y., Kawabata T., Kawase S., Kisamori K., Lee C.S., Lee H.C., Maeda Y., Michimasa S., Miki K., Miya H., Noji S., Ota S., Sakaguchi S., Sasamoto Y., Shimoura S., Suzuki T., Takahisa K., Tamii A., Yako K., Yokota N., Yokoyama R., Zenihiro J., "Study of the neutron rich nuclei via heavy-ion double charge exchange reaction", Direct Reactions with Exotic Beams (DREB2012), Mar. 26-29, 2012, Aula Magna, Faculty of SMFN, Pisa, Italy.

S. Shimoura (invited): "Detectors for Nuclear Physics", The Technology and Instrumentation in Particle Physics 2011 (TIPP 2011), June. 9–14, 2011, Chicago, USA.

S. Kawase, "Proton spin-orbit splitting in ^{18}O studied by the (polp,2p) reaction at 200 MeV", The international Conference on Advances in Radioactive Isotope Science (ARIS), May, 29– Jun. 3, Leuven, Belgium

H. Yamaguchi, "Studies related to ^{7}Be", Review Meeting on CRIB Activities, Jun 21-22, 2011, Center for Nuclear Study, University of Tokyo, Wako, Japan.

S. Kubono, "Summary of Research Activities at CRIB and the Scope", Review Meeting on CRIB Activities, Jun 21-22, 2011, Center for Nuclear Study, University of Tokyo, Wako, Japan.

S. Hayakawa, "Direct measurement of the 11C(alpha, p)14N reaction", Review Meeting on CRIB Activities, Jun 21-22, 2011, Center for Nuclear Study, University of Tokyo, Wako, Japan.

H. Yamaguchi, "Alpha-induced reaction studies using low-energy RI beams at CRIB", The 11th. International Symposium on Origin of Matter and Evolution of the Galaxies (OMEG11), Nov 14-18, 2011, Center for Nuclear Study, University of Tokyo, Wako, Japan.

S. Kubono, "Nuclear Physics Problems for Explosive Nucleosynthesis" The 11th. International Symposium on Origin of Matter and Evolution of the Galaxies (OMEG11), Nov 14-18, 2011, Center for Nuclear Study, University of Tokyo, Wako, Japan.

(Domestic Conference)

Hisayuki Torii, "ハードプローブの最先端",Heavy Ion Cafe/Pub 合同研究会 QDC 物質の最先端」June 8, 2011, Nagoya University, Japan

S.Ota, "Nucleon correlation and pickup reaction",RCNP 研究会リングサイクロトロン施設の将来-大強度超高品質ビームで切り拓く原子核科学のフロンティア」, Mar 21-23, RCNP, Osaka University, Japan

S. Kawase, "陽子ノックアウト反応による酸素同位体のスピン軌道分離の研究", the JPS fall meeting, Sep. 16–19, 2011,Hirosaki, Japan

Y. Kubota, T. Uesaka, S. Ota, M. Dozono, Y. Kikuchi, "不安定核実験のための高位置分解能中性子トラッカーの開発", at the JPS fall meeting, 16–19 Sep. 2011, Hirosaki University, Japan

T. Gunji for the ALICE Collaboration, "Dielectron measurement in p+p and Pb+Pb Collisions at LHC-ALICE", at the JPS Spring meeting, Mar. 24–27, 2012, Kansai-Gakuin University, Japan

T. Gunji, "日本核物理の将来：高エネルギー重イオンレポート", at the JPS fall meeting, symposium on "日本の核物理の将来・', Setp. 16–19, 2011, Hirosaki University, Japan

T. Gunji for the ALICE Collaboration, "Heavy Quarkonium Production in p+p and Pb+Pb Collisions at LHC-ALICE", at the JPS fall meeting, Setp. 16–19, 2011, Hirosaki University, Japan

S. Hayashi, H.Hamagaki, T.Gunji, M.Tanaka, H.Ikeda, M.Kurokawa, Y.Katayose: "Development of a Front-end ASIC for Forward Calorimeter in LHC-ALICE experiment" at the JPS fall meeting, Setp. 16–19, 2011, Hirosaki University, Japan

S. Hayashi, H.Hamagaki, T.Gunji, M.Tanaka, H.Ikeda, M.Kurokawa, Y.Katayose: "Development of a Front-end ASIC for Forward Calorimeter in LHC-ALICE experiment" at the JPS Spring meeting, Mar. 24–27, 2012, Kansei Gakuin University, Japan

R. Akimoto for the PHENIX Collaboration, "Performance of the silicon vertex tracker for the RHIC-PHENIX experiment", at the JPS fall meeting, Setp. 16–19, 2011, Hirosaki University, Japan

R. Akimoto for the PHENIX Collaboration "Current status of heavy quark measurement by using silicon vertex tracker at RHIC-PHENIX experiment", at the JPS Spring meeting, Mar. 24–27, 2012, Kwansei Gakuin University, Japan

Y.Hori for the ALICE collaboration, "The measurement of strange hadron elliptic flow and higher harmonics in sqrts$_{NN}$=2.76TeV Pb-Pb collisions at LHC", at the JPS fall meeting, Setp. 16–19, 2011, Hirosaki University, Japan

Y.Hori for the ALICE collaboration, "Charge dependent azimuthal correlation at sqrts$_{NN}$=2.76TeV Pb-Pb collisions at LHC-ALICE experiment", at the JPS Spring meeting, Mar. 24–27, 2012, Kwansei Gakuin University, Japan

T. Tsuji for the ALICE Collaboration, "Measurements of π^0 with respect to reaction plane in Pb+Pb collsions at $\sqrt{s_{NN}} = 2.76$ TeV", at the JPS Spring meeting, Mar. 24–27, 2012, Kansei Gakuin University, Japan

Y.Sekiguchi, *et al*, "Development and measurement of basic properties of Glass GEM" at the JPS Spring meeting, Mar. 24–27, 2012, Kansei Gakuin University, Japan

A. Takahara for the PHENIX Collaboration, "Study of J/ψ photoproduction in ultra-peripheral Au+Au collisions at $\sqrt{s_{NN}}$ =200GeV using the PHENIX detector"', at the JPS fall meeting, Setp. 16–19, 2011, Hirosaki University, Japan

H. Torii for the ALICE Collaboration, "QGP through hard probes at LHC-ALICE", at the JPS Autumn meeting, Sep. 17, 2011, Hirosaki University, Japan

H. Torii for the ALICE Collaboration, "Neutral meson production in p+p collisions at $\sqrt{s}$=0.9, 2.76, and 7TeV", at the JPS Spring meeting, Mar. 26, 2012, Kansai-Gakuin University, Japan

Y. Yamaguchi for the PHENIX collaboration, "Nuclear effects on direct photon production in 200GeV d+Au collisions measured at the PHENIX experiment" at the JPS annual meeting, Mar. 24–27, 2012, Kwansei Gakuin University, Hyogo, Japan

A. Nukariya, H.Hamagaki, Y.Tanaka, T.Fusayasu, T.Kawaguchi, "GEM を用いた新型 X 線検出器のデータ処理部の開発" at the JPS fall meeting, Setp. 16–19, 2011, Hirosaki University, Japan

item Ideguchi E., "Study of high-spin states by using energy degraded RI beams", Nuclear Physics with Energy-degraded RI Beam at RIBF, May 25, 2011, Wako, Japan.

Michimasa S., "Alpha-inducled transfer reactions with degraded beams", Nuclear Physics with Energy-degraded RI Beam at RIBF, May 25, 2011, Wako, Japan.

Michimasa S., " Gamma-ray Spectroscopy of neutron-rich Mg isotopes by using proton inelastic scattering ", RIBF ULIC and CNS Symposium on Frontier of Gamma-ray Spectroscopy (Gamma11), June 30 – July 2, 2011, Wako, Japan.

Sasamoto Y., "The super-allowed Fermi type charge exchange reaction (^{10}C,^{10}Bγ) for studies of isovector non-spin-flip monopole resonance", RIBF ULIC and CNS Symposium on Frontier of Gamma-ray Spectroscopy (Gamma11), June 30 – July 2, 2011, Wako, Japan.

Go S., "Digital pulse shape analysis method to extract interaction position for CNS-GRAPE", RIBF ULIC and CNS Symposium on Frontier of Gamma-ray Spectroscopy (Gamma11), June 30 – July 2, 2011, Wako, Japan.

Nakajima D., "First results of the HypHI Phase 0 experiment", RIBF ULIC and CNS Symposium on Frontier of Gamma-ray Spectroscopy (Gamma11), June 30 – July 2, 2011, Wako, Japan.

Ideguchi I., "Superdeformed Band in Asymmetric $N > Z$ Nucleus, ^{40}Ar, and High-Spin Level Structures in $A \sim 40$ Nuclei", RIBF ULIC and CNS Symposium on Frontier of Gamma-ray Spectroscopy (Gamma11), June 30 – July 2, 2011, Wako, Japan.

Michimasa S., "In-beam gamma-ray spectroscopy combined with transfer reactions" RCNP 研究会「リングサイクロトロン施設の将来 — 大強度超高品質ビームで切り拓く原子核科学のフロンティア —, Mar. 21–23, RCNP, Osaka University, Japan.

Shimoura S., "Physics by Brilliant project" RCNP 研究会「リングサイクロトロン施設の将来」— 大強度超高品質ビームで切り拓く原子核科学のフロンティア —, Mar. 21–23, RCNP, Osaka University, Japan.

Shimoura S., Ikeuchi Y., Otsuka T., "Analysis of gamma-ray emitting nuclides in the soils of Fukushima and surrounding area" 日本原子力学会,2012 年春の年会, Mar.19–21, Fukui University

Yokoyama R., Nishibata H., Hamatani N., Shimota T., Odahara A., Ito Y., Takatsu J., Tajiri K., Ideguchi E., "インビーム￥gamma 線核分光における蒸発粒子反跳効果の補正", the JPS Autumn meeting, Sep. 16–19, 2011, Hirosaki University, Aomori, Japan.

"4 中性子系質量欠損核分光実験に向けた、検出器読み出しシステムの開発と性能評価" Kisamori K., Shimoura S., Michimasa S., Ota S., Noji S., Tokieda H., Yokoyama R., Baba H., "4 中性子系質量欠損核分光実験に向けた、検出器読み出しシステムの開発と性能評価" the JPS Autumn meeting, Sep. 16–19, 2011, Hirosaki University, Aomori, Japan.

Shimoura S., "高アイソスピン核における一粒子冷気状態", the JPS Autumn meeting, Sep. 16–19, 2011, Hirosaki University, Aomori, Japan.

Ideguchi E., Go S., Miya H., Kisamori K., Takaki M., Ota S., Michimasa S., Shimoura S., Koike T., Yamamoto T., Shirotori K., Ito Y., Takatsu J., Suzuki T., Morikawa T., Shinozuka T., Yang S., Shizuma T., Oshima M., Koizumi M., Toh Y., Hatsukawa Y., Kimura A., Furutaka K., Nakamura S., Kitadani F., Harada H., Sugawara M., Watanabe Y.X., Hirayama Y., Oi M., "質量数 30 領域の高スピン状態の研究", the JPS Autumn meeting, Sep. 16–19, 2011, Hirosaki University, Aomori, Japan.

Takaki M., Matsubara H., Uesaka T., Aoi N., Ota S., Kawase S., Kawabata T., Kikuchi Y., Kisamori K., Kubota Y., Sakaguchi S., Sasamoto Y., Shimoura S., Suzuki T., Zenihiro J., Lee H.C., Takahisa K., Tamii A., Lee C.S., Dozono M., Tokieda H., Noji S., Hashimoto T., Fujii T., Maeda Y., Miki K., Michimasa S., Miya H., Yako K., Yokota K., Yokoyama R., Tang Leung Tsz, " 重イオン二重荷電交換反応を用いた ^{12}Be の研究", the JPS Autumn meeting, Sep. 16–19, 2011, Hirosaki University, Aomori, Japan.

Michimasa S., Yanagisawa Y., Inafuku K., Aoi N., Elekes Z., Fulop Zs., Ichikawa Y., Iwasa N., Kurita K., Kurokawa M., Machida T., Motobayashi T., Nakamura T., Nakabayashi T., Notani M., Ong H.J., Onishi T.K., Otsu H., Sakurai H., Shinohara M., Sumikama T., Takauchi S., Tanaka K., Togano Y., Yamada K., Yamaguchi M., Yoneda K., "陽子非弾性散乱を用いた Island of inversion 核の低励起状態の研究". the JPS Autumn meeting, Sep. 16–19, 2011, Hirosaki University, Aomori, Japan.

Fujii T., Ota S., Shimoura S., Aoi N., Takeshita E., Takeuchi S., Suzuki H., Baba H., Fukuchi T., Fukui T., Hashimoto Y., Ideguchi E., Ieki K., Iwasa N., Iwasaki H., Kanno S., Kondo Y., Kubo T., Kurita K., Minemura T., Michimasa S., Motobayashi T., Murakami T., Nakabayashi T., Nakamura T., Niikura J., Okumura T., Onishi T., Sakurai H., Shinohara M., Suzuki D., Suzuki M., Tamaki M., Tanaka K., Togano Y., Wakabayashi Y., Yamada I., "^{32}Mg 近傍不安定核の α 非弾性散乱", JPS Spring Meeting, March 24–27, 2012, Kwansei Gakuin University, Osaka, Japan.

Shimoura S., "土壌放射線マップの作成", JPS Spring Meeting, March 24–27, 2012, Kwansei Gakuin University, Osaka, Japan.

Takaki M., Matsubara H., Uesaka T., Aoi N., Ota S., Kawase S., Kawabata T., Kikuchi Y., Kisamori K., Kubota Y., Sakaguchi S., Sasamoto Y., Shimoura S., Suzuki T., Zenihiro J., Lee H.C., Takahisa K., Tamii A., Lee C.S., Dozono M., Tokieda H., Noji S., Hashimoto T., Fujii T., Maeda Y., Miki K., Michimasa S., Miya H., Yako K., Yokota K., Yokoyama R., Tang Leung Tsz, "超多重項間遷移を用いた ^{12}C(^{18}O,^{18}Ne 測定による ^{12}Be 核の研究", JPS Spring Meeting, March 24–27, 2012, Kwansei Gakuin University, Osaka, Japan.

Lee C.S., Uesaka T., Ota S., Sasano M., "重イオン蓄積リングの核反応実験への適用可能性の検討", JPS Spring Meeting, March 24–27, 2012, Kwansei Gakuin University, Osaka, Japan.

Tokieda H., Ota S., Dozono M., Michimasa S., Hashimoto T., Matsubara H., Kawase S., Kikuchi Y., Kubota Y., Lee C.S., Gunji T., Yamaguchi H., Kahl D.M., Akimoto R., Hamagaki H., Kubono S., Uesaka T., "重水素ガスを用いた GEM の応答", JPS Spring Meeting, March 24–27, 2012, Kwansei Gakuin University, Osaka, Japan.

Kikuchi Y., Ota S., Matsubara H., Kubota Y., Lee C.S., Uesaka T., "大強度不安定核ビーム実験のための Imm 核プラスチックシンチレータを用いたホドスコープの開発", JPS Spring Meeting, March 24–27, 2012, Kwansei Gakuin University, Osaka, Japan.

Ideguchi E.,, Sarantites D.G., Reviol W., Chiara C.J., Devlin M., Baktash C., Janssens R.V.F., Rudolph D., Axelsson A., Carpenter M.P., Galindo-Uribarri A., LaFosse D.R., Lauritsen T., Lerma F., Lister C.J., Reiter P., Seweryniak D., Weiszflog M., Wilson J.N., "^{42}Ca の高スピン状態の研究", JPS Spring Meeting, March 24–27, 2012, Kwansei Gakuin University, Osaka, Japan.

Shimoura S., "原子核と放射線ー放射線って何？それはどこから、どうして、どのように？ー学校の先生のための放射線勉強会", May 8 and July 16, 2011, University of Tokyo, Tokyo, Japan.

Shimoura S., "土壌中のガンマ線放出核種分析による福島周辺放射線マップ" 理学系研究科シンポジウム "大震災復興へ向けての理学者の役割",Feb. 3, 2012, University of Tokyo, Tokyo, Japan.

Shimoura S., "放射線とは何か" 東京大学理工医農 4 研究科横断抗議 "放射線を知る",Nov. 11, 2012, University of Tokyo, Tokyo, Japan.

松原礼明

"sd 殻領域の M1 遷移強度分布とクエンチング",May 20, 2011, Chiba University, Chiba, Japan.

T. Gunji, "Experimental Studies of Hot and Dense QCD medium at LHC-ALICE" at the 20th Hadron Seminar at JAEA, Oct. 5t 2012, JAEA, Japan

H. Hamagaki, "New progress in the experimental study of high-energy heavy-ion collisions", presented in the colloquium of Research group Physics II, the Graduate School of Science, Kyoto University, 28 June 2011.

H. Torii, "クォークグルーオンプラズマ物性研究が開く扉", 東大駒場核理論研究室セミナー, July 6, 2011, Tokyo University, Japan

H. Hamagaki, "Ultra-hot QCD matter studied using high-energy heavy-ion collisions", a series of lectures, made for the Division of Physics and Astronomy, the Graduate School of Science, Kyoto University, 28 - 30 June 2011.

Radioactive nuclear beam R&D group
IPNS (Institute for Particle and Nuclear Studies)
KEK (High Energy Accelerator Research Organization)

Publications

[Journal]

(Original Papers) *Subject to Peer Review

Imai N., Hirayama Y., Watanabe Y.X., Teranishi T., Hashimoto T., Hayakawa S., Ichikawa Y., Ishiyama H., Jeong S.C., Kahl D., Kubono S., Miyatake H., Ueno H., Yamaguchi H., Yoneda K., Yoshimi A.: "Isobaric analog resonances of the N = 21 nucleus ^{35}Si", Phys. Rev. C**85** (2012) 034313,*

Hirayama Y., Mihara M., Wanatabe Y.X., Jeong S.C., Miyatake H., Momota S., Hashimoto T., Imai N., Matsuta K. Ishiyama H.,, Ichikawa S., Ishii T., Izumikawa T., katayama I., kawakami H., Kawamura H., Nishinaka I., Nishio K., Makii H., Mitsuoka S., Osa A., Otokawa Y., Sato T.K.: "Tilted–foil technique for produceing a spin–polarized radioactive isotope beam", Eur. Phy. J. A. **48** (2012) 54,*

Okada M., Niki K., Hirayama Y., Imai N., Ishiyama H., Jeong S.C., Katayama I., Miyatake H., Oyaizu M., Watanabe Y.X., Arai S., Makii H., Wakabayashi Y., "Low–background prebunching system for heavy–ion beams at the Tokai radioactive ion accelerator complex", Phys. Rev. ST Accel. Beams **15** (2012) 030101,*

Ishiyama .H, Yamaguchi K., Mizoi Y., Watanabe Y.X., Das S.K., Hashimoto T., Miyatake H., Hirayama Y., Imai N., Oyaizu M., Jeong S.C., Fukuda T., Mitsuoka S., Makii H., Sato T.K.,: "GEM–MSTPC: An active–target type detector in low–pressure He/CO2 mixed gas", J. Instrum. **7** (2012) C03036,*

Jeong S.C., Oyaizu M., Imai N., Hirayama Y., Ishiyama H., Miyatake H., Niki K., Okada M., Watanabe Y.X., Otokawa Y., Osa A., ichikawa S., "Wall–loss distribution of charge breeding ions in an electron cyclotron resonance ion source", Rev. Sci. Insturm. **83** (2012) 02A910,*

Hirayama Y., Mihara M., Wanatabe Y.X., Jeong S.C., Imai N., Matsuta K., Miyatake H., Hashimoto T., Ishiyama H., Ichikawa S., Ishii T., Izumikawa T., katayama I., kawakami H., Nishinaka I., Nishio K., Makii H., Mitsuoka S., Momota S., Osa A., Otokawa Y., Sato T.K., Wakabayashi Y.: "Spin–polarization of radioactive $^{123}In_{g.s.}$ by the tilted–foil method", Eur. Phys. J. A. **47**, (2011) 138,*

Sugai I., Takeda Y., Kawakami H., Ohta N., Makii H., Miyatake H.: "Adhesion improvement HIVIPP ^{12}C targets on Au backings", Nucl. Instrum. Methods A **655**, (2011) 24,*

Kura K., Tajiri K., Shimoda T., Odahara A., Hori T., Kazato M,: Masue T,: Suga M,: Takashima A,: Suzuki T,: Fukuchi T,: Hirayama Y,: Imai N,: Miyatake H,: Pearson M,: Levy C.D.P.,: Jackson K.P.: "Structure of ^{28}Mg studies by β–decay spectroscopy of spin–polarized ^{28}Na: The first step of systematic studies on neutron–rich Mg isotopes", Phys. Rev. C **85**, (2012) 034310,*

[Book・ Proceedings]

(Original Papers) *Subject to Peer Review

鄭 淳讃, "Radioisotopes – Applications in Physical Science (Chapter 4)", Oct. 2011, INTEC Co., ISBM = 978–953–307–510–5

Oral Presentations

(International Conference etc.)

Hirayama Y.,: Miyatake H.,: Jeong S.C.,: Ishiyama H.,: Imai N.,: Watanabe Y.X.,: Oyaizu M.,: Niki K.,: Okada M.,: Wada M.,: Sonoda T.,: Takamini A.,: Ito Y.,: Matsuo Y.,: Furukawa T.,: Van Duppen P.,: Kudryavtsev Y.,: Huyse M.: "Beta-decay spectroscopy of r–process nuclei using KEK isotope separation system", The first international conference on Advances in Radioactive Isotpoe Science (ARIS–2011), 29 May – 3 June, 2011, Leuven, Bergium

Sonoda T.,: Wada M.,: Matsuo Y.,: Kubo T.,: BigRIPS team .,: Tomita H.,: Sakamoto C.,: Shinozuka T.,: Wakui T.,: Ito Y.,: Nakamura S.,: Schry P.,: Miyatake H.,: Imai N.,: Ishiyama H.,: Hirayama Y.,: Watanabe Y.X.,: Jeong S.C.,: Furukawa T.,: Okada K.,: Takamine A.,: Huyse M.,: Kudryavtsev Y.,: Van Duppen P.,: "Development of the resonance ionization laser ion source for parasitic RI–beam production and in–gas–cell/ jet laser spectroscopy as SLOWRI RIKEN", The first international conference on Advances in Radioactive Isotpoe Science (ARIS–2011), 29 May – 3 June, 2011, Leuven, Bergium

Watanabe Y.X.: "Experimental project for production of heavy neutron–rich nuclie by multinucleon transfer reaction (KISS project", YIPQS Long –term workshop Dynamics and Correlations in Exotic Nuclei (DCEN2011), 20 –28 October, 2011, Yukawa Institute for Theoretical Physics, Kyoto, Japan

Makii H.: "Measurement of the 12C(alpha, gamma)16O reaction at TRIAC", The 11th International Symposium on Origin of Matter and Evolution of Galaxies (OMEG11), 14-17, November 2011, RIKEN, Japan

Ishiyama H.: "Experimental studies of astrophysical reaction rates using low–energy radioactive nuclear beams", Korea-Japan Common Symposium on 2011 Korea Physics Society, 20, October 2011, Pusan, Korea

Ishiyama H., Yamaguchi K., Mizoi Y., Watanabe Y.X., Das S.K., Hashimoto T., Miyatake H., Hirayama Y., Imai N., Oyaizu M., Jeong S.C., Fukuda T., Mitsuoka S., Makii H., Sato T.K.: "GEM-MSTPC: An active–target type detector in low–pressure He/CO2 mixed gas", 2nd International Conferenece on Micro Pattern Gaseous Detectors (MPGD2011), 29 August–1 September 2011, Koube, Japan

VIII. LIST OF PREPRINTS

(2011 April ～2012 March)

RIKEN-MP

17 H. Ohno, S. Aoki et al. "Charmonium spectral functions with the variational method in zero and finit" Apr, 2011

18 Y. Hidaka, D. Satow et al. "Ultrasoft Fermionic Mode in Yukawa Theory at High Temperature nuclei" May, 2011

19 Y. Kanada-En'yo, Y. Hidaka "Alpha-cluster structure and density wave in oblate nuclei" Apr, 2011

20 T. Jittoh, K. Kohri et al. "Big-bang nucleosynthesis with a long-lived charged massive particle includi" May, 2011

21 T. Kimura "Matrix model from N = 2 orbifold partition function" May, 2011

22 H. Saito, S. Ejiri et al. "Phase structure of finite temperature QCD in the heavy quark region" June, 2011

23 T. Azeyanagi, T. Kobayashi et al. "D term and gaugino masses in gauge mediation" June, 2011

24 T. Kojo, Y. Hidaka et al. "Interweaving Chiral Spirals" July, 2011

25 M. Eto, K. Hashimoto et al. "Anomaly-induced charges in baryons" Sep, 2011

26 T. Kimura, M. Nitta "Vortices on Orbifolds" Aug, 2011

27 F. Halzen, K. Igi et al. "Total Hadronic Cross Sections and π^¥mp π^+ Scattering" Oct, 2011

28 T. Kimura "Beta-ensembles for toric orbifold partition function" Sep, 2011

29 D. Satow, Y. Hidaka "Fermion Spectrum at Ultrasoft Region in a Hot QED/QCD Plasma" Sep, 2011

30 T. Kimura, T. Nishioka "The Chiral Heat Effect" Sep, 2011

31 Y. Maezawa "Heavy quark free energy and ..." Dec, 2011

33 T. Misumi, M. Creutz et al. "Aoki Phases in Staggered-Wilson Fermions" Oct, 2011

34 T. Kimura, M. Creutz et al. "Index Theorem and Overlap Formalism with Naive and Minimally Doubled Fermio" Aug, 2011

35 Y. Hidaka, N. Yamamoto "No-Go Theorem for Critical Phenomena in Large-Nc QCD" Oct, 2011

36 T. Kimura, S. Komatsu et al. "Revisiting symmetries of lattice fermions via spin-flavor representation" Nov, 2011

37 Y. Hidaka, D. Satow et al. "Ultrasoft Fermionic Modes at High Temperature" Nov, 2011

38 M. Murata, M. Schnabl "Multibrane Solutions in Open String Field Theory" Dec, 2011

39 T. Kimura "Spinless basis for spin-singlet FQH states" Jan, 2012

41 K. Hashimoto, N. Iizuka "A Comment on Holographic Luttinger Theorem" Mar, 2012

42 S. Aoki, K. Hashimoto et al. "Matrix Theory for Baryons: An Overview of Holographic QCD for Nuclear Physics" Mar, 2012

43 Y. Hidaka "Counting rule for Nambu-Goldstone modes in nonrelativistic systems" Mar, 2012

RIKEN-NC-NP

56 K. Iida, S. Koide et al. "Proton inelastic diffraction by a black nucleus and the size of excited nuclei" June, 2011

57 N. Hinohara, K. Sato et al. "Shape fluctuations in the ground and excited 0+ states of 30Mg and 32Mg" Sep, 2011

58 S. Ebata, T. Nakatsukasa and T. Inakura "Study of pygmy dipole resonance with a new time-dependent mean field theory" Oct, 2011

59 K. Sato, N. Hinohara et al. "Microscopic approach to large-amplitude deformation dynamics with local QRP" Oct, 2011

60 S. Ebata, T. Nakatsukasa and T. Inakura "Systematic study of low-lying E1 strength using the time-dependent mean fie" Jan, 2012

61 Y. Togano, Y. Yamada et al. "Hindered proton collectivity in 28S: Possible magic number at Z=16" Jan, 2012

63 N.D. Dang "Damping of giant dipole resonances in hot rotating nuclei" Feb, 2012

64 N.D. Dang "Viscosity of hot nuclei" Sep, 2011

67 S. Sakaguchi, T. Uesaka et al. "Elastic Scattering of Neutron-Rich Helium Isotopes" May, 2011

RIKEN-QHP

1 T. Aoyama, M. Hayakawa et al. "Tenth-order lepton anomalous magnetic moment -- Sixth-order vertices containg vacuum-polarization subdiagrams" May, 2011

2 M. G. Endres, D. B. Kaplan et al. "Noise, sign problems, and statistics" Jun, 2011

3 M. G. Endres, D. B. Kaplan et al. "Lattice Monte Carlo calculations for unitary fermions in a harmonic trap" Jun, 2011

5 H. Saito, S. Ejiri et al. "Phase structure of finite temperature QCD in the heavy quark region" Jun, 2011

6 T. Doi, S. Aoki et al. "Exploring three-nucleon forces in lattice QCD" Jun, 2011

7 S. Kamata and H. Suzuki "Numerical simulation of the N=(2,2) Landau-Ginzburg model" Jul, 2011

8 S. Aoki, N. Ishii et al. "Extraction of Hadron Interactions above Inelastic Threshold in Lattice QCD" Jun, 2011

9 Y. Akamatsu, H. Hamagaki et al. "Can transport peak explain the low-mass enhancement of dileptons at RHIC?" Jun, 2011

10 Y. Akamatsu, H. Hamagaki et al. "Low-mass dilepton production through transport process in quark-gluon plasma" Jul, 2011

11 A. Rothkopf, T. Hatsuda et al. "Complex heavy-quark potential at finite temperature from lattice QCD" Aug, 2011

12 T. Aoyama, M. Hayakawa et al. "Tenth-order QED lepton anomalous magnetic moment---Eighth-order vertices containing a second-order vacuum polarization" Jan, 2011

13 J. Lee, Michael M. G. Endres et al. "Extended study for unitary fermions on a lattice using the cumulant expansion technique" Nov, 2011

14 T. Aoyama, M. Hayakawa et al. "Tenth-order QED contribution to the lepton anomalous magnetic moment -- Sixth-order vertices containing an internal light-by-light-scattering subdiagram" Jan, 2012

15 H.Suzuki "Supersymmetry, chiral symmetry and the generalized BRS transformation in lattice formulations of 4D N=1 SYM" Feb, 2012

16 M. G. Endres, D. B. Kaplan et al. "Lattice Monte Carlo calculations for unitary fermions in a finite box" Mar, 2012

33 T. Umeda, S. Aoki et al. "Equation of state in 2+1 flavor QCD with improved Wilson quarks by the fixed scale approach" Mar, 2012

34 H. Saito, S. Aoki et al. "Finite density QCD phase transition in the heavy quark region" Feb, 2012

35 N. Ishii et al. "Hadron-Hadron Interactions from Imaginary-time Nambu-Bethe-Salpeter Wave Function on the Lattice" Mar, 2012

36 S. Ejiri, S. Aoki et al. "Numerical study of QCD phase diagram at high temperature and density by a histogram method" Mar, 2012

37 K. Hamaguchi, T.Hatsuda et al. "Stau-catalyzed d-t Nuclear Fusion" Feb, 2012

41 T. Hatsuda "Hadron interactions from lattice QCD" Jan, 2011

CNS-REP

87 H. Yamaguchi, T. Hashimoto, S. Hayakawa, D.N. Binh, D. Kahl, S. Kubono, Y. Wakabayashi, T. Kawabata and T. Teranishi, "Alpha resonance structure in ^{11}B studied via resonant scattering of $^{7}Li+\alpha$" CNS-REP 87 Feb. 2011

88 T. Gunji "CNS Annual Report 2010" CNS-REP 88 Feb. 2012

IX. LIST OF SYMPOSIA
& WORKSHOPS

(2011 April ~2012 March)

1 "International Symposium on Functional Materials Science(ISFMS 2011)" Bali, Indonesia Apr. 27-28

2 "RBRC workshop on Opportunities for Drell-Yan Physics at RHIC" RBRC May 11-13

3 "E(U)RICA International Workshop" RNC May 23-24

4 "Quarkonium Workshop" RBRC Jun. 6-17

5 "Hadron and Nuclear Physics at J-PARC" KEK Jun. 10-11

6 "Frontier of gamma-ray spectroscopy (gamma11)" RNC Jun. 30-Jul. 2

7 "PHENIX Spinfest 2011" RNC Jul.1-31

8 "Methodology in Heavy Ion Science" at Oiso, Kanagawa Jul. 4-6

9 "The 10th CNS International Summer School" CNS Wako Campus Sep. 26-Oct.01

10 "RBRC workshop on Opprotunities for Polarized He-3 in RHIC and EIC" RBRC Sep. 28-30

11 "Future Directions in High Energy QCD" RNC Oct. 20-22

12 "The 11th International Symposium on Origin of Matter and Evolution of Galaxies (OMEG11)" RNC Nov. 14-17

13 "The 11th International Symposium on Origin of Matter and Evolution of Galaxies" RNC Nov. 14-17

14 "RBRC workshop on Fluctuations, Correlations and RHIC low Energy Runs" RBRC Oct. 3-5

15 "RBRC workshop at Wako on Future Directions in High Energy QCD" RBRC Oct. 20-22

16 "Uncovering 10 fundamental issues in mathematical sciences" RIKEN Dec. 26-29

17 "The 3rd Joint ISIS/RIKEN Muon Facility Development Workshop" Abingdon Dec.7

18 "The next step to advanced mutagenesis in modern genome science era" RIKEN Jan. 19-20

19 "Review Meeting on CRIB Activities." CNS Wako Campus Jun. 21-22

X. LIST OF SEMINARS

(2011 April ~2012 March)

Theoretical Research Division

1 Walter F. Henning (RNC) "Towards the Extremesof the Nuclear Landscape" Apr. 07

2 Paul D. Stevenson (University of Surrey) "Skyrme Tensor Force in Collisions and Resonances" Apr. 13

3 Tohru Kojo (RBRC) "Quarkyonic Matter" Apr. 15

4 Hideki Takayasu (Sony Computer Science Laboratories Inc. and Meiji Institute for Advanced Study of Mathematical Sciences) "Langevin's view of financial markets" Apr. 18

5 Tadahiro Suhara (Kyoto University) "Various cluster structures in C isotopes" Apr. 27

6 Kouji Kashiwa (RBRC) "Investigation of QCD phase structure from imaginary chemical potential" May 09

7 Tadahiro Suhara (Hokkaido University) "Shape Coexistence and Shell Erosion of N=28 System - the case of 43S - " May 11

8 Masaki Fukushima (University of Tokyo) "Recent progress in the observation of the highest energy cosmic rays" May 17

9 Kimitoshi Kono (Low Temperature Physics Laboratory) "Rotating "super"solid He: an evidence for supersolidity" May 23

10 Masaaki Kimura (Hokkaido University) "Shape Coexistence and Shell Erosion of N=28 System - the case of 43S -" May 31

11 Akihiro Tanaka (National Institute for Materials Science) "Emergent Riemann-Cartan spacetime in topological insulators" Jun. 13

12 Tatsuo Azeyanagi (RIKEN) "Recent progress in Large N reduction" Jun. 15

13 Naoto Tanji (KEK) "Dynamics of non-perturbative particle production in strong electromagnetic fields" Jun. 20

14 Yasushi Matsuo (University of Tokyo) "Review Meeting on CRIB Activities" Jun. 21-22

15 Yutaka Matsuo "A Non-Abelian Self-Dual Gauge Theory in 5+1 Dimensions" Jun. 27

16 Kazuo Hosomichi (Kyoto University) "LeSUSY Gauge Theories on Squashed Three-Spheres" Jun. 27

17 Hiroshi Toki (RCNP) "New multiconductor transmission-line theory and the mechanism ofnoise reduction" Jun. 29

18 Hiroshi Toki (RCNP) "Extended Brueckner-Hartree-Fock theory in many body system - Importance of pion in nuclei -" Jun. 30

19 Takahiro Sagawa (Kyoto University) "Thermodynamics of Information Processing and Maxwell's Demon" Jul. 4-5

20 Ugajin Tomonori (University of Tokyo) "Holographic Conductivity in Disordered Systems" Jul. 11

21 Tunoru Shintake (Innovative Light Sources Division) "SACLA: SPring-8 Angstrom Compact free electron Laser, history of technical development and future" Jul. 19

22 Satoru Hirenzaki (Nara Women's University) "Mesic Atoms and Mesic Nuclei" Jul. 21

23 Ken Sekimoto (Universite Paris-Didero (Paris7)/ESPCI) "Disentanglement of energetics and momentum transfer in non-equilibrium steady states" Sep. 06

24 Norihiro Iizuka (CERN) "What is the gravity dual of the confinement/deconfinementtransition in holographic QCD?" Sep. 26

25 Norihiro Iizuka (CERN) "Black Holes and Non-Fermi Liquids" Sep. 26

26 Taro Kimura (RIKEN /University of Tokyo) "Chiral heat effect" Oct. 17

27 Toshiyuki Azuma (Atomic, Molecular & Optical Physics Lab.) "Frontier of AMO (Atomic, Molecular and Optical) physics" Oct. 25

28 Yasuro Funaki (RNC) "Alpha clustering and condensation in 16O" Oct. 26

29 Hideaki Iida (RNC) "A review and our study on finite density QC" Nov. 14

30 Shigehiro Yasui (KEK) "Non-Abelian statistics of quantum vortices with Majorana and Dirac zero modes" Nov. 14

31 Yasunori Yamazaki (Atomic Physics Laboratory, ASI, RIKEN) "Recent progress on cold antihydrogen research" Nov. 22

32 Shingo Kobayashi (University of Tokyo) "Vortex core states in spinor Bose-Einstein condansates" Dec. 09

33 Toshiko Kojita (Kyoto University) "Winding number in string field theory" Dec. 12

34 Yoshiro Takahashi (Kyoto University) "Ultracold ytterbium Atoms : Application to Quantum Simulation and Precision Measurement" Dec. 20

35 Yoshifumi Shimizu (Kyushu University) "Study of tetrahedral nuclear states by quantum number projection method" Dec. 22

36 Hideko Nagahiro (Nara Women's University) "Composite and elementary natures of hadrons -- Study of mixing properties of a1(1260) --" Dec. 22

37 Tatsuma Nishioka (Kyoto University) "On gauge theories on three-sphere" Jan. 10

38 Sumio Iijima (Meijo University, AIST/NTRC, NEC Co.) "Nano Carbon: Science and Applications" Jan. 17

39 Tetsutaro Higaki (RIKEN) "Moduli Stabilization and Supersymmetry Breaking for String Phenomenology" Jan. 23

40 Shoji Asai (University of Tokyo) "The Latest Results of LHC" Jan. 24

41 Aleksey Cherman (University of Cambridge) "Sneaking up on dense QCD using large N methods" Feb. 06

42 Martin Schnabl (Institute of Physics ASCR) "The landscape of Open String Field Theory" Feb. 13

43 Hiroyuki Sakuragi (Osaka City University) "Microscopic interaction models for heavy-ion reactions - present status and future perspective -" Feb. 14

44 Mitsutoshi Fujita (University of Washington) "SL(2,Z) duality on AdS/BCFT" Feb. 24

45 Taizan Watari (University of Tokyo) "Studying Generalized Parton Distribution in Holographic QCD" Feb. 27

46 Andrew W. Steiner (University of Washington) "Monthly Colloquium:Neutron Stars as a Laboratory for the Nuclear Symmetry Energy" Feb. 28

47 Masaki Oshikawa (University of Tokyo) "Gauge invariance, commensurability and Luttinger's theorem" Mar. 02

48 Shigehiro Nagataki (Kyoto University) "General Relativistic Magneto-Hydrodynamic Simulations of Gamma-Ray Bursts" Mar. 5

49 Hirohiko Shimada (Ecole Normale Superieure) "Aspects of Replica Method and Renormalization Group for Disordered Systems" Mar. 15

50 Kengo Maeda (Shibaura tech.) "Non-linear or anisotropic black hole solutions in asymptotically AdS spacetime" Mar. 21

Sub Nuclear Research Division

1 Masanori Hanada (University of Washington) "Nuclear theory/RIKEN seminar" Apr. 01

2 Xiangdong Ji (University of Maryland) "Gauge symmetry and spin structure of the proton" Apr. 06

3 Eduardo Pontón (Columbia University) "Warped Radion Dark Matter" Apr. 06

4 Joachim Bartels (Hamburg University) "RIKEN Lunch Seminar" Apr. 07

5 Elisabetta Furlan (BNL) "Lunch Seminar" Apr. 08

6 Laura Tolos (Barcelona) "Nuclear theory/RIKEN seminar" Apr. 12

7 Risdiana (RNC) "mSR Study of Charge Carrier Diffusion in Regioregular Poly (3-alkylthiophene)" Apr. 12

8 Yanou Cui (Harvard) "New Perspectives on Dark Matter-Baryon Coincidence" Apr. 13

9 Heechang Na (Ohio State University) "Heavy-light meson decays from HPQCD" Apr. 20

10 Prasad Hegde (BNL) "RIKEN Lunch Seminar" Apr. 21

11 Prerit Jaiswal (BNL/YITP) "Lunch Seminar" Apr. 22

12 Jim Lattimer (Stony Brook University) "Nuclear theory/RIKEN seminar" Apr. 22

13 Boris Kerbikov (ITEP) "Quark matter conductivity in strong magnetic field" Apr. 29

14 Ricardo Torres Andrés (Madrid University) "Isospin breaking and chiral symmetry restoration" May 05

15 Frank Petriello (Northwestern University & Argonne National Laboratory) "Nuclear theory/RIKEN seminar" May 06

16 Stefania Gori (University of Chicago) "Flavor transitions in two Higgs doublet models" May 18

17 Christine Davies (University of Glasgow) "Joint RIKEN/HET lunch seminar" May 19

18 Yasumichi Aoki (Nagoya) "Lunch Seminar" May 20

19 Bernd Kniehl (Hamburg University) "Testing NRQCD factorization in J/Psi production at NLO" May 27

20 Kazuki Ueno (RNC) "Gamma-ray imaging camera based on gaseous tracking detector" Jun. 03

21 Jessie Shelton (Yale University) "The Top Forward-Backward Asymmetry at Tevatron and the LHC" Jun. 15

22 Toru Kojo (RBRC) "Interweaving Chiral Spirals at large density" Jun. 23

23 Shaouly Bar-Shalom (Technion) "4th generation & 2HDMs - Models for TeV-scale compositeness" Jun. 24

24 Brian Tiburzi (MIT) "Lattice QCD in External Fields" Jun. 27

25 Leo Stodolsky (Max Planck) "Recent Results of the CRESST Dark Matter Search" Jun. 29

26 Giorgio Torrieri (Frankfurt University) "The phase diagram in T-mu-Nc space" Jun. 30

27 Eigo Shintani (RBRC) "HET/RIKEN" Jul. 01

28 Adam Szczepaniak (Indiana University) "Nuclear theory/RIKEN seminar" Jul. 01

29 Leo Stodolsky (Max Planck) "The photon number integral." Jul. 06

30 Andrey Leonidov (Lebedev Institute) "Color decoherence in QCD jets and gluon Cherenkov radiation in dense medium" Jul. 07

31 Ivan Horvath (Kentucky) "HET/RIKEN Lunch Seminar" Jul. 08

32 Giovanni Chirilli (Lawrence Berkeley National Laboratory) "Nuclear theory/RIKEN seminar" Jul. 08

33 Tsukasa Tada (RNC) "Defying Gravity --Quest for the ultimate theory of the universe" Jul. 12

34 Qamar Usmani (University Malaysia Perlis) "Nuclear Matter Properties, Clustering at the Nuclear Surface and Symmetry Energy" Jul. 15

35 Yasufumi Araki (University of Tokyo) "Chiral symmetry restoration in monolayer graphene by Kekule distortion" Jul. 21

36 Pilar Staig & Edward Shuryak (Stony Brook University) "Acoustic oscillations in higher harmonics of Big and Little Bans" Jul. 22

37 John Laiho (Glasgo University) "Asymptotic Safety and Lattice Quantum Gravity" Jul. 28

38 Michael Lublinsky (Ben Gurion University) "Nuclear theory/RIKEN seminar" Jul. 29

39 Taichi Kawanai (University of Tokyo) "Interquark potential for the charmonium system with almost physical quark masses" Aug. 04

40 David Atwood (Iowa State Universtiy) "HET/RIKEN LUNCH SEMINAR" Aug. 05

41 Hiromichi Nishimura (Washington University) "Phases of QCD-like Theories on R3 X S1" Aug. 05

42 Angel Gomez Nicola (Universidad Complutense) "Chiral Symmetry and meson gases: recent developments" Aug. 12

43 Shigemi Ohta (RBRC) "RIKEN Lunch Seminar" Aug. 18

44 Antal Jakovac (Technical University Budapest) "Quasiparticle description of the hadronic phase and the chiral transition" Aug. 19

45 Ernest Ma (UC-Riverside) "Observable Scalars from Neutrino Mixing" Aug. 24

46 Sean Gavin (Wayne State University) "RIKEN Lunch Seminar" Aug. 25

47 Hong Liu (Massachusetts Institute of Technology) "Nuclear theory/RIKEN seminar" Aug. 26

48 Alan Drew (Queen Mary Univiersity) "Local probe investigation of spin transport and dynamics in organic semiconductors" Sep. 07

49 Mohammed Mia (Columbia University) "A holographic model for large N thermal QCD" Sep. 09

50 Jian-ping Chen (Jefferson Lab) "Transverse Spin and Transverse Structure of the Nucleon" Sep. 15

51 Masakiyo Kitazawa (Osaka University) "RIKEN Lunch Seminar" Sep. 22

52 Yuji Hirono (University of Tokyo) "Interaction of non-Abelian vortices with quasiparticles in high density QCD" Sep. 29

53 David Lin (NCTS) "Strong yukawa models on the lattice" Sep. 30

54 Peter Arnold (University of Virginia) "New results on "jet" stopping in AdS/CFT" Sep. 30

55 Ethan T. Neil (Fermilab) "Searching for (Nearly) Conformal Dynamics on the Lattice" Oct. 05

56 Shinji Ejiri (Niigata University) "Histogram method for the calculation of QCD equation of state at finite density" Oct. 07

57 Adam Bzdak (RBRC) "Symmetric forward-backward correlations as seen at RHIC" Oct. 13

58 Miller Mendoza Jimenez (ETH, Zurich) "Solving the Boltzmann Equation for Relativistic Systems" Oct. 14

59 Tobias Toll (BNL) "Calculating the incoherent and total cross-sections in exclusive diffractive vector " Oct. 27

60 Vladimir Skokov (BNL) "Probing QCD phase diagram with charge fluctuations" Nov. 03

61 Eigo Shintani (RBRC) "HET/RIKEN LUNCH Seminar" Nov. 04

62 Tomomi Ishikawa (RBRC) "Exploring dynamical QED effects with the reweighting method" Nov. 10

63 Ted Rogers (Stony Brook) "Factorization with transverse momentum dependent parton distribution functions" Nov. 17

64 Zyun F. Ezawa (Tohoku University) "Noncommutative Geometry and Josephson Effects in Bilayer Quantum Hall System" Nov. 28

65 Yu Maezawa (BNL) "Anomaly-induced charges in nucleons" Dec. 01

67 Philip King (ISIS, STFC) "Overview of Rutherford Appleton Laboratory and the RIKEN-RAL future perspective" Dec. 01

68 Naoki Yamamoto (University of Washington) "QCD phase diagram: universality and continuity" Dec. 02

69 Claudio Rebbi (Boston University) "Hybrid Monte Carlo simulation of graphene" Dec. 07

70 Yan-Qing Ma (BNL) "Understanding the heavy quarkonia production at hadron colliders within NRQCD factorization" Dec. 08

71 Aleksi Kurkela (McGill University) "Thermalization in collisions of extremely large nuclei at extremely large energies" Dec. 09

72 Anastasios Taliotis (Crete University) "Nuclear Theory/RIKEN Seminar" Dec. 16

73 Su Huong Lee (Yonsei University) "A look again at eta' in medium" Dec. 19

74 Purushottam Dixit (BNL) "Ions in biology: Water and Proteins" Jan. 12

75 Scott Pratt (Michigan State University) "Correlations from charge and momentum conservation -- How they can be used to determine fundamental properties of the QGP" Jan. 13

76 Dru B. Renner (Jefferson Lab.) "Nonperturbative QCD vacuum polarization corrections" Jan. 18

77 Mike Creutz (BNL) "HET/RIKEN LUNCH Seminar" Jan. 20

78 Abhishek Agarwal (American Physical Society) "Mass-Gaps, Gluon mass-terms and Supersymmetry in Three Dimensions" Jan. 20

79 Jakub Wagner (National Center for Nuclear Research) "Generalized Parton Distibutions in Ultraperipheral Production of Lepton Pairs" Jan. 27

80 Gockce Basar (Stony Brook) "Instantons and sphalerons in magnetic field" Feb. 02

81 Kresimir Kumericki (University of Zagreb) "Studying 3D structure of proton with neural networks" Feb. 03

82 Takao Sakaguchi (BNL) "Direct photon physics in heavy ion collisions: Current status and Future" Feb. 09

83 Tom DeGrand (University of Colorado at Boulder) "Lattice vs. Technicolor" Feb. 22

84 Frasher Loshaj (Stony Brook) "Jet Fragmentation From Two Dimensional Field Theory" Feb. 23

85 Dieter Mueller (BNL) "Deeply Virtual Compton Scattering at a proposed high-luminosity Electron-Ion-Collider" Feb. 24

86 Adrian Dumitru (CUNY and RBRC) "KNO scaling of fluctuations in pp and pA, and higher-order eccentricities in heavy-ion collisions" Mar. 01

87 Berndt Mueller (Duke University) "Hydrodynamic Fluctuations in Relativistic Heavy Ion Collisions" Mar. 02

88 Kenji Morita (Kyoto University) "Baryon number probability distribution near a phase transition" Mar. 08

89 Dietrich Bodeker (Bielefeld) "Thermal production of relativistic right-handed neutrinos" Mar. 14

90 Christopher Herzog (YITP of Stony Brook) "The Spin of Holographic Electrons at Nonzero Temperature and Density" Mar. 15

91 Jamal Jalilian-Marian (Baruch College) "Di-hadron angular correlations in Color Glass Condensate formalism: multi-gluon correlators" Mar. 16

92 Ralf Rapp (Texas A&M) "Heavy Flavor in Hot/Dense Matter " Mar. 23

93 David Vegh (Stony Brook) "RIKEN Lunch Seminar" Mar. 29

94 Taku Izubuchi (BNL) "HET/RIKEN Lunch Seminar" Mar. 30

RIBF Research Division

1 Eiji Ideguchi (University of Tokyo) "Superdeformed Band in Asymmetric N>Z Nucleus, 40Ar, and High-Spin Level Structures in A～40 Nuclei" Apr. 19

2 Tetsuo Hatsuda (U. Tokyo/ RNC) "Nuclear Force from Lattice QCD" Apr. 26

3 Takanori Sakamoto (University of Maryland) "Gamma-ray Burst Observations and Future Prospect" Apr. 28

4 Hiroshi Toki (RCNP) "The theory of multiconductor transmission line and the reduction of electromagnetic noise" May 10

5 Yasuyuki Suzuki (Niigata University) "Introduction to Glauber Theory and its application" May 12

6 Tetsuya Ohnishii (RNC) "Search for new neutron-rich isotopes using in-flight fission of 238U beam at 345 MeV/u" May 19

7 Kazuko Uno (Louis Pasteur Center for Medical Research) "Affects of Low-dose radiation : The body's acquired defense systems against radiation damage" Jun. 06

8 Hiromitsu Haba (RNC) "Superheavy element nuclear chemistry at RIKEN" Jun. 14

9 Hiroyuki Ichida (Stanford University) "Regulatory mechanisms of symbiosis by DNA methylation in rhizobial genome" Jun. 28

10 Satoru Katsuda (RNC) "Real-time Evolution of Supernova Remnants revealed with X-ray images" Jul. 07

11 Sadao Momota (Kochi U. Tech.) "Momentum distribution and production cross section of projectile-like fragments at intermediate energies" Jul. 12

12 Tomohiro Uesaka (RNC) "Spin in Isospin Physics" Jul. 26

13 Youichiro Hoshino (Hokkaido University) "Analysis of sexual reproduction process and its application for plant breeding by using wild genetic" Aug. 11

14 Atsushi Tamii (RCNP) "Complete Electric Dipole Response and the Neutron Skin in 208Pb" Sep. 08

15 Filip. G. Kondev (ANL) "Physics with Rare Isotope Sources" Sep. 22

16 Indranil Mazumdar (Tata Institute of Fundamental Research) "Halo World: The Story according to Faddeev, Efimov and Fano" Sep. 29

17 Toru Tamagawa (RNC) "Commentary on the 2011 Nobel Prize in Physics: Is the expansion of our universe really accelerating?" Oct. 18

18 Hiroaki Utsunomiya (Konan University) "Determination of radiative neutron capture cross sections for unstable nuclei by Coulomb dissociation" Nov. 01

19 Hisayoshi Yurimoto (Hokkaido University) "Characteristics of asteroid Itokawa from Hayabusa return samples" Nov. 15

20 Tadashi Sato (Tohoku University) "Is root-type breeding the key to improve problem-soil tolerance in rice?" Nov. 24

21 Shinya Yamada (RNC) "X-ray Observations of Black-hole Binaries" Nov. 24

22 Tomoko Abe (RNC) "Extreme innovation in mutation breeding by ion beam radiation" Nov. 24

23 Tadashi Sato (Tohoku University) "Is root-type breeding the key to improve problem-soil tolerance in rice?" Nov. 24

24 Shizuka Mori (Yamagata University) "Study of damage in rice plant exposed to salty winds of typhoon." Nov. 24

25 Tomoko Abe (RNC) "The next step to advanced mutagenesis in modern genome science era" Nov. 24

26 Satoshi N. Nakamura (Tohoku University) "Study of Lambda hypernuclei with electron beams" Nov. 29

27 Fumihiko Usui (Japan Aerospace Exploration Agency) "AKARI Asteroid Catalogue" Dec. 01

28 Thierry Stora (CERN) "New radioactive ion beams at CERN-ISOLDE : Target and ion source developments" Dec. 02

29 Masayuki Aikawa (Hokkaido University) "Current Status and Future Plans of Nulcear Reaction Data Centre (JCPRG)" Dec. 13

30 Charlotte Elster (Ohio University) "Microscopic Optical Potentials for the Reaction Helium-6(p,p)Helium-6" Dec. 16

31 Toshiyuki Sumikama (Tokyo University of Science) "Structural evolution of neutron-rich nuclei around 108Zr" Jan. 10

32 Xiao-Dong Tang (University of Nortre Dame) "Carbon Burning in the Universe and the Laboratory" Jan. 13

33 Yasuyuki Suzuki (Niigata University) "Introduction to the Glauber theory and its application Lecture Series on Nuclear Physics, Course IX" Jan. 31

34 Yuji Hasegawa (Vienna University of Technology) "Uncertain relation studied in neutron’s successive spin-measurements" Feb. 07

35 Minghui Huang (Chinese Academy of Sciences) "Researches in the SHN Group of IMP" Feb. 24

36 Masatoshi Itoh (Tohoku University) "Evidence for the new excited state in 12C and its structure" Feb. 24

37 Nobuyuki Nakamura (University of Electro-Communications) "Studies of highly charged ions with an electron beam ion trap" Feb. 28

38 Sigurd Hofmann (GSI) "Special Seminar: Status and perspectives of research on superheavy-nuclei" Mar. 01

39 Emiko Hiyama (RNC) "Weakly-bound few-body systems with strong short-range correlation" Mar. 06

40 Masaki Sasano (RNC) "A new experimental technique to measure the charge-exchange (p,n) reaction with RI beams" Mar. 13

41 Yuko Motizuki (RNC), Kazuya Takahashi (RNC), Yoichi Nakai (RNC), Kentaro Sekiguchi (RNC), Ai Shimada (RNC), .etc "The First NEXT Joint Meeting on ”Solar activity in the last 2000 years studied with Antarctic ice cores”" Mar. 13-14

42 Andrei Andreyev (University of the West of Scotland) "Fission of proton-rich nuclei in the lead region" Mar. 19

43 Abhay Deshpande (RBRC) "Physics and the Prospects of EIC/eRHIC Project" Mar. 29

KEK

1 Kazuyuki Ogata (Osaka University), "New understanding of the formation of 12C" Apr.27

2 Kouhei Washiyama (Free University of Brussels) "Description of the heavy-ion fusion reactions near the Coulomb barrier based on the mean field approximation" Jul. 25

3 Alexande St. Murphy (University of Edinburgh), "Measurements of key nuclear astrophysical reaction in novae and x-ray bursts" Feb. 17

AUTHOR INDEX

RIKEN Accelerator Progress Report *vol.* **45**

独立行政法人理化学研究所加速器年次報告　第45巻 (2012)

印　刷　平成24年（2012）　9月30日
発　行　平成24年（2012）10月31日

発行者　独立行政法人理化学研究所　仁科加速器研究センター
代表者　延　與　秀　人
〒351-0198　埼玉県和光市広沢2番1号
progress@ribf.riken.jp

編集者　独立行政法人理化学研究所　仁科加速器研究センター
加速器年次報告編集委員会

印刷所　株式会社デジタル印刷
〒300-4405　茨城県桜川市真壁町桜井307-1